| | |
|---|---|
| Report Title: | **Advanced Systems for Preprocessing and Characterizing Coal-Biomass Mixtures as Next-Generation Fuels and Feedstocks** |
| Type of Report: | **Final Scientific/Technical Report** |
| Reporting Period: | **October 1, 2010 – June 30, 2014** |
| Principal Authors: | **Michael Karmis, Gerald Luttrell, Nino Ripepi, Robert Bratton and Erich Dohm** |
| Date Report Issued: | **September 30, 2014** |
| DOE Award Number: | **DE-FE0005451** |
| Submitting Organization: | **Virginia Polytechnic Institute & State University**<br>**Office of Sponsored Programs**<br>**North End Center, Suite 4200**<br>**300 Turner Street NW**<br>**Blacksburg, VA 24061** |

# Disclaimer

"This report was prepared as an account of work sponsored by an agency of the United States Government. Neither the United States Government nor any agency thereof, nor any of their employees, makes any warranty, express or implied, or assumes any legal liability or responsibility for the accuracy, completeness, or usefulness of any information, apparatus, product, or process disclosed, or represents that its use would not infringe privately owned rights. Reference herein to any specific commercial product, process, or service by trade name, trademark, manufacturer, or otherwise does not necessarily constitute or imply its endorsement, recommendation, or favoring by the United Sates Government or any agency thereof. The views and opinions of authors expressed herein do not necessarily state or reflect those of the United States Government or any agency thereof."

# Abstract

The research activities presented in this report are intended to address the most critical technical challenges pertaining to coal-biomass briquette feedstocks. Several detailed investigations were conducted using a variety of coal and biomass feedstocks on the topics of (1) coal-biomass briquette production and characterization, (2) gasification of coal-biomass mixtures and briquettes, (3) combustion of coal-biomass mixtures and briquettes, and (4) conceptual engineering design and economic feasibility of briquette production. The briquette production studies indicate that strong and durable co-firing feedstocks can be produced by co-briquetting coal and biomass resources commonly available in the United States. It is demonstrated that binderless coal-biomass briquettes produced at optimized conditions exhibit very high strength and durability, which indicates that such briquettes would remain competent in the presence of forces encountered in handling, storage and transportation. The gasification studies conducted demonstrate that coal-biomass mixtures and briquettes are exceptional gasification feedstocks, particularly with regard to the synergistic effects realized during devolatilization of the blended materials. The mixture combustion studies indicate that coal-biomass mixtures are exceptional combustion feedstocks, while the briquette combustion study indicates that the use of blended briquettes reduces $NO_x$, $CO_2$, and CO emissions, and requires the least amount of changes in the operating conditions of an existing coal-fired power plant. Similar results were obtained for the physical durability of the pilot-scale briquettes compared to the bench-scale tests. Finally, the conceptual engineering and feasibility analysis study for a commercial-scale briquetting production facility provides preliminary flowsheet and cost simulations to evaluate the various feedstocks, equipment selection and operating parameters.

# Table of Contents

I. INTRODUCTION AND BACKGROUND ..... 1

1. Research Motivations and Objectives ..... 2
1.1 Research Motivations ..... 2
1.1.1 United States Energy Consumption ..... 2
1.1.2 Greenhouse Gas Emissions ..... 3
1.1.3 Domestic Energy Independence ..... 4
1.1.4 Co-Gasification of Coal and Biomass ..... 6
1.2 Research Objectives ..... 7

2. Scientific Merit Review ..... 8
2.1 Co-Gasification Benefits ..... 8
2.2 Co-Gasification Challenges ..... 10
2.3 Gasification Processes ..... 11
2.3.1 Types of Gasifiers ..... 14
2.3.2 Thermochemical Reactions ..... 21
2.3.3 Kinetic Modeling ..... 23
2.4 Coal and Biomass Properties Relevant to Gasification ..... 27
2.4.1 Chemical Composition ..... 28
2.4.2 Physical Properties ..... 33
2.4.3 Thermal Properties ..... 38
2.4.4 Mechanical Properties ..... 44
2.5 Agglomeration of Coal-Biomass Mixtures ..... 50
2.5.1 Agglomeration Theory ..... 50
2.5.2 Tumble/Growth Agglomeration ..... 58
2.5.3 Pressure Agglomeration ..... 66

II. BRIQUETTING AND PELLETIZATION ACTIVITIES ..... 80

3. Briquette Characterization Methods ..... 81
3.1 Abstract ..... 81
3.2 Introduction ..... 81

3.2.1 Problem Statement ..... 81
3.2.2 Briquette Properties ..... 82
3.2.3 Research Objective ..... 93
3.3 Experimental ..... 94
3.3.1 Materials ..... 94
3.3.2 Briquette Production ..... 97
3.3.3 Evaluation and Refinement Procedures ..... 98
3.4 Results and Discussion ..... 111
3.4.1 Tensile Strength ..... 111
3.4.2 Crushing Strength ..... 113
3.4.3 Elasticity ..... 116
3.4.4 Mechanical Durability ..... 120
3.4.5 Attritability ..... 123
3.4.6 Friability ..... 127
3.4.7 Water Content ..... 130
3.4.8 Particle Density ..... 131
3.4.9 Bulk Density ..... 132
3.4.10 Water Resistance ..... 134
3.5 Summary and Conclusions ..... 136

4. Moisture Optimization in Coal-Biomass Briquette Production ..140
4.1 Abstract ..... 140
4.2 Introduction ..... 141
4.2.1 Problem Statement ..... 141
4.2.2 Moisture Optimization ..... 141
4.2.3 Research Objectives ..... 144
4.3 Experimental ..... 144
4.3.1 Materials ..... 144
4.3.2 Briquette Production ..... 148
4.3.3 Briquette Characterization ..... 151
4.4 Results and Discussion ..... 153
4.4.1 Hydraulic Press Moisture Optimization ..... 153
4.4.2 Roll Press Moisture Optimization ..... 158
4.4.3 Correlations between Briquette Properties ..... 162
4.5 Summary and Conclusions ..... 172

5. Evaluation of Coal-Biomass Briquette Production Variables ..... 175
5.1 Abstract ..... 175
5.2 Introduction ..... 176
5.2.1 Problem Statement ..... 176
5.2.2 Roll Press Briquette Production ..... 177
5.2.3 Research Objectives ..... 182
5.3 Experimental ..... 183
5.3.1 Materials ..... 183
5.3.2 Briquette Production ..... 191
5.3.3 Briquette Characterization ..... 197
5.4 Results and Discussion ..... 203
5.4.1 Evaluation of Feedstock Variables – Bituminous Coal ..... 203
5.4.2 Evaluation of Additive Variables – Bituminous Coal ..... 242
5.4.3 Evaluation of Mixture Variables – Sub-Bituminous Coal ..... 259
5.4.4 Evaluation of Roll Press Operating Parameters ..... 280
5.4.5 Detailed Characterization of Optimum Briquettes ..... 299
5.5 Summary and Conclusions ..... 306

6. Production of Water-Resistant Coal-Biomass Briquettes ..... 309
6.1 Abstract ..... 309
6.2 Introduction ..... 310
6.2.1 Problem Statement ..... 310
6.2.2 Briquette Water Resistance ..... 310
6.2.3 Research Objective ..... 312
6.3 Experimental ..... 312
6.3.1 Materials ..... 312
6.3.2 Briquette Production ..... 315
6.3.3 Briquette Characterization ..... 318
6.4 Results and Discussion ..... 321
6.4.1 Conventional Binder Evaluations ..... 321
6.4.2 Preliminary Coating Evaluations ..... 326
6.4.3 Detailed Coating Evaluations ..... 331
6.5 Summary and Conclusions ..... 335

7. Sequential Pelletization, Drying and Briquetting ..... 337
7.1 Abstract ..... 337

7.2 Introduction ..... 337
7.3 Experimental ..... 339
7.3.1 Materials ..... 339
7.3.2 Pelletization, Drying and Briquetting Equipment ..... 343
7.3.3 Laboratory Procedures ..... 346
7.4 Results and Discussion ..... 350
7.4.1 Moisture Optimization Study ..... 350
7.4.2 Preliminary Comparisons of Briquettes Formed with Hot and Ambient Temperature Feedstocks ..... 354
7.4.3 Confirmation of the Impact of Pre-pelletization and Hot versus Cold Briquetting ..... 363
7.4.4 Co-Briquetting of Pelletized Coal and Biomass ..... 376
7.5 Summary and Conclusions ..... 391

8. Bio-Oil and Biochar Briquetting Evaluations ..... 393
8.1 Abstract ..... 393
8.2 Introduction ..... 393
8.3 Experimental ..... 396
8.3.1 Materials ..... 396
8.3.2 Pyrolysis Reactor ..... 396
8.3.3 Bio-Oil and Biochar Production Procedures ..... 397
8.3.4 Briquette Production ..... 399
8.3.5 Briquette Evaluation Procedures ..... 400
8.4 Results and Discussion ..... 401
8.5 Summary and Conclusions ..... 404

9. Coal Particle Size Briquetting Evaluations ..... 406
9.1 Abstract ..... 406
9.2 Introduction ..... 406
9.3 Experimental ..... 408
9.3.1 Materials ..... 408
9.3.2 Major Equipment ..... 411
9.3.3 Briquette Production ..... 411
9.3.4 Briquette Evaluations ..... 412
9.4 Results and Discussion ..... 413
9.5 Summary and Conclusions ..... 419

10. Pilot-Scale Briquetting Test Work ..... 421
10.1 Abstract ..... 421
10.2 Introduction ..... 421
10.3 Detailed Characterization of Optimum Briquettes ..... 422
10.3.1 Characterization of Physical Properties ..... 423
10.3.2 Pilot-Scale Briquette Evaluations ..... 426
10.4 Summary and Conclusions ..... 427

III. GASIFICATION AND COMBUSTION ACTIVITIES ..... 430

11. Thermogravimetric Analysis of Coal-Biomass Blends ..... 431
11.1 Abstract ..... 431
11.2 Introduction ..... 432
11.3 Experimental ..... 434
11.4 Results and Discussion ..... 436
11.4.1 Thermal Evolution Profiles – Blends with Corn Stover ..... 436
11.4.2 Thermal Evolution Profiles – Blends with Switchgrass ..... 440
11.4.3 Single Fuels – Effect of Heating Rates ..... 442
11.4.4 Analysis of Synergistic Interactions in Blends ..... 445
11.5 Kinetic Analysis ..... 449
11.5.1 Parallel First Order Reactions Model – Approximation of Temperature Integral 449
11.5.2 Distributed Activation Energy Model – Gaussian Distribution of Activation Energy ..... 455
11.5.3 Matrix Inversion Method ..... 462
11.5.4 Results and Discussion – Matrix Inversion Method ..... 465
11.6 Reactivity in $CO_2$ Atmosphere ..... 477
11.6.1 Kinetic Analysis of Boudouard Reaction – Single First Order Model ..... 479
11.6.2 Kinetic Analysis of Boudouard Reaction – Matrix Inversion Algorithm ..... 482
11.7 Summary and Conclusions ..... 484

12. Experimental Moving Bed Gasification of Coal-Biomass Blends ..... 486
12.1 Laboratory Scale Moving Bed Gasifier: Design & Operation ..... 486
12.2 Gasification with Varying Oxygen/Steam Ratio ..... 489
12.2.1 Quartz Insulation ..... 489

12.2.2 Stainless Steel Reactor ..... 492
12.3 Gasification with Varying Oxygen Partial Pressure ..... 497
12.4 Gasification of Briquettes ..... 502
12.4.1 Product Gas Analysis – Briquette Gasification ..... 503
12.5 Summary and Conclusions ..... 510

13. Source Apportionment of Carbon using Stable Carbon Isotope Analysis ..... 511
13.1 Abstract ..... 511
13.2 Introduction ..... 512
13.2.1 Background ..... 512
13.2.2 Theory ..... 513
13.3 Experimental ..... 515
13.3.1 Materials ..... 515
13.3.2 Process Parameters and Reactions ..... 516
13.3.3 Apparatus ..... 517
13.4 Results and Discussion ..... 519
13.4.1 Blends with Corn Stover ..... 523
13.4.2 Blends with Switchgrass ..... 526
13.5 Statistical Significance of Experimental Data ..... 529
13.6 Isotope Equilibrium ..... 530
13.7 Carbon Sourcing ..... 532
13.8 Summary and Conclusions ..... 534

14. Physiochemical Characterization of Coal and Biomass Feedstocks ..... 536
14.1 Introduction ..... 536
14.2 Experimental ..... 538
14.2.1 Materials and Preparation ..... 538
14.2.2 Instrumentation and Procedure ..... 539
14.3 Results and Discussion ..... 541
14.3.1 Biomass Leaching ..... 541
14.3.2 Coal and Biomass Comparison ..... 547
14.3.3 Coal-Biomass Moisture Interactions ..... 550
14.4 Summary and Conclusions ..... 551

15. Pyrolysis Chemical Kinetics of Coal and Biomass Feedstocks ..552
15.1 Introduction ..... 552
15.1.1 Pyrolysis Process ..... 552
15.1.2 Kinetics Analysis Approaches ..... 553
15.1.3 Biomass Pyrolysis ..... 555
15.1.4 Coal-Biomass Co-Pyrolysis ..... 558
15.2 Experimental ..... 560
15.3 Results and Discussion ..... 561
15.3.1 Gravimetric Response of Fuels ..... 561
15.3.2 Model Development and Kinetic Parameters ..... 564
15.4 Summary and Conclusions ..... 568

16. Pyrolysis and Combustion Energetics of Coal and Biomass Feedstocks ..... 570
16.1 Introduction ..... 570
16.2 Experimental ..... 571
16.3 Energetic Models ..... 574
16.3.1 Pyrolysis Model ..... 574
16.3.2 Combustion Model ..... 575
16.4 Energetic Signals ..... 576
16.4.1 STA Signal Analysis ..... 576
16.4.2 MCC Signal Analysis ..... 578
16.5 Energetic Properties Evaluation ..... 581
16.5.1 Heat of Pyrolysis and Heat of Gasification ..... 581
16.5.2 Heat of Pyrolysis Gas Combustion and Heat of Char Combustion ..... 584
16.6 Summary and Conclusions ..... 586

17. Combustion Performance of Coal and Biomass Feedstocks ..... 587
17.1 Introduction ..... 587
17.2 Experimental ..... 589
17.3 Fuel Performance Model ..... 589
17.4 Results and Discussion ..... 591
17.4.1 Fuel Pyrolysis Performance ..... 591
17.4.2 Char Combustion and Cumulative Performance ..... 595
17.5 Summary and Conclusions ..... 597

18. Combustion Characterization of Coal-Biomass Briquettes.....599
18.1 Introduction ..... 599
18.2 Experimental..... 601
18.2.1 Materials and Preparation ..... 601
18.2.2 Instrument and Procedure ..... 602
18.3 Results and Discussion ..... 605
18.3.1 Flammability and Combustion Performance ..... 605
18.3.2 Ignitability and Burn Duration..... 609
18.3.3 Emission Gas Profiles and Yields..... 613
18.4 Summary and Conclusions ..... 620

IV. FEASIBILITY ASSESSMENT AND CONCLUSIONS.....622

19. Feasibility Assessment.....623
19.1 Abstract..... 623
19.2 Circuit Simulation..... 623
19.3 Conceptual Circuit Design..... 624
19.4 Processing Simulations..... 625
19.4.1 Coal and Biomass Feedstock Properties ..... 625
19.4.2 Briquetting Process Flowsheet Simulations..... 625
19.5 Economic Feasibility ..... 626
19.6 Feasibility Study Results ..... 634
19.7 Summary and Conclusions ..... 637

20. Conclusions and Recommendations .....639
20.1 Summary of Research Activities ..... 639
20.2 Original Contributions..... 647
20.3 Final Conclusions ..... 649
20.4 Recommendations for Further Investigation ..... 659

Appendix A. Additional Mathematical Models for Coal-Biomass Briquette Production .....690
A.1 EM-SG Model..... 690
A.2 EM-MC Model..... 694
A.3 EM-WS Model ..... 698

A.4 EM-SD Model ..... 702

Appendix B. Briquette Flow Properties Report ..... 706

Appendix C. MATLAB Codes used for Estimating Gasification Kinetic Parameters ..... 756

C.1 Distributed Activation Energy Model – Gaussian Distribution of Activation Energy 756

C.2 Matrix Inversion Algorithm ..... 758

# List of Figures

Figure 1-1. United States energy consumption in 2011 (U.S. Energy Information Administration, 2012) ..... 2

Figure 2-1. Gasification unit operations and processes (modified from Kumar et al., 2009) ..... 13

Figure 2-2. Products obtainable from syngas (modified from Higman & van der Burgt, 2003) ..... 14

Figure 2-3. Dry ash and slagging moving bed gasifier schematics and temperature profiles (modified from Kristiansen, 1996 and Simbeck et al., 1993 as cited in Carpenter, 2008) ..... 16

Figure 2-4. Fluidized bed gasifier schematic and temperature profile (modified from Kristiansen, 1996 and Simbeck et al., 1993 as cited in Carpenter, 2008) ..... 18

Figure 2-5. Entrained flow gasifier schematic and temperature profile (modified from Kristiansen, 1996 and Simbeck et al., 1993 as cited in Carpenter, 2008) ..... 20

Figure 2-6. Flow function classification and lines of constant flow behavior (modified from Schulze, 2008) ..... 47

Figure 2-7. Particle binding mechanisms in agglomeration processes (modified from Pietsch, 2002) ..... 51

Figure 2-8. Mechanisms of size change in tumble/growth agglomeration (modified from Pietsch, 2002) ..... 60

Figure 2-9. Disc pelletizer schematic diagram (modified from Capes, 1980) ..... 61

Figure 2-10. Particle flow pattern in disc pelletizers (modified from Pietsch, 2002) ..... 62

Figure 2-11. Drum pelletizer schematic diagram and particle flow pattern (modified from Pietsch, 2002) ..... 63

Figure 2-12. Mechanisms of compaction in pressure agglomeration (modified from Pietsch, 2002) ..... 68

Figure 2-13. Schematic diagram of (a) gravity fed roll press with smooth rollers and (b) force fed roll press with pocket rollers (modified from Pietsch, 2002) ..... 70

Figure 2-14. Schematic diagram of the nip region between two smooth counter-rotating rollers (modified from Pietsch, 2002 and Capes, 1980) ..... 71

Figure 2-15. Komarek B-100R roll press schematic diagram (modified from Guigon & Simon, 2003) ..... 73

Figure 3-1. Forces briquettes encounter in handling, storage and transportation ..... 83

Figure 3-2. Apparatus for measurement of particle density specified in En 15150 (2011) ..... 90

Figure 3-3. Particle-size distribution of bituminous coals ..... 95

Figure 3-4. Equipment used for biomass size reduction: (a) tub grinder (b) hammer mill and (c) knife mill ..... 96

Figure 3-5. Komarek B-100R roll press (a) schematic diagram (modified from Guigon & Simon, 2003) and (b) laboratory installation ..... 97

Figure 3-6. (a) Mark-10 force gauge and test stand schematic drawing, (b) Mark-10 TSA750 manual test stand and force gauge installation and (c) Mark-10 M5-500 digital force gauge ..... 98

Figure 3-7. Briquette orientations and plungers utilized for indirect tensile strength tests: (a) 'tall' diametrical compression, (b) 'short' diametrical compression, (c) parallel wedge indentation, (d) perpendicular wedge indentation and (e) point indentation ..... 99

Figure 3-8. Briquette orientation and plunger utilized for crushing strength tests (a) prior to crushing and (b) after crushing ..... 100

Figure 3-9. (a) Mark-10 ESM001 digital travel display fitted to the manual test stand for elasticity tests and (b) force-displacement data point selection example ..... 101

Figure 3-10. Mechanical durability cylinder (a) schematic drawing and (b) laboratory installation ..... 103

Figure 3-11. Modified ASTM shatter test device for friability testing ..... 104

Figure 3-12. Particle density apparatus (a) schematic drawing and (b) laboratory installation ..... 106

Figure 3-13. Boxes of varying size for bulk density measurement: (left) 1 $ft^3$, (middle) 0.50 $ft^3$ and (right) 0.24 $ft^3$ ..... 107

Figure 3-14. (a) Initial briquette overflow for bulk density measurement (b) bulk density container after removing excess briquettes with a straightedge and (c) weight platform assembly for compressibility measurement ..... 108

Figure 3-15. Water resistance apparatus (a) schematic drawing and (b) laboratory installation ..... 109

Figure 3-16. Example of briquette arrangement on filter paper for water resistance measurement ..... 110

Figure 3-17. Distribution of indirect tensile strength results for (a) point indentation test, (b) parallel wedge indentation test, (c) perpendicular wedge indentation test, (d) tall diametrical compression test and (e) short diametrical compression test ..... 112

Figure 3-18. Distribution of crushing strength data recorded with the manual test stand ..... 113

Figure 3-19. Example of briquette compression beyond the break point with the manual test stand ..... 114

Figure 3-20. Example of briquette compression with the aluminum bar incorporated to the manual test stand configuration (a) prior to crushing and (b) beyond the break point ..... 115

Figure 3-21. Distribution of crushing strength data recorded by incorporating the aluminum bar to the manual test stand configuration ..... 116
Figure 3-22. Distribution of calculated spring constant values for (top) linear force-displacement evaluations and (bottom) peak force-displacement evaluations ..... 118
Figure 3-23. Sample force-displacement curve for spring constant calculation ..... 119
Figure 3-24. Mechanical durability results for different numbers of briquettes tested ..... 120
Figure 3-25. Mechanical durability residual values for different numbers of briquettes tested ..... 121
Figure 3-26. Mechanical durability results for different rotational speeds and different numbers of cylinder rotations ..... 122
Figure 3-27. Exponential regression line fitted to mechanical durability results for different rotational speeds and different numbers of cylinder rotations ..... 123
Figure 3-28. Attritability results for different screening times with different numbers of briquettes ..... 124
Figure 3-29. Attritability results for different numbers of briquettes ..... 126
Figure 3-30. Attritability results for different sieve sizes ..... 127
Figure 3-31. Friability results for different drop heights ..... 128
Figure 3-32. Friability results for different numbers of briquettes tested ..... 129
Figure 3-33. Friability residual values for different numbers of briquettes tested ..... 129
Figure 3-34. Graphical representation of particle density results for different test configurations [Error bars indicate plus and minus one standard deviation from the mean] ..... 132
Figure 3-35. Bulk density results for different container volumes [Error bars indicate plus and minus one standard deviation from the mean] ..... 133
Figure 3-36. Bulk density results for different consolidation pressures ..... 134
Figure 3-37. Graphical representation of water uptake measurements for different water spray durations ..... 135
Figure 4-1. (a) Dry density versus water content as determined by the Proctor Test for soils and (b) proctor curve and zero air voids curve for soils ..... 143
Figure 4-2. Particle-size distribution of coal samples ..... 146
Figure 4-3. (a) Pellet press schematic drawing, (b) Carver pellet press laboratory installation and (c) Carver pellet mold ..... 149
Figure 4-4. Komarek B-100R roll press (left) schematic diagram (modified from Guigon & Simon, 2003) and (right) laboratory installation ..... 151
Figure 4-5. Correlation between water content and dry density for all hydraulic press briquettes ..... 156

Figure 4-6. Correlation between water content and normalized dry density for the bituminous coal briquettes produced with the hydraulic press ..... 158

Figure 4-7. Correlation between water content and dry density for (a) TC-SD briquettes, (b) MR-SD briquettes, (c) EM-SD briquettes and (d) EB-SD briquettes ..... 161

Figure 4-8. Correlation between water content and normalized dry density for the bituminous coal briquettes produced with the roll press ..... 162

Figure 4-9. Correlation between water content and mechanical durability for all roll press briquettes ..... 163

Figure 4-10. Correlation between water content and crushing strength for all roll press briquettes ..... 164

Figure 4-11. Linear correlation between mechanical durability and dry density for (a) TC-SD briquettes, (b) MR-SD briquettes, (c) EM-SD briquettes and (d) EB-SD briquettes ..... 166

Figure 4-12. (a) Linear correlation between mechanical durability and dry density for the combined data from the three bituminous coals and (b) linear correlation between normalized mechanical durability and normalized dry density for the combined data from the three bituminous coals ..... 167

Figure 4-13. Linear correlations between mechanical durability and dry density of EB-SD briquettes for increasing and decreasing dry density values ..... 168

Figure 4-14. Linear correlation between crushing strength and dry density for (a) TC-SD briquettes, (b) MR-SD briquettes, (c) EM-SD briquettes and (d) EB-SD briquettes ..... 169

Figure 4-15. (a) Linear correlation between crushing strength and dry density for the combined data from the three bituminous coals and (b) linear correlation between normalized crushing strength and normalized dry density for the combined data from the three bituminous coals ..... 170

Figure 4-16. Linear correlations between crushing strength and dry density of EB-SD briquettes for increasing and decreasing dry density values ..... 171

Figure 4-17. Exponential correlation between mechanical durability and crushing strength for (a) TC-SD briquettes, (b) MR-SD briquettes, (c) EM-SD briquettes and (d) EB-SD briquettes ..... 172

Figure 5-1. Particle binding mechanisms in briquette production (modified from Pietsch, 2002) ..... 177

Figure 5-2. Mechanisms of compaction in briquette production (modified from Pietsch, 2002) ..... 178

Figure 5-3. Schematic diagram of (a) force fed roll press with pocket rollers (modified from Pietsch, 2002) and (b) nip region between two smooth counter-rotating rollers (modified from Pietsch, 2002 and Capes, 1980) ..... 179

Figure 5-4. Particle-size distribution of coal feedstocks ..... 185

Figure 5-5. Equipment used for biomass size reduction: (a) knife mill, (b) tub grinder and (c) hammer mill ..... 189

Figure 5-6. Komarek B-100R roll press (left) schematic diagram (modified from Guigon & Simon, 2003) and (right) laboratory installation ..... 192

Figure 5-7. Example of an experimental design constructed in Design-Expert® 8 ..... 193

Figure 5-8. Schematic drawing of bench-scale moving bed gasifier used to characterize the gasification behavior of coal-biomass briquettes (Bhagavatula, 2013) ..... 202

Figure 5-9. Effect of feed water content on particle density of briquettes composed of Emerald (bituminous) coal and (a) corn stover, (b) switchgrass, (c) miscanthus, (d) wheat straw and (e) sawdust ..... 209

Figure 5-10. Effect of feed water content on crushing strength of briquettes composed of Emerald (bituminous) coal and (a) corn stover, (b) switchgrass, (c) miscanthus, (d) wheat straw and (e) sawdust ..... 210

Figure 5-11. Effect of feed water content on mechanical durability of briquettes composed of Emerald (bituminous) coal and (a) corn stover, (b) switchgrass, (c) miscanthus, (d) wheat straw and (e) sawdust ..... 211

Figure 5-12. Effect of biomass content on particle density of briquettes composed of Emerald (bituminous) coal and (a) corn stover, (b) switchgrass, (c) miscanthus, (d) wheat straw and (e) sawdust ..... 214

Figure 5-13. Effect of biomass content on crushing strength of briquettes composed of Emerald (bituminous) coal and (a) corn stover, (b) switchgrass, (c) miscanthus, (d) wheat straw and (e) sawdust ..... 215

Figure 5-14. Effect of biomass content on mechanical durability of briquettes composed of Emerald (bituminous) coal and (a) corn stover, (b) switchgrass, (c) miscanthus, (d) wheat straw and (e) sawdust ..... 216

Figure 5-15. Effect of biomass top size on particle density of briquettes composed of Emerald (bituminous) coal and (a) corn stover, (b) switchgrass, (c) miscanthus, (d) wheat straw and (e) sawdust ..... 219

Figure 5-16. Effect of biomass top size on crushing strength of briquettes composed of Emerald (bituminous) coal and (a) corn stover, (b) switchgrass, (c) miscanthus, (d) wheat straw and (e) sawdust ..... 220

Figure 5-17. Effect of biomass top size on mechanical durability of briquettes composed of Emerald (bituminous) coal and (a) corn stover, (b) switchgrass, (c) miscanthus, (d) wheat straw and (e) sawdust ..... 221

Figure 5-18. Diagnostic graphs for visual inspection of ANOVA results for EM-CS particle density model: (a) normal probability plot of studentized results and (b) predicted versus actual values plot ..... 224

Figure 5-19. Diagnostic graphs for visual inspection of ANOVA results for EM-CS crushing strength model: (a) normal probability plot of studentized results and (b) predicted versus actual values plot ..... 226

Figure 5-20. Diagnostic graphs for visual inspection of ANOVA results for EM-CS mechanical durability model: (a) normal probability plot of studentized results and (b) predicted versus actual values plot ..... 227

Figure 5-21. Influence of feed water content on modeled responses for particle density, crushing strength and mechanical durability for briquettes composed of Emerald (bituminous) coal and corn stover ..... 229

Figure 5-22. Influence of biomass content on modeled responses for particle density, crushing strength and mechanical durability for briquettes composed of Emerald (bituminous) coal and corn stover ..... 230

Figure 5-23. Influence of biomass top size on modeled responses for particle density, crushing strength and mechanical durability for briquettes composed of Emerald (bituminous) coal and corn stover ..... 231

Figure 5-24. Comparison of particle density results for briquettes composed of bituminous coal and (a) miscanthus, (b) switchgrass, (c) sawdust, (d) corn stover and (e) wheat straw [Error bars indicate plus and minus one standard deviation from the mean] ..... 236

Figure 5-25. Comparison of crushing strength results for briquettes composed of bituminous coal and (a) miscanthus, (b) switchgrass, (c) sawdust, (d) corn stover and (e) wheat straw [Error bars indicate plus and minus one standard deviation from the mean] ..... 239

Figure 5-26. Comparison of mechanical durability results for briquettes composed of bituminous coal and (a) corn stover, (b) switchgrass, (c) miscanthus, (d) wheat straw and (e) sawdust ..... 241

Figure 5-27. Effect of binder content of briquettes composed of Emerald (bituminous) coal, corn stover and pregelatinized wheat starch on (a) particle density, (b) crushing strength and (c) mechanical durability ..... 244

Figure 5-28. Effect of cure time of briquettes composed of Emerald (bituminous) coal, corn stover and pregelatinized wheat starch on (a) particle density, (b) crushing strength and (c) mechanical durability ..... 246

Figure 5-29. Effect of biomass content of briquettes composed of Emerald (bituminous) coal, corn stover and pregelatinized wheat starch on (a) particle density, (b) crushing strength and (c) mechanical durability ..... 247

Figure 5-30. Diagnostic graphs for visual inspection of ANOVA results for EM-CS-PGWS particle density model: (a) normal probability plot of studentized results and (b) predicted versus actual values plot ..... 250

Figure 5-31. Diagnostic graphs for visual inspection of ANOVA results for EM-CS-PGWS crushing strength model: (a) normal probability plot of studentized results and (b) predicted versus actual values plot ..... 252

Figure 5-32. Diagnostic graphs for visual inspection of ANOVA results for EM-CS-PGWS mechanical durability model: (a) normal probability plot of studentized results and (b) predicted versus actual values plot ..... 253

Figure 5-33. Influence of binder content on modeled responses for particle density, crushing strength and mechanical durability for briquettes composed of Emerald (bituminous) coal, corn stover and pregelatinized wheat starch ..... 255

Figure 5-34. Influence of cure time on modeled responses for particle density, crushing strength and mechanical durability for briquettes composed of Emerald (bituminous) coal, corn stover and pregelatinized wheat starch..... 256

Figure 5-35. Influence of biomass content on modeled responses for particle density, crushing strength and mechanical durability for briquettes composed of Emerald (bituminous) coal, corn stover and pregelatinized wheat starch ..... 257

Figure 5-36. Effect of feed water content on (a) particle density, (b) crushing strength and (c) mechanical durability for briquettes composed of Eagle Butte (sub-bituminous) coal, corn stover and pregelatinized wheat starch ..... 261

Figure 5-37. Effect of biomass content on (a) particle density, (b) crushing strength and (c) mechanical durability for briquettes composed of Eagle Butte (sub-bituminous) coal, corn stover and pregelatinized wheat starch ..... 264

Figure 5-38. Effect of binder content on (a) particle density, (b) crushing strength and (c) mechanical durability for briquettes composed of Eagle Butte (sub-bituminous) coal, corn stover and pregelatinized wheat starch ..... 266

Figure 5-39. Diagnostic graphs for visual inspection of ANOVA results for EB-CS-PGWS particle density model: (a) normal probability plot of studentized results and (b) predicted versus actual values plot ..... 268

Figure 5-40. Diagnostic graphs for visual inspection of ANOVA results for EB-CS-PGWS crushing strength model: (a) normal probability plot of studentized results and (b) predicted versus actual values plot ..... 270

Figure 5-41. Diagnostic graphs for visual inspection of ANOVA results for EB-CS-PGWS mechanical durability model: (a) normal probability plot of studentized results and (b) predicted versus actual values plot ..... 271

Figure 5-42. Influence of feed water content on modeled responses for particle density, crushing strength and mechanical durability for briquettes composed of Eagle Butte (sub-bituminous) coal, corn stover and pregelatinized wheat starch..... 274

Figure 5-43. Influence of biomass content on modeled responses for particle density, crushing strength and mechanical durability for briquettes composed of Eagle Butte (sub-bituminous) coal, corn stover and pregelatinized wheat starch..... 275

Figure 5-44. Influence of binder content on modeled responses for particle density, crushing strength and mechanical durability for briquettes composed of Eagle Butte (sub-bituminous) coal, corn stover and pregelatinized wheat starch..... 276

Figure 5-45. Effect of biomass type on (a) particle density, (b) crushing strength and (c) mechanical durability for briquettes composed of Eagle Butte (sub-

bituminous) coal and each type of biomass [Error bars indicate plus and minus one standard deviation from the mean] ..... 279

Figure 5-46. Effect of Komarek B100R roll force on (a) particle density, (b) crushing strength and (c) mechanical durability for briquettes composed of McClure River (bituminous) coal and corn stover ..... 281

Figure 5-47. Effect of Komarek B100R roll torque on (a) particle density, (b) crushing strength and (c) mechanical durability for briquettes composed of McClure River (bituminous) coal and corn stover ..... 284

Figure 5-48. Effect of Komarek B100R roll speed on (a) particle density, (b) crushing strength and (c) mechanical durability for briquettes composed of McClure River (bituminous) coal and corn stover ..... 286

Figure 5-49. Diagnostic graphs for visual inspection of ANOVA results for Komarek B100R roll press particle density model: (a) normal probability plot of studentized results and (b) predicted versus actual values plot ..... 289

Figure 5-50. Diagnostic graphs for visual inspection of ANOVA results for Komarek B100R roll press crushing strength model: (a) normal probability plot of studentized results and (b) predicted versus actual values plot ..... 291

Figure 5-51. Diagnostic graphs for visual inspection of ANOVA results for Komarek B100R roll press mechanical durability model: (a) normal probability plot of studentized results and (b) predicted versus actual values plot ..... 292

Figure 5-52. Influence of Komarek B100R roll force on modeled responses for particle density, crushing strength and mechanical durability for briquettes composed of McClure River (bituminous) coal and corn stover ..... 295

Figure 5-53. Influence of Komarek B100R roll torque on modeled responses for particle density, crushing strength and mechanical durability for briquettes composed of McClure River (bituminous) coal and corn stover ..... 296

Figure 5-54. Influence of Komarek B100R roll speed on modeled responses for particle density, crushing strength and mechanical durability for briquettes composed of McClure River (bituminous) coal and corn stover ..... 297

Figure 5-55. Flow function for determination of required hopper opening sizes for Emerald-sawdust (EM-SD) briquettes [Values are listed in U.S. standard units as provided by Solids Handling Technologies] ..... 301

Figure 5-56. Flow function for determination of required hopper opening sizes for Eagle Butte-corn stover (EB-CS) briquettes [Values are listed in U.S. standard units as provided by Solids Handling Technologies] ..... 302

Figure 6-1. Particle-size distribution of coal samples ..... 314

Figure 6-2. Komarek B-100R roll press (left) schematic diagram (modified from Guigon & Simon, 2003) and (right) laboratory installation ..... 316

Figure 6-3. Dry density of briquettes with conventional binder application ..... 323

Figure 6-4. Crushing strength of briquettes with conventional binder application ..... 324

Figure 6-5. Mechanical durability of briquettes with conventional binder application..... 325
Figure 6-6. Water uptake of briquettes with conventional binder application ..... 326
Figure 6-7. Water uptake of coated briquettes (Set 1) ..... 328
Figure 6-8. Water uptake of coated briquettes (Set 2) ..... 329
Figure 6-9. Mechanical durability of coated briquettes ..... 330
Figure 6-10. Briquette samples after durability and water uptake tests..... 331
Figure 7-1. Particle size distributions for the various study coals and the EtOH biochar sample ..... 343
Figure 7-2. Schematic of thermal dryer used for drying coal pellets..... 345
Figure 7-3. 75-kW thermal dryer used for drying coal pellets ..... 346
Figure 7-4. Thirty minute crushing strengths for briquettes made from thermally dried coal pellets that were formed with or without binder as indicated ..... 351
Figure 7-5. Thirty minute crushing strengths for briquettes made from thermally dried coal pellets that were formed with the indicated binders..... 352
Figure 7-6. Seven day crushing strengths for the briquetted samples that exhibited the highest crushing strengths for each of the pelletized coal-binder blends ..... 353
Figure 7-7. Mechanical durability values of the briquetted samples that exhibited the highest crushing strengths for each of the pelletized coal-binder blends ..... 354
Figure 7-8. Comparison of 7 day crushing strengths for briquettes made from thermally dried coal pellets that were either immediately briquetted while hot or cooled to ambient temperature before briquetting and shown as a function of the binder added..... 356
Figure 7-9. Comparison of 7 day crushing strengths for briquettes made from thermally dried coal pellets that were either immediately briquetted while hot or cooled to ambient temperature before briquetting and shown as a function of the binder added..... 357
Figure 7-10. Comparison of mechanical durability results for briquettes made from thermally dried coal pellets that were briquetted hot versus equivalent pellets that were thermally dried then cooled to ambient temperature before briquetting..... 359
Figure 7-11. Seven day crushing strengths as a function of binder type ..... 372
Figure 7-12. Average mechanical durability from duplicate samples of briquettes made with air dried fines, air dried pellets, and hot thermally dried pellets ..... 375
Figure 7-13. Thirty minute, 24 hour, and 7 day crushing strengths for various biomass types co-briquetted with air dried PCC coal pellets made with 3 wt% wheat starch..... 377
Figure 7-14. Mechanical durability values for various biomass types co-briquetted with air dried PCC coal pellets made with 3 wt% wheat starch ..... 378

Figure 7-15. Thirty minute, 24 hour, and 7 day crushing strengths for various biomass types co-briquetted with air dried RVSB coal pellets that contained 3-wt% wheat starch ..... 380

Figure 7-16. Mechanical durability values for different biomass types co-briquetted with RVSB coal/wheat starch pellets at concentrations of 10 wt% (top) and 30 wt% (bottom) biomass ..... 381

Figure 7-17. Thirty minute crushing strengths for briquettes made from fine coal/3% starch pellets blended with 10 wt% biomass ..... 384

Figure 7-18. Seven day crushing strengths for briquettes made from fine coal/3% starch pellets blended with 10 wt% biomass ..... 385

Figure 7-19. Mechanical durability of briquettes made from fine coal/3% starch pellets blended with 10 wt% biomass ..... 387

Figure 7-20. Thirty minute and 7 day crushing strengths for briquettes made with thermally dried PCC fines/starch pellets that were blended with either 0% or 10 wt% biomass ..... 388

Figure 7-21. Thirty minute and 7 day crushing strengths for briquettes made with thermally dried RVSB fines/3% starch that were blended with either 0% or 10 wt% biomass ..... 389

Figure 7-22. Thirty minute and 7 day crushing strengths for briquettes made with thermally dried MRC fines/3% starch pellets that were blended with either 0% or 10 wt% biomass ..... 390

Figure 8-1. Schematic of 5.5 liter batch reactor used to produce bio-oil and biochar ..... 397

Figure 8-2. Steady-shear viscosities of the as-collected (top) and HVBO bio-oils (bottom) ..... 399

Figure 8-3. Crushing strengths following a 7 day cure for briquettes made with RVSB coal fines and 10% biomass comprised of bio-oil, biochar, wheat starch, corn stover, and/or miscanthus as indicated ..... 403

Figure 8-4. Mechanical durability results following a 7 day cure for briquettes made with RVSB coal fines and 10% biomass comprised of bio-oil, biochar, wheat starch, corn stover, and/or miscanthus as indicated ..... 403

Figure 9-1. Particle-size distribution for the three study coals plotted against the average diameter of the 8 size ranges to which the particles partitioned ..... 413

Figure 9-2. Linear combinations of the particle-size distributions for blends of MRC and Alden coals on top and for the MRC and PCC coals on bottom. ..... 414

Figure 9-3. Twenty-four hour crushing strengths (top) and mechanical durability (bottom) for blends of MRC and Alden coal fines ..... 415

Figure 9-4. Average weight of briquettes made with Alden and MRC coals and coal blends ..... 416

Figure 9-5. Twenty-four hour crushing strength and mechanical durability of briquettes produced from blends of MRC and PCC coal fines and 10% wheat straw

(WS) and 10% corn stover (CS) both with and without addition of a gelatinized wheat starch binder (WG) ..... 417

Figure 9-6. Average briquette weights for briquettes made with the PCC/MRC coal blends. ..... 418

Figure 10-1. Komarek Model B400B Briquetting Machine (courtesy K R Komarek, Inc.). ..... 423

Figure 10-2. EM-SD (left) and EB-CS (right) pilot-scale briquettes..... 423

Figure 11-1. Weight loss curves on a moisture free basis during the pyrolysis of PCC Bituminous coal, corn stover and their blends at 5 °C/min ..... 436

Figure 11-2. Weight loss curves on a moisture free basis during the pyrolysis of BT Sub-Bituminous coal, corn stover and their blends at 5 °C/min ..... 437

Figure 11-3. Differential thermogravimetric curves of pyrolysis of PCC-CS blends at 5 °C/min..... 438

Figure 11-4. Differential thermogravimetric curves of pyrolysis of BT-CS blends at 5 °C/min..... 438

Figure 11-5. Weight loss curves and DTG profiles during the pyrolysis of PCC Bituminous coal, switchgrass and their blends at 20 °C/min ..... 441

Figure 11-6. Weight loss curves and DTG profiles during the pyrolysis of BT Sub-Bituminous coal, switchgrass and their blends at 20 °C/min ..... 441

Figure 11-7. Weight loss profiles and DTG curves of pyrolysis of PCC Bituminous coal at four different heating rates ranging from 5 °C/min to 40 °C/min ..... 443

Figure 11-8. Weight loss profiles and DTG curves of pyrolysis of BT Sub-Bituminous coal at four different heating rates ranging from 5 °C/min to 40 °C/min..... 443

Figure 11-9. Weight loss profiles and DTG curves of pyrolysis of Corn Stover at four different heating rates ranging from 5 °C/min to 40 °C/min..... 444

Figure 11-10. Weight loss profiles and DTG curves of pyrolysis of switchgrass at four different heating rates ranging from 5 °C/min to 40 °C/min..... 444

Figure 11-11. Disparity in the experimental and predicted curves during the release of volatile matter with increasing concentration of corn stover..... 446

Figure 11-12. Comparison of the experimental and predicted weight loss curves for, (a) Blends of PCC Bituminous Coal and Corn Stover, and (b) Blends of BT Sub-Bituminous Coal and Corn Stover ..... 447

Figure 11-13. Comparison of the experimental and predicted DTG curves for (a) 10% CS + 90% PCC blend, (b) 20% CS + 80% PCC blend, and (c) 30% CS + 70% PCC blend..... 447

Figure 11-14. Comparison of the experimental and predicted DTG curves for (a) 10% CS + 90% BT blend, (b) 20% CS + 80% BT blend, and (c) 30% CS + 70% BT blend..... 448

Figure 11-15. Disparity in the experimental and predicted curves during the release of volatile matter with increasing concentration of switchgrass..... 448

Figure 11-16. Comparison of the experimental and predicted weight loss and DTG curves for (a) 10% SG + 90% PCC blend, and (b) 30% SG + 70% PCC blend ..... 449

Figure 11-17. Comparison of the experimental and predicted weight loss and DTG curves for (a) 10% SG + 90% BT blend, and (b) 30% SG + 70% BT blend ..... 449

Figure 11-18. Analysis of the thermal evolution profiles and temperature ranges for pyrolysis of (a) PCC Bituminous coal, (b) Corn Stover and (c) 10% CS and 90% PCC blend ..... 452

Figure 11-19. Estimation of kinetic parameters for pyrolysis of (a) PCC Bituminous coal, (b) Corn Stover, and (c) 10% CS and 90% PCC blend ..... 453

Figure 11-20. Plot for estimating the activation energy and Arrhenius constant for pyrolysis of PCC Bituminous coal at various heating rates and conversion points using DAEM ..... 458

Figure 11-21. Plot for estimating the relationship between V/Vf and activation energy for pyrolysis of PCC Bituminous coal using DAEM ..... 459

Figure 11-22. Plot for estimating the relationship between f (E) and activation energy for pyrolysis of PCC Bituminous coal using DAEM ..... 460

Figure 11-23. Plot for estimating the relationship between Arrhenius constant and activation energy for pyrolysis of PCC Bituminous coal using DAEM ..... 460

Figure 11-24. Comparison between experimental and calculated devolatilization weight loss of PCC Bituminous coal with increasing temperature using DAEM ..... 461

Figure 11-25. Mass fraction of fuel associated with each reaction during devolatilization of PCC Bituminous coal ..... 466

Figure 11-26. Plot of activation energy vs mass fraction remaining for pyrolysis of PCC Bituminous coal describing the values of activation energy for each parallel reaction ..... 467

Figure 11-27. Plot of pre-exponential factor vs mass fraction remaining for pyrolysis of PCC Bituminous coal describing the values of pre-exponential factor for each parallel reaction ..... 468

Figure 11-28. Comparison of experimental and predicted values for devolatilization of PCC Bituminous coal for two heating rates (10 °C/min and 20 °C/min) used in the matrix inversion algorithm: (a) weight loss vs temperature, and (b) derivative weight loss vs temperature ..... 469

Figure 11-29. Comparison of experimental and predicted values for devolatilization of PCC Bituminous coal for two heating rates (5 °C/min and 40 °C/min) not used in the matrix inversion algorithm: (a) weight loss vs temperature, and (b) derivative weight loss vs temperature ..... 470

Figure 11-30. Mass fraction of fuel associated with each reaction during devolatilization of Corn Stover ..... 471

Figure 11-31. Plot of activation energy vs mass fraction remaining for pyrolysis of Corn Stover describing the values of activation energy for each parallel reaction ..... 471

Figure 11-32. Comparison of experimental and predicted values for devolatilization of Corn Stover for two heating rates (20 °C/min and 40 °C/min) used in the matrix inversion algorithm: (a) weight loss vs temperature, and (b) derivative weight loss vs temperature ..... 472

Figure 11-33. Comparison of experimental and predicted values for devolatilization of Corn Stover for the heating rate (5 °C/min) not used in the matrix inversion algorithm: (a) weight loss vs temperature, and (b) derivative weight loss vs temperature ..... 473

Figure 11-34. Mass fraction of fuel associated with each reaction during devolatilization of 10% Corn Stover blended with 90% PCC Bituminous coal ..... 474

Figure 11-35. Plot of activation energy vs mass fraction remaining for pyrolysis of 10% Corn Stover-90% PCC Bituminous coal describing the values of activation energy for each parallel reaction ..... 474

Figure 11-36. Comparison of experimental and predicted values for devolatilization of 10% Corn Stover-90% PCC Bituminous coal for two heating rates (10 °C/min and 20 °C/min) used in the matrix inversion algorithm: (a) weight loss vs temperature, and (b) derivative weight loss vs temperature ..... 475

Figure 11-37. Comparison of experimental and predicted values for devolatilization of 10% Corn Stover-90% PCC Bituminous coal blend for heating rates (5 °C/min and 40 °C/min) not used in the matrix inversion algorithm: (a) weight loss vs temperature, and (b) derivative weight loss vs temperature ..... 476

Figure 11-38. Weight loss profiles and DTG curves of Bituminous coal, Corn Stover and PCC-CS blends at a 5 °C/min heating rate in a $CO_2$ atmosphere ..... 478

Figure 11-39. Weight loss profiles and DTG curves of Sub-bituminous coal, Corn Stover and BT-CS blends at a 5 °C/min heating rate in a $CO_2$ atmosphere ..... 478

Figure 11-40. Plot for estimating the activation energy for Boudouard reaction of PCC Bituminous coal, Corn Stover and blends of PCC Bituminous coal with Corn Stover at various heating rates ..... 480

Figure 11-41. Plot for estimating the activation energy for Boudouard reaction of BT Sub-bituminous coal, Corn Stover and blends of BT Sub-bituminous coal with Corn Stover at various heating rates ..... 480

Figure 11-42. Variation in activation energy of Boudouard reaction with increasing percentage of Corn Stover in blends with Bituminous and Sub-bituminous coals ..... 481

Figure 11-43. Stem plot of mass fraction of fuel associated with each reaction occurring during decomposition of PCC Bituminous coal in $CO_2$ atmosphere obtained using DAEM (matrix inversion algorithm) ..... 483

Figure 12-1. Schematic of the laboratory scale moving bed gasification system ..... 487

Figure 12-2. Average compositions of the product gases obtained during gasification of bituminous coal with varying steam to oxygen ratios ..... 490

Figure 12-3. Average ratios of the product gases obtained during gasification of sub-bituminous coal with varying steam to oxygen ratios ..... 491

Figure 12-4. Maximum ratios of the product gases and efficiency obtained during gasification of sub-bituminous coal with varying steam to oxygen ratios ..... 492

Figure 12-5. Average carbon monoxide concentration in exit stream obtained during gasification of bituminous coal with varying oxygen partial pressures..... 499

Figure 12-6. Average carbon dioxide concentration in exit stream during gasification of bituminous coal with varying oxygen partial pressures..... 500

Figure 12-7. Average CO:$CO_2$ ratios in the exit gas stream obtained during gasification of sub bituminous coal with varying oxygen partial pressures ..... 500

Figure 12-8. Average hydrogen concentration obtained during gasification of sub bituminous coal with varying oxygen partial pressures..... 501

Figure 12-9. Energy conversion efficiency obtained during gasification of sub bituminous coal with varying oxygen partial pressures..... 501

Figure 12-10. Average compositions of the product gases obtained during gasification of EM-SD briquettes with varying steam to oxygen ratios..... 505

Figure 12-11. Average ratios of the product gases obtained during gasification of EM-SD briquettes with varying steam to oxygen ratios ..... 506

Figure 12-12. Average compositions of the product gases obtained during gasification of EM-SD briquettes with varying steam to oxygen ratios at a constant air flow rate of 1400 ml/min..... 507

Figure 12-13. Average ratios of the product gases obtained during gasification of EM-SD briquettes with varying steam to oxygen ratios ..... 507

Figure 12-14. Comparison of cold gas efficiencies for gasification of EM-SD briquettes ..... 508

Figure 13-1. Typical GC-C-IRMS chromatogram of the gasification products (CO elutes at t = 318 s followed by $CH_4$ at 606 s and $CO_2$ at 1350 s)..... 522

Figure 13-2. Effect of increasing percentage of corn stover and varying oxygen/steam ratios on the isotopic signatures of product gases in its blends with PCC Bituminous coal: (a) Isotopic signature of CO, and (b) Isotopic signature of $CO_2$..... 525

Figure 13-3. Effect of increasing percentage of corn stover and varying oxygen/steam ratios on the isotopic signatures of product gases in its blends with BT Sub-Bituminous coal: (a) Isotopic signature of CO, and (b) Isotopic signature of $CO_2$..... 525

Figure 13-4. Effect of increasing percentage of switchgrass and varying oxygen/steam ratios on the isotopic signatures of product gases in its blends with PCC Bituminous coal: (a) Isotopic signature of CO, and (b) Isotopic signature of $CO_2$..... 527

Figure 13-5. Effect of increasing percentage of switchgrass and varying oxygen/steam ratios on the isotopic signatures of product gases in its blends with BT Sub-

Bituminous coal: (a) Isotopic signature of CO, and (b) Isotopic signature of $CO_2$ ..... 527

Figure 13-6. Comparison of Isotopic Signatures at an $O_2$:steam ratio of 2:1: (a) and (b): Blends with Corn Stover, and (c) and (d): Blends with Switchgrass ..... 528

Figure 13-7. Individual contribution of each biomass source towards generation of product gases at different $O_2$/steam ratios: (a) Contribution in the generation of CO in blends with PCC Bituminous coal, (b) Contribution in the generation of $CO_2$ in blends with PCC Bituminous coal, (c) Contribution in the generation of CO in blends with BT Sub-Bituminous coal, and (d) Contribution in the generation of $CO_2$ in blends with BT Sub-Bituminous coal ..... 534

Figure 14-1. Quanta 600 FEG ESEM ..... 540

Figure 14-2. Switchgrass biomass at 100X magnification on top of a carbon tape: (a) Raw, and (b) Water leached ..... 541

Figure 14-3. SG particle at 1000X magnification with Si element X-ray scan in the inset: (a) SG-Raw, and (b) SG-Leached ..... 542

Figure 14-4. Effect of water leaching on major inorganic element concentrations of biomass samples: (a) SG, and (b) CS ..... 543

Figure 14-5. Pyrolyzed leached biomass samples: (a) SG-Leached char at 100X magnification, (b) SG-Leached char sample at 1000X magnification with Si (Green) and O (Red) element X-ray scans in the inset, and (c) CS-Leached char at 1000X magnification ..... 545

Figure 14-6. Ash samples at 1000X magnification: (a) SG-Leached ash with Ca and Si element X-ray scans in the inset, and (b) CS-Leached ash particle ..... 546

Figure 14-7. Major compounds in leached biomass ash samples ..... 547

Figure 14-8. ESEM images for EC sample at 100X magnification: (a) Un-pyrolyzed EC, (b) EC char, and (c) EC ash ..... 548

Figure 14-9. (a) C/O ratio for EC, SG leach and CS leach samples in unpyrolyzed, char and ash states, and (b) C% for EC, SG leach and CS leach samples in unpyrolyzed, char and ash states ..... 549

Figure 14-10. Effect of EC and leached SG biomass co-pyrolysis: (a) SEM image of char from EC and SG-Leached mixture pyrolysis, and (b) C%, O% and C/O ratio of EC-char, SG-Leached char and char sample from co-pyrolysis of EC and SG-Leached sample in 80:20 mass ratio ..... 550

Figure 15-1. Types of decomposition models: (a) One-step global model (simplified), (b) One-stage multi reaction model (primary reactions), and (c) Two-stage semi global model (primary and secondary reactions) ..... 557

Figure 15-2. Biomass pyrolysis models: (a) Cozzani et al. (2009), (b) Kansa et al. (1977) and Kanury et al. (1970), (c) Milosavljevic et al. (1995), and (d) Shafizadeh (1968) ..... 558

Figure 15-3. TG and DTG analysis of fuel pyrolysis at 20 K/min heating rate: SG-Raw, SG-Leached and EC samples ..... 562

Figure 15-4. TG and DTG signals for pyrolysis of EC-SG-Leached mixture (80:20 by mass) ..... 563

Figure 15-5. TG runs at multiple heating rates and kinetic fit estimation for biomass samples using non-linear regression: (a) CS Raw, and (b) CS-Leached ..... 565

Figure 15-6. TG runs and kinetic fit estimation for fuel samples: (a) EC with three $n^{th}$ order independent parallel reaction model, and (b) EC & CS-Leached mixture at 80:20 initial mass ratio using five $n^{th}$ order independent parallel reaction model ..... 567

Figure 16-1. Instruments for energetic properties: (a) STA, (b) MCC, and (c) MCC schematic ..... 572

Figure 16-2. DSC and DTG signals for pyrolysis of CS-Raw and CS-Leached samples ..... 577

Figure 16-3. DSC and DTG signals for pyrolysis of EC and CS-Leached samples ..... 577

Figure 16-4. DSC signals for EC and CS-Leached mixture pyrolysis at 20 K/min heating rate ..... 578

Figure 16-5. HRR for pyrolysis gas combustion of CS-Raw, CS-Leached and EC samples ..... 579

Figure 16-6. HRR for pyrolysis gas combustion of EC and CS-Leached mixture pyrolysis at 20 K/min heating rate ..... 580

Figure 16-7. Char combustion heat release rate signals for CS-Raw, CS-Leached and EC samples ..... 581

Figure 17-1. Temperature dependent fuel pyrolysis performance parameter $\eta_p$: (a) Glycerol, PS, SG-Raw and EC samples, and (b) EC & SG-Leached mixture in 80:20 ratio ..... 592

Figure 17-2. Temperature dependent fuel pyrolysis performance parameter $\eta_p$: (a) Glycerol, PS, SG-Raw and EC samples, and (b) EC & SG-Leached mixture in 80:20 ratio ..... 595

Figure 17-3. Temperature dependent cumulative fuel performance ($\eta_{cum}$) ..... 596

Figure 18-1. Fuel samples tested in this study, as shown from left to right: (a) EC, SG-Raw and CS-Raw, and (b) EC briquette, EC & SG-Raw 80:20 blend briquette and EC briquette, EC & CS-Raw 80:20 blend briquette ..... 601

Figure 18-2. (a) Bench-scale fixed bed reactor inside the cone calorimeter, and (b) Stainless steel open grate system with aluminum pan at bottom (The system is painted with high temperature high emissivity black paint) ..... 603

Figure 18-3. Three types of test conditions using EC fuel: (a) Raw fuel in Al foil, (b) Briquettes in Al foil, and (c) Briquettes in open grate system ..... 604

Figure 18-4. After-combustion three types of test conditions using EC fuel: (a) Raw fuel in Al foil, (b) Briquettes in Al foil, and (c) Briquettes in open grate system ..... 606

Figure 18-5. After-combustion three types of test conditions using EC fuel upon ash removal from upper surface: (a) Raw fuel in Al foil, (b) Briquettes in Al foil, and (c) Briquettes in open grate system ..... 606

Figure 18-6. After-combustion two types of test conditions using blend briquettes upon ash removal: (a) EC and SG-Raw briquette, and (b) EC and CS-Raw briquette ..... 607

Figure 18-7. $NO_x$ profiles (in ppb) as a function of time for various experiments (All experiments conducted with Al foil except for last legend) ..... 615

Figure 18-8. HRR profiles (in $kW/m^2$) as a function of time for various experiments (All experiments conducted with Al foil except for last legend) ..... 617

Figure 18-9. $CO_2$ profiles (in volume %) as a function of time for various experiments (All experiments conducted with Al foil except for last legend)..... 618

Figure 18-10. CO profiles (in ppm) as a function of time for various experiments (All experiments conducted with Al foil except for last legend) ..... 619

Figure 19-1. Flowhseet simulation for the EM-SD feedstock with 30% biomass..... 628

Figure 19-2. Flowhseet simulation for the EM-SD feedstock with 20% biomass..... 629

Figure 19-3. Flowhseet simulation for the EM-SD feedstock with 10% biomass..... 630

Figure 19-4. Flowhseet simulation for the EB-CS feedstock with 30% biomass..... 631

Figure 19-5. Flowhseet simulation for the EB-CS feedstock with 20% biomass..... 632

Figure 19-6. Flowhseet simulation for the EB-CS feedstock with 10% biomass..... 633

# List of Tables

Table 2-1. General characteristics of gasification reactors (modified from Ratafia-Brown et al., 2002 as cited in Fernando, 2009 and from Simbeck et al., 1993 as cited in Higman & van der Burgt, 2003) ..... 15

Table 2-2. Standard test methods for determining coal and biomass properties relevant to gasification ..... 27

Table 2-3. True density of selected elements (modified from Weast, 1960 as cited in Jenkins, 1989) ..... 36

Table 3-1. Chemical properties of coal and biomass feedstocks ..... 95

Table 3-2. Water content accuracy and precision results ..... 130

Table 3-3. Particle density results for different test configurations ..... 131

Table 3-4. Water uptake measurements for all variables studied ..... 135

Table 4-1. Physical properties of coal feedstocks ..... 145

Table 4-2. Chemical properties of coal and biomass feedstocks ..... 146

Table 4-3. Summary of water content optimization results for TC-SD hydraulic press briquettes ..... 154

Table 4-4. Summary of water content optimization results for MR-SD hydraulic press briquettes ..... 154

Table 4-5. Summary of water content optimization results for EM-SD hydraulic press briquettes ..... 155

Table 4-6. Summary of water content optimization results for EB-SD hydraulic press briquettes ..... 155

Table 4-7. Summary of water content optimization results for TC-SD roll press briquettes ..... 159

Table 4-8. Summary of water content optimization results for MR-SD roll press briquettes ..... 159

Table 4-9. Summary of water content optimization results for EM-SD roll press briquettes ..... 159

Table 4-10. Summary of water content optimization results for EB-SD roll press briquettes ..... 160

Table 5-1. Physical properties of coal feedstocks ..... 185

Table 5-2. Chemical properties of coal feedstocks ..... 186

Table 5-3. Chemical properties of biomass feedstocks ..... 190

Table 5-4. Summary of characterization results for briquettes composed of Emerald coal and corn stover ..... 204

Table 5-5. Summary of characterization results for briquettes composed of Emerald coal and switchgrass ..... 204
Table 5-6. Summary of characterization results for briquettes composed of Emerald coal and miscanthus ..... 205
Table 5-7. Summary of characterization results for briquettes composed of Emerald coal and wheat straw ..... 205
Table 5-8. Summary of characterization results for briquettes composed of Emerald coal and sawdust ..... 206
Table 5-9. ANOVA results for EM-CS particle density model ..... 223
Table 5-10. ANOVA results for EM-CS crushing strength model ..... 225
Table 5-11. ANOVA results for EM-CS mechanical durability model ..... 227
Table 5-12. Numerical optimization results for EM-CS mathematical models ..... 232
Table 5-13. Summary of briquette characterization results for McClure River coal verification tests ..... 233
Table 5-14. Summary of briquette characterization results for Toms Creek coal verification tests ..... 233
Table 5-15. Summary of briquette characterization results for briquettes composed of Emerald (bituminous) coal, corn stover and pregelatinized wheat starch ..... 242
Table 5-16. ANOVA results for EM-CS-PGWS particle density model ..... 250
Table 5-17. ANOVA results for EM-CS-PGWS crushing strength model ..... 251
Table 5-18. ANOVA results for EM-CS-PGWS mechanical durability model ..... 253
Table 5-19. Numerical optimization results for EM-CS-PGWS mathematical models ..... 259
Table 5-20. Summary of characterization results for briquettes composed of Eagle Butte (sub-bituminous) coal, corn stover and pregelatinized wheat starch ..... 260
Table 5-21. ANOVA results for EB-CS-PGWS particle density model ..... 268
Table 5-22. ANOVA results for EB-CS-PGWS crushing strength model ..... 269
Table 5-23. ANOVA results for EB-CS-PGWS mechanical durability model ..... 271
Table 5-24. Numerical optimization results for EB-CS-PGWS mathematical models ..... 277
Table 5-25. Summary of briquette characterization results for Eagle Butte biomass verification tests ..... 278
Table 5-26. Summary of briquette characterization results for evaluation of Komarek B100R roll press operating parameters ..... 280
Table 5-27. ANOVA results for Komarek B100R roll press particle density model ..... 289
Table 5-28. ANOVA results for Komarek B100R roll press crushing strength model ..... 290
Table 5-29. ANOVA results for Komarek B100R roll press mechanical durability model ..... 292

Table 5-30. Numerical optimization results for Komarek B100R roll press mathematical models ..... 299

Table 5-31. Summary of physical characterization results for Emerald-sawdust (EM-SD) and Eagle Butte-corn stover (EB-CS) briquettes ..... 300

Table 5-32. Required hopper outlet sizes to ensure reliable flow of Emerald-sawdust (EM-SD) and Eagle Butte-corn stover (EB-CS) briquettes ..... 303

Table 5-33. Required hopper angles to ensure reliable mass flow for Emerald-sawdust (EM-SD) and Eagle Butte-corn stover (EB-CS) briquettes ..... 304

Table 5-34. Bulk density and compressibility results for Emerald-sawdust (EM-SD) and Eagle Butte-corn stover (EB-CS) briquettes ..... 305

Table 5-35. Summary of gasification characterization results for Emerald-sawdust (EM-SD) and Eagle Butte-corn stover (EB-CS) briquettes (adapted from Bhagavatula, 2013) ..... 305

Table 6-1. Chemical properties of coal and biomass feedstocks ..... 314

Table 6-2. Summary of conventional binder evaluation results ..... 322

Table 6-3. Summary of preliminary coating evaluation results ..... 327

Table 6-4. Summary of detailed coating evaluation results ..... 332

Table 7-1. Proximate, ultimate, and calorific analysis of biomass samples (as-received basis) ..... 340

Table 7-2. Major elements in ash and trace elements in biomass samples (as-received basis) ..... 341

Table 7-3. Proximate, ultimate, and calorific analysis of coal samples (as-analyzed basis) ..... 342

Table 7-4. Major elements in ash and trace elements in coal samples (as-analyzed basis) ..... 342

Table 7-5. The average increase in 30 minute and 7 day crushing strengths for briquettes formed with thermally dried pellets that were briquetted while hot versus equivalent pellets that were cooled to ambient temperature before briquetting ..... 358

Table 7-6. Increase in fines generated during mechanical durability testing for briquettes formed with thermally dried pellets that were cooled before briquetting versus equivalent pellets that were briquetted hot ..... 360

Table 7-7. Comparison of relative changes in crushing strengths and fines generation during mechanical durability testing for briquettes made with thermally dried hot pellets, thermally dried cool pellets, air dried pellets, and air dried un-pelletized fines ..... 363

Table 7-8. Comparison of binderless briquettes made from air dried fines, air dried pellets, and thermally dried pellets ..... 365

Table 7-9. Comparison of briquettes made from air dried fines, air dried pellets, and thermally dried pellets, all of which were blended with 2.4 wt% gelatinized wheat starch binder ..... 366

Table 7-10. Comparison of briquettes made from air dried fines, air dried pellets, and thermally dried pellets, all of which were blended with 3.1 wt% of Binder 2 ..... 367

Table 7-11. Comparison of briquettes made from air dried fines, air dried pellets, and thermally dried pellets blended with 3.0 wt% Binder1 ..... 368

Table 7-12. Comparison of briquettes made from air dried fines, air dried pellets, and thermally dried pellets, all blended with Lignin/Lime binder (2.6% / 1.3%)..... 369

Table 7-13. Comparison of the average 7 day crushing strengths as a function of the binder added..... 370

Table 7-14. Comparison of mechanical durability results for briquettes made from the PCC, RVSB, and MRC coals that were briquetted as air dried fines, air dried pellets, and hot thermally dried pellets ..... 373

Table 8-1. Composition and properties of briquettes made from RVSB coal co-briquetted with various combinations of wheat starch, corn stover, miscanthus, biochar, and bio-oil binder..... 402

Table 9-1. Chemical analysis of study coals shown on an as-received basis ..... 410

Table 9-2. Proximate analysis, ultimate analysis, and calorific values of biomass samples ..... 410

Table 10-1. Summary of physical characterization results comparing bench-scale and pilot-scale Emerald-sawdust (EM-SD) and Eagle Butte-corn stover (EB-CS) briquettes..... 426

Table 11-1. Proximate and elemental analysis of feedstocks ..... 435

Table 11-3. Pyrolysis temperature range, maximum weight loss rates and peak temperatures of all feedstocks determined by TGA ..... 437

Table 11-4. Maximum weight loss rates and peak temperatures attained during the devolatilization of individual feedstocks at different heating rates ..... 445

Table 11-5. Obtained pyrolysis kinetic parameters, temperature and conversion ranges for all feedstocks at a heating rate of 5 °C/min ..... 454

Table 11-6. Obtained pyrolysis kinetic parameters for single fuels and blended feedstocks using distributed activation energy model (Gaussian distribution of activation energies)..... 462

Table 11-7. Pyrolysis kinetic parameters and number of devolatilization reactions obtained for various feedstocks using matrix inversion algorithm..... 477

Table 11-8. Peak temperatures at various heating rates and activation energies for heat treatment of Coal-Corn Stover blends in a $CO_2$ atmosphere obtained using thermogravimetric analysis..... 481

Table 12-1. Average composition of product gases obtained during gasification of PCC Bituminous coal with varying oxygen to steam ratios..... 489

Table 12-2. Calculated energy efficiency during gasification of PCC Bituminous coal with varying oxygen to steam ratios ..... 489

Table 12-3. Average composition of product gases obtained during gasification of bituminous coal at varying $O_2$/steam ratios in the lab scale stainless steel moving bed gasifier ..... 493

Table 12-4. Average composition of product gases obtained during gasification of blends of bituminous coal and corn stover at varying $O_2$/steam ratios in the lab scale stainless steel moving bed gasifier..... 494

Table 12-5. Average composition of product gases obtained during gasification of blends of sub-bituminous coal and corn stover at varying $O_2$/steam ratios in the lab scale stainless steel moving bed gasifier..... 495

Table 12-6. Average composition of product gases obtained during gasification of blends of PCC bituminous coal and switchgrass at varying $O_2$/steam ratios in the lab scale stainless steel moving bed gasifier..... 496

Table 12-7. Average composition of product gases obtained during gasification of blends of BT sub-bituminous coal and switchgrass at varying $O_2$/steam ratios in the lab scale stainless steel moving bed gasifier..... 497

Table 12-8. Average composition of product gases obtained during gasification of sub bituminous coal with varying oxygen partial pressures..... 498

Table 12-9. Calculated energy efficiency during gasification of bituminous coal with varying oxygen partial pressures ..... 498

Table 12-10. Average composition of product gases obtained during gasification of EM-SD briquettes with varying oxygen to steam ratios ..... 504

Table 12-11. Average composition of product gases obtained during gasification of EM-SD-G97 briquettes with varying oxygen to steam ratios..... 508

Table 12-12. Average composition of product gases obtained during gasification of EB-CS briquettes with varying oxygen to steam ratios ..... 509

Table 12-13. Average composition of product gases obtained during gasification of EB-CS-G97 briquettes with varying oxygen to steam ratios ..... 509

Table 13-1. Product gas compositions for CO and $CO_2$ produced during the gasification of various coal/biomass blends at different $O_2$/steam ratios..... 520

Table 13-2. $\delta^{13}C$ values of various feedstock materials..... 521

Table 13-3. Carbon isotope ratios for CO and $CO_2$ produced during the gasification of various coal/biomass blends at different $O_2$/steam ratios ..... 523

Table 13-4. Analysis of Variance (ANOVA) for models generated based on experimental data and estimating the statistical significance (p-values) between treatment factors and response variables ..... 530

Table 13-5. Comparison of isotopic equilibrium temperatures of $CO_2$-CO product gases and experimental gasifier temperatures ..... 532

Table 14-1: Proximate analysis (dry basis) of coal and biomass samples..... 538

Table 14-2: Ultimate analysis (dry basis) of coal and biomass samples ..... 538

Table 14-3: Effect of leaching on biomass (C%, O% and C/O in mass percentage) ..... 543

Table 14-4. Elemental composition of EC, SG-Leached and CS-Leached ash samples ..... 549

Table 15-1. Kinetic parameters for pyrolysis of biomass and EC samples ..... 565

Table 16-1. Pyrolysis energetic properties of fuel samples pyrolysis at 20 K/min heating rate ..... 581

Table 16-2. Weighted additions of $\Delta h_{pyr}$ and $\Delta h_{gas}$ properties for individual fuel samples to estimate the energetic properties for the two fuel mixture test cases ..... 583

Table 16-3. Energetic combustion properties of fuel samples from MCC ..... 584

Table 16-4. Weighted additions of $\Delta h_{comb,p}$ and $\Delta h_{comb,cc}$ properties for individual fuel samples to estimate the energetic properties for the two fuel mixture test cases. Additions in initial mass ratio (80:20) and volatile mass ratio (54:46) basis ..... 585

Table 17-1. Pyrolysis performance indicating energetic properties of fuel samples ..... 593

Table 17-2. Fuel pyrolysis performance ranking order as per different criteria ..... 593

Table 17-3. Pyrolysis performance evaluation of fuel blends ..... 594

Table 17-4. Fuel combustion performance parameters for coal and biomass fuels ..... 597

Table 18-1. Test matrix for fuel briquetting study ..... 605

Table 18-2. Effective heat of combustion for different blended fuel tests ..... 608

Table 18-3. Final mass yield for different blended fuel tests ..... 609

Table 18-4. The $t_{off}$, $t_{ig}$ and $t_{burn}$ parameters for all fuels tested using Al foil setup ..... 611

Table 18-5. Yield data for $NO_x$, $CO_2$ and CO gases for various experiments ..... 620

Table 19-1. Summary of feedstock properties and operating parameters used for the flowsheet simulations. ..... 627

Table 19-2. Results of the flowsheet simulations for the eastern region (Emerald/sawdust, A1-A3) and the western region (Eagle Butte/corn stover, B1-B3) ..... 635

Table 19-3. Feasibility analysis for the eastern region (EM-SD) facility. ..... 636

Table 19-4. Feasibility analysis for the western region (EB-CS) facility. ..... 637

# Executive Summary

Co-utilization of biomass with coal in existing coal-fired facilities presents a unique opportunity to reduce greenhouse gas emissions and increase energy production from renewable resources. The research activities presented in this report are intended to address the most critical technical challenges pertaining to coal-biomass briquette feedstocks. The primary technical challenge regarding coal-biomass briquettes is achieving and maintaining a high level of physical quality from production to utilization. Additional challenges include developing a proper understanding of the co-firing behavior of blended coal-biomass fuels, and optimizing the operation of advanced gasification systems for converting coal-biomass blends into useable energy. To address these challenges, several detailed research investigations were conducted on the following topics using a variety of coal and biomass feedstocks:

1. Coal-biomass briquette production and characterization
2. Gasification of coal-biomass mixtures and briquettes
3. Combustion of coal-biomass mixtures and briquettes
4. Conceptual engineering design and economic feasibility of briquette production

The coal-biomass briquette production studies indicate that strong and durable gasification feedstocks can be produced by co-briquetting coal and biomass resources commonly available in the United States. In these studies, selected mixtures of bituminous coals, sub-bituminous coal, corn stover, wheat straw, miscanthus, switchgrass, sawdust, and biochar were evaluated as potential briquette feedstocks over a range of material properties and mixture ratios. This report proves that binderless coal-biomass briquettes produced at optimized conditions exhibit very high crushing strength (> 2,000 N) and mechanical durability (> 90%), which indicate that such briquettes would largely remain intact in the presence of forces encountered in handling, storage and transportation. However, such optimal binderless coal-biomass briquettes exhibit poor water resistance, which indicates that additional investigation of this matter is required.

Moisture content was found to have the greatest influence on binderless briquette strength and durability. As a result, the Briquette Proctor Test was developed to quickly optimize feedstock water content for briquette production, which significantly reduces time and material requirements. Additionally, a novel pre-pelletization, drying, and briquetting process was developed to improve fine coal drying and to further enhance the quality of coal-biomass briquettes. Finally, this report contains specific recommendations on briquette characterization methods, as well as material properties and roll press operating conditions for development of a wide range of high quality coal-biomass briquette formulations.

Additional briquette production evaluations were performed to assess gelatinized wheat starch, bio-oil, molasses/lime, lignin/lime, and two proprietary chemicals as binding additives for coal-biomass briquette production. It was determined that the gelatinized wheat starch and proprietary binders provide the greatest briquette strength and durability, while the bio-oil that was produced and tested does not appear to be suitable for use as a binder in this application. Several proprietary wood-derived chemicals were also studied in an attempt to improve the water resistance of coal-biomass briquettes. The results of this study indicate that wood-derived

chemicals can be applied to the exterior of coal-biomass briquettes as a coating to improve the water resistance by up to 97% and the weathered mechanical durability by up to 400%.

The gasification studies demonstrate that coal-biomass mixtures are exceptional gasification feedstocks. TGA experiments revealed a non-linearity in the evolution of volatile matter with increasing percentage of corn stover in blends with bituminous coal, which indicates synergistic behavior. Moving bed gasification tests showed that a high energy conversion efficiency (~36%) and $CO:CO_2$ ratio (~3:1) can be achieved using a mixture of nitrogen and oxygen in the feed gas stream. A novel stable carbon isotope analysis method was developed to distinguish and quantify the individual contributions of coal and biomass feedstock materials in the generation of carbon containing gases during gasification. This tool verifies that an increase in the amount of biomass in the feed leads to a steady increase in the isotopic value of the carbon containing gases, which further exemplifies the presence of synergistic effects between the blended materials.

The mixture combustion studies indicate that coal-biomass mixtures are exceptional combustion feedstocks. Using temperature dependent performance parameters, it is demonstrated that different fuels produce peak performance at different temperatures, thus the mixing of various fuels helps blended fuels in generating consistent performance over a wider temperature range, which in turn can be advantageous for power plant operation. The blending of coal and leached biomass fuels in 80:20 ratio shows that the blending of biomass increases the pyrolysis performance of coal by 21-33%. However, the blending of biomass decreases the char combustion performance of coal samples by 28%. Thus, blending of biomass decreases the cumulative fuel combustion performance of coal by 22%, which signifies the additional mass of mixture fuel that would need to be fed into a co-firing plant to obtain the same performance as coal-alone combustion.

The coal-biomass briquette combustion study indicates that the use of blended briquettes requires the least amount of changes in the operating conditions of an existing coal-fired power plant. Specifically, the flammability and combustion performance of blended briquettes is better than those of raw blended fuels. The off-gassing time, ignitability and burn duration of coal-biomass briquette combustion is similar to that of coal combustion. Also, the heat release rate profile for blended briquettes is higher and more uniform than the heat release rate profile for coal-biomass mixtures. Furthermore, the use of blended briquettes provides lower peak $NO_x$ values than raw blends of coal and biomass, and the $CO_2$ and CO yields from coal-biomass briquette combustion is lower than that from raw coal and biomass blend combustion.

The pilot-scale briquette production and physical performance study indicates that the pilot-scale briquettes were very comparable in performance to the bench-scale briquettes. The result suggests that screening various briquette formulations (coals, biomasses, reagents, coatings, etc.) on a bench-scale level provides opportunities for more in-depth studies and minimizes resources (briquetting equipment, manpower, time).

The conceptual engineering and economic feasibility study indicates that a commercial-scale briquetting production facility with a capacity of 100 tph of dry briquettes can be developed and constructed for an estimated capital cost of $5.9 million. The estimated operating cost for a facility in the eastern U.S. processing premium thermal (bituminous) coals and wood related biomass is $7-$8 per ton of briquettes. The estimated operating cost for a facility in the western U.S. processing low rank (subbituminous) coals and agricultural related biomass is $30-$40 per

ton of briquettes, with the higher cost due primarily to the high reagent consumption required for the high (inherent) moisture content coal.

As a result of the research presented in this report, additional studies are recommended to investigate the market potential for coal-biomass briquettes in the areas of logistics, biomass sustainability, and economic feasibility to determine the potential role of coal-biomass briquettes in the global energy market. Additionally, further investigation is recommended to enhance the understanding of (1) the effect of inherent moisture content and coal particle-size distribution on briquette quality, (2) devolatilization kinetics and energetics of coal-biomass briquettes, (3) high pressure gasification performance, and (4) emission gas behavior correlations. Finally, further development is recommended to improve the wood-derived chemical coating application technology, and to improve the bio-oil and biochar production process to enhance the potential for use as briquette binders and fillers, respectively.

# SECTION I

# INTRODUCTION AND BACKGROUND

# Chapter 1

# Research Motivations and Objectives

## 1.1 Research Motivations

### 1.1.1 United States Energy Consumption

In 2011, total energy consumption in the United States was 1.027 x $10^{20}$ joules (97.3 quadrillion Btu). As depicted in Figure 1-1, the electric power sector was the largest consumer of energy, followed by the transportation, industrial, and residential and commercial sectors (U.S. Energy Information Administration, 2012). Although a portion of the energy demand is currently met by nuclear power and renewable energy sources, fossil fuels continue to dominate the United States energy portfolio, contributing more than eighty percent to the total energy demand. Fossil fuels offer many benefits over non-fossil energy sources, including high energy density, widespread availability and affordability (DiPeso, 2011). However, there are a number of growing domestic and international concerns regarding current and future consumption of fossil energy.

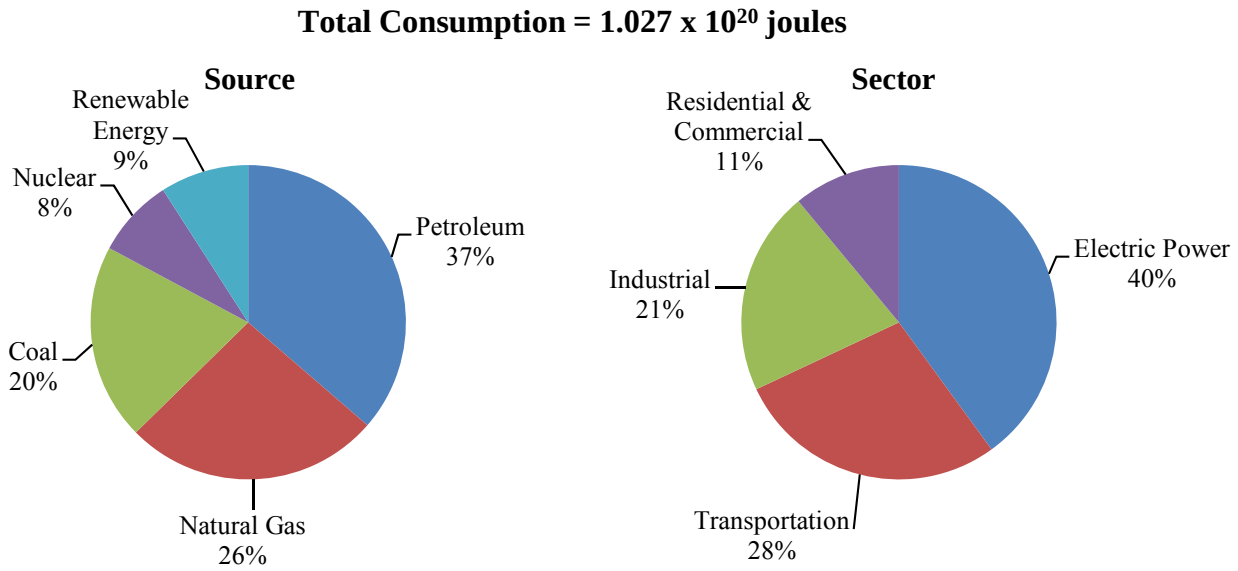



Figure 1-1. United States energy consumption in 2011 (U.S. Energy Information Administration, 2012)

### 1.1.2 Greenhouse Gas Emissions

The release of greenhouse gases from fossil fuel utilization has received considerable attention in recent years. Greenhouse gases include water vapor, carbon dioxide ($CO_2$), methane ($CH_4$), nitrous oxide ($N_2O$) and halocarbons. Carbon dioxide is the second most prevalent greenhouse gas, accounting for approximately 25 percent of the greenhouse effect (Casper, 2010). In 2011, carbon dioxide emissions from energy consumption in the United States totaled 5,481 million metric tons (6,042 million short tons). Of this total, 42 percent was contributed by petroleum, 34 percent by coal and 24 percent by natural gas (U.S. Energy Information Administration, 2012). In an effort to reduce domestic carbon dioxide emissions, the United States Environmental Protection Agency (EPA) is increasing regulatory pressure on stationary emission sources. The most recent rule proposed by the EPA would establish a new source performance standard (NSPS) for carbon dioxide. The proposed standard would establish an emissions limit of 453.6 kilograms (1,000 pounds (lb)) of carbon dioxide per megawatt-hour of electricity generated for new fossil fuel-fired electric generating units larger than 25 megawatts (33,526 horsepower (hp)) (U.S. Environmental Protection Agency, 2012). If passed, this new rule could reduce coal-fired power generation, increase energy prices and destroy jobs and investments throughout the United States (Crooks, 2012).

In 2011, the electric power sector accounted for 92 percent of total domestic coal consumption, which was used to produce 46 percent of the total power generated in the United States (U.S. Energy Information Administration, 2012). Due to the current regulatory environment, many electric utilities have investigated options to reduce carbon dioxide emissions from coal-fired power stations. One near-term method that has gained considerable interest is co-firing, which involves substituting a portion of the coal feed with a renewable and carbon-neutral feedstock such as biomass (Sami et al., 2001). Biomass co-firing is an attractive option because it offers an immediate reduction of carbon dioxide emissions and does not require a significant capital investment (Basu et al., 2011). In addition to greenhouse gas mitigation, electric utilities can implement biomass co-firing to contribute to states' renewable portfolio standards in regions that do not possess sufficient wind, solar or other renewable resources (Nussbaumer, 2003).

As of 2009, more than 150 coal-fired power stations across the world reported co-firing coal and biomass on a commercial or trial basis (Fernando, 2009). In 2011, there were 40 power stations co-firing coal and biomass in the United States alone, with the majority located in the

eastern and mid-western regions of the country (Basu et al., 2011). However, most industrial co-firing operations have used less than ten percent biomass on a heat input basis, while more than fifty percent would be required to meet the carbon dioxide emission limit proposed by the EPA. Unfortunately, industrial co-firing experiences have revealed a number of technical issues that can be detrimental to achieving this goal. These issues include biomass availability, transportation, storage, handling, and fouling and corrosion of the combustor (Basu et al., 2011; Fernando, 2009; Sami et al., 2001). Therefore, it is anticipated that other capital-intensive modifications to the traditional coal-fired power station, such as efficiency improvements or installation of a carbon capture system, would be necessary to comply with EPA regulations.

### 1.1.3 Domestic Energy Independence

Another major concern regarding the current United States energy portfolio is the reliance on foreign sources of energy. Historically, the United States has imported large quantities of petroleum from politically unstable regions of the world, including the Middle East and South America. Petroleum is imported primarily to meet the rising demand of the transportation and industrial sectors for the production of liquid fuels and chemicals. In 2011, petroleum imports to the United States totaled $1.002 \times 10^6$ cubic meters (8.4 million barrels) per day, or approximately 45 percent of total petroleum consumption (U.S. Energy Information Administration, 2012). These imports pushed the foreign trade deficit past $500 billion in 2011 and have greatly influenced foreign policy in the Middle East (Snow, 2012). In light of this challenge, there is significant political and industrial interest in technologies to increase domestic energy independence.

An established technology that has gained interest in recent years is gasification, which is a chemical process that converts carbonaceous materials into syngas for the production of chemicals, synthetic fuels and power (Basu, 2010). Specifically, interest in coal gasification has increased significantly due to fluctuations in the price of crude oil and concerns about domestic energy independence. The growing interest in gasification can also be attributed to the development of new applications such as gas-to-liquids processes, the prospect of increased efficiency and environmental performance in power generation, and the ability to process low-value or waste feedstocks (Higman & van der Burgt, 2003).

As of 2010, worldwide gasification capacity was 7.082 x $10^4$ megawatts-thermal ($MW_{th}$) (9.497 x $10^7$ hp) of syngas from 144 operating plants (U.S. Department of Energy, 2010). Additionally, 48 gasification plants with a projected capacity of 5.129 x $10^4$ $MW_{th}$ (6.878 x $10^7$ hp) are in the planning or construction phases and should be operational by 2016. The majority of these new gasification plants (40 of 48) are designed to use coal as the primary feedstock. In the United States, gasification capacity was 6.166 x $10^3$ $MW_{th}$ (8.202 x $10^6$ hp) from 18 operating plants in 2010 and an additional 18 plants are set to begin operating by 2016. These new gasification plants are projected to increase domestic gasification capacity by more than 500 percent to 3.341 x $10^3$ $MW_{th}$ (4.480 x $10^7$ hp). By 2016, coal will be used as the primary feedstock in the production of 1.778 $MW_{th}$ (2.385 x $10^7$ hp) in the United States, or roughly 53 percent of the total gasification capacity. About 45 percent of domestic coal gasification will be used to produce gaseous or liquid fuels, 42 percent to generate power, and 8 percent for the production of chemicals (U.S. Department of Energy, 2010).

One motivation for the gasification of coal is to replace petroleum as the primary feedstock for the production of chemicals and liquid fuels. Syngas produced from coal gasification is typically composed of 25 to 30 percent hydrogen ($H_2$) and 30 to 60 percent carbon monoxide (CO) (Ratafia-Brown et al., 2002). Pure hydrogen can be used to produce ammonia and other chemicals, while a mixture of hydrogen and carbon monoxide can be used to produce chemicals such as methanol. Similarly, pure carbon monoxide can be used to produce acetic acid and other chemicals (Higman & van der Burgt, 2003). Additional liquid fuels can be produced by catalytically combining hydrogen and carbon monoxide. For example, diesel fuel can be produced using the Fischer-Tropsch process or gasoline can be produced by methanol synthesis. Finally, syngas produced by coal gasification can also be used to produce synthetic natural gas composed primarily of methane (Fernando, 2008).

Interest in the gasification of coal for power generation began in the 1970s due to economic and environmental considerations. Current motivations for reducing greenhouse gas emissions have enhanced the prospects of power generation from an integrated gasification combined cycle (IGCC) plant (Fernando, 2008). The IGCC plant was developed in the 1980s by integrating gasification technology with a combined cycle power plant, which uses hot gas exiting a gas turbine as a heat source for a steam cycle in a heat recovery steam turbine (Higman & van der Burgt, 2003). Such IGCC coal-fired plants can achieve higher efficiencies than

traditional pulverized coal combustion plants. In addition, carbon dioxide capture is considerably easier in the IGCC plant because the concentration and pressure of carbon dioxide is much greater in syngas than in the flue gas produced in a pulverized coal combustion plant (Fernando, 2008). Due to these advantages, the IGCC plant is a promising technology for future power generation using the vast coal reserves in the United States.

### 1.1.4 Co-Gasification of Coal and Biomass

Coal gasification and biomass co-firing offer significant environmental and economic benefits to the current United States energy portfolio. However, both the efficiency improvement of IGCC and biomass co-firing in coal-fired boilers will not provide adequate reduction in carbon dioxide emissions to meet the proposed EPA standard for power generation. In each case, the power plant would need to install a carbon capture and storage system to comply with the regulation (U.S. Environmental Protection Agency, 2012). Currently, significant government funding and tax incentives are needed to justify the installation of such as system, which would add considerably to the overall cost of electricity generation. Moving forward, the United States must still strive to improve greenhouse gas mitigation and domestic energy independence without sacrificing the nation's abundant, affordable and secure coal resources.

One area of considerable research interest in recent years is the co-gasification of coal and biomass, which incorporates the benefits of traditional biomass co-firing with the versatility of coal gasification. Aside from the environmental benefits, many studies to date have found a number of thermochemical synergies in the co-gasification of coal and biomass, including an improvement in the syngas $H_2$/CO ratio, faster reaction rates, increased carbon conversion and higher thermal efficiency (Long & Wang, 2011; Pan et al., 2000; Sjostrom et al., 1999). Unfortunately, there are also many technical challenges to co-gasification that can be very costly if not properly addressed. These challenges include upstream issues, such as biomass availability, transportation, storage, and handling, as well as problems encountered within the gasifier, such as fouling, corrosion, inconsistent feeding and segregation (Fernando, 2009). Further research is needed in the field of preprocessing coal and biomass mixtures to alleviate these technical challenges for co-gasification to gain industrial support (Koppejan & Brem, 2008; Reed, 1981).

## 1.2 Research Objectives

The ultimate objective of the research detailed in this report is to support the development of coal and biomass co-gasification by addressing feedstock technical challenges advancing the understanding of the devolatilization process. Research activities were designed to identify and alleviate technical and economic barriers associated with preprocessing and thermal utilization of coal and biomass mixtures. Specifically, this research investigates the laboratory-scale production, physical characterization, and thermal characterization of coal-biomass briquettes composed of various coal and biomass feedstocks. Additional work was conducted to evaluate pilot-scale briquette production and to evaluate the economic feasibility of commercial production of coal-biomass briquette feedstocks. Specific objectives of this research are to:

1. Identify, develop and refine methods to characterize physical properties of coal-biomass briquettes;
2. Develop a methodology to quickly and easily identify the optimum water content of coal-biomass blends prior to briquette production;
3. Evaluate the influence of the most significant feedstock variables, additive variables and roll press operating variables in the production of coal-biomass briquettes from various coal and biomass feedstocks;
4. Develop and evaluate methods to improve the water resistance of coal-biomass briquettes using proprietary wood-derived chemicals;
5. Develop a novel sequential coal pelletization, drying, and briquetting process to improve the strength and durability of coal-biomass briquettes;
6. Evaluate the potential to use bio-oil and biochar produced from the pyrolysis of woody biomass as a coal-biomass briquette binder and filler, respectively;
7. Evaluate the impact of coal particle-size distribution on the strength and durability of coal-biomass briquettes;
8. Validate the results of selected laboratory-scale briquetting test work by conducting a series of pilot-scale briquetting tests;
9. Evaluate the thermal evolution profiles and estimate the kinetic parameters for pyrolysis and Boudouard reaction of coal-biomass blends using thermogravimetric analysis;
10. Conduct a series of experimental moving bed gasification tests on coal-biomass blends;

11. Evaluate the source apportionment of carbon during gasification of coal-biomass mixtures using stable carbon isotope analysis;
12. Characterize the physiochemical effects of biomass leaching, differences in individual coal and biomass samples, and the impact of blending coal and biomass fuels;
13. Characterize the kinetic parameters of coal and biomass fuels, including water leached biomass, using thermal analysis of the fuels while undergoing devolatilization;
14. Characterize the pyrolysis and combustion energetics of coal, biomass, and coal-biomass blends using a STA and a micro-scale combustion calorimeter (MCC);
15. Quantify the combustion performance index of coal, biomass, and coal-biomass blends by developing a model based on gravimetric, pyrolysis and combustion energetics data;
16. Investigate the effect of briquetting on the flammability, ignitability, combustion performance, burn duration, and emissions of coal briquettes and coal-biomass briquettes; and
17. Determine the economic feasibility of a commercial-scale coal-biomass briquette production facility.

# Chapter 2

# Scientific Merit Review

## 2.1 Co-Gasification Benefits

Growing concerns over rising greenhouse gas emissions and foreign petroleum imports have generated significant interest in cleaner and more secure technologies for the production of power, liquid fuels and chemicals. One of the more promising near-term options to address these challenges is co-gasification of coal and biomass. Co-gasification involves substituting a portion of the primary gasifier feed, such as coal, with a renewable and carbon-neutral feedstock, such as biomass (Sami et al., 2001). In addition to a net reduction in carbon dioxide ($CO_2$) emissions, the incorporation of biomass can also reduce the emission of sulfur oxides ($SO_x$) and nitrogen oxides

($NO_x$) due to the low sulfur and nitrogen levels typically present in biomass (Fernando, 2009; Demirbas, 2003).

For example, Long & Wang (2011) reported a reduction in harmful emissions from a 250-MW IGCC plant by incorporating up to fifty percent biomass in the coal feed. The concentration of $CO_2$ in the syngas was reduced from 14.88% with coal only to 13.97% by adding fifty percent biomass (weight basis) to the feed. Similarly, hydrogen sulfide ($H_2S$) in the syngas was reduced from 0.27% to 0.15% under the same conditions. Pinto et al. (2010) investigated the abatement of sulfur and nitrogen compounds by catalytic treatment of syngas produced from the co-gasification of coal and biomass. They found that syngas treatment using dolomite and a nickel-based catalyst led to a 97 percent net reduction in $H_2S$ and ammonia ($NH_3$), which are the primary precursors to $SO_x$ and $NO_x$ emissions.

Aside from the environmental benefits of co-gasification, recent studies have found a number of improvements in process efficiency and syngas composition that are attributed to coal and biomass synergies during thermochemical conversion (Brar et al., 2012). Kumabe et al. (2007) studied the co-gasification of woody biomass and coal with air and steam in a moving bed gasifier at 900 degrees Celsius. Experiments were conducted to determine the effects of biomass content on the molar ratio of $H_2$, CO and $CO_2$ in the produced syngas. The results showed an increase in carbon conversion in the syngas as the biomass ratio was increased, whereas the conversion to char and tar decreased. Based on the molar ratios of $H_2$, CO and $CO_2$ in the produced syngas, the authors concluded that a low biomass ratio is favorable for the synthesis of methanol and liquid fuels and a high biomass ratio if favorable for dimethyl ether synthesis (Kumabe et al., 2007).

Pan et al. (2000) investigated the co-gasification of low-grade Spanish coals and pine chips at different ratios in a bench scale fluidized bed reactor operating at 840 to 910 degrees Celsius. The results showed an increase in the molar ratio of CO in the syngas as well as an increase in $H_2$ for blends with less than 25 percent pine chips. Carbon conversion was found to increase from 63.0% with coal alone to 75.3% by adding 25 percent pine chips to the feed. The overall thermal efficiency of the system increased from 40 to 61 percent under the same conditions (Pan et al., 2000). These significant improvements highlight the potential to convert low-grade coals into premium fuels by co-gasification.

Sjostrom et al. (1999) observed a number of synergies in the co-gasification of woody biomass and coal with oxygen in a pressurized fluidized bed reactor operating at 700 to 900 degrees Celsius and 0.4 MPa. Experiments were conducted by varying the content of coal and biomass in the gasifier feed and comparing the results to the gasification of the individual fuels. The study found an unexpectedly high reaction rate and low char yield, which led to an increase in syngas production. Moreover, tar and ammonia yields were lower than the sum of yields from the gasification of the individual fuels (Sjostrom et al., 1999).

## 2.2 Co-Gasification Challenges

Although there are a number of benefits to co-gasification of coal and biomass, there are also several challenges presented that can be very costly and detrimental to industrial operations if not properly addressed (Basu et al., 2011). As a standalone gasification fuel, biomass faces many economic and technical challenges. When compared to fossil fuels, biomass generally benefits from renewability and decreased harmful emissions ($CO_2$, $NO_x$, $SO_x$); however, the dominant tradeoff is a significant loss in energy density and seasonal availability (Sami et al., 2001). Consequently, more biomass is needed to attain the same energy output as fossil fuels. This problem is compounded when considering the added transportation and handling costs required to distribute the additional material (Smith & Rousaki, 2002; Taulbee et al., 2010). Depending on the distance, the reduction in gasification emissions may be offset by the increase in transportation emissions (Fernando, 2005). Additionally, since many agriculturally-based biomass fuels undergo a yearly cycle of growth, supply may be restricted to only a couple months per year (Fernando, 2009).

Aside from economic and supply issues, many technical issues constrain standalone biomass use. The chemical behavior of biomass is quite different from coal. Typically, biomass has a much higher moisture, ash, and chlorine content than even low rank coals. These differences can cause agglomeration issues during gasification and may add to equipment corrosion (Demirbas, 2003). Furthermore, fuel storage can be problematic since biomass is hygroscopic (i.e. readily absorbs and retains moisture) and can become reactive. For example, when wood chips exceed twenty percent moisture, biologic activity begins to deteriorate the fuel (i.e. rotting), leading to a significant loss in heat value (Fernando, 2005). While biomass generally gasifies at a similar temperature as coal, biomass ash is generally more aggressive and

has a lower melting point than coal ash. Consequently, fouling and slagging can be significant if the ash becomes soft and sticky. Biomass particles are typically characterized by high aspect ratios and a fibrous, non-friable nature, which leads to difficulties in size reduction (Couch 2008). In addition, biomass size reduction can be quite expensive and energy intensive and often requires a separate pulverizer in addition to the standard coal pulverizer (Fernando, 2009).

To alleviate many of the technical and economic constraints of standalone biomass use, many industrial facilities have experimented with co-gasification of biomass with coal (Fernando, 2009; Smith, 2001). By combining specific mixtures of coal and biomass, a plant can achieve increased sustainability and reduced harmful emissions while avoiding the drawbacks of inconsistent supply and diminished thermodynamic efficiency. Furthermore, if the feed fuels are properly engineered, little if any retrofitting is required for existing plants. Direct co-firing, where biomass and coal are gasified together in the same reactor, is the simplest and most widely accepted practice, since the process can easily be accommodated using existing equipment (Fernando, 2005; Demirbas, 2003).

While more advantageous than standalone biomass gasification, direct co-gasification is still limited by inherent technical constraints. When independent feeds of biomass and coal are introduced into a moving bed or fluidized bed gasifier, a natural segregation occurs due to the density difference between coal and biomass. This segregation of fuel types can lead to thermal inconsistencies throughout the vessel and reduce gasification efficiency. If the biomass is excessively moist, further disturbance to the reactor heat balance can proliferate, leading to reduced biomass consumption and net accumulation in the reactor (Fernando, 2005). Additionally, the low melting point, increased alkalinity, and aggressive quality nature of the biomass ash can cause fouling and slagging problems along with extensive corrosion at relatively low temperatures (Sami et al., 2001).

## 2.3 Gasification Processes

To adequately appreciate the benefits and challenges of coal and biomass co-gasification, a basic understanding of gasification processes is required. Collot (2002) defines gasification as "the reaction of solid fuels with air, oxygen, steam, carbon dioxide or a mixture of these gases at a temperature exceeding 700 degrees Celsius to yield a gaseous product suitable for use either as a source of energy or as a raw material for the synthesis of chemicals, liquid fuels or other

gaseous fuels." In other words, gasification is a thermochemical process that converts carbonaceous materials into synthetic gas (syngas) with recoverable heating value (Mulvaney & Robbins, 2011).

The principal mechanism of syngas production is partial oxidation of carbon, which occurs when fuel particles are heated in the presence of an oxidant typically composed of oxygen, air and/or steam (Fernando, 2008). The resultant syngas is comprised primarily of hydrogen, carbon monoxide and other light hydrocarbons that can be used directly for power generation or as a feedstock to produce chemicals, liquid fuels or other gaseous fuels (Higman & van der Burgt, 2003). Gasification differs from combustion in a number of fundamental aspects; most notably is the lack of useful heating value in the gaseous product from combustion. In addition, combustion occurs in an oxidizing environment which converts the potential energy within a feedstock into thermal energy. In contrast, gasification occurs in a reducing environment which converts the energy stored within a material into chemical energy (Basu, 2010).

As shown in Figure 2-1, gasification processes can be divided into three major unit operations: upstream processing, thermochemical gasification, and downstream processing (Kumar et al., 2009). Upstream processing includes acquisition and on-site storage of the fuel source and can also include particle size reduction and drying to ensure reliable, consistent feeding and optimal syngas composition. For dry feed entrained flow gasifiers, coal is pulverized in a ring-roller mill to reduce the particle size to an acceptable level. In contrast, rod mills are generally used for size reduction upstream of coal-water slurry gasifiers (Higman & van der Burgt, 2003). Drying is usually required to ensure consistent coal moisture content for dry feed gasifiers. Similar to the systems used in conventional pulverized coal boilers, the dryer is integrated in a recycle loop with the mill and heated with a gas burner.

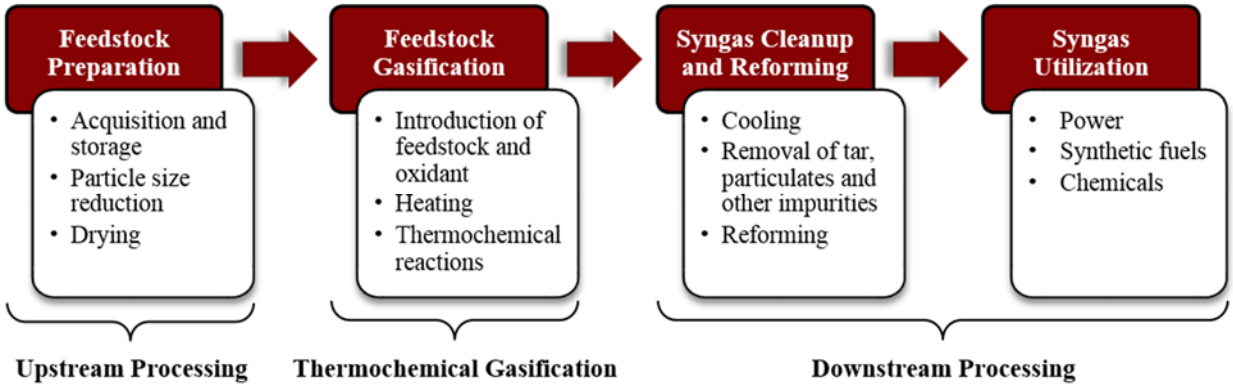



Figure 2-1. Gasification unit operations and processes (modified from Kumar et al., 2009)

Size reduction of agricultural and wood biomass is often accomplished with tub grinders, hammer mills and knife mills (Kumar et al., 2009). Due to the high moisture content inherent to many types of biomass, a drying process is often required. This process is energy intensive so waste heat must be recovered and utilized to maintain the plant efficiency at an acceptable level. Commercially available biomass dryers include perforated floor bin dryers, band conveyor dryers, rotary cascade dryers, fluidized bed steam dryers and pneumatic conveying steam dryers (Cummer & Brown, 2002).

Downstream processing operations include syngas cleanup, reforming and utilization (Kumar et al., 2009). Depending on the intended end product, these operations require a number of different complex processes and pieces of equipment. Syngas cleanup operations generally involve raw gas cooling, particulate, tar and acid gas removal and sulfur recovery (Mondal et al., 2011). Syngas reforming operations include the water gas shift reaction and separation of the constituents ($H_2$, CO, $CO_2$) for purification or separate uses in a polygeneration plant. Detailed descriptions of syngas cleanup and reforming operations are available in a number of publications (Bell et al., 2011; Mondal et al., 2011; Speight, 2008; Higman & van der Burgt, 2003; Ozum et al., 1993; Bennett, 1981).

There are many useful applications for syngas derived from the gasification of carbonaceous fuels. As displayed in Figure 2-2, a wide range of products are directly obtainable by reforming hydrogen and carbon monoxide, the two main components of syngas. These products are generally classified as power, synthetic fuels and chemicals (Higman & van der Burgt, 2003). Power from syngas is obtained by direct firing in gas turbines to generate electric power. Synthetic fuels from syngas include Fischer-Tropsch fuels, synthetic natural gas (SNG),

town gas and reduction gas. Chemicals directly obtainable from syngas include ammonia, methanol, hydrogen, carbon monoxide and oxo-alcohols. Many of these direct products are further processed and refined to produce more useful consumer products like polyurethanes and acetates (Higman & van der Burgt, 2003).

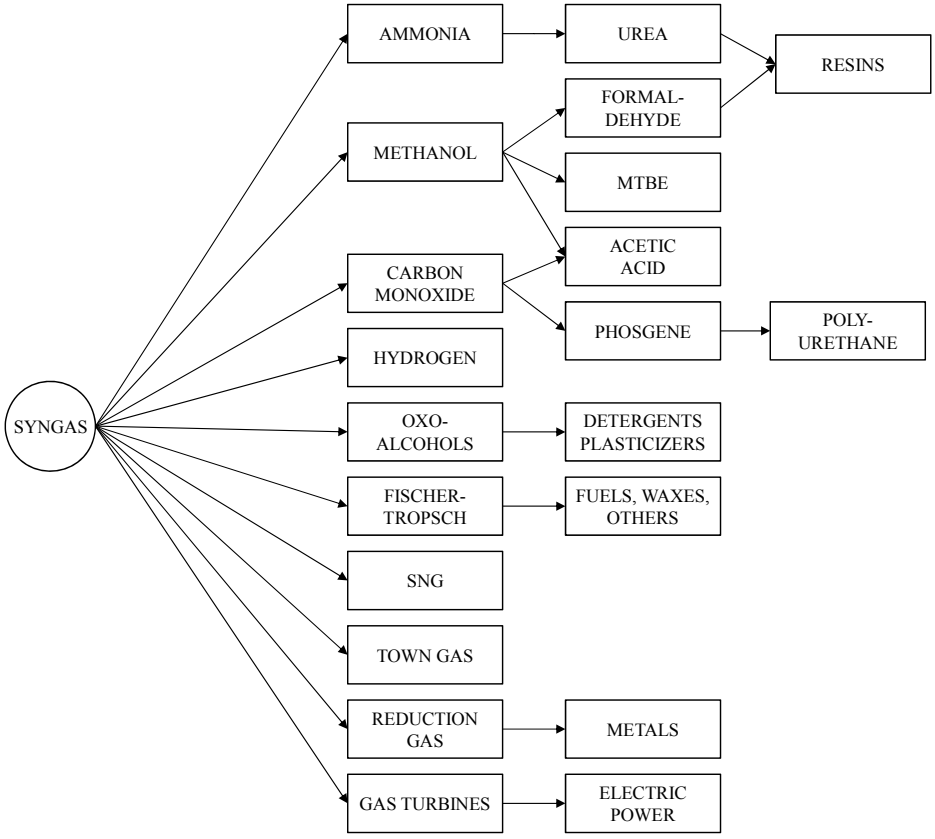



Figure 2-2. Products obtainable from syngas (modified from Higman & van der Burgt, 2003)

## 2.3.1 Types of Gasifiers

At the core of the gasification process is the gasifier, which brings the fuel and oxidant into contact at elevated temperatures. Each reactor must be uniquely designed and operated to accommodate specific feedstock conditions and the desired composition of the resultant syngas. The primary design and operating parameters of the gasifier include the reactor type and geometry, temperature profile, feed rate of the fuel and oxidant, and the type and amount of catalysts added to the system (Kumar et al., 2009).

Many different reactor types have been developed for coal gasification, which generally follow one of three generic processes: moving bed (also known as fixed bed), fluidized bed and entrained flow (Fernando, 2009). The physical configuration of each type of reactor varies,

which affects how the fuel and oxidant are brought into contact within the system. Each reactor type is also distinct with respect to feed condition sensitivity, operating conditions and the characteristics of the resultant syngas. For example, a major distinction between gasifiers is whether the ash is removed from the system in a dry form or as slag. Additionally, each process is designed for specific types of feedstocks which must be fed to the system in either slurry form, as a dry powder, as granules or in lump form. The operating temperature and pressure within the gasifier and the resultant syngas temperature can also vary for each type of process (Couch, 2008). A summary of these and other important characteristics of moving bed, fluidized bed and entrained flow reactors are summarized in Table 2-1.

Table 2-1. General characteristics of gasification reactors (modified from Ratafia-Brown et al., 2002 as cited in Fernando, 2009 and from Simbeck et al., 1993 as cited in Higman & van der Burgt, 2003)

| Category | Moving Bed | | Fluidized Bed | | Entrained Flow |
|---|---|---|---|---|---|
| Ash condition | Dry | Slagging | Dry | Agglomerating | Slagging |
| Commercial versions | Lurgi | BGL | HTW, KRB | KRW, U-Gas | GE, E-Gas, Shell, Siemens, MHI, EAGLE, PRENFLO |
| **Feed Characteristics** | | | | | |
| Size limits | 5-80 mm | 5-80 mm | < 6 mm | < 6 mm | < 0.1 mm |
| Acceptability of caking coals | Possibly | Yes | Possibly | Yes | Yes |
| Ash content limits | No limits | < 25% preferred | No limits | No limits | < 25% preferred |
| Ash melting temperature | > 1200 °C | < 1300 °C | > 1100 °C | > 1100 °C | < 1300 °C |
| Preferred feedstock | Lignite, reactive bituminous, anthracite, biomass, wastes | Bituminous, anthracite, petcoke, biomass, wastes | Lignite, reactive bituminous, wastes | Lignite, bituminous, cokes, biomass, wastes | Lignite, sub-bituminous, bituminous, anthracite, petcoke |
| **Operating Characteristics** | | | | | |
| Syngas temperature | 425-650 °C | 425-650 °C | 900-1050 °C | 900-1050 °C | 1200-1600 °C |
| Gasification pressure | 3 MPa | > 3 MPa | 0.1 MPa | 0.1-3 MPa | 2-8 MPa |
| Oxidant requirement | Low | Low | Moderate | Moderate | High |
| Steam requirement | High | Low | Moderate | Moderate | Low |
| Unit capacities | 10-350 MWh | 10-350 MWh | 100-700 MWh | 20-150 MWh | up to 700 MWh |
| Key technical issue | Use of fines and hydrocarbons | | Carbon conversion | | Raw gas cooling |
| Distinguishing characteristic | Hydrocarbons in raw gas | | Large char recycle | | High heat in raw gas |

#### 2.3.1.1 Moving Bed Gasifiers

As the first commercially available gasifiers, moving bed reactors played an important role in the early production of syngas from coal and coke (Higman & van der Burgt, 2003). In moving bed gasifiers, relatively large fuel particles are fed into the top of the vessel and the oxidant is introduced at the bottom, producing a countercurrent flow. As shown in Figure 2-3, the fuel particles move downward under gravity, forming a bed, and the ash is removed from the

bottom of the reactor. As the oxidant enters the bottom of the vessel, it absorbs heat and reacts with the fuel as it moves upward through the bed of particles. Before exiting the gasifier, the hot syngas preheats and pyrolyses the downward flowing fuel, which results in high carbon conversion and hence high thermal efficiency (Fernando, 2008; Waitzman et al., 1975).

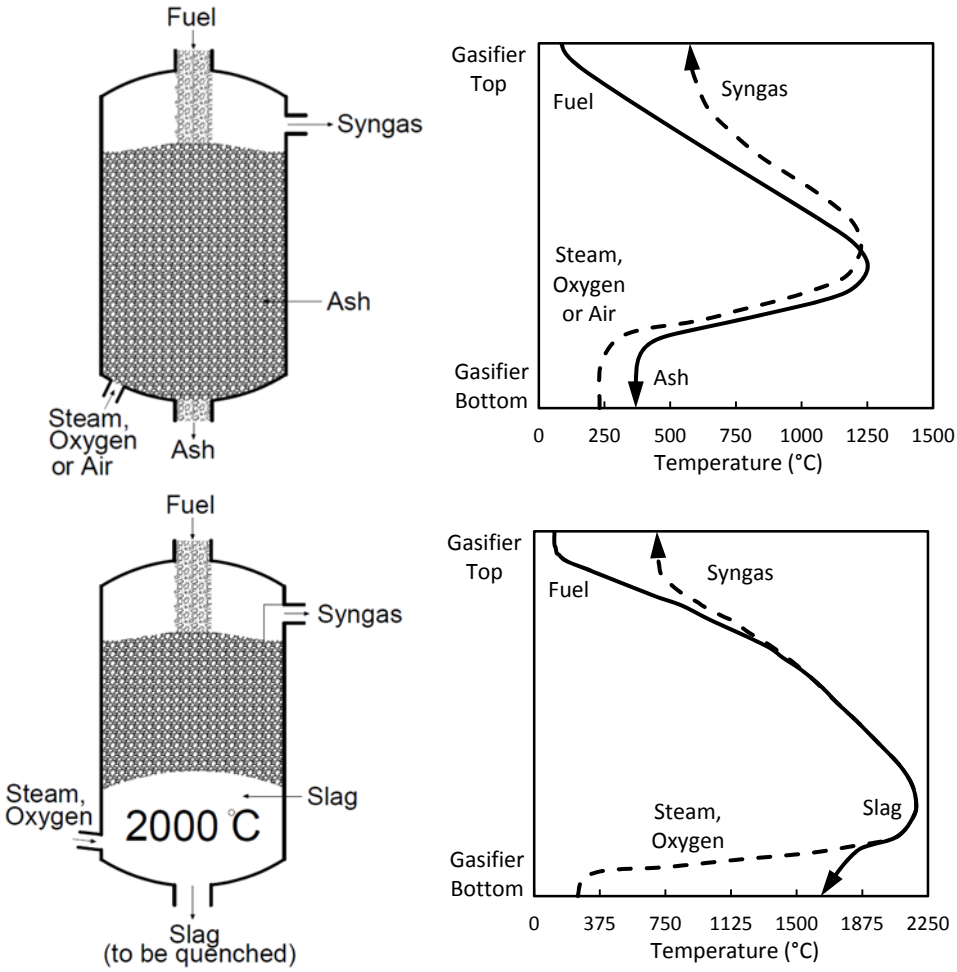



Figure 2-3. Dry ash and slagging moving bed gasifier schematics and temperature profiles (modified from Kristiansen, 1996 and Simbeck et al., 1993 as cited in Carpenter, 2008)

The gasification process can be divided into four distinct zones within the reactor: drying, pyrolysis, reduction, and oxidation (Brar et al., 2012; Mondal et al., 2011). The drying zone is located at the top of the reactor where the feed is introduced and the syngas is cooled before exiting the system. As the particles descend downward they are further heated and enter the pyrolysis zone. Next, the particles enter the reduction zone where they are gasified by reacting with steam and carbon dioxide. In the combustion zone, located toward the bottom of the reactor, the highest temperatures are reached as oxygen reacts with the residual char. Finally, ash is

formed at the bottom of the vessel either in the form of dry ash or slag and is removed from the system (Carpenter, 2008). Excess steam is introduced to keep the temperature below the ash fusion temperature in the dry ash process, while much less steam is used and higher temperatures are achieved in the slagging process (Fernando, 2009; Brar et al., 2012).

Moving bed reactors are generally used to gasify solid fuels in the range of 5-80 mm, including coals, biomass and waste materials. Fuel particles less than 5 mm tend to pack into the reactor bed, thus reducing the total surface area of the fuel and decreasing the overall efficiency of the reactor. It is also possible for fine particles to follow the countercurrent gas flow and blow back into the feed mechanism or cake onto the syngas exit opening. This problem is intensified when dealing with caking or moist feedstocks (Fernando, 2009). The residence time of the fuel within the gasifier is dictated by the operating pressure and the type of oxidant used. For example, residence time in atmospheric steam/air gasifiers is typically several hours yet high pressure steam/oxygen gasifiers only require 15 to 60 minutes.

Moving bed gasifiers are most commonly used for the production of synthetic fuels and chemicals, although there are instances where they have been used for power generation in the integrated gasification combined cycle (IGCC) plant. There are two main commercial versions of the moving bed gasifier, the Lurgi dry ash gasifier and the British Gas/Lurgi (BGL) slagging gasifier. These systems differ in a number of fundamental aspects including ash conditions, feed sensitivity, maximum throughput and syngas composition (Fernando, 2008). For example, the Lurgi dry ash gasifier is characterized by low oxygen consumption and high steam demand, which is in direct contrast to the BGL slagging gasifier. Detailed descriptions of these systems, including process flowsheets, performance data and typical applications, are discussed by Bell et al. (2011), Basu (2010), Fernando (2008) and Higman & van der Burgt (2003).

#### 2.3.1.2 Fluidized Bed Gasifiers

In fluidized bed gasifiers, fine fuel particles are gasified as a suspended bed that is created by an upward flow of fluidizing gases. As displayed in Figure 2-4, this is achieved by feeding the fuel into the side of the vessel and injecting the oxidant at the bottom with enough velocity to fully suspend the bed of particles as they move downward under gravity. This configuration creates intense back mixing, where feed particles are mixed with the particles already undergoing gasification. As a result, fluidized bed gasifiers offer a consistent temperature

profile throughout the vessel, which promotes both heat and mass transfer (Higman & van der Burgt, 2003). Depending on the degree of fluidization and bed height, fluidized bed gasifiers are classified as circulating fluidized bed, bubbling fluidized bed and transport reactors. Another distinguishing feature of fluidized bed systems is the nature of the ash, which can be dry or agglomerated (Fernando, 2008).

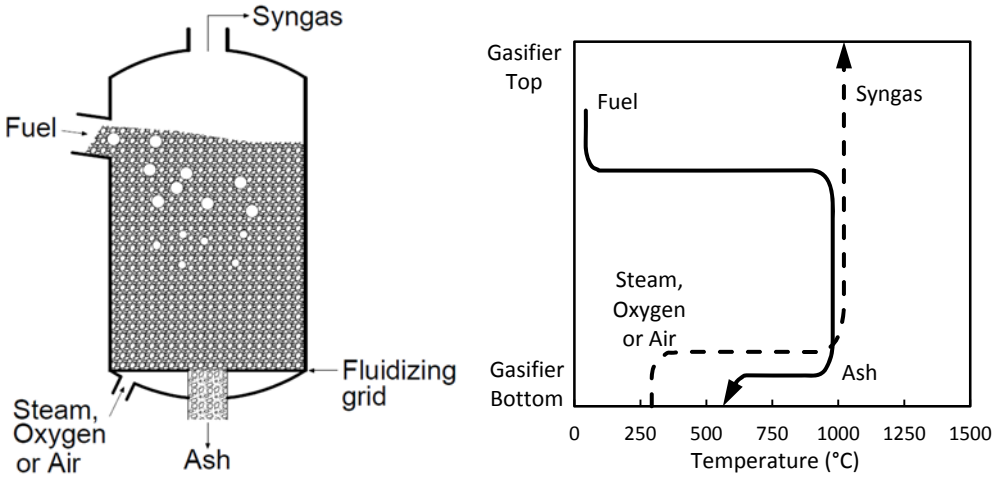



Figure 2-4. Fluidized bed gasifier schematic and temperature profile (modified from Kristiansen, 1996 and Simbeck et al., 1993 as cited in Carpenter, 2008)

Fuel residence time in fluidized bed gasifiers is typically on the order of 10-100 seconds, which enables much higher throughputs than achievable in moving bed reactors (Fernando, 2008). To reach maximum thermal efficiency, particle size of the feed must be constantly monitored and controlled. One common issue arises when superfine particles (<0.5 mm) become entrained in the rising syngas and flow out of the top of the vessel. To alleviate this problem, a cyclone is typically installed downstream to capture and return these particles to the bed. In contrast, particles that are too large (>6 mm) fail to fluidize and disrupt the bed formation (Minchener, 2005). These issues can limit the carbon conversion and thermal efficiency of the system (Fernando, 2008).

The temperature within fluidized bed reactors must be maintained below the ash fusion temperature as ash melting will cause clinker formation and destabilize the suspended bed (Gomz-Barea, 2010). This specification makes fluidized bed gasifiers best suited to handle relatively reactive fuels such as low grade coals and biomass (Fernando, 2008). Other technical challenges encompass the process of ash removal. In a fluidized bed, overly dense ash eventually moves to the bottom of the vessel where it drops through a grate. Ash that has a low fusion

temperature, high free swelling index or a high alkali concentration will agglomerate at high temperatures. These agglomerations can destabilize the bed, stick to discharge openings, and hinder process efficiency in dry ash systems (Couch, 2008).

The most widely used commercial versions of the dry ash fluidized bed process include the High Temperature Winkler (HTW) bubbling fluidized bed gasifier and the Kellogg Brown and Root (KBR) transport gasifier. More recently, there has been commercial interest in the development of agglomerated ash fluidized bed reactors that can increase carbon conversion by preferentially separating low-carbon ash from the bed. Commercial reactors that use the agglomerated ash technique include the Kellogg Rust Westinghouse (KRW) fluidized bed gasifier and the U-Gas bubbling fluidized bed gasifier. Detailed descriptions of these systems, including process flowsheets, performance data and typical applications, are presented by Bell et al. (2011), Basu (2010), Fernando (2008) and Higman & van der Burgt (2003).

#### 2.3.1.3 Entrained Flow Gasifiers

In entrained flow gasifiers, fuel particles and oxidant are introduced at the top of the vessel and flow downward together under gravity as depicted in Figure 2-5. This co-current flow regime results in the oxidant surrounding or entraining the fuel particles as they flow down through the reactor. Entrained flow gasifiers are operated at high temperatures (1250-1600 °C) and pressures (2-8 MPa) to melt the ash into inert slag (Higman & van der Burgt, 2003). The temperature must be kept relatively high to ensure that the ash behaves as a liquid throughout the vessel (Gomez-Barea, 2010). Ultrafine fuel particles (<0.1 mm) are fed to the vessel in dry form or as a slurry to promote mass transfer and entrainment within the gas. The fine feed and high operating temperature produce very high carbon conversion rates and thus residence time is low, on the order of a few seconds (Fernando, 2008).

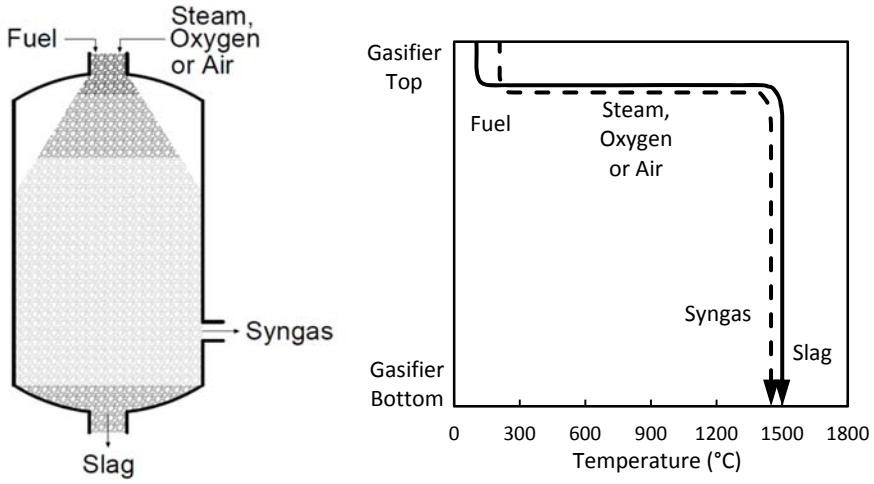



Figure 2-5. Entrained flow gasifier schematic and temperature profile (modified from Kristiansen, 1996 and Simbeck et al., 1993 as cited in Carpenter, 2008)

After the short residence time, both the syngas and the ash are removed from the bottom of the vessel. Typically, consistent ash content is desired, as the ash provides added insulation which prevents heat loss. Ash fusion temperature of the fuel must be low enough for slag formation to enable the inert material to flow down the reactor walls and exit the vessel under standard operating temperatures (Bell et al., 2011). If insufficient ash melting is experienced, fluxes such as limestone can be introduced with the feed to improve slag formation. Additionally, excessive impurities in the ash (e.g. sulfur, chlorine) may cause downstream blockage and added corrosion (Fernando, 2009). Although entrained flow gasifiers produce relatively clean syngas free of tar and phenols, there are large amounts of sensible heat in the raw gas that must be recovered downstream to maximize the thermal efficiency of the system (Basu, 2010).

Entrained flow gasifiers are often characterized as the most versatile type of reactor because they can efficiently gasify essentially all coal types (Fernando, 2008; Higman & van der Burgt, 2003). As a result of this and other advantages, entrained flow gasifiers are the most widely used industrial gasification technology throughout the world. The most popular commercial systems that employ dry feed entrained flow technology include the Shell Coal Gasification Process (SCGP), Siemens Fuel Gasification (SFG), Mitsubishi Heavy Industries (MHI), Energy Application for Gas, Liquid and Electricity (EAGLE), and Pressurized Entrained Flow (PRENFLO). In contrast, the most significant commercial slurry feed entrained flow gasifiers are the GE reactor and ConocoPhillips E-Gas reactor. Detailed descriptions of these

systems, including process flowsheets, performance data and typical applications, are presented by Bell et al. (2011), Fernando (2008) and Higman & van der Burgt (2003).

### 2.3.2 Thermochemical Reactions

The thermochemistry of coal gasification has been widely studied and is well established. Although biomass gasification has not been studied as extensively, it is generally described by the same basic thermochemical reactions as coal gasification. However, the chemistry of coal and biomass co-gasification is not well understood. Several different thermochemical reactions take place within a gasifier during the conversion of coal or biomass to syngas. This section provides a general overview of gasification thermochemistry for carbonaceous materials but does not examine the thermodynamic or kinetic characteristics of gasification, which together dictate the rate and efficiency of the process and regulate the composition of the resultant syngas. However, detailed descriptions of gasification thermodynamics and kinetics are available in a number of publications (Bell et al., 2011; Basu, 2010; Higman & van der Burgt, 2003; Desrosiers, 1981; Graboski, 1981).

The first process that takes place when a carbonaceous material enters a gasifier is vaporization of surface and inherent moisture. This reaction can be formally written as:

$$H_2O_{(l)} \rightarrow H_2O_{(g)} \;\; \Delta H = +44\ MJ/kmol \qquad \text{(R. 2-1)}$$

where ΔH is the associated heat of reaction. A positive sign (+) indicates that heat is absorbed and a negative sign (−) indicates that heat is released. The water phase transition can have a significant effect on gasification thermodynamics due to the resulting steam mixing with the gases introduced to the system. This effect is particularly apparent with high-moisture feedstocks and in slurry-fed gasifiers (Bell et al., 2011).

As the carbonaceous material increases beyond the vaporization temperature in a restricted oxygen environment, it is pyrolyzed, or decomposed into char and hydrogen-rich volatile matter such as hydrocarbon gases, tars and phenols (Fernando, 2008). This reaction can be written as:

$$Feedstock_{(s)} \rightarrow Char_{(s)} + Volatiles_{(s,g)} \;\; \Delta H = positive, variable \qquad \text{(R. 2-2)}$$

The gasification of char begins with the following combustion reactions which occur as oxygen is fed to the gasifier (Higman & van der Burgt, 2003).

$$2C_{(s)} + O_{2(g)} \rightarrow 2CO_{(g)} \;\; \Delta H = -222\ MJ/kmol \qquad \text{(R. 2-3)}$$

$$C_{(s)} + O_{2(g)} \rightarrow CO_{2(g)} \ \Delta H = -394\ MJ/kmol \quad \text{(R. 2-4)}$$

Oxygen may also react with hydrogen to produce water vapor. This reaction can be formally written as:

$$2H_{2(g)} + O_{2(g)} \rightarrow 2H_2O_{(g)} \ \Delta H = -484\ MJ/kmol \quad \text{(R. 2-5)}$$

Reactions 2-3, 2-4 and 2-5 provide the heat necessary for subsequent gasification reactions, which include the steam gasification reaction, the Boudouard reaction and the methanation reaction (Bell et al., 2011). The steam gasification reaction, also known as the water gas reaction, can be formally written as:

$$C_{(s)} + H_2O_{(g)} \rightarrow CO_{(g)} + H_{2(g)} \ \Delta H = +131\ MJ/kmol \quad \text{(R. 2-6)}$$

The reaction of carbon and steam is endothermic and is generally characterized by high temperatures and low pressures (Fernando, 2008). The Boudouard reaction involves gasification with carbon dioxide and can be formally written as:

$$C_{(s)} + CO_{2(g)} \rightarrow 2CO_{(g)} \ \Delta H = +173\ MJ/kmol \quad \text{(R. 2-7)}$$

The Boudouard reaction is also endothermic although it typically takes place slower than the steam gasification reaction. The methanation reaction involves gasification with hydrogen and can formally be written as:

$$C_{(s)} + 2H_{2(g)} \rightarrow CH_{4(g)} \ \Delta H = -75\ MJ/kmol \quad \text{(R. 2-8)}$$

This reaction is very slow except at high pressures (Fernando, 2008). Reactions 2-6, 2-7 and 2-8 can be reduced to two homogeneous gas reactions which occur spontaneously as a result of high reaction temperature. The first reaction is the water gas shift reaction, which affects the $H_2$/CO ratio and can be formally written as:

$$CO_{(g)} + H_2O_{(g)} \rightarrow CO_{2(g)} + H_{2(g)} \ \Delta H = -41\ MJ/kmol \quad \text{(R. 2-9)}$$

The second reaction is the steam methane reforming reaction which can be formally written as:

$$CH_{4(g)} + H_2O_{(g)} \rightarrow CO_{(g)} + 3H_{2(g)} \ \Delta H = +206\ MJ/kmol \quad \text{(R. 2-10)}$$

Reactions 2-3 through 2-8 describe the possible pathways to gasification for all carbonaceous materials. However, most gasification processes depend on a balance between Reactions 2-3 (partial oxidation) and 2-6 (water gas reaction). The overall gasification reaction for fossil fuels, which also contain hydrogen, can be formally written as:

$$C_xH_{y_{(s)}} + x/2\ O_{2(g)} = xCO_{(g)} + y/2\ H_{2(g)} \quad \text{(R. 2-11)}$$

In this reaction, *x* and *y* are a function of the type of feedstock and specific material properties (Higman & van der Burgt, 2003). For coal, the ratio *x*/*y* is approximately equal to 1; therefore *x* and *y* are equal to one.

The gasification of biomass is similar to that of coal; however, coal is primarily composed of carbon, while biomass contains a mixture of more complex compounds including cellulose, hemicellulose and lignin (Brar et al., 2012). These large polymeric molecules are broken down into gases ($H_2$, CO, $CH_4$ and lighter hydrocarbons), char, ash, tar and minor contaminants in the presence of heat and oxidant during gasification (Kumar et al., 2009). Char and tar production are undesirable in the process and occur as a result of incomplete conversion of the biomass material. Kumar et al. present the overall gasification reaction for biomass as:

$$CH_xO_{y_{(s)}} + O_{2(g)} + H_2O_{(g)} = CO_{(g)} + H_{2(g)} + C_{(s)} + tar_{(s)} \quad \text{(R. 2-12)}$$

where *x* and *y* are a function of the type of biomass and specific material properties.

### 2.3.3 Kinetic Modeling

One of the main objectives of this research is to establish the synergistic effects of coal-biomass blends in making co-gasification a useful and economical process. Kinetic modeling of the devolatilization behavior of coal and biomass is an important step to assess the contribution of single materials and their interactions during the devolatilization stage. The understanding of kinetics of pyrolysis of blends of biomass and coals is far from clear and it is important in design and operation of co-gasification processes.

Thermogravimetric analysis (TGA) can be used to investigate thermal events and kinetics of pyrolysis and oxidation of the solid raw materials. Thermogravimetric analysis provides a measurement of weight loss of the sample as a function of time and temperature. The kinetics of the thermal events can then be determined by the application of the Arrhenius equation corresponding to the separate slopes of constant mass degradation in each thermal event with different reaction order, activation energy and frequency factor. Thermogravimetric analysis experiments can be carried out either isothermally, where the sample is heated at a constant temperature, or non-isothermally, where the sample is heated at a constant rate. Isothermal experiments are cumbersome due to the fact that the sample might take a long time to reach even 50% conversion at relatively low temperatures of 500 ºC or less apart from the fact that multiple experiments are required for predicting the kinetic parameters. On the contrary, the kinetic

parameters can be predicted using only a single experimental run in the non-isothermal mode apart from achieving close to complete conversion in a much shorter period of time.

Coal devolatilization is a process involving complex decomposition and the exact description of the kinetics involved is not yet available. Several authors have approximated the overall process as a first-order decomposition occurring uniformly throughout the particle [26-29]. Therefore, the pyrolysis reaction equation can be conveniently represented as:

$$dX/dt = k(1 - X) \quad \text{(Eq. 2-1)}$$

$$X = ((W_O - W_t)/(W_O - W_f)) \quad \text{(Eq. 2-2)}$$

and

$$k = Aexp(-E/RT) \quad \text{(Eq. 2-3)}$$

where $X$ is the pyrolysis conversion, $k$ is the reaction rate constant, $W_0$ is the original mass of the test sample, $W_t$ is the mass of the test sample at time $t$, $W_f$ is the final mass at the end of pyrolysis, $E$ is the activation energy, $T$ is the temperature, $A$ is the pre-exponential factor and $R$ is the universal gas constant.

Solution of Equation 2-3, via integration subject to the condition that conversion is zero at initial time, yields the following result:

$$-ln(1 - X) = kt \quad \text{(Eq. 2-4)}$$

Hence, the rate constant ($k$) can be determined from the slope of a plot of $-ln(1-X)$ versus time. Subsequently, the values of activation energy and pre-exponential factor can be estimated from the slope and intercept, respectively, of an Arrhenius plot of $ln(k)$ versus $1/T$ represented by Equation 2-3. Equations 2-1 through 2-4 represent the pyrolysis reaction as a global one step kinetic chemical reaction model under isothermal conditions.

For pyrolysis or oxidation reactions under non-isothermal conditions, the heating rate ($H$) plays a very important role in determining the kinetic parameters (Cai et al., 2008; Sima-Ella et al., 2005; Coats & Redfern, 1964). For a first-order reaction at constant heating rate, $H = dT/dt$, a combination of Equations 2-1 and 2-3 yields the following result:

$$dX/dT = [A(1 - X)/H]\, exp(-E/RT) \quad \text{(Eq. 2-5)}$$

As in the case of isothermal analysis, solution of Equation 2-5, via integration subject to the condition that conversion is zero at initial temperature, $T_0$, yields the following result:

$$ln(1 - X) = -(A/H) \int_{T_0}^{T} exp(-E/RT)\, dT \quad \text{(Eq. 2-6)}$$

Since, there is no conversion at initial temperature, $T_0$, the limits of the integral in Equation 2-6 can be conventionally changed to $\int_0^T \exp(-E/RT)$, thereby introducing a new function as represented in Equation 2-7:

$$f(y) = \int_y^\infty (e^{-y}/y^2)\ dy \qquad \text{(Eq. 2-7)}$$

where $y = (-E/RT)$. Therefore, Equation 2-6 reduces to:

$$ln(1-X) = -(A/H)\, f(y) \qquad \text{(Eq. 2-8)}$$

Since Equation 2-7 cannot be solved analytically, the function *f(y)* can be approximated using two theories: Doyle's approximation and Coats-Redfern approximation. The use of these approximations would help in transforming Equation 2-7 into simple linear forms and thus obtaining the activation energy (*E*) and pre-exponential factor (*A*) as shown in Equations 2-9 through 2-13.

In Doyle's approximation, *f(y)* is obtained by assuming a linear relationship between *ln(f(y))* and *y* as shown in Equation 2-8, while in Coats-Redfern approximation an asymptotic expansion of *f(y)* is assumed wherein only the first term is utilized. Doyle's approximation is represented as:

$$f(y) \cong exp(-5.33 - y) \qquad \text{(Eq. 2-9)}$$

and $$ln[ln(1-X)] = ln(-AE/HR) - 5.33 - 1.052(E/RT) \qquad \text{(Eq. 2-10)}$$

Coats-Redfern approximation is represented as:

$$f(y) = e^{-y}/y^2\ [1 - (2!/y) + (3!/y^2) - (4!/y^3) + \ldots] \qquad \text{(Eq. 2-11)}$$

or $$f(y) \approx e^{-y}/y^2 \qquad \text{(Eq. 2-12)}$$

and $$ln[-ln(1-X)/T^2] = ln(AR/HE) - E/RT \qquad \text{(Eq. 2-13)}$$

The theory presented using Equations 2-1 through 2-13 models the pyrolysis and oxidation reactions assuming them to be first-order decomposition reactions. But, in reality, these reactions need to be modeled for an unknown reaction order. For an $n^{th}$ order reaction, a similar theory as to the one presented above can be utilized to determine the kinetic parameters (Yaman & Haykiri-Acma, 2007; Hatakeyama & Quinn, 1999), wherein Equation 2-13 can be modified as:

$$ln[(1 - (1-X)^{1-n})/(1-n)T^2] = ln(AR/HE) + E/RT \qquad \text{(Eq. 2-14)}$$

Kinetic parameters obtained using the single first order reaction models are actually a starting point in the devolatilization modeling. More accurate and specific models are required to meet

the experimental results of each material, one model being the distributed activation energy model (Biagini et al., 2002; Anthony & Howard, 1976).

The distributed activation energy model treats the thermal decomposition process as a large number of independent, parallel rate processes. The thermal decomposition of a single organic species can be described as an irreversible first-order reaction with respect to the amount of unreacted material remaining. Thus, the rate at which the volatiles are produced by a particular reaction can be defined according to the mass balance on the reactant species.

$$dV_i/dt = k_i(V_i^\infty - V_i) \quad \text{(Eq. 2-15)}$$

$$V_i^\infty - V_i = V_i^\infty \, exp\left(-At \, exp(-E/RT)\right)_i \quad \text{(Eq. 2-16)}$$

where $V_i^\infty$ is the final quantity of volatile matter for the generic species ($i$), and $k_i$ is the rate constant of the reaction expressed according to the Arrhenius law.

This type of kinetic model requires that the amount of volatiles and kinetic parameters known for all the single reactions. To estimate these parameters from experimental data for all the reactions is practically not possible. The problem can be simplified if it is assumed that the rate constants for all the reactions differ only in the activation energy. The number of reactions is large enough so that the activation energy can be expressed as a continuous Gaussian distribution function *f(E)* and *f(E) dE*, representing the potential loss of volatile fraction with activation energy between the intervals $E$ and $E + dE$. Thus,

$$V_i^\infty = dV^\infty = V^\infty f(E)dE \quad \text{(Eq. 2-17)}$$

The total amount of volatile material unreleased is obtained by summing the contribution from each reaction, that is, by integrating Equation 2-16 over all values of E using Equation 2-17. Finally, the yield of volatiles can be calculated using Equation 2-18:

$$(V^\infty - V)/V^\infty = \left[\int_0^\infty \exp\left(-\left(\int_0^t k \, dt\right) f(E)dE\right)\right] \quad \text{(Eq. 2-18)}$$

and

$$f(E) = (\sigma(2\pi)^{0.5})^{-1} \exp[-(E - E_0)^2/2\sigma^2] \quad \text{(Eq. 2-19)}$$

where $V^\infty$ is the global volatile quantity of the material, $E_0$ is the mean activation energy and σ is the standard deviation of the activation energy. This approach avoids the low values of the activation energies which result when a single first-order reaction model is applied to fit a temperature dependence that arises from the occurrence of different reactions in different temperature intervals (Di Blasi, 2008). The theories presented in this section form a basis for analyzing the experimental data discussed in subsequent chapters.

## 2.4 Coal and Biomass Properties Relevant to Gasification

There are many different coal and biomass properties relevant to gasification processes. These properties can be divided into four categories: chemical composition, thermal properties, physical properties, and mechanical properties (Berkowitz, 1994; Speight, 2005). The chemical composition, thermal characteristics and physical properties are generally of greatest relevance to the thermochemical gasification process and downstream operations. In contrast, the mechanical properties discussed are of greater significance to upstream processing operations. Standard test methods have been developed to directly measure many of these coal and biomass properties; however, further research is needed to determine the suitability of applying other methods that are not specifically intended for coal and biomass (Basu, 2010; Higman & van der Burgt, 2003). Table 2-2 lists some of the published standard test methods that can be used to determine coal and biomass properties relevant to gasification.

Table 2-2. Standard test methods for determining coal and biomass properties relevant to gasification

| Category | Coal | Biomass | | |
|---|---|---|---|---|
| | ASTM | ASTM | CEN | ASABE |
| **Proximate Analysis** | D3172-07a | E870-82[4] | -- | -- |
| Moisture | D3173-11, D3302/D3302M-12 | E871-82[5] | EN 14774[7] | ASAE S358.3[8] |
| Volatile Matter | D3175-11 | E872-82[5] | EN 15148[7] | -- |
| Ash | D3174-12 | E1755-01, E1534-93[5] | EN 14775[7] | -- |
| Fixed Carbon | D3172-07a | -- | -- | -- |
| **Ultimate Analysis** | D3176-09 | E870-82[4] | -- | -- |
| Carbon | D5373-08 | E777-08[6] | EN 15104[7] | -- |
| Hydrogen | D5373-08 | E777-08[6] | EN 15104[7] | -- |
| Sulfur | D3177-02 | E775-87[6] | EN 15289[7] | -- |
| Nitrogen | D5373-08 | E778-08[6] | EN 15104[7] | -- |
| Oxygen | D3176-09 | -- | -- | -- |
| **Physical Properties** | | | | |
| Particle Size | D4749-87 | -- | EN 15149-2[7] | ASAE S424.1[8] |
| True Density | D167-93[1] | -- | -- | -- |
| Apparent Density | D167-93[1] | -- | EN 15150[7] | -- |
| Bulk Density | D291-07, D7481-09[2] | E870-82[4] | EN 15103[7] | -- |
| Porosity | D167-93[1] | -- | -- | -- |
| **Thermal Properties** | | | | |
| Calorific Value | D5865-12 | E870-82[4] | EN 14918[7] | -- |
| Specific Heat | D2766-95[3] | D2766-95[3] | -- | -- |
| Thermal Conductivity | C518-10[10] | C518-10[10] | -- | -- |
| Thermal Diffusivity | E1461-11[11] | E1461-11[11] | -- | -- |
| Thermoplasticity | D2639-08, D720-91, D5515-97 | -- | -- | -- |
| Ash Fusibility | D1857/D1857M-04 | -- | CEN/TS 15370-1[7] | -- |
| **Mechanical Properties** | | | | |
| Grindability | D409/409M-12 | -- | -- | -- |
| Flow Behavior | D6128-06[2], D6773-08[2], D6683[2] | D6128-06[2], D6773-08[2], D6683[2] | -- | ASAE D274.1[9] |

[1]lump coke [2]powder [3]liquid and solid [4]wood fuel [5]particulate wood fuel [6]refuse-derived fuel [7]solid biofuels [8]forage material [9]grain and seed [10]flat slab [11]isotropic solid material

Precise knowledge of feedstock properties is essential to the proper design and efficient operation of gasification systems, as evidenced by numerous journal publications on this topic (Tremel et al., 2012; Voitkevich et al., 2012; Montagnaro et al., 2011; Song et al., 2011; Song et al., 2010b; Collot, 2006; Geyer et al., 2000; Mills & Rhine, 1989a; Mills & Rhine, 1989b; van Heek & Muhlen, 1987; van Heek & Muhlen, 1985). The following sections describe the most important gasification-related properties of coal and biomass and highlight some published results on the gasification of different coal and biomass types.

## 2.4.1 Chemical Composition

### 2.4.1.1 Proximate Analysis

Proximate analysis of coal or biomass is an assay of the moisture, volatile matter, ash and fixed carbon content of the material determined by a series of standard tests (Basu, 2010; Speight, 2005). This series of tests provides an initial indication of fuel quality for the design of gasification systems and is relatively simple and inexpensive to perform. Methods for performing the proximate analysis of coal have been established by each of the major standards institutions (e.g. ASTM, ISO, CEN) with slight procedural differences, so it is important to specify the method used when reporting results (Petrakis & Grandy, 1980). Proximate analysis of coals is specified by ASTM D3172-07a (2007); however, there is not an ASTM standard for proximate analysis that encompasses all types of biomass, although ASTM E870-82 (2006) describes the procedure for particulate wood fuels.

Coal and biomass moisture content is an important gasification property because the evaporation of moisture consumes a significant amount of the deliverable energy from a gasification plant. Therefore, moisture content must be known to properly design the system for minimal energy loss (Basu, 2010). Moisture content also affects bulk handling and conveying operations upstream of the gasifier. For example, Liang et al. (2011) found that the mass flow rate of a pneumatic conveyor feeding a pressurized entrained flow gasifier decreased with an increase in lignite moisture content (3.24 to 8.18%). However, the mass flow rate was found to increase at first, then decrease with a rise in subbituminous coal moisture content (0.40 to 6.18%) under the same operating conditions (Liang et al., 2011).

Determination of coal and biomass moisture content is complicated by its presence in two separate forms: surface (free) moisture and inherent (equilibrium) moisture (Allardice & Evans,

1978). As the name implies, surface moisture is the moisture present on the surface of the coal or biomass particle, which is ordinarily deposited during processing, transportation and storage. In contrast, inherent moisture is the moisture absorbed within the coal matrix or biomass cell walls (Speight, 2005). Total moisture is defined as the sum of the surface and inherent moisture and can be expressed on a wet basis or a dry basis. The wet basis moisture content of coal and biomass is calculated as:

$$M_{wet} = 100\left(\left(m_{wet} - m_{dry}\right)/m_{wet}\right) \quad \text{(Eq. 2-20)}$$

where $M_{wet}$ is the wet basis moisture content expressed as a percentage, $m_{wet}$ is the wet weight and $m_{dry}$ is the dry weight (Basu, 2010). The dry basis moisture content is calculated as:

$$M_{dry} = 100\left(\left(m_{wet} - m_{dry}\right)/m_{dry}\right) \quad \text{(Eq. 2-21)}$$

where $M_{dry}$ is the dry basis moisture content expressed as a percentage. Finally, the wet basis and dry basis moisture contents are related as:

$$M_{dry} = M_{wet}/(100 - M_{wet}) \quad \text{(Eq. 2-22)}$$

ASTM D3173-11 (2011) and ASTM D3302/D3302M-12 (2012) specify standard procedures for determining and reporting coal moisture content. Similarly, ASTM E871-82 (2006) specifies a method for determining and reporting the moisture content of wood fuels, while ASAE S358.3 (2008) specifies a method for forage materials and EN 14774 (2009) specifies a method for solid biofuels. Typically, these methods involve drying materials in an oven at a temperature of 105 degrees Celsius until constant mass is achieved and moisture content is calculated from the loss in mass of the sample.

Volatile matter content is a measure of the condensable and noncondensable vapor (excluding water vapor) produced while heating coal or biomass under specified conditions (Speight, 2005). The determination of this value depends on a number of factors including the maximum temperature reached (typically 950 °C), the heating rate, the type of heating equipment, and the size, shape and composition of the crucible in which the material is heated (Basu, 2010). The applicable ASTM standards for determination of volatile matter are D3175-11 (2011) for coal and E872-82 (2006) for particulate wood fuels. Volatile matter content is important to consider when designing a gasification system because it will be released within in the gasifier and transported downstream with the syngas.

Ash content is a measure of the inorganic solid residue remaining after the combustion of coal or biomass under designated conditions. The applicable ASTM standards for determination

of ash content are D3174-12 (2012) for coal, E1755-01 (2007) for biomass, and E1534-93 (2006) for particulate wood fuels. It is also important to determine the major and minor elements that comprise the ash, which can be determined for coal by ASTM D3682-01 (2006). The elemental composition of ash is complex and varies with the mineral composition of a material and the incineration conditions employed. Some typical ash constituents include silica, aluminum, iron, calcium, magnesium, titanium, sodium and potassium (Basu, 2010; Higman & van der Burgt, 2003). Ash composition has a major impact on the occurrence of fouling and slagging within a gasifier. For example, ash with high alkali-oxide content often creates fouling and slagging problems due to the reduction of ash melting temperature (Speight, 2005). Ash composition also affects gasification reactivity and the rate of carbon conversion. Specifically, calcium, magnesium, sodium and potassium have been found to catalytically enhance carbon conversion during gasification of various rank coals (Hattingh et al., 2011; Nattermann & Hutinger, 1994). Finally, ash composition influences the ash fusion temperature, which is an important thermal property discussed in *Section 2.4.3* (Song et al., 2010a).

Fixed carbon content is a measure of the material remaining after the determination of moisture, volatile matter and ash present in coal or biomass as outlined above (Speight, 2005). It is calculated by subtracting the mass percentage of each component from 100 and can be formally written as:

$$FC = 100 - (M + VM + ASH) \quad \text{(Eq. 2-23)}$$

where $FC$ is the mass percentage of fixed carbon, $M$ is the mass percentage of moisture, $VM$ is the mass percentage of volatile matter and $ASH$ is the mass percentage of ash in a given material (Basu, 2010). Fixed carbon content is an important parameter for gasification analysis because the conversion of fixed carbon to syngas is the last reaction to occur within the gasifier. As a result, it dictates the gasification rate and syngas yield and is used to determine the required size of the gasifier. The procedure to determine fixed carbon content of coal is specified by ASTM D3172-07a (2007), while fixed carbon content of biomass is simply determined by Equation 2-23.

#### 2.4.1.2 Ultimate Analysis

Ultimate analysis of coal or biomass is an assay of the elemental composition, ash content and moisture content of the material as determined by a series of standard tests (Higman & van der Burgt, 2003). Elemental composition is the weight percentage of carbon, hydrogen,

sulfur, nitrogen, and oxygen in the fuel. Moisture and ash contents are determined using the same methods specified for the proximate analysis to convert the elemental composition to a dry ash-free basis. In addition to the components covered by ultimate analysis, the determination of chlorine content is important for biomass materials because it can be present at rather high levels and can cause fouling and corrosion within the gasifier (Graboski & Bain, 1981). Standard methods to determine chlorine content of biomass is covered by EN 15289 (2011). Chlorine content in coal is typically less than one percent by weight, although some coals can contains as much as 2.5 percent. Coal chlorine content is determined by ASTM D4208-02 (2007).

Methods for performing the ultimate analysis of coal have been established by each of the major standards institutions (e.g. ASTM, ISO, CEN) with slight procedural differences, so it is important to specify the method used when reporting results (Petrakis & Grandy, 1980). Ultimate analysis of coals is specified by ASTM D3176-09 (2009); however, there is not an ASTM standard for ultimate analysis that encompasses all types of biomass, although ASTM E870-82 (2006) describes the procedure for particulate wood fuels. These tests provide more detailed and useful information than proximate analysis for the design of gasification systems (Speight, 2005). For example, elemental composition can be used to predict syngas composition and estimate the true density of coal and biomass. However, ultimate analysis is more difficult and expensive to perform than proximate analysis (Basu, 2010).

Carbon is the largest component of coal, accounting for 70 to 95 percent by weight on a dry ash-free basis, while hydrogen typically accounts for 2 to 6 percent (Speight, 2005). Most of the carbon and hydrogen in coal is contained in complex organic compounds, although some carbon is trapped in mineral carbonates and hydrogen is also present in surface and inherent moisture. The determination of carbon and hydrogen in coal is specified by ASTM D5373-08 (2008). Biomass materials typically have a lower carbon content and similar hydrogen content compared to coal on a dry ash-free basis (Graboski & Bain, 1981). Carbon and hydrogen content determination is specified by EN 15104 (2011) for biomass and by ASTM E777-08 (2008) for refuse-derived fuels.

Sulfur content is an important consideration in coal and biomass gasification because of the production of sulfur oxides during the combustion phase. The release of these compounds to the environment is problematic because of their contribution to acid rain, and therefore sulfur oxide emissions are strictly regulated (Speight, 2008). Additionally, sulfur oxides can cause

equipment corrosion and unwanted slagging within the gasifier that can lead to downtime and production losses (Speight, 2005). As a result, there are a number of publications detailing efforts to improve the precision and accuracy of sulfur determination (Gorbaty et al., 1992; Ahmed & Whalley, 1978).

The sulfur content of coal is typically 0.5 to 6.0 percent by weight, depending on rank and formation (Higman & van der Burgt, 2003). Sulfur can be present in three different forms within coal: pyritic sulfur, organically bound sulfur, and inorganic sulfates (Speight, 2005). In coals with high sulfur content, the majority of the sulfur is present in the form of pyrite. The determination of sulfur in coal is specified by ASTM D3177-02 (2007). The sulfur content of biomass is generally much lower than coal, with typical values less than one percent by weight (Basu, 2010). As a result, biomass energy conversion does not significantly contribute to the emission of sulfur oxides, which is one of the major motivations for biomass co-firing. Sulfur content determination is specified by EN 15289 (2011) for biomass and by ASTM E775-87 (2008) for refuse-derived fuels.

Nitrogen content is another important consideration in coal and biomass gasification because it directly influences ammonia production and due to environmental concerns over nitrogen oxides emissions that result from syngas combustion. Coal generally contains 0.5 to 2.5 percent nitrogen by weight, of which a portion is converted to ammonia ($NH_3$) and the remainder is converted to elemental nitrogen ($N_2$) (Higman & van der Burgt, 2003). The determination of nitrogen in coal is specified by ASTM D5373-08 (2008). The nitrogen content of most biomass fuels varies from 0.2 to 1.0 percent by weight (Jenkins et al., 1998). Zhou et al. (2000) reported that more than ninety percent of the fuel-bound nitrogen in agricultural and woody biomass is converted to ammonia and elemental nitrogen. Nitrogen content determination is specified by EN 15104 (2011) for biomass and by ASTM E778-08 (2008) for refuse-derived fuels.

No reasonable test methods exist to measure the oxygen content of a fuel. As a result, it is calculated by subtracting the mass percentage of each of the other calculated components from 100 and can be formally written as:

$$O = 100 - (C + H + N + S + M + ASH) \quad \text{(Eq. 2-24)}$$

where $O$ is the mass percentage of oxygen, $C$ is the mass percentage of carbon, $H$ is the mass percentage of hydrogen, $N$ is the mass percentage of nitrogen, $M$ is the mass percentage of moisture and $ASH$ is the mass percentage of ash in a given material (Basu, 2010). The procedure

to determine oxygen content of coal is specified by ASTM D3176-09 (2009), while oxygen content of biomass is simply determined using Equation 2-24.

## 2.4.2 Physical Properties

### 2.4.2.1 Particle Size

Certain physical properties of coal and biomass influence the design and performance of the gasification process. Often, the first physical property that must be considered is the size of individual particles in the gasifier feed. Standard methods for measuring particle size by sieve analysis are available for both coal (ASTM D4749-87, 2002) and biomass (EN 15149-2, 2010; ANSI/ASAE S424.1, 1992). Particle size is important because it directly relates to the surface area of the fuel particles and therefore has a large impact on the rate at which chemical reactions take place within the gasifier (Collot, 2002).

The selection of the proper type of gasifier is largely influenced by particle size because each type of gasifier is uniquely suited for a particular particle size range. For example, commercial moving bed reactors are generally used to gasify fuel particles in the range of 5-80 mm, fluidized bed reactors are generally used to gasify particles less than 6 mm and entrained flow reactors are generally used to gasify particles less than 0.1 mm (Fernando, 2008; Collot, 2006; Higman & van der Burgt, 2003, Simbeck et al., 1993). Once the proper gasifier has been identified for a particular feed particle size, further research is often conducted to determine the effects of particle size on the performance of a particular system. Most of the research to date on coal and biomass co-gasification has been focused on optimizing gasifier operating conditions and determining the influence of different ratios of coal and biomass. However, there has been considerable research on the effect of particle size for independent coal gasification and biomass gasification.

Kim et al. (2011) studied the effects of coal type and particle size on the performance of char-$CO_2$ gasification in a laboratory-scale moving bed reactor. The tests were conducted over a range of operating temperatures (1050-1400 °C) with four mean coal particle sizes (0.045, 0.09, 0.18, and 0.274 mm). The results showed that the effect of particle size on the reactivity of the char was larger at the highest operating temperatures and that char reactivity decreased as the particle size increased. Additionally, the authors found that the shrinking core model (SCM) was

more accurate for modeling the kinetic behavior of larger particles while the volume reaction model (VRM) was better suited for smaller particle sizes (Kim et al., 2011).

Hanson et al. (2002) investigated the relation between initial coal particle size and char particle size evolution during pyrolysis and steam gasification in an air-blown system. The study focused on coal particle sizes in the range of 0.5-2.8 mm and determined that the larger size fractions of coal were more likely to fragment during gasification while the smaller size fractions had a greater tendency to produce char particles larger than the initial coal particles. Testing the reactivity of the produced char indicated that particle size does not play a large role in the pyrolysis and gasification performance within the range of particles sizes investigated (Hanson et al., 2002).

Gaston et al. (2011) investigated the effects of white oak sawdust particle size on the yield of light gas and tar compounds in a laboratory-scale fluidized bed gasifier. The sawdust was milled into four size classes with mean diameters of 6, 13, 18 and 25 mm for the study. The authors found that light gas yield increased and char content decreased as the mean particle size of the sawdust increased. Additionally, mass spectrometry measurements indicated that tar and polycyclic aromatic hydrocarbon formation increased with particle size. The results of this study highlight the potential restrictions on heat and mass transport for the gasification of sawdust with larger particle sizes (Gaston et al., 2011).

Luo et al. (2009) examined the effects of particle size and bed temperature on the gasification performance of a laboratory-scale moving bed reactor using ultrafine pine sawdust. The sawdust was separated into five size classes (<0.075, 0.075-0.15, 0.15-0.3, 0.3-0.6, and 0.6-1.2 mm), individually gasified and the composition of the produced syngas was determined. The study found that the dry gas formation, hydrogen yield and carbon conversion efficiency increased with a corresponding decrease in particle size, while tar and char content decreased. However, at the highest temperatures the change in gasification performance due to varying particle size was not significant. The hydrogen and carbon monoxide content of the syngas reached maximum values of 51.2% and 22.4% respectively at 900 degrees Celsius with the smallest size fraction and the values decreased with each incremental increase in particle size (Luo et al., 2009).

Yin et al. (2003) studied the effect of particle size on the gasification performance of a pilot-scale moving bed reactor using peach tree prunings as the feedstock. The prunings were

separated into five size classes (<10, 10-20, 20-40, 40-60 and 60-80 mm) and the resulting gas and hydrocarbon compositions were analyzed by gas chromatography and gas chromatography-mass spectrometry. The results indicated that gas yield and lower heating value increase with a corresponding increase in particle size while tar and dust content decrease. The hydrogen and carbon dioxide content of the syngas reached maximum values of 16.1% and 14.4% respectively with the smallest size fraction and the values decreased with each incremental increase in particle size (Yin et al., 2003).

#### 2.4.2.2 Density and Specific Gravity

Coal and biomass densities are important to consider when examining energy content on a volumetric basis. This property is particularly important when sizing a gasifier and feed conveyor to meet desired production. Density must also be considered for operations upstream of the gasifier such as fuel transportation, bulk handling and storage (Graboski & Bain, 1981). Coal and biomass density can be reported in three principal ways: true density, apparent density and bulk density. These density values differ due to the method in which the volume of the material is calculated and reported. In addition, density can be reported relative to the density of water as specific gravity (*SG*), which is calculated as:

$$SG = \rho/\rho_{water} \quad \text{(Eq. 2-25)}$$

where $\rho$ is the density of the material and $\rho_{water}$ is the density of water.

The true density of coal and biomass is a measure of the mass per unit volume occupied by the solid constituent of an individual particle (Basu, 2010). To calculate true density, the total mass is divided by the actual volume of the solid content. This can be formally written as:

$$\rho_{true} = n_{total}/v_{true} \quad \text{(Eq. 2-26)}$$

where $m_{total}$ is the total mass and $v_{true}$ is the true solid volume. For porous solids such as coal and biomass, the precise determination of true density is often challenging because it is difficult to measure the true solid volume without including pore volume. To determine true solid volume of a material, the entire pore structure must be filled with a fluid that has no interaction with the solid component. For coal, true density is commonly determined by helium displacement because helium can penetrate the pores within the coal structure without any chemical interaction (Speight, 2005). This density measurement, often referred to as helium density, is performed by placing a weighed sample of coal into a gas pycnometer of known volume, introducing a known quantity of helium and measuring the pressure of the helium at a given temperature, which gives

the volume of the solid component of the coal. However, there is evidence that a portion of the coal pore structure may be inaccessible to the helium (Berkowitz, 1994). Another possible way to calculate the true density of coal is to use the standard test method for true specific gravity of lump coke (ASTM D167-93, 2004). This method specifies the use of a Hogarth's specific gravity bottle to calculate the true density of coke particles less than 0.075 mm.

True density can also be estimated for a given material by determining the ultimate analysis and multiplying the weight percent of each constitutive element by the element's true density (Basu, 2010). The true density of coal can be estimated from its elemental composition by the following equation:

$$\rho_{He} = 1.534 - 0.05196H + 0.007375O - 0.02472N + 0.003853S \quad \text{(Eq. 2-27)}$$

where $\rho_{He}$ is the helium density and $H$, $O$, $N$ and $S$ are the calculated weight percent of hydrogen, oxygen, nitrogen and sulfur on a dry mineral-matter-free basis (Speight, 2005). Due to significant variations in the elemental composition of different biomass types, a generic correlation between true density and elemental composition has not been established for biomass. However, the values provided in Table 2-3 can be used to approximate the true density of biomass given the elemental composition of a particular material.

Table 2-3. True density of selected elements (modified from Weast, 1960 as cited in Jenkins, 1989)

| Element | C | Ca | Fe | K | Mg | Na | P | S | Si | Zn |
|---|---|---|---|---|---|---|---|---|---|---|
| True Density ($g/cm^3$) | 1.80-2.10 | 1.54 | 7.86 | 0.86 | 1.74 | 0.97 | 1.82-2.70 | 2.07 | 2.32 | 7.14 |

Apparent density, or particle density, of porous solids is a measure of the mass per unit volume occupied by the solid, including pores and cracks (Mahajan & Walker, 1978). To calculate apparent density, the total mass is divided by the external volume of the solid (Basu, 2010). This can be formally written as:

$$\rho_{apparent} = m_{total}/v_{external} \quad \text{(Eq. 2-28)}$$

where $m_{total}$ is the total mass and $v_{external}$ is the external solid volume. For regularly shaped particles, stereometric methods can be used to approximate external solid volume. Stereometric methods are based on the measurement of particle dimensions (e.g. length, width, height, diameter) by means of a mechanical instrument (e.g. micrometer, caliper, ruler). The volume of the solid is then estimated by calculating the volume of the closest geometric shape using the recorded dimensions (Rabier et al., 2006). Due to the irregular shape of coal and biomass

particles, this method is rarely used. Apparent density of coal and biomass is more commonly determined by calculating external particle volume using one of three methods: mercury displacement (Gan et al., 1972); salinization (Ettinger & Zhupakhina, 1960) or gas flow (Ergun, 1951). Apparent density is used more often than true density in engineering design because it provides the actual volume occupied by a particle in a system and its measurement is relatively straight forward.

Bulk density of coal and biomass is a measure of the mass per unit volume occupied by a group of particles, including interstitial volume between the particles (Berkowitz, 1994). Many factors influence bulk density, including apparent density, particle size and shape, surface and inherent moisture, and degree of compaction (Speight, 2005). To calculate bulk density ($\rho_{bulk}$), the total mass of particles is divided by the volume of the container in which they are placed (Basu, 2010). This can be formally written as:

$$\rho_{bulk} = m_{total}/v_{container} \quad \text{(Eq. 2-29)}$$

where $m_{total}$ is the total mass and $v_{container}$ is the total volume of the container. The precise measurement of this property is important because it is often used to design bulk handling, transportation and storage systems upstream of the gasifier. As a result, standard methods have been developed for bulk density determination of both coal (ASTM D291-07, 2012) and biomass (ASTM E870-82, 2006). There is also a method to determine the loose and tapped bulk densities of powders that can potentially be applied to particulate coal and biomass particles (ASTM D7481-09, 2009).

#### 2.4.2.3 Porosity

Porosity is the fraction of a volume of coal or biomass that is occupied by pore space. Similarly to particle size, the surface area of fuel particles is a function of porosity and therefore this property has a large impact on the rate at which chemical reactions take place within the gasifier (Speight, 2005). There are two types of porosity to define: particle porosity and bulk (or bed) porosity (Basu, 2010). Particle porosity is calculated by dividing the volume of pore space within an individual particle by the total solid volume. Particle porosity is mathematically related to true and apparent density by:

$$\varepsilon_{particle} = 100 - 100\left(\rho_{apparent}/\rho_{true}\right) \quad \text{(Eq. 2-30)}$$

where $\varepsilon_{particle}$ is the particle porosity expressed as a percentage. The standard method for determining true specific gravity of lump coke (ASTM D167-93, 2004) also outlines the procedure for determining particle porosity using Equation 2-25. Bulk porosity is calculated by dividing the volume of interstitial space within a bed of particles by the bulk volume of the bed. Bulk porosity is mathematically related to bulk and apparent density by:

$$\varepsilon_{bulk} = 100 - 100\left(\rho_{bulk}/\rho_{apparent}\right) \quad \text{(Eq. 2-31)}$$

where $\varepsilon_{bulk}$ is the bulk porosity expressed as a percentage.

## 2.4.3 Thermal Properties

### 2.4.3.1 Calorific Value

The calorific value of a fuel is the heat produced when a unit quantity undergoes complete combustion in the presence of oxygen under a specified set of conditions (Speight, 2005). The value is calculated in units of calories per gram and can be easily converted to other units appropriate for specific applications (i.e. 1.0 cal/g = 4.187 kJ/kg = 1.8 Btu/lb). Calorific value can be reported as either the gross calorific value (GCV) or the net calorific value (NCV), which differ with respect to the latent heat of vaporization of water (Basu, 2010). Gross calorific value is particularly important for gasification systems in the North America because thermal efficiency is reported with respect to the gross calorific value of the fuel. However, many European countries define the efficiency of thermal systems in terms of the net calorific value (Basu, 2010).

Gross calorific value, also known as higher heating value (HHV), accounts for the latent heat of vaporization of steam in the combustion product as determined by returning all of the combustion products to the pre-combustion temperature (typically 25 °C). The gross calorific value is determined using either an isoperibol or adiabatic bomb calorimeter as specified by ASTM D5865-12 (2012) for coal and by ASTM E870-82 (2006) for wood fuels. If these experimental methods cannot be performed, gross calorific value can be estimated from empirical correlations. For example, the Dulong equation relates the elemental composition of coal to gross calorific value by:

$$GCV = 338.6C + 1444(H - O/80) + 94.28S \quad \text{(Eq. 2-32)}$$

where $GCV$ is expressed in kJ/kg, and $C$, $H$, $O$ and $S$ are the mass percentage (dry ash-free basis) of the elements determined by ultimate analysis (Perry & Chilton, 1973). Similarly, Channiwala

and Parikh (2002) developed an empirical correlation that relates elemental composition and ash content to gross calorific value, which can be used to approximate both coal and biomass calorific values. This correlation is presented as:

$$GCV = 349.1C + 1178.3H + 100.5S - 15.1N - 103.4O - 21.1ASH \quad \text{(Eq. 2-33)}$$

where *GCV* is expressed in kJ/kg, *C*, *H*, *S*, *N*, *O* and *ASH* are the mass percentage (dry basis) of the constituents determined by ultimate and proximate analyses (Channiwala & Parikh, 2002).

Net calorific value, also known as lower heating value (LHV), is the difference between the gross heat released and the latent heat of vaporization of steam produced during combustion (Speight, 2005). The latent heat of vaporization of steam is usually not recovered because the combustion products are rarely cooled to the pre-combustion temperature (Basu, 2010). Thus, net calorific value is a measure of the effective heat stored in a fuel that can actually be converted to energy, which is less than the chemical energy stored in the fuel. Basu (2010) relates net calorific value to gross calorific value by:

$$NCV = HHV - h_g(9H/100 + M/100) \quad \text{(Eq. 2-34)}$$

where $h_g$ is the latent heat of vaporization of steam in kJ/kg and *H* and *M* are the mass percentage of hydrogen and moisture, respectively, in the sample.

#### 2.4.3.2 Specific Heat

Specific heat is the ratio of the heat capacity of a substance to the heat capacity of water at 15 degrees Celsius, and thus it is a dimensionless quantity. Heat capacity is the heat required to produce a given temperature change within a unit quantity of a substance, with units of joules per kilogram per Kelvin (J/kg-K) or Btu per pound per degree Fahrenheit (Btu/lb-°F) (Speight, 2005). Knowledge of this thermal property is essential for the effective design and operation of both coal and biomass gasification systems (Collazo et al., 2012). However, methods for the measurement of specific heat of coal and biomass are not standardized so it can be challenging to obtain accurate and precise values.

Specific heat and heat capacity are numerically equal because the heat capacity of water is 4,187 J/kg-K (1.0 Btu/lb-°F). As a result, these two terms are often used interchangeably. The specific heat of coal and biomass can be measured by ASTM D2766-95 (2009), which specifies the standard test method for specific heat measurement of liquids and solids. Specific heat of coal is generally between 0.25-0.37 and typically increases with moisture and volatile content yet

decreases with carbon content (Baughman, 1978). Specific heat can also be estimated as the sum of the specific heats of the major elements in coal by:

$$C_p = 0.189C + 0.847H + 0.215S + 0.491N + 0.360O \quad \text{(Eq. 2-35)}$$

where $C_p$ is the specific heat and $C$, $H$, $S$, $N$ and $O$ are the mass percentage (dry ash-free basis) of the elements determined by ultimate analysis (Speight, 2005). Jenkins (1989) correlates the specific heat of dry wood species and temperature over the range of 0 to 106 degrees Celsius. This equation is formally presented as:

$$C_p = 0.266 + 0.00116T \quad \text{(Eq. 2-36)}$$

where $C_p$ is the specific heat and $T$ is the temperature in degrees Celsius.

#### 2.4.3.3 Thermal Conductivity

The thermal conductivity of a material is the time rate of heat transfer by conduction across a unit area of unit thickness for a unit temperature gradient, as calculated by:

$$Q = (kA\Delta t)/d \quad \text{(Eq. 2-37)}$$

where $Q$ is the heat transfer rate, $k$ is the thermal conductivity, $A$ is the area, and $\Delta t$ is the temperature gradient for the distance $d$ (Carslaw & Jaeger, 1959). The rate of heat transfer through a material is typically expressed in units of W/m-K or Btu/hr-ft-°F (Speight, 2005). Heat transfer rate, and thus thermal conductivity, is very important to the rate and efficiency of syngas production in modern gasification systems. Thermal conductivity of a material can be measured by ASTM C518-10 (2010), which specifies the standard method for determination of steady-state thermal transmission properties by means of the heat flow meter apparatus.

Although thermal conductivity is a well-understood concept, the determination of a single value for anisotropic materials such as coal and biomass is very difficult, if not impossible to obtain. The difficulty arises due to banding and bedding planes in coals and the fibrous nature of biomass, which significantly affect the conduction of heat through the materials (Speight, 2005; Jenkins, 1989). For example, the longitudinal thermal conductivity of wood is roughly 2.25-2.75 times the conductivity across the grain, with the conductivity in the tangential direction slightly less than that in the radial direction (Jenkins, 1989). The thermal conductivity of different wood types ranges from 0.039-0.172 W/m-K depending on the species and composition, while the thermal conductivity of U.S. coal ranges from 0.22-0.55 W/m-K depending on rank and composition (Herrin & Deming, 1996). The thermal conductivity of coal typically increases with

apparent density, volatile matter, ash content and temperature and is lower perpendicular to the bedding than parallel to the bedding (Cercone et al., 1996; Speight, 1994).

#### 2.4.3.4 Thermal Diffusivity

The thermal diffusivity is the rate at which temperature change can occur through a material. It is related to steady-state thermal conductivity by:

$$\alpha = k/(\rho C_p) \quad \text{(Eq. 2-38)}$$

where $\alpha$ is the thermal diffusivity, $k$ is the thermal conductivity, $C_p$ is the specific heat and $\rho$ is the density of the material (Speight, 2005). From Equation 2-38 it is apparent that thermal diffusivity increases with thermal conductivity and decreases with specific heat. As with thermal conductivity, thermal diffusivity of coal is typically higher parallel to the bedding than perpendicular to the bedding. Jenkins (1989) reports that the average value of thermal diffusivity of wood is $1.74 \cdot 10^{-7}$ cubic meters per second, but cautions that the value depends on the direction tested relative to the grain. The thermal diffusivity of coal and biomass can be measured by ASTM E1461-11 (2011), which specifies the standard test method for thermal diffusivity by the flash method. However, this test is recommended for primarily homogeneous isotropic materials, which indicates that it could be difficult to obtain accurate and precise measurements.

#### 2.4.3.5 Thermoplasticity

The term thermoplasticity is used to describe the caking, agglomerating and swelling behavior of coals under the influence of heat, which is of great importance to the gasification process (Speight, 2005). These thermoplastic properties influence particle size in fluidized bed and entrained flow gasifiers, which in turn affects heat and mass transfer and the overall carbon conversion within the reactor. In moving bed gasifiers, thermoplastic behavior can cause undesired agglomeration of coal particles that can lead to adherence to surfaces and plugging of the reactor (van Heek & Muhlen, 1987). For example, to efficiently gasify caking coals in moving bed reactors, a stirrer must be installed at the top to prevent agglomeration of coal particles once the temperature exceeds the softening point. However, the stirrer is only effective for mildly caking coals, whereas heavily caking coals require prior oxidative treatment for use in moving bed systems (Higman & van der Burgt, 2003).

In addition to chemical changes that all coals undergo in the presence of heat, caking coals soften, melt, fuse, swell and resolidify within a specific temperature range, known as the

plastic range (Berkowitz, 1994). It is in this temperature range that agglomeration occurs. The caking behavior of coal is directly related to chemical composition, including volatile matter, mineral matter, carbon, hydrogen and oxygen content. Specifically, caking tendency increases with volatile matter content up to 35 percent and decreases beyond that range. Similarly, caking behavior increases with carbon content up to around 89 percent and decreases beyond that point. As a result, anthracite and semianthracite coals generally do not exhibit any caking behavior. The caking tendency of coal also has been shown to increase with hydrogen content and decrease with mineral matter and oxygen content (Speight, 2005).

The thermoplastic properties of coal can be measured with a constant-torque Gieseler plastometer, as specified by ASTM D2639-08 (2008). The coal properties normally determined by this test are the initial softening temperature, maximum fluid temperature, solidification temperature and maximum fluidity (Speight, 2005). Another useful indication of the thermoplastic properties of coal is the agglomerating index, which is a qualitative designation of the appearance of coal residue produced from the determination of volatile matter content by ASTM D3175-11 (2011).

The swelling behavior of coal when heated under specified conditions can be used as a rather definitive measurement of thermoplastic properties. The empirical method for determining swelling behavior, referred to as the free-swelling index, is specified by ASTM D720-91 (2010). This procedure requires heating approximately one gram of coal in a crucible to 820 degrees Celsius to produce a coke button, which is then compared to a series of standard coke button profiles with corresponding free-swelling indices (Berkowitz, 1994). The swelling properties of bituminous coal can also be determined by ASTM D5515-97 (2010) using a dilatometer. However, this test method is limited in applicability to coals with a free-swelling index greater than or equal to one.

#### 2.4.3.6 Ash Fusibility

Ash fusibility refers to the softening and melting behavior of the noncombustible mineral residue that is produced during the combustion of coal and biomass (Berkowitz, 1994). This is one of the most important variables to consider for gasification processes because each reactor is specifically designed for particular ash removal conditions. For example, dry ash moving bed gasifiers and fluidized bed gasifiers require feedstocks with high ash softening and melting

temperatures to ensure that the ash does not form a slag and plug the reactor. In contrast, a low ash softening and melting point is preferred for slagging moving bed gasifiers and entrained flow gasifiers to ensure maximum process efficiency (Higman & van der Burgt, 2003).

The determination of ash fusibility of coals is specified by ASTM D1857/D1857M-04 (2010). By this method, several temperature points are measured by observing the behavior of triangular ash cones formed in a standard mold and subjected to heat in a controlled atmosphere. The temperatures that are determined include the initial deformation temperature ($T_i$), softening temperature ($T_s$), hemispherical temperature ($T_h$) and fluid temperature ($T_f$). The softening temperature is often used to distinguish between slagging coals ($T_s$ < 1200 °C) and nonslagging coals ($T_s$ > 1425 °C). Coals with ash softening temperatures between these limits are generally suitable for use in both slagging and nonslagging gasifiers (Berkowitz, 1994). For gasification applications, it is important that these properties are determined under reducing conditions due to considerable differences typically experienced under oxidizing conditions (Higman & van der Burgt, 2003). The determination of biomass ash melting behavior is specified by CEN/TS 15370-1 (2006). Additionally, ash fusibility determination has been reported for woody and agricultural biomass materials by the ASTM method specified for coal (Jenkins, 1989).

An additional property that is important for slagging gasifiers is the slag viscosity-temperature relationship, which affects the flow and removal of slag from the gasifier (Higman & van der Burgt, 2003). This relationship must be determined empirically for each coal type and gasifier type to optimize the gasifier operating conditions. As a result, there have been numerous publications detailing the viscosity and flow properties of coal ash slags (e.g. Montagnaro et al., 2011; Song et al., 2011; Song et al., 2010b; Hurst et al., 1999; Seggiani, 1998; Nowok, 1994). It is generally accepted that slag viscosity less than 25 Pa·s is required for continuous reliable removal from gasifiers, although this value can vary depending on system specific variables such as geometry. The relationship between slag viscosity and temperature varies for different slags. For example, some slags are characterized by exponential slag-temperature relationships while others behave more linearly (Higman & van der Burgt, 2003).

## 2.4.4 Mechanical Properties

### 2.4.4.1 Grindability

Grindability is a measure of the energy required to reduce the particle size and increase the surface area of a particular substance. The most commonly used method to measure the grindability of coals is ASTM D409/D409M-12 (2012), which specifies the use of the Hardgrove machine to calculate the Hardgrove Grindability Index (HGI). This test method covers the determination of the relative grindability or ease of pulverization of coals relative to coals chosen as standards. The theoretical basis for the method is the proposition that the work required to pulverize a material is proportional to the new surface area produced (Berkowitz, 1994). In this test, a representative 50 gram sample of 16-30 mesh coal is ground by 8 steel balls in the Hardgrove machine for 60 revolutions. The material is then removed from the machine and the mass of minus 200 mesh material is used to determine the Hardgrove Grindability Index from a calibration chart, which must be created by grinding standard reference samples of coal for 40, 60, 80 and 110 rotations (Speight, 2005; Berkowitz, 1994).

The grindability of coal is dependent on a number of factors including rank, friability and thermoplasticity (Speight, 2005). A general relationship between coal rank and grindability is presented in Speight (2005) and Berkowitz (1994) where anthracites and lignites have the lowest Hardgrove Grindability Index and bituminous coals exhibit the highest value. However, grindability varies from seam to seam and within seams, so each coal must be tested independently to ensure accurate values. A strong correlation exists between coal friability and grindability to the extent that highly friable coal generally is found to have a high Hardgrove Grindability Index. The relation between grindability and thermoplasticity is due to plastic deformation from the heat produced by grinding, which leads to agglomeration of small particles and effectively reduces the fraction of minus 200 mesh material (Berkowitz, 1994).

Grindability is particularly important for feed preparation prior to gasification in entrained flow reactors, which require a feed size less than 0.1 millimeters for faster and more complete carbon conversion (Higman & van der Burgt, 2003). Unfortunately, grinding is energy intensive and can reduce the overall efficiency of a gasification plant if the process is not optimized or if significant changes in feed composition are experienced (Sami et al., 2001). Another difficulty concerning co-gasification of coal and biomass is the lack of knowledge on the grinding characteristics of coal-biomass blends and the underlying mechanisms that affect

size reduction. Doroodchi et al. (2013) investigated the milling characteristics of blends of bituminous coal and hardwood chips and determined that the output particle-size distribution is the arithmetic average of the input particle-size distributions for blends containing up to fifty percent (by mass) woodchips. This information could be used to predict the grindability of coal-biomass blends prior to co-gasification.

#### 2.4.4.2 Flow Behavior

The flow behavior of coal and biomass (also referred to as flowability or handleability) is important to consider for handling, storage and processing operations upstream of the gasifier to ensure consistent feed availability. For example, several industrial co-firing operations have experienced flow issues with equipment such as hoppers, silos and gravity stockpile reclaim when attempting to incorporate biomass with coal feed (Hunt et al., 1997; Boylan, 1996). Common flow problems include arching, ratholing, erratic flow, limited live storage capacity, flooding and segregation. These issues can lead to decreased production, increased maintenance costs and even equipment failure (Khambekar et al., 2010).

Arching is the formation of a cavity in the shape of an arch over a discharge outlet that prevents material flow and forms due to cohesion or mechanical interlocking of particles. In contrast, ratholing is the formation of a vertical cavity surrounded by stagnant material that forms down through an outlet and also prevents material flow. When a combination of arching and ratholing occurs and obstructs flow the condition is known as erratic flow (Prescott & Barnum, 2000). Limited live storage capacity is the reduction in storage capacity in a stockpile, silo or hopper as a result of the buildup of stagnant material. Flooding can arise when fine material becomes aerated and pours out of a discharge chute uncontrollably, similar to fluid flow. Finally, segregation can occur in mixtures of particles with a wide size distribution or variations in density. The primary mechanism of segregation is particle sifting, which produces localized regions of particles with similar physical properties (Schulze, 2008).

Flow behavior is a multidimensional characteristic that is influenced by both material parameters and processing equipment. The fundamental theory on flow behavior of particulate solids was originally developed by Jenike (1964) and has since been applied to nearly every industry that involves powder or bulk solids handling, including powder coating, food, cement, coal, ore, clay, and biomass (Schulze, 2008). For reliable handling and storage of coal and

biomass particles, the geometry and materials of construction of equipment must be designed to suit the flow behavior of the particular material, which is influenced by common properties such as particle-size distribution, particle shape, chemical composition, moisture, and temperature. Thus, critical flow properties must be determined to design a reliable and effective handling system (Khambekar et al., 2010).

Flow of bulk solids is defined as plastic deformation due to an applied load. The magnitude of the load necessary to induce flow, measured by a uniaxial compression test, can give a preliminary indication of the flow behavior of a material (Schulze, 2008). For the uniaxial compression test, a hollow cylinder is filled with material and a consolidating load ($\sigma_1$) is applied, then the consolidated material is removed from the cylinder and an increasing vertical compressive load is applied until the material yields. The compressive stress that causes the material to yield is known as the unconfined yield strength ($\sigma_c$). This procedure is repeated for different consolidating loads to generate pairs of values ($\sigma_1$, $\sigma_c$). The values are then plotted to determine the flow function ($ff_c$) of the material, where:

$$ff_c = \sigma_1/\sigma_c \quad \text{(Eq. 2-39)}$$

Classification of flow function values with lines of constant flow behavior are displayed in Figure 2-6, where larger flow function values correspond to better flow behavior. An example of the flow function of a material (A) is also plotted in Figure 2-6, which shows that flow behavior is clearly dependent on consolidation stress. The flow function can be analyzed to determine the minimum outlet diameter for bins and hoppers to prevent arching and ratholing (Prescott & Barnum, 2000). Unfortunately, the uniaxial compression test is problematic for extremely fine-grained bulk solids because unconfined yield strength values are lower than expected and preparation of the hollow cylinder to obtain frictionless walls is difficult and time consuming (Schwedes & Schulze, 1990).

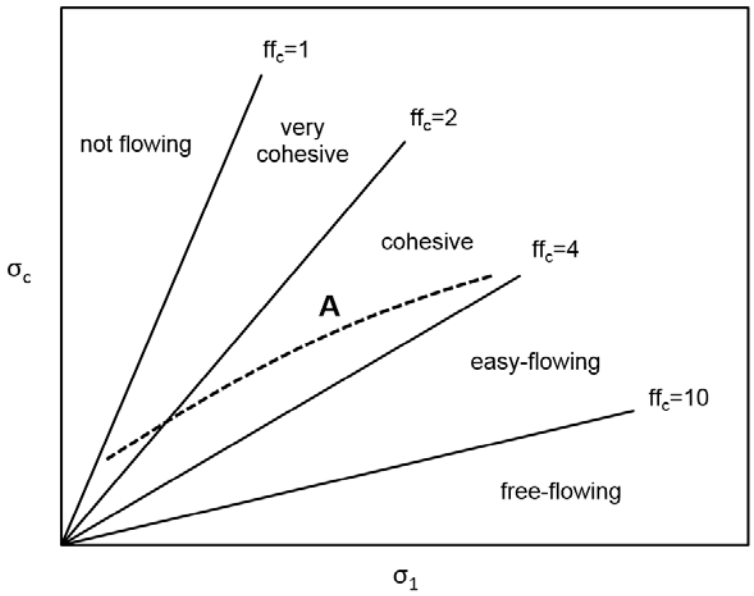



Figure 2-6. Flow function classification and lines of constant flow behavior (modified from Schulze, 2008)

The most commonly used method to accurately determine the flow behavior of fine-grained materials in advanced bulk solids technology is shear testing, which is specified by ASTM D6128-06 (2006) using the Jenike shear cell and ASTM D6773-08 (2008) by the Schulze ring shear tester. These tests calculate the shear force required for a material to yield as a function of consolidating pressure to develop the flow function for a material (Schulze, 2008). The information obtained from shear testing can be analyzed to determine material properties indicative of flow behavior, such as cohesive strength and internal angle of friction (Prescott & Barnum, 2000). Shear testing can also be used to determine the friction between particles and the walls of a bin or hopper, referred to as the wall friction angle or the coefficient of sliding friction. This property is determined by sliding a material sample across a stationary wall surface in a shear tester. Wall friction angles can be used to determine required hopper angles to ensure reliable and consistent flow (Khambekar et al., 2010).

Another material property that is commonly determined to analyze the flow behavior of bulk solids is the variation of bulk density as a function of consolidating pressure. The apparatus and procedure for determining the range of bulk density values is specified by ASTM D6683-08 (2008). The range of values is often expressed as a straight line on a log-log plot of consolidating pressure versus bulk density where the slope of the line is the compressibility of the material.

The results obtained from this test can be used to properly design processing, storage and transfer equipment to accommodate desired capacities (Khambekar et al., 2010).

Flow behavior is also influenced by the permeability of bulk solids during discharge from bins and hoppers, which is measured as a function of bulk density. The permeability of a material controls the maximum achievable discharge rate and thus must be considered when designing the size of bin outlets and transfer chutes to sustain desired flow rates. Permeability values are typically determined by measuring the rate of air flow at a constant pressure drop through numerous samples of varying bulk density. The range of values is often expressed as a straight line on a log-log plot. This relationship can then be used to calculate the required orifice size to achieve desired discharge rates (Prescott & Barnum, 2000).

Although shear testing to assess flow behavior is well-established and fundamentally sound, there are a number of drawbacks to its application to real-time analysis of coal and biomass at industrial facilities. The drawbacks include the complexity of shear testing equipment and procedures, the time and cost associated with analyses and the need for an experienced operator to interpret the results (Brown et al., 1997). In addition, shear testing can only be performed on samples less than 1 millimeter, so preparation of the material (e.g. screening, crushing) is typically required for testing. Hence, shear testing has not been widely adopted in the coal industry (Brown & Miles, 2004). As a result, a number of simpler techniques and devices have been developed specifically for the rapid assessment of coal and biomass flow behavior. The techniques and devices developed for coal assessment include the Durham Cone, the Nottingham Handleability Monitor, the Edinburgh Cohesion Tester and the avalanching technique. The only method that was identified for the assessment of biomass flow behavior is ASAE D274.1 (1992), which gives equations and graphs to estimate the flow rate of specific grains and oilseeds through horizontal and vertical orifices.

The Durham Cone was originally developed in the United Kingdom by the National Coal Board to assess the ease of discharge of fine coal blends (up to 50 mm) from 29 tonne (32 short ton) HAA rail wagons (Hall and Cutress, 1960). Mikka and Smitham (1985) evaluated the influence of moisture, fines and clay content on the results obtained from the Durham Cone. Their results showed that moisture content largely influenced coal handleability when a significant portion of fines were present but the effect was not apparent at a very low fines content. In addition, they showed that the coal size distribution influenced the extent to which

handleability was affected by moisture and fines content. Finally, by comparing the results obtained from Durham Cone to those from the Jenike shear cell for two different coals, the authors concluded that the Durham Cone gave a better prediction of coal handleability (Mikka & Smitham, 1985). The advantages of the Durham Cone for coal handleability assessment are that it is relatively quick to perform (approximately 15 minutes), it can handle coal up to 50 millimeters in size and it does not require a skilled operator to interpret results. However, the main disadvantage of this method is that the results have been shown to exhibit poor repeatability and reproducibility (Brown & Miles, 2004).

The Nottingham Handleability Monitor was developed at the University of Nottingham for reliable on-line measurement of coal handleability using an extrusion trough (Brown et al., 1997). The device was designed to measure the maximum hydraulic pressure required to move coal through a circular tube with a venturi arrangement. The pressure reading is considered to be a measure of coal handleability and is known as the Extrusion Trough Handleability Index (Brown & Miles, 2004). The repeatability and reproducibility of the Nottingham Handleability Monitor was found to be a significant improvement over the Durham Cone in a comparative study (Brown & Atkin, 2000). Another advantage of this technique is the ability to handle large coal particles (up to 50 mm) and perform tests quickly and continuously.

The Edinburgh Cohesion Tester was developed at Edinburgh University to enable real time measurements of coal cohesion to prevent flow problems commonly encountered in coal bunkers at power stations (U.K. Department of Trade and Industry, 2002). This device was designed to measure the unconfined yield strength (cohesive strength) of coal particles after the application of a known consolidating pressure, similar to the uniaxial compression test. The Edinburgh Cohesion Tester incorporates several critical features that address the major drawbacks of uniaxial compression testing. For example, a three piece mold is used to minimize disturbance when removing the sample from the mold. This mold is supported by a soft elastic base which minimizes wall friction effects during vertical consolidation. Brown and Miles (2004) concluded that the Edinburgh Cohesion Tester is useful for predicting the occurrence of coal flow problems in bunkers and repeatable results can be obtained with very little operator training and experience.

Brown and Miles (2004) also present a novel technique for assessing the handleability of coals, known as the avalanching technique. This method was developed based on the work

presented by Rastogi and Klinzing (1994), which recognized that the avalanching of powders could be a useful method to characterize and monitor flow behavior. To assess coal handleability, the avalanching behavior is monitored as the mass flow rate of material using an apparatus comprised of a variable speed feed conveyor, an avalanche ramp and an electronic balance connected to a computer to continuously retrieve data. Further testing and development of this technique will be undertaken to investigate the potential for use as an on-stream assessment of handleability at industrial facilities (Brown & Miles, 2004).

## 2.5 Agglomeration of Coal-Biomass Mixtures

Many of the challenges associated with co-gasification of coal and biomass can be mitigated by agglomeration of coal-biomass mixtures. Size enlargement by agglomeration is defined as any process in which small particles are combined to form larger particles (Capes, 1980). Agglomeration processes are used across many different industries in a wide variety of applications to improve the bulk properties of particulate solids. The objectives and benefits of agglomeration for the co-utilization of coal and biomass include increased bulk density, improved storage and handling properties, improved flow properties, improved homogeneity of blends, reduced dust losses and improved particle bed heat transfer (Browning, 1967). Pietsch (2002) and Capes (1980) have written extensive reviews on all aspects of agglomeration processes, to which the interested reader is directed for additional details. The following section is intended to simply provide an overview of significant aspects of agglomeration theory, tumble/growth agglomeration processes and pressure agglomeration processes.

### 2.5.1 Agglomeration Theory

#### 2.5.1.1 Particle Binding Mechanisms

Size enlargement by agglomeration is differentiated from other grain growth technologies by the types of mechanisms that bind small particles together to form larger particles. The binding mechanisms in agglomeration process are generally classified into five major groups by the nature of particle-particle interactions: (1) solid bridges, (2) adhesion and cohesion forces, (3) surface tension and capillary pressure, (4) attraction forces between solids and (5) interlocking bonds (Rumpf, 1962). These groups of forces can be further divided into several subgroups, and in practice, a combination of forces act simultaneously within agglomerates to bond individual

particles to one another. Figure 2-7 depicts the particle binding mechanisms in agglomeration processes.

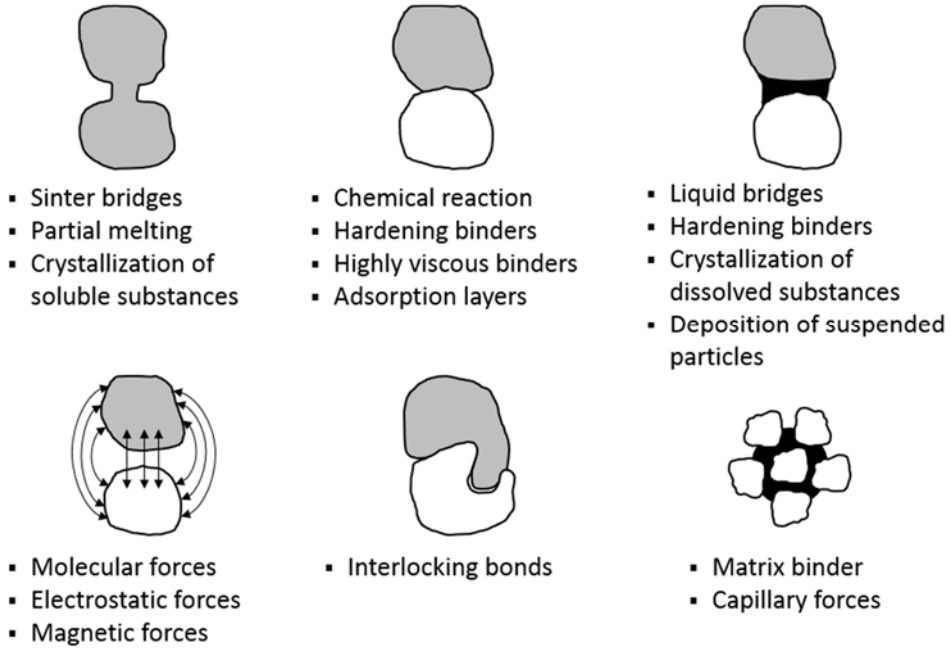



Figure 2-7. Particle binding mechanisms in agglomeration processes (modified from Pietsch, 2002)

Solid bridges can form between particles by the diffusion of atoms or molecules at points of contact as a result of elevated temperatures and pressures that occur in some agglomeration processes. The rate of diffusion of these bridges, known as sinter bridges, increase with a corresponding increase in pressure, temperature and contact area. Another type of solid bridge mechanism is partial melting, in which edges of particles melt from friction or pressure and quickly resolidify. Solid bridges may also form as a result of chemical reactions, hardening of binders and recrystallization of dissolved substances (Pietsch, 2002). Kaliyan and Morey (2008) determined that solid bridges are formed in corn stover and switchgrass briquettes and pellets from hardening of natural binders. This occurs when water soluble carbohydrates, lignin, protein starch and fat are activated in the presence of water under high pressures and temperatures. The solid bridges are formed when pressure is removed and the binder materials cool.

Adhesion and cohesion forces act to bind individual particles when a highly viscous binder (e.g. bitumen, pitch or molasses) is utilized. In this process, adhesion forces are present at the interfaces between the solid particles and binding material, while the cohesion forces act within the binder to strengthen the agglomerate. Another example of adhesion and cohesion

forces are immobile adsorption layers (< 3 nm) that form around particles from the attraction of free atoms or molecules within a system. These layers strengthen the bond between particles by enabling molecular attractive forces due to the decreased distance between particles. In addition, adsorption layers can improve agglomerate strength through the deformation of solid particles at contact points, wherein surface roughness is decreased and the contact area between particles is increased (Pietsch, 2002).

Surface tension and capillary forces often improve interparticle bonding in wet agglomeration processes. For example, liquid bridges can form between particles as a result of free moisture within the system or from capillary condensation. Liquid bridge formation is often a precursor to the formation of solid bridges, thus this interaction plays an important role in the development of agglomerate strength. Another significant interparticle bonding mechanism is the negative capillary pressure that forms as a result of total saturation of the agglomerate pore structure. In general, both of these mechanisms act in wet agglomeration process to bond individual particle to one another (Pietsch, 2002).

Several different types of attraction forces between solid particles can occur within the structure of an agglomerate. The strength of these mechanisms, which include molecular, electric and magnetic forces, are highly dependent on the distance between particles. Molecular forces consist of van der Waals forces, free chemical bonds (valence forces) and hydrogen bonds. Van der Waals forces, which occur naturally at the surface of all solid particles due to electric polarization induced by the presence of other particles, generally provide the greatest attractive energy of the molecular forces. Van der Waals forces exert a magnitude on the order of $1.602 \times 10^{-20}$ joules (0.1 eV), have a maximum range of 100 nanometers and decrease significantly with the distance between particles. When the surfaces of two particles contact one another, electrostatic attractive forces form electric double layers due to the difference in electron work functions, which in turn induce permanent bonding. Magnetic forces can also contribute to agglomerate strength if ferromagnetic particles are present in a particulate system (Pietsch, 2002).

Interlocking bonds can form between elongated, fibrous materials (e.g. fibers, threads, lamellae) when particles bend, twist or weave together during agglomeration processes. These bonds can also be formed when a plastic material wraps around the exterior of a more rigid material due to the application of high pressure. This phenomena generally produces a very

durable bond similar to that of a matrix binder (Pietsch, 2002). Due to the fibrous nature of many biomass materials, interlocking bonds are thought to contribute to the strength of biomass agglomerates. For example, Pickard et al. (1961) concluded that interlocking bonds may contribute to the formation of durable hay briquettes due to the interlacing of stem and leaf materials.

#### 2.5.1.2 Binders, Lubricants and Other Additives

Particle size enlargement operations often require the addition of binders, lubricants or other additives to improve the quality of agglomerates when sufficient bonding cannot be achieved through natural binding mechanisms (Capes, 1980). The use of additives is also required in applications where a specific product characteristic must be obtained (e.g. water resistance) and with agglomeration of relatively large particles. Binders are components added to a particulate system prior to or during agglomeration processes to improve the strength of interparticle bonds, and thus improve the overall strength of agglomerates. Similarly, lubricants are components added prior to or during agglomeration to increase the density of agglomerates, which is achieved by a reduction in porosity as a result of a decrease in the coefficient of friction between particles. Many other types of additives can be combined with particulate solids prior to or during agglomeration to produce a desired functional property that is otherwise unattainable (Pietsch, 2002).

The selection of a binder for a specific agglomeration process depends on a number of considerations, most notably the desired agglomerate strength, cost and availability of additives and compatibility with the intended end use of the agglomerate. As a result, the development of binder formulations is usually very specific to a particular industrial application. However, all binders can be classified according to chemical type and function regardless of the intended application (Capes, 1980). The functions of binders are generally classified as matrix, film or chemical type according to the bonding mechanism utilized. For example, matrix type binders embed solid particles in a continuous matrix whereas film type binders are usually solutions or dispersions such as starch gels. In contrast, chemical type binders produce a chemical reaction between the binder and the solid particles or between binder components (e.g. Portland cement). Binders can be further classified as organic or inorganic based on their chemical composition. Examples of inorganic binders employed in agglomeration processes include lime, sodium

silicates, bentonite, gypsum, salts, cement and magnesia. In contrast, examples of organic binders used in agglomeration processes include alcohols, asphalt, coal tar, dextrin, gelatin, lignosulfonates, molasses, petroleum residues, starches and sucrose (Pietsch, 2002; Messman, 1977). In compaction processes, binders often serve a dual purpose by improving agglomerate strength and also providing adequate lubrication to achieve a desired level of compaction.

The selection of a lubricant for agglomeration processes is dependent upon the same considerations as binder selection: desired strength, cost, availability and compatibility. Lubricants can be classified by the physical state and intended function of the additive. For example, liquid lubricants that have been used in agglomeration processes include water, glycerin, oils, silicones and ethylene glycol. In contrast, solid lubricants include paraffin, graphite, stearic acid and other waxes (Pietsch, 2002). The function employed by lubricants can be characterized as internal or external types. Internal lubricants are added to solid particles to increase the density of agglomerates by reducing the coefficient of friction between particles and to assist in removal of the agglomerate from a confined space, as is common in compaction processes. Conversely, external lubricants are additives applied directly to a mold or die in compaction processes to prevent friction and wear of surfaces (Capes, 1980).

#### 2.5.1.3 Agglomerate Quality

The most important and widely used indicator of agglomerate quality is the strength of bonds between particles (Pietsch, 2002). The only scientifically defined method to characterize the strength of agglomerates that provides information on the fundamental nature of interparticle bonds is tensile strength measurement. Tensile strength is defined as the tensile force at failure divided by the cross-sectional area of the agglomerate. In cases where the agglomerate does not have a uniform shape, the area of the failure plane that results from this test can be used in place of cross-sectional area. Universal equations and theoretical models for approximation of the tensile strength of agglomerates is discussed in detail by Pietsch (2002).

In practice, the tensile strength of agglomerates can be accurately and reproducibly measured with a variety of specially designed and general purpose devices. Typically these devices are comprised of three main components for (1) gripping the sample, (2) applying a deforming load and (3) measuring the applied deforming load (Capes, 1980). Tensile strength measurement devices can include other features to measure deformation and peak load during

testing, which can provide additional information about the strength and durability of particle bonds within an agglomerate. However, there is no standard device or procedure for measuring the tensile strength of agglomerates due to the many different shapes and sizes of agglomerated products. In any case, the major issue surrounding tensile strength measurement is the difficulty involved in mounting and gripping individual agglomerates without impacting the strength or integrity of the sample.

Many different devices and procedures have been used over the past fifty years to measure agglomerate tensile strength. For example, Rumpf (1962) reported a method for determining the tensile strength of spherical pellets that requires several different sample preparation steps prior to evaluation. In this procedure, two parallel plane surfaces are first cut on opposite ends of each pellet. Next, the surfaces are coated with a lacquer and an adhesive to facilitate attachment of metal adaptors to each end of the pellet. The pellet is then turned down to a cylindrical shape (0.18-mm diameter) in a lathe and the finished sample is mounted to a tensile strength measurement device through the metal adaptors. Unfortunately, this procedure is labor intensive and requires great care when cutting and machining the pellets to ensure that the strength is not impacted by the preparation process. Also, since the outer portion of the pellets is removed prior to tensile strength measurement, this method would not provide an accurate result for agglomerates with an unequal strength distribution (Capes, 1980).

A number of indirect tensile strength measurement techniques have been developed to address the difficulties of traditional methods. For example, Berenbaum and Brodie (1959) investigated three alternative methods for measuring tensile strengths of brittle materials, including a bending test, an indentation test and a test in which disks are compressed diametrically. It was determined that the results from the indentation test and the diametrical compression test are in reasonable agreement with traditional tensile strength results. The diametrical compression test was used to evaluate the tensile strength of agglomerates by Fell and Newton (1968) in a study on the strength of lactose tablets.

Although tensile strength measurement is the only scientifically defined and fundamentally understood method to measure agglomerate strength, these methods are rarely used in practical and industrial applications due to the complexity of the procedures and the required interpretation of results. As a result, a wide variety of industry-specific methods have been developed to simulate the forces that agglomerates are subjected to during handling,

transportation and storage. Unfortunately, the results obtained from these types of tests are empirical and not theoretically predictable because the fundamental failure mechanisms are not understood. Nonetheless, these types of strength and durability measurements are important to consider because of their simplicity and industrial acceptance.

A comprehensive review of reported strength and durability evaluation methods for all types of agglomerates is beyond the scope of this discussion. Therefore, this review is limited to method used to evaluate coal and biomass solid fuels. Over the past several decades, researchers involved in the development of fuel briquette formulations and processes have reached a consensus regarding the most important physical properties that should be measured to indicate the quality of briquettes. The identified physical properties are impact-shatter resistance, compressive strength, and attrition resistance (Taulbee et al., 2010; Honaker et al., 2005; Richards, 1990; Eckerd, 1967; Moore, 1957; Prostel, 1953; Boley & Rice, 1949). The measurement of these three parameters can be used to indicate the extent to which briquettes will remain intact during handling, transportation and storage.

Briquettes continually experience impact-shatter forces, compressive forces and attrition forces from formation to utilization. Impact-shatter is defined as breaking violently into pieces from a sudden impact. Impact-shatter forces are encountered when briquettes drop in stockpiling, at conveyor transfer points and from bins and chutes. Compression is defined as the act, process or result of pressing or squeezing together. Briquettes experience compressive forces in bins, stockpiles and railcars from the load applied by other briquettes. Attrition is defined as wearing or grinding down by friction. Briquettes are subjected to attrition forces during transportation and at loading and unloading points.

Although researchers generally agree on the most important physical properties concerning briquette durability, specific test methods to quantify these parameters are highly variable. Generally, researchers independently develop assessment procedures appropriate to the nature of the particular investigations performed at their laboratories. For example, many researchers have designed assessment procedures for attrition and impact-shatter resistance to mirror existing ASTM procedures for coal and coke, yet there is still very little consistency between the procedures employed at separate laboratories.

The only documented procedures that have been used to quantify the durability of coal-biomass briquettes are those that have been in use at the University of Kentucky's Center for

Applied Energy Research (CAER) over the last decade. Taulbee et al. (2010) and Patil et al. (2009) describe methods to quantify the 'compressive' strength and attrition index of briquettes prepared from blends of biomass and fine coal. Patil et al. (2009) and Honaker et al. (2005) describe a drop test method that is used to determine the impact-shatter resistance of briquettes made from blends of coal fines and sawdust. This method consists of averaging the number of drops to failure for four briquettes dropped from a height of 0.46 meters (1.5 ft) onto a steel plate. However, this method was eventually abandoned due to an inherently high level of data scatter and the time consuming nature of these evaluations. In addition, this method requires the technician to visibly determine when the briquette has split into two or more significant pieces, which is a subjective decision that could vary from one person to another.

The importance of impact-shatter evaluation has also been realized by the coal industry. ASTM D440-07 (2012) describes a drop shatter test for coal that was established to indicate the extent to which lump coal will break in conventional transit and handling operations. This standard specifies dropping fifty kilograms of coal from a box equipped with a false bottom that is positioned 1.83 meters (6 ft) above a steel plate. The coal is dropped from the box by releasing the false bottom, recovered from the steel plate and dropped a second time to further break the coal. The broken coal is then hand screened through nested sieves (203, 152, 102, 76, 51, 38, 25, 19, 13, 6, and 3 mm apertures). The results reported are the mass percentage in each class to the nearest 0.1% and the percentage size stability of each class to the nearest 0.5%.

Taulbee et al. (2010) and Patil et al. (2009) describe a method to measure briquette 'compressive' strength using either a Mark-10 EG-200 force gauge (890 N capacity) or a Lloyd Instruments LRX Plus load cell (4,448 N capacity). Each gauge is mounted to an automated test stand and equipped with a 19 millimeter (0.75 in) diameter plunger which travels downward at a rate of 25.4 millimeters (1 in) per minute. This ability to control the rate of loading is very important to ensure the accuracy and reproducibility of test results (Capes, 1980). The force gauges are configured with a break detect feature which stops the movement of the plunger once the applied force drops to 95 percent of the maximum force attained during the test. The plunger then reverses direction and the maximum force attained during the test is designated as the compressive strength of the briquette. Measurements are recorded along the axis used to apply force during briquette formation and reported values represent the average of a minimum of 15 measurements. Values less than 222 newtons (50 $lb_f$) are classified as poor, between 222 and 445

newtons (50-100 $lb_f$) as marginal, between 445 and 667 newtons (100-150 $lb_f$) as good, and greater than 667 newtons (150 $lb_f$) as excellent. Although the measurement recorded following this procedure provides important information regarding the strength of briquettes, the use of the term 'compressive' strength is not scientifically valid (Pietsch, 2002).

Taulbee et al. (2010) and Patil et al. (2009) also describe a method to measure attrition indices for briquettes that have cured for seven days in a controlled-environment chamber. Approximately 200 gram samples (20 to 25 briquettes) are placed into a 0.305 meter (1 ft) diameter Plexiglas cylinder equipped with three, 51 millimeter (2 in) lifters; tumbled for five minutes at 40 rotations per minute; and screened through a 4.75 millimeter (U.S. Standard 4 mesh) sieve in a Ro-Tap sieve shaker for two minutes. The attrition index is reported as the fraction of the starting briquette weight retained on the 4.75 millimeter sieve. Attrition Indices less than 0.80 are considered poor, 0.80 to 0.90 marginally acceptable, 0.90 to 0.95 good, and greater than 0.95 excellent. This and the other methods described provide a solid foundation for coal-biomass briquette evaluations. However, optimization and standardization of coal-biomass briquette evaluation procedures is an important area that requires further investigation.

### 2.5.2 Tumble/Growth Agglomeration

The most basic particle size enlargement technique is tumble/growth agglomeration (Pietsch, 2002). This process is characterized by the collision and coalescence of fine particles as a result of some form of agitation in the presence of natural or supplemental binding mechanisms. The most widely used method of bulk particle agitation in the mineral processing industry to induce agglomeration is tumbling in rotating discs, drums and cones (Capes, 1980). In this context, tumbling refers to irregular, turbulent motion of all particulate solids in a defined environment. Typically, agglomerates produced by these methods are spherical in shape with diameters ranging from 4 to 6 millimeters. Other technologies for tumble/growth agglomeration include mixer agglomeration, drying of solutions and suspensions, low density particle clouds and agglomeration in liquid suspensions. This section provides a general overview of tumble/growth agglomeration mechanisms, disc and drum agglomeration technology and some practical applications of these concepts in solid fuel production.

#### 2.5.2.1 Process Overview

The process of tumble/growth agglomeration begins when individual particles within a particulate system collide and stick together as a result of agitation. A nuclei (or seed) is formed when the strength of the activated binding mechanisms is greater than the sum of the ambient separation forces (e.g. gravity, inertia, drag) within the system acting on the nuclei. This process, referred to as nucleation, is the most delicate stage of tumble/growth agglomeration because the adhesive forces that develop from the collision of particles are relatively weak (Pietsch, 2002). As a result, nucleation is an inherently time consuming process as many nuclei disintegrate and only a small proportion survive at any given time. After nucleation, size change within a system of particulates can take place by a number of different mechanisms, including coalescence, layering, abrasion transfer, shatter, breakage and attrition (Capes, 1980). These mechanisms are visually depicted in Figure 2-8.

Pietsch (2002) proposes that the tendency for adhesion of particles in tumble/growth agglomeration processes can be expressed as:

$$T_a = \sum B_i(x) / \sum F_{jy}(x) \qquad \text{(Eq. 2-40)}$$

where $T_a$ is the adhesion tendency of two particles, $B_i(x)$ is the sum of all active binding forces and $F_{jy}(x)$ is the active sum of all separation forces within the system. For successful adhesion between two or more particles, the adhesion tendency ($T_a$) must be greater than or equal to one. The particle size ($x$) has a very large influence on the magnitude of adhesive forces and ambient system forces, and thus on the adhesion tendency of two or more particles.

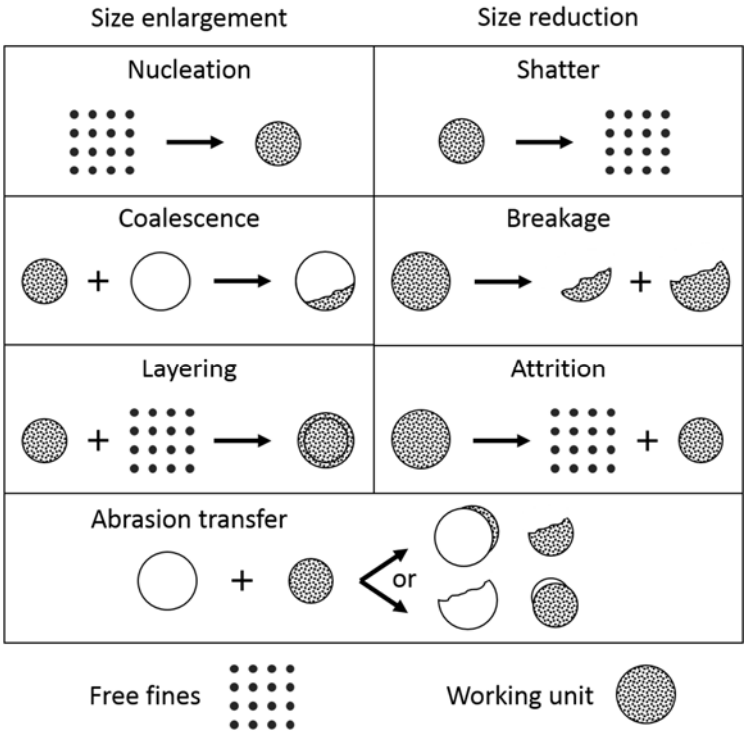



Figure 2-8. Mechanisms of size change in tumble/growth agglomeration (modified from Pietsch, 2002)

Addition of supplemental binders is typically required for tumble/growth agglomeration processes unless the average particle diameter is less than ten microns (Pietsch, 2002). The strength of naturally occurring binding mechanisms (e.g. van der Waals forces, electrostatic forces) in a system of nano-sized particles can equal or exceed other system forces, even with little or no presence of moisture. As a result, the adhesion tendency of fine particles increases with a corresponding decrease in particle size. In more common tumble/growth agglomeration processes, green agglomerates (moist or wet) are formed through coalescence and layering as a result of binder addition. If the solid particles contain a significant amount of moisture, a solid binder can be used, but in most industrial applications a liquid binder is required (Pietsch, 2005).

The strength of green agglomerates is primarily attributed to bridges formed by freely movable liquids, capillary pressure at the surface of particles or adhesive forces produced by viscous binders (Pietsch, 2002). Green agglomerates generally require a post-treatment (curing) process after formation to remove excess moisture, which often reduces market appeal, and to improve the strength of bonds. The curing process results in the formation of solid bridges though sintering, chemical reactions, partial melting or recrystallization.

#### 2.5.2.2 Disc and Drum Agglomerators

The most widely used tumble/growth agglomeration devices in mineral processing applications are inclined disc and rotary drum pelletizers. The operating principle of these devices is the formation of spherical pellets by rotating a cylindrical vessel containing a mixture of particulate solids and binders (Pietsch, 2005). As a result of the rotation of the vessel, the mixture is continuously subjected to irregular, turbulent motion until particles of a desired size are formed and removed from the system. These systems can be configured as batch or continuous processes to facilitate a wide variety of applications across many different industries (Capes, 1980).

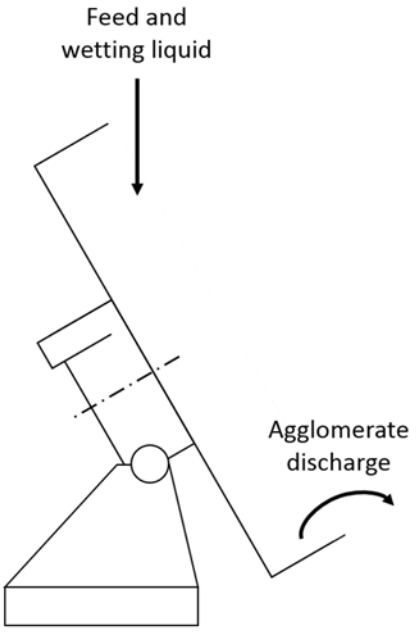



Figure 2-9. Disc pelletizer schematic diagram (modified from Capes, 1980)

Disc pelletizers (also referred to as pan or dish pelletizers) are characterized by a round, flat-bottomed, inclined shallow pan that rotates about the center point (Figure 2-9). Solid feed particles are gravity fed to the center of the rotating disc from above and the formed agglomerates discharge over the bottom rim of the disc. The ratio of rim height to the rim diameter is typically in the range of 0.1-0.2 for shallow disc pelletizers, although many modified pan designs have been developed (Pietsch, 2002). An expanded metal liner or an abrasive coating is fixed to the interior of the disc to reduce wear and prolong the operational life of the disc. Adjustable spray nozzles are mounted to a frame that is attached to the base of the pelletizer

for the addition of water or other liquid binders. Scrapers or plows are also mounted to the frame to agitate stagnant material and to control the flow pattern of solids within the disc. The inclination of the disc can be adjusted between 40 and 70 degrees to the horizontal to optimize the process for a particular feed and desired agglomerate characteristics. Disc rotation is driven by a fixed-speed or variable-speed motor mounted to the base of the pelletizer. Variable-speed motors provide greater control over agglomerate formation and quality (Capes, 1980). The diameter of disc pelletizers can range from 0.5 meters for laboratory or small-scale applications to more than 10 meters for high-tonnage industrial operations (Pietsch, 2002).

The most distinguishing characteristic of disc pelletizers is the size classification of agglomerates that occurs as a result of the unique flow pattern within the pan. As displayed in Figure 2-10, larger agglomerates move to the top of the bed by natural segregation and discharge over the rim as additional feed is added to the system. The seed agglomerates and individual particles are concentrated in the bottom of the bed for additional agglomerate formation. Due to this classification effect, the size particle size of agglomerates discharged from the disc is rather uniform and there is often no need for an additional screening operation (Capes, 1980). Under clockwise rotation, the distribution of solids is restricted primarily to the left side of the pan. Due to the coefficient of friction of the solids, particles are carried clockwise from the bottom to the top of the pan. Once the particles reach the top portion of the pan, gravity causes the particles to cascade down to the bottom of the pan, where the cycle is continued (Pietsch, 2002).

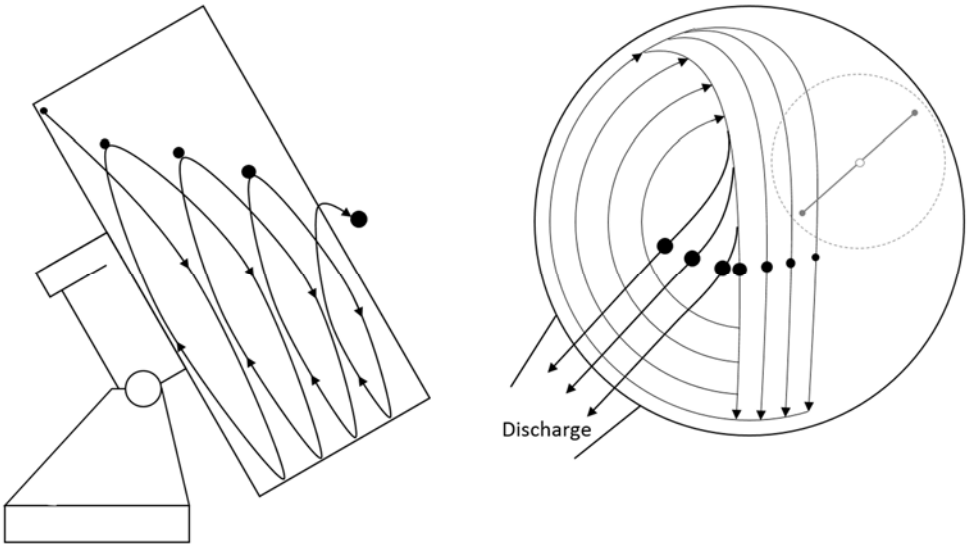



Figure 2-10. Particle flow pattern in disc pelletizers (modified from Pietsch, 2002)

Aside from feed and binder properties, a number of system operating variables influence the size, shape and density of tumbled agglomerates (Capes, 1980). The flow rate of added liquid and the position of the spray nozzles influences the shape of agglomerates. The proper configuration for liquid addition to a disc pelletization system promotes growth by layering, in which dry fines are collected on the surface of established agglomerates that have been wetted by the sprays. In contrast, addition of too much liquid will result in the undesirable production of abnormally shaped particles. Agglomerate size is controlled by liquid addition rate and retention time in the disc. Retention time can be increased by reducing the particle feed rate, decreasing the angle of inclination of the disc or by increasing the height of the rim. Each of these options can be employed to increase agglomerate particle size.

The density of agglomerates is primarily influenced by disc diameter, angle of inclination and the liquid addition rate. Sufficient liquid must be added to the system to for agglomerate growth and densification by the formation of liquid bridges and other interparticle bonds. Disc diameter and angle of inclination have a similar effect on agglomerate density in that an increase in both parameters results in the increase of the kinetic energy of cascading particles. This in turn produces greater compaction stresses upon impact with other particles and the rim, and thus higher density agglomerates are formed. However, it must be considered that as the angle of inclination increases, agglomerate residence time is reduced, which will result in a reduction in agglomerate particle size (Capes, 1980).

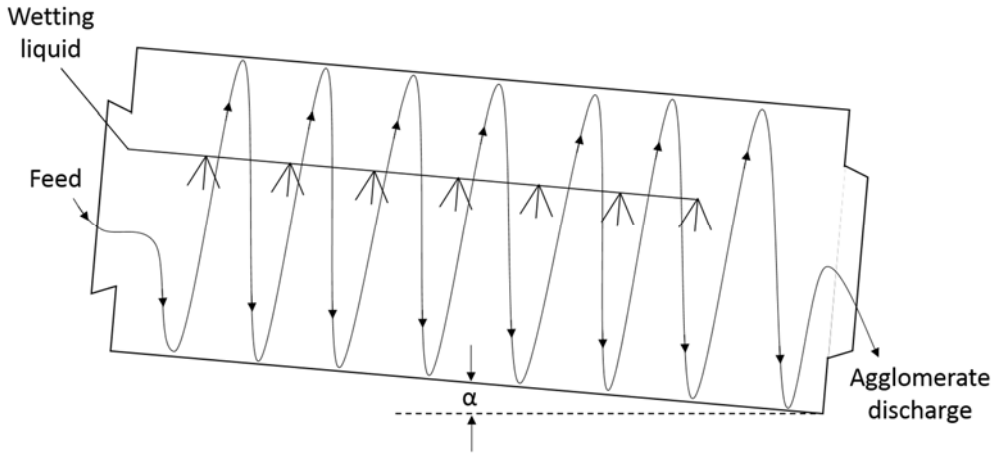



Figure 2-11. Drum pelletizer schematic diagram and particle flow pattern (modified from Pietsch, 2002)

Drum pelletizers are more commonly used than disc pelletizers for high-tonnage applications such as iron ore pelletization and fertilizer granulation. These devices are

characterized by a large rotating steel cylinder with a slight inclination (α, up to 10°) to the discharge end that is driven by a fixed-speed or variable-speed drive (Figure 2-11). Feed material is introduced to the inclined end of the drum and is tumbled down the length of the drum. This irregular, turbulent motion leads to the formation of spherical pellets in the presence of liquid, which can be added prior to, or with the feed (Pietsch, 2002). To prevent spill-back of feed material, a retaining ring is commonly installed to the feed end of the drum. Additionally, a dam ring can be installed to the discharge end of the drum to increase bed depth and residence time, which is beneficial in many applications. Similar to disc pelletizers, the interior of drum pelletizers is often lined with an expanded metal liner or an abrasive coating to reduce wear and facilitate proper tumbling motion. Scrapers or plows are also mounted to the interior of the drum to limit material build-up and control the uniformity of the drum surface (Capes, 1980).

Although the configuration of drum pelletizers is quite different from disc pelletizers, the material flow pattern in drums is very similar to that of discs. However, the main difference is that particle discharge from drum pelletizers is largely due to gravity, whereas natural segregation discharges larger particles from disc pelletizers. The result is a much wider distribution of agglomerate particle size in the discharged product from drum pelletizers. Consequently, most drum pelletization operations require a recycle loop where fine material is screened from the produce and returned to the feed end of the drum (Capes, 1980). The size, shape and density of agglomerates produced in drum pelletizers are influenced by the same parameters as products of disc pelletization: liquid addition rate, retention time, drum diameter and drum inclination. These effect of these parameters is very similar in both types of tumbling agglomeration, and thus optimization of operating variables must be conducted for every unique application.

#### 2.5.2.3 Solid Fuel Applications

The most significant solid fuel application of tumble/growth agglomeration is the pelletization of wet coal fines. Modern coal mining and preparation operations produce large tonnages of wet coal fines due to the methods used for coal extraction and cleaning. Due to the unfavorable economics of cleaning and drying wet coal fines, vast quantities of fine coal have been deposited in slurry impoundments in coal mining regions. For example, it is estimated that more than 2 billion tonnes of recoverable fine coal is contained in slurry impoundments in the

eastern United States alone (Pietsch, 2005). An additional 30 to 50 million tonnes are added to slurry impoundments in this region every year. This has led to significant interest in methods to reconstitute and dry fine coal to improve the marketability of this valuable waste product.

Tumbling/growth agglomeration is the only economical method to reconstitute ultra-fine filter cake coal, which is formed when water is removed from the flotation product of a modern coal preparation plant (Holley & Antonetti, 1977). The advantage of this method over other agglomeration process (e.g. pressure agglomeration) is that the moisture content of filter cake upon discharge from the vacuum filter is in the ideal range for coal pelletization. Thus, there is no need for a preliminary drying stage prior to agglomeration. However, high-moisture coal pellets formed by tumble/growth agglomeration methods require drying after formation to improve the strength and durability. This process can be accomplished with many commercially available dryers (e.g. fixed bed) without production of harmful pollutants. In comparison, pressure agglomeration processes require a feed material that is much drier, and commercially available technologies for drying fine coal can no longer be permitted due to air quality regulations. However, there are many innovative fine coal drying technologies currently being developed which may increase the feasibility of pressure agglomeration of coal fines in the future.

Holley & Antonetti (1977) described a coal pelletization pilot-plant that was built to agglomerate coal obtained from a tailings impoundment. The purpose of the pilot-plant was to determine if construction and operation of a production plant was economically feasible. For the pilot-plant evaluations, coal was recovered from the impoundment, cleaned by two-stage froth flotation and dewatered with a vacuum filter. Several batches of pellets were produced with different binders (lignosulfonate and coal tar) at a rate of 227 kilograms (500 lb) per hour of product. The coal and binder was mixed in 45 kilogram (100 lb) batches and fed to a 0.91 meter (3 ft) diameter disc pelletizer, in which 12.7 millimeter (0.5 in) diameter pellets were formed. The pellets were discharged directly onto a fluidized-bed vibratory dryer operated at 149 degrees Celsius (300 °F) to reduce the pellet moisture below 6 percent. The quality of the pellets was measured by a modified drop shatter test. The lignosulfonate binder was found to be far superior to the coal tar in this application.

Mehrotra (1980) investigated the kinetics and strength aspects of coal pelletization for 14 different coal samples. In batch pelletization experiments, it was observed that the moisture

content of the feed coal had the most significant impact on pellet growth kinetics. Specifically, the pellet growth rate increased with increasing water content. The fineness of the coal samples was also found to have a large impact on the growth rate of pellets. For example, pellet growth rate was found to decrease with increasing fineness for anthracite and bituminous coals. Mehrotra also observed that the strength of pellets tends to decrease with a corresponding decrease in the ash and sulfur content of the feed coal, whereas pellet strength increases with an increase in the fineness of the feed. Moreover, it was found that pellet strength was independent of the feed moisture content. Finally, this study found that corn starch is more effective than asphalt and bentonite for improving the strength of the coal pellets and that binder addition led to a small reduction in the growth rate of pellets.

A more recent application of coal pelletization is described in a patent claim by Taulbee (2012). This document claims that briquette production can be enhanced by the sequential pelletization and briquetting of coal fines. The first step of this process is the formation of spherical pellets in a disc or drum pelletizer from mixtures of wet coal fines, biomass and/or binders. Next, the pellets are conveyed to a fixed-bed dryer to reduce the moisture content below ten percent. This allows quick and efficient drying of the coal fines due to the high porosity of the green pellets. After drying, the pellets are conveyed to a briquetting machine where an additional 2 to 30 percent biomass and 1 to 15 percent binder are mixed with the pellets prior to briquette production. The briquettes produced following this procedure are shown to exhibit good initial strength and durability. However, the strongest and most durable briquettes are produced when the pellets are still hot during the briquetting process. Briquetting processes are covered extensively in the following section on pressure agglomeration.

### 2.5.3 Pressure Agglomeration

The most versatile and widely used technique for size enlargement of particulate solids is pressure agglomeration. This process is characterized by the compaction and densification of particulate solids by application of external forces in a confined space (Capes, 1980). Pressure agglomeration technologies can be classified by the level of forces exerted during densification and shaping, which affect the strength and other properties of the compacted products. In low-pressure agglomeration processes, feed materials with high moisture and plasticity are formed by pressing through a structurally weak die, and thus generally require a post-treatment process to

improve strength and durability. In medium-pressure agglomeration (also known as pelleting), inherent plasticity of drier feed materials is activated by a conditioning process prior to extrusion through perforated dies. This technology has seen significant application in the biomass fuel industry, particularly in the production of wood pellets for home heating and industrial power generation. High-pressure agglomeration techniques are characterized by deformation and destruction of dry feed materials in the presence of high forces, which results in the production of durable densified products with high green strength (Pietsch, 2002). The most commonly used high-pressure agglomeration technology for fine coal reconstitution is roll press briquetting. This section provides a general overview of pressure agglomeration processes, roll pressing technology and some practical applications of these concepts in solid fuel production.

#### 2.5.3.1 Process Overview

The mechanisms of solid particle compaction in pressure agglomeration processes can be divided into two stages. In the initial stage, low pressures cause bulk particles to settle and rearrange, which results in a reduction of porosity and an increase in bulk density. The total surface area of contact between particles also increases during this stage and bonds are formed through liquid bridges and capillary pressure (Drzymala, 1993). At this point, agglomerates are relatively weak and require additional compaction pressure to improve strength and durability. In the second stage, much higher pressures are exerted on the densified mass, which results in the fracture of brittle particles and/or plastic deformation of malleable materials (Pietsch, 2002). Additional bonds are formed during this stage by activation of interparticle adhesive forces, which occurs when the surface area of contact between particles is further increased and the distance between particles becomes extremely small. A schematic representation of these processes is provided in Figure 2-12.

The top half of this figure shows the structural change of particulate solids with the progression of compaction, densification, fragmentation and plastic deformation that occurs with increasing pressure in a confined space or die. The bottom half of the figure depicts the increase in pressing force at a constant compression rate over a period of time until the maximum pressure ($P_{max}$) is reached. The reason for a sharp reduction in pressing force beyond this point depends on the agglomeration technique. For example, in a roll press system, the maximum force is applied to a material as it passes through the center of the rolls. A sharp decrease in pressing

force is immediately observed as the material is ejected from the rolls. Similarly, in a punch and die agglomeration system, the maximum force applied to a material is defined by the predefined displacement of the punch, after which the punch is retracted and the force applied to the material sharply declines. Another important phenomena in pressure agglomeration processes is listed in the bottom right corner of Figure 2-12: expansion of compressed air and elastic spring-back. These mechanisms cause cracking and weakening of agglomerates, the magnitude of which is determined by material properties and operating conditions. If not adequately addressed, these mechanisms can cause partial or complete destruction of agglomerates. One method to reduce the effects of elastic spring-back and expansion of compressed air is to reduce the speed of compaction, which in turn increases the amount of time material remains confined under the influence of the load. This parameter is referred to as dwell time (Pietsch, 2002).

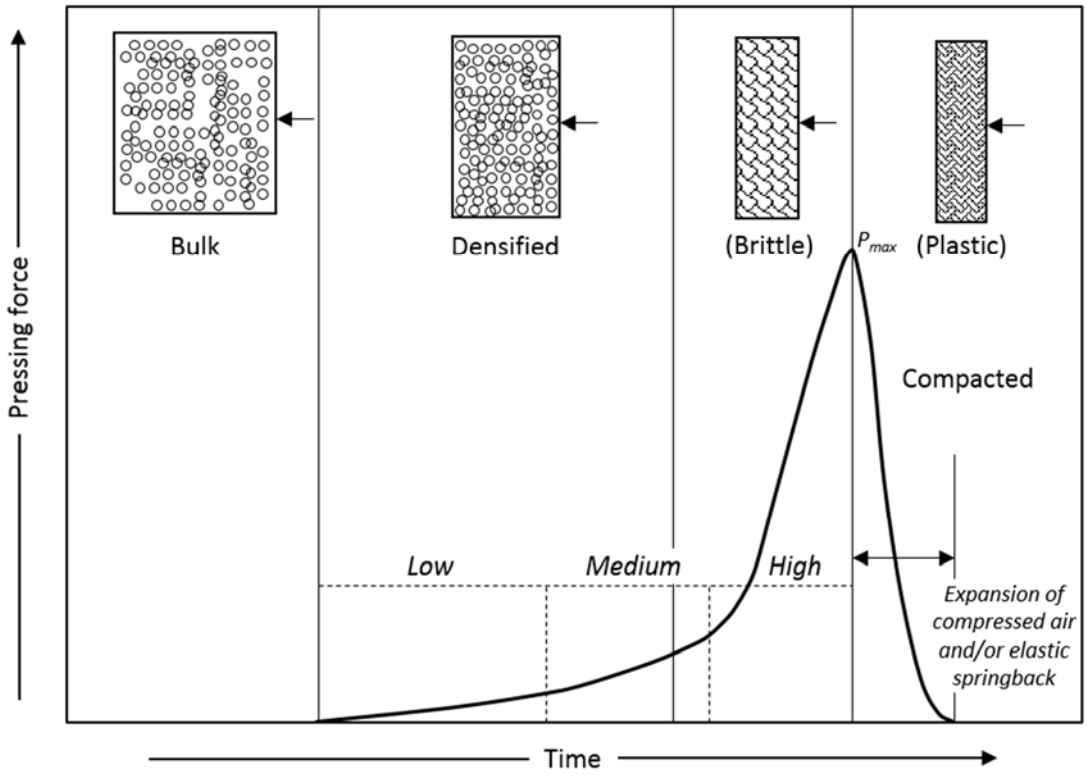



Figure 2-12. Mechanisms of compaction in pressure agglomeration (modified from Pietsch, 2002)

The primary goal of pressure agglomeration is to improve the density of particulate solids by applying external pressure to a system of particles in a confined space. Thus, a common method to evaluate a pressure agglomeration process is to measure the apparent density of the formed products. Comparison of this value with the true density of the solid particles gives a

clear indication of the level of densification achieved. Specifically, the ratio of the apparent density of an agglomerate to the true density of the constituent solids is often measured. This agglomerate characteristic, referred to as packing density, is influence by particle size, shape, surface roughness and internal structure for any given densification system (Standish et al., 1991). In high pressure agglomeration systems, the internal structure (or strength) of materials greatly influences particle fragmentation, which in turn influences the size and shape of particles within a system. For example, the fragmentation of brittle solids during compaction reduces packing density due to the development of hydrostatic pressure and the high strength exhibited by smaller particles (Pietsch, 2002).

Without fragmentation or plastic deformation of particles, the maximum theoretical packing density of perfect spheres is 74 percent (i.e. $\sqrt{2}\,\pi/6 = 0.7405$). This value increases to 86 percent if a smaller size fraction of spheres is added to the material that occupy the void spaces between the larger particles (Scott & Kilgour, 1969). Similarly, if third and fourth size fraction is added that fills the new void spaces between the larger particles then the theoretical packing density approaches 90 to 92 percent and 95 to 97 percent, respectively (Drzymala, 1993). For real-world applications, these theoretical packing densities are generally not achievable due to the irregular shape and inconsistent size of common materials. However, fine-grained materials with regular shape, low surface roughness and compact structure can realistically achieve packing densities up to 90 percent. When additional densification beyond that achievable by particle size manipulation is desired, lubricants are commonly added to reduce interparticle friction and saturate the pore volume. However, the addition of lubricants often degrades the quality of agglomerates, so this parameter must be optimized to balance agglomerate density with desired quality.

#### 2.5.3.2 Roll Press Compactors

The most widely used pressure agglomeration technology for size enlargement of particulate solids in the mineral processing industry is roll pressing. Roll presses were originally developed in the mid-19$^{th}$ century as an economic method to produce strong agglomerates from large quantities of coal fines (Pietsch, 2002). Roll presses are characterized by two identical counter-rotating rolls held together by an applied force that compact particulate material as it is

drawn between the rolls. Figure 2-13 provides a schematic diagram of two different roll press configurations.

In the most simple roll press configuration, particulate solids are fed by gravity through smooth rollers to produce dense sheets of material (Figure 2-13a). Fluted, corrugated and waffled rollers can also be used to form dense sheets, which are typically crushed and screened after production to create a granular product (Capes, 1980). In a different roll press configuration, particulate solids are force fed by a rotating screw through pocket rollers to produce briquettes of uniform size and shape (Figure 2-13b). This process produces a 'web' or 'flash' material on the edges of the briquettes due to the flat area around each pocket. The majority of the web material is typically removed by screening the briquettes after formation and recycled back into the feed to minimize the production of fines during handling. Roll presses can be built with any combinations of feeding mechanism and roll type. Vertical feed systems can also be substituted by horizontal force feed systems, which are desirable for some applications.

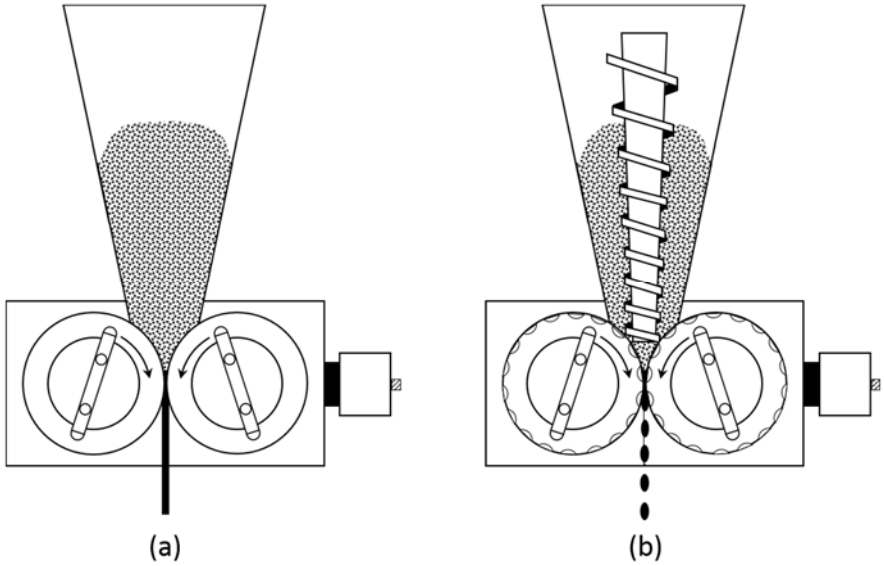



Figure 2-13. Schematic diagram of (a) gravity fed roll press with smooth rollers and (b) force fed roll press with pocket rollers (modified from Pietsch, 2002)

As particulate solids enter the nip region between the rollers and compaction begins, three distinct zones can be defined: the feed zone, the compaction zone and the release zone (Pietsch, 2002). Figure 2-14 depicts the movement of material through these zones for a gravity fed system with two smooth counter-rotating rollers. In the feed zone, material is drawn into the nip region by the combination of gravity and friction between the rollers and the particulate

solids. This zone is defined by the width of the rectangular feed opening ($h_O$), the angle of delivery ($\alpha_F$) and the angle of nip ($\alpha_C$). As shown in the pressure-displacement diagram on the right side of Figure 2-14, low pressure forces are developed in the feed zone, which leads to preliminary densification by particle rearrangement. From here material continues into the compaction zone, defined by the area between the angle of nip ($\alpha_C$) and the neutral angle ($\alpha_N$), where a sharp increase in pressure leads to the fragmentation and plastic deformation of particles. Beyond the neutral angle ($\alpha_N$), the densified product enters the release zone, in which particles are subjected to the maximum pressure ($P_{Max}$) within the system and the maximum sheet density is attained with a thickness ($h_A$) equal to the width between the rollers. Finally, the frictional force is reversed and the agglomerate is ejected from the rollers. Immediately following ejection, the final sheet thickness ($h_S$) slightly increases due to the expansion of compressed air and elastic spring-back. The complexity of material flow through the nip region is greatly enhanced in the case of roll press briquetting with pocket rollers (Pietsch, 2002).

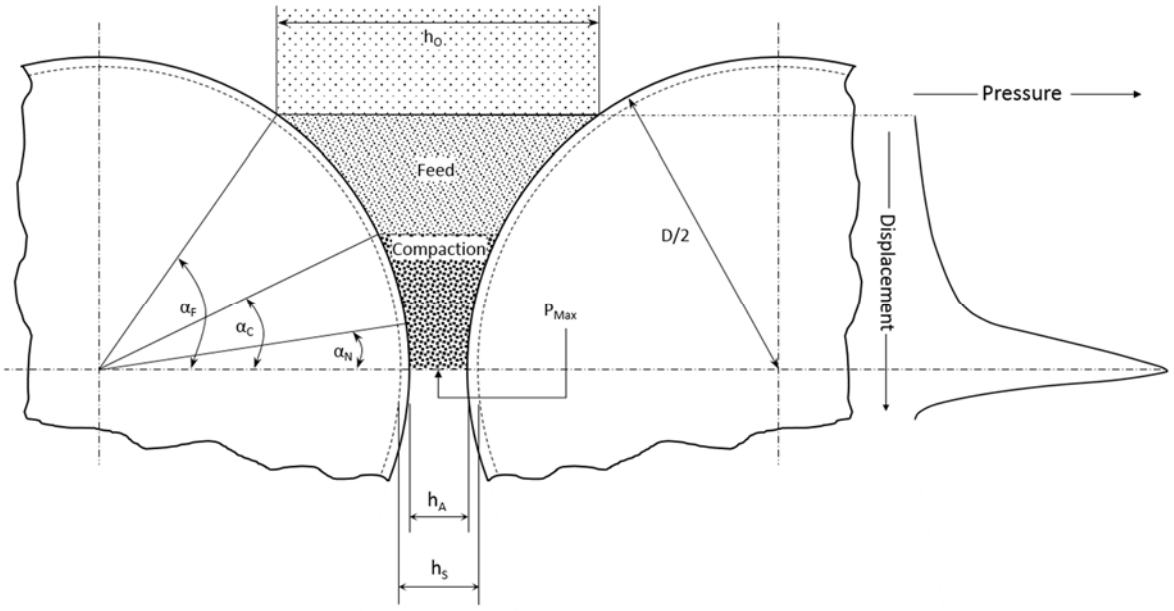



Figure 2-14. Schematic diagram of the nip region between two smooth counter-rotating rollers (modified from Pietsch, 2002 and Capes, 1980)

As previously stated, roll presses can be configured vertically, horizontally or at an incline. In any case, roll presses consist of three major components: a frame, a roller-pressurization system, and a feeding system. Two frame designs are commonly employed in roll press systems, which are distinguished by the position of the rollers with respect to the frame. A

common frame design for smaller machines is a cantilevered shaft assembly, where rollers are mounted in a bearing block on the end of a shaft that provides easy access for maintenance. This design is contrasted by a multi-shaft assembly, in which rollers are mounted in the middle of a shaft between two bearing blocks (Guigon & Simon, 2003). The roller and pressurization system is comprised of two countercurrent rotating rolls that are mounted to individual bearing blocks and driven by a fixed-speed or variable-speed motor with a reduction gear. Spacers are placed between the bearing blocks to prevent wear that would result if the rollers were touching. The rollers are brought into close contact by a hydraulic piston system, which in turn dictates the width of the gap between rollers.

A variety of feeding systems can be used to provide a continuous and uniform flow of material to the nip region of the rollers. For free-flowing solids in a vertical roll press configuration, gravity feed systems are often utilized. A device can also be installed upstream of the rollers in a gravity feed system to control the feed rate of material to the nip region (e.g. adjustable gate). In fine powder pressing applications, a force feeding system (e.g. tapered screw) is often required to deaerate, pre-compact and pressurize the feed as it enters the nip. In these systems, the feed rate to the nip can be precisely controlled by a variable-speed drive (Capes, 1980). An additional device can be installed to provide an even distribution of material to the screw (e.g. paddle feeder), which also assists in deaeration of the feed. Force feed systems are typically required in all horizontal and inclined press configurations.

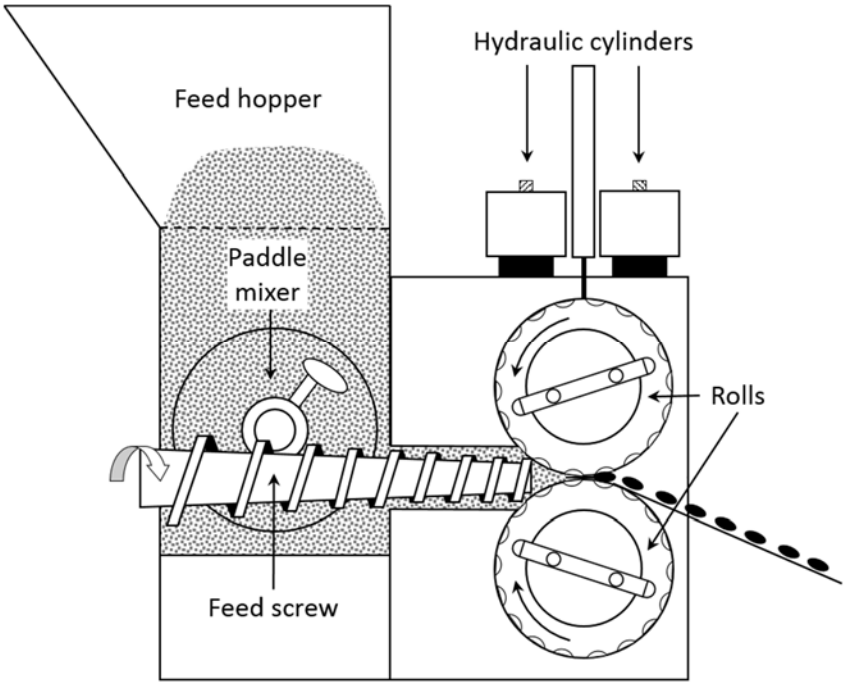



Figure 2-15. Komarek B-100R roll press schematic diagram (modified from Guigon & Simon, 2003)

Figure 2-15 shows the configuration of the Komarek B-100R laboratory roll press, which is commonly used for optimization and scale-up of briquette production processes. This machine is configured horizontally with two counter rotating rolls on cantilevered shafts, two hydraulic cylinders, a horizontal tapered screw and a paddle feeder. The hydraulic cylinders control the position of the upper roll and thus control the gap between the rolls. The paddle feeder is driven by a fixed speed motor and distributes the material to the horizontal screw that in turn feeds material to the rolls. The counter rotating rolls and the horizontal screw are driven by variable speed motors, which enable adjustment of the torque applied to the material from the rolls and screw.

Roll press compaction presents several advantages over other pressure agglomeration methods. For example, the configuration of roll press systems facilitates continuous production at very high capacities. When multiple units are operated in a parallel circuit, several hundred tonne per hour production rates can be achieved. Additionally, energy consumption is low since the only power consumed is for driving the rollers and, in feed force systems, for driving the screw. This results in low compaction costs, which is necessary in high tonnage industries such as fertilizer and mining/minerals, and in the compaction of waste materials. Finally, roll pressing can be used to process hot materials up to 1,000 degrees Celsius, which is often challenging with

other pressure agglomeration technologies (Guigon & Simon, 2003). However, there are also some challenges to roll press agglomeration. For instance, particulate solids can be lost by leakage in the nip region, which is typically addressed by installing a vacuum deaeration system to recover and recycle fines back to the feed. Deaeration systems serve a dual purpose by also improving agglomerate quality and production throughput. Further, geometry and stress distribution of briquettes produced in pocket rollers is more irregular than extruded products, which can lead to downstream handling issues.

#### 2.5.3.3 Solid Fuel Applications

The oldest and most common method of size enlargement and densification of solid fuels is pressure agglomeration. The growing demand for solid fuels in the 19$^{th}$ century led to a drastic increase in coal production throughout the western world, which in turn generated large quantities of unmarketable coal fines. In light of this development and the high cost of coal mining in Europe, significant effort was directed to the development of novel high-quality products from coal fines. Many different methods were developed to convert coal fines into marketable products by pressure agglomeration. These products, commonly referred to as briquettes, featured many advantages over particulate coal fines, including enlarged particle size, reduced dust losses, improved flow properties and increased bulk density (Pietsch, 2005). Coal briquette production reached a peak in the western world shortly after World War II. Due to growing environmental concerns surrounding smoke and other air pollution that resulted from the high content of tar and/or pitch used to bind coal fines together, a steep decline in coal briquette production occurred. Although several new applications for briquetting technology are currently being considered, industrial briquetting of solid fuels is at a historic low in the developed world (Pietsch, 2005).

Nonetheless, research interest in briquetting solid fuels has remained strong as the production of unmarketable coal fines has increased rapidly in the past 50 years. In addition, a tremendous emphasis has been placed on energy production from renewable resources throughout Europe and North America as traditional fossil fuel resources continue to deplete and greenhouse gas emissions continue to rise. As a result, hundreds of papers have been published over the past century that address the application of roll press briquetting to the densification of coal and biomass feedstocks. It is well beyond the scope of this review to attempt to summarize

all of the studies that have been conducted on these topics. Therefore, the following section will address select findings related to the influence of material variables and operating conditions on the quality of briquettes and recent developments in binder formulations.

Most early studies on coal briquetting focused on the improvement of briquette strength and durability by evaluating different types of binders. For example, Mills (1908) investigated a wide variety of organic and inorganic binders to produce satisfactory quality briquettes at the lowest possible price. The inorganic binders evaluated in this study included clay, lime, magnesia, magnesia cement, plaster of Paris (gypsum), Portland cement, natural cement, slag cement and water gas. Many more organic binders were tested, including wood products, sugar factory residues, starches, slaughter house refuse, tars and pitches from coal, natural asphalts and petroleum products, for a total of 35 different substances. It was found that organic binders generally improve the coherence of coal briquettes more than inorganic binders. However, due to the higher price of most organic binders, it was concluded that the selection of an ideal binder must be made based on the desired briquette quality for every specific application. In a more recent study, Taulbee et al. (2009) evaluated 50 binder formulations in the production of briquettes from blends of fine coal and sawdust. Based on the results of the study, guar gum and wheat starch were identified as the most suitable binders for the pulverized coal market and lignosulfonate/lime was identified as the best binder for the stoker market.

More recent studies have been focused on the effects of material properties and process conditions on the strength and durability of briquettes. For example, Taulbee et al. (2009) evaluated numerous briquetting parameters in the production of briquettes from blends of fine coal and sawdust. The parameters investigated include binder content, sawdust content, sawdust type, briquetting pressure and dwell time, coal and sawdust particle size, clay content, moisture content, cure temperature and cure time. It was found that binder content, sawdust content, sawdust type and curing conditions exerted the greatest influence on the quality of briquettes. In contrast, briquetting pressure and dwell time were found to have the smallest impact on briquette quality. In another study published by the same authors, Patil et al. (2009) investigated the effect of particle-size distribution on the production of briquettes from blends of coal fines and sawdust. Using a modified Proctor density test, it was determined that the packing density of coal-only blends reached a maximum with seventy to eighty percent coarse coal. However, the maximum compressive strength of the briquettes was found with one hundred percent fine

flotation coal. The packing density and compressive strength results for briquettes produced with sawdust were very similar. One difference in the results was that the greatest compressive strength of the coal-sawdust briquettes was obtained with twenty to fifty percent fine coal, rather than one hundred percent.

In another study, Mangena & du Cann (2007) investigated the effect of coal properties in binderless briquetting of various South African coking coals and weathered bituminous coals. The vitrinite-rich coking and blend coking coals were found to produce the highest quality binderless briquettes, which is thought to be a result of stronger bonding from the deformation and subsequent consolidation of the vitrinite macerals in the coals. It was also determined that weathering of bituminous coal fines has an adverse effect on the ability to produce good briquettes. The authors suggest that the negative influence of weathered coal fines can be alleviated by the addition of kaolinite to the coal feed prior to briquette production.

Another area of significant interest in recent years is lignite briquetting. Beker (1997) evaluated the effects of moisture content and briquetting pressure in production of briquettes from Turkish lignites and waste materials. The optimum moisture content and briquetting pressure were found to be 15% and 550 MPa, respectively. At these conditions, sawdust and paper mill waste were found to be good binders that produce briquettes with good strength and high calorific value. Furthermore, Beker et al. (1998) studied the optimization of briquetting conditions for blends of Turkish lignite and bituminous coals with and without binders. It was determined that the addition of bituminous coal decreased the mechanical strength of the lignite briquettes. In an effort to improve the strength of the briquettes, sawdust, sunflower shell and molasses were added as binders, which in turn increased the mechanical stability of the briquettes. Finally, it was found that all of the briquettes produced in this study were not water resistant, which imposes challenges for storage and transportation.

A continual topic of significant interest is the identification of cost-effective binders to improve the strength, durability and other qualities of fuel briquettes. This is largely due to the significant limitations of many traditional binders for solid fuel applications. For example, inorganic binders such as sodium silicate and bentonite increase the ash content and reduce the heating value of feedstocks. However, inorganic binders are generally less expensive than organic materials. Briquettes made using starch-based binders have poor water-proofing properties and tend to fall apart when exposed to moisture during transportation and storage

(Taulbee et al., 2010). Further, asphalt-based binders produce additional emissions when heated during thermochemical conversion processes. More importantly, conventional binders require a very high dose (5-10% by dry weight) to provide adequate strength and durability. These binders are usually derived from useful and often expensive raw materials; therefore, they add significantly to the overall cost of production. The high dose can be attributed to the fact that conventional binders are typically matrix or film type, which only perform an adhesive function by physically binding the coal particles together to form a large mass. No chemical reaction takes place to strengthen the bond between the binder and coal particles (Messman, 1977). Therefore, there is still a need to find improved binders for agglomeration applications.

During the past two decades, efforts to improve the quality of briquettes have been focused on improving the performance of conventional binders. Goleczka et al. (1988) invented a process for cold briquetting by using a binder composed of molasses and an inorganic hardening agent obtained from calcium carbonate, calcium phosphate, iron oxide and aluminum oxide. Hale et al. (1989) also disclosed a binder incorporating molasses/phosphoric acid and magnesium oxide. The briquettes produced with these mixtures showed good initial shatter resistance, improved hot compressive strength and excellent water resistance. Major and Radu (1998) disclosed a new synergistic binder composition composed of asphalt, sodium carbonate pulping liquor and nonylphenol ethoxylate that can produce a waterproof, self-curing briquette. White (1999) invented a binder that is produced by direct liquefaction of biomass with the addition of pyrolysis tar, petroleum asphalt, reinforcing fibers, extender, fillers, and cross-linking agents if necessary. Kriech and Dobbs (2003) recently disclosed a binder composition including a distillable petroleum hydrocarbon emulsified with a surfactant and water. This binder can increase the hydrophobic characteristics of coal particles and bring about a significant change in their chemistry. Grigorova and Kuzev (2003) tested starch modified with cophony as a brown coal briquetting binder for improved water resistance.

More recently, new methods for reducing binder dosage and for improving the bond strength at the binder-particle interface have been explored by some researchers. For example, Miller and Martin (1980) patented a new briquetting process that uses organic Lewis-base solvents to pretreat coal fines prior to compaction to produce coal briquettes without adding additional binders. The solvents claimed in this patent are capable of electron donor action, and include acetone, methyl ethyl ketone, and ethylene diamine. It is believed that an unassociated

electron pair may perform an important function in the interaction between the coal and the solvent. However, a large amount of solvent (20-50% by dry weight) is required for this process, which must be recovered and reused for the process to remain cost-effective. Studies have also been performed by adding liquid oxidants (e.g. $H_2O_2$) to coal tar to promote the release of oxygen radicals during curing and to strengthen the interfacial bonds between the binder and coal. The interfacial bonds can also be improved by adding other types of additives such as phosphoric acid (Plancher et al., 2002).

Another limitation to coal briquette production is the absorption of water and subsequent disintegration of briquettes during storage and transportation. In light of this difficulty, there is a growing interest in the development of economically feasible methods to sustain the physical and mechanical integrity of fuel briquettes in the presence of water, as evidenced by a number of publications on this topic (Wang et al., 2011; Motaung et al., 2007; Saglam et al., 1990). Several different methods have been investigated to improve the water resistance of fuel briquettes. The most commonly employed method is coating individual fuel particles with a chemical binder prior to briquette production. For example, Bratton et al. (2010) evaluated a novel fine coal briquetting process that included the application of a proprietary binder to improve the strength and weathering properties of coal briquettes. It was determined that a wetting and drying cycle had minimal impact on the durability of coal briquettes produced with the proprietary binder. However, the cost of the novel binder is not discussed and thus is likely a limiting factor to this approach. Furthermore, Taulbee et al. (2009) investigated twelve different binders including molasses, guar gum, corn starch, wheat starch and paper sludge to improve the strength and water resistance of briquettes produced with fine coal and sawdust. The study found that the compressive strength of the coal-sawdust briquettes was significantly reduced after submergence in water for eight hours. These and other water soluble binders are generally not recommended to improve the water resistance of fuel briquettes (Mills, 1908).

Another method that has been investigated to improve the water resistance of fuel briquettes is coating with water insoluble chemicals. Coating materials can be applied by many different techniques including dipping, brushing, flow coating, roller coating and spraying (Freitag, 1996). Of these methods, dipping and spraying present the greatest opportunity for fuel briquette coating due to the size and shape of briquettes. Both methods generally require heating the material to reduce the viscosity, which leads to a reduction in film thickness and thus a

reduction in chemical consumption. When the materials are heated prior to application, these techniques are referred to as hot dipping and hot spraying (Freitag, 1996).

Specific techniques for coating briquettes have been disclosed in patents filed in the United States and Australia. Goss (1938) patented a hot spraying mechanism for applying paraffin wax to wood briquettes for the purpose of protecting against the absorption of moisture. Lundwall (1939) developed a machine that employs the dipping technique to coat briquettes composed of metal cuttings with a mixture of water and Portland cement. Furthermore, Trechock (1973) described a spray coating method to overcome the problem of airborne dust associated with rail shipment of coke briquettes. Using this method, the briquettes are treated with an aqueous dispersion of solid film former such as sodium silicate, blackstrap molasses, turpentine resins and pitches derived from black coal or petroleum. Bates et al. (1988) disclosed a method of coating briquettes composed of brown coal, bituminous coal, anthracite or other carbonaceous materials such as wood. The patent describes a water based emulsion comprising an acrylic polymer based on acrylic ester monomer that can be applied by spraying or dipping. Finally, Shimasaki et al. (2003) developed a method of producing coal briquettes with high strength and excellent water resistance by mixing starch with the coal particles prior to briquette production and coating the surface of the briquettes with a heavy oil component simultaneously with or after briquette formation.

# SECTION II

# BRIQUETTING AND PELLETIZATION ACTIVITIES

# Chapter 3

# Briquette Characterization Methods

## 3.1 Abstract

A major limitation to industrial utilization of coal-biomass briquette feedstocks is the absence of standard methods to characterize important physical and mechanical properties of coal-biomass briquettes. To address this challenge, a detailed review of briquette properties was conducted to determine the most important properties for characterization of coal-biomass briquettes. The briquette properties that were identified as most significant are: (1) tensile strength, (2) crushing strength, (3) elasticity, (4) mechanical durability, (5) attritability, (6) friability, (7) water content, (8) particle density, (9) bulk density and (10) water resistance. Crushing strength and mechanical durability appear to be the most important of these properties, and thus should be measured for all experimental and industrial coal-biomass briquette formulations. The other identified properties are still very important and should be considered in detailed evaluations of coal-biomass briquettes when requested by a client or customer. Experimental evaluations were conducted to adapt, evaluate and refine established methods that appeared suitable for coal-biomass briquette evaluations by directly testing coal-biomass briquettes and analyzing the results. Additionally, work was conducted to develop novel characterization methods to quantify briquette properties when suitable established methods were not applicable or available. Recommendations are provided for specific methods and procedures to characterize coal-biomass briquettes based on the results of this study.

## 3.2 Introduction

### 3.2.1 Problem Statement

Co-utilization of biomass with coal in existing coal-fired facilities presents a unique opportunity to reduce greenhouse gas emissions and increase energy production from renewable resources. Significant interest in this opportunity has led to more than 150 coal-fired power

stations across the world co-firing biomass with coal on a commercial or trial basis as of 2009 (Fernando, 2009). These co-firing experiences have revealed a number of technical challenges including upstream issues, such as biomass availability, transportation, storage, and handling, as well as problems encountered during energy conversion, such as fouling, corrosion, inconsistent feeding and segregation (Basu et al., 2011; Sami et al., 2001). Recent studies suggest that many of these challenges can be mitigated by reconstituting coal-biomass mixtures into larger particles. Specifically, roll press briquetting has been investigated to produce homogeneous, free-flowing feedstocks that minimize handling and segregation problems often encountered with combustion and gasification systems (Taulbee et al., 2010; Honaker et al., 2005). However, a major limitation to industrial utilization of these feedstocks is the absence of standard methods to characterize important physical and mechanical properties of coal-biomass briquettes.

## 3.2.2 Briquette Properties

### 3.2.2.1 Strength and Durability

The most important and widely used indicator of briquette quality is the strength of bonds between particles (Pietsch, 2002). The only scientifically defined method to characterize the strength of briquettes that provides information on the fundamental nature of interparticle bonds is tensile strength measurement. Tensile strength is defined as the tensile force at failure divided by the cross-sectional area of the briquette. In cases where the briquette does not have a uniform shape, the area of the failure plane that results from this test can be used in place of cross-sectional area. Universal equations and theoretical models for approximation of the tensile strength of briquettes is discussed in detail by Pietsch (2002).

In practice, the tensile strength of briquettes can be accurately and reproducibly measured with a variety of specially designed and general purpose devices. Typically these devices are comprised of three main components for (1) gripping the sample, (2) applying a deforming load and (3) measuring the applied deforming load (Capes, 1980). Tensile strength measurement devices can include other features to measure deformation and peak load during testing, which can provide additional information about the strength and durability of particle bonds within a briquette. However, there is no standard device or procedure for measuring tensile strength due to the many different shapes and sizes of briquettes. In any case, the major issue concerning tensile strength measurement is the difficulty involved in mounting and gripping individual

briquettes without impacting the strength or integrity of the sample. Due to this difficulty, tensile strength measurement is rarely used to characterize briquettes in laboratory and industrial applications. Instead, a wide variety of industry-specific methods have been developed to simulate the forces that briquettes are subjected to during handling, transportation and storage. Unfortunately, the results obtained from these types of tests are empirical and not theoretically predictable because the fundamental failure mechanisms are not understood. Nonetheless, these types of strength and durability measurements are important to consider because of their simplicity and industrial acceptance.

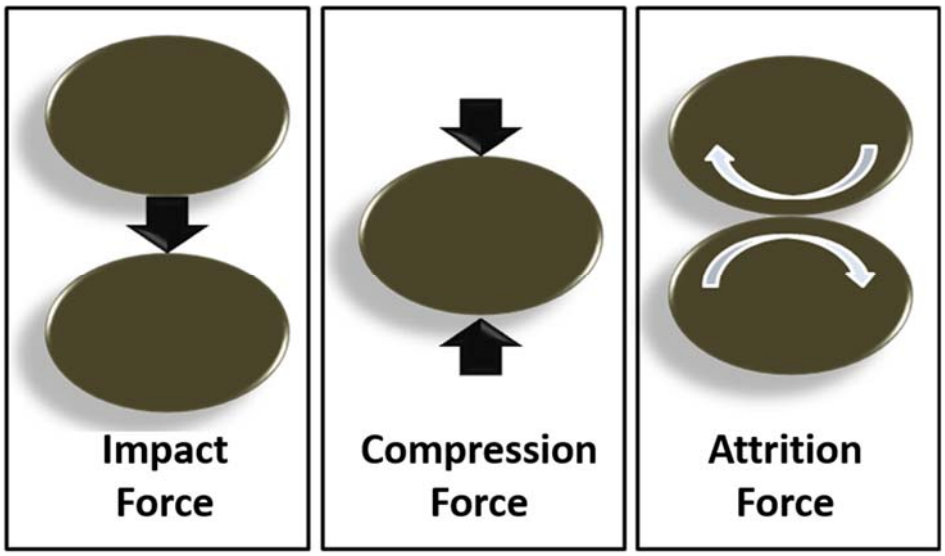



Figure 3-1. Forces briquettes encounter in handling, storage and transportation

Over the past several decades, researchers involved in the development of fuel briquette formulations and processes have reached a consensus regarding the most important physical properties that should be measured to indicate the quality of briquettes. The identified physical properties are friability, crushing (or break) strength, and attritability (Taulbee et al., 2010; Honaker et al., 2005; Richards, 1990; Eckerd, 1967; Moore, 1957; Prostel, 1953; Boley & Rice, 1949). The measurement of these three parameters can be used to indicate the extent to which briquettes will degrade during handling, transportation and storage. Briquettes continually experience impact forces, compression forces and attrition forces from production to utilization (Figure 3-1). Impact forces cause sudden breakage into small pieces from a sudden impact. These forces are encountered when briquettes drop in stockpiling, at conveyor transfer points and from bins and chutes. Friability is the term used to describe the tendency of an object to resist

impact forces. Briquettes can be crushed by compression forces encountered in bins, stockpiles and railcars from the load applied by other briquettes. Attrition is defined as wearing or grinding down by friction. Briquettes are subjected to attrition forces during transportation and at loading and unloading points.

Although researchers generally agree on the most important physical properties concerning briquette strength and durability, specific test methods to quantify these parameters are highly variable. It is common for researchers to independently develop assessment procedures appropriate to the nature of the particular investigations performed at their laboratories. For example, many researchers have designed assessment procedures for attritability and friability to mirror existing ASTM procedures for coal and coke, yet there is still very little consistency between the procedures employed at separate laboratories.

The only documented procedures that have been used to quantify the durability of coal-biomass briquettes are those that have been in use at the University of Kentucky's Center for Applied Energy Research (CAER) over the last decade. Taulbee et al. (2010) and Patil et al. (2009) describe methods to quantify the crushing strength and attritability of briquettes prepared from blends of biomass and fine coal. Patil et al. (2009) and Honaker et al. (2005) describe a drop test method that is used to determine the friability of briquettes made from blends of coal fines and sawdust. This method consists of averaging the number of drops to failure for four briquettes dropped from a height of 0.46 meters (1.5 ft) onto a steel plate. However, this method was eventually abandoned due to an inherently high level of data scatter and the time consuming nature of these evaluations. In addition, this method requires the technician to visibly determine when the briquette has split into two or more significant pieces, which is a subjective decision that could vary from one person to another.

The importance of friability measurement has also been realized by the coal industry. ASTM D440-07 (2012) describes a drop-shatter test for coal that was established to indicate the extent to which lump coal will break in conventional transit and handling operations. This standard specifies dropping fifty kilograms of coal from a box equipped with a false bottom that is positioned 1.83 meters (6 ft) above a steel plate. The coal is dropped from the box by releasing the false bottom, recovered from the steel plate and dropped a second time to further break the coal. The broken coal is then hand screened through nested sieves (203, 152, 102, 76, 51, 38, 25,

19, 13, 6, and 3 mm apertures). The results are reported as the mass percentage in each size class and the friability of each size class.

Taulbee et al. (2010) and Patil et al. (2009) describe a method to measure briquette crushing strength using either a Mark-10 EG-200 force gauge (890 N, 200 $lb_f$ capacity) or a Lloyd Instruments LRX Plus load cell (4,448 N, 1,000 $lb_f$ capacity). Each gauge is mounted to an automated test stand and equipped with a 19 millimeter (0.75 in) diameter plunger which travels downward at a rate of 25.4 millimeters (1 in) per minute. This ability to control the rate of loading is very important to ensure the accuracy and reproducibility of test results (Capes, 1980). The force gauges are configured with a break detect feature which stops the movement of the plunger once the applied force drops to 95 percent of the maximum force attained during the test. The plunger then reverses direction and the maximum force attained during the test is designated as the "compressive strength" of the briquette. Measurements are recorded along the axis used to apply force during briquette formation and reported values represent the average of a minimum of 15 measurements. Values less than 222 newtons (50 $lb_f$) are classified as poor, between 222 and 445 newtons (50-100 $lb_f$) as marginal, between 445 and 667 newtons (100-150 $lb_f$) as good, and greater than 667 newtons (150 $lb_f$) as excellent. Although the measurement recorded following this procedure provides important information regarding the strength of briquettes, the use of the term 'compressive strength' is not scientifically valid (Pietsch, 2002). A more appropriate term for this type of characterization method is crushing strength.

This test procedure can be easily adapted to measure the elasticity of individual briquettes, which is directly related to the application of compression forces. The elasticity of an object is its tendency to return to original shape after application of a deforming load (Sadd, 2009). When an elastic object is subjected to an external deforming load, the internal structure of the object opposes the deformation, and after the force is removed, restores the object to its original size and shape. Elasticity of a material can be expressed according to various elastic moduli, such as Young's modulus, shear modulus and bulk modulus. Each of these values are indicative of the inherent stiffness of a material for different types of deformation. For instance, the shear modulus applies to deformation in shearing and the Young's modulus applies to deformation that results from uniaxial compression or extension. The elasticity of many materials is defined by the linear relation between stress and strain, known as Hooke's law, which is described by:

$$F = -kx \quad \text{(Eq. 3-1)}$$

where $F$ is the force applied to an object, $x$ is the resultant internal displacement of the object, and $k$ is the rate or spring constant, which is an inherent material property. Due to the simplicity of this relationship, this appears to be a good approach to measure the elasticity of coal-biomass briquettes.

Taulbee et al. (2010) and Patil et al. (2009) also describe a method to measure forces that coal-biomass briquettes encounter in handling, and transportation, which is considered a measure of attritability. Following this procedure, 20 to 25 briquettes (approximately 200 grams) are placed into a 0.305 meter (1 ft) diameter Plexiglas cylinder equipped with three, 51 millimeter (2 in) lifters and tumbled for five minutes at 40 rotations per minute. The briquettes are then removed from the cylinder and screened through a 4.75-millimeter (U.S. Standard 4 mesh) sieve in a Ro-Tap sieve shaker for two minutes. The attrition index ($A_I$) is calculated by:

$$A_I = m_r/m_i \quad \text{(Eq. 3-2)}$$

where $m_r$ is the mass of briquettes retained on the 4.75-millimeter sieve and $m_i$ is the initial mass of the briquettes prior to testing. By this method, attrition indices less than 0.80 are considered poor, between 0.80 and 0.90 are considered marginally acceptable, between 0.90 and 0.95 are considered good and greater than 0.95 are considered excellent. This method is a good measure of briquette durability but it is not a measure of true attritability. Attrition is defined as wearing or grinding down an object by friction, and this test method incorporates impact forces in addition to attrition forces. Therefore, this test method will be referred to as "mechanical durability" from this point forward to conform with the terminology used in EN 15210-2 (2010), which presents a standard method for determining the mechanical durability of biomass briquettes by tumbling in a similar device. However, an additional method to measure the true attritability of coal-biomass briquettes should still be considered. In addition to these important properties indicative of briquette quality, there are several other feedstock properties that should be considered for co-firing processes.

#### 3.2.2.2 Moisture Content

Moisture content is an important property because the evaporation of moisture during energy conversion consumes a significant amount of the deliverable energy in a feedstock. Therefore, moisture content must be known to properly design a system for minimal energy loss (Basu, 2010). Determination of coal-biomass briquette moisture content is complicated by its

presence in two separate forms: surface (free) moisture and inherent (equilibrium) moisture. As the name implies, surface moisture is the moisture present on the surface of the coal or biomass particles, which is ordinarily deposited during processing, transportation and storage. In contrast, inherent moisture is the moisture absorbed within the coal matrix or biomass cell walls (Speight, 2005). Total moisture is defined as the sum of the surface and inherent moisture and can be expressed on a wet basis or a dry basis. The wet basis moisture content of coal and biomass is calculated as:

$$M_{wet} = 100\big((m_{wet} - m_{dry})/m_{wet}\big) \quad \text{(Eq. 3-3)}$$

where $M_{wet}$ is the wet basis moisture content expressed as a percentage, $m_{wet}$ is the wet weight and $m_{dry}$ is the dry weight (Basu, 2010). The dry basis moisture content is calculated as:

$$M_{dry} = 100\big((m_{wet} - m_{dry})/m_{dry}\big) \quad \text{(Eq. 3-4)}$$

where $M_{dry}$ is the dry basis moisture content expressed as a percentage. Finally, the wet basis and dry basis moisture contents are related as:

$$M_{dry} = M_{wet}/(100 - M_{wet}) \quad \text{(Eq. 3-5)}$$

ASTM D3302/D3302M-12 (2012) specifies a standard procedure for determining and reporting the total moisture in coal. In this method, coal samples are dried at 107 ± 3 degrees Celsius in a drying oven until constant mass is achieved. Constant mass is defined as a change in mass less than or equal to 0.1 percent of the total loss in mass over a period of one hour. The total moisture of the coal sample ($M$) is calculated by:

$$M = [R(100 - ADL)/100] + ADL \quad \text{(Eq. 3-6)}$$

where $R$ is the residual moisture weight percent and $ADL$ is the air dry loss weight percent, which is calculated as the loss in weight in air drying divided by the gross sample weight.

Similarly, ASTM E871-82 (2006) specifies a method for determining and reporting the moisture content of wood fuels, wherein a sample is dried in an oven at 103 ± 1 degrees Celsius until the total weight change of the sample varies less than 0.2 percent over a period of two hours. The moisture content of wood fuels ($M$) is calculated by:

$$M = 100 \times \big(m_i - m_f\big)/(m_i - m_c) \quad \text{(Eq. 3-7)}$$

where $m_i$ is the initial sample mass, $m_f$ is the final sample mass and $m_c$ is the mass of the drying container. Finally, EN 14774 (2009) specifies a method for determining and reporting the total moisture content of solid biofuels. In this method, biofuel samples are dried at 105 ± 2 degrees Celsius in a drying oven until constant mass is achieved. Constant mass is defined by this

standard as a change in mass less than or equal to 0.2 percent of the total loss in mass over a period of one hour. The total as-received moisture content ($M_{ar}$) of solid biofuels is calculated by:

$$M_{ar} = 100 \times (m_2 - m_3 + m_4)/(m_2 - m_1 + m_4) \quad \text{(Eq. 3-8)}$$

where $m_1$ is the mass of the empty container, $m_2$ is the mass of the drying container and sample before drying, $m_3$ is the mass of the drying container and sample after drying and $m_4$ is the mass of the moisture associated with packing. It is often useful to report moisture content as a fraction rather than a percentage. In such a case, the term 'water content' is used to describe the amount of water present in a sample of interest. Water content ($w$) is calculated by:

$$w = m_w/m_s \quad \text{(Eq. 3-9)}$$

where $m_w$ is the mass of water in the sample and $m_s$ is the mass of dry solids. This relationship is particularly useful when examining the relationship between the water content and density of compacted solids. Thus, the total amount of water present in coal-biomass briquettes will be calculated by Equation 3-9 and reported as water content throughout the remainder of this study.

#### 3.2.2.3 Particle and Bulk Density

Density is another important property to consider for briquette production and utilization. This property is particularly important when sizing a gasifier and feed conveyor to meet desired production. Density must also be considered for operations upstream of the gasifier such as fuel transportation, bulk handling and storage (Graboski & Bain, 1981). The density of coal-biomass briquettes can be reported as particle density and bulk density, depending on the method that the volume of the material is calculated and reported. Particle density (or apparent density) of briquettes is a measure of the mass per unit volume occupied by individual briquettes, including pores and cracks (Mahajan & Walker, 1978). This property is particularly important for briquettes and other agglomerates because strength and durability typically increase with particle density (Pietsch, 2002). To calculate particle density, the total mass is divided by the external volume of the briquette (Basu, 2010).

For regularly shaped particles, stereometric methods can be used to approximate the external volume of a sample to calculate particle density. In contrast, the density of irregularly shaped particles can be determined by liquid or solid displacement methods. Density determination by solid displacement can be accomplished with a powder pycnometer, in which the apparent volume of a sample is determined by the displacement of a powder. Liquid

displacement methods (hydrostatic and buoyancy) are based on the Archimedes principle, which states that the buoyancy of an object immersed in a fluid is equal to the weight of the fluid that the body displaces. According to the hydrostatic method, the mass of liquid displaced by a sample is recorded and particle density ($\rho_p$) is calculated by:

$$\rho_p = (m_{air}/m_{dis})\rho_w \quad \text{(Eq. 3-10)}$$

where $m_{air}$ is the weight of the sample in air, $m_{dis}$ is the weight of the liquid displaced by the sample and $\rho_w$ is the density of the liquid. In the buoyancy method, the buoyancy of a sample is determined by measuring the difference between the mass of the sample in air and the apparent mass of the sample while submerged in a liquid of known density. By this method, particle density ($\rho_p$) is calculated by:

$$\rho_p = (m_{air}/(m_{air} - m_w))\rho_w \quad \text{(Eq. 3-11)}$$

where $m_{air}$ is the weight of the sample in air, $m_w$ is the weight of the sample in liquid and $\rho_w$ is the density of the liquid. According to Rabier et al. (2006), liquid displacement methods are more accurate and precise than stereometric methods for the determination of the particle density of fuel briquettes, which often vary in size and shape.

A standard method for measuring the particle density of biomass pellets and briquettes using the buoyancy method is presented in EN 15150 (2011). This standard describes an apparatus and procedures to calculate the particle density of pellets (diameter ≤ 25 millimeters) that is easily adaptable to coal-biomass briquette evaluations. The apparatus consists of a balance, a density determination rig and a glass beaker (Figure 3-2). The density determination rig consists of a bridge platform, a supporting frame and a submergence tray. The supporting frame rests on the weight cell of the balance and the bridge platform is placed over the supporting frame and the balance so that neither are loaded by the bridge. The glass beaker is filled with water, placed on the bridge platform and the submergence tray is hung from the supporting frame into the glass beaker. The bottom of the submergence tray must have perforated openings to allow liquid to fill the dish from below during submergence. In addition, the submergence tray must be positioned so that it does not touch the bottom or sides of the glass beaker. Typically, brackets can be installed along the top of the supporting frame that form a narrow groove for the submergence tray to rest in place.

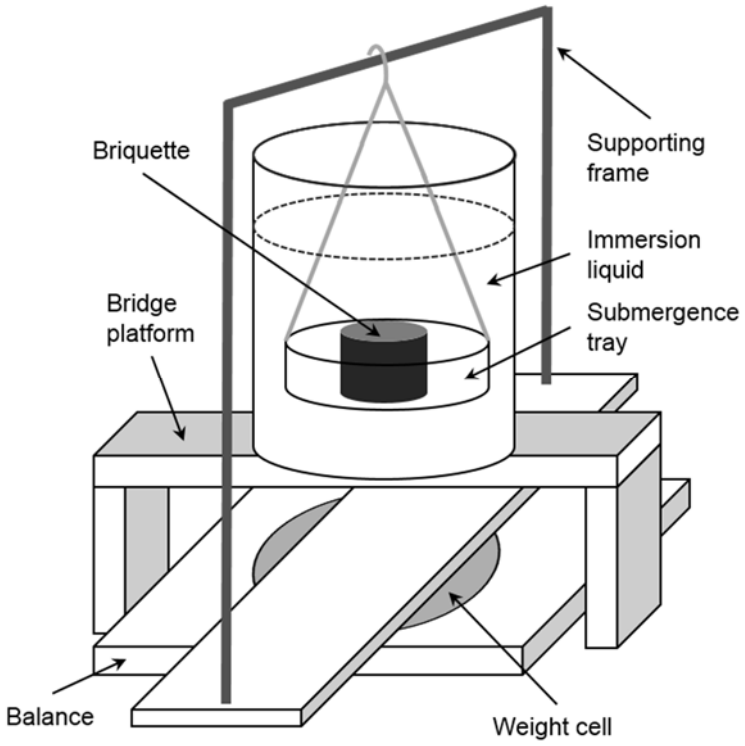



Figure 3-2. Apparatus for measurement of particle density specified in En 15150 (2011)

After assembly of the apparatus is complete, the scale must be tared with the empty submergence tray in place. The mass of four pellets is recorded to the nearest 0.001 grams by placing them on the supporting frame. Next, the submergence tray is removed from the supporting frame and the four pellets are placed in the tray. The tray is then carefully placed back in the groove between the brackets of the supporting frame to submerge the pellets in the liquid. While the pellets are submerged, the mass on the balance display is recorded to the nearest 0.001 grams. Due to the hygroscopic nature of biomass particles, the standard recommends recording the mass reading from the balance immediately after submergence to prevent water absorption and disintegration. The mass should be recorded approximately three to five seconds after placing the tray back on the supporting frame when the reading on the balance display reaches a constant value. Immediately after recording the mass of the submerged pellets, the submergence tray is lifted off of the supporting frame and out of the glass beaker to prevent contamination of the liquid by disintegration of the pellets. This procedure is repeated for nine additional four-pellet samples for a total of ten replications and the moisture content of a portion of the initial sample material is calculated according to EN 14774 (2009). Finally, the particle density of the pellets at a given moisture content ($\rho_p$) is calculated as:

$$\rho_p = (m_a/(m_a - m_l))\rho_l \quad \text{(Eq. 3-12)}$$

where $m_a$ is the weight of the pellets in air, $m_l$ is the weight of the pellets while submerged in water and $\rho_l$ is the density of the liquid in which the pellets are submerged.

Due to the rapid disintegration of many briquette formulations in water and the surface tension present at the briquette-water interface, it is recommended in EN 15150 that a wetting agent is added to the water and/or a coating agent is applied to the surface of the briquette prior to submergence. The recommended wetting agent is t-Octylphenoxypolyethoxyethanol; polyethylene glycol tertoctylphenyl ether (trade mark Triton X-100®) at a concentration of 1.5 grams per liter of water and the recommended coating agent is paraffin wax with a melting point of 52 to 54 degrees Celsius. However, Rabier et al. (2006) determined that if a coating agent is applied before submersion in liquid, a correction for the amount of the coating agent penetrating the sample is required. A simple assumption that all of the coating agent remains outside of the briquette is unacceptable. Therefore, a correction factor must be derived using a powder pycnometer or similar device. However, the authors did not find any improvement in the precision or accuracy of results when using paraffin wax to coat samples. Therefore, it was concluded that applying the coating agent and correcting for the amount that penetrates the sample is not worth the additional effort.

Bulk density is a measure of the mass per unit volume occupied by a group of particles, including interstitial volume between the particles (Berkowitz, 1994). Many factors influence bulk density, including particle density, particle size and shape, surface and inherent moisture, and degree of compaction (Speight, 2005). The bulk density of coal-biomass briquettes is an important property to consider from a materials handling and storage perspective. This property is used to predict the required size of bins and hoppers and to predict the flow behavior of solids. Contrary to the common misconception in many industries, bulk solids do not simply have loose and packed densities. Rather, they exhibit a range of bulk densities that is a function of the consolidating pressure applied to the material. For highly compressible materials, this range of values is often expressed as a straight line on a log-log plot of consolidating pressure versus bulk density, where the slope of the line is the compressibility of the material. The results obtained from this test can be used to properly design processing, storage and transfer equipment to accommodate desired production capacities.

Several different standard methods are available for measuring bulk density that could be applicable to coal-biomass briquette evaluations. These methods include ASTM D291-07 (2012), which covers the determination of cubic foot weight of crushed bituminous coal, ASTM E873-82 (2013), which covers the determination of bulk density of densified particulate biomass, and ASTM D6683-08 (2008), which covers the measurement of bulk density of powders and other bulk solids as a function of compressive stress. The concept of bulk density measurement is fairly simple in all of these methods: the mass of bulk solids that occupies a standard volume container (i.e. 1 $ft^3$) is measured and the bulk density is calculated as mass divided by volume. This relationship is formally written as:

$$\rho_b = m_t / v_c \quad \text{(Eq. 3-13)}$$

where $\rho_b$ is the bulk density, $m_t$ is the total mass and $v_c$ is the total volume of the container. According to ASTM D291-07 (2012), the uncompacted bulk density of coal samples is determined by discharging coal into a one cubic foot box from a conical hopper situated one foot and ten inches above the bottom of the box. Excess material is removed from the box using a straight edge and the bulk density is determined by measuring the weight of the filled box. Similarly, ASTM E873-82 (2006) specifies the measurement of bulk density of densified particulate biomass fuels, in which material is poured into a one cubic foot box from a height of two feet above the top edge. The box is then dropped five times onto a nonresilient surface from a height of six inches and excess material is removed from the box using a straight edge. Finally, the bulk density of the biomass fuel is calculated by dividing the net weight of the sample by the volume of the measuring box.

#### 3.2.2.4 Water Resistance

The absorption of water and subsequent disintegration of coal-biomass briquettes is a major limitation to the design of low-cost storage and transportation systems for co-firing operations. As a result, water resistance is a very important property to consider for the production and utilization of coal-biomass briquettes. Over the years, many methods have been reported in the literature for measuring the water resistance of fuel briquettes. For example, Wright (1911) measured the water absorption tendency of coal briquettes by immersing them in water for varying time periods up to several weeks. The results of this test are reported as the time immersed, the total percentage of water absorbed and the percentage of water absorbed in

the first four days of the test. Similarly, Richards (1990) adopted a water immersion test to evaluate the water absorption and disintegration of coal briquettes. By this method, briquettes are immersed in water for thirty minutes and then weighed to measure the mass of water absorbed. The results are reported qualitatively with respect to tendency and time to disintegrate, in addition to percent absorption. Yildirim & Ozbayoglu (2002) measured the water resistance of coal briquettes by immersing briquettes in water for 24 hours. After drying, the percentage of minus 10 millimeter material was reported as the water disintegration index. Finally, Taulbee et al. (2009) measured the water resistance of briquettes composed of fine coal and sawdust by submerging four briquettes in water for eight hours, curing overnight in an environmental chamber and measuring the compressive strength the following day. Each of these methods involve submerging briquettes in water for an extended period of time. While these provide a good foundation for further development of water resistance test methods for coal-biomass briquettes, it is unlikely that briquettes will ever be fully submerged in water. Further, it is unlikely that there will ever be an economically feasible method to waterproof briquettes, which is what these multi-hour submergence tests truly measure. Therefore, efforts of this study will be directed toward development of a method to measure water resistance during some type of simulated rainfall event.

### 3.2.3 Research Objective

Many different methods are reported in the literature to characterize various physical and mechanical properties of coal and biomass feedstocks. However, a major limitation to industrial utilization of coal-biomass briquette feedstocks is the absence of standard characterization methods. Therefore, the objective of this research was to adapt, evaluate and refine established methods that appear suitable for coal-biomass briquette evaluations by directly testing coal-biomass briquettes and analyzing the results. Additionally, work was conducted to develop novel characterization methods to quantify briquette properties when suitable established methods were not applicable or not available. Ultimately, the results of this study will be used to develop a manual of standard test methods and procedures to guide industrial characterization of coal-biomass briquette formulations.

## 3.3 Experimental

### 3.3.1 Materials

All briquettes produced for this study were composed of bituminous coal and milled biomass. The two bituminous coals used in this study were obtained from preparations plants in the Appalachian coal basin of the eastern United States. Specifically, the coal samples were obtained from Alpha Natural Resources' Emerald mine preparation plant in Waynesburg, Pennsylvania (referred to as Emerald coal) and Alpha Natural Resources' McClure River preparation plant in McClure, Virginia (referred to as McClure River coal). The Emerald coal was obtained from the clean coal stockpile at the preparation plant and was subjected to further processing prior to briquette production. Size reduction of the Emerald coal was accomplished by successive crushing in a jaw crusher, roll crusher and grinder. The coal was then screened to a top size of one millimeter using a Uniflex two-deck screen, air-dried for one week, split into two-kilogram lots and stored in sealed plastic bags. The moisture content of the coal prior to briquette production was 1.60% (dry basis), which was determined by oven drying at 105 degrees Celsius for 24 hours. The size distribution of the crushed coal was measured by wet screening and analyzed using the Rosin-Rammler equation (Figure 3-3). Based on this analysis, the Emerald coal was found to have a mass median diameter of 301 microns, a size modulus of 0.43 and a distribution modulus of 1.02. Ultimate and proximate analyses were also conducted to characterize the chemical composition of the Emerald coal (Table 3-1). Notable results of the analyses include a moisture and ash free heating value of 35,513 kJ/kg (15,268 Btu/lb), an ash content of 9.37% (dry basis) and a sulfur content of 3.04% (dry basis).

The McClure River coal was a clean coal flotation product sampled from a vacuum disk filter in the preparation plant. This coal was air-dried for one week prior to briquette production to reach a total moisture content of 1.10% (dry basis). The size distribution of this coal was also measured by wet screening and analyzed using the Rosin-Rammler equation (Figure 3-3). Based on this analysis, the McClure River coal was found to have a mass median diameter of 73 microns, a size modulus of 0.10 and a distribution modulus of 1.09. Ultimate and proximate analyses were also conducted to characterize the chemical composition of the McClure River coal (Table 3-1). Notable results of the analyses include a moisture and ash free heating value of

36,574 kJ/kg (15,724 Btu/lb), an ash content of 10.50% (dry basis) and a sulfur content of 0.88% (dry basis).

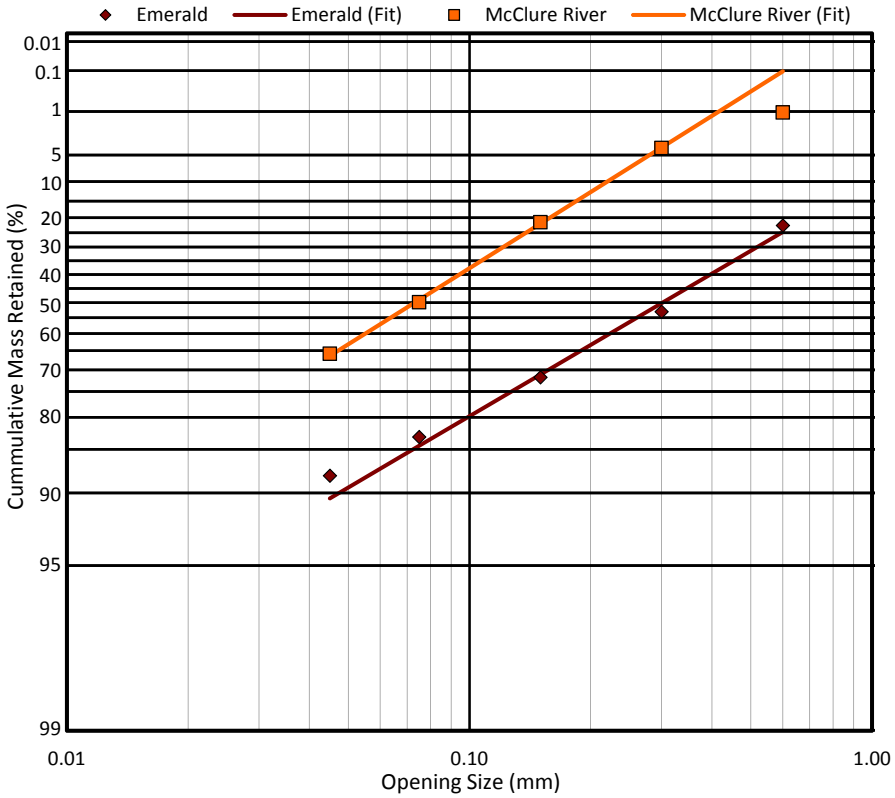



Figure 3-3. Particle-size distribution of bituminous coals

Table 3-1. Chemical properties of coal and biomass feedstocks

| Chemical Property | Emerald Coal | | McClure River Coal | | Corn Stover | | Switchgrass | |
|---|---|---|---|---|---|---|---|---|
| | As Received | Dry Basis | As Received | Dry Basis | As Received | Dry Basis | As Received | Dry Basis |
| Moisture (%) | 4.28 | -- | 28.38 | -- | 12.95 | -- | 14.79 | -- |
| Ash (%) | 8.97 | 9.37 | 7.52 | 10.50 | 4.36 | 5.01 | 2.44 | 2.86 |
| Sulfur (%) | 3.04 | 3.18 | 0.63 | 0.88 | 0.09 | 0.10 | 0.07 | 0.08 |
| Volatiles (%) | 37.59 | 39.27 | 20.25 | 28.28 | 71.49 | 82.13 | 70.37 | 82.58 |
| Fixed Carbon (%) | 49.16 | 51.36 | 43.85 | 61.22 | 11.19 | 12.86 | 12.41 | 14.56 |
| Carbon (%) | 74.26 | 77.58 | 58.91 | 82.26 | 46.37 | 53.27 | 41.59 | 48.81 |
| Hydrogen (%) | 4.91 | 5.13 | 6.58 | 4.75 | 4.94 | 5.67 | 6.32 | 7.04 |
| Nitrogen (%) | 1.39 | 1.45 | 1.12 | 1.56 | 0.54 | 0.62 | 0.35 | 0.30 |
| Oxygen (%) | 3.15 | 3.29 | 25.24 | 0.05 | 30.75 | 35.33 | 41.58 | 48.57 |
| HHV (kJ/kg) | 30,808 | 32,185 | 23,444 | 32,734 | 16,347 | 18,778 | 16,082 | 18,873 |
| MAF HHV (kJ/kg) | -- | 35,513 | -- | 36,574 | -- | 19,769 | -- | 19,429 |

The biomass used for this study was milled switchgrass and corn stover. The switchgrass sample was obtained as large round bales from Piedmont Bioproducts in Gretna, Virginia. The bales were successively processed through a Sperry New Holland tub grinder (Figure 3-4a) and a Bliss Industries hammer mill (Figure 3-4b) equipped with a 6.35 millimeter screen, and stored in a sealed bulk bag prior to use. Particle-size distribution was not determined for the switchgrass sample because previous attempts to collect this information has indicated that the results are skewed due to the elongated particle shape of milled grass (i.e. elongated particles tend to screen differently than round particles). Prior to briquette production the moisture content of the switchgrass was 17.50% (dry basis), which was determined by oven drying at 105 degrees Celsius for 24 hours. Ultimate and proximate analyses were conducted on the switchgrass sample with the results presented in Table 3-1. Notable results of the analyses include a moisture and ash free heating value of 19,429 kJ/kg (8,353 Btu/lb), an ash content of 2.86% (dry basis) and a sulfur content of 0.08% (dry basis).



(a) (b) (c)

Figure 3-4. Equipment used for biomass size reduction: (a) tub grinder (b) hammer mill and (c) knife mill

The corn stover used for this study was obtained as large round bales from a farm in Blacksburg, Virginia operated by Virginia Tech. The bales were processed in a Jordan Reduction Solutions knife mill (Figure 3-4c) equipped with a 4.76 millimeter screen and stored in a sealed bulk bag prior to use. Again, particle-size distribution was not determined due to the inherently low accuracy of the procedure. Prior to briquette production the moisture content of the corn stover was 11.35% (dry basis), which was determined by oven drying at 105 degrees Celsius for 24 hours. The ultimate and proximate analyses results for the corn stover sample are also

displayed in Table 3-1. Notable results of the analyses include a moisture and ash free heating value of 19,769 kJ/kg (8,499 Btu/lb), an ash content of 5.01% (dry basis) and a sulfur content of 0.10% (dry basis).

### 3.3.2 Briquette Production

Pill-shaped briquettes (approximately 43 x 19 x 14 mm) were produced with a Komarek B-100R laboratory roll press equipped with 13-centimeter diameter rolls. The machine is comprised of two counter-rotating rolls, two hydraulic cylinders, a horizontal tapered screw and a paddle feeder (Figure 3-5). The hydraulic cylinders control the position of the upper roll and thus control the gap between the rolls. The paddle feeder is driven by a fixed speed motor and distributes the material to the horizontal screw that in turn feeds material to the rolls. The counter-rotating rolls and the horizontal screw are driven by variable speed motors, which enable adjustment of the torque applied to the material from the rolls and screw.

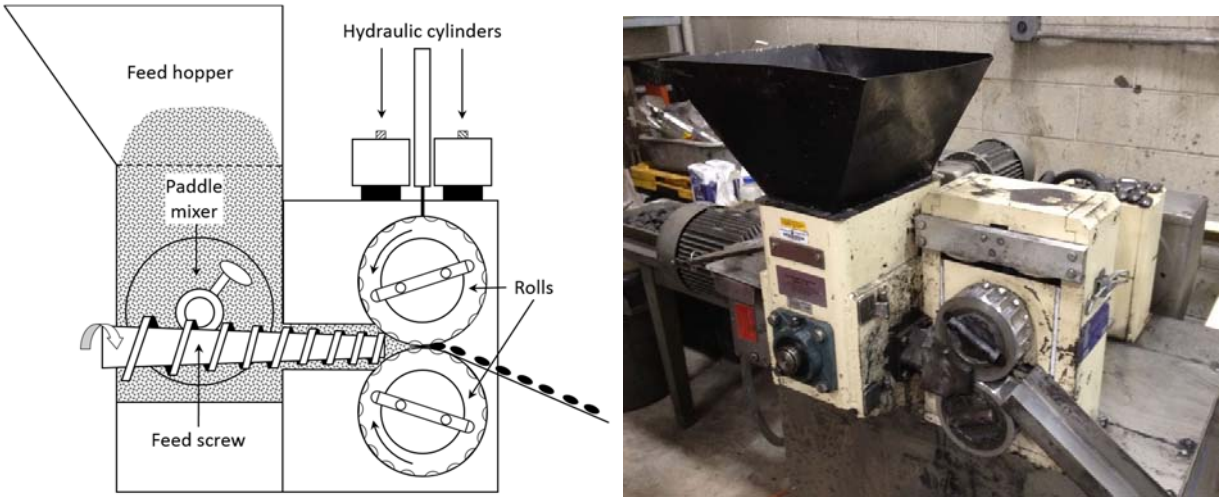
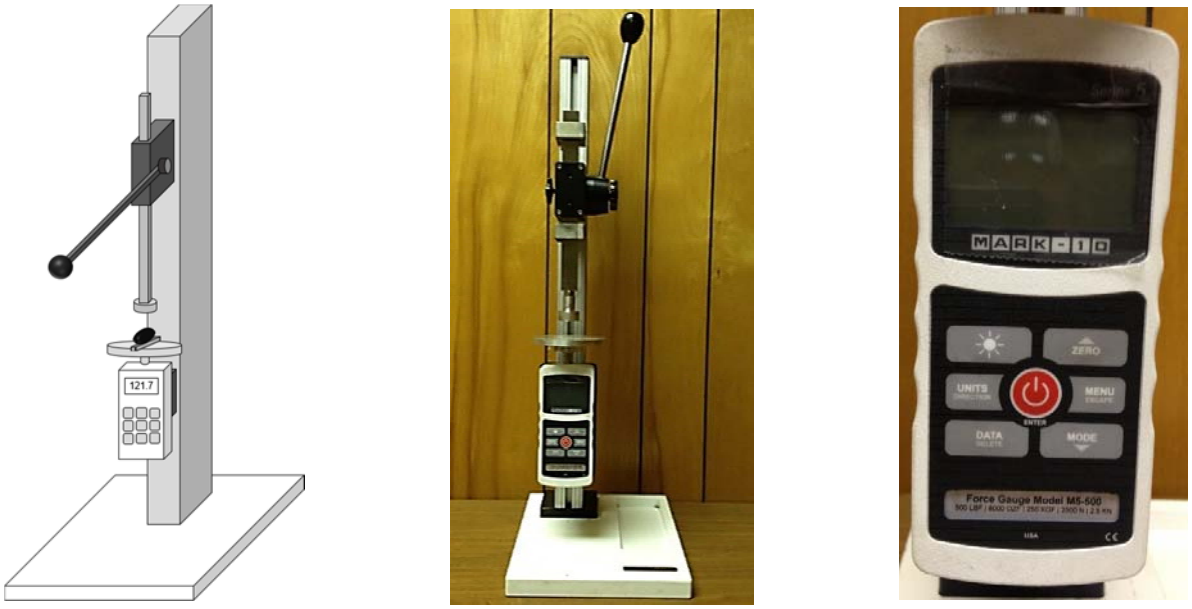



Figure 3-5. Komarek B-100R roll press (a) schematic diagram (modified from Guigon & Simon, 2003) and (b) laboratory installation

For all laboratory experiments, the rolls of the B-100R were driven at a motor speed of 450 rotations per minute with a hydraulic force of 100 kilonewtons. The horizontal screw speed was adjusted during briquette production to maintain a roll torque of approximately 1,500 to 1,800 newton-meters. Two types of briquettes were produced for this study, based on the availability of materials at the time of evaluations: (1) Emerald coal – corn stover briquettes (referred to as EM-CS) and (2) McClure River coal – switchgrass briquettes (referred to as MR-

SG). In both cases, the briquettes were produced in five-kilogram batches with 20% biomass (dry basis) and 80% bituminous coal (dry basis). The coal and biomass were mixed for five minutes in a Hobart A200 18.9 liter (5 gal) commercial mixer and directly co-briquetted in the Komarek B-100R. Immediately after formation, the briquettes were screened across a Sweco vibrating separator equipped with a 12.7 millimeter (0.5 in) screen to remove excess fines. Finally, the briquettes were stored in sealed 18.9 liter (5 gal) buckets for 24 hours prior to use for evaluating the configuration of several characterization methods.




(a) (b) (c)

Figure 3-6. (a) Mark-10 force gauge and test stand schematic drawing, (b) Mark-10 TSA750 manual test stand and force gauge installation and (c) Mark-10 M5-500 digital force gauge

## 3.3.3 Evaluation and Refinement Procedures

### 3.3.3.1 Tensile Strength

A Mark-10 M5-500 digital force gauge with a 2,224 newton (500 $lb_f$) capacity and 0.4 newton (0.1 $lb_f$) resolution was used to evaluate several indirect tensile strength measurement techniques. As shown in Figure 3-6, the force gauge was fitted with a 101.6 millimeter (4 in) diameter aluminum plate and mounted to a Mark-10 TSA750 manual test stand. The manual test stand has the advantage of lower capital investment, but the precision of this device is inferior to an automated test stand. For evaluations, the digital force gauge was configured with a break detect feature that stopped data acquisition once the applied force dropped to 95 percent of the

maximum force attained during each test. The tensile strength of each briquette was then reported as the maximum force attained during each test. Evaluations were performed on 25 EM-CS briquettes for each indirect tensile test and the tensile strength was reported as the average of the 25 values.

Several different plungers and briquette configurations were evaluated to determine the most significant and repeatable method to indirectly measure the tensile strength of coal-biomass briquettes. Figure 3-7 shows each configuration that was tested with different plunger types and briquette orientations. Initially, two diametrical compression tests were performed on the EM-CS briquettes, in which force was applied between two parallel plates to briquettes along the axis of formation (i.e. the axis between the two roller pockets during formation). The first of these tests was performed with the briquette standing 'tall' with the long axis parallel to the axis of force application during the evaluation (Figure 3-7a). The second test was performed with the briquette standing 'short' with the long axis perpendicular to the axis of force application (Figure 3-7b).

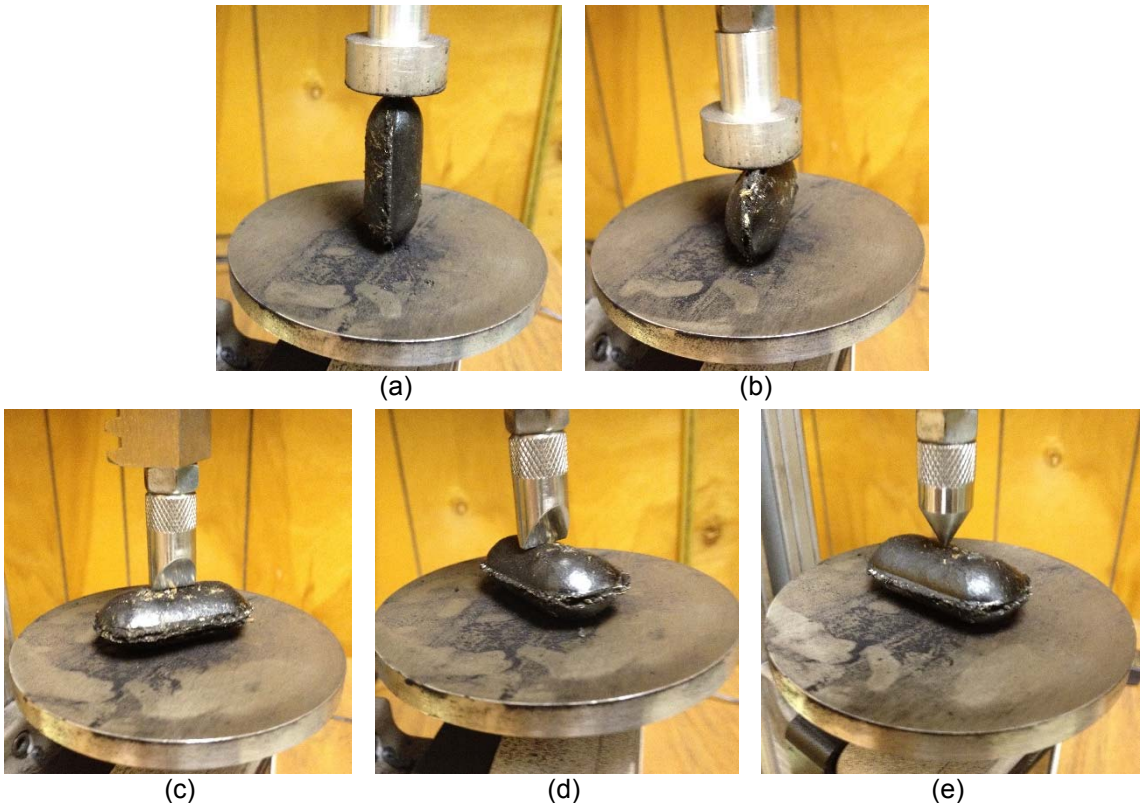



Figure 3-7. Briquette orientations and plungers utilized for indirect tensile strength tests: (a) 'tall' diametrical compression, (b) 'short' diametrical compression, (c) parallel wedge indentation, (d) perpendicular wedge indentation and (e) point indentation

In addition, three indention tests were performed by applying a force to the smooth 'pocket' surface of the briquettes. The first two indention tests were performed with a wedge-shaped indention tool that was applied parallel to the long axis of the briquette (Figure 3-7c) and perpendicular to the long axis of the briquette (Figure 3-7d). The final test configuration employed a conical indention tool (Figure 3-7e) to apply a point load to the center of briquettes. Results of these evaluations are presented in Section 3.4.1.

#### 3.3.3.2 Crushing Strength

To evaluate and refine the crushing strength test method reported by Taulbee et al. (2010) and Patil et al. (2009), the Mark-10 digital force gauge and test stand configuration was again utilized. In this instance, the test stand was fitted with a 25.4 millimeter (1 in) cylindrical aluminum plunger that was used to apply force to the center of the pocket surface of briquettes until failure (Figure 3-8). The gauge was again configured with a break detect feature that stopped data acquisition once the applied force dropped to 95 percent of the maximum force attained during each test. The crushing strength of each briquette was then reported as the maximum force attained during each test. Evaluations were performed by crushing 50 MR-SG briquettes to determine the precision of results obtained from this method and any improvements that could be made. Results of these evaluations are presented in Section 3.4.2.



(a) (b)

Figure 3-8. Briquette orientation and plunger utilized for crushing strength tests (a) prior to crushing and (b) after crushing

#### 3.3.3.3 Elasticity

To measure the elasticity of coal-biomass briquettes using the fundamental theory presented by Hooke's Law (i.e. Equation 3-1), the same equipment and procedure that was

described for crushing strength evaluations was utilized. However, in this instance the test stand was fitted with a Mark-10 ESM001 digital travel display to record the displacement of briquettes while the load was applied by the plunger (Figure 3-9a). This installation was required to determine the spring constant (*SC*) of the briquettes, which is calculated by:

$$SC = (F_2 - F_1)/(x_2 - x_1) \quad \text{(Eq. 3-14)}$$

where $F_2$ is the maximum force applied during elastic deformation, $F_1$ is the minimum force applied during elastic deformation, $x_2$ is the displacement that corresponds with $F_2$, and $x_1$ is the displacement that corresponds with $F_1$ (see Figure 3-9b). These values are obtained from the force versus displacement curve that is produced during testing. The force gauge was configured to record two force and displacement data points per second with the break detect feature activated. To improve the accuracy of readings, an aluminum bar (51 x 8 x 8 mm) was placed upon the aluminum plate with each briquette then placed atop and parallel to the bar for testing (the motivation for this approach is discussed in detail in Section 3.4.2).

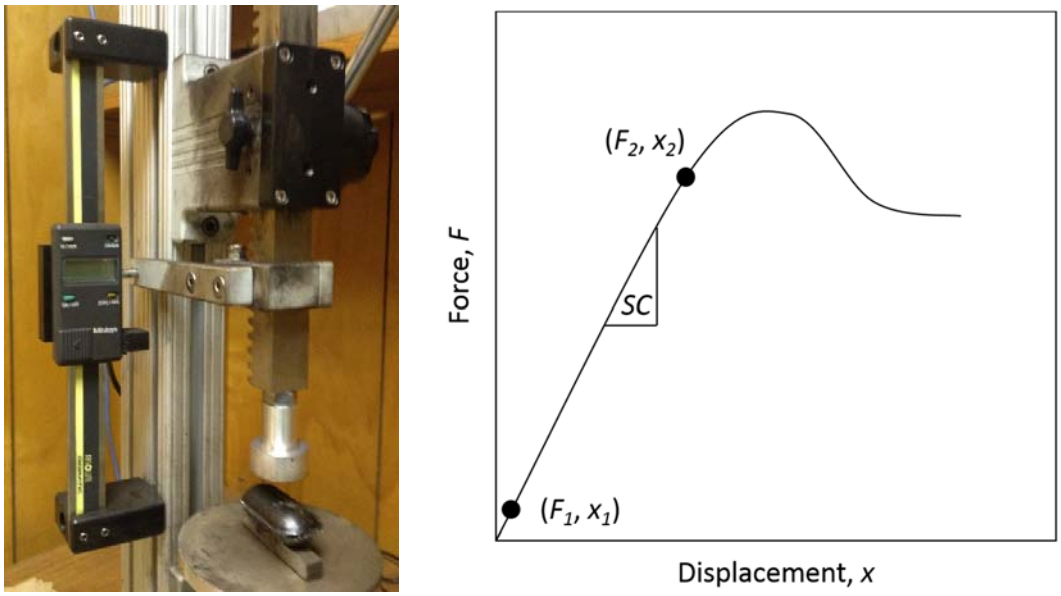



Figure 3-9. (a) Mark-10 ESM001 digital travel display fitted to the manual test stand for elasticity tests and (b) force-displacement data point selection example

Evaluation of this method was conducted to determine the impact of data point selection on the calculated spring constant values (i.e. selection of $F_1$ and $F_2$ from the force-displacement curve in Figure 3-9b). The selection of the ($F_2$, $x_2$) data point is complicated because it is often difficult to determine the upper extent of the linear portion of the curve due to the low sampling frequency (i.e. two samples per second) and the inherent error from using a manual test stand.

Therefore, two separate approaches were evaluated for selection of the ($F_2$, $x_2$) data point to determine the method that provides the best combination of accuracy and precision: (1) selection of a force-displacement data point that appears to form the upper extent of the linear portion of the curve (as shown in Figure 3-9b) and (2) selection of the peak force-displacement data point (i.e. yield point). The inherent advantage of the first method is that the calculated spring constant is derived from the elastic deformation (i.e. linear) portion of the force-displacement curve. However, the inherent disadvantage of this approach is the ambiguity of selection of the upper extent of the linear portion of the curve. In contrast, the inherent advantage of the second approach is that the force-displacement data point can be easily selected from identifying the maximum force attained during each individual test. However, the disadvantage associated with this method is that the calculated spring constant values are fundamentally inaccurate because the peak force typically occurs after a period of inelastic deformation that exists beyond the elastic (linear) displacement region. Nonetheless, both methods were evaluated by crushing 25 EM-CS briquettes, recording the two prescribed sets of data points, and calculating the spring constant using Equation 3-14. Finally, each of the 25 values were averaged and the spring constant was reported as the calculated average value. Results of these evaluations are presented in Section 3.4.3.

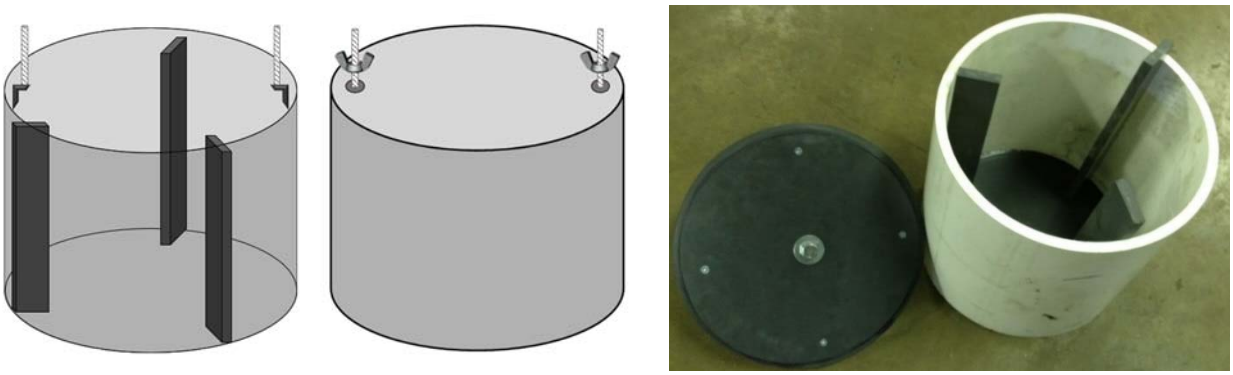
#### 3.3.3.4 Mechanical Durability

Evaluation of the attritability characterization method reported by Taulbee et al. (2010) and Patil et al. (2009) was performed using a 0.305 meter (1 ft) diameter PVC cylinder equipped with three 50.8 millimeter (2 in) lifters (Figure 3-10). As previously discussed, this method is a good measure of briquette durability but it is not a measure of true attritability. Therefore, this test method is now referred to as “mechanical durability” to conform to the terminology used in EN 15210-2 (2010) and to differentiate between this briquette characteristic and true attritability. To evaluate the configuration of the mechanical durability test, several series of experiments were designed to determine the influence and optimum conditions of three key process variables. The variables studied were the number of cylinder rotations, the cylinder rotational speed (rpm) and the number of briquettes loaded into the cylinder. For each experiment, MR-SG briquettes were tumbled under prescribed conditions and subsequently screened over a 4.75-millimeter

sieve in a Ro-Tap sieve shaker for two minutes. The mechanical durability (*MD*) of the briquettes was then calculated by:

$$MD = 100 \times \left(m_{final}/m_{initial}\right) \quad \text{(Eq. 3-15)}$$

where $m_{final}$ is the mass of briquettes retained on the 4.75-millimeter sieve and $m_{initial}$ is the initial mass of the briquettes prior to durability testing. Results of these evaluations are presented in Section 3.4.4.



(a) (b)

Figure 3-10. Mechanical durability cylinder (a) schematic drawing and (b) laboratory installation

#### 3.3.3.5 Attritability

Due to the lack any published methods to measure true attritability of briquettes, a novel method was developed to measure the attritability of coal-biomass briquettes. The principle of this method is that a group of briquettes are screened in a Ro-Tap sieve shaker for a prescribed period of time over a specified sieve size. During this screening period in the sieve shaker, the briquettes are subjected to true attrition forces as they continually rub against one another and the inside surface of the sieve. This action produces frictional forces that wear the briquettes down over time. Using this method, the attritability (*A*) of briquettes is calculated by:

$$A = 100 \times \left(m_{final}/m_{initial}\right) \quad \text{(Eq. 3-16)}$$

where $m_{final}$ is the mass of briquettes retained on the sieve after the screening period and $m_{initial}$ is the initial mass of the briquettes prior to attritability testing. Optimization of this method was accomplished by conducting evaluations on MR-SG briquettes to determine the ideal configuration of three key variables: (1) the number of briquettes loaded on the sieve during testing, (2) the screening time employed and (3) the sieve size used for screening. Results of these evaluations are presented in Section 3.4.5.

#### 3.3.3.6 Friability

A modified version of the ASTM shatter test device was built to evaluate the applicability of ASTM D440-07 (2012) to characterize the friability of coal-biomass briquettes (Figure 3-11). The machine was built with a PVC box (0.20 x 0.20 x 0.20 m, 0.67 x 0.67 x 0.67 ft) equipped with a false bottom that held the briquettes prior to drop testing. The box rests above a 25.4 millimeter (1 in) thick, 0.57 meter (22.5 in) diameter steel plate with a wooden frame placed on it. The wooden frame (0.35 m [14.0 in] tall x 0.39 m [15.3 in] long x 0.39 m [15.3 in] wide) is used to contain the briquettes after contact with the steel plate. Evaluations were performed with MR-SG briquettes to maximize the precision and significance of the results obtained from this method by evaluating the influence of various drop heights and the number of briquettes dropped. After two sequential drops the MR-SG briquettes were screened over a 4.75-millimeter sieve in a Ro-Tap sieve shaker for two minutes to determine the friability of the briquettes ($F$), which was calculated by:

$$F = 100 \times \left(m_{final}/m_{initial}\right) \quad \text{(Eq. 3-17)}$$

where $m_{final}$ is the mass of briquettes retained on the 4.75-millimeter sieve and $m_{initial}$ is the initial mass of the briquettes prior to friability testing. Results of these evaluations are presented in Section 3.4.6.



Figure 3-11. Modified ASTM shatter test device for friability testing

#### 3.3.3.7 Water Content

Since each of the identified standard methods for determining water content are based on the same fundamental principle and employ very similar methods, the decision was made to measure the water content of coal-biomass briquettes by drying at 105 ± 4 degrees Celsius in a drying oven for 24 hours. To evaluate the precision of such measurements, the water content of six EM-CS briquettes was calculated after 24 hours using Equation 3-9, and the standard deviation of the results was determined. To evaluate the accuracy of water content measurements after a period of 24 hours, the six briquettes were placed back into the oven for an additional two hours to determine the change in the calculated water content value with additional drying time. After this period of time, the briquettes were reweighed and the water content was again calculated. Finally, the results of this second measurement (i.e. 26 hour drying period) and the 24 hour drying period were compared. These results are presented and discussed in Section 3.4.7.

#### 3.3.3.8 Particle Density

To measure particle density of briquettes, an apparatus was constructed to record the apparent weight of an individual briquette while submerged in a liquid of known density (Figure 3-12). The design of this apparatus and the procedure followed were adapted from the buoyancy method outlined in EN 15150 (2011). The rig constructed for briquette evaluations is slightly larger than that described in EN 15150, but is composed of the same three major components: (1) a frame that rests on the weight cell of a balance and supports a submergence tray, (2) a submergence tray with perforations in the bottom to allow the liquid to fill the dish, and (3) a bridge platform that supports a glass beaker filled with liquid that overstretches the weight cell of the balance to prevent loading by the beaker. To measure the particle density of briquettes, the scale was tared with the empty submergence tray in place and the mass of individual briquettes was determined by placing them on the supporting frame. Next, the submergence tray was removed from the supporting frame and the briquette was placed in the tray. The tray was then carefully placed back in the groove between the brackets of the supporting frame to submerge the briquette in the liquid. During the first three to five seconds of submergence when the reading on the balance display reached a constant value, the mass on the balance display was recorded to the nearest 0.01 grams. Immediately after recording the mass of the submerged

briquette, the submergence tray was lifted off of the supporting frame and out of the glass beaker to prevent contamination of the liquid by disintegration of the briquette.

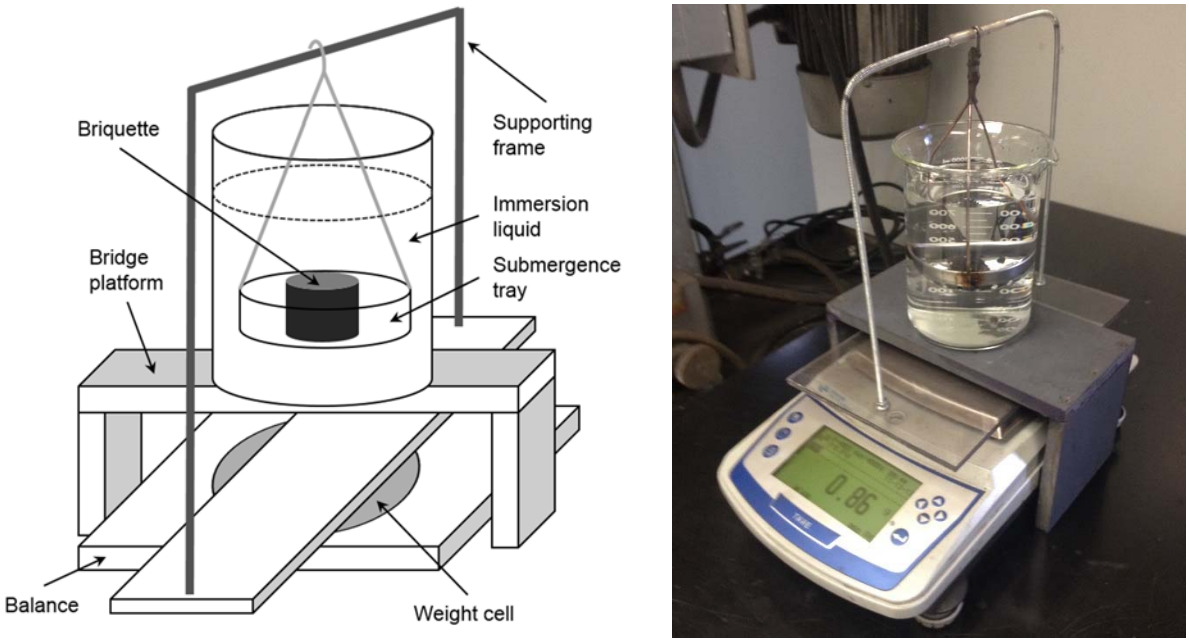



Figure 3-12. Particle density apparatus (a) schematic drawing and (b) laboratory installation

The buoyancy of each briquette was calculated by subtracting the sample's apparent mass in water from its measured mass in air. The particle density ($\rho_p$) is then calculated by:

$$\rho_p = \rho_w \times m_a/(m_a - m_b) \quad \text{(Eq. 3-18)}$$

where $m_a$ is the mass of the briquette in air, $m_b$ is the mass of the briquette in water and $\rho_w$ is the density of the immersion liquid. A number of configurations were evaluated to determine the most accurate and precise method to measure particle density of coal-biomass briquettes. For each configuration, the mass of 12 EM-CS briquettes was recorded in air and apparent mass was measured in water to calculate the average wet particle density, the standard deviation and the relative standard deviation. Initially, water was used as the submergence liquid to determine if any wetting agent or coating was necessary. Next, Triton® X-100 was added to the water at a concentration of 1.5 grams per liter to determine if any improvement could be made by adding a wetting agent. Due to the complexity of continually heating paraffin wax for coating briquettes, an aerosol polyurethane was evaluated instead for its potential applicability. A final set of tests was conducted with the combination of water, Triton® X-100 and the polyurethane. Results of these evaluations are presented in Section 3.4.8.

### 3.3.3.9 Bulk Density

A major problem with adapting standard bulk density measurement methods to laboratory evaluations of coal-biomass briquettes is the large amount of briquettes required to occupy a one cubic foot container. This corresponds to a substantial amount of materials, which require time-consuming preparation (i.e. crushing, screening and drying) prior to briquette production. As a result, three wooden containers were constructed with varying volumes (6.80 x $10^{-3}$ $m^3$ [0.24 $ft^3$], 1.42 x $10^{-2}$ $m^3$ [0.50 $ft^3$], 2.83 x $10^{-2}$ $m^3$ [1.00 $ft^3$]) to determine if a smaller container can be used to obtain accurate bulk density measurements for coal-biomass briquettes (Figure 3-13). Each containers was designed with cubic interior dimensions for simplicity (i.e. 0.24 $ft^3$ = $7.5^3$ $in^3$, 0.50 $ft^3$ = $9.5^3$ $in^3$, 1.00 $ft^3$ = $12.0^3$ $in^3$). For each container size, multiple measurements were recorded to determine the precision of the bulk density results.



Figure 3-13. Boxes of varying size for bulk density measurement: (left) 1 $ft^3$, (middle) 0.50 $ft^3$ and (right) 0.24 $ft^3$

To measure bulk density, EM-CS briquettes were poured into the wooden containers of known mass from a height of 0.61 meters (2 ft) above the bottom of the interior of the container. As shown in Figure 3-14a, sufficient material was poured so that the briquettes overflowed the top of the container. Next, a straight edge was used to remove the overflowing material from the top of the container. This was accomplished by swiping the straight edge along the top of the container from left to right, top to bottom, right to left and bottom to top until the straight edge no longer came into contact with any briquettes (Figure 3-14b). The container was then reweighed and the bulk density was calculated by:

$$\gamma = \left(m_f - m_e\right)/V_c \qquad \text{(Eq. 3-19)}$$

where $\gamma$ is bulk density, $m_f$ is the mass of the filled container, $m_e$ is the mass of the empty container and $V_c$ is the volume of the container. This procedure was repeated a minimum of six times to measure the apparent bulk density of the EM-CS briquettes for each container size. Results of these evaluations are presented in Section 3.4.9.



(a) (b) (c)

Figure 3-14. (a) Initial briquette overflow for bulk density measurement (b) bulk density container after removing excess briquettes with a straightedge and (c) weight platform assembly for compressibility measurement

Bulk compressibility was measured by applying an increasing consolidation pressure to EM-CS briquettes loaded into the 6.80 x $10^{-3}$ $m^3$ (0.24 $ft^3$) container. To accomplish this, the briquettes were initially poured into the container from a height of 0.61 meters (2 ft) above the bottom of the interior of the container. Next, a straight edge was used to remove the overflowing material from the top of the container as previously described. Weights were then added in 2.27 kilogram (5 lb) increments to a platform that rests on top of the briquettes and fits inside the cubic container as the briquettes are compressed (Figure 3-14c). The container was then topped off with additional briquettes by again pouring from a height of two feed above the bottom of the interior of the container and the straight edge was again used to remove the overflowing material in the same manner described above. To calculate the compressibility of the briquettes, the container was reweighed after each successive 2.27 kilogram addition to determine the apparent change in bulk density with confining pressure. Results of these evaluations are also presented in Section 3.4.9.

### 3.3.3.10 Water Resistance

A device was constructed to measure the water resistance of coal-biomass briquettes that simulates precipitation that briquettes may encounter during storage and transportation (Figure 3-15). The device consists of a perforated stainless steel platform upon which briquettes are placed. The platform sits above a sump which contains fresh water. A pump was used to cycle the water from the sump through a pipe and out a spray nozzle located approximately 0.46 meters (1.5 ft) above the briquettes. The pump was equipped with a variable frequency drive so the flow rate of water onto the briquettes could be controlled. Finally, a flow meter was installed in the pipe to enable measurement of the water flow rate.

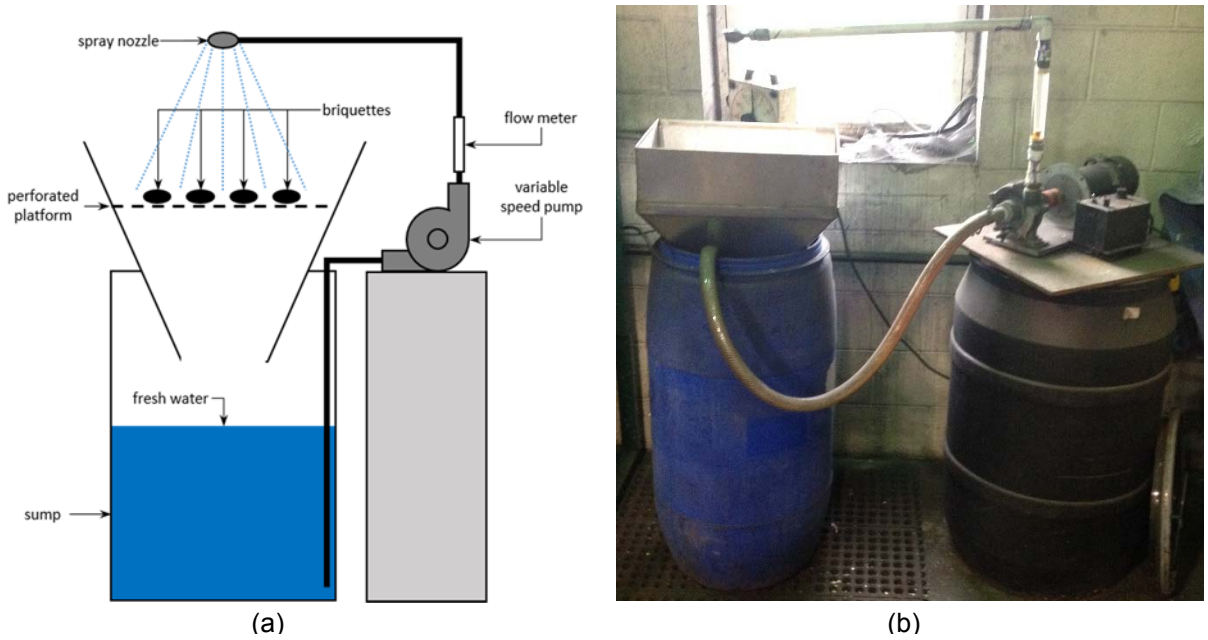



Figure 3-15. Water resistance apparatus (a) schematic drawing and (b) laboratory installation

Using this device, the water resistance of coal-biomass briquettes was defined as the water absorbed during a specified duration of water spray (i.e. water uptake), which is reported as a percentage of the initial mass of briquettes. To measure water uptake, the mass of a specified number of briquettes was initially recorded. Next, the briquettes were placed on a filter paper which was then placed on the perforated platform of the device (Figure 3-16). The filter paper was used to retain any pieces of the briquettes that become loose during the simulated precipitation that would otherwise wash down into the sump. The pump was then started at a specified speed to achieve a desired flow rate through the spray nozzle. After a specified period

of time, the pump was turned off and the filter paper with the briquettes was removed from the perforated platform. Finally, the briquettes were removed from the filter paper and the wet mass of the briquettes was recorded after a period of one minute. The water uptake ($WU$) is then calculated by:

$$WU = 100 \times \left(m_{wet} - m_{dry}\right)/m_{dry} \quad \text{(Eq. 3-20)}$$

where $m_{dry}$ is the initial mass of the briquettes prior to testing and $m_{wet}$ is the final mass of briquettes after the spraying period.



Figure 3-16. Example of briquette arrangement on filter paper for water resistance measurement

A series of tests were conducted to determine the optimal spray duration, water flow rate and number of briquettes for water uptake evaluations. The first group of tests was conducted on lots of 5, 10, 20 and 40 EM-CS briquettes at a water flow rate of 11.4 liters per minute (3 gal/min) with a spray duration of 15 seconds to determine the effect of the number of briquettes tested on water uptake measurements. The next series of tests were conducted on lots of five briquettes with spray durations of 5, 15, 30, 60 and 120 seconds at a water flow rate of 11.4 liters per minute (3 gal/min) to determine the impact of spray duration on water uptake measurements. The final series of tests were conducted on lots of five briquettes with water flow rates of 3.8, 7.6, 11.4, 15.1, and 18.9 liters per minute (1, 2, 3, 4, and 5 gal/min) with a spray duration of 15 seconds to analyze the impact of water flow rate on water uptake measurements. Results of these evaluations are presented in Section 3.4.10.

## 3.4 Results and Discussion

### 3.4.1 Tensile Strength

The recorded strength values for each of the five indirect tensile strength tests are presented in Figure 3-17. The average force reading was 244.9 N (55.0 $lb_f$) for the tall diametrical compression tests, 239.6 N (53.9 $lb_f$) for the short diametrical compression tests, 578.4 N (130.0 $lb_f$) for the parallel wedge tests, 500.9 N (112.6 $lb_f$) for the perpendicular wedge tests and 212.6 N (47.8 $lb_f$) for the point indention tests. The average force reading from the point indentation test and the two diametrical compression tests were very similar. In contrast, the results from the two wedge indention tests were very different from the other three tests, yet similar to one another. None of the distributions of results presented in Figure 3-17 closely resemble a normal distribution. However, the results of the tall diametrical compression tests are most similar to a normal distribution, which indicates that this method gives the most precise results. At this point, it is unknown whether or not any of the values obtained from these indirect tensile strength tests fundamentally describe the cohesive strength of individual particles within the briquettes. Nonetheless, it is possible that the true tensile strength of the tested briquettes falls within one of the ranges of similar values (i.e. 212.6-244.9 N [47.8-55.0 $lb_f$] or 500.9-578.4 N [112.6-130.0 $lb_f$]).

If tensile strength measurement of coal-biomass briquettes is desired in future applications, the tall diametrical compression test would be recommended. However, additional investigations should be conducted to develop a more suitable method to obtain theoretically significant tensile strength results and to determine if any data manipulation could improve the measured results. Although tensile strength is the only material property that describes the fundamental nature of bonds between particles in a material, this property is rarely measured in practical and industrial applications. As a result, a wide variety of industry-specific methods have been developed to simulate the forces that briquettes are subjected to during handling, transportation and storage, which are important to consider because of their simplicity and industrial acceptance.

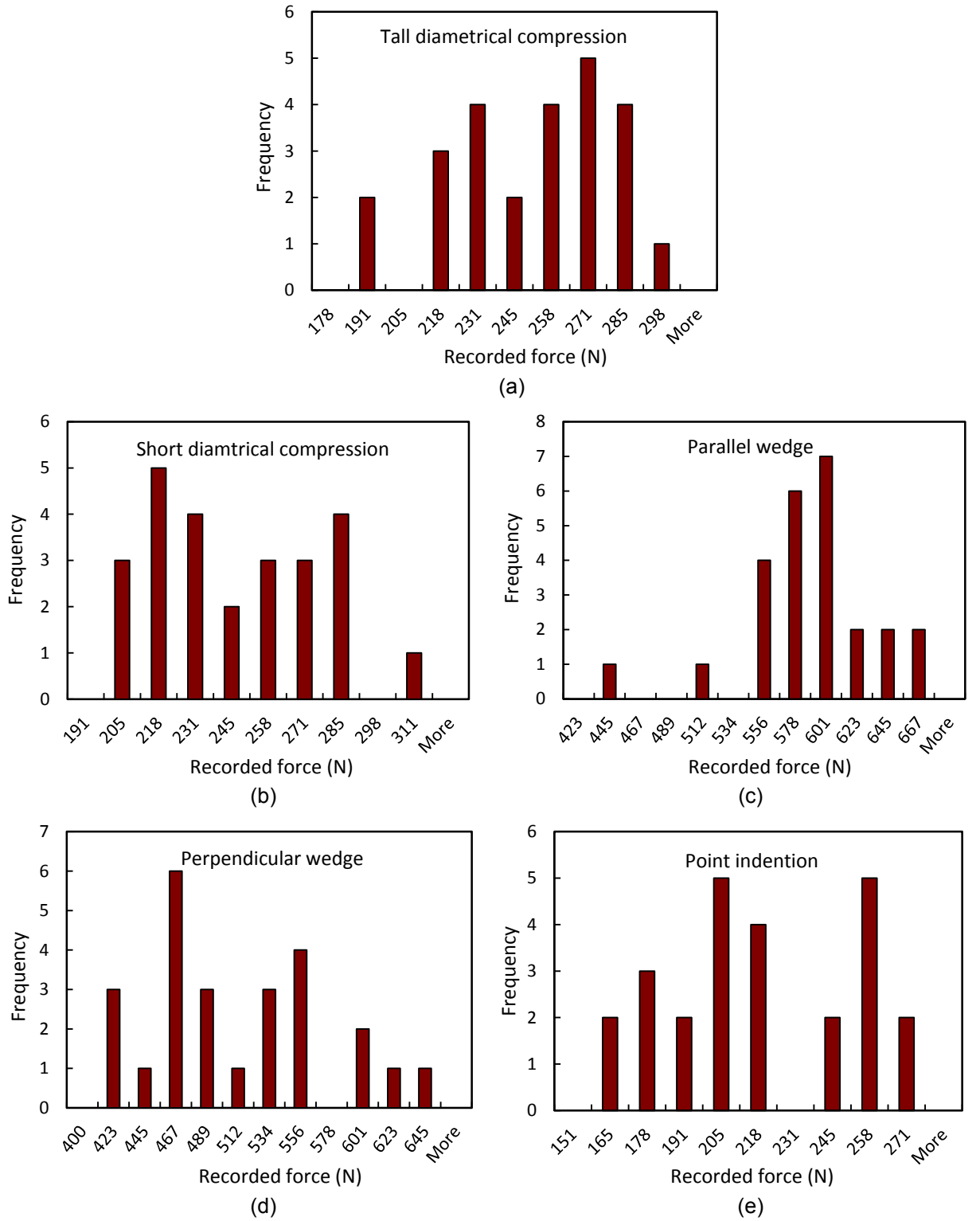



Figure 3-17. Distribution of indirect tensile strength results for (a) point indentation test, (b) parallel wedge indentation test, (c) perpendicular wedge indentation test, (d) tall diametrical compression test and (e) short diametrical compression test

### 3.4.2 Crushing Strength

To evaluate the precision of the crushing strength test method reported by Taulbee et al. (2010) and Patil et al. (2009) when conducted with a manual test stand rather than an automated test stand, 50 MR-SG briquettes were tested. The distribution of recorded briquette crushing strength values are presented in Figure 3-18. It can be seen that there is considerable scatter in the data and the results do not fit a normal distribution. The crushing strength values ranged from 46.3 to 2,454.1 N (10.4-551.7 $lb_f$) with a mean of 1,134.3 N (255.0 $lb_f$) and a standard deviation of 762.9 N (171.5 $lb_f$). The block of 27 data points depicted on the right side of Figure 3-18 represent the large number of briquettes for which the break detect feature of the machine did not detect briquette failure. When failure was not detected by the force gauge, the briquette was further compressed and the value obtained from the test was much higher than the true crushing strength of the briquette.

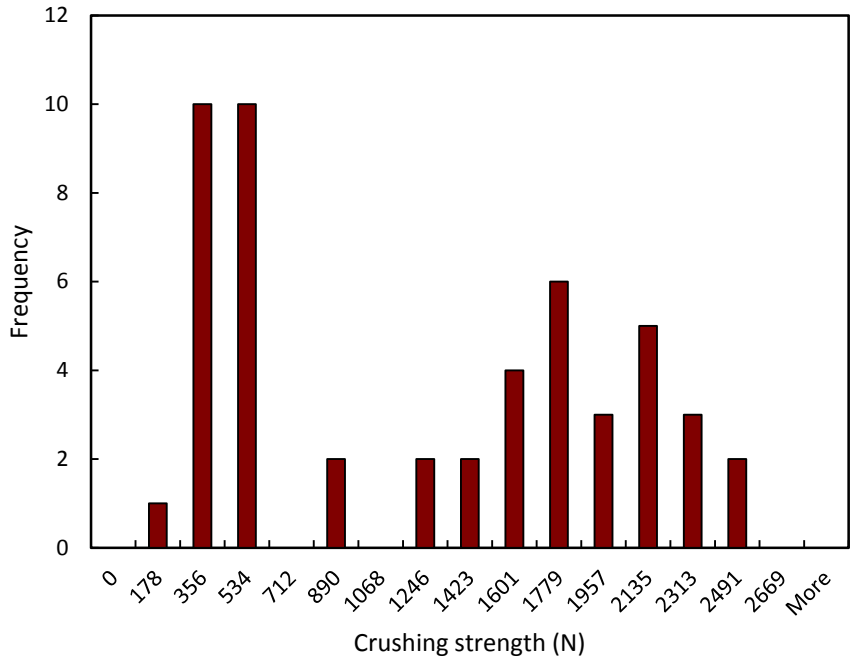



Figure 3-18. Distribution of crushing strength data recorded with the manual test stand

Although it is difficult to see in Figure 3-18, the true distribution of crushing strength values exists between 0 and 890 N (0-200 $lb_f$). In practice, a technician performing this test would reject the measurements greater than 1,067.6 N (240 $lb_f$) because the briquette would have visibly fractured prior to the completion of the test (i.e. Figure 3-19). The number of data points

that would be rejected is thought to be a function of the elasticity of briquettes. For example, a very inelastic briquette will tend to fail very suddenly once the force applied by the plunger exceeds the load that the briquette can support. In this case, the break detect feature is able to clearly detect when the applied force drops to 95 percent of the maximum force attained during the test. Therefore, very few (if any) data points would be rejected. In contrast, a very elastic briquette will not fail suddenly. Instead, it will compress between the plunger and plate as the force is increased until the briquette is visibly destroyed. Consequently, the applied force never drops to 95 percent of the maximum force attained during the test and the data point must be rejected. This case is particularly apparent with uncured briquettes and briquettes produced with high biomass content.



Figure 3-19. Example of briquette compression beyond the break point with the manual test stand

The constant compression speed of an automated test stand alleviates this problem to a large extent. When using an automated test stand, crushing strengths for coal-biomass briquettes typically exhibit relative standard deviations in the range of 10 to 20 percent. Similarly, the portion of briquettes which do not trigger a break point range from zero percent for most samples to less than 10 percent for worst-case scenarios. This is in stark contrast to the results obtained with the use of a manual test stand, in which a break point was not detected for more than half the briquettes tested. While an automated test stand may improve the sensitivity to break-point detection, such units are expensive and not always readily available. In the absence of such an

apparatus, a simple, cost-effective solution was developed to improve the sensitivity to break point detection that can be easily incorporated into any force gauge-manual test stand arrangement. An aluminum bar (51 x 8 x 8 mm) was placed on the 101.6 millimeter (4 in) diameter aluminum plate with each briquette then placed atop and parallel to the bar for testing (see Figure 3-20a). This configuration was then used with the break detect feature enabled to determine the crushing strength of 50 MR-SG briquettes from the same batch that was tested without the aluminum bar. The distribution of briquette crushing strength values recorded with the new configuration is displayed in Figure 3-21. These values ranged from 87.6 to 1,035.5 N (19.7-232.8 $lb_f$), with a mean of 507.5 N (114.1 $lb_f$) and a standard deviation of 180.6 N (40.6 $lb_f$).

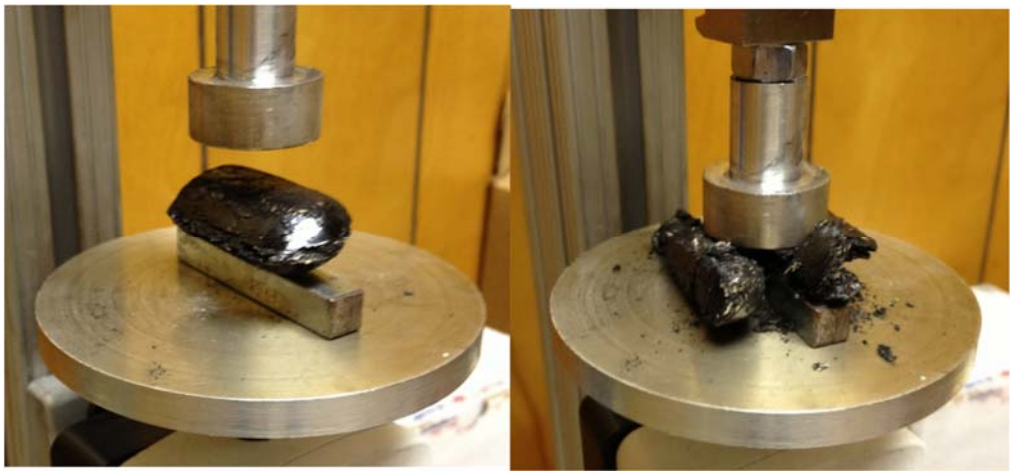


Figure 3-20. Example of briquette compression with the aluminum bar incorporated to the manual test stand configuration (a) prior to crushing and (b) beyond the break point

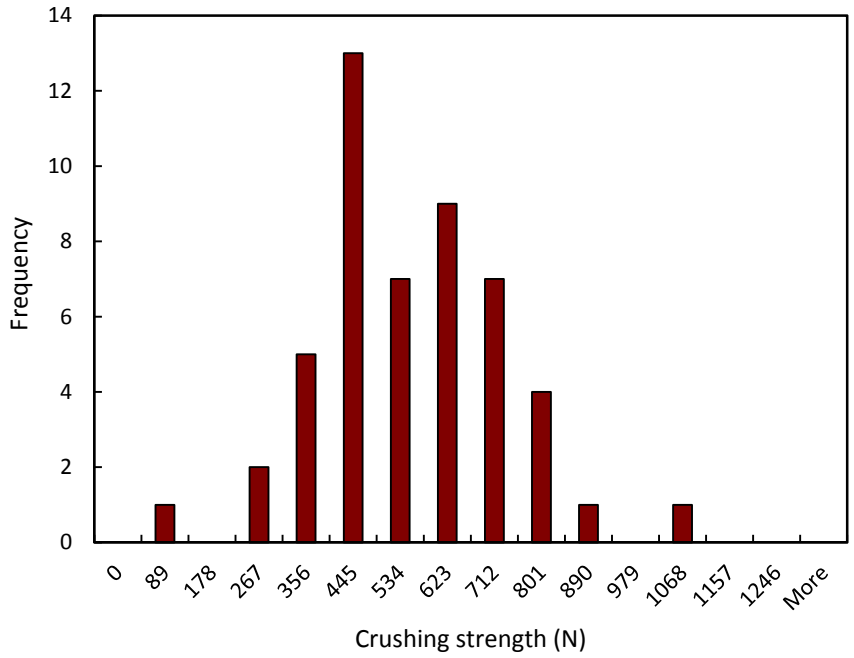



Figure 3-21. Distribution of crushing strength data recorded by incorporating the aluminum bar to the manual test stand configuration

It is evident from Figure 3-18 and Figure 3-21 that the addition of the aluminum bar to the manual test stand configuration resulted in a dramatic increase in the precision of the test results without the rejection of any data points. Specifically, the addition of the aluminum bar reduced the standard deviation of the data by more than 75 percent. This dramatic improvement was realized because the applied force dropped significantly as soon as the briquette reached the break point, as a result of the briquette no longer resting on the aluminum bar (see Figure 3-20b). Figure 3-21 also shows that the crushing strength values fit a normal distribution with the addition of aluminum bar. A similar distribution exists toward the left side of Figure 3-18 for the data obtained without the aluminum bar; however, the data in Figure 3-18 is skewed to lower crushing strength values. This is likely due to the loss of more than half of the data points from the range of true crushing strength values during the tests with the aluminum bar. These results show that this crushing strength method is well suited for coal-biomass briquette evaluations using a manual test stand and an aluminum bar.

### 3.4.3 Elasticity

A histogram of the results from both sets of elasticity evaluations are provided in Figure 3-22. It is clearly shown by this figure that the spring constant values obtained from the linear

force-displacement evaluations (top) closely resemble a normal distribution. In contrast, the spring constants obtained from the peak force-displacement evaluations (bottom) appear to follow a much more random distribution. The result was fairly surprising as the difficulty associated with the selection of the upper extent of the linear portion of the curve did not appear to have any significant impact on the precision of the measurements. As a result of the fundamental significance (i.e. derivation from Hooke's law) of spring constant results obtained using the linear force-displacement method and the improved precision of the calculated results, the linear force-displacement method appears to be better suited for characterizing the elasticity of coal-biomass briquettes.

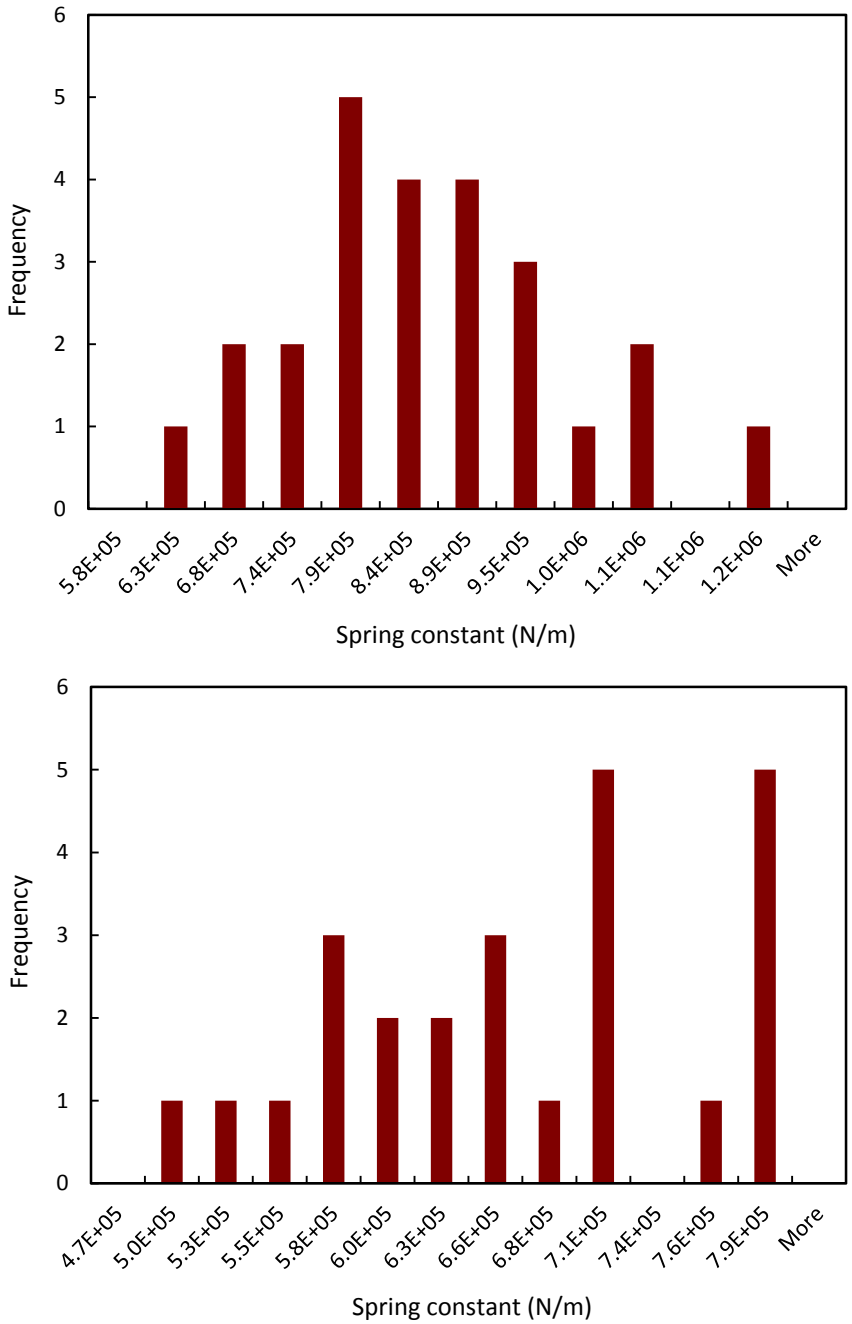



Figure 3-22. Distribution of calculated spring constant values for (top) linear force-displacement evaluations and (bottom) peak force-displacement evaluations

Another interesting observation is the difference in the mean spring constant values for each set of evaluations. The average spring constant for the peak load and displacement evaluations is 6.53 x $10^5$ N/m (3,730 $lb_f$/in), as compared to 8.31 x $10^5$ N/m (4,747 $lb_f$/in) for the linear force and displacement evaluations. The reason for this increase in measured spring constant values for the linear force and displacement evaluations can be understood by

examining a sample force-displacement diagram, as shown in Figure 3-23. From this figure, two different sets of force-displacement data can be obtained to calculate the spring constant of a briquette. The data point corresponding to the peak force and displacement is represented by the purple star and the data point corresponding to the linear force and displacement is represented by the green star. Using Hooke's Law, the spring constant corresponding to the peak force and displacement (slope of purple line) is 4.69 x $10^5$ N/m (2679 $lb_f$/in), and the spring constant corresponding to the linear force and displacement (slope of green line) is 7.25 x $10^5$ N/m (4138 $lb_f$/in). This example shows why the average spring constant values are considerably larger for the linear force-displacement evaluations than for the peak force-displacement evaluations. Based on these results, this method appears to be acceptable for measuring the spring constant of coal-biomass briquettes.

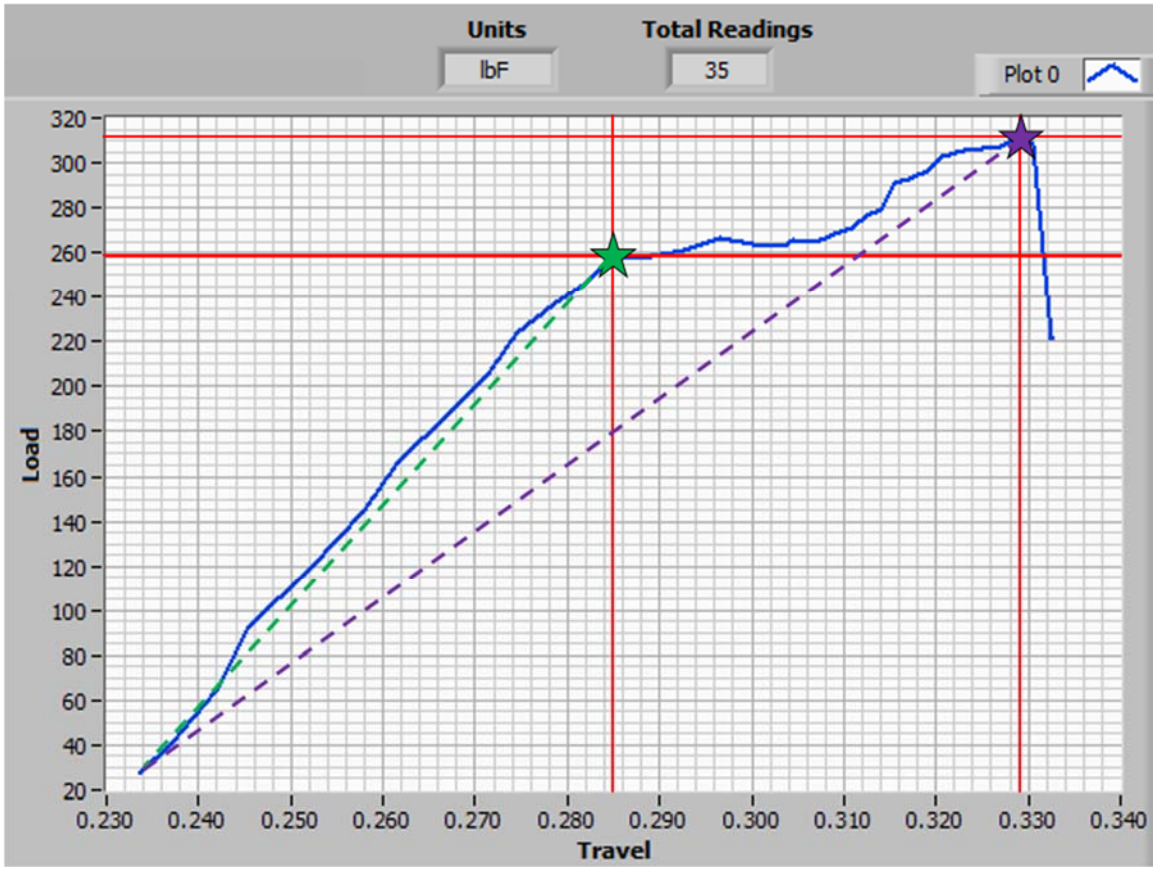



Figure 3-23. Sample force-displacement curve for spring constant calculation

### 3.4.4 Mechanical Durability

The first variable studied to evaluate the mechanical durability method reported by Taulbee et al. (2010) and Patil et al. (2009) was the number of briquettes loaded in the cylinder. Four separate series of tests were performed by tumbling different numbers of briquettes for five minutes at 40 rotations per minute to determine how mechanical durability results are impacted by cylinder loading (i.e. volume of briquettes to volume of the cylinder). It is important to note that the moisture content of the McClure River coal varied for each series of tests (i.e. 0.98 to 1.70%) due to variable drying conditions, which directly impacted the measured mechanical durability values. Figure 3-24 displays the results obtained for the four series of tests. Test 1 was performed with the highest moisture coal, while the lowest moisture coal was used for Test 4. For each of the four series of tests, the measured mechanical durability of the briquettes increased with a cylinder loading greater than 60 briquettes.

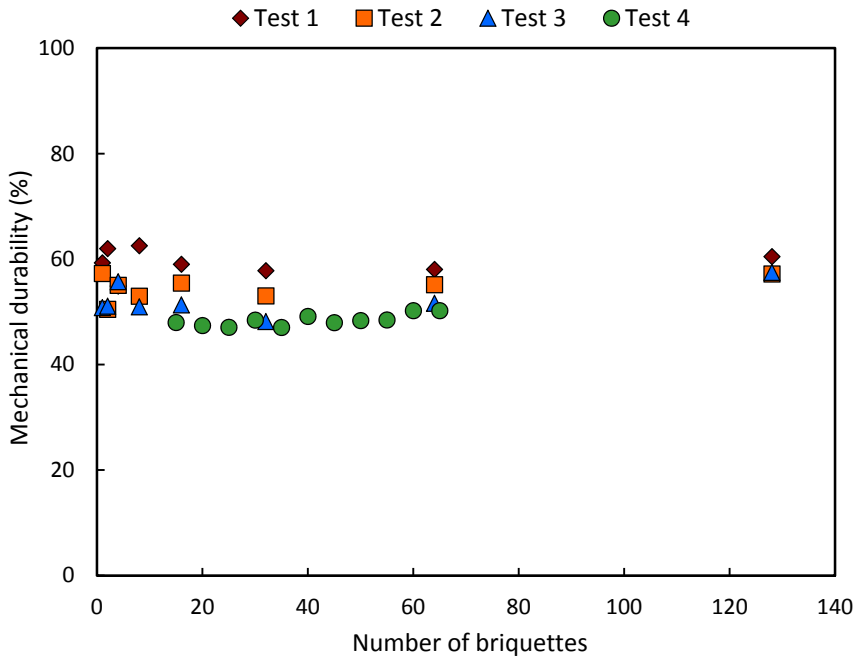



Figure 3-24. Mechanical durability results for different numbers of briquettes tested

This trend can be seen more clearly with the mechanical durability residual values plotted as a function of the number of briquettes loaded in the cylinder (Figure 3-25). The residual value is the difference between the sample and the estimated function value, which is the average of all data points for each test. High residual values represent large deviation from the average while

values close to zero represent small deviation. The residual values were very high (-4.38 to 3.56) for cylinder loading between one and eight briquettes, but remained close to zero between 16 and 64 briquettes. The increase in mechanical durability with a greater number of briquettes is thought to be the result of a cushioning effect from a high cylinder loading factor. From the data in Figure 3-24 and Figure 3-25, the ideal cylinder loading for measurement of mechanical durability was determined to be 20 briquettes. This is supported by the low residual values calculated in the range of 16 to 64 briquettes and the desire to limit the number of briquettes required for each evaluation.

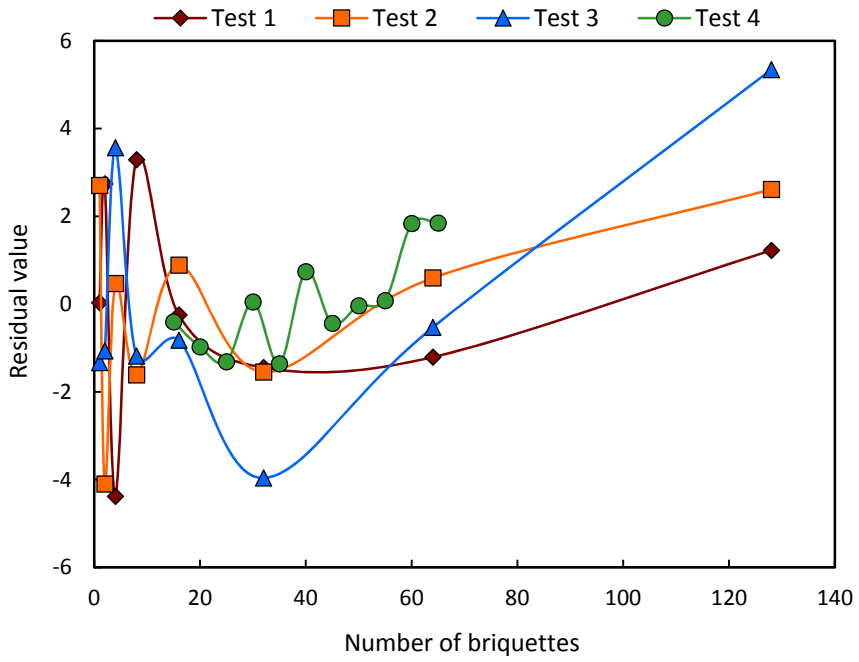



Figure 3-25. Mechanical durability residual values for different numbers of briquettes tested

The other variables examined to evaluate and refine the mechanical durability method were the number of cylinder rotations and the rotational speed of the cylinder (rpm). Evaluations were performed on 20 MR-SG briquettes at cylinder rotational speeds of 10, 20, 40 and 60 rpm. For each speed, five different numbers of rotations were examined (i.e. 20, 40, 80, 160 and 320 rotations). The results of these evaluations are displayed in Figure 3-26. Through 80 rotations, mechanical durability decreased with a corresponding decrease in the rotational speed of the cylinder. For example, the most minus 4.75-millimeter material was produced from tumbling at 10 rpm, while the least minus 4.75-millimeter material was produced from tumbling at 60 rpm. This occurred because at higher rotational speeds the briquettes are carried by the lifters inside

the cylinder so they do not experience as many drops as briquettes tumbled at lower speeds. However, there was some variation in this trend once the number of rotations was increased to 160 and 320. The least breakage still occurred at 60 rpm while the most breakage unexpectedly occurred at 20 rpm.

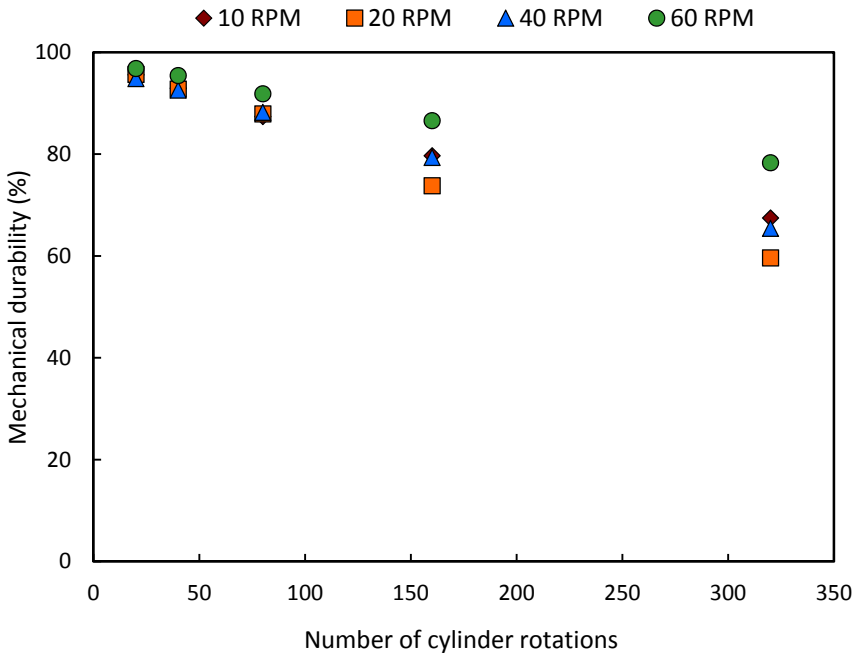



Figure 3-26. Mechanical durability results for different rotational speeds and different numbers of cylinder rotations

An exponential statistical model was fitted to the data which relates the mechanical durability of the briquettes to the number of cylinder rotations for each rotational speed (Figure 3-27). The exponential model was selected because the briquette particles that are most easily removed come off quickly while the remaining particle becomes more resistant to degradation over time, which is indicative of exponential decay. The coefficient of determination ($R^2$) was calculated for each exponential regression curve and is displayed in Figure 3-27. The coefficient of determination provides a measure of how likely future outcomes will be predicted by a statistical model, with values ranging from zero to one. In this case, a high coefficient of determination means that for an individual rotational speed, data is more likely to fall in line with the statistical model that describes briquette decay over time. The rotational speed with the highest coefficient of determination was 40 rpm, with an $R^2$ value of 0.9997. In contrast, the 60 rpm statistical model has the lowest $R^2$ value at 0.9945. Due to the highest $R^2$ value and to align

with the method reported in the literature, a rotational speed of 40 rpm is suggested for coal-biomass briquette evaluations. It can also be observed from Figure 3-27 that greater differentiation between individual mechanical durability values is achieved when briquettes are subjected to larger numbers of rotations. Therefore, 200 cylinder rotations should be performed to reduce the time required for evaluations while still maintaining sufficient sample differentiation and alignment with the method reported in the literature. An additional outcome of this study was the decision to only screen briquettes in the Ro-Tap sieve shaker for 30 seconds after mechanical durability testing. This decision was made due to the realization that briquettes experience additional degradation during screening, which is discussed in Section 3.4.5. A screening time of 30 seconds was chosen because this amount of time ensured all of the broken particles passed through the sieve without producing a significant quantity of additional fine material.

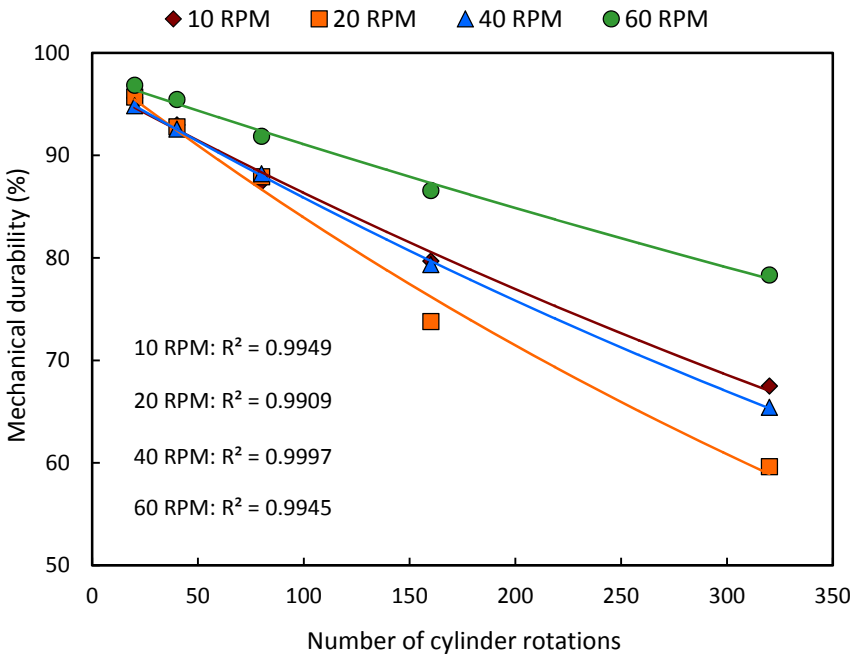



Figure 3-27. Exponential regression line fitted to mechanical durability results for different rotational speeds and different numbers of cylinder rotations

## 3.4.5 Attritability

To optimize the screening time and number of briquettes for the attritability evaluation method, a series of tests were conducted in which different numbers of MR-SG briquettes (i.e. 5, 10, 15, 20, 25, and 30) were screened for different periods of time (i.e. 10, 20, 40, 80, 160, and

320 seconds). This was accomplished by weighing a specified number of briquettes and then initially screening them in a Ro-Tap sieve shaker over a 4.75-millimeter sieve for 10 seconds. The sieve was then removed from the Ro-Tap and the mass of briquettes retained on the sieve was recorded. Next, the sieve was placed back in the Ro-Tap and the briquettes were screened for an additional 10 seconds. The sieve was again removed from the Ro-Tap and the mass of the briquettes retained on the screen was recorded. This value was designated the 20 second screening time value since the briquettes were subjected to a total of 20 seconds throughout the course of the two tests. Again, the sieve was placed back in the Ro-Tap and the briquettes were screened for an additional 20 seconds (i.e. a total screening time of 40 seconds). This screening and weighing procedure was continued until the briquettes were screened for a total of 320 seconds. The results of these evaluations for each screening time with different numbers of briquettes are presented in Figure 3-28.

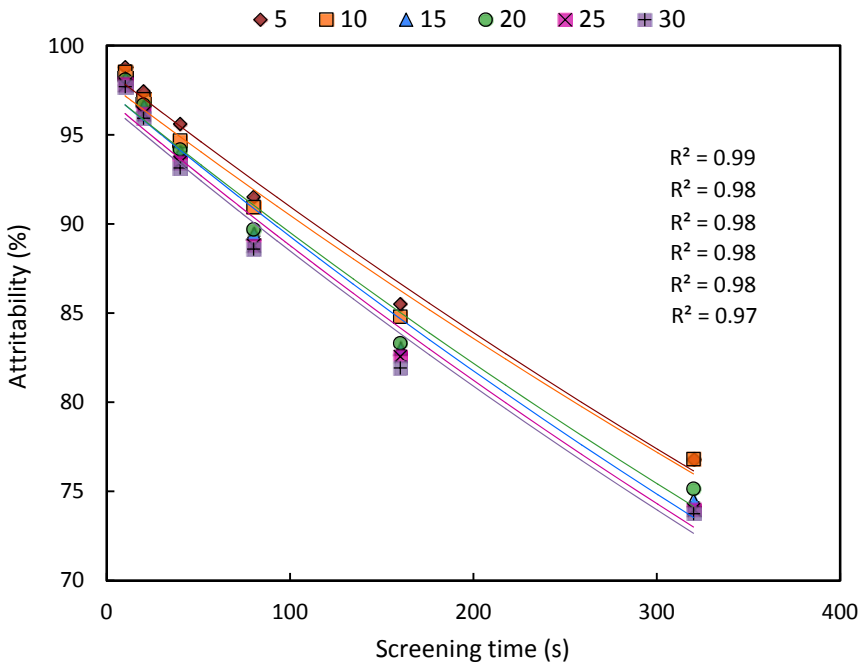



Figure 3-28. Attritability results for different screening times with different numbers of briquettes

To analyze the relationship between the measured attritability of the briquettes over time, an exponential regression line was fitted to the data for each number of briquettes tested. This type of regression was chosen because attrition is thought to be an exponential decay process, wherein the outer surface of the briquettes is removed most easily and the attrition rate decreases with time. This relationship proved to be quite accurate, which is demonstrated by the high

coefficient of determination ($R^2$) values calculated for each data set. It can also be observed from Figure 3-28 that the differentiation between individual attritability results is greater when briquettes are subjected to a longer screening duration. Therefore, it is suggested that briquettes are screened for 300 seconds (i.e. 5 minutes) to provide a significant differentiation between the results for different briquette formulations.

To provide additional insight into the relationship between attritability values and the number of briquettes tested, attritability is plotted versus number of briquettes in Figure 3-29. For this example, the screening time was held constant at three minutes and a 4.75-millimeter sieve was utilized. Evaluations were performed with 1, 2, 4, 8, 16 and 32 briquettes, each of which was repeated three times. The standard deviation of the results is also provided in Figure 3-29 as error bars. The lowest standard deviation (0.39%) was found for evaluations with 16 briquettes. This value increased to 0.70% when the number of briquettes tested was increased to 32. As a result, it is suggested that evaluations are performed with 20 briquettes due to the low standard deviation in this region and because 20 is a good sample size for statistically significant results. Another interesting finding was that the attritability values and the number of briquettes tested were found to be related to one another by a power law. In this instance, the data fit a power function extremely well (i.e. $R^2 = 1.00$). The power determined by the regression (i.e. 0.02) relates the attritability of one briquette to that of any number of briquettes ($x$) for the three minute screening time evaluated.

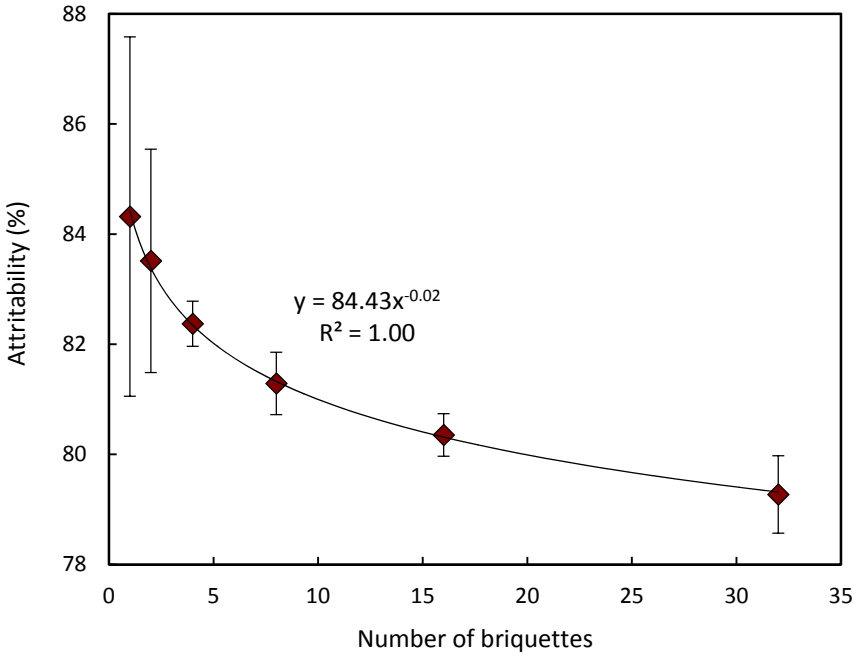



Figure 3-29. Attritability results for different numbers of briquettes

The final set of evaluations were performed to determine the impact of sieve size on the measured attritability values. This was accomplished by screening 20 MR-SG briquettes for three minutes in the Ro-Tap sieve shaker using 10 different sieve sizes (i.e. 6.70, 4.75, 3.35, 2.36, 1.70, 1.18, 0.84, 0.59, 0.43 and 0.21 mm). The results of these evaluations are provided in Figure 3-30, which clearly shows that an increase in sieve size leads to a decrease in attritability values. This finding stands to reason since more broken particles can fall through a larger sieve than a smaller one. For example, a very high attritability value (96.9%) was measured for the 0.21-millimeter sieve size, which indicates that only a small percentage of minus 0.21-millimeter particles were produced from attrition. In contrast, the attritability value was substantially lower (87.7%) for briquettes screened over the 6.70-millimeter sieve because all of the particles with an effective diameter less than 6.70 millimeters fell through the sieve openings. The results of this series of tests suggest that sieve size should be selected based on the minimum acceptable size of particles for downstream handling and processing. Therefore, a sieve size of 4.75 millimeters is recommended for coal-biomass briquettes because this particle size is often referred to as the minimum desirable particle size for downstream handling and processing operations in the coal industry.

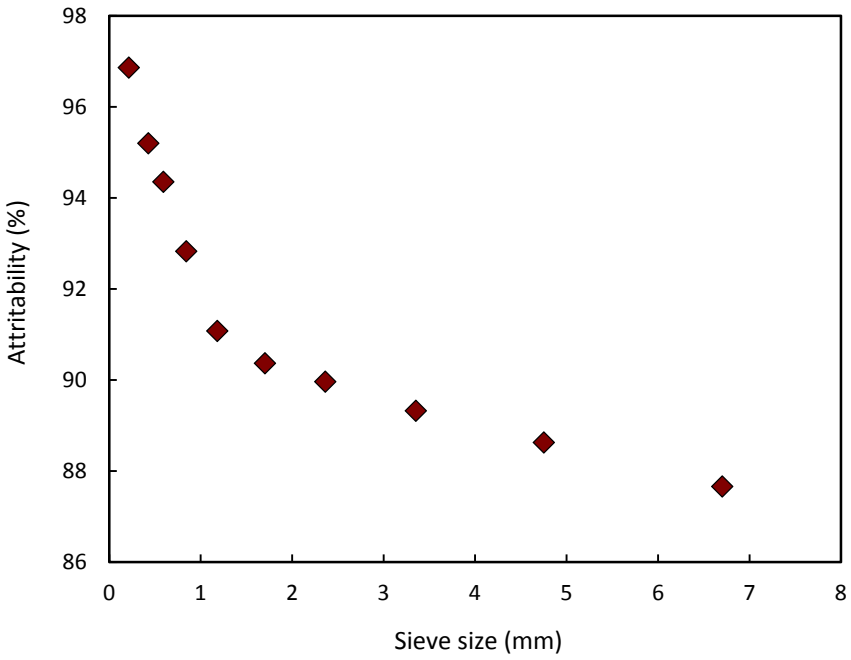



Figure 3-30. Attritability results for different sieve sizes

## 3.4.6 Friability

Evaluations were performed to determine the optimum drop height and number of briquettes to use for the modified drop-shatter test that was modified from ASTM D440-07 (2012). This method specifies dropping 22.7 kilograms (50 lb) of material, which is not practical for laboratory-scale briquette evaluations. Therefore, the decision was made to examine the difference in briquette friability measurements when different numbers of briquettes are tested (i.e. 10, 20, 40 and 80 briquettes). Each number of briquettes was dropped twice from a height of 1.2, 1.8, and 2.6 meters (4, 6, and 8.4 ft) to determine the drop height with the most consistent results. The data from these evaluations is displayed in Figure 3-31 as a function of drop height and in Figure 3-32 as a function of the number of briquettes dropped.

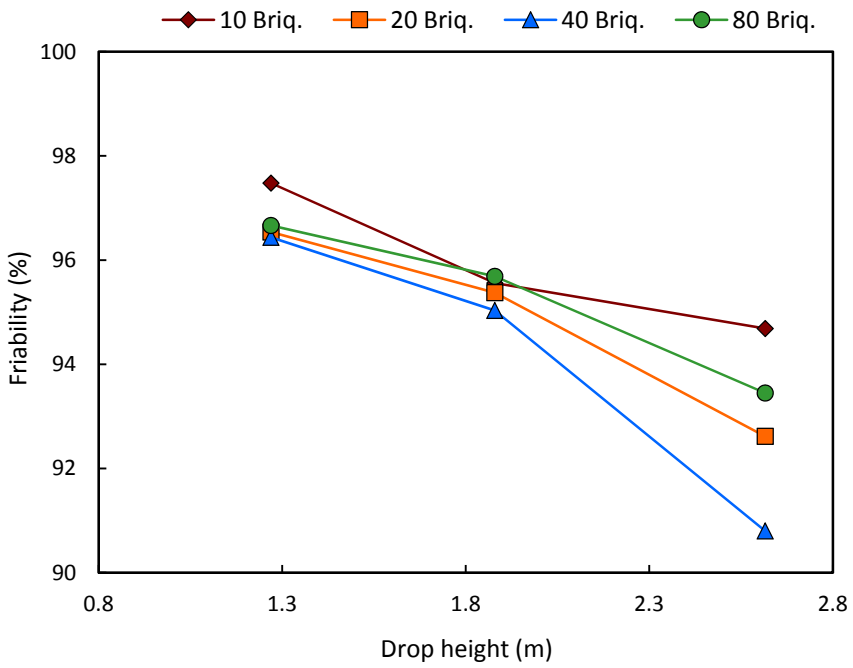



Figure 3-31. Friability results for different drop heights

From Figure 3-31 and Figure 3-32, it can be observed that the least breakage occurred at a drop height of 1.2 meters (4 ft) with a sample size of 10 briquettes, while the most breakage occurred at a drop height of 2.6 meters (8.4 ft) with a sample size of 40 briquettes. An interesting observation was that an increase in the briquette sample size could not be directly correlated to the friability results (i.e. the most breakage occurred with 40 rather than 80 briquettes). However, it can be seen that an increase in drop height directly corresponds to more breakage. The drop height with the most consistent results regardless of the number of briquettes dropped was 1.8 meters (6 ft). At this height, friability measurements ranged from 95.03 to 95.69%. In contrast, the most scatter of results was seen at a drop height of 2.6 meters (8.4 ft) with a friability range of 90.80 to 94.69%. Therefore, it appears that briquettes should be dropped from a height of 1.8 meters (6 ft) to reduce the influence of drop height on the friability results.

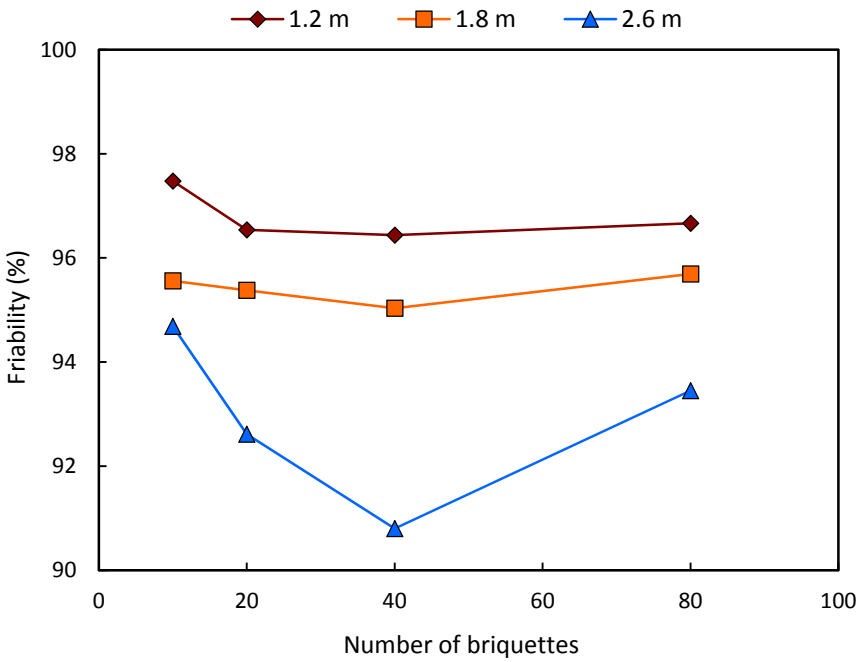



Figure 3-32. Friability results for different numbers of briquettes tested

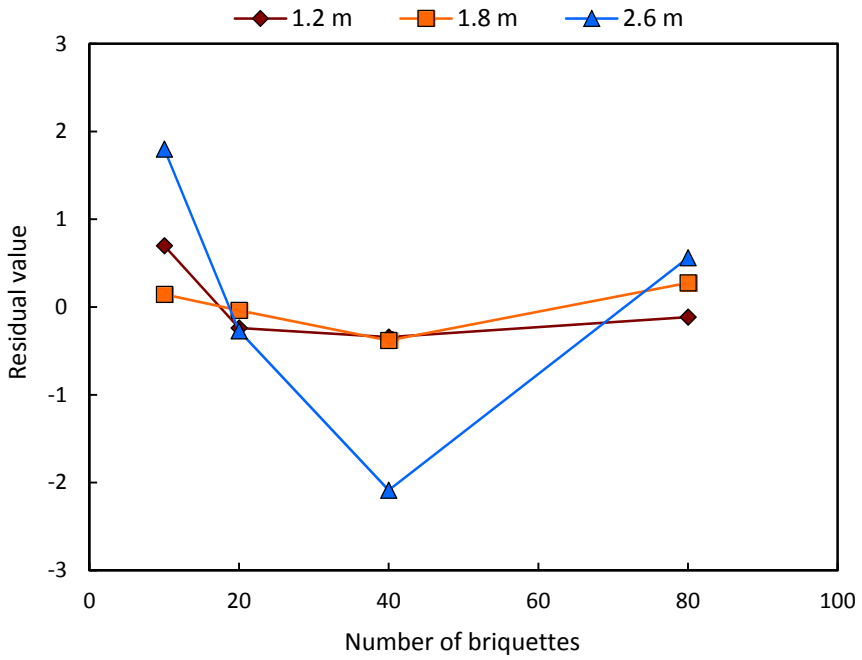



Figure 3-33. Friability residual values for different numbers of briquettes tested

From Figure 3-33, it is clear that a sample size of 20 briquettes produced residual values closest to zero (-0.04 to -0.27). It can also be seen that with 10 and 80 briquettes the residual value is typically greater than zero (-0.12 to 1.80), while with 40 briquettes the residual is much lower than zero (-0.34 to -2.09). Therefore, it appears that 20 briquettes should be used for

friability evaluations to minimize the influence of the number of briquettes tested on the results of this test. An additional outcome of this study was the decision to only screen briquettes in the Ro-Tap sieve shaker for 30 seconds after friability testing. This decision was made due to the realization that briquettes experience additional degradation during screening, which is discussed in Section 3.4.5.

### 3.4.7 Water Content

To evaluate the accuracy and precision of the proposed water content evaluation procedure, six EM-CS briquettes were dried at 105 ± 4 degrees Celsius in a drying oven for 24 hours. The results of these evaluations are presented in Table 3-2. In addition, the standard deviation and relative standard deviation were calculated for the group of six measurements to determine the precision of the method. The average water content value for the six measurements was 0.0382 and the standard deviation was 0.0030. This equated to a relative standard deviation of 7.78%. The low relative standard deviation result indicates that this method is very precise, especially considering the inherent variability among individual products of agglomeration processes.

Table 3-2. Water content accuracy and precision results

| Measurement Number | Initial Wet Mass (g) | 24 hours | | | 26 hours | | | Change in Water Content (%/hr) |
|---|---|---|---|---|---|---|---|---|
| | | Dry Mass (g) | Water Mass (g) | Water Content | Dry Mass (g) | Water Mass (g) | Water Content | |
| 1 | 9.844 | 9.463 | 0.381 | 0.0403 | 9.462 | 0.382 | 0.0404 | 0.14 |
| 2 | 9.651 | 9.299 | 0.352 | 0.0379 | 9.298 | 0.353 | 0.0380 | 0.15 |
| 3 | 9.771 | 9.470 | 0.301 | 0.0318 | 9.469 | 0.302 | 0.0319 | 0.17 |
| 4 | 9.418 | 9.055 | 0.363 | 0.0401 | 9.054 | 0.364 | 0.0402 | 0.14 |
| 5 | 9.595 | 9.226 | 0.369 | 0.0400 | 9.224 | 0.371 | 0.0402 | 0.28 |
| 6 | 9.572 | 9.213 | 0.359 | 0.0390 | 9.212 | 0.360 | 0.0391 | 0.14 |
| Avg. | | | | 0.0382 | | | 0.0383 | 0.17 |
| Std. Dev. | | | | 0.0030 | | | 0.0033 | 0.05 |
| Std. Dev. (%): | | | | 7.78 | | | 7.79 | 29.75 |

To evaluate the accuracy of water content measurements after a period of 24 hours, each of the briquettes were dried for an additional two hours to determine the change in the calculated water content value with additional drying time. As presented in Table 3-2, the average change in the calculated water content of the six briquettes over the additional two hour period was

found to be 0.17% per hour of the total loss in mass. This value is less than the value commonly recommended by the existing standards for moisture content determination (i.e. 0.2% per hour of the total loss in mass). For this reason, the prescribed period of 24 hours is certainly acceptable for accurately measuring the water content of coal-biomass briquettes.

### 3.4.8 Particle Density

For each particle density test configuration, the mass of 12 EM-CS briquettes was recorded in air and the apparent mass was measured in water. The calculated particle densities and standard deviations for each set of tests are presented numerically in Table 3-3 and graphically in Figure 3-34. One clear observation is that the particle density value was found to be lowest with the water-only evaluations. This was most likely due to the adherence of air bubbles on the surface of the briquettes, which reduced the effective mass of the briquettes in water, thereby reducing the calculated particle density.

Table 3-3. Particle density results for different test configurations

| Test Configuration | Number of Evaluations | Average Particle Density ($g/cm^3$) | Standard Deviation ($g/cm^3$) | Standard Deviation (%) |
|---|---|---|---|---|
| Water only | 12 | 1.105 | 0.010 | 0.883 |
| Water and polyurethane | 12 | 1.120 | 0.006 | 0.575 |
| Water and detergent | 12 | 1.132 | 0.010 | 0.846 |
| Water, detergent and polyurethane | 12 | 1.128 | 0.009 | 0.808 |

The lowest standard deviation (0.006) and relative standard deviation (0.575%) values were found with the polyurethane coated samples tested in water. However, since this coating method is not recommended by EN 15150 (2011) and because of the necessity to account for the amount of polyurethane that penetrates the sample, this method is not ideal. The samples tested with the detergent added to the water were found to have a higher particle density (1.132 $g/cm^3$) and lower relative standard deviation (0.846%) than the samples tested in water alone (1.105 $g/cm^3$, 0.883%). The higher particle density is believed to be more accurate than the density calculated in water alone because the adherence of air bubbles to the surface of the briquettes

was eliminated by incorporating the detergent. Due to the high degree of precision associated with the water and detergent test configuration and the conformity with EN 15150 (2011), this configuration appears to be the best method for measuring the particle density of coal-biomass briquettes.

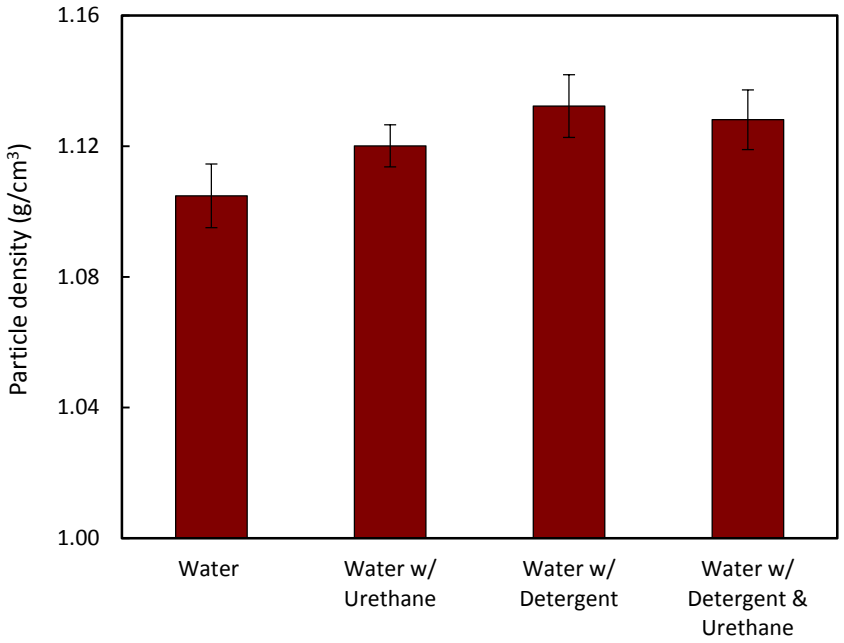



Figure 3-34. Graphical representation of particle density results for different test configurations [Error bars indicate plus and minus one standard deviation from the mean]

## 3.4.9 Bulk Density

Figure 3-35 shows the experimentally determined bulk density values and standard deviations for EM-CS briquettes corresponding to each container size. From this figure, it can be observed that the bulk density values increased slightly with an increase in container volume. For example, the average bulk density of briquettes in the 6.80 x $10^{-3}$ $m^3$ (0.24 $ft^3$) container was 647.9 kg/$m^3$ (40.5 lb/$ft^3$), as compared to 653.2 kg/$m^3$ (40.8 lb/$ft^3$) and 654.2 kg/$m^3$ (40.8 lb/$ft^3$) in the 1.42 x $10^{-2}$ $m^3$ (0.50 $ft^3$) and 2.83 x $10^{-2}$ $m^3$ (1.00 $ft^3$) containers, respectively. Although there was a measurable difference in the apparent bulk density of briquettes when the container size was increased from 6.80 x $10^{-3}$ to 2.83 x $10^{-2}$ $m^3$ (0.24 to 1.00 $ft^3$), the increase was very small, accounting for less than a one percent increase in apparent bulk density. The standard deviation of the bulk density measurements was 7.8 kg/$m^3$ (0.5 lb/$ft^3$) for the 6.80 x $10^{-3}$ $m^3$ (0.24 $ft^3$) container, 11.7 kg/$m^3$ (0.7 lb/$ft^3$) for the 1.42 x $10^{-2}$ $m^3$ (0.50 $ft^3$) container, and 4.0 kg/$m^3$

(0.3 lb/ft$^3$) for the 2.83 x 10$^{-2}$ m$^3$ (1.00 ft$^3$) container. Although the best precision was found with the 2.83 x 10$^{-2}$ m$^3$ (1.00 ft$^3$) container, there was no clear trend indicating that the precision of bulk density measurements increases with container size. From these findings it can be concluded that a 6.80 x 10$^{-3}$ m$^3$ (0.24 ft$^3$) container can be used to accurately and precisely measure the bulk density of pill-shaped coal biomass briquettes. However, if larger briquettes are produced and tested, a larger container may be necessary to accurately measure bulk density.

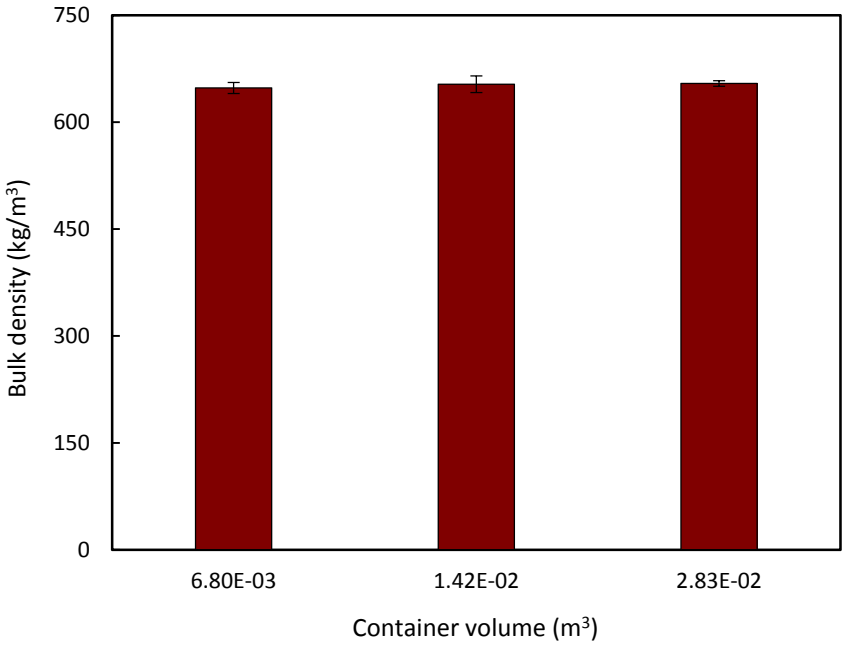



Figure 3-35. Bulk density results for different container volumes [Error bars indicate plus and minus one standard deviation from the mean]

The measured changes in bulk density with consolidation pressure from the compressibility tests are shown in Figure 3-36. From this figure it can be seen that an increase in consolidation pressure led to a slight increase in bulk density from the initial value of 650.0 kg/m$^3$ (40.6 lb/ft$^3$) to a final value of 672.8 kg/m$^3$ (42.0 lb/ft$^3$). Based on the data collected, the compressibility of the briquettes was found to be 0.03 m$^{-1}$ (0.01 ft$^{-1}$). This data suggests that coal-biomass briquettes are generally expected to have low values of bulk compressibility and that this method is acceptable to measure briquette compressibility.

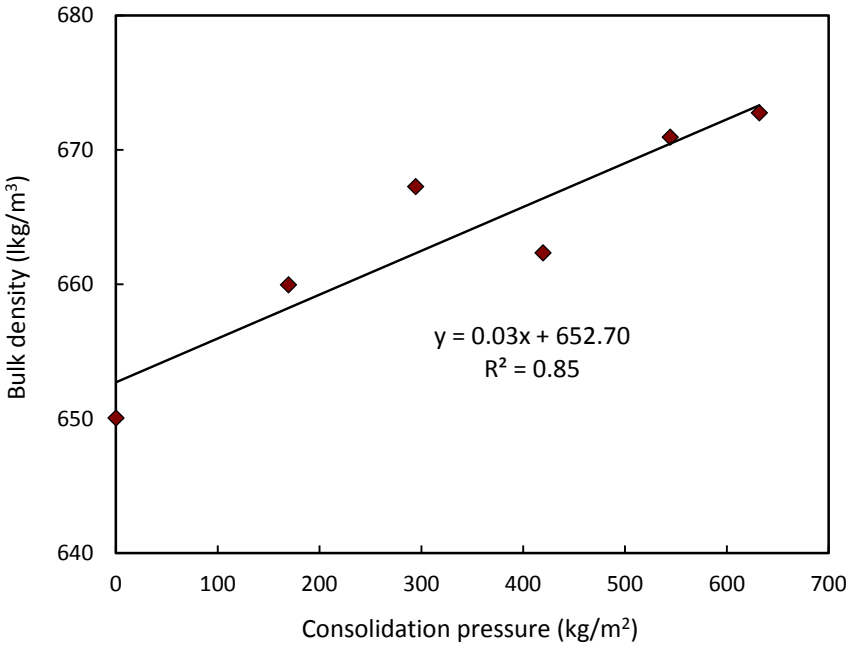



Figure 3-36. Bulk density results for different consolidation pressures

### 3.4.10 Water Resistance

The results of the first series of tests to determine the effect of the number of briquettes tested on water uptake measurements are presented in Table 3-4. These results suggest that the number of briquettes tested does not have a large impact on water uptake values. This is evident by the narrow range of values (21.68 to 22.89%) and the low relative standard deviation (2.95%) among the conditions evaluated. As a result of these findings, and in an effort to reduce material requirements, five briquettes was selected as the optimal number for water uptake tests. However, this decision is not intended to limit the number of briquettes tested to five if a higher number of briquettes is desired. For example, if it is desirable to evaluate the mechanical durability of briquettes after exposure to water, then it would be suggested to simultaneously test 20 briquettes for water uptake and subsequently test for mechanical durability, rather than testing four separate lots of five briquettes for water uptake.

Table 3-4. Water uptake measurements for all variables studied

| Number of Briquettes Tested | Water Uptake (%) | Spray Duration (sec) | Water Uptake (%) | Water Flow Rate (l/min) | Water Uptake (%) |
|---|---|---|---|---|---|
| 5 | 22.87 | 5 | 21.46 | 3.8 | 17.89 |
| 10 | 21.79 | 15 | 27.21 | 7.6 | 17.47 |
| 20 | 21.68 | 30 | 32.06 | 11.4 | 19.84 |
| 40 | 22.89 | 60 | 34.34 | 14.1 | 17.98 |
| -- | -- | 120 | 44.57 | 18.9 | 24.48 |
| Average: | 22.31 | Average: | 31.93 | Average: | 19.53 |
| Std. Dev: | 0.66 | Std. Dev: | 8.62 | Std. Dev: | 2.91 |
| Std. Dev (%): | 2.95 | Std. Dev (%): | 27.00 | Std. Dev (%): | 14.90 |

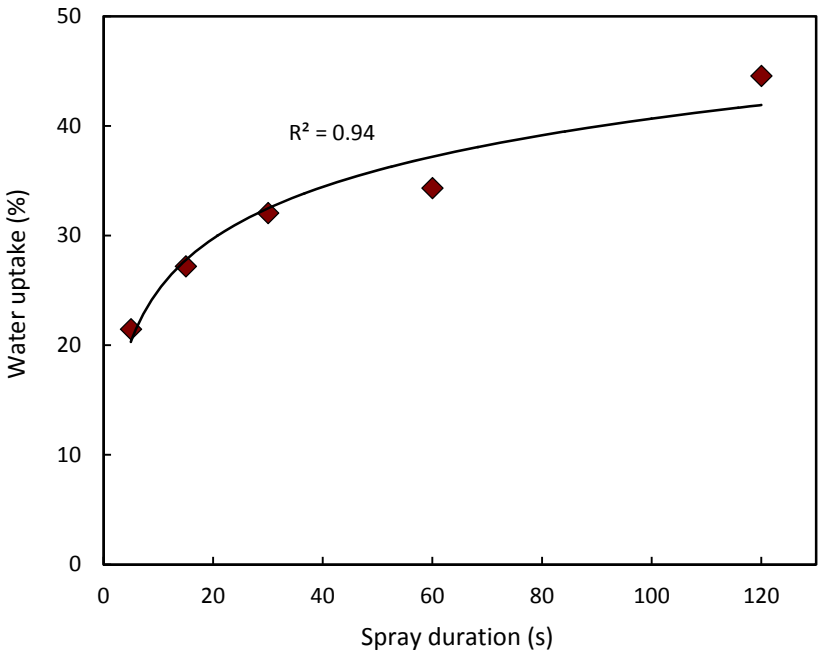



Figure 3-37. Graphical representation of water uptake measurements for different water spray durations

The results of the second series of tests to determine the impact of spray duration on water uptake measurements are also presented in Table 3-4. A very clear and predictable trend ($R^2$=0.94) was observed that relates the spray duration to the water uptake measurement, as shown in Figure 3-37. An interesting observation was how quickly these briquettes took up water. After only five seconds, a water uptake greater than 20% was recorded. This implies that a water uptake measurement can be conducted after only a short spray duration without sacrificing a substantial differentiation of results (i.e. if after five seconds the water uptake value was only a small fraction of the value after 120 seconds, then a substantial differentiation of results would

be sacrificed by choosing to only spray for five seconds). Therefore, in an effort to minimize the time required for evaluations and achieve statistically significant differentiation of results, a spray duration of 15 seconds appears to be most suitable for coal-biomass briquette water uptake evaluations.

The results of the final series of tests to analyze the impact of water flow rate on water uptake measurements are also displayed in Table 3-4. The measured water uptake values were found to be quite consistent (17.47 to 19.84%) for water flow rates between 3.8 and 14.1 liters per minute (1-4 gal/min). However, the measured water uptake at a water flow rate of 18.9 liters per minute (5 gal/min) was significantly higher (24.48%). It is unknown if this finding is significant or if the variation is a statistical outlier resulting from inconsistent briquettes between tests or loss of material due to the high impact force of the water spray at 18.9 liters per minute (5 gal/min). Regardless of the source of this discrepancy, it appears that a water flow rate of 11.4 liters per minute (3 gal/min) is ideal because at this value the spray profile provided complete coverage of the perforated stainless steel plate and the water pressure did not cause any significant loss of sample into the sump.

## 3.5 Summary and Conclusions

A major limitation to industrial utilization of coal-biomass briquette feedstocks is the absence of standard methods to characterize important physical and mechanical properties of coal-biomass briquettes. To address this challenge, a detailed review of briquette properties was initially conducted to determine the most important properties for characterization of coal-biomass briquettes. The briquette properties that were identified as most significant are: (1) tensile strength, (2) crushing strength, (3) elasticity, (4) mechanical durability, (5) attritability, (6) friability, (7) water content, (8) particle density, (9) bulk density and (10) water resistance. Crushing strength and mechanical durability appear to be the most important of all these properties, and thus should be measured for all experimental and industrial coal-biomass briquette formulations. The other identified properties are still very important and should be considered in detailed evaluations of coal-biomass briquettes when requested by a client or customer.

Experimental evaluations were conducted to adapt, evaluate and refine established methods that appeared suitable for coal-biomass briquette evaluations by directly testing coal-

biomass briquettes and analyzing the results. Additionally, work was conducted to develop novel characterization methods to quantify briquette properties when suitable established methods were not applicable or available. The following section outlines the recommended methods and procedures to characterize coal-biomass briquettes based on the results of this study.

1. Tensile strength – To measure tensile strength, individual coal-biomass briquettes are compressed with the briquette standing tall (i.e. with the long axis of the briquette parallel to the axis of force application) between flat compression plates. This is carried out using a digital force gauge and a manual or automatic test stand. A break detect feature is utilized that stops data acquisition after the applied force drops to 95 percent of the maximum force attained during each test. Tensile strength is then designated as this maximum force. This procedure is repeated for a minimum of 25 briquettes until the relative standard deviation of results is below 20 percent. The average tensile strength of all conducted measurements is reported as the briquette crushing strength, along with the standard deviation of the measured results.

2. Crushing strength – To measure crushing strength, individual coal-biomass briquettes are compressed along the smooth pocket surface (i.e. surface of force application during formation) using a digital force gauge and a manual or automatic test stand equipped with flat compression plates. When using a manual test stand, briquettes are placed atop and parallel to an aluminum bar to improve the accuracy of readings. In both instances, a break detect feature is utilized that stops data acquisition after the applied force drops to 95 percent of the maximum force attained during each test. Crushing strength is then designated as this maximum force. This procedure is repeated for a minimum of 25 briquettes until the relative standard deviation of results is below 20 percent. The average crushing strength of all conducted measurements is reported as the briquette crushing strength, along with the standard deviation of the measured results.

3. Elasticity – To measure elasticity, individual coal-biomass briquettes are compressed following the method outlined for crushing strength measurements. However, force application is measured with respect to briquette displacement using a digital travel display or a similar measurement device. Elasticity is reported as the spring constant of the

briquettes, which is calculated as the slope of the linear portion of the force-displacement diagram. This measurement is conducted for a minimum of 25 briquettes until the relative standard deviation of the results is below 20 percent. The average spring constant of all conducted measurements is reported as the briquette elasticity, along with the standard deviation of the calculated results.

4. Mechanical durability – To measure mechanical durability, 20 coal-biomass briquettes are tumbled for five minutes at 40 rotations per minute in a 0.3 meter (1 ft) diameter PVC or Plexiglas cylinder equipped with three 50.8 millimeter (2 in) lifters. The briquettes are then removed from the cylinder and screened for 30 seconds over a 4.75-millimeter sieve in a Ro-Tap sieve shaker. Mechanical durability is reported as the percentage of the initial mass of briquettes retained on the 4.75-millimeter sieve.

5. Attritability – To measure attritability, 20 coal-biomass briquettes are screened for five minutes over a 4.75-millimeter sieve in a Ro-Tap sieve shaker. Attritability is reported as the percentage of the initial mass of briquettes retained on the 4.75-millimeter sieve.

6. Friability – To measure friability, 20 coal-biomass briquettes are dropped twice from a height of 1.8 meters (6 ft) onto a steel plate using a modified shatter test machine. The briquettes are then screened for 30 seconds over a 4.75-millimeter sieve in a Ro-Tap sieve shaker. Friability is reported as the percentage of the initial mass of briquettes retained on the 4.75-millimeter sieve.

7. Water content – To measure water content, coal-biomass briquettes are dried for 24 hours at 105 ± 4 degrees Celsius in a drying oven. Water content is reported as the fraction of water in the sample on a dry basis.

8. Particle density – To measure particle density, the apparent weight of individual coal-biomass briquettes is measured while submerged in a solution of water and detergent using an apparatus similar to that described in EN 15150 (2011). The detergent to be used is Triton® X-100 at a concentration of 1.5 grams per liter of water. Particle density is calculated by the product of the liquid density and the ratio of the mass of the briquette in air to the difference between the mass of the briquette in air and the mass of the briquette in

water. This measurement is conducted for a minimum of 10 briquettes until the relative standard deviation of the results is below 20 percent. The average particle density of all conducted measurements is reported as the briquette particle density, along with the standard deviation of the calculated results.

9. Bulk density – To measure bulk density, coal-biomass briquettes are poured into a 6.80 x $10^{-3}$ $m^3$ (0.24 $ft^3$) box from a height of 0.6 meters (2 ft) above the bottom of the interior of the container so that the briquettes overflow the top of the container. A straight edge is used to remove the overflow material from the top of the container. Bulk density is calculated by dividing the net weight of the briquettes in the filled container by the volume of the container. Variation in bulk density with increasing consolidation pressure, known as compressibility, is measured by incrementally adding weight to a platform that rests on top of the briquettes and calculating the new bulk density for each consolidation pressure. Compressibility is reported as the slope of the line of bulk density versus consolidation pressure.

10. Water resistance – To measure water resistance, five coal-biomass briquettes are subjected to a 15 second water spray at a flow rate of 11.4 liters per minute (3 gal/min) from a height of 0.5 meters (1.5 ft) above the briquettes. Water resistance is reported as the water uptake of the briquettes that results from this spray test, which is reported as the water absorbed as a percentage of the initial mass of the briquettes.

# Chapter 4

# Moisture Optimization in Coal–Biomass Briquette Production

## 4.1 Abstract

Existing experimental methodologies to identify optimum moisture levels for briquette production are time consuming, labor intensive and fail to address fundamental theory. To address this challenge, the Briquette Proctor Test was developed, which is a novel low-cost method to quickly determine the optimum water content of coal-biomass mixtures for briquette production. This test is theoretically derived from the Proctor Test for clay soils, but utilizes a hydraulic press and pellet mold to determine optimum water content. The results obtained using the Briquette Proctor Test showed a clear relationship between water content and the dry density of coal-biomass briquettes. Specifically, a clear optimum water content was experimentally determined for each bituminous coal type, and a range of optimum values was identified for the sub-bituminous coal. This influence of water content on briquette production determined by the Briquette Proctor Test proved to be very representative of the results obtained for briquettes produced with a roll press. This suggests that the Briquette Proctor Test can be used to run a preliminary series of scoping tests prior to performing roll press briquetting tests. Additionally, a strong positive correlation was observed between the dry density, mechanical durability, and crushing strength of briquettes, which suggests that an exhaustive experimental study on roll press briquetting coal-biomass mixtures could be streamlined by simply determining the water content that results in the highest dry density, because the maximum strength and durability likely exist at or near this value as well. The Briquette Proctor Test also reduces material requirements, as significantly fewer briquettes are required to locate optimum conditions. Another major implication of these findings is the realization that bituminous coals with similar water contents exhibit very similar compaction behavior regardless of the physical and chemical

properties of the coals. However, sub-bituminous coals exhibit very different compaction behavior than bituminous coals, and thus require independent investigation.

## 4.2 Introduction

### 4.2.1 Problem Statement

Co-utilization of biomass with coal in existing coal-fired facilities presents a unique opportunity to reduce greenhouse gas emissions and increase energy production from renewable resources. Significant interest in this opportunity has led to more than 150 coal-fired power stations across the world co-firing coal and biomass on a commercial or trial basis as of 2009 (Fernando, 2009). These co-firing experiences have revealed a number of technical challenges including upstream issues, such as biomass availability, transportation, storage, and handling, as well as problems encountered during energy conversion, such as fouling, corrosion, inconsistent feeding and segregation (Basu et al., 2011; Sami et al., 2001). Recent studies suggest that many of these challenges can be mitigated by reconstituting coal-biomass mixtures into larger particles. Specifically, roll press briquetting has been investigated to produce homogeneous, free-flowing feedstocks that minimize handling and segregation problems often encountered with combustion and gasification systems (Taulbee et al., 2010; Honaker et al., 2005).

However, the degradation of coal-biomass briquettes during handling, transportation and storage is a significant limitation to industrial utilization of these feedstocks. As the cost of raw binder materials continues to rise and the outlook for coal prices remains bleak, there is a growing interest in alternative methods to improve the strength and durability of coal-biomass briquettes. With several new technologies to economically dry fine coal on the horizon, moisture optimization of feed materials could emerge as a viable alternative to binder addition in the briquette production process. Unfortunately, existing experimental methodologies to identify optimum moisture levels for briquette production are time consuming, labor intensive and fail to address fundamental aspects of this issue.

### 4.2.2 Moisture Optimization

In the context of densified products, such as briquettes and pellets, optimum material properties are referred to as the conditions that produce the greatest strength and durability of the final densified product (Kaliyan & Morey, 2009). Strength and durability is very important to

consider because briquettes must withstand the forces encountered in handling, storage and transportation operations to justify the cost of briquette production. Many researchers involved in laboratory evaluation of briquette and pellet formulations have noted the significant influence of water content on the strength and durability of densified products (Tumuluru et al., 2011; Kaliyan & Morey, 2009; Taulbee et al., 2009; Mangena & Cann, 2007; Mani et al., 2003). However, there is very little fundamental understanding of the relationship between feedstock moisture content and the strength and durability of briquettes due to the complex mechanics of roll press briquetting and the number of variables present in these systems. As a result, a shotgun approach is commonly used to identify optimum conditions in the laboratory, wherein many batches of briquettes are produced at various conditions, tested for strength and durability, and the optimum is identified by the conditions that exhibit the highest strength and durability. The downside to this approach is that there is no way to verify that the best recorded results are indeed the best possible results. The only solid conclusions that can be drawn using this method are the presence of relative optimum conditions with respect to other conditions tested. Another downside to this approach is the large amount of materials (i.e. coal and biomass) and long time required to perform such an exhaustive experimental study.

An important fundamental characteristic of briquettes and other agglomerates is the significant influence of porosity on strength and durability. Specifically, briquettes exhibit the greatest strength at the lowest achievable porosity, or in other words, at the highest particle density (Pietsch, 2002). Based on this relationship, the standard Proctor Test used in soil mechanics was identified as a potential method to optimize the moisture content of coal-biomass briquettes. The purpose of the Proctor Test is to determine the water content of clay soils that corresponds to the maximum compacted density. In this test, 2.5 kilograms of soil are compacted in a cylindrical mold of known diameter by a specified number of hammer blows. The compacted dry density ($\rho_d$) of the soil is then calculated by:

$$\rho_d = m_s / V_t \quad \text{(Eq. 4-1)}$$

where $m_s$ is the mass of solids and $V_t$ is the total volume (i.e. volume of solid, liquid and gas). This procedure is repeated for various water contents by adding a specified mass of water for each repetition and calculating the precise water content by:

$$w = m_w / m_s \quad \text{(Eq. 4-2)}$$

where $w$ is the water content, $m_w$ is the mass of water and $m_s$ is the mass of solids. By measuring the dry density for each calculated water content, a plot can be constructed similar to that shown in Figure 4-1a. The maximum value identified from this plot establishes the maximum dry density ($\rho_d^*$) and optimum water content ($w^*$) for the given soil (Lindeburg, 1989).

Complete saturation of the soil occurs with perfect compaction at a given water content since all air is expelled (Lindeburg, 1989). The saturation densities corresponding to each water content can be plotted versus water content to construct a curve known as the zero air voids curve (Figure 4-1b). This curve always lies above the Proctor Test curve since it is not actually possible to expel all air from the compacted material. The theoretical maximum density of the zero air voids curve is calculated as:

$$\rho_z = \rho_w/(w + (1/SG)) \quad \text{(Eq. 4-3)}$$

where $\rho_z$ is the zero air voids density, $\rho_w$ is the density of water, $w$ is the water content and $SG$ is the specific gravity of the solid. The maximum value of the zero air voids density ($\rho_{zd}$) occurs at a water content of zero. At this point, the maximum dry zero air voids density is equal to the density of the solid itself. It should also be noted that the maximum dry density ($\rho_d^*$) will always be less than the zero air voids density ($\rho_{zd}$) since air voids can never be completely eliminated (Lindeburg, 1989).

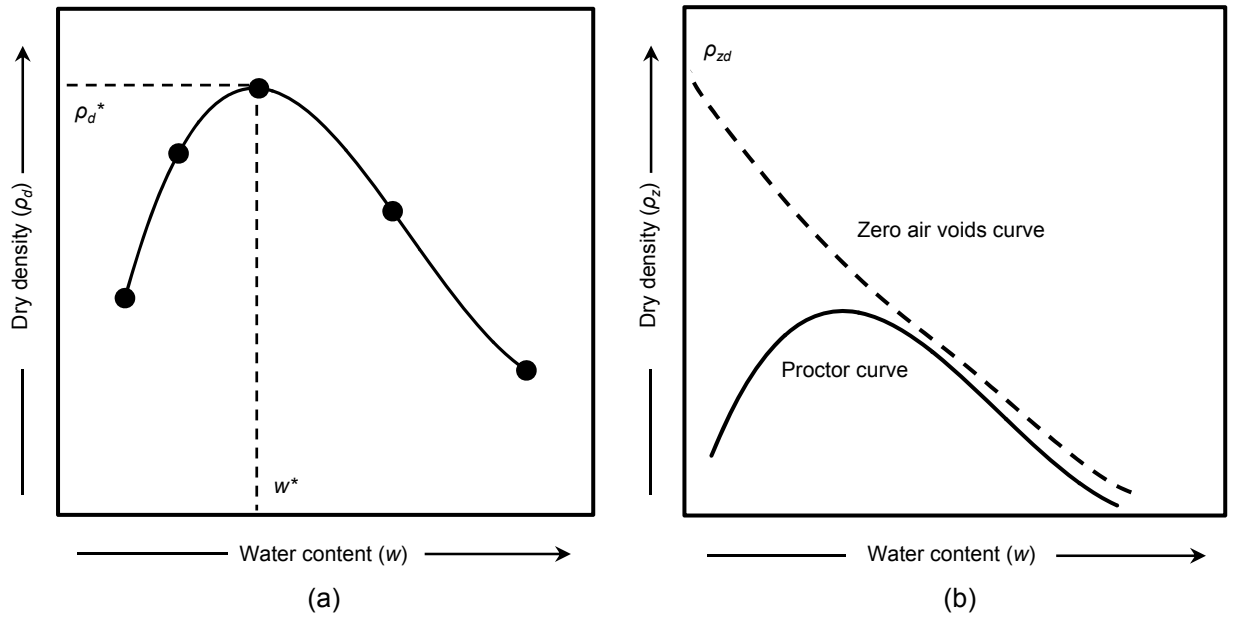



Figure 4-1. (a) Dry density versus water content as determined by the Proctor Test for soils and (b) proctor curve and zero air voids curve for soils

### 4.2.3 Research Objectives

Existing experimental methodologies to identify optimum moisture levels for briquette production are time consuming, labor intensive and fail to address fundamental aspects of this issue. Therefore, the objective of this study was to develop a methodology that minimizes time and materials required to identify the optimum water content of coal-biomass blends prior to briquette production. The fundamental theory presented in the standard Proctor Test for clay soils was adapted to coal-biomass briquette production to evaluate a number of hypotheses:

1. Water content of coal-biomass blends directly influences the dry density, strength and durability of briquettes;
2. Batch briquette production using a hydraulic press with a pellet mold can be used to predict optimum material properties for continuous roll press briquette production; and
3. Dry density is directly related to the crushing strength and mechanical durability of coal-biomass briquettes.

The secondary objective of this study was to compare and contrast the briquetting performance of three bituminous coals and one sub-bituminous coal. This was accomplished by evaluating the three hypotheses listed above for each of the coals studied, comparing the results of the evaluations and determining the sources of any inconsistencies.

## 4.3 Experimental

### 4.3.1 Materials

All briquettes produced for this study were composed of bituminous or sub-bituminous coal and sawdust. The three bituminous coals investigated for this study were obtained from preparations plants operated by Alpha Natural Resources in the Appalachian coal basin of the eastern United States and the sub-bituminous coal was obtained from a mine operated by Alpha Natural Resources in the Powder River Basin in the western United States. Specifically, the coal samples evaluated were:

1. Toms Creek: a high-volatile bituminous coal obtained from the Toms Creek preparation plant in Coeburn, Virginia;
2. McClure River: a medium-volatile bituminous coal obtained from the McClure River preparation plant in McClure, Virginia;

3. Emerald: a high-volatile, high-sulfur bituminous coal obtained from the Emerald mine preparation plant in Waynesburg, Pennsylvania; and
4. Eagle Butte: a sub-bituminous coal obtained from the Eagle Butte mine in Gillette, Wyoming.

The Toms Creek coal was a combined spiral and flotation clean product sampled from a screen bowl centrifuge in the preparation plant. Prior to briquette production, this coal was screened to a top size of one millimeter using a Uniflex two-deck screen, air dried for one week, split into two-kilogram lots and stored in sealed plastic bags. Several evaluations were performed to determine important physical properties of the coal, the results of which are included in Table 4-1. The moisture content of the coal prior to briquette production was 1.03% (dry basis), which was determined by oven drying at 105 degrees Celsius for 24 hours. The true density of the Toms Creek coal was 1.33 g/cm$^3$, which was determined by water displacement in a 250 milliliter volumetric flask. The size distribution of the crushed coal was measured by wet screening and analyzed using the Rosin-Rammler equation (Figure 4-2). Based on this analysis, the Toms Creek coal was found to have a mass median diameter of 239 microns, a size modulus of 0.36 and a distribution modulus of 0.88. Ultimate and proximate analyses were also conducted to characterize the chemical composition of the coal (Table 4-2). Notable results of the analyses include a moisture and ash free heating value of 35,472 kJ/kg (15,250 Btu/lb), an ash content of 11.30% (dry basis), and a sulfur content of 0.93% (dry basis).

Table 4-1. Physical properties of coal feedstocks

| Physical Property | Toms Creek | McClure River | Emerald | Eagle Butte |
|---|---|---|---|---|
| Moisture Content (%) | 1.03 | 0.93 | 1.60 | 1.80 |
| True Density (g/cm$^3$) | 1.33 | 1.27 | 1.27 | 1.27 |
| Mass Median Diameter (μm) | 239 | 266 | 301 | 295 |
| Size Modulus | 0.36 | 0.40 | 0.43 | 0.41 |
| Distribution Modulus | 0.88 | 0.91 | 1.02 | 1.16 |

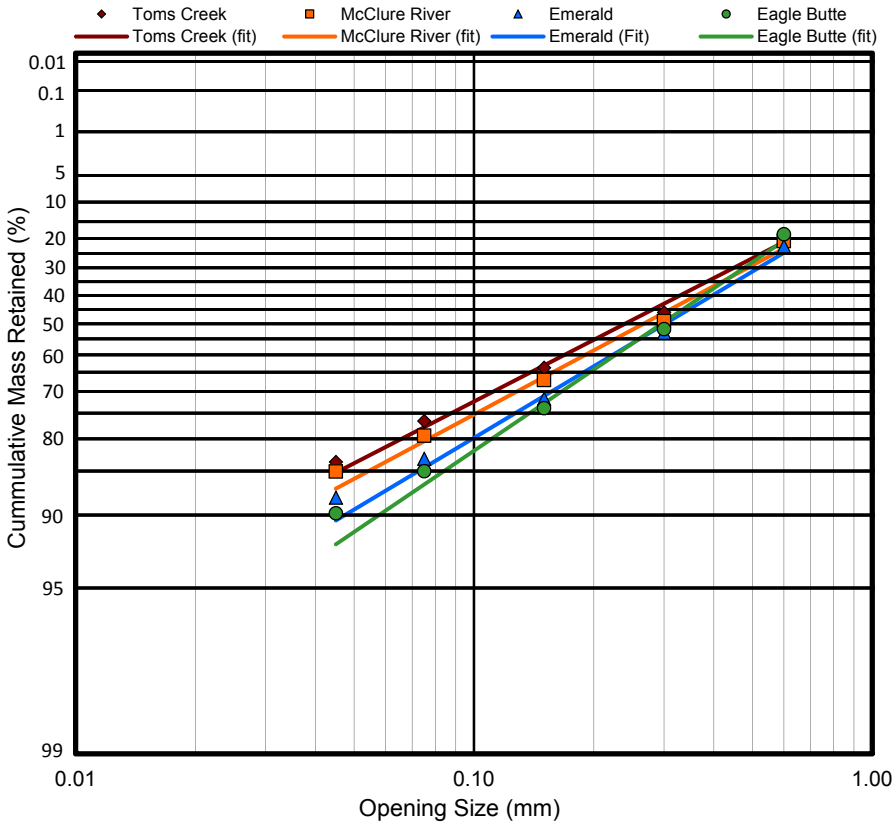



Figure 4-2. Particle-size distribution of coal samples

Table 4-2. Chemical properties of coal and biomass feedstocks

| Chemical Property | Toms Creek | | McClure River | | Emerald | | Eagle Butte | | Sawdust | |
|---|---|---|---|---|---|---|---|---|---|---|
| | As Received | Dry Basis | As Received | Dry Basis | As Received | Dry Basis | As Received | Dry Basis | As Received | Dry Basis |
| Moisture (%) | 13.73 | -- | 7.89 | -- | 4.28 | -- | 29.08 | -- | 9.42 | -- |
| Ash (%) | 9.75 | 11.30 | 5.73 | 6.22 | 8.97 | 9.37 | 5.60 | 7.89 | 0.87 | 0.96 |
| Sulfur (%) | 0.80 | 0.93 | 0.81 | 0.88 | 3.04 | 3.18 | 0.64 | 0.90 | 0.05 | 0.05 |
| Volatiles (%) | 27.24 | 31.57 | 26.17 | 28.41 | 37.59 | 39.27 | 40.89 | 57.66 | 83.23 | 91.89 |
| Fixed Carbon (%) | 49.29 | 57.13 | 59.80 | 64.92 | 49.16 | 51.36 | 24.43 | 34.45 | 6.48 | 7.15 |
| Carbon (%) | 66.19 | 76.72 | 75.77 | 82.26 | 74.26 | 77.58 | 47.08 | 66.38 | 50.23 | 55.45 |
| Hydrogen (%) | 3.85 | 4.46 | 4.38 | 4.75 | 4.91 | 5.13 | 4.00 | 5.64 | 5.43 | 5.99 |
| Nitrogen (%) | 1.36 | 1.58 | 1.44 | 1.56 | 1.39 | 1.45 | 0.70 | 0.99 | 0.09 | 0.10 |
| Oxygen (%) | 4.32 | 5.01 | 0.05 | 0.05 | 3.15 | 3.29 | 12.91 | 18.20 | 33.92 | 37.45 |
| HHV (kJ/kg) | 27,144 | 31,464 | 30,152 | 32,734 | 30,808 | 32,185 | 18,955 | 26,726 | 17,952 | 19,820 |
| MAF HHV (kJ/kg) | -- | 35,472 | -- | 36,574 | -- | 35,513 | -- | 29,015 | -- | 20,013 |

The McClure River coal was obtained from the clean coal stockpile at the preparation plant and was subjected to further processing prior to briquette production. Size reduction of the coal was accomplished by successive crushing in a jaw crusher, roll crusher and grinder. The

coal was then screened to a top size of one millimeter using a Uniflex two-deck screen, air-dried for one week, split into two-kilogram lots and stored in sealed plastic bags. Again, several evaluations were performed to determine important physical properties of the coal, the results of which are included in Table 4-1. The moisture content of the coal prior to briquette production was 0.93% (dry basis), which was determined by oven drying at 105 degrees Celsius for 24 hours. The true density of the McClure River coal was 1.27 g/cm$^3$, which was determined by water displacement in a 250 milliliter volumetric flask. The size distribution of this coal was also measured by wet screening and analyzed using the Rosin-Rammler equation (Figure 4-2). Based on this analysis, the McClure River coal was found to have a mass median diameter of 266 microns, a size modulus of 0.40 and a distribution modulus of 0.91. Ultimate and proximate analyses were also conducted to characterize the chemical composition of the McClure River coal (Table 4-2). Notable results of the analyses include a moisture and ash free heating value of 36,574 kJ/kg (15,724 Btu/lb), an ash content of 6.22% (dry basis), and a sulfur content of 0.88% (dry basis).

The Emerald coal was obtained from the clean coal stockpile at the preparation plant and was subjected to further processing prior to briquette production. Size reduction of the Emerald coal was accomplished by successive crushing in a jaw crusher, roll crusher and grinder. The coal was then screened to a top size of one millimeter using a Uniflex two-deck screen, air-dried for one week, split into two-kilogram lots and stored in sealed plastic bags. Again, several evaluations were performed to determine important physical properties of the coal, the results of which are included in Table 4-1. The moisture content of the coal prior to briquette production was 1.60% (dry basis), which was determined by oven drying at 105 degrees Celsius for 24 hours. The true density of the Emerald coal was 1.27 g/cm$^3$, which was determined by water displacement in a 250 milliliter volumetric flask. The size distribution of the crushed coal was measured by wet screening and analyzed using the Rosin-Rammler equation (Figure 4-2). Based on this analysis, the Emerald coal was found to have a mass median diameter of 301 microns, a size modulus of 0.43 and a distribution modulus of 1.02. Ultimate and proximate analyses were also conducted to characterize the chemical composition of the Emerald coal (Table 4-2). Notable results of the analyses include a moisture and ash free heating value of 35,513 kJ/kg (15,268 Btu/lb), an ash content of 9.37% (dry basis), and a sulfur content of 3.04% (dry basis).

The Eagle Butte coal was obtained from the raw coal stockpile of the Eagle Butte mine. Prior to briquette production, this coal was successively crushed in a jaw crusher, roll crusher and a grinder. The coal was then screened to a top size of one millimeter using a Uniflex two-deck screen, air dried for one week, oven dried at 105 degrees Celsius for 48 hours, split into two-kilogram lots and stored in sealed plastic bags. Again, several evaluations were performed to determine important physical properties of the coal, the results of which are included in Table 4-1. The moisture content of the Eagle Butte coal prior to briquette production was 1.80% (dry basis), which was determined by oven drying at 105 degrees Celsius for 24 hours. The true density of the Eagle Butte coal was 1.27 g/cm$^3$, which was determined by water displacement in a 250 milliliter volumetric flask. The size distribution was again analyzed using the Rosin-Rammler equation (Figure 4-2), which indicated that the coal had a mass median diameter of 295 microns, a size modulus of 0.41 and a distribution modulus of 1.16. Ultimate and proximate analyses were also conducted to characterize the chemical composition of the Eagle Butte coal (Table 4-2). Notable results of the analyses include a moisture and ash free heating value of 29,015 kJ/kg (12,474 Btu/lb), an ash content of 7.89% (dry basis), and a sulfur content of 0.90% (dry basis).

The sawdust used for this study was maple wood obtained from a cabinet manufacturing facility in Christiansburg, Virginia. The sawdust was collected by a vacuum filter during the fine sanding process and was transported to the research laboratory in a sealed bulk bag. A split of the sample was then subjected to moisture analysis using the same procedure specified for the coal sample. The moisture content of the sawdust was found to be 5.45% (dry basis). Particle-size distribution was not determined for the ultra-fine sawdust because previous attempts to collect this information has indicated that the results are lack adequate precision and accuracy. However, ultimate and proximate analyses were conducted on a split of the sawdust sample (Table 4-2). Notable results of the analyses include a moisture and ash free heating value of 20,013 kJ/kg (8,604 Btu/lb), an ash content of 0.96% (dry basis), and a sulfur content of 0.05% (dry basis).

### 4.3.2 Briquette Production

The theoretical approach to the standard Proctor Test for soils was adapted to design a procedure to maximize the dry density of coal-biomass briquettes by optimizing the water

content of coal-biomass mixtures prior to briquette production. Unfortunately, the Proctor Test procedure was deemed unsuitable for experimental briquette production because it conflicts with several objectives of this study: (1) repeated hammer blows are not representative of the forces present in the roll press; (2) the size of the densified product is not comparable to the size of briquettes produced by the roll press; and (3) the mass of material required (i.e. 2.5 kg) does not minimize material requirements. Therefore, a modified approach to obtaining the plot of dry density versus water content was designed that better conforms to the objectives of this study. This modified approach, referred to as the Briquette Proctor Test, consists of producing individual briquettes in a manual hydraulic press using a pellet mold (Figure 4-3a) and subsequently measuring water content and dry density. The hydraulic press used in this study was a Carver Model C bench-top manual press with a maximum clamping force of 106,757 newtons (24,000 $lb_f$) (Figure 4-3b). The pellet mold used in combination with the press was a Carver No. 2090 stainless steel test cylinder with an interior diameter of 28.6 millimeters (1.125 in), which produces pellets with a surface area of 6.4 x $10^{-4}$ $m^2$ (1 $in^2$) (Figure 4-3c).

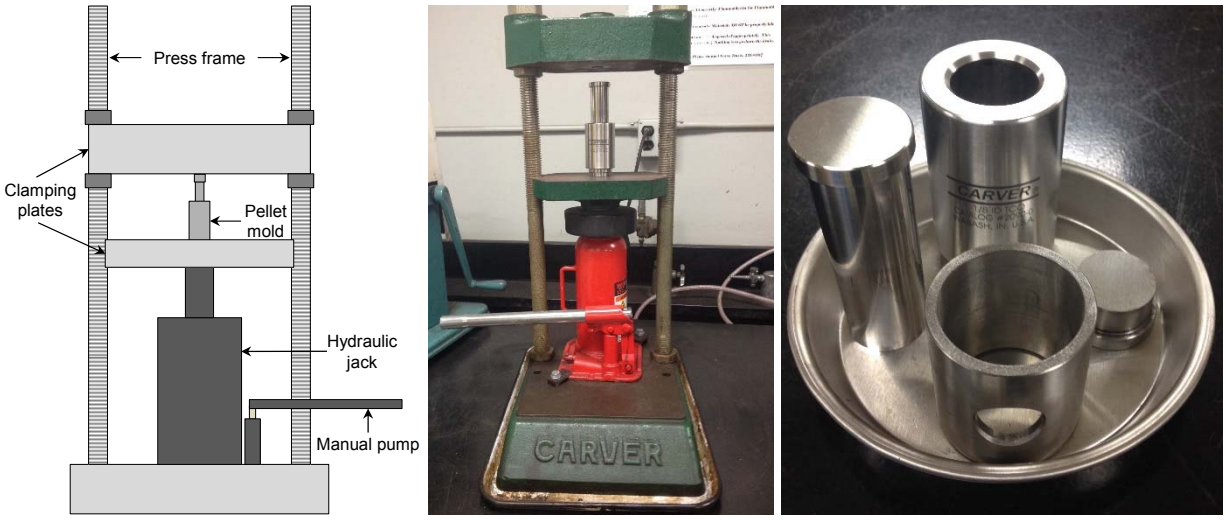



Figure 4-3. (a) Pellet press schematic drawing, (b) Carver pellet press laboratory installation and (c) Carver pellet mold

To evaluate the applicability of the Briquette Proctor Test, briquettes were produced with a total dry mass of 15 grams with 80 percent coal (dry basis) and 20 percent sawdust (dry basis). The water content of the blend was varied over a range of 0.01 to 0.15 for each of the three sets of bituminous coal-sawdust briquettes and over a range of 0.02 to 0.25 for the sub-bituminous

coal-sawdust mixture. The sub-bituminous coal was evaluated over an elevated range of water contents because some preliminary data indicates that the optimum water content for sub-bituminous coal-biomass briquettes is higher than the range studied for bituminous coal-biomass briquettes.

For each individual briquette produced, between 12.11 and 12.22 grams of coal (depending on the water content of the specific coal) were homogenized with 3.16 grams of sawdust and a specified mass of water for five minutes in a KitchenAid 4.7 liter (1.25 gal) stand mixer. Next, the mixture was carefully poured into the pellet mold and placed onto the Carver hydraulic press. The mold was then compressed until the force reading on the press reached approximately 89,000 newtons (20,000 $lb^f$). The pellet was immediately ejected to simulate a very low dwell time, as is common with roll press briquette production. Immediately after ejection from the mold, the pellet was tested for either water content or wet density, which was later corrected to dry density ($\rho_d$) by:

$$\rho_d = \rho_{wet}/(1 + w) \quad \text{(Eq. 4-4)}$$

where $\rho_{wet}$ is the calculated wet density and $w$ is the calculated water content. It should be noted that two identical pellets were produced for each targeted water content because an individual pellet could not be tested for both water content and wet density.

To examine the relationship between results of the Briquette Proctor Test and roll press briquette production, pill-shaped briquettes (approximately 43 x 19 x 14 mm) were produced with a Komarek B-100R laboratory roll press equipped with 13-centimeter diameter rolls. The machine is comprised of two counter-rotating rolls, two hydraulic cylinders, a horizontal tapered screw and a paddle feeder (Figure 5-6). The hydraulic cylinders control the position of the upper roll and thus control the gap between the rolls. The paddle feeder is driven by a fixed speed motor and distributes the material to the horizontal screw that in turn feeds material to the rolls. The counter rotating rolls and the horizontal screw are driven by variable speed motors, which enable adjustment of the torque applied to the material from the rolls and screw. For all briquettes produced with the B100R throughout this study, the rolls were driven at a motor speed of 450 rotations per minute with 100 kilonewtons of hydraulic force. The horizontal screw speed was adjusted during briquette production to maintain a roll torque of approximately 1000 to 1200 newton-meters.

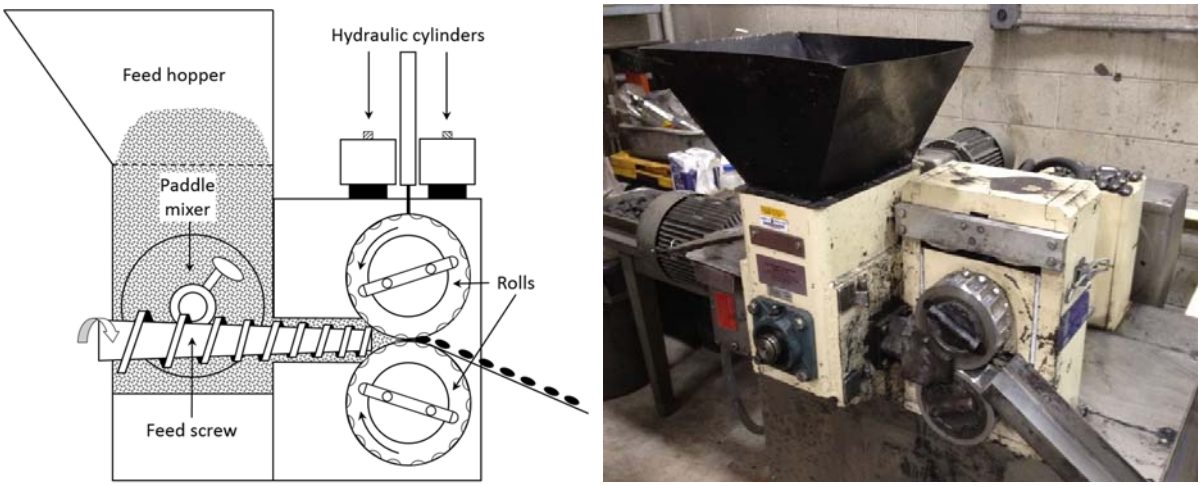



Figure 4-4. Komarek B-100R roll press (left) schematic diagram (modified from Guigon & Simon, 2003) and (right) laboratory installation

For roll press production, briquettes were produced in two kilogram batches with 80 percent coal and 20 percent sawdust on a dry mass basis. A calculated mass of water was added to each batch to reach a targeted water content. The water content of the blend was varied over a range of 0.007 to 0.082 for each of the three sets of bituminous coal-sawdust briquettes and over a range of 0.025 to 0.225 for the sub-bituminous coal-sawdust mixture. Next, the coal, biomass and water were homogenized for five minutes in a Hobart A200 18.9 liter (5 gal) commercial mixer. After mixing, a five-gram sub-sample of the homogenized feed was tested for water content, and the rest of the material was briquetted in the Komarek B-100R. Immediately after formation, the briquettes were screened across a Sweco vibrating separator equipped with a 12.7 millimeter (0.5 in) screen to remove excess fines. The briquettes were then placed in an aluminum dish and immediately evaluated for water content, dry density, mechanical durability and crushing strength.

## 4.3.3 Briquette Characterization

### 4.3.3.1 Water Content

The water content of briquettes was determined by drying for 24 hours at 105 degrees Celsius in a drying oven. The mass of water in the briquettes was calculated by subtracting the dry mass of the briquettes from the initial mass before drying. The water content was then calculated by dividing the mass of water by the dry mass of the sample, as outlined in Equation 4-2. The water content of the briquettes produced with the roll press was measured immediately

after briquette production and again roughly three hours later, after durability and strength measurements were conducted, to monitor the change in water content over time. In both instances, measurements were conducted on 10 individual briquettes and the average of the 10 values was reported as the water content. Water content of the feed material was measured prior to briquette production using an AND MF-50 moisture analyzer set at 105 degrees Celsius. Feed samples were dried until the change in mass was reduced to 0.05 percent per minute, at which point the displayed value was reported as the water content of the feed.

#### 4.3.3.2 Dry Density

The dry density (i.e. dry particle density) of briquettes was calculated by first measuring the initial (wet) density and then calculating the dry density ($\rho_d$) based on the measured water content as outlined in Equation 4-4. To accomplish this, a density determination rig was used to measure the apparent mass of briquettes in a solution of water and detergent. The wet density ($\rho_{wet}$) was then calculated by:

$$\rho_{wet} = (m_a/(m_a - m_b))\rho_w \quad \text{(Eq. 4-5)}$$

where $m_a$ is the mass of the briquette in air, $m_b$ is the apparent mass of the briquette in water and $\rho_w$ is the density of the liquid. The dry density of the briquettes produced with the roll press was calculated immediately after briquette production and again roughly three hours later, after durability and strength measurements were conducted, to monitor the change in dry density over time. In both instances, the procedure was repeated for 10 briquettes produced with the roll press and the average of the 10 values was reported as the dry density. For both cases, the procedure was repeated for 10 briquettes and the average of the 10 values was reported as the dry density.

#### 4.3.3.3 Mechanical Durability

The mechanical durability of briquettes was measured by tumbling 20 briquettes for five minutes at 40 rotations per minute in a 0.3 meter (1 ft) diameter PVC cylinder equipped with three 50.8 millimeter (2 in) lifters. The briquettes were then removed from the cylinder and screened in a Ro-tap sieve shaker for 30 seconds over a 4.75-millimeter sieve. The mechanical durability ($MD$) of the briquettes was then calculated by:

$$MD = 100 \times \left(m_{final}/m_{initial}\right) \quad \text{(Eq. 4-6)}$$

where $m_{final}$ is the mass of briquettes retained on the 4.75-millimeter sieve and $m_{initial}$ is the initial mass of the briquettes prior to durability testing. This procedure was repeated two times to ensure that the results were within two percent agreement.

#### 4.3.3.4 Crushing Strength

The crushing strength of briquettes was determined using a Mark-10 M5-500 digital force gauge fitted with a 101.6 millimeter (4 in) diameter aluminum plate. The force gauge was mounted to a Mark-10 TSA750 manual test stand equipped with a 25.4 millimeter (1 in) diameter aluminum plunger that was used to apply force to the briquettes until failure. The force gauge was configured with a break detect feature which stops data acquisition once the applied force drops to 95 percent of the maximum force attained during each test. The crushing strength of each briquette was then reported as the maximum force attained during each test. To improve the accuracy of readings, an aluminum bar (51 x 8 x 8 millimeters) was placed upon the aluminum plate with each briquette then placed atop and parallel to the bar for testing. Evaluations were performed on 50 briquettes and the crushing strength was reported as the average of the 50 values.

## 4.4 Results and Discussion

### 4.4.1 Hydraulic Press Moisture Optimization

The results obtained using the Briquette Proctor Test are presented in Table 4-3 through Table 4-6 for each of the four coal types. These tables list the calculated water contents and dry densities of the coal-sawdust briquettes that were produced with the hydraulic press. The water contents of the produced briquettes typically varied by 10 to 20 percent from the target values due to the inherent variability of the coal and biomass feedstocks. The dry density of the Toms Creek-sawdust (TC-SD) briquettes ranged from 1.045 g/cm$^3$ at a water content of 0.010 to 0.923 g/cm$^3$ at a water content of 0.133, with a maximum value of 1.103 g/cm$^3$ at a water content of 0.037 (Table 4-3). Similarly, the dry density of the McClure River-sawdust (MR-SD) briquettes ranged from 0.997 g/cm$^3$ at a water content of 0.011 to 0.914 g/cm$^3$ at a water content of 0.125, with a maximum value of 1.066 g/cm$^3$ at a water content of 0.033 (Table 4-4). Moreover, the dry density of the Emerald-sawdust (EM-SD) briquettes ranged from 0.997 g/cm$^3$ at a water content of 0.011 to 0.901 g/cm$^3$ at a water content of 0.129, with a maximum value of 1.060 g/cm$^3$ at a

water content of 0.025 (Table 4-5). The dry density of the TC-SD briquettes was clearly the highest of the three bituminous coal briquettes. This is most likely a direct result of the higher true density of the TC coal (i.e. 1.33 g/cm$^3$) as compared to the MR and EM coals (i.e. 1.27 g/cm$^3$). In contrast to results obtained for the three bituminous coals, the dry density of the Eagle Butte-sawdust (EB-SD) briquettes ranged from 0.862 g/cm$^3$ at a water content of 0.019 to 0.818 g/cm$^3$ at a water content of 0.238, with a maximum value of 0.922 g/cm$^3$ at a water content of 0.111 (Table 4-6).

Table 4-3. Summary of water content optimization results for TC-SD hydraulic press briquettes

| Test ID | Water Content | | Dry Density (g/cm$^3$) |
|---|---|---|---|
| | Target | Actual | |
| TC-SD-1H | 0.01 | 0.010 | 1.045 |
| TC-SD-2H | 0.02 | 0.022 | 1.069 |
| TC-SD-3H | 0.03 | 0.026 | 1.096 |
| TC-SD-4H | 0.04 | 0.037 | 1.103 |
| TC-SD-5H | 0.05 | 0.042 | 1.091 |
| TC-SD-6H | 0.06 | 0.055 | 1.087 |
| TC-SD-8H | 0.08 | 0.072 | 1.044 |
| TC-SD-10H | 0.10 | 0.089 | 1.001 |
| TC-SD-15H | 0.15 | 0.133 | 0.923 |

Table 4-4. Summary of water content optimization results for MR-SD hydraulic press briquettes

| Test ID | Water Content | | Dry Density (g/cm$^3$) |
|---|---|---|---|
| | Target | Actual | |
| MR-SD-1H | 0.01 | 0.011 | 0.997 |
| MR-SD-2H | 0.02 | 0.018 | 1.043 |
| MR-SD-3H | 0.03 | 0.025 | 1.049 |
| MR-SD-4H | 0.04 | 0.033 | 1.066 |
| MR-SD-5H | 0.05 | 0.039 | 1.065 |
| MR-SD-6H | 0.06 | 0.050 | 1.051 |
| MR-SD-8H | 0.08 | 0.063 | 1.022 |
| MR-SD-10H | 0.10 | 0.082 | 0.982 |
| MR-SD-15H | 0.15 | 0.125 | 0.914 |

Table 4-5. Summary of water content optimization results for EM-SD hydraulic press briquettes

| Test ID | Water Content | | Dry Density ($g/cm^3$) |
|---|---|---|---|
| | Target | Actual | |
| EM-SD-1H | 0.01 | 0.011 | 0.997 |
| EM-SD-2H | 0.02 | 0.018 | 1.033 |
| EM-SD-3H | 0.03 | 0.025 | 1.060 |
| EM-SD-4H | 0.04 | 0.033 | 1.059 |
| EM-SD-5H | 0.05 | 0.043 | 1.047 |
| EM-SD-6H | 0.06 | 0.049 | 1.041 |
| EM-SD-8H | 0.08 | 0.068 | 1.021 |
| EM-SD-10H | 0.10 | 0.083 | 0.962 |
| EM-SD-15H | 0.15 | 0.129 | 0.901 |

Table 4-6. Summary of water content optimization results for EB-SD hydraulic press briquettes

| Test ID | Water Content | | Dry Density ($g/cm^3$) |
|---|---|---|---|
| | Target | Actual | |
| EB-SD-2H | 0.02 | 0.019 | 0.862 |
| EB-SD-4H | 0.04 | 0.037 | 0.906 |
| EB-SD-6H | 0.06 | 0.057 | 0.920 |
| EB-SD-8H | 0.08 | 0.080 | 0.919 |
| EB-SD-10H | 0.10 | 0.095 | 0.914 |
| EB-SD-12H | 0.12 | 0.111 | 0.922 |
| EB-SD-15H | 0.15 | 0.146 | 0.921 |
| EB-SD-20H | 0.20 | 0.189 | 0.883 |
| EB-SD-25H | 0.25 | 0.238 | 0.818 |

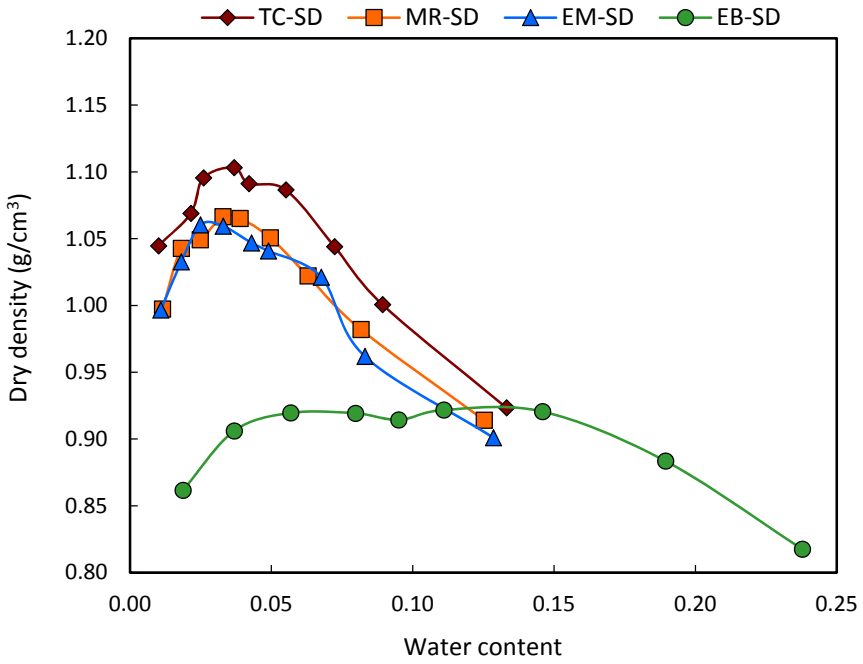



Figure 4-5. Correlation between water content and dry density for all hydraulic press briquettes

The calculated water content and dry density values for each of the four coals are displayed graphically in Figure 4-5. In this figure and throughout the remainder of this analysis, maroon diamonds represent TC-SD data, orange squares represent MR-SD data, blue triangles represent EM-SD data and green circles represent EB-SD, unless otherwise specified. It is evident from this figure that the water content of the feed greatly influenced the dry density of the briquettes. As predicted, the Briquette Proctor Test results depicted in Figure 4-5 for the three bituminous coal briquettes (i.e. TC-SD, MR-SD and EM-SD) are very similar to the standard Proctor curve for clay soils. Conversely, the correlation between water content and dry density of the sub-bituminous coal briquettes (i.e. EB-SD) is more obscure and appears to have a wide range of optimum water content values.

Although maximum dry density values were easily determined using the Briquette Proctor Test, there was actually a range of water content values that produced briquettes within a narrow band of near-optimum dry density values. For example, the dry density of the TC-SD briquettes varied between 1.087 g/cm$^3$ and 1.10$^3$ g/cm3 for water contents of 0.026, 0.037, 0.042 0.055. This suggests that a range of water contents can be targeted to approach the maximum dry density for briquettes produced with the hydraulic press. As a result, the selection of the optimum water content for a particular application could be chosen based on other

considerations, such as the economic tradeoff between an incremental increase in dry density (i.e. quality) and the incremental cost of drying materials to a particular water content. It is also evident from Figure 4-5 that water contents outside of the optimum range produce briquettes with much lower dry densities. For example, the minimum dry density of the TC-SD briquettes was found to be 0.923 g/cm$^3$ at a water content of 0.133, which represents a decrease of 16.3 percent from the maximum achieved dry density. Similarly, the dry density of the MR-SD briquetted decreased by 14.3 percent from the maximum to the minimum value, while the dry density of the EM-SD briquettes decreased by 15.0 percent and the dry density of the EB-SD briquettes decreased by 11.3 percent.

To further investigate the similarity of the three bituminous coals with respect to the water content and dry density of briquettes produced with a hydraulic press, normalized dry density values were calculated and compared. Normalizing the dry density results enables the direct comparison of the compaction behavior of the three coals without regarding the differences in true density, size modulus and bulk modulus. Each of these properties influence the measured dry density values, but are not believed to have any effect on the relationship between water content and dry density in compaction processes. Measured dry density values were normalized by dividing the individual dry density values by the maximum achieved dry density for each coal type. The result is displayed in Figure 4-6, which clearly shows the high degree of similarity in the compaction behavior of the three coals. This indicates that the fundamental compaction mechanisms are the same for bituminous coals, even though individual properties can impact dry density values.

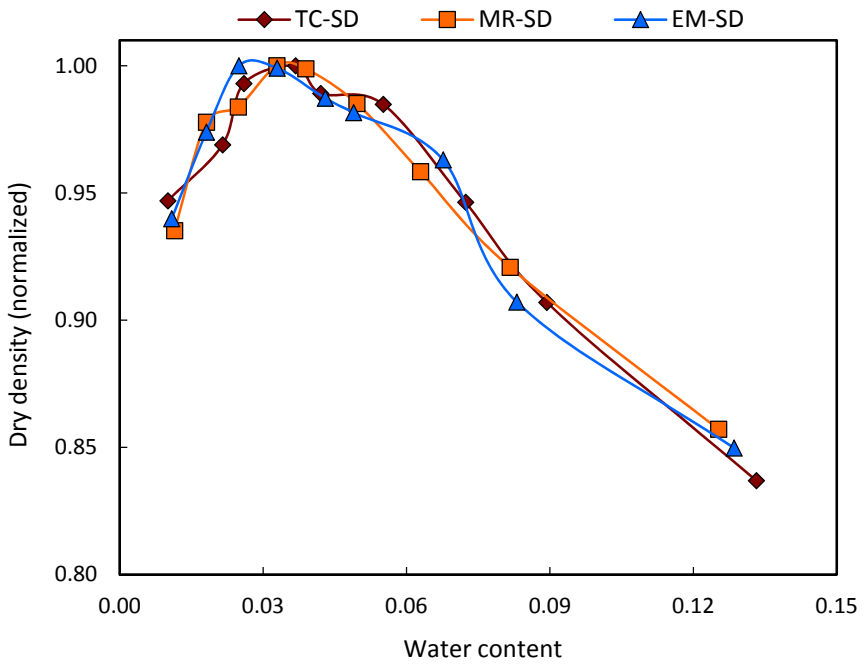



Figure 4-6. Correlation between water content and normalized dry density for the bituminous coal briquettes produced with the hydraulic press

## 4.4.2 Roll Press Moisture Optimization

The results of the continuous roll press briquetting tests are presented in Table 4-7 through Table 4-10 for each of the four coal types. These tables list the calculated water content, dry density, mechanical durability and crushing strength values of the coal-sawdust briquettes as determined by the procedures outlined in 4.3.3. The briquette water content and dry density values listed in each table represent the average dry density and water content values for the initial tests and those conducted roughly three hours after briquette production. The water content of the homogenized feed material typically varied by 10 to 20 percent from the target feed moisture, which is thought to be a result of imperfect mixing and sampling, as well as the inherent variability of the coal and biomass feedstocks. Another interesting observation was that the water content of the briquettes was consistently lower than the water content of the feed material. The source of this discrepancy is most likely a combination of water evaporation from heat produced during roll press briquette production and water loss due to air-drying prior to briquette evaluations.

Table 4-7. Summary of water content optimization results for TC-SD roll press briquettes

| Test ID | Feed Water Content | | Briquette Water Content | Dry Density ($g/cm^3$) | Mechanical Durability (%) | Crushing Strength (N) |
|---|---|---|---|---|---|---|
| | Target | Actual | | | | |
| TC-SD-0.7R | 0.007 | 0.008 | 0.006 | 1.10 | 85.4 | 645.9 |
| TC-SD-1.5R | 0.015 | 0.016 | 0.014 | 1.14 | 91.9 | 803.3 |
| TC-SD-2.2R | 0.022 | 0.023 | 0.018 | 1.16 | 92.9 | 975.0 |
| TC-SD-3.7R | 0.037 | 0.039 | 0.029 | 1.14 | 92.5 | 938.1 |
| TC-SD-5.2R | 0.052 | 0.049 | 0.038 | 1.12 | 88.2 | 798.5 |
| TC-SD-6.7R | 0.067 | 0.068 | 0.050 | 1.10 | 76.9 | 484.0 |
| TC-SD-8.2R | 0.082 | 0.083 | 0.063 | 1.06 | 63.1 | 268.7 |

Table 4-8. Summary of water content optimization results for MR-SD roll press briquettes

| Test ID | Feed Water Content | | Briquette Water Content | Dry Density ($g/cm^3$) | Mechanical Durability (%) | Crushing Strength (N) |
|---|---|---|---|---|---|---|
| | Target | Actual | | | | |
| MR-SD-0.7R | 0.007 | 0.011 | 0.011 | 1.12 | 93.3 | 844.7 |
| MR-SD-1.5R | 0.015 | 0.016 | 0.014 | 1.13 | 94.4 | 854.5 |
| MR-SD-2.2R | 0.022 | 0.022 | 0.017 | 1.15 | 95.1 | 1,198.4 |
| MR-SD-3.7R | 0.037 | 0.038 | 0.028 | 1.12 | 94.3 | 1,121.0 |
| MR-SD-5.2R | 0.052 | 0.045 | 0.037 | 1.10 | 89.8 | 892.8 |
| MR-SD-6.7R | 0.067 | 0.060 | 0.051 | 1.04 | 81.0 | 485.7 |
| MR-SD-8.2R | 0.082 | 0.075 | 0.065 | 1.01 | 69.4 | 265.1 |

Table 4-9. Summary of water content optimization results for EM-SD roll press briquettes

| Test ID | Feed Water Content | | Briquette Water Content | Dry Density ($g/cm^3$) | Mechanical Durability (%) | Crushing Strength (N) |
|---|---|---|---|---|---|---|
| | Target | Actual | | | | |
| EM-SD-0.7R | 0.007 | 0.007 | 0.007 | 1.12 | 94.0 | 1,070.7 |
| EM-SD-1.5R | 0.015 | 0.018 | 0.014 | 1.14 | 94.7 | 1,189.9 |
| EM-SD-2.2R | 0.022 | 0.025 | 0.021 | 1.15 | 95.2 | 1,241.9 |
| EM-SD-3.7R | 0.037 | 0.044 | 0.032 | 1.14 | 95.0 | 1,331.8 |
| EM-SD-5.2R | 0.052 | 0.052 | 0.043 | 1.11 | 92.2 | 1,052.4 |
| EM-SD-6.7R | 0.067 | 0.069 | 0.048 | 1.09 | 85.1 | 631.2 |
| EM-SD-8.2R | 0.082 | 0.082 | 0.070 | 1.03 | 73.0 | 361.6 |

Table 4-10. Summary of water content optimization results for EB-SD roll press briquettes

| Test ID | Feed Water Content | | Briquette Water Content | Dry Density ($g/cm^3$) | Mechanical Durability (%) | Crushing Strength (N) |
|---|---|---|---|---|---|---|
| | Target | Actual | | | | |
| EB-SD-2.5R | 0.025 | 0.040 | 0.029 | 0.96 | 54.2 | 381.2 |
| EB-SD-4.0R | 0.040 | 0.049 | 0.047 | 1.00 | 65.7 | 475.5 |
| EB-SD-5.5R | 0.055 | 0.053 | 0.058 | 1.03 | 71.0 | 527.1 |
| EB-SD-7.0R | 0.070 | 0.072 | 0.065 | 1.03 | 75.2 | 594.7 |
| EB-SD-8.5R | 0.085 | 0.084 | 0.074 | 1.03 | 77.7 | 654.3 |
| EB-SD-10.0R | 0.100 | 0.100 | 0.087 | 1.04 | 81.1 | 741.1 |
| EB-SD-12.5R | 0.125 | 0.127 | 0.111 | 1.03 | 85.7 | 981.7 |
| EB-SD-15.0R | 0.150 | 0.143 | 0.132 | 1.03 | 86.8 | 1,044.4 |
| EB-SD-17.5R | 0.175 | 0.169 | 0.151 | 1.00 | 87.3 | 919.0 |
| EB-SD-20.0R | 0.200 | 0.170 | 0.166 | 0.94 | 84.0 | 584.1 |
| EB-SD-22.5R | 0.225 | 0.188 | 0.189 | 0.90 | 71.3 | 447.0 |

The calculated water content and dry density values of the roll press briquettes and the hydraulic press briquettes for each of the four coals are displayed graphically in Figure 4-7. A visible shift in the location of the optimum dry density and water content of the roll press briquettes is apparent. For example, the maximum dry density of the TC-SD briquettes (Figure 4-7a) was 1.16 $g/cm^3$, which occurred at a water content of 0.018. Although this shift to higher dry density and lower water content was found, the data points for briquettes produced with the roll press appear to fall on the same zero air voids curve as the data from briquettes produced with the hydraulic press. This suggests that the maximum value of the zero air voids density is very similar for briquettes produced with both types of presses. It is believed that the shift in optimum values occurred due to differences in the mechanisms of compression present in the roll press and hydraulic press. Specifically, the only force applied by the hydraulic press is a uniaxial compression force. In contrast, briquettes produced with the roll press are fed by a variable speed screw into rotating rolls held together by a uniaxial compression force, which creates torque. During this dynamic process, friction forces produce heat that also aids in the compaction and densification process. Nonetheless, these finding suggest that the Briquette Proctor Test can be used to determine a range of water content values for coal-biomass blends in which the optimum water content for roll press briquette production likely exists.

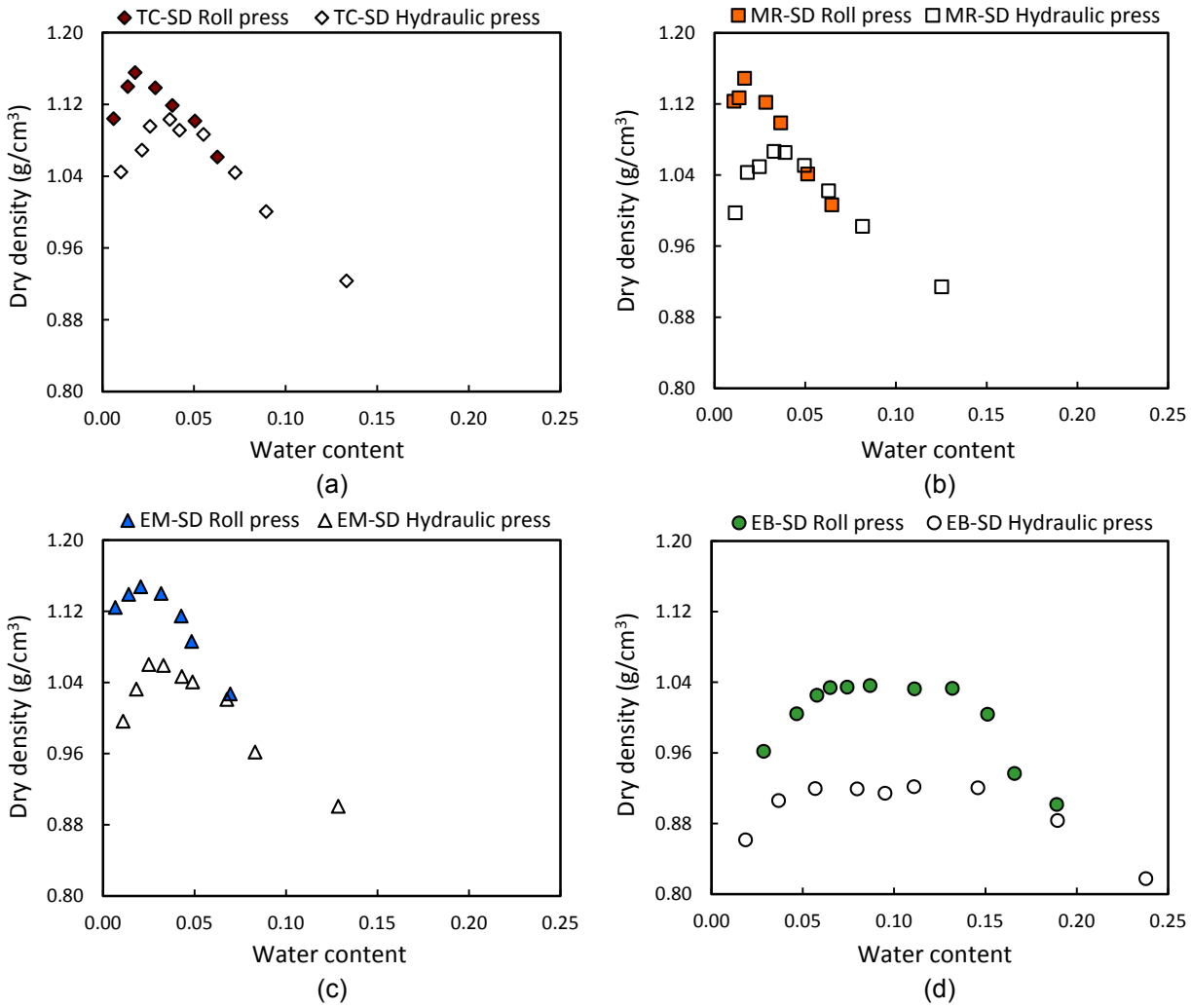



Figure 4-7. Correlation between water content and dry density for (a) TC-SD briquettes, (b) MR-SD briquettes, (c) EM-SD briquettes and (d) EB-SD briquettes

The results of the roll press briquetting tests further validate the similarity in the compaction behavior of the three bituminous coals investigated. As with the results presented in the previous section, the TC-SD roll press briquettes (Figure 4-7a), MR-SD roll press briquettes (Figure 4-7b) and EM-SD roll press briquettes (Figure 4-7c) all exhibit the same relationship between water content and dry density, wherein the maximum dry density occurs at a slightly higher dry density and lower water content than the results from the hydraulic press tests indicated. Specifically, the maximum dry densities of the three bituminous coal briquettes ranged from 1.15 g/cm$^3$ to 1.16 g/cm$^3$ over a water content range of 0.017 to 0.021. Another similarity of these results and the hydraulic press results is that the dry density of the TC-SD briquettes was again the highest of the three bituminous coal samples. In contrast to the bituminous coal results,

the maximum dry density of the EB-SD roll press briquettes was 1.04 g/cm$^3$, which occurred at a water content of 0.087 (Figure 4-7d). This result further exemplifies the difference in the compaction behavior of sub-bituminous coal as compared to bituminous coal.

Normalized dry density values were calculated and compared to further investigate the similarity of the three bituminous coals with respect to briquette water content and dry density. As shown in Figure 4-8, the normalized dry density values for the three bituminous coals are very comparable over the range of water contents evaluated. However, the visual similarity of these results is not as pronounced as the results presented for the hydraulic press briquettes (i.e. Figure 4-6), even though the location of the maximum dry density is very similar. The most probable reason for the decreased similarity in the relationship between briquette water content and dry density is the greater forces present in roll press systems, which leads to a greater discernment between samples.

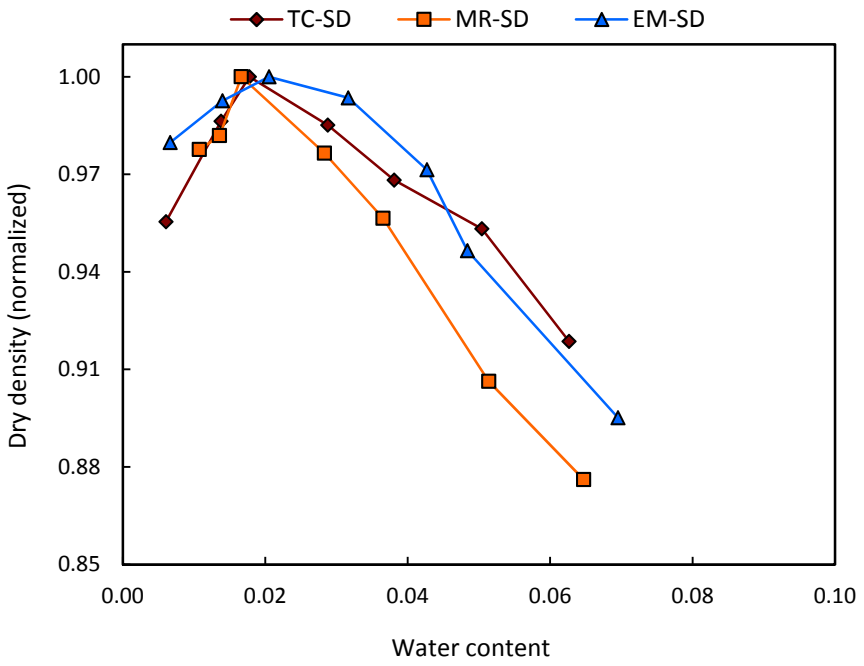



Figure 4-8. Correlation between water content and normalized dry density for the bituminous coal briquettes produced with the roll press

## 4.4.3 Correlations between Briquette Properties

Crushing strength and mechanical durability were measured for each batch of briquettes produced with the roll press to determine the influence of water content and dry density on these quality indicators. The water content of each type of briquettes is plotted versus mechanical

durability in Figure 4-9. The highest mechanical durability value for the TC-SD briquettes was 92.9%, which occurred at a water content of 0.018. Similarly, the highest mechanical durability values for the MR-SD (95.1%) and EM-SD briquettes (95.2%) occurred at water contents of 0.017 and 0.021, respectively. In contrast, the maximum mechanical durability of the EB-SD briquettes was 87.3%, which occurred at a water content of 0.151. It is evident from Figure 4-9 that mechanical durability values decrease significantly when water content is varied outside of a small range of near-optimum values. For example, an increase in the water content of TC-SD briquettes from 0.018 to 0.063 resulted in a 32.1 percent decrease in mechanical durability and a decrease in the water content of EB-SD briquettes from 0.151 to 0.029 led to a 37.9 percent decrease in mechanical durability. Moreover, an increase in the water content of MR-SD briquettes from 0.017 to 0.065 resulted in a 27.0 percent decrease in mechanical durability and an increase in the water content of EM-SD briquettes from 0.021 to 0.070 led to a 23.3 percent decrease in mechanical durability.

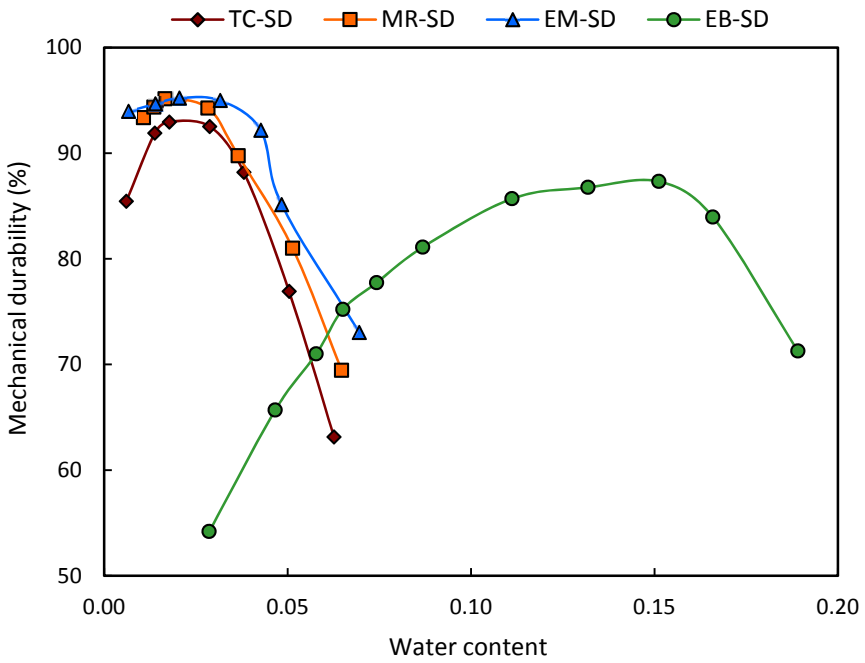



Figure 4-9. Correlation between water content and mechanical durability for all roll press briquettes

The water content of each type of briquettes is plotted versus crushing strength in Figure 4-10. The highest crushing strength value for the TC-SD briquettes was 975.0 N (219.2 $lb_f$), which occurred at a water content of 0.018. Similarly, the highest crushing strength values for the MR-SD (1,198.4 N; 269.4 $lb_f$) and EM-SD briquettes (1,331.8 N; 299.4 $lb_f$) occurred at water

contents of 0.017 and 0.032, respectively. The maximum crushing strength of the EB-SD briquettes (1,044.4 N; 234.8 $lb_f$) was similar in magnitude to the bituminous coal briquettes, but it occurred at a water content of 0.132. It is evident from Figure 4-10 that a dramatic decrease in crushing strength occurs when water content is varied outside of a small range of near-optimum values. For example, an increase in the water content of TC-SD briquettes from 0.018 to 0.063 resulted in a 72.4 percent decrease in crushing strength and a decrease in the water content of EB-SD briquettes from 0.132 to 0.029 led to a 63.5 percent decrease in crushing strength. Moreover, an increase in the water content of MR-SD briquettes from 0.017 to 0.065 resulted in a 77.9 percent decrease in crushing strength and an increase in the water content of EM-SD briquettes from 0.032 to 0.070 led to a 72.8 percent decrease in crushing strength.

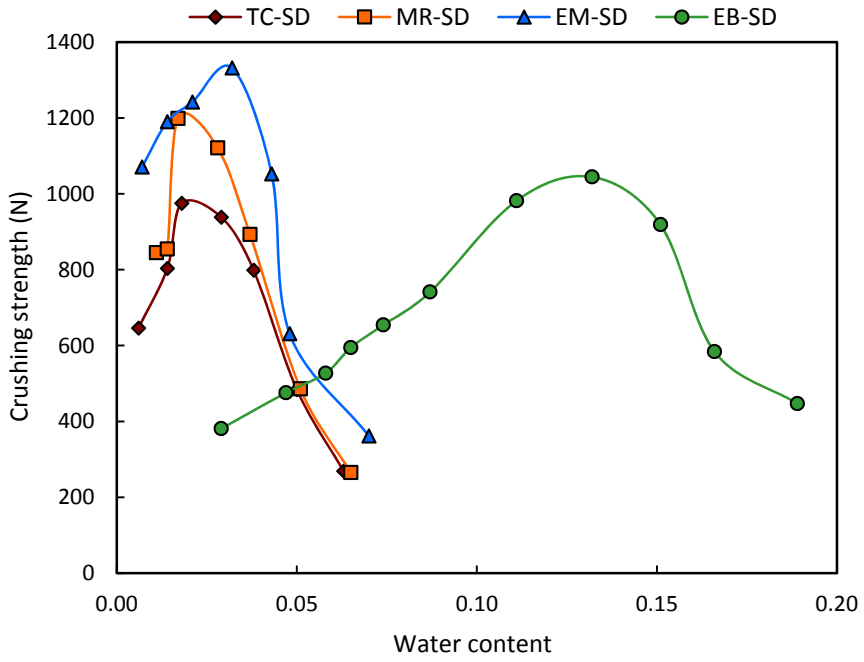



Figure 4-10. Correlation between water content and crushing strength for all roll press briquettes

The reason for significant variances in the mechanical durability and crushing strength of the different types of bituminous coal briquettes cannot be definitively determined. However, it appears that the distribution modulus, which is the measure of the spread of particle size distribution as calculated by the Rosin-Rammler equation, and ash content are the major sources of these variations. Specifically, the distribution modulus appears to have the largest impact on strength and durability, with higher distribution moduli corresponding to greater strength and durability of briquettes. For example, the distribution modulus of the Emerald coal was the

highest of the three coal samples (1.02), and the EM-SD briquettes had the greatest crushing strength (1,331.8 N; 299.4 $lb_f$) and mechanical durability (95.2%). In contrast, the distribution modulus of the McClure River coal was 0.91, and the MR-SD briquettes exhibited lower crushing strength (1,198.4 N; 269.4 $lb_f$) and mechanical durability (95.1%). Similarly, the distribution modulus of the Toms Creek coal was the lowest of the three bituminous coal samples (0.88), and the TC-SD briquettes were found to have the lowest strength (975.0 N; 219.2 $lb_f$) and durability (92.9%).

Further examination revealed that the difference in maximum strength and maximum durability of MR-SD briquettes and TC-SD briquettes (i.e. 223.3 N [50.2 $lb_f$] and 2.2%) is much greater than the difference observed between MR-SD briquettes and EM-SD briquettes (i.e. 133.4 N [30 $lb_f$] and 0.01%). However, the difference in the distribution modulus of McClure River coal and Toms Creek coal (i.e. 0.03) is significantly less than the difference in the distribution modulus of McClure River coal and Emerald coal (i.e. 0.11). Therefore, the distribution modulus is not the only significant factor that influences briquette strength and durability. The other significant variable appears to be ash content, which would account for the significant difference in strength and durability of MR-SD briquettes (MR ash = 6.22%) and TC-SD briquettes (TC ash = 11.30%), despite a very small difference in the calculated distribution moduli. Thus, it appears that ash content is inversely related to briquette strength and durability. Still, the data does not indicate that ash content has as large of an influence on briquette strength and durability as distribution modulus. This is supported by the fact that the EM-SD briquettes are superior to the MR-SD briquettes in both strength and durability, yet the ash content of the Emerald coal (i.e. 9.37%) is higher than that of the McClure River coal (i.e. 6.22%).

An interesting correlation is that between dry density and the mechanical durability of the coal-biomass briquettes. To visualize this correlation, the measured mechanical durability values were plotted versus the calculated dry density values, as shown in Figure 4-11. A least squares linear regression was performed to model the relationship between these two variables. The results of the regression analysis are provided in Figure 4-11 for each type of coal. The coefficient of determination ($R^2$) was calculated for each trend line to quantify the fit of the data to the linear regression model. These results are provided in Figure 4-11a for the TC-SD briquettes, Figure 4-11b for the MR-SD briquettes, Figure 4-11c for the EM-SD briquettes and Figure 4-11d for the EB-SD briquettes.

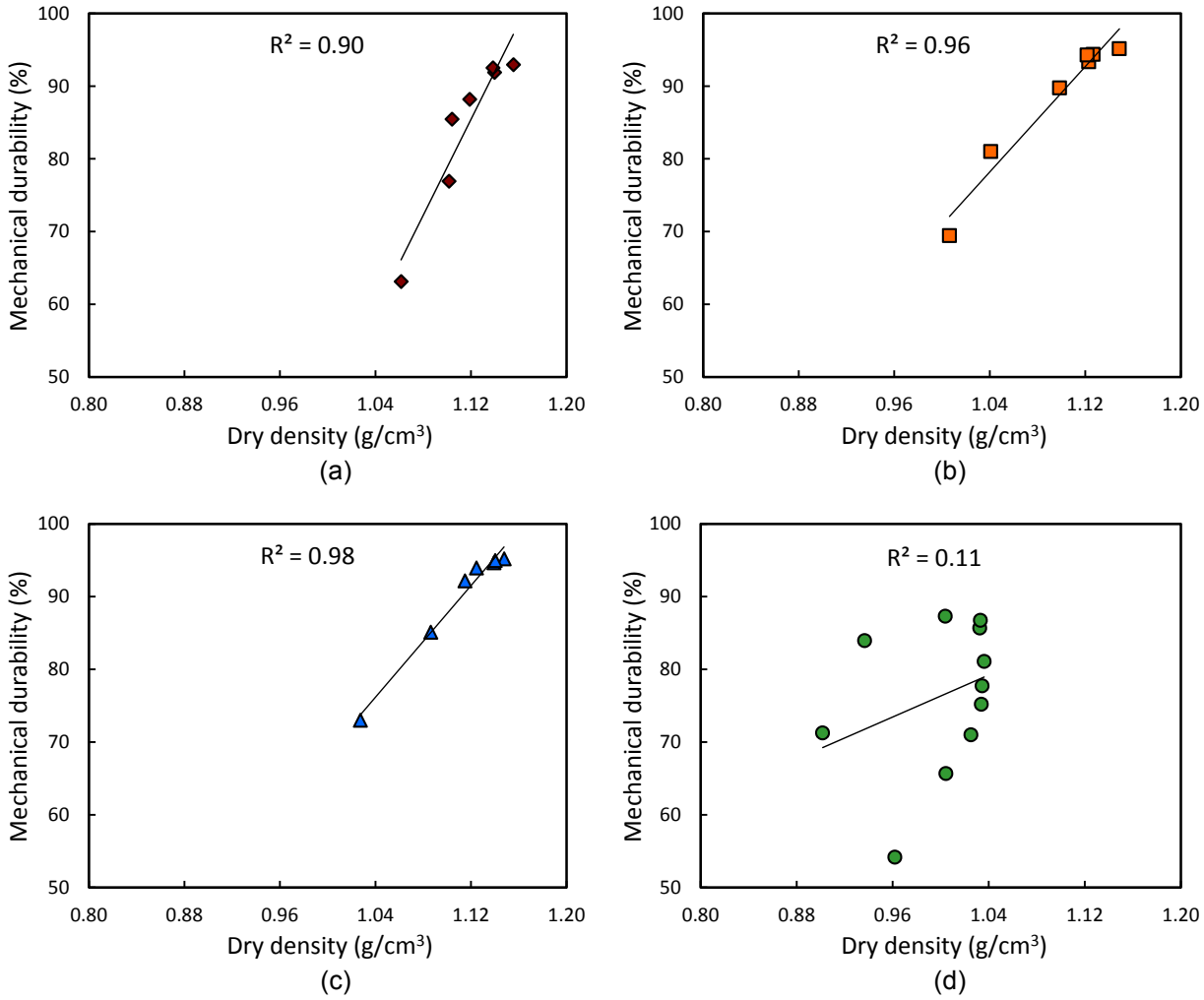



Figure 4-11. Linear correlation between mechanical durability and dry density for (a) TC-SD briquettes, (b) MR-SD briquettes, (c) EM-SD briquettes and (d) EB-SD briquettes

The individual R-squared values for each bituminous coal type were very high, which indicates that a strong linear correlation exists between the dry density and mechanical durability of each set of briquettes. Specifically, the EM-SD briquettes were found to have the highest R-squared value (0.98) followed closely by the MR-SD briquettes (0.96) and the TC-SD briquettes (0.90). To determine if a correlation exists between all of the bituminous coal briquette data, the 21 pairs of dry density and mechanical durability data displayed in Figure 4-11a through Figure 4-11c were combined into a single data set (Figure 4-12a) and a linear regression was again performed. The coefficient of determination of the data fit to this model was 0.74, which indicates that the dry density and mechanical durability of bituminous coal-biomass briquettes fits a generalized linear model fairly well, regardless of the physical and chemical properties of

the coal. For reference, the derived empirical equation is included in Figure 4-12a. To provide additional insight to this relationship, the dry density and mechanical durability values of the 21 bituminous coal data pairs were normalized and a linear regression was again performed (Figure 4-12b). The calculated $R^2$ value for this model was 0.82, which represents a 10.8 percent improvement in the fit of the model to the data. Again, the derived empirical formula is included in Figure 4-12b for reference.

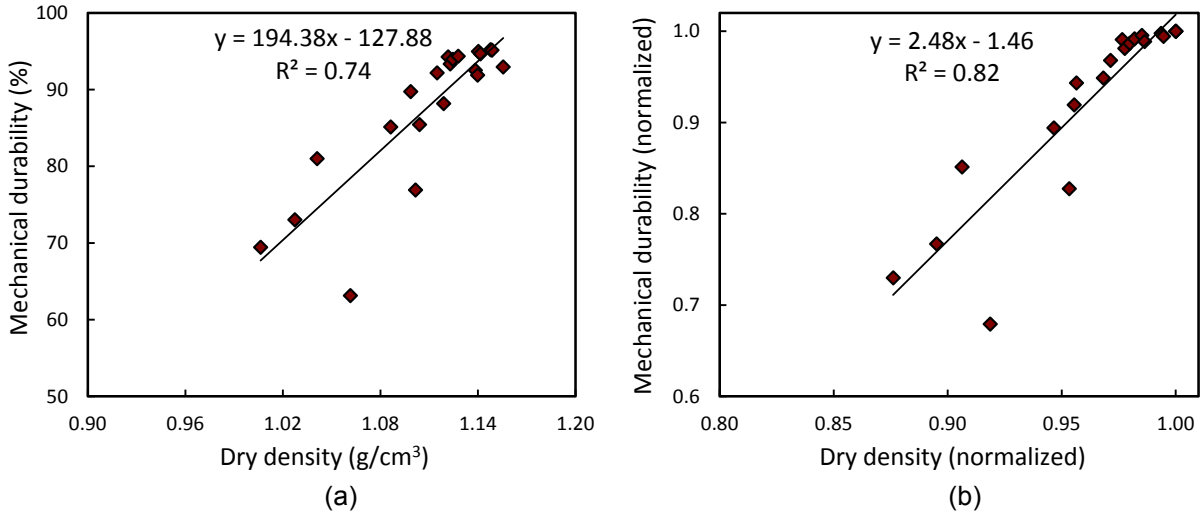



Figure 4-12. (a) Linear correlation between mechanical durability and dry density for the combined data from the three bituminous coals and (b) linear correlation between normalized mechanical durability and normalized dry density for the combined data from the three bituminous coals

In contrast to the findings for the bituminous coals, the EB-SD briquettes were found to have a very low R-squared value (0.11), which suggests that little or no correlation exists between dry density and mechanical durability of sub-bituminous coal-biomass briquettes. However, further investigation of the trend displayed in Figure 4-11d reveals that a correlation does exist between the dry density and mechanical durability of the EB-SD briquettes. To visualize this correlation, the dry density and mechanical durability data was divided into two sets: (1) increasing dry density values, which include the first six test results in Table 4-10 (i.e. water contents of 0.029 to 0.087), and (2) decreasing dry density values, which include the last six test results in Table 4-10 (i.e. water contents of 0.087 to 0.189). A linear regression was then performed independently on each data set to determine if an independent linear correlation exists between briquettes of increasing and decreasing dry densities. As displayed in Figure 4-13, the two sets of data fit the independent linear models much better than the single model presented in

Figure 4-11d, as evidenced by an $R^2$ value of 0.94 for the increasing dry density data and an R-squared value of 0.51 for the decreasing dry density data. This clearly demonstrates that linear correlations do exist between dry density and mechanical durability values for sub-bituminous coal-biomass briquettes.

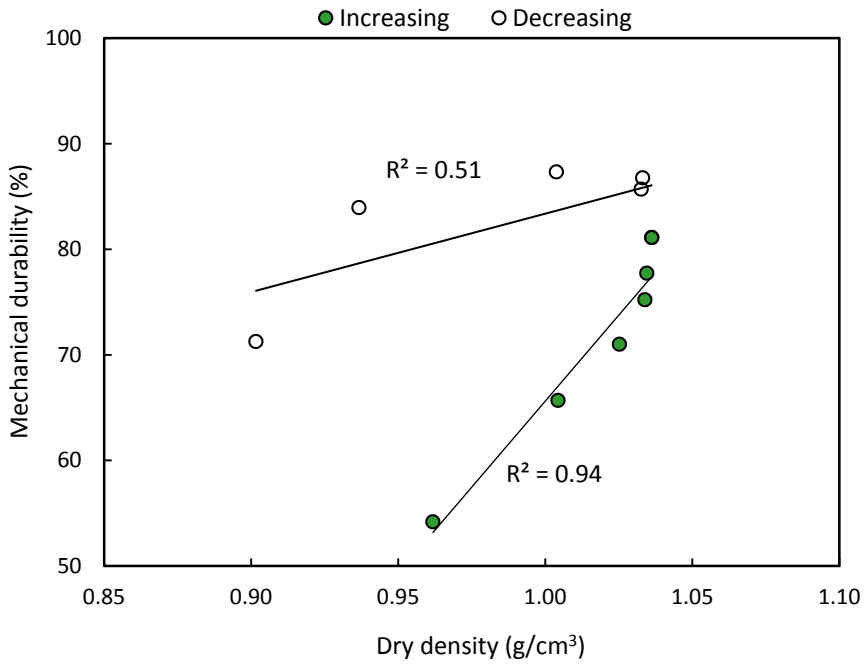



Figure 4-13. Linear correlations between mechanical durability and dry density of EB-SD briquettes for increasing and decreasing dry density values

Another interesting observation is the correlation between dry density and the crushing strength of the coal-biomass briquettes. To visualize this correlation, the measured crushing strength values were plotted versus the calculated dry density values, as shown in Figure 4-14. A least squares linear regression was performed to model the relationship between these two variables. The results of the regression analysis are provided in Figure 4-14 for each type of coal. The coefficient of determination was calculated for each trend line to quantify the fit of the data to the linear regression model. These results are provided in Figure 4-14a for the TC-SD briquettes, Figure 4-14b for the MR-SD briquettes, Figure 4-14c for the EM-SD briquettes and Figure 4-14d for the EB-SD briquettes. The R-squared values for each bituminous coal type were very high, which indicates that a strong linear correlation exists between the dry density and crushing strength for each coal type. Specifically, the EM-SD briquettes were found to have the

highest R-squared value (0.94) followed closely by the TC-SD briquettes (0.92) and the MR-SD briquettes (0.89).

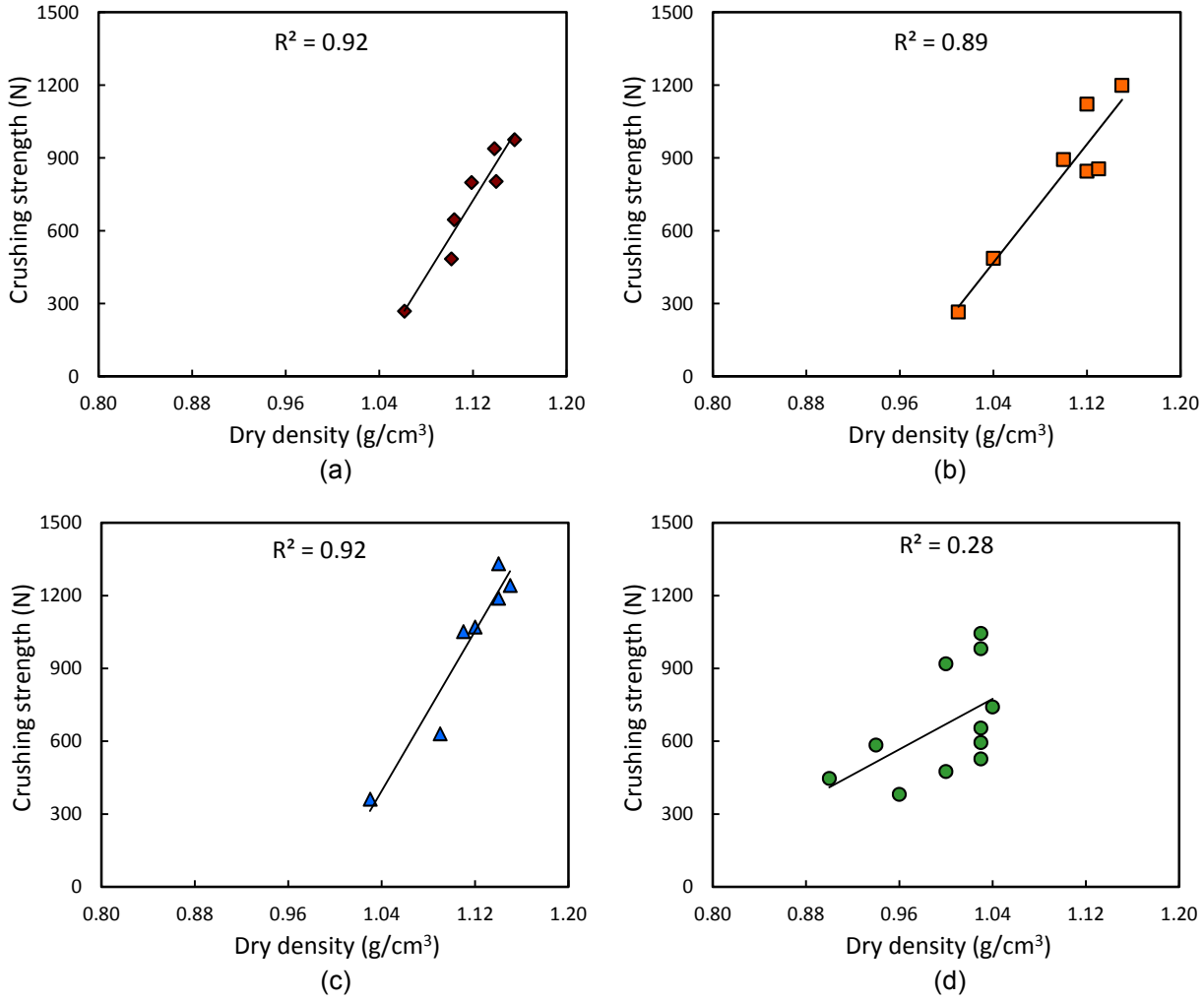



Figure 4-14. Linear correlation between crushing strength and dry density for (a) TC-SD briquettes, (b) MR-SD briquettes, (c) EM-SD briquettes and (d) EB-SD briquettes

To determine if a correlation exists between all of the bituminous coal briquette data, the 21 pairs of dry density and crushing strength data displayed in Figure 4-14a through Figure 4-14c were combined into a single data set (Figure 4-15a) and a linear regression was again performed. The coefficient of determination of the data fit to this model was 0.73, which indicates that the dry density and crushing strength of bituminous coal-biomass briquettes fits a generalized linear model fairly well, regardless of the physical and chemical properties of the coal. For reference, the derived empirical equation is included in Figure 4-15a. To provide additional insight to this relationship, the dry density and crushing strength values of the 21

bituminous coal data pairs were normalized and a linear regression was again performed (Figure 4-15b). The calculated R-squared value for this model was 0.88, which represents a 20.5 percent improvement in the fit of the model to the data. Again, the derived empirical formula is included in Figure 4-15b for reference.

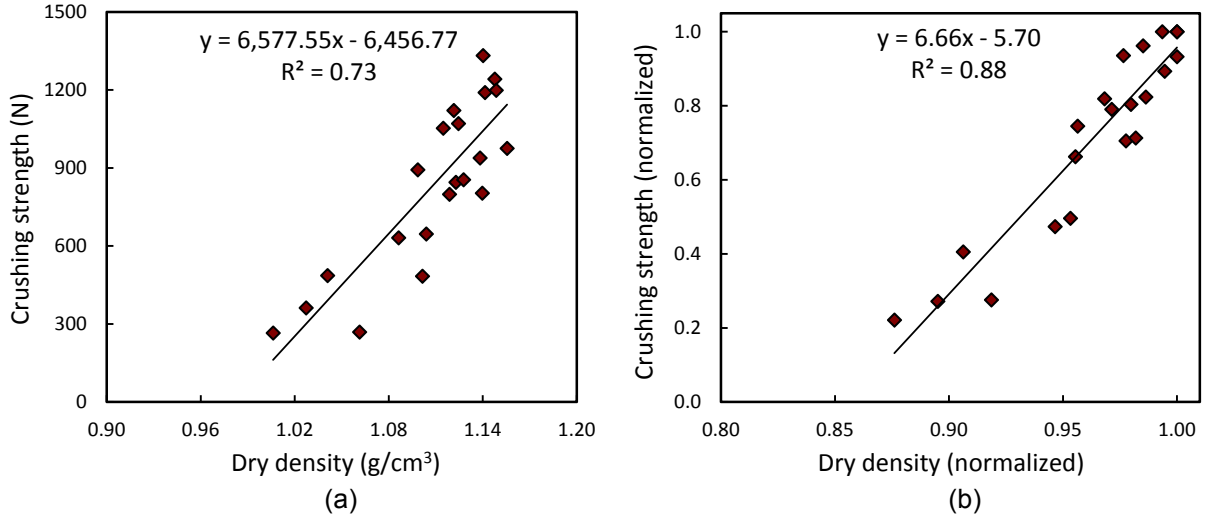



Figure 4-15. (a) Linear correlation between crushing strength and dry density for the combined data from the three bituminous coals and (b) linear correlation between normalized crushing strength and normalized dry density for the combined data from the three bituminous coals

In contrast to the findings for the bituminous coals, the EB-SD briquettes were found to have a very low R-squared value (0.29), which suggests that little or no correlation exists between dry density and mechanical durability of sub-bituminous coal-biomass briquettes. However, further investigation of the trend displayed in Figure 4-14d reveals that a correlation does exist between the dry density and mechanical durability of the EB-SD briquettes. To visualize this correlation, the dry density and mechanical durability data was divided into two sets: (1) increasing dry density values, which include the first six test results in Table 4-10 (i.e. water contents of 0.029 to 0.087), and (2) decreasing dry density values, which include the last six test results in Table 4-10 (i.e. water contents of 0.087 to 0.189). A linear regression was then performed independently on each data set to determine if an independent linear correlation exists between briquettes of increasing and decreasing dry densities. As displayed in Figure 4-16, the two sets of data fit the independent linear models much better than the single model presented in Figure 4-14d, as evidenced by an R-squared value of 0.77 for both the increasing and decreasing

dry density data. This clearly demonstrates that linear correlations do exist between dry density and mechanical durability values for sub-bituminous coal-biomass briquettes.

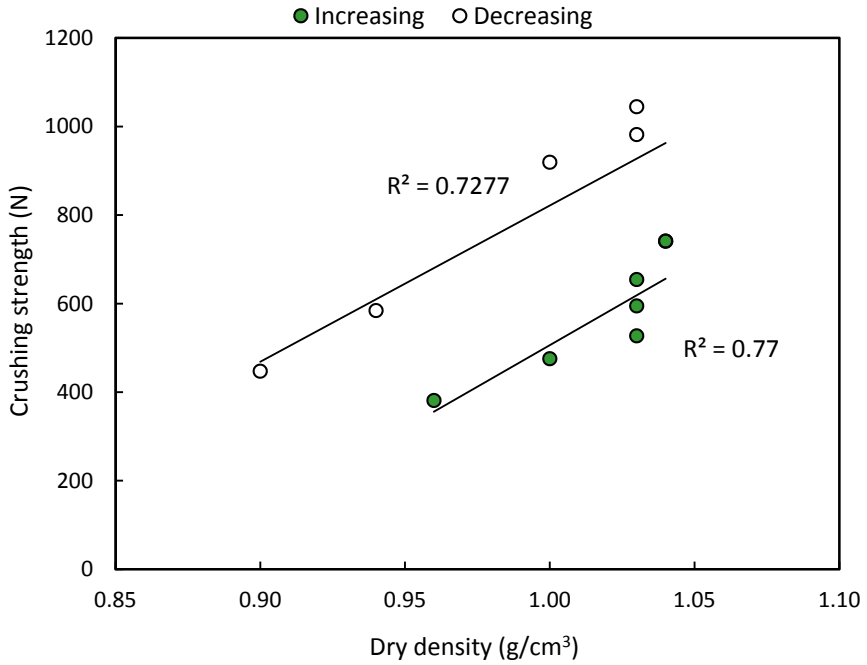



Figure 4-16. Linear correlations between crushing strength and dry density of EB-SD briquettes for increasing and decreasing dry density values

To analyze the relationship between mechanical durability and crushing strength, the two quality indicators were plotted against one another for each coal type, as shown in Figure 4-17. An exponential regression was performed to model the relationship between these two quality indicators. The results of the regression analysis are provided in Figure 4-11 for each type of coal. The coefficient of determination was calculated for each trend line to quantify the fit of the data to the exponential regression model. These results are provided in Figure 4-17a for the TC-SD briquettes, Figure 4-17b for the MR-SD briquettes, Figure 4-17c for the EM-SD briquettes and Figure 4-17d for the EB-SD briquettes. The individual $R^2$ values for each coal type were very high, which indicates that a strong exponential correlation exists between the mechanical durability and crushing strength of the briquettes. Specifically, the TC-SD briquettes were found to have the highest R-squared value (0.99) followed closely by the EM-SD briquettes (0.98) and the MR-SD briquettes (0.95). For the EB-SD briquettes, the fit of the data to the exponential model was not as precise, as evidenced by an R-squared value of 0.80. Nonetheless, the strong correlation between mechanical durability and crushing strength indicates that as the mechanical

durability of coal-biomass briquettes increases in a moisture optimization process, the crushing strength typically increases at an exponential rate. This suggests that measurement of both crushing strength and mechanical durability is not needed to locate optimum moisture with respect to briquette quality.

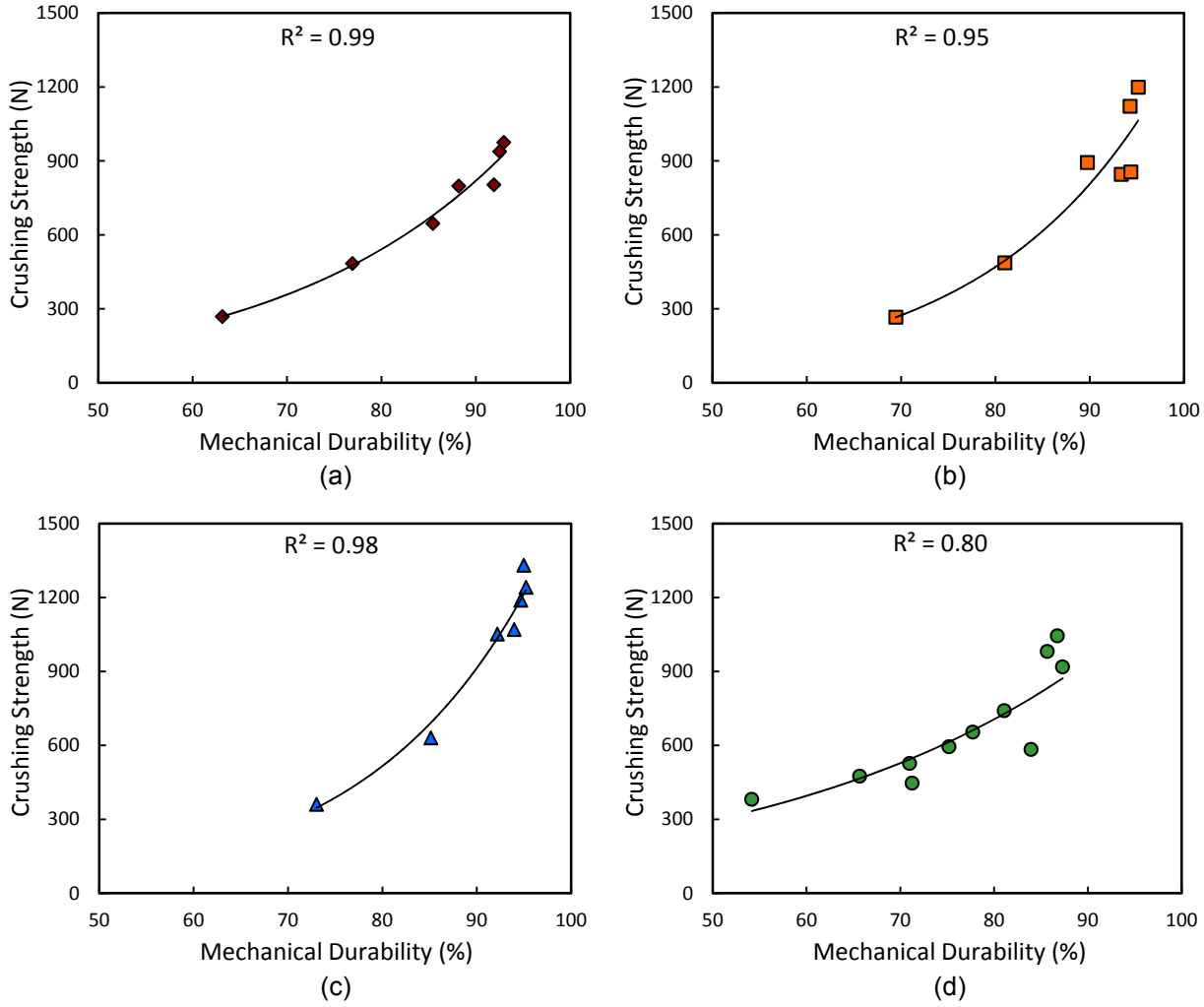



Figure 4-17. Exponential correlation between mechanical durability and crushing strength for (a) TC-SD briquettes, (b) MR-SD briquettes, (c) EM-SD briquettes and (d) EB-SD briquettes

## 4.5 Summary and Conclusions

The primary objective of this study was to develop a methodology that minimizes time and materials required to identify the optimum water content of coal-biomass blends prior to briquette production. In support of this effort, the Briquette Proctor Test was developed based on the theoretical compaction concepts employed by the Proctor Test for clay soils. Accordingly,

three hypotheses were formulated and evaluated to determine the applicability of this novel test method. The secondary objective of this study was to compare and contrast the briquetting performance of three bituminous coals and one sub-bituminous coal. This was accomplished by evaluating the three hypotheses for each of the coals studied, comparing the results of the evaluations and determining the sources of any inconsistencies.

The first hypothesis stated that the water content of coal-biomass blends directly influences the dry density, crushing strength and mechanical durability of briquettes. A peak in dry density was easily identified for each coal type at a particular water content for the roll press and hydraulic press briquettes. The water content that corresponded to the maximum dry density of the bituminous coal-sawdust briquettes was in the range of 0.017 to 0.021. In contrast, the water content that corresponded to the maximum dry density of the sub-bituminous coal-sawdust briquettes was in the range of 0.058 to 0.132. The results obtained by the Briquette Proctor Test proved that water content does indeed influence the dry density of coal-biomass briquettes very similarly to the influence of water content on the dry density of compacted clay soils as determined by the Proctor Test. Additionally, a peak in mechanical durability and crushing strength values was easily observed for each coal type. The major sources of inconsistencies in the dry density, mechanical durability and crushing strength of the bituminous coal-sawdust briquettes was determined to be the distribution modulus and ash content. Specifically, it was determined that a positive correlation exists between distribution modulus and each briquette quality and a negative correlation exists between ash content and each briquette quality.

The second hypothesis stated that batch briquette production using a hydraulic press with a pellet mold is representative of continuous roll press briquette production. From the dry density versus water content results for briquettes produced with both types of presses, it is clear that the hydraulic press gives a good indication of the results that would be expected with the roll press. However, the peak value of dry density calculated for briquettes produced with the roll press occurred at a lower water content and was greater in magnitude than the values recorded for briquettes produced with the hydraulic press. Although this shift was observed, both sets of data appear to fall on the same zero air voids curve, which suggests that the maximum value of the zero air voids density is very similar for both data sets. This shift is thought to be a result of a temperature increase and the presence of other forces that occurs with roll press briquette production.

The final hypothesis stated that dry density is directly related to the crushing strength and mechanical durability of coal-biomass briquettes. To test this theory, the calculated values of dry density were plotted versus the measured crushing strength and mechanical durability values for each coal type and a linear regression model was fitted to each data set. For each of the bituminous coals studied, a very high coefficient of determination was calculated for both crushing strength and mechanical durability. To determine the similarity of the compaction behavior of the three bituminous coals, the data sets were combined and fitted with a linear regression model, which found fairly decent correlations between dry density and mechanical durability ($R^2 = 0.74$), and between dry density and crushing strength ($R^2 = 0.73$). Although these values could have been higher, they are deemed acceptable due to the inherent variability of coal-biomass briquettes.

These findings suggest that an exhaustive experimental moisture optimization study for roll press briquetting coal-biomass mixtures could be streamlined by simply determining the water content that results in the highest dry density. It is likely that the maximum crushing strength and mechanical durability of the briquettes exist at or near this value as well. In addition to reducing the time required to perform evaluations, the Briquette Proctor Test also reduces material requirements as significantly fewer briquettes are required to locate optimum conditions. Another major implication of these findings is the realization that bituminous coals with similar water contents exhibit very similar compaction behavior regardless of the physical and chemical properties of the coals. However, sub-bituminous coals exhibit very different compaction behavior than bituminous coals, and thus require independent investigation. Ultimately, moisture optimization will improve the quality of briquettes and promote the co-utilization of coal-biomass feedstocks.

# Chapter 5

# Evaluation of Coal–Biomass Briquette Production Variables

## 5.1 Abstract

Experimental optimization of coal-biomass briquette production is an essential task to improve the strength and durability of briquettes. In support of this challenge, an exhaustive bench-scale study was conducted to examine the most significant feedstock, additive, and roll press variables in coal-biomass briquette production. Additional work was performed to identify optimum process conditions for each variable, which were defined for this study as the conditions that contribute to production of coal-biomass briquettes with the greatest crushing strength and mechanical durability. In addition, work was conducted to compare and contrast the quality of briquettes composed of four coal types and five biomass types. Lastly, a comprehensive series of tests were conducted to characterize the physical properties, flow properties and gasification behavior of selected coal-biomass briquettes to verify the enhanced quality of co-briquetted feedstocks. The results of this study show that biomass content and water content are the most statistically significant mixture variables with regard to the crushing strength and mechanical durability of coal-biomass briquettes. The results also confirm that starch content is a very statistically significant mixture variable with regard to the crushing strength and mechanical durability of coal-biomass briquettes. Another important finding is that roll torque is the most statistically significant roll press operating variable with regard to the particle density, crushing strength and mechanical durability of coal-biomass briquettes. Finally, it is shown that binderless coal-biomass briquettes produced at optimized conditions exhibit very high crushing strength and mechanical durability values, which indicate that the briquettes would remain competent in the presence of forces encountered in handling, storage and transportation. Binderless coal-biomass briquettes produced at optimized conditions also exhibit excellent

gasification behavior. This confirms that coal-biomass briquettes are exceptional gasification feedstocks for the co-production of power and synthetic fuels.

## 5.2 Introduction

### 5.2.1 Problem Statement

Co-utilization of biomass with coal in existing coal-fired facilities presents a unique opportunity to reduce greenhouse gas emissions and increase energy production from renewable resources. Significant interest in this opportunity has led to more than 150 coal-fired power stations across the world co-firing coal and biomass on a commercial or trial basis as of 2009 (Fernando, 2009). These co-firing experiences have revealed a number of technical challenges including upstream issues, such as biomass availability, transportation, storage, and handling, as well as problems encountered during energy conversion, such as fouling, corrosion, inconsistent feeding and segregation (Basu et al., 2011; Sami et al., 2001). Recent studies suggest that many of these challenges can be mitigated by reconstituting coal-biomass mixtures into larger particles. Specifically, roll press briquetting has been investigated to produce homogeneous, free-flowing feedstocks that minimize handling and segregation problems often encountered with combustion and gasification systems (Taulbee et al., 2010; Honaker et al., 2005).

One of the major challenges surrounding this technology is the degradation of coal-biomass briquettes during handling, transportation and storage. Fortunately, the strength and durability of briquettes can be greatly improved by optimizing the briquette production process. Despite its perceived simplicity, roll press briquetting is a complex process that is characterized by a number of design variables, which makes theoretical prediction of briquette quality extremely difficult. As a result, optimization of roll press briquetting is best accomplished by a series of laboratory tests, from which empirical models can be developed for particular feedstocks (Dec & Komarek, 1997). Therefore, experimental optimization of the briquetting process is essential to enhance the quality and marketability of coal-biomass briquettes.

## 5.2.2 Roll Press Briquette Production

### 5.2.2.1 Compaction Theory

The potential binding mechanisms employed in briquette production processes are generally classified into five major groups by the nature of particle-particle interactions: (1) solid bridges, (2) adhesion and cohesion forces, (3) surface tension and capillary pressure, (4) attraction forces between solids and (5) interlocking bonds (Rumpf, 1962). These groups of forces can be further divided into several subgroups, and in practice, a combination of forces act simultaneously within briquettes to bond individual particles to one another. Figure 2-7 depicts the potential particle binding mechanisms in briquette production processes.

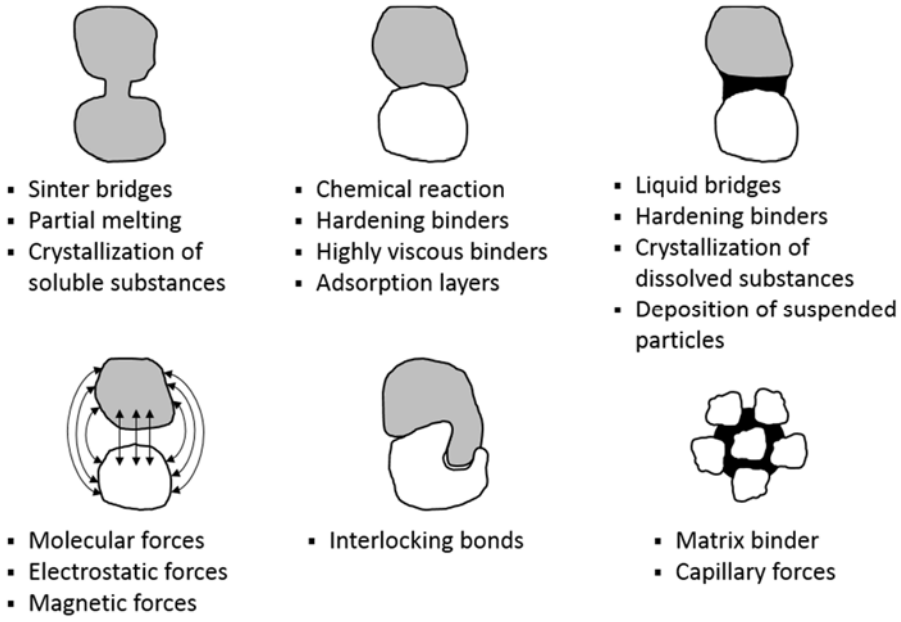



Figure 5-1. Particle binding mechanisms in briquette production (modified from Pietsch, 2002)

The mechanisms of compaction in briquette production can be divided into two stages. In the initial stage, low pressures cause bulk particles to settle and rearrange, which results in a reduction of porosity and an increase in bulk density. The total surface area of contact between particles also increases during this stage and bonds are formed through liquid bridges and capillary pressure (Drzymala, 1993). At this point, briquettes are relatively weak and require additional compaction pressure to improve strength and durability. In the second stage, much higher pressures are exerted on the densified mass, which results in the fracture of brittle particles and/or plastic deformation of malleable materials (Pietsch, 2002). Additional bonds are

formed during this stage by activation of interparticle adhesive forces, which occurs when the surface area of contact between particles is further increased and the distance between particles becomes extremely small. Figure 2-12 provides a schematic representation of these processes.

The top half of this figure shows the structural change of particulate solids with the progression of compaction, densification, fragmentation and plastic deformation that occurs with increasing pressure. The bottom half of the figure depicts the increase in pressing force at a constant compression rate over a period of time until the maximum pressure ($P_{max}$) is reached. Beyond this point, the pressure drops and expansion of compressed air and/or elastic spring-back can crack and weaken briquettes, which can lead to partial or complete degradation if not adequately addressed. One method to reduce the effects of elastic spring-back and expansion of compressed air is to reduce the speed of compaction, which in turn increases the amount of time material remains confined under the influence of the load. This parameter is referred to as dwell time (Pietsch, 2002). Another method to reduce the effects of these mechanisms is deaeration of the feed material prior to briquette formation. This is typically accomplished by selection of the proper feeding mechanism (e.g. paddle feeder and tapered screw) for a particular application.

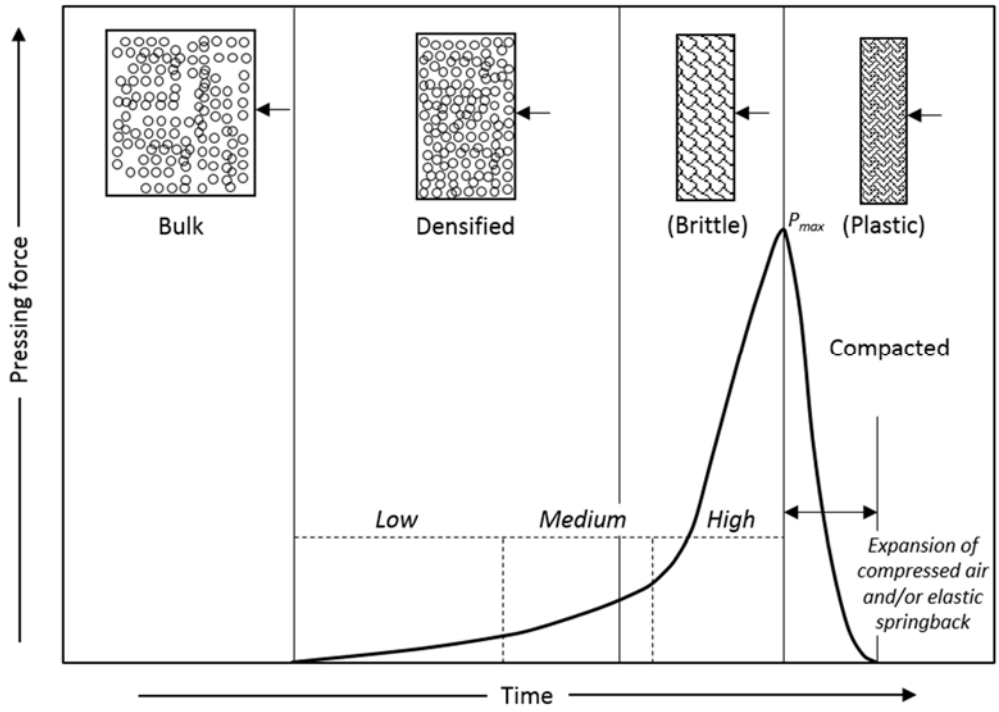



Figure 5-2. Mechanisms of compaction in briquette production (modified from Pietsch, 2002)

#### 5.2.2.2 Roll Press Machines

Roll pressing is the most widely used pressure agglomeration technology for size enlargement of particulate solids in the mineral processing industry. Originally developed to agglomerate coal fines, roll presses are characterized by two identical counter-rotating rolls held together by an applied force that compact particulate material as it is drawn between the rolls. In roll press briquetting machines, particulate solids are force or gravity fed through pocket rollers to produce briquettes of uniform size and shape (Figure 5-3a). This process produces a 'web' or 'flash' material on the edges of the briquettes due to the flat area around each pocket. The majority of the web material is typically removed by screening the briquettes after formation and recycled back into the feed to minimize the production of fines during handling.

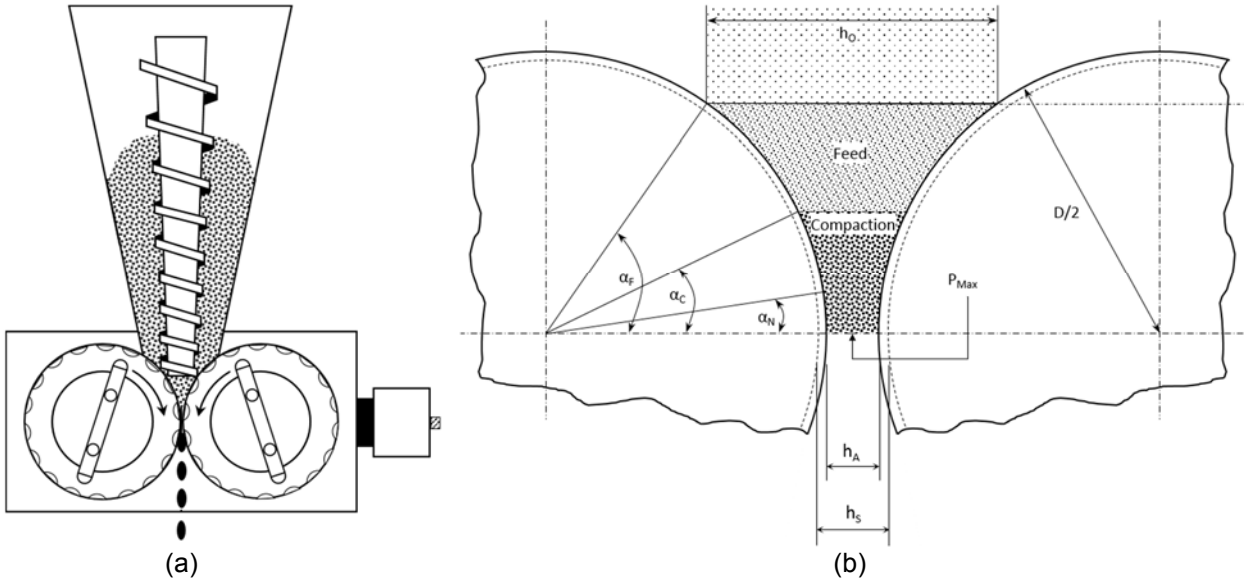



Figure 5-3. Schematic diagram of (a) force fed roll press with pocket rollers (modified from Pietsch, 2002) and (b) nip region between two smooth counter-rotating rollers (modified from Pietsch, 2002 and Capes, 1980)

As particulate solids enter the nip region between the rollers and compaction begins, three distinct zones can be defined: the feed zone, the compaction zone and the release zone (Pietsch, 2002). Figure 5-3b depicts the movement of material through these zones for a gravity fed system with two smooth counter-rotating rollers. In the feed zone, material is drawn into the nip region by the combination of gravity and friction between the rollers and the particulate solids. This zone is defined by the width of the rectangular feed opening ($h_O$), the angle of delivery ($\alpha_F$) and the angle of nip ($\alpha_C$). During the compaction process, low pressure forces are

developed in the feed zone, which leads to preliminary densification by particle rearrangement. From here material continues into the compaction zone, defined by the area between the angle of nip ($\alpha_C$) and the neutral angle ($\alpha_N$), where a sharp increase in pressure leads to the fragmentation and plastic deformation of particles. Beyond the neutral angle ($\alpha_N$), the densified product enters the release zone, in which particles are subjected to the maximum pressure ($P_{Max}$) within the system and the maximum particle density is attained with a thickness ($h_A$) equal to the width between the rollers. Finally, the frictional force is reversed and the briquette is ejected from the rollers. Immediately following ejection, the final particle thickness ($h_S$) slightly increases due to the expansion of compressed air and elastic spring-back. The complexity of material flow through the nip region is greatly enhanced in the case of roll press briquetting with pocket rollers (Pietsch, 2002).

#### 5.2.2.3 Briquette Production Variables

Roll press briquette production is a complex process that is characterized by a number of important design variables. These variables can be divided into three groups: (1) operating parameters, (2) feedstock variables and (3) additive variables. The most important roll press operating parameters are compaction pressure, roll torque, and roll rotational speed (Dec & Komarek, 1997). Each of these parameters influences the degree of compaction of a material and the quality of briquettes produced. Specifically, compaction pressure and roll torque affect the shear and hydrostatic stresses developed within individual briquettes, which greatly influence briquette strength and durability (Dec & Komarek, 1997). The roll torque applied to a material in a roll press system can be adjusted by varying the feed rate of material to the rolls, which rotate at a fixed speed. Although it is difficult to maintain a constant value for this parameter, measurement of roll torque is easily accomplished in most roll press machines using an integrated torque transducer.

The compaction pressure applied to a material during briquette production in a roll press is typically adjusted by varying the roll separating force applied by an integrated hydraulic system. In contrast to roll torque measurement, interpretation and measurement of compaction pressure is a much greater challenge. The pressure applied by the rolls on a material during briquette production depends on material properties (i.e. stress-strain relationship), friction conditions and the design of the pressing system (Dec & Komarek, 1997). Compaction pressure

could be measured with a pressure transducer at the roll surface, but this component is generally not incorporated in roll press systems because of the cost and technical complexity of such systems. As a result, true compaction pressure is not typically measured. However, compaction pressure can be estimated and reported as two different variables: (1) force factor, wherein roll separating force is divided by the width of the rolls and (2) briquette calculated (or mean) pressure, wherein roll separating force is divided by the surface determined by the circumferential length of the briquette and the roll width (Dec & Komarek, 1997).

The other important roll press operating parameter is roll rotational speed. This parameter affects both the quality of briquettes and the production rate of the machine. As roll speed is decreased, the negative effects of elastic spring-back and expansion of compressed air are reduced as permanent material bonds form with an increase in dwell time. However, due to desired production rates in industrial processes, roll speed must be optimized to balance production rate with briquette quality. For example, roll speed is often limited in fine powder applications by deaeration and precompaction requirements to maintain briquette quality. Since roll speed is an adjustable parameter on modern roll press machines, measurement is very straightforward.

Feedstock variables also have a large influence on the strength and durability of briquettes produced by roll pressing. For any given material, the most important of these variables are moisture content and particle-size distribution (Komarek, 2001). Both properties can greatly influence the packing density, and thus the quality, of coal-biomass briquettes. In experimental optimization of coal-biomass briquetting, the impact of these variables should be considered for every specific combination of coal and biomass investigated. This includes every combination of different types of coal and biomass, as well as every ratio of coal to biomass in the blended feed. Although these parameters are not true material variables, they are classified as such for the purpose of this study.

The impact of moisture content on the particle density, strength and durability of coal-biomass briquettes was discussed in detail in Chapter 4. Specifically, several sets of laboratory tests were conducted for different coal types, the results of which proved that water content has a very significant influence on the quality of coal-biomass briquettes. A clear optimum water content was experimentally determined for each bituminous coal type, and a range of optimum values was identified for the sub-bituminous coal studied. Additionally, a strong positive

correlation was found between the dry density, mechanical durability and crushing strength of coal-biomass briquettes. However, the one aspect this study did not address is the combined influence of water content and other material variables.

The importance of particle-size distribution in briquette production is largely a function of the achievable packing density of particles and the number of contact points for the formation of particle bonds. For instance, the maximum theoretical packing density of perfect spheres is 74 percent (i.e. $\sqrt{2}\pi/6 = 0.7405$). This value increases to 86 percent if a smaller size fraction of spheres is added to the material that occupy the void spaces between the larger particles (Scott & Kilgour, 1969). Similarly, if third and fourth size fraction is added that fills the new void spaces between the larger particles then the theoretical packing density approaches 90 to 92 percent and 95 to 97 percent, respectively (Drzymala, 1993). In an investigation on the effect of particle-size distribution on the production of briquettes composed of fine coal and sawdust, Patil et al. (2009) determined that packing density can be maximized by combining 70 to 80 percent coarse coal recovered from a spiral separator (1.18 x 0.15 mm) with 20 to 30 percent fine coal recovered from a flotation cell (<0.15 mm). However, the maximum compressive strength of the briquettes occurred with 100 percent fine coal, and thus no strong correlation between density and strength were noted.

When binders or lubricants are combined with coal and biomass to improve briquette properties, additional variables concerning these additives must also be considered. Specifically, the influence of the amount of additive used and briquette cure time are particularly important to consider in these applications. For example, Taulbee et al. (2009) determined that binder content and cure time have a significant impact on the quality of briquettes produced from blends of fine coal and sawdust. This study determined that increased binder content and cure time generally improved the quality of the coal-biomass briquettes.

### 5.2.3 Research Objectives

Experimental optimization of coal-biomass briquette production is an essential task to improve the strength and durability of briquettes. In support of this challenge, an exhaustive bench-scale study was conducted to examine the most significant process variables and to identify optimum process conditions. The specific objectives of this study were to:

1. Evaluate and analyze the influence of material variables (i.e. water content, biomass content and biomass top size) on the density, strength and durability of briquettes composed of different types of coal and biomass feedstocks;
2. Evaluate and analyze the influence of additive variables (i.e. binder content and curing time) on the density, strength and durability of coal-biomass briquettes;
3. Evaluate and analyze the influence of roll press operating parameters (i.e. roll force, roll torque and roll rotational speed) on the density, strength and durability of coal-biomass briquettes;
4. Determine the optimum combination of feedstock variables, additive variables and roll press variables for industrial production of coal-biomass briquette feedstocks; and
5. Conduct an extensive characterization study on important physical properties, flow properties and gasification behavior of selected coal-biomass briquettes to verify the enhanced quality of co-briquetted feedstocks.

## 5.3 Experimental

### 5.3.1 Materials

Several different coal and biomass feedstocks were collected to address the objectives of this research. Processing was required to prepare each bulk feedstock for briquetting experiments. Specifically, size reduction and screening operations were conducted to obtain a desired top size for each of the feedstocks. A top size of one millimeter was selected for the coal feedstocks because coal particles less than this size are typically difficult to handle and transport. Large quantities of this size fraction are produced during the mechanical excavation of coal in modern coal mines. Thus, coal particles less than one millimeter in diameter present a significant opportunity for agglomeration into larger particles by briquetting. Several different biomass top sizes (i.e. 1.20, 2.38 and 4.75 mm) were selected to evaluate the impact of biomass size reduction on the quality of coal-biomass briquettes. Additional preparation was conducted to dry the coal and biomass feedstocks so that briquettes could be produced at target moisture levels for further investigation of this material property. The only additive evaluated in this study was pregelatinized wheat starch, which did not require any preparation prior to briquette production.

#### 5.3.1.1 Coal Feedstocks

The coal feedstocks investigated in this study included three high-rank bituminous coals and one low-rank sub-bituminous coal. These coals were chosen because they represent the vast majority of proven coal resources in the United States and because they dominate the country's current coal production portfolio. The bituminous coals were obtained from preparations plants operated by Alpha Natural Resources throughout the Appalachian coal basin of the eastern United States. In contrast, the sub-bituminous coal was obtained from a mine operated by Alpha Natural Resources in the Powder River Basin in the western United States. Specifically, the coal samples obtained for briquetting evaluations were:

1. Emerald: a high-volatile, high-sulfur bituminous coal obtained from the Emerald mine preparation plant in Waynesburg, Pennsylvania;
2. McClure River: a medium-volatile bituminous coal obtained from the McClure River preparation plant in McClure, Virginia;
3. Toms Creek: a high-volatile bituminous coal obtained from the Toms Creek preparation plant in Coeburn, Virginia; and
4. Eagle Butte: a sub-bituminous coal obtained from the Eagle Butte mine in Gillette, Wyoming.

The Emerald coal sample was obtained from the clean coal stockpile at the preparation plant and was subjected to further processing to prepare the coal for briquette production. Size reduction of the sample was accomplished by successive crushing in a jaw crusher, roll crusher and grinder. The coal was then screened to a top size of one millimeter using a Uniflex two-deck screen, air-dried for one week, split into two kilogram lots and stored in sealed plastic bags. Several evaluations were performed to determine important physical properties of coal, the results of which are included in Table 4-1. The moisture content of the coal prior to briquette production was 1.60% (dry basis), which was determined by oven drying at 105 degrees Celsius for 24 hours. The true density of the Emerald coal was 1.27 g/cm$^3$, which was determined by water displacement in a 250 milliliter volumetric flask. The size distribution of the crushed coal was measured by wet screening and analyzed using the Rosin-Rammler equation (Figure 4-2). Based on this analysis, the Emerald coal was found to have a mass median diameter of 301 microns, a size modulus of 0.43 and a distribution modulus of 1.02. Ultimate and proximate analyses were also conducted to characterize the chemical composition of the Emerald coal

(Table 4-2). Notable results of the analyses include a moisture and ash free heating value of 35,513 kJ/kg (15,268 Btu/lb), an ash content of 9.37% (dry basis), and a sulfur content of 3.04% (dry basis).

Table 5-1. Physical properties of coal feedstocks

| Physical Property | Emerald | McClure River | Toms Creek | Eagle Butte |
|---|---|---|---|---|
| Moisture Content (%) | 1.60 | 0.93 | 1.03 | 1.80 |
| True Density (g/cm$^3$) | 1.27 | 1.27 | 1.33 | 1.27 |
| Mass Median Diameter (μm) | 301 | 266 | 239 | 295 |
| Size Modulus | 0.43 | 0.40 | 0.36 | 0.41 |
| Distribution Modulus | 1.02 | 0.91 | 0.88 | 1.16 |

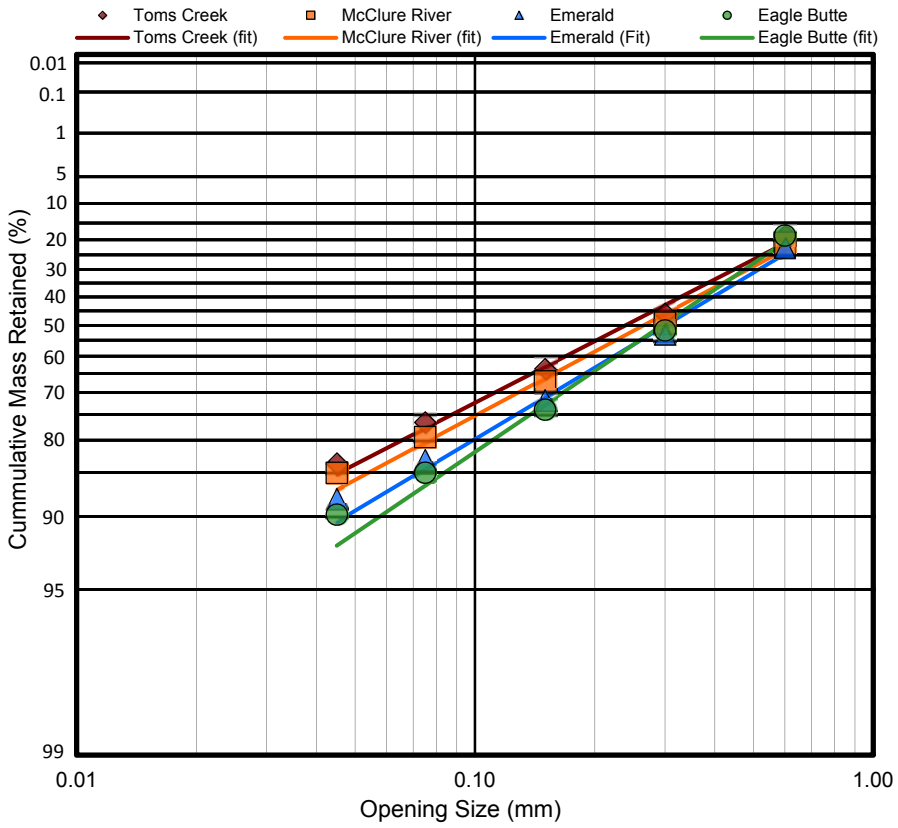



Figure 5-4. Particle-size distribution of coal feedstocks

Table 5-2. Chemical properties of coal feedstocks

| Chemical Property | Emerald | | McClure River | | Toms Creek | | Eagle Butte | |
|---|---|---|---|---|---|---|---|---|
| | As Received | Dry Basis | As Received | Dry Basis | As Received | Dry Basis | As Received | Dry Basis |
| Moisture (%) | 4.28 | -- | 7.89 | -- | 13.73 | -- | 29.08 | -- |
| Ash (%) | 8.97 | 9.37 | 5.73 | 6.22 | 9.75 | 11.30 | 5.60 | 7.89 |
| Sulfur (%) | 3.04 | 3.18 | 0.81 | 0.88 | 0.80 | 0.93 | 0.64 | 0.90 |
| Volatiles (%) | 37.59 | 39.27 | 26.17 | 28.41 | 27.24 | 31.57 | 40.89 | 57.66 |
| Fixed Carbon (%) | 49.16 | 51.36 | 59.80 | 64.92 | 49.29 | 57.13 | 24.43 | 34.45 |
| Carbon (%) | 74.26 | 77.58 | 75.77 | 82.26 | 66.19 | 76.72 | 47.08 | 66.38 |
| Hydrogen (%) | 4.91 | 5.13 | 4.38 | 4.75 | 3.85 | 4.46 | 4.00 | 5.64 |
| Nitrogen (%) | 1.39 | 1.45 | 1.44 | 1.56 | 1.36 | 1.58 | 0.70 | 0.99 |
| Oxygen (%) | 3.15 | 3.29 | 0.05 | 0.05 | 4.32 | 5.01 | 12.91 | 18.20 |
| HHV (kJ/kg) | 30,808 | 32,185 | 30,152 | 32,734 | 27,144 | 31,464 | 18,955 | 26,726 |
| MAF HHV (kJ/kg) | -- | 35,513 | -- | 36,574 | -- | 35,472 | -- | 29,015 |

The McClure River coal sample was also obtained from the clean coal stockpile at the preparation plant and subjected to further processing to prepare the coal for briquette production. Size reduction of the coal was accomplished by successive crushing in a jaw crusher, roll crusher and grinder. The coal was then screened to a top size of one millimeter using a Uniflex two-deck screen, air-dried for one week, split into two-kilogram lots and stored in sealed plastic bags. Again, several evaluations were performed to determine important physical properties of coal, the results of which are included in Table 4-1. The moisture content of the coal prior to briquette production was 0.93% (dry basis), which was determined by oven drying at 105 degrees Celsius for 24 hours. The true density of the McClure River coal was 1.27 g/cm$^3$, which was determined by water displacement in a 250 milliliter volumetric flask. The size distribution of this coal was also measured by wet screening and analyzed using the Rosin-Rammler equation (Figure 4-2). Based on this analysis, the McClure River coal was found to have a mass median diameter of 266 microns, a size modulus of 0.40 and a distribution modulus of 0.91. Ultimate and proximate analyses were also conducted to characterize the chemical composition of the McClure River coal (Table 4-2). Notable results of the analyses include a moisture and ash free heating value of 36,574 kJ/kg (15,724 Btu/lb), an ash content of 6.22% (dry basis), and a sulfur content of 0.88% (dry basis).

The Toms Creek coal sample was a combined spiral and flotation clean product sampled from a screen bowl centrifuge in the preparation plant. In preparation for briquette production, the coal was screened to a top size of one millimeter using a Uniflex two-deck screen, air dried

for one week, split into two-kilogram lots and stored in sealed plastic bags. Again, several evaluations were performed to determine important physical properties of coal, the results of which are included in Table 4-1. The moisture content of the coal prior to briquette production was 1.03% (dry basis), which was determined by oven drying at 105 degrees Celsius for 24 hours. The true density of the Toms Creek coal was 1.33 g/cm$^3$, which was determined by water displacement in a 250 milliliter volumetric flask. The size distribution of the crushed coal was measured by wet screening and analyzed using the Rosin-Rammler equation (Figure 4-2). Based on this analysis, the Toms Creek coal was found to have a mass median diameter of 239 microns, a size modulus of 0.36 and a distribution modulus of 0.88. Ultimate and proximate analyses were also conducted to characterize the chemical composition of the coal (Table 4-2). Notable results of the analyses include a moisture and ash free heating value of 35,472 kJ/kg (15,250 Btu/lb), an ash content of 11.30% (dry basis), and a sulfur content of 0.93% (dry basis).

The Eagle Butte coal sample was obtained from the raw coal stockpile of the Eagle Butte mine. In preparation for briquette production, the coal was successively crushed in a jaw crusher, roll crusher and grinder. The coal was then screened to a top size of one millimeter using a Uniflex two-deck screen, air dried for one week, oven dried at 105 degrees Celsius for 48 hours, split into two-kilogram lots and stored in sealed plastic bags. Again, several evaluations were performed to determine important physical properties of coal, the results of which are included in Table 4-1. The moisture content of the Eagle Butte coal prior to briquette production was 1.80% (dry basis), which was determined by oven drying at 105 degrees Celsius for 24 hours. The true density of the Eagle Butte coal was 1.27 g/cm$^3$, which was determined by water displacement in a 250 milliliter volumetric flask. The size distribution was again analyzed using the Rosin-Rammler equation (Figure 4-2), which indicated that the coal had a mass median diameter of 295 microns, a size modulus of 0.41 and a distribution modulus of 1.16. Ultimate and proximate analyses were also conducted to characterize the chemical composition of the Eagle Butte coal (Table 4-2). Notable results of the analyses include a moisture and ash free heating value of 29,015 kJ/kg (12,474 Btu/lb), an ash content of 7.89% (dry basis), and a sulfur content of 0.90% (dry basis).

#### 5.3.1.2 Biomass Feedstocks

The biomass feedstocks investigated in this study included five total samples of corn stover, grasses and wood that represent the wide spectrum of renewable biomass resources available in the United States. A particular focus was placed on agricultural residues, forestry residues and perennial grasses that are viable energy crops. Specifically, the biomass samples obtained for briquetting evaluations were:

1. Corn stover: an agricultural by-product of corn production (i.e. stalk, leaf, husk and cob) obtained from a farm in Blacksburg, Virginia operated by Virginia Tech;
2. Switchgrass: a perennial warm season bunchgrass native to North America, obtained from Piedmont Bioproducts in Gretna, Virginia;
3. Miscanthus: a large perennial warm season bunchgrass, obtained from Piedmont Bioproducts in Gretna, Virginia;
4. Wheat straw: an agricultural by-product of wheat production (i.e. dry stalks after grain is removed), obtained from a farm in Riner, Virginia; and
5. Sawdust: a forestry by-product produced by cutting, drilling or sanding wood, obtained from Turman Sawmill in Hillsville, Virginia.

The corn stover sample evaluated in this study was obtained as large round bales, which were processed in a Jordan Reduction Solutions knife mill (Figure 3-4a) equipped with a 6.35-millimeter screen. The corn stover was then screened to three different top sizes (i.e. 1.20, 2.38, 4.75 mm) using a Sweco vibrating separator and stored in sealed 18.9 liter (5 gal) buckets. A portion of each size class was oven dried at 105 degrees Celsius for 48 hours to facilitate low moisture content evaluations. An additional bale of the corn stover was processed in the Jordan Reduction Solutions knife mill with a 4.76-millimeter screen to produce a large quantity of material that did not require any screening, for use in evaluations where biomass top size was not varied. Particle-size distribution was not determined for the processed biomass materials because previous attempts to collect this information has indicated that the results are skewed due to the elongated shape of the milled particles (i.e. elongated particles tend to screen differently than round particles). Prior to briquette production, the moisture content of the oven dried and as-received corn stover was 1.40% (dry basis) and 11.35% (dry basis) respectively, as determined by oven drying at 105 degrees Celsius for 24 hours. Ultimate and proximate analyses were conducted on the corn stover sample, the results of which are presented in Table 5-3. Notable

results of the analyses include a moisture and ash free heating value of 19,769 kJ/kg (8,499 Btu/lb), an ash content of 5.01% (dry basis), and a sulfur content of 0.10% (dry basis).



(a) (b) (c)

Figure 5-5. Equipment used for biomass size reduction: (a) knife mill, (b) tub grinder and (c) hammer mill

The switchgrass sample examined in this study was obtained as large round bales, which were successively processed through a Sperry New Holland tub grinder (Figure 3-4b) and a Bliss Industries hammer mill (Figure 3-4c) equipped with a 6.35-millimeter screen. The switchgrass was then screened to three different top sizes (i.e. 1.20, 2.38, 4.75 mm) using a Sweco vibrating separator and stored in sealed 18.9 liter (5 gal) buckets. A portion of each size class was oven dried at 105 degrees Celsius for 48 hours to facilitate low moisture content evaluations. Prior to briquette production, the moisture content of the oven dried and as-received switchgrass was 1.00% (dry basis) and 17.50% (dry basis) respectively, as determined by oven drying at 105 degrees Celsius for 24 hours. Ultimate and proximate analyses were conducted on the switchgrass sample with the results presented in Table 5-3. Notable results of the analyses include a moisture and ash free heating value of 19,429 kJ/kg (8,353 Btu/lb), an ash content of 2.86% (dry basis), and a sulfur content of 0.08% (dry basis).

Table 5-3. Chemical properties of biomass feedstocks

| Chemical Property | Corn Stover | | Switchgrass | | Miscanthus | | Wheat Straw | | Sawdust | |
|---|---|---|---|---|---|---|---|---|---|---|
| | As Received | Dry Basis | As Received | Dry Basis | As Received | Dry Basis | As Received | Dry Basis | As Received | Dry Basis |
| Moisture (%) | 12.95 | -- | 14.79 | -- | 11.65 | -- | 12.14 | -- | 14.08 | -- |
| Ash (%) | 4.36 | 5.01 | 2.44 | 2.86 | 2.38 | 2.69 | 3.07 | 3.49 | 0.22 | 0.26 |
| Sulfur (%) | 0.09 | 0.10 | 0.07 | 0.08 | 0.05 | 0.06 | 0.06 | 0.07 | 0.03 | 0.03 |
| Volatiles (%) | 71.49 | 82.13 | 70.37 | 82.58 | 74.07 | 83.84 | 70.24 | 79.95 | 78.64 | 81.53 |
| Fixed Carbon (%) | 11.19 | 12.86 | 12.41 | 14.56 | 11.90 | 13.47 | 14.55 | 16.56 | 7.05 | 8.21 |
| Carbon (%) | 46.37 | 53.27 | 41.59 | 48.81 | 42.44 | 48.04 | 41.81 | 47.59 | 51.66 | 60.12 |
| Hydrogen (%) | 4.94 | 5.67 | 6.32 | 7.04 | 5.43 | 6.15 | 5.38 | 6.12 | 5.40 | 6.28 |
| Nitrogen (%) | 0.54 | 0.62 | 0.35 | 0.30 | 0.14 | 0.16 | 0.40 | 0.46 | 0.02 | 0.02 |
| Oxygen (%) | 30.75 | 35.33 | 41.58 | 48.57 | 37.90 | 42.90 | 37.14 | 42.27 | 28.60 | 33.29 |
| HHV (kJ/kg) | 16,347 | 18,778 | 16,082 | 18,873 | 16,915 | 19,145 | 16,977 | 19,322 | 18,864 | 21,955 |
| MAF HHV (kJ/kg) | -- | 19,769 | -- | 19,429 | -- | 19,676 | -- | 20,020 | -- | 22,013 |

The miscanthus sample evaluated in this study was obtained as large round bales, which were successively processed through a Sperry New Holland tub grinder and a Bliss Industries hammer mill equipped with a 6.35-millimeter screen. The miscanthus was then screened to three different top sizes (i.e. 1.20, 2.38, 4.75 mm) using a Sweco vibrating separator and stored in sealed 18.9 liter (5 gal) buckets. A portion of each size class was oven dried at 105 degrees Celsius for 48 hours to facilitate low moisture content evaluations. Prior to briquette production, the moisture content of the oven dried and as-received miscanthus was 1.25% (dry basis) and 16.30% (dry basis) respectively, as determined by oven drying at 105 degrees Celsius for 24 hours. Ultimate and proximate analyses were conducted on the switchgrass sample with the results presented in Table 5-3. Notable results of the analyses include a moisture and ash free heating value of 19,676 kJ/kg (8,459 Btu/lb), an ash content of 2.69% (dry basis), and a sulfur content of 0.06% (dry basis).

The wheat straw sample examined in this study was obtained as small rectangular bales, which processed in a Jordan Reduction Solutions knife mill equipped with a 6.35-millimeter screen. The corn stover was then screened to three different top sizes (i.e. 1.20, 2.38, 4.75 mm) using a Sweco vibrating separator and stored in sealed 18.9 liter (5 gal) buckets. A portion of each size class was oven dried at 105 degrees Celsius for 48 hours to facilitate low moisture content evaluations. Prior to briquette production, the moisture content of the oven dried and as-received wheat straw was 1.65% and 12.25% (dry basis) respectively, as determined by oven drying at 105 degrees Celsius for 24 hours. Ultimate and proximate analyses were conducted on

the switchgrass sample with the results presented in Table 5-3. Notable results of the analyses include a moisture and ash free heating value of 20,020 kJ/kg (8,607 Btu/lb), an ash content of 3.49% (dry basis), and a sulfur content of 0.07% (dry basis).

The sawdust sample evaluated in this study was kiln-dried eastern white pine dust and shavings. To prepare the sawdust for briquette production, the bulk sample was screened to three different top sizes (i.e. 1.20, 2.38, 4.75 mm) using a Sweco vibrating separator and stored in sealed 18.9 liter (5 gal) buckets. A portion of each size class was oven dried at 105 degrees Celsius for 48 hours to facilitate low moisture content evaluations. Prior to briquette production, the moisture content of the oven dried and as-received sawdust was 1.35% (dry basis) and 10.60% (dry basis) respectively, as determined by oven drying at 105 degrees Celsius for 24 hours. The ultimate and proximate analyses results for the sawdust sample are displayed in Table 5-3. Notable results of the analyses include a moisture and ash free heating value of 22,013 kJ/kg (9,464 Btu/lb), an ash content of 0.26% (dry basis), and a sulfur content of 0.03% (dry basis).

#### 5.3.1.3 Additives

The only additive used to improve the quality of briquettes throughout this study was wheat starch. A pretreated form of the carbohydrate was obtained from Archer Daniels Midland Company in a 22.7 kilogram (50 lb) bag. This starch was cooked in the presence of water and heat to break down intermolecular bonds in a process known as starch gelatinization. The gelatinized starch was then dried, which rendered it cold water soluble. This type of commercially available starch is commonly known as pregelatinized wheat starch. This organic, water soluble matrix binder was chosen for this study because it has been proven to improve the quality of coal-biomass briquettes and is readily available throughout the United States (Taulbee et al., 2009; Shimasaki et al., 2003).

### 5.3.2 Briquette Production

Throughout this study, pill-shaped briquettes (approximately 43 x 19 x 14 mm) were produced with a Komarek B-100R laboratory roll press equipped with 13-centimeter diameter pocketed rolls. The machine is comprised of two counter-rotating rolls, two hydraulic cylinders, a horizontal tapered screw and a paddle feeder. A schematic diagram of the roll press and the laboratory installation are depicted in Figure 5-6. The hydraulic cylinders control the position of the upper roll and thus control the gap between the rolls. The paddle feeder is driven by a fixed

speed motor and distributes the material to the horizontal screw that in turn feeds material to the rolls. The counter-rotating rolls and the horizontal screw are driven by variable speed motors, which enable adjustment of the torque applied to the material from the rolls and screw.

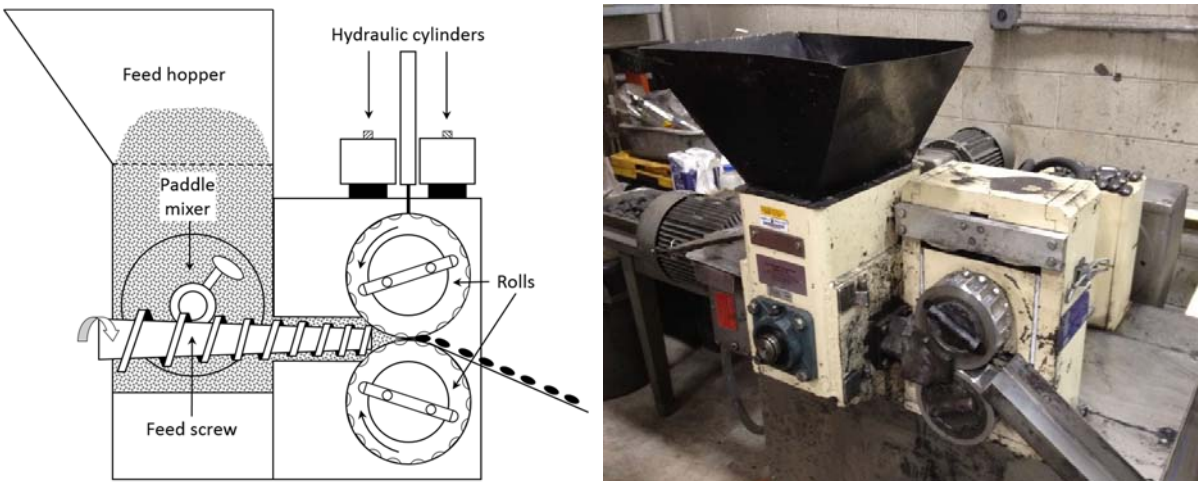



Figure 5-6. Komarek B-100R roll press (left) schematic diagram (modified from Guigon & Simon, 2003) and (right) laboratory installation

#### 5.3.2.1 Evaluations of Feedstock and Additive Variables

Several series of tests were designed to evaluate the influence of feedstock variables, additive variables and machine parameters on the quality of coal-biomass briquettes. The specifications for each series of tests were developed in Design-Expert® 8 using a Box-Behnken experimental design. This approach facilitated the creation of response surfaces and empirical models that relate variables of interest to measured responses, while minimizing the number of required tests. The first series of evaluations were designed to determine the influence of feedstock variables (i.e. water content, biomass content and biomass top size) on the dry density, crushing strength and mechanical durability of binderless bituminous coal-biomass briquettes. Due to the similar compaction behavior of bituminous coals during roll press briquetting, as discussed in Chapter 4, it was determined that the most efficient course of action was to initially evaluate the influence of material variables for a single bituminous coal blended with each of the five types of biomass. The data obtained from these tests was used to compare the relative briquetting performance of each biomass type. Next, a series of verification tests were designed using the other two bituminous coals to verify that the optimum material variables from the initial exhaustive study are indeed similar for each coal. This experimental design reduced the

amount of time and materials required to determine the influence of feedstock variables on quality indicators for each coal-biomass combination.

File Edit View Display Options Design Tools Help Tips

Notes for Mixture Testing [
Design (Actual)
Summary
Graph Columns
Evaluation
Analysis
R1:Dry density (Emp
R2:Crushing strengt
R3:Mechanical dura
Optimization
Numerical
Graphical
Point Prediction
Confirmation

| Select | Std | Run | Factor 1 A:Water con... % | Factor 2 B:Biomass to... mm | Factor 3 C:Biomass c... % | Response 1 Dry density g/cm3 | Response 2 Crushing str... lbf | Response 3 Mechanical d... % |
|---|---|---|---|---|---|---|---|---|
| | 11 | 1 | 5.00 | 1.20 | 30.00 | | | |
| | 9 | 2 | 5.00 | 1.20 | 10.00 | | | |
| | 14 | 3 | 5.00 | 2.38 | 20.00 | | | |
| | 12 | 4 | 5.00 | 4.75 | 30.00 | | | |
| | 7 | 5 | 2.00 | 2.38 | 30.00 | | | |
| | 8 | 6 | 8.00 | 2.38 | 30.00 | | | |
| | 15 | 7 | 5.00 | 2.38 | 20.00 | | | |
| | 13 | 8 | 5.00 | 2.38 | 20.00 | | | |
| | 2 | 9 | 8.00 | 1.20 | 20.00 | | | |
| | 5 | 10 | 2.00 | 2.38 | 10.00 | | | |
| | 10 | 11 | 5.00 | 4.75 | 10.00 | | | |
| | 3 | 12 | 2.00 | 4.75 | 20.00 | | | |
| | 1 | 13 | 2.00 | 1.20 | 20.00 | | | |
| | 6 | 14 | 8.00 | 2.38 | 10.00 | | | |
| | 4 | 15 | 8.00 | 4.75 | 20.00 | | | |

Figure 5-7. Example of an experimental design constructed in Design-Expert® 8

The Emerald coal was selected for the initial series of tests because it produced briquettes with the greatest compressive strength and mechanical durability in the moisture optimization study presented in Chapter 4. Using the Box-Behnken experimental design with three center points, a series of 15 briquetting tests were designed for the Emerald coal and each type of biomass. An example of the experimental design layout produced in Design-Expert® 8 is displayed in Figure 5-7. For every individual test, briquettes were produced in 1.5 kilogram (dry) batches with a target water content (i.e. 0.02, 0.05, or 0.08), target biomass content (i.e. 10, 20 or 30%), and target biomass top size (i.e. 1.20, 2.38 or 4.75 mm). To accomplish this, a calculated mass of coal, biomass and water were homogenized for five minutes in a Hobart A200 18.9 liter (5 gal) commercial mixer. The mixture was then fed to the Komarek B-100R, which was operated at a roll motor speed of 450 rotations per minute, a roll force of 100 kilonewtons and a roll torque of approximately 1500 newton-meters. Immediately after formation, the briquettes were screened across a Sweco vibrating separator equipped with a 12.7 millimeter (0.5 in) screen

to remove excess fines and subsequently evaluated for water content, dry density, mechanical durability and crushing strength.

Next, a series of verification tests were designed to evaluate the McClure River and Toms Creek coals. The objective of these tests was to verify that the optimum combinations of feedstock variables identified for each Emerald coal-biomass mixture can also produce strong and durable briquettes with the other bituminous coals, and to validate that an exhaustive optimization study is not required for each bituminous coal type. A secondary objective of these tests was to give a clear indication to the effect of coal and biomass type on the quality of coal-biomass briquettes. To accomplish this, a single set of feedstock variables (e.g. 0.02 water content, 1.20 mm biomass top size, 20% biomass content) was selected for each of the five biomass types that corresponded with the best combination of measured crushing strength and mechanical durability in the Emerald coal tests. For each of the five tests, briquettes were produced in 1.5 kilogram (dry) batches with a calculated mass of coal, biomass and water. These materials were homogenized for five minutes in a Hobart A200 18.9 liter (5 gal) commercial mixer and fed to the Komarek B-100R, which was operated at a roll motor speed of 450 rotations per minute, a roll force of 100 kilonewtons and a roll torque of approximately 1500 newton-meters. Immediately after formation, the briquettes were screened across a Sweco vibrating separator equipped with a 12.7 millimeter (0.5 in) screen to remove excess fines and subsequently evaluated for water content, dry density, mechanical durability and crushing strength.

The third series of tests that were designed to determine the combined impacts of additive variables (i.e. starch content and cure time) on the dry density, crushing strength and mechanical durability of bituminous coal-biomass briquettes produced with different biomass contents. Using the Box-Behnken experimental design with three center points, a series of 15 briquetting tests were specified. For each test, briquettes were produced in 1.5 kilogram (dry) batches at a target water content of 0.05, a biomass top size of 4.75 millimeters, a specified biomass content (i.e. 10, 20 or 30%) and a specified pregelatinized wheat starch content (i.e. 0.0, 2.5 or 5.0%). To accomplish this, a calculated mass of Emerald coal, corn stover, pregelatinized wheat starch and water were homogenized for five minutes in a Hobart A200 18.9 liter (5 gal) commercial mixer. The mixture was then fed to the Komarek B-100R, which was operated at a roll motor speed of 450 rotations per minute, a roll force of 100 kilonewtons and a roll torque of approximately 1500

newton-meters. Immediately after formation, the briquettes were screened across a Sweco vibrating separator equipped with a 12.7 millimeter (0.5 in) screen to remove excess fines. Finally, the briquettes were cured for a specified period of time (i.e. 0, 1 or 7 days) prior to evaluations for water content, dry density, mechanical durability and crushing strength.

The fourth series of tests were designed to determine the combined influence of feedstock and additive variables (i.e. water content, biomass content and binder content) on the dry density, crushing strength and mechanical durability of sub-bituminous coal-biomass briquettes. Based on the insignificant influence of biomass top size on the quality of Emerald coal-biomass briquettes as discussed in Section 5.4.1, the biomass top size variable was excluded from these evaluations. Using the Box-Behnken experimental design with three center points, a series of 15 briquetting tests were planned to evaluate the quality of briquettes produced from mixtures of Eagle Butte coal and corn stover. For each test, briquettes were produced in 1.5 kilogram (dry) batches with a specified water content (i.e. 0.10, 0.15 or 0.20), corn stover content (i.e. 10, 20 or 30%) and pregelatinized wheat starch content (i.e. 0.0, 2.5 or 5.0%). To accomplish this, a calculated mass of Emerald coal, corn stover (minus 4.76 mm), pregelatinized wheat starch and water were homogenized for five minutes in a Hobart A200 18.9 liter (5 gal) commercial mixer. The mixture was then fed to the Komarek B-100R, which was operated at a roll motor speed of 450 rotations per minute, a roll force of 100 kilonewtons and a roll torque of approximately 1500 newton-meters. Immediately after formation, the briquettes were screened across a Sweco vibrating separator equipped with a 12.7 millimeter (0.5 in) screen to remove excess fines. Finally, the briquettes were cured for 24 hours prior to evaluations for water content, dry density, mechanical durability and crushing strength.

A final series of evaluations of feedstock variables were designed to evaluate the quality of binderless briquettes produced with sub-bituminous coal and all five biomass types. The objective of these tests was to verify the binderless briquetting potential of sub-bituminous coal-biomass mixtures at the optimum binderless conditions (i.e. 0.0% binder content) determined from the previous series of tests. For each test, briquettes were produced in 1.5 kilogram (dry) batches at a target water content of 0.15, a biomass content of 30 percent, and a biomass top size of 4.75 millimeters. To accomplish this, a calculated mass of Eagle Butte coal, biomass (minus 4.75 mm) and water were homogenized for five minutes in a Hobart A200 18.9 liter (5 gal) commercial mixer. The mixture was then fed to the Komarek B-100R, which was operated at a

roll motor speed of 450 rotations per minute, a roll force of 100 kilonewtons and a roll torque of approximately 1500 newton-meters. Immediately after formation, the briquettes were screened across a Sweco vibrating separator equipped with a 12.7 millimeter (0.5 in) screen to remove excess fines and subsequently evaluated for water content, dry density, mechanical durability and crushing strength.

#### 5.3.2.2 Evaluations of Roll Press Operating Parameters

A separate series of tests were designed to determine the combined impacts of the Komarek B-100R roll press operating parameters (i.e. roll speed, roll force and roll torque) on the dry density, crushing strength and mechanical durability of coal-biomass briquettes. Using the Box-Behnken experimental design with three center points, a series of 15 tests were planned to evaluate the quality of briquettes produced from mixtures of bituminous coal and corn stover. For each test, briquettes were produced in 1.5 kilogram (dry) batches at a target water content of 0.03, a biomass content of 20 percent and a biomass top size of 4.75 millimeters. To accomplish this, a calculated mass of McClure River coal, corn stover (minus 4.76 mm) and water were homogenized for five minutes in a Hobart A200 18.9 liter (5 gal) commercial mixer. The mixture was then fed directly to the Komarek B-100R, which was operated at a specified roll motor speed (i.e. 300, 600 or 900 rpm), a specified roll force (i.e. 50, 75 or 100 kN) and a specified roll torque (i.e. 600, 1200 or 1800 N-m). Immediately after formation, the briquettes were screened across a Sweco vibrating separator equipped with a 12.7 millimeter (0.5 in) screen to remove excess fines and subsequently evaluated for water content, dry density, mechanical durability and crushing strength.

#### 5.3.2.3 Detailed Characterization Study

A final series of briquettes were produced for a detailed characterization study of the physical properties, flow properties and gasification behavior of selected types of optimum coal-biomass briquettes. The purpose of this study was to verify the enhanced quality of the co-briquetted feedstocks and to provide additional information that may be useful to industrial consumers of coal-biomass briquettes. Two types of briquettes were produced for the detailed characterization study. The first type of briquettes were composed of the Emerald coal and sawdust, while the second type of briquettes were composed of Eagle Butte coal and corn stover. These combinations were chosen because of the geographical proximity of bituminous coal to

forestry operations in the eastern United States and the geographical proximity of the nation's largest sub-bituminous coal producing region (i.e. Powder River basin) to the nation's largest corn producing states in the Midwest.

The bituminous coal-sawdust briquettes were produced in a single 20-kilogram batch with 70 percent Emerald coal and 30 percent sawdust (minus 1.20 mm) at a target water content of 0.0022. Similarly, the sub-bituminous coal-corn stover briquettes were produced in a single eight-kilogram batch with 70 percent Eagle Butte coal and 30 percent corn stover (minus 4.75 mm) at a target water content of 0.1850. These feedstock parameters (i.e. water content, biomass content and biomass top size) were selected using an optimization tool in Design-Expert® 8, which used the mathematical models developed for each coal-biomass combination to maximize the predicted values of mechanical durability and crushing strength. For briquette production, a calculated mass of coal, biomass and water (total mixture mass of 2 kg) were homogenized for five minutes in a Hobart A200 18.9 liter (5 gal) commercial mixer. This process was repeated ten times for each coal-biomass combination to produce 20 kilograms of mixed feed material. The mixture was then fed directly to the Komarek B-100R, which was operated at a roll motor speed of 900 rotations per minute, a roll force of 100 kilonewtons and a roll torque of approximately 1800 newton-meters. These roll press operating parameters were also selected using an optimization tool in Design-Expert® 8, which used the empirical model developed for the roll press to maximize the predicted values of mechanical durability and crushing strength. Immediately after formation, the briquettes were screened across a Sweco vibrating separator equipped with a 12.7 millimeter (0.5 in) screen and subsequently evaluated for tensile strength, crushing strength, elasticity, mechanical durability, attritability, friability, water content, particle density, water resistance and chemical dosage. All additional briquettes were sent to specialized external laboratories for analysis of flow properties and gasification behavior.

## 5.3.3 Briquette Characterization

### 5.3.3.1 Water Content

The water content of briquettes was determined by drying five briquettes for 24 hours at 105 degrees Celsius in a drying oven. The mass of water in the briquettes was calculated by subtracting the dry mass of the briquettes from the initial mass before drying. The water content was then calculated by:

$$w = m_w / m_s \quad \text{(Eq. 5-1)}$$

where $w$ is the water content, $m_w$ is the mass of water and $m_s$ is the dry mass of the briquettes. Water content of the feed material was measured prior to briquette production using an AND MF-50 moisture analyzer set at 105 degrees Celsius. Feed samples were dried until the change in mass was reduced to 0.05 percent per minute, at which point the displayed value was reported as the water content of the feed.

#### 5.3.3.2 Particle Density

The particle density of briquettes was calculated by first measuring the initial (wet) density and then calculating the dry density ($\rho_d$) based on the measured water content by:

$$\rho_d = \rho_{wet} / (1 + w) \quad \text{(Eq. 5-2)}$$

where $\rho_{wet}$ is the calculated wet density and $w$ is the calculated water content. A density determination rig was used to measure the apparent mass of briquettes in a solution of water and detergent. Wet density ($\rho_{wet}$) was then calculated by:

$$\rho_{wet} = (m_a / (m_a - m_b))\rho_w \quad \text{(Eq. 5-3)}$$

where $m_a$ is the mass of the briquette in air, $m_b$ is the apparent mass of the briquette in water and $\rho_w$ is the density of the liquid. Wet density was measured after the 24-hour curing period for the conventional binder tests and after the one hour cooling period for the coating tests. For both cases, the procedure was repeated for 10 briquettes and the average of the 10 values was reported as the dry particle density.

#### 5.3.3.3 Mechanical Durability

The mechanical durability of briquettes was measured by tumbling 20 briquettes for five minutes at 40 rotations per minute in a 0.3 meter (1 ft) diameter PVC cylinder equipped with three 50.8 millimeter (2 in) lifters. The briquettes were then removed from the cylinder and screened in a Ro-tap sieve shaker for 30 seconds over a 4.75-millimeter sieve. The mechanical durability ($MD$) of the briquettes was then calculated by:

$$MD = 100 \times \left(m_{final} / m_{initial}\right) \quad \text{(Eq. 5-4)}$$

where $m_{final}$ is the mass of briquettes retained on the 4.75-millimeter sieve and $m_{initial}$ is the initial mass of the briquettes prior to durability testing. Weathered mechanical durability values were also measured for selected briquettes by performing a series of mechanical durability and water

uptake tests. This series of tests included an initial mechanical durability test followed by water uptake evaluation of the plus 4.75-millimeter material, followed by another mechanical durability test, followed by another water uptake evaluation of the plus 4.75-millimeter material, followed by a final mechanical durability test. The weathered mechanical durability was then calculated by the product of the values obtained from each mechanical durability test.

#### 5.3.3.4 Crushing Strength

The crushing strength of briquettes was determined using a Mark-10 M5-500 digital force gauge fitted with a 101.6 millimeter (4 in) diameter aluminum plate. The force gauge was mounted to a Mark-10 TSA750 manual test stand equipped with a 25.4 millimeter (1 in) diameter aluminum plunger that was used to apply force to the briquettes until failure. The force gauge was configured with a break detect feature which stops data acquisition once the applied force drops to 95 percent of the maximum force attained during each test. The crushing strength of each briquette was then reported as the maximum force attained during each test. To improve the accuracy of readings, an aluminum bar (51 x 8 x 8 mm) was placed upon the aluminum plate with each briquette then placed atop and parallel to the bar for testing. Evaluations were performed on 25 briquettes and the crushing strength was reported as the average of the 25 values.

#### 5.3.3.5 Water Resistance

The water resistance of briquettes was determined using an apparatus designed to simulate precipitation that briquettes may encounter during storage and transportation. To calculate water resistance, five briquettes were subjected to a 15-second water spray at a flow rate of 11.4 liters per minute (3 gal/min) from a height of 0.5 meters (1.5 ft) above the briquettes. Water resistance was reported as the water uptake of the briquettes that resulted from this spray test, with water uptake ($u$) calculated by:

$$u = \left(m_f - m_i\right)/m_i \quad \text{(Eq. 5-5)}$$

where $m_i$ is the initial mass of briquettes and $m_f$ is the mass of briquettes after the water spray. Weathered water uptake values were also determined in conjunction with the weathered mechanical durability tests as the product of the values obtained from the two water uptake tests.

#### 5.3.3.6 Friability

The friability of briquettes was measured by dropping 20 briquettes twice from a height of 1.8 meters (6 ft) onto a steel plate using a modified shatter test device. The briquettes were then screened for 30 seconds in a Ro-tap sieve shaker over a 4.75-millimeter sieve. The friability (*F*) of the briquettes was then calculated by:

$$F = 100 \times \left(m_{final}/m_{initial}\right) \quad \text{(Eq. 5-6)}$$

where $m_{final}$ is the mass of briquettes retained on the 4.75-millimeter sieve and $m_{initial}$ is the initial mass of the briquettes prior to friability testing.

#### 5.3.3.7 Attritability

The attritability of briquettes was measured by screening 20 briquettes for five minutes in a Ro-tap sieve shaker over a 4.75-millimeter sieve. The attritability (*A*) of the briquettes was then calculated by:

$$A = 100 \times \left(m_{final}/m_{initial}\right) \quad \text{(Eq. 5-7)}$$

where $m_{final}$ is the mass of briquettes retained on the 4.75-millimeter sieve and $m_{initial}$ is the initial mass of the briquettes prior to attritability testing.

#### 5.3.3.8 Tensile Strength

To measure tensile strength, individual briquettes were crushed between two flat compression plates with the briquette standing tall (i.e. with the long axis of the briquette parallel to the axis of force application). This was accomplished using a Mark-10 M5-500 digital force gauge fitted with a 101.6 millimeter (4 in) diameter aluminum plate. The force gauge was mounted to a Mark-10 TSA750 manual test stand equipped with a 25.4 millimeter (1 in) diameter aluminum plunger that was used to apply force to the briquettes until failure. The force gauge was configured with a break detect feature which stops data acquisition once the applied force drops to 95 percent of the maximum force attained during each test. Tensile strength of each briquette was then designated as this maximum force. Evaluations were performed on 25 briquettes and the tensile strength was reported as the average of the 25 values.

#### 5.3.3.9 Elasticity

To measure the elasticity of briquettes, the same equipment and procedure that was described for crushing strength evaluations was utilized. However, in this instance the test stand

was fitted with a Mark-10 ESM001 digital travel display to record the displacement of briquettes while the load was applied by the plunger. This installation was required to determine the spring constant (*SC*) of the briquettes, which is calculated by:

$$SC = (F_2 - F_1)/(x_2 - x_1) \quad \text{(Eq. 5-8)}$$

where $F_2$ is the maximum force applied during elastic deformation, $F_1$ is the minimum force applied during elastic deformation, $x_2$ is the displacement that corresponds with $F_2$, and $x_1$ is the displacement that corresponds with $F_1$. These values are obtained from the force versus displacement curve that is produced during data acquisition. The force gauge was configured to record two force and displacement data points per second with the break detect feature activated. Evaluations were performed on 25 briquettes and the elasticity was reported as the average calculated spring constant value for all 25 measurements.

#### 5.3.3.10 Flow Properties

To measure briquette flow properties and determine the hopper dimensions needed to ensure reliable material flow, two 18.9 liter (5 gal) buckets of each briquette type were sent to Solids Handling Technologies in Rock Hill, South Carolina for a series of extensive evaluations. Although flow properties of bulk solids are typically determined using a Jenike Shear Tester, this device is not recommended for particles larger than 6.35 millimeters because they cannot be properly sheared, which leads to significant error and inaccurate results. Therefore, a modified approach was used for coal-biomass briquette evaluations due to the size of the pill-shaped briquettes (i.e. 43 x 19 x 14 mm). In this modified approach, the cohesive properties of briquettes were determined using a hopper with variable sized openings (i.e. gates), which is specially designed for large particles. This was accomplished by filling the hopper in stages and applying consolidation weights for a short period of time to ensure even consolidation of the briquettes. After filling and consolidating, the gates were successively removed to determine the opening size required for material flow, which is referred to as the arching dimension for a particular consolidation pressure. Additional tests were conducted at varying consolidation pressure to generate a flow function for the briquettes. In addition to these cohesive properties, wall friction values were determined for each type of coal-biomass briquettes to determine the hopper slopes required for mass flow. Finally, the bulk density of the briquettes was measured as a function of consolidation pressure (i.e. compressibility), which is useful for calculating bin loads and required hopper angles and opening sizes.

#### 5.3.3.11 Gasification Behavior

The gasification behavior of selected coal-biomass briquettes was examined to verify the quality of these feedstocks in co-gasification processes. Gasification experiments were conducted at the University of Kentucky using a laboratory-scale updraft moving bed gasification system (Figure 5-8). The gasifier is a stainless steel cylinder with a height of 0.9 meters (3 ft) and an internal diameter of 34.8 millimeters (1.37 in). Crushed briquettes were fed at a variable rate to the top of the gasifier onto a stainless steel grate at the bottom of the cylinder. The oxidant and steam were introduced at the bottom of the system and moved up through the bed of particles. The syngas was then removed through a port located at the top of the vessel and transported to a condenser to clean the gas of impurities. Finally, the syngas was analyzed in a GOW-MAC Series 600 gas chromatograph to measure the composition of hydrogen, carbon monoxide, methane and carbon dioxide.

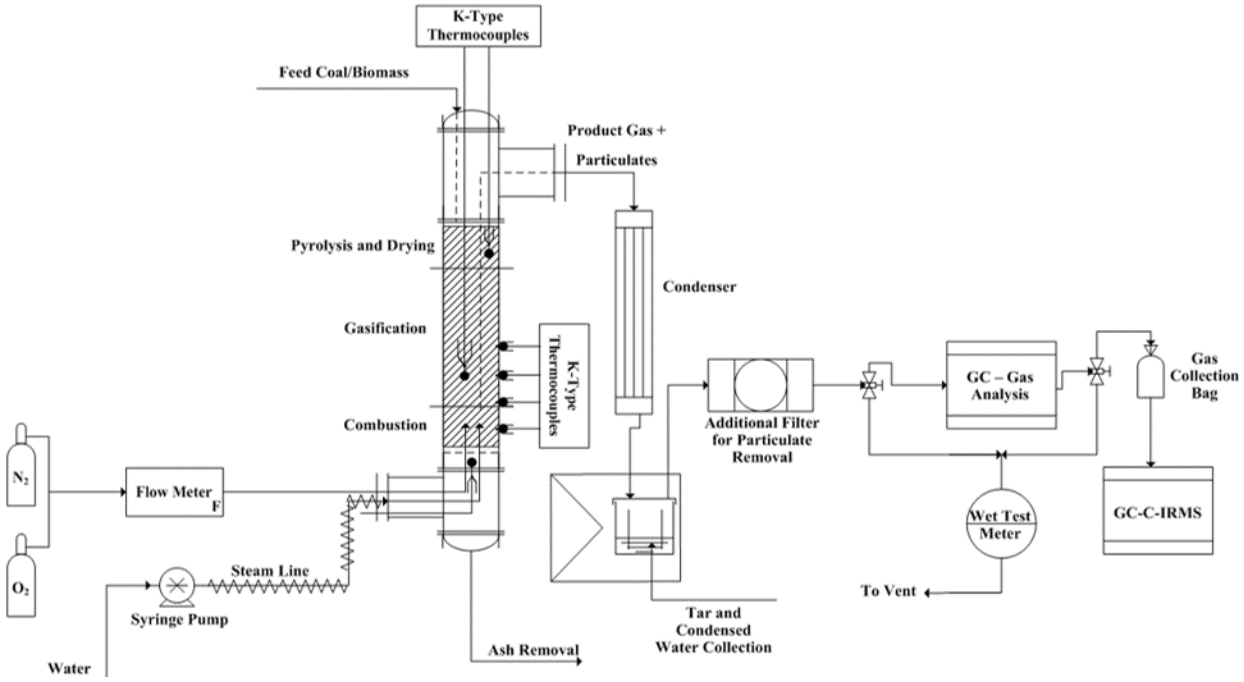



Figure 5-8. Schematic drawing of bench-scale moving bed gasifier used to characterize the gasification behavior of coal-biomass briquettes (Bhagavatula, 2013)

All gasification experiments were performed at atmospheric pressure with a fixed steam to oxygen ratio of 2 to 1. This configuration was selected to minimize the production of carbon dioxide and to maximize the production of hydrogen and carbon monoxide. Experiments were conducted separately with pure oxygen air as the oxidant to determine the resultant

concentrations of the product gasses. In addition, the energy content of the product gas was measured to calculate the cold gas efficiency of each gasification process.

# 5.4 Results and Discussion

## 5.4.1 Evaluation of Feedstock Variables – Bituminous Coal

### 5.4.1.1 Summary of Results

The results of the Emerald coal-biomass briquette evaluations are summarized in Table 5-4 for corn stover, Table 5-5 for switchgrass, Table 5-6 for miscanthus, Table 5-7 for wheat straw, and Table 5-8 for sawdust. Each test is identified in these tables by coal type (i.e. EM = Emerald coal), biomass type (i.e. CS = corn stover, SG = switchgrass, MC = miscanthus, WS = wheat straw and SD = sawdust) and the standard test number assigned in Design-Expert® 8 according to the target water content, biomass top size and biomass content (i.e. 01 = target water content of 0.02, biomass content of 20% and biomass top size of 1.20 mm). In the following sections, correlations between each feedstock variable and each response (i.e. briquette property) are presented and discussed. The results were then analyzed using the Design-Expert® 8 statistical analysis tools to fit mathematical models to each response, which can be used to predict briquette quality. In addition, contour graphs of the models are presented to visually interpret and evaluate the results. Finally, numerical optimization of the model was conducted to determine the combination of feedstock conditions that produce the highest quality briquettes.

Table 5-4. Summary of characterization results for briquettes composed of Emerald coal and corn stover

| Test ID | Feed Water Content | Biomass Content (%) | Biomass Top Size (mm) | Briquette Water Content | Particle Density (g/cm$^3$) | Crushing Strength (N) | Mechanical Durability (%) |
|---|---|---|---|---|---|---|---|
| EM-CS-01 | 0.0180 | 20 | 1.20 | 0.013 | 1.12 | 1,267.3 | 88.0 |
| EM-CS-02 | 0.0810 | 20 | 1.20 | 0.061 | 1.04 | 542.7 | 64.9 |
| EM-CS-03 | 0.0165 | 20 | 4.75 | 0.012 | 1.11 | 1,237.9 | 88.6 |
| EM-CS-04 | 0.0865 | 20 | 4.75 | 0.057 | 1.06 | 568.9 | 46.6 |
| EM-CS-05 | 0.0210 | 10 | 2.38 | 0.015 | 1.16 | 1,049.8 | 91.9 |
| EM-CS-06 | 0.0840 | 10 | 2.38 | 0.065 | 1.10 | 146.3 | 19.1 |
| EM-CS-07 | 0.0165 | 30 | 2.38 | 0.012 | 1.04 | 1,469.7 | 77.0 |
| EM-CS-08 | 0.0870 | 30 | 2.38 | 0.068 | 1.00 | 1,354.5 | 75.2 |
| EM-CS-09 | 0.0465 | 10 | 1.20 | 0.036 | 1.11 | 654.3 | 80.4 |
| EM-CS-10 | 0.0585 | 10 | 4.75 | 0.029 | 1.12 | 707.7 | 79.7 |
| EM-CS-11 | 0.0455 | 30 | 1.20 | 0.041 | 1.06 | 1,845.1 | 89.4 |
| EM-CS-12 | 0.0600 | 30 | 4.75 | 0.033 | 1.08 | 2,000.4 | 90.2 |
| EM-CS-13 | 0.0405 | 20 | 2.38 | 0.034 | 1.13 | 1,285.1 | 87.0 |
| EM-CS-14 | 0.0605 | 20 | 2.38 | 0.038 | 1.10 | 1,246.4 | 86.7 |
| EM-CS-15 | 0.0500 | 20 | 2.38 | 0.039 | 1.10 | 1,236.6 | 85.8 |

Table 5-5. Summary of characterization results for briquettes composed of Emerald coal and switchgrass

| Test ID | Feed Water Content | Biomass Content (%) | Biomass Top Size (mm) | Briquette Water Content | Particle Density (g/cm$^3$) | Crushing Strength (N) | Mechanical Durability (%) |
|---|---|---|---|---|---|---|---|
| EM-SG-01 | 0.020 | 20 | 1.20 | 0.014 | 1.12 | 1,380.3 | 89.7 |
| EM-SG-02 | 0.077 | 20 | 1.20 | 0.065 | 1.00 | 112.1 | 17.0 |
| EM-SG-03 | 0.019 | 20 | 4.75 | 0.013 | 1.11 | 1,250.8 | 86.0 |
| EM-SG-04 | 0.084 | 20 | 4.75 | 0.066 | 1.05 | 80.1 | 12.8 |
| EM-SG-05 | 0.020 | 10 | 2.38 | 0.012 | 1.15 | 939.9 | 90.1 |
| EM-SG-06 | 0.082 | 10 | 2.38 | 0.065 | 1.08 | 62.3 | 5.9 |
| EM-SG-07 | 0.020 | 30 | 2.38 | 0.015 | 1.03 | 1,815.8 | 83.2 |
| EM-SG-08 | 0.071 | 30 | 2.38 | 0.066 | 0.98 | 596.5 | 38.3 |
| EM-SG-09 | 0.046 | 10 | 1.20 | 0.036 | 1.07 | 356.3 | 48.6 |
| EM-SG-10 | 0.052 | 10 | 4.75 | 0.036 | 1.09 | 375.9 | 40.2 |
| EM-SG-11 | 0.042 | 30 | 1.20 | 0.037 | 1.04 | 1,792.2 | 84.0 |
| EM-SG-12 | 0.046 | 30 | 4.75 | 0.032 | 1.04 | 1,799.7 | 82.6 |
| EM-SG-13 | 0.040 | 20 | 2.38 | 0.040 | 1.05 | 902.1 | 68.6 |
| EM-SG-14 | 0.056 | 20 | 2.38 | 0.042 | 1.03 | 963.0 | 71.3 |
| EM-SG-15 | 0.039 | 20 | 2.38 | 0.035 | 1.05 | 886.5 | 67.3 |

Table 5-6. Summary of characterization results for briquettes composed of Emerald coal and miscanthus

| Test ID | Feed Water Content | Biomass Content % | Biomass Top Size mm | Briquette Water Content | Particle Density (g/cm$^3$) | Crushing Strength (N) | Mechanical Durability (%) |
|---|---|---|---|---|---|---|---|
| EM-MC-01 | 0.023 | 20 | 1.20 | 0.015 | 1.13 | 1,388.7 | 89.0 |
| EM-MC-02 | 0.076 | 20 | 1.20 | 0.062 | 1.09 | 114.8 | 15.6 |
| EM-MC-03 | 0.024 | 20 | 4.75 | 0.015 | 1.13 | 1,211.3 | 89.2 |
| EM-MC-04 | 0.080 | 20 | 4.75 | 0.066 | 1.09 | 177.9 | 13.6 |
| EM-MC-05 | 0.021 | 10 | 2.38 | 0.015 | 1.18 | 899.4 | 91.0 |
| EM-MC-06 | 0.076 | 10 | 2.38 | 0.066 | 1.12 | 71.6 | 5.1 |
| EM-MC-07 | 0.024 | 30 | 2.38 | 0.014 | 1.07 | 1,946.1 | 86.1 |
| EM-MC-08 | 0.077 | 30 | 2.38 | 0.067 | 1.01 | 845.6 | 46.5 |
| EM-MC-09 | 0.048 | 10 | 1.20 | 0.039 | 1.13 | 298.5 | 36.7 |
| EM-MC-10 | 0.047 | 10 | 4.75 | 0.037 | 1.13 | 308.7 | 32.4 |
| EM-MC-11 | 0.050 | 30 | 1.20 | 0.039 | 1.06 | 1,789.5 | 85.0 |
| EM-MC-12 | 0.036 | 30 | 4.75 | 0.036 | 1.07 | 2,026.2 | 83.2 |
| EM-MC-13 | 0.051 | 20 | 2.38 | 0.039 | 1.09 | 864.3 | 66.3 |
| EM-MC-14 | 0.045 | 20 | 2.38 | 0.039 | 1.09 | 1,011.1 | 72.5 |
| EM-MC-15 | 0.053 | 20 | 2.38 | 0.040 | 1.07 | 923.9 | 65.3 |

Table 5-7. Summary of characterization results for briquettes composed of Emerald coal and wheat straw

| Test ID | Feed Water Content | Biomass Content (%) | Biomass Top Size (mm) | Briquette Water Content | Particle Density (g/cm$^3$) | Crushing Strength (N) | Mechanical Durability (%) |
|---|---|---|---|---|---|---|---|
| EM-WS-01 | 0.021 | 20 | 1.20 | 0.016 | 1.15 | 1,141.0 | 90.5 |
| EM-WS-02 | 0.084 | 20 | 1.20 | 0.066 | 1.04 | 322.1 | 42.8 |
| EM-WS-03 | 0.026 | 20 | 4.75 | 0.015 | 1.14 | 1,278.0 | 87.2 |
| EM-WS-04 | 0.077 | 20 | 4.75 | 0.065 | 1.06 | 540.5 | 41.3 |
| EM-WS-05 | 0.022 | 10 | 2.38 | 0.014 | 1.18 | 943.0 | 91.7 |
| EM-WS-06 | 0.079 | 10 | 2.38 | 0.065 | 1.11 | 149.0 | 21.0 |
| EM-WS-07 | 0.024 | 30 | 2.38 | 0.016 | 1.06 | 1,613.4 | 77.0 |
| EM-WS-08 | 0.080 | 30 | 2.38 | 0.071 | 0.98 | 837.6 | 74.1 |
| EM-WS-09 | 0.049 | 10 | 1.20 | 0.042 | 1.13 | 418.6 | 63.5 |
| EM-WS-10 | 0.055 | 10 | 4.75 | 0.039 | 1.12 | 526.2 | 52.9 |
| EM-WS-11 | 0.059 | 30 | 1.20 | 0.047 | 1.09 | 1,413.6 | 86.1 |
| EM-WS-12 | 0.056 | 30 | 4.75 | 0.045 | 1.09 | 2,099.6 | 88.1 |
| EM-WS-13 | 0.050 | 20 | 2.38 | 0.041 | 1.09 | 1,107.6 | 81.0 |
| EM-WS-14 | 0.057 | 20 | 2.38 | 0.046 | 1.10 | 1,063.1 | 79.9 |
| EM-WS-15 | 0.051 | 20 | 2.38 | 0.041 | 1.10 | 1,036.0 | 84.9 |

Table 5-8. Summary of characterization results for briquettes composed of Emerald coal and sawdust

| Test ID | Feed Water Content | Biomass Content (%) | Biomass Top Size (mm) | Briquette Water Content | Particle Density (g/cm$^3$) | Crushing Strength (N) | Mechanical Durability (%) |
|---|---|---|---|---|---|---|---|
| EM-SD-01 | 0.022 | 20 | 1.20 | 0.016 | 1.14 | 1,356.7 | 92.7 |
| EM-SD-02 | 0.084 | 20 | 1.20 | 0.066 | 0.97 | 66.7 | 16.0 |
| EM-SD-03 | 0.021 | 20 | 4.75 | 0.014 | 1.14 | 1,277.5 | 92.0 |
| EM-SD-04 | 0.089 | 20 | 4.75 | 0.065 | 1.04 | 86.3 | 16.5 |
| EM-SD-05 | 0.023 | 10 | 2.38 | 0.015 | 1.15 | 990.2 | 92.5 |
| EM-SD-06 | 0.081 | 10 | 2.38 | 0.064 | 1.08 | 107.2 | 20.0 |
| EM-SD-07 | 0.022 | 30 | 2.38 | 0.017 | 1.10 | 1,671.6 | 91.3 |
| EM-SD-08 | 0.088 | 30 | 2.38 | 0.064 | 0.97 | 171.3 | 30.7 |
| EM-SD-09 | 0.052 | 10 | 1.20 | 0.038 | 1.05 | 238.9 | 46.8 |
| EM-SD-10 | 0.058 | 10 | 4.75 | 0.039 | 1.09 | 264.2 | 44.4 |
| EM-SD-11 | 0.055 | 30 | 1.20 | 0.041 | 1.04 | 924.8 | 80.5 |
| EM-SD-12 | 0.057 | 30 | 4.75 | 0.042 | 1.04 | 1,115.2 | 78.8 |
| EM-SD-13 | 0.055 | 20 | 2.38 | 0.041 | 1.03 | 560.5 | 65.9 |
| EM-SD-14 | 0.052 | 20 | 2.38 | 0.040 | 1.05 | 610.7 | 68.4 |
| EM-SD-15 | 0.056 | 20 | 2.38 | 0.039 | 1.03 | 597.4 | 68.0 |

#### *5.4.1.1.1 Feed Water Content Correlations*

The correlation between feed water content and each measured briquette property were evaluated for all five types of biomass by linear regression analysis. To investigate these correlations, feed water content was plotted versus each measured briquette property with the data points grouped by biomass content (i.e. 10, 20 and 30%). This approach was used because little or no correlation existed for the entire data sets due to the influence of the other two feedstock variables (i.e. biomass content and biomass top size). The feed water content correlations were initially investigated with the data grouped separately by biomass content and biomass top size. From these investigations, it was found that water content correlations were greatest with the data grouped by biomass content.

Figure 5-9 displays the correlations between feed water content and particle density for each of the five types of biomass. Specifically, the water content correlations are shown in Figure 5-9a for corn stover, Figure 5-9b for switchgrass, Figure 5-9c for miscanthus, Figure 5-9d for wheat straw and Figure 5-9e for sawdust. It is clear from these charts that feed water content has a negative correlation with the particle density of briquettes. For each of the five biomass types, an increase in water content led to a general reduction in particle density at each biomass content. For briquettes produced with 10 percent biomass, the maximum particle density

occurred at the minimum water content for all five types of biomass. However, this was not always the case for briquettes produced with 30 percent biomass. The particle density of briquettes produced with corn stover, switchgrass and wheat straw initially increased with an increase in water content. The particle density reached a maximum value in the water content range of 0.04 to 0.06, and then dropped off when the water content approached or exceeded 0.08. In contrast, the briquettes composed of sawdust exhibited a strong negative correlation (i.e. $R^2$ = 0.99) at 30 percent biomass. These findings suggest that the ideal feed water content with respect to dry density is lowest for briquettes composed of 10 percent biomass. However, the optimum water content increases as biomass content is increased for each biomass type except sawdust.

Figure 5-10 illustrates the correlations between feed water content and crushing strength for each of the five types of biomass. Specifically, the water content correlations are shown in Figure 5-10a for corn stover, Figure 5-10b for switchgrass, Figure 5-10c for miscanthus, Figure 5-10d for wheat straw and Figure 5-10e for sawdust. It is clear from these charts that feed water content generally exhibits a negative correlation with briquette crushing strength. At 10 and 20 percent biomass, an increase in feed water content led to a reduction in crushing strength for all five biomass types (i.e. maximum crushing strength occurred at minimum water content). In contrast, the crushing strength of briquettes composed of 30 percent biomass initially increased with an increase in water content, and reached a maximum value in the water content range of 0.03 to 0.06. However, this correlation at 30 percent biomass was not observed for the briquettes composed of sawdust. These results further confirm the findings of the particle density correlations, in which the ideal feed water content was determined to be lowest for briquettes composed of 10 percent biomass and highest for briquettes composed of 30 percent biomass, with the lone exception occurring with sawdust briquettes. The low crushing strength values recorded at a water content of 0.08 suggest that binderless briquetting of coal-biomass mixtures is not feasible at or above this water content.

Figure 5-11 shows the correlations between feed water content and mechanical durability for each of the five biomass types. Specifically, the water content correlations are shown in Figure 5-11a for corn stover, Figure 5-11b for switchgrass, Figure 5-11c for miscanthus, Figure 5-11d for wheat straw and Figure 5-11e for sawdust. As expected, the feed water content generally exhibits a negative correlation with the mechanical durability of briquettes. At 10 and 20 percent biomass, an increase in feed water content led to a reduction in mechanical durability

for all five biomass types (i.e. maximum mechanical durability occurred at minimum water content). In contrast, the mechanical durability of briquettes composed of 30 percent biomass initially increased with an increase in water content, and reached a maximum value in the water content range of 0.03 to 0.06. However, this correlation at 30 percent biomass was not observed for the briquettes composed of sawdust. These results further confirm the findings of the particle density and crushing strength correlations, in which the ideal feed water content was determined to be lowest for briquettes composed of 10 percent biomass and highest for briquettes composed of 30 percent biomass, with the lone exception occurring with sawdust briquettes. The low mechanical durability values recorded at a water content of 0.08 suggest that binderless briquetting of coal-biomass mixtures is not feasible at or above this water content.

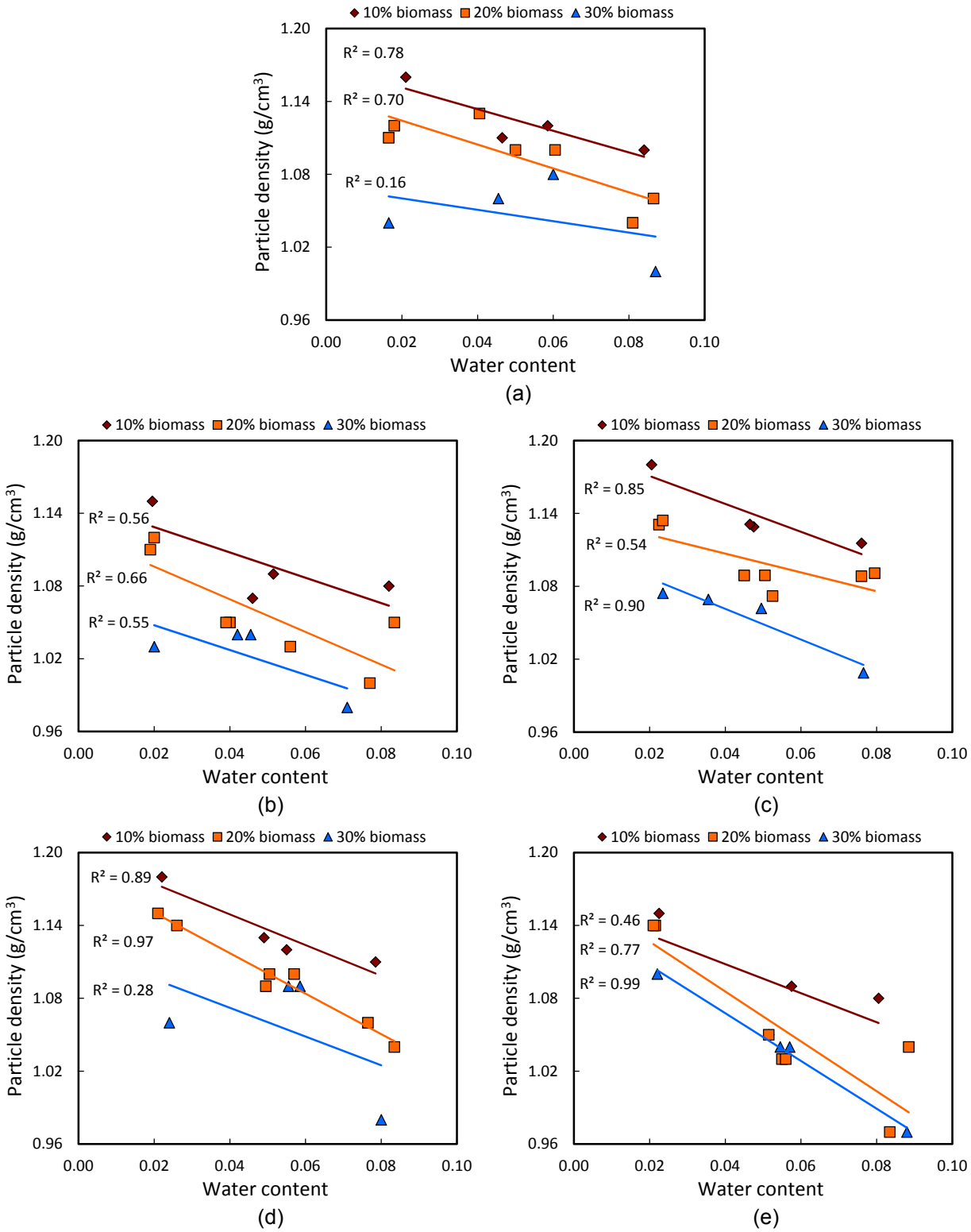



Figure 5-9. Effect of feed water content on particle density of briquettes composed of Emerald (bituminous) coal and (a) corn stover, (b) switchgrass, (c) miscanthus, (d) wheat straw and (e) sawdust

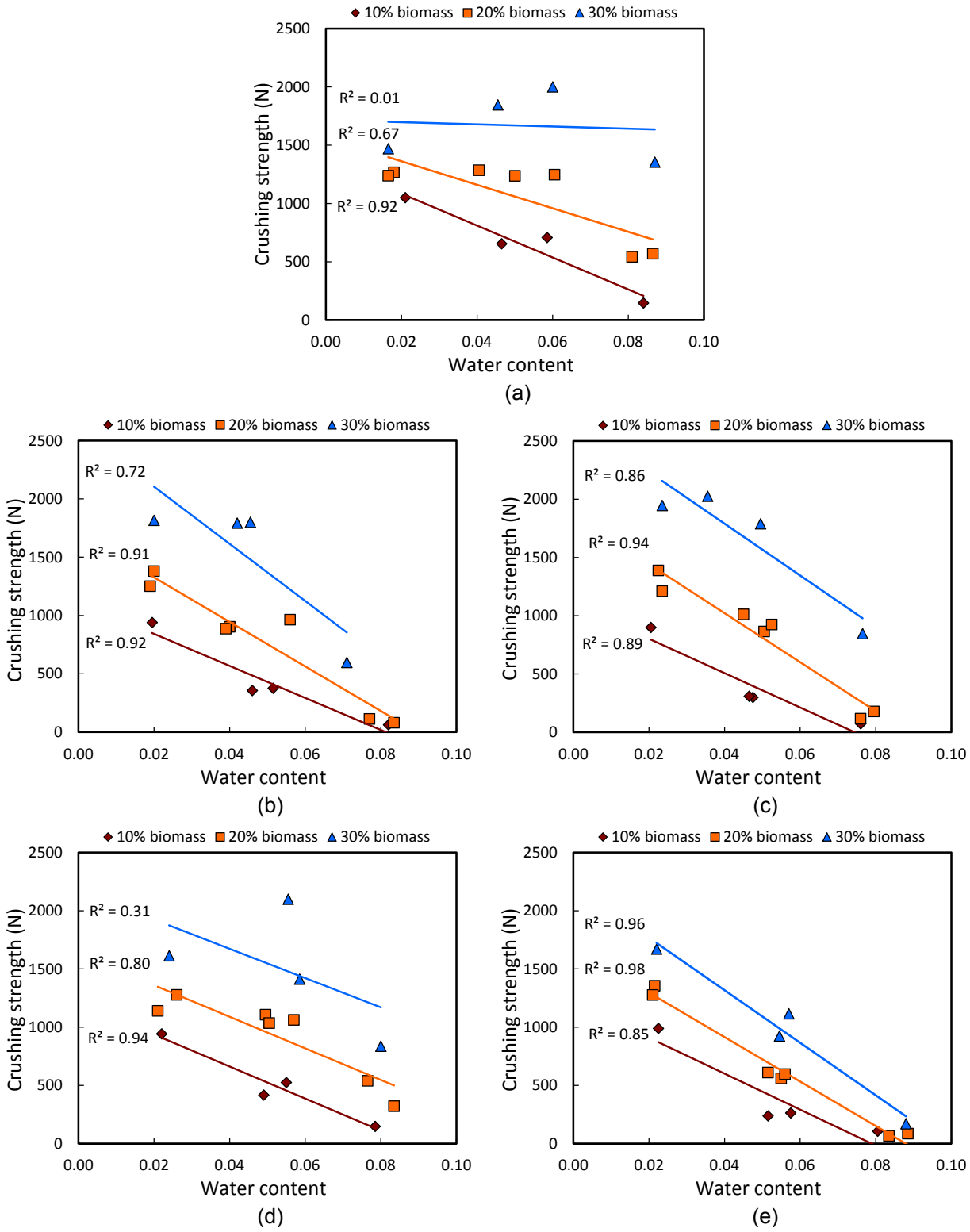



Figure 5-10. Effect of feed water content on crushing strength of briquettes composed of Emerald (bituminous) coal and (a) corn stover, (b) switchgrass, (c) miscanthus, (d) wheat straw and (e) sawdust

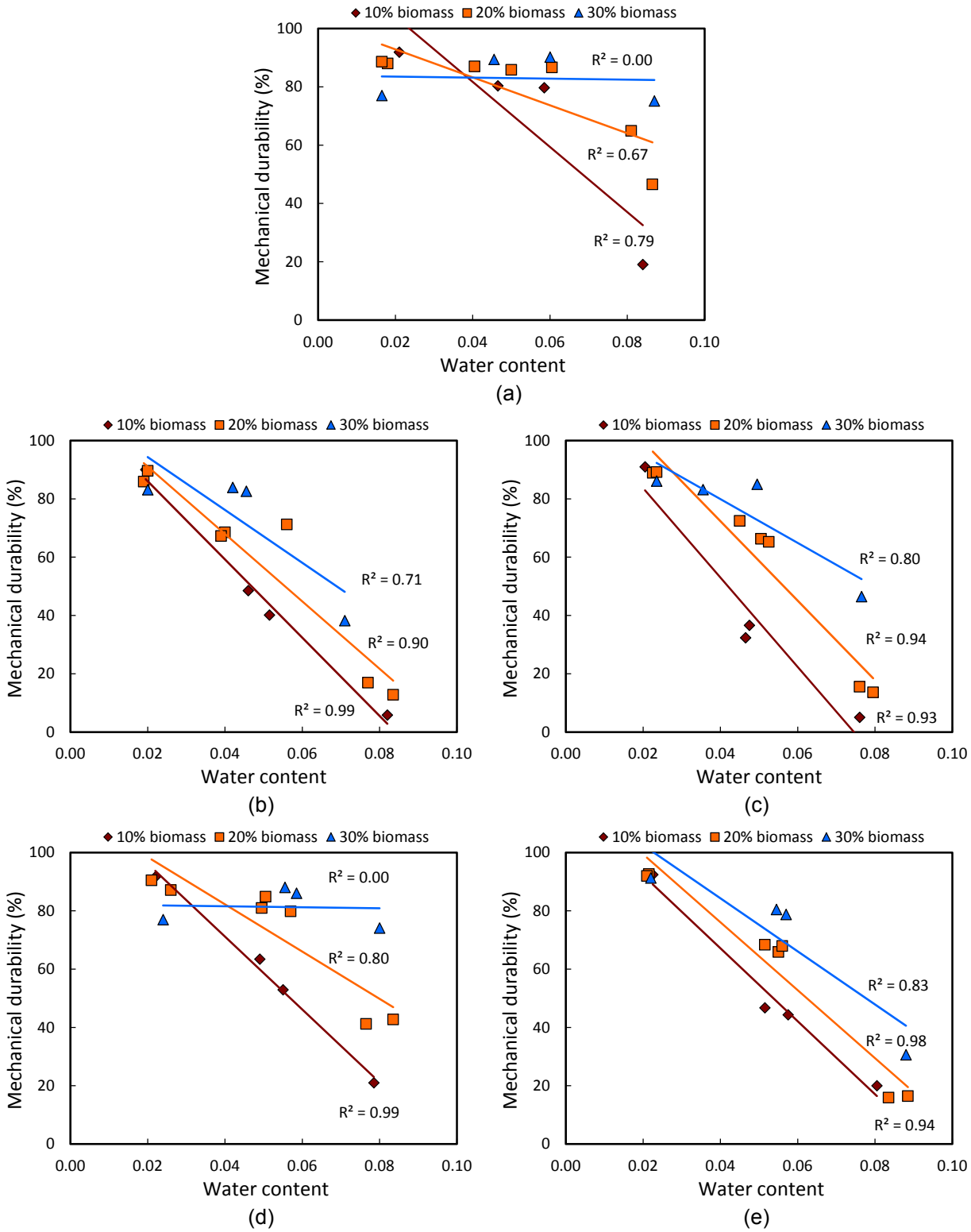



Figure 5-11. Effect of feed water content on mechanical durability of briquettes composed of Emerald (bituminous) coal and (a) corn stover, (b) switchgrass, (c) miscanthus, (d) wheat straw and (e) sawdust

*5.4.1.1.2 Biomass Content Correlations*

The correlation between biomass content and each measured briquette property were also evaluated for all five biomass types by linear regression analysis. To investigate these correlations, biomass content was plotted versus each measured briquette property with the data points grouped by the target feed water content (i.e. 0.02, 0.05 and 0.08). This approach was used because little or no correlation existed for the entire data sets due to the influence of the other two feedstock variables (i.e. water content and biomass top size). The biomass content correlations were initially investigated with the data grouped separately by water content and biomass top size. From these investigations, it was found that biomass content correlations were greatest with the data grouped by water content.

Figure 5-12 displays the correlations between biomass content and particle density for each of the five types of biomass. Specifically, the biomass content correlations are shown in Figure 5-12a for corn stover, Figure 5-12b for switchgrass, Figure 5-12c for miscanthus, Figure 5-12d for wheat straw and Figure 5-12e for sawdust. It is clear from these charts that biomass content has a negative correlation with the particle density of briquettes. For each of the five biomass types, an increase in biomass content directly reduced the particle density at each water content. This finding was expected since the addition of additional biomass with a true density much lower than coal will reduce the composite density of the mixture prior to briquette production. This correlation was very strong for briquettes produced with a water content of 0.02, which is evident by an average coefficient of determination ($R^2$) of 0.92. In contrast, the weakest average correlation ($R^2 = 0.65$) was found at a water content of 0.05. Another interesting observation is that the correlations for the briquettes composed of sawdust were weaker than those for the other four types of biomass. Nonetheless, these findings prove that an increase in biomass content directly reduces the particle density of coal-biomass briquettes.

Figure 5-13 illustrates the correlations between biomass content and crushing strength for each of the five types of biomass. Specifically, the biomass content correlations are shown in Figure 5-13a for corn stover, Figure 5-13b for switchgrass, Figure 5-13c for miscanthus, Figure 5-13d for wheat straw and Figure 5-13e for sawdust. It is clear from these charts that biomass content has a positive correlation with the crushing strength of briquettes. For each of the five biomass types, an increase in biomass content directly increased the crushing strength at each water content. The average correlations were very strong for water contents of 0.02 ($R^2 = 0.97$)

and 0.05 ($R^2$ = 0.95), but were not as apparent at a water content of 0.08 ($R^2$ = 0.73). These findings suggest that addition of biomass to coal briquettes improves the crushing strength of feedstocks and that low biomass content briquettes are typically lower in strength. This phenomena is thought to be a result of mechanical interlocking bonds that form between elongated biomass particles during briquette production.

Figure 5-14 shows the correlations between biomass content and mechanical durability for each of the five biomass types. Specifically, the biomass content correlations are shown in Figure 5-14a for corn stover, Figure 5-14b for switchgrass, Figure 5-14c for miscanthus, Figure 5-14d for wheat straw and Figure 5-14e for sawdust. These charts show that an increase in biomass content reduces the mechanical durability of briquettes produced at a water content of 0.02. In contrast, an increase in biomass content improves the mechanical durability of briquettes produced at a water content of 0.05 and 0.08. Another interesting observation is that the mechanical durability at 30 percent biomass is highest for briquettes produced with a water content of 0.05. However, this correlation was not observed for the briquettes produced with sawdust, which further exemplifies the difference between sawdust and the other types of biomass with regard to briquetting optimization.

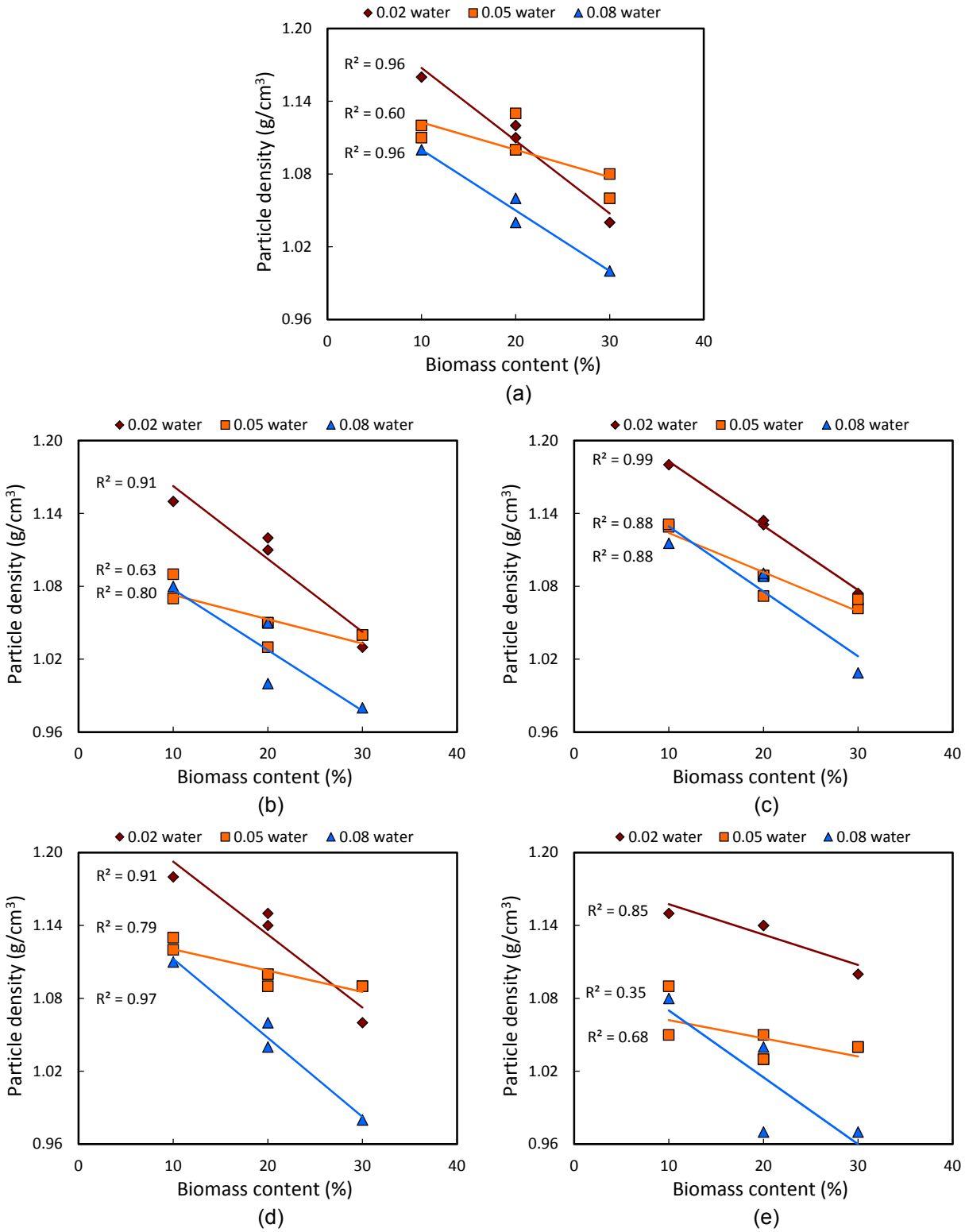



Figure 5-12. Effect of biomass content on particle density of briquettes composed of Emerald (bituminous) coal and (a) corn stover, (b) switchgrass, (c) miscanthus, (d) wheat straw and (e) sawdust

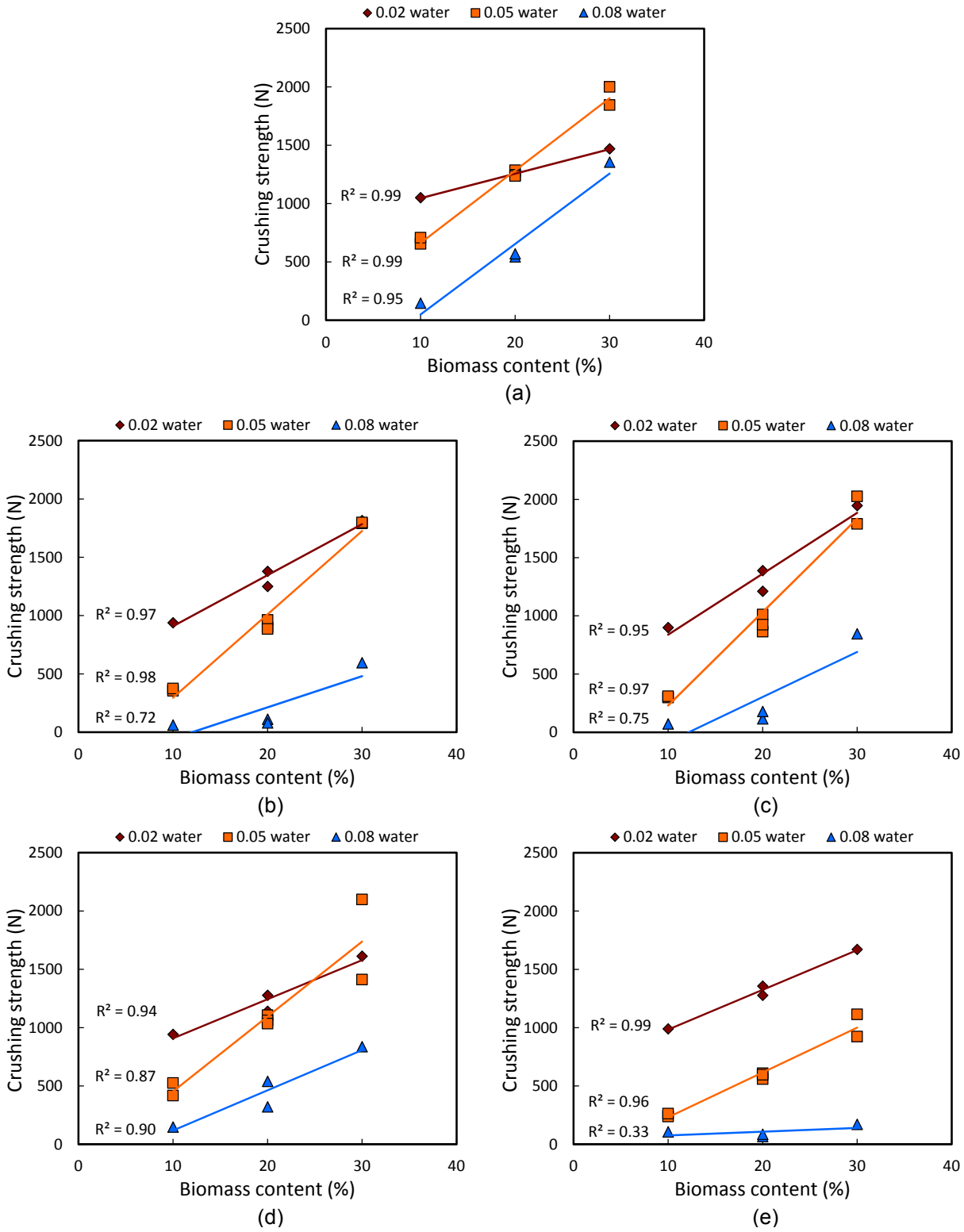



Figure 5-13. Effect of biomass content on crushing strength of briquettes composed of Emerald (bituminous) coal and (a) corn stover, (b) switchgrass, (c) miscanthus, (d) wheat straw and (e) sawdust

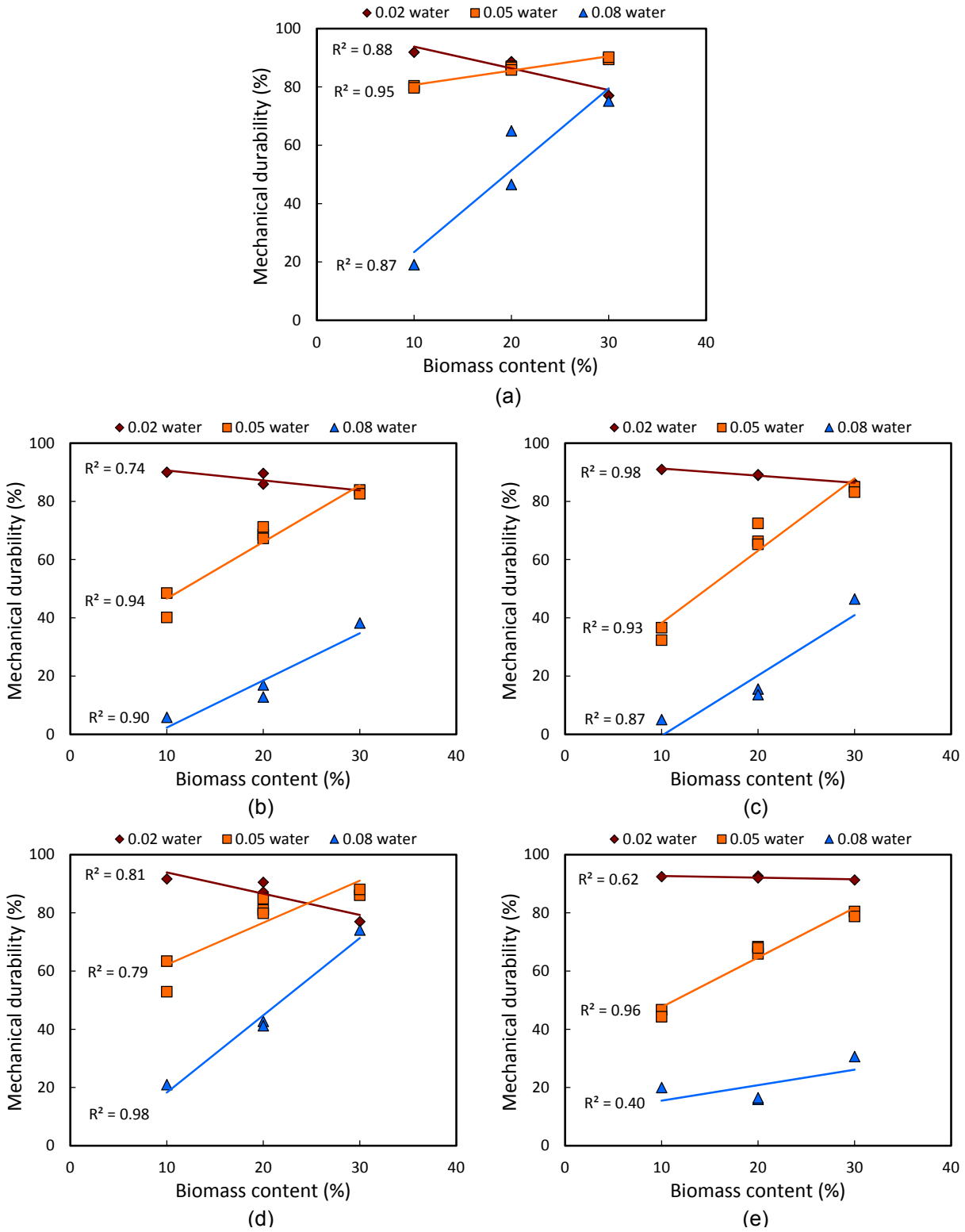



Figure 5-14. Effect of biomass content on mechanical durability of briquettes composed of Emerald (bituminous) coal and (a) corn stover, (b) switchgrass, (c) miscanthus, (d) wheat straw and (e) sawdust

*5.4.1.1.3 Biomass Top Size Correlations*

The correlations between biomass top size and each measured briquette property also were evaluated for all five biomass types by linear regression analysis. To investigate these correlations, biomass top size was plotted versus each measured briquette property with the data points grouped by the target feed water content (i.e. 0.02, 0.05 and 0.08). This approach was used because little or no correlation existed for the entire data sets due to the influence of the other two feedstock variables (i.e. water content and biomass content). The biomass top size correlations were initially investigated with the data grouped separately by water content and biomass content. From these investigations, it was found that biomass top size correlations were greatest with the data grouped by water content, although neither resulted in any significant correlations.

Figure 5-15 displays the correlations between biomass top size and particle density for each of the five types of biomass. Specifically, the biomass top size correlations are shown in Figure 5-15a for corn stover, Figure 5-15b for switchgrass, Figure 5-15c for miscanthus, Figure 5-15d for wheat straw and Figure 5-15e for sawdust. It is clear from these charts that there is very little correlation between biomass top size and particle density. This is supported by average coefficient of determination values of 0.00, 0.07 and 0.09 for water contents of 0.02, 0.05 and 0.08, respectively. However, these findings do suggest that the slight influence of biomass top size on particle density increases with a corresponding increase in water content.

Figure 5-16 illustrates the correlations between biomass top size and crushing strength for each of the five types of biomass. Specifically, the biomass top size correlations are shown in Figure 5-16a for corn stover, Figure 5-16b for switchgrass, Figure 5-16c for miscanthus, Figure 5-16d for wheat straw and Figure 5-16e for sawdust. It is clear from these charts that there is very little correlation between biomass top size and crushing strength. This is supported by average coefficient of determination values of 0.02 for each water content.

Figure 5-17 shows the correlations between biomass top size and mechanical durability for each of the five biomass types. Specifically, the biomass top size correlations are shown in Figure 5-17a for corn stover, Figure 5-17b for switchgrass, Figure 5-17c for miscanthus, Figure 5-17d for wheat straw and Figure 5-17e for sawdust. It is clear from these charts that there is very little correlation between biomass top size and mechanical durability. This is supported by

average coefficient of determination values of 0.06, 0.02 and 0.03 for water contents of 0.02, 0.05 and 0.08, respectively.

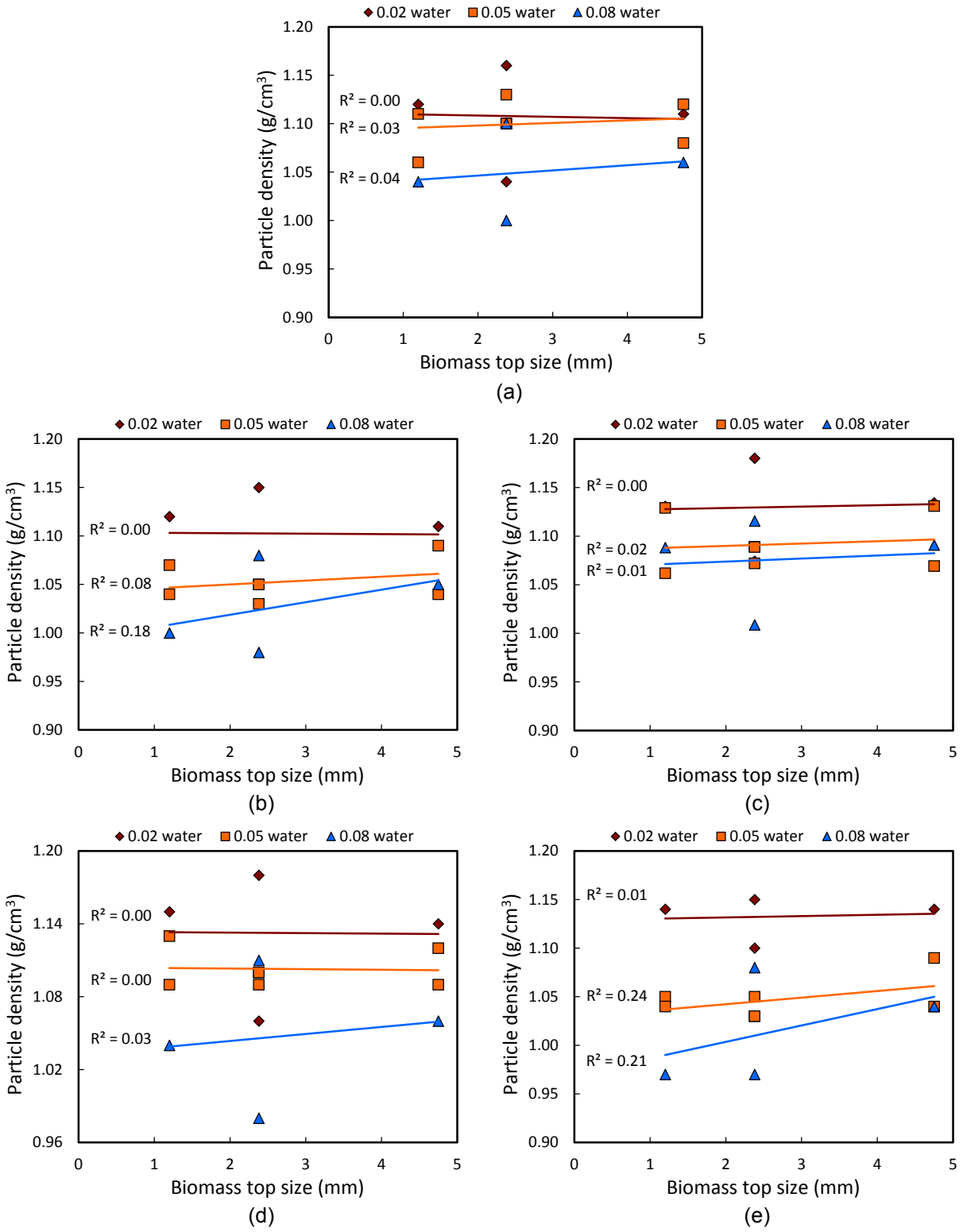



Figure 5-15. Effect of biomass top size on particle density of briquettes composed of Emerald (bituminous) coal and (a) corn stover, (b) switchgrass, (c) miscanthus, (d) wheat straw and (e) sawdust

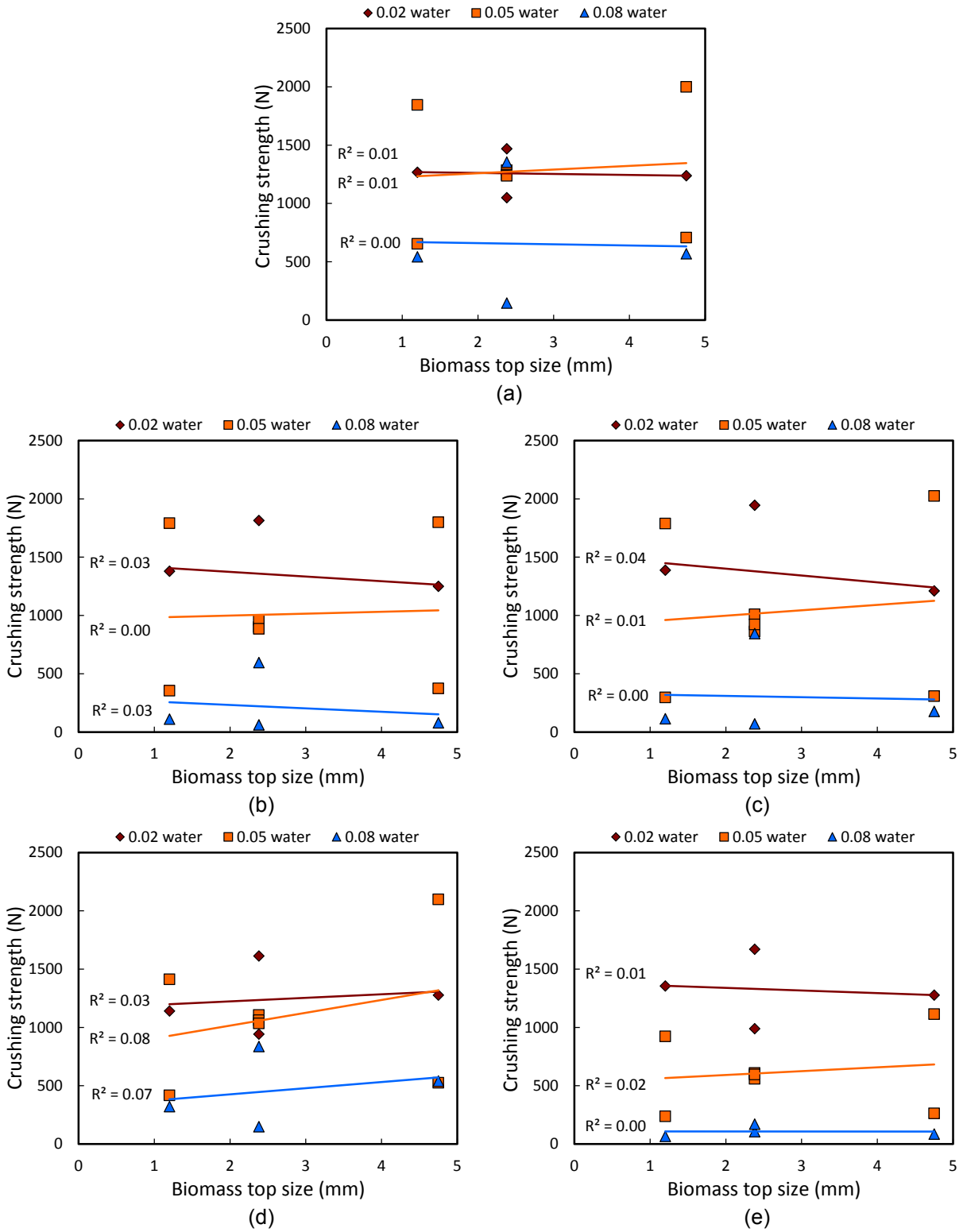



Figure 5-16. Effect of biomass top size on crushing strength of briquettes composed of Emerald (bituminous) coal and (a) corn stover, (b) switchgrass, (c) miscanthus, (d) wheat straw and (e) sawdust

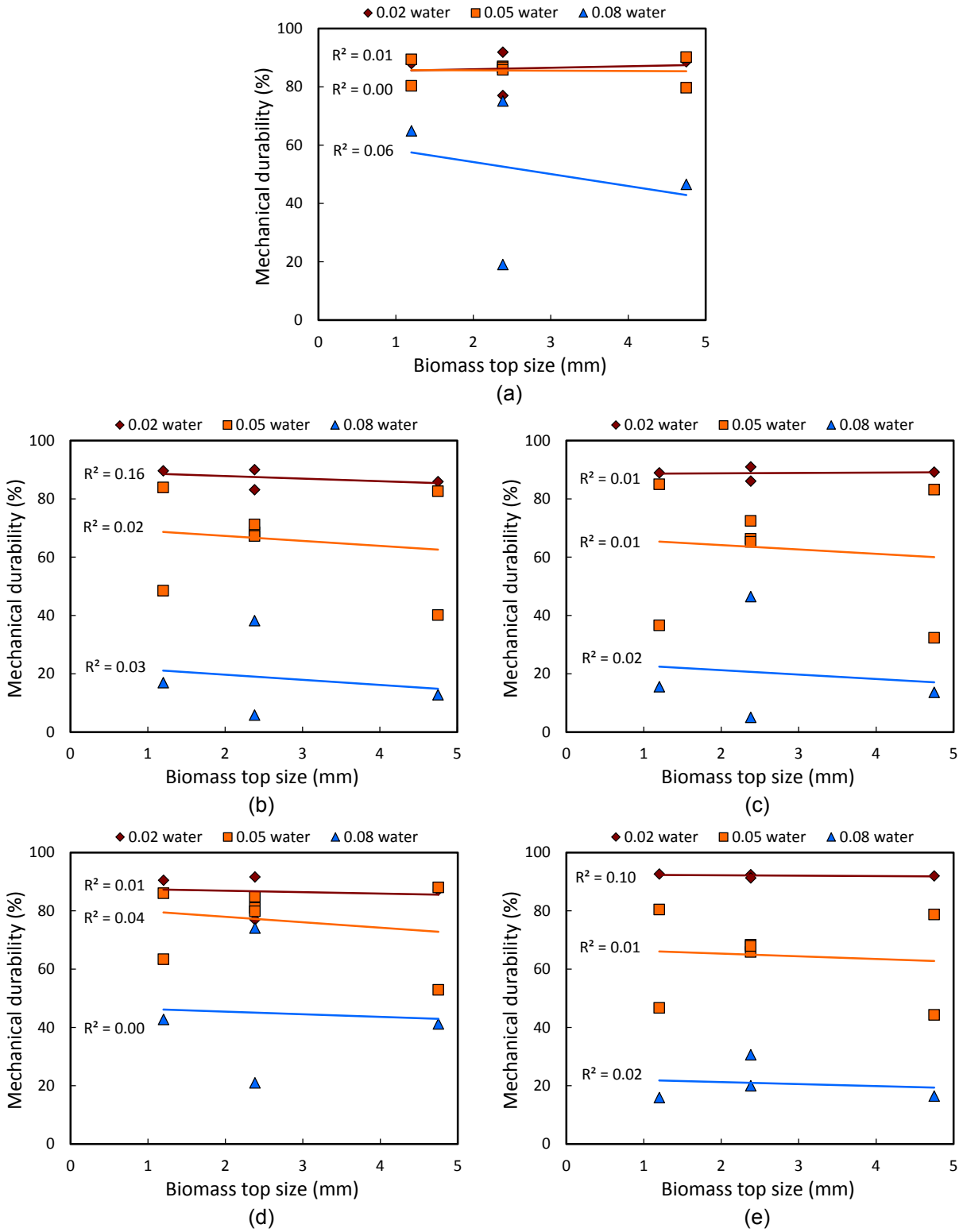



Figure 5-17. Effect of biomass top size on mechanical durability of briquettes composed of Emerald (bituminous) coal and (a) corn stover, (b) switchgrass, (c) miscanthus, (d) wheat straw and (e) sawdust

#### 5.4.1.2 Statistical Analyses

The data sets presented in Table 5-4 through Table 5-8 were examined using the statistical analysis tools included in Design-Expert® 8 to determine the influence of each feedstock variable and to optimize the quality of briquettes. For each combination of Emerald coal and biomass, mathematical models were developed that relate the feedstock variables (i.e. water content, biomass content and biomass top size) to the measured briquette properties (i.e. particle density, crushing strength, and mechanical durability). The first step of model development was selection of the process order (e.g. linear, quadratic) of the mathematical model. This was accomplished by determining the process order with the lowest lack of fit p-value and the highest adjusted R-squared and predicted R-squared values. The selected model was then analyzed using the analysis of variance (ANOVA) function to determine the statistical significance of the entire model and of each individual term. All insignificant terms were then removed from the model, except those required to maintain hierarchy. Next, the fit of the model to the data was evaluated using various diagnostics tools. The following sections present the empirical mathematical models developed for briquettes composed of Emerald coal and corn stover and summarize the results of the statistical analyses. The results for the remaining four types of briquettes composed of Emerald coal and biomass are included in Appendix A.

##### *5.4.1.2.1 Particle Density Model*

A linear mathematical model was constructed that relates feed water content, biomass content and biomass top size to the particle density of briquettes composed of Emerald coal and corn stover. According to the model, the predicted particle density of briquettes is calculated by:

$$\rho = 1.20 - 0.85w + 0.0042s - 0.0039c \quad \text{(Eq. 5-9)}$$

where $\rho$ is the particle density (g/cm$^3$), $w$ is the feed water content, $s$ is the biomass top size (mm) and $c$ is the biomass content (%). The statistical significance of this model, in terms of its fit to the data from which it was derived, was analyzed using a number of numerical and graphical tools.

The ANOVA results were first inspected to numerically measure the statistical significance of the model. A summary of the results of this analysis are provided in Table 5-9. The most important statistical measure analyzed was the p-value, which represents the probability of obtaining a test statistic as extreme as the observed value, assuming the null

hypothesis is true. As the p-value decreases, it becomes more likely that a model (or term) is causing an effect, and less likely that an effect is the result of chance. In common practice, the null hypothesis is rejected for models (or terms) with p-values less than 0.05, which in turn implies that the model (or term) is statistically significant. P-values greater than 0.10 imply that the model (or term) is not significant, while the significance of terms with p-values between 0.05 and 0.10 must be determined on a case-by-case basis. The p-value of the particle density model is 0.0007, which indicates that the predicted particle density values would be highly unlikely under the null hypothesis and verifies that the model is indeed statistically significant. The p-values of the three model terms are 0.0039 (water content), 0.3568 (biomass top size) and 0.0005 (biomass content). This implies that water content and biomass content are statistically significant model terms, and thus have a major impact on accurate prediction of the particle density of briquettes. In contrast, biomass top size is not a significant model term, which implies that its impact on particle density quantified in the model is not statistically significant. This term was needed to maintain the hierarchy of the model, otherwise it would have been removed to improve the model. For example, a secondary term in a quadratic model would be removed if it were found to have a p-value greater than 0.10. This process is referred to as model reduction.

Table 5-9. ANOVA results for EM-CS particle density model

| Source | Sum of Squares | df | Mean Square | F Value | p-value Prob > F |
|---|---|---|---|---|---|
| Model | 0.019 | 3 | 6.28E-03 | 12.4493 | 0.0007 |
| A-Water content | 6.65E-03 | 1 | 6.65E-03 | 13.1991 | 0.0039 |
| B-Biomass top size | 4.66E-04 | 1 | 4.66E-04 | 0.92513 | 0.3568 |
| C-Biomass content | 0.012 | 1 | 0.012 | 23.9591 | 0.0005 |
| Residual | 5.55E-03 | 11 | 5.04E-04 | -- | -- |
| Cor Total | 0.024 | 14 | -- | -- | -- |

Following the ANOVA, a number of diagnostic graphs were inspected to visually examine the residuals, which are differences in the actual measured particle density values and those predicted by the model. The purpose of examining the residuals is to look for any patterns that would indicate that anything other than noise is present in the data. One of the major ANOVA assumptions is that the residuals are normally distributed. Thus, this assumption was visually examined in a normal probability plot of studentized results, which is the recommended method to confirm the normality assumption. If the residuals are indeed normally distributed, the

residuals will follow an approximately straight line. Figure 5-18a shows the normal probability plot of studentized residuals for the particle density model. It is clear from this figure that the residuals do indeed follow an approximately straight line, and thus are normally distributed. A plot of predicted versus actual particle density values was also examined to visually analyze the relationship between the measured particle density values and those predicted by the model. In this plot, a line drawn at 45 degrees (i.e. predicted = actual) should go through the middle of the data over the entire range of data points. Point clusters below or above the line indicated problems with the model over or under predicting responses. The predicted versus actual values plot is displayed in Figure 5-18b for the particle density model, which shows the desired data scatter about the line is present. This further exemplifies the statistical significance of the particle density model and indicates that it is well suited for prediction of briquette quality.

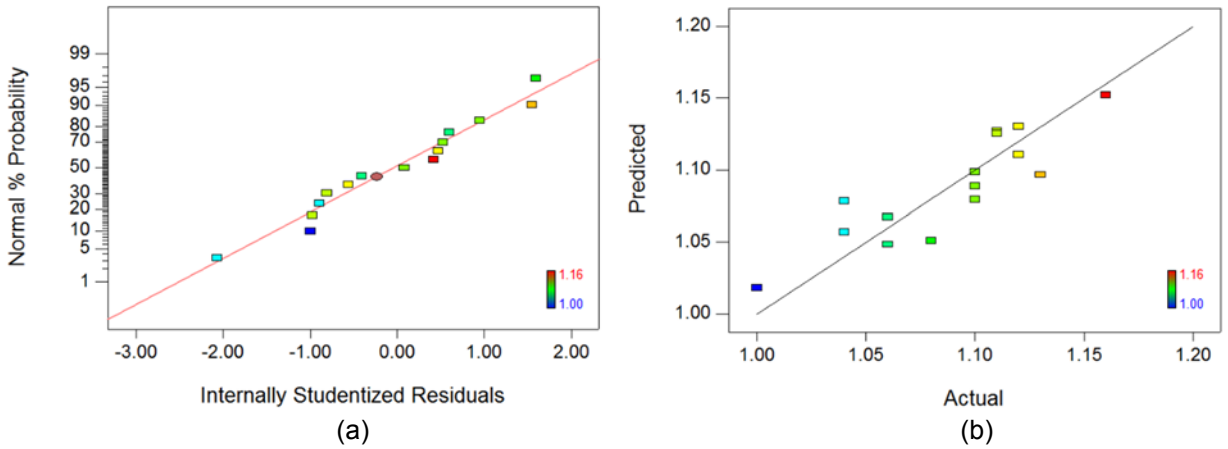



Figure 5-18. Diagnostic graphs for visual inspection of ANOVA results for EM-CS particle density model: (a) normal probability plot of studentized results and (b) predicted versus actual values plot

#### *5.4.1.2.2 Crushing Strength Model*

A quadratic mathematical model was constructed that relates feed water content, biomass content and biomass top size to the crushing strength of briquettes composed of Emerald coal and corn stover. According to the model, the predicted crushing strength of briquettes is calculated by:

$$\sigma = 419.14 + 10631.24w + 38.61s + 20.59c + 625.57wc - 311509.89w^2 \quad \text{(Eq. 5-10)}$$

where $\sigma$ is the crushing strength (N), $w$ is the feed water content, $s$ is the biomass top size (mm) and $c$ is the biomass content (%). The statistical significance of this model, in terms of its fit to the data from which it was derived, was analyzed using the same numerical and graphical tools

previously described. A summary of the ANOVA is provided in Table 5-10 for the crushing strength model. The p-value of the model is less than 0.0001, which indicates that the predicted crushing strength values would be highly unlikely under the null hypothesis and verifies that the model is indeed statistically significant. The p-values of the model terms are 0.0003 (water content), 0.1807 (biomass top size), less than 0.0001 (biomass content), 0.0122 (water content x biomass content) and 0.0010 (water content$^2$). This implies that all of the model terms are statistically significant (except biomass top size), and thus have a major impact on accurate prediction of the crushing strength of briquettes. In contrast, biomass top size is not a significant model term, which implies that its impact on crushing strength quantified in the model is not statistically significant.

Table 5-10. ANOVA results for EM-CS crushing strength model

| Source | Sum of Squares | df | Mean Square | F Value | p-value Prob > F |
|---|---|---|---|---|---|
| Model | 3378773 | 5 | 675755 | 36.60 | < 0.0001 |
| A-Water content | 577934 | 1 | 577934 | 31.30 | 0.0003 |
| B-Biomass top size | 38874 | 1 | 38874 | 2.11 | 0.1807 |
| C-Biomass content | 2113279 | 1 | 2113279 | 114.46 | < 0.0001 |
| AC | 180565 | 1 | 180565 | 9.78 | 0.0122 |
| $A^2$ | 416389 | 1 | 416389 | 22.55 | 0.0010 |
| Residual | 166168 | 9 | 18463 | -- | -- |
| Cor Total | 3544941 | 14 | -- | -- | -- |

To confirm the ANOVA normality assumption for the crushing strength model, the residuals were visually examined in a normal probability plot of studentized results. Figure 5-19a shows the normal probability plot of studentized residuals for the crushing strength model. It is clear from this figure that the residuals follow an approximately straight line, and thus are normally distributed. A plot of predicted versus actual values was also examined to visually analyze the relationship between the measured crushing strength values and those predicted by the model. The predicted versus actual plot is displayed in Figure 5-19b for the crushing strength model, which shows the desired data scatter about the 45 degree line is present. This further exemplifies the statistical significance of the crushing strength model and indicates that it is well suited for prediction of briquette quality.

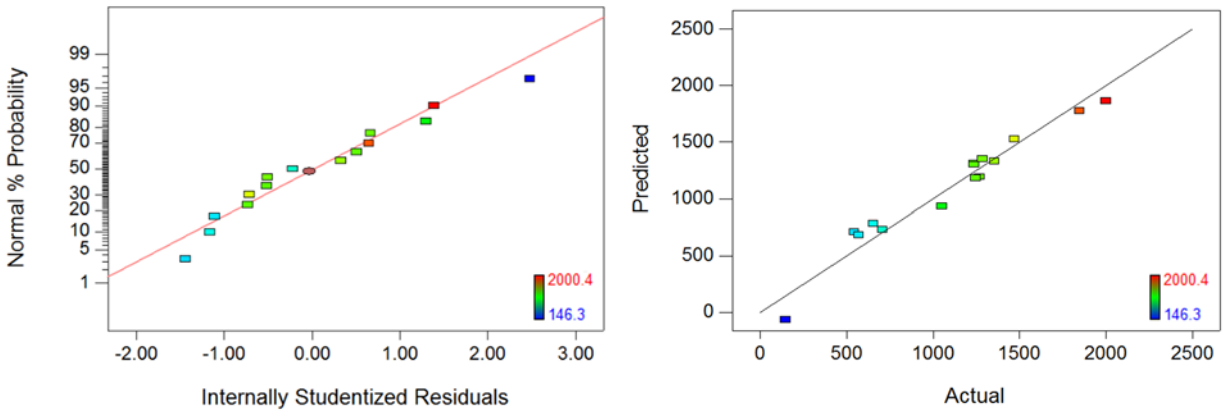



Figure 5-19. Diagnostic graphs for visual inspection of ANOVA results for EM-CS crushing strength model: (a) normal probability plot of studentized results and (b) predicted versus actual values plot

#### *5.4.1.2.3 Mechanical Durability Model*

A quadratic mathematical model was constructed that relates feed water content, biomass content and biomass top size to the mechanical durability of briquettes composed of Emerald coal and corn stover. According to the model, the predicted mechanical durability of briquettes is calculated by:

$$MD = 108.87 + 43.20w + 0.57s - 1.93c + 53.27wc - 15946.36w^2 \quad \text{(Eq. 5-11)}$$

where *MD* is the mechanical durability (%), $w$ is the feed water content, $s$ is the biomass top size (mm) and $c$ is the biomass content (%). The statistical significance of this model, in terms of its fit to the data from which it was derived, was analyzed using the same numerical and graphical tools previously described. A summary of the ANOVA is provided in Table 5-11 for the mechanical durability model. The p-value of the model is less than 0.0001, which indicates that the predicted mechanical durability values would be highly unlikely under the null hypothesis and verifies that the model is indeed statistically significant. The p-values of the model terms are less than 0.0001 (water content), 0.6454 (biomass top size), 0.0085 (biomass content), 0.0002 (water content x biomass content) and 0.0004 (water content$^2$). This implies that all of the model terms are statistically significant (except biomass top size), and thus have a major impact on accurate prediction of the mechanical durability of briquettes. In contrast, biomass top size is not a significant model term, which implies that its impact on mechanical durability quantified in the model is not statistically significant.

Table 5-11. ANOVA results for EM-CS mechanical durability model

| Source | Sum of Squares | df | Mean Square | F Value | p-value Prob > F |
|---|---|---|---|---|---|
| Model | 5192 | 5 | 1038 | 27.68 | < 0.0001 |
| A-Water content | 2129 | 1 | 2129 | 56.74 | < 0.0001 |
| B-Biomass top size | 9 | 1 | 9 | 0.23 | 0.6454 |
| C-Biomass content | 422 | 1 | 422 | 11.25 | 0.0085 |
| AC | 1309 | 1 | 1309 | 34.91 | 0.0002 |
| $A^2$ | 1091 | 1 | 1091 | 29.09 | 0.0004 |
| Residual | 338 | 9 | 38 | | |
| Cor Total | 5529 | 14 | | | |

To confirm the ANOVA normality assumption for the mechanical durability model, the residuals were visually examined in a normal probability plot of studentized results. Figure 5-20a shows the normal probability plot of studentized residuals for the mechanical durability model. It is clear from this figure that the residuals follow an approximately straight line, and thus are normally distributed. A plot of predicted versus actual values was also examined to visually analyze the relationship between the measured mechanical durability values and those predicted by the model. The predicted versus actual plot is displayed in Figure 5-20b for the mechanical durability model, which shows the desired data scatter about the 45 degree line is present. This further exemplifies the statistical significance of the mechanical durability model and indicates that it is well suited for prediction of briquette quality.

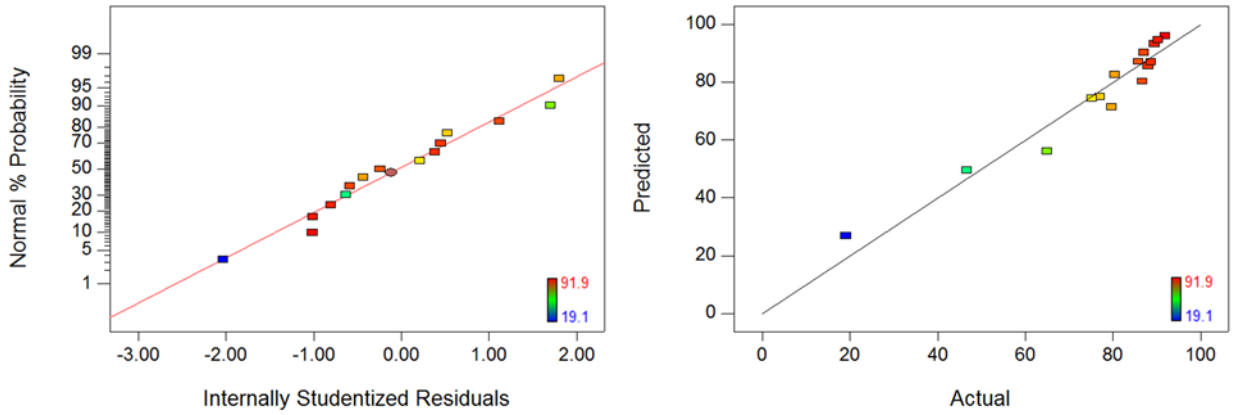



Figure 5-20. Diagnostic graphs for visual inspection of ANOVA results for EM-CS mechanical durability model: (a) normal probability plot of studentized results and (b) predicted versus actual values plot

#### 5.4.1.3 Model Graphs

Following the development and statistical analysis of each mathematical model, several contour graphs were constructed to visually interpret and evaluate the results. To provide a clear interpretation of the influence of each feedstock variable on each briquette property, the contour graphs are assembled by common model terms. This section presents and discusses the contour graphs for the models developed for briquettes composed of Emerald coal and corn stover. The graphs for the remaining four types of briquettes composed of Emerald coal and biomass are included in Appendix B.

The influence of feed water content on the modeled responses for particle density, crushing strength and mechanical durability are presented in Figure 5-21. From this figure it is evident that the maximum particle density values (i.e. > 1.16 g/cm$^3$) occur at a water content of 0.02 with 10 percent biomass at a top size of 4.75 millimeters. In contrast, the minimum particle density (i.e. < 1.04 g/cm$^3$) values occur at a water content of 0.08 with 30 percent biomass at a top size of 1.20 millimeters. Figure 5-21 also clearly indicates that briquette crushing strength reaches a maximum value (i.e. > 1,800 N) at a water content of 0.05 with 30 percent biomass at a top size of 4.75 millimeters and reaches a minimum value (i.e. < 200 N) at a water content of 0.08 with 10 percent biomass at a top size of 1.20 millimeters. Finally, this figure shows that the mechanical durability of briquettes reaches a maximum value (i.e. > 95%) at a water content of 0.02 with 10 percent biomass at a top size of 4.75 millimeters. The figure also indicates that a mechanical durability value in excess of 95 percent is achievable at a water content of 0.05 with 30 percent biomass at a top size of 4.75 millimeters.

The modeled responses for particle density, crushing strength and mechanical durability with respect to biomass content and biomass top size are presented in Figure 5-22 and Figure 5-23, respectively. These figures present the same data that is displayed in Figure 5-21, but offer a different perspective that may be desirable in certain circumstances. Regardless of the chart examined, graphical evaluation of these mathematical models indicate the optimum values of feedstock variables with respect to the crushing strength and mechanical durability of briquettes composed of Emerald coal and corn stover. These values are a water content of 0.05, a biomass content of 30 percent and a biomass top size of 4.75 millimeters, which predict a crushing strength in excess of 1,800 newtons and a mechanical durability in excess of 95 percent. Numerical optimization of the feedstock variables can be conducted to verify this result.

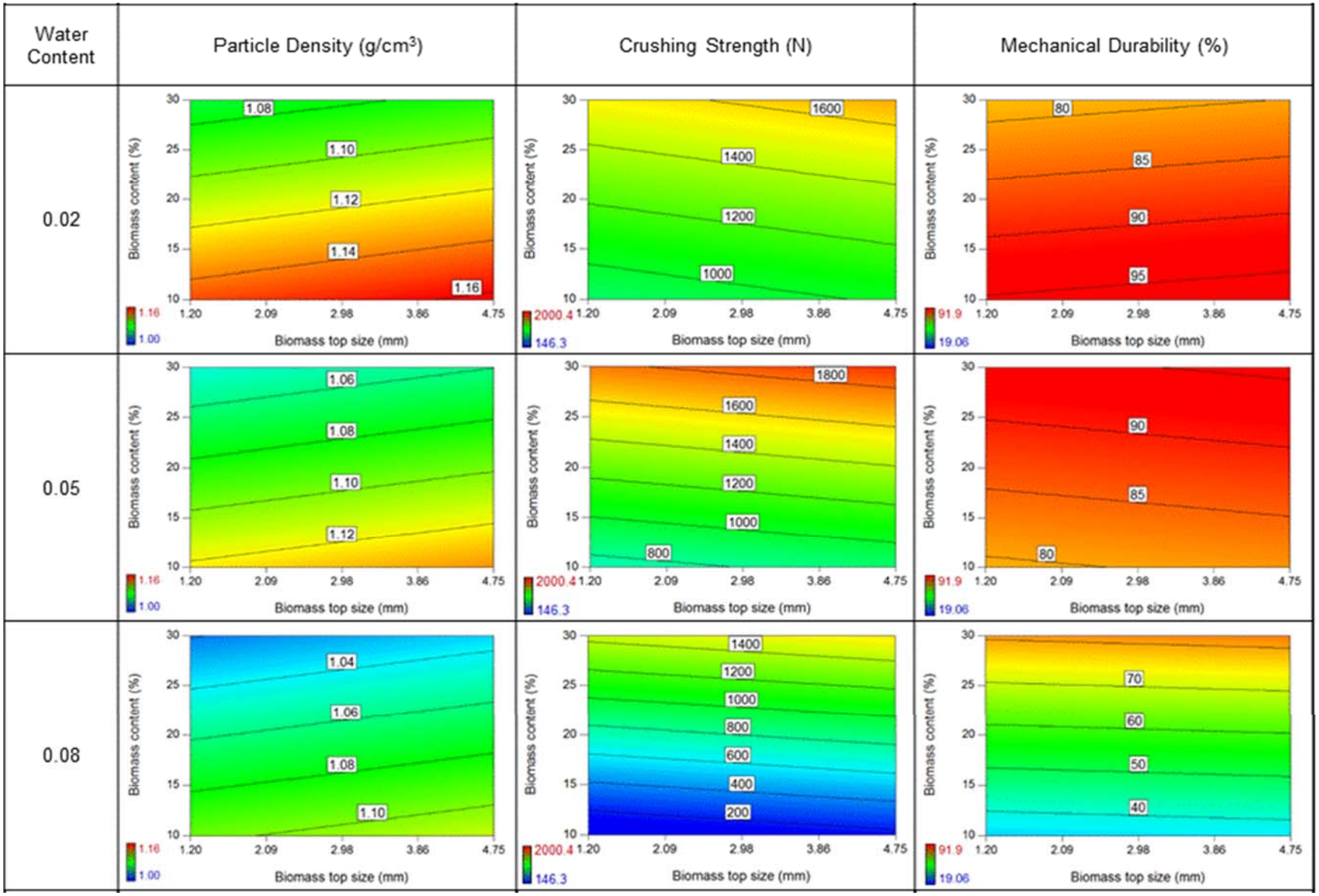



Figure 5-21. Influence of feed water content on modeled responses for particle density, crushing strength and mechanical durability for briquettes composed of Emerald (bituminous) coal and corn stover

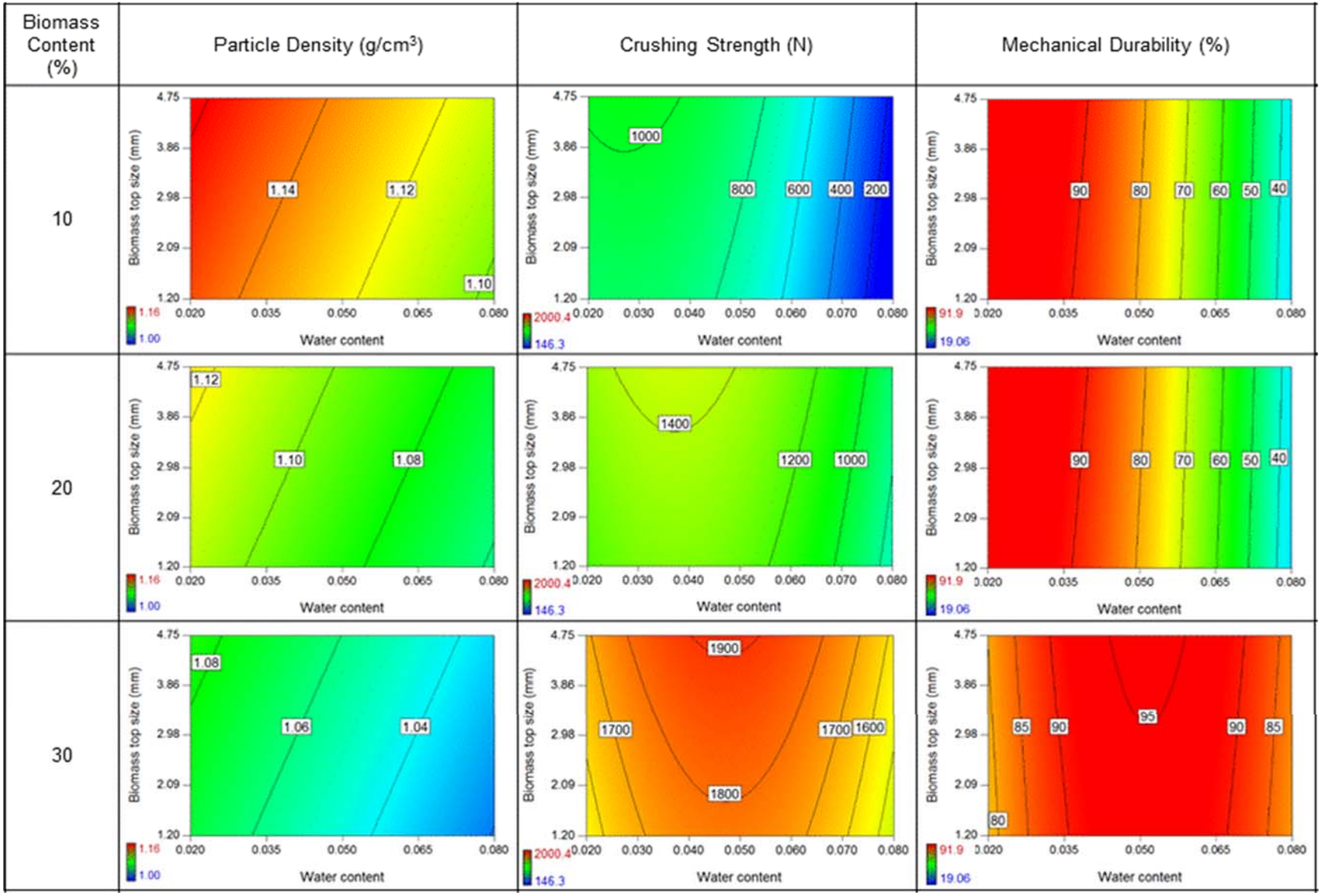



Figure 5-22. Influence of biomass content on modeled responses for particle density, crushing strength and mechanical durability for briquettes composed of Emerald (bituminous) coal and corn stover

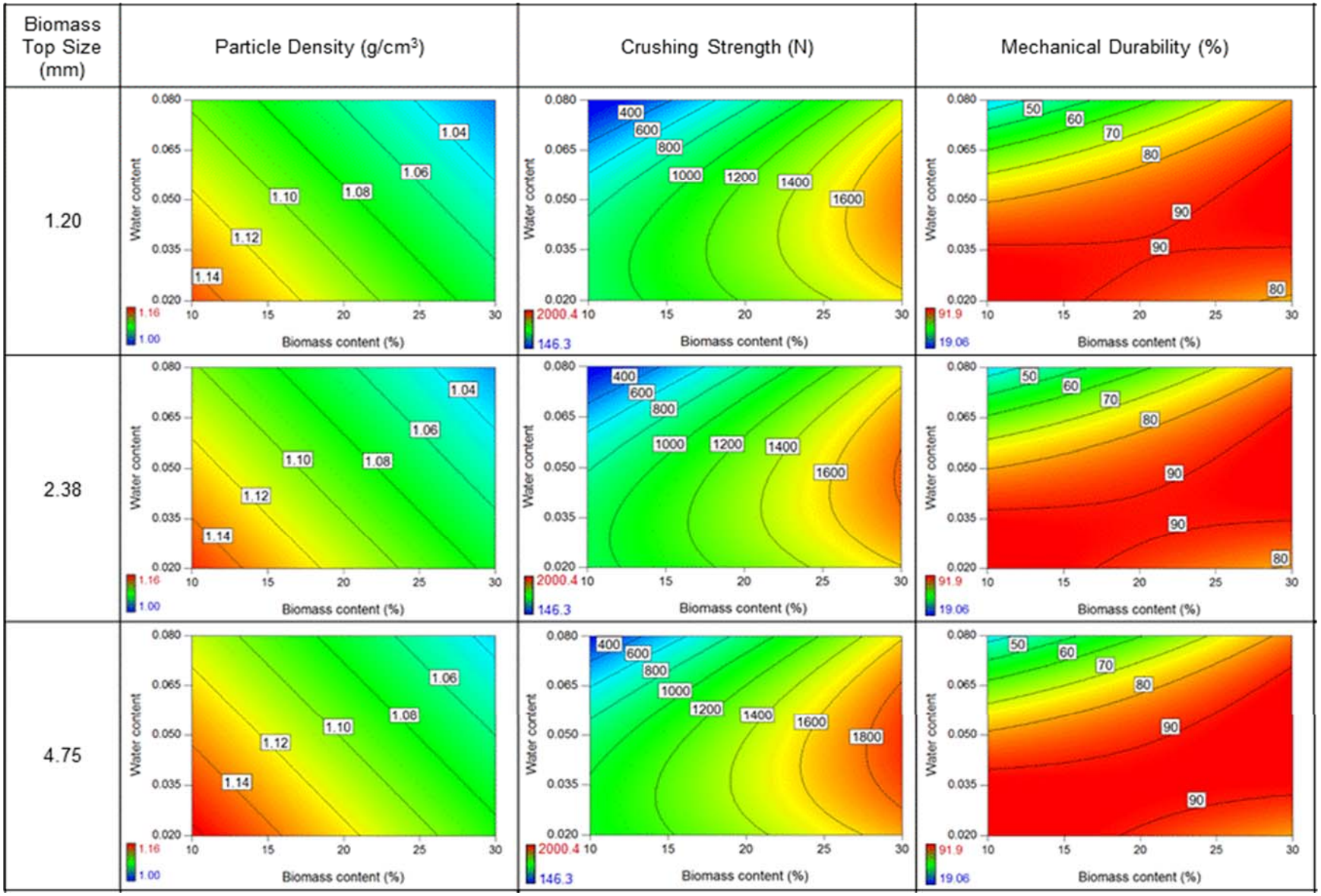



Figure 5-23. Influence of biomass top size on modeled responses for particle density, crushing strength and mechanical durability for briquettes composed of Emerald (bituminous) coal and corn stover

#### 5.4.1.4 Numerical Optimization

Numerical optimization of the feedstock variables was conducted in Design-Expert® 8 using the tool included in the analysis package. This tool allows for specification of optimization criteria (i.e. goals), which can include maximizing or minimizing predicted responses and process variables, as well as setting target values for each parameter. The tool also allows for adjustment of the importance of each goal on a scale from one to five (1 being the least important, 5 being the most important). The results of the optimization routine include a specified value for each of the process (i.e. feedstock) variables, as well as the predicted values for each response (e.g. crushing strength). A desirability value is calculated for each solution to the optimization routine to provide a method to rank the solutions and to indicate the extent to which the combination of responses approaches a perfect solution (i.e. desirability = 1).

Optimization of the mathematical models developed for briquettes comprised of Emerald coal and corn stover was accomplished by specifying a maximization goal for both crushing strength and mechanical durability. The importance of the mechanical durability goal was set to five and the importance of the crushing strength goal was set to three. This configuration was selected after experimenting with the effect of the importance setting on the desirability of the solutions to the optimization routine. The routine generated 21 optimized solutions, which indicated a crushing strength in excess of 1,900 newtons and a mechanical durability in excess of 94 percent is achievable. As shown in Table 5-12, the most desirable solutions occur at a water content of 0.05 with 30 percent biomass at a top size of 4.75 millimeters.

Table 5-12. Numerical optimization results for EM-CS mathematical models

| Number | Water Content | Biomass Top Size (mm) | Biomass Content (%) | Crushing Strength (N) | Mechanical Durability (%) | Desirability |
|---|---|---|---|---|---|---|
| 1 | 0.050 | 4.75 | 30 | 1911.4 | 95.9 | 0.950 |
| 2 | 0.050 | 4.75 | 30 | 1912.3 | 95.8 | 0.950 |
| 3 | 0.051 | 4.75 | 30 | 1910.5 | 95.9 | 0.950 |
| 4 | 0.050 | 4.75 | 30 | 1910.5 | 95.9 | 0.950 |
| 5 | 0.050 | 4.67 | 30 | 1909.2 | 95.8 | 0.950 |
| 6 | 0.047 | 4.75 | 30 | 1914.1 | 95.6 | 0.949 |
| 7 | 0.050 | 4.75 | 30 | 1906.1 | 95.8 | 0.949 |
| 8 | 0.050 | 4.44 | 30 | 1898.9 | 95.7 | 0.949 |
| 9 | 0.049 | 4.75 | 30 | 1900.7 | 95.6 | 0.949 |
| 10 | 0.050 | 4.39 | 30 | 1897.2 | 95.7 | 0.949 |

#### 5.4.1.5 Comparison of Bituminous Coals

A series of verification tests were designed to evaluate the McClure River and Toms Creek coals. The objective of these tests was to verify that the optimum combinations of feedstock variables identified for each Emerald coal-biomass mixture can also produce strong and durable briquettes with the other bituminous coals, and to validate that an exhaustive optimization study is not required for each bituminous coal type. A secondary objective of these tests was to give a clear indication to the effect of coal and biomass type on the quality of coal-biomass briquettes. To accomplish this, an optimum set of feedstock variables was chosen for each biomass type from the 15 conditions evaluated for the Emerald coal evaluations. The optimum set of feedstock variables for the corn stover and wheat straw corresponded to standard test 12, which included a target water content of 0.05, a biomass content of 30 percent and a biomass top size of 4.75 millimeters. In contrast the optimum set of feedstock variables for the switchgrass, miscanthus and sawdust corresponded to standard test 01, which included a target water content of 0.02, a biomass content of 20 percent and a biomass top size of 1.20 millimeters. The results of the five sets of tests are summarized in Table 5-13 for the McClure River coal and in Table 5-14 for the Toms Creek coal.

Table 5-13. Summary of briquette characterization results for McClure River coal verification tests

| Test ID | Feed Water Content | Biomass Content (%) | Biomass Top Size (mm) | Briquette Water Content | Particle Density (g/cm$^3$) | Crushing Strength (N) | Mechanical Durability (%) |
|---|---|---|---|---|---|---|---|
| MR-MC-01 | 0.024 | 20 | 1.20 | 0.015 | 1.11 | 1346.5 | 89.7 |
| MR-SG-01 | 0.023 | 20 | 1.20 | 0.016 | 1.11 | 1230.8 | 88.3 |
| MR-SD-01 | 0.023 | 20 | 1.20 | 0.015 | 1.14 | 1193.9 | 92.4 |
| MR-CS-12 | 0.068 | 30 | 4.75 | 0.049 | 1.07 | 2114.2 | 84.0 |
| MR-WS-12 | 0.060 | 30 | 4.75 | 0.040 | 1.07 | 1961.7 | 83.0 |

Table 5-14. Summary of briquette characterization results for Toms Creek coal verification tests

| Test ID | Feed Water Content | Biomass Content (%) | Biomass Top Size (mm) | Briquette Water Content | Particle Density (g/cm$^3$) | Crushing Strength (N) | Mechanical Durability (%) |
|---|---|---|---|---|---|---|---|
| TC-MC-01 | 0.022 | 20 | 1.20 | 0.015 | 1.13 | 978.6 | 77.1 |
| TC-SG-01 | 0.021 | 20 | 1.20 | 0.016 | 1.11 | 919.9 | 80.4 |
| TC-SD-01 | 0.021 | 20 | 1.20 | 0.014 | 1.15 | 917.2 | 88.1 |
| TC-CS-12 | 0.060 | 30 | 4.75 | 0.046 | 1.10 | 1988.4 | 74.0 |
| TC-WS-12 | 0.046 | 30 | 4.75 | 0.045 | 1.09 | 1665.0 | 68.3 |

To visualize the similarities in the measures responses for briquettes comprised of the three bituminous coals, the measured quality parameters for each coal type were plotted in a single chart. Figure 5-24 shows the similarities in the particle density of bituminous coal briquettes comprised of each biomass type. Specifically, the results are shown in Figure 5-24a for miscanthus, Figure 5-24b for switchgrass, Figure 5-24c for sawdust, Figure 5-24d for corn stover and Figure 5-24e for wheat straw. The measured particle density values for the briquettes composed of miscanthus ranged from 1.11 to 1.13 g/cm$^3$ for the three bituminous coals. The minimum value was attained with the McClure River coal, while both the Emerald and Toms Creek coals produced the maximum particle density value. Similarly, the measured particle density values for the briquettes composed of switchgrass ranged from 1.11 to 1.12 g/cm$^3$, with the maximum value corresponding to the Emerald coal briquettes and the minimum value corresponding to both the McClure River and the Toms Creek coal briquettes. The particle density values for the briquettes composed of sawdust and bituminous coal ranged from 1.14 to 1.15 g/cm$^3$, with the maximum value attained with the Toms Creek coal and the minimum value attained with both the Emerald and McClure River coal. These initial sets of results indicate that the three bituminous coals behave very similar with respect to the particle density of briquettes produced with biomass. These results also indicate that briquettes produced with sawdust generally have a greater particle density than briquettes composed of miscanthus and switchgrass. This result is certainly plausible due to the fact that woody biomass has a greater true density than agricultural biomass.

The measured particle density values for the briquettes composed of corn stover ranged from 1.07 to 1.10 g/cm$^3$ for the three bituminous coals. The minimum value was attained with the McClure River coal, while the Toms Creek coals produced the maximum particle density value. It is clear that these density values are substantially lower than the values obtained for the other agricultural biomass types (i.e. miscanthus and switchgrass). This result was due to the higher biomass content of the corn stover briquettes (i.e. 30%), as compared to the miscanthus and switchgrass briquettes (i.e. 20%). The incremental addition of biomass with a true density much lower than coal will clearly reduce the particle density of briquettes. Similarly, the measured particle density values for the briquettes composed of wheat straw ranged from 1.07 to 1.09 g/cm$^3$, with the maximum value corresponding to both the Emerald and Toms Creek coal briquettes and the minimum value corresponding to the McClure River coal briquettes. The

results presented in Figure 5-24 clearly validate the similarity in particle density of the bituminous coal briquettes.

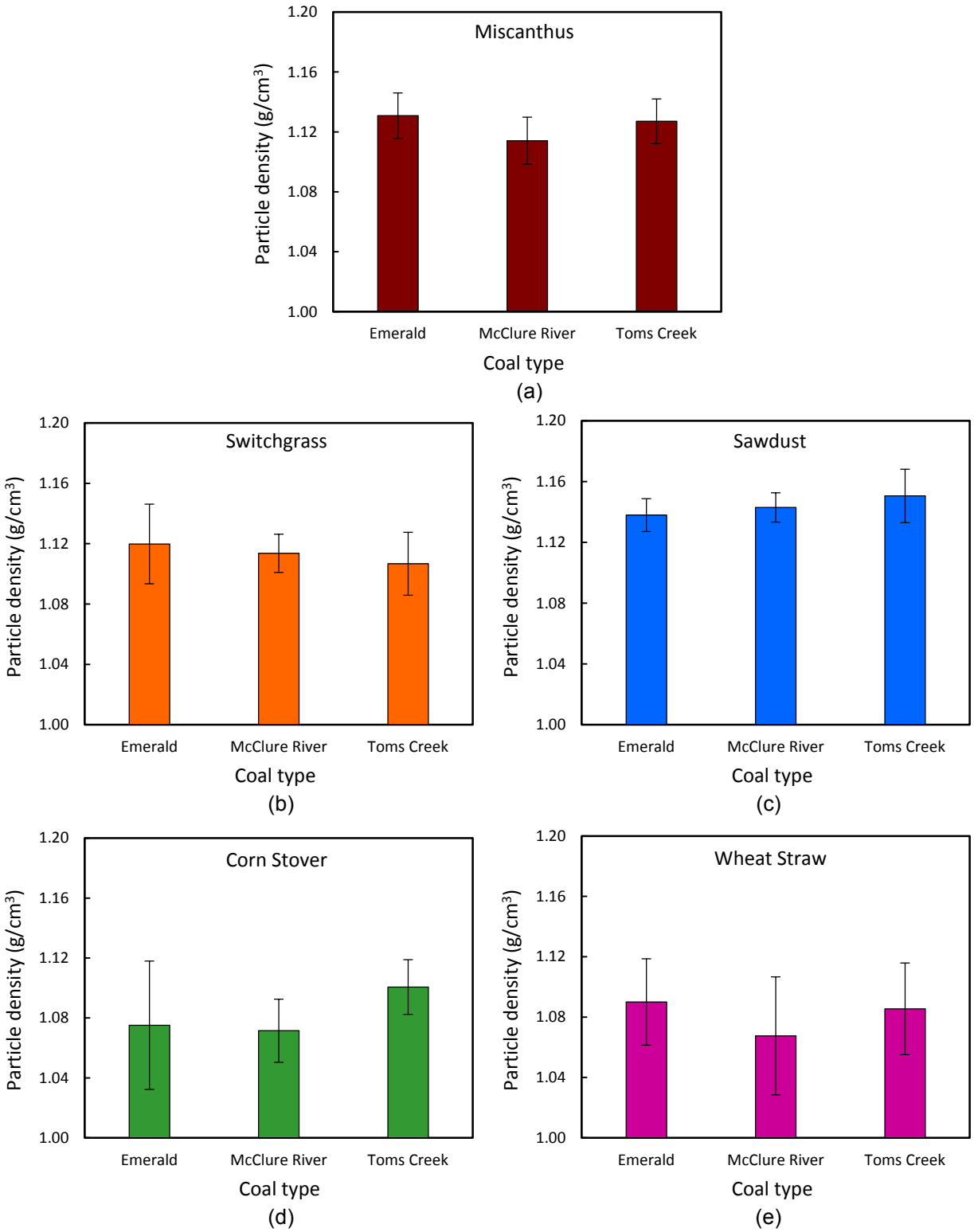



Figure 5-24. Comparison of particle density results for briquettes composed of bituminous coal and (a) miscanthus, (b) switchgrass, (c) sawdust, (d) corn stover and (e) wheat straw [Error bars indicate plus and minus one standard deviation from the mean]

Figure 5-25 shows the similarities in the crushing strength of bituminous coal briquettes comprised of each biomass type. Specifically, the results are shown in Figure 5-25a for miscanthus, Figure 5-25b for switchgrass, Figure 5-25c for sawdust, Figure 5-25d for corn stover and Figure 5-25e for wheat straw. The measured crushing strength values for the briquettes composed of miscanthus ranged from 979 to 1,389 N (220.0-312.2 $lb_f$) for the three bituminous coals. The minimum value was attained with the Toms Creek coal, while the Emerald coal produced the maximum crushing strength value. Similarly, the measured crushing strength values for the briquettes composed of switchgrass ranged from 920 to 1,380 N (206.8-310.3 $lb_f$), with the maximum value corresponding to the Emerald coal briquettes and the minimum value corresponding to the Toms Creek coal briquettes. The crushing strength values for the briquettes composed of sawdust and bituminous coal ranged from 917 to 1,357 N (206.2-305.0 $lb_f$). The maximum value was again attained with the Emerald coal and the minimum value was again attained with the Toms Creek coal. This reoccurring trend in briquette crushing strength values (i.e. Emerald = highest, Toms Creek = lowest) is likely the result of differences in the distribution modulus and ash content of the coals. As discussed in Chapter 4, this relative ranking of coal types with respect to crushing strength was anticipated. These results also indicate that briquettes produced with miscanthus, switchgrass and sawdust generally exhibit similar crushing strengths.

The measured crushing strength values for the briquettes composed of corn stover ranged from 1,988 to 2,114 N (447.0-475.3 $lb_f$) for the three bituminous coals. As anticipated, the minimum value was attained with the Toms Creek coal, while the McClure River coal unexpectedly produced the maximum crushing strength. It is clear that these crushing strengths are substantially higher than the values obtained for the other agricultural biomass types (i.e. miscanthus and switchgrass). This result was due to the higher biomass content of the corn stover briquettes (30%), as compared to the miscanthus and switchgrass briquettes (20%). This was expected since the incremental addition of biomass was previously shown to increase the crushing strength of briquettes. Similarly, the measured crushing strength values for the briquettes composed of wheat straw ranged from 1,665 to 2,100 N (374.3-472.0 $lb_f$), with the maximum and minimum values corresponding to the Emerald and Toms Creek coal briquettes, respectively. The results presented in Figure 5-25 clearly show the similarities in the crushing strength of bituminous coal briquettes. While differences do exist in the measured values, they

can be explained by further examination of the distribution modulus and ash content of each coal.

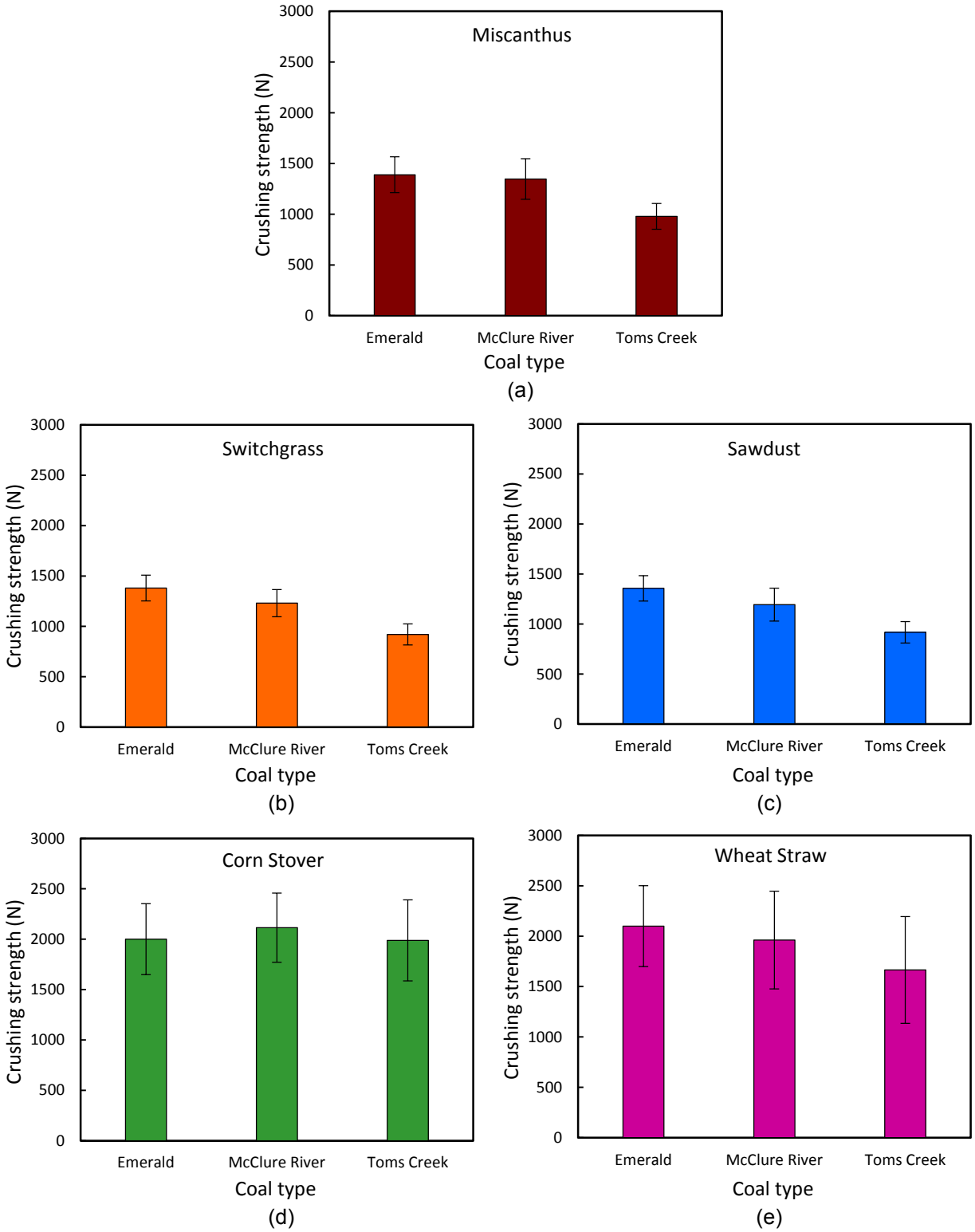



Figure 5-25. Comparison of crushing strength results for briquettes composed of bituminous coal and (a) miscanthus, (b) switchgrass, (c) sawdust, (d) corn stover and (e) wheat straw [Error bars indicate plus and minus one standard deviation from the mean]

Figure 5-26 shows the similarities in the mechanical durability of bituminous coal briquettes comprised of each biomass type. Specifically, the results are shown in Figure 5-26a for miscanthus, Figure 5-26b for switchgrass, Figure 5-26c for sawdust, Figure 5-26d for corn stover and Figure 5-26e for wheat straw. The mechanical durability values for the briquettes composed of miscanthus ranged from 77.1 to 89.7% for the three bituminous coals. The minimum value was attained with the Toms Creek coal, while the McClure River coal produced the maximum mechanical durability. Similarly, the mechanical durability values for the briquettes composed of switchgrass ranged from 80.4 to 89.7%, with the maximum value corresponding to the Emerald coal briquettes and the minimum value corresponding to the Toms Creek coal briquettes. The mechanical durability values for the briquettes composed of sawdust and bituminous coal ranged from 88.1 to 92.7%. The maximum value was again attained with the Emerald coal and the minimum value was again attained with the Toms Creek coal. This reoccurring trend in briquette mechanical durability values (i.e. Emerald = highest, Toms Creek = lowest) is likely the result of differences in the distribution modulus and ash content of the coals. As discussed in Chapter 4, this relative ranking of coal types with respect to the mechanical durability of briquettes was anticipated. These results also indicate that briquettes produced with sawdust generally exhibit greater mechanical durability than briquettes composed of miscanthus and switchgrass.

The mechanical durability of briquettes composed of corn stover ranged from 74.0 to 90.2% for the three bituminous coals. As anticipated, the minimum value was attained with the Toms Creek coal and the maximum value was attained with the Emerald coal. The effect of the higher biomass content of the corn stover briquettes compared to the miscanthus and switchgrass briquettes is not definitive. However, it appears that a wider range of mechanical durability values are attained with 30 percent biomass. Similarly, the mechanical durability of the briquettes composed of wheat straw ranged from 68.3 to 88.1%, with the maximum value corresponding to both the Emerald coal briquettes and the minimum value corresponding to the Toms Creek coal briquettes. The results presented in Figure 5-26 clearly show the similarities in the mechanical durability of bituminous coal briquettes. While differences do exist in the measured values, they can be explained by further examination of the distribution modulus and ash content of each individual coal type. Nonetheless, the Emerald coal appears to be the best bituminous coal for production of coal-biomass briquettes.

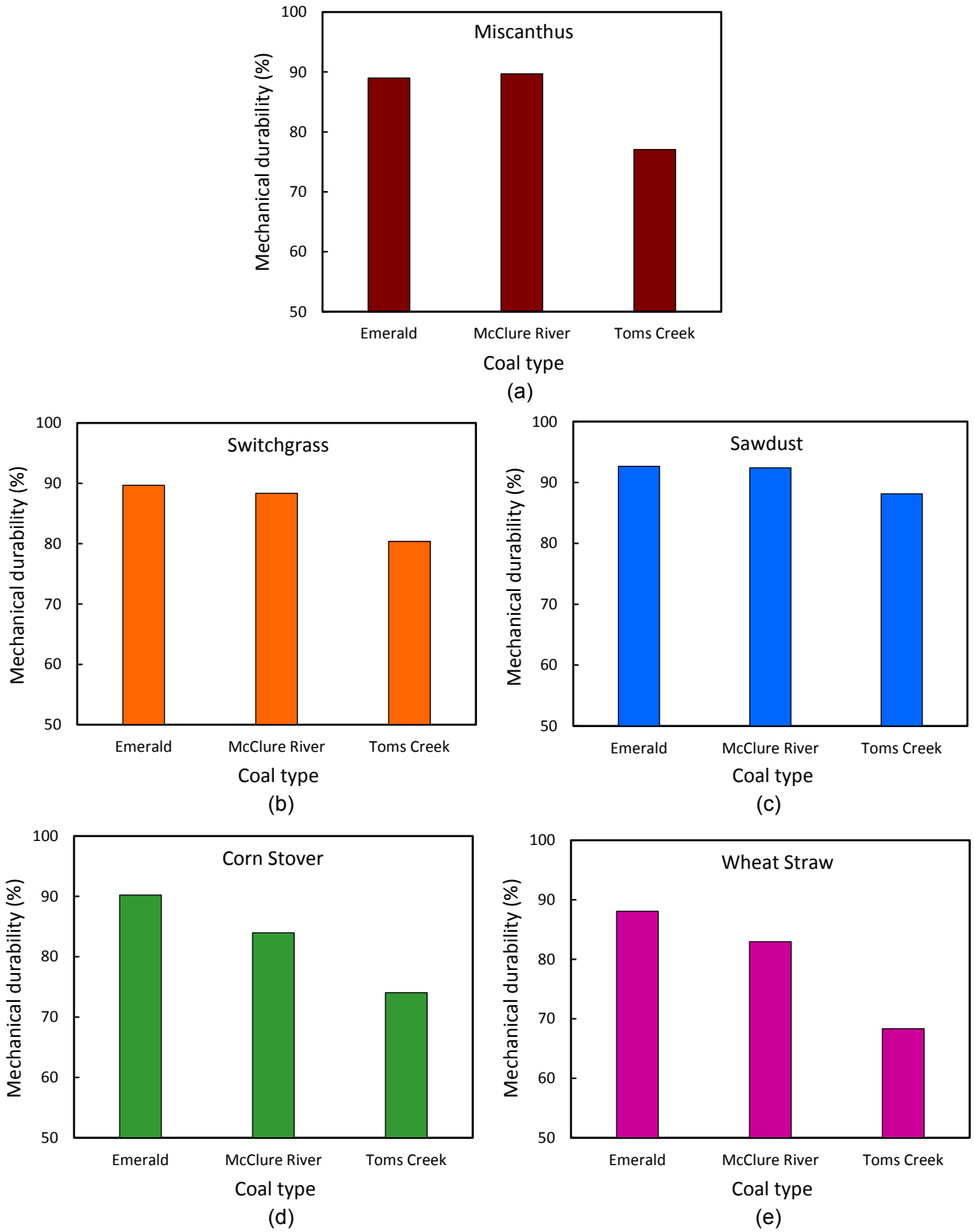



Figure 5-26. Comparison of mechanical durability results for briquettes composed of bituminous coal and (a) corn stover, (b) switchgrass, (c) miscanthus, (d) wheat straw and (e) sawdust

## 5.4.2 Evaluation of Additive Variables – Bituminous Coal

### 5.4.2.1 Summary of Results

The results of the additive variables evaluations for briquettes composed of Emerald coal, corn stover and pregelatinized wheat starch are summarized in Table 5-15. Each test that was conducted is identified by the standard test number assigned in Design-Expert® 8 according to the biomass content, starch content and cure time (i.e. 01 = biomass content of 10%, starch content of 0.0% and cure time of 1 day). In the following sections, correlations between each additive variable and the measured briquette properties are presented and discussed. Analysis of the results is also covered, including mathematical models developed for each response using the Design-Expert® 8 statistical analysis tools. In addition, contour graphs of the models are presented to visually interpret and evaluate the results. Finally, numerical optimization of the model was conducted to determine the combination of additive variables that produces the highest quality briquettes.

Table 5-15. Summary of briquette characterization results for briquettes composed of Emerald (bituminous) coal, corn stover and pregelatinized wheat starch

| Test ID | Biomass Content (%) | Starch Content (%) | Cure Time (days) | Briquette Water Content | Particle Density (g/cm$^3$) | Crushing Strength (N) | Mechanical Durability (%) |
|---|---|---|---|---|---|---|---|
| EM-CS-PGWS-01 | 10 | 0.0 | 1 | 0.019 | 1.15 | 689.0 | 76.4 |
| EM-CS-PGWS-02 | 30 | 0.0 | 1 | 0.039 | 1.11 | 1812.7 | 89.6 |
| EM-CS-PGWS-03 | 10 | 5.0 | 1 | 0.026 | 1.17 | 1343.8 | 97.4 |
| EM-CS-PGWS-04 | 30 | 5.0 | 1 | 0.042 | 1.12 | 2226.8 | 93.7 |
| EM-CS-PGWS-05 | 10 | 2.5 | 0 | 0.035 | 1.16 | 804.7 | 95.0 |
| EM-CS-PGWS-06 | 30 | 2.5 | 0 | 0.044 | 1.12 | 1913.6 | 91.8 |
| EM-CS-PGWS-07 | 10 | 2.5 | 7 | 0.021 | 1.17 | 1033.8 | 95.2 |
| EM-CS-PGWS-08 | 30 | 2.5 | 7 | 0.040 | 1.12 | 2096.0 | 94.7 |
| EM-CS-PGWS-09 | 20 | 0.0 | 0 | 0.044 | 1.12 | 1047.1 | 84.9 |
| EM-CS-PGWS-10 | 20 | 5.0 | 0 | 0.040 | 1.15 | 1678.3 | 94.9 |
| EM-CS-PGWS-11 | 20 | 0.0 | 7 | 0.029 | 1.13 | 1234.8 | 88.4 |
| EM-CS-PGWS-12 | 20 | 5.0 | 7 | 0.032 | 1.17 | 1715.2 | 96.1 |
| EM-CS-PGWS-13 | 20 | 2.5 | 1 | 0.032 | 1.15 | 1477.7 | 94.3 |
| EM-CS-PGWS-14 | 20 | 2.5 | 1 | 0.029 | 1.16 | 1494.6 | 94.2 |
| EM-CS-PGWS-15 | 20 | 2.5 | 1 | 0.031 | 1.16 | 1540.0 | 95.1 |

*5.4.2.1.1 Binder Content Correlations*

The correlation between binder content and each measured briquette property were evaluated by linear regression analysis. To investigate these correlations, binder content was plotted versus each measured briquette property with the data points grouped by biomass content (i.e. 10, 20 and 30%). This approach was used because little or no correlation existed for the entire data set due to the influence of the other two mixture variables (i.e. biomass content and cure time). The binder content correlations were initially investigated with the data grouped separately by biomass content and cure time. From these investigations, it was found that binder content correlations were greatest with the data grouped by biomass content.

Figure 5-27a displays the correlation between binder content and the particle density of the briquettes. It is clear from this chart that binder content exhibits a positive correlation with particle density. For each of the three biomass contents, an increase in starch content led to a rise in the particle density of the briquettes. This was particularly apparent when the starch content was increased from 0.0 to 2.5 percent. However, when the starch content was increased from 2.5 to 5.0 percent, the particle density values remained fairly constant, particularly at a biomass content of 10 and 30 percent. The strength of these linear correlations was measured by determining the coefficient of determination for each data set grouped by biomass content. The strongest linear correlation was found for the briquettes produced with 30 percent biomass (i.e. $R^2 = 0.86$). The strength of this correlation successively declined with a reduction in biomass content. Specifically, the coefficient of determination for briquettes produced with 20 and 10 percent biomass was 0.68 and 0.54, respectively.

Figure 5-27b illustrates the correlation between binder content and the crushing strength of the briquettes. It is clear from this chart that binder content exhibits a strong positive correlation with crushing strength. Specifically, an increase in starch content led to a direct rise in the crushing strength of the briquettes for each of the three biomass contents. This correlation was expected, considering the sole purpose of starch addition to briquette feedstocks is the improvement of briquette quality. The strength of these linear correlations was measured by determining the coefficient of determination for each data set grouped by biomass content. The strongest linear correlation was found for the briquettes produced with 20 percent biomass (i.e. $R^2 = 0.90$), followed closely by briquettes produced with 10 and 30 percent biomass with coefficients of determination of 0.86 and 0.84, respectively.

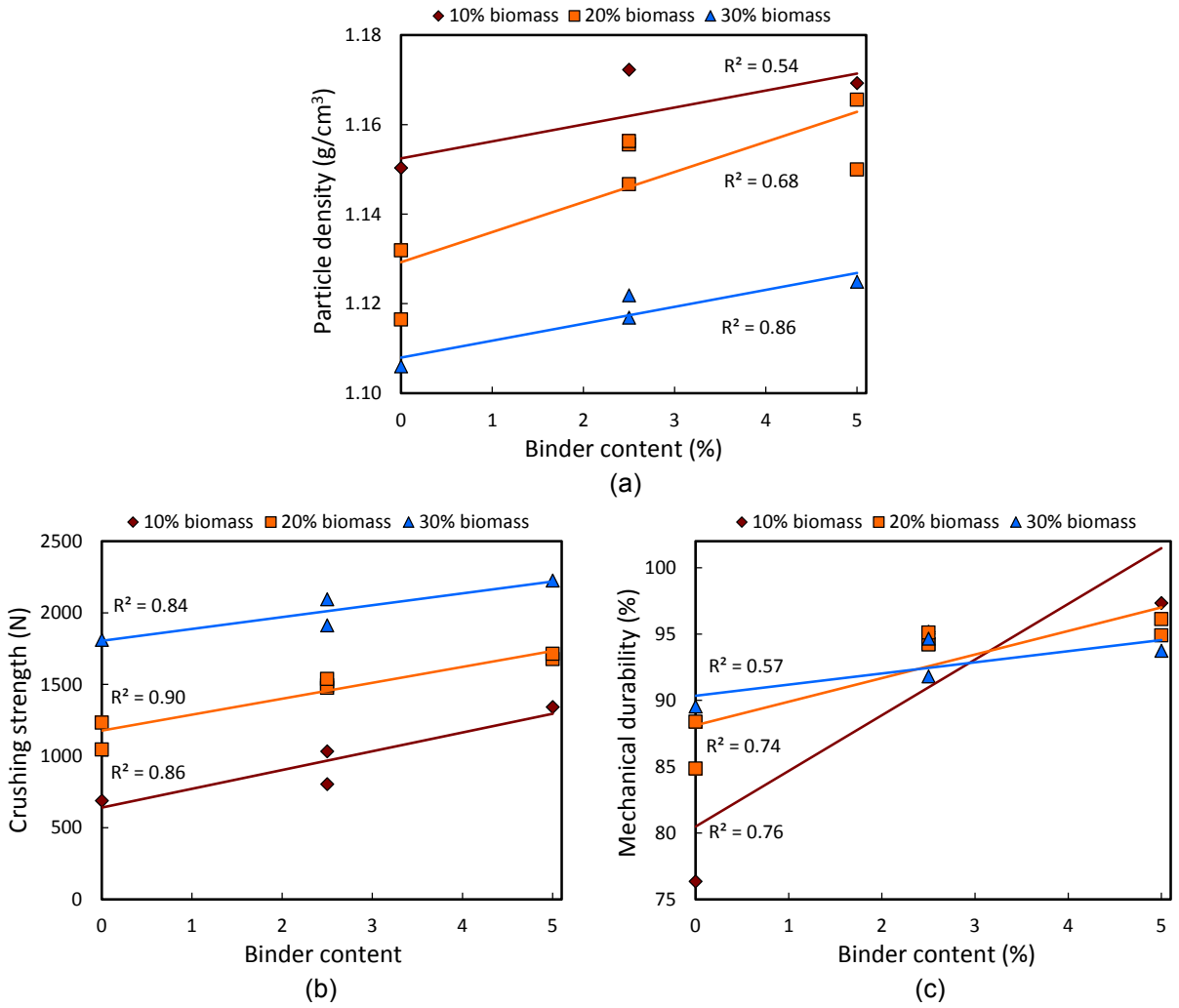



Figure 5-27. Effect of binder content of briquettes composed of Emerald (bituminous) coal, corn stover and pregelatinized wheat starch on (a) particle density, (b) crushing strength and (c) mechanical durability

Figure 5-27c shows the correlation between binder content and the mechanical durability of the briquettes. It is clear from this chart that binder content exhibits a positive correlation with mechanical durability. Specifically, an increase in starch content led to an overall increase in the mechanical durability of the briquettes for each of the three biomass contents. The strength of these linear correlations was measured by determining the coefficient of determination for each data set grouped by biomass content. The strongest linear correlation was found for the briquettes produced with 10 percent biomass (i.e. $R^2 = 0.76$). The strength of this correlation successively declined with an increase in biomass content to a coefficient of determination of 0.74 and 0.57 for briquettes produced with 20 and 30 percent biomass, respectively.

*5.4.2.1.2 Cure Time Correlations*

The correlation between briquette cure time and each measured property were also evaluated by linear regression analysis. To investigate these correlations, cure time was plotted versus each measured briquette property with the data points grouped by biomass content (i.e. 10, 20 and 30%). This approach was used because little or no correlation existed for the entire data set due to the influence of the other two mixture variables (i.e. biomass content and binder content). The cure time correlations were initially investigated with the data grouped separately by binder content and biomass content. From these investigations, it was found that cure time correlations were greatest with the data grouped by biomass content, although neither resulted in any significant correlations.

Figure 5-28a displays the correlation between cure time and the particle density of the briquettes. It is clear from this chart that there is very little correlation between briquette cure time and particle density, although a slight correlation exists for briquettes composed of 10 percent biomass. This is supported by coefficient of determination values of 0.45, 0.03 and 0.12 for biomass contents of 10, 20 and 30 percent, respectively. The most probable reason for the absence of any significant correlations is the interaction between binder content and particle density, which is concealed in this simple correlation investigation.

Figure 5-28b illustrates the correlation between cure time and the crushing strength of the briquettes. It is clear from this chart that there is also very little correlation between briquette cure time and crushing strength. This is supported by coefficient of determination values of 0.04, 0.01 and 0.11 for biomass contents of 10, 20 and 30 percent, respectively. The most probable reason for the absence of any noteworthy correlations is the significant interaction between binder content and crushing strength, which is concealed in this analysis.

Figure 5-28c shows the correlation between cure time and the mechanical durability of the briquettes. It is clear from this chart that there is also very little correlation between briquette cure time and crushing strength. This is supported by coefficient of determination values of 0.05, 0.00 and 0.41 for biomass contents of 10, 20 and 30 percent, respectively. The most probable reason for the absence of any significant correlations is the interaction between binder content and mechanical durability, which is concealed in this analysis.

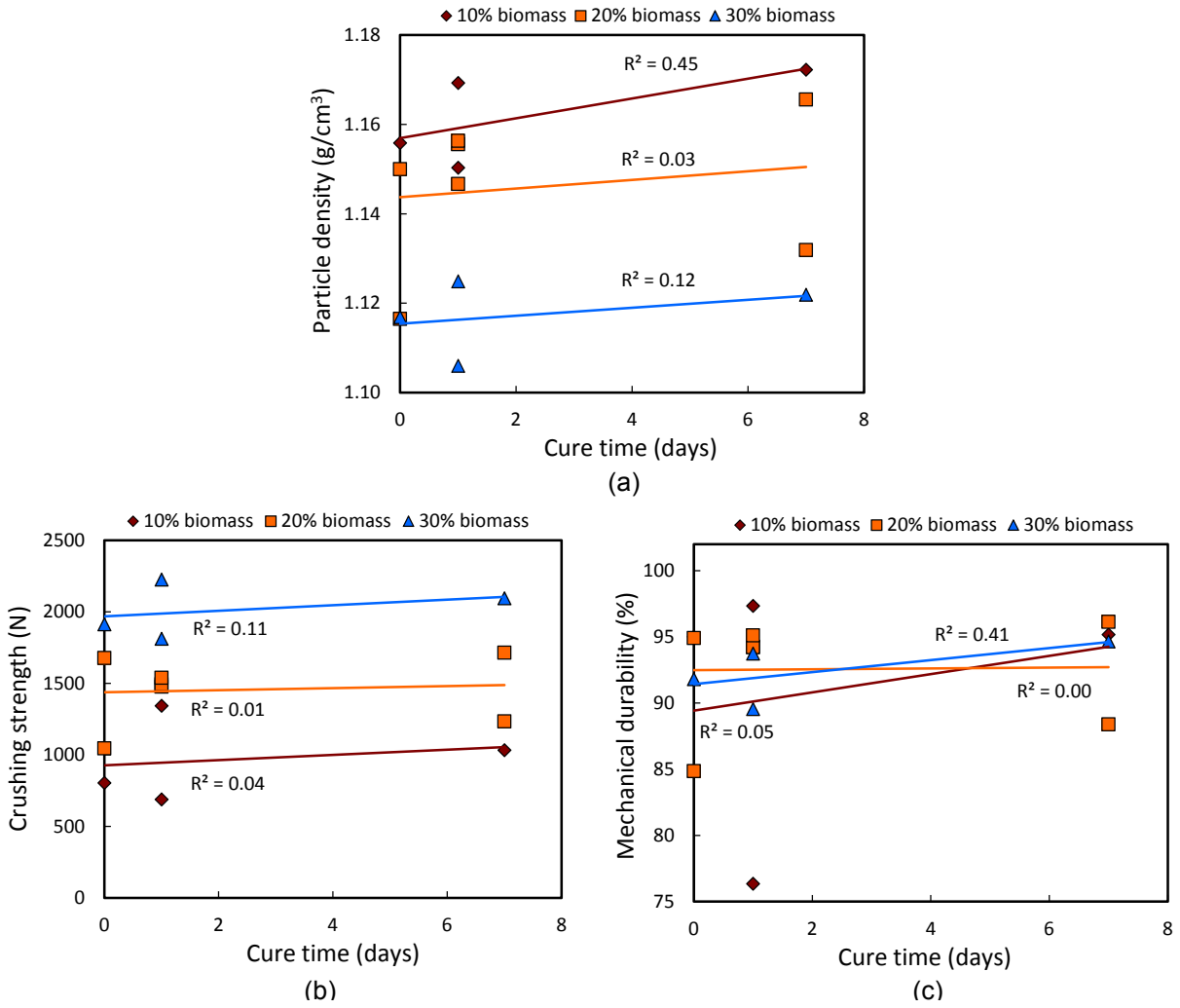



Figure 5-28. Effect of cure time of briquettes composed of Emerald (bituminous) coal, corn stover and pregelatinized wheat starch on (a) particle density, (b) crushing strength and (c) mechanical durability

### *5.4.2.1.3 Biomass Content Correlations*

The correlation between biomass content and each measured property were also evaluated by linear regression analysis. To investigate these correlations, biomass content was plotted versus each measured briquette property with the data points grouped by binder content (i.e. 0.0, 2.5 and 5.0%). This approach was used because little or no correlation existed for the entire data set due to the influence of the other two mixture variables (i.e. binder content and briquette cure time). The biomass content correlations were initially investigated with the data grouped separately by binder content and briquette cure time. From these investigations, it was determined that biomass content correlations were greatest with the data grouped by binder content.

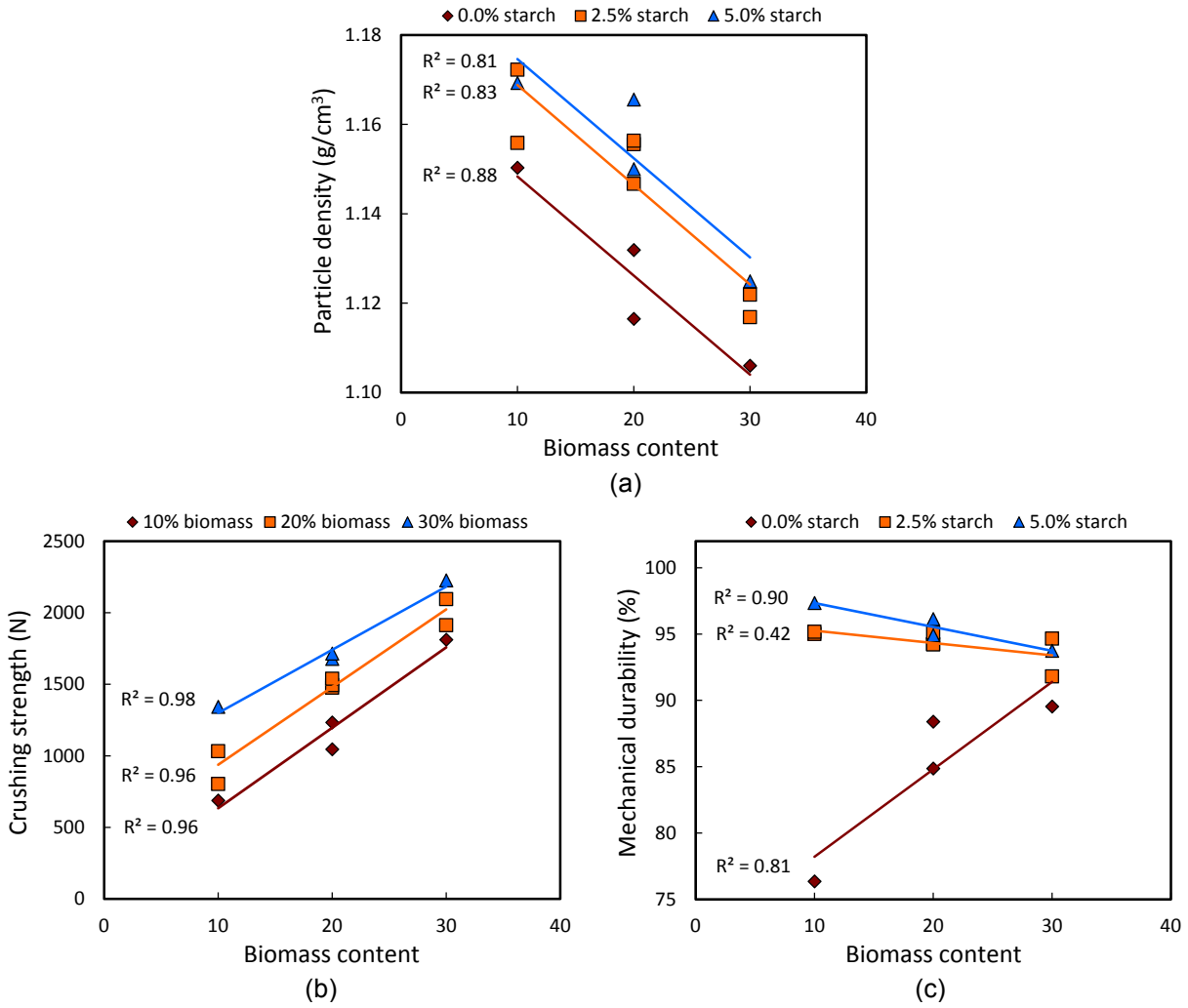



Figure 5-29. Effect of biomass content of briquettes composed of Emerald (bituminous) coal, corn stover and pregelatinized wheat starch on (a) particle density, (b) crushing strength and (c) mechanical durability

Figure 5-29a displays the correlation between biomass content and the particle density of the briquettes. It is clear from this chart that biomass content exhibits a fairly strong negative correlation with particle density. For each of the three binder contents, an increase in biomass content caused a direct reduction in the particle density of the briquettes. This finding was expected since the addition of additional biomass with a true density much lower than coal will reduce the composite density of the mixture prior to briquette production. The strength of these linear correlations was measured by determining the coefficient of determination for each data set grouped by binder content. The strongest linear correlation was found for the briquettes produced with no starch (i.e. $R^2 = 0.88$). The strength of this correlation successively declined with an increase in starch content. Specifically, the coefficient of determination for briquettes

produced with 2.5 and 5.0 percent starch was 0.83 and 0.81, respectively. These findings further prove that an increase in biomass content directly reduces the particle density of coal-biomass briquettes.

Figure 5-29b illustrates the correlation between biomass content and the crushing strength of the briquettes. It is clear from this chart that biomass content has a very strong positive correlation with crushing strength. Specifically, an increase in biomass content led to a direct rise in the crushing strength of the briquettes for each of the three binder contents. The strength of these linear correlations was measured by determining the coefficient of determination for each data set grouped by binder content. The strongest linear correlation was found for the briquettes produced with 5.0 percent starch (i.e. $R^2 = 0.98$), followed closely by briquettes produced with 2.5 and 0.0 percent starch (i.e. $R^2 = 0.96$ for both). These findings further validate that addition of biomass to coal briquettes improves the crushing strength of feedstocks and that low biomass content briquettes are typically lower in strength.

Figure 5-29c shows the correlation between biomass content and the mechanical durability of the briquettes. It is clear from this chart that the correlation between biomass content and mechanical durability depends heavily on binder content. Specifically, an increase in biomass content led to a sharp increase in the mechanical durability of the briquettes produced without starch (i.e. starch content = 0.0 %). In contrast, an increase in biomass content resulted in a modest decline in mechanical durability for briquettes produced with 2.5 and 5.0 percent starch. The strength of these linear correlations was measured by determining the coefficient of determination for each data set grouped by binder content. The strongest linear correlation was found for the briquettes produced with 5.0 percent starch (i.e. $R^2 = 0.90$), which was followed closely by briquettes produced without starch (i.e. $R^2 = 0.81$). However, the strength of this was significantly lower for briquettes produced with 2.5 percent starch (i.e. $R^2 = 0.42$). These findings suggest that addition of biomass to coal briquettes with a starch binder leads to a decrease in mechanical durability.

#### 5.4.2.2 Statistical Analyses

The results of the additive variables evaluations were examined using the statistical analysis tools included in Design-Expert® 8 to determine the influence of each mixture variable and to optimize the quality of briquettes. Mathematical models were developed that relate the

additive variables (i.e. binder content and cure time) and biomass content to the measured briquette properties (i.e. particle density, crushing strength, and mechanical durability). The first step of model development was selection of the process order (e.g. linear, quadratic) of the mathematical model. This was accomplished by determining the process order with the lowest lack of fit p-value and the highest adjusted R-squared and predicted R-squared values. The selected model was then analyzed using the analysis of variance (ANOVA) function to determine the statistical significance of the entire model and of each individual term. All insignificant terms were then removed from the model, except those required to maintain hierarchy. Next, the fit of the model to the data was evaluated using various diagnostics tools. The following sections present the empirical mathematical models developed for briquettes composed of Emerald coal, corn stover and pregelatinized wheat starch, and summarize the results of the statistical analyses.

#### *5.4.2.2.1 Particle Density Model*

A linear mathematical model was constructed that relates binder content, cure time and biomass content to the particle density of briquettes composed of Emerald coal, corn stover and pregelatinized wheat starch. According to the model, the predicted particle density of briquettes is calculated by:

$$\rho = 1.17 + 0.0050b + 0.0009t - 0.0023c \quad \text{(Eq. 5-12)}$$

where $\rho$ is the particle density (g/cm$^3$), $b$ is the binder content (%), $t$ is the cure time (days) and $c$ is the biomass content (%). The statistical significance of this model, in terms of its fit to the data from which it was derived, was analyzed using ANOVA to evaluate a number of variables. A summary of the ANOVA is provided in Table 5-16 for the particle density model. The p-value of the particle density model is 0.0002, which indicates that the predicted density values would be highly unlikely under the null hypothesis and verifies that the model is indeed statistically significant. The p-values of the model terms are less than 0.0001 (biomass content), 0.0055 (binder content) and 0.3518 (cure time). This implies that biomass content and binder content are statistically significant model terms, and thus have a major impact on accurate prediction of the particle density of briquettes. In contrast, cure time is not a significant model term, which implies that its impact on particle density quantified in the model is not statistically significant. This term

was needed to maintain the hierarchy of the model, otherwise it would have been removed to improve the model.

Table 5-16. ANOVA results for EM-CS-PGWS particle density model

| Source | Sum of Squares | df | Mean Square | F Value | p-value Prob > F |
|---|---|---|---|---|---|
| Model | 5.40E-03 | 3 | 1.80E-03 | 17.06 | 0.0002 |
| A-Biomass content | 4.05E-03 | 1 | 4.05E-03 | 38.40 | < 0.0001 |
| B-Starch content | 1.25E-03 | 1 | 1.25E-03 | 11.85 | 0.0055 |
| C-Cure time | 9.97E-05 | 1 | 9.97E-05 | 0.95 | 0.3518 |
| Residual | 1.16E-03 | 11 | 1.05E-04 | -- | -- |
| Lack of Fit | 1.09E-03 | 9 | 1.22E-04 | 3.65 | 0.2338 |
| Pure Error | 6.67E-05 | 2 | 3.33E-05 | -- | -- |
| Cor Total | 6.56E-03 | 14 | -- | -- | -- |

To confirm the ANOVA normality assumption for the particle density model, the residuals were visually examined in a normal probability plot of studentized results. Figure 5-30a shows the normal probability plot of studentized residuals for the crushing strength model. It is clear from this figure that the residuals follow an approximately straight line, and thus are normally distributed. A plot of predicted versus actual values was also examined to visually analyze the relationship between the measured particle density values and those predicted by the model. The predicted versus actual plot is displayed in Figure 5-30b for the particle density model, which shows the desired data scatter about the 45 degree line is present. This further exemplifies the statistical significance of the particle density model and indicates that it is well suited for prediction of briquette quality.

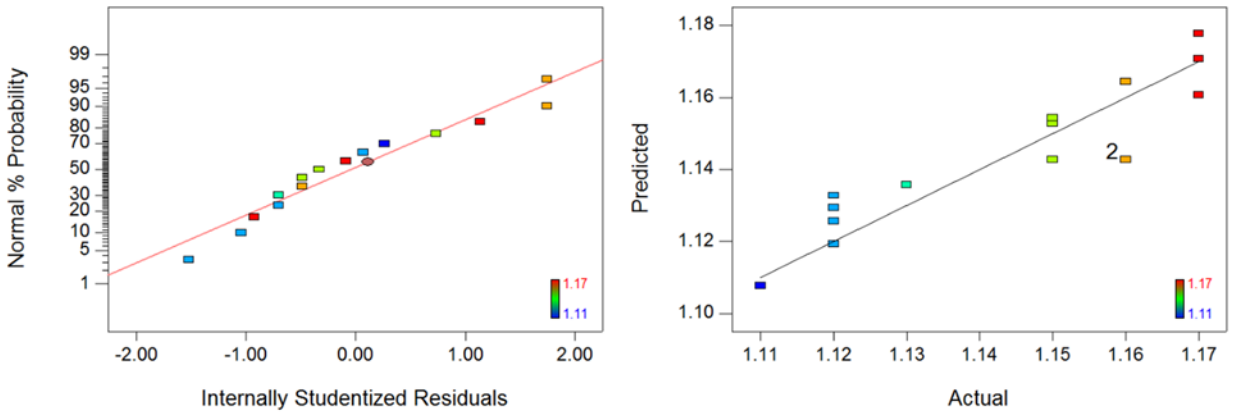



Figure 5-30. Diagnostic graphs for visual inspection of ANOVA results for EM-CS-PGWS particle density model: (a) normal probability plot of studentized results and (b) predicted versus actual values plot

*5.4.2.2.2 Crushing Strength Model*

A quadratic mathematical model was constructed that relates binder content, cure time and biomass content to the crushing strength of briquettes composed of Emerald coal and corn stover. According to the model, the predicted crushing strength of briquettes is calculated by:

$$\sigma = -76.40 + 157.16b + 172.55t + 58.24c - 2.41bc - 21.40t^2 \quad \text{(Eq. 5-13)}$$

where $\sigma$ is the crushing strength (N), $b$ is the binder content (%), $t$ is the cure time (days) and $c$ is the biomass content (%). The statistical significance of this model, in terms of its fit to the data from which it was derived, was analyzed using ANOVA to evaluate a number of variables. A summary of the ANOVA is provided in Table 5-17 for the crushing strength model. The p-value of the model is less than 0.0001, which indicates that the predicted crushing strength values would be highly unlikely under the null hypothesis and verifies that the model is indeed statistically significant. The p-values of the model terms are less than 0.0001 (biomass content), less than 0.0001 (starch content), 0.0011 (cure time), 0.0322 (biomass content x starch content) and 0.0011 (cure time$^2$). This implies that all of the model terms are statistically significant, and thus have a major impact on accurate prediction of the crushing strength of briquettes.

Table 5-17. ANOVA results for EM-CS-PGWS crushing strength model

| Source | Sum of Squares | df | Mean Square | F Value | p-value Prob > F |
|---|---|---|---|---|---|
| Model | 2.86E+06 | 5 | 572053 | 253.13 | < 0.0001 |
| A-Biomass content | 2.18E+06 | 1 | 2.18E+06 | 965.39 | < 0.0001 |
| B-Starch content | 5.94E+05 | 1 | 5.94E+05 | 262.99 | < 0.0001 |
| C-Cure time | 50577 | 1 | 50577 | 22.38 | 0.0011 |
| AB | 14478 | 1 | 14478 | 6.41 | 0.0322 |
| $C^2$ | 49734 | 1 | 49734 | 22.01 | 0.0011 |
| Residual | 20339 | 9 | 2260 | -- | -- |
| Lack of Fit | 18265 | 7 | 2609 | 2.52 | 0.3137 |
| Pure Error | 2074 | 2 | 1037 | -- | -- |
| Cor Total | 2.88E+06 | 14 | -- | -- | -- |

To confirm the ANOVA normality assumption for the crushing strength model, the residuals were visually examined in a normal probability plot of studentized results. Figure 5-31a shows the normal probability plot of studentized residuals for the crushing strength model. It is clear from this figure that the residuals follow an approximately straight line, and thus are normally distributed. A plot of predicted versus actual values was also examined to visually

analyze the relationship between the measured crushing strength values and those predicted by the model. The predicted versus actual plot is displayed in Figure 5-31b for the crushing strength model, which shows the desired data scatter about the 45 degree line is present. This further exemplifies the statistical significance of the crushing strength model and indicates that it is well suited for prediction of briquette quality.

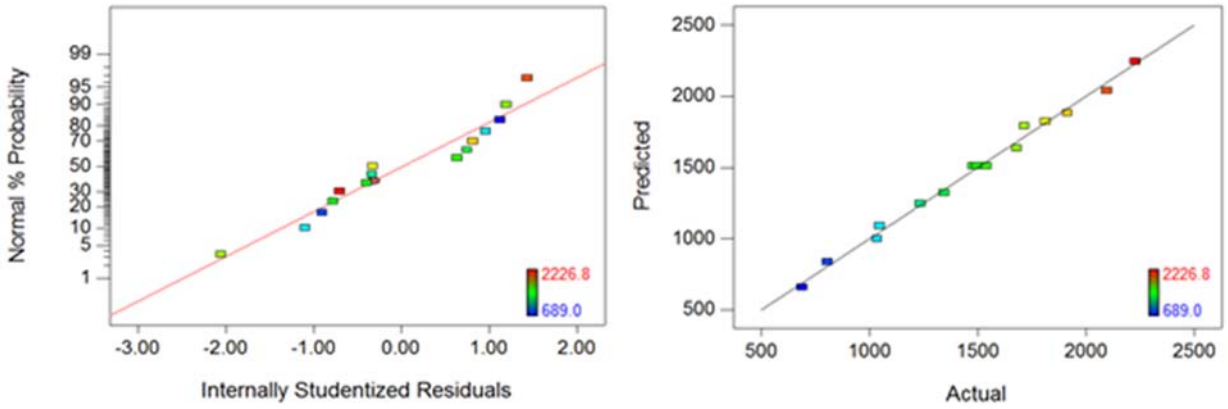



Figure 5-31. Diagnostic graphs for visual inspection of ANOVA results for EM-CS-PGWS crushing strength model: (a) normal probability plot of studentized results and (b) predicted versus actual values plot

*5.4.2.2.3 Mechanical Durability Model*

A quadratic mathematical model was constructed that relates binder content, cure time and biomass content to the mechanical durability of briquettes composed of Emerald coal and corn stover. According to the model, the predicted mechanical durability of briquettes is calculated by:

$$MD = 74.29 + 8.79b + 0.29t + 0.49c - 0.17bc - 0.66b^2 \quad \text{(Eq. 5-14)}$$

where *MD* is the mechanical durability (%), $b$ is the binder content (%), $t$ is the cure time (days) and $c$ is the biomass content (%). The statistical significance of this model, in terms of its fit to the data from which it was derived, was analyzed using ANOVA to evaluate a number of variables. A summary of the ANOVA is provided in Table 5-18 for the mechanical durability model. The p-value of the model is 0.0002, which indicates that the predicted mechanical durability values would be highly unlikely under the null hypothesis and verifies that the model is indeed statistically significant. The p-values of the model terms are 0.3360 (biomass content), less than 0.0001 (starch content), 0.1556 (cure time), 0.0026 (biomass content x starch content) and 0.0037 (starch content$^2$). This implies that the majority of the model terms are statistically

significant (except biomass content and cure time), and thus have a major impact on accurate prediction of the mechanical durability of briquettes. In contrast, biomass content and cure time are not significant model terms, which implies that the impact of these variables on mechanical durability quantified in the model is not statistically significant.

Table 5-18. ANOVA results for EM-CS-PGWS mechanical durability model

| Source | Sum of Squares | df | Mean Square | F Value | p-value Prob > F |
|---|---|---|---|---|---|
| Model | 380.25 | 5 | 76.05 | 18.24 | 0.0002 |
| A-Biomass content | 4.31 | 1 | 4.31 | 1.03 | 0.3360 |
| B-Starch content | 230.80 | 1 | 230.80 | 55.35 | < 0.0001 |
| C-Cure time | 10.02 | 1 | 10.02 | 2.40 | 0.1556 |
| AB | 70.48 | 1 | 70.48 | 16.90 | 0.0026 |
| $B^2$ | 63.00 | 1 | 63.00 | 15.11 | 0.0037 |
| Residual | 37.53 | 9 | 4.17 | -- | -- |
| Lack of Fit | 37.02 | 7 | 5.29 | 20.70 | 0.0468 |
| Pure Error | 0.51 | 2 | 0.26 | -- | -- |
| Cor Total | 417.78 | 14 | -- | -- | -- |

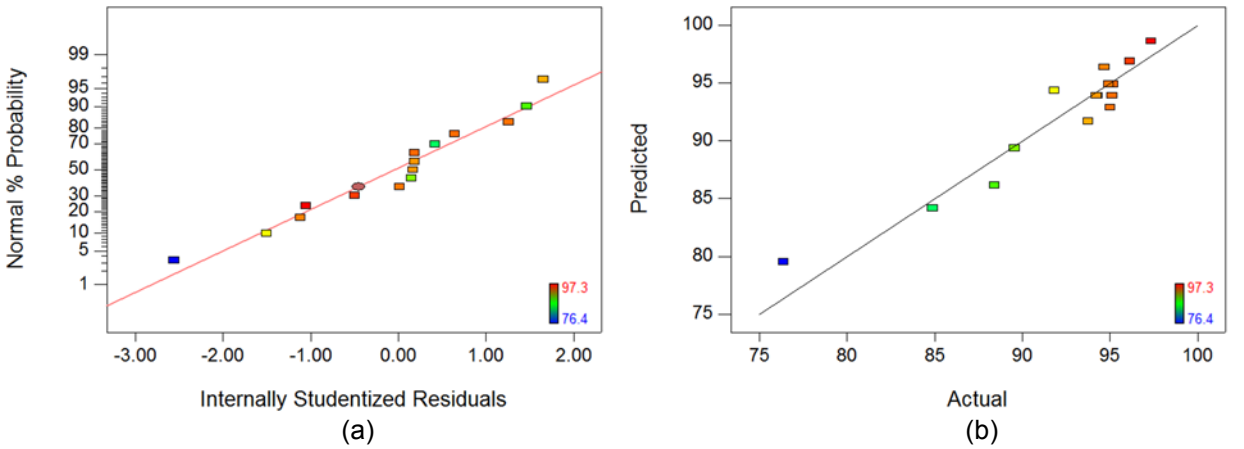



Figure 5-32. Diagnostic graphs for visual inspection of ANOVA results for EM-CS-PGWS mechanical durability model: (a) normal probability plot of studentized results and (b) predicted versus actual values plot

To confirm the ANOVA normality assumption for the mechanical durability model, the residuals were visually examined in a normal probability plot of studentized results. Figure 5-32a shows the normal probability plot of studentized residuals for the mechanical durability model. It is clear from this figure that the residuals follow an approximately straight line, and thus are normally distributed. A plot of predicted versus actual values was also examined to visually analyze the relationship between the measured mechanical durability values and those predicted

by the model. The predicted versus actual plot is displayed in Figure 5-32b for the mechanical durability model, which shows the desired data scatter about the 45 degree line is present. This further exemplifies the statistical significance of the mechanical durability model and indicates that it is well suited for prediction of briquette quality.

#### 5.4.2.3 Model Graphs

Following the development and statistical analysis of each mathematical model, several contour graphs were constructed to visually interpret and evaluate the results. To provide a clear interpretation of the influence of each mixture variable on each briquette property, the contour graphs are assembled by common model terms. The influence of binder content on the modeled responses for particle density, crushing strength and mechanical durability are presented in Figure 5-33. From this figure it is evident that the maximum particle density values (i.e. > 1.18 g/cm$^3$) occur at a starch content of 5.0 percent with 10 percent biomass and a cure time of 7 days. In contrast, the minimum particle density (i.e. < 1.11 g/cm$^3$) values occur with no starch, 30 percent biomass and no cure time. Figure 5-33 also clearly indicates that briquette crushing strength reaches a maximum value (i.e. > 2,400 N [540 lb$_f$]) at a starch content of 5.0 percent with 30 percent biomass and a cure time of 4 to 5 days, and reaches a minimum value (i.e. < 600 N [135 lb$_f$]) with no starch, 10 percent biomass and a cure time of 0 days. Finally, this figure shows that the mechanical durability of briquettes reaches a maximum value (i.e. 100%) at a starch content of 5.0 percent with 10 percent biomass and a cure time of 7 days, and reaches a minimum value with no starch, 10 percent biomass and no cure time. The figure also indicates that a mechanical durability value in excess of 96 percent is achievable at a starch content of 2.5 percent with 30 percent biomass and a cure time of 7 days.

The modeled responses for particle density, crushing strength and mechanical durability with respect to cure time and biomass content are presented in Figure 5-34 and Figure 5-35, respectively. These figures present the same data that is displayed in Figure 5-33, but offer a different perspective that may be desirable in certain circumstances. Regardless of the chart examined, a clear optimum set of mixture variables, with respect to both crushing strength and mechanical durability, is not evident for this briquette formulation. As a result, numerical optimization of the mixture variables is necessary to determine the ideal value for each variable and to predict the strength and durability of such optimum briquette formulations.

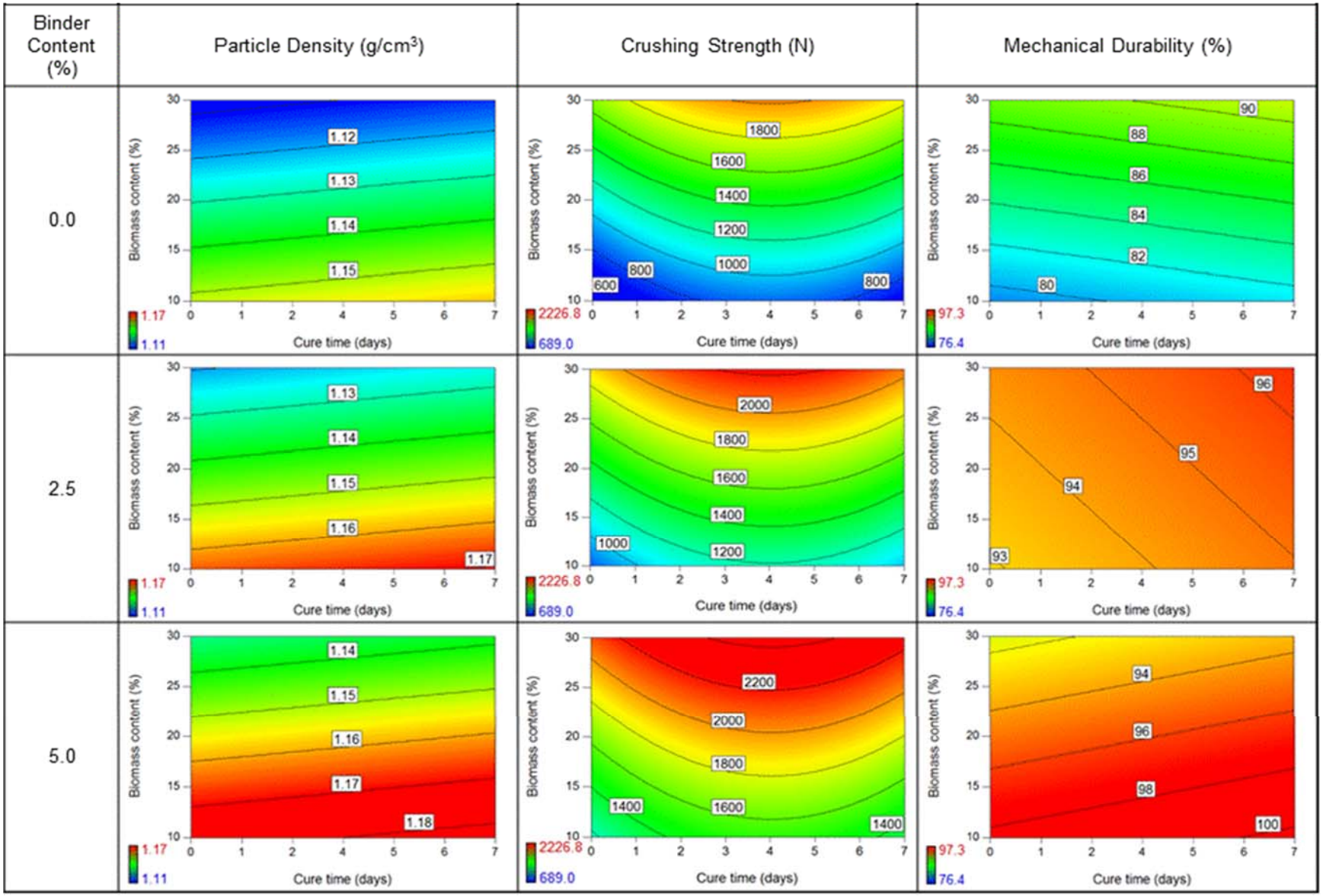



Figure 5-33. Influence of binder content on modeled responses for particle density, crushing strength and mechanical durability for briquettes composed of Emerald (bituminous) coal, corn stover and pregelatinized wheat starch

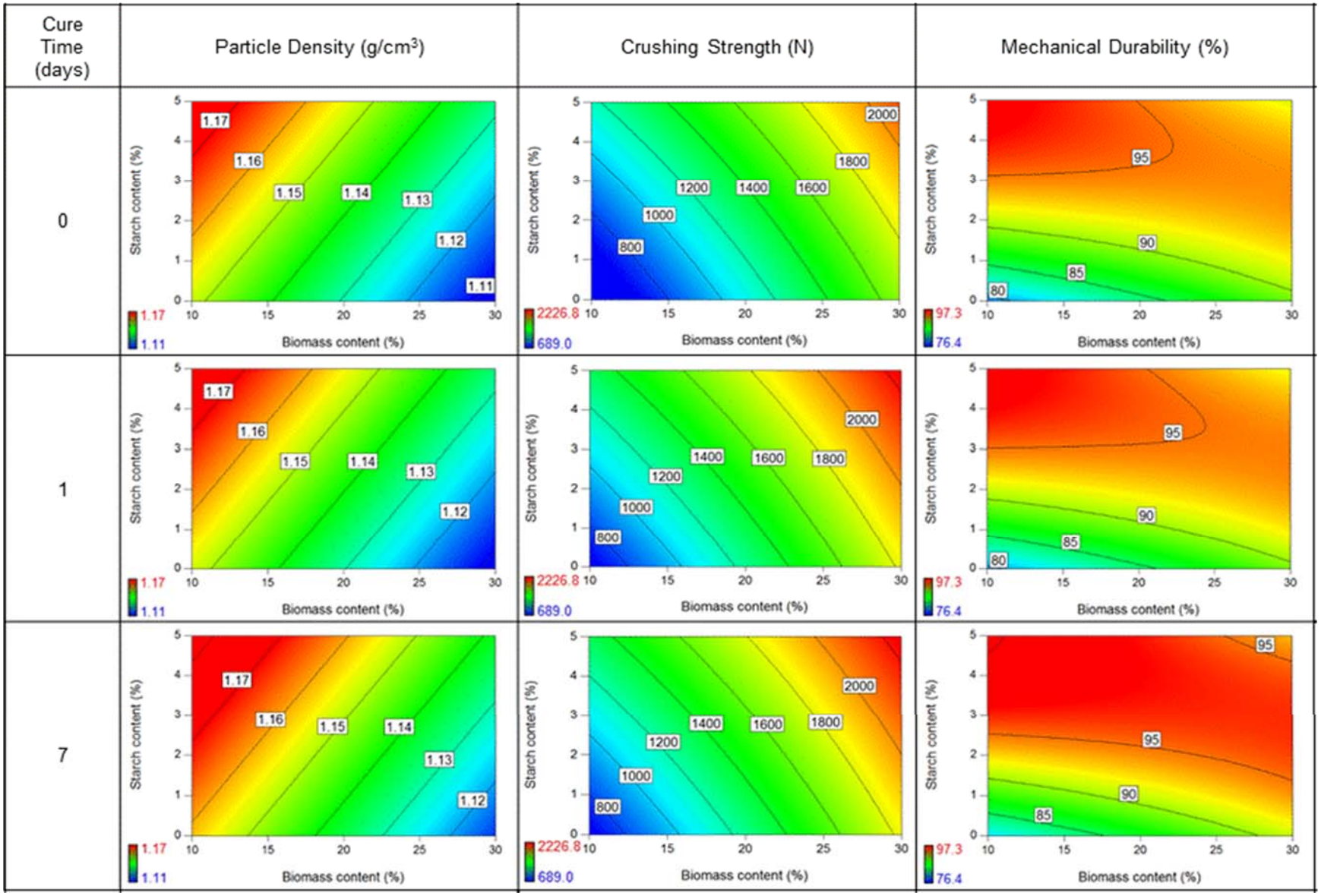



Figure 5-34. Influence of cure time on modeled responses for particle density, crushing strength and mechanical durability for briquettes composed of Emerald (bituminous) coal, corn stover and pregelatinized wheat starch

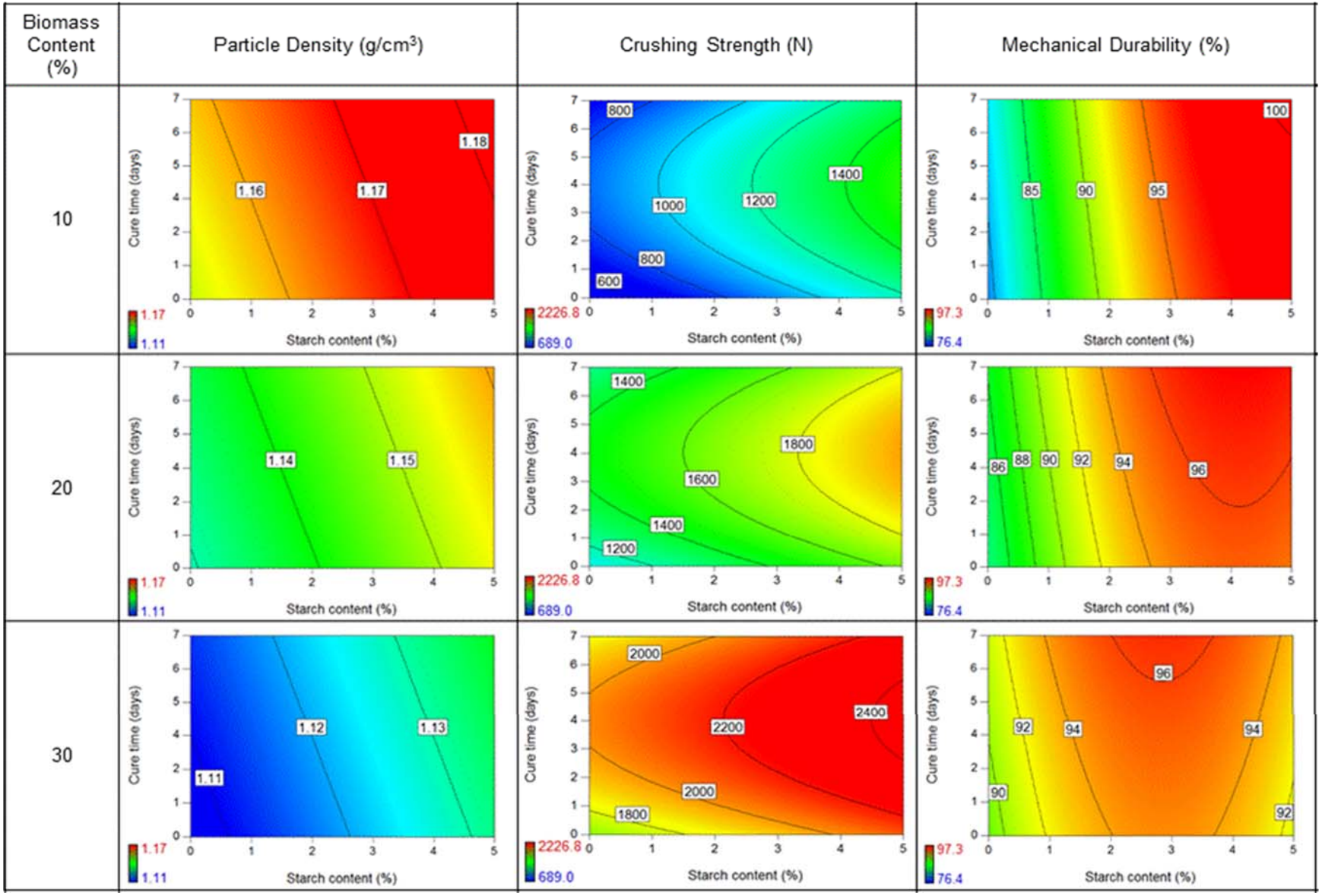



Figure 5-35. Influence of biomass content on modeled responses for particle density, crushing strength and mechanical durability for briquettes composed of Emerald (bituminous) coal, corn stover and pregelatinized wheat starch

#### 5.4.2.4 Numerical Optimization

Numerical optimization of the mixture variables was conducted in Design-Expert® 8 using the tool included in the analysis package. This tool allows for specification of optimization criteria (i.e. goals), which can include maximizing or minimizing predicted responses and process variables, as well as setting target values for each parameter. The tool also allows for adjustment of the importance of each goal on a scale from one to five (1 being the least important, 5 being the most important). The results of the optimization routine include a specified value for each of the process variables, as well as the predicted values for each response. A desirability value is calculated for each solution to the optimization routine to provide a method to rank the solutions and to indicate the extent to which the combination of responses approaches a perfect solution.

Optimization of the mathematical models developed for briquettes comprised of Emerald coal, corn stover and pregelatinized wheat starch was accomplished by specifying a maximization goal for both crushing strength and mechanical durability. The importance of the mechanical durability goal was set to five and the importance of the crushing strength goal was set to three. This configuration was selected after experimenting with the effect of the importance setting on the desirability of the solutions to the optimization routine. The routine generated 16 optimized solutions, all of which specified a biomass content of 30 percent, a starch content in the range of 2.73 to 3.48 percent and a cure time of 3.9 to 6.1 days. As shown in Table 5-19, the top ten most desirable solutions were predicted to produce briquettes with a crushing strength greater than 2,225 newtons (500 $lb_f$) and a mechanical durability in excess of 95 percent.

Table 5-19. Numerical optimization results for EM-CS-PGWS mathematical models

| Number | Biomass Content (%) | Starch Content (%) | Cure Time (days) | Crushing Strength (N) | Mechanical Durability (%) | Desirability |
|---|---|---|---|---|---|---|
| 1 | 30 | 3.13 | 5.7 | 2226.8 | 96.0 | 0.891 |
| 2 | 30 | 3.11 | 5.6 | 2226.8 | 96.0 | 0.891 |
| 3 | 30 | 3.15 | 5.7 | 2226.8 | 96.0 | 0.891 |
| 4 | 30 | 3.18 | 5.7 | 2226.8 | 96.0 | 0.891 |
| 5 | 30 | 3.05 | 5.6 | 2226.8 | 96.0 | 0.891 |
| 6 | 30 | 3.16 | 5.5 | 2226.8 | 96.0 | 0.890 |
| 7 | 30 | 3.19 | 5.9 | 2213.9 | 96.1 | 0.890 |
| 8 | 30 | 3.48 | 6.1 | 2226.3 | 95.9 | 0.889 |
| 9 | 30 | 3.22 | 5.2 | 2226.8 | 95.9 | 0.887 |
| 10 | 30 | 2.73 | 3.9 | 2250.4 | 95.6 | 0.878 |

## 5.4.3 Evaluation of Mixture Variables – Sub-Bituminous Coal

### 5.4.3.1 Summary of Results

The results of the mixture variables evaluations for briquettes composed of Eagle Butte sub-bituminous coal, corn stover and pregelatinized wheat starch are summarized in Table 5-20. Each test that was conducted is identified by the standard test number assigned in Design-Expert® 8 according to the target feed water content, biomass content and starch content (i.e. 01 = target feed water content of 0.10, biomass content of 10% and starch content of 2.5%). In the following sections, correlations between each mixture variable and the measured briquette properties are presented and discussed. Analysis of the results is also covered, including mathematical models developed for each response using the Design-Expert® 8 statistical analysis tools. In addition, contour graphs of the models are presented to visually interpret and evaluate the results. Finally, numerical optimization of the model was conducted to determine the combination of mixture variables that produces the highest quality briquettes.

Table 5-20. Summary of characterization results for briquettes composed of Eagle Butte (sub-bituminous) coal, corn stover and pregelatinized wheat starch

| Test ID | Feed Water Content | Biomass Content (%) | Starch Content (%) | Briquette Water Content | Particle Density ($g/cm^3$) | Crushing Strength (N) | Mechanical Durability (%) |
|---|---|---|---|---|---|---|---|
| EB-CS-PGWS-01 | 0.110 | 10 | 2.5 | 0.100 | 1.06 | 832.7 | 80.2 |
| EB-CS-PGWS-02 | 0.212 | 10 | 2.5 | 0.157 | 1.01 | 1096.5 | 95.5 |
| EB-CS-PGWS-03 | 0.093 | 30 | 2.5 | 0.096 | 1.00 | 1167.7 | 82.7 |
| EB-CS-PGWS-04 | 0.242 | 30 | 2.5 | 0.146 | 0.98 | 1515.1 | 96.8 |
| EB-CS-PGWS-05 | 0.101 | 20 | 0.0 | 0.095 | 1.02 | 882.5 | 68.2 |
| EB-CS-PGWS-06 | 0.214 | 20 | 0.0 | 0.147 | 0.98 | 909.2 | 84.9 |
| EB-CS-PGWS-07 | 0.103 | 20 | 5.0 | 0.094 | 1.02 | 1080.5 | 85.1 |
| EB-CS-PGWS-08 | 0.249 | 20 | 5.0 | 0.160 | 1.00 | 1564.9 | 98.1 |
| EB-CS-PGWS-09 | 0.151 | 10 | 0.0 | 0.124 | 1.05 | 1060.9 | 83.0 |
| EB-CS-PGWS-10 | 0.153 | 30 | 0.0 | 0.122 | 0.99 | 1350.5 | 87.4 |
| EB-CS-PGWS-11 | 0.156 | 10 | 5.0 | 0.126 | 1.07 | 1819.8 | 98.1 |
| EB-CS-PGWS-12 | 0.163 | 30 | 5.0 | 0.128 | 1.01 | 2010.6 | 97.6 |
| EB-CS-PGWS-13 | 0.170 | 20 | 2.5 | 0.122 | 1.04 | 1369.6 | 92.2 |
| EB-CS-PGWS-14 | 0.155 | 20 | 2.5 | 0.129 | 1.03 | 1558.7 | 93.2 |
| EB-CS-PGWS-15 | 0.162 | 20 | 2.5 | 0.122 | 1.03 | 1343.4 | 91.2 |

#### *5.4.3.1.1 Feed Water Content Correlations*

The correlation between feed water content and each measured briquette property were evaluated by linear regression analysis. To investigate these correlations, water content was plotted versus each measured briquette property with the data points grouped by biomass content (i.e. 10, 20 and 30%). This approach was used because little or no correlation existed for the entire data set due to the influence of the other two mixture variables (i.e. biomass content and binder content). The water content correlations were initially investigated with the data grouped separately by biomass content and binder content. From these investigations, it was found that feed water content correlations were greatest with the data grouped by biomass content. Nonetheless, the correlations were not very strong due to the significant influence of both biomass content and binder content.

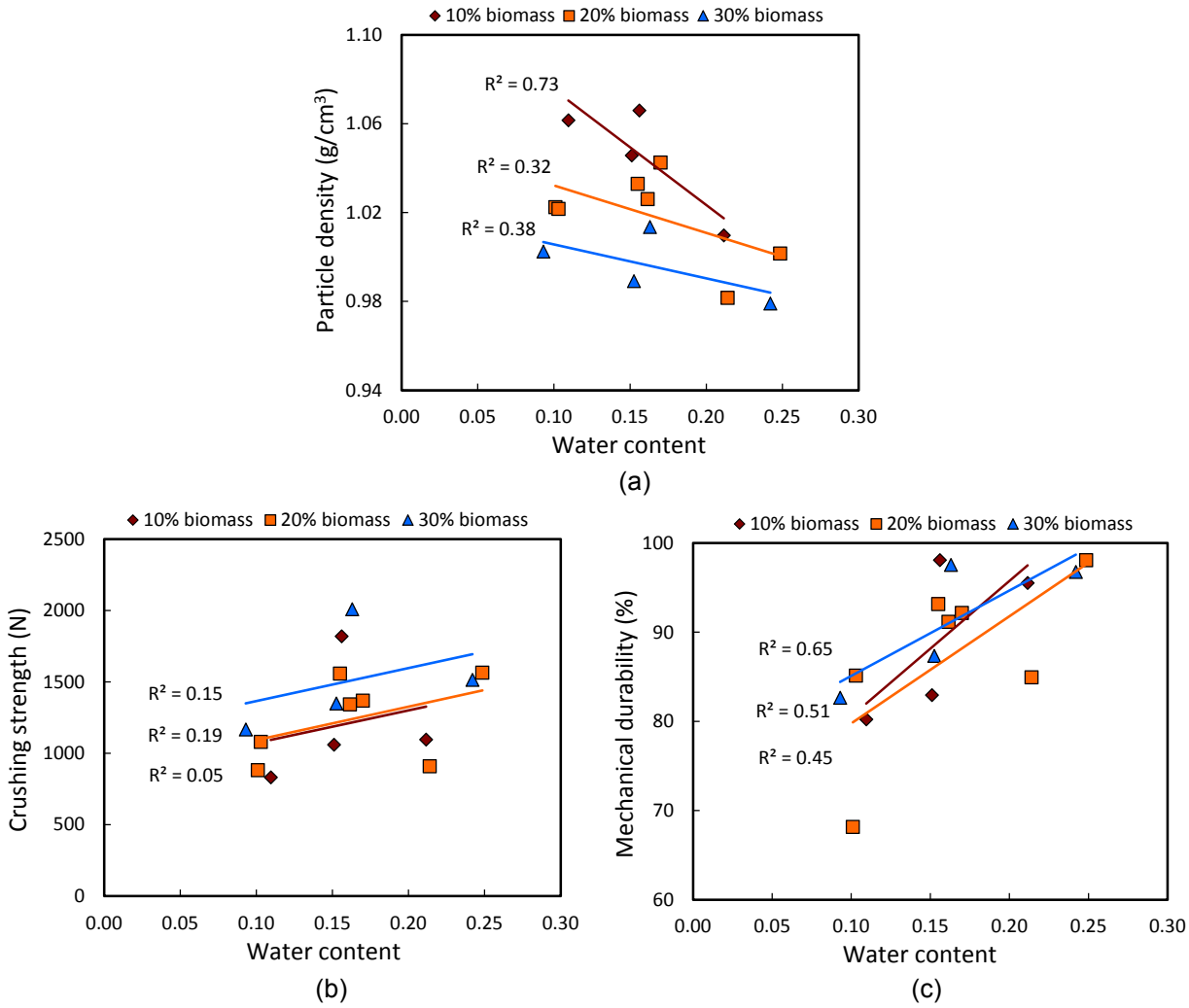



Figure 5-36. Effect of feed water content on (a) particle density, (b) crushing strength and (c) mechanical durability for briquettes composed of Eagle Butte (sub-bituminous) coal, corn stover and pregelatinized wheat starch

Figure 5-36a displays the correlation between feed water content and the particle density of the briquettes. It is clear from this chart that water content generally exhibits a negative correlation with particle density. From the minimum to the maximum water content, the particle density of the briquettes dropped for all three biomass contents. However, the particle density reached a maximum value in the water content range of 0.15 to 0.17, and then dropped off when the water content approached or exceeded 0.20. The strength of these linear correlations was measured by determining the coefficient of determination for each data set grouped by biomass content. The strongest linear correlation was found for the briquettes produced with 10 percent biomass (i.e. $R^2 = 0.73$). The strength of the correlation was much lower for the briquettes with

higher biomass content. Specifically, the coefficient of determination for briquettes produced with 20 and 30 percent biomass was 0.32 and 0.38, respectively.

Figure 5-36b illustrates the correlation between feed water content and the crushing strength of the briquettes. No obvious correlations exist in this data set due to the significant interaction between binder content and crushing strength, which is concealed in this analysis. However, it is fairly clear from this chart that maximum crushing strength values are achieved at approximately the same water content (i.e. 0.15-0.16) for all biomass content data sets. This suggests that this range of feed water contents is ideal for briquettes produced with sub-bituminous coal and biomass. The strength of the linear correlations was measured by determining the coefficient of determination for each data set grouped by biomass content. The strongest linear correlation was found for the briquettes produced with 20 percent biomass (i.e. $R^2 = 0.19$). In contrast, the coefficient of determination for briquettes produced with 10 and 30 percent biomass was 0.05 and 0.15, respectively.

Figure 5-36c shows the correlation between feed water content and the mechanical durability of briquettes. It is clear from this chart that a general positive correlation exists between water content and mechanical durability. The maximum mechanical durability values occurred between water contents of 0.15 and 0.16 for biomass contents of 10 and 30 percent. In contrast, the maximum mechanical durability for briquettes composed of 20 percent biomass occurred at a water content of 0.25. The most likely cause of this discrepancy is the difference in binder content for each data point, which is concealed in this analysis. The strongest correlation was found for briquettes produced with 30 percent biomass (i.e. $R^2 = 0.65$), which was followed closely by briquettes produced with 20 percent (i.e. $R^2 = 0.51$) and 10 percent (i.e. $R^2 = 0.45$) biomass.

*5.4.3.1.2 Biomass Content Correlations*

The correlation between biomass content and each measured briquette property were also evaluated by linear regression analysis. To investigate these correlations, biomass content was plotted versus each measured briquette property with the data points grouped by water content (i.e. 0.10, 0.15 and 0.20). This approach was used because little or no correlation existed for the entire data set due to the influence of the other two mixture variables (i.e. water content and binder content). The biomass content correlations were initially investigated with the data grouped separately by water content and binder content. From these investigations, it was found

that feed water content correlations were greatest with the data grouped by water content. Nonetheless, the correlations were not very prominent due to the significant influence of both water content and binder content.

Figure 5-37a displays the correlation between biomass content and the particle density of the briquettes. It is clear from this chart that biomass content exhibits a negative correlation with particle density. For each of the three water contents, an increase in biomass content caused a direct reduction in the particle density of the briquettes. This finding was expected since the addition of additional biomass with a true density much lower than coal will reduce the composite density of the mixture prior to briquette production. The strength of these linear correlations was measured by determining the coefficient of determination for each data set grouped by water content. The strongest linear correlation was found for the briquettes with a feed water content of 0.10 (i.e. $R^2 = 0.95$). The strength of this correlation successively declined with an increase in water content. Specifically, the coefficient of determination for briquettes produced with a water content of 0.15 and 0.20 was 0.81 and 0.69, respectively. These findings further prove that an increase in biomass content directly reduces the particle density of coal-biomass briquettes.

Figure 5-37b illustrates the correlation between biomass content and the crushing strength of the briquettes. It is clear from this chart that biomass content generally exhibits a positive correlation with crushing strength. However, there were some discrepancies in the data, particularly at a water content of 0.15, where an increase in biomass content appears to initially reduce and then increase the crushing strength of the briquettes. This was likely due to the significant interaction between binder content and crushing strength, which is concealed in this analysis. The strongest linear correlation was found for briquettes produced with a water content of 0.10 (i.e. $R^2 = 0.74$). In contrast, the coefficient of determination for briquettes produced with water contents of 0.15 and 0.20 was 0.09 and 0.28, respectively.

Figure 5-37c shows the correlation between biomass content and the mechanical durability of briquettes. No obvious correlations exist in this data set due to the significant interaction between binder content and mechanical durability, which is concealed in this analysis. This lack of correlation is supported by average coefficient of determination values of 0.02, 0.02 and 0.01 for water contents of 0.10, 0.15 and 0.20, respectively.

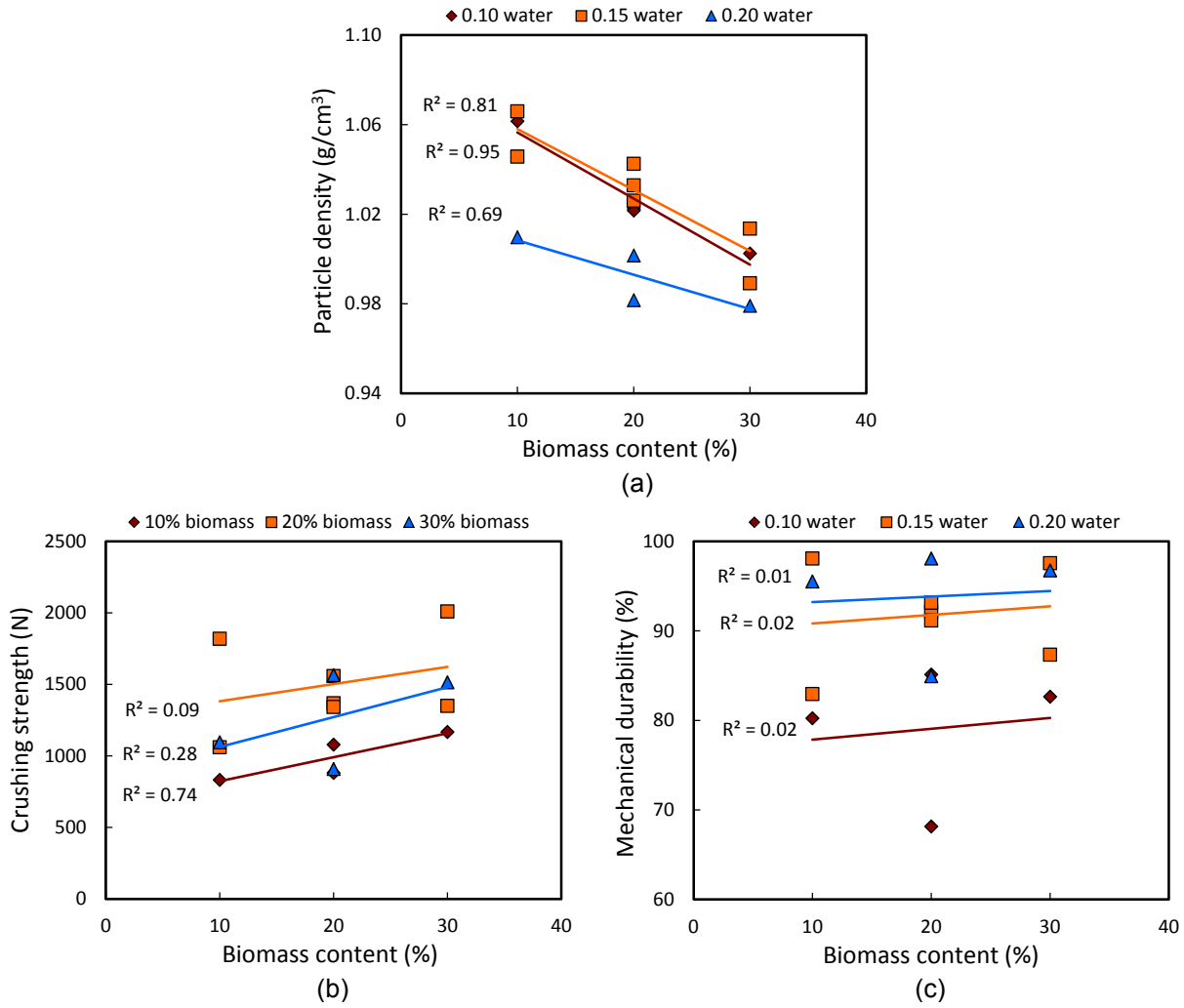



Figure 5-37. Effect of biomass content on (a) particle density, (b) crushing strength and (c) mechanical durability for briquettes composed of Eagle Butte (sub-bituminous) coal, corn stover and pregelatinized wheat starch

### *5.4.3.1.3 Binder Content Correlations*

The correlation between binder content and each measured briquette property were evaluated by linear regression analysis. To investigate these correlations, binder content was plotted versus each measured briquette property with the data points grouped by feed water content (i.e. 0.10, 0.15 and 0.20). This approach was used because little or no correlation existed for the entire data set due to the influence of the other two mixture variables (i.e. water content and biomass content). The binder content correlations were initially investigated with the data grouped separately by water content and biomass content. From these investigations, it was found that binder content correlations were greatest with the data grouped by water content.

Figure 5-38a displays the correlation between binder content and the particle density of the briquettes. No obvious correlations exist in this data set due to the significant interaction between biomass content and particle density, which is concealed in this analysis. This lack of correlation is supported by average coefficient of determination values of 0.14, 0.00 and 0.29 for water contents of 0.10, 0.15 and 0.20, respectively.

Figure 5-38b illustrates the correlation between binder content and the crushing strength of briquettes. It is clear from this chart that binder content generally exhibits a positive correlation with crushing strength. Specifically, an increase in starch content led to a direct rise in the crushing strength of the briquettes for each of the three biomass contents. This correlation was expected, considering the sole purpose of starch addition to briquette feedstocks is the improvement of briquette quality. However, there was some scatter in the data as a result of the significant interaction between biomass content and crushing strength, which is concealed in this analysis. The strength of these linear correlations was measured by determining the coefficient of determination for each data set grouped by biomass content. The strongest linear correlation was found for the briquettes produced at a water content of 0.15 (i.e. $R^2 = 0.81$), followed closely by briquettes produced at a water content of 0.20 (i.e. $R^2 = 0.70$). In contrast, the coefficient of determination for briquettes produced with a water content of 0.10 was 0.26.

Figure 5-38c shows the correlation between binder content and the mechanical durability of briquettes. It is clear from this chart that binder content exhibits a strong positive correlation with mechanical durability. Specifically, an increase in starch content led to a sharp increase in the mechanical durability of the briquettes, regardless of the water content. The strength of these linear correlations was measured by determining the coefficient of determination for each data set grouped by biomass content. The strongest linear correlation was found for the briquettes produced with a water content of 0.15 (i.e. $R^2 = 0.93$), which was followed closely by briquettes produced with water contents of 0.10 (i.e. $R^2 = 0.85$) and 0.20 (i.e. $R^2 = 0.79$).

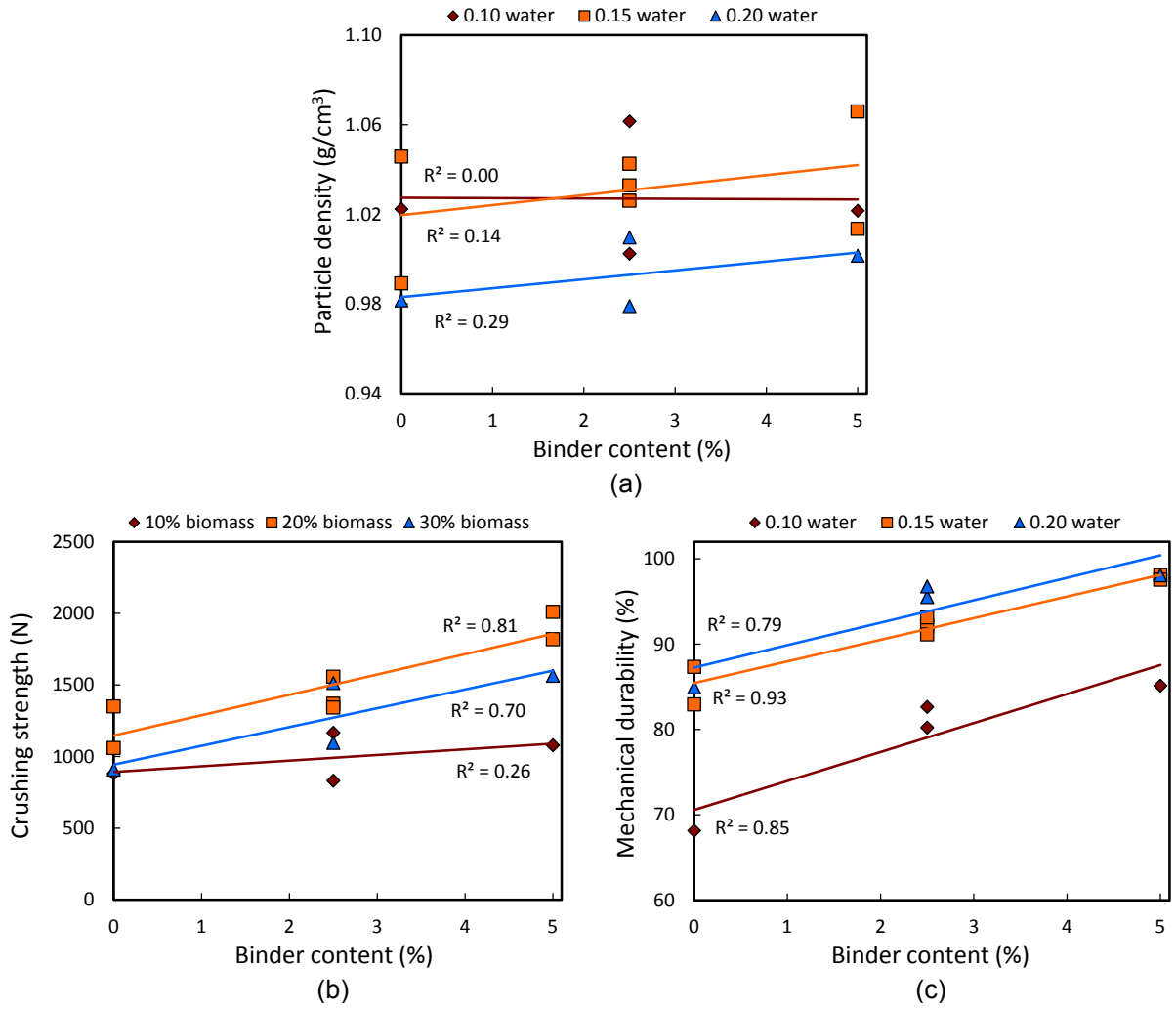



Figure 5-38. Effect of binder content on (a) particle density, (b) crushing strength and (c) mechanical durability for briquettes composed of Eagle Butte (sub-bituminous) coal, corn stover and pregelatinized wheat starch

### 5.4.3.2 Statistical Analyses

The results of the mixture variables evaluations were examined using the statistical analysis tools included in Design-Expert® 8 to determine the influence of each variable and to optimize the quality of briquettes. Mathematical models were developed that relate the mixture variables (i.e. water content, biomass content and binder content) to the measured briquette properties (i.e. particle density, crushing strength, and mechanical durability). The first step of model development was selection of the process order (e.g. linear, quadratic) of the mathematical model. This was accomplished by determining the process order with the lowest lack of fit p-value and the highest adjusted R-squared and predicted R-squared values. The selected model was then analyzed using the analysis of variance (ANOVA) function to determine the statistical

significance of the entire model and of each individual term. All insignificant terms were then removed from the model, except those required to maintain hierarchy. Next, the fit of the model to the data was evaluated using various diagnostics tools. The following sections present the empirical mathematical models developed for briquettes composed of Eagle Butte coal, corn stover and pregelatinized wheat starch, and summarize the results of the statistical analyses.

*5.4.3.2.1 Particle Density Model*

A linear mathematical model was constructed that relates feed water content, biomass content and binder content to the particle density of briquettes composed of Eagle Butte coal, corn stover and pregelatinized wheat starch. According to the model, the predicted particle density of briquettes is calculated by:

$$\rho = 1.10 - 0.25w - 0.0026c + 0.0036b \quad \text{(Eq. 5-15)}$$

where $\rho$ is the particle density (g/cm$^3$), $w$ is the feed water content, $c$ is the biomass content (%) and $b$ is the binder content (%). The statistical significance of this model, in terms of its fit to the data from which it was derived, was analyzed using ANOVA to evaluate a number of variables. A summary of the ANOVA is provided in Table 5-21 for the particle density model. The p-value of the particle density model is 0.0013, which indicates that the predicted density values would be highly unlikely under the null hypothesis and verifies that the model is indeed statistically significant. The p-values of the model terms are 0.0147 (water content), 0.0007 (biomass content) and 0.1296 (binder content). This implies that water content and biomass content are statistically significant model terms, and thus have a major impact on accurate prediction of the particle density of briquettes. In contrast, binder content is not a significant model term, which implies that its impact on particle density quantified in the model is not statistically significant. This term was needed to maintain the hierarchy of the model, otherwise it would have been removed to improve the model.

Table 5-21. ANOVA results for EB-CS-PGWS particle density model

| Source | Sum of Squares | df | Mean Square | F Value | p-value Prob > F |
|---|---|---|---|---|---|
| Model | 8.01E-03 | 3 | 2.67E-03 | 10.92 | 0.0013 |
| A-Water content | 2.04E-03 | 1 | 2.04E-03 | 8.36 | 0.0147 |
| B-Biomass content | 5.22E-03 | 1 | 5.22E-03 | 21.38 | 0.0007 |
| C-Binder content | 6.56E-04 | 1 | 6.56E-04 | 2.68 | 0.1296 |
| Residual | 2.69E-03 | 11 | 2.44E-04 | -- | -- |
| Cor Total | 1.07E-02 | 14 | -- | -- | -- |

To confirm the ANOVA normality assumption for the particle density model, the residuals were visually examined in a normal probability plot of studentized results. Figure 5-39a shows the normal probability plot of studentized residuals for the crushing strength model. It is clear from this figure that the residuals follow an approximately straight line, and thus are normally distributed. A plot of predicted versus actual values was also examined to visually analyze the relationship between the measured particle density values and those predicted by the model. The predicted versus actual plot is displayed in Figure 5-39b for the particle density model, which shows the desired data scatter about the 45 degree line is present. This further exemplifies the statistical significance of the particle density model and indicates that it is well suited for prediction of briquette quality.

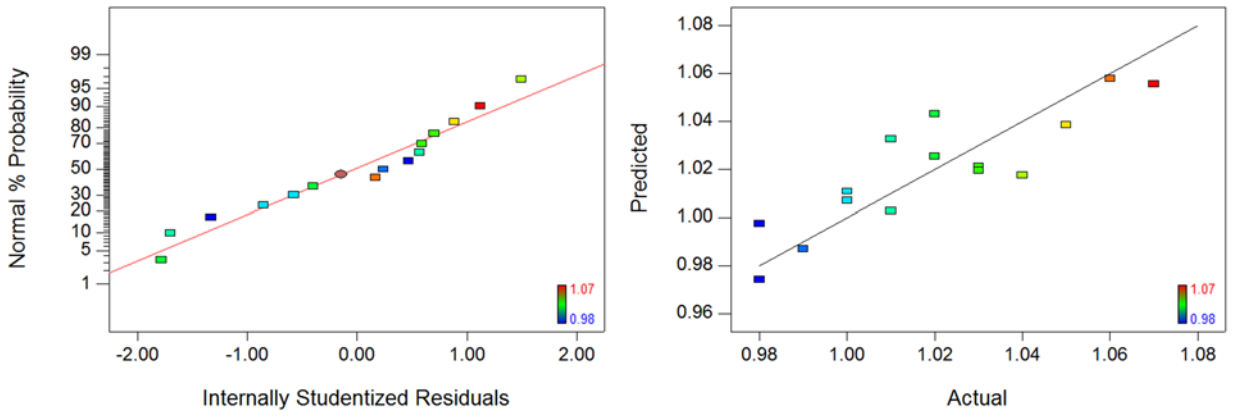



Figure 5-39. Diagnostic graphs for visual inspection of ANOVA results for EB-CS-PGWS particle density model: (a) normal probability plot of studentized results and (b) predicted versus actual values plot

### *5.4.3.2.2 Crushing Strength Model*

A quadratic mathematical model was constructed that relates feed water content, biomass content and binder content to the crushing strength of briquettes composed of Eagle Butte coal,

corn stover and pregelatinized wheat starch. According to the model, the predicted crushing strength of briquettes is calculated by:

$$\sigma = -1482.60 + 27920.42w + 20.90c - 64.57b + 1182.36wb - 87045.49w^2 \quad \text{(Eq. 5-16)}$$

where $\sigma$ is the crushing strength (N), $w$ is the feed water content, $c$ is the biomass content (%) and $b$ is the binder content (%). The statistical significance of this model, in terms of its fit to the data from which it was derived, was analyzed using ANOVA to evaluate a number of variables. A summary of the ANOVA is provided in Table 5-22 for the crushing strength model. The p-value of the model is 0.0005, which indicates that the predicted crushing strength values would be highly unlikely under the null hypothesis and verifies that the model is indeed statistically significant. The p-values of the model terms are 0.0011 (water content), 0.0031 (biomass content), 0.0005 (binder content), 0.0320 (water content x binder content) and 0.0007 (water content$^2$). This implies that all of the model terms are statistically significant, and thus have a major impact on accurate prediction of the crushing strength of briquettes.

Table 5-22. ANOVA results for EB-CS-PGWS crushing strength model

| Source | Sum of Squares | df | Mean Square | F Value | p-value Prob > F |
|---|---|---|---|---|---|
| Model | 1.49E+06 | 5 | 2.98E+05 | 14.37 | 0.0005 |
| A-Water content | 4.65E+05 | 1 | 4.65E+05 | 22.39 | 0.0011 |
| B-Biomass content | 3.31E+05 | 1 | 3.31E+05 | 15.94 | 0.0031 |
| C-Binder content | 5.96E+05 | 1 | 5.96E+05 | 28.71 | 0.0005 |
| AC | 1.33E+05 | 1 | 1.33E+05 | 6.42 | 0.0320 |
| $A^2$ | 5.20E+05 | 1 | 5.20E+05 | 25.07 | 0.0007 |
| Residual | 1.87E+05 | 9 | 20745 | -- | -- |
| Cor Total | 1.68E+06 | 14 | -- | -- | -- |

To confirm the ANOVA normality assumption for the crushing strength model, the residuals were visually examined in a normal probability plot of studentized results. Figure 5-40a shows the normal probability plot of studentized residuals for the crushing strength model. It is clear from this figure that the residuals follow an approximately straight line, and thus are normally distributed. A plot of predicted versus actual values was also examined to visually analyze the relationship between the measured crushing strength values and those predicted by the model. The predicted versus actual plot is displayed in Figure 5-40b for the crushing strength model, which shows the desired data scatter about the 45 degree line is present. This further

exemplifies the statistical significance of the crushing strength model and indicates that it is well suited for prediction of briquette quality.

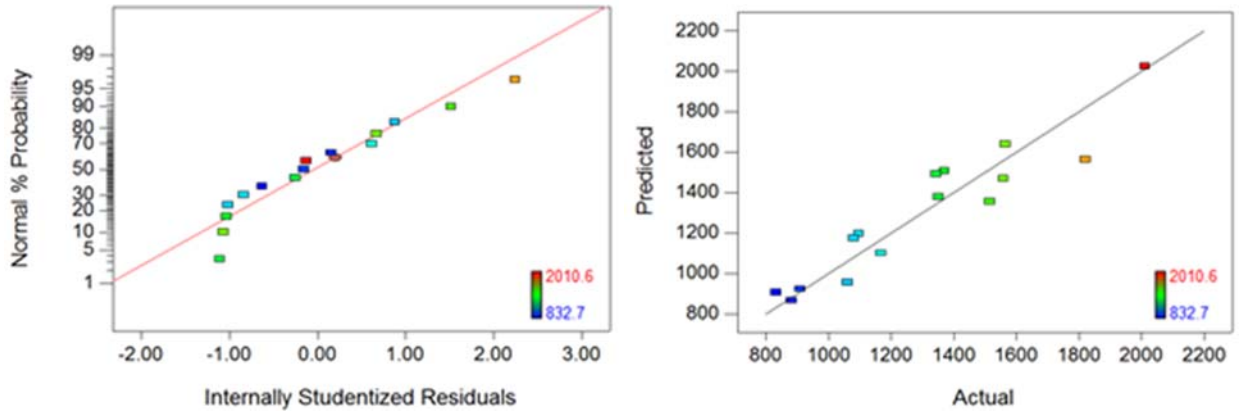



Figure 5-40. Diagnostic graphs for visual inspection of ANOVA results for EB-CS-PGWS crushing strength model: (a) normal probability plot of studentized results and (b) predicted versus actual values plot

#### *5.4.3.2.3 Mechanical Durability Model*

A quadratic mathematical model was constructed that relates feed water content, biomass content and binder content to the mechanical durability of briquettes composed of Eagle Butte coal, corn stover and pregelatinized wheat starch. According to the model, the predicted mechanical durability of briquettes is calculated by:

$$MD = 35.34 + 561.56w - 0.89c + 2.74b - 1344.23w^2 + 0.03c^2 \quad \text{(Eq. 5-17)}$$

where *MD* is the mechanical durability (%), $w$ is the feed water content, $c$ is the biomass content (%) and $b$ is the binder content (%). The statistical significance of this model, in terms of its fit to the data from which it was derived, was analyzed using ANOVA to evaluate a number of variables. A summary of the ANOVA is provided in Table 5-23 for the mechanical durability model. The p-value of the model is less than 0.0001, which indicates that the predicted mechanical durability values would be highly unlikely under the null hypothesis and verifies that the model is indeed statistically significant. The p-values of the model terms are less than 0.0001 (water content) 0.1061 (biomass content), less than 0.0001 (starch content), 0.0010 (water content$^2$) and 0.0702 (biomass content$^2$). This implies that all of the model terms are statistically significant (except biomass content), and thus have a major impact on accurate prediction of the mechanical durability of briquettes. In contrast, biomass content is not a significant model term,

which implies that the impact of this variable on mechanical durability quantified in the model is not statistically significant.

Table 5-23. ANOVA results for EB-CS-PGWS mechanical durability model

| Source | Sum of Squares | df | Mean Square | F Value | p-value Prob > F |
|---|---|---|---|---|---|
| Model | 941 | 5 | 188 | 31.04 | < 0.0001 |
| A-Water content | 515 | 1 | 515 | 84.87 | < 0.0001 |
| B-Biomass content | 20 | 1 | 20 | 3.22 | 0.1061 |
| C-Binder content | 364 | 1 | 364 | 60.01 | < 0.0001 |
| $A^2$ | 137 | 1 | 137 | 22.57 | 0.0010 |
| $B^2$ | 26 | 1 | 26 | 4.22 | 0.0702 |
| Residual | 55 | 9 | 6 | -- | -- |
| Cor Total | 996 | 14 | -- | -- | -- |

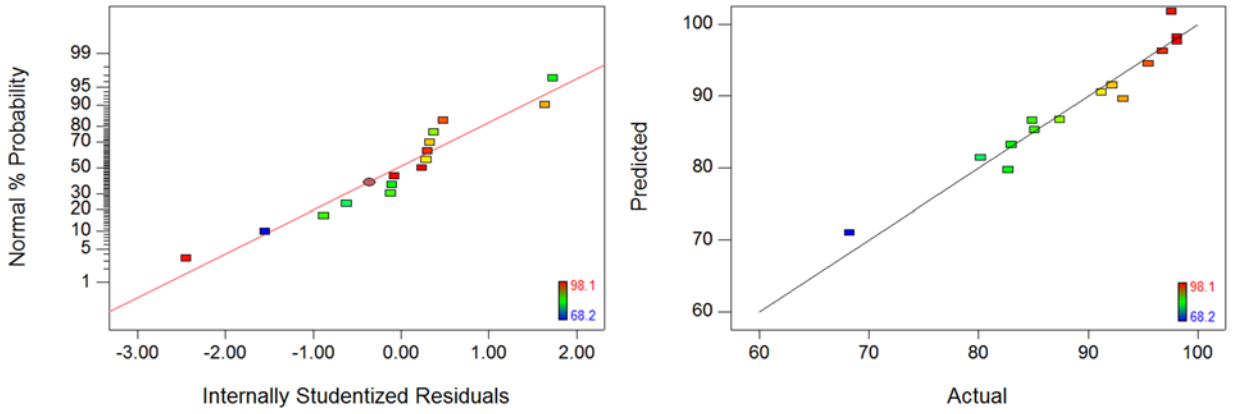



Figure 5-41. Diagnostic graphs for visual inspection of ANOVA results for EB-CS-PGWS mechanical durability model: (a) normal probability plot of studentized results and (b) predicted versus actual values plot

To confirm the ANOVA normality assumption for the mechanical durability model, the residuals were visually examined in a normal probability plot of studentized results. Figure 5-41a shows the normal probability plot of studentized residuals for the mechanical durability model. It is clear from this figure that the residuals follow an approximately straight line, and thus are normally distributed. A plot of predicted versus actual values was also examined to visually analyze the relationship between the measured mechanical durability values and those predicted by the model. The predicted versus actual plot is displayed in Figure 5-41b for the mechanical durability model, which shows the desired data scatter about the 45 degree line is present. This

further exemplifies the statistical significance of the mechanical durability model and indicates that it is well suited for prediction of briquette quality.

#### 5.4.3.3 Model Graphs

Following the development and statistical analysis of each mathematical model, several contour graphs were constructed to visually interpret and evaluate the results. To provide a clear interpretation of the influence of each mixture variable on each briquette property, the contour graphs are assembled by common model terms. The influence of water content on the modeled responses for particle density, crushing strength and mechanical durability are presented in Figure 5-42. From this figure it is evident that the maximum particle density values (i.e. > 1.06 $g/cm^3$) occur at a water content of 0.10 with 10 percent biomass and a starch content of 5 percent. In contrast, the minimum particle density (i.e. < 0.98 $g/cm^3$) values occur at a water content of 0.20 with 30 percent biomass and no starch.

Figure 5-42 also clearly indicates that briquette crushing strength reaches a maximum value (i.e. > 2,000 N [450 $lb_f$]) at a water content of 0.20 with 30 percent biomass and a starch content of 5 percent, and reaches a minimum value (i.e. < 700 N [160 $lb_f$]) at a water content of 0.10 with 10 percent biomass and no starch. Finally, this figure shows that the mechanical durability of briquettes reaches a maximum value (i.e. 100%) at a water content of 0.20 with both 10 and 30 percent biomass at a starch content of 5 percent, and reaches a minimum value at a water content of 0.10 with 10 to 20 percent biomass and no starch. The figure also indicates that very high crushing strength (i.e. > 1,800 N [400 $lb_f$]) and mechanical durability (i.e. > 95%) values are achievable at a water content of 0.15 with 30 percent biomass and a starch content of 5 percent.

The modeled responses for particle density, crushing strength and mechanical durability with respect to biomass content and binder content are presented in Figure 5-43 and Figure 5-44, respectively. These figures present the same data that is displayed in Figure 5-42, but offer a different perspective that may be desirable in certain circumstances. Regardless of the chart examined, a clear optimum set of mixture variables, with respect to both crushing strength and mechanical durability, appears to be achievable at a water content of 0.20 with 30 percent biomass and 5 percent starch. At these conditions, the models predict a crushing strength in

excess of 2,000 newtons (450 $lb_f$) and a mechanical durability near 100 percent. Numerical optimization of the mixture variables was conducted to verify this result.

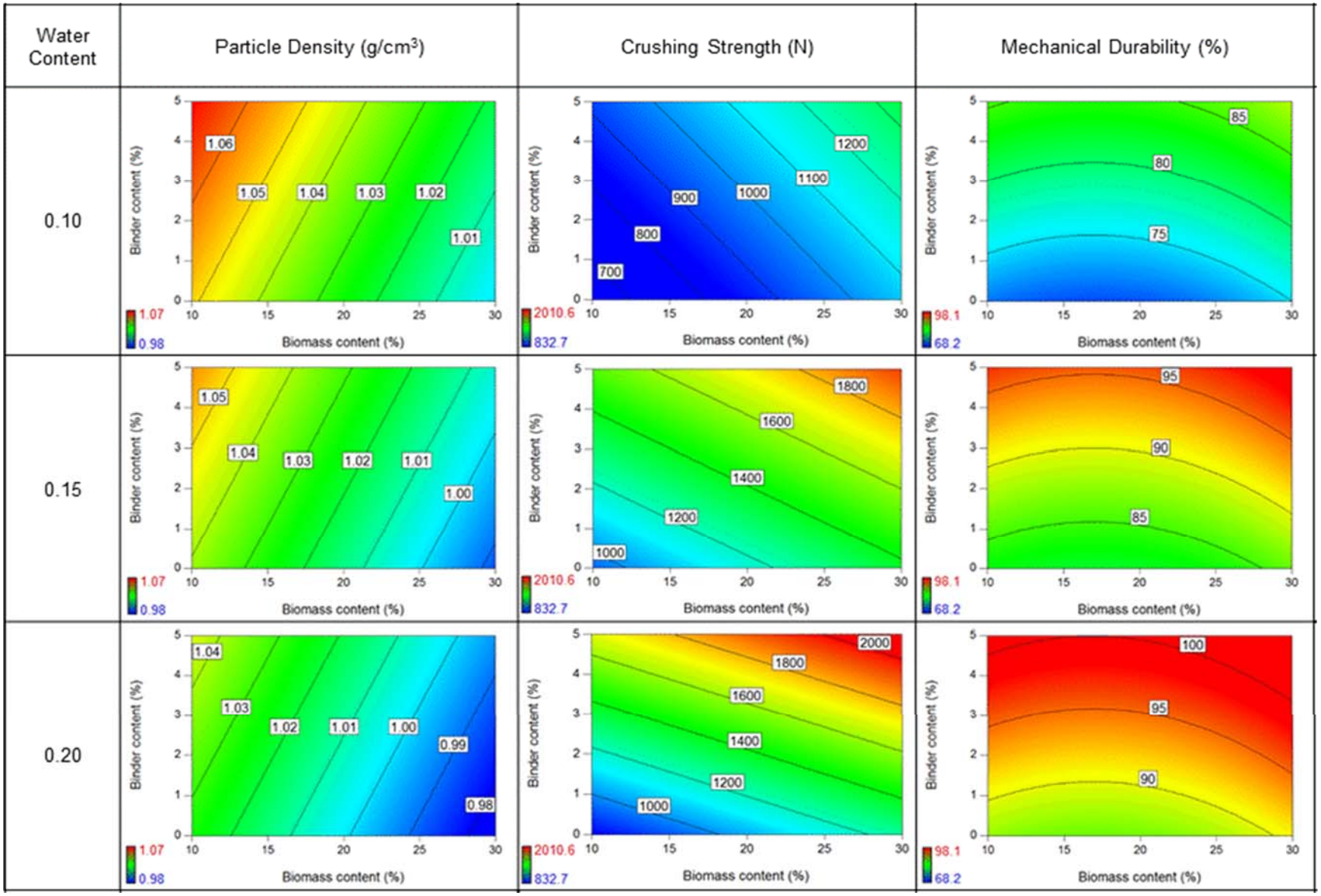



Figure 5-42. Influence of feed water content on modeled responses for particle density, crushing strength and mechanical durability for briquettes composed of Eagle Butte (sub-bituminous) coal, corn stover and pregelatinized wheat starch

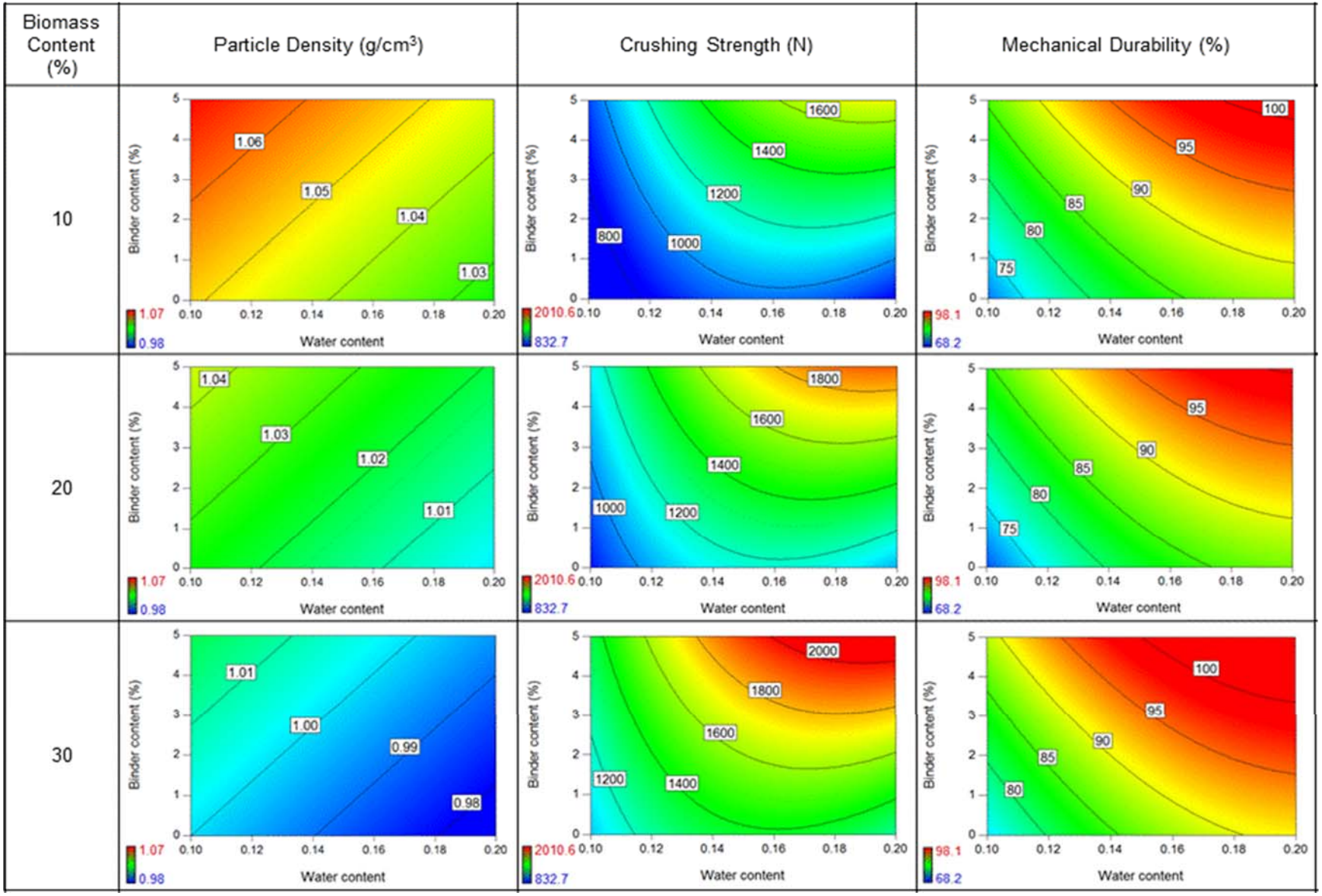



Figure 5-43. Influence of biomass content on modeled responses for particle density, crushing strength and mechanical durability for briquettes composed of Eagle Butte (sub-bituminous) coal, corn stover and pregelatinized wheat starch

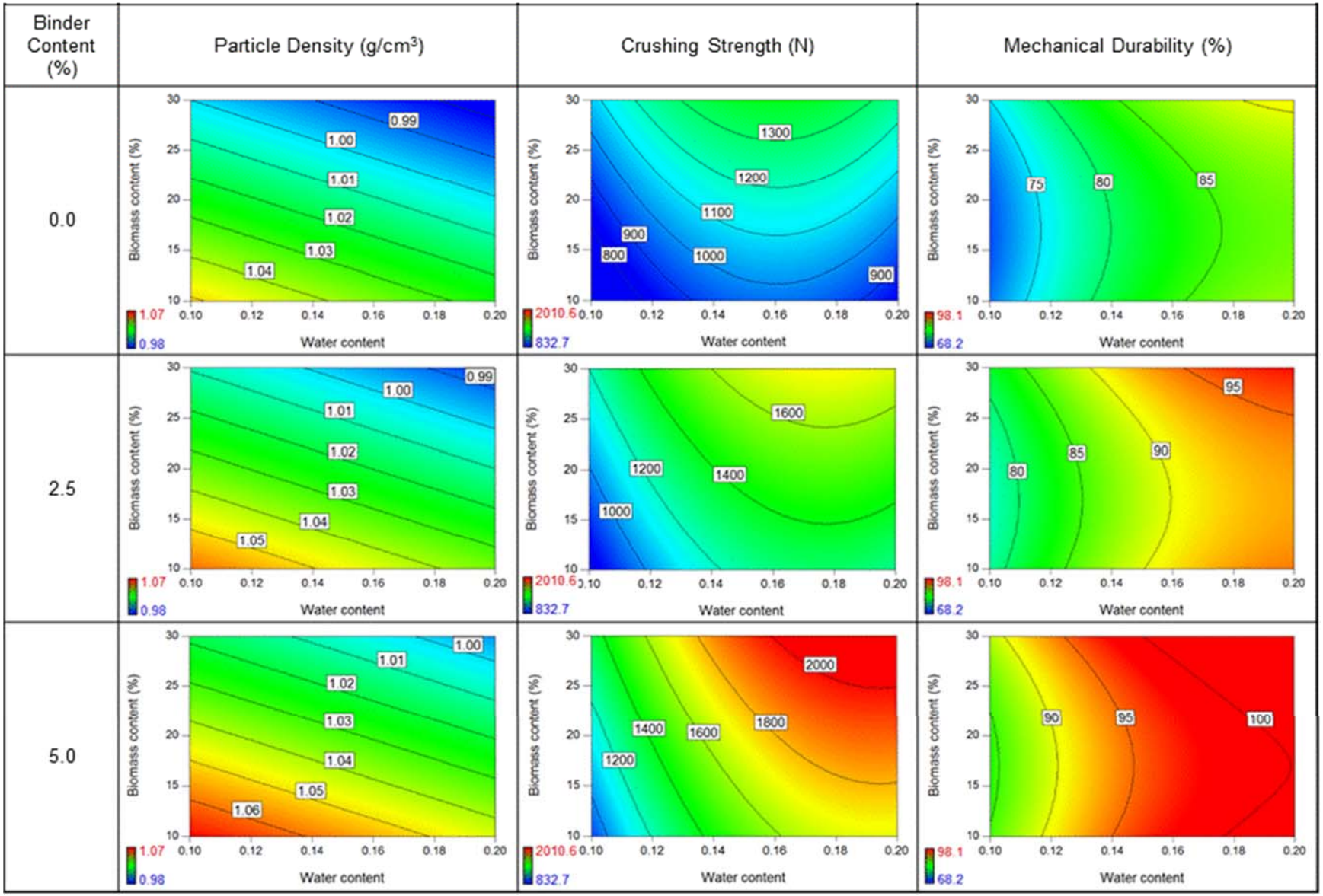



Figure 5-44. Influence of binder content on modeled responses for particle density, crushing strength and mechanical durability for briquettes composed of Eagle Butte (sub-bituminous) coal, corn stover and pregelatinized wheat starch

#### 5.4.3.4 Numerical Optimization

Numerical optimization of the mixture variables was conducted in Design-Expert® 8 using the tool included in the analysis package. This tool allows for specification of optimization criteria (i.e. goals), which can include maximizing or minimizing predicted responses and process variables, as well as setting target values for each parameter. The tool also allows for adjustment of the importance of each goal on a scale from one to five (1 being the least important, 5 being the most important). The results of the optimization routine include a specified value for each of the process variables, as well as the predicted values for each response. A desirability value is calculated for each solution to the optimization routine to rank and evaluate the solutions.

Optimization of the mathematical models developed for briquettes comprised of Eagle Butte coal, corn stover and pregelatinized wheat starch was accomplished by specifying a maximization goal for both crushing strength and mechanical durability. The importance of the mechanical durability goal was set to five and the importance of the crushing strength goal was set to three. The routine generated 31 optimized solutions, all of which specified a water content of approximately 0.20, a biomass content of 30 percent, and a starch content of approximately 5 percent. As shown in Table 5-24, the top ten most desirable solutions were predicted to produce briquettes with a crushing strength in excess of 2,100 newtons (472 $lb_f$) and a mechanical durability in excess of 100 percent. However, it is not possible to achieve mechanical durability values this high, but nonetheless high durability would be expected.

Table 5-24. Numerical optimization results for EB-CS-PGWS mathematical models

| Number | Water Content | Biomass Content (%) | Binder Content (%) | Crushing Strength (N) | Mechanical Durability (%) | Desirability |
|---|---|---|---|---|---|---|
| 1 | 0.194 | 30 | 5.00 | 2108.9 | 104.3 | 0.968 |
| 2 | 0.195 | 30 | 5.00 | 2108.9 | 104.4 | 0.968 |
| 3 | 0.196 | 30 | 5.00 | 2108.9 | 104.4 | 0.968 |
| 4 | 0.197 | 30 | 5.00 | 2108.5 | 104.4 | 0.968 |
| 5 | 0.198 | 30 | 5.00 | 2108.0 | 104.5 | 0.968 |
| 6 | 0.195 | 30 | 4.99 | 2106.7 | 104.3 | 0.968 |
| 7 | 0.193 | 30 | 4.98 | 2105.8 | 104.2 | 0.967 |
| 8 | 0.194 | 30 | 4.98 | 2105.3 | 104.3 | 0.967 |
| 9 | 0.195 | 30 | 4.97 | 2103.6 | 104.3 | 0.967 |
| 10 | 0.193 | 30 | 4.96 | 2103.1 | 104.2 | 0.966 |

#### 5.4.3.5 Comparison of Biomass Types

An additional series of tests were designed to evaluate the quality of briquettes produced with sub-bituminous coal and other types of biomass. The objective of these tests was to verify that the optimum combination of mixture variables identified for the Eagle Butte corn stover briquettes can also produce strong and durable briquettes with the other biomass types. To provide additional information on binderless briquetting mixtures of sub-bituminous coal and biomass, the decision was made to conduct the tests at optimum binderless conditions. The chosen optimum set of conditions was a target feed water content of 0.15, a biomass content of 30 percent and binder content of 0.0 percent, which corresponded to Standard Test 10 in the Design-Expert® 8 software. The results of these tests for each of the five types of biomass are summarized in Table 5-25.

Table 5-25. Summary of briquette characterization results for Eagle Butte biomass verification tests

| Test ID | Feed Water Content | Biomass Content (%) | Binder Content (%) | Briquette Water Content | Particle Density (g/cm$^3$) | Crushing Strength (N) | Mechanical Durability (%) |
|---|---|---|---|---|---|---|---|
| EB-MC-PGWS-10 | 0.133 | 30 | 0.0 | 0.129 | 0.96 | 1380.7 | 71.0 |
| EB-SG PGWS-10 | 0.130 | 30 | 0.0 | 0.132 | 0.94 | 1062.2 | 64.0 |
| EB-SD PGWS-10 | 0.130 | 30 | 0.0 | 0.130 | 0.95 | 866.1 | 70.7 |
| EB-CS PGWS-10 | 0.152 | 30 | 0.0 | 0.134 | 0.97 | 1615.6 | 80.2 |
| EB-WS PGWS-10 | 0.150 | 30 | 0.0 | 0.132 | 0.95 | 1152.5 | 70.5 |

To visualize the similarities and differences in the measured results, the particle density, crushing strength and mechanical durability values for each biomass type are plotted in Figure 5-45. The particle density results for each biomass types are presented in Figure 5-45a. This chart shows the average measured value and the calculated standard deviation of the measurements. From this chart, it is clear that the particle density of the sub-bituminous coal-biomass briquettes is very similar regardless of the type of biomass used. However, the mean particle density of briquettes composed of switchgrass was clearly the lowest (i.e. 0.94 g/cm$^3$). In contrast, the particle density of the briquettes composed of corn stover was the highest (i.e. 0.97 gcm$^3$).

Figure 5-45b illustrates the crushing strength results for each biomass type. This chart shows the average measured value and the calculated standard deviation of the measurements. The range of mean crushing strength values for the five biomass types was 866 to 1,616 newtons

(195-363 $lb_f$). The biomass type with the lowest crushing strength was the sawdust, while the corn stover exhibited the highest crushing strength. Clearly, biomass type has a fairly significant impact on the crushing strength of sub-bituminous coal briquettes. Figure 5-45c shows the mechanical durability results for each biomass type. The range of the measured values for the five biomass types was 64.0 to 80.2 percent. Once again, the corn stover exhibited the highest result, while the switchgrass was found to have the lowest mechanical durability. These results indicate that corn stover is the best type of biomass with respect to the quality of briquettes composed of sub-bituminous coal and biomass.

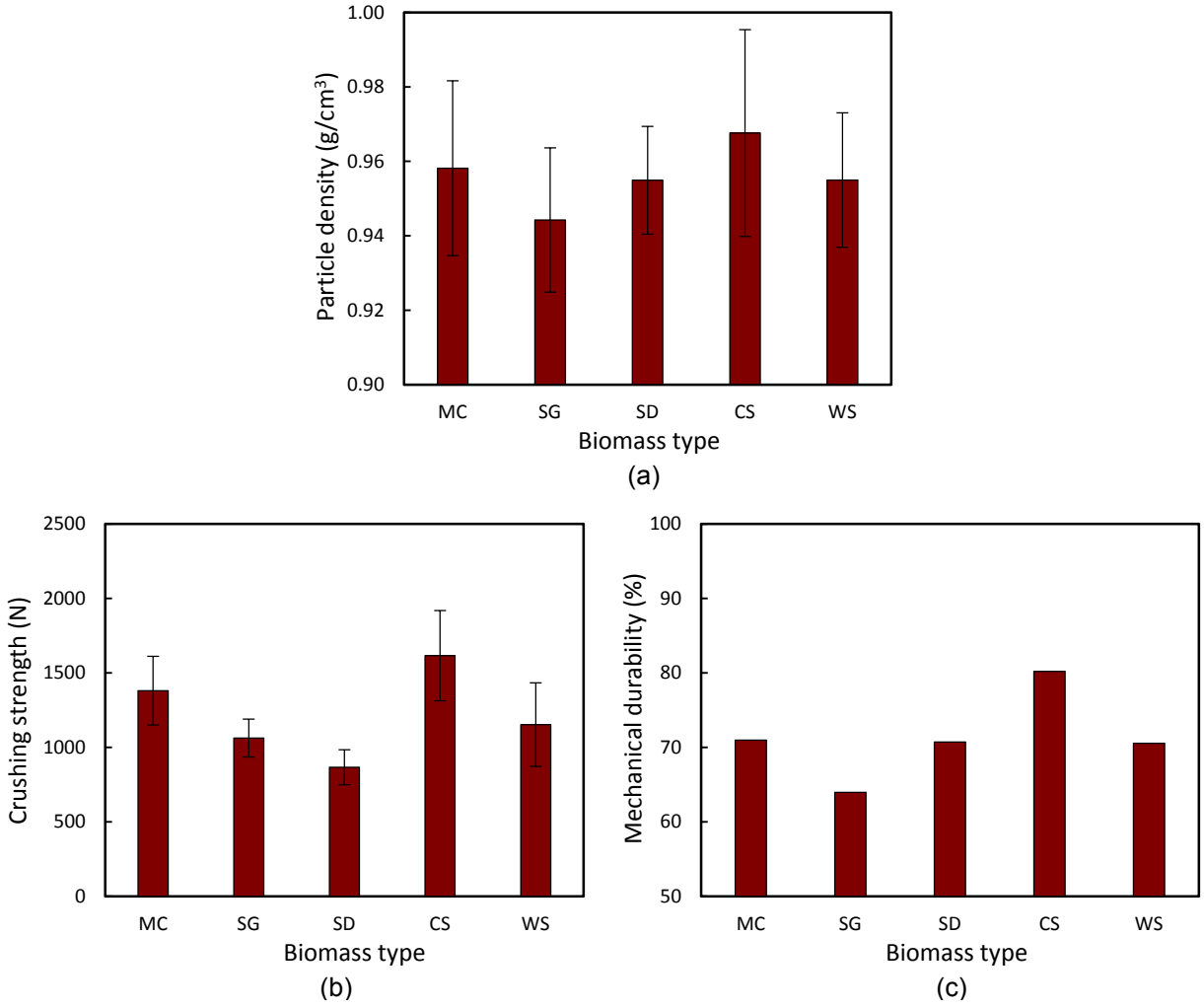



Figure 5-45. Effect of biomass type on (a) particle density, (b) crushing strength and (c) mechanical durability for briquettes composed of Eagle Butte (sub-bituminous) coal and each type of biomass [Error bars indicate plus and minus one standard deviation from the mean]

## 5.4.4 Evaluation of Roll Press Operating Parameters

### 5.4.4.1 Summary of Results

The results of the operating parameters evaluations for the Komarek B100R roll press are summarized in Table 5-26. Each test that was conducted is identified by the standard test number assigned in Design-Expert® 8 according to the roll force, roll torque and roll motor speed (i.e. 01 = roll force of 50 kN, roll torque of 1200 N-m and roll motor speed of 300 rpm). It should be noted that a roll torque of 1800 newton-meters was not sustainable at a roll force of 50 kilonewtons. Therefore, a roll torque of 1200 newton-meters was evaluated in the tests that initially specified these conditions. In the following sections, correlations between each operating variable and the measured briquette properties are presented and discussed. Analysis of the results is also covered, including mathematical models developed for each response using the Design-Expert® 8 statistical analysis tools. In addition, contour graphs of the models are presented to visually interpret and evaluate the results. Finally, numerical optimization of the model was conducted to determine the combination of operating parameters that produces the highest quality briquettes.

Table 5-26. Summary of briquette characterization results for evaluation of Komarek B100R roll press operating parameters

| Test ID` | Roll Force (kN) | Roll Torque (N-m) | Roll Speed (rpm) | Briquette Water Content | Particle Density (g/cm$^3$) | Crushing Strength (N) | Mechanical Durability (%) |
|---|---|---|---|---|---|---|---|
| MR-CS-MP-01 | 50 | 1200 | 300 | 0.020 | 1.09 | 870.1 | 81.5 |
| MR-CS-MP-02 | 50 | 1200 | 900 | 0.024 | 1.07 | 949.7 | 81.5 |
| MR-CS-MP-03 | 100 | 1200 | 300 | 0.027 | 1.12 | 1057.8 | 84.7 |
| MR-CS-MP-04 | 100 | 1200 | 900 | 0.026 | 1.11 | 1148.5 | 85.0 |
| MR-CS-MP-05 | 75 | 600 | 300 | 0.024 | 1.06 | 921.2 | 64.3 |
| MR-CS-MP-06 | 75 | 600 | 900 | 0.024 | 1.01 | 871.0 | 54.0 |
| MR-CS-MP-07 | 75 | 1200 | 300 | 0.028 | 1.09 | 1077.4 | 84.4 |
| MR-CS-MP-08 | 75 | 1800 | 900 | 0.019 | 1.12 | 1316.2 | 92.5 |
| MR-CS-MP-09 | 50 | 600 | 600 | 0.022 | 1.05 | 735.7 | 70.3 |
| MR-CS-MP-10 | 100 | 600 | 600 | 0.026 | 1.06 | 953.3 | 63.1 |
| MR-CS-MP-11 | 50 | 1200 | 600 | 0.020 | 1.08 | 974.6 | 83.0 |
| MR-CS-MP-12 | 100 | 1800 | 600 | 0.021 | 1.16 | 1316.2 | 93.7 |
| MR-CS-MP-13 | 75 | 1200 | 600 | 0.024 | 1.11 | 1040.9 | 86.6 |
| MR-CS-MP-14 | 75 | 1200 | 600 | 0.024 | 1.10 | 1052.9 | 87.7 |
| MR-CS-MP-15 | 75 | 1200 | 600 | 0.022 | 1.11 | 1076.0 | 88.6 |

#### *5.4.4.1.1 Roll Force Correlations*

The correlation between roll force and each measured briquette property were evaluated by linear regression analysis. To investigate these correlations, roll force was plotted versus each measured briquette property with the data points grouped by roll torque values (i.e. 600, 1200 and 1800 N-m). This approach was used because little or no correlation existed for the entire data set due to the influence of the other operating parameters (i.e. roll torque and roll speed). The roll force correlations were initially investigated with the data grouped separately by roll torque and roll speed. From these investigations, it was found that roll force correlations were greatest with the data grouped by roll torque.

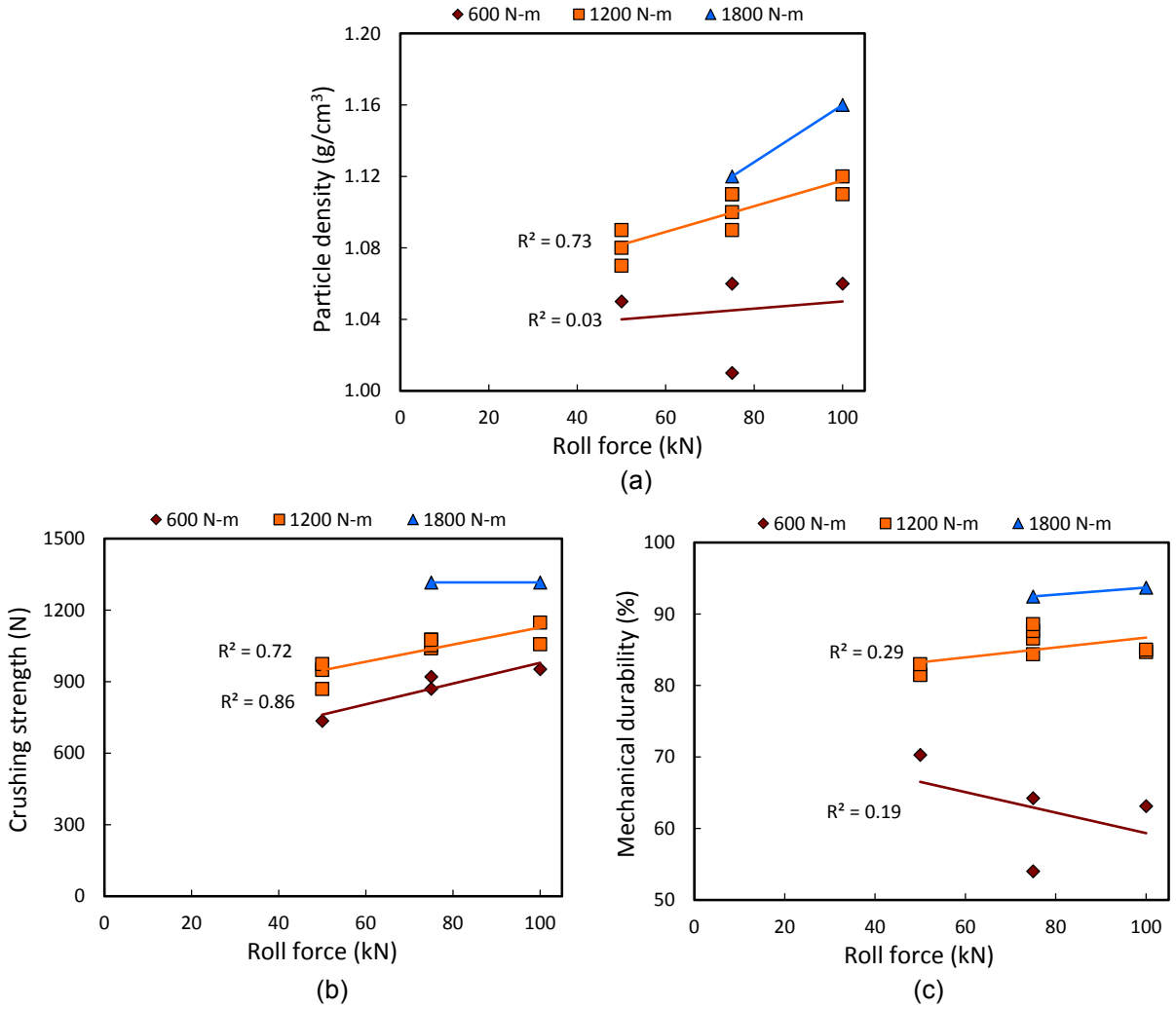



Figure 5-46. Effect of Komarek B100R roll force on (a) particle density, (b) crushing strength and (c) mechanical durability for briquettes composed of McClure River (bituminous) coal and corn stover

Figure 5-46a displays the correlation between roll force and the particle density of briquettes produced with the Komarek B100R roll press. It is clear from this chart that roll force generally exhibits a positive correlation with particle density. For each of the three roll torques tested, an increase in roll force led to an increase in the particle density of the briquettes, with the exception of one data point at a roll torque of 600 newton-meters. The strength of these linear correlations was measured by determining the coefficient of determination for each data set grouped by roll torque. However, this value was not determined for the briquettes produced at a roll torque of 1800 newton-meters since there were only two recorded data points. At a roll torque of 1200 newton-meters, the coefficient of determination was 0.73. In contrast, this value was only 0.03 for the briquettes produced at a roll torque of 600 newton-meters. These coefficients indicate that roll force and roll torque are not the only variables that influence the particle density of coal-biomass briquettes.

Figure 5-46b illustrates the correlation between roll force and the crushing strength of the briquettes. This chart clearly shows that there is a strong positive correlation between roll force and crushing strength for briquettes produced at roll torque values of 600 and 1200 newton-meters. In contrast, there is no clear correlation between roll force and crushing strength for the briquettes produced at a roll torque of 1800 newton-meters. The uncertainty of this result is amplified by the lack of data points at this operating condition. The strength of the linear correlations for the briquettes produced at roll torque values of 600 and 1200 newton-meters was determined by calculating the coefficient of determination values. The strongest linear correlation was found for the briquettes produced at a roll torque of 600 newton-meters (i.e. $R^2$ = 0.86). In comparison, the coefficient of determination for briquettes at a roll torque of 1200 newton-meters was 0.72.

Figure 5-46c shows the correlation between roll force and the mechanical durability of briquettes. It appears from this chart that there is a slight positive correlation between roll force and mechanical durability for briquettes produced with a roll torque of 1200 and 1800 newton-meters. Conversely, the mechanical durability of briquettes produced with a roll torque of 600 newton-meters exhibited a slight negative correlation with roll force. The strength of the linear correlations for the briquettes produced at roll torque values of 600 and 1200 newton-meters was determined by measuring the coefficient of determination values. The coefficient of

determination values for the briquettes produced at a roll torque of 600 and 1200 newton-meters was 0.19 and 0.29, respectively.

*5.4.4.1.2 Roll Torque Correlations*

The correlation between roll torque and each measured briquette property were also evaluated by linear regression analysis. To investigate these correlations, roll torque was plotted versus each measured briquette property with the data points grouped by roll force values (i.e. 50, 75 and 100 kN). This approach was used because little or no correlation existed for the entire data set due to the influence of the other operating parameters (i.e. roll force and roll speed). The roll torque correlations were initially investigated with the data grouped separately by roll force and roll speed. From these investigations, it was found that roll torque correlations were greatest with the data grouped by roll force.

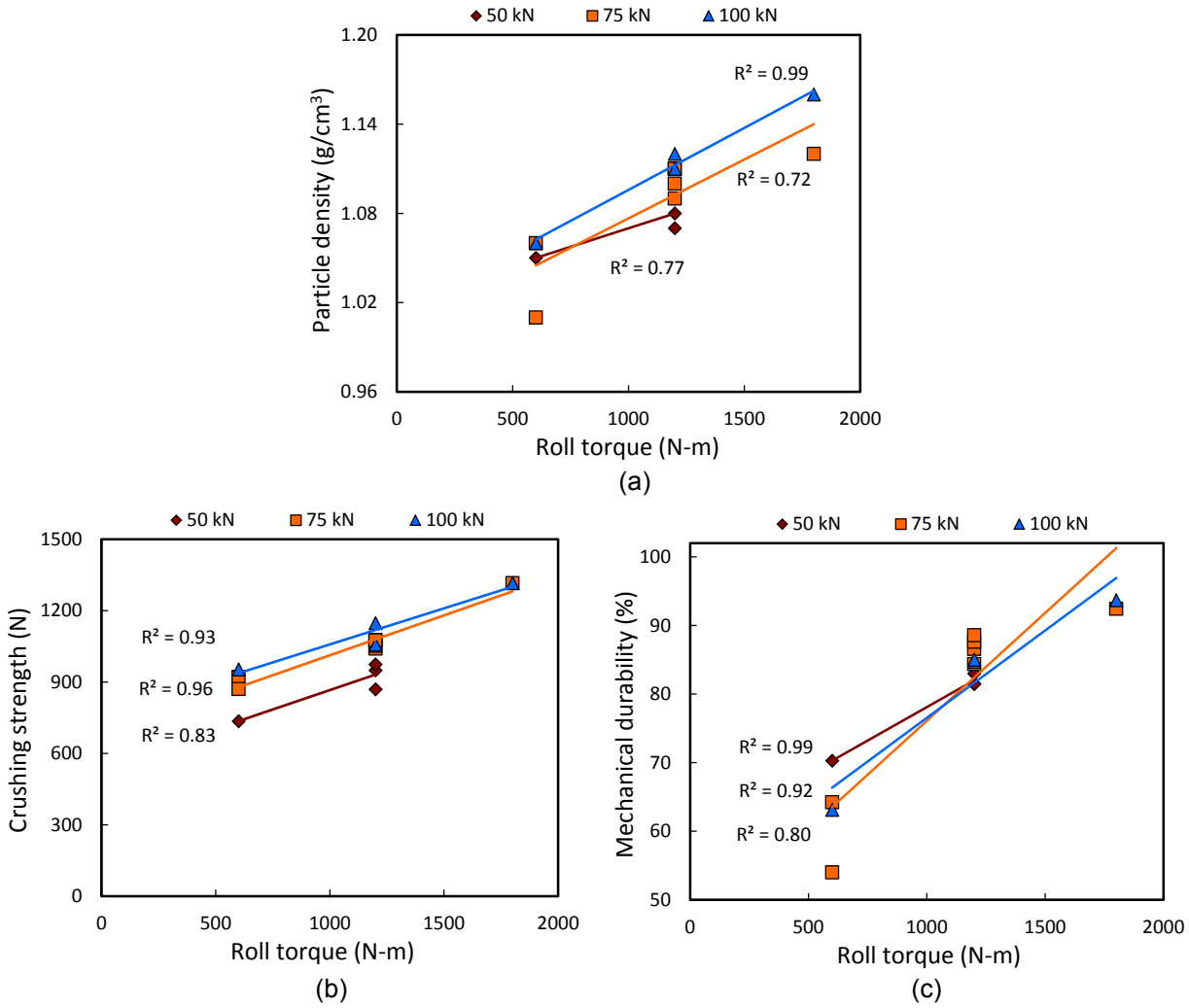



Figure 5-47. Effect of Komarek B100R roll torque on (a) particle density, (b) crushing strength and (c) mechanical durability for briquettes composed of McClure River (bituminous) coal and corn stover

Figure 5-47a displays the correlation between roll torque and the particle density of briquettes produced with the Komarek B100R roll press. It is clear from this chart that there is a fairly strong positive correlation between roll torque and the particle density of the briquettes. For each of the roll forces evaluated, an increase in roll torque led to a direct increase in the particle density of the briquettes. The strength of these linear correlations was measured by determining the coefficient of determination for each data set grouped by roll force. The strongest correlation was observed for the briquettes produced with a roll force of 100 kilonewtons (i.e. $R^2 = 0.99$). In contrast, the coefficient of determination values for briquettes produced with roll forces of 75 and 50 kilonewtons were 0.72 and 0.77, respectively.

Figure 5-47b illustrates the correlation between roll torque and the crushing strength of the briquettes. This chart clearly shows that there is a positive correlation between roll torque and briquette crushing strength. An increase in roll torque directly corresponded to an increase in the crushing strength of the briquettes for each of the roll forces evaluated. The strength of these linear correlations was determined by calculating the coefficient of determination for each set of roll forces. Each of the values was high, which indicates that the linear correlation between roll torque and briquette crushing strength is strong. Specifically, the coefficient of determination values for briquettes produced at 50, 75 and 100 kilonewtons were 0.83, 0.96 and 0.93, respectively. These results suggest that the crushing strength of coal-biomass briquettes can be improved by increasing the roll torque applied during briquette production.

Figure 5-47c shows the correlation between roll torque and the mechanical durability of briquettes. As with the previous chart, it appears from this chart that there is a positive correlation between roll torque and the mechanical durability of briquettes. An increase in roll torque directly corresponded to an increase in the mechanical durability of the briquettes for each of the roll forces evaluated. The strength of these linear correlations was determined by calculating the coefficient of determination for each set of roll forces. The strongest linear correlation was found for the briquettes produced at a roll force of 50 kilonewtons (i.e. $R^2$ = 0.99). The strength of this correlation successively declined with an increase in roll force. Specifically, the coefficient of determination for briquettes produced at a roll force of 75 and 100 kilonewtons was 0.92 and 0.80, respectively. These results suggest that the mechanical durability of coal-biomass briquettes can be improved by increasing the roll torque applied during briquette production.

*5.4.4.1.3 Roll Speed Correlations*

The correlation between the roll motor speed and each measured briquette property were also evaluated by linear regression analysis. To investigate these correlations, roll speed was plotted versus each measured briquette property with the data points grouped by roll torque values (i.e. 600, 1200 and 1800 N-m). This approach was used because little or no correlation existed for the entire data set due to the influence of the other operating parameters (i.e. roll force and roll torque). The roll speed correlations were initially investigated with the data grouped

separately by roll force and roll torque. From these investigations, it was found that roll speed correlations were greatest with the data grouped by roll torque.

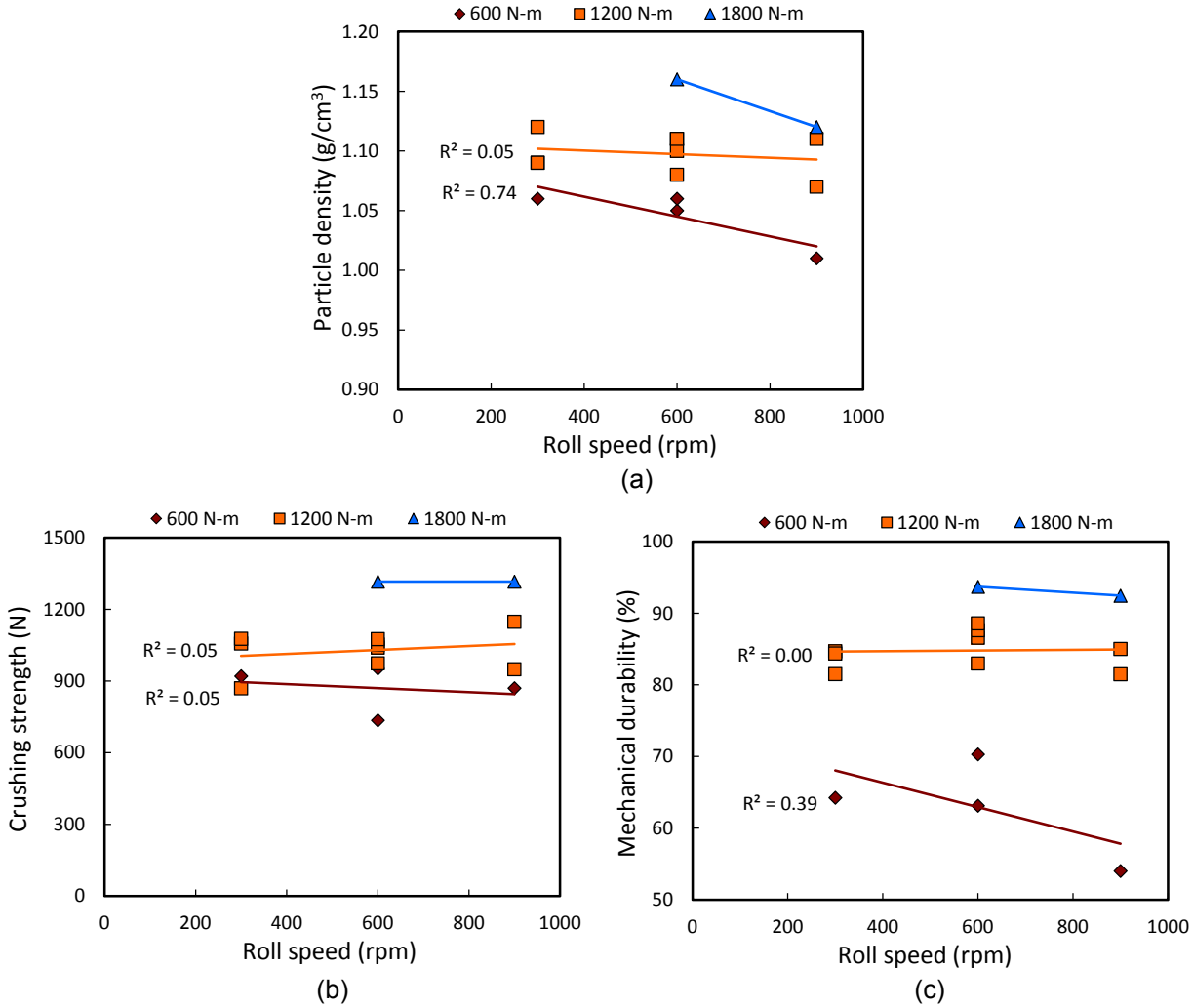



Figure 5-48. Effect of Komarek B100R roll speed on (a) particle density, (b) crushing strength and (c) mechanical durability for briquettes composed of McClure River (bituminous) coal and corn stover

Figure 5-48a displays the correlation between roll speed and the particle density of briquettes produced with the Komarek B100R roll press. From this char, it appears that a slight negative correlation exists between roll speed and particle density. For each of the three roll torques tested, an increase in roll speed led to a slight decrease in the particle density of the briquettes. The strength of these linear correlations was measured by determining the coefficient of determination for each data set grouped by roll torque. However, this value was not determined for the briquettes produced at a roll torque of 1800 newton-meters since there were only two recorded data points. At a roll torque of 1200 newton-meters, the coefficient of

determination was 0.05, which indicates that the correlation is not significant. However, the coefficient of determination for the briquettes produced at a roll torque of 600 newton-meters was 0.74, which indicates that the linear correlation is much stronger for briquette produced under this condition.

Figure 5-48b illustrates the correlation between roll speed and the crushing strength of the briquettes. It is clear from this chart that there is very little correlation between roll speed and the crushing strength of briquettes. This is supported by coefficient of determination values of 0.05 for roll torque values of 600 and 1200 newton-meters. Again, this coefficient was not calculated for the briquettes produced at a roll torque of 1800 newton-meters since there were only two recorded data points. These results suggest that roll speed has no quantifiable impact on the crushing strength of coal-biomass briquettes.

Figure 5-48c shows the correlation between roll speed and the mechanical durability of briquettes. It appears from this chart that there is no correlation between roll speed and mechanical durability for briquettes produced with a roll torque of 1200 and 1800 newton-meters. Conversely, the mechanical durability of briquettes produced with a roll torque of 600 newton-meters exhibited a slight negative correlation with roll speed. The strength of the correlations for the briquettes produced with at roll toques of 600 and 1200 newton-meters was determined by calculating the coefficient of determination for each data set. The briquettes produced at a roll torque of 600 newton-meters were found to have a coefficient of determination 0.39. In contrast, the coefficient of determination for the briquettes produced at a roll torque of 1200 newton-meters was 0.00. These results suggest that roll speed has no quantifiable impact on the mechanical durability of briquettes produced at high torque values. However, roll speed may have an impact on the quality of briquettes produced at lower torque values. In this case, slower roll speed likely enables better aeration of the feed prior to briquette formation, which has a positive effect on briquette quality.

#### 5.4.4.2 Statistical Analyses

The results of the operating parameter evaluations for the Komarek B100R roll press were examined using the statistical analysis tools included in Design-Expert® 8 to determine the influence of each variable and to optimize the quality of briquettes. Mathematical models were developed that relate the roll press operating parameters (i.e. roll force, roll torque and roll

speed) to the measured briquette properties (i.e. particle density, crushing strength, and mechanical durability). The first step of model development was selection of the process order (e.g. linear, quadratic) of the mathematical model. This was accomplished by determining the process order with the lowest lack of fit p-value and the highest adjusted R-squared and predicted R-squared values. The selected model was then analyzed using the analysis of variance (ANOVA) function to determine the statistical significance of the entire model and of each individual term. All insignificant terms were then removed from the model, except those required to maintain hierarchy. Next, the fit of the model to the data was evaluated using various diagnostics tools. The following sections present the empirical mathematical models developed for briquettes produced with the Komarek B100R roll press and summarize the results of the statistical analyses.

#### *5.4.4.2.1 Particle Density Model*

A linear mathematical model was constructed that relates roll force, roll torque and roll speed to the particle density of briquettes produced with the Komarek B100R roll press. According to the model, the predicted particle density of briquettes is calculated by:

$$\rho = 0.98 + 0.00056f + 0.000081t - 0.000041s \quad \text{(Eq. 5-18)}$$

where $\rho$ is the particle density (g/cm$^3$), $f$ is the roll torque (kN), $t$ is the roll torque (N-m) and $s$ is the roll motor speed (rpm). The statistical significance of this model, in terms of its fit to the data from which it was derived, was analyzed using ANOVA to evaluate a number of variables. A summary of the ANOVA is provided in Table 5-27 for the particle density model. The p-value of the particle density model is less than 0.0001, which indicates that the predicted density values would be highly unlikely under the null hypothesis and verifies that the model is indeed statistically significant. The p-values of the model terms are 0.0265 (roll speed), 0.0142 (roll force) and less than 0.0001 (roll torque). This implies that each of the operating parameters are statistically significant model terms, and thus have a major impact on accurate prediction of the particle density of briquettes. However, it should be distinguished that roll torque is the most statistically significant model parameter, and thus has the greatest effect on the particle density of coal-biomass briquettes according to this model.

Table 5-27. ANOVA results for Komarek B100R roll press particle density model

| Source | Sum of Squares | df | Mean Square | F Value | p-value Prob > F |
|---|---|---|---|---|---|
| Model | 1.63E-02 | 3 | 5.44E-03 | 30.18 | < 0.0001 |
| A-Roll speed | 1.18E-03 | 1 | 1.18E-03 | 6.56 | 0.0265 |
| B-Roll force | 1.52E-03 | 1 | 1.52E-03 | 8.46 | 0.0142 |
| C-Roll torque | 1.28E-02 | 1 | 1.28E-02 | 71.04 | < 0.0001 |
| Residual | 1.98E-03 | 11 | 1.80E-04 | -- | -- |
| Lack of Fit | 1.92E-03 | 9 | 2.13E-04 | 6.38 | 0.1427 |
| Pure Error | 6.67E-05 | 2 | 3.33E-05 | -- | -- |
| Cor Total | 1.83E-02 | 14 | -- | -- | -- |

To confirm the ANOVA normality assumption for the particle density model, the residuals were visually examined in a normal probability plot of studentized results. Figure 5-49a shows the normal probability plot of studentized results for the crushing strength model. It is clear from this figure that the residuals follow an approximately straight line, and thus are normally distributed. A plot of predicted versus actual values was also examined to visually analyze the relationship between the measured particle density values and those predicted by the model. The predicted versus actual plot is displayed in Figure 5-49b for the particle density model, which shows the desired data scatter about the 45 degree line is present. This further exemplifies the statistical significance of the particle density model and indicates that it is well suited for prediction of briquette quality.

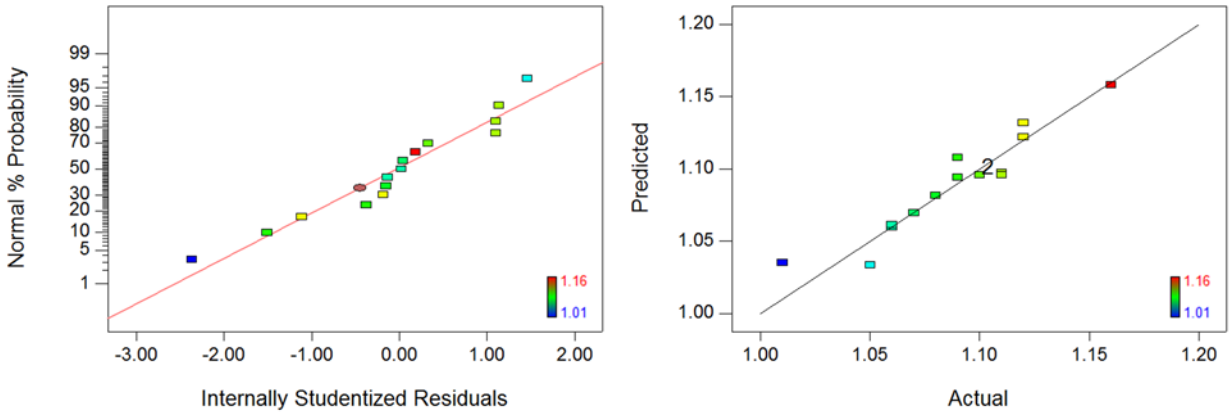



Figure 5-49. Diagnostic graphs for visual inspection of ANOVA results for Komarek B100R roll press particle density model: (a) normal probability plot of studentized results and (b) predicted versus actual values plot

*5.4.4.2.2 Crushing Strength Model*

A linear mathematical model was constructed that relates roll force, roll torque and roll speed to the crushing strength of briquettes produced with the Komarek B100R roll press. According to the model, the predicted crushing strength of briquettes is calculated by:

$$\sigma = 345.04 + 3.78f + 0.32t + 0.07s \quad \text{(Eq. 5-19)}$$

where $\sigma$ is the crushing strength (N), $f$ is the roll force (kN), $t$ is the roll torque (N-m) and $s$ is the roll motor speed (rpm). The statistical significance of this model, in terms of its fit to the data from which it was derived, was analyzed using ANOVA to evaluate a number of variables. A summary of the ANOVA is provided in Table 5-28 for the crushing strength model. The p-value of the model is less than 0.0001, which indicates that the predicted crushing strength values would be highly unlikely under the null hypothesis and verifies that the model is indeed statistically significant. The p-values of the model terms are 0.2302 (roll speed), 0.0001 (roll force) and less than 0.0001 (roll torque). This implies that roll force and roll torque are statistically significant model terms, and thus have a major impact on accurate prediction of the crushing strength of briquettes. In contrast, roll speed is not a significant model term, which implies that its impact on crushing strength quantified in the model is not statistically significant. This term was needed to maintain the hierarchy of the model, otherwise it would have been removed to improve the model.

Table 5-28. ANOVA results for Komarek B100R roll press crushing strength model

| Source | Sum of Squares | df | Mean Square | F Value | p-value Prob > F |
|---|---|---|---|---|---|
| Model | 3.24E+05 | 3 | 1.08E+05 | 49.32 | < 0.0001 |
| A-Roll speed | 3530 | 1 | 3530 | 1.61 | 0.2302 |
| B-Roll force | 69976 | 1 | 69976 | 31.98 | 0.0001 |
| C-Roll torque | 1.96E+05 | 1 | 1.96E+05 | 89.52 | < 0.0001 |
| Residual | 24071 | 11 | 2188 | -- | -- |
| Lack of Fit | 23433 | 9 | 2604 | 8.16 | 0.1139 |
| Pure Error | 638 | 2 | 319 | -- | -- |
| Cor Total | 3.48E+05 | 14 | -- | -- | -- |

To confirm the ANOVA normality assumption for the crushing strength model, the residuals were visually examined in a normal probability plot of studentized results. Figure 5-50a shows the normal probability plot of studentized results for the crushing strength model. It is clear from this figure that the residuals follow an approximately straight line, and thus are

normally distributed. A plot of predicted versus actual values was also examined to visually analyze the relationship between the measured crushing strength values and those predicted by the model. The predicted versus actual plot is displayed in Figure 5-50b for the crushing strength model, which shows the desired data scatter about the 45 degree line is present. This further exemplifies the statistical significance of the crushing strength model and indicates that it is well suited for prediction of briquette quality.

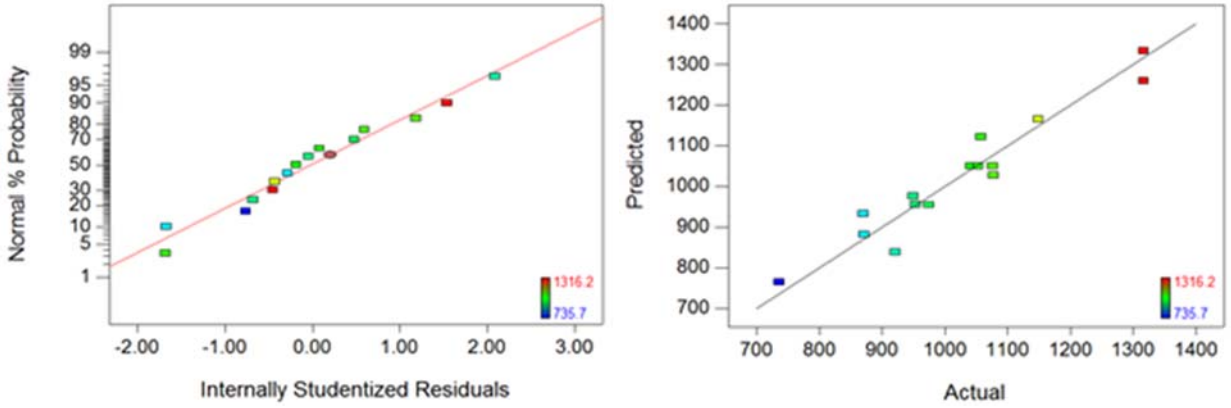



Figure 5-50. Diagnostic graphs for visual inspection of ANOVA results for Komarek B100R roll press crushing strength model: (a) normal probability plot of studentized results and (b) predicted versus actual values plot

#### *5.4.4.2.3 Mechanical Durability Model*

A quadratic mathematical model was constructed that relates roll force, roll torque and roll speed to the mechanical durability of briquettes produced with the Komarek B100R roll press. According to the model, the predicted mechanical durability of briquettes is calculated by:

$$MD = 51.18 - 0.30f + 0.05t + 0.02s + 0.00030ft + 0.000034ts - 0.000029t^2 - 0.000047s^2$$

(Eq. 5-20)

where *MD* is the mechanical durability (%), $f$ is the roll torque (kN), $t$ is the roll torque (N-m) and $s$ is the roll motor speed (rpm). The statistical significance of this model, in terms of its fit to the data from which it was derived, was analyzed using ANOVA to evaluate a number of variables. A summary of the ANOVA is provided in Table 5-29 for the mechanical durability model. The p-value of the model is less than 0.0001, which indicates that the predicted mechanical durability values would be highly unlikely under the null hypothesis and verifies that the model is indeed statistically significant. The p-values of the model terms are 0.6877 (roll speed), 0.0882 (roll force), less than 0.0001 (roll torque), 0.0046 (roll speed x roll torque), 0.0186 (roll force x roll

torque), 0.0057 (roll speed$^2$) and 0.0002 (roll torque$^2$). This implies that the majority of the model terms are statistically significant (except roll speed), and thus have a major impact on accurate prediction of the mechanical durability of briquettes. In contrast, roll speed is not a significant model term, which implies that the impact of this variable on mechanical durability quantified in the model is not statistically significant.

Table 5-29. ANOVA results for Komarek B100R roll press mechanical durability model

| Source | Sum of Squares | df | Mean Square | F Value | p-value Prob > F |
|---|---|---|---|---|---|
| Model | 1870.12 | 7 | 267.16 | 63.90 | < 0.0001 |
| A-Roll speed | 0.73 | 1 | 0.73 | 0.18 | 0.6877 |
| B-Roll force | 16.38 | 1 | 16.38 | 3.92 | 0.0882 |
| C-Roll torque | 398.35 | 1 | 398.35 | 95.28 | < 0.0001 |
| AC | 70.25 | 1 | 70.25 | 16.80 | 0.0046 |
| BC | 38.92 | 1 | 38.92 | 9.31 | 0.0186 |
| $A^2$ | 64.40 | 1 | 64.40 | 15.40 | 0.0057 |
| $C^2$ | 209.10 | 1 | 209.10 | 50.02 | 0.0002 |
| Residual | 29.26 | 7 | 4.18 | -- | -- |
| Lack of Fit | 27.26 | 5 | 5.45 | 5.45 | 0.1623 |
| Pure Error | 2.00 | 2 | 1.00 | -- | -- |
| Cor Total | 1899.39 | 14 | -- | -- | -- |

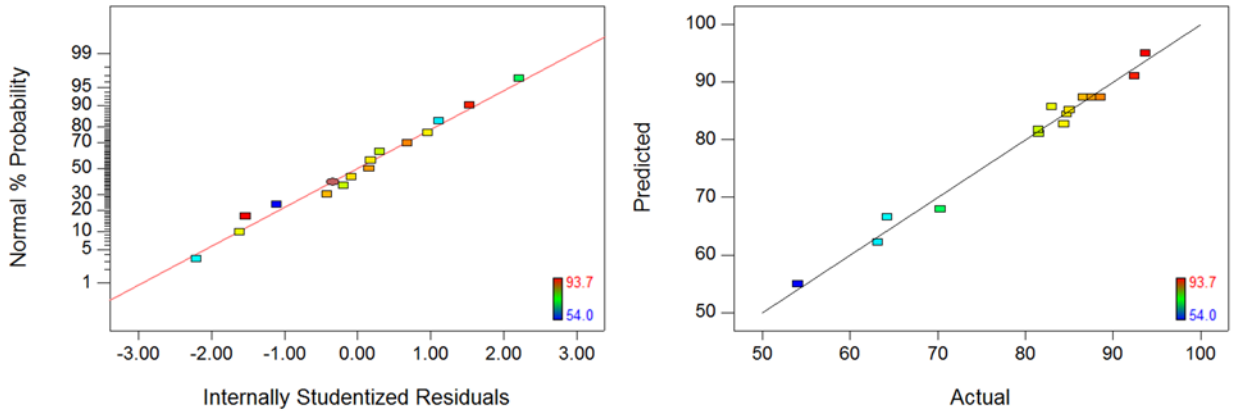



Figure 5-51. Diagnostic graphs for visual inspection of ANOVA results for Komarek B100R roll press mechanical durability model: (a) normal probability plot of studentized results and (b) predicted versus actual values plot

To confirm the ANOVA normality assumption for the mechanical durability model, the residuals were visually examined in a normal probability plot of studentized results. Figure 5-51a shows the normal probability plot of studentized results for the mechanical durability model. It is

clear from this figure that the residuals follow an approximately straight line, and thus are normally distributed. A plot of predicted versus actual values was also examined to visually analyze the relationship between the measured mechanical durability values and those predicted by the model. The predicted versus actual plot is displayed in Figure 5-51b for the mechanical durability model, which shows the desired data scatter about the 45 degree line is present. This further exemplifies the statistical significance of the mechanical durability model and indicates that it is well suited for prediction of briquette quality.

#### 5.4.4.3 Model Graphs

Following the development and statistical analysis of each mathematical model, several contour graphs were constructed to visually interpret and evaluate the results. The influence of water content on the modeled responses for particle density, crushing strength and mechanical durability are presented in Figure 5-52. From this figure it is evident that the maximum particle density values (i.e. > 1.16 g/cm$^3$) occur at a roll force of 100 kN, a roll speed of 300 rpm and a roll torque of 1800 N-m. In contrast, the minimum particle density (i.e. < 1.04 g/cm$^3$) values occur at a roll force of 50 kN, a roll speed of 900 rpm and a roll torque of 600 N-m. This figure also clearly indicates that briquette crushing strength reaches a maximum value (i.e. > 1,300 N [300 lb$_f$]) at a roll force of 100 kN, a roll speed of 900 rpm and a roll torque of 1800 N-m, and reaches a minimum value (i.e. < 800 N [180 lb$_f$]) at a roll force of 50 kN, a roll speed of 300 rpm and a roll torque of 600 N-m. Finally, this figure shows that the mechanical durability of briquettes reaches a maximum value (i.e. > 95%) at a roll force of 100 kN, a roll speed of 900 rpm and a roll torque of 1800 N-m. In contrast, the minimum mechanical durability occurs at a roll force of 50 kN, a roll speed of 300 rpm and roll torque of 600 N-m.

The modeled responses for particle density, crushing strength and mechanical durability with respect to biomass content and binder content are presented in Figure 5-53 and Figure 5-54, respectively. These figures present the same data that is displayed in Figure 5-52, but offer a different perspective that may be desirable in certain circumstances. Regardless of the chart examined, a clear optimum set of mixture variables, with respect to both crushing strength and mechanical durability, appears to be achievable at a roll force of 100 kN, a roll speed of 900 rpm and roll torque of 1800 N-m. At these conditions, the models predict a crushing strength in

excess of 1,300 newtons (300 $lb_f$) and a mechanical durability greater than 95 percent. Numerical optimization of the mixture variables was conducted to verify this result.

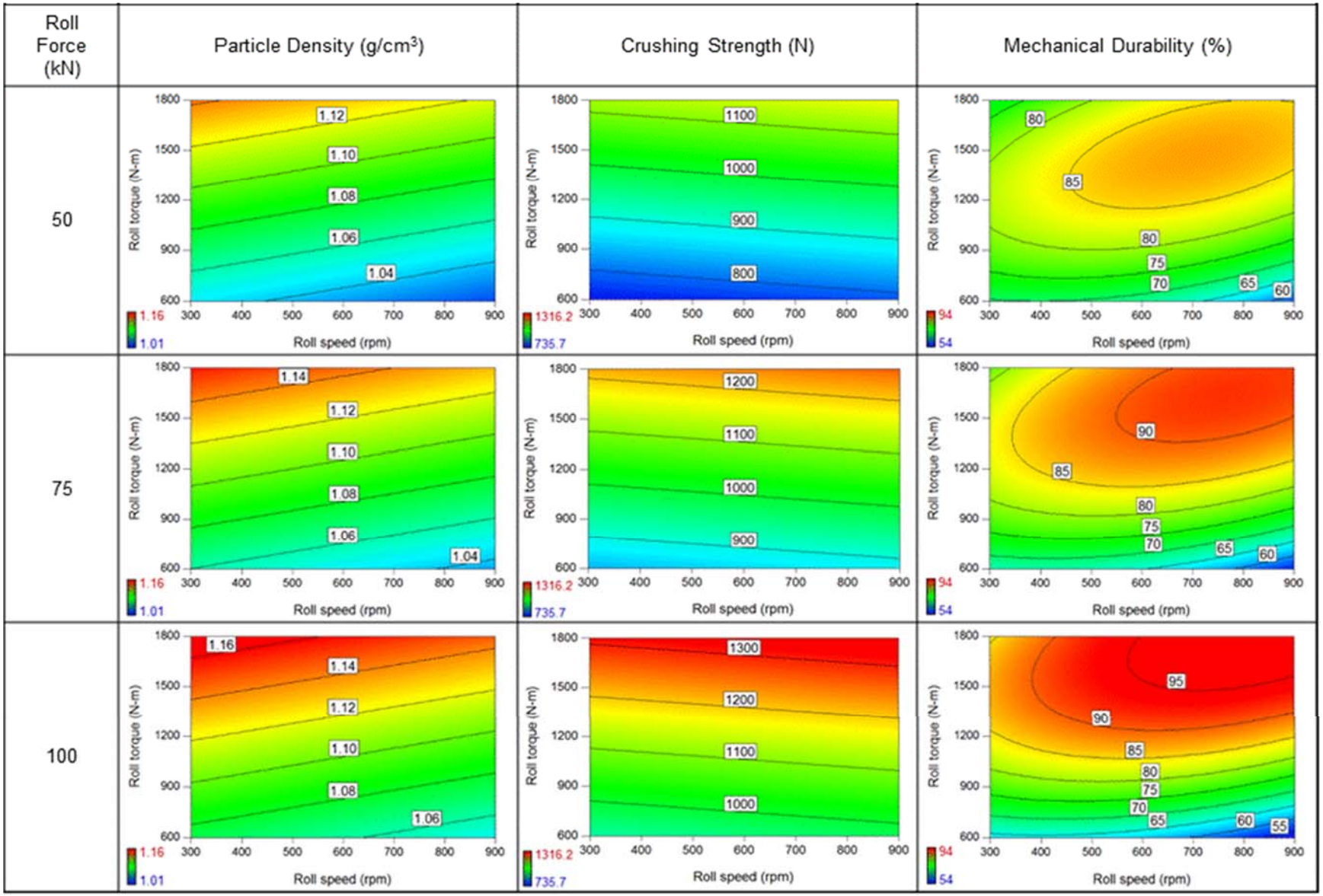



Figure 5-52. Influence of Komarek B100R roll force on modeled responses for particle density, crushing strength and mechanical durability for briquettes composed of McClure River (bituminous) coal and corn stover

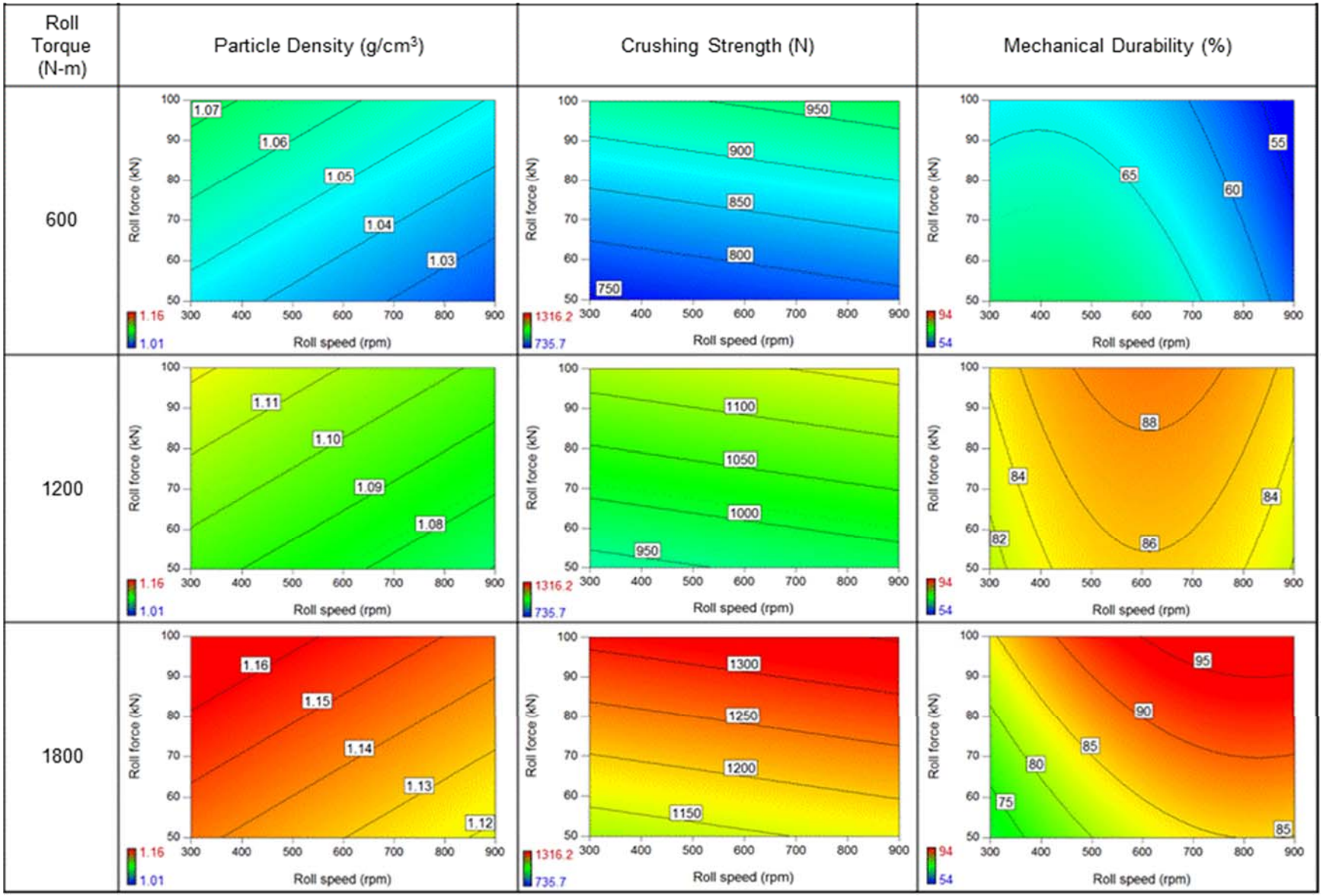



Figure 5-53. Influence of Komarek B100R roll torque on modeled responses for particle density, crushing strength and mechanical durability for briquettes composed of McClure River (bituminous) coal and corn stover

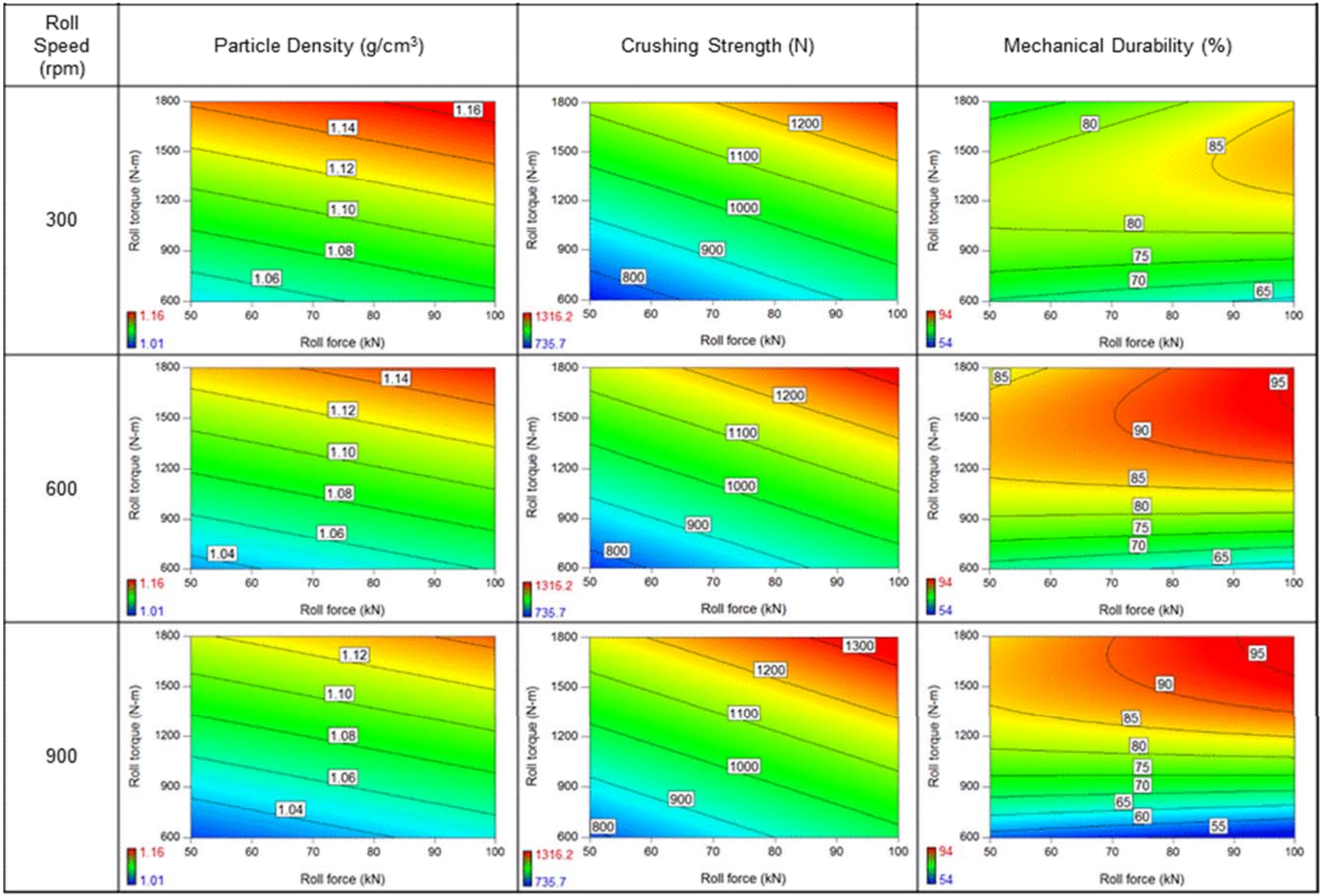



Figure 5-54. Influence of Komarek B100R roll speed on modeled responses for particle density, crushing strength and mechanical durability for briquettes composed of McClure River (bituminous) coal and corn stover

#### 5.4.4.4 Numerical Optimization

Numerical optimization of the feedstock variables was conducted in Design-Expert® 8 using the tool included in the analysis package. This tool allows for specification of optimization criteria (i.e. goals), which can include maximizing or minimizing predicted responses and process variables, as well as setting target values for each parameter. The tool also allows for adjustment of the importance of each goal on a scale from one to five (1 being the least important, 5 being the most important). The results of the optimization routine include a specified value for each of the process variables, as well as the predicted values for each response. A desirability value is calculated for each solution to the optimization routine to provide a method to rank the solutions and to indicate the extent to which the combination of responses approaches a perfect solution.

Optimization of the mathematical models developed for the Komarek B100R machine was accomplished by specifying a maximization goal for both crushing strength and mechanical durability. The importance of the mechanical durability goal was set to five and the importance of the crushing strength goal was set to three. This configuration was selected after experimenting with the effect of the importance setting on the desirability of the solutions to the optimization routine. The routine generated 19 optimized solutions, all of which specified a roll force of 100 kN, a roll torque of 1800 N-m and a roll speed of 819 to 840 rpm. As shown in Table 5-30, the top ten most desirable solutions were predicted to produce briquettes with a crushing strength in excess of 1,340 newtons (300 $lb_f$) and a mechanical durability in excess of 97.5 percent.

Table 5-30. Numerical optimization results for Komarek B100R roll press mathematical models

| Number | Roll Speed (rpm) | Roll Force (kN) | Roll Torque (N-m) | Crushing Strength (N) | Mechanical Durability (%) | Desirability |
|---|---|---|---|---|---|---|
| 1 | 829 | 100 | 1800 | 1349.1 | 97.6 | 0.966 |
| 2 | 826 | 100 | 1800 | 1348.7 | 97.6 | 0.966 |
| 3 | 833 | 100 | 1800 | 1349.1 | 97.6 | 0.966 |
| 4 | 837 | 100 | 1800 | 1349.6 | 97.5 | 0.966 |
| 5 | 819 | 100 | 1797 | 1347.8 | 97.5 | 0.966 |
| 6 | 832 | 100 | 1793 | 1346.9 | 97.5 | 0.966 |
| 7 | 829 | 100 | 1792 | 1346.5 | 97.5 | 0.966 |
| 8 | 840 | 100 | 1793 | 1347.8 | 97.5 | 0.966 |
| 9 | 832 | 100 | 1786 | 1344.7 | 97.5 | 0.966 |
| 10 | 823 | 100 | 1782 | 1342.9 | 97.5 | 0.966 |

## 5.4.5 Detailed Characterization of Optimum Briquettes

A detailed characterization study was conducted to investigate important properties of two selected optimum types of coal-biomass briquettes. The purpose of this study was to verify the enhanced quality of the co-briquetted feedstocks and to provide additional information that may be useful for industrial consumers or other end users of coal-biomass briquettes. Two types of briquettes were examined for the detailed characterization study. The first type of briquettes were composed of the Emerald coal and sawdust, while the second type of briquettes were composed of Eagle Butte coal and corn stover. Both types of briquettes were subjected to a range of tests to fully characterize their physical properties, flow properties and gasification behavior. The following section present and discuss the results of these evaluations.

### 5.4.5.1 Characterization of Physical Properties

A summary of the results of the comprehensive physical evaluations of the two types of briquettes are included in Table 5-31. From these results, it is fairly clear that the EM-SD briquettes are superior in quality to the EB-CS briquettes. For example, the crushing strength and tensile strength of the EM-SD briquettes was 1,590 newtons (357 $lb_f$) and 256 newtons (57.5 $lb_f$), as compared to 1,225 newtons (275.3 $lb_f$) and 206 newtons (46.3 $lb_f$) for the EB-CS briquettes. This corresponds to 29.8% higher crushing strength and a 24.2% higher tensile strength for the EM-SD briquettes. Nonetheless, the crushing strength of the EB-CS briquettes indicates that these briquettes are very strong, and thus high quality in this regard.

The mechanical durability of the EM-SD and EB-CS briquettes was 92.8% and 91.1%, respectively. These values were very similar and were both very good, which indicates that the briquettes would largely remain intact in the presence of attrition and impact forces encountered during handling and transportation. However, the weathered mechanical durability of the EM-SD (i.e. 39.4%) and EB-CS briquettes (i.e. 7.7%) was much lower, which indicates that the briquettes would experience a high degree of degradation in the presence of water. This is most likely a direct result of the water uptake values for the briquettes. For example, the initial and weathered water uptake of the EM-SD briquettes was 8.3% and 20.4%, respectively. In comparison, the initial and weathered water uptake of the EB-CS briquettes was 14.3% and 58.6%, respectively. These results suggest that a water resistant binder or some other post-production process would be required to reduce the water uptake of briquettes that will be exposed to precipitation or other moisture for any extended period of time.

Table 5-31. Summary of physical characterization results for Emerald-sawdust (EM-SD) and Eagle Butte-corn stover (EB-CS) briquettes

| Briquette Property | Units | EM-SD | EB-CS |
|---|---|---|---|
| Tensile strength | N | 255.8 | 206.0 |
| Crushing strength | N | 1589.8 | 1224.6 |
| Spring constant | N/m | 8.14E+05 | 4.98E+05 |
| Mechanical durability | % | 92.8 | 91.1 |
| Weathered mechanical durability | % | 39.4 | 7.7 |
| Attritability | % | 97.4 | 96.9 |
| Friability | % | 97.1 | 98.4 |
| Water content | -- | 0.018 | 0.163 |
| Particle density | $g/cm^3$ | 1.13 | 0.94 |
| Water uptake | % | 8.3 | 14.3 |
| Weathered water uptake | % | 20.4 | 58.6 |

The attritability and friability of the EM-SD briquettes was 97.4% and 97.1%, respectively. Similarly, the EB-CS briquettes exhibited attritability and friability values of 96.9% and 98.4%, respectively. These results indicate that the briquettes would withstand attrition forces in handling and impact forces from drops encountered on conveyors or at other points prior to utilization. Another observation was the significant difference in the particle density of the two types of briquettes. Specifically, the EM-SD briquettes were determined to have a particle density of 1.13 $g/cm^3$, as compared to only 0.94 $g/cm^3$ for the EB-CS briquettes. This

result was likely due to a combination of factors, including the higher true density of sawdust and the higher porosity of the EB-CS briquettes. The difference in porosity can be attributed to the higher water content of the EB-CS briquettes (i.e. w = 0.163) compared to the EM-SD briquettes (i.e. w = 0.018), which leads to increased air voids after drying the samples to calculate dry particle density.

#### 5.4.5.2 Characterization of Flow Properties

Several tests were conducted by Solids Handling Technologies to quantify the flow behavior of the EM-SD and EB-CS briquettes. Cohesive property tests and wall friction tests were performed to determine the opening sizes required to prevent arching and the required angle for mass flow. In addition, a compressibility test was performed to determine the relationship between bulk density and confining pressure. The cohesive properties of the briquettes are summarized by their respective flow functions, as shown in Figure 5-55 and Figure 5-56 for the EM-SD and EB-CS briquettes, respectively. Detailed results of the flow property tests conducted by Solids Handling Technologies are provided in Appendix B.

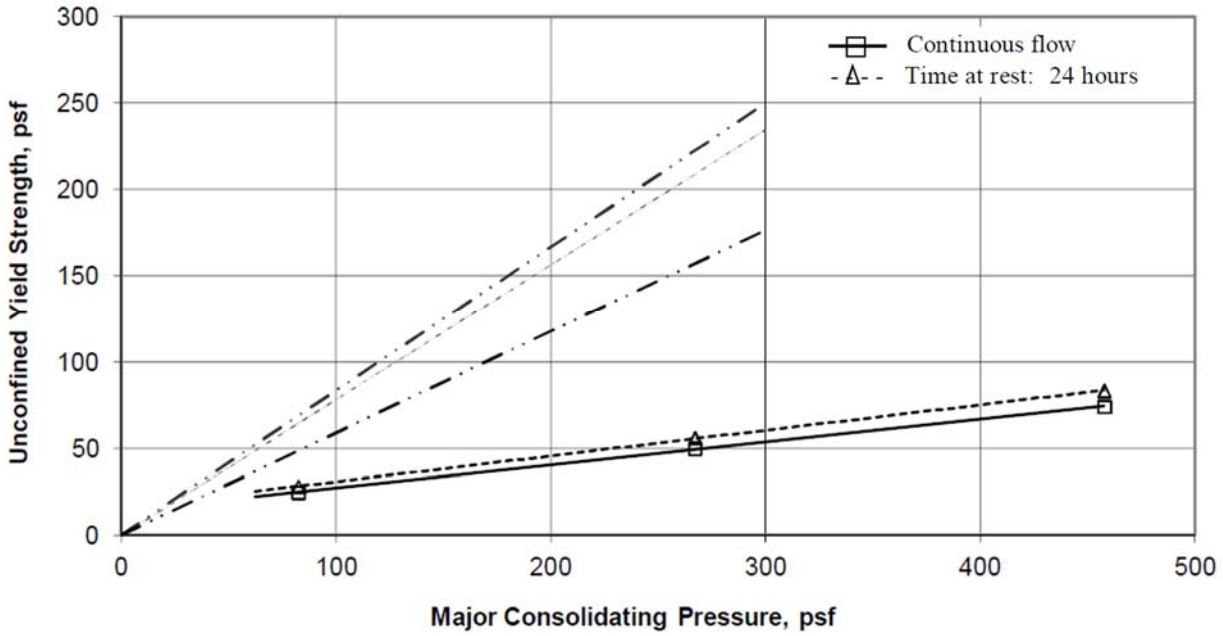



Figure 5-55. Flow function for determination of required hopper opening sizes for Emerald-sawdust (EM-SD) briquettes [Values are listed in U.S. standard units as provided by Solids Handling Technologies]

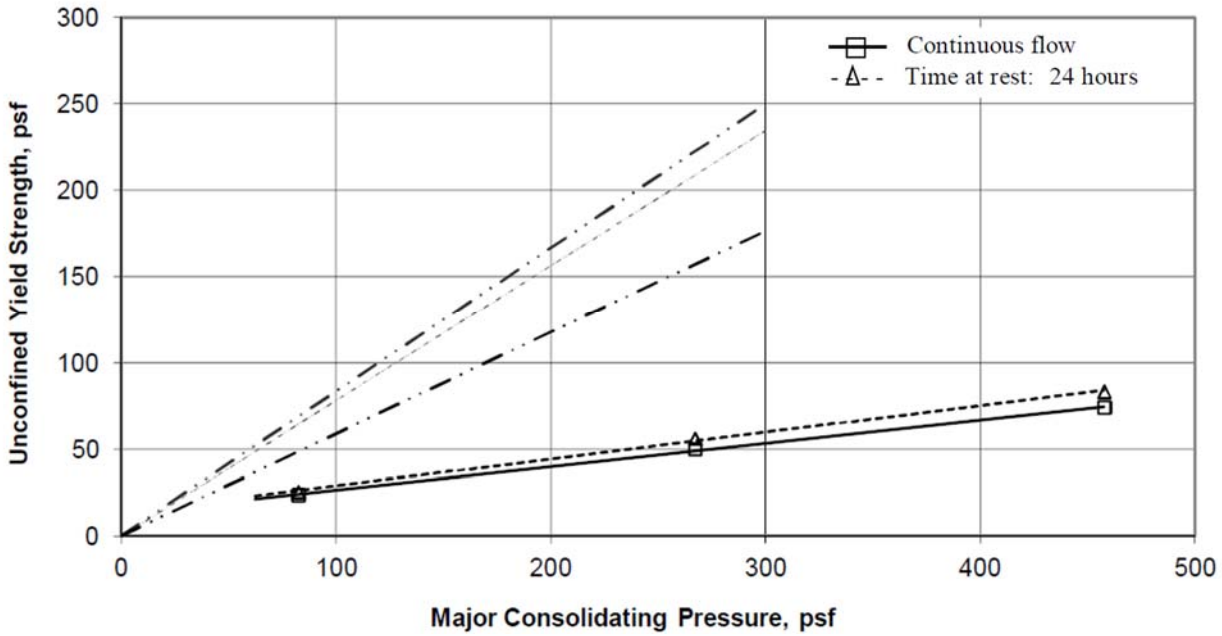



Figure 5-56. Flow function for determination of required hopper opening sizes for Eagle Butte-corn stover (EB-CS) briquettes [Values are listed in U.S. standard units as provided by Solids Handling Technologies]

In the figures above, the developed flow function for each material is plotted for continuous flow (i.e. no time at rest) and for a consolidation period of 24 hours. It is clearly shown that the unconfined yield strength required to cause flow of the briquettes is very low and increases at a slow rate with an increase in consolidation pressure. These results indicate that both the EM-SD and EB-CS briquettes exhibit superior flow properties, and thus are unlikely to exhibit poor flow characteristics such as ratholing and arching. However, suitable hopper outlet sizes must be selected to ensure reliable flow for specific applications. The required outlet size must be selected with consideration to the temperature of the briquettes and the consolidating load (or effective head) applied by briquettes on one another. An example of the required hopper outlet dimensions to prevent ratholing in a funnel flow pattern and to prevent arching in a mass flow pattern are provided in Table 5-32 for the EM-SD and EB-CS briquettes. These values were calculated based on a temperature of 22 degrees Celsius (72 °F) and an effective head of three meters (10 ft).

Table 5-32. Required hopper outlet sizes to ensure reliable flow of Emerald-sawdust (EM-SD) and Eagle Butte-corn stover (EB-CS) briquettes

| Briquette Sample | Time at Rest (hr) | Funnel Flow | Mass Flow | |
|---|---|---|---|---|
| | | Conical Opening (m) | Conical Opening (m) | Slot Opening (m) |
| EM-SD | 0 | 2.3 | 0.3 | 0.2 |
| | 24 | 2.7 | 0.3 | 0.2 |
| EB-CS | 0 | 2.3 | 0.3 | 0.2 |
| | 24 | 2.5 | 0.3 | 0.2 |

There is very little difference in the conical opening required for the two types of briquettes to prevent arching in a funnel flow pattern. Specifically, the EM-SD briquettes require an opening with a diameter of 2.3 meters (7.7 ft) and the EB-SD briquettes require an opening with a diameter of 2.3 meters (7.4 ft). However, it is important to point out that both types of briquettes require a slightly larger opening size to ensure reliable flow after 24 hours at rest. It is also clear from this analysis that a much larger conical opening is required to ensure reliable flow in a funnel flow pattern than in a mass flow pattern. The EM-SD and EB-SD briquettes only require a conical opening with a diameter of 0.3 meters (1 ft) to prevent arching in a mass flow pattern, which represents a significant reduction in outlet size. The required opening size is further reduced to prevent arching in a wedge shaped hoppers with a slot outlet (i.e. 0.2 m).

In addition to proper outlet size, mass flow hoppers must be designed with an appropriate hopper angle to ensure a reliable flow pattern. The required hopper angle depends on the determined outlet size, storage time at rest and the friction between briquettes and the wall surface. To determine the required hopper angle, a series of wall friction tests are conducted to determine the angle of sliding friction between the wall surface and the briquettes. An example of the required hopper angles to prevent arching in a mass flow pattern is provided in Table 5-33 for the EM-SD and EB-CS briquettes. These values were calculated for flow through a circular opening with a diameter of 0.3 meters (1 ft), or a slot opening with a length of 0.5 meters (1.5 ft) and width of 0.2 meters (0.5 ft), at a temperature of 22 degrees Celsius (72 °F).

Table 5-33. Required hopper angles to ensure reliable mass flow for Emerald-sawdust (EM-SD) and Eagle Butte-corn stover (EB-CS) briquettes

| Briquette Sample | Wall Surface Material | Conical Hopper Angle (deg. from vertical) | Wedge Hopper Angle (deg. from vertical) |
|---|---|---|---|
| EM-SD | 2B Stainless Steel | 28 | 40 |
| | Carbon Steel | 12 | 22 |
| EB-CS | 2B Stainless Steel | 30 | 42 |
| | Carbon Steel | 19 | 29 |

These results show that a steeper hopper angle is required to ensure reliable flow for the EM-SD briquettes than the EB-CS briquettes. For example, a conical hopper constructed out of or lined with 2B stainless steel must have an angle of 28 degrees (from vertical) to ensure reliable flow of the EM-SD briquettes, as compared to a required angle of 30 degrees for the EB-SD briquettes. These results also prove that a steeper angle is required for a carbon steel surface than one fabricated from stainless steel. In addition, it is clearly shown that conical hoppers require steeper angles of inclination than wedge-shaped hoppers. For example, EM-SD briquettes against a 2B stainless steel surfaces require an additional 12 degrees of slope (i.e. 28 versus 40 degrees from vertical) for a conical hopper as compared to a wedge-shaped hopper.

The final variable that must be determined to design hoppers of required size and strength is the bulk density of briquettes as a function of confining pressure. Bulk density values are used to calculate the required opening sizes and hopper angles in addition to bin and feeder load requirements. The compressibility of briquettes can be defined as the change in bulk density divided by the change in confining pressure. The range of bulk density values for different confining pressure and the calculated compressibility for the EM-SD and EB-CS briquettes is displayed in Table 5-34. The EM-SD briquettes exhibit a higher range of bulk densities (740.1-746.5 kg/m$^3$ [46.2-46.6 lb/ft$^3$]) than the EB-CS briquettes (661.6-671.2 kg/m$^3$ [41.3-41.9 lb/ft$^3$]). This was result was anticipated as the particle density of the EM-SD briquettes is substantially higher than the EB-CS briquettes, yet the shape is very similar. However, the compressibility of the EB-CS briquettes was found to be significantly greater than that of the EM-SD briquettes. Nonetheless, these results suggest that both types of briquettes exhibit excellent flow properties. As a result, design of bins and hoppers for reliable flow of coal-biomass briquettes is quite simple using the procedures outlined above.

Table 5-34. Bulk density and compressibility results for Emerald-sawdust (EM-SD) and Eagle Butte-corn stover (EB-CS) briquettes

| Briquette Sample | Consolidating Pressure ($kg/m^2$) | Bulk Density ($kg/m^3$) | Compressibility ($m^{-1}$) |
|---|---|---|---|
| EM-SD | 220 | 740.1 | 5.15E-05 |
| | 3003 | 743.3 | |
| | 11791 | 746.5 | |
| EB-CS | 220 | 661.6 | 7.71E-05 |
| | 3003 | 664.8 | |
| | 11791 | 671.2 | |

### 5.4.5.3 Characterization of Gasification Behavior

The gasification of the EM-SD and EB-CS briquettes was studied in a moving bed reactor with both pure oxygen and air as the oxidant at an oxygen to steam ratio of 2 to 1 (i.e. 1,400 ml/min of air is approximately equal to 300 ml/min of oxygen). For the pure oxygen tests, oxygen was fed to the gasifier at a rate of 650 milliliters per minute and steam was fed at a rate of 1,300 milliliters per minute. In contrast, air was fed to the gasifier at a rate of 1400 milliliters per minute for the second set of tests, while steam was fed at a rate of 600 milliliters per minute. The syngas was analyzed to determine the composition of hydrogen, carbon monoxide, methane and carbon dioxide. In addition, the energy content of the product gas was measured to calculate the cold gas efficiency of each gasification process. The results of these evaluations are provided in Table 5-35.

Table 5-35. Summary of gasification characterization results for Emerald-sawdust (EM-SD) and Eagle Butte-corn stover (EB-CS) briquettes (adapted from Bhagavatula, 2013)

| Briquette Sample | Oxidizing Conditions | | | Product Gas Composition | | | | Cold Gas Efficiency (%) |
|---|---|---|---|---|---|---|---|---|
| | Air Flow Rate (ml/min) | Oxygen Flow Rate (ml/min) | Steam Flow Rate (ml/min) | $H_2$ (%) | CO (%) | $CH_4$ (%) | $CO_2$ (%) | |
| EM-SD | -- | 650 | 1300 | 11.20 | 18.25 | 9.37 | 47.14 | 28.12 |
| | 1400 | -- | 600 | 7.45 | 7.11 | 0.00 | 10.73 | 43.04 |
| EB-CS | -- | 650 | 1300 | 19.47 | 24.80 | 3.81 | 49.20 | 45.48 |
| | 1400 | -- | 600 | 13.98 | 10.14 | 0.00 | 10.48 | 63.50 |

The syngas produced from the reaction of pure oxygen and steam with the EM-SD briquettes had a composition of 11.20% hydrogen, 18.25% carbon monoxide, 9.37% methane and 47.14% carbon dioxide. In contrast, the syngas produced from the reaction of the same briquettes with air and steam had a composition of 7.45% hydrogen, 7.11% carbon monoxide,

0.00% methane and 10.73% carbon dioxide. Although the absolute value of the hydrogen and carbon monoxide concentrations decreased with air gasification, the ratio of hydrogen and carbon monoxide to carbon dioxide produced (i.e. [$H_2$+CO]: $CO_2$) increased from 0.62 to 1.36. As a result, the cold gas efficiency of the system increased from 28.12% to 43.04%. These product gas concentrations and cold gas efficiencies indicate that the EM-SD briquettes are a good gasification feedstock for the co-production of power and synthetic fuels (Bhagavatula, 2013).

The syngas produced from the reaction of pure oxygen and steam with the EB-CS briquettes had a composition of 19.47% hydrogen, 24.80% carbon monoxide, 3.81% methane and 49.20% carbon dioxide. In contrast, the syngas produced from the reaction of the same briquettes with air and steam had a composition of 13.98% hydrogen, 10.14% carbon monoxide, 0.00% methane and 10.48% carbon dioxide. Although the absolute value of the hydrogen and carbon monoxide concentrations decreased with air gasification, the ratio of hydrogen and carbon monoxide to carbon dioxide produced increased from 0.90 to 2.30. As a result, the cold gas efficiency of the system increased from 45.48% to 63.50%. The EB-CS feedstock is clearly superior to the EM-SD feedstock with respect to gasification performance. This is a direct result of the higher volatile matter content of sub-bituminous coal as compared to bituminous coal, which dramatically increases the energy conversion efficiency of the process. Also, the higher porosity of the EB-CS briquettes aids in the thermal decomposition of the feedstock, which in turn increases the cold gas efficiency. These product gas concentrations and cold gas efficiency values indicate that the EB-CS briquettes are an exceptional gasification feedstock for the co-production of power and synthetic fuels.

## 5.5 Summary and Conclusions

Experimental optimization of coal-biomass briquette production is an essential task to improve the strength and durability of briquettes. In support of this challenge, an exhaustive bench-scale study was conducted to examine the most significant feedstock, additive and roll press variables in coal-biomass briquette production. Additional work was performed to identify optimum process conditions for each variable, which were defined for this study as the conditions that contribute to production of coal-biomass briquettes with the greatest crushing strength and mechanical durability. In addition, work was conducted to compare and contrast the

quality of briquettes composed of four coal types (i.e. 3 bituminous and 1 sub-bituminous) and five biomass types (i.e. corn stover, switchgrass, miscanthus, wheat straw, and sawdust). Lastly, a comprehensive series of tests were conducted to characterize the physical properties, flow properties, and gasification behavior of selected coal-biomass briquettes to verify the enhanced quality of co-briquetted feedstocks.

As a result of this study, the following conclusions can be drawn regarding bench-scale production of coal-biomass briquettes over the range of variables evaluated:

- Biomass content is the most statistically significant mixture variable with regard to the particle density of coal-biomass briquettes. For all types of coal and biomass evaluated, an increase in biomass content causes a direct reduction in particle density.
- Biomass content is the most statistically significant mixture variable with regard to the crushing strength of binderless coal-biomass briquettes. For all types of coal and biomass evaluated, an increase in biomass content causes a direct increase in crushing strength.
- Water content is the most statistically significant mixture variable with regard to the mechanical durability of binderless coal-biomass briquettes. For all types of coal and biomass evaluated, a clear optimum water content can be identified where mechanical durability reaches a maximum value.
- Biomass top size is not a statistically significant mixture variable with regard to the particle density, crushing strength and mechanical durability of coal-biomass briquettes.
- Differences in the quality of coal-biomass briquettes composed of different types of bituminous coal with identical top sizes can be attributed to differences in the distribution modulus and ash content of the coals. Briquette quality increases with a corresponding increase in distribution modulus and a corresponding decrease in ash content.
- Starch content is a very statistically significant mixture variable with regard to the crushing strength and mechanical durability of coal-biomass briquettes. An increase in starch content causes a direct increase in crushing strength and mechanical durability.
- Cure time is a statistically significant process variable with regard to the crushing strength of coal-biomass briquettes. A period of 6 days is recommended to cure the briquettes for which this variable was studied.
- Corn stover exhibits the best properties of the biomass types studied with regard to the crushing strength and mechanical durability of coal-biomass briquettes.

- Roll torque is the most statistically significant roll press operating variable with regard to the particle density, crushing strength and mechanical durability of coal-biomass briquettes. An increase in roll torque causes a direct increase in particle density, crushing strength and mechanical durability.
- Roll force is a statistically significant roll press operating variable with regard to the particle density, crushing strength and mechanical durability of coal-biomass briquettes. An increase in roll torque causes a direct increase in particle density, crushing strength and mechanical durability.
- Roll speed is a statistically significant roll press operating variable with regard to the particle density of coal-biomass briquettes. An increase in roll speed causes a direct reduction in particle density.
- Binderless coal-biomass briquettes produced at optimized conditions exhibit very high crushing strength and mechanical durability values, which indicate that the briquettes would largely remain competent in the presence of forces encountered in handling, storage and transportation.
- Binderless coal-biomass briquettes produced at optimized conditions exhibit poor water resistance, which indicates that additional investigation of this matter is required.
- Binderless coal-biomass briquettes produced at optimized conditions exhibit excellent flow properties, which indicates that proper hopper design is straightforward.
- Binderless coal-biomass briquettes produced at optimized conditions exhibit excellent gasification behavior with regard to product gas composition and cold gas efficiency. This confirms that coal-biomass briquettes are exceptional gasification feedstocks for the co-production of power and synthetic fuels.

# Chapter 6

# Production of Water-Resistant Coal-Biomass Briquettes

## 6.1 Abstract

A study was conducted to evaluate the potential for several proprietary wood-derived chemicals to improve the water resistance of coal-biomass briquettes. Two methods for application of the chemicals were examined: (1) conventional binder application as a powder prior to briquette production and (2) briquette coating. For the conventional binder application method, five of the six wood-derived chemicals significantly improved the water resistance of the coal-biomass briquettes. The best performing wood-derived chemical improved the water resistance of the briquettes by 63% and 77% at binder contents of 2.5% and 5.0%, respectively. For the briquette coating technique, initial results indicated that each of the wood-derived chemicals outperformed briquettes with no coating and four of the five chemicals outperformed briquettes with a paraffin wax coating. The best performing wood-derived chemical with respect to water resistance improved the water resistance of the briquettes by 97%. Similarly, the final mechanical durability of briquettes was improved by approximately 400% with the best performing wood-derived chemical. A series of detailed coating evaluations were performed which further exemplify the benefits of the wood-derived chemical coatings and validated the results of the preliminary tests. The detailed evaluations also provide insight to the influence of the chemical coatings on other important properties of coal-biomass briquettes. Furthermore, the results of the detailed evaluations provide evidence that these coatings can be successfully used to improve the durability and water resistance of briquettes comprised of different coal types (i.e. bituminous and sub-bituminous) and different biomass types (i.e. sawdust and corn stover). However, selection of the optimum wood-derived chemical for any coal-biomass briquette application depends primarily on the cost of each chemical and the desired level of briquette

durability and water resistance. Therefore, it is recommended that the chemical coating type and application method be chosen independently for every unique coal-biomass briquette operation.

## 6.2 Introduction

### 6.2.1 Problem Statement

Co-utilization of biomass with coal in existing coal-fired facilities presents a unique opportunity to reduce greenhouse gas emissions and increase energy production from renewable resources. Significant interest in this opportunity has led to more than 150 coal-fired power stations across the world co-firing coal and biomass on a commercial or trial basis as of 2009 (Fernando, 2009). These co-firing experiences have revealed a number of technical challenges including upstream issues, such as biomass availability, transportation, storage, and handling, as well as problems encountered during energy conversion, such as fouling, corrosion, inconsistent feeding and segregation (Basu et al., 2011; Sami et al., 2001). Recent studies suggest that many of these challenges can be mitigated by reconstituting coal-biomass mixtures into larger particles. Specifically, roll press briquetting has been investigated to produce homogeneous, free-flowing feedstocks that minimize handling and segregation problems often encountered with combustion and gasification systems (Taulbee et al., 2010; Honaker et al., 2005). However, the absorption of water and subsequent disintegration of coal-biomass briquettes remains a major limitation to the design of low-cost storage and transportation systems for co-firing operations. As a result, there is a growing interest in the development of economically feasible methods to sustain the physical and mechanical integrity of fuel briquettes in the presence of water (Wang et al., 2011; Motaung et al., 2007; Saglam et al., 1990).

### 6.2.2 Briquette Water Resistance

Several different methods have been investigated to improve the water resistance of fuel briquettes. The most commonly employed method is coating individual fuel particles with a chemical binder prior to briquette production. For example, Bratton et al. (2010) evaluated a novel fine coal briquetting process that included the application of a proprietary binder to improve the strength and weathering properties of coal briquettes. The authors found that a wetting and drying cycle had minimal impact on the durability of coal briquettes produced with the proprietary binder. However, the cost of the novel binder is not discussed and thus is likely a

limiting factor to this approach. Furthermore, Taulbee et al. (2009) investigated twelve different binders including molasses, guar gum, corn starch, wheat starch and paper sludge to improve the strength and water resistance of briquettes produced with fine coal and sawdust. The study found that the compressive strength of the coal-sawdust briquettes was significantly reduced after submergence in water for eight hours. These and other water soluble binders are generally not recommended to improve the water resistance of fuel briquettes (Mills, 1908).

Another method that has been investigated to improve the water resistance of fuel briquettes is coating with water insoluble chemicals. Chemical coatings can be applied by many different techniques including dipping, brushing, flow coating, roller coating and spraying (Freitag, 1996). Of these methods, dipping and spraying present the greatest opportunity for fuel briquette coating due to the size and shape of briquettes. Both methods generally require heating the material to reduce the viscosity, which leads to a reduction in film thickness and thus a reduction in chemical consumption. When the materials are heated prior to application, these techniques are referred to as hot dipping and hot spraying (Freitag, 1996).

Specific techniques for coating briquettes have been disclosed in patents filed in the United States and Australia. Goss (1938) patented a hot spraying mechanism for applying paraffin wax to wood briquettes for the purpose of protecting against the absorption of moisture. Lundwall (1939) developed a machine that employs the dipping technique to coat briquettes composed of metal cuttings with a mixture of water and Portland cement. Furthermore, Trechock (1973) described a spray coating method to overcome the problem of airborne dust associated with rail shipment of coke briquettes. Using this method, the briquettes are treated with an aqueous dispersion of solid film former such as sodium silicate, blackstrap molasses, turpentine resins and pitches derived from black coal or petroleum. Bates et al. (1988) disclosed a method of coating briquettes composed of brown coal, bituminous coal, anthracite or other carbonaceous materials such as wood. The patent describes a water based emulsion comprising an acrylic polymer based on acrylic ester monomer that can be applied by spraying or dipping. Finally, Shimasaki et al. (2003) developed a method of producing coal briquettes with high strength and excellent water resistance by mixing starch with the coal particles prior to briquette production and coating the surface of the briquettes with a heavy oil component simultaneously with or after briquette formation.

### 6.2.3 Research Objective

The purpose of this study was to evaluate the potential for several proprietary wood-derived chemicals to improve the water resistance of coal-biomass briquettes. A preliminary screening study was conducted to examine the technical feasibility of two application methods for each wood-derived chemical: (1) conventional binder application, wherein chemicals were mixed with coal and biomass particles prior to briquette production, and (2) coating application, wherein coal-biomass briquettes were dipped in heated chemicals to coat the exterior surface of the briquettes. To establish the relative performance of each wood-derived chemical for both application methods, additional evaluations were performed without chemicals and with commonly used chemicals. An additional series of detailed coating evaluations were conducted on optimal co-firing briquette formulations to validate the performance of the wood-derived chemical coatings and to measure several additional properties of the coated briquettes.

## 6.3 Experimental

### 6.3.1 Materials

All briquettes produced for the preliminary screening study were composed of bituminous coal and corn stover. The coal was obtained from the clean coal stockpile of Alpha Natural Resources' Emerald mine preparation plant in Waynesburg, Pennsylvania (referred to as Emerald coal). Prior to briquetting, the coal was successively crushed in a jaw crusher, roll crusher and a grinder. The coal was then screened to a top size of one millimeter using a Uniflex two-deck screen, air dried for one week, split into two kilogram lots and stored in sealed plastic bags. The moisture content of the coal prior to briquette production was 1.60% (dry basis), which was determined by oven drying at 105 degrees Celsius for 24 hours. The size distribution of the crushed coal was measured by wet screening and analyzed using the Rosin-Rammler equation (Figure 6-1). Based on this analysis, the Emerald coal was found to have a mass median diameter of 301 microns, a size modulus of 0.43 and a distribution modulus of 1.02. Ultimate and proximate analyses were also conducted to characterize the chemical composition of the coal (Table 6-1). Notable results of the analyses include a moisture and ash free heating value of 35,513 kJ/kg (15,268 Btu/lb), an ash content of 9.37% (dry basis) and a sulfur content of 3.04% (dry basis).

Two types of briquettes were produced for the detailed coating evaluations. The first type of briquettes were composed of the Emerald coal and sawdust, while the second type of briquettes were composed of a sub-bituminous coal and corn stover. The sub-bituminous coal was obtained from the raw coal stockpile of Alpha Natural Resources' Eagle Butte mine in Gillette, Wyoming (referred to as Eagle Butte coal). Prior to briquetting, this coal was successively crushed in a jaw crusher, roll crusher and grinder. The coal was then screened to a top size of one millimeter using a Uniflex two-deck screen, air dried for one week, oven dried at 105 degrees Celsius for 48 hours, split into two-kilogram lots and stored in sealed plastic bags. The moisture content of the Eagle Butte coal prior to briquette production was 1.70% (dry basis), which was determined by oven drying at 105 degrees Celsius for 24 hours. The size distribution was again analyzed using the Rosin-Rammler equation (Figure 6-1), which indicated that the coal had a mass median diameter of 295 microns, a size modulus of 0.41 and a distribution modulus of 1.16. Ultimate and proximate analyses were also conducted to characterize the chemical composition of the Eagle Butte coal (Table 6-1). Notable results of the analyses include a moisture and ash free heating value of 29,015 kJ/kg (12,474 Btu/lb) and an ash content of 7.89% (dry basis).

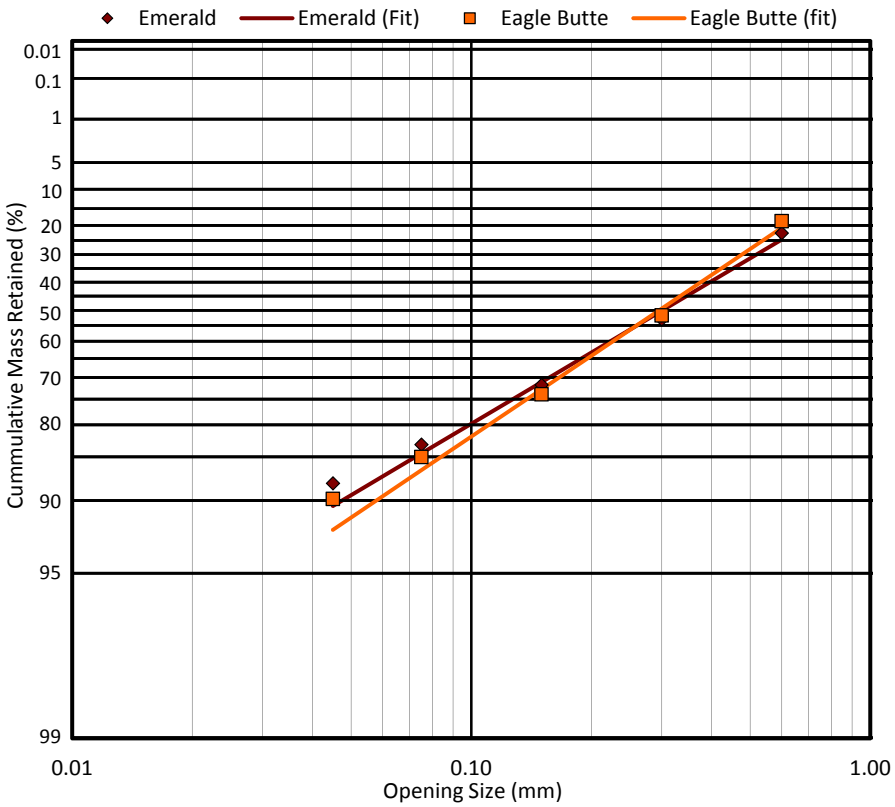



Figure 6-1. Particle-size distribution of coal samples

Table 6-1. Chemical properties of coal and biomass feedstocks

| Chemical Property | Emerald | | Eagle Butte | | Corn Stover | | Sawdust | |
|---|---|---|---|---|---|---|---|---|
| | As Received | Dry Basis | As Received | Dry Basis | As Received | Dry Basis | As Received | Dry Basis |
| Moisture (%) | 4.28 | -- | 29.08 | -- | 12.95 | -- | 14.08 | -- |
| Ash (%) | 8.97 | 9.37 | 5.60 | 7.89 | 4.36 | 5.01 | 0.22 | 0.26 |
| Sulfur (%) | 3.04 | 3.18 | 0.64 | 0.90 | 0.09 | 0.10 | 0.03 | 0.03 |
| Volatiles (%) | 37.59 | 39.27 | 40.89 | 57.66 | 71.49 | 82.13 | 78.64 | 81.53 |
| Fixed Carbon (%) | 49.16 | 51.36 | 24.43 | 34.45 | 11.19 | 12.86 | 7.05 | 8.21 |
| Carbon (%) | 74.26 | 77.58 | 47.08 | 66.38 | 46.37 | 53.27 | 51.66 | 60.12 |
| Hydrogen (%) | 4.91 | 5.13 | 4.00 | 5.64 | 4.94 | 5.67 | 5.40 | 6.28 |
| Nitrogen (%) | 1.39 | 1.45 | 0.70 | 0.99 | 0.54 | 0.62 | 0.02 | 0.02 |
| Oxygen (%) | 3.15 | 3.29 | 12.91 | 18.20 | 30.75 | 35.33 | 28.60 | 33.29 |
| HHV (kJ/kg) | 30,808 | 32,185 | 18,955 | 26,726 | 16,347 | 18,778 | 18,864 | 21,955 |
| MAF HHV (kJ/kg) | -- | 35,513 | -- | 29,015 | -- | 19,769 | -- | 22,013 |

The corn stover used for this study was obtained as large round bales from a farm in Blacksburg, Virginia operated by Virginia Tech. The bales were processed in a Jordan Reduction Solutions knife mill equipped with a 4.75-millimeter screen and stored in a sealed bulk bag prior to use. Particle-size distribution was not determined for the processed corn stover because

previous attempts to collect this information has indicated that the results are skewed due to the elongated shape of the milled particles (i.e. elongated particles tend to screen differently than round particles). Prior to briquette production the moisture content of the corn stover was 11.35% (dry basis), which was determined by oven drying at 105 degrees Celsius for 24 hours. Ultimate and proximate analyses were conducted on the corn stover sample, the results of which are presented in Table 6-1. Notable results of the analyses include a moisture and ash free heating value of 19,769 kJ/kg (8,499 Btu/lb), an ash content of 5.01% (dry basis) and a sulfur content of 0.10% (dry basis).

The sawdust used for this study was kiln-dried eastern white pine dust and shavings, which was obtained in bulk bags from Turman Sawmill in Hillsville, Virginia. Prior to briquette production, the sawdust was screened to a top size of 1.2 millimeters using a Sweco vibrating separator and stored in 18.9 liter (5 gal) buckets. Again, particle-size distribution was not determined due to the inherently low accuracy of such measurements. The moisture content of the sawdust was reduced to 0.20% by oven drying at 105 degrees Celsius for 24 hours. The ultimate and proximate analyses results for the sawdust sample are displayed in Table 6-1. Notable results of the analyses include a moisture and ash free heating value of 22,013 kJ/kg (9,464 Btu/lb), an ash content of 0.26% (dry basis) and a sulfur content of 0.03% (dry basis).

Several different chemicals were evaluated throughout this study for the ability to improve the water resistance of coal-biomass briquettes. For conventional binder tests, the chemicals evaluated included pregelatinized wheat starch, obtained from Archer Daniels Midland Company, and six proprietary wood-derived chemicals provided by Georgia-Pacific Chemicals (G16, G88, G89, G90, G97 and G98). All of the wood-derived chemicals were solid at room temperature except G16, which was a highly viscous liquid at room temperature. For briquette coating tests, the chemicals evaluated included paraffin wax and the five solid-state chemicals provided by Georgia-Pacific (G88, G89, G90, G97 and G98). The G97 chemical was used for the additional detailed coating evaluations because of the performance and relative cost of this chemical.

### 6.3.2 Briquette Production

Pill-shaped briquettes (approximately 43 x 19 x 14 mm) were produced with a Komarek B-100R laboratory roll press equipped with 13-centimeter diameter rolls. The machine is

comprised of two counter rotating rolls, two hydraulic cylinders, a horizontal tapered screw and a paddle feeder. A schematic diagram of the roll press and the laboratory installation are depicted in Figure 5-6.

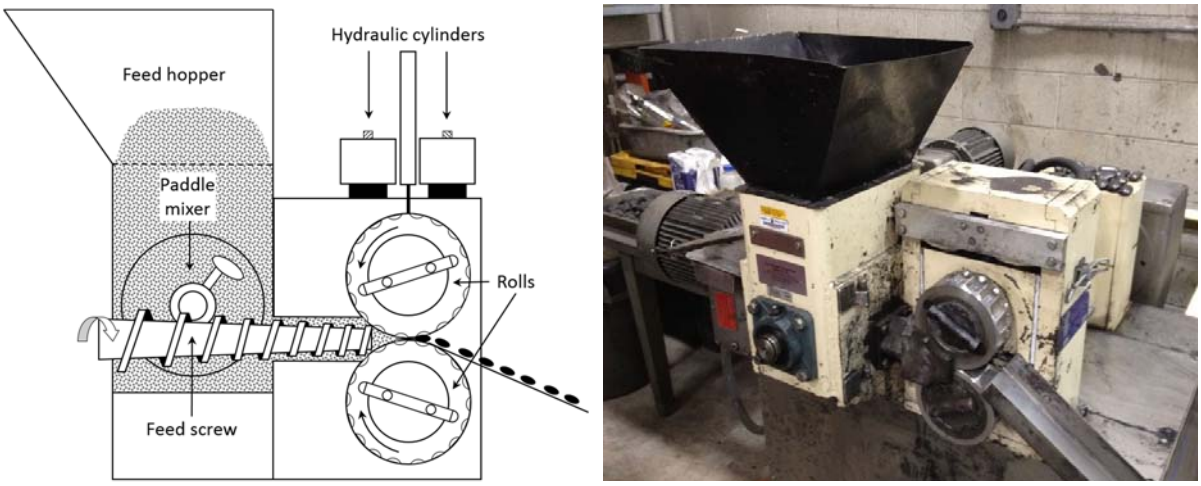



Figure 6-2. Komarek B-100R roll press (left) schematic diagram (modified from Guigon & Simon, 2003) and (right) laboratory installation

The hydraulic cylinders control the position of the upper roll and thus control the gap between the rolls. The paddle feeder is driven by a fixed speed motor and distributes the material to the horizontal screw that in turn feeds material to the rolls. The counter rotating rolls and the horizontal screw are driven by variable speed motors, which enable adjustment of the torque applied to the material from the rolls and screw. For all laboratory experiments, the rolls of the B-100R were driven at a motor speed of 450 rotations per minute with 100 kilonewtons of hydraulic force. The horizontal screw speed was adjusted during briquette production to maintain a roll torque of approximately 1800 newton-meters.

For conventional binder evaluations, briquettes were produced in two kilogram batches at a target moisture content of 5 percent with 20 percent corn stover and either 80 percent coal (no binder), 77.5 percent coal (2.5 percent binder) or 75 percent coal (5 percent binder). Prior to briquette production, each wood-derived chemical was crushed and screened to a top size of one millimeter to facilitate mixing in powder form. The coal, corn stover and binding additives were mixed for five minutes in a Hobart A200 18.9 liter (5 gal) commercial mixer and directly co-briquetted in the Komarek B-100R. Immediately after formation, the briquettes were screened across a Sweco vibrating separator equipped with a 12.7 millimeter (0.5 in) screen to remove excess fines. Finally, the briquettes were set out for 24 hours to facilitate curing of the binder

prior to evaluations for water content, particle density, mechanical durability, crushing strength and water resistance. The results of these evaluations are discussed in Section 6.4.1.

For the preliminary briquette coating evaluations, a single six kilogram batch of briquettes was produced with 20 percent corn stover and 80 percent coal at a target moisture content of five percent. The coal and corn stover were mixed for five minutes in a Hobart A200 18.9 liter (5 gal) commercial mixer and briquetted in the Komarek B-100R. As outlined above, these briquettes were also screened immediately after formation to remove excess fines and set out for 24 hours to maintain consistency in the experimental approach. For each chemical evaluated, coating of briquettes was conducted in two batches for two separate series of evaluations: (1) water uptake tests and (2) a series of sequential mechanical durability and water uptake tests. Each chemical was heated in a 250-milliliter glass beaker to 160 degrees Celsius in a laboratory oven operated at 200 degrees Celsius. Briquettes were submerged individually into the heated chemical for approximately two seconds and placed on a perforated platform inside the oven for ten minutes. Next, the perforated platform was removed from the oven, each briquette was flipped over and the platform was placed back into the oven for an additional five minutes. The purpose of placing the briquettes on the perforated platform inside the oven was to allow excess material to drip off the briquettes to reduce the applied chemical dosage. Finally, the coated briquettes were removed from the oven and set out for one hour to permit cooling of the applied chemical prior to evaluations for water resistance, mechanical durability and chemical dosage. Results of these evaluations are discussed in Section 6.4.2.

For the detailed coating evaluations, Emerald-sawdust (EM-SD) and Eagle Butte-corn stover (EB-CS) briquettes were produced in eight kilogram batches with 70 percent coal and 30 percent biomass. The EM-SD and EB-CS briquettes were produced at target moisture contents of 2.20 and 18.50 percent, respectively. These moisture contents were selected using the optimization tools featured in the statistical models presented in Chapter 5. After production, the briquettes were split into two separate batches: one for coating and the other for directly testing without a coating. Six batches of 50 briquettes were coated with the G97 chemical following the same procedure described for the preliminary coating tests. After cooling for one hour, both the coated and uncoated briquettes were evaluated for tensile strength, crushing strength, elasticity, mechanical durability, attritability, friability, water content, particle density, water resistance and chemical dosage. Results of these evaluations are discussed in Section 6.4.3.

## 6.3.3 Briquette Characterization

### 6.3.3.1 Water Content

The water content of briquettes was determined by drying five briquettes for 24 hours at 105 degrees Celsius in a drying oven. The mass of water in the briquettes was calculated by subtracting the dry mass of the briquettes from the initial mass before drying. The water content was then calculated by:

$$w = m_w/m_s \quad \text{(Eq. 6-1)}$$

where $w$ is the water content, $m_w$ is the mass of water and $m_s$ is the dry mass of the briquettes. Water content was measured after the 24-hour curing period for the conventional binder tests and after the one hour cooling period for the coating tests. Water content of the feed material was measured prior to briquette production using an AND MF-50 moisture analyzer set at 105 degrees Celsius. Feed samples were dried until the change in mass was reduced to 0.05 percent per minute, at which point the displayed value was reported as the water content of the feed.

### 6.3.3.2 Particle Density

The particle density of briquettes was calculated by first measuring the initial (wet) density and then calculating the dry density ($\rho_d$) based on the measured water content by:

$$\rho_d = \rho_{wet}/(1 + w) \quad \text{(Eq. 6-2)}$$

where $\rho_{wet}$ is the calculated wet density and $w$ is the calculated water content. A density determination rig was used to measure the apparent mass of briquettes in a solution of water and detergent. Wet density ($\rho_{wet}$) was then calculated by:

$$\rho_{wet} = (m_a/(m_a - m_b))\rho_w \quad \text{(Eq. 6-3)}$$

where $m_a$ is the mass of the briquette in air, $m_b$ is the apparent mass of the briquette in water and $\rho_w$ is the density of the liquid. Wet density was measured after the 24-hour curing period for the conventional binder tests and after the one hour cooling period for the coating tests. For both cases, the procedure was repeated for 10 briquettes and the average of the 10 values was reported as the dry particle density.

### 6.3.3.3 Mechanical Durability

The mechanical durability of briquettes was measured by tumbling 20 briquettes for five minutes at 40 rotations per minute in a 0.3 meter (1 ft) diameter PVC cylinder equipped with three 50.8 millimeter (2 in) lifters. The briquettes were then removed from the cylinder and

screened in a Ro-tap sieve shaker for 30 seconds over a 4.75-millimeter sieve. The mechanical durability (*MD*) of the briquettes was then calculated by:

$$MD = 100 \times \left(m_{final}/m_{initial}\right) \quad \text{(Eq. 6-4)}$$

where $m_{final}$ is the mass of briquettes retained on the 4.75-millimeter sieve and $m_{initial}$ is the initial mass of the briquettes prior to durability testing.

#### 6.3.3.4 Crushing Strength

The crushing strength of briquettes was determined using a Mark-10 M5-500 digital force gauge fitted with a 101.6 millimeter (4 in) diameter aluminum plate. The force gauge was mounted to a Mark-10 TSA750 manual test stand equipped with a 25.4 millimeter (1 in) diameter aluminum plunger that was used to apply force to the briquettes until failure. The force gauge was configured with a break detect feature which stops data acquisition once the applied force drops to 95 percent of the maximum force attained during each test. The crushing strength of each briquette was then reported as the maximum force attained during each test. To improve the accuracy of readings, an aluminum bar (51 x 8 x 8 mm) was placed upon the aluminum plate with each briquette then placed atop and parallel to the bar for testing. Evaluations were performed on 25 briquettes and the crushing strength was reported as the average of the 25 values.

#### 6.3.3.5 Water Resistance

The water resistance of briquettes was determined using an apparatus designed to simulate precipitation that briquettes may encounter during storage and transportation. To calculate water resistance, five briquettes were subjected to a 15 second water spray at a flow rate of 11.4 liters per minute (3 gal/min) from a height of 0.5 meters (1.5 ft) above the briquettes. Water resistance was reported as the water uptake of the briquettes that resulted from this spray test, with water uptake ($u$) calculated by:

$$u = \left(m_f - m_i\right)/m_i \quad \text{(Eq. 6-5)}$$

where $m_i$ is the initial mass of briquettes and $m_f$ is the mass of briquettes after the water spray.

#### 6.3.3.6 Chemical Dosage

For coating tests, the chemical dosage applied to the briquettes was determined by calculating the mass of briquettes before and after the application of the chemical coating. The

mass of each chemical coating was calculated by subtracting the coated mass of the briquettes from the initial mass. The chemical dosage (*d*) was then calculated by:

$$d = m_c / m_b \quad \text{(Eq. 6-6)}$$

where $m_c$ is the mass of the chemical coating and $m_b$ is the initial mass of the briquettes. Chemical dosage was measured immediately after the one hour cooling period.

#### 6.3.3.7 Friability

The friability of briquettes was measured by dropping 20 briquettes twice from a height of 1.8 meters (6 ft) onto a steel plate using a modified shatter test device. The briquettes were then screened for 30 seconds in a Ro-tap sieve shaker over a 4.75-millimeter sieve. The friability (*F*) of the briquettes was then calculated by:

$$F = 100 \times \left(m_{final} / m_{initial}\right) \quad \text{(Eq. 6-7)}$$

where $m_{final}$ is the mass of briquettes retained on the 4.75-millimeter sieve and $m_{initial}$ is the initial mass of the briquettes prior to friability testing.

#### 6.3.3.8 Attritability

The attritability of briquettes was measured by screening 20 briquettes for five minutes in a Ro-tap sieve shaker over a 4.75-millimeter sieve. The attritability (*A*) of the briquettes was then calculated by:

$$A = 100 \times \left(m_{final} / m_{initial}\right) \quad \text{(Eq. 6-8)}$$

where $m_{final}$ is the mass of briquettes retained on the 4.75-millimeter sieve and $m_{initial}$ is the initial mass of the briquettes prior to attritability testing.

#### 6.3.3.9 Tensile Strength

To measure tensile strength, individual briquettes were crushed between two flat compression plates with the briquette standing tall (i.e. with the long axis of the briquette parallel to the axis of force application). This was accomplished using a Mark-10 M5-500 digital force gauge fitted with a 101.6 millimeter (4 in) diameter aluminum plate. The force gauge was mounted to a Mark-10 TSA750 manual test stand equipped with a 25.4 millimeter (1 in) diameter aluminum plunger that was used to apply force to the briquettes until failure. The force gauge was configured with a break detect feature which stops data acquisition once the applied force drops to 95 percent of the maximum force attained during each test. Tensile strength of

each briquette was then designated as this maximum force. Evaluations were performed on 25 briquettes and the tensile strength was reported as the average of the 25 values.

#### 6.3.3.10 Elasticity

To measure the elasticity of briquettes, the same equipment and procedure that was described for crushing strength evaluations was utilized. However, in this instance the test stand was fitted with a Mark-10 ESM001 digital travel display to record the displacement of briquettes while the load was applied by the plunger. This installation was required to determine the spring constant (*SC*) of the briquettes, which is calculated by:

$$SC = (F_2 - F_1)/(x_2 - x_1) \quad \text{(Eq. 6-9)}$$

where $F_2$ is the maximum force applied during elastic deformation, $F_1$ is the minimum force applied during elastic deformation, $x_2$ is the displacement that corresponds with $F_2$, and $x_1$ is the displacement that corresponds with $F_1$. These values are obtained from the force versus displacement curve that is produced during data acquisition. The force gauge was configured to record two force and displacement data points per second with the break detect feature activated. Evaluations were performed on 25 briquettes and the elasticity was reported as the average calculated spring constant value for all 25 measurements.

## 6.4 Results and Discussion

### 6.4.1 Conventional Binder Evaluations

A series of conventional binder tests were conducted for the preliminary performance evaluation of six wood-derived chemicals in powder form when mixed with coal and biomass prior to briquette formation. For comparison, two additional sets of briquettes were produced with pregelatinized wheat starch and one additional batch was produced with no binder. For each chemical evaluated, briquettes were produced with a binder content of 2.5 percent and 5.0 percent. The evaluations performed for the conventional binder tests included water content, dry density, crushing strength, mechanical durability and water uptake. A detailed summary of the results of these evaluations are presented in Table 6-2. One observation from briquette production and evaluation was the poor performance of the G16 binder. Although the water content of the G16 briquettes was similar to others, the liquid state of the G16 binder shifted the

location of optimum moisture for maximum compaction density and thus reduced the strength and durability of the briquettes.

Table 6-2. Summary of conventional binder evaluation results

| Chemical Binder | Binder Content (%) | Water Content | | Particle Density ($g/cm^3$) | Crushing Strength (N) | Mechanical Durability (%) | Water Uptake (%) |
|---|---|---|---|---|---|---|---|
| | | Feed | Briquettes | | | | |
| No binder | 0.0 | 0.051 | 0.027 | 1.16 | 1,312 | 92.5 | 15.8 |
| Starch | 2.5 | 0.053 | 0.032 | 1.15 | 1,610 | 95.4 | 19.6 |
| Starch | 5.0 | 0.050 | 0.034 | 1.16 | 1,806 | 96.0 | 21.7 |
| G16 | 2.5 | 0.038 | 0.029 | 1.02 | 494 | 29.9 | 165.2 |
| G16 | 5.0 | 0.038 | 0.028 | 1.01 | 271 | 26.3 | 190.6 |
| G88 | 2.5 | 0.049 | 0.030 | 1.13 | 1,183 | 90.5 | 6.4 |
| G88 | 5.0 | 0.045 | 0.027 | 1.13 | 1,085 | 90.2 | 7.0 |
| G89 | 2.5 | 0.046 | 0.026 | 1.15 | 1,334 | 93.5 | 6.4 |
| G89 | 5.0 | 0.050 | 0.026 | 1.15 | 1,352 | 93.8 | 5.9 |
| G90 | 2.5 | 0.048 | 0.029 | 1.14 | 1,250 | 90.3 | 5.8 |
| G90 | 5.0 | 0.049 | 0.023 | 1.14 | 1,228 | 88.7 | 3.7 |
| G97 | 2.5 | 0.045 | 0.026 | 1.14 | 1,343 | 92.3 | 9.0 |
| G97 | 5.0 | 0.044 | 0.027 | 1.14 | 1,495 | 91.4 | 5.8 |
| G98 | 2.5 | 0.049 | 0.027 | 1.15 | 1,303 | 91.0 | 6.4 |
| G98 | 5.0 | 0.044 | 0.027 | 1.12 | 1,499 | 90.7 | 5.4 |

Figure 6-3 shows the dry density values for each binder type and dosage. From this figure it is clear that the binderless briquettes had the greatest dry density (1.16 $g/cm^3$) and the addition of each binder led to a reduction in dry density. One possible explanation for this result is the reduction in average particle density that results from addition of binding additives with a lower density than coal. The only exception to this finding occurred with the addition of five percent starch, which also produced a dry density of 1.16 $g/cm^3$. For five of the seven binder types, the increase in binder content from 2.5 percent to 5.0 percent resulted in a reduction of the dry density of the briquettes. This further exemplifies the conclusion that the addition of a lower density wood-derived chemical will reduce the dry density of coal-biomass briquettes. Again, the only significant exception was the starch briquettes, which increased in density with an increase in binder content from 2.5 percent to 5.0 percent. Overall, the starch binder outperformed each of the wood-derived chemicals with respect to dry density. However, binderless briquetting with feed moisture optimization remains the best technique to maximize the dry density of coal-biomass briquettes.

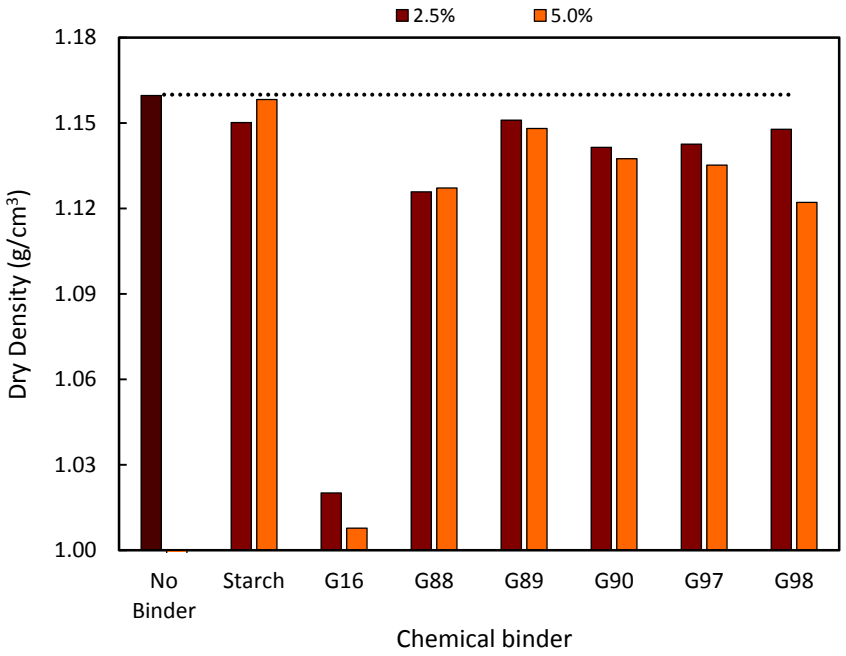



Figure 6-3. Dry density of briquettes with conventional binder application

The variations in briquette crushing strength that resulted from addition of each chemical binder are displayed in Figure 6-4. Several of the briquettes with added binder exhibited higher crushing strength than the binderless briquettes (1,312 N [295 $lb_f$]), including those produced with starch (1,610 N [362 $lb_f$], 1,806 N [406 $lb_f$]), G89 (1,334 N [300 $lb_f$], 1,352 N [304 $lb_f$]), G97 (1,343 N [302 $lb_f$], 1,495 N [336 $lb_f$]) and G98 (1,303 N [293 $lb_f$], 1,499 N [337 $lb_f$]). The crushing strength of briquettes produced with the G16 chemical was significantly lower than each of the other batches (494 N [111 $lb_f$], 271 N [61 $lb_f$]), which again is thought to be the direct result of a shift in the location of optimum moisture for maximum compaction due to the liquid state of the chemical. The incremental addition of the wood-derived chemicals from 2.5 percent to 5.0 percent showed mixed results with respect to briquette crushing strength. Crushing strength of briquettes produced with three of the chemicals (i.e. G16, G88 and G90) decreased with a corresponding increase in binder content. Conversely, the crushing strength of briquettes produced with the other three wood-derived chemicals (i.e. G89, G97 and G98) increased with an increase in binder content. This shows that briquettes produced with binders that exceed the strength of their binderless counterpart at a low binder dosage will continue to increase in strength with an increase in binder content. Likewise, briquettes produced with binders that exhibit inferior strength than their binderless counterpart at low binder dosages will continue to

decrease in strength with an increase in binder content. Overall, the starch binder outperformed each of the wood-derived chemicals with respect to crushing strength.

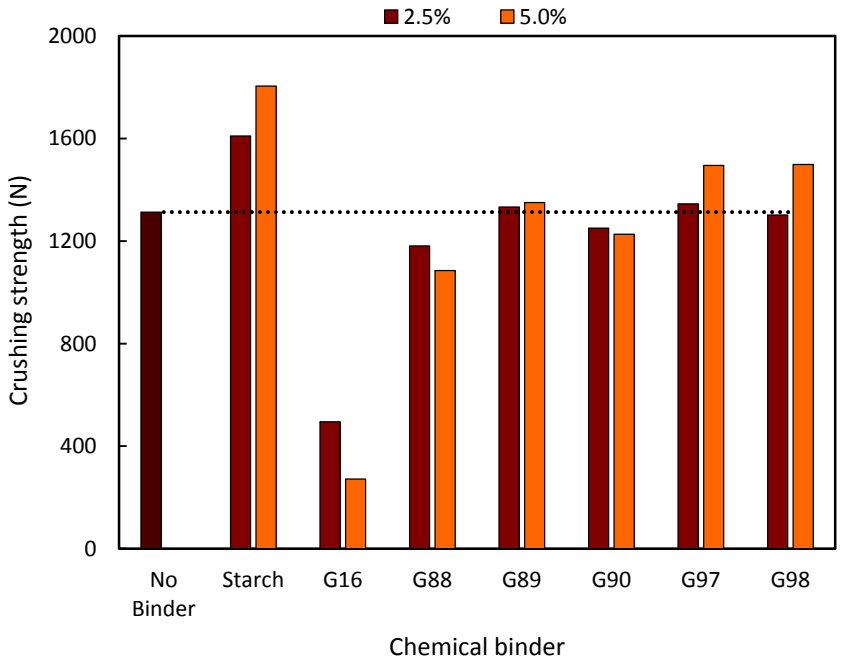



Figure 6-4. Crushing strength of briquettes with conventional binder application

The mechanical durability results for each chemical binder are displayed in Figure 6-5. Only the starch (95.4, 96.0%) and G89 (93.5, 93.8%) briquettes exhibited greater mechanical durability than the binderless briquettes (92.5%). Except for the G16 chemical, all of the other wood-derived chemicals produced briquettes with a mechanical durability slightly less than the binderless briquettes (88.7-92.3%). Similar to the crushing strength results, briquettes produced with binders that exceed the durability of their binderless counterpart at a low binder dosage continue to increase in durability with an increase in binder content. Likewise, briquettes produced with binders that exhibit inferior durability than their binderless counterpart at low binder dosages continue to decrease in durability with an increase in binder content. Overall, the starch binder outperformed each of the wood-derived chemicals with respect to mechanical durability.

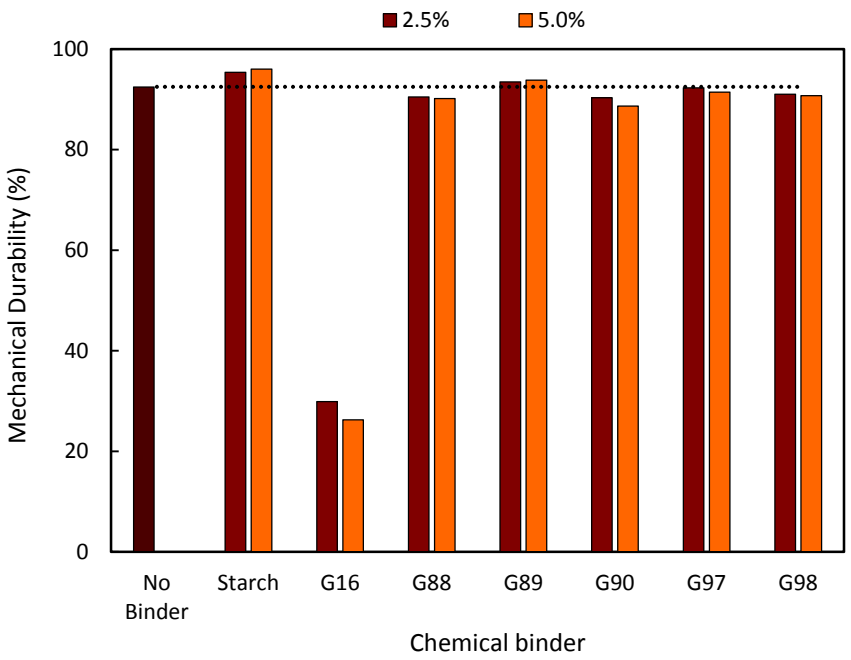



Figure 6-5. Mechanical durability of briquettes with conventional binder application

Figure 6-6 provides a visual representation of the water uptake results for binderless briquettes and those produced with each of the chemical binders. In this chart, a lower value is desirable as it corresponds to less water absorbed during the simulated rainfall period. The binderless briquettes absorbed less water (15.8%) than the starch briquettes (19.6, 21.7%) and the G16 briquettes (165.2, 190.6%). Conversely, briquettes produced with the other five wood-derived chemicals absorbed less water than the binderless briquettes, and thus improved the water resistance. The best performing wood-derived chemical was G90. This chemical produced briquettes with a water uptake of 5.8% and 3.7% at binder contents of 2.5 percent and 5.0 percent, respectively. This represents a 63% improvement in water resistance at 2.5 percent binder content and a 77% improvement in water resistance at a binder content of 5.0 percent. Although the briquettes produced with wood-derived chemicals were outperformed by the starch briquettes with respect to density, strength and durability, the significant improvement in water resistance achieved by the addition of G88, G89, G90, G97 and G98 presents a unique opportunity to improve coal-biomass briquette quality in the presence of water.

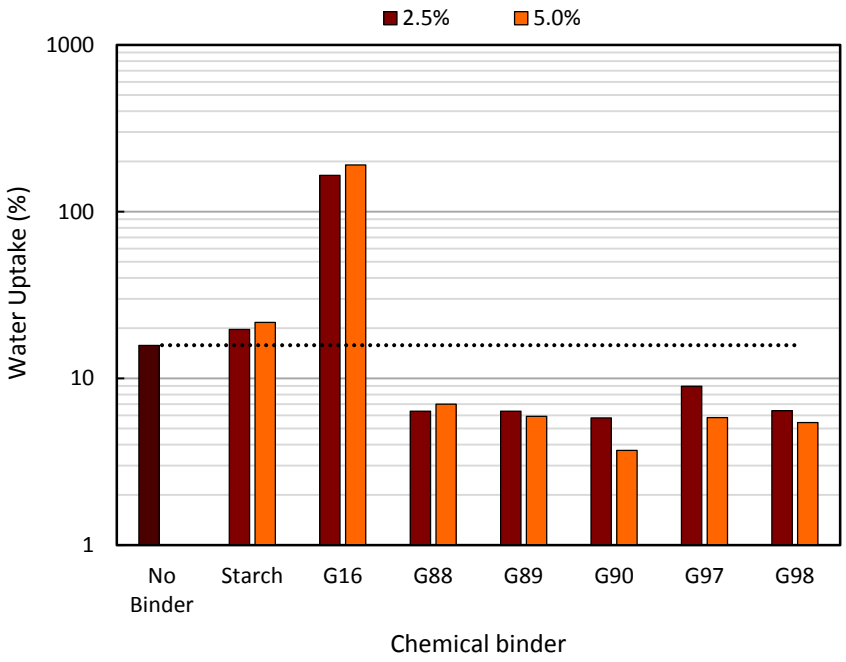



Figure 6-6. Water uptake of briquettes with conventional binder application

## 6.4.2 Preliminary Coating Evaluations

An additional series of tests were conducted to evaluate the performance of the five solid-state wood-derived chemicals as a coating agent applied to the exterior of coal-biomass briquettes. For comparison, additional tests were performed with no coating and with paraffin wax as the coating agent. For each type of chemical coating, two sets of evaluations were conducted: (1) chemical dosage and water uptake measurements for five briquettes, and (2) chemical dosage and a series of mechanical durability and water uptake measurements for 20 briquettes. The series of durability and water uptake tests included an initial mechanical durability test followed by water uptake evaluation of the plus 4.75-millimeter material, followed by another durability test, followed by another water uptake evaluation of the plus 4.75-millimeter material, followed by a final mechanical durability test. The results of these evaluations are included in Table 6-3. The weathered mechanical durability values listed in Table 6-3 represent the total durability of the briquettes after the series of water uptake and durability tests, as calculated by the product of each mechanical durability test result. Similarly, the weathered water uptake values listed in Table 6-3 represent the total water uptake of the briquettes after the series of water uptake and mechanical durability tests, as calculated by the product of the two water uptake test results.

Table 6-3. Summary of preliminary coating evaluation results

| Chemical Coating | Set 1 | | Set 2 | | | | |
|---|---|---|---|---|---|---|---|
| | Chemical Dosage (%) | Water Uptake (%) | Chemical Dosage (%) | Mechanical Durability (%) | Weathered Mechanical Durability (%) | Water Uptake (%) | Weathered Water Uptake (%) |
| No coating | 0.0 | 17.2 | 0.0 | 92.1 | 19.5 | 12.4 | 32.3 |
| Paraffin wax | 1.5 | 0.7 | 2.0 | 90.6 | 78.0 | 0.8 | 1.8 |
| G88 | 6.8 | 1.3 | 9.9 | 98.8 | 96.3 | 0.6 | 1.2 |
| G89 | 9.1 | 0.7 | 5.6 | 94.7 | 66.2 | 1.2 | 5.9 |
| G90 | 9.0 | 0.9 | 8.8 | 97.1 | 93.0 | 0.4 | 1.0 |
| G97 | 5.9 | 1.0 | 8.0 | 98.9 | 97.6 | 0.7 | 1.4 |
| G98 | 5.8 | 1.0 | 6.5 | 98.3 | 96.8 | 0.7 | 1.7 |

The chemical dosage and water uptake results for the initial set of evaluations on five briquettes are displayed in Figure 6-7. From this figure, it is clearly shown that the briquettes with no coating exhibited the highest water uptake (17.2%). In contrast, the highest water uptake measured for the briquettes with a chemical coating was 1.3%, which occurred with the G88 coating. Each of the other water uptake vales were equal to or below 1.0%. The paraffin wax coating exhibited the greatest water resistance by limiting briquettes to a water uptake of 0.7%. This result was particularly notable given the lowest chemical dosage associated with the application of paraffin wax (1.5%). Although these results appear to be very promising, the wood-derived chemical dosage applied to the briquettes using this coating technique (5.8-9.1%) could be too costly for industrial applications, depending on the price of the chemicals. Nonetheless, coating briquettes with the wood-derived chemicals significantly improved briquette water resistance compared to no coating and conventional binder application. For example, the range of water uptake values for conventional binder application (5.0%) of G88, G89, G90, G97 and G98 was 3.7% to 7.0%. Conversely, the range of water uptake values for coating application of the same chemicals was 0.7% to 1.3%. However, the impact of water uptake on the mechanical integrity of briquettes requires further investigation.

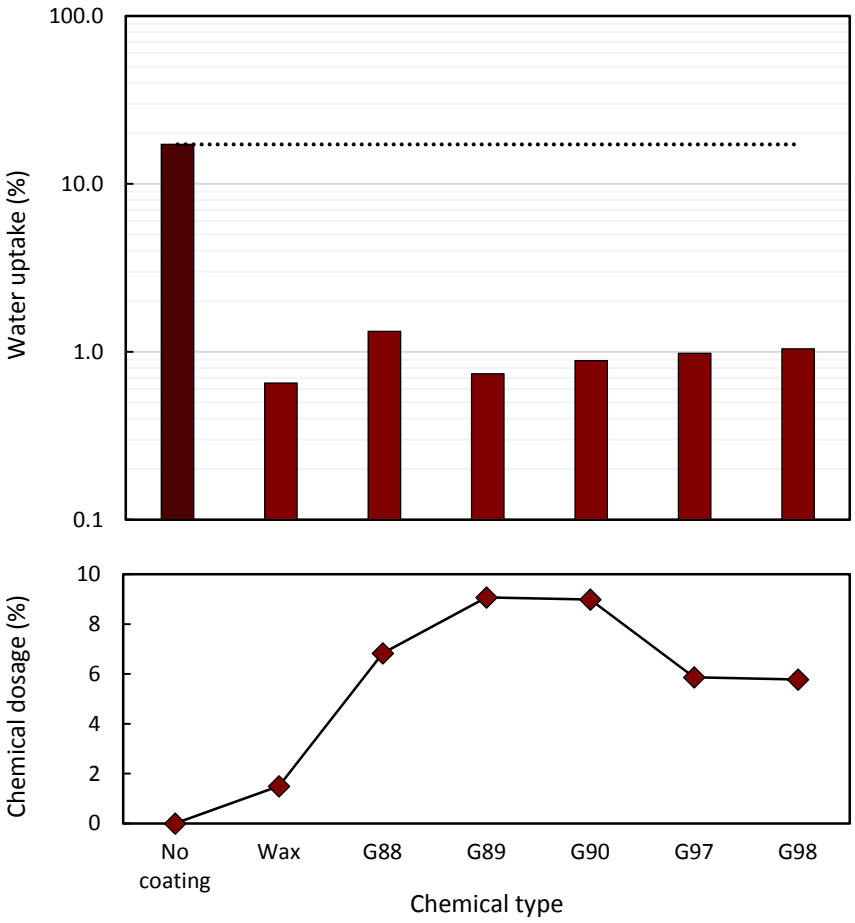



Figure 6-7. Water uptake of coated briquettes (Set 1)

The second set of coating evaluations were specifically designed to examine the impact of water uptake on the mechanical integrity of coal-biomass briquettes. Figure 6-8 shows the initial water uptake and the weathered water uptake values of briquettes with each type of chemical coating and without a coating. It is clearly shown that the initial (12.4%) and weathered (32.3%) water uptake of the briquettes with no coating are significantly higher than each of the coated briquette samples. All of the chemical coatings except G89 reduced the initial briquette water uptake below 1.0% and the weathered water uptake below 2.0%. The chemical coating with the greatest performance was G90, which improved the initial and weathered water resistance of the briquettes by 97%. As with the previous set of tests, the dosage of the paraffin wax was significantly lower than that of the wood-derived chemicals. This was likely due to the higher viscosity of the wood-derived chemicals at 160 degrees Celsius as compared to the

paraffin wax. The G89 briquettes had the lowest chemical dosage (5.6%) of the wood-derived chemical batches, whereas the G88 briquettes were found to have the highest dosage (9.9%).

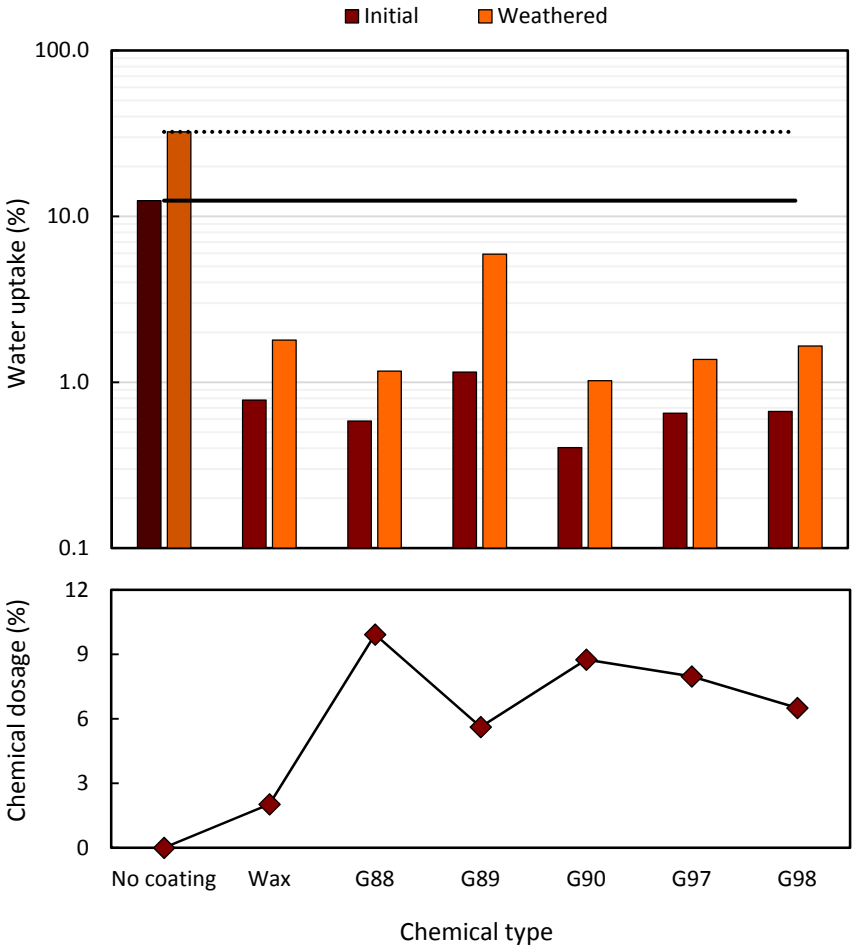



Figure 6-8. Water uptake of coated briquettes (Set 2)

Figure 6-9 shows the initial and weathered mechanical durability of the coated briquettes after the series of durability and water uptake evaluations. From this figure it is evident that the initial durability of briquettes with the wood-derived chemical coatings were greater than the durability of briquettes with no coating (92.1%) and the paraffin wax coating (90.6%). Briquettes coated with the G97 chemical exhibited the greatest initial mechanical durability (98.9%), followed closely by G88 (98.8%), G98 (98.3%), G90 (97.1%) and G89 (94.7%). The measured durability of each of these coated briquette samples are considered excellent (i.e. ≥95%). The weathered durability of the briquettes with no coating was 19.5%, which is considered very poor (i.e. <60%). However, the weathered durability of the coated briquettes showed significant

improvement. For example, the weathered durability of briquettes coated with four of the wood-derived chemicals (G88, G90, G97 and G98) remained greater than the initial durability of the briquettes with no coating (i.e. >92.1%). The final durability of the G88 (96.3%), G97 (97.6%) and G98 (96.8%) briquettes remained classified as excellent, and therefore these chemicals are well suited for use as a coating agent to improve the integrity of coal-biomass briquettes in the presence of water.

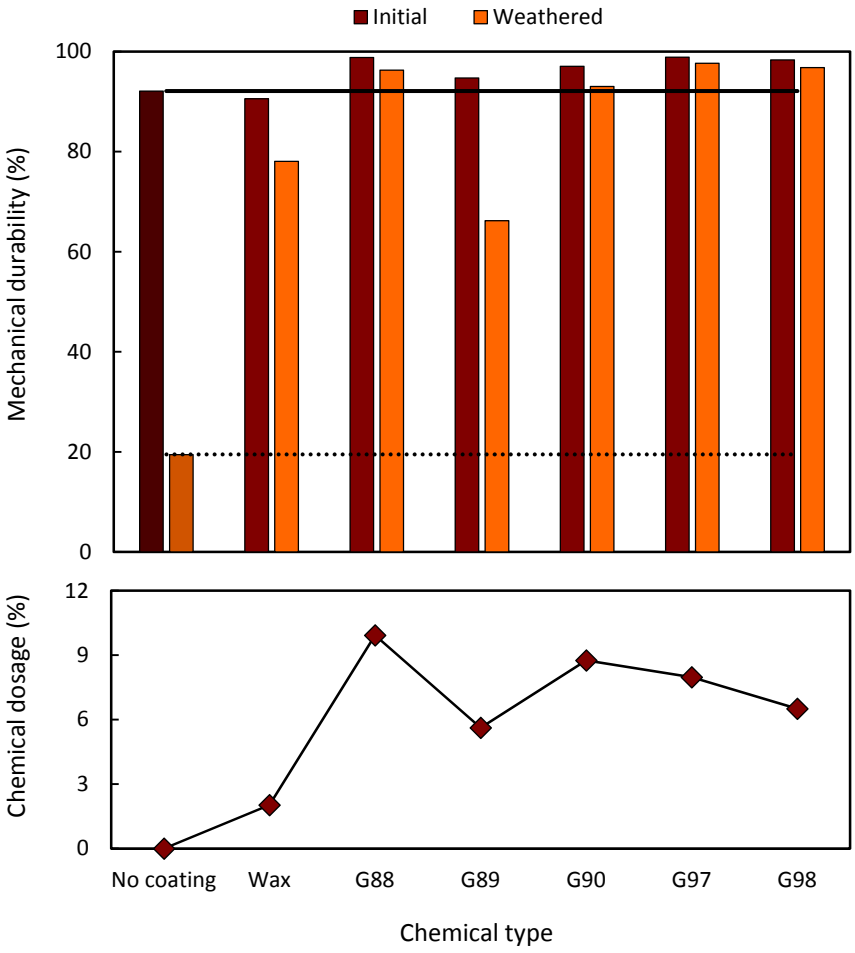



Figure 6-9. Mechanical durability of coated briquettes

To provide a greater appreciation for the results presented in Figure 6-8 and Figure 6-9, images of the actual briquette samples after the series of mechanical durability and water uptake evaluations are provided in Figure 6-10. Here it is clearly shown that the briquettes with no coating experienced a high degree of fragmentation during the evaluations (i.e. final durability = 19.5%). In contrast, briquettes coated with paraffin wax, G89 and G90 chemicals appear partially

degraded, yet still much less degraded than the briquettes with no coating. Finally, briquettes coated with the G88, G97 and G98 chemicals appear fully intact, which corresponds with weathered mechanical durabilities of 96.3%, 97.6% and 96.8%, respectively. Due to the similar performance of G88, G97 and G98 with respect to mechanical durability and water uptake, the choice of the optimum chemical for coal-biomass briquette coating must be made with consideration to the market price of each chemical.

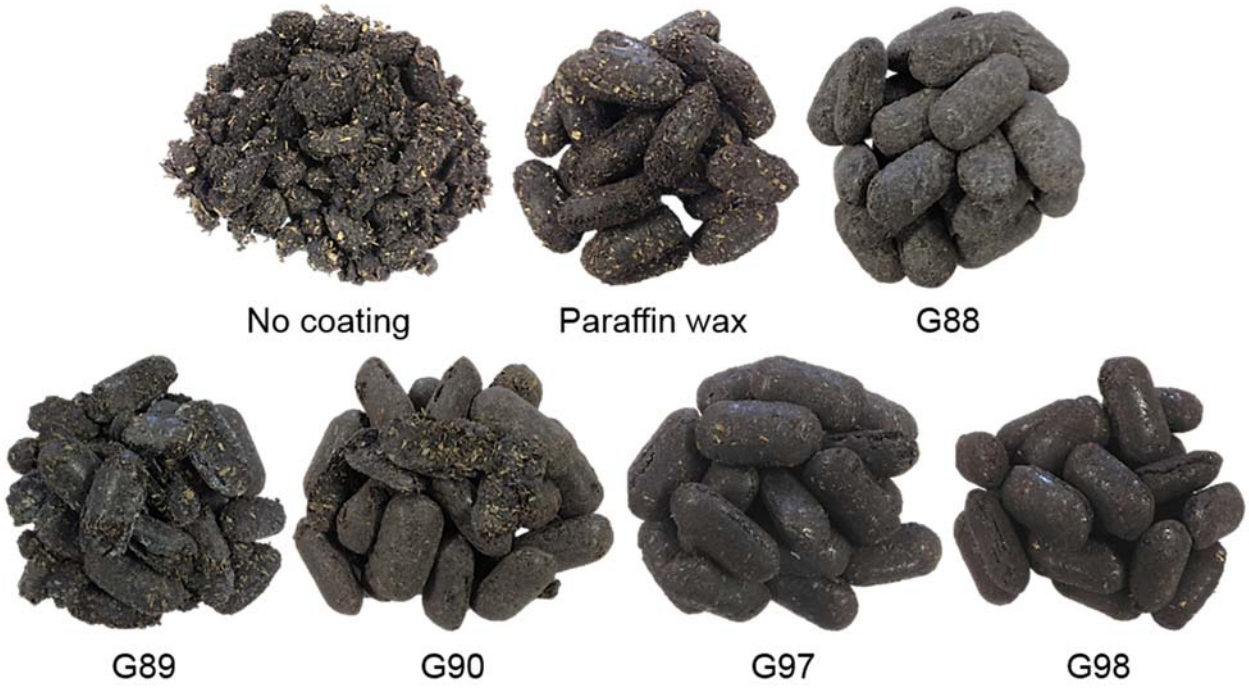



Figure 6-10. Briquette samples after durability and water uptake tests

## 6.4.3 Detailed Coating Evaluations

A series of detailed coating evaluations were performed to validate the performance of a selected wood-derived chemical coating and to measure several additional properties of the coated briquettes. The G88, G97 and G98 chemicals exhibited the best performance with respect to weathered mechanical durability and weathered water uptake. Through discussions with Georgia-Pacific, it was determined that the cost of the G97 chemical is approximately 30 percent less than the G88 chemical and approximately seven percent less than the G98 chemical. For this reason, the G97 chemical was selected for the detailed coating evaluations. These tests were performed with 30 percent biomass to determine the maximum achievable water resistance for briquettes with the greatest proportion of hygroscopic biomass material. The coal-biomass

combinations selected for detailed evaluations were Emerald coal-sawdust (EM-SD) and Eagle Butte-corn stover (EB-CS), which were chosen to reflect the distribution of readily available coal and biomass resources in the United States (i.e. sawdust and bituminous coal are readily available in the east; corn stover and sub-bituminous coal are readily available in the west). To determine the impact of the G97 coating on the overall quality of coal-biomass briquettes, detailed evaluations were also performed on an uncoated portion of both types of briquettes. The results of these four series of detailed evaluations are presented in Table 6-4.

Table 6-4. Summary of detailed coating evaluation results

| Briquette Property | EM-SD | | | EB-CS | | |
|---|---|---|---|---|---|---|
| | No Coating | G97 Coating | Change (%) | No Coating | G97 Coating | Change (%) |
| Tensile strength (N) | 255.8 | 455.5 | 78.3 | 206.0 | 498.2 | 142.1 |
| Crushing strength (N) | 1,589.8 | 1,391.8 | -12.4 | 1,224.6 | 1,270.0 | 3.7 |
| Spring constant (N/m) | 524.9 | 389.8 | -25.7 | 321.1 | 203.8 | -36.5 |
| Mechanical durability (%) | 92.8 | 97.7 | 5.3 | 91.1 | 97.6 | 7.2 |
| Weathered mechanical durability (%) | 39.4 | 89.4 | 126.9 | 7.7 | 94.7 | 1126.9 |
| Attritability (%) | 97.4 | 99.5 | 2.1 | 96.9 | 99.5 | 2.7 |
| Friability (%) | 97.1 | 99.3 | 2.3 | 98.4 | 99.5 | 1.1 |
| Water content | 0.018 | 0.022 | 21.0 | 0.163 | 0.131 | -19.8 |
| Particle density ($g/cm^3$) | 1.13 | 1.11 | -1.9 | 0.94 | 0.96 | 2.1 |
| Water uptake (%) | 8.3 | 1.0 | -88.3 | 14.3 | 0.9 | -93.7 |
| Weathered water uptake (%) | 20.4 | 1.5 | -92.4 | 58.6 | 0.9 | -98.4 |
| Chemical dosage (%) | 0.0 | 9.8 | -- | 0.0 | 14.4 | -- |

In addition to the results of each evaluation reported in Table 6-4, the percent change of each value is reported. This metric makes it easier to assess the impact of the G97 coating on each of the measured briquette properties. The tensile strength of the EM-SD briquettes and the EB-CS briquettes was significantly improved by the application of the chemical coating. Specifically, the tensile strength of the coated EM-SD briquettes increased by 78.3% to 455.5 N (102.4 $lb_f$) and the tensile strength of the coated EB-CS briquetted increased by 142.1% to 498.2 N (112.0 $lb_f$). Another interesting result was that the tensile strength was higher for the uncoated EM-SD briquettes than the uncoated EB-CS briquettes, yet when the G97 coating was applied this finding was reversed. At this point, the fundamental cause of this occurrence is unknown.

The influence of the G97 coating on crushing strength showed mixed results. Specifically, the crushing strength of the coated EM-SD briquettes decreased by 12.4% to

1,391.8 N (312.9 $lb_f$). In contrast, the crushing strength of the coated EB-CS briquettes increased by 3.7% to 1,270 N (285.5 $lb_f$). Nonetheless, these crushing strength values are very high and indicative of extremely strong briquettes. Therefore, the reduced crushing strength value for the EM-SD briquettes is not particularly alarming. For both the coated and uncoated briquettes, the bituminous coal briquettes (EM-SD) exhibited higher crushing strengths than the sub-bituminous coal briquettes (EB-CS). This finding is in agreement with the statistical models discussed in Chapter 5.

The application of the G97 coating also resulted in a fairly significant decrease in the spring constant of the briquettes. Specifically, the spring constant of the coated EM-SD briquettes decreased by 25.7% to 389.8 N/m (3450 $lb_f$/in) and the spring constant of the coated EB-CS briquettes decreased by 36.5% to 203.8 N/m (1804 $lb_f$/in). For both the coated and uncoated briquette evaluations, the EM-SD briquettes exhibited higher spring constant values than the EB-CS briquettes. This was most likely due to the difference in elasticity of the corn stover and sawdust. For example, corn stover has a much lower particle density than sawdust due to the internal pore structure of corn stalks. Therefore, raw corn stover can be compressed more easily than sawdust, which appears to also be the case when co-briquetted with coal.

A very promising result of these evaluations was the increase in mechanical durability that was measured for the coated briquettes. Specifically, the mechanical durability of the coated EM-SD briquettes increased by 5.3% to 97.7% and the mechanical durability of the EB-CS briquettes increased by 7.2% to 97.6%. Although this was a very encouraging result, a more important finding was the increase in weathered mechanical durability for the coated briquettes. The weathered mechanical durability of the coated EM-SD briquettes increased by 126.9% to 89.4% and the weathered mechanical durability of the coated EB-CS briquettes increased by 1126.9% to 94.7%. These weathered durability values are very good and indicate that these briquettes would remain a high-quality product in the presence of rain or other precipitation. These results validate the results of the preliminary coating evaluations.

Attritability and friability were also improved for bother briquette formulations by adding the G97 coating. For instance, attritability increased by 2.1% (EM-SD) and 2.7% (EB-CS) to 99.5% for both types of briquettes. This value is extremely high and indicates that attrition has a very minimal impact on the production of fine material for briquettes coated with the G97 chemical. A similar result was observed for briquette friability, wherein the measured values

increased by 2.3% and 1.1% to 99.3% and 99.5% for the EM-SD and EB-CS briquettes, respectively. Similarly, this indicates that impact forces are not likely to significantly degrade the quality of coal-biomass briquettes coated with G97.

As expected, the G97 coating greatly improved the initial and weathered water resistance of both types of briquettes. Specifically, the initial and weathered water uptake of the coated EM-SD briquettes decreased by 88.3% and 92.4%, respectively. This equated to an initial water uptake of 1.0% and a weathered water uptake of 1.5%. Similarly, the initial and weathered water uptake of the coated EB-CS briquettes decreased by 93.7% and 98.4%, respectively. This equated to an initial and weathered water uptake of 0.9%. Both of these results further demonstrate the great potential for the G97 chemical to dramatically improve the water resistance of coal-biomass briquettes when applied as a coating to the exterior surface. In addition, these results further validate the results of the preliminary coating evaluations. Thus, it is likely that the other promising Georgia-Pacific wood-derived chemicals (i.e. G88, G98) would also exhibit very promising results in a series of validation tests.

Another interesting observation was the influence of the G97 coating on the particle density of the briquettes. Specifically, the particle density of the coated EM-SD briquettes decreased by 1.9% to 1.11 g/cm$^3$. Conversely, the particle density of the coated EB-CS briquettes increased by 2.1% to 0.96 g/cm$^3$. The reason for this occurrence is thought to be a direct result of the addition of the G97 chemical, which has a specific gravity of approximately 1.0. Therefore, it stands to reason that addition of this chemical to individual briquettes would increase the particle density of briquettes with an initial particle density less than 1.00 g/cm$^3$ and decrease the particle density of briquettes with an initial particle density greater than 1.00 g/cm$^3$. Furthermore, the change in particle density as a result of application of the G97 chemical was greater for the EB-CS briquettes (2.1%) than for the EM-SD briquettes (1.9%). This is likely a direct result of the higher chemical dosage measured for the EB-CS briquettes (14.4%) than the EM-SD briquettes (9.8%).

An unexpected and negative result of these tests was the increased chemical dosage measured for these two batches of briquettes compared to the chemical dosages measured for the preliminary coating evaluations. Since chemical dosage is directly linked to production cost, an increase in this value is particularly disconcerting. However, since this result is directly linked to the chemical application method employed for this study and the size of the pill-shaped

briquettes produced, chemical dosage can certainly be reduced by improving the application method (i.e. spraying instead of dipping) and by increasing the ratio of briquette mass to surface area (i.e. using larger roll pockets). Based on the results of the preliminary coating evaluations and this detailed study, it appears that a decrease in chemical dosage would not necessarily result in decreased weathered mechanical durability and increased weathered water uptake. This assertion is only feasible if the thickness of the chemical coating is reduced by reducing the chemical dosage. In contrast, if the chemical dosage is reduced by not providing uniform coating to the entire surface of the briquettes, it is anticipated that weathered mechanical durability and weathered water uptake would suffer.

## 6.5 Summary and Conclusions

There is currently a growing interest in the development of economically feasible methods to sustain the physical and mechanical integrity of coal-biomass briquettes in the presence of water In light of this issue, a study was performed to evaluate the potential for several proprietary wood-derived chemicals to improve the water resistance of coal-biomass briquettes. Two methods for application of the chemicals were examined: (1) conventional binder application wherein chemicals were mixed with coal and biomass particles prior to briquette production, and (2) coating application wherein coal-biomass briquettes were dipped in heated chemicals to coat the exterior surface. Additional evaluations were performed without chemicals and with commonly used chemicals to establish the relative performance of each wood-derived chemical.

For the conventional binder application method, five of the six wood-derived chemicals significantly improved the water resistance of the coal-biomass briquettes. The best performing wood-derived chemical (G90) produced briquettes with a water uptake of 5.8% and 3.7% at binder contents of 2.5 percent and 5.0 percent, respectively. This represents a 63% and 77% improvement in water resistance as compared to the binderless briquettes. Although the briquettes produced with wood-derived chemicals were outperformed by the starch briquettes with respect to density, strength and durability, the significant improvement in water resistance from addition of the wood-derived chemicals presents a unique opportunity to improve coal-biomass briquette quality in the presence of water.

For the briquette coating technique, each of the wood-derived chemicals outperformed briquettes with no coating, and four of the five chemicals outperformed briquettes with the paraffin wax coating. The wood-derived chemical with the greatest water resistance potential (G90) produced an initial briquette water uptake of 0.4% and a final water uptake of 1.0%. This represents a 97% improvement in water uptake for both initial and weathered water uptake. Briquettes coated with G97 exhibited the greatest initial (98.9%) and final (97.6%) mechanical durability. This represents a 7% increase in initial durability and a 401% increase in weathered durability. One concern with the results of the briquette coating evaluations is the high dosage (5-10%) of the wood-derived chemicals. This issue is thought to be a result of the dipping technique employed and the high viscosity of the heated chemicals.

The results of the detailed coating evaluations further exemplified the benefits of the G97 coating with respect to initial and weathered durability and water resistance. In addition, these evaluations provided insight to the influence of the G97 coating on other important properties of coal-biomass briquettes. These evaluations also provided evidence that the G97 coating can be successfully used to improve the durability and water resistance of briquettes comprised of different coal types (i.e. bituminous and sub-bituminous) and different biomass types (i.e. sawdust and corn stover). However, a major shortcoming of coating briquettes with wood-derived chemicals such as G97 is the high chemical dosage that was applied to the surface of the briquettes using the technique outlined in this study.

Briquette coating methods require further investigation to determine if the chemical dosage could be reduced by modifying the dipping technique or by implementing a hot spraying technique. The selection of the optimum wood-derived chemical for coal-biomass briquette coating applications depends primarily on the cost of each chemical and the desired level of briquette durability and water resistance. Therefore, it is recommended that the chemical coating type and application method be chosen independently for every unique coal-biomass briquette operation as a balance between desired quality and production cost.

# Chapter 7

# Sequential Pelletization, Drying and Briquetting

## 7.1 Abstract

Forming wet coal fines into spherical pellets before thermally drying and briquetting the pellets at an elevated temperature offers several advantages over direct briquetting of wet or dry coal fines, not the least of which is substantial improvement in briquette durability. Accordingly, the work described in this chapter focuses on comparisons of the durability of briquettes made from various combinations of thermally dried coal pellets, air dried coal pellets, and air dried coal fines. The impact of various binders blended with these feedstocks was investigated and the study concludes with formation of coal-biomass briquettes in which selected biomass types were blended in-situ within the briquette press hopper with both hot and cool thermally dried pellets. Not only does pelletizing the wet fines provide an agglomerate that is amenable to drying in a moving bed but the results clearly demonstrate that substantial improvements in briquette durability is obtained, both with and without biomass, by briquetting hot, thermally dried coal pellets versus briquetting air or thermally dried coal fines or coal pellets at ambient temperature.

## 7.2 Introduction

One of the biggest obstacles to briquetting of fine coal recovered from preparation plants or slurry impoundments is their high moisture content. Not only does the moisture reduce the net heating value of the fines but it also results in poor flow properties that lead to bridging, run stoppages, and a generally inconsistent feed rate. When briquettes can be produced, they typically exhibit unacceptably low green strengths. Thus, before high-moisture fine coal can be briquetted, the moisture needs to be sufficiently reduced to permit for a consistent feed rate and acceptable green strengths.

Dewatering high-moisture fine coal to a range that is amenable to briquetting is not trivial. Historically, the method of choice has been fluidized-bed drying. However, fluidized bed dryers are highly problematic to operate and pose serious fire and explosion hazards. Due to these latter hazards, fluid bed dryers for fine coal are effectively no longer being permitted in the United States.

An alternate to fluidized bed dryers is a moving bed (conveyed bed) dryer in which a perforated belt is used to transport the wet fines through a drying oven as hot flue gas or other gaseous drying medium is passed upward and/or downward through the bed. However, the low porosity of a packed bed of wet coal fines dictates that only a shallow bed be used, which limits throughput. Further, attempts to dry coal fines in a shallow bed results in entrainment of the fines when the hot flue gas is passed upward through the bed or plugging of the belt perforations when the flue gas is passed downward through the bed.

Forming the fine coal into spherical pellets in a pan pelletizer prior to drying in a moving-bed system can avoid these issues by increasing bed porosity, thus lowering the pressure drop required to route hot flue gas through the packed bed. Further, the larger sized pellets suppress the upward entrainment of fines or downward escape or plugging of the perforated belt, permitting for larger perforations in the belt. Pre-pelletizing the wet fines with a binder also offers the potential to obtain a more uniform binder coverage compared to adding and blending a binder with dried fines. This can potentially reduce the amount of binder required to obtain a targeted strength in the final product. After passing through the conveyed bed dryer, the dried pellets are a free-flowing material with fewer fugitive dust issues compared to dried fines. The dried pellets also provide an ideal briquetting feedstock as they can be loaded and fed in a consistent manner. They can also be co-fed to a briquette press hopper with biomass where a paddle mixer and feed auger crush and effectively blend the fine coal and biomass in situ into a homogeneous blend immediately before forming into coal-biomass briquettes (Taulbee et al., 2012). Finally, if the dried pellets are immediately briquetted on exiting the dryer while hot, the briquettes formed have a significantly higher crushing strength compared to briquettes formed from otherwise equivalent ambient temperature briquettes (Taulbee et al., 2014). Most importantly, permits can still be obtained for moving bed dryers in the United States.

While pre-pelletizing fine coal prior to drying introduces an additional processing step, pan pelletization is a relatively inexpensive, high-throughput, and simple form of agglomeration

(Mehta, 1996). Importantly, pan pelletization can be applied to fine coals with a moisture content ranging to about 30% (Conkle, 1992). Thus, when one considers the advantages of pelletizing, drying, and briquetting of high-moisture coal fines compared to drying and briquetting wet coal fines, the additional pelletization step appears to be justified.

Accordingly, the work reported in this chapter focuses on pelletizing, drying, and subsequent briquetting of high-moisture fine coal samples. The fine coal samples evaluated include three products recovered from screen bowl decanters as a combination of clean product from flotation and spiral circuits and an ultra-fine product from froth flotation cells and dewatered by vacuum disk filtration. A preliminary study was focused on identifying the optimum pellet moisture for briquetting pelletized coals. This was followed by comparisons of briquettes made with and without a binder from various feedstocks including thermally dried pellets that were briquetted while hot, thermally dried pellets that were briquetted after cooling, air dried pellets, and air dried fines. The study concludes with a comparison of briquettes made with both hot and ambient temperature pellets co-briquetted with various biomass types.

## 7.3 Experimental

### 7.3.1 Materials

#### 7.3.1.1 Biomass Feedstocks

The biomass feedstocks used for briquette production throughout the course of this study included:

- CS - Corn Stover. The CS sample was locally harvested and provided as square bales by the University of Kentucky Biosystems and Agricultural Engineering Department. Prior to use, the CS samples was processed through a knife mill fitted with a 6.35 mm (0.25 in) screen.
- WS - Wheat Straw. Procured and processed same as for corn stover
- MS - Miscanthus. Procured and processed same as for corn stover
- SG - Switchgrass. Procured and processed same as for corn stover
- Green SD - mixed hardwood sawdust. Multiple barrels of sawdust comprised primarily of red oak and poplar were collected from White Lumber, Inc. Morehead, KY. The green SD sample was screened to pass a 6.35 mm screen (0.25 in) prior to use.

- Kiln SD – kiln dried sawdust. Kiln-dried mixed hardwoods, comprised primarily of poplar and red oak sawdust collected from White Lumber, Inc., Morehead, KY. The Kiln SD was also screened to minus 6.35 mm (0.25 in) prior to use.
- EtOH BC. The EtOH bio-char was produced by gasification of mixed northern hardwood chips at the Chippewa Valley Ethanol plant in Benson, Minnesota. The Chippewa bio-char sample was a high moisture (>30 wt%), small particle-size material (~80% <150 μm).
- Pine BC. The pine bio-char sample was generated by gasification of mixed pine-wood chips by Bio-Char Engineering Corporation, Golden CO. The pine BC was a low density, low moisture, and relatively large particle-size char that was reduced to approximately minus 2.38 mm (8 mesh) in a hammer mill prior to use.

Laboratory analyses of the biomass samples are given in Table 7-1 and Table 7-2. Note the unusually high calorific value for the pine bio-char compared to the other biomass or biomass-derived samples (Table 7-1). This pine BC sample is also low in oxygen and volatile matter and high in fixed carbon making it more similar in composition to coal (Table 7-3) than to the other biomass types. In contrast, the calorific content of the EtOH BC sample is unusually low for bio-char, attributed to its high moisture and ash content. There are other significant differences among the various biomass samples, particularly in total ash and the concentrations of Si and Ca in the ash. Otherwise, the biomass chemical composition is unremarkable.

Table 7-1. Proximate, ultimate, and calorific analysis of biomass samples (as-received basis)

| Abbreviated ID | Sample ID | Ash % | Moisture % | C % | H % | N % | $S_{tot}$ % | O % | % Vol Matter | % Fixed C | GCV kJ/kg |
|---|---|---|---|---|---|---|---|---|---|---|---|
| WS | Wheat straw | 4.30 | 9.40 | 44.11 | 6.51 | 1.03 | 0.29 | 43.76 | 74.32 | 11.98 | 16373 |
| CS | Corn stover | 2.58 | 8.48 | 45.79 | 6.05 | 2.28 | 0.14 | 43.16 | 78.06 | 10.88 | 16696 |
| SG | Switchgrass | 1.53 | 8.28 | 46.40 | 6.51 | 1.02 | 0.14 | 44.40 | 81.35 | 8.84 | 17054 |
| MS | Miscanthus | 2.36 | 9.20 | 43.69 | 5.77 | 0.98 | 0.13 | 47.07 | 78.25 | 10.19 | 16889 |
| SD | Green sawdust | 0.47 | 19.52 | 39.66 | 6.85 | 0.17 | 0.05 | 52.80 | 71.90 | 8.11 | 15612 |
| Kiln SD | Kiln dried SD | 0.28 | 12.42 | 45.13 | 6.78 | 1.26 | 0.06 | 46.49 | 76.97 | 10.33 | 15905 |
| Pine BC | Pine BC | 9.29 | 9.07 | 74.29 | 2.73 | <0.10 | 0.02 | 13.67 | 13.00 | 68.64 | 27835 |
| EtOH BC | Chippewa BC | 24.59 | 30.79 | 35.29 | 4.47 | <0.10 | 0.02 | 35.63 | 16.89 | 27.73 | 12212 |

Table 7-2. Major elements in ash and trace elements in biomass samples (as-received basis)

| Abbreviated ID | $SiO_2$ % | $Al_2O_3$ % | $Fe_2O_3$ % | CaO % | MgO % | $Na_2O$ % | $K_2O$ % | $P_2O_5$ % | $TiO_2$ % | $SO_3$ % | V ppm | Cr ppm | Mn ppm |
|---|---|---|---|---|---|---|---|---|---|---|---|---|---|
| WS | 60.20 | 1.68 | 0.69 | 4.42 | 3.17 | 0.18 | 18.32 | 9.98 | 0.14 | 1.14 | <1 | 38 | 403 |
| CS | 41.53 | 3.87 | 1.44 | 7.22 | 4.41 | 0.24 | 28.01 | 6.03 | 0.30 | 2.66 | <1 | 53 | 768 |
| SG | 54.18 | 2.16 | 1.51 | 17.47 | 10.03 | 0.31 | 5.55 | 6.33 | 0.24 | 3.53 | <1 | 67 | 1855 |
| MIS | 55.89 | 1.86 | 0.91 | 11.61 | 9.94 | 0.53 | 9.66 | 8.39 | 0.17 | 2.88 | <1 | 49 | 1100 |
| SD | 15.22 | 4.58 | 10.32 | 18.43 | 10.44 | 0.25 | 15.08 | 1.49 | 0.26 | 18.08 | <1 | 79 | 5170 |
| Kiln SD | 5.43 | 2.25 | 2.67 | 50.86 | 3.96 | 0.05 | 21.29 | 2.65 | 0.16 | 1.96 | <1 | 29 | 2435 |
| Pine BC | 55.83 | 12.66 | 5.12 | 13.15 | 3.92 | 1.20 | 5.16 | 1.44 | 0.52 | 0.75 | 55 | 87 | 2023 |
| EtOH BC | 37.08 | 4.46 | 1.86 | 42.41 | 4.48 | 0.88 | 4.77 | 1.22 | 0.24 | 0.55 | <1 | 52 | 1414 |
| **Abbreviated ID** | **Co ppm** | **Ni ppm** | **Cu ppm** | **Zn ppm** | **As ppm** | **Rb ppm** | **Sr ppm** | **Zr ppm** | **Mo ppm** | **Cd ppm** | **Sb ppm** | **Ba ppm** | **Pb ppm** |
| WS | <1 | 32 | 57 | 309 | 18 | 385 | <1 | 22 | <1 | <1 | 8 | 784 | 52 |
| CS | <1 | 33 | 62 | 255 | 37 | 355 | <1 | 20 | <1 | 1 | 10 | 134 | 40 |
| SG | 3 | 52 | 104 | 588 | 22 | 191 | 159 | 18 | 53 | 1 | 5 | 170 | 46 |
| MIS | 1 | 43 | 104 | 658 | 18 | 336 | 78 | 20 | 5 | <1 | 7 | 134 | 52 |
| SD | 29 | 186 | 93 | 831 | 97 | 255 | 677 | 14 | <1 | 1 | 12 | 3126 | 38 |
| Kiln SD | <1 | 48 | 109 | 138 | 75 | 255 | 1207 | 20 | <1 | 1 | 13 | 1655 | 20 |
| Pine BC | 15 | 46 | 85 | 364 | 39 | 288 | 740 | 13 | <1 | 1 | 7 | 874 | 51 |
| EtOH BC | <1 | 30 | 77 | 435 | 98 | 358 | 276 | 22 | <1 | 1 | 12 | 526 | 49 |

#### 7.3.1.2 Coal Feedstocks

All coal samples used in this and other studies conducted at the University of Kentucky's Center for Applied Energy Research were of bituminous rank and obtained from either the Appalachian or Illinois Basin coal fields. The coals included:

- PCC. Screen-bowl fines collected from Teco Coal's Perry County Preparation Plant near Hazard in Eastern Kentucky. The sample was a combination of spiral and flotation fines from approximate 1:1 blends of Elkhorn 4 and Hazard 5/5A seams with nominal particle size of 595 x 44 μm (-28 x +325 mesh). The PCC sample was evaluated without further size reduction.
- RVSB. Illinois Basin screen-bowl fines collected from the River View Preparation Plant near Waverly, in Western Kentucky. The sample was a combination of spiral and flotation fines from a 1:1 blend of the Kentucky 9 and Kentucky 11 seams with a nominal particle size of 1.0 x 0.044 mm (-16 x +325 mesh). The sample was evaluated without further size reduction.

- ASB. A sample of screen bowl fines collected at the Alden Resources' Preparation Plant near Williamsburg in Southeast Kentucky. The ASB was a combination of fines recovered from spiral and flotation circuits that originated from the Blue Gem seam with a nominal particle size of minus 6.35 mm (0.25 in). The ASB sample was evaluated without further size reduction.
- MRC. A vacuum disk filter sample of flotation fines from Alpha Natural Resources' McClure River Preparation Plant located east of Abington, VA. The nominal particle size was minus 150 μm (100 mesh). This sample was evaluated without further size reduction.

Proximate, ultimate, and calorific value along with major and trace elements are shown on an as-received basis for the five study coals in Table 7-3 and Table 7-4. Note the relatively low ash content of the Alden coal sourced from the high-value Blue Gem seam from southern Kentucky. Also note the lower sulfur and oxygen contents and higher calorific value of the three coals from the Appalachian field compared to the two River View samples from the Illinois Basin. Otherwise, the chemical composition of the various samples is also relatively unremarkable.

Table 7-3. Proximate, ultimate, and calorific analysis of coal samples (as-analyzed basis)

| Abbreviated ID | Ash % | Moisture % | C % | H % | N % | $S_{tot}$ % | O % | % Vol Matter | % Fixed C | GCV kJ/kg |
|---|---|---|---|---|---|---|---|---|---|---|
| MRC | 11.00 | 0.87 | 77.98 | 4.90 | 1.41 | 0.89 | 3.82 | 27.83 | 60.30 | 31657 |
| PCC | 6.86 | 1.03 | 77.97 | 5.24 | 1.50 | 0.75 | 7.68 | 34.60 | 57.51 | 31720 |
| RVSB | 13.42 | 1.00 | 67.18 | 4.10 | 1.41 | 2.70 | 11.19 | 32.06 | 53.52 | 26242 |
| ASB | 3.65 | 1.12 | 79.27 | 5.43 | 1.84 | 0.84 | 8.97 | 36.26 | 58.97 | 32152 |

Table 7-4. Major elements in ash and trace elements in coal samples (as-analyzed basis)

| Abbreviated ID | $SiO_2$ % | $Al_2O_3$ % | $Fe_2O_3$ % | CaO % | MgO % | $Na_2O$ % | $K_2O$ % | $P_2O_5$ % | $TiO_2$ % | $SO_3$ % | V ppm | Cr ppm | Mn ppm |
|---|---|---|---|---|---|---|---|---|---|---|---|---|---|
| MRC | 54.08 | 27.94 | 8.80 | 1.91 | 1.72 | 0.52 | 3.36 | 0.24 | 1.50 | 1.49 | 498 | 142 | 369 |
| PCC | 53.84 | 29.71 | 6.61 | 2.30 | 1.27 | 0.66 | 2.65 | 0.09 | 1.89 | 2.29 | 714 | 155 | 364 |
| RVSB | 43.62 | 16.35 | 15.39 | 10.29 | 1.03 | 0.64 | 2.17 | 0.59 | 0.86 | 9.76 | 546 | 158 | 394 |
| ASB | 50.28 | 26.33 | 11.25 | 3.21 | 1.78 | 0.36 | 3.43 | 0.26 | 1.23 | 2.93 | 662 | 170 | 320 |
| **Abbreviated ID** | **Co ppm** | **Ni ppm** | **Cu ppm** | **Zn ppm** | **As ppm** | **Rb ppm** | **Sr ppm** | **Zr ppm** | **Mo ppm** | **Cd ppm** | **Sb ppm** | **Ba ppm** | **Pb ppm** |
| MRC | 41 | 119 | 166 | 5 | 98 | 30 | 1138 | 207 | 60 | 1 | 1 | 1053 | 82 |
| PCC | 49 | 222 | 221 | 269 | 108 | 10 | 1921 | <1 | 73 | 1 | <1 | 954 | 96 |
| RVSB | 47 | 107 | 54 | 248 | 70 | 46 | 82 | 16 | 32 | 1 | 6 | 764 | 39 |
| ASB | 63 | 184 | 218 | 321 | 136 | 24 | 2121 | 2 | 50 | 1 | 3 | 1199 | 85 |

Particle-size distributions, obtained by a combination of wet (minus 1 mm size fractions) and dry (plus 1 mm size fractions) sieve analysis, are shown for the four study coals and the EtOH biochar sample in Figure 7-1. There were significant differences in the particle size distributions of the various coals samples with nearly 60% of the Alden screen bowl samples comprised of particles larger than 600 µm compared to the MRC disk filter sample, which was comprised of 46 wt% less than 75 µm (200 mesh). The remaining two screen bowl samples, PCC and RVSB, were very similar in particle size distribution and fell between these two extremes with nearly half of the weight of each partitioning to 150-600 µm range (30 x 100 mesh). The EtOH BC particle size distribution is included to emphasize how similar in size distribution for this sample compared to the ultra-fine MRC coal sample.

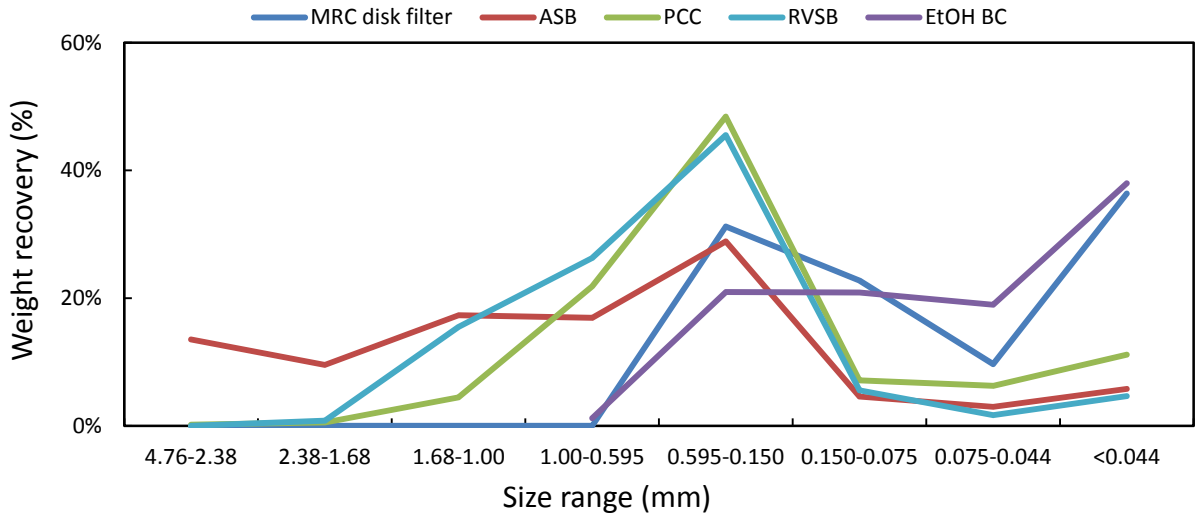



Figure 7-1. Particle size distributions for the various study coals and the EtOH biochar sample

## 7.3.2 Pelletization, Drying and Briquetting Equipment

### 7.3.2.1 Briquetter

All briquettes were formed in a Komarek B-100 continuous roll briquetter with a roller force of 85-90 kN targeted for all runs. Roller speed was fixed for the vast majority of run at a nominal setting of 25 Hz, which equates to an approximate production rate of 45 kg/hr (100 lbs/hr). The feed auger was controlled manually during each run to provide a force of approximately 90 N-m.

#### 7.3.2.2 Vibrating Screen

All newly formed briquettes were passed across a 61-cm (2 ft) diameter Sweco mechanical screener equipped with a 6.35mm (0.25 in) screen to remove fines immediately after production.

#### 7.3.2.3 Pelletizers

Smaller-sized pelletized coal samples were formed in an unbranded 40 cm (16 in) disk pelletizer. Larger-scale pellet samples were produced in a Mars Mineral, model P-30, 91 mm (3 ft) diameter disk pelletizer.

#### 7.3.2.4 Controlled Environment Chambers

To eliminate variations in briquette properties attributable to variation in ambient temperature and humidity conditions, all briquetted samples were stored in one of three Caron controlled-environment chambers (models 6010, 6020, and 6030) from formation until the completion of physical evaluations. All three chambers were maintained at simulated ambient conditions of 22.3 °C (72 °F) and 70% relative humidity during the project.

#### 7.3.2.5 Knife Mill

With the exception of the sawdust sample, the majority of the biomass samples were reduced in particle size by processing through a model G1012 Granulator (knife mill) fitted with a 6.35 mm (0.25 in) screen. The mill was manufactured by Jordan Reduction Solutions, Birmingham, Alabama, and had a rated capacity of 90 kg/hr (200 lb/hr).

#### 7.3.2.6 Thermal Dryer

A forced-air thermal dryer that was fabricated in house was used to heat and dry the green coal pellets. The thermal dryer incorporated a variable speed blower that pulls air into a 75 kW electrical-resistance duct-heater and forces it out through a packed bed of coal pellets loaded to 20.3 cm diameter (8 in), 2.38 mm (8 mesh) screen that was equipped with a 15 cm (6 in) chimney. The blower and heater were independently controlled, allowing for targeted combinations of flow velocity and temperature. The blower speed was manually selected while gas temperature is controlled via a feedback loop with a Farnam 7550 series process controller. The 20 cm (8 in) diameter, 2.38 mm (8 mesh) screen/pellet holder was designed to quickly attach

and detach, permitting for accurate management of residence time and measurement of weight loss. The blower motor has a nominal capacity of 38.4 $m^3$/min (1355 scf/min), equating to a linear velocity of 4.87 m/s through the 20.3-cm diameter pellet holder at STP. The in-duct electrical-resistance heater (Farnam Flow Torch$^{TM)}$ has a nominal maximum temperature output of 482 °C. The dryer was instrumented with type K thermocouples and pitot static tubes for measuring temperatures and air velocity, respectively. Data was continuously recorded with a DATAQ USB DI-718B data acquisition system and WinDaq software. A schematic and photograph of the thermal dryer are shown in Figure 7-2 and Figure 7-3, respectively.

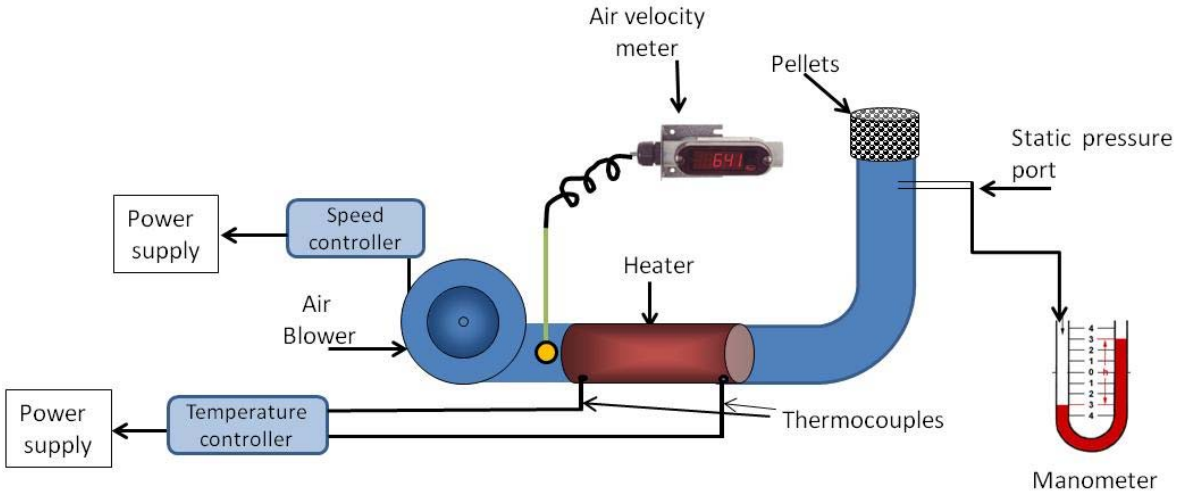



Figure 7-2. Schematic of thermal dryer used for drying coal pellets

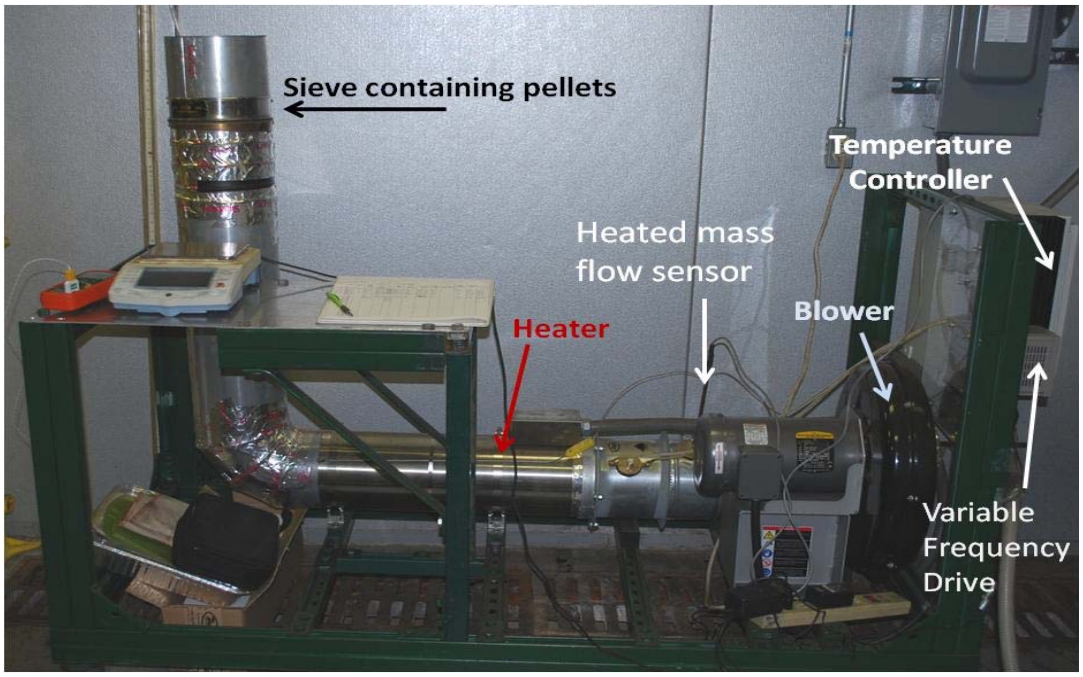



Figure 7-3. 75-kW thermal dryer used for drying coal pellets

## 7.3.3 Laboratory Procedures

### 7.3.3.1 Briquette Evaluations

#### *7.1.1.1.1 Initial Briquette Moisture*

Initial briquette moisture was determined by collecting 6 to 8 briquettes from the briquetter discharge chute into a tared beaker, immediately weighing the briquettes, and then oven-drying overnight at 105 °C.

#### *7.1.1.1.2 Average Crushing Strength*

Average crushing strengths were determined at 30 minutes, 24 hours, and 7 days on briquettes that were maintained at a constant temperature and relative humidity of 22.3 °C and 70%, respectively. A minimum of 25 briquettes were crushed at each time interval. Briquettes were placed on a flat surface and a downward force applied at a rate of 2.5 cm/min (1 in/min) with a 1.9-cm (0.75 in) diameter plunger along the same axis that force was applied by the roll pockets during formation. Force was applied until the failure was detected and recorded with a Lloyd Instruments LRX Plus compressive meter mounted to an automated test stand (upper limit 450 $kg_f$).

*7.1.1.1.3 Mechanical Durability*

Mechanical durability of briquettes was measured following a 7 day cure at 22.3 °C (72 °F) and 70% relative humidity. Approximately 200 g of briquetted sample were placed into a 30.5-cm diameter (12 in) Plexiglas cylinder equipped with three, 5 cm (2 in) lifters; tumbled for five minutes at 40 rpm; and mechanically screened for 3 minutes in a Ro-Tap vibrator fitted with a 4.76 mm (4 mesh) screen. The average mechanical durability was reported as the fraction of the starting briquette weight retained on the 4 mesh screen. Mechanical durability values less than 0.80 are considered poor, 0.80-0.90 marginally acceptable, 0.90-0.95 good, and greater than 0.95 excellent.

*7.1.1.1.4 Resistance to Water Degradation*

Resistance to water degradation was determined by weighing 10 briquettes, submerging the briquettes in a water-filled glass beaker for one hour and then visually classifying the briquettes as fully degraded, mostly degraded, mostly intact, or intact. Briquettes that classified as intact were retrieved and dried in room air for 30 minutes, reweighed to determine water uptake, and then crushed to determine a post-submersion crushing strength.

### 7.3.3.2 Pelletization

For the thermal-drying experiments, the fine coal was formed into spherical pellets in either a 40 cm or a 91 cm diameter pan pelletizer at 30-35 degrees from vertical. Coal was loaded manually while water was sprayed in a manner to optimize production of pellets in the range of 6 to 20 mm (0.25-0.75 in) diameter. For pellets made with binder, the coal and binder were blended in a 60 liter dough-style blender before loading to the pelletizer.

### 7.3.3.3 Pellet Drying

Pellets were either thermally dried or weighed to an open tray and placed into a fume hood where they were air dried to a targeted moisture determined by monitoring weight loss. For thermally dried pellets, the thermal dryer was first preheated to the target temperature of either 175 or 200 °C. Three to four kg of green pellets were weighed to the 20-cm diameter (8 in) pellet holder and dried at a drying-gas velocity of 2 m/s ambient. The pellet holder was periodically removed and weighed until a targeted weight loss was achieved.

#### 7.3.3.4 Briquetting

For most briquetting runs, 3 to 4 kg batches of dried coal pellets, dried coal pellets and biomass, dried coal fines, or dried coal fines and biomass were loaded to the briquette press feed hopper and briquetted. For coal pellets that were made with a binder, the binder was blended with the coal fines prior to pelletization. For the briquetting of coal fines or coal fines and biomass with binder, the binder was pre-blended with the coal fines or coal fines and biomass prior to loading to the briquette press feed hopper. For briquetting experiments with thermally dried pellets without biomass, the dried pellets were either loaded immediately to the briquette press hopper or allowed to cool to room temperature prior to briquetting. For thermally dried pellets that were to be co-briquetted with biomass, the hot pellets and biomass were blended in a heated 20 liter mixing bowl and then briquetted immediately while hot or allowed to cool to before briquetting

Briquettes were formed at a roller force of 80 kN, a roller speed of 25 Hz (nominal production rate of 45 kg/hr [100 lbs/hr]), and a targeted feed-auger torque of 90 Nm. Immediately following formation, each batch of briquettes was processed through to a Sweco mechanical screener fitted with a 61-cm (2 ft) diameter, 4.76 mm (4 mesh) screen to remove fines. The entire batch of briquettes were collected from the exit chute of the mechanical screener and stored in a controlled-environment chamber until tested.

#### 7.3.3.5 Moisture Optimization

To determine the optimum moisture content for briquetting, the four high moisture study coals were formed into spherical pellets in the 40 cm pelletizer and then thermally dried to varying degrees. Pellets were formed both without a binder and with six binder formulations that were pre-blended with each coal on a cost-equivalent basis of $15/ton[1]. Approximately 25 kg of pellets were prepared for each coal-binder blend and stored in sealed buckets until tested. Approximately 3 kg subsamples of each of the pelletized samples were loaded to the thermal dryer and dried at 200 °C and an ambient drying-air velocity of 2 m/s. After drying for a targeted time interval, the sample was removed, weighed, and immediately briquetted prior to cooling. Due to differences in packing density and run-to-run drying-gas velocities as well as variations in

[1] The addition rate for the WG binder was not based on the prohibitively high market price of pre-gelatinized wheat starch but rather on a conservative assumption that un-gelatinized wheat starch could be modified on site for $100/ton.

the initial pellet moistures, the final moisture attained was not highly correlated with drying time making it difficult to accurately attain the target moisture.

The initial moisture content for each briquetted sample was determined by collecting 6-8 briquettes from the briquetter discharge chute during each run, immediately weighing, and then placing into a drying oven overnight at 105 °C. Unexpectedly, the weight of several of the thermally dried samples increased slightly during the oven-drying step resulting in a negative value for the initial briquette moistures. This increase in mass happened most often with the MRC coal followed by the ASB coal (only one of the PCC samples and none of the RVSB samples exhibited an increase in weight during drying) and was most pronounced in those samples formed with the molasses/slaked lime binder (as high 1.7% increase in mass in one sample). As for the larger weight gain in briquettes made with calcined lime, it is possible the calcined lime dehydrated during drying then reabsorbed moisture overnight or alternatively, incorporated atmospheric $CO_2$, leading to a gain in mass. Attempts to measure the initial briquette moisture by drying the briquettes at a reduced temperature under vacuum were found to lessen but not eliminate the weight gain for those pellets that were dried to very low moisture levels before briquetting. The reason for the increase in mass is unknown but may result from absorption or incorporation of an atmospheric gas ($H_2O$, $O_2$, or $CO_2$) as the briquettes cooled in the environmental chamber. However, the more likely reason for this weight gain is thought to be due to having dried the pellets to a moisture level that was lower than the equilibrium moisture at 105 °C, resulting in the re-absorption of atmospheric moisture within the drying oven.

#### 7.3.3.6 Briquette Production from Hot and Cooled Blends of Biomass and Coal Pellets

Several 12 kg batches of coal pellets were made in the 40 cm disk pelletizer from blends of 3 wt% wheat starch and either PCC, RVSB, or MRC coal fines. Next, 3-kg subsamples of green pellets from each batch were loaded to the thermal dryer operating at 175 °C and 3 m/s drying-gas velocity and dried to 1-2 wt% moisture. After drying, the pellets were blended with 10 wt% biomass in a 20 liter dough-style blender and allowed to cool before forming into briquettes. A second 3-kg split of each of the pelletized coal was dried and blended with biomass in an identical manner, only this time, mixing with biomass was conducted in a heat-traced mixing bowl to suppress heat loss and the coal-biomass blends were quickly briquetted while

hot. This hot versus ambient temperature briquetting procedure was repeated for all 15 combinations of coal (MRC, PCC, and RVSB) and biomass (corn stover, wheat straw, miscanthus, EtOH bio-char, and kiln dried sawdust) as well as for the three coal samples without biomass, yielding a total of 36 briquetted samples for comparison.

## 7.4 Results and Discussion

### 7.4.1 Moisture Optimization Study

Moisture content is a critical parameter for controlling briquette durability, particularly green strength. Prior to initiating a study of sequential pelletization-drying-briquetting, it was deemed important to first determine the optimum moisture for briquetting pellets made with the four study coals. Further, considering that coal is the major component of the coal-biomass briquettes to be produced, the study to identify the optimum coal moisture was undertaken without the additional complication of biomass addition.

As described in the Experimental section, master samples of pellets were prepared with each of the four high-moisture study coals, both with and without binder. Several splits of each of the master samples were then dried to various moisture levels in order to determine the range of moisture that provided the strongest briquettes for each coal[2].

Green crushing strengths determined 30 minutes after formation are shown in Figure 7-4 and Figure 7-5 as a function of binder types and initial briquette moisture[3]. There is significant scatter in these data that is likely amplified by the relatively close spacing of moisture values on the low end coupled with potential inaccuracies in the moisture determinations. For a given coal, the strongest briquettes were obtained with the WG binder followed by two proprietary binders (Binder 1 and Binder 2) while the binderless briquettes exhibited the lowest strengths. For a given binder, the MRC coal generally exhibited the highest or near highest strengths.

[2] As an aside, during preparation of the coal pellets, it was observed that the small-particle-size MRC coal pelletized the most easily regardless of the binder added while the larger-particle-size ASB coal proved to be the most challenging.

[3] The moisture content for briquetted samples that exhibited a weight gain during the overnight drying as discussed in the Experimental section are plotted as 0%.

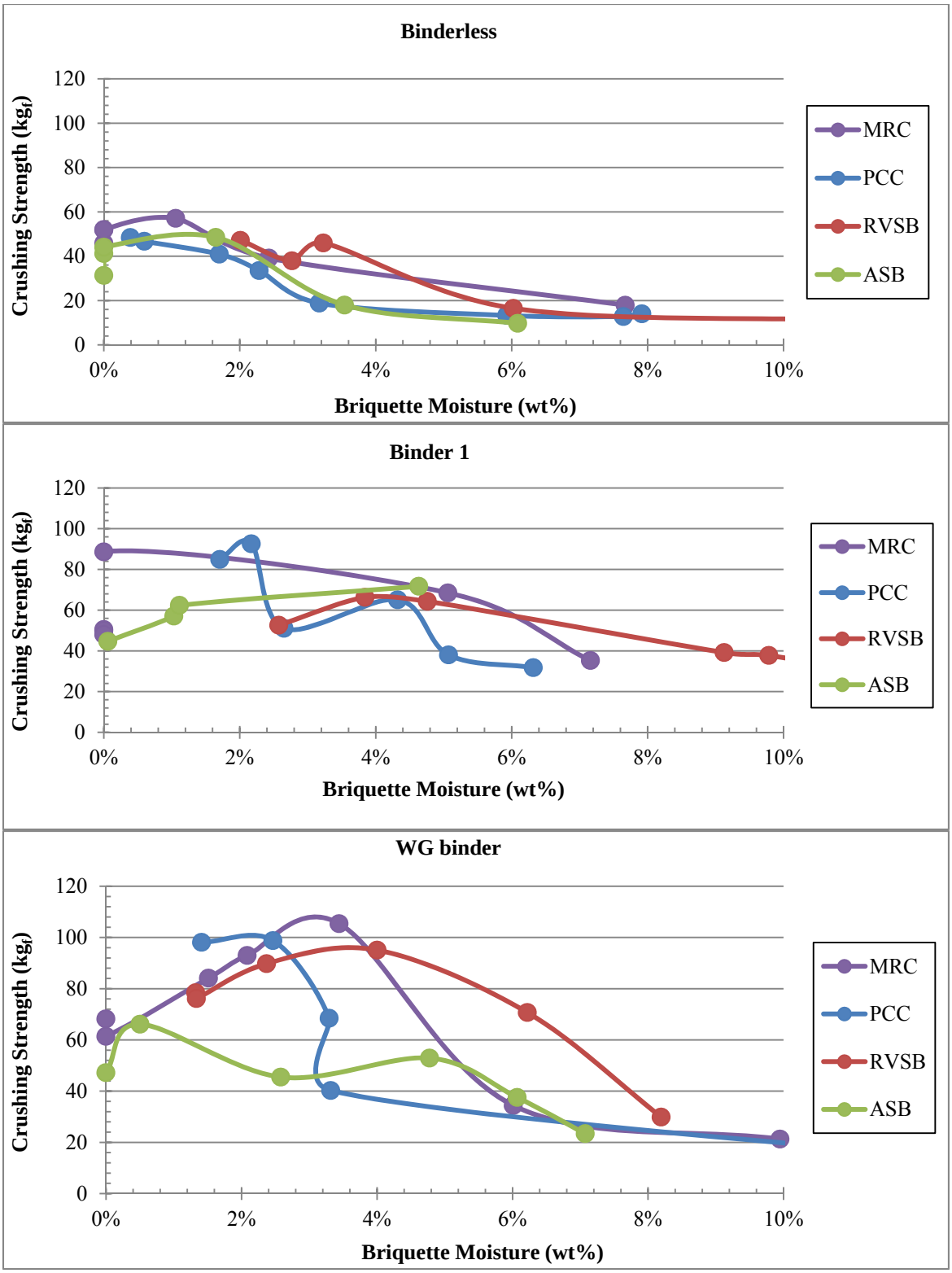



Figure 7-4. Thirty minute crushing strengths for briquettes made from thermally dried coal pellets that were formed with or without binder as indicated

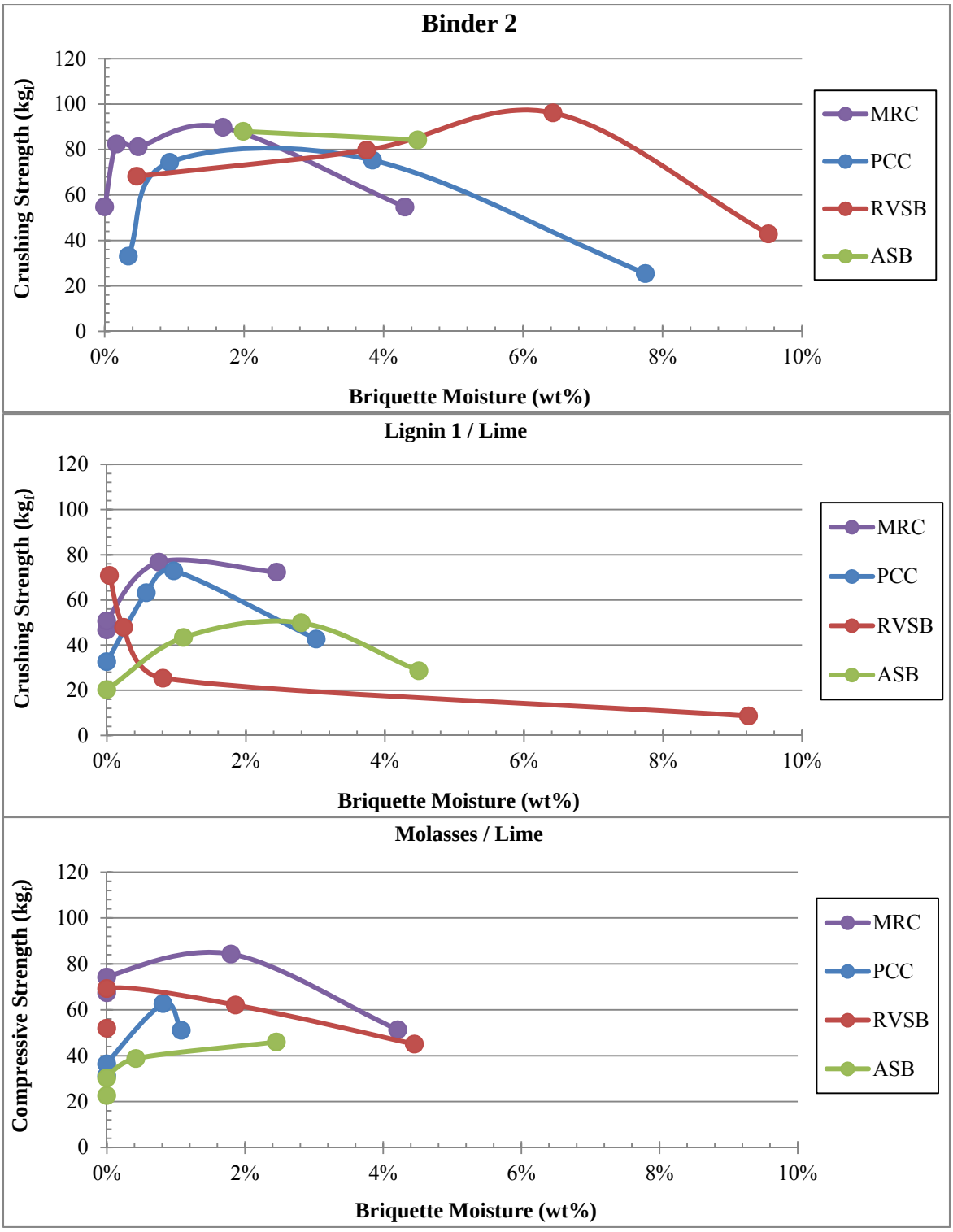



Figure 7-5. Thirty minute crushing strengths for briquettes made from thermally dried coal pellets that were formed with the indicated binders

Cured crushing strengths determined 7 days after formation are shown for briquettes made with each of the coal-binder blends in Figure 7-6. This plot reveals that the strongest

briquettes were obtained with the smaller-particle-size MRC coal regardless of the binder used while the larger particle size ASB coal consistently produced briquettes with the lowest strengths. Most of the briquetted samples exhibited small increases in strength as the briquettes cured with the most pronounced increase in strength exhibited by the MRC briquettes. The strongest briquettes were obtained with the WG binder for two of the coals while Binder 2 provided the strongest briquettes with the other two coals.

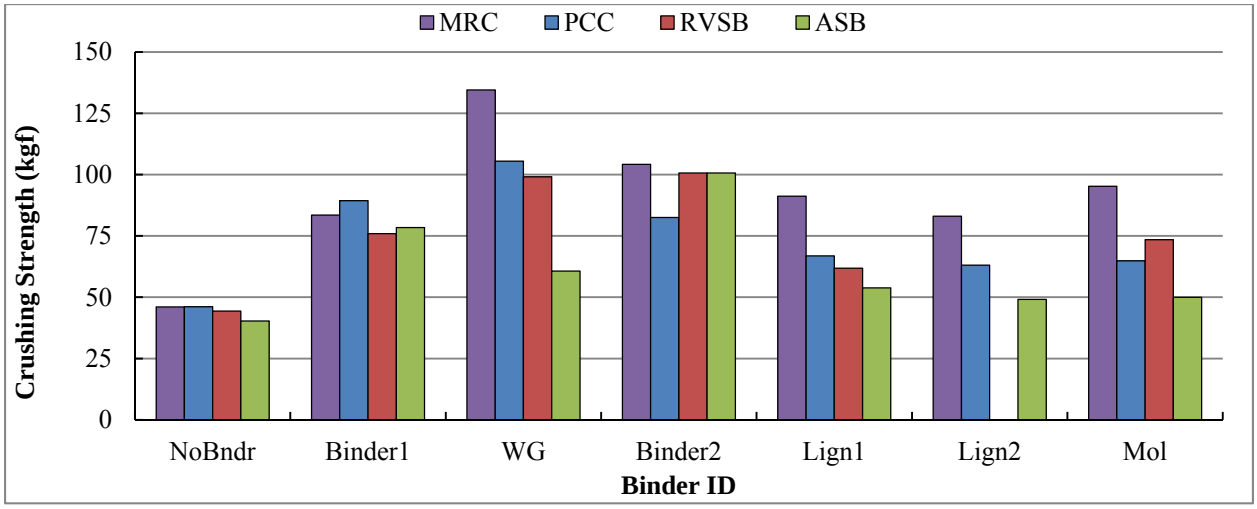



Figure 7-6. Seven day crushing strengths for the briquetted samples that exhibited the highest crushing strengths for each of the pelletized coal-binder blends

The corresponding mechanical durability values are shown in Figure 7-7. Similar to crushing strengths, the best mechanical durability for a given binder was generally obtained with the small particle size MRC coal, with the larger-sized ASB fines generally exhibiting the lowest durability values. While the binderless briquettes consistently exhibited the lowest mechanical durability values for all four study coals, note that the binderless briquettes formed with the MRC coal exhibited a value of 0.83, which classifies as acceptable. Several of the samples exhibited mechanical durability values that classified as good (>0.90) with the briquettes made with Binder 2 providing the highest durability values for three of the four coals evaluated and the WG and Binder 1 binders providing the highest durability values with the fourth coal (PCC).

While there is a great deal of scatter in the data, the plots shown in Figure 7-4 through Figure 7-7 indicate that the strongest briquettes were formed when a binder was added from coal pellets with moisture contents in the range of about 1 to 4%, with strengths generally decreasing above and below these levels. For binderless briquettes, the optimum moisture tended to be in

the range of about 2% or less. Optimum moisture was generally about the same for the three coals from the Appalachian field but tended to be somewhat higher for the slightly lower rank coal and higher inherent moisture RVSB coal from the Illinois Basin.

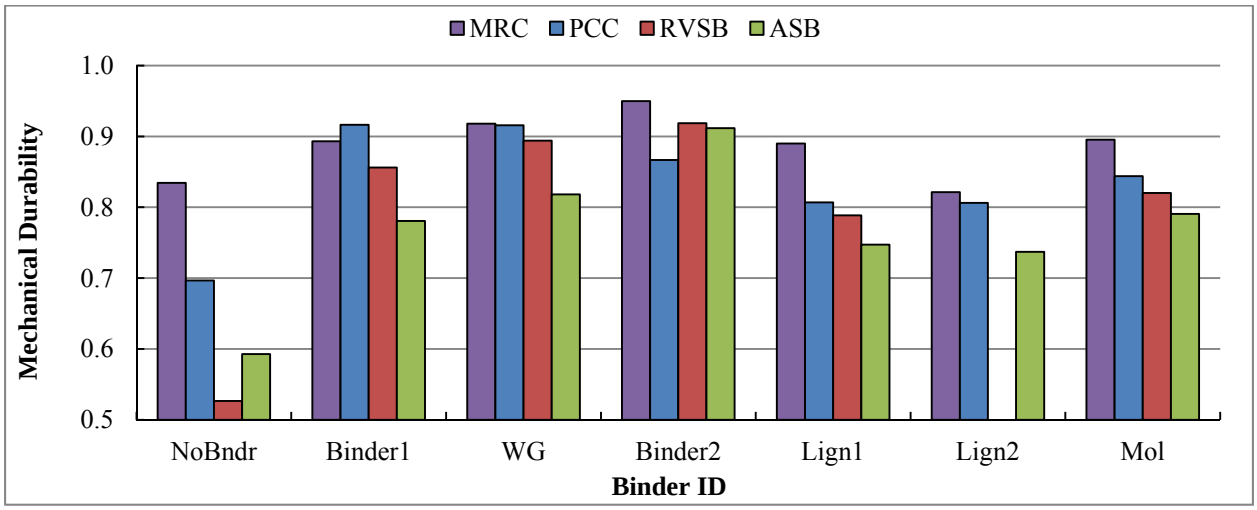



Figure 7-7. Mechanical durability values of the briquetted samples that exhibited the highest crushing strengths for each of the pelletized coal-binder blends

## 7.4.2 Preliminary Comparisons of Briquettes Formed with Hot and Ambient Temperature Feedstocks

In addition to the potential for obtaining more-uniform binder coverage with a pre-pelletization step, results from the moisture-optimization study suggest that briquetting a heated feedstock provided a more durable briquette than did briquetting an equivalent feedstock at ambient temperature. Since conventional coal-fines drying technologies rely on thermal processes, there is a potential to significantly improve briquette durability by briquetting the coal fines as they exit a thermal dryer while hot versus briquetting the fines after they have cooled (e.g. following silo storage).

To investigate this potential, a series of experiments were conducted to compare properties of briquettes made from hot, thermally dried pellets to the properties of briquettes made with ambient temperature feedstocks including thermally dried pellets that were air cooled before briquetting, air dried fines, and air dried pellets. The feedstocks used for this study were obtained from splits of the 25 kg samples of pelletized coals that were thermally dried and briquetted hot for the moisture optimization study described in the preceding section. One split was allowed to air dry to equilibrium moisture while a second split was thermally dried and

allowed to cool in room air before briquetting. For comparison, a third set of briquette samples was prepared from the same coals using un-pelletized fines that had been air dried to equilibrium moisture prior to adding binder and briquetting.

Comparisons of seven-day crushing strengths for briquettes made with hot versus ambient temperature pellets are shown in Figure 7-8 and Figure 7-9. The data in these figures that represents briquettes made with hot pellets corresponds to the briquetted samples from the moisture optimization study whose moisture content most closely matched that of the briquettes formed from their ambient-temperature counterparts.

A comparison of the 7 day crushing strengths in Figure 7-8 and Figure 7-9 demonstrates that a significantly higher strength was obtained with all four of the pelletized coals when the briquettes were made with hot pellets versus when made from otherwise equivalent pellets that were cooled to ambient-temperature before briquetting. This increase is particularly striking for the briquettes made with the Binder 2 and Lignin 1/Lime binders in which crushing strengths increased on average by ~84% and ~94%, respectively. The smallest increase in strength for hot- versus cool-pellet briquetting was exhibited by the binderless briquettes, which averaged a more modest increase of ~12%.

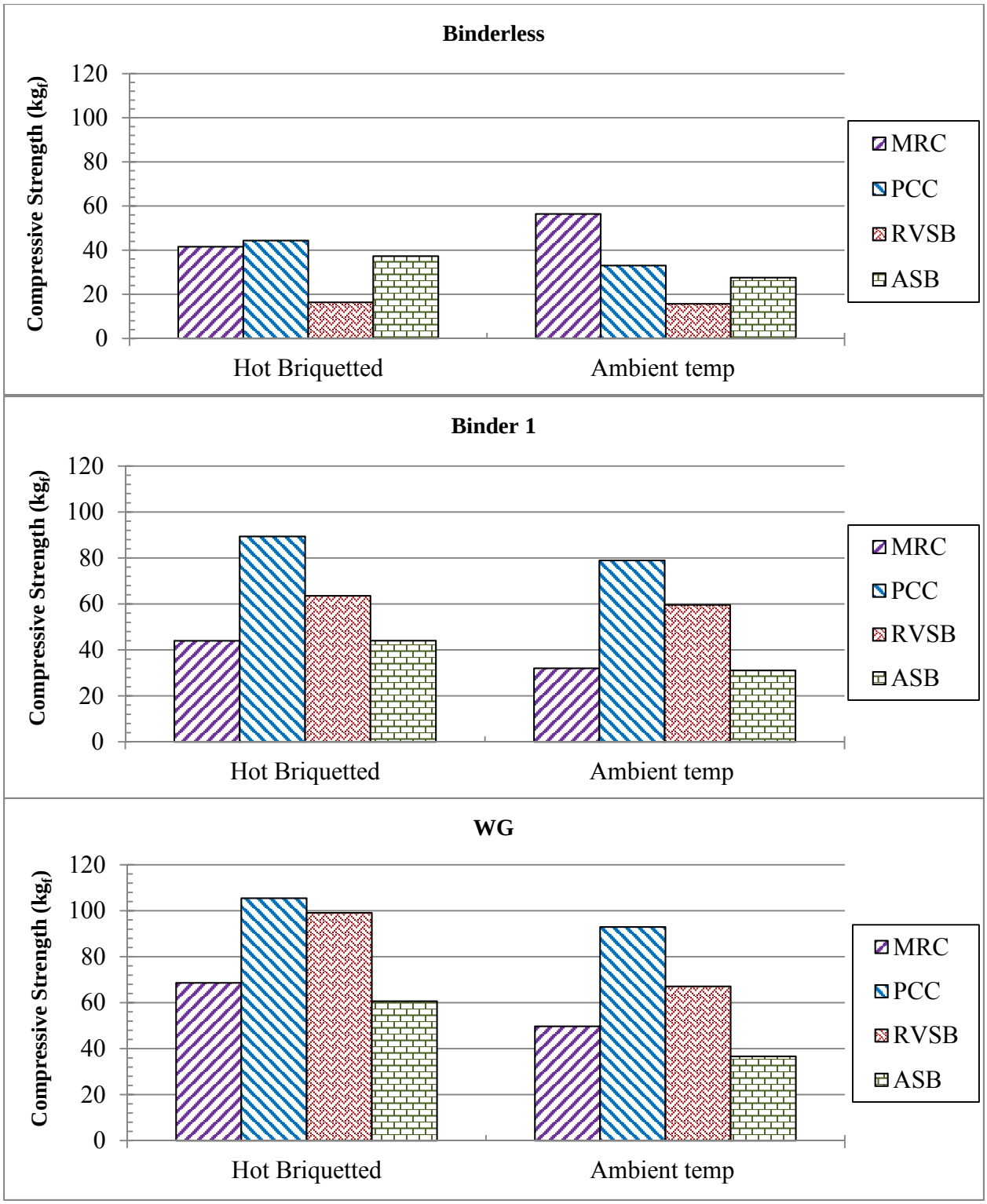



Figure 7-8. Comparison of 7 day crushing strengths for briquettes made from thermally dried coal pellets that were either immediately briquetted while hot or cooled to ambient temperature before briquetting and shown as a function of the binder added

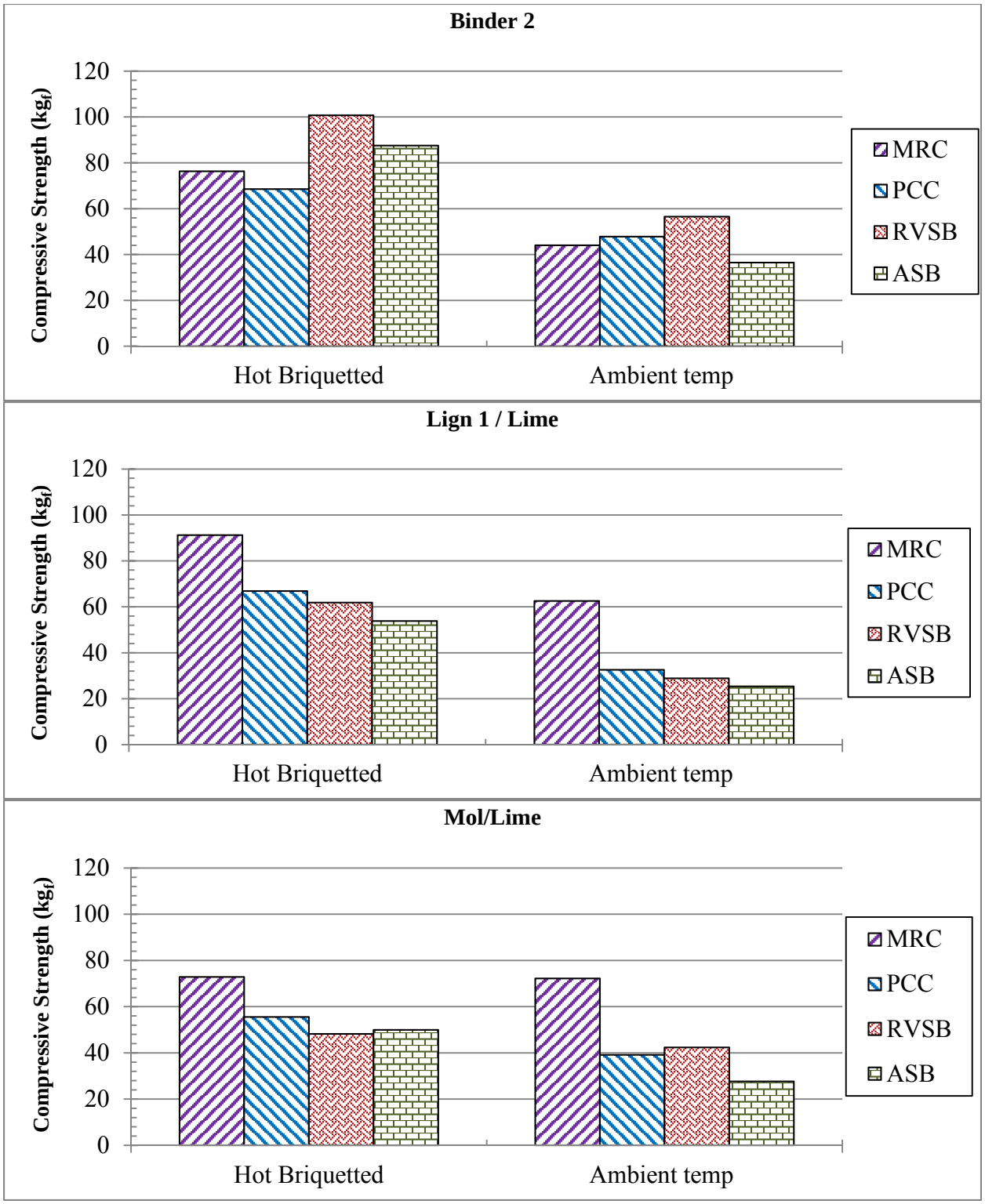



Figure 7-9. Comparison of 7 day crushing strengths for briquettes made from thermally dried coal pellets that were either immediately briquetted while hot or cooled to ambient temperature before briquetting and shown as a function of the binder added

The average increase in the 30 minute and 7 day crushing strengths for briquettes made with hot versus ambient temperature pellets are grouped according to the binder added were averaged for all four pelletized coals and shown in Table 7-5. These data show that when the thermally dried coal pellets were briquetted hot versus after cooling, the average 30 minute and 7 day crushing strengths increased by 44% and 48%, respectively. When only those briquette that were made with a binder are considered, the average increase was 49% and 56%, respectively.

Table 7-5. The average increase in 30 minute and 7 day crushing strengths for briquettes formed with thermally dried pellets that were briquetted while hot versus equivalent pellets that were cooled to ambient temperature before briquetting

| **Binder** | **30 Minute Crushing Strength (% increase)** | **7 Day Crushing Strength (% increase)** |
|---|---|---|
| No Binder | 17.7% | 11.9% |
| Binder 1 | 26.8% | 24.7% |
| Wheat starch | 26.5% | 41.2% |
| Binder 2 | 72.7% | 83.6% |
| Lignin 1 / Lime | 95.1% | 94.4% |
| Molasses/Lime | 22.4% | 34.3% |

Note that there are substantial differences in the magnitude of increase in crushing strengths as a function of the binder added in Table 7-5. This would suggest that certain binders (i.e., Binder 2 and Lignin1/Lime) were substantially more effective when thermally dried and briquetted while hot. Also note that the increase in strength for the briquettes made with all five binders was greater than the average increase in strength for briquettes made without a binder indicating that all the binders evaluated benefited from hot briquetting.

The corresponding mechanical durability values for briquettes made with four of the briquette samples are shown in Figure 7-10. Similar to the trends in crushing strength, the mechanical durability of the briquettes made with hot pellets were consistently higher than those made from equivalent pellets that were cooled before briquetting. The average increase in the weight of fines (less than 4.76 mm [4 mesh]) generated during the mechanical durability test for briquettes made with pellets that were cooled to ambient temperature versus equivalent pellets that were briquetted hot are shown in Table 7-6. These data represent the average for all four

pelletized coals grouped according to the binder that was added[4]. Similar to the trends noted for crushing strength, briquettes that were made without a binder exhibited the smallest improvement in mechanical durability when the pellets were briquetted hot rather than after cooling. Also, similar to the trends in crushing strength, there were substantial differences in the mechanical durability of briquettes made with hot versus cool pellets as a function of the binder added.

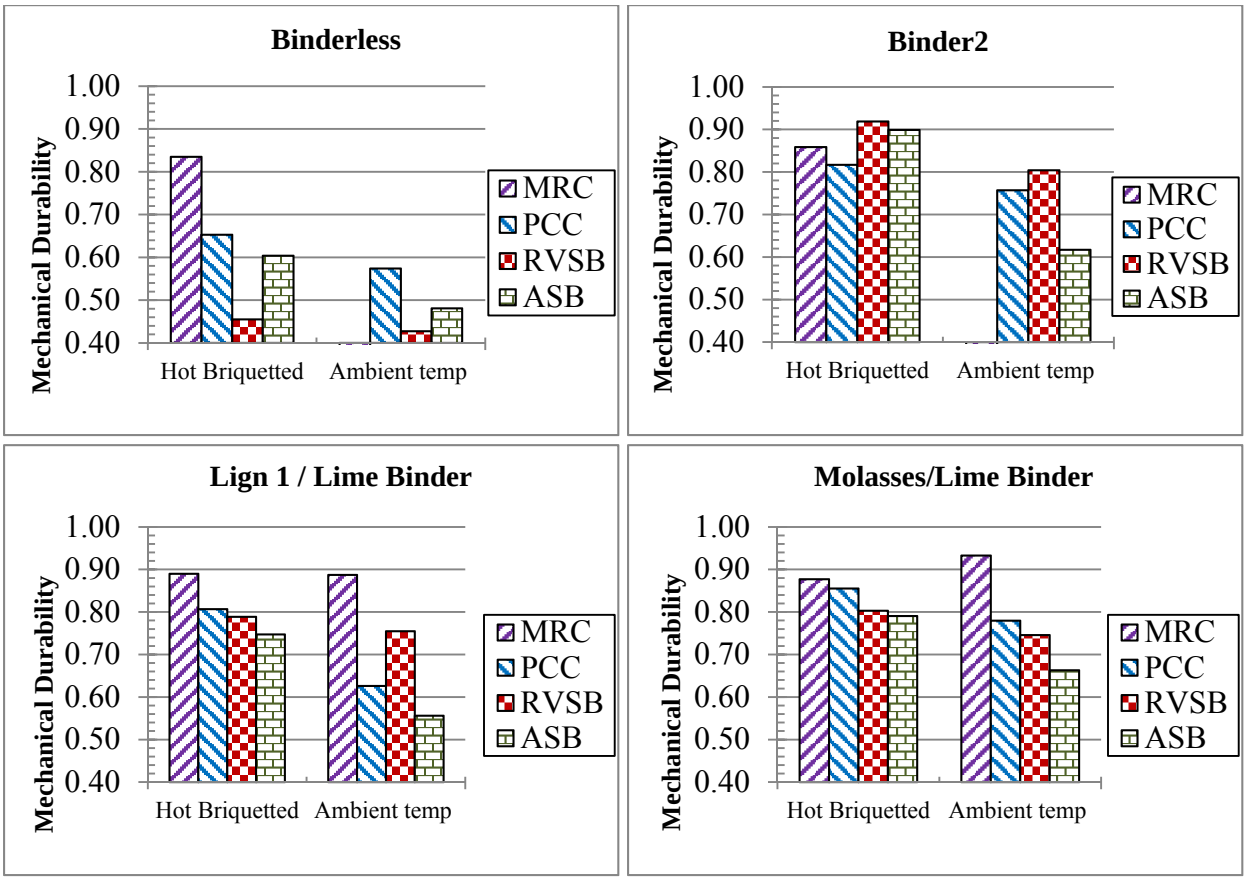



Figure 7-10. Comparison of mechanical durability results for briquettes made from thermally dried coal pellets that were briquetted hot versus equivalent pellets that were thermally dried then cooled to ambient temperature before briquetting

[4] Four coals formed into pellets with 5 binders or without a binder equates to 24 potential hot versus ambient sample pairs. However, only 19 sample pairs were evaluated, as briquetting was not conducted after cooling for five of the pelletized coal samples.

Table 7-6. Increase in fines generated during mechanical durability testing for briquettes formed with thermally dried pellets that were cooled before briquetting versus equivalent pellets that were briquetted hot

| Binder | Increase of -4 mesh Fines Generated during Durability Testing of Briquettes made from Cooled vs Hot Pellets |
|---|---|
| No Binder | 19.6% |
| Binder 1 | 21.7% |
| Wheat starch | 108.6% |
| Binder 2 | 151.0% |
| Lignin 1 / Lime | 46.9% |
| Molasses/Lime | 24.3% |

#### 7.4.2.1 Comparison of Briquettes made with Hot, Thermally Dried Coal Pellets versus those made with Air Dried, Ambient Temperature Pellets

In the next study, the durability of briquettes made with thermally dried pellets that were briquetted hot was compared to the durability of briquettes made with equivalent pellets that were air dried and briquetted at ambient temperature. The increase in the average 30 minute and 7 day crushing strengths for briquettes made with hot pellets relative to those made with air dried pellets was 26.1% and 38.8%, respectively[5]. The weight of material smaller than 4.76 mm (4 mesh) generated during mechanical durability testing was on average 66.5% greater for the air dried pellets compared to the briquettes made with the thermally dried, high temperature pellets. However, while the differences in strength and durability characteristics were large, it must be noted that there were inconsistencies and substantial scatter in these data and many of the coal-binder combinations were not included in these preliminary investigations. Therefore, a decision was made to repeat this comparison in a follow up study described later in this chapter.

#### 7.4.2.2 Comparison of Briquettes formed from Air Dried Pellets versus Un-pelletized Air Dried Fines

The objective of the next comparison was to determine if pelletizing fine coal and binder provided more durable briquettes than obtained by briquetting un-pelletized fine coal and binder. For this study, blends were prepared for briquetting from splits of each of the four coals by either

[5] These data represent the overall average changes measured from comparisons of all four high-moisture coals for 5 of the 6 binders evaluated. Data for the binderless briquettes and the Lignin 2/Lime binder are omitted as several of the potential sample pairs for these sample sets were not prepared and tested.

blending with a binder then pelletizing and air drying the pellets or by air drying the fine coal and blending it with a binder without pelletizing.

The average increase in 30 minute and 7 day crushing strength for the air dried pellets versus the un-pelletized fines was a meager 6.2 and 3.2%, respectively[6]. On the other hand, there was a more substantial average increase of 26.2% in the weight of fines generated during mechanical durability testing by the briquettes made from the air dried fines relative to those made with air dried pellets. Unfortunately as before, data from about half the potential sample pairs was not obtained and there were again inconsistencies and substantial scatter in the data due in part to problems associated with obtaining comparable levels of moisture in the matching sample pairs that were being compared. Accordingly, it was decided this comparison should also be more fully repeated as will be presented later in this chapter.

#### 7.4.2.3 Comparison of Briquettes formed from Hot, Thermally Dried Coal Pellets versus Un-pelletized Air Dried Coal Fines

The objective in this final round of preliminary comparisons was to determine the full extent to which briquette durability might be enhanced by the combination of pelletizing, with its potential to improve binder dispersion, and hot briquetting, which appears to improve durability[7].

In this comparison, the average increase in the 30 minute and 7 day crushing strengths for briquettes made with hot, thermally dried pellets containing a binder[8] was 32.8 and 32.6%, respectively, compared to equivalent formulations made with air dried fines and binder. Likewise, the increase in the weight of -4 mesh fines generated during mechanical durability testing averaged 41.8% for the briquettes made with binder and air dried fines versus equivalent formulations that were pelletized, thermally dried, and briquetted hot. In contrast, briquettes that were formed without a binder with the air dried fines were both stronger and more durable than those made with otherwise equivalent binderless coal pellets that were thermally dried and briquetted hot[9]. When the binderless data are included in the averages, the increase in the 30 minute and 7 day crushing strength for the hot-briquetted pellets drops to 24.4% and 26.2%,

[6] Results from the binderless briquettes were not included in these average values.
[7] Possible reasons for the observed improvement in briquette performance following thermal drying and hot briquetting include thermal-activation of one or more of the binders, improved binder dispersion, or softening of the coal particles leading to more efficient packing.
[8] The molasses/lime binder was not evaluated in this comparison.
[9] Data for the ASB coal are omitted as binderless pellets could not be formed with the larger-particle-size ASB coal fines.

while the increase in -4 mesh fines generated by the un-pelletized fines declines to 28.1%. These results would suggest that perhaps either thermal activation or heat-induced binder dispersion was the reason for the improvement in briquette properties. However, as before, a significant portion of the sample pairs were not included in these first round tests (only 9 of the 20 possible sample pair combinations were evaluated) and there were inconsistencies and substantial scatter in the data, again attributed in part to problems associated with obtaining comparable levels of moisture in the matching sample pairs.

A summary of the average increases in crushing strengths and fines generation for the preliminary evaluations described above is given in Table 7-7. The data represent averages for all available sample pairs evaluated regardless of binder type. The increase in average crushing strength refers to the first sample named in column 1 relative to the second. The increase in fines generated refers to the second sample named in column 1 relative to the first. From these preliminary studies of pre-briquetting drying methods, it was concluded that briquettes made with coal/binder blends that were pelletized, thermally dried and briquetted hot consistently exhibited higher crushing strengths and mechanical durability results relative to briquettes formed from analogous pellets that were thermally dried and cooled, pellets that were air dried, or fines that were air dried.

Missing data points combined with inconsistent results led to a decision to essentially repeat the entire preliminary study, as is described in the next section. While the data from the preliminary studies was somewhat sparse and often inconsistent, the results are nonetheless congruent with results from the repeat tests. The data obtained in the repeat experiments is much more complete, consistent, and reliable and could been presented without the preliminary test data. However, a decision was made to include the preliminary data as they provide strong support that the results and conclusions drawn in the in the next section are accurate.

Table 7-7. Comparison of relative changes in crushing strengths and fines generation during mechanical durability testing for briquettes made with thermally dried hot pellets, thermally dried cool pellets, air dried pellets, and air dried un-pelletized fines

| Comparison | Increase in Crushing Strength (hot vs ambient) | | Increase in -4 mesh fines generation (ambient vs hot) |
|---|---|---|---|
| | 30 min | 7 day | |
| Hot vs cooled thermally dried pellets | 43.5% | 48.4% | 62.0% |
| Hot pellets vs air dried pellets | 26.1% | 38.8% | 66.5% |
| Hot pellets vs un-pelletized fines | 24.4% | 26.2% | 28.1% |
| Air dried pellets vs un-pelletized fines[a] | 6.2% | 3.2% | 26.2% |

[a] Binderless briquette data were omitted for the comparison of air dried pellets vs un-pelletized fines (last row) in an effort to determine if pelletizing the coal with binder ultimately improves briquette durability due to more uniform binder dispersion.

## 7.4.3 Confirmation of the Impact of Pre-pelletization and Hot versus Cold Briquetting

Experiments described in the preceding section indicated that briquette durability was improved when the wet coal fines were formed into pellets before drying and briquetting compared to briquettes that were made directly from dried, un-pelletized coal fines. This improvement was more apparent when a binder was added, presumably due to more uniform distribution of the binder during pelletizing. There was an even greater improvement when the fines were pelletized, thermally dried, and briquetted hot versus when they were allowed to cool before briquetting.

Due to the potential significance of these results coupled with the substantial scatter and missing data associated with the initial evaluations, an effort was made to improve the reliability of the data by preparing and testing each sample in duplicate. These confirmation experiments focused on a comparison of briquettes made from three of the high-moisture fine coal samples that were formed from either (1) air dried, un-pelletized fines, (2) air dried spherical pellets briquetted at room temperature, or (3) spherical pellets that were thermally dried and briquetted hot.

### 7.4.3.1 Sample Preparation

The ASB sample was dropped while the three remaining high-moisture fine coal samples were selected for re-evaluation (River View screen bowl [RVSB], Perry County screen bowl [PCC], and McClure River disk filter [MRC]). Molasses/lime binder was dropped and each coal was processed either without a binder or blended with one of the four remaining binders that

were added on a cost-equivalent basis of $15/t[10] (wheat starch [WG], Lignin1/Lime [LL], or proprietary binders 1 and 2). Binders were either mixed with the air dried coal fines immediately before briquetting or mechanically mixed with the wet coal fines prior to pelletization.

The initial step in preparing blends for briquetting was to weigh out 22 kg of each coal. Approximately 1/3 of each of these samples (~7.5 kg) was spread onto plastic trays to air dry to equilibrium moisture while the remaining sample (~15 kg) was formed into spherical pellets in a 40-cm diameter (16 in) pan pelletizer. Each pelletized sample was then split into two equal portions with one split sealed in a 19 liter (5 gal) bucket and the second split also spread onto plastic trays to air dry to equilibrium moisture.

Approximately one week after formation, 3 kg splits of each of the air dried samples were briquetted in a pair duplicate briquetting runs. The wet pellets that had been stored in the 19 liter buckets were also split and loaded to the thermal dryer where they were dried in duplicate runs at 200 °C and an ambient drying-gas velocity of 2 m/s. During thermal drying, the pellet bed was intermittently removed and weighed. Drying was stopped when moisture loss approached that which had been recorded for the matching samples of air dried pellets and fines and the thermally dried pellets were immediately briquetted while hot.

#### 7.4.3.2 Comparison of Briquettes formed from Air Dried Fines, Air Dried Pellets, and Thermally Dried Pellets

Test results for briquettes prepared from air dried fines, air dried pellets, and thermally dried pellets are shown in Table 7-8 through Table 7-12, with each table representing results for a different binder (e.g. binderless, wheat starch, Binder1, Binder2, and lignin/lime). With few exceptions, most notably the two runs shown as strike-through data in Table 7-8 and Table 7-12 in which thermal drying was stopped well short of attaining the target moisture, the data for each pair of replicate runs are remarkably similar (typically within 5%). The consistency of these data was significantly better than the data from the preliminary comparisons leading to a greater confidence in the results.

[10]A conservative assumption was made that the un-gelatinized wheat starch could be modified on site at a cost of $100/ton, which was added to the prevailing market price for un-gelatinized wheat starch for this calculation.

Table 7-8. Comparison of binderless briquettes made from air dried fines, air dried pellets, and thermally dried pellets

| Run | Briquette Moisture | Crushing Strength ($kg_f$) | | | Moisture Degradation | | | |
|---|---|---|---|---|---|---|---|---|
| | | 30 min | 24 hr | 7 day | Mechanical Durability | Avg Briq Wt (g) | Wet Str ($kg_f$) | Water Uptake |
| **PCC-Air Dried Fines** | | | | | | | | |
| Run #1 | 1.7% | 36 | 33 | 35 | 0.63 | 9.10 | 48 | 8.9% |
| Run #2 | 1.3% | 31 | 31 | 31 | 0.56 | 9.10 | 38 | 8.8% |
| Average | 1.5% | 33 | 32 | 33 | 0.60 | 9.10 | 43 | 8.8% |
| **PCC-Air Dried Pellets** | | | | | | | | |
| Run #1 | 1.5% | | | | 0.50 | 8.92 | 33 | 9.9% |
| Run #2 | 1.5% | 25 | 23 | 23 | 0.50 | 8.91 | 33 | 10.2% |
| Average | 1.5% | 26 | 24 | 24 | 0.50 | 8.91 | 33 | 10.1% |
| **PCC-Thermally Dried Pellets** | | | | | | | | |
| Run #1 | 0.3% | 53 | — | 49 | 0.71 | 9.11 | 81 | 7.4% |
| Run #2 | 0.8% | 51 | — | 43 | 0.66 | 8.97 | 69 | 9.2% |
| Average | 0.6% | 52 | — | 46 | 0.69 | 9.04 | 75 | 8.3% |
| **RVSB-Air Dried Fines** | | | | | | | | |
| Run #1 | 3.2% | 18 | 14 | 14 | 0.31 | 8.16 | 13 | 12.5% |
| Run #2 | 3.1% | 16 | 13 | 14 | 0.29 | 8.17 | 13 | 12.5% |
| Average | 3.2% | 17 | 13 | 14 | 0.30 | 8.16 | 13 | 12.5% |
| **RVSB-Air Dried Pellets** | | | | | | | | |
| Run #1 | 2.4% | 18 | 16 | 16 | 0.33 | 8.67 | 15 | 11.4% |
| Run #2 | 2.6% | 17 | 13 | 16 | 0.31 | 7.96 | 10 | 7.2% |
| Average | 2.5% | 17 | 14 | 16 | 0.32 | 8.31 | 12 | 9.3% |
| **RVSB-Thermally Dried Pellets** | | | | | | | | |
| ~~Run #1~~ | ~~6.3%~~ | ~~9~~ | ~~11~~ | ~~11~~ | ~~0.18~~ | — | — | — |
| Run #2 | 3.9% | 18 | 17 | 16 | 0.28 | 8.74 | 15 | 22.1% |
| Average | 3.9% | 18 | 17 | 16 | 0.28 | 8.74 | 15 | 22.1% |
| **MRC-Air Dried Fines** | | | | | | | | |
| Run #1 | 0.9% | 38 | 37 | 32 | 0.67 | 8.16 | 35 | 7.7% |
| Run #2 | 0.9% | 35 | 32 | 34 | 0.68 | 8.53 | 39 | 6.5% |
| Average | 0.9% | 36 | 34 | 33 | 0.68 | 8.34 | 37 | 7.1% |
| **MRC-Air Dried Pellets** | | | | | | | | |
| Run #1 | 1.1% | 44 | 40 | 37 | 0.78 | 8.43 | 53 | 6.2% |
| Run #2 | 0.9% | 42 | 43 | 44 | 0.81 | 8.74 | 51 | 5.8% |
| Average | 1.0% | 43 | 42 | 41 | 0.80 | 8.58 | 52 | 6.0% |
| **MRC-Thermally Dried Pellets** | | | | | | | | |
| Run #1 | 0.6% | 57 | 40 | 50 | 0.85 | 8.74 | 57 | 3.2% |
| Run #2 | 0.6% | 58 | 43 | 51 | 0.85 | 8.56 | 63 | 4.4% |
| Average | 0.6% | 58 | 42 | 51 | 0.85 | 8.65 | 60 | 3.8% |

Table 7-9. Comparison of briquettes made from air dried fines, air dried pellets, and thermally dried pellets, all of which were blended with 2.4 wt% gelatinized wheat starch binder

| Run | Briquette Moisture | Crushing Strength ($kg_f$) | | | Moisture Degradation | | | |
|---|---|---|---|---|---|---|---|---|
| | | 30 min | 24 hr | 7 day | Mechanical Durability | Avg Briq Wt (g) | Wet Str ($kg_f$) | Water Uptake |
| **PCC-Air Dried Fines** | | | | | | | | |
| Run #1 | 2.1% | 68 | 75 | 71 | 0.89 | 9.72 | — | — |
| Run #2 | 2.3% | 67 | 70 | 70 | 0.90 | 9.56 | — | — |
| Average | 2.2% | 67 | 73 | 71 | 0.89 | 9.64 | — | — |
| **PCC-Air Dried Pellets** | | | | | | | | |
| Run #1 | 2.0% | 83 | 89 | 85 | 0.91 | 10.10 | — | — |
| Run #2 | 2.1% | 74 | 82 | 79 | 0.91 | 9.83 | — | — |
| Average | 2.0% | 79 | 86 | 82 | 0.91 | 9.97 | — | — |
| **PCC-Thermally Dried Pellets** | | | | | | | | |
| Run #1 | 1.2% | 98 | 96 | 92 | 0.89 | 9.39 | 19 | 14.0% |
| Run #2 | 1.5% | 89 | 90 | 87 | 0.90 | 9.37 | 18 | 13.8% |
| Average | 1.4% | 94 | 93 | 89 | 0.90 | 9.38 | 18 | 13.9% |
| **RVSB-Air Dried Fines** | | | | | | | | |
| Run #1 | 2.7% | 51 | 52 | 51 | 0.79 | 9.14 | 1 | 33.8% |
| Run #2 | 2.5% | 47 | 46 | 40 | 0.73 | 9.15 | 3 | 33.8% |
| Average | 2.6% | 49 | 49 | 46 | 0.76 | 9.15 | 2 | 33.8% |
| **RVSB-Air Dried Pellets** | | | | | | | | |
| Run #1 | 3.5% | 57 | 57 | 57 | 0.81 | 9.60 | 4 | 31.7% |
| Run #2 | 3.5% | 59 | 53 | 52 | 0.80 | 9.57 | 5 | 30.2% |
| Average | 3.5% | 58 | 55 | 55 | 0.80 | 9.59 | 4 | 31.0% |
| **RVSB-Thermally Dried Pellets** | | | | | | | | |
| Run #1 | **1.9%** | 75 | 75 | 75 | 0.84 | 9.17 | 35 | 14.5% |
| Run #2 | 2.3% | 83 | 75 | 78 | 0.85 | 8.97 | 21 | 17.6% |
| Average | 2.1% | 79 | 75 | 76 | 0.85 | 9.07 | 28 | 16.1% |
| **MRC-Air Dried Fines** | | | | | | | | |
| Run #1 | 1.6% | 78 | 82 | 82 | 0.92 | 8.67 | 8 | 23.1% |
| Run #2 | 1.7% | 60 | 66 | 68 | 0.88 | 8.49 | 6 | 21.5% |
| Average | 1.6% | 69 | 74 | 75 | 0.90 | 8.58 | 7 | 22.3% |
| **MRC-Air Dried Pellets** | | | | | | | | |
| Run #1 | 0.7% | 70 | 84 | 88 | 0.91 | 8.95 | 30 | 14.5% |
| Run #2 | 1.8% | 72 | 75 | 89 | 0.92 | 8.68 | 16 | 16.6% |
| Average | 1.2% | 71 | 80 | 88 | 0.91 | 8.82 | 23 | 15.5% |
| **MRC-Thermally Dried Pellets** | | | | | | | | |
| Run #1 | 0.3% | 86 | 84 | 91 | 0.87 | 8.67 | 89 | 2.4% |
| Run #2 | 0.4% | 79 | 98 | 89 | 0.88 | 8.37 | 83 | 2.5% |
| Average | 0.3% | 82 | 91 | 90 | 0.87 | 8.52 | 86 | 2.4% |

Table 7-10. Comparison of briquettes made from air dried fines, air dried pellets, and thermally dried pellets, all of which were blended with 3.1 wt% of Binder 2

| Run | Briquette Moisture | Crushing Strength ($kg_f$) | | | Moisture Degradation | | | |
|---|---|---|---|---|---|---|---|---|
| | | 30 min | 24 hr | 7 day | Mechanical Durability | Avg Briq Wt (g) | Wet Str ($kg_f$) | Water Uptake |
| **PCC-Air Dried Fines** | | | | | | | | |
| Run #1 | 2.1% | 33 | 31 | 33 | 0.58 | 9.36 | — | — |
| Run #2 | 2.2% | 35 | 35 | 35 | 0.62 | 9.37 | — | — |
| Average | 2.2% | 34 | 33 | 34 | 0.60 | 9.37 | — | — |
| **PCC-Air Dried Pellets** | | | | | | | | |
| Run #1 | 2.1% | 38 | 34 | 38 | 0.63 | 9.58 | — | — |
| Run #2 | 2.3% | 37 | 37 | 36 | 0.65 | 9.66 | 3 | 27.9% |
| Average | 2.2% | 38 | 35 | 37 | 0.64 | 9.62 | — | — |
| **PCC-Thermally Dried Pellets** | | | | | | | | |
| Run #1 | 0.0% | 55 | 55 | 49 | 0.76 | 8.96 | 14 | 18.4% |
| Run #2 | 0.8% | 66 | 63 | 58 | 0.81 | 9.53 | 9 | 19.3% |
| Average | 0.4% | 60 | 59 | 53 | 0.78 | 9.24 | 12 | 18.8% |
| **RVSB-Air Dried Fines** | | | | | | | | |
| Run #1 | 5.8% | 23 | 25 | 28 | 0.50 | 8.33 | — | — |
| Run #2 | 5.7% | 27 | 24 | 27 | 0.51 | 8.42 | — | — |
| Average | 5.8% | 25 | 25 | 28 | 0.51 | 8.38 | — | — |
| **RVSB-Air Dried Pellets** | | | | | | | | |
| Run #1 | 5.6% | 26 | 28 | 27 | 0.51 | 8.74 | — | — |
| Run #2 | 6.2% | 32 | 35 | 34 | 0.61 | 8.88 | — | — |
| Average | 5.9% | 29 | 31 | 30 | 0.56 | 8.81 | — | — |
| **RVSB-Thermally Dried Pellets** | | | | | | | | |
| Run #1 | **5.9%** | 76 | 74 | 82 | 0.89 | 8.74 | 5 | 24.0% |
| Run #2 | 5.0% | 69 | 76 | 75 | 0.91 | 8.86 | 5 | 23.5% |
| Average | 5.4% | 73 | 75 | 79 | 0.90 | 8.80 | 5 | 23.7% |
| **MRC-Air Dried Fines** | | | | | | | | |
| Run #1 | 1.5% | 54 | — | 54 | 0.79 | 8.50 | 15 | 18.5% |
| Run #2 | 1.5% | 49 | 55 | 45 | 0.72 | 8.60 | 11 | 17.3% |
| Average | 1.5% | 51 | 55 | 49 | 0.75 | 8.55 | 13 | 17.9% |
| **MRC-Air Dried Pellets** | | | | | | | | |
| Run #1 | 1.6% | 36 | 36 | 34 | 0.69 | 8.16 | 6 | 18.6% |
| Run #2 | 1.6% | 40 | 36 | 32 | 0.68 | 8.38 | 8 | 17.0% |
| Average | 1.6% | 38 | 36 | 33 | 0.68 | 8.27 | 7 | 17.8% |
| **MRC-Thermally Dried Pellets** | | | | | | | | |
| Run #1 | 0.4% | 63 | — | 49 | 0.78 | 8.42 | 31 | 7.9% |
| Run #2 | 0.3% | 82 | — | 79 | 0.85 | 9.06 | 65 | 2.6% |
| Average | 0.4% | 73 | — | 64 | 0.82 | 8.74 | 48 | 5.2% |

Table 7-11. Comparison of briquettes made from air dried fines, air dried pellets, and thermally dried pellets blended with 3.0 wt% Binder1

| Run | Briquette Moisture | Crushing Strength ($kg_f$) | | | Moisture Degradation | | | |
|---|---|---|---|---|---|---|---|---|
| | | 30 min | 24 hr | 7 day | Mechanical Durability | Avg Briq Wt (g) | Wet Str ($kg_f$) | Water Uptake |
| **PCC-Air Dried Fines** | | | | | | | | |
| Run #1 | 2.0% | 36 | 40 | 35 | 0.64 | 9.52 | — | — |
| Run #2 | 2.1% | 43 | 46 | 49 | 0.69 | 9.77 | — | — |
| Average | 2.0% | 39 | 43 | 42 | 0.66 | 9.65 | — | — |
| **PCC-Air Dried Pellets** | | | | | | | | |
| Run #1 | 1.9% | 43 | 37 | 41 | 0.66 | 9.67 | — | — |
| Run #2 | 2.0% | 43 | 44 | 43 | 0.68 | 9.72 | — | — |
| Average | 2.0% | 43 | 40 | 42 | 0.67 | 9.69 | — | — |
| **PCC-Thermally Dried Pellets** | | | | | | | | |
| Run #1 | 0.3% | 63 | 63 | 57 | 0.80 | 9.53 | 36 | 8.8% |
| Run #2 | 0.7% | 92 | 92 | 85 | 0.89 | 9.32 | 31 | 14.0% |
| Average | 0.5% | 77 | 78 | 71 | 0.85 | 9.42 | 33 | 11.4% |
| **RVSB-Air Dried Fines** | | | | | | | | |
| Run #1 | 2.7% | 14 | 15 | 16 | 0.33 | 8.23 | — | — |
| Run #2 | 2.7% | 17 | 15 | 13 | 0.30 | 8.73 | — | — |
| Average | 2.7% | 15 | 15 | 15 | 0.32 | 8.48 | — | — |
| **RVSB-Air Dried Pellets** | | | | | | | | |
| Run #1 | 3.8% | 30 | 23 | 21 | 0.38 | 8.20 | — | — |
| Run #2 | 3.8% | 20 | 18 | 17 | 0.36 | 7.81 | — | — |
| Average | 3.8% | 25 | 20 | 19 | 0.37 | 8.01 | — | — |
| **RVSB-Thermally Dried Pellets** | | | | | | | | |
| Run #1 | **1.3%** | 41 | 36 | 37 | 0.66 | 8.50 | — | — |
| Run #2 | 2.2% | 43 | 44 | 39 | 0.71 | 8.23 | — | — |
| Average | 1.7% | 42 | 40 | 38 | 0.69 | 8.36 | — | — |
| **MRC-Air Dried Fines** | | | | | | | | |
| Run #1 | 1.6% | 37 | 27 | 35 | 0.61 | 8.31 | 6 | 21.8% |
| Run #2 | 1.6% | 32 | 32 | 30 | 0.63 | 7.85 | 0 | 24.4% |
| Average | 1.6% | 35 | 30 | 32 | 0.62 | 8.08 | 3 | 23.1% |
| **MRC-Air Dried Pellets** | | | | | | | | |
| Run #1 | 1.7% | 41 | 59 | 60 | 0.77 | 8.44 | 7 | 23.9% |
| Run #2 | 1.7% | 49 | 51 | 57 | 0.82 | 8.78 | 8 | 21.2% |
| Average | 1.7% | 45 | 55 | 59 | 0.79 | 8.61 | 7 | 22.6% |
| **MRC-Thermally Dried Pellets** | | | | | | | | |
| Run #1 | 0.3% | 68 | 81 | 65 | 0.81 | 8.78 | 57 | 3.4% |
| Run #2 | 0.4% | 64 | 66 | 71 | 0.80 | 8.51 | 50 | 6.3% |
| Average | 0.3% | 66 | 74 | 68 | 0.81 | 8.64 | 53 | 4.9% |

Table 7-12. Comparison of briquettes made from air dried fines, air dried pellets, and thermally dried pellets, all blended with Lignin/Lime binder (2.6% / 1.3%)

| Run | Briquette Moisture | Crushing Strength ($kg_f$) | | | Moisture Degradation | | | |
|---|---|---|---|---|---|---|---|---|
| | | 30 min | 24 hr | 7 day | Mechanical Durability | Avg Briq Wt (g) | Wet Str ($kg_f$) | Water Uptake |
| **PCC-Air Dried Fines** | | | | | | | | |
| Run #1 | 2.2% | 34 | 40 | 34 | 0.71 | 9.41 | 17 | 11.2% |
| Run #2 | 2.3% | 38 | 38 | 36 | 0.71 | 9.35 | 17 | 11.0% |
| Average | 2.2% | 36 | 39 | 35 | 0.71 | 9.38 | 17 | 11.1% |
| **PCC-Air Dried Pellets** | | | | | | | | |
| Run #1 | 2.2% | 32 | 32 | 32 | 0.64 | 8.88 | 13 | 11.3% |
| Run #2 | 2.2% | 34 | 31 | 32 | 0.65 | 8.82 | 14 | 11.2% |
| Average | 2.2% | 33 | 32 | 32 | 0.65 | 8.85 | 13 | 11.3% |
| **PCC-Thermally Dried Pellets** | | | | | | | | |
| Run #1 | 1.0% | 57 | 55 | 54 | 0.78 | 9.19 | 26 | 10.0% |
| Run #2 | 0.1% | 56 | 55 | 59 | 0.70 | 9.35 | 24 | 10.2% |
| Average | 0.6% | 56 | 55 | 56 | 0.74 | 9.27 | 25 | 10.1% |
| **RVSB-Air Dried Fines** | | | | | | | | |
| Run #1 | 3.3% | 28 | 23 | 22 | 0.52 | 9.04 | 11 | 12.9% |
| Run #2 | 3.5% | 27 | 24 | 23 | 0.55 | 8.77 | 12 | 12.7% |
| Average | 3.4% | 27 | 24 | 23 | 0.54 | 8.90 | 11 | 12.8% |
| **RVSB-Air Dried Pellets** | | | | | | | | |
| Run #1 | 2.8% | 27 | 25 | 28 | 0.59 | 9.21 | 12 | 13.6% |
| Run #2 | 2.7% | 33 | 30 | 29 | 0.62 | 9.61 | 14 | 12.8% |
| Average | 2.8% | 30 | 28 | 29 | 0.60 | 9.41 | 13 | 13.2% |
| **RVSB-Thermally Dried Pellets** | | | | | | | | |
| Run #1 | **2.5%** | 34 | 33 | 32 | 0.60 | 8.86 | 12 | 11.8% |
| ~~Run #2~~ | ~~4.5%~~ | ~~26~~ | ~~22~~ | ~~24~~ | ~~0.47~~ | ~~8.22~~ | ~~9~~ | ~~12.8%~~ |
| Average | 2.5% | 34 | 33 | 32 | 0.60 | 8.86 | 12 | 11.8% |
| **MRC-Air Dried Fines** | | | | | | | | |
| Run #1 | 1.7% | 52 | 64 | 56 | 0.85 | 8.73 | 29 | 8.1% |
| Run #2 | 1.6% | 57 | 68 | 61 | 0.84 | 8.92 | 28 | 7.6% |
| Average | 1.6% | 54 | 66 | 59 | 0.84 | 8.83 | 28 | 7.9% |
| **MRC-Air Dried Pellets** | | | | | | | | |
| Run #1 | 1.5% | 60 | 68 | 67 | 0.85 | 8.82 | 29 | 7.8% |
| Run #2 | 1.5% | 61 | 65 | 62 | 0.83 | 8.58 | 28 | 8.5% |
| Average | 1.5% | 61 | 66 | 64 | 0.84 | 8.70 | 28 | 8.2% |
| **MRC-Thermally Dried Pellets** | | | | | | | | |
| Run #1 | 1.7% | 76 | 75 | 79 | 0.86 | 8.63 | 29 | 8.1% |
| Run #2 | 1.3% | 75 | 73 | 78 | 0.87 | 8.70 | 32 | 7.6% |
| Average | 1.5% | 75 | 74 | 78 | 0.87 | 8.67 | 31 | 7.8% |

To facilitate comparisons, the data in Table 7-8 through Table 7-12 are summarized and condensed in Table 7-13. Column 2 of Table 7-13 shows the average crushing strengths for briquettes made at ambient temperature with air dried fines grouped according to the binder added (if any). Column 3 shows the percent change in crushing strength for briquettes made with air dried pellets versus those made with the air dried fines of column 2. Column 4 shows a similar comparison of the thermally dried pellets that were briquetted hot to the air dried fines (column 2).

Table 7-13. Comparison of the average 7 day crushing strengths as a function of the binder added

| **Binder** | **Average Crushing Strength for Briquettes made with Air Dried Fines[a] ($kg_f$)** | **Change in Strength for Air Dried Pellets[b] (%)** | **Change in Strength for Thermally Dried Pellets[b] (%)** |
|---|---|---|---|
| Binderless | 26.6 | 3.1% | 36.3% |
| Wheat Starch | 63.8 | 18.0% | 37.8% |
| Binder 2 | 36.9 | -4.6% | 90.4% |
| Binder 1 | 29.7 | 37.4% | 113.4% |
| Lignin/lime | 38.7 | 9.0% | 45.7% |
| **Averages** | **39.1** | **12.6%** | **64.7%** |

[a] Crushing strengths and comparisons are for average data for the three study coals grouped according to binder type.
[b]Relative to air dried fines data in column 2

The overall averages shown in the last row of Table 7-13 indicate a relatively modest but measurable improvement (12.6%) in crushing strength for the briquettes made with air dried pellets compared to those made with air dried fines. Since the primary difference in these two briquette feedstocks was the manner in which the binder was applied (i.e. mechanically mixed with dry fines versus co-pelletizing with wet fines), this increase in strength would suggest better dispersion of the binder due to the pelletization step. An alternate explanation is that the dry pellets tended to feed to the briquette press in a more consistent manner than the dry fines (i.e. the roller and feed auger torques are more easily held constant)[11].

Briquettes made with thermally dried pellets that were briquetted hot exhibited a much larger increase in the average strengths (64.7%) compared to those made from air dried fines, which is in agreement with the results from the initial round of comparisons presented in the

[11] Maintaining a consistent feed rate was a particular problem with the ultra-fine MRC sample, which was significantly more difficult to feed at a constant roller or feed-screw torque that dry RVSB or PCC fines.

previous section. This increase cannot be explained as improved binder dispersion since the strengths obtained were much larger than was obtained with the equivalent air dried pellets. Therefore, the results provide evidence that hot briquetting improves briquette strength relative to ambient temperature briquetting. However, note these increases were not uniform as there were large differences in the relative improvement for the different binders. Improvements in crushing strengths ranged as high as 113% and 90% for Binders 1 and 2, respectively, and as low as 36% and 38% for briquettes made without a binder or with the wheat starch binder, respectively. The particularly large increase in strengths with Binders 1 and 2 suggest these materials may have been activated during thermal drying. The reason for the smaller but still significant increase in strength for the binderless briquettes is speculated as stemming from softening and more efficient packing of the coal particles when briquetted at a higher temperature.

The 7 day crushing strength data are plotted for the individual samples as a function of coal and binder type in the three plots of Figure 7-11. These plots visually illustrate the general trend of increasing strength as one moves from left to right for briquettes made with air dried fines, to briquettes made with air dried pellets, to those made with thermally dried and hot briquetted pellets. The increase in strength for briquettes made with hot, thermally dried pellets versus those made with air dried pellets was generally substantial, whereas the increase in strength for air dried pellets versus their air dried fines analogues was on average much smaller.

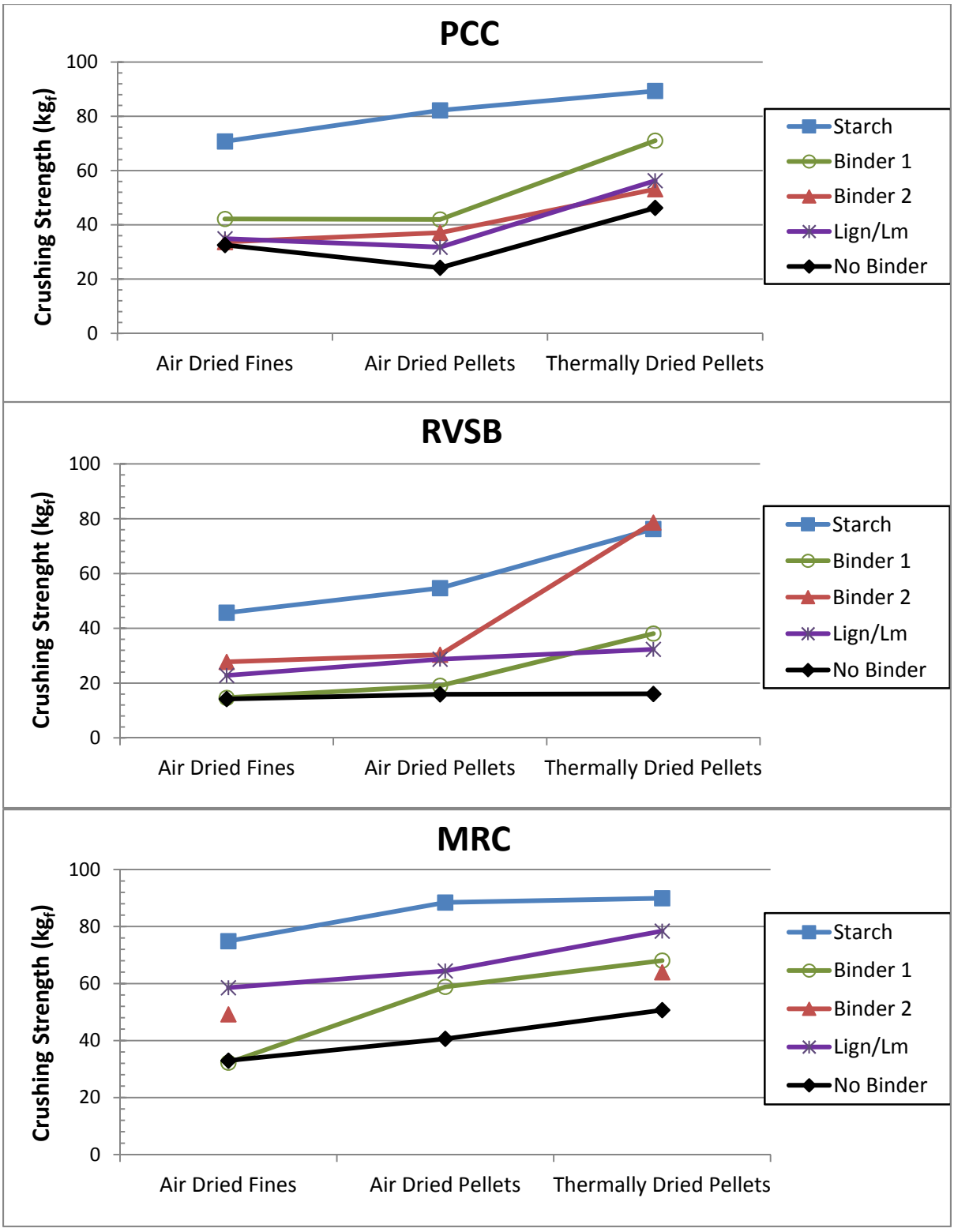



Figure 7-11. Seven day crushing strengths as a function of binder type

For a given binder, the 7 day crushing strengths were most often highest for briquettes made with the MRC fines followed closely by those made with the PCC fines. Also note that for

briquettes made with both the air dried fines and air dried pellets, the starch binder provided briquette strengths that were consistently greater than obtained with the other binders under evaluation which was not always the case for briquettes made from hot thermally dried pellets.

Table 7-14 shows comparisons of average mechanical durability data that is grouped according to binder type for the same samples described above. The average mechanical durability for briquettes made with thermally dried pellets (column 2) reveal that the highest average durability was obtained for briquettes made with the starch binder (0.87) followed by those made with proprietary Binder 2 (0.83), both of which are considered acceptable. In contrast, the average mechanical durability for briquettes made with hot pellets without a binder was unacceptably low at 0.60 as was the average durability for briquettes made with either Binder 1 or Lignin/Lime (0.78 and 0.74, respectively).

Table 7-14. Comparison of mechanical durability results for briquettes made from the PCC, RVSB, and MRC coals that were briquetted as air dried fines, air dried pellets, and hot thermally dried pellets

| Binder | Mechanical Durability of Thermally Dried Pellets | Change in Fines generated for Air Dried Fines (%) | Change in Fines generated for Air Dried Pellets (%) |
|---|---|---|---|
| Binderless | 0.60 | 46.0 | 29.2 |
| Starch | 0.87 | 12.4 | -6.4 |
| Binder2 | 0.83 | 173.8 | 162.0 |
| Binder1 | 0.78 | 110.1 | 74.4 |
| Lignin/Lime | 0.74 | 15.6 | 18.8 |
| **Averages** | **0.77** | **71.6** | **55.6** |

The 3rd and 4th columns respectively show the average percent increase in the weight of fines generated during mechanical durability testing of briquettes made from air dried fines and air dried pellets relative to the weight of fines generated from hot thermally dried pellets. The data in the last row of Table 7-14 reveal that the overall increase in the weight of fines generated by briquettes made from air dried pellets compared to the hot briquetted pellets was a 55.6% averaged for all samples. While this finding is substantial, the equivalent increase in fines generated for briquettes made from air dried fines sample was even greater (71.6%). Data in these latter two columns again provide evidence that even for ambient temperature briquetting, a more durable briquette is produced when a blend of coal and binder is pelletized and dried before it is briquetted than when an equivalent dry blend is briquetted directly without pelletizing.

The largest change in the fraction of fines generated by briquettes made with dried fines versus made with hot pellets was exhibited by the briquettes made with Binders 1 and 2, again reflecting an apparent activation of these binders during thermal drying. In comparison, the analogous change in fines generated for the briquettes made with the starch binder was minor, which is consistent with a relatively small improvement in the performance when this binder is processed at an elevated versus ambient temperature as was shown before.

Mechanical durability results for these same briquetted samples are plotted for each coal as a function of binder type in Figure 7-12. Similar to the results obtained for crushing strengths, the best mechanical durability results were obtained with briquettes made with MRC fines, followed closely by those made with the PCC fines. However, there was not a substantial difference in the durability as a function of briquetting hot versus an ambient temperature feedstock for the MRC coal. For the PCC and RVSB coals, only briquettes made with Binders 1 and 2 exhibited consistent and significant improvements in durability characteristics for briquettes made with hot pellets versus ambient temperature fines or pellets. Unlike the briquettes made with the PCC and RVSB coals, all five sets of briquette samples made from thermally dried MRC pellets exhibited essentially the same mechanical durability regardless of the binder added. Further, the mechanical durability for all of the briquette samples made with pelletized MRC fines, both air and thermally dried, classified as acceptable to good, which is in contrast to the briquettes made with the PCC and RVSB coals which generally classified as poor (<0.80), particularly those made at ambient temperature. Finally, and in agreement with the corresponding crushing strengths above, briquettes made with the wheat starch binder consistently exhibited the highest durability.

In summary, the crushing strength and mechanical durability comparisons in Figure 7-11, Figure 7-12, Table 7-13, and Table 7-14 consistently indicate that briquette durability is improved by pelletizing a give blend of coal fines and binder prior to briquetting, while an even more substantial improvement is obtained if the pellets are thermally dried and briquetted while hot. The magnitude of improvement in briquette performance obtained via thermal treatment appears to be governed largely by the nature of the binder use. The wheat starch binder consistently provides the best overall durability regardless of how the fines were processed prior to briquetting. However, following thermal drying and hot briquetting, briquettes made with Binders 1 and 2 perform about as well as the wheat starch binder.

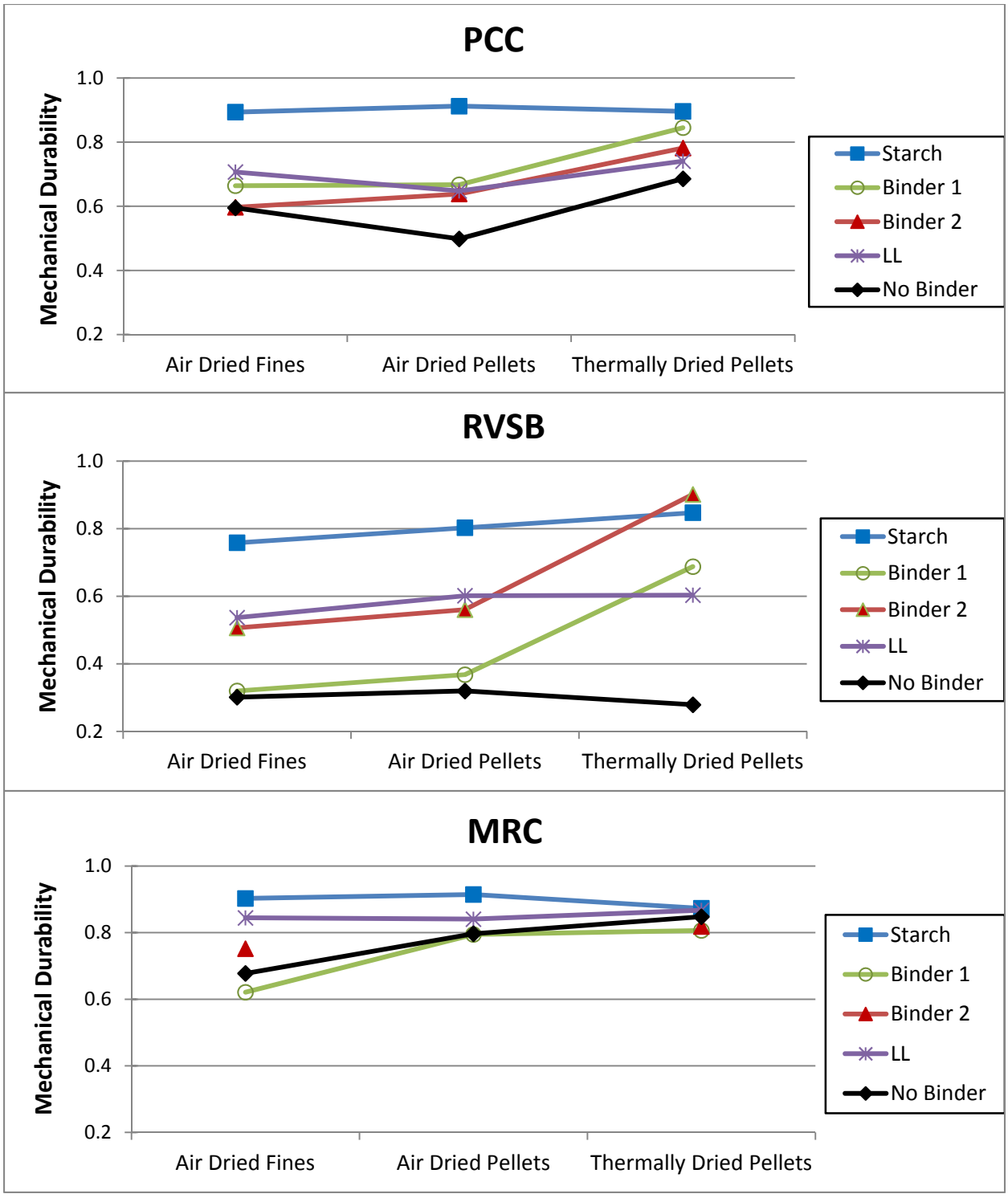



Figure 7-12. Average mechanical durability from duplicate samples of briquettes made with air dried fines, air dried pellets, and hot thermally dried pellets

## 7.4.4 Co-Briquetting of Pelletized Coal and Biomass

### 7.4.4.1 Co-Briquetting of Biomass with Air Dried Coal Pellets

After determining that briquetting fine coal pellets resulted in the production of more durable briquettes, a series of evaluations were conducted to determine if a similar improvement could be obtained following the addition of biomass and if so, to determine which biomass type provided the most improvement.

Several biomass types were selected for evaluation including wheat straw (WS), corn stover (CS), switch grass (SG), miscanthus (MS), green sawdust (SD), kiln-dried sawdust (kiln SD), and two bio-chars (pine and EtOH). Two master batches of coal pellets were made in a 90 cm pan pelletizer from 3% wheat starch binder blended with either the RVSB or the PCC screen-bowl coals. The pelletized coals were air dried to equilibrium moisture over a period of several days before homogenizing and storing in sealed drums. Subsamples of the dried pellets were subsequently crushed and blended with each biomass type at biomass concentrations of 10% and 30% by weight and briquetted.

Figure 7-13 shows crushing strengths for briquettes made with the PCC/starch pellets that were co-briquetted with both 10 and 30 wt% biomass[12]. Note that the crushing strengths for the 10% biomass briquettes were far more consistent than for their 30% counter-parts. This is not surprising considering they were essentially comprised of about 90 wt% coal, and thus the addition of different types of biomass had less of an impact on briquette properties. Also note that with the exception of the briquettes formed with the two bio-chars samples, the crushing strengths of the 30% biomass briquettes were generally higher than their 10% biomass analogues. This was despite the fact that the absolute binder concentration in the 30% biomass briquettes was significantly lower than in the 10% biomass briquettes (2.1% vs 2.7%) due to greater dilution of the 3% starch pellets when a higher concentration of biomass was added.

[12]Results for the 30% green sawdust briquettes are not shown in Figure 7-13 as they disintegrated when they were passed over a vibrating screen to remove fines.

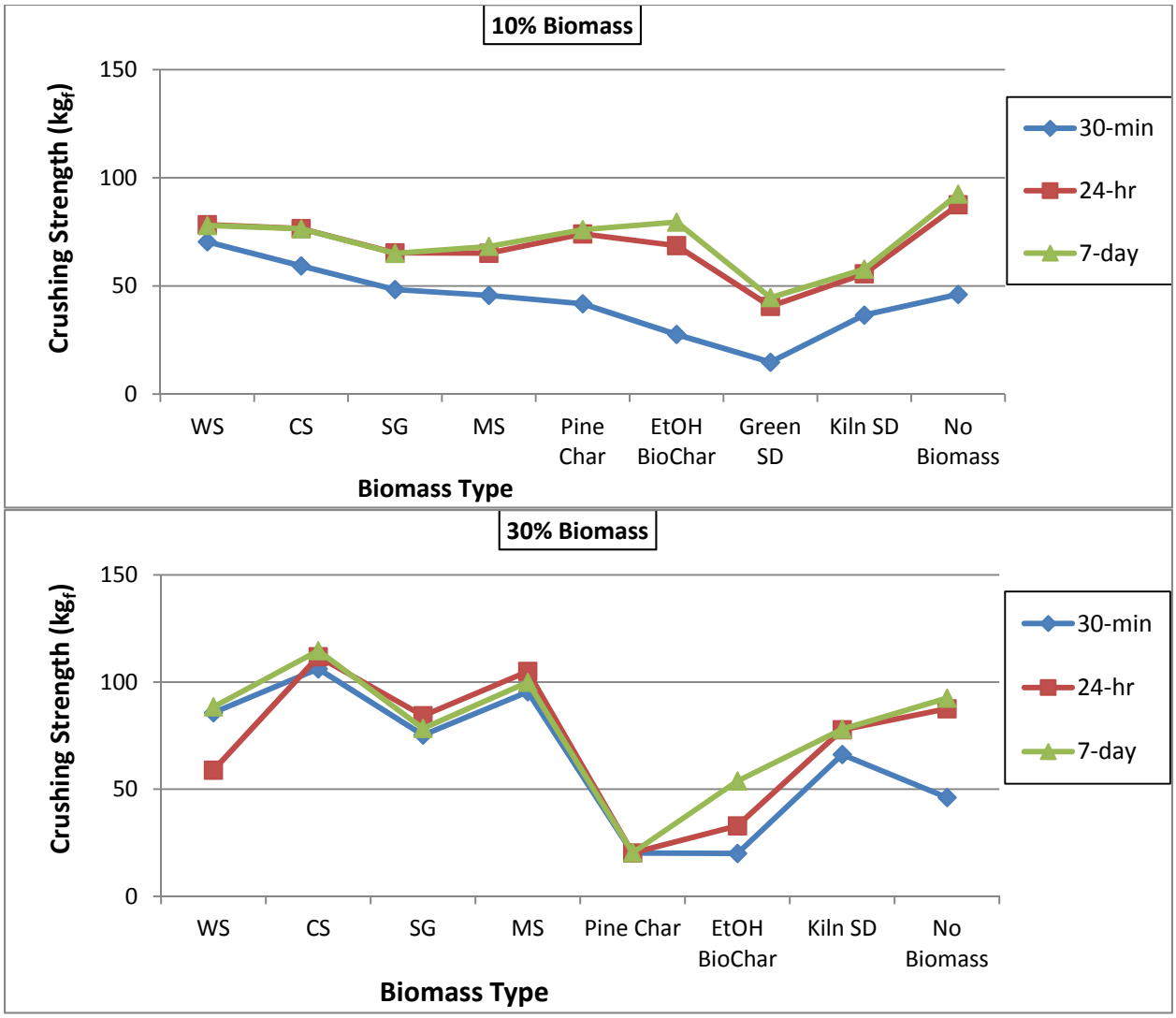



Figure 7-13. Thirty minute, 24 hour, and 7 day crushing strengths for various biomass types co-briquetted with air dried PCC coal pellets made with 3 wt% wheat starch

Crushing strengths for the 10% biomass briquettes tended to improve as the briquettes cured whereas the strengths for the 30% biomass briquettes remained relatively constant over the same cure interval. The largest increases in strength during curing were exhibited by briquettes made without biomass, which was followed by briquettes made with either 10% or with 30% EtOH bio-char[13]. Further, despite their relatively low green strength, by day 7 the crushing strengths of briquettes formed without biomass were higher than that of any of the 10% biomass briquettes and were equivalent to or stronger than the majority of the 30% biomass briquettes. This difference in behavior as the briquettes cure is attributed to the elastic characteristics of raw

[13] EtOH biochar particles are more rigid than raw biomass. Thus, the two briquettes samples made with the EtOH biochar would be expected to exhibit less rebound or re-expansion following formation.

biomass, resulting in swelling and a weakening of the briquette over time. This type of elastic behavior is not as prominent for the more rigid coal or biochar particles, which likely explains why briquettes made with coal only or with coal and biochar tend to get stronger with time compared to briquettes that contain raw biomass.

Mechanical durability results for the same briquetted samples are shown in Figure 7-14. As before, the durability values for the 10% biomass briquettes were far more similar for the different biomass types than were those for the 30% biomass briquettes. Except for briquettes made with the green sawdust, the 10% biomass briquettes exhibited mechanical durability values that classified as good.

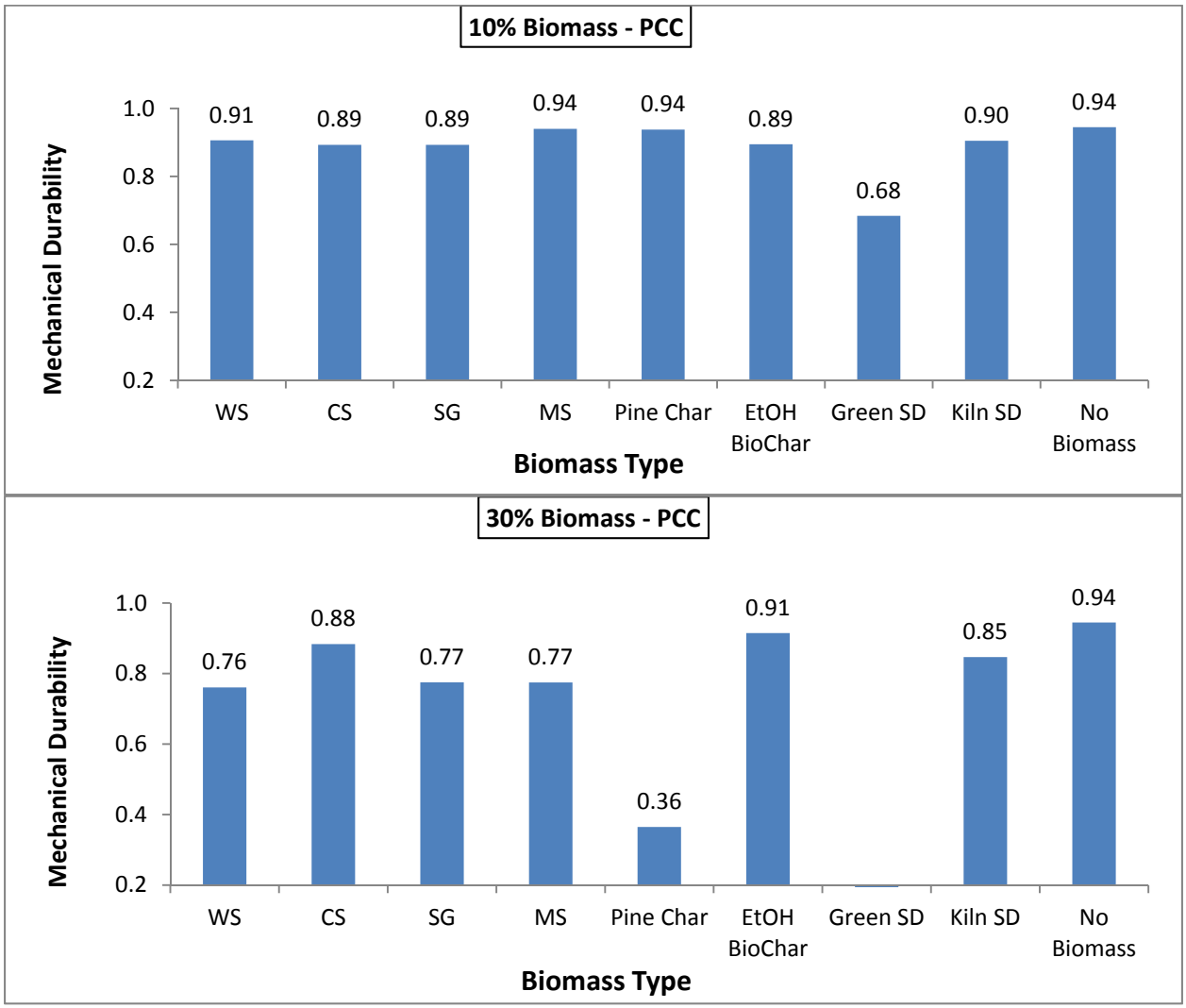



Figure 7-14. Mechanical durability values for various biomass types co-briquetted with air dried PCC coal pellets made with 3 wt% wheat starch

In contrast, only briquettes formed with 30 wt% corn stover, EtOH bio-char, or kiln-dried sawdust exhibited durability that classified as acceptable to good (>0.80), while the mechanical durability of the remainder of the 30% biomass samples classified as poor (<0.80). With the exception of a small improvement in the durability of the 30% EtOH bio-char briquettes, the 30% biomass briquettes exhibited mechanical durability values that were consistently lower than the values of their 10% counterparts, which is opposite to the trends noted in crushing strengths where the 30% biomass briquettes were generally stronger.

Finally, the only briquettes that exhibited resistance to water degradation during submersion were those formed either without biomass, with 10% pine bio-char, or with 10% or 30% EtOH bio-char. Thus, while the briquettes formed with bio-char generally did not compare well in terms of crushing strengths, particularly when added at 30 wt%, they did outperform the other biomass types with respect to resistance to water degradation.

Analogous crushing strengths and mechanical durability results for briquettes made with air dried RVSB coal pellets containing 3 wt% wheat starch are shown in Figure 7-15 and Figure 7-16, respectively. Data for briquettes containing 30% pine char, green SD, or kiln SD are not plotted, as the briquettes made with these biomass types were too weak to survive mechanical screening during the fines removal step.

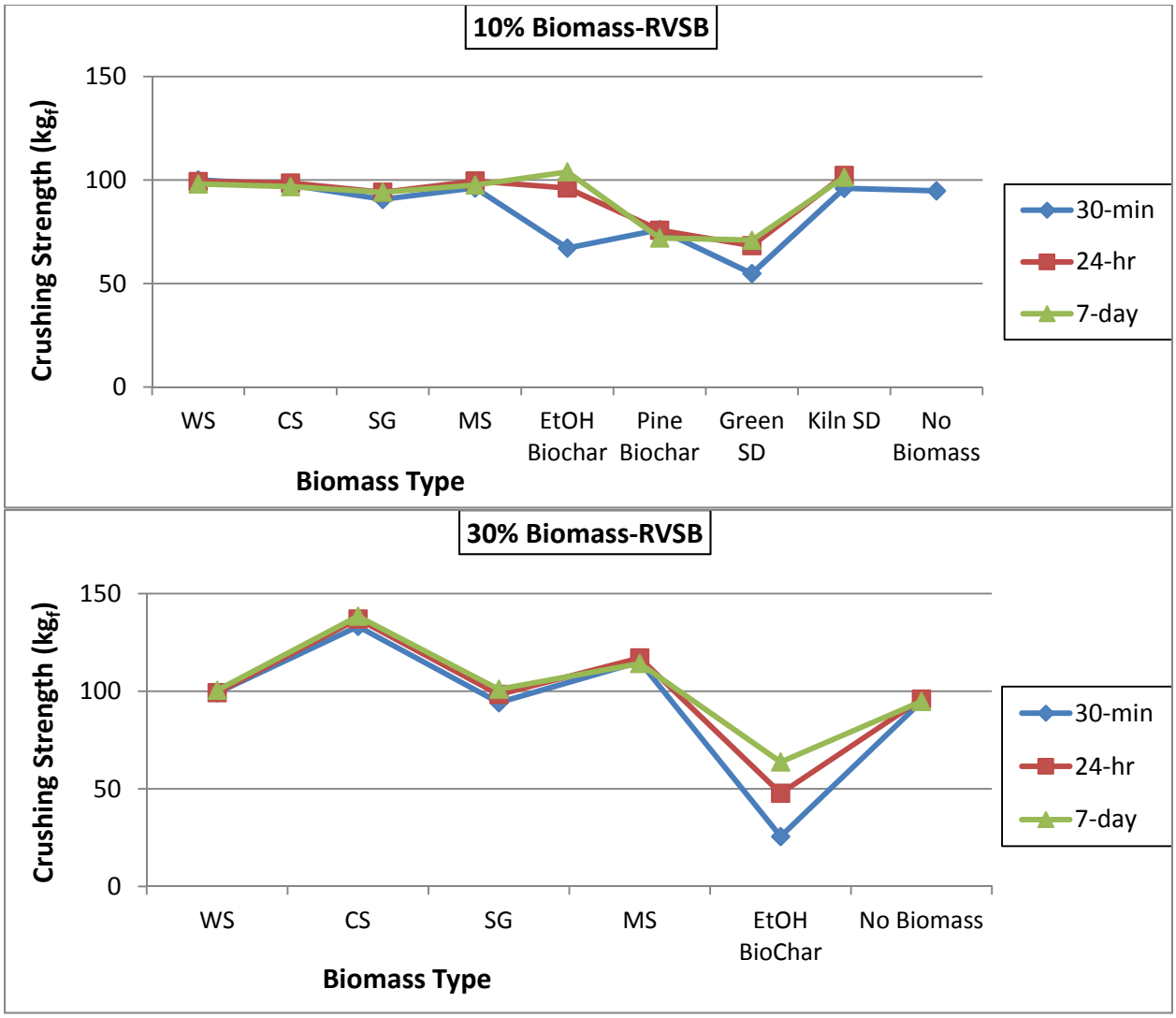



Figure 7-15. Thirty minute, 24 hour, and 7 day crushing strengths for various biomass types co-briquetted with air dried RVSB coal pellets that contained 3-wt% wheat starch

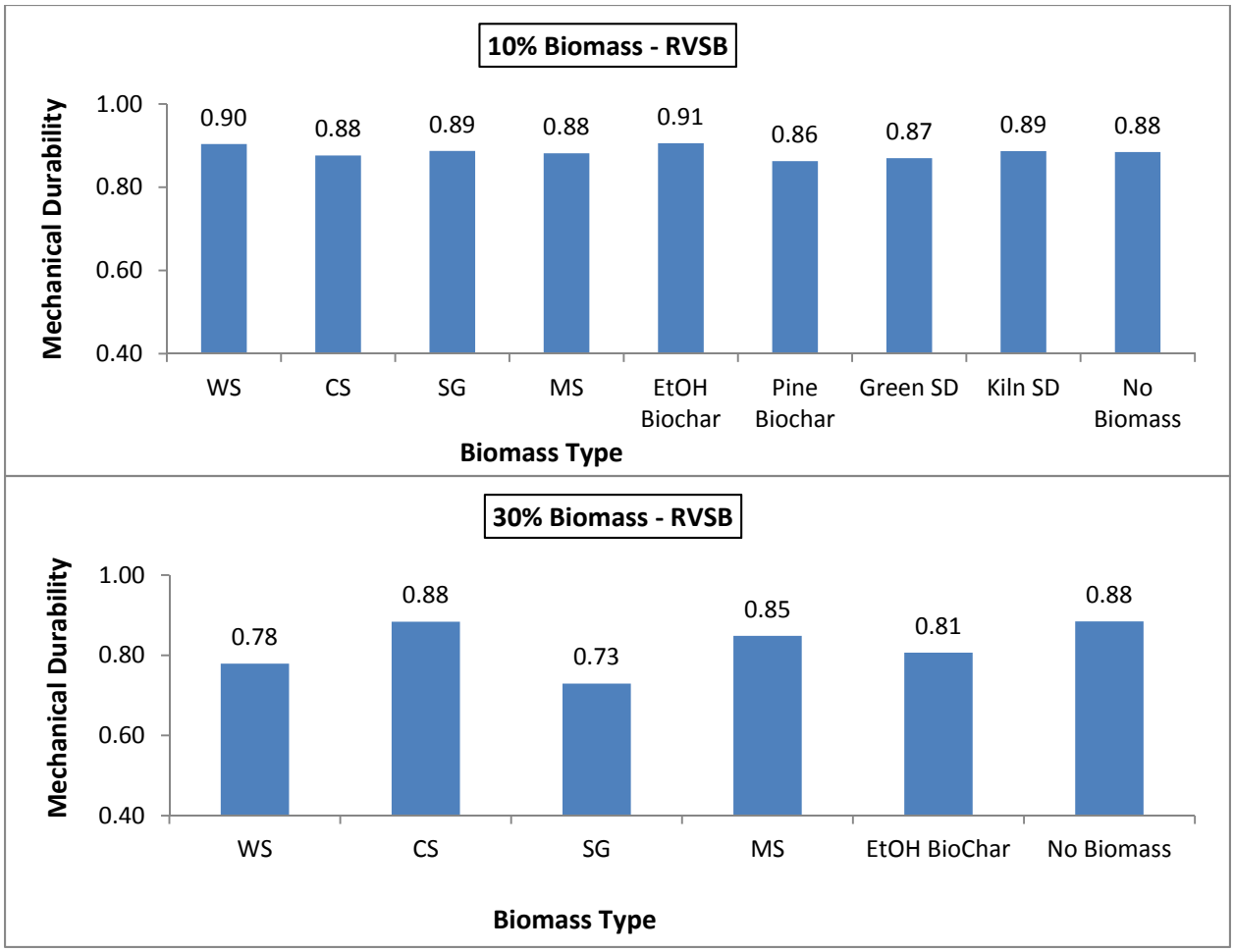



Figure 7-16. Mechanical durability values for different biomass types co-briquetted with RVSB coal/wheat starch pellets at concentrations of 10 wt% (top) and 30 wt% (bottom) biomass

In general, the coal-biomass briquettes made with the RVSB coal pellets exhibited slightly higher crushing strengths and lower mechanical durability values than analogous briquettes made with the PCC coal pellets. Several trends noted for the PCC briquettes are again apparent in the RVSB briquettes including:

- Crushing strength and mechanical durability values exhibited less variation for the 10% than for the 30% biomass briquettes regardless of the biomass added;
- Crushing strengths were generally higher for the 30% biomass briquettes compared to their 10% counterparts;
- The mechanical durability values for all of the 10% biomass briquettes classified as acceptable to good whereas the durability values for 30% biomass briquettes classified as acceptable to poor;

- Briquettes made with 30% corn stover or 30% miscanthus again exhibited the highest crushing strength;
- Addition of bio-char or sawdust generally resulted in briquettes with low crushing strengths or which fell apart during the fines removal step; and
- The only briquettes made with the RVSB coal pellets that exhibited resistance to water degradation during submersion were those formed either without biomass, with 10% pine bio-char, or with both 10 and 30% EtOH bio-char.

In summary, for a given biomass concentration, briquettes formed with dried PCC and RVSB coal pellets were reasonably similar in durability. For both coals, crushing strengths were generally higher and mechanical durability values lower in the briquettes made with 30% biomass versus those made with 10% biomass. Most briquetted samples exhibited similar crushing strengths and mechanical durability values at a 10% biomass addition rate, regardless of the type of biomass added, but differed substantially at a 30% addition rate. For briquettes made with 30 wt% biomass, corn stover and miscanthus provided the highest crushing strengths for both coals. With the exception of EtOH bio-char co-briquetted with the PCC coal pellets, addition of 30% bio-char or 30% sawdust produced briquettes that were either very weak or that disintegrated over the mechanical screener during fines removal.

The only briquettes that exhibited resistance to water degradation in this study were those made without biomass, with 10% pine char, and with 10% or 30% EtOH bio-char. Thus, while briquettes formed with bio-char did not compare favorably with the other biomass types in terms of durability, the briquettes made with bio-char were the only biomass-coal briquettes that exhibited any measured resistance to water degradation.

#### 7.4.4.2 Co-Briquetting of Biomass with Thermally Dried Coal Pellets at Ambient versus Elevated Temperature

Results presented earlier in this chapter demonstrated that in the absence of biomass, more-durable coal briquettes were produced when fine coal was formed into pellets, the pellets heated to reduce moisture, and then briquetted before cooling. Accordingly, additional experiments were initiated to determine if more durable coal-biomass briquettes could be formed if the briquetting was conducted at an elevated rather than at ambient temperature. For these experiments, pellets made with three of the high-moisture coals (PCC, RVSB, and MRC) were thermally dried and blended with one of five biomass types. The blends were then either

briquetted hot or allowed to cool before briquetting. Briquettes were also made in a similar manner with the three pelletized coals without biomass for comparison.

Details of the production procedure are described in Section 7.3.3.6. Briefly, master batches of pelletized coal were made from blends of 3 wt% wheat starch and either PCC, RVSB, or MRC coal fines. Splits from each batch were dried in the thermal dryer to about 1-2 wt% moisture. After drying, one split of the hot coal pellets was blended with 10 wt% biomass, cooled to room temperature, and then formed into briquettes while a second split was blended with 10 wt% biomass in a heat-traced mixing bowl and immediately briquetted before cooling. This hot versus ambient temperature briquetting procedure was repeated for all 15 combinations of three coals and five biomass types (corn stover, wheat straw, miscanthus, EtOH bio-char, and kiln dried sawdust), plus the three pelletized coals without biomass, yielding a total of 18 sample pairs for comparison.

Thirty minute and 7 day crushing strengths for paired briquette samples made with dried coal pellets and 10% biomass are shown in Figure 7-17 and Figure 7-18, respectively. For a given biomass type, the highest green strengths were consistently obtained with the ultra-fine MRC coal followed by briquettes made with RVSB sample. For a given coal, the briquettes made with corn stover and kiln-dried sawdust consistently exhibited the highest crushing strengths, while briquettes made with EtOH bio-char or made without biomass exhibited the lowest strengths.

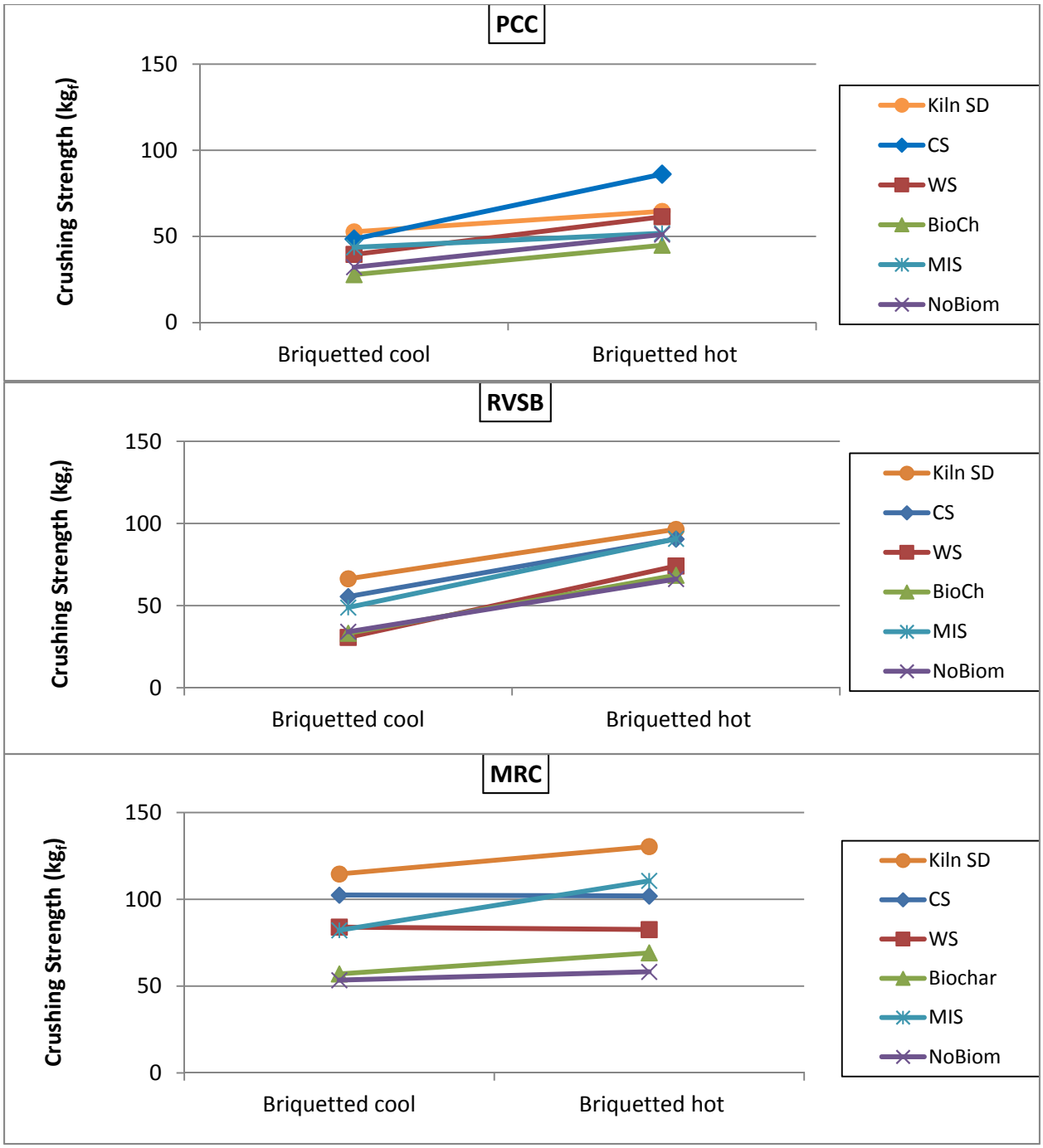



Figure 7-17. Thirty minute crushing strengths for briquettes made from fine coal/3% starch pellets blended with 10 wt% biomass

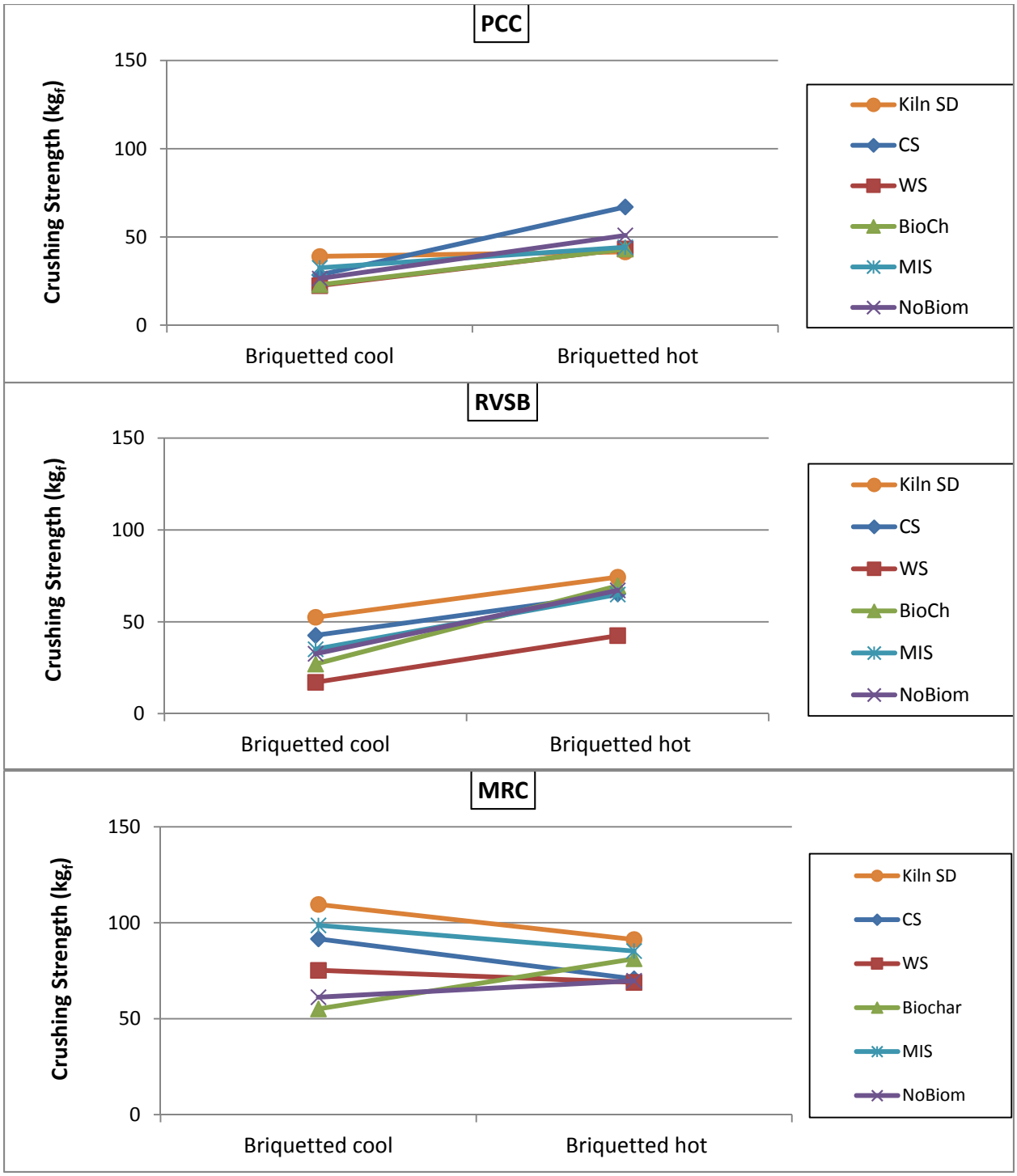



Figure 7-18. Seven day crushing strengths for briquettes made from fine coal/3% starch pellets blended with 10 wt% biomass

Note that for the PCC and RVSB coals, green strengths were higher when the coal pellet/biomass blends were briquetted hot rather than after they had cooled. However, this was not always the case for the briquettes made with the MRC coal pellets, particularly 7 day

strengths which were often higher in the briquettes formed at ambient temperature compared to their hot briquetted counterparts. Part of the reason for this discrepancy might stem from the fact that controlling the feed-screw torque was more difficult when briquetting the MRC sample than for the other two coals due to the ultra-fine particle size of the MRC coal. Even when operated at maximum speed, the feed auger torque often fell below the 90 N-m target for the MRC pellets, particularly when feeding the hot MRC pellets.

In contrast, the target feed auger torque could be achieved for the larger-particle-size PCC and RVSB coals at auger speeds much lower than maximum. The lack of adequate torque for the MRC sample, even at the maximum feed-auger speed, would suggest that the ultra-fine MRC particles were slipping between the feed auger and the feed cylinder walls countercurrent to the force being applied. Further, the feed screw speed needed to maintain the target torque was more dependent on the sample depth within the feed hopper for the MRC sample than it was for the larger particle-size coals. Thus, it is not known if the lack of correlation between briquette strength and the temperature at which the briquettes were formed was due to differences in feed-auger torques or was due to the chemical/physical nature of the MRC fines.

The mechanical durability results of these same briquette samples are shown in Figure 7-19. For the most part, durability results mirrored the crushing strengths in that the best mechanical durability values were consistently obtained with the MRC pellets regardless of which biomass type was added. For example, 22 of the 24 briquette samples made with PCC and RVSB fines exhibited durability values that classified as poor (<0.80) in contrast to those made with the MRC fines, nearly all of which classified as acceptable to good (0.80-0.95). Another similarity was that mechanical durability values for the PCC and RVSB coals were consistently better when the biomass/coal pellet blends were briquetted hot rather than after cooling. Again, this was not the case for briquettes made with the MRC coal for which there was little difference in the mechanical durability for blends that were briquetted at elevated versus ambient temperature. However, in contrast to the low crushing strengths exhibited by briquettes made with bio-char or made without biomass, these latter briquette samples exhibited the highest mechanical durability.

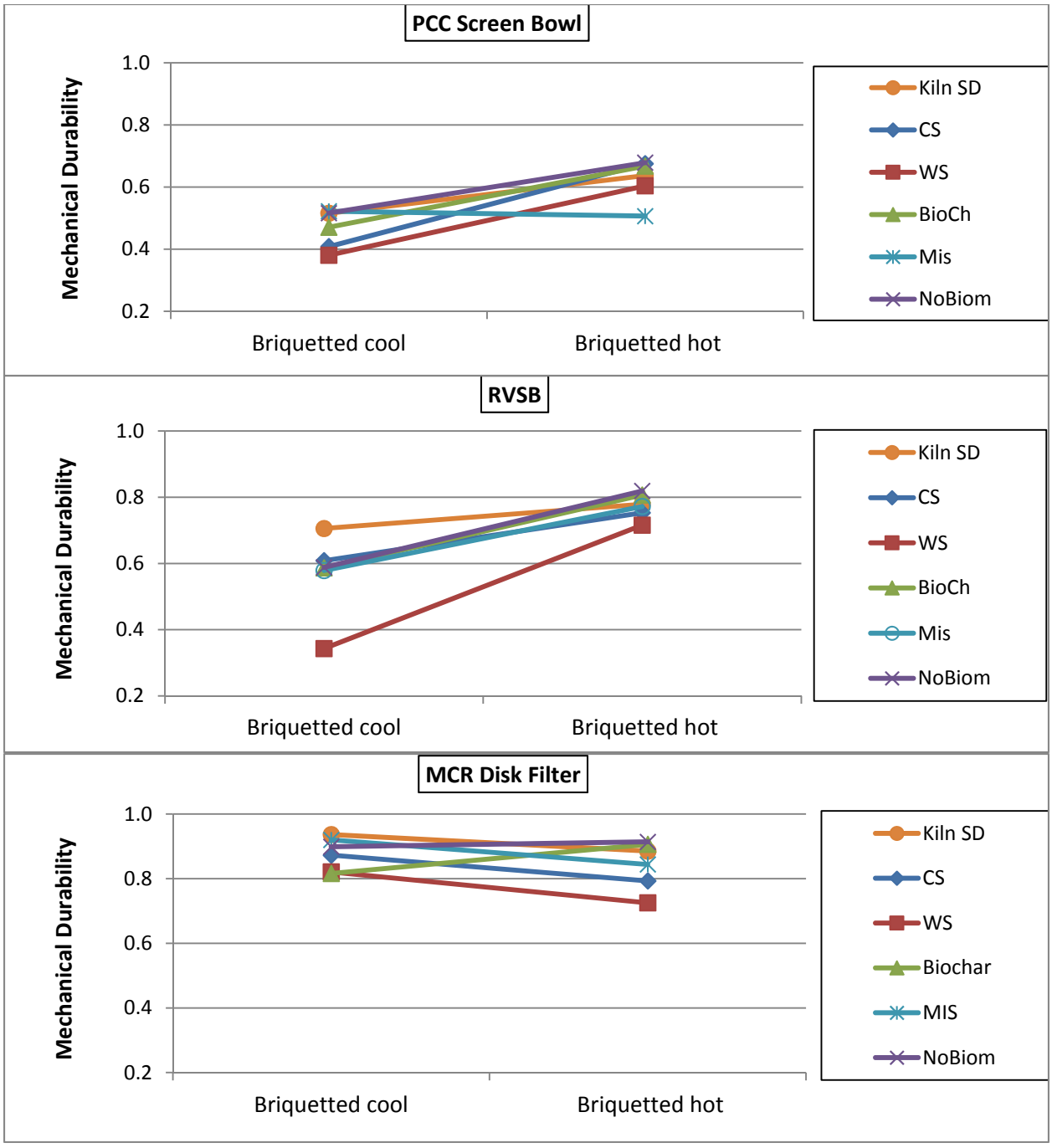



Figure 7-19. Mechanical durability of briquettes made from fine coal/3% starch pellets blended with 10 wt% biomass

Crushing strengths for these same hot versus cool-briquetted blends are re-plotted as a function of cure time for the PCC, RVSB, and MRC coals in Figure 7-20 through Figure 7-22, respectively. While these are the same data as were plotted in Figure 7-17 and Figure 7-18, the improvement in strength for coal-biomass blends that were briquetted hot (dashed lines) versus

at ambient temperature (solid lines of matching color) is more apparent when plotted in this manner. What is also revealed by these plots is that with minor exceptions involving bio-char or briquettes made without biomass, crushing strengths consistently declined between 30 minutes and 7 days for all 3 coals regardless of whether the pellet/biomass blends were briquetted hot or were briquetted after cooling. The most reasonable explanation for the loss in strength is that the compressed biomass tends to relax and expand over time, possibly accelerated by moisture absorption by the biomass as the briquettes cure.

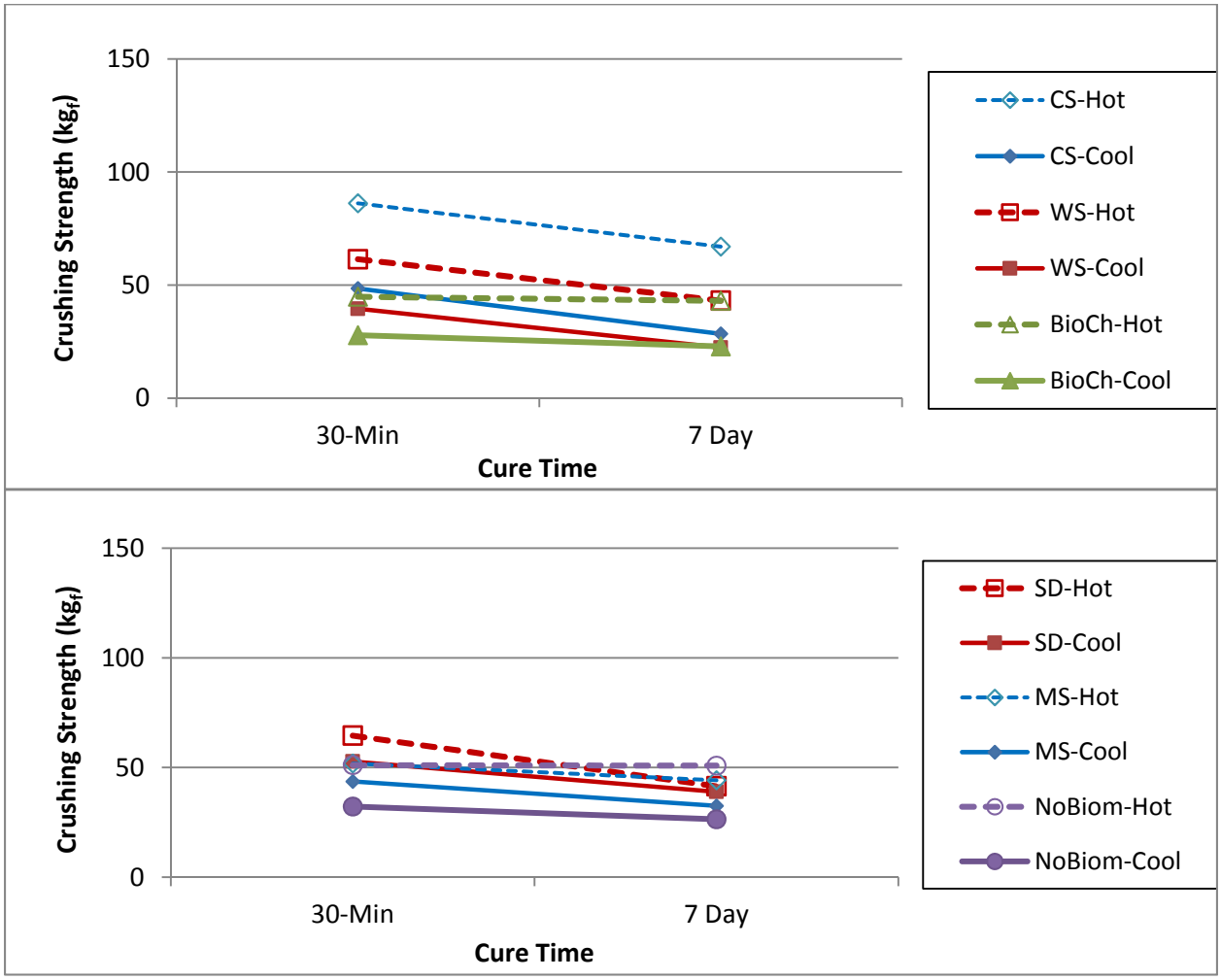



Figure 7-20. Thirty minute and 7 day crushing strengths for briquettes made with thermally dried PCC fines/starch pellets that were blended with either 0% or 10 wt% biomass

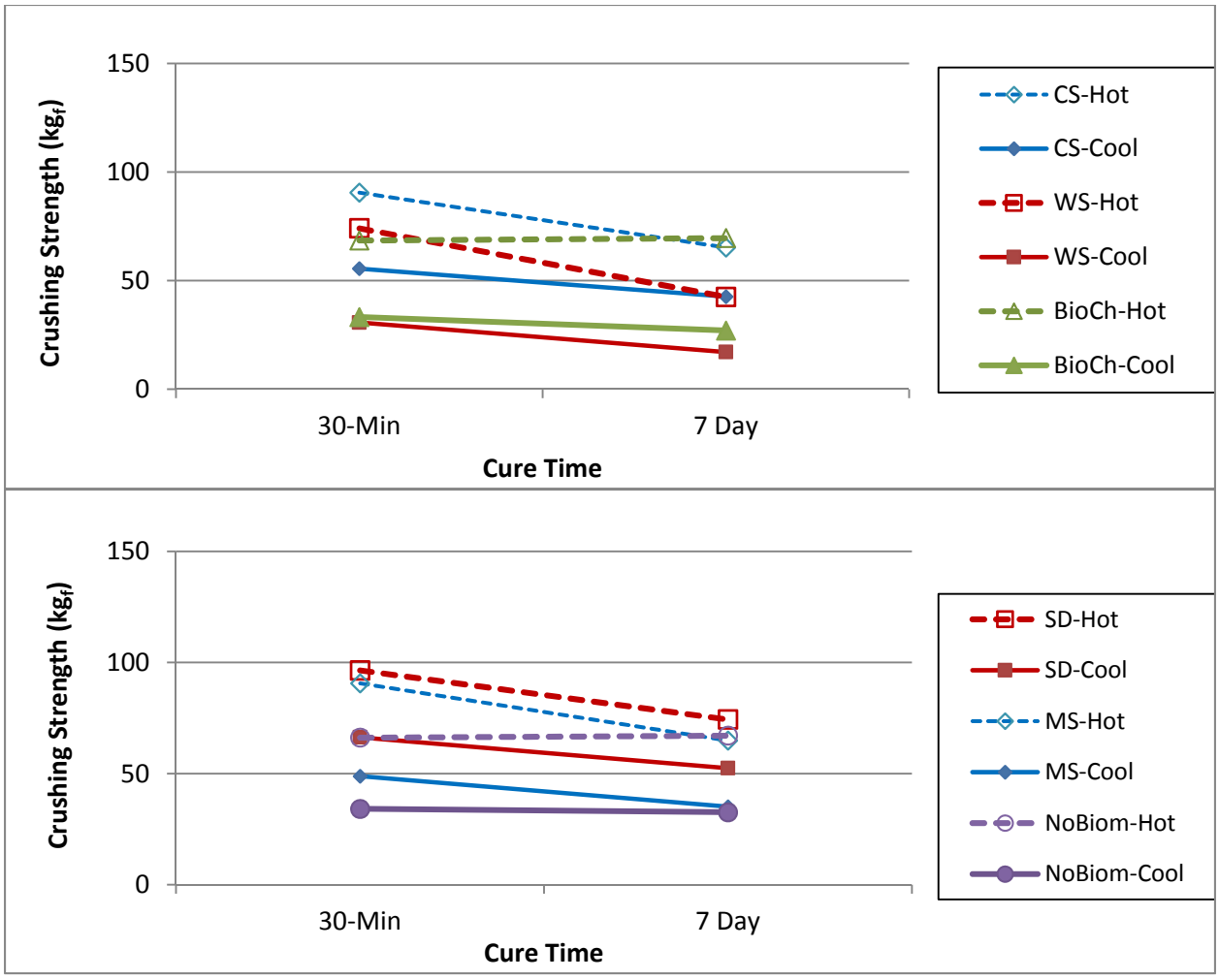



Figure 7-21. Thirty minute and 7 day crushing strengths for briquettes made with thermally dried RVSB fines/3% starch that were blended with either 0% or 10 wt% biomass

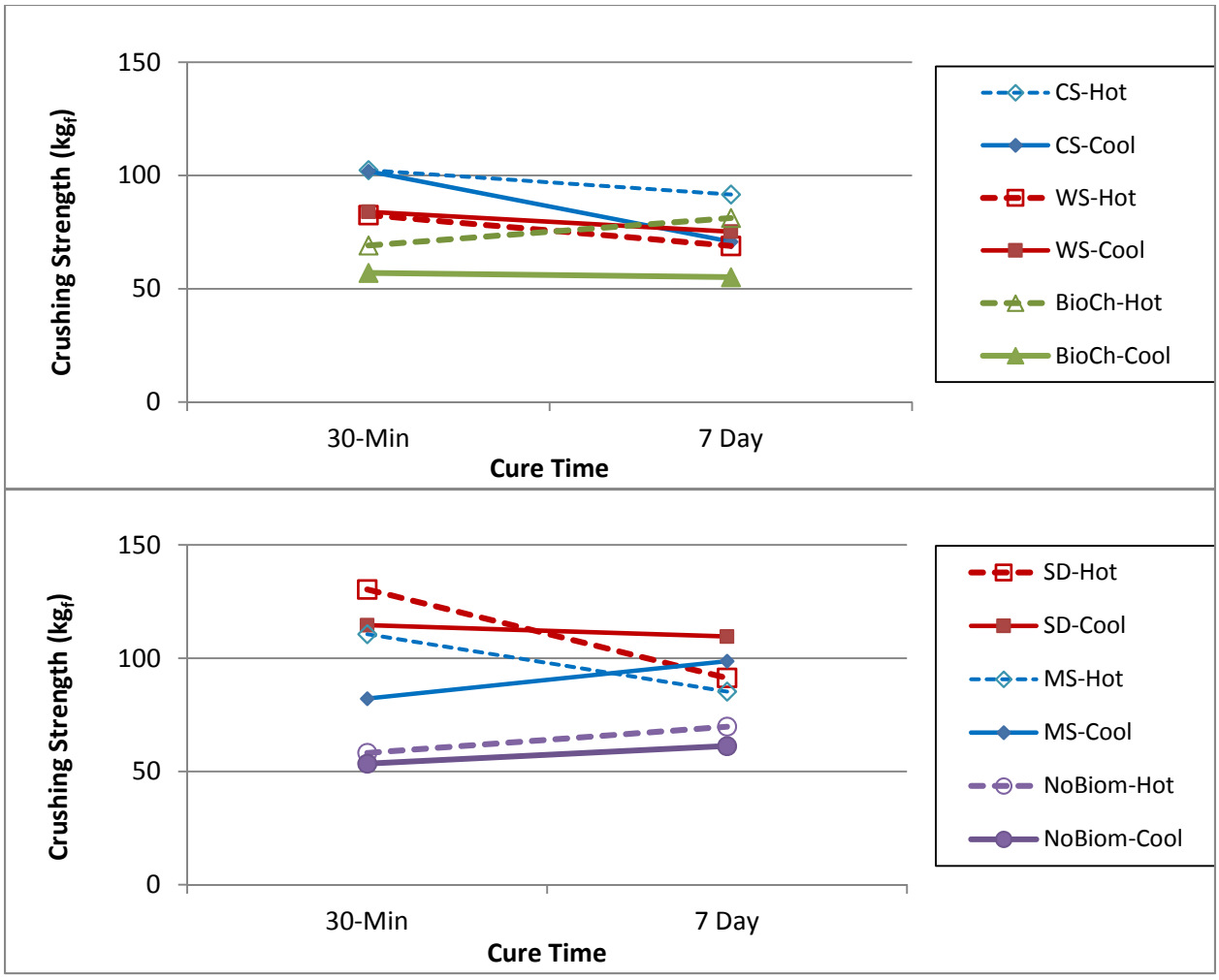



Figure 7-22. Thirty minute and 7 day crushing strengths for briquettes made with thermally dried MRC fines/3% starch pellets that were blended with either 0% or 10 wt% biomass

As evidence that the decline in strengths was due to the addition of biomass, note that the briquettes that were made without biomass exhibited little or no decline in strength between 30 minutes and 7 days for the PCC and RVSB coals and minor increases for briquettes made with MRC fines. Also note that unlike the loss in strength exhibited by briquettes made with raw biomass, the briquettes that were made with bio-char exhibited little or no change in crushing strength as the briquettes cured. This latter behavior is attributed to the fact that bio-char is in some ways more similar to coal than to raw biomass, including having been thermally altered in a manner to render it more aromatic, and thus more rigid, as well as more hydrophobic as demonstrated by its superior resistance to water degradation. Thus, the alteration of the biomass structure and accompanying increase in hydrophobicity renders bio-char less prone to expand, and/or absorb moisture relative to raw biomass.

## 7.5 Summary and Conclusions

Due to the many potential advantages offered by pan pelletization of wet coal fines prior to drying and briquetting, an extensive study was undertaken to characterize the impact of pelletization on briquette durability. Numerous comparisons were made including comparisons of briquettes made with air dried coal fines, with air dried coal pellets, and with thermally dried coal pellets that were briquetted both hot and after cooling. The impact of adding a binder and biomass to these feedstocks was also evaluated. Selected findings include:

- The optimum moisture for producing the strongest briquettes from pelletized coal fines ranged from about 1 to 4% for the four bituminous coals evaluated.
- At ambient temperature, crushing strength and mechanical durability were improved by forming blends of binder and fine coal into pellets and then drying prior to briquetting as opposed to briquetting dried blends of fines and binder directly, presumably due to more uniform dispersal of the binder attributable to pelletization.
- In general, substantial improvements in durability were obtained for briquettes that were made from thermally dried coal pellets that were briquetted while hot as compared to briquettes made from analogous blends briquetted at ambient temperature in the form of air-died fines, air dried pellets, and thermally dried pellets.
    - These improvements were more pronounced for briquettes that were made with a binder and for briquettes made with the larger particle size coals.
    - The magnitude of improvement was highly dependent on the binder added suggesting that several of the binders under evaluation were thermally activated.
- When added on an equivalent cost basis, the strongest briquettes were most often obtained with gelatinized wheat starch and two proprietary binders.
- The least durable briquettes were those made without a binder and with the largest particle size coal.
- Coal-biomass briquettes made with 30 wt% corn stover or 30 wt% miscanthus exhibited the highest crushing strength.
- For a given biomass type, the highest green strengths were consistently obtained with the ultra-fine MRC coal.

- For a given biomass type, mechanical durability mirrored crushing strengths in that the best mechanical durability values were generally obtained with the ultra-fine MRC coal.
- The durability of briquettes made with fine coal and raw biomass declined as the briquettes cured versus briquettes made with fine coal without biomass or made with fine coal and bio-char, which remained relatively constant or increased slightly as the briquettes cured.
- In general, briquettes made with the two screen bowl coals, River View (RVSB) from the Illinois basin and the slightly higher rank Perry County Coal (PCC) from the Appalachian Field, exhibited similar trends during briquetting including:
    - Without exception, green strengths were higher when the coal pellet/biomass blends were briquetted hot rather than after they had cooled
    - Crushing strength and mechanical durability values exhibited less variation for briquettes made with 10 wt% biomass than for those made with 30 wt% biomass regardless of the biomass type added.
    - Crushing strengths were generally higher for the 30 wt% biomass briquettes compared to their 10% counterparts.
    - Opposite trends were noted for mechanical durability results, which generally classified as acceptable to good for briquettes made with 10 wt% biomass versus acceptable to poor for briquettes made with 30 wt% biomass.
    - Briquettes made with 30% corn stover or 30% miscanthus exhibited the highest crushing strengths of the biomass types evaluated.
    - Briquettes made with bio-char or sawdust exhibited the lowest durability, often disintegrating during fines removal over a vibrating screen.
    - While briquettes formed with bio-char did not compare favorably with the other biomass types in terms of durability, the briquettes made with bio-char were the only coal-biomass briquettes that exhibited significant resistance to water degradation.

# Chapter 8

# Bio-Oil and Biochar Briquetting Evaluations

## 8.1 Abstract

A scoping evaluation was conducted to assess the potential to use biomass-derived oil and char produced during pyrolysis of woody biomass as a briquette binder and filler, respectively. Kilogram quantities of bio-oil and biochar were produced in a series of batch reactor runs using a kiln dried sawdust feedstock. The bio-oil sample was tested both as collected and after thermal treatment intended to remove lighter components and increase viscosity. Briquettes that contained either 10 or 30 wt% biomass were made from various combinations of screen-bowl coal fines, the two bio-oil binders, and the sawdust biochar. For comparison, briquettes were also made with a conventional wheat starch binder, miscanthus, and corn stover. While the higher viscosity bio-oil was more effective as a binder than the as-collected bio-oil, the durability of briquettes formed with either bio-oil was no better and more often, worse than that of analogous briquettes made without a binder. However, both bio-oils did impart resistance to water degradation, which was not obtained with the conventional wheat starch binder. Briquettes formed with 10 wt% biochar exhibited crushing strengths and mechanical durability results that were substantially lower than analogous briquettes made with miscanthus or corn stover. Attempts to form briquettes with 30 wt% sawdust biochar were unsuccessful as the briquettes disintegrated during fines removal over a vibrating screen. It was concluded that the bio-oil used in this evaluation would require significant modification before it could be used as an effective binder while the production of a suitable biochar for co-briquetting would likely benefit from a different feedstock and production at a temperature significantly lower than the ~500 °C used in his study.

## 8.2 Introduction

Two of the obstacles that could potentially impede commercial development of a coal-

biomass briquetting industry are the availability of adequate quantities of binder and biomass. Further, the conventional binders and raw biomass that are available are often either economically or physically unsuitable for co-firing with coal. Because biomass obtains its carbon from the atmosphere during its growth cycle, combustion of biomass to produce energy is generally considered to be carbon neutral, particularly combustion of a waste biomass such as agricultural residue, which is ultimately destined to release its carbon as $CO_2$ as it decays. Further, other pollutants that plague coal use such as sulfur, mercury, or arsenic are absent or in low concentrations in biomass, and in turn, in biochar. Thus, when biochar is co-fired with coal, fewer of these pollutants and less net $CO_2$ is emitted per unit of energy produced.

While co-firing raw biomass with coal can reduce net $CO_2$ emissions, there are a number of impediments to co-firing raw biomass, including a low bulk energy density which limits the distance it can be economically transported, susceptibility to rot, the added costs to store, convey, and pulverize raw biomass at the utility, and de-rating of the boiler at higher rates of co-firing. However, most of these obstacles can be reduced or eliminated by pyrolyzing or pre-charring the biomass in a process known as torrefaction (Koppejan, 2012; Dutta & Leon, 2011). In torrefaction, biomass is heated in an inert or autogenous atmosphere to moderate temperatures of ~220 to 320 °C, driving off mostly water and carbon dioxide along with a small amount of volatile matter. Because the loss of weight during torrefaction is substantially greater than the loss of heating value, the char that remains has a calorific value that is more similar to that of coal. The biomass also undergoes chemical reaction during torrefaction, particularly destruction of hemicellulose, leaving behind a solid that is more brittle and thus more easily ground (Phanphanich & Mani, 2012) as well as being more hydrophobic and resistant to microbial degradation (Koppejan, 2012).

Since weight decreases during torrefaction while volume is essentially unchanged, a net decline in density results. Densifying the torrefied biomass, most commonly by applying high pressures to form pellets (extrusion) or pucks (piston and dye), increases the char's bulk energy density which decreases transportation costs, decreases fugitive and explosive-dust issues, and facilitates handling and processing. Further, depending on how the biochar is produced and pelletized, the pellets are often water resistant meaning they can be stored without cover, which offers a significant advantage relative to raw biomass (Wild, 2014).

Because of the advantages of torrefied versus raw biomass, research and development has focused chiefly on the production of pelletized biochar fuels with no published accounts of co-briquetting torrefied biomass and coal. This is somewhat surprising considering that coal-biochar briquettes offer the same benefits as biochar pellets with several additional advantages including, a broader range of suitable torrefaction temperatures; fewer freezing or fugitive dust issues compared to cleaned coal fines; reduced respiratory and dust-explosion hazards during production and handling; and the option to use roll briquetting instead of extrusion or puck production. In terms of process economics, this latter can advantage can be quite significant as compared to extrusion or puck production, briquetting requires substantially less energy, results in less machine wear, and generally provides higher production rates. Production of a coal-biochar briquette (or extrudate) can also potentially provide an avenue to market the waste coal fines stored in gob piles and slurry impoundments around the U.S. as well as prove to be more appealing to the coal-plant operator as the handling, processing, and combustion behavior of coal-biochar briquettes should be virtually indistinguishable from coal.

The production of a high energy density coal-biochar briquette that would emit fewer pollutants per unit of power produced, and that could be stored, ground, and combusted without modifying existing infrastructure would represent a premium fuel that would command a premium price. Accordingly, one of the two major objectives of the scoping evaluation was to assess the potential to produce a durable and water resistant briquetted fuel from a blend of coal and biochar.

With respect to binders, numerous binder formulations have been proposed or used to produce coal or coal-biomass briquettes (Bratton et al., 2010a; Taulbee et al., 2009; Honaker et al., 2005). Some of the more common conventional binders that have been proposed for coal briquetting include starch, molasses/lime, lignosulfonate, pitch, asphalt, sodium silicate, and bentonite. However, all of these have one or more undesirable characteristics such as cost, limited availability, lack of water resistance, addition of inorganic components, etc. For example, one of the more effective binders for coal briquetting in terms of strength and durability is starch. However, starch does not provide the desired level of water resistance and the price for starch renders this material marginally suitable at best as a binding agent for coal. Further, due to its limited availability, a commercial scale coal-biomass briquetting industry would soon drive the cost of starch above a level that could be economically justified.

The ability to produce an effective bio-oil binder during pyrolysis of biomass could resolve many of the impediments posed by conventional binders. A bio-oil binder would have a high heating value, would not increase the inorganic component of the fuel briquette, could potentially impart resistance to water degradation, and would be produced in quantities that were proportional to the biochar being added. Accordingly, the second major objective of the study was to assess the potential to use the bio-oil that is co-produced during the pyrolytic production of sawdust char as a binder for coal/biochar and for coal/raw biomass briquettes.

## 8.3 Experimental

### 8.3.1 Materials

The following coal and biomass samples were used to produce briquettes throughout this study:

- Kiln SD – kiln dried sawdust. Multiple barrels of kiln dried mixed hardwoods, comprised primarily of milled poplar and red oak, were collected from White Lumber, Inc., Morehead, KY. This Kiln SD was screened to minus 6.35 mm (0.25 in) prior to use.
- CS - Corn Stover. The CS sample was locally harvested and provided as square bales by the University of Kentucky Biosystems and Agricultural Engineering Department. Prior to use, the CS samples were reduced in particle size by processing through a knife mill fitted with a 6.35 mm (0.25 in) screen.
- MIS - Miscanthus. Procured and processed in same manner as corn stover sample.
- RVSB. Several barrels of screen-bowl coal fines were collected from the River View prep plant near Waverly, in Western Kentucky. The sample was a combination of spiral and flotation fines from a 1:1 blend of the Kentucky 9 and Kentucky 11 seams. Nominal particle size was minus 1.0 x 0.044 mm (16 x 325 mesh). The sample was evaluated without additional size reduction.

### 8.3.2 Pyrolysis Reactor

Bio-oil and biochar samples were produced by heating sawdust in a stainless steel 5.5 liter batch reactor positioned inside of a fire-brick lined electrically-heated kiln. Off gases and oil vapors were routed out of the kiln using stainless steel transfer lines and into a downstream

condensation train submerged in an ice bath. A schematic of the apparatus used to process the sawdust into oil and char is shown in Figure 8-1.

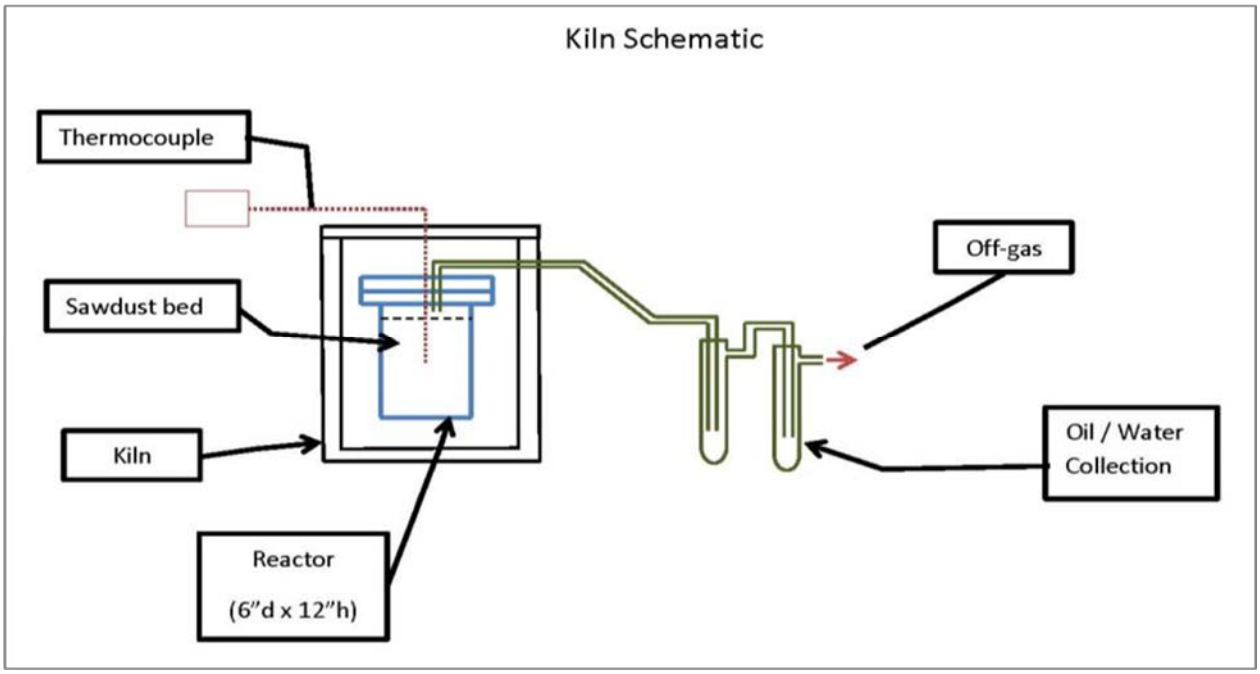



Figure 8-1. Schematic of 5.5 liter batch reactor used to produce bio-oil and biochar

## 8.3.3 Bio-Oil and Biochar Production Procedures

The procedure for producing the bio-oil and biochar for evaluation entailed loading 1.2 kg of kiln dried sawdust to the pyrolysis reactor, inserting a type K thermocouple into the middle of the sawdust bed, and positioning the assembled reactor inside of an electrically-heated kiln (Figure 8-1). After loading, the kiln was ramped to 225 °C at 20 °C/min and held as water evolved and was collected downstream in a pair of cold traps[14] submerged in an ice bath. After an approximate one hour hold at 225 °C, the condensed water was removed from the traps and weighed. The condensation train was reassembled and the kiln temperature ramped to 400 °C at a rate of 20 °C/min. Due to the low thermal conductivity of sawdust and the evolution of water, which suppressed the temperature inside the reactor, the temperature of the sawdust bed lagged the kiln temperature, typically requiring over an hour to reach 200 °C after the kiln temperature had reached the 400 °C target. However, on attaining a bed temperature of approximately 200

[14]The cold traps resulted in an intentional inefficient trapping of oil vapors under the assumption that the more readily condensed heavy oil components would provide more suitable binding characteristics than would a lighter oil that would be recovered with a more efficient oil collection train.

°C, exothermic pyrolysis reactions increased and the sawdust bed temperature increased rapidly, reaching 500 °C in approximately 10 minutes at which time the kiln was switched off. Oil and water collection was continued approximately 10 minutes until evolution had visible slowed. The cold traps were then removed and the condensed oil and water were centrifugally separated and weighed. The reactor was permitted to cool overnight after which the reactor was disassembled and the char was recovered and weighed.

Several batches of the kiln dried sawdust were pyrolyzed in this manner in a series of replicate runs with the oil and char produced in these replicate runs composited to provide a total of ~1.35 kg of as-collected bio-oil and about 7 kg of biochar. The as-collected bio-oil (ACBO) flowed freely at room temperature, exhibiting a viscosity similar in magnitude to that of water despite the use of an intentionally-inefficient oil collection train intended to favor recovery of the heavier oil components. In an effort to generate a sample of bio-oil with a higher viscosity, about 1 liter of the ACBO was tared to an open 2 liter beaker and placed onto a hot plate to evaporate a portion of the more volatile components. Over a three day period, the bio-oil temperature was slowly increased from 70 °C to a final temperature of 230 °C, during which time the liquid volume was reduced from ~1 liter to ~500 ml. After 3 days of open air heating, the oil that remained was significantly more viscous than the ACBO. This higher viscosity oil is referenced here as the high-viscosity bio-oil (HVBO). The initial and final bio-oil viscosities for the ACBO and HVBO samples, obtained from steady-shear viscosity analyses, as shown in Figure 8-2, reveal an increase in viscosity of over three orders of magnitude for the HVBO compared to the ACBO.

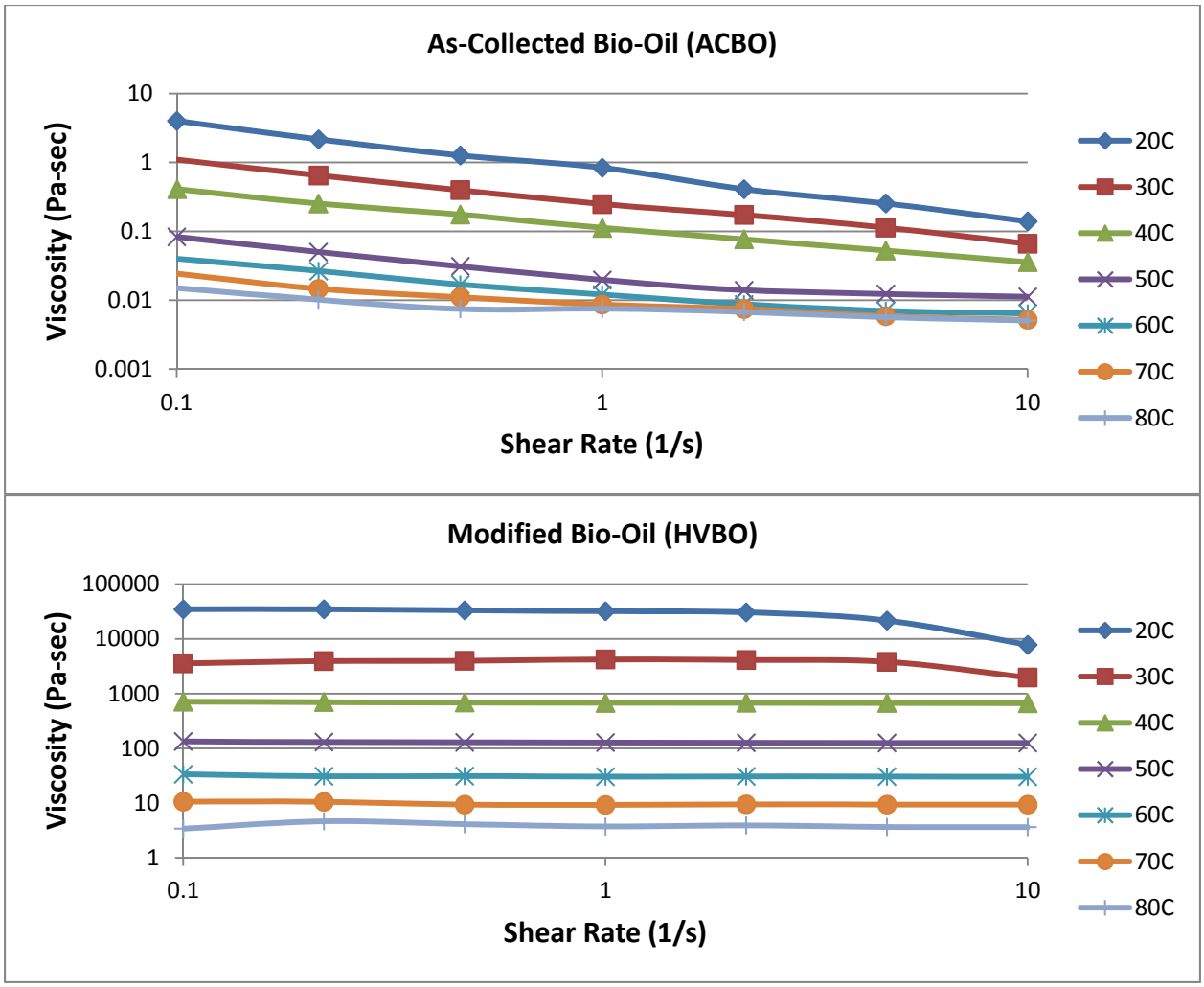



Figure 8-2. Steady-shear viscosities of the as-collected (top) and HVBO bio-oils (bottom)

## 8.3.4 Briquette Production

Targeted weights of both the ACBO and HVBO binders were applied to selected coal and biomass blends using a Sure Shot model A 0.9 kg (2 lb) sprayer as the blends were mixed in a 19 liter (20 qt) Hobart blender. The ACBO sample was applied at ambient temperature by pressurizing the sprayer to 0.62 Mpa (90 lb/in$^2$) prior to application. Unlike the low viscosity ACBO, the HVBO sample was near solid at room temperature requiring that it be warmed before loading to the sprayer. After loading, the HVBO was heated to ~110°C and then pressurized and sprayed onto the coal/biomass blends as described for the ACBO sample above.

For most briquette-production runs, targeted combinations of coal, biochar, and/or binder were blended and processed in 2.5 to 4 kg batches with each blend containing a total of either 10

or 30 wt% biomass[15]. Briquettes were formed at a roller force of 80 kN, a roller speed of 25 Hz (nominal production rate of ~45 kg/hr [100 lbs/hr]), and a targeted feed auger torque of ~90 N-m. During each run, 6-8 briquettes were collected into a tared beaker as they exited the briquette press, immediately weighed, and then dried overnight at 105 °C to determine initial briquette moisture. Immediately following formation, each batch of briquettes was passed across a Sweco mechanical screener fitted with a 61 cm (2 ft) diameter, 4.76 mm (4 mesh) screen to remove fines. On exiting the mechanical screener, the entire batch of briquettes were collected and placed into a controlled-environment chamber. However, it should be noted that none of the briquettes made with 30 wt% biomass survived the fines removal step.

## 8.3.5 Briquette Evaluation Procedures

### 8.3.5.1 Initial Briquette Moisture

During each briquetting run, 6-8 briquettes were collected from the briquette press discharge chute in a tared beaker, immediately weighed, and then oven-dried overnight at 105 °C to determine moisture at the time of briquette formation.

### 8.3.5.2 Crushing Strength

Average crushing strengths were determined at 30 minutes, 24 hours, and 7 days following formation. Typically, 25 briquettes were crushed at each time interval using a Lloyd Instruments, LRX Plus compressive meter fitted with a 1.9-cm (0.75 in) diameter plunger. The briquettes were placed on a flat surface and force was applied to the flatter side, perpendicular to the longer axis of the briquette (i.e. force applied along the same axis as applied by the roll pockets during formation). The compressive meter was mounted to an automated test stand that sensed and recorded the force applied at failure. The test stand had an upper limit of 450 $kg_f$ (1,000 $lb_f$) and was operated at a downward speed of 2.5 cm/min (1 in/min).

### 8.3.5.3 Mechanical Durability

Mechanical durability of briquettes was determined following a 7 day cure in a controlled-environment chamber. Approximately 200 g samples were placed into a 30.5-cm diameter (1 ft) Plexiglas cylinder equipped with three, 5 cm (2 in) lifters; tumbled for five minutes at 40 rpm; and mechanically screened for 3 minutes in a Ro-Tap sieve shaker fitted with

[15] Total biomass consisted of biomass-based binder plus either raw biomass or biochar.

a 4.76 mm (4 mesh) screen. The mechanical durability was reported as the fraction of the starting briquette weight that was retained on the 4 mesh screen. Mechanical durability values less than 0.80 are considered poor, 0.80-0.90 as marginally acceptable, 0.90-0.95 as good, and greater than 0.95 as excellent.

#### 8.3.5.4 Resistance to Water Degradation

Following a 7 day cure, 10 briquettes were weighed and submerged in a glass beaker filled with water. After one hour, the briquettes were visually classified as fully intact, partially intact, or fully degraded. Briquettes that classified as fully intact were retrieved, dried in room air for 30 minutes, reweighed to determine water uptake, and immediately crushed to determine the post-submersion crushing strength.

## 8.4 Results and Discussion

The two bio-oil binders (ACBO and HVBO), a wheat starch binder, and three biomass types (biochar, corn stover, and miscanthus) were combined with RVSB coal fines in various ratios to generate sixteen, 2.5 kg sample blends for briquetting. Twelve of the samples were prepared with 10 wt% biomass + binder and 90 wt% coal while the remaining four were prepared with 30 wt% biomass + binder and 70 wt% coal. The wheat starch binder and the corn stover and miscanthus biomass types were included to provide baseline data for evaluating the bio-oil and biochar, respectively.

The composition and test results for the briquettes made from the 16 test blends are shown in **Error! Reference source not found.**. As was noted in Section 8.3, briquettes made with 30% biochar did not survive the fines removal step over a mechanical screener, including the sample made with biochar and a wheat starch binder, which is normally a highly-effective binder. Considering that even briquettes that may be considered too weak to be commercially viable often survive the fines removal step, the data in **Error! Reference source not found.** would suggest that the sawdust biochar is unsuitable for use as a filler material for production of fuel briquettes when blended with coal at 30 wt%.

Table 8-1. Composition and properties of briquettes made from RVSB coal co-briquetted with various combinations of wheat starch, corn stover, miscanthus, biochar, and bio-oil binder

| Biomass ID | Biomass Content (wt%) | Binder ID[c] | Binder[b] Content (wt%) | Briquette Moisture (wt%) | Crushing Strength[d] | | | Mechanical Durability | Average Briq Wt (g) | Visual Appearance FI, PI, D[a] | Wet Strength ($kg_f$) |
|---|---|---|---|---|---|---|---|---|---|---|---|
| | | | | | 30 min ($kg_f$) | 24 hr ($kg_f$) | 7 day ($kg_f$) | | | | |
| Biochar | 6.0% | ACBO | 4.0% | 7.3% | 9 | 12 | 12 | 0.22 | 7.61 | FI | 7.3 |
| Biochar | 6.0% | HVBO | 4.0% | 6.8% | 18 | 23 | 27 | 0.45 | 9.03 | FI | 15.8 |
| Biochar | 6.0% | WSt | 4.0% | 7.1% | 30 | 31 | 39 | 0.63 | | FD | |
| Biochar | 10.0% | NBndr | --- | 7.0% | 9 | 11 | 13 | 0.14 | | FD | |
| Corn Stover | 6.0% | ACBO | 4.0% | 8.0% | 17 | 24 | 25 | 0.34 | 8.05 | PI | |
| Corn Stover | 6.0% | HVBO | 4.0% | 7.3% | 29 | 37 | 39 | 0.62 | 8.79 | PI | 2.6 |
| Corn Stover | 6.0% | WSt | 4.0% | 7.3% | 57 | 67 | 72 | 0.83 | | FD | |
| Corn Stover | 10.0% | NBndr | --- | 7.5% | 31 | 42 | 42 | 0.53 | | FD | |
| Miscanthus | 6.0% | ACBO | 4.0% | 8.1% | 10 | 12 | 15 | 0.30 | 6.95 | PI | 5.0 |
| Miscanthus | 6.0% | HVBO | 4.0% | 7.6% | 25 | 38 | 38 | 0.58 | 9.13 | PI | 4.7 |
| Miscanthus | 6.0% | WSt | 4.0% | 7.0% | 54 | 57 | 68 | 0.82 | | FD | |
| Miscanthus | 10.0% | NBndr | --- | 7.7% | 25 | 32 | 35 | 0.47 | | FD | |
| Biochar | 26.0% | ACBO | 4.0% | *All of the 30% biomass briquettes made with biochar disintegrated during the fines removal step* | | | | | | | |
| Biochar | 26.0% | HVBO | 4.0% | | | | | | | | |
| Biochar | 26.0% | WSt | 4.0% | | | | | | | | |
| Biochar | 30.0% | NBndr | --- | | | | | | | | |

[a] FI-Fully intact, PI-partially intact, FD-fully degraded
[b] All three binders evaluated are biomass derived and thus are considered part of the biomass component of the briquette
[c] ACBO-as collected bio-oil; HVBO-high viscosity bio-oil; WSt-wheat starch; NBndr-no binder
[d] Data shown in red indicate values that are equal to or greater than minimally acceptable

Crushing strength and mechanical durability results are shown for the 10% biomass briquettes in **Error! Reference source not found.** and plotted in Figure 8-3 and Figure 8-4, respectively. These data reveal that briquettes made with the ACBO binder exhibited lower crushing strengths and were less durable than briquettes made with the same coal and biomass without a binder. That is, the ACBO exhibited properties more akin to those of a lubricant than to those of a binder. Briquettes made with the higher viscosity HVBO binder fared better as they consistently exhibited strengths and durability values that were equal to or greater than analogous values obtained for their binderless analogues, particularly compared to the binderless briquettes that were made with biochar. However, despite their unacceptably low durability, all of the briquetted samples made with either of the two bio-oil binders exhibited resistance to

water degradation during submersion. This property was in contrast to that of the binderless briquettes or to that of the briquettes made with a wheat starch binder, which fully disintegrated during water submersion.

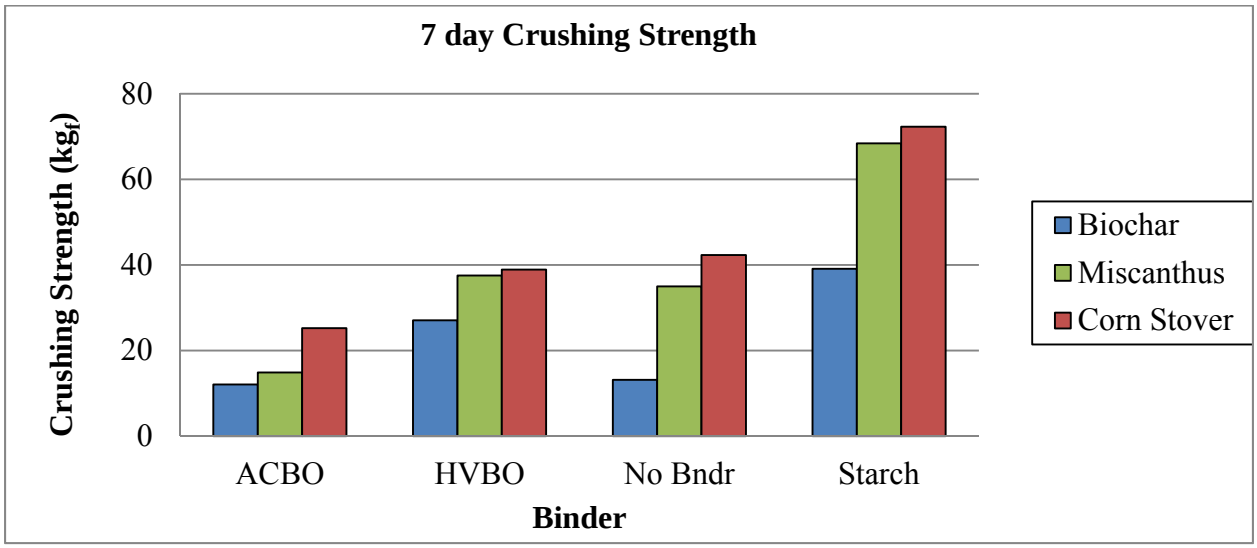



Figure 8-3. Crushing strengths following a 7 day cure for briquettes made with RVSB coal fines and 10% biomass comprised of bio-oil, biochar, wheat starch, corn stover, and/or miscanthus as indicated

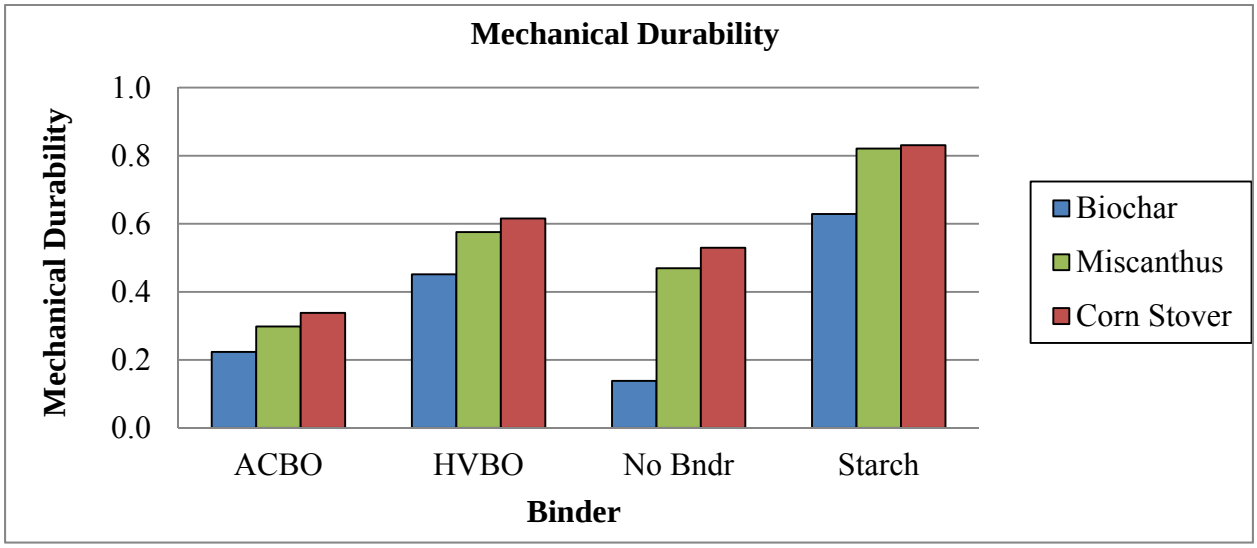



Figure 8-4. Mechanical durability results following a 7 day cure for briquettes made with RVSB coal fines and 10% biomass comprised of bio-oil, biochar, wheat starch, corn stover, and/or miscanthus as indicated

With respect to the impact of biochar addition, both the crushing strength and mechanical durability were found to be lower for briquettes made with biochar compared to otherwise

analogous briquettes made with 10 wt% corn stover or miscanthus. This trend held regardless of whether the briquettes were made with a bio-oil or wheat starch binder or made without a binder.

None of the briquetted samples made with biochar and/or bio-oil for this evaluation exhibited an average crushing strength greater than 23 $kg_f$ (50 $lb_f$) or a mechanical durability greater than 0.8, both of which are considered to be minimally acceptable values. This was the case even when wheat starch, which normally is a highly effective binder, was substituted for the bio-oil and briquetted using the biochar filler as well as when corn stover and miscanthus were substituted for biochar and briquetted with the bio-oil binders. In fact, the bio-oil and biochar used in these scoping evaluations fared so poorly that additional evaluations planned for these materials was abandoned. However, additional work was conducted with two biochars from alternate sources, which performed better than the sawdust biochar produced for the study. That work is reported in the Chapter 7.

## 8.5 Summary and Conclusions

Briquettes made with a sawdust derived bio-oil binder exhibited good resistance to water degradation as opposed to otherwise analogous briquettes that were made without a binder or that were made with a wheat starch binder. Further, thermally modifying the as-collected bio-oil to remove a portion of the more volatile oil components resulted in an increase in oil viscosity and subsequent improvement in binding characteristics. However, the crushing strength and mechanical durability of briquettes made with either of the two bio-oils evaluated were no better, and more often were worse than obtained without a binder. Thus, despite its ability to impart water resistance and the improvement in effectiveness following thermal modification, it was concluded that the two bio-oils that were evaluated exhibited characteristics that were more akin to those of a lubricant than to those of a binder and they were deemed unacceptable for further consideration as binding agents.

Pyrolysis oil produced from woody biomass typically has a significant amount of oxygen incorporated into its structure, chiefly in the form of phenols, cresols, and other hydroxyl-containing compounds. Since oxygen groups are polar and generally improve binding characteristics, the total lack of effectiveness as a binder in this study was a bit surprising and thought perhaps to be due to a relatively low average molecular weight. Thus, the most promising avenue for future research intended to produce a more effective bio-oil binder is

thought to be in the area of treatments to increase the average molecular weight as well as viscosity of the bio-oil by more aggressively removing the lighter components and/or inducing cross-linking reactions.

With respect to briquettes made with 10 wt% biomass, the briquettes made with sawdust-derived biochar filler exhibited an unacceptably low crushing strength and mechanical durability on both an absolute and on a relative basis compared to the strength and durability of briquettes made with equivalent amounts of miscanthus or corn stover. Attempts to produce coal/biochar briquettes with 30 wt% biochar plus binder were unsuccessful as the briquettes that were produced did not survive the fines removal step across a mechanical screener, even when a normally effective starch binder was added. Thus, based on results from both the 10 and 30% biomass briquettes, the sawdust-derived biochar used in this study was also deemed unsuitable for producing coal-biomass briquettes.

Before dismissing biochar as unsuitable for co-briquetting with coal, it should be noted that the batch reactor used to produce the sawdust biochar had inherent design limitations. Chief among these limitations was an inability to control the final pyrolysis temperature. As described in the Section 8.3, when the sawdust reached a bed temperature of ~200 °C, exothermic pyrolysis reactions began to dominate and the sawdust-bed temperature quickly climbed to over 500 °C. This rapid rise in temperature could not be controlled or significantly slowed in the highly insulated pyrolysis kiln. In contrast, the temperature range typically reported as optimum for the production of high strength biochar pellets is in the ~220-320 °C range with pellet durability declining at higher production temperatures (Koppejan, 2012; Dutta & Leon, 2011). There is little doubt that the surface chemistry of biochar produced in the 220-320 °C range will differ from that of char produced at >500 °C. Therefore, there is a good possibility that the poor performance of briquettes made with the sawdust biochar produced for this study was due to an unsuitable surface chemistry resulting from the high production temperature. Further, while the char surface chemistry likely plays a major role in governing briquette durability, it is also believed that the small, angular shape of the sawdust-char particles contributed to the poor performance. Thus, the two areas considered most promising for future biochar research center on production of biochar at a lower temperature and production of biochars from feedstocks that have shapes that may be more suitable for producing more durable coal-biochar briquettes (e.g. wheat straw or miscanthus).

# Chapter 9

# Coal Particle Size Briquetting Evaluations

## 9.1 Abstract

In a scoping evaluation of the impact of the coal particle-size distribution on briquette durability, an ultra-fine coal sample (MRC) was systematically blended with two larger size screen-bowl coal samples (Alden and PCC) at targeted ratios. There was a good deal of overlap in the particle-size distributions between the MRC and PCC coals but very little between the MRC and Alden coals. Two biomass types that differed in shape and texture (corn stover and wheat straw) were added at 10 wt% to each of the blended coal samples and briquetted, both with and without a binder. For a given fine coal blend, there was little difference in the briquette quality as a function of which biomass was added. However, there were differences in durability as a function of the proportion of the ultra-fine MRC coal that was present. For the blends made with the ultra-fine MRC coal and the relatively large particle size Alden coal, both strength and mechanical durability were directly proportional to the fraction of MRC coal in the blend, both with and without a binder. Similar trends in strength and durability behavior were noted for the binderless briquettes made with the MRC and PCC coals. However, when a binder was added, the strength and mechanical durability remained relatively constant or declined as the proportion of MRC coal increased. Possible reasons for these trends are discussed.

## 9.2 Introduction

Higher bulk packing densities for coal and other particles is best achieved with a wider rather than a narrower particle-size distribution (Yu et al., 1995; Yu & Standish 1993; Standish et al., 1991a; Standish et al., 1991b). The equations that are used to model particle packing are typically unitless, meaning they are dependent more on the relative size distribution rather than the absolute size distribution. However, while a higher bulk density may correlate to some extent with briquette strength, briquette strength is far from being fully described by the same

parameters as packing density. For example, a collection of larger coal particles will have fewer contact points than an equivalent weight of smaller particles. When pressed together without the addition of a binder, the larger particles will form a very weak agglomerate that is more likely to fall apart when the force is removed compared to a cluster of smaller particles where there are more numerous particle interactions in the form of electrostatic and/or van der Waal attractions. Thus, while the larger particles may provide a higher packing density, they will not necessarily provide the strongest briquettes. Filling the voids between larger particles can improve the integrity of the agglomerate by providing a physical support as well as additional points of contact for particle interactions. In some respects, this in-filling can be described by the equations that describe how packing density is increased by using a wide versus a narrow particle-size distribution. However, when a binder is added, the optimum particle-size distribution for obtaining stronger briquettes can shift from smaller toward larger particles. This is because larger particles have less surface area per unit weight meaning less binder is needed to uniformly cover the particles to an effective thickness.

When one further considers the impact of parameters such as moisture content, friability[16], particle shape, surface chemistry, mineral matter and dispersion, the nature of the binder added, and so forth, it becomes obvious that modeling the relation between particle-size distribution and briquette durability for a complex feedstock such as coal is not trivial. Further, the optimum particle-size distribution for producing the strongest briquettes may also vary in day to day operations due to variation of parameters such as the force being applied, the adherence of flocculants on the particle surface, surface moisture or oxidation, how effectively the coal and binder were blended, and so on.

Despite the many significant variables, it is noted that in this as well as prior work, that while a distribution in particle sizes is needed, when a binder is not added, smaller particles in general make better briquettes while very strong briquettes can be made from larger particles when using a binder. However, with few exceptions (e.g., ferro-silicate or stoker coal), there is little or no reason to consider briquetting particles larger than about 5 mm, particularly for the steam market as coal particles larger than about 5 mm can be dried and shipped with relative

[16] During briquetting, higher friability can lead to greater fines production and/or production of fissures between particles with no binder coverage, both of which can impact briquette durability.

ease. Further, considering that briquetting larger particles generally requires adding an expensive binder, a realistic upper limit is more on the order of about 1 mm or less.

With the exception of sawdust, most forms of biomass must be reduced in size prior to co-briquetting with coal. In contrast, samples of fine coal are often available from prep plants or slurry impoundments at a particle size that is both suitable and can benefit from briquetting. For bituminous coals, the most common method for generating fine coal in this size range at the prep plant is to combine the products from spiral and froth flotation cleaning circuits and then run them through a screen bowl decanter to reduce the moisture content. Since particles smaller than about 45 μm simply pass through the decanter due to insufficient settling time or are removed via cyclones and discarded with the tailings, screen bowl fines with a nominal particle size range of between about 45 and 600 μm (28 x 325 mesh) tend to be the norm, though depending on the plant configuration and operation, somewhat larger size or smaller distributions may be produced (Records & Sutherland, 2001). While less common, samples of fine coal produced by froth flotation are also available. The particles recovered by froth flotation are nominally less than about 150 μm in diameter and thus too small to be dewatered in a screen bowl decanter, instead, requiring moisture reduction via pressure and/or vacuum filtration (Osborne, 1988).

These two clean coal product streams, combined spiral and flotation product and the ultra-fine froth flotation product, represent the two most common fine coal samples produced in coal preparation plants that are of a suitable size range for direct briquetting. Accordingly, the objective of this study was to conduct a scoping evaluation of the impact of particle size on briquette durability using these types of fine coal samples.

# 9.3 Experimental

## 9.3.1 Materials

### 9.3.1.1 Coal Feedstocks

The three fine coal samples used in this evaluation were of bituminous rank and all were obtained from the Appalachian coal field.

- PCC – The PCC screen-bowl fines were collected from Teco Coal's Perry County Prep plant near Hazard in Eastern Kentucky. The sample was a combination of spiral and flotation fines from an approximate 1:1 blend of Elkhorn 4 and Hazard 5/5A seams with

a nominal particle size of 595 x 44 μm (28 x 325 mesh). The sample was evaluated without additional size reduction.

- Alden – The Alden screen-bowl fines were collected from the Alden Resources' preparation plant near Williamsburg in Southeast Kentucky. This sample was also a combination of fines recovered from spiral and flotation circuits recovered during processing of coal from the Blue Gem Seam. The Alden sample had a larger nominal particle size of 6.35 x 0 mm (<1/4 in) and was evaluated without additional size reduction.
- MRC – The MRC fines were collected from a disk filter during dewatering of flotation fines at the McClure River Coal prep plant located east of Abington, Virginia. The MRC sample had a nominal particle size of minus 150 μm (100 mesh) and was evaluated without additional size reduction.

Particle-size distributions were obtained by a combination of wet (minus 1 mm size fractions) and dry (plus 1 mm size fractions) U.S. sieve analysis. There were significant differences in the particle-size distributions of the three fine coal samples, with nearly 60 wt% of the Alden screen bowl sample comprised of particles larger than ~600 μm (30 mesh), nearly half of the weight of the PCC sample comprised of particles between about150 and 600 μm in diameter (30 x 100 mesh), and 46 wt% of the MRC disk filter sample comprised of particles less than about 75 μm in diameter (200 mesh). Further, there was a good deal of overlap in the particle-size distributions for the PCC and MRC fines, but a gap in the particle-size distribution around 0.5 mm for the Alden and MRC samples.

The three study coals were used to prepare two sets of master samples for briquetting. Samples within each of the two sets of master blends were prepared with the PCC and MRC coal or with the Alden and MRC coals at concentrations that ranged from 100 wt% of each screen bowl sample (PCC or Alden) to 100 wt% MRC. Each of the master blends was then briquetted with either 10 wt% corn stover or 10 wt% wheat straw both with and without a starch binder. The impact on crushing strength and mechanical durability were then evaluated for each set of briquettes as a function binder type, biomass type, and the concentration of screen bowl versus disk filter coal. The work conducted here was similar to a previous study in which the Proctor density for blends of decanter coal, froth flotation coal, and sawdust were determined and related

to the durability of briquettes prepared with those blends (Patil et. al., 2009). The results obtained are strikingly similar.

Proximate and ultimate analysis results, along with calorific values for the three study coals are shown on an as-received basis in Table 9-1. While the Alden sample was lower in ash than the PCC fines, these two screen-bowl samples were otherwise similar in terms of fixed carbon, volatile matter, and calorific value. In comparison, the MRC was higher in ash and lower in volatile matter.

Table 9-1. Chemical analysis of study coals shown on an as-received basis

| Sample ID | Abbreviated ID | Ash % | Moisture % | C % | H % | N % | $S_{tot}$ % | O % | % Vol Matter | % Fixed C | GCV kJ/kg |
|---|---|---|---|---|---|---|---|---|---|---|---|
| McClure River | MRC | 11.00 | 0.87 | 77.98 | 4.90 | 1.41 | 0.89 | 3.82 | 27.83 | 60.30 | 30610 |
| Perry Co Screen Bowl | PCC | 6.86 | 1.03 | 77.97 | 5.24 | 1.50 | 0.75 | 7.68 | 34.60 | 57.51 | 31720 |
| Alden Screen Bowl | Alden | 3.65 | 1.12 | 79.27 | 5.43 | 1.84 | 0.84 | 8.97 | 36.26 | 58.97 | 32152 |

#### 9.3.1.2 Biomass Feedstocks

The following biomass samples were used for briquette production throughout the course of this study:

- CS – Corn Stover was locally harvested and provided as square bales by the University of Kentucky Biosystems and Agricultural Engineering Department. Prior to use, the CS samples was processed through a knife mill fitted with a 6.35 mm (0.25 in) screen.
- WS – Wheat Straw was procured and processed in same manner as described for corn stover.

Proximate and ultimate analysis results, along with calorific values for the two biomass samples are shown on an as-received basis in Table 9-2.

Table 9-2. Proximate analysis, ultimate analysis, and calorific values of biomass samples

| Abbreviated ID | Sample ID | Ash % | Moisture % | C % | H % | N % | $S_{tot}$ % | O % | % Vol Matter | % Fixed C | GCVg kJ/kg |
|---|---|---|---|---|---|---|---|---|---|---|---|
| WS | Wheat straw | 4.30 | 9.40 | 44.11 | 6.51 | 1.03 | 0.29 | 43.76 | 74.32 | 11.98 | 16373 |
| CS | Corn stover | 2.58 | 8.48 | 45.79 | 6.05 | 2.28 | 0.14 | 43.16 | 78.06 | 10.88 | 16696 |

## 9.3.2 Major Equipment

### 9.3.2.1 Briquette Press

All briquettes were formed in a Komarek B-100 continuous roll briquette press using a targeted roll force of 80-85 kN, which is less than the 85-90 kN force that was normally used during the project[17]. Roller speed was fixed at a nominal setting of 25 Hz, which equates to a production rate of approximately 45 kg/hr (100 lbs/hr). The feed auger was controlled manually during each run to provide a force of approximately 85 N-m, which again is lower than the 90 N-m that was normally targeted during the project[2].

### 9.3.2.2 Controlled Environment Chambers

To eliminate variations in briquette properties due to variations in ambient temperature and humidity conditions over the course of the project, all briquetted samples were stored in one of three Caron controlled-environment chambers (models 6010, 6020, and 6030), which were maintained at simulated ambient conditions of 22.3 °C (72 °F) and 70% relative humidity. Briquettes were placed into the chamber immediately after production and retained until the physical evaluations were complete.

### 9.3.2.3 Knife Mill

The corn stover and wheat straw samples were reduced in particle size by processing through a model G1012 Granulator (knife mill) manufactured by Jordan Reduction Solutions in Birmingham, Alabama. The mill was fitted with a 6.35 mm (0.25 in) screen and had a rated capacity of ~90 kg/hr (200 lb/hr).

## 9.3.3 Briquette Production

Samples of the PCC, RVSB, and MRC coals were air-dried to equilibrium moisture then used to prepare eleven master coal samples consisting of 100% MRC, 100% Alden, 100% PCC and 4 combinations each of MRC/Alden and MRC/PCC coals blended at weight ratios of 20/80, 40/60, 60/40, and 80/20. The master samples were then used to prepare forty-four blends for briquetting by blending 2,700 g of each of the 11 master sample with (1) 300 g of corn stover, (2) 300 g of wheat straw, (3) 300 g of corn stover plus 150 g of gelatinized wheat starch, and (4)

[17]While these changes were relatively small, they resulted in a substantial decline in briquette strength, particularly green strength, and mechanical durability.

300 g of wheat straw plus 150 g of gelatinized wheat starch. Each of the 44 blends were briquetted and the briquettes retained in a controlled-environment chamber at 22.3 °C and 70% relative humidity until tested for crushing strength (30 min, 24 hrs, and 7 days after formation), mechanical durability (7 days), and resistance to water degradation (7 days). As noted above, the briquette press roller and feed auger torques were reduced for these evaluations relative to the torques normally used resulting in a significant decrease in overall briquette durability. This modification was made in an effort to allow for a more-valid comparison of the impact of changing particle-size distribution at feed and roller torques that are more representative of those that might be used commercially.

For those briquetting runs in which a binder was used, the binder was pre-blended with the coal fines and biomass prior to loading to the briquette press feed hopper. Briquettes were formed in a Komarek B-100 continuous briquette roll press at a roll force of 80 kN, a roller speed of 25 Hz (nominal production rate of ~45 kg/hr, i.e, ~100 lbs/hr), and a targeted feed-auger torque of ~85 N-m. Each batch of briquettes passed across a Sweco mechanical screener fitted with a 61-cm (2 ft) diameter, 4.76 mm (4 mesh) screen to remove fines. The entire batch of briquettes was collected from the Sweco exit chute and stored in a controlled-environment chamber until tested.

## 9.3.4 Briquette Evaluations

### 9.3.4.1 Crushing Strength

Average crushing strengths were determined at 30 minutes, 24 hours, and 7 days following formation. Thirty briquettes were crushed at each time interval using a Lloyd Instruments, LRX Plus compressive meter fitted with a 1.9-cm (0.75 in) diameter plunger and was mounted to an automated test stand. The test stand had an upper limit of 450 $kg_f$ (1,000 $lb_f$) and was operated at a downward speed of 2.5 cm/min (1 in/min). Briquettes were placed on a flat surface and force was applied perpendicular to the flatter side and longer axis of the briquette (i.e., force applied along the same axis as applied by the roll pockets during formation). The compressive meter sensed and displayed the maximum force applied at failure.

### 9.3.4.2 Mechanical Durability

Mechanical durability of briquettes was determined following a 7 day cure in a controlled

environment chamber. Approximately 200 g of briquettes (20-25 briquettes) were placed into a 30.5-cm (1 ft) diameter Plexiglas cylinder equipped with three, 5 cm (2 in) lifters; tumbled for five minutes at 40 rpm, and screened for 3 minutes in a Ro-Tap sieve shaker fitted with a 4.76 mm (4 mesh) screen. The average mechanical durability was reported as the fraction of the starting briquette weight retained on the 4 mesh screen. Mechanical durability values less than 0.80 are considered poor, 0.80-0.90 marginally acceptable, 0.90-0.95 good, and greater than 0.95 excellent.

## 9.4 Results and Discussion

Particle-size distributions for the three study coals as determined from a combination of wet and dry sieve analyses are shown in Figure 9-1. In this plot, the weight percent recovery for each mesh range is plotted against the midpoint diameter for that range[18]. For example, the average particle diameter of 4 x 12 mesh material was assigned a value of 3.2 mm, which is midway between the 4.76 mm (4 mesh) and 1.68 mm (12 mesh) sieve openings. While this is a crude approximation, it is considered adequate for illustrating the significant differences in particle-size distribution for the three parent coals, particularly the ultra-fine MRC coal compared to the two screen bowl samples.

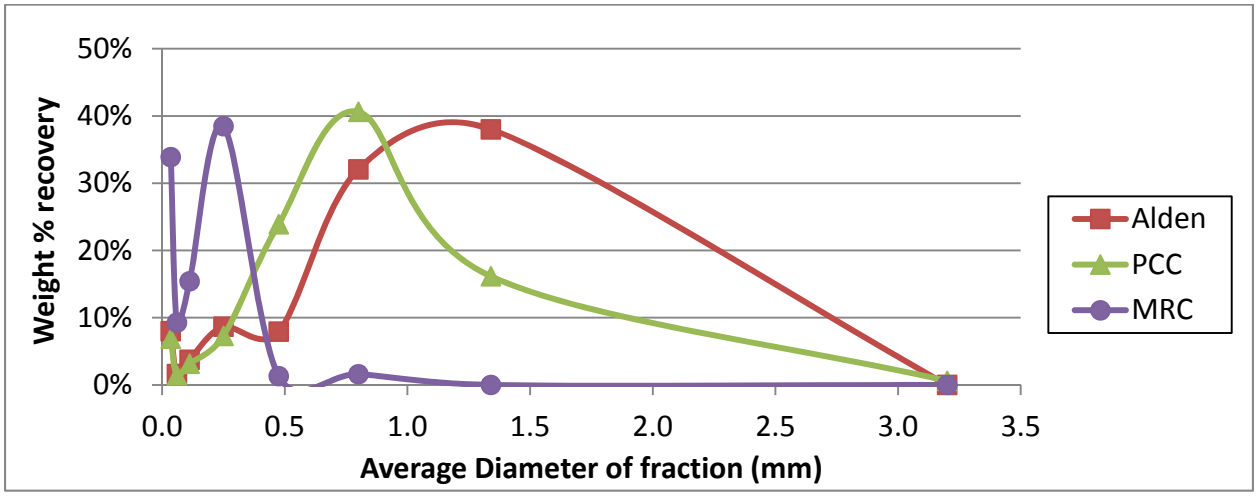



Figure 9-1. Particle-size distribution for the three study coals plotted against the average diameter of the 8 size ranges to which the particles partitioned

[18] As an aside, while there are substantial differences in the weight recovery curves, between 93% and 95% of the total number of particles in all three coals are smaller than 44 µm (325 mesh).

In an effort to evaluate the relation between coal particle size and briquette properties, samples with a range of size distributions were prepared by blending the ultra-fine MRC sample with the coarser PCC and Alden coals as described in Section 9.3. Figure 9-2 depicts the calculated particle-size distributions of the resulting blends calculated as linear combinations of the empirically determined distributions of the parent coals.

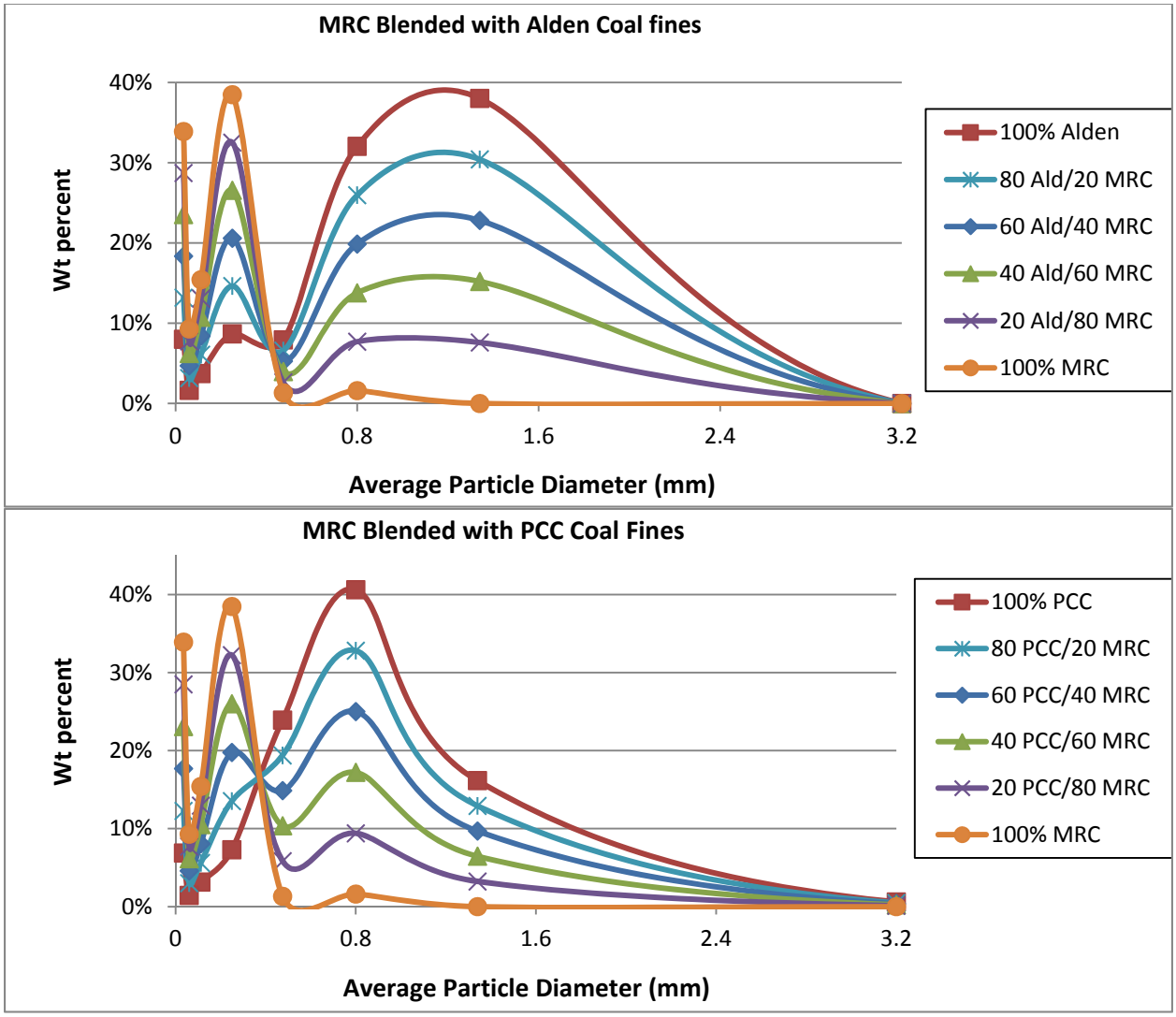



Figure 9-2. Linear combinations of the particle-size distributions for blends of MRC and Alden coals on top and for the MRC and PCC coals on bottom.

Crushing strengths for blends of Alden and MRC coal co-briquetted with either corn stover or wheat straw are shown in Figure 9-3. As expected, the briquettes made with a binder were consistently stronger and more durable than were their binderless counterparts. Also note that there is very little difference in the durability of briquettes made with corn stover versus

those made with wheat straw despite the significant differences in morphology and surface texture for these two biomass types. This suggests that at low addition rates of biomass, changing the particle size of the coal component has a greater impact on briquette properties than does changing the type of biomass added.

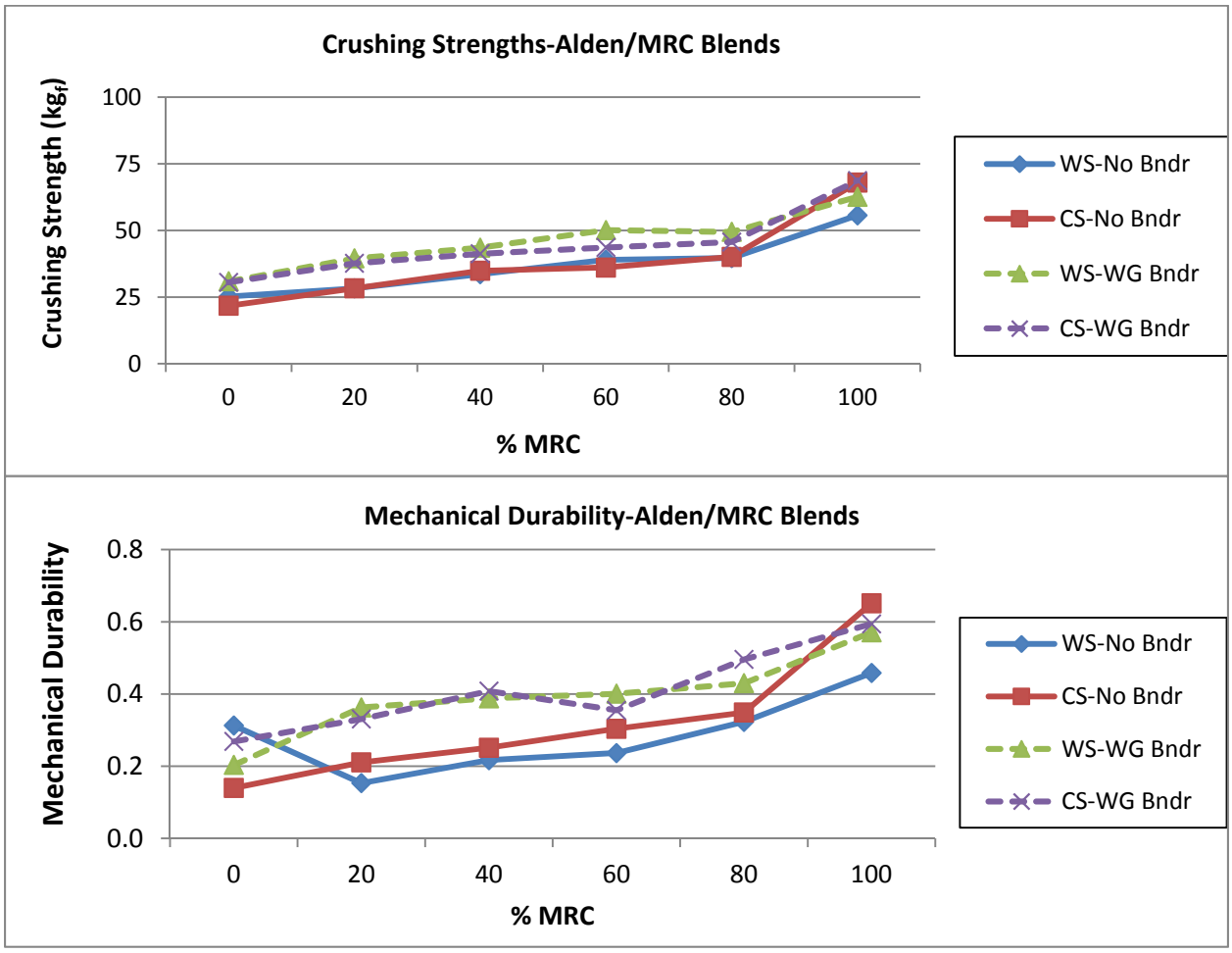



Figure 9-3. Twenty-four hour crushing strengths (top) and mechanical durability (bottom) for blends of MRC and Alden coal fines

The plots in Figure 9-3 reveal that with relatively minor exceptions, there was a continuous improvement in both crushing strength and mechanical durability as the proportion of the ultra-fine MRC in the briquettes was increased. Thus, regardless of which of the two biomass types was added or whether the briquettes were formed with or without adding a starch binder, there was essentially no improvement in briquette durability obtained by blending the Alden and MRC coals to broaden the coal particle-size distribution.

The average briquette weight for the four briquetted samples made with each of the six Alden/MRC master blends is plotted in Figure 9-4. Average briquette weight is expected to correlate with briquette density since the briquette press roller pockets are of fixed volume. However, this is at best a crude approximation for several reasons including a higher roller torque can force the rollers apart and stronger briquettes tend to retain more of the webbing that forms between the briquette roller pockets, both of which, effectively increase the briquette volume. Further, briquettes with lower mechanical durability lose more material during the fines removal step effectively reducing their weight. Nonetheless, to a first approximation, it is reasonable to assume there is a general correlation between briquette density and briquette durability, particularly when the change in briquette weight is of such magnitude as exhibited by the data in Figure 9-4 where the average briquette weight increased by about 50% as the coal component transitions from 100% PCC to 100% MRC. A comparison of the data in Figure 9-4 to that in Figure 9-3 reveals a direct correlation between briquette density and briquette durability.

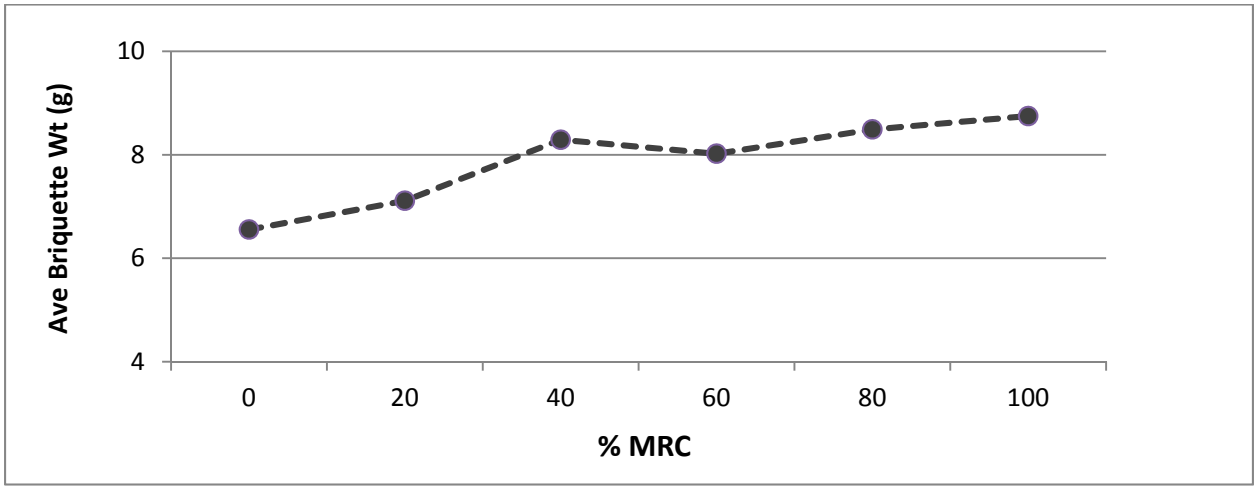



Figure 9-4. Average weight of briquettes made with Alden and MRC coals and coal blends

Analogous crushing strength, durability, and density plots are shown for briquettes made with varying proportions of the PCC and MRC coals in Figure 9-5 and Figure 9-6, respectively. Similar to the MRC/Alden blends, for briquettes made without a binder, there is little difference in strength or mechanical durability for briquettes made with corn stover versus those made with wheat straw as a function of the proportion of MRC versus PCC coal. For a given blend, there was little or no difference for the briquettes made corn stover versus wheat straw for the briquette pairs made with binder or for the briquette pairs made without binder. However, the

trends in briquette strength and mechanical durability as a function of the relative proportion of PCC versus MRC coal in the briquettes were different for briquettes made with a binder compared to otherwise analogous binderless briquettes. For the briquettes made without binder, crushing strength and mechanical durability steadily improved as the proportion of MRC coal increased, similar to the trend observed for the Alden/MRC blends. In contrast, when a starch binder was added, mechanical durability steadily decreased while crushing strengths remained relatively constant or decreased slightly as the proportion of the MRC coal was increased.

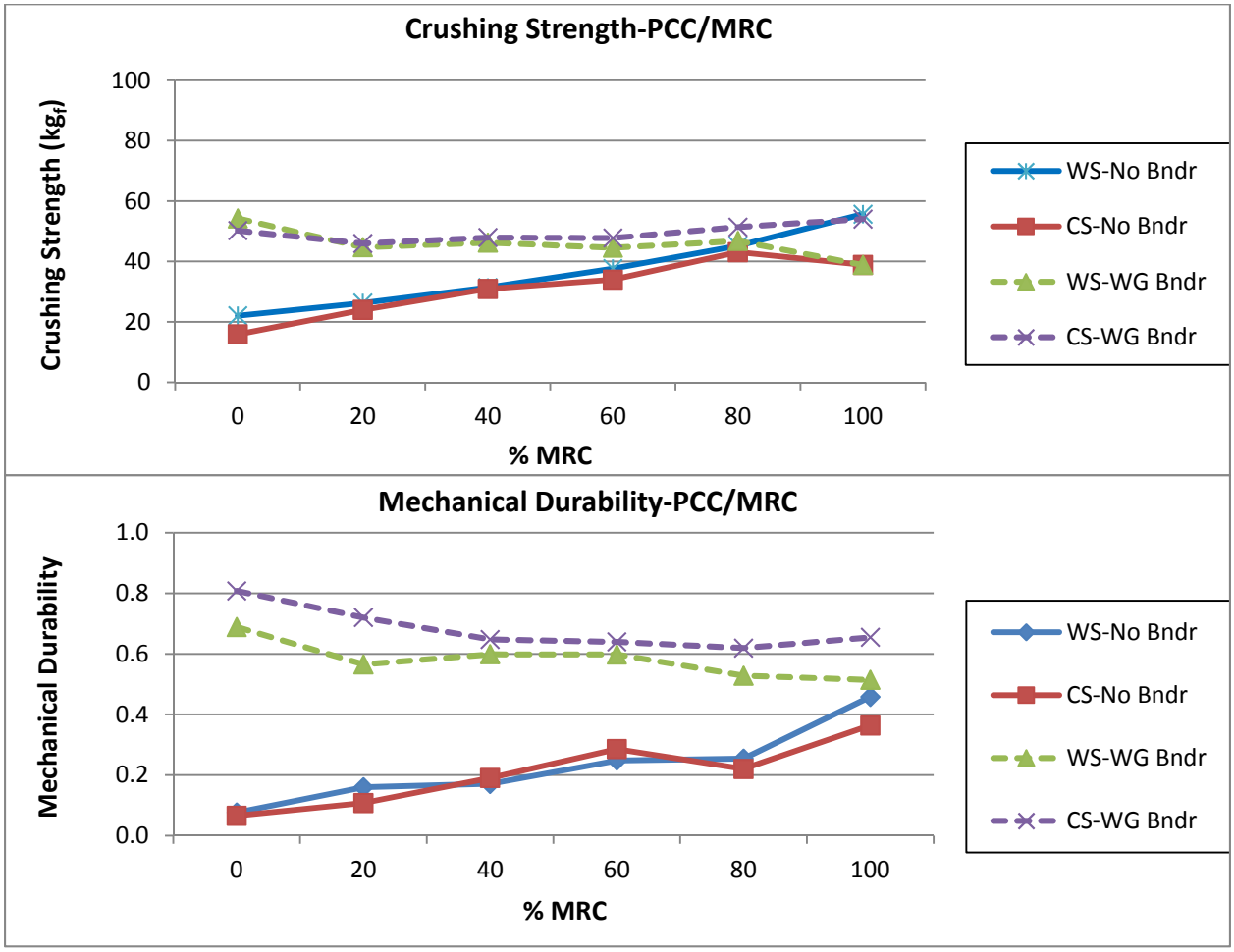



Figure 9-5. Twenty-four hour crushing strength and mechanical durability of briquettes produced from blends of MRC and PCC coal fines and 10% wheat straw (WS) and 10% corn stover (CS) both with and without addition of a gelatinized wheat starch binder (WG)

Average briquette weights for the MRC/PCC briquettes are shown in Figure 9-6. Unlike Figure 9-4 where all four sets of briquettes were used to calculate an overall average briquette weight, in Figure 9-6, the average briquette weight for the two sets of binderless briquettes is

plotted separately from the average briquette weight for the two sets of briquette samples made with wheat starch. Even though the trends in strength and durability differ depending on whether a binder was or was not added, the correlation between the average briquette weights (i.e., apparent density) in Figure 9-6 and the briquette durability plots shown in Figure 9-5 is apparent, just as it was for the briquettes made with the MRC/Alden blends.

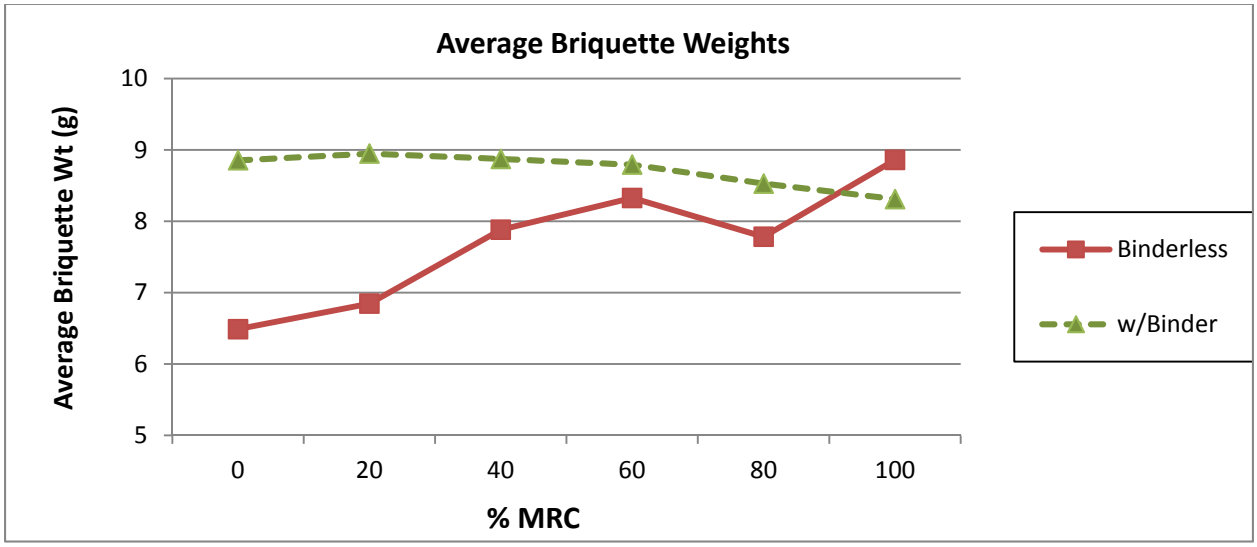



Figure 9-6. Average briquette weights for briquettes made with the PCC/MRC coal blends.

As discussed above, a higher proportion of the ultra-fine MRC coal provided stronger binderless briquettes for both the PCC/MRC and the Alden /MRC blends. This is not surprising as adding a higher proportion of the ultra-fine MRC coal is anticipated to result in a more efficient particle packing resulting in more electrostatic and Van der Waals interactions. However, when a binder is added, blends that contain higher proportions of the larger-sized PCC or Alden coal have a lower surface area per unit weight and would therefore require less binder to uniformly cover the particle surfaces. This may explain why when a binder is added, having a higher proportion of the larger PCC coal particles in the blend results in briquettes with crushing strengths and mechanical durability values that are as good as or better than briquettes made with higher proportions of MRC coal. By extension, an argument can be made that adding the larger Alden coal particles should result in similar or larger improvements. However, this is not in agreement with the results in which higher proportions of Alden coal resulted in lower briquette durability. One explanation for these divergent trends is that the Alden particles are simply too large relative to the MRC particles to allow for efficient particle packing and/or utilization of the

binder. That is, when a blend containing the larger Alden particles is compressed, there are fewer contact points between the larger particles to allow the binder to work effectively. Further, as shown in Figure 9-2, there is a gap at about 5 μm in the particle-size distribution between the larger Alden fines and the ultra-fine MRC coal. It is possible that the larger Alden particles hinder the complete infilling of the voids between the larger Alden particles during compression due to the absence of particles in this range. Perhaps higher compression forces would eliminate the latter but the briquettes made for these comparisons were produced at a relatively low roller force and this oversight was not recognized until well after the project was completed.

These explanations for the dissimilar behavior of briquettes made with binder and the MRC/PCC versus MRC/Alden blends are clearly speculative. However, it is also clear that these differences are real as the trends were consistent for all four sets of briquetted samples that were evaluated with multiple samples over a wide range of blending ratios. Further, these trends are also in agreement with a prior study (Patil et. al., 2009) in which the proctor density (packing density) of decanter coal blended with a froth flotation fines and sawdust were determined and compared to the crushing strength of briquettes made with the same blends. Similar to the current study, that study revealed that without a binder, briquetting sawdust with 100% flotation coal yielded the highest briquette crushing strengths, but when a binder was added the highest strengths were obtained when the decanter fines were blended with an ultra-fine flotation coal.

## 9.5 Summary and Conclusions

The results presented in this study indicate that at relatively low biomass addition rates, the particle-size distribution of the coal component has a greater impact on briquette properties than does the type of biomass added. The results also demonstrate that without the addition of a binder, stronger briquettes are produced with ultra-fine flotation coal compared to briquettes formed with larger particle size screen bowl samples. Even blending of the ultra-fine flotation coal with a larger sized screen bowl coal to broaden the particle size did not improve briquette durability when a binder was not added. Thus, it would appear that a small particle-size distribution is a requirement for binderless briquetting if acceptable briquettes are to be formed at ambient temperature. However, it should be noted that the relative contribution to improved durability by the smaller coal particles versus the higher clay content of the MRC could not be differentiated.

In contrast to the binderless coal-biomass briquettes, significant improvements in briquette durability were obtained with a binder for blends of the MRC flotation fines and PCC screen-bowl fines compared to binderless briquettes made from the same blends. This difference was more pronounced as the proportion of the larger-sized PCC fines was increased. The reason for the difference in durability trends with a binder and without a binder is attributed to good overlap of the particle-size distributions of the MRC and PCC coals. This allowed for efficient particle packing and a reduction in the total surface area, which required less binder to obtain a uniform and effective particle coverage. A similar trend was not observed for the Alden/MRC blends. The reason for this difference in behavior for the MRC/PCC versus the MRC/Alden blends is speculated as being due to a gap in the particle-size distribution between the MRC and Alden samples, which may have resulted in inefficient in-filling of the voids between the larger Alden coal particles during compression. This speculation is supported by the fact that for all of the blends evaluated in the study, the average briquette weight (i.e. apparent density) correlated directly with briquette strength. Thus, the lower density of the briquettes made with higher proportions of Alden fines is indicative of less-efficient particle packing.

The results of the particle size studies provide some guidance as possible avenues to maximize briquette strength while minimizing binder requirements. Future work in this area could benefit from studies focused on differentiating the impact of clay content versus the coal particle-size distribution and on an evaluation of the impact of the roller force used during briquetting of samples with a broad particle-size distribution.

# Chapter 10

# Pilot-Scale Briquetting Test Work

## 10.1 Abstract

A study was conducted to evaluate the physical performance of two batches of pilot-scale briquettes produced with a commercial briquetting machine at the GreenFields Coal Company facility in McDowell County, West Virginia. The two batches represented optimum types of coal-biomass briquettes selected for detailed evaluation and discussed in Chapter 6. The batches for the pilot-scale briquettes were 1) 70% Emerald Coal with 30% fine sawdust and 2) 70% Eagle Butte coal with 30% corn stover. The pilot-scale briquettes are a "pillow-style" briquette, approximately 32 mm square x 19 mm thick at the center and are more typical of the type that would be commercially produced. The test results indicated that the pilot-scale briquette properties are similar to the bench-scale properties, and that the Emerald coal/sawdust batch exhibited slightly better performance than the Eagle Butte/corn stover batch for most of the tests. The Eagle Butte/corn stover batch showed somewhat better performance for crushing strength and water take-up. Therefore, it appears appropriate to evaluate briquetting formulation options on a bench-scale level to provide valid physical performance data to minimize testing at a commercial-scale production level.

## 10.2 Introduction

Co-utilization of biomass with coal in existing coal-fired facilities presents a unique opportunity to reduce greenhouse gas emissions and increase energy production from renewable resources. Significant interest in this opportunity has led to more than 150 coal-fired power stations across the world co-firing coal and biomass on a commercial or trial basis as of 2009 (Fernando, 2009). These co-firing experiences have revealed a number of technical challenges including upstream issues, such as biomass availability, transportation, storage, and handling, as well as problems encountered during energy conversion, such as fouling, corrosion, inconsistent

feeding and segregation (Basu et al., 2011; Sami et al., 2001). Recent studies suggest that many of these challenges can be mitigated by reconstituting coal-biomass mixtures into larger particles. Specifically, roll press briquetting has been investigated to produce homogeneous, free-flowing feedstocks that minimize handling and segregation problems often encountered with combustion and gasification systems (Taulbee et al., 2010; Honaker et al., 2005). However, the absorption of water and subsequent disintegration of coal-biomass briquettes remains a major limitation to the design of low-cost storage and transportation systems for co-firing operations. As a result, there is a growing interest in the development of economically feasible methods to sustain the physical and mechanical integrity of fuel briquettes in the presence of water (Wang et al., 2011; Motaung et al., 2007; Saglam et al., 1990).

## 10.3 Detailed Characterization of Optimum Briquettes

A detailed characterization study was conducted to investigate important properties of two selected optimum types of pilot-scale coal-biomass briquettes. The purpose of this study was to verify the enhanced quality of the co-briquetted feedstocks at the pilot-scale level and to provide additional information that may be useful for industrial consumers or other end users of coal-biomass briquettes. Two batches of briquettes were examined for the detailed characterization study. The first batch of briquettes was composed of 70% Emerald coal and 30% sawdust (EM-SD), while the second batch of briquettes was composed of 70% Eagle Butte coal and 30% corn stover (EB-CS). The pilot-scale briquettes were produced at the GreenFields Coal Company facility in McDowell County, West Virginia. The mixtures were developed to align the eastern coal with biomass sourced from wood products and to align the western coal with agricultural products. Approximately 100 kg was prepared for each batch. The moisture content of the coals and the biomass was adjusted to provide the best conditions for producing the pilot-scale briquettes, based on the performance testing of the bench-scale briquettes. The moisture content for the EM-SD batch was ~1.0% and the moisture content for the EB-CS batch was ~6%.

The pilot-sale briquetting machine at the GreenFields site, shown in Figure 10-1, is a 2 ton/hr Komarek Model. Short test runs were conducted with material from each batch to adjust the machine parameters to obtain a “good” briquette. The machine produced a “pillow-style” briquette, approximately 32 mm square x 19 mm thick at the center, as shown in Figure 10-2.

Approximately one barrel (55-gallon) of pilot-scale briquettes was produced for each batch. The briquettes were produced without using a binding reagent. Both batches of briquettes were subjected to a range of tests similar to the bench-scale testing to characterize their physical properties. The following sections present and discuss the results of these evaluations.



Figure 10-1. Komarek Model B400B Briquetting Machine (courtesy K R Komarek, Inc.).



Figure 10-2. EM-SD (left) and EB-CS (right) pilot-scale briquettes.

### 10.3.1 Characterization of Physical Properties

A detailed review of briquette properties was conducted to determine the most important properties for characterization of coal-biomass briquettes. The briquette properties that were identified as most significant for the pilot-scale briquettes are: (1) tensile strength, (2) crushing strength, (3) mechanical durability, (4) attritability, (5) friability, (6) water content, (7) particle density, (8) bulk density and (9) water resistance. Crushing strength and mechanical durability appear to be the most important of all these properties, and thus should be measured for all experimental and industrial coal-biomass briquette formulations. The other identified properties

are still very important and should be considered in detailed evaluations of coal-biomass briquettes when requested by a client or customer.

Experimental evaluations were conducted to evaluate and compare the pilot-scale coal-biomass briquettes with the results for the bench-scale tests in an effort to gain confidence in evaluations and analysis that directly test bench-scale coal-biomass briquettes. The following section outlines the methods and procedures used to characterize the pilot-scale coal-biomass briquettes. The briquettes for the individual tests were randomly selected from the batch production run.

1. Tensile strength – To measure tensile strength, individual coal-biomass briquettes were compressed with the briquette standing on edge (i.e. with the plane through the corners of the briquette parallel to the axis of force application) between flat compression plates. This was carried out using a digital force gauge and a manual test stand. A break detect feature was utilized that stops data acquisition after the applied force drops to 95 percent of the maximum force attained during each test. Tensile strength is then designated as this maximum force. This procedure was repeated for 25 briquettes. The average of all conducted tensile strength measurements was reported as the briquette tensile strength.

2. Crushing strength – To measure crushing strength, individual coal-biomass briquettes were compressed along the smooth pocket surface (i.e. surface of force application during formation) using a digital force gauge and a manual test stand equipped with flat compression plates. A break detect feature was utilized that stops data acquisition after the applied force drops to 95 percent of the maximum force attained during each test. Crushing strength was then designated as this maximum force. This procedure was repeated for a minimum of 25 briquettes. The average of all conducted crushing strength measurements was reported as the briquette crushing strength.

3. Mechanical durability – To measure mechanical durability, 5 coal-biomass briquettes were tumbled for five minutes at 40 rotations per minute in a 12-inch diameter PVC cylinder equipped with three 2-inch lifters. The briquettes were then removed from the cylinder and screened for 30 seconds over a 4.75-millimeter sieve in a Ro-Tap sieve shaker. Mechanical

durability was reported as the percentage of the initial mass of briquettes retained on the 4.75-millimeter sieve.

4. Attritability – To measure attritability, 5 coal-biomass briquettes were screened for five minutes over a 4.75-millimeter sieve in a Ro-Tap sieve shaker. Attritability was reported as the percentage of the initial mass of briquettes retained on the 4.75-millimeter sieve.

5. Friability – To measure friability, 12 coal-biomass briquettes were dropped two times from a height of six feet onto a steel plate using a modified shatter test machine. The briquettes were then screened for 30 seconds over a 4.75-millimeter sieve in a Ro-Tap sieve shaker. Friability was reported as the percentage of the initial mass of briquettes retained on the 4.75-millimeter sieve.

6. Water content – To measure water content, 12 coal-biomass briquettes were dried for 24 hours at 105 ± 4 degrees Celsius in a drying oven. Water content was reported as the fraction of water in the sample on a dry basis.

7. Particle density – To measure particle density, the apparent weight of individual coal-biomass briquettes was measured while submerged in a solution of water and detergent using an apparatus similar to that described in EN 15150 (2011). The detergent used was Triton® X-100 at a concentration of 1.5 grams per liter of water. Particle density was calculated by the product of the liquid density and the ratio of the mass of the briquette in air to the difference between the mass of the briquette in air and the mass of the briquette in water/detergent solution. This measurement was conducted for 15 briquettes. The average particle density of all conducted measurements was reported as the briquette particle density.

8. Bulk density – To measure bulk density, coal-biomass briquettes were poured into a 28.32-liters (1-$ft^3$) box from a height of 0.61 meter (2 feet) above the bottom of the interior of the container so that the briquettes overflowed the top of the container. A straight edge was used to remove the overflow material from the top of the container. Bulk density was calculated by dividing the net weight of the briquettes in the filled container by the volume of the container.

9. Water resistance – To measure water resistance, five coal-biomass briquettes are subjected to a 15 second water spray at a flow rate of three gallons per minute from a height of 0.46 m (18 inches) above the briquettes. Water resistance was reported as the water uptake of the briquettes that results from this spray test, which was reported as the water absorbed as a percentage of the initial mass of the briquettes.

## 10.3.2 Pilot-Scale Briquette Evaluations

A summary of the results of the comprehensive physical evaluations of the two types of briquettes are included in Table 5-31. From these results, it is fairly clear that the EM-SD briquettes are similar in quality to the EB-CS briquettes. For example, the tensile and crushing strength of the EM-SD briquettes was 876 newtons (197 $lb_f$) and 1,204 newtons (271 $lb_f$), as compared to 212 newtons (48 $lb_f$) and 1,433 newtons (322 $lb_f$) for the EB-CS briquettes, respectively. The EM-SD exhibits a significant higher tensile strength, but slightly lower crushing strength. Nonetheless, the crushing strength of the briquettes indicates that these briquettes are very strong, and thus high quality in this regard.

Table 10-1. Summary of physical characterization results comparing bench-scale and pilot-scale Emerald-sawdust (EM-SD) and Eagle Butte-corn stover (EB-CS) briquettes.

| | | EM-SD | | EB-CS | |
|---|---|---|---|---|---|
| **Briquette Property** | **Units** | **Bench-Scale Briquettes** | **Pilot-Scale Briquettes** | **Bench-Scale Briquettes** | **Pilot-Scale Briquettes** |
| Tensile strength | N | 255.8 | 875.9 | 206.0 | 211.5 |
| Crushing strength | N | 1589.8 | 1203.7 | 1224.6 | 1432.9 |
| Mechanical durability | % | 92.8 | 90.6 | 91.1 | 60.9 |
| Attritability | % | 97.4 | 97.2 | 96.9 | 86.9 |
| Friability | % | 97.1 | 97.3 | 98.4 | 89.9 |
| Water content | -- | 0.018 | 0.036 | 0.163 | 0.157 |
| Particle density | $g/cm^3$ | 1.13 | 1.23 | 0.94 | 1.12 |
| Bulk density | $g/cm^3$ | - | 0.64 | - | 0.55 |
| Water uptake | % | 8.3 | 12.2 | 14.3 | 2.3 |

The mechanical durability of the EM-SD and EB-CS briquettes was 90.6% and 60.9%, respectively. These values indicate the EM-SD briquettes are comparable to the bench-scale briquettes and that the briquettes would largely remain intact in the presence of attrition and impact forces encountered during handling and transportation. However, the EB-CS briquettes

had a significantly lower resistance in the presence of attrition and impact forces encountered during handling and transportation. This is most likely a direct result of the "push-back" effect from the larger particle size for the corn stover in the batch.

The attritability and friability for the EM-SD pilot-scale briquettes were 97.2% and 97.3%, respectively, which compares very closely to the bench scale results. The attritability and friability for the EB-CS pilot-scale briquettes were 86.9% and 89.9%, respectively, which was slightly lower than the bench-scale results. These results indicate that the briquettes would withstand attrition forces in handling and impact forces from drops encountered on conveyors or at other points prior to utilization. Another observation was the slight difference in the particle density of the two types of briquettes. Specifically, the EM-SD briquettes were determined to have a particle density of 1.23 g/cm$^3$, as compared to only 1.12 g/cm$^3$ for the EB-CS briquettes. As with the bench-scale briquettes, this result was likely due to a combination of factors, including the higher true density of sawdust and the higher porosity of the EB-CS briquettes. The difference in porosity can be attribute to the higher water content of the EB-CS briquettes (i.e. w = 0.157) compared to the EM-SD briquettes (i.e. w = 0.036).

## 10.4 Summary and Conclusions

Experimental optimization of coal-biomass briquette production is an essential task to improve the strength and durability of briquettes. Meeting this challenge requires an exhaustive bench-scale study conducted to examine the most significant feedstock blends, reagent(s) and roll press variables in coal-biomass briquette production to identify the conditions that contribute to the production of coal-biomass briquettes with the greatest crushing strength and mechanical durability. In addition, the development of bench-scale evaluations that provide valid indications for the performance of full-scale briquettes would greatly minimize the time and costs to optimize the feedstock blends and processing variables for full-scale production operations.

A pilot-scale production run was conducted for two batches of coal-biomass feedstocks, based on the optimal blends identified in the bench-scale evaluations. One batch consisted of 70% Emerald coal and 30% sawdust identified as EM-SD. The second batch consisted of 70% Eagle Butte coal and 30% corn stover identified as EB-CS. The commercial-size "pillow-style" briquettes (approximately 32 mm square by 19 mm thick) were produced at the GreenFields Coal Company facility in McDowell, West Virginia using a 2 ton/hr Komarek Model B400B

briquetting machine. Each batch, without any binding reagent, produced approximately 100 kg of briquettes.

The objective for producing the pilot-scale briquettes was to compare the physical performance characteristics of the briquettes with the results from the bench-scale testing. The briquette properties that were identified as most significant for the pilot-scale briquettes are: (1) tensile strength, (2) crushing strength, (3) mechanical durability, (4) attritability, (5) friability, (6) water content, (7) particle density, (8) bulk density and (9) water resistance. Crushing strength and mechanical durability appear to be the most important of all these properties, and thus should be measured for all experimental and industrial coal-biomass briquette formulations. The other identified properties are still very important and should be considered in detailed evaluations of coal-biomass briquettes as necessary.

The results of the various physical tests for the pilot-scale briquettes, as shown in Table 10-1, indicates that the performance was very similar to the performance for the bench-scale tests. The crushing strength and tensile strength compared well, with significantly higher crushing strength exhibited for the EM-SD briquettes. The mechanical durability, attritability and friability for the EM-SD briquettes nearly matched the performance for the bench-scale tests. The mechanical durability, attritability and friability for the EB-CS briquettes was slightly lower than the bench-scale tests. The particle density for both blends was slightly higher than the bench-scale tests. The water resistance tests showed a significant difference for both blends. The EM-SD briquettes had a high water take-up, but the EB-CS briquettes had a lower water take-up compared to the bench-scale tests.

As a result of this study, the following conclusions can be drawn regarding the production and evaluation of the pilot-scale coal-biomass briquettes over the range of performance variables tested:

- Selected bench-scale physical performance testing procedures can be used to predict the performance for full-scale commercial briquettes.
- Performance testing at the bench-scale level allows for a wider range of feedstock blends, operating variables and reagent conditions to be evaluated using a minimum amount of material for the samples and laboratory resources.

- Bench-scale screening tests can provide a reduced set of test conditions that minimizes the required testing on a pilot- or production-scale basis, thus reducing the time and costs for evaluations.

# SECTION III

# GASIFICATION AND COMBUSTION ACTIVITIES

# Chapter 11

# Thermogravimetric Analysis of Coal–Biomass Blends

## 11.1 Abstract

The thermal evolution profiles and kinetic parameters for the pyrolysis of two coals (PCC Bituminous coal and BT Sub-Bituminous coal), one biomass sample (corn stover) and their blends (10%, 20% and 30% by weight of corn stover) have been investigated at a heating rate of 5 °C/min in an inert nitrogen atmosphere, using thermogravimetric analysis. The weight loss profiles observed illustrate that the thermal evolution profiles of the single fuels are different from that of the blends. The thermal evolution profiles of PCC Bituminous coal (PCC) and BT Sub-Bituminous coal (BT) display only one major peak over a wide temperature distribution, 152-814 °C for PCC and 175-818 °C for BT, whereas the thermal decomposition profile for corn stover (CS) falls in a much narrower band than that of the coals (226-608 °C). The non-linearity in the evolution of volatile matter with increasing percentage of corn stover in the blends verifies the possibility of synergistic behavior in the blends with bituminous coal where deviations from the predicted yield ranging between 2-7% were observed, whereas very little deviations (1-3%) from predicted yield were observed in blend with sub-bituminous coal, indicating no significant interactions with corn stover. In addition, a single first order reaction model using the Coats-Redfern approximation was utilized to predict the kinetic parameters of the pyrolysis reaction. The kinetic analysis indicated that each thermal evolution profile may be represented as a single first order reaction. Three temperature regimes were identified for each of the coals, while corn stover and the blends were analyzed using two and four temperature regimes respectively. The kinetic parameters were also obtained through two other distributed activated energy models and the results were compared effectively. Ultimately, it this study shows that using the distributed activation energy models, in particular matrix inversion algorithms, is extremely effective and

robust in predicting devolatilization kinetics as compared to simply using single first order models.

## 11.2 Introduction

The past few years have seen an upsurge in the interest of gasification of biomass. The primary motivations for biomass gasification include (1) reduction in greenhouse gas emissions caused by the combustion of fossil fuels; (2) a need for energy independence due to the depleting resources and fluctuating prices of oil and natural gas; and (3) developing interest in renewable energy resources (Basu, 2010).

Although there is an abundance of coal in the United States and several other countries and it will continue to be a major source of energy for many years to come, there is still great interest in replacing part of the coal used in energy generation with renewable biomass (Brown, 2003). Many countries have initiated incentives in recent years to encourage the co-utilization of biomass and coal for energy production (Fernando, 2009). The term biomass is used to encompass any plant-derived organic matter available on a renewable basis (Brown, 2003). Biomass fuels (BF) are to be sustainable natural resources if they renew themselves at such a rate that they will be available for future use. That is, if the rate of consumption of BF is less than or equal to the rate at which it is generated. These BF resources can be either grown and harvested biomass such as switchgrass or waste biomass such as corn stover, wood wastes from forestry and lumbering operations, wastes from paper production, and landscaping wastes (Brown, 2003). As is well known, the emission of $CO_2$ during the burning of BF is neutralized by the removal of $CO_2$ from the atmosphere by the process of photosynthesis during biomass growth.

The idea of gasifying mixtures of coal and biomass is relatively new with almost zero commercial experience since the properties of coal and biomass differ significantly from each other (Gordillo et at., 2009; Di Blasi et al., 1999; Klass, 1998). Many gasifiers can gasify biomass, but most of them are small scale, operate at lower temperatures and pressures, and use air instead of oxygen. Under these less severe conditions, pyrolysis dominates and produces light hydrocarbons, bio-oils, tars, and char, in addition to carbon monoxide. Prins et al. (2007) reported that fuels with higher oxygen to carbon ratios have larger energy losses due to their high ratio of available chemical energy to heating value. Also, such fuels are over-oxidized (combusted) in the gasifier in order to reach the required gasification temperature. Therefore,

highly oxygenated fuels are not ideal for gasifiers keeping in view the energy losses that can be incurred and hence, solid biomass can be more readily gasified if it is co-gasified with coal (Fernando, 2009).

Pyrolysis or devolatilization (used interchangeably) is the first zone of the gasification process. The chemical components in the raw coal decompose by heating to a relatively low temperature (350-800°C) in the absence of oxygen. Coal can be considered as a complex polymer network consisting of aromatic clusters and aliphatic bridges. During the process of pyrolysis, the complex structure of coal is broken down in to several small fragments whose vapor pressure is high enough to form volatile matter. The duration of evolution of volatiles is relatively shorter for biomass than coal (Sadhukhan et al., 2008). The products include: pyrolysis gases (CO, $H_2$, $CH_4$, and $H_2O$), tar, oil, naphtha, and residual solid char (Liu et al., 2010; Basu, 2010; Higman and van der Burgt, 2008). A complete description of the characteristics of pyrolysis is complicated, but for a given sample, the pyrolysis behavior depends on the heating rate, final decomposition temperature, vapor residence time, the environment under which the pyrolysis takes place, pressure, coal particle size, and coal rank (Dutta et al., 1977). The structure and the composition of the char obtained are also greatly affected by the pyrolysis conditions. This can be considered as the starting point for all heterogeneous gasification reactions.

Kinetic modeling of the devolatilization behavior of coal and biomass is, therefore, an important step in assessing the contribution of single materials and their interactions during the devolatilization stage. The understanding of kinetics of co-pyrolysis of blends of biomass and coals, particularly the mixtures of western coals and corn stover used in this study, is far from clear and, hence, it is important in design and operation of co-gasification processes.

Thermogravimetric analysis (TGA) can be used to investigate thermal events and kinetics of pyrolysis and oxidation of the solid raw materials. TGA analysis provides a measurement of weight loss of the sample as a function of time and temperature. The kinetics of the thermal events can then be determined by the application of the Arrhenius equation corresponding to the separate slopes of constant mass degradation in each thermal event with different reaction order, activation energy, and frequency factor. TGA experiments can be carried out either isothermally, where the sample is heated at a constant temperature, or non-isothermally, where the temperature of the sample is increased at a constant rate. Isothermal experiments are typically slower since the sample might take a long time to reach even 50% conversion at temperatures of 500º C or

less and multiple experiments are required for determining the kinetic parameters. On the contrary, the kinetic parameters can be determined using only a single experimental run in the non-isothermal mode which can achieve complete conversion in a much shorter period of time (Sima-Ella et al., 2005). As described previously, the devolatilization of coal-biomass blends is a complex process and the exact description of the kinetics is not yet available.

## 11.3 Experimental

The thermal behavior of pure coal, biomass which includes corn stover (CS) and switchgrass (SG) and their blends using thermogravimetric analysis would be discussed extensively in this chapter. For the purpose of this work, biomass (CS and SG) was blended individually up to 30% by weight with two different ranks of coals, namely, PCC Bituminous coal (PCC) and BT Sub-Bituminous coal (BT). The samples were crushed and sieved to 150 μm before blending to limit the effects of intra-particle heat transfer. The coal-biomass blends were prepared in appropriate proportions and homogenized by constant stirring in the sample holders to ensure sufficient dispersion. Subsequently, their non-isothermal weight loss profiles were evaluated and co-pyrolysis kinetic parameters were determined using the integral method. These coals were chosen based on economic considerations, their low sulfur content, and high percentage of carbon present since the ultimate goal is to gasify these blends in a moving bed reactor for the production of syngas that can be used as feedstock for downstream processes such as Fischer-Tropsch Synthesis used for producing liquid fuels. Also, keeping in view of the overall gasification process, blends of higher percentages of biomass (in excess of 30% by weight) was not possible for the conditions at which the gasifier was operated since biomass is a low density, low heating value fuel and addition of more biomass would make the gasification process less efficient. Hence, a maximum of 30% by weight of biomass was chosen for this study. The proximate and elemental analyses of the individual fuels are presented in Table 11-1.

Table 11-1. Proximate and elemental analysis of feedstocks

| Feedstock | Proximate Analysis (As Received Basis) | | | | Elemental Analysis (As Received Basis) | | | | |
|---|---|---|---|---|---|---|---|---|---|
| | % Moisture | % Fixed Carbon | % Volatile Matter | % Ash | % C | % H | % N | % S | % O |
| PCC Bituminous Coal | 1.48 | 55.74 | 34.58 | 8.24 | 75.78 | 5.68 | 1.62 | 0.93 | 7.75 |
| BT Sub-Bituminous Coal | 6.44 | 44.01 | 41.18 | 8.37 | 62.95 | 5.47 | 0.95 | 0.53 | 21.73 |
| Corn Stover | 5.66 | 10.32 | 76.15 | 7.87 | 42.33 | 6.71 | 0.73 | 0.30 | 42.06 |
| Switchgrass | 4.87 | 9.35 | 83.62 | 2.16 | 45.76 | 8.09 | 0.32 | 0.08 | 42.87 |

As a part of this, pyrolysis of the different feedstocks was carried out in non-isothermal mode using a TA-SDT-Q600 thermogravimetric analyzer. The weight of the samples used for these experiments was about 30 mg for the coal samples and about 10 mg for the biomass samples on an as received basis (which is approximately 25 mg for coal samples and 8 mg for biomass on a dry basis). Pure nitrogen was used as the purge gas. Flow of pure nitrogen through the system negates sample oxidation and also removes the volatile pyrolysis products, thus ensuring an inert atmosphere during the run.

In the non-isothermal mode, once the sample is inserted into the furnace, the temperature of the furnace was increased from room temperature to 127 °C and held at that temperature for 15 minutes to ensure drying. Subsequently, the furnace temperature was raised to 900 °C at constant heating rates ranging between 5 °C/min and 40 °C/min. An inert nitrogen atmosphere was employed throughout the process and the nitrogen flow rate was maintained constant at 100 ml/min. Upon reaching a temperature of 900 °C, air was introduced into the furnace to burn off the remaining char and obtain the percentage of ash in the respective samples. Also, the heat transfer limitations may be ignored due to the fact that the furnace heats up slowly combined with a low weight of the sample being pyrolyzed. The process was repeated four times to ensure reproducibility of the weight loss profiles for each sample (error < 5% for all samples).

## 11.4 Results and Discussion

### 11.4.1 Thermal Evolution Profiles – Blends with Corn Stover

The weight loss curves (dry ash free basis) during the non-isothermal pyrolysis at a heating rate of 5 °C/min for all the feedstocks containing corn stover are shown in Figure 11-1 and Figure 11-2. The weight loss increases with increasing reaction temperature for all samples. Also, the weight loss profiles of the coal-biomass blends fall between those of the isolated single fuels. Figure 11-3 and Figure 11-4 depict the differential thermogravimetric (DTG) curves of the samples used in this work, as a function of pyrolysis temperature, at a heating rate of 5 °C/min. It can be seen that the samples display one peak at temperatures less than 150 °C representing the removal of moisture from the samples (Idris et al., 2010). Above this temperature, varied peaks are observed for the coals, corn stover and their blends. Table 11-2 summarizes some of the pyrolysis parameters, such as, pyrolysis temperature range ($T_i$ is the temperature of initial weight loss and $T_f$ is the temperature at the end of the reaction), maximum weight loss rates and corresponding maximum DTG peak temperatures.

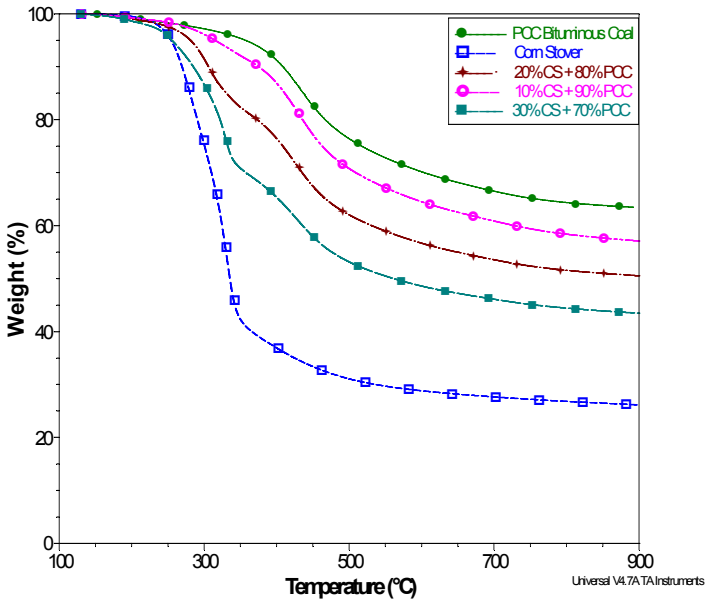



Figure 11-1. Weight loss curves on a moisture free basis during the pyrolysis of PCC Bituminous coal, corn stover and their blends at 5 °C/min

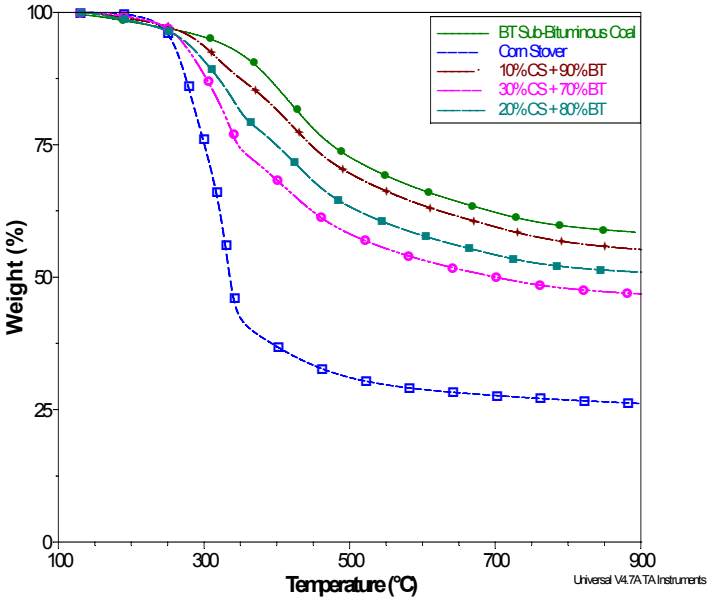



Figure 11-2. Weight loss curves on a moisture free basis during the pyrolysis of BT Sub-Bituminous coal, corn stover and their blends at 5 °C/min

Table 11-2. Pyrolysis temperature range, maximum weight loss rates and peak temperatures of all feedstocks determined by TGA

| Feedstock Materials | Pyrolysis T Range, °C | | Maximum Weight Loss Rate, $(\%/min)_{max}$ | | Peak Temperature, $T_{max}$, °C | |
|---|---|---|---|---|---|---|
| | $T_i$ | $T_f$ | Peak 1 (CS) | Peak 2 (Coal) | $T_{max,1}$ | $T_{max,2}$ |
| PCC Bituminous Coal (PCC) | 152 | 814 | - | 0.889 | - | 433 |
| BT Sub-Bituminous Coal (BT) | 175 | 818 | - | 0.668 | - | 419 |
| Corn Stover (CS) | 226 | 608 | 4.492 | - | 331 | - |
| 10% CS + 90% PCC | 207 | 787 | 0.251 | 0.819 | 330 | 430 |
| 20% CS + 80% PCC | 204 | 765 | 1.492 | 0.500 | 326 | 419 |
| 30% CS + 70% PCC | 190 | 755 | 2.332 | 0.561 | 330 | 427 |
| 10% CS + 90% BT | 176 | 815 | 0.550 | 0.603 | 318 | 423 |
| 20% CS + 80% BT | 201 | 785 | 0.941 | 0.599 | 327 | 411 |
| 30% CS + 70% BT | 199 | 755 | 1.550 | 0.552 | 336 | 413 |

The thermal evolution profiles of PCC Bituminous coal (PCC) and BT Sub-Bituminous coal (BT) display only one major peak over a wide temperature distribution, 152-814 °C for PCC and 175-818 °C for BT. This peak represents the release of carbon containing volatile matter

from both coals (Idris et al., 2010). The maximum peak temperature for this major peak is approximately 433 °C and 419 °C, respectively, for PCC and BT. It is worth noting that the maximum weight loss rate of BT is much lower than that of PCC. This can attributed to the fact that the volatile matter or the immobile phase present in BT coal are bonded together with much higher molecular bond energy than that of PCC coal and hence will be removed with a slower rate at similar temperatures.

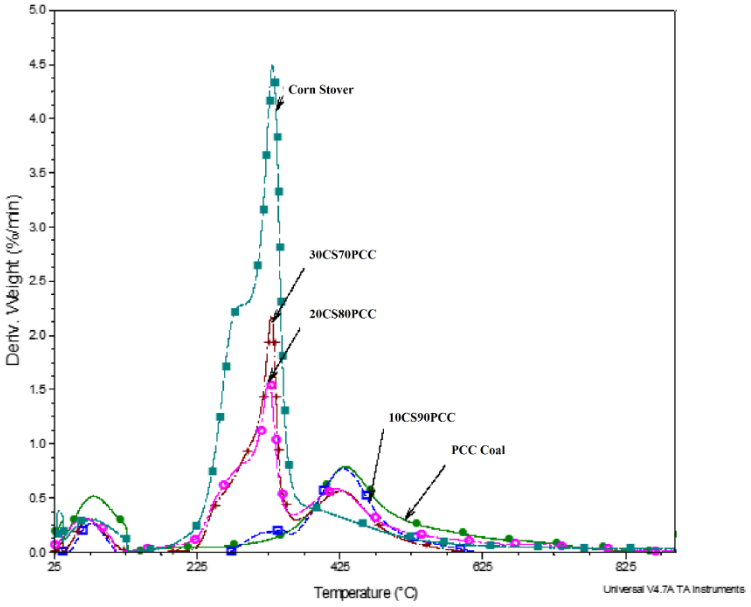



Figure 11-3. Differential thermogravimetric curves of pyrolysis of PCC-CS blends at 5 °C/min

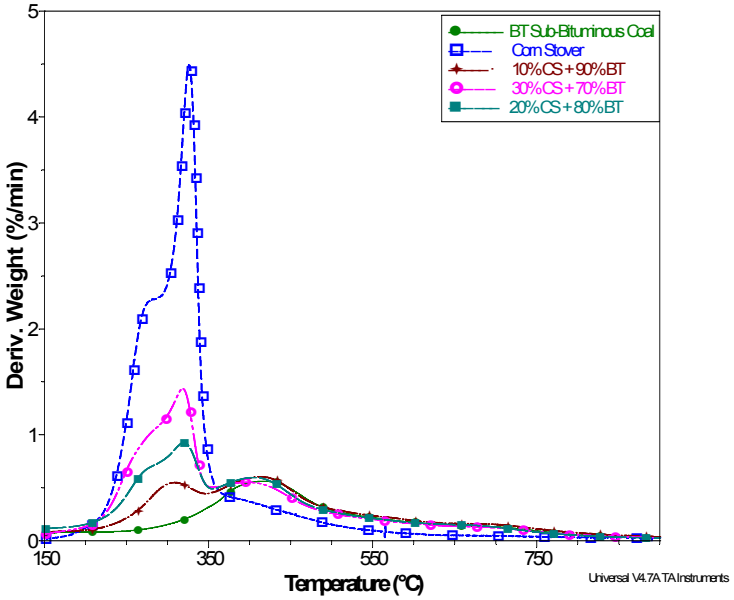



Figure 11-4. Differential thermogravimetric curves of pyrolysis of BT-CS blends at 5 °C/min

Also, the maximum weight loss rates for the coals occur in a temperature range of 400-500 °C corresponding to the data reported by Sun et al (2011). In the case of corn stover (CS), the thermal evolution profile can be divided into three more stages apart from moisture removal corresponding to the removal of hemicellulose, cellulose and lignin components of corn stover. The decomposition of the hemicellulose and cellulose components of corn stover can also be termed as the active pyrolysis zone while the slow decomposition of the lignin component represents the passive pyrolysis zone. This is generally the case for all ligno-cellulosic materials (Jeguirim & Trouve, 2009). As it can be seen, the thermal decomposition profile for CS falls in a much narrower band than that of the coals (226-608 °C). This is mainly due to the high volatile content and lower fixed carbon content of CS as compared with that of the coals.

This difference is also attributed to the strength of the molecular structure of the fuels. The immobile phase present in coal structure comprises dense polycyclic aromatic hydrocarbons linked together by aromatic rings with very high bond energy of about 1000 kJ/mol (Cai et al., 2008). In contrast, the polymers of hemicellulose, cellulose and lignin which constitute the macromolecular structure of biomass and other woody materials are linked together by relatively weak bonds with a bond energy of about 380-420 kJ/mol (Vuthaluru, 2004). These bonds are less resistant to heat at low temperatures. As a consequence, a much higher mass loss rate results in biomass samples as compared with coal as can be seen from Table 11-2. The maximum weight loss rate of CS is almost an order of magnitude higher than both coals. As observed, the DTG profile of CS results in a split peak in the temperature range of 226-375 °C. The lower temperature shoulder represents the decomposition of the hemicellulose component with a peak temperature of 286 °C and a weight loss rate of 2.28%/min while the higher temperature peak represents the decomposition of the cellulose component with a maximum weight loss rate of 4.50%/min at a temperature of 331 °C. This decomposition continues up to a temperature of approximately 375 °C. Above this temperature, the slow decomposition of the lignin component begins continuing up to a temperature of about 608 °C beyond which very little change in the weight occurs.

As for the blends of both coals with corn stover, the DTG curves are represented in Figure 11-3 and Figure 11-4. The DTG evolution profiles for different blends of CS with PCC and BT showed two distinct peaks in the temperature range of approximately 176-815 °C. For blends of CS and PCC, the first peak occurs at a maximum peak temperature of approximately

326-330 °C representing the devolatilization of CS (evolution of hemicellulose and cellulose components) while the second peak occurs at a maximum peak temperature of 419-430 °C representing the devolatilization of PCC. Similar trends are observed for blends of CS and BT with maximum peak temperatures ranging from 318-336 °C for the devolatilization of CS and 411-423 °C for the devolatilization of BT. Also, it can be observed that the maximum weight loss rate (%/min) for the CS devolatilization profile increased with increasing concentration of CS in the blends and vice versa for the coal devolatilization profile, without an apparent change in the shape and position of the peaks when compared to that of the single fuels. This may be attributed to the fact that the release of volatiles containing oxygenated components during the devolatilization of CS, generally, does not affect the devolatilization of coal at higher temperatures (Aboyade et al., 2013; Idris et al., 2010; Biagini et al., 2002). But, it must be noted here that the change in the maximum devolatilization rate is not linear with the increase in corn stover percentage indicating the possibility of interactions between the blended fuels.

### 11.4.2 Thermal Evolution Profiles – Blends with Switchgrass

The thermal evolution profiles of switchgrass and blends of both coals with switchgrass during devolatilization at a heating rate of 20 °C/min are shown in Figure 11-5 and Figure 11-6, respectively. These weight loss curves follow a similar pattern as that of blends with corn stover described in the previous section. The devolatilization interval for switchgrass starts around 175 °C with the decomposition of hemicellulose and ends around 650 °C with the slow decomposition of lignin. The low temperature shoulder, attributed towards the peak hemicellulose decomposition, occurs at 305 °C. The region between 305 °C and 405 °C is attributed towards the decomposition of the cellulose component of switchgrass, with peak decomposition occurring around 360 °C.

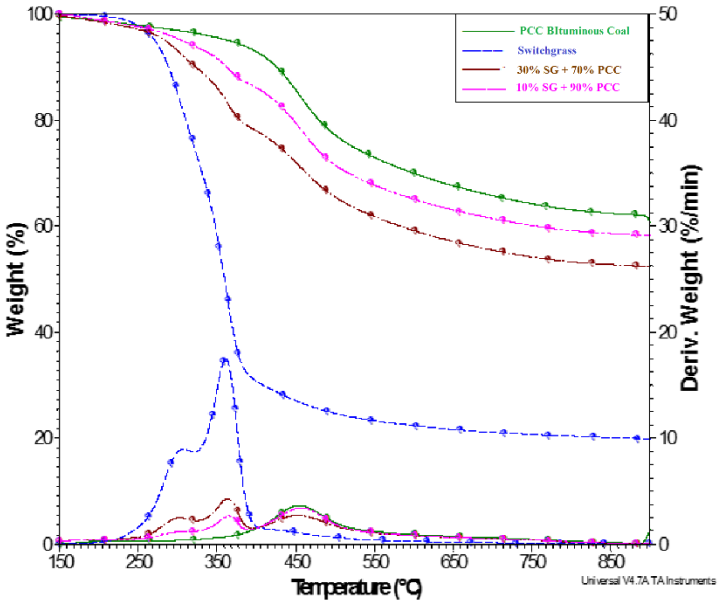



Figure 11-5. Weight loss curves and DTG profiles during the pyrolysis of PCC Bituminous coal, switchgrass and their blends at 20 °C/min

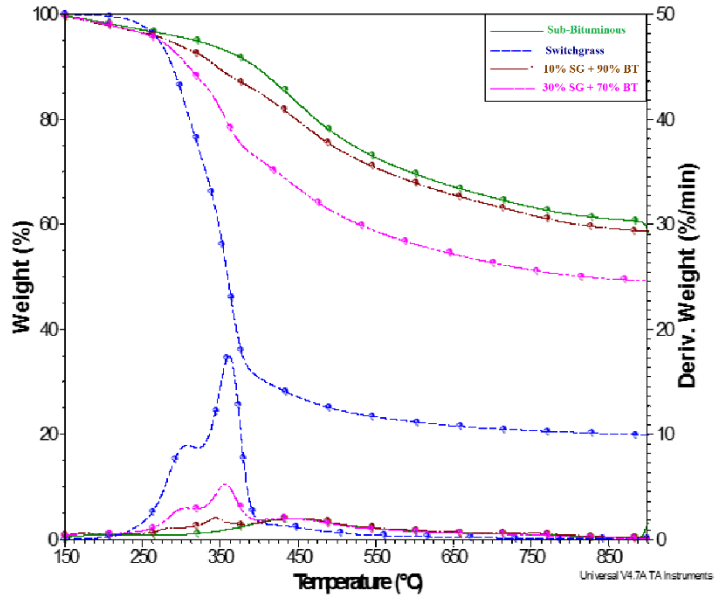



Figure 11-6. Weight loss curves and DTG profiles during the pyrolysis of BT Sub-Bituminous coal, switchgrass and their blends at 20 °C/min

When compared with blends of corn stover, a clear distinction in the DTG profiles can be observed. For these blends of coals and switchgrass, three different peaks are clearly observed, where the low temperature peaks can be attributed to the decomposition of switchgrass while the high temperature peak is for the decomposition of coals. This is different from those observed in blends with corn stover, where the two low temperature peaks merge which is an indication that

some components in coal are interacting with corn stover in the low temperature range of around 220-380 °C. Since there is a clear distinction in the hemicellulose and cellulose peaks when switchgrass is blended with coal, suggests the fact that no significant interactions are occurring and that the two components are decomposing separately.

### 11.4.3 Single Fuels – Effect of Heating Rates

The effect of various heating rates ranging from 5-40 °C/min on the devolatilization of single fuels (Figure 11-7 through Figure 11-10) is described in this section. The values of $T_{max}$ and maximum peak heights at various heating rates for all the single feedstocks are shown in Table 11-3. Evidently, the maximum peak height and the temperatures at which maximum devolatilization occurs increases with increasing heating rates. In other words, an increase in reactivity of devolatilization is observed with increasing heating rates. Different temperatures affect the point coordinates and thus the slope and intercept of the linear fit. This in turn affects the activation energy, E, and the pre-exponential factor, $k_0$. It may be inferred from the weight loss profiles and DTG curves of various feedstocks that a possible reason for this shift in temperatures could be because of the fact that less heat is required for the cracking of solid fuel particles into products. At higher heating rates, this process occurs later at slightly higher temperatures due to the fact that heat transfer is not as effective as it were at lower heating rates, where the solid fuel particles are more gradually heated resulting in an effective transfer of heat to the inner portions and within the particles themselves. Therefore, heating rates and temperatures play a crucial role during devolatilization processes.

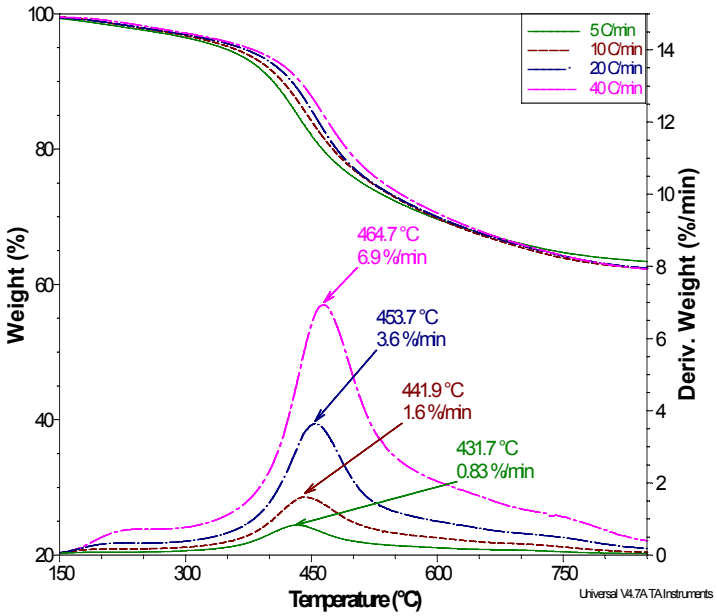



Figure 11-7. Weight loss profiles and DTG curves of pyrolysis of PCC Bituminous coal at four different heating rates ranging from 5 °C/min to 40 °C/min

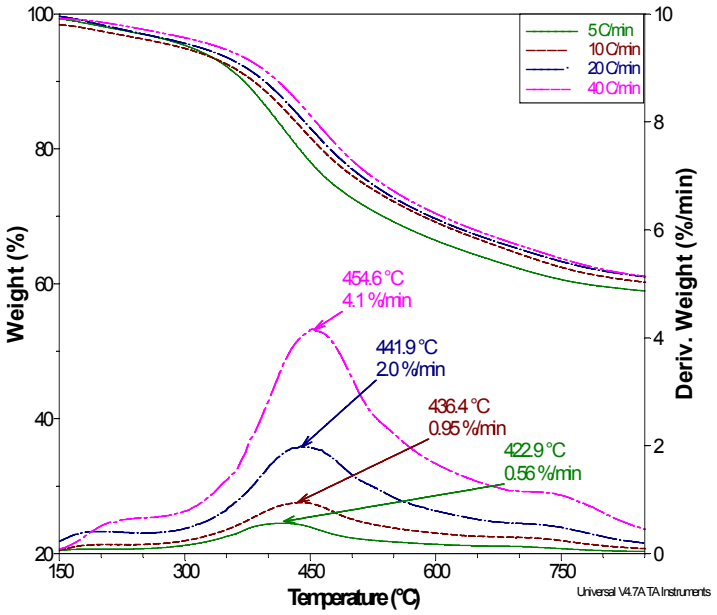



Figure 11-8. Weight loss profiles and DTG curves of pyrolysis of BT Sub-Bituminous coal at four different heating rates ranging from 5 °C/min to 40 °C/min

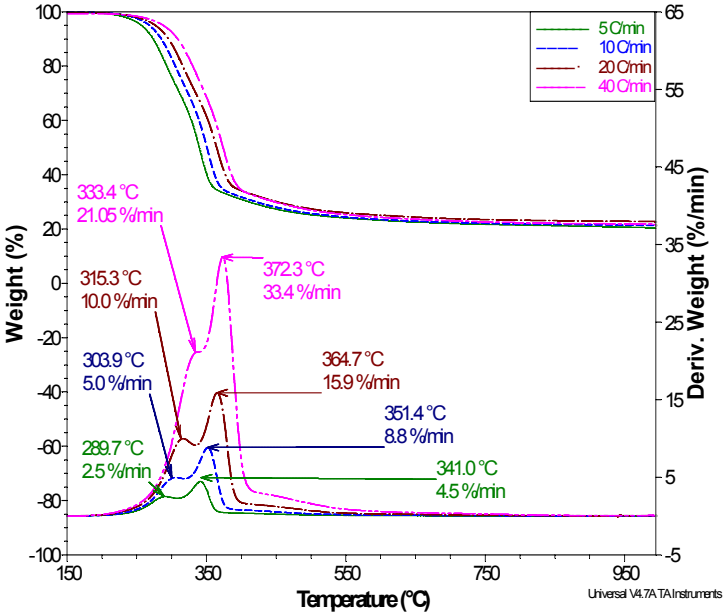



Figure 11-9. Weight loss profiles and DTG curves of pyrolysis of Corn Stover at four different heating rates ranging from 5 °C/min to 40 °C/min

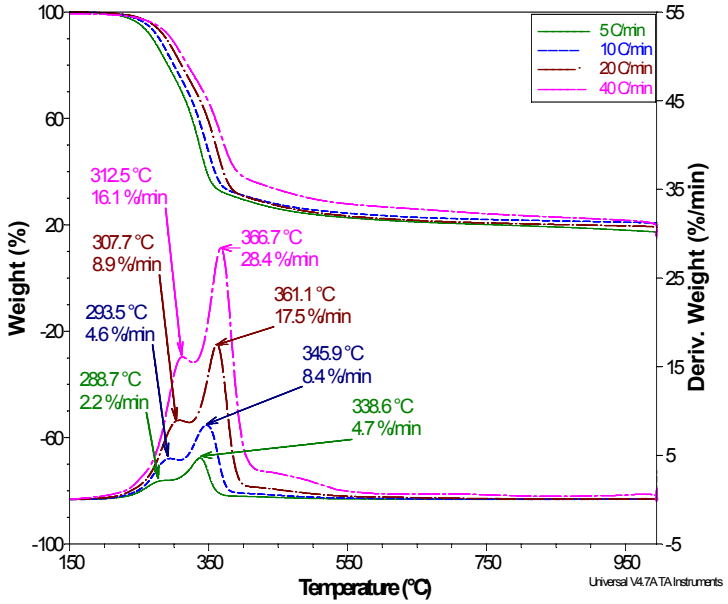



Figure 11-10. Weight loss profiles and DTG curves of pyrolysis of switchgrass at four different heating rates ranging from 5 °C/min to 40 °C/min

Table 11-3. Maximum weight loss rates and peak temperatures attained during the devolatilization of individual feedstocks at different heating rates

| **Feedstock Materials** | **Heating Rates °C/min** | **Maximum Weight Loss Rate, $(\%/min)_{max}$** | | **Peak Temperature, $T_{max}$, °C** | |
|---|---|---|---|---|---|
| PCC Bituminous Coal | 5 | 0.83 | | 432 | |
| | 10 | 1.60 | | 442 | |
| | 20 | 3.60 | | 454 | |
| | 40 | 6.90 | | 465 | |
| BT Sub-Bituminous Coal | 5 | 0.56 | | 423 | |
| | 10 | 0.95 | | 436 | |
| | 20 | 2.00 | | 442 | |
| | 40 | 4.10 | | 454 | |
| Corn Stover (CS) | | **Peak 1** | **Peak 2** | **$T_{max}$ 1** | **$T_{max}$ 2** |
| | 5 | 2.50 | 4.50 | 290 | 341 |
| | 10 | 5.00 | 8.80 | 304 | 351 |
| | 20 | 10.00 | 15.90 | 315 | 365 |
| | 40 | 21.05 | 33.40 | 333 | 372 |
| Switchgrass (SG) | 5 | 2.20 | 4.70 | 289 | 339 |
| | 10 | 4.60 | 8.40 | 294 | 346 |
| | 20 | 8.90 | 17.50 | 308 | 361 |
| | 40 | 16.10 | 28.40 | 313 | 367 |

## 11.4.4 Analysis of Synergistic Interactions in Blends

To investigate the synergistic behavior between the coals and biomass in the blends, the disparity in the amount of volatile matter released was evaluated between the experimental and calculated curves as shown in Figure 11-11 and Figure 11-12. In order to better analyze the synergistic behavior between the blended fuels, an additional experimental run consisting of 40% biomass was also performed. The predicted amount of volatile matter released was calculated using a simple additive relationship, as shown in Equation 11-1 (Yaman & Haykiri-Acma, 2010; Yaman & Haykiri-Acma, 2007). Here, for the pyrolysis of blends of coal and biomass, if the interaction between the two blended feedstocks shows a faster reaction rate than the sum of the rate of each pure feedstock individually (weighted according to their mixture mass ratio) accounting for experimental uncertainty, then a positive synergistic effect or synergy is noted between the pair. On the contrary, if the interaction of two chars shows no effect on the reaction rate or shows a slower reaction rate than the sum of the weighted rates based on the individual chars, a negative synergistic effect is demonstrated, as defined by:

$$VM_{Calc,\ Blend} = X_{Coal} * VM_{Coal,\ Obs} + X_{CS} * VM_{CS,\ Obs} \quad \text{(Eq. 11-1)}$$

where, $X_i$ refers to the fraction of each material in the blend and $VM_i$ is the percentage of volatile matter evolved. As shown in Figure 11-11, for the TGA experimental runs performed, the percentage of volatile matter evolved increases with an increase in the percentage of corn stover in the blend which is an expected result due to the fact that corn stover has higher volatile content inherently.

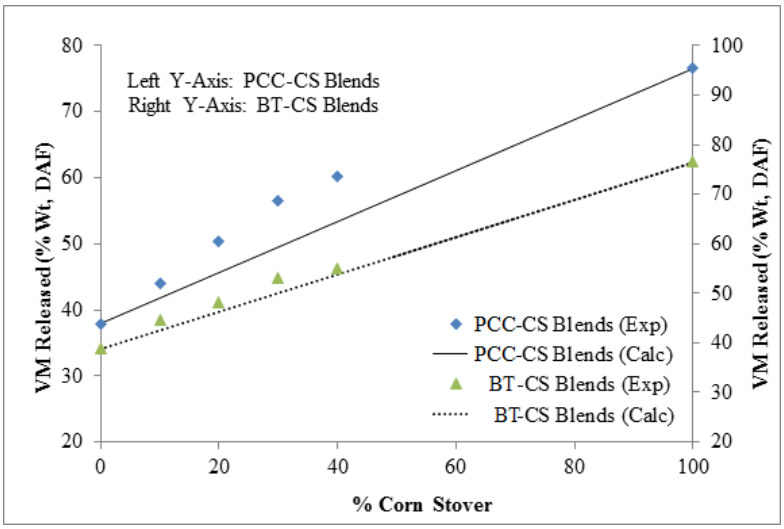
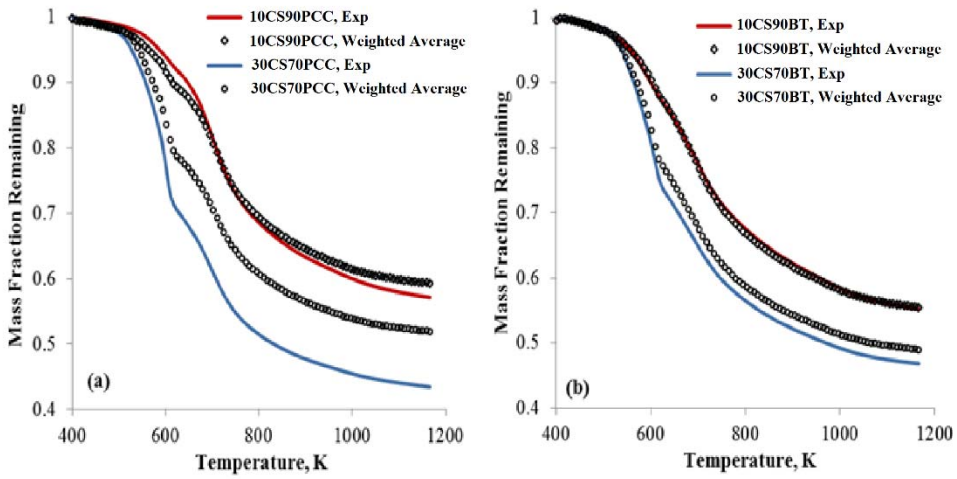



Figure 11-11. Disparity in the experimental and predicted curves during the release of volatile matter with increasing concentration of corn stover

However, it is noteworthy that this increase in volatile matter with increasing corn stover concentration in the blends of corn stover with bituminous coal is not linear with deviations from the predicted yield ranging between 2-7%, indicating some kind of synergistic behavior between the blended materials unlike some previous works indicated in literature (Vuthaluru, 2004; Meesri & Moghtaderi, 2002). On the contrary, for blends of corn stover with sub-bituminous coal, the deviations from the predicted yield are much lower (1-3%), implying, very little synergistic interactions between corn stover and sub-bituminous coal. In order to further verify this assumption and delve deeper into the synergistic behavior between the materials, the calculated and experimental DTG curves were plotted as shown in Figure 11-13 and Figure 11-14. The calculated DTG curves were estimated using an equation similar to Equation 11-1 by replacing the percent of volatile matter evolved with the weight loss rate of the material. The DTG curves for PCC and CS blends show that the predicted and experimental curves match closely at temperatures above 500 °C indicating that synergy between the materials exists at

lower temperatures (230-450 °C). Also, increasing the percentage of CS in the blend lowers the temperature (380 °C) until when synergistic behavior is observed. In the case of CS and BT blends, the disparity in the predicted and experimental DTG curves is quite apparent at lower concentrations of CS. The synergistic behavior for 10% CS and 90% BT starts at about 320 °C continuing until the end of pyrolysis. However, increasing the CS percentage to 30% drastically reduces the synergistic behavior. This can be observed only at higher temperatures (380-680 °C), albeit, with very less deviations in both curves.




(a) (b)

Figure 11-12. Comparison of the experimental and predicted weight loss curves for, (a) Blends of PCC Bituminous Coal and Corn Stover, and (b) Blends of BT Sub-Bituminous Coal and Corn Stover

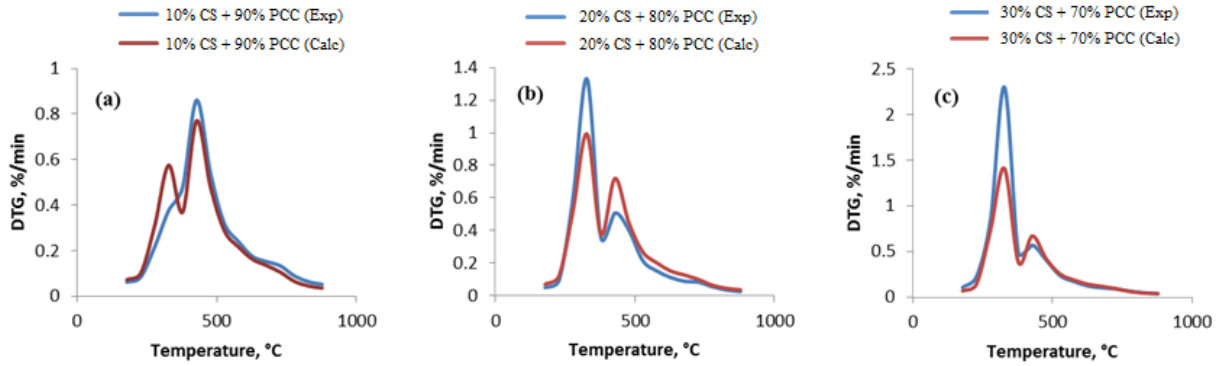



Figure 11-13. Comparison of the experimental and predicted DTG curves for (a) 10% CS + 90% PCC blend, (b) 20% CS + 80% PCC blend, and (c) 30% CS + 70% PCC blend

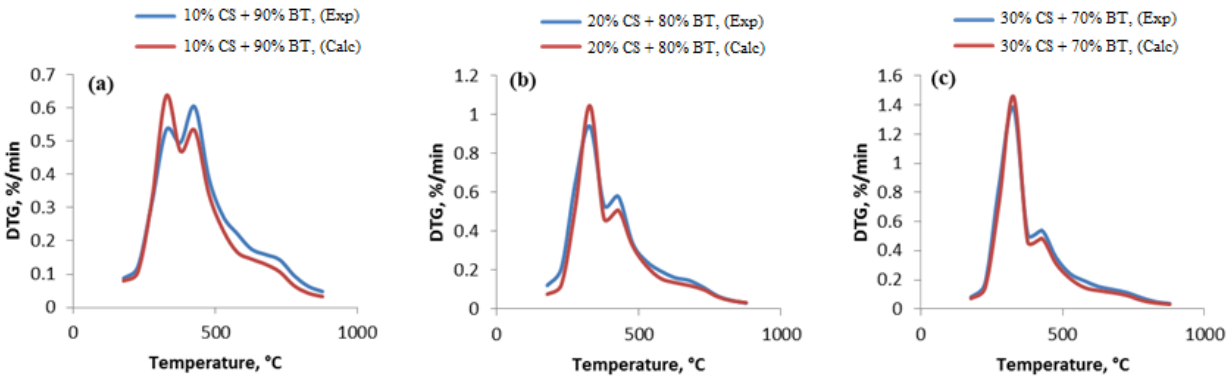



Figure 11-14. Comparison of the experimental and predicted DTG curves for (a) 10% CS + 90% BT blend, (b) 20% CS + 80% BT blend, and (c) 30% CS + 70% BT blend

Similar to corn stover blends, the blends containing switchgrass also show a clear increase in the amount of volatile matter with increasing percentage of switchgrass in the blend. But, clearly, from Figure 11-15, it can be stated that the deviations from the predicted and experimental yield is minimal suggesting that no significant interactions are present during devolatilization of blends of coals and switchgrass.

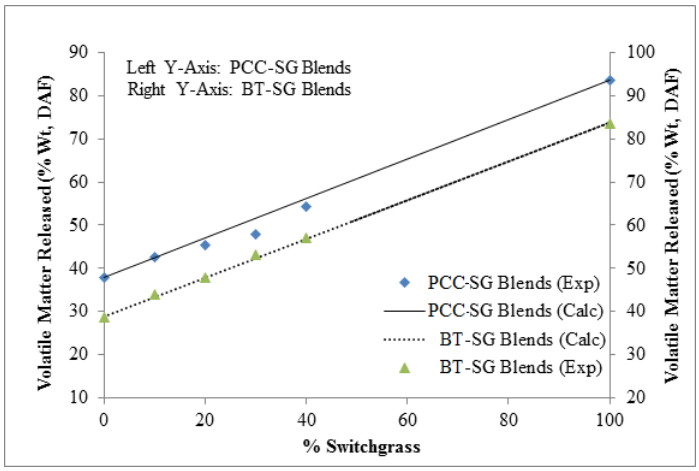



Figure 11-15. Disparity in the experimental and predicted curves during the release of volatile matter with increasing concentration of switchgrass

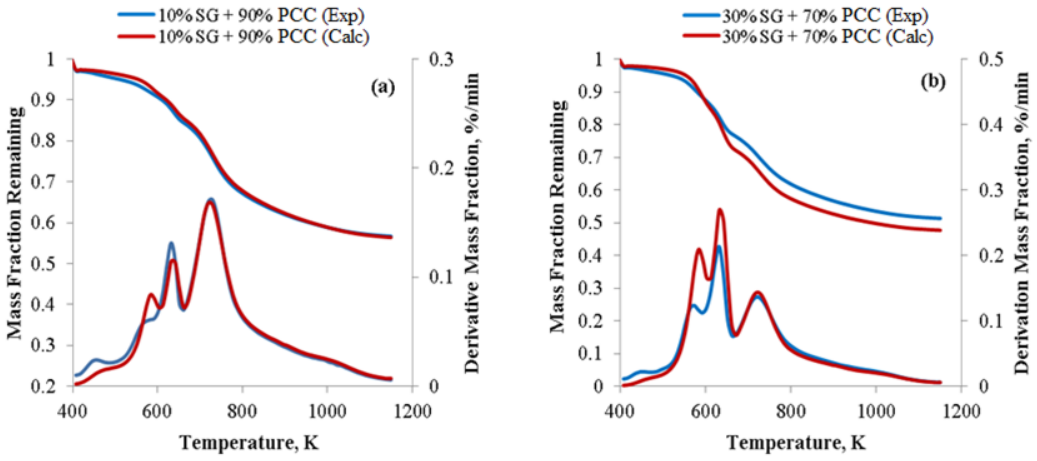



Figure 11-16. Comparison of the experimental and predicted weight loss and DTG curves for (a) 10% SG + 90% PCC blend, and (b) 30% SG + 70% PCC blend

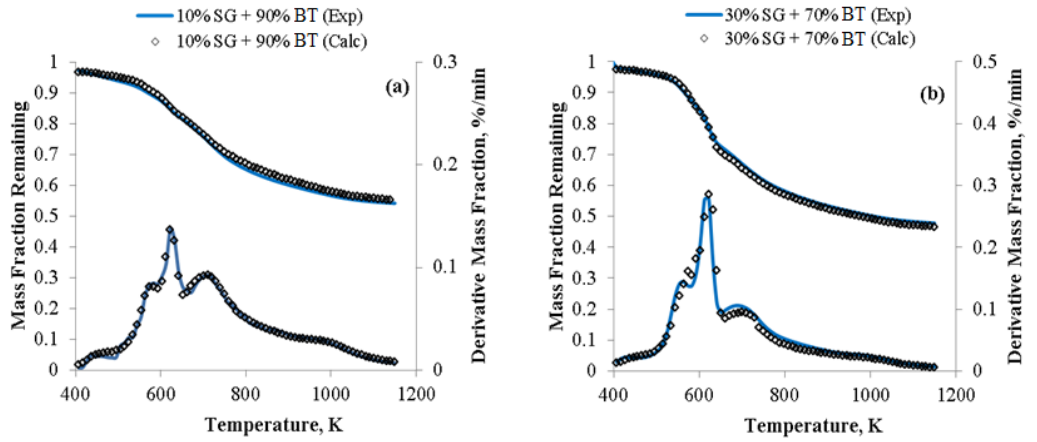



Figure 11-17. Comparison of the experimental and predicted weight loss and DTG curves for (a) 10% SG + 90% BT blend, and (b) 30% SG + 70% BT blend

## 11.5 Kinetic Analysis

### 11.5.1 Parallel First Order Reactions Model – Approximation of Temperature Integral

Several authors have approximated the overall process of pyrolysis as a first-order decomposition occurring uniformly throughout the coal and biomass particles (Cai et al., 2008; Di Blasi, 2008; Sadhukhan et al., 2008; Jong et al., 2007; Zhou et al., 2006; Ahuja et al., 1996; Koufopanos & Papayannakos, 1991; Coats & Redfern, 1964). For pyrolysis or oxidation reactions under non-isothermal conditions, the heating rate H plays a very important role in determining the kinetic parameters (Cai et al., 2008; Zhou et al., 2006; Sima-Ella et al., 2005;

Hatakeyama & Quinn, 1999; Coats & Redfern, 1964). For a first-order reaction at constant heating rate, $H = dT/dt$:

$$dX/dT = [A(1-X)/H]\, exp\left(-E/RT\right) \quad \text{(Eq. 11-2)}$$

where, $A$ is pre-exponential factor and $E$ is the activation energy.

Integration of the above equation subject to the condition that conversion is zero at initial temperature, $T_0$, leads to the following result:

$$ln(1-X) = -\left(A/H\right) \int_{T_0}^{T} exp\left(-E/RT\right)\, dT \quad \text{(Eq. 11-3)}$$

Since, there is no conversion at initial temperature, $T_0$, the limits of the integral in Equation 11-3 can be conventionally changed to:

$$\int_0^T \exp\left(-E/RT\right) \quad \text{(Eq. 11-4)}$$

thereby introducing a new function as represented in Equation 11-5:

$$f(y) = \int_y^\infty \left(e^{-y}/y^2\right) dy \quad \text{(Eq. 11-5)}$$

where $y = -E/RT$. Therefore, Equation 11-3 reduces to:

$$ln(1-X) = -\left(A/H\right) f(y) \quad \text{(Eq. 11-6)}$$

Since Equation 11-5 cannot be solved analytically, several authors have used different approaches to solve the function *f (y)* (Jerez, 1983; Coats & Redfern, 1964; Freeman & Carroll, 1958; Kissinger, 1957). Coats-Redfern approximation has been used in this study to determine the approximate value of the temperature integral because of the fact that this method provides the best linearity of the data as opposed to other analytical model-fitting methods (Gopalakrishnan & Sujatha, 2011; Syed et al., 2011; Fermoso et al., 2010; Sima-Ella et al., 2005). This method is widely used and accepted for the calculation of kinetic parameters. The use of this approximation would help in transforming Equation 11-5 into simple linear forms and thus obtaining the activation energy, $E$ and pre-exponential factor, $A$ as shown in Equations 11-7 through 11-9. In this approximation, *f(y)* is obtained by assuming an asymptotic expansion wherein only the first two terms are utilized.

Coats-Redfern approximation states:

$$f(y) = e^{-y}/y^2 \left[1 - \left(2!/y\right) + \left(3!/y^2\right) - \left(4!/y^3\right) + \ldots\right] \quad \text{(Eq. 11-7)}$$

or,

$$f\,(y) \approx e^{-y}/y^2 \left(1 - \frac{2}{y}\right) \quad \text{(Eq. 11-8)}$$

and,

$$ln\left[{-ln(1-X)}/{T^2}\right] = ln\left[\left(1-\frac{2RT}{E}\right){AR}/{HE}\right] - {E}/{RT} \quad \text{(Eq. 11-9)}$$

As described in Equations 11-2 through 11-9, using Coats-Redfern approximation, the kinetic parameters, activation energy and pre-exponential factor, were determined for both single fuels as well as the blends. From the pyrolysis data obtained, it is evident that different constituents of the sample pyrolyze at different temperatures and each temperature regime may be represented with a specific set of kinetic parameters. Each zone or temperature regime was estimated through inflection points or tangents drawn along the weight loss curves once moisture has been removed. The points corresponding to the tangents were marked as the beginning of a particular temperature zone of the total pyrolysis regime. Figure 11-18 shows the first order plot of $ln[-ln(1-X)/T^2]$ versus $1/T$. The activation energy can be estimated from the slope of this plot while the pre-exponential factor can be estimated from the intercept by taking the temperature at which $W_t = (W_0 + W_f)/2$.

The pyrolysis of PCC Bituminous coal may be described as a process with three consecutive first order reactions. In order to apply Equation 11-9, the conversion was recalculated for each zone separately to determine the kinetic parameters for the respective zones. A similar procedure was carried out for estimating the kinetic parameters of BT Sub-Bituminous coal and blends of both coals with corn stover. BT coal also has three zones where the first-order analysis can be applied while the corn stover has two independent zones and the blends contain at least four different zones (Bhagavatula et al., 2014). As an illustration, Figure 11-19 depicts the kinetic analysis for the pyrolysis of PCC Bituminous coal, corn stover, and 10% CS and 90% PCC blend.

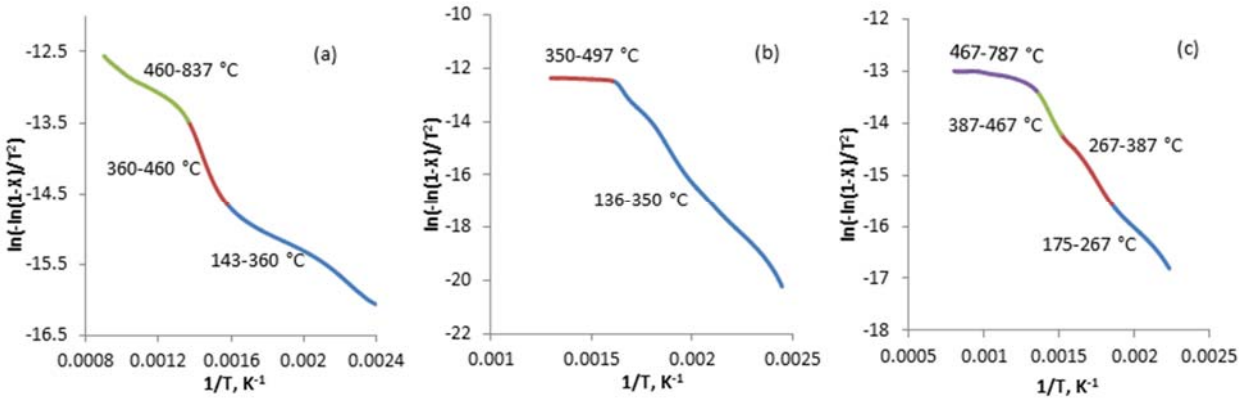



Figure 11-18. Analysis of the thermal evolution profiles and temperature ranges for pyrolysis of (a) PCC Bituminous coal, (b) Corn Stover and (c) 10% CS and 90% PCC blend

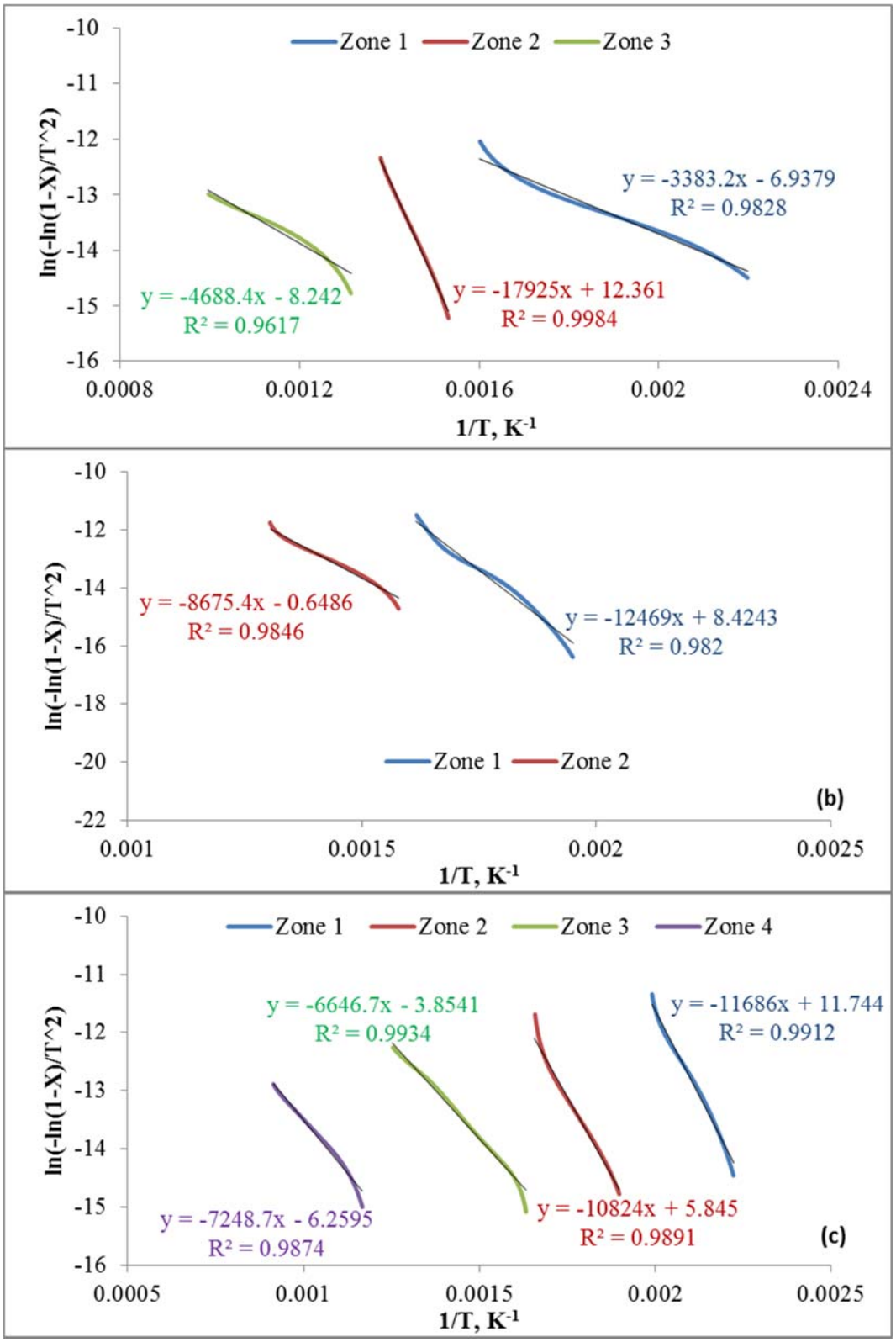



Figure 11-19. Estimation of kinetic parameters for pyrolysis of (a) PCC Bituminous coal, (b) Corn Stover, and (c) 10% CS and 90% PCC blend

Table 11-4. Obtained pyrolysis kinetic parameters, temperature and conversion ranges for all feedstocks at a heating rate of 5 °C/min

| Feedstock Materials | Temperature °C | Conversion Range, % | Activation Energy E, KJ/mol | Arrhenius Constant, $min^{-1}$ | Correlation Coefficient, $R^2$ |
|---|---|---|---|---|---|
| PCC Bituminous Coal | 143 - 360 | 2-16 | 28.13 | 2.46E+01 | 0.9828 |
| | 360 - 460 | 16 - 53 | 149.03 | 2.27E+10 | 0.9984 |
| | 460 - 837 | 53-98 | 38.98 | 9.55E+00 | 0.9616 |
| BT Sub-bituminous Coal | 175-281 | 2-9 | 56.96 | 8.37E+04 | 0.9973 |
| | 281-457 | 9-55 | 78.15 | 1.13E+05 | 0.9948 |
| | 457-791 | 55-97 | 41.75 | 1.40E+01 | 0.9909 |
| Corn Stover (CS) | 136 - 350 | 3-77 | 103.67 | 3.13E+08 | 0.9820 |
| | 350 - 497 | 77-92 | 72.13 | 2.69E+04 | 0.9846 |
| 10% CS + 90% PCC | 175-267 | 1-5 | 67.90 | 1.36E+06 | 0.9886 |
| | 267-387 | 5-25 | 82.47 | 1.20E+06 | 0.9907 |
| | 387-467 | 25-57 | 179.16 | 3.37E+12 | 0.9905 |
| | 467-787 | 57-97 | 25.69 | 1.18E+00 | 0.9785 |
| 20% CS + 80% PCC | 150-244 | 1-5 | 57.39 | 1.92E+05 | 0.9984 |
| | 244-360 | 5-38 | 107.69 | 6.30E+08 | 0.9893 |
| | 360-496 | 38-75 | 107.07 | 9.69E+06 | 0.9913 |
| | 496-843 | 75-97 | 45.85 | 1.88E+01 | 0.9814 |
| 30% CS + 70% PCC | 166-231 | 1-5 | 97.16 | 8.02E+09 | 0.9912 |
| | 231-332 | 5-43 | 89.99 | 2.09E+07 | 0.9891 |
| | 332-550 | 43-86 | 55.26 | 8.89E+02 | 0.9934 |
| | 550-854 | 86-97 | 60.27 | 9.31E+01 | 0.9874 |
| 10% CS + 90% BT | 156-265 | 1-7 | 53.61 | 9.52E+04 | 0.9915 |
| | 265-338 | 7-22 | 138.82 | 9.92E+11 | 0.9967 |
| | 338-451 | 20-53 | 100.42 | 1.29E+07 | 0.9921 |
| | 451-853 | 53-98 | 28.71 | 3.63E+00 | 0.9895 |
| 20% CS + 80% BT | 156-224 | 2-6 | 64.59 | 2.69E+06 | 0.9905 |
| | 224-308 | 6-18 | 126.01 | 2.06E+11 | 0.9927 |
| | 308-437 | 18-61 | 96.90 | 3.02+03 | 0.9892 |
| | 437-835 | 61-97 | 30.37 | 1.53E+00 | 0.9872 |
| 30% CS + 70% BT | 171-245 | 1-5 | 87.10 | 2.85E+08 | 0.9889 |
| | 245-342 | 5-45 | 99.15 | 1.22E+08 | 0.9933 |
| | 342-455 | 45-71 | 93.14 | 1.81E+06 | 0.9888 |
| | 455-880 | 71-98 | 34.98 | 4.53E+00 | 0.9790 |

Thus, the coal devolatilization process can be divided into three stages (Cai et al., 2008; Zhou et al., 2006; Vuthalura, 2004). For PCC Bituminous coal, in the first stage, for temperatures less than 360 ºC or until a conversion level of approximately 16%, only the peripheral parts and the mobile phase of the macromolecular structure of coal decompose. This zone will have relatively lower activation energy as shown in Table 11-4. In the second stage, for temperatures between 360 ºC and 460 ºC (conversion between 16 and 53%), pyrolysis liquids

and gases are the main products. As explained earlier, this zone mainly comprises the immobile phase of the coal structure which is more resistant to heat. Therefore, only a small amount of fragmented polycyclic aromatic compounds are produced during this phase. Hence, the activation energy of this phase is much higher than that of the first phase.

In the last stage, for temperatures greater than 460 ºC, the remaining macromolecular structure of coal is further decomposed. The activation energy in this case is much lower than that of the second phase indicating that during the third stage, repolymerization or cross-linking reaction resulting in the formation of char as the pyrolysis product occurs more easily since most of the volatiles or oxygen containing functional groups have been removed in the previous stages. Apart from this, it can be seen that the kinetic zones for the coal-biomass blend are slightly different from that of coals. For coal-biomass blends, four independent reactions are used to describe the co-pyrolysis process. It can be noted that the conversion range for the first stage is only up to 7% indicating that the main decomposition of the coal-biomass blend occurs at higher temperatures. As seen from Table 11-4, the kinetic parameters for the different thermal evolution profiles during the co-pyrolysis of coal and corn stover blends have been predicted. The good correlation factor indicates that each thermal evolution profile may be represented as a single first order reaction.

### 11.5.2 Distributed Activation Energy Model – Gaussian Distribution of Activation Energy

Kinetic parameters obtained using the single first order reaction models are actually a starting point in the devolatilization modeling. Although simple and used as a starting point for more complex models, a single first order reaction model utilized for estimating the devolatilization kinetics of complex materials is only applicable over a limited range of experimental conditions. The kinetic parameters obtained through such a model may not be used as global parameters and that the parameters such as activation energy and pre-exponential factor change for different heating rates (i.e. the parameters obtained through one experimental condition may not be extrapolated to an unknown heating rate). More accurate and specific models are required to meet the experimental results of each material, one model being the distributed activation energy model (Biagini et al., 2002; Anthony & Howard, 1976).

Since coal and biomass are complex fuels with a wide variety of chemical groups, the distributed activation energy model treats the thermal decomposition process as a large number of independent, parallel rate processes or decomposition of many different chemical groups where each group is characterized uniquely by its activation energy. The thermal decomposition of a single organic species can be described as an irreversible first-order reaction with respect to the amount of unreacted material remaining. Thus, the rate at which the volatiles are produced by a particular reaction can be defined according to the mass balance on the reactant species.

$$dV_i/_{dt} = k_i(V_i^* - V_i) \quad \text{(Eq. 11-10)}$$

$$V_i^* - V_i = V_i^* \, exp\left(-At \, exp\left(-E/_{RT}\right)\right)_i \quad \text{(Eq. 11-11)}$$

where $V_i^*$ is the final quantity of volatile matter for the generic species, $i$, and $k_i$ is the rate constant of the reaction expressed according to the Arrhenius law.

This type of kinetic model requires that the amount of volatiles and kinetic parameters known for all the single reactions. To estimate these parameters from experimental data for all the reactions is practically not possible. The problem can be simplified if it is assumed that the rate constants for all the reactions differ only in the activation energy. The number of reactions is large enough so that the activation energy can be expressed as a continuous Gaussian distribution function *f(E)* and *f(E)dE* representing the potential loss of volatile fraction with activation energy between the intervals $E$ and $E + dE$. Thus,

$$V_i^* = dV^* = V^* f(E)dE \quad \text{(Eq. 11-12)}$$

The total amount of volatile material unreleased is obtained by summing the contribution from each reaction, that is, by integrating Equation 11-11 over all values of $E$ using Equation 11-12. Finally, the yield of volatiles can be calculated using Equation 2.4.11.

$$(V^* - V)/_{V^*} = \left[\int_0^\infty \exp\left(-\left(\int_0^t k \, dt\right) f(E)dE\right)\right] \quad \text{(Eq. 11-13)}$$

where,

$$k = A \, Exp\left(-E/_{RT}\right) \quad \text{(Eq. 11-14)}$$

and,

$$f(E) = (\sigma(2\pi)^{0.5})^{-1} \exp\left[-(E - E_0)^2/_{2\sigma^2}\right] \quad \text{(Eq. 11-15)}$$

where, $V^*$ is the global volatile quantity of the material, $E_0$ is the mean activation energy and $\sigma$ is the standard deviation of the activation energy. This approach avoids the low values of the

activation energies which result when a single first-order reaction model is applied to fit a temperature dependence that arises from the occurrence of different reactions in different temperature intervals (Di Blasi, 2008).

In this work, Miura's method is used to estimate *f(E)* and *A* values for all the feedstock materials (Li et al., 2009). Both *f(E)* and *A* are obtained from at least three thermogravimetric experiments using different heating profiles without assuming any functional forms for *f(E)* and *A* (Miura & Maki, 1998). The procedure used to estimate *f(E)* and *A* is summarized as:

1. Measure *V/V** vs. *T* using at least three different heating rates on a dry and ash-free basis.
2. Calculate the values of $ln\ (H/T^2)$ and $1/(RT)$ at the same *V/V**, where *H* is the heating rate.
3. Plot $ln(H/T^2)$ and $1/(RT)$ at the selected *V/V** ratio and then determine the activation energies, *E*, from the slopes and *A* from the intercept as shown in Equation 11-16.

$$ln\left(\frac{H}{T^2}\right) = ln\left(\frac{AR}{E}\right) + 0.6075 - \frac{E}{RT} \quad \text{(Eq. 11-16)}$$

4. Plot *V/V** and *E* and differentiate the *V/V** vs. *E* relationship by *E* to obtain *f(E)*.
5. Pre-exponential factor, *A*, can be expressed as a function of activation energy using the following expression:

$$A = \alpha\ Exp\ (E\beta) \quad \text{(Eq. 11-17)}$$

where, $\alpha$ and $\beta$ are constants dependent on the reacting material (Li et al., 2009; Miura & Maki, 1998).

For illustration of the distributed activated energy model (DAEM), Figure 11-20 through Figure 11-23 describe the method for establishing the kinetic parameters during the pyrolysis of PCC Bituminous coal. For different heating rates ranging from 5-40 °C/min, Figure 11-20 describes the linear relationship between $ln(H/T^2)$ and $1/T$ at various conversions. The idea is that, with increase in heating rates, the temperature required to attain a particular conversion increases and hence, the kinetic parameters can be determined at each conversion point.

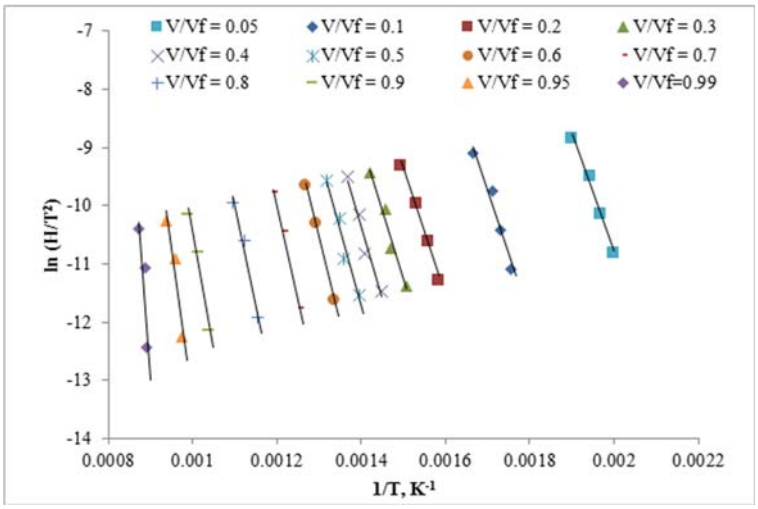



Figure 11-20. Plot for estimating the activation energy and Arrhenius constant for pyrolysis of PCC Bituminous coal at various heating rates and conversion points using DAEM

Once the activation energies at selected conversions are determined, the relationship between conversion ($V/V_f$) and activation energies needs to be established. For this, a plot of $V/V_f$ versus $E$ is shown in Figure 11-21. The relationship between $V/V_f$ and $E$ is fitted with a logistic distribution curve using Equation 11-18:

$$\frac{V}{V_f} = A_2 + \frac{(A_1 - A_2)}{\left(1 + \left(E/E_0\right)^p\right)} \qquad \text{(Eq 11-18)}$$

where $A_1$ and $A_2$ are the intial and final conversion points, $E_0$ is the mean activation energy and $p$ is a constant. The values of these constant are obtained by fitting the experimental data with Equation 11-18.

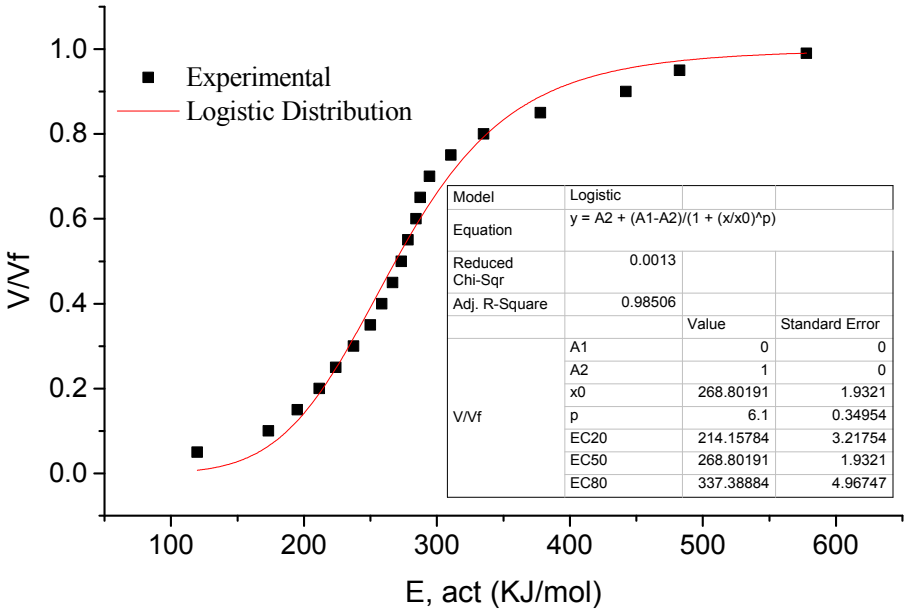



Figure 11-21. Plot for estimating the relationship between V/Vf and activation energy for pyrolysis of PCC Bituminous coal using DAEM

Once the relationship between $V/V_f$ and $E$ is established and the unknown constants obtained, Equation 11-18 can be differentiated with respect to $E$ to obtain the values for the function $f(E)$. Finally, a plot of the obtained $f(E)$ values with respect to the activation energy shown in Figure 11-22, can be fitted using a Gaussian distribution function and that the complex devolatilization reaction kinetics of carbonaceous materials may not be represented by only a single first order reaction, but the reaction is made up of several parallel reactions occurring simultaneously with increasing temperatures.

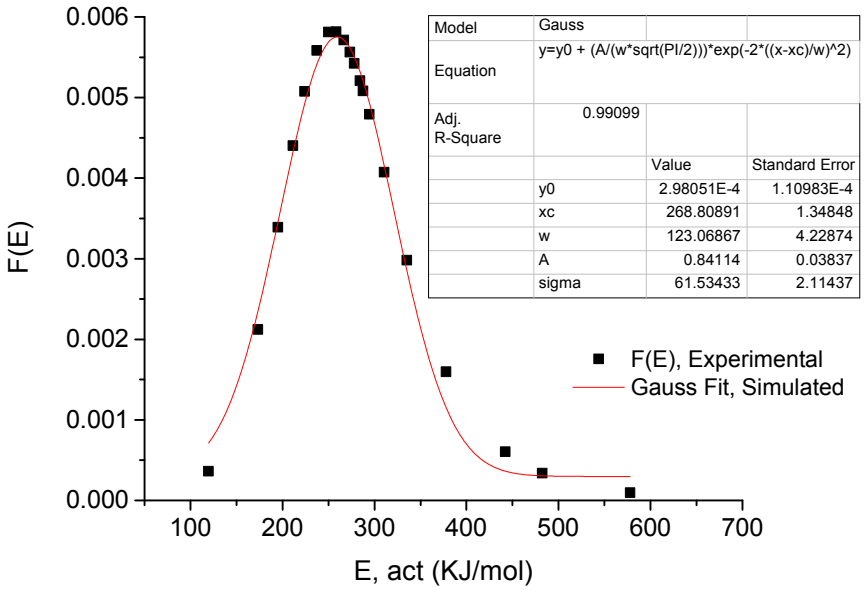



Figure 11-22. Plot for estimating the relationship between f (E) and activation energy for pyrolysis of PCC Bituminous coal using DAEM

As seen from Figure 11-22, for PCC Bituminous coal, the peak of *f(E)* occurs at 0.00575 kJ/mol corresponding to an activation energy of approximately 269 kJ/mol and the distribution of activation energies follows an approximate Gaussian function ($R^2$ = 0.99). The range of activation energies is between 120-578 kJ/mol within the devolatilization conversion interval of 5-99%.

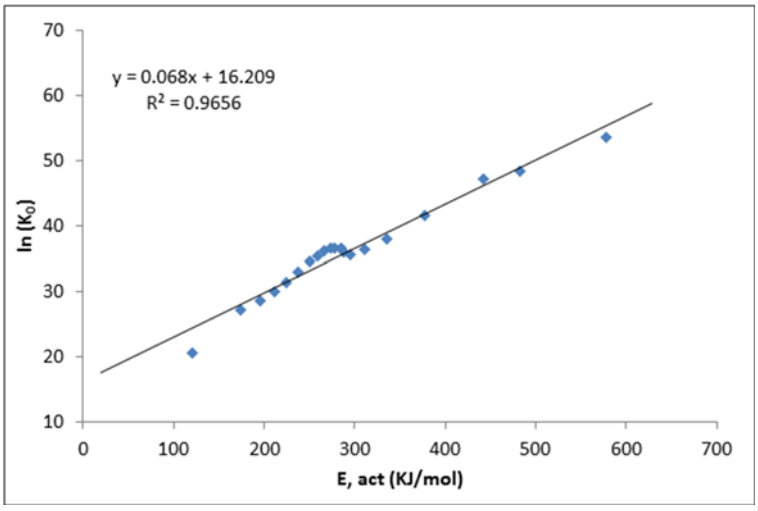



Figure 11-23. Plot for estimating the relationship between Arrhenius constant and activation energy for pyrolysis of PCC Bituminous coal using DAEM

From Figure 11-23, it may be observed that a linear relationship with reasonable correlation coefficient ($R^2$ = 0.97) exists between $ln(k_0)$ and activation energy. For the devolatilization interval, the values of $k_0$ range between $e^{20}$ – $e^{53}$ $min^{-1}$ for PCC Bituminous coal, corresponding well to the values available in literature for coals with similar properties (Li et al., 2009; Miura & Maki, 1998).

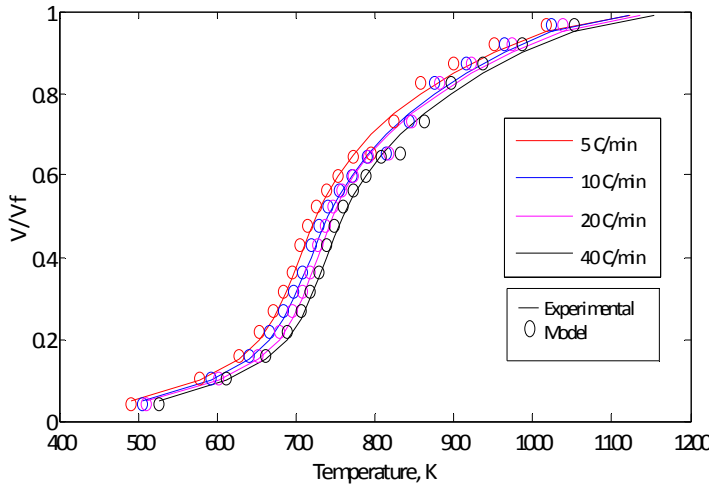



Figure 11-24. Comparison between experimental and calculated devolatilization weight loss of PCC Bituminous coal with increasing temperature using DAEM

Using the kinetic parameters thus obtained, Equation 11-13 is then solved using the quadrature function of MATLAB to predict the weight loss or conversion profiles during devolatilization at all heating rates and compared with the experimental data as shown in Figure 11-24. From Figure 11-24, it can be observed that the weight loss profiles can be predicted with greater accuracy when compared with that of Method 1. A similar procedure has been utilized for analyzing the devolatilization kinetic parameters of all the feedstock materials and these values are shown in Table 11-5.

Table 11-5. Obtained pyrolysis kinetic parameters for single fuels and blended feedstocks using distributed activation energy model (Gaussian distribution of activation energies)

| Feedstock Materials | Activation Energy Range KJ/mol | Peak f (E), KJ/mol | Peak Activation Energy, KJ/mol | Arrhenius Constant Range, $min^{-1}$ |
|---|---|---|---|---|
| PCC Bituminous Coal | 120-578 | 0.00575 | 269 | $e^{20}$- $e^{53}$ |
| BT Sub-Bituminous Coal | 100-446 | 0.00936 | 210 | $e^{19}$-$e^{43}$ |
| Corn Stover (CS) | 91-256 | 0.00859 | 171 | $e^{14}$-$e^{40}$ |
| 10% CS + 90% PCC | 118-374 | 0.0042 | 220 | $e^{23}$- $e^{46}$ |
| 30% CS + 70% PCC | 110-350 | 0.0061 | 175 | $e^{17}$- $e^{46}$ |
| 10% CS + 90% BT | 95-396 | 0.0047 | 226 | $e^{27}$- $e^{42}$ |
| 30% CS + 70% BT | 92-320 | 0.00875 | 154 | $e^{17}$- $e^{26}$ |

## 11.5.3 Matrix Inversion Method

As described in Section 11.5.2, the devolatilization mass loss of a complex carbonaceous material can be uniquely characterized within an activation energy interval of $E$ and $E + dE$ at any particular time $t$ (Scott et al., 2006a; Scott et al., 2006b; Please et al., 2003). If the decomposition is considered to be first order, then Equation 11-13 can be rewritten in the following form:

$$m(E,t) = m_0(E)\ \Psi\ (E,t) \quad \text{(Eq 11-19)}$$

and,

$$\Psi\ (E,t) = Exp\left[-A(E)\ \int_0^t Exp\left(-E/RT\right) dt\right] \quad \text{(Eq 11-20)}$$

where, $m(E,t)$ is the mass density function of the volatile material at any time $t$ and $m_0(E)$ is the initial mass of volatile material within the interval $E$ and $E + dE$.

Since $m(E,t)$ cannot be measured quantitatively, integrating Equation 11-19 over all activation energies enables the calculation of total amount of material decomposed, $M_v(t)$, at any time $t$.

$$\frac{M_v\ (t)}{M_{v0}} = \frac{M_{v0} - V\ (t)}{M_{v0}} = \int_0^\infty g\ (E)\ \Psi\ (E,t)\ dE \quad \text{(Eq 11-20)}$$

and,

$$g\ (E) = \frac{m_0\ (E)}{\int_0^\infty m_0\ (E)\ dE} \quad \text{(Eq 11-21)}$$

where, $M_v(t)$ is the mass of volatiles at any time $t$, $M_{vo}$ is the initial mass of volatile matter, $V(t)$ is the yield of volatiles and $g(E)$ is the underlying initial distribution of activation energies.

Since, $g(E)$ is unknown, calculation of activation energies and pre-exponential factors for each parallel reaction is more complex. In order to overcome this complexity, a mathematical inversion method which does not rely on any assumption of the initial distribution of activation energies is utilized in this research for estimating the kinetic parameters. This method was successfully tested by Scott et al. (2006b) for evaluating the kinetic parameters of pyrolysis of sewage sludge. This method, which is virtually an extension of Miura's method, is used for determining the number of reactions occurring during the process of devolatilization, in addition to determining the values of activation energies and pre-exponential factors.

If it is assumed that a volatile component of the fuel with an initial mass fraction of $f_{i,0}$ reacts with an activation energy of $E_i$ and pre-exponential factor of $A_i$, Equation 11-18 can then be expressed as:

$$f_i = f_{i,0}\,\Psi_i \qquad \text{(Eq 11-22)}$$

where $f_i$ is the fraction of the $i^{th}$ component remaining as the fuel is devolatilized and $\Psi_i$ is the double exponential term. For a material decomposing via several parallel first-order reactions, Equation 11-20 can therefore be expressed as:

$$\frac{M(t)}{M_0} = W + \sum_{All\ Reactions,i} f_{i,0}\ \Psi_i \qquad \text{(Eq 11-23)}$$

where $W$ is the fraction of inert material.

The problem is therefore to estimate $f_{i,0}$, $E_i$ and $A_i$. The distributed activation energy model can be stated to be a special case of this general problem which can be generated by increasing the number of reactions to infinity with a constraint that each of the reactions is uniquely characterized by its activation energy. It is to be noted that while the DAEM is ill-posed when the number of reactions is finite and the reactions do not overlap, the problem stated above is well-posed and can be solved. This is because of the fact that during the conversion process, the will be a point when a particular reaction is dominant and hence, its values of $E$ and $A$ can be directly evaluated without interference from other reactions. Equation 11-23, therefore, would be a linear problem so that the mass of solid fuel remaining at a given time would be the sum of the masses of each of the components remaining. Therefore, Equation 11-23 can be interpreted in a matrix form as follows:

$$\frac{1}{M_0}\begin{bmatrix} M(t_0) \\ M(t_1) \\ M(t_2) \\ \vdots \\ M\,(t_n) \end{bmatrix} = \begin{bmatrix} \Psi_1\,(t_0) & \Psi_2\,(t_0) & \cdots\cdots & \Psi_n\,(t_0) & 1 \\ \Psi_1\,(t_1) & \Psi_2\,(t_1) & \cdots\cdots & \Psi_n\,(t_1) & 1 \\ \Psi_1\,(t_2) & \Psi_2\,(t_2) & \cdots\cdots & \Psi_n\,(t_2) & 1 \\ \vdots & \vdots & \cdots\cdots & \vdots & 1 \\ \Psi_1\,(t_n) & \Psi_2\,(t_n) & \cdots\cdots & \Psi_n\,(t_n) & 1 \end{bmatrix} \times \begin{bmatrix} f_{1,0} \\ f_{2,0} \\ f_{3,0} \\ \vdots \\ W \end{bmatrix} \qquad \text{(Eq 11-23)}$$

Equation 11-23 can therefore be termed as a modified form of the distributed activation energy model. For a constant heating rate experiment (i.e. $dT/dt = H$ and initial temperature $T_0$), the double exponential term, $\Psi$ can be expressed as:

$$\Psi_i\,(t) = \Psi_i\,(T) = Exp\left[-\frac{A_i}{H}\int_{T_0}^{T} Exp\left(-E_i/_{RT}\right)\,dT\right] \qquad \text{(Eq 11-24)}$$

and,

$$f_i\,(T) = f_{i,0}\,\Psi_i\,(T) \qquad \text{(Eq 11-25)}$$

Thermogravimetric experiments conducted at two different heating rates, $H_1$ and $H_2$, can be used for calculating the values of $E_i$ and $A_i$. Assuming that the i$^{th}$ reaction is the only reaction occurring at the same conversion in both experiments, then,

$$f_i\,(H_1, T_1) = f_i\,(H_2, T_2) \qquad \text{(Eq 11-26)}$$

and subsequently,

$$\Psi_i\,(H_1, T_1) = \Psi_i\,(H_2, T_2) \qquad \text{(Eq 11-27)}$$

Substituting for $\Psi_i$ from equation 11-24 and taking natural logarithms on each side yields:

$$\frac{1}{H_1}\left[T_0\,Exp\left(-\frac{E_i}{RT_0}\right) - \frac{-E_i}{R}\int_{\frac{E}{RT_0}}^{\infty}\frac{Exp\,(-u)}{u}du - T_1\,Exp\left(-\frac{E_i}{RT_1}\right) + \frac{E_i}{R}\int_{\frac{E}{RT_1}}^{\infty}\frac{Exp\,(-u)}{u}du\right] =$$

$$\frac{1}{H_2}\left[T_0\,Exp\left(-\frac{E_i}{RT_0}\right) - \frac{-E_i}{R}\int_{\frac{E}{RT_0}}^{\infty}\frac{Exp\,(-u)}{u}du - T_2\,Exp\left(-\frac{E_i}{RT_2}\right) + \frac{E_i}{R}\int_{\frac{E}{RT_2}}^{\infty}\frac{Exp\,(-u)}{u}du\right] \qquad \text{(Eq 11-28)}$$

Equation 11-28 is a non-linear equation, which can be solved analytically for estimating unknown $E_i$. This calculated value of activation energy using Equation 11-28 will be accurate due to the fact that only one reaction would be dominating the overall mass loss at a chosen conversion point. Deviations in activation energy are observed, when several reactions occur simultaneously at the same conversion. Once the activation energy, $E_i$, is determined, pre-exponential factor, $A_i$, can be calculated by assuming that the conversion of the individual

component i of the dominating reaction reaches a particular conversion. For this method, it is assumed that the conversion is:

$$X_i = 1 - e^{-1} \Rightarrow \Psi_i = e^{-1} \Rightarrow \ln(\Psi_i) = -1 \quad \text{(Eq 11-29)}$$

Also, this value of $\Psi_i$ corresponds to the conversion at which the rate of decomposition is at a maximum. Combining Equations 11-24 and 11-28, $A_i$ can then be estimated.

The matrix inversion method is thus different from Method 2 in the sense that this method does not require that each reaction be uniquely characterized by its activation energy and does not use a step function approximation, which is central to Method 2 (Miura's method) for estimating the amount of each reaction occurring. The procedure for solving Equation 11-23 can thus be summarized as follows:

1. Perform at least two thermogravimetric experiments at different constant rates of heating and measure the values of mass as a function of temperature.
2. Consider n points of conversion during the decomposition temperature interval where the kinetic parameters, $E_i$ and $A_i$, are to be evaluated.
3. At each conversion point, evaluate $E_i$ and $A_i$ using a combination of Equations 11-24 and 11-28 to obtain n values of the kinetic parameters.
4. Using the set of n reactions with known values of $E_i$ and $A_i$, create the matrix $\Psi$ in Equation 11-23.
5. Once the matrix $\Psi$ is created, the mass fraction of each reaction, $f_i$, can be evaluated by inverting Equation 11-23: $f_i = \Psi^{-1} m$

This type of analysis has been used before for the determination of pyrolysis characteristics of dried sewage sludge and high ash, inertinite-rich, medium rank C South African coal (Saloojee, 2011; Scott et al., 2006a). In this work, the modified distributed activated energy model has been extended for determining the kinetic parameters of single fuels as well as blends of coal and biomass.

## 11.5.4 Results and Discussion – Matrix Inversion Method

### 11.5.4.1 PCC Bituminous Coal

The results of the real TGA devolatilization experiments using the Matrix Inversion method are presented and discussed in this section. Figure 11-25 through Figure 11-27 describe the inversion algorithm results for PCC Bituminous coal. The inversion algorithm was applied to

the TGA data at various heating rates and kinetic parameters were obtained at various conversions. The obtained kinetic parameters were then used to model the reactions at unknown heating rates that were not used in the algorithm. The obtained weight loss data was then compared with real TGA data for comparison and accuracy of the method.

As discussed earlier, this inversion algorithm is advantageous over Miura's method due to the fact that only two TGA curves are required and less data needs to be processed overall, thereby, significantly reducing the processing times and also the ability to predict the reaction curves at unknown heating rates. For PCC Bituminous coal, TGA data for heating rates 10 °C/min and 20 °C/min were used in the inversion algorithm for determining the kinetic parameters and the obtained parameters were then used to predict the weight loss curves at 5 °C/min and 40 °C/min.

MATLAB codes used for calculations in this method are presented in Appendix C. The weight loss data sets from TGA experiments were reduced by linear interpolation to further simplify the computation. From these reduced data sets, a total of 50 conversions were chosen where the kinetic parameters were to be calculated. One candidate reaction is generated at each value of conversion and for cases where more than one real reaction occurs at a particular conversion, the values of $E$ and $A$ generated (using Step 3) would be incorrect. Therefore, using the second stage of the algorithm (Steps 4 and 5), the values of $f_{i,0}$ of such unrealistic reactions can be set to zero, thereby determining the total number of reactions during devolatilization.

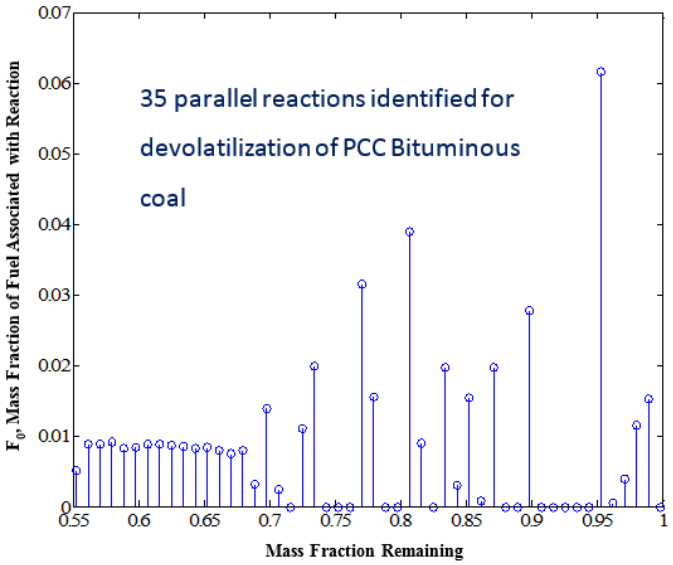



Figure 11-25. Mass fraction of fuel associated with each reaction during devolatilization of PCC Bituminous coal

Figure 11-25 shows the values of $f_{i,0}$ for PCC Bituminous coal. Upon examination of these values, 35 parallel reactions have been identified for the devolatilization of PCC Bituminous coal. Increasing the number of conversion points to a number greater than 50 would not make a difference because the total number of parallel reactions occurring in this case falls within the number of conversion points chosen. For example, when the number of conversion points were increased from 50 to 100, the number of parallel reactions occurring was still the same and no change in the activation energy range was observed.

It should be noted here that only the decomposition reactions, starting with removal of moisture, are taken into consideration during this method and hence, fixed carbon content and ash content are not included in Figure 11-25 through Figure 11-27. The values of activation energy and pre-exponential factor for each reaction are shown in Figure 11-26 and Figure 11-27. It can be observed from Figure 11-26 and Figure 11-27 that the values of kinetic parameters increase with increasing weight loss until a maxima is achieved when the mass fraction of the fuel (PCC Bituminous coal) remaining is approximately 55%, indicating the completion of the devolatilization process.

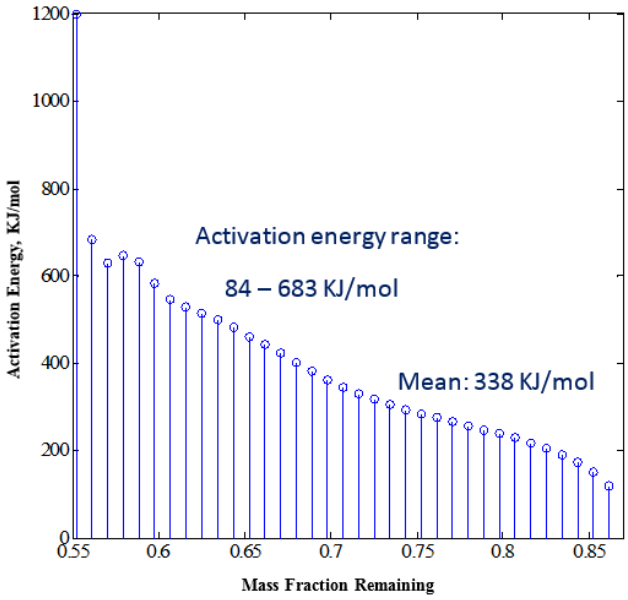



Figure 11-26. Plot of activation energy vs mass fraction remaining for pyrolysis of PCC Bituminous coal describing the values of activation energy for each parallel reaction

Activation energy values occurring during pyrolysis of PCC Bituminous coal have a range between 84-683 kJ/mol with a mean activation energy of approximately 338 kJ/mol while

the values of pre-exponential factor are not constant for all reactions but have a large range between 9E+5 $min^{-1}$ and 5E+32 $min^{-1}$. The kinetic parameters thus obtained were used to model the TGA curves. A comparison of the actual TGA curves and the predicted curves are shown in Figures Figure 11-28 and Figure 11-29.

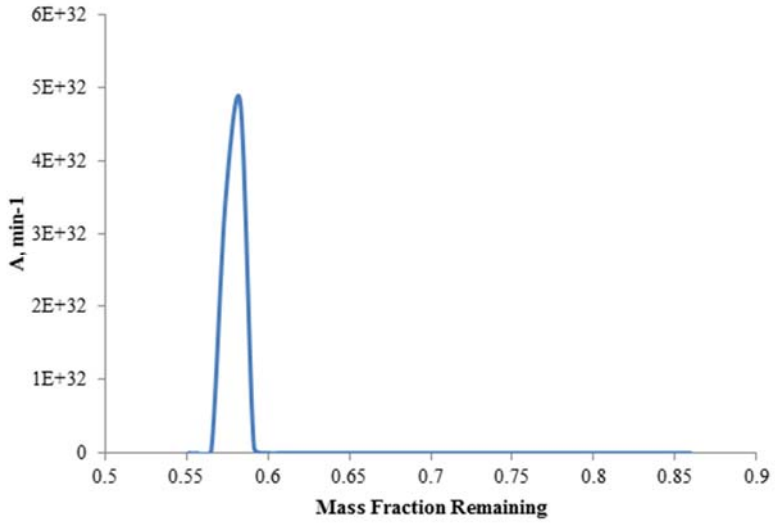



Figure 11-27. Plot of pre-exponential factor vs mass fraction remaining for pyrolysis of PCC Bituminous coal describing the values of pre-exponential factor for each parallel reaction

From Figure 11-28, it can be clearly seen that for the two heating rates used in the algorithm, the model predicts the weight loss data and derivative weight loss data excellently with standard error of less than 0.5% between the experimental and predicted values. The kinetic parameters obtained were then used for modeling the devolatilization reaction at two heating rates, 5 °C/min and 40 °C/min, not used in the algorithm in order to verify if the model could be extrapolated to unknown heating rates. This is important to verify since the process of devolatilization occurs instantaneously at the top of a moving bed reactor during gasification where the heating rates tend to be much higher, in the order of 100 °C/sec. For the thermogravimetric analyzer used in this work (TA SDT Q600), a linear increase in furnace temperature was not possible at heating rates higher than 40 °C/min. Hence, it must be noted here that the maximum heating rates utilized in this work is 40 °C/min.

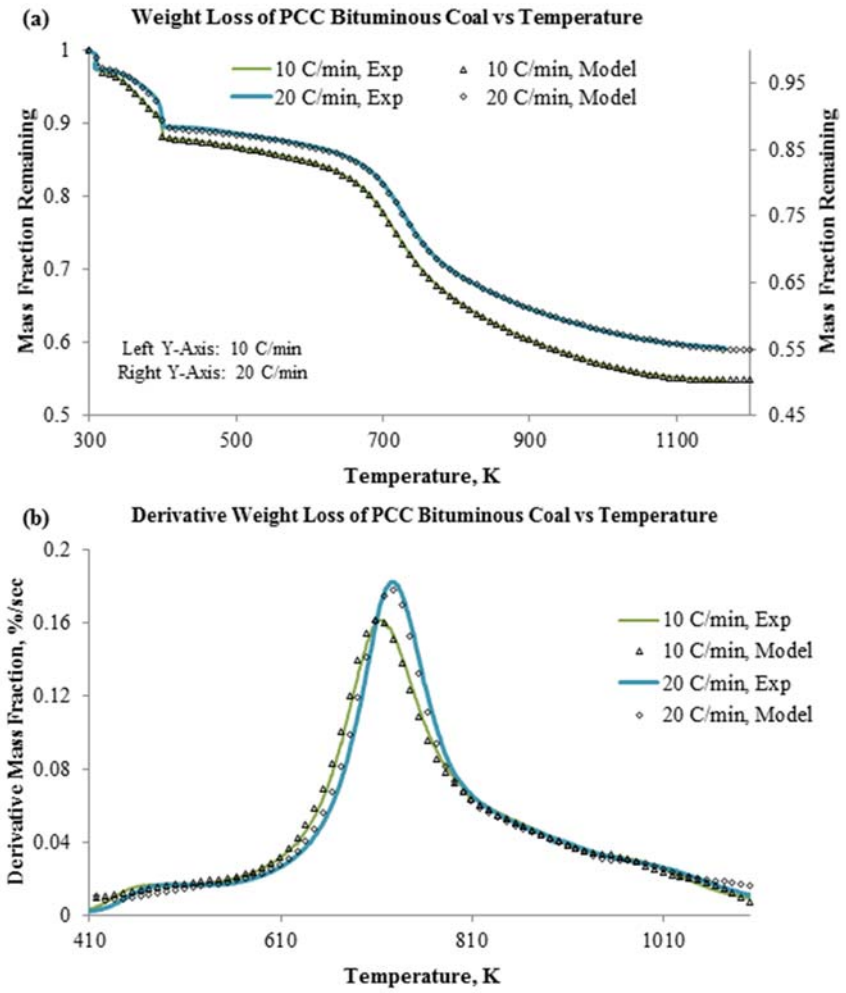



Figure 11-28. Comparison of experimental and predicted values for devolatilization of PCC Bituminous coal for two heating rates (10 °C/min and 20 °C/min) used in the matrix inversion algorithm: (a) weight loss vs temperature, and (b) derivative weight loss vs temperature

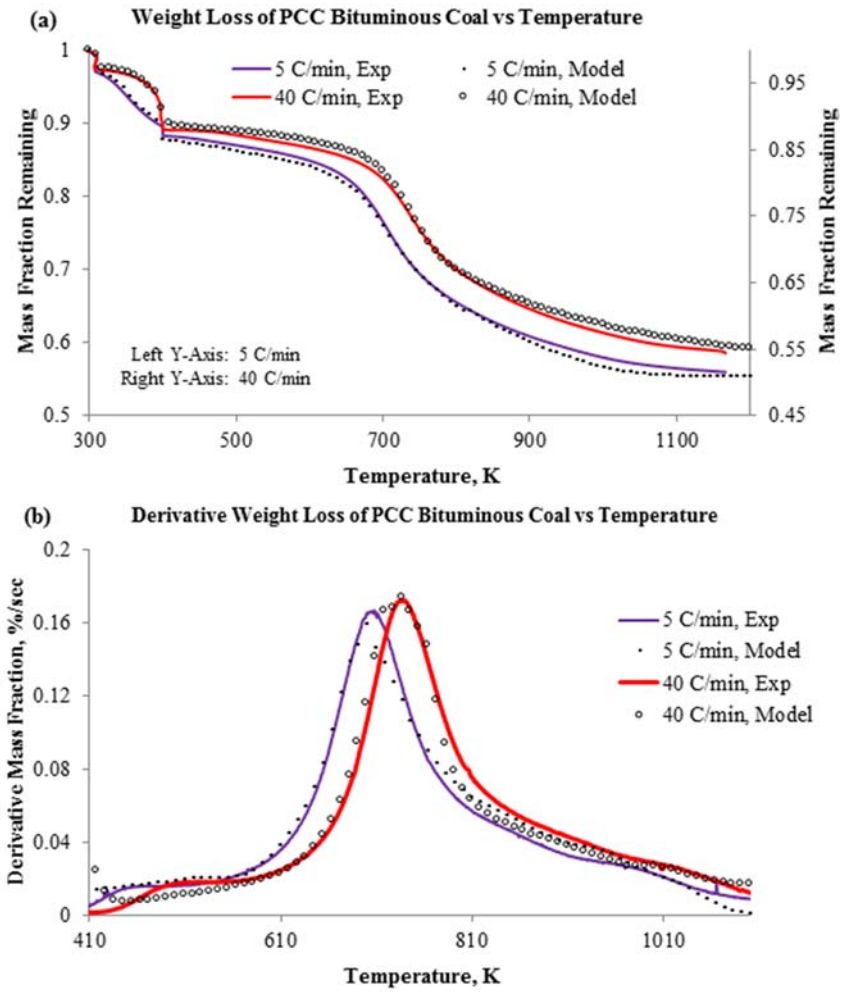



Figure 11-29. Comparison of experimental and predicted values for devolatilization of PCC Bituminous coal for two heating rates (5 °C/min and 40 °C/min) not used in the matrix inversion algorithm: (a) weight loss vs temperature, and (b) derivative weight loss vs temperature

It can be observed from Figure 11-29, that the model can be utilized for predicting weight loss data for unknown heating rates also. As seen from Figure 11-29, the predicted weight loss values and derivative weight loss values fall within 1% of the actual experimental curves suggesting that this model can be successfully utilized for predicting the devolatilization reaction even at extremely high heating rates that are achieved in industrial reactors. It is also important to understand if this model can be extended to various feedstocks with different compositions of moisture, volatile matter and fixed carbon content. Therefore, for this purpose and for comparison with other models described earlier, devolatilization of the two biomass materials (CS and SG) and blends of biomass with the two coals are analyzed further using the matrix inversion method in the following sections.

### 11.5.4.2 Kinetics of Corn Stover Devolatilization – Matrix Inversion Method

The kinetics parameters for corn stover devolatilization were obtained via the matrix inversion method by utilizing the TGA data for heating rates 20 °C/min and 40 °C/min in the inversion algorithm and the obtained parameters were then used to predict the weight loss curves at a lower heating rate of 5 °C/min. From Figure 11-30, it is evident that there are far fewer reactions occurring during the devolatilization of corn stover when compared to that of sub-bituminous coal. The values of $f_{i,0}$ in Figure 11-30 suggest that the devolatilization of corn stover can be represented by a total of 7 reactions which includes removal of moisture.

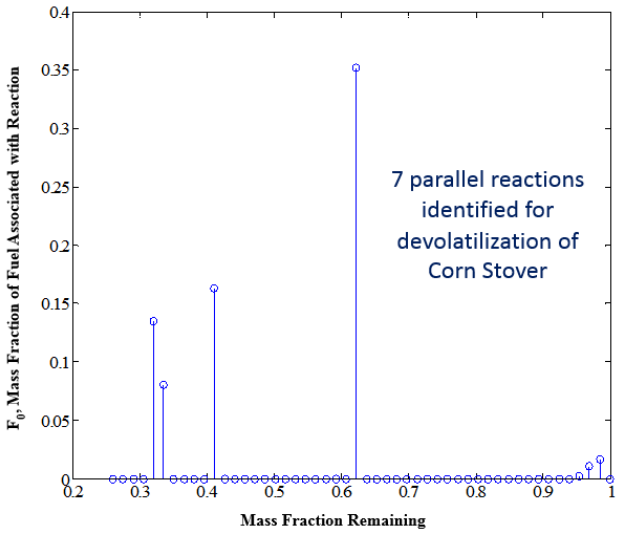



Figure 11-30. Mass fraction of fuel associated with each reaction during devolatilization of Corn Stover

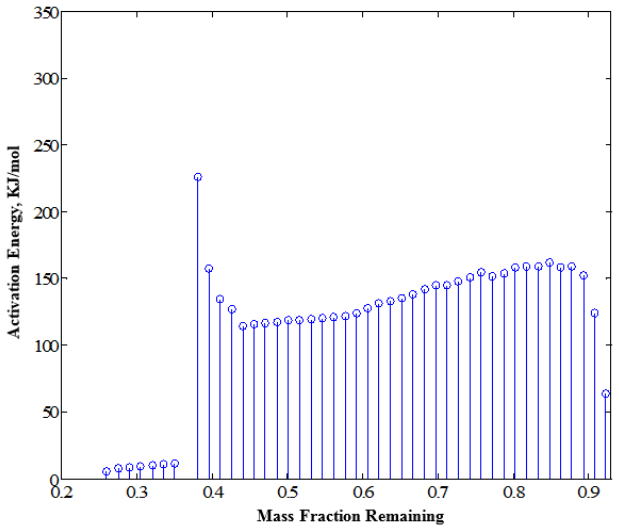



Figure 11-31. Plot of activation energy vs mass fraction remaining for pyrolysis of Corn Stover describing the values of activation energy for each parallel reaction

The range of activation energy values obtained (55-225 kJ/mol), are also comparable to the values obtained using Methods 1 and 2 described in previous sections of this chapter. Likewise, the values of pre-exponential factor have a large range of approximately 2- 1.08E+17 $min^{-1}$. From Figure 11-32 and Figure 11-33, it is evident that this method can also be used for predicting the devolatilization kinetics of high volatile biomass materials such as corn stover.

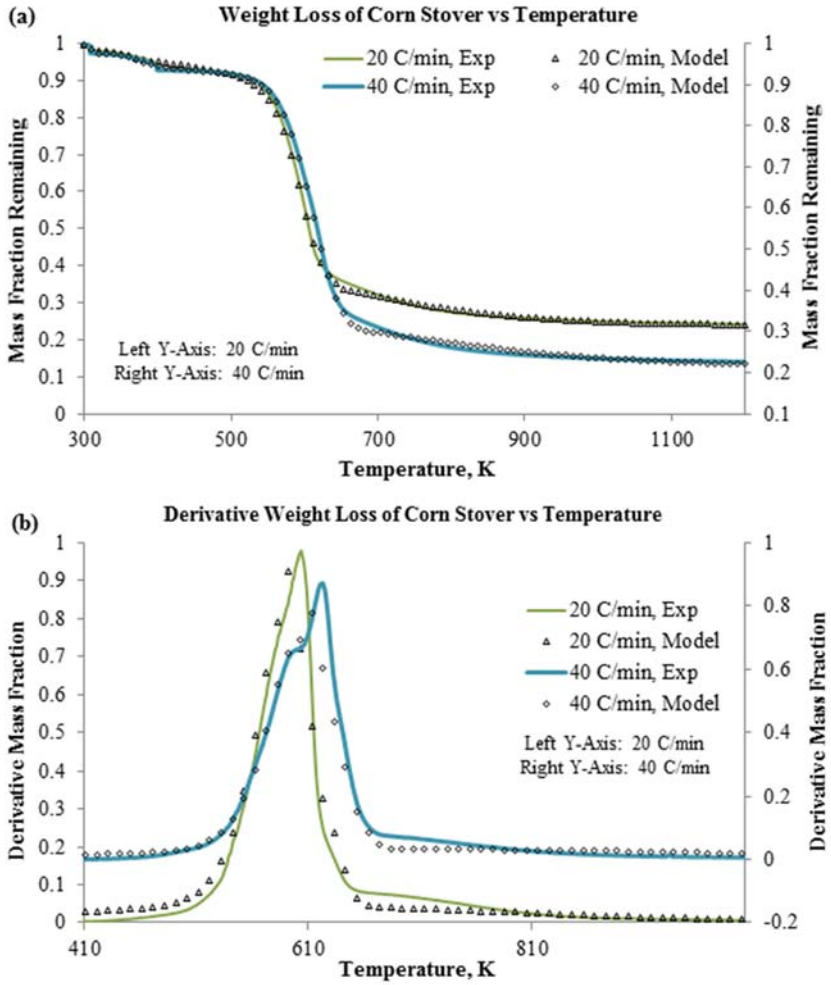



Figure 11-32. Comparison of experimental and predicted values for devolatilization of Corn Stover for two heating rates (20 °C/min and 40 °C/min) used in the matrix inversion algorithm: (a) weight loss vs temperature, and (b) derivative weight loss vs temperature

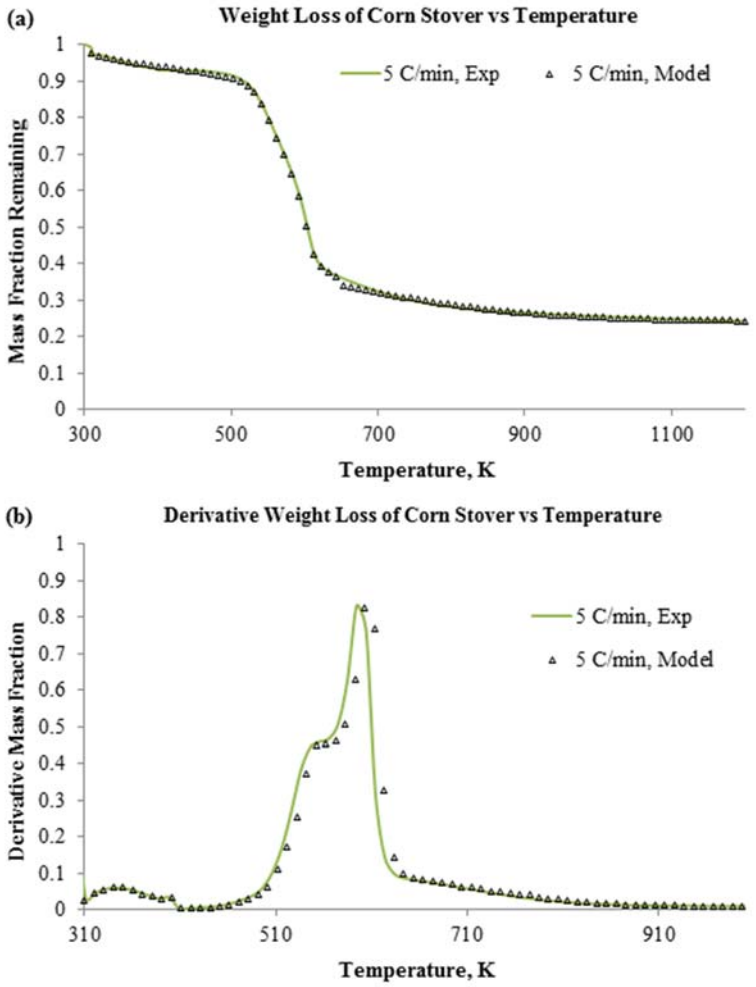



Figure 11-33. Comparison of experimental and predicted values for devolatilization of Corn Stover for the heating rate (5 °C/min) not used in the matrix inversion algorithm: (a) weight loss vs temperature, and (b) derivative weight loss vs temperature

### 11.5.4.3 Devolatilization Kinetics of 10CS90PCC Blend – Matrix Inversion Method

Once the devolatilization kinetics of single fuels were analyzed, the matrix inversion algorithm was tested on the blends of those single fuels. For illustration, the analysis of 10% corn stover blended with 90% PCC Bituminous coal is discussed in this section. The activation energy curve for the blended feedstock follows a slightly different pattern when compared to that of the single fuels, again, indicating the fact that there are certain interactions between the single fuels during devolatilization as described in previous sections. The kinetic parameters obtained even for the blended feedstocks represent the weight loss data excellently, with errors of less than 0.5% for all heating rates. This proves the effectiveness and robustness of the matrix inversion

method in representing the devolatilization of various materials when compared with other methods discussed previously.

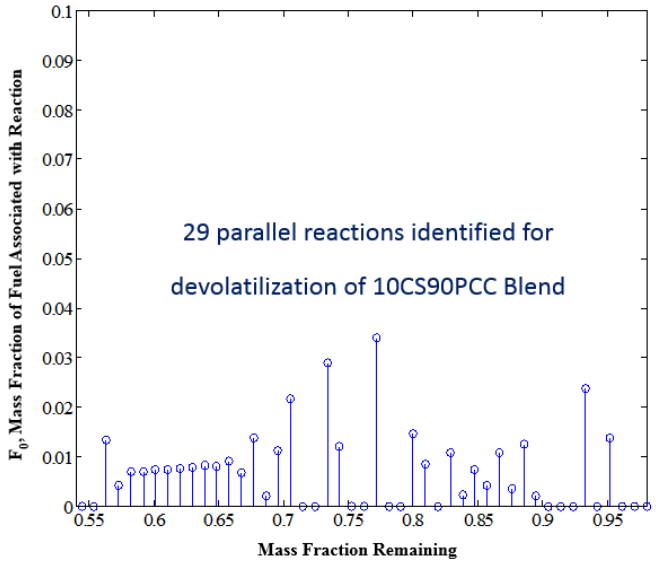



Figure 11-34. Mass fraction of fuel associated with each reaction during devolatilization of 10% Corn Stover blended with 90% PCC Bituminous coal

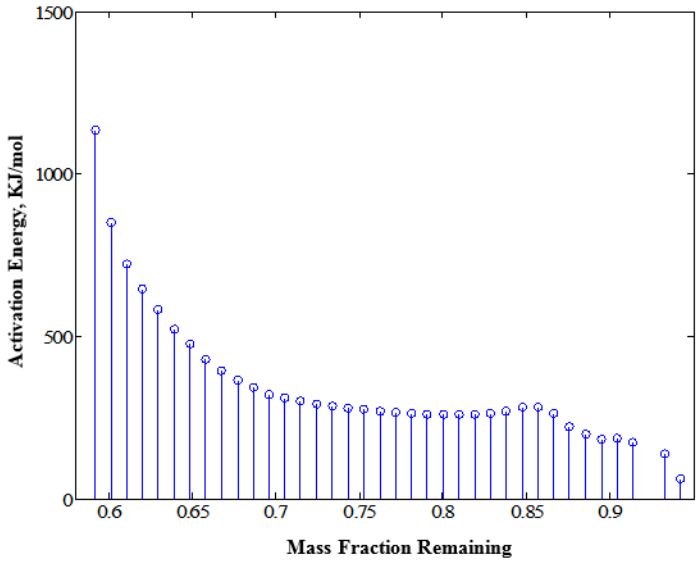



Figure 11-35. Plot of activation energy vs mass fraction remaining for pyrolysis of 10% Corn Stover-90% PCC Bituminous coal describing the values of activation energy for each parallel reaction

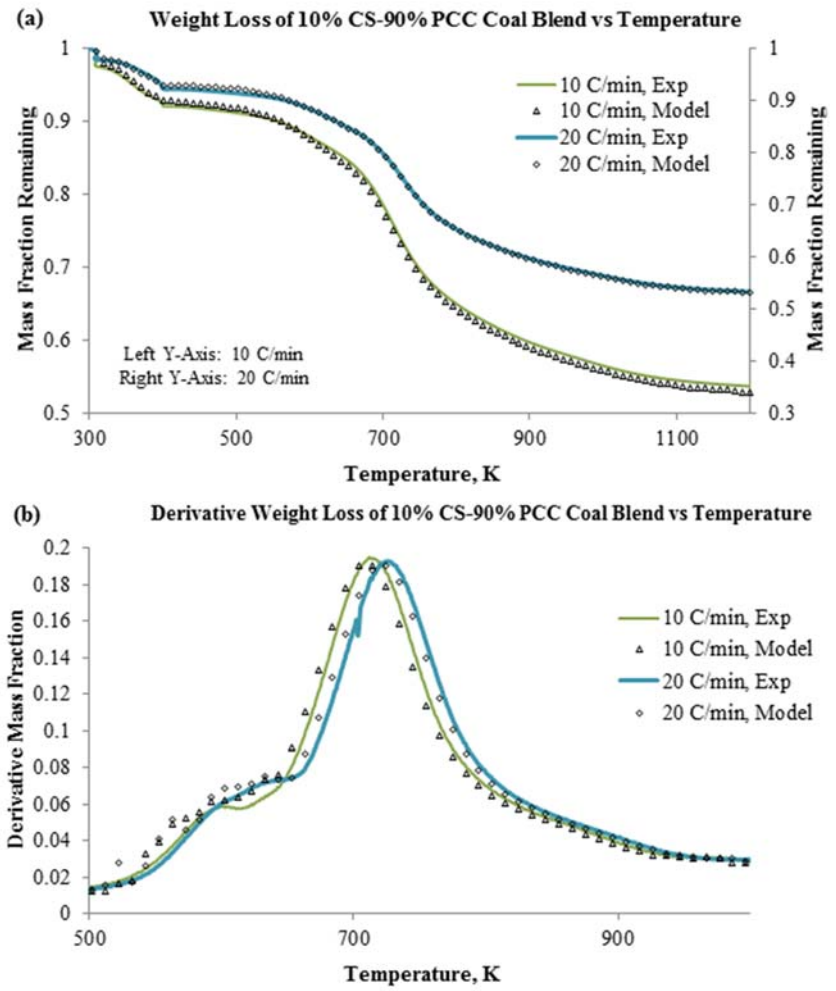



Figure 11-36. Comparison of experimental and predicted values for devolatilization of 10% Corn Stover-90% PCC Bituminous coal for two heating rates (10 °C/min and 20 °C/min) used in the matrix inversion algorithm: (a) weight loss vs temperature, and (b) derivative weight loss vs temperature

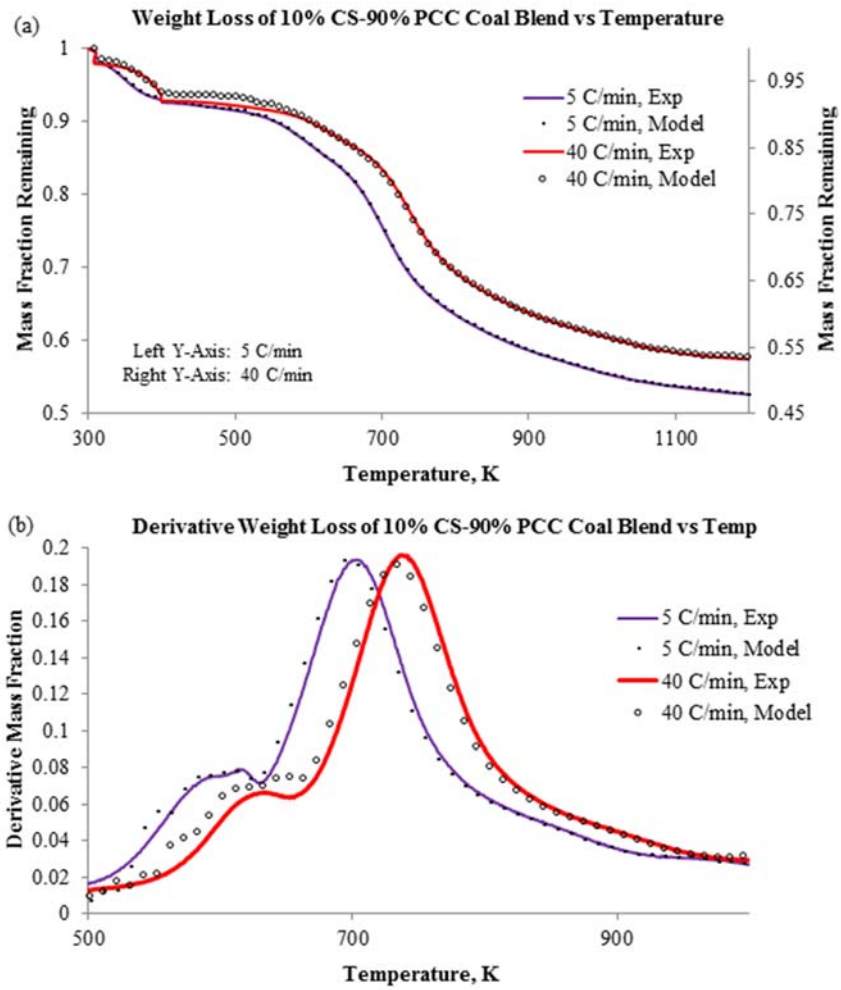



Figure 11-37. Comparison of experimental and predicted values for devolatilization of 10% Corn Stover-90% PCC Bituminous coal blend for heating rates (5 °C/min and 40 °C/min) not used in the matrix inversion algorithm: (a) weight loss vs temperature, and (b) derivative weight loss vs temperature

It is expected that the number of reactions occuring during the devolatilization of blended materials would be between those that would occur during the devolatilization of single fuels and that the number would gradually decrease with increase of high volatile matter content fuels in the blend, i.e., corn stover and switchgrass in this case. For a 10% corn stover blend with bituminous coal, as shown in Figure 11-34, the number of devolatilization reactions is 29, while only 20 reactions were observed in 30% blend of corn stover with bituminous coal as shown in Table 11-6.

Table 11-6. Pyrolysis kinetic parameters and number of devolatilization reactions obtained for various feedstocks using matrix inversion algorithm

| Feedstock Materials | No. of Reactions | Activation Energy Range, kJ/mol | Arrhenius Constant Range, $sec^{-1}$ |
|---|---|---|---|
| PCC Bituminous Coal | 35 | 84-683 | 9E+5 – 5E+32 |
| BT Sub-Bituminous Coal | 29 | 93-300 | 2E+8 – 2E+14 |
| Corn Stover (CS) | 7 | 55-226 | 7E+4 – 4E+13 |
| Switchgrass (SG) | 11 | 40-175 | 1E+0 – 2E+13 |
| 10% CS + 90% PCC | 29 | 75-722 | 2E+9 – 5E+41 |
| 30% CS + 70% PCC | 20 | 89-607 | 2E+7 – 5E+45 |
| 10% CS + 90% BT | 25 | 67-356 | 2E+5 – 6E+15 |
| 30% CS + 70% BT | 22 | 78-320 | 3E+9 – 2E+22 |
| 10% SG + 90% PCC | 28 | 112-796 | 2E+8-2E+51 |
| 30% SG + 70% PCC | 24 | 41-673 | 1E+3-8E+31 |
| 10% SG + 90% BT | 28 | 59-237 | 1E+3-4E+29 |
| 30% SG + 70% BT | 24 | 40-231 | 1E+0-5E+17 |

## 11.6 Reactivity in $CO_2$ Atmosphere

To examine and compare the results of pyrolysis and gasification reactions, the feedstock samples were subjected to heat treatment in a carbon dioxide atmosphere. Seven feedstock samples were utilized for this purpose which include both coals and blends of these coals with up to 30% by weight of corn stover (similar to the feedstocks utilized for pyrolysis experiments). The flow rate of carbon dioxide utilized in these experiments was 100 ml/min while the heating rates varied between 5 °C/min and 40 °C/min. The feedstock samples were homogenized and placed in the TGA crucible and heated from room temperature to 1000 °C in a $CO_2$ atmosphere and weight loss characteristics were analyzed. The weight loss profiles thus obtained for each feedstock material were used in estimating the kinetic parameters of char-$CO_2$ reaction or Boudouard reaction. The weight loss profiles and DTG curves (moisture free basis) with respect temperature at a heating rate of 5 °C/min for all the feedstock materials are shown in Figure 11-38 and Figure 11-39 respectively.

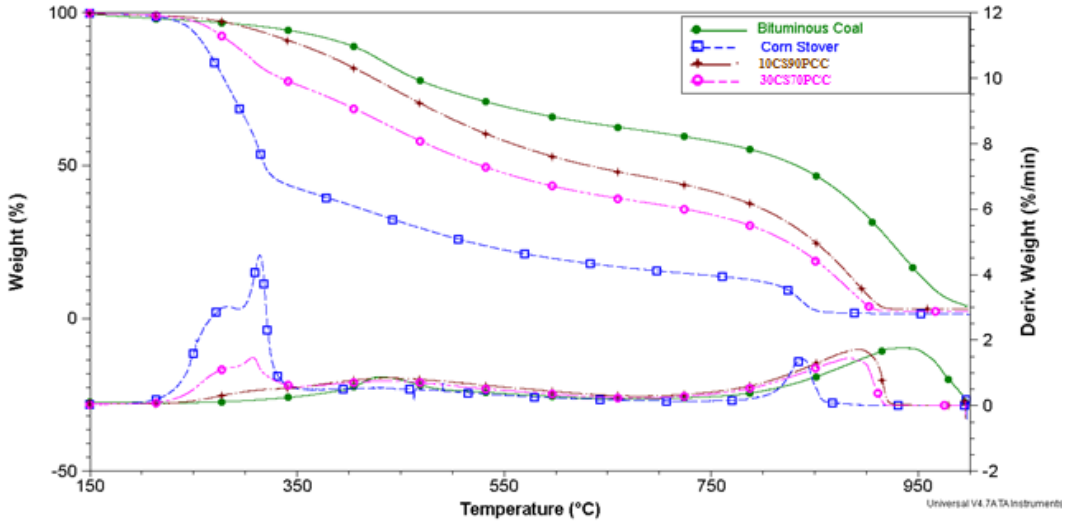



Figure 11-38. Weight loss profiles and DTG curves of Bituminous coal, Corn Stover and PCC-CS blends at a 5 °C/min heating rate in a $CO_2$ atmosphere

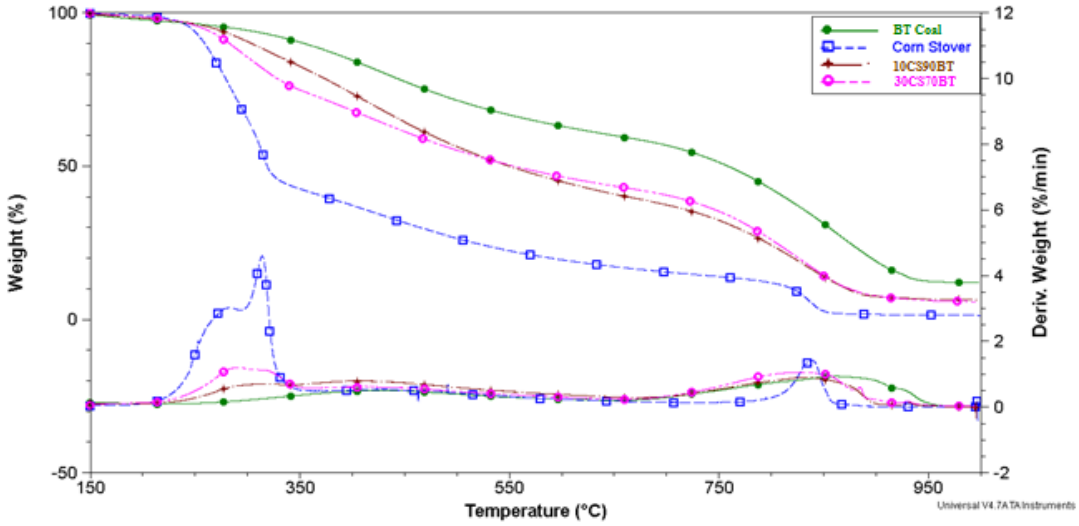



Figure 11-39. Weight loss profiles and DTG curves of Sub-bituminous coal, Corn Stover and BT-CS blends at a 5 °C/min heating rate in a $CO_2$ atmosphere

When compared with devolatization of the feedstock materials utilizing a $N_2$ atmosphere, it can be observed that the TGA curves with respect to temperature follow a similar pattern until approximately 500 °C even when pure $CO_2$ is utilized as the sweeping gas. Although the mass loss rates at low temperatures are higher in pure $CO_2$ atmosphere, the differences are only marginal. At higher temperatures, however, a significant increase in mass loss rate is observed in pure $CO_2$ atmosphere. This may be understood by the stages of coal pyrolysis process. In case of 100% $N_2$ environment, the coal pyrolysis process has two stages: release of moisture content and

devolatilization but the process of coal pyrolysis in pure $CO_2$ environment can be divided into three stages: moisture release, devolatilization and char gasification or Boudouard reaction with $CO_2$ to form CO in high temperature zone (> 500 °C) . Also, this difference may be explained due to the density difference and transport properties of these gases which are quite different (the mass of the $CO_2$ molecule is different from that of $N_2$). Moreover, the formation of char particles is larger and its surface area is also higher than that of the $N_2$ char particles. Hence, the weight loss observed in $CO_2$ environment is much higher.

### 11.6.1 Kinetic Analysis of Boudouard Reaction – Single First Order Model

Using heat flow equations based on a second order partial differential equation, Kissinger derived an equation relating the DTA peak temperature to the rate of heating, as shown in Equation 11-30 (Barkia et al., 2004; Kissinger, 1957).

$$\left. d\left(ln\left(\frac{H}{T_m^2}\right)\right) \middle/ d\left(\frac{1}{T_m}\right) \right. = -{E_a}/{R} \qquad \text{(Eq. 11-30)}$$

or,

$$ln\left(\frac{H}{T_m^2}\right) = \left(-{E_a}/{RT_m}\right) + ln\left({AR}/{E_a}\right) \qquad \text{(Eq. 11-31)}$$

where, $H$ is the rate of heating (°C/min), $T_m$ is the peak temperature, $E_a$ is the energy of activation (kJ/mol).

The Kissinger equation has been widely used to determine activation energies of reactions from DTA data. The method is based on the assumption that the DTA peak temperature corresponds to the temperature of maximum reaction rate. Nevertheless studies on metallurgical cokes and other carbons using simultaneous TG/DTG/DTA have shown that these two temperatures are very close (Barkia et al., 2004). Plots of $ln(H/T_m^2)$ vs peak temperatures for coal-corn stover blends are shown in Figure 11-40 and Figure 11-41. The activation energies and pre-exponential factors can then be obtained from the slope and intercept of each plot respectively.

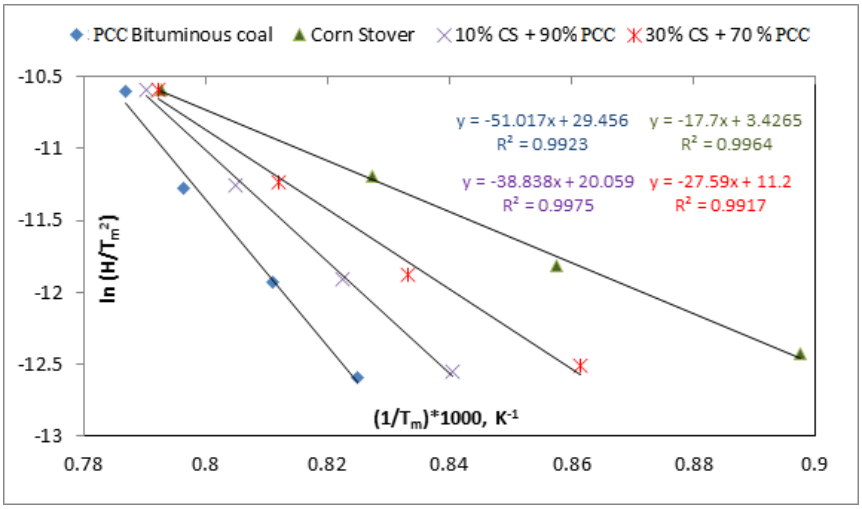



Figure 11-40. Plot for estimating the activation energy for Boudouard reaction of PCC Bituminous coal, Corn Stover and blends of PCC Bituminous coal with Corn Stover at various heating rates

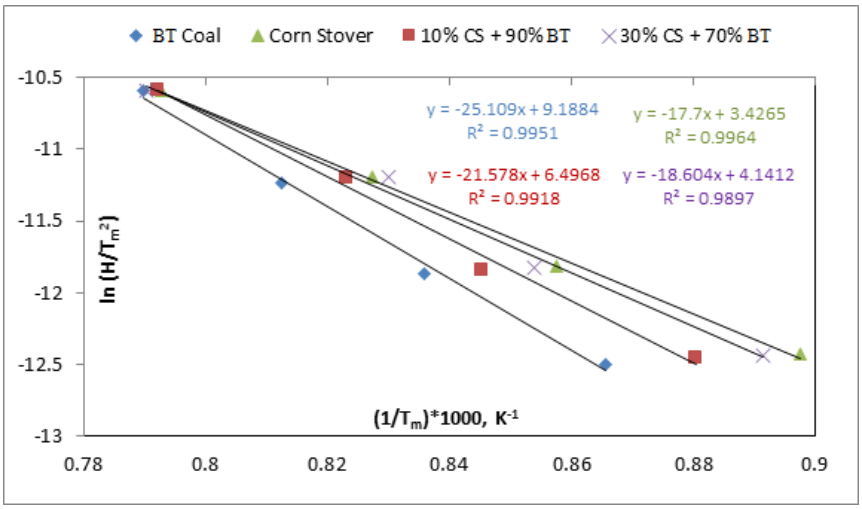



Figure 11-41. Plot for estimating the activation energy for Boudouard reaction of BT Sub-bituminous coal, Corn Stover and blends of BT Sub-bituminous coal with Corn Stover at various heating rates

The kinetic analysis performed is similar to the method described in Section 11.5.2 for devolatilization reaction, the only difference being that at high temperatures, char gasification in $CO_2$ can be represented as a single reaction as opposed to several parallel reactions which was the case while estimating devolatilization kinetics. The linear fits of the obtained experimental data, with regression coefficients greater than 0.99, suggest that the Boudouard reaction follows first order kinetics and that the assumption of using maximum peak temperatures is reasonable. The kinetic parameters obtained for each material is listed in Table 11-7.

Table 11-7. Peak temperatures at various heating rates and activation energies for heat treatment of Coal-Corn Stover blends in a $CO_2$ atmosphere obtained using thermogravimetric analysis

| Feedstock | Heating rate, °C/min | Peak Temperature $T_m$, K | Pre-Exponential Factor, $min^{-1}$ | Activation Energy, kJ/mol |
|---|---|---|---|---|
| PCC Bituminous Coal | 5 | 1212.29 | 3.2E+14 | 424.16 |
| | 10 | 1233.19 | | |
| | 20 | 1255.48 | | |
| | 40 | 1270.97 | | |
| BT Sub-Bituminous Coal | 5 | 1155.34 | 2.5E+05 | 208.76 |
| | 10 | 1196.19 | | |
| | 20 | 1230.86 | | |
| | 40 | 1266.13 | | |
| Corn Stover (CS) | 5 | 1114.17 | 5.4E+02 | 147.16 |
| | 10 | 1166.19 | | |
| | 20 | 1208.86 | | |
| | 40 | 1261.31 | | |
| 10% CS + 90% PCC | 5 | 1189.91 | 2.0E+10 | 322.90 |
| | 10 | 1215.82 | | |
| | 20 | 1242.30 | | |
| | 40 | 1265.16 | | |
| 30% CS + 70% PCC | 5 | 1160.81 | 2.0E+06 | 229.38 |
| | 10 | 1200.10 | | |
| | 20 | 1231.64 | | |
| | 40 | 1262.40 | | |
| 10% CS + 90% BT | 5 | 1135.67 | 1.4E+04 | 179.40 |
| | 10 | 1182.96 | | |
| | 20 | 1214.87 | | |
| | 40 | 1262.30 | | |
| 30% CS + 70% BT | 5 | 1121.67 | 1.2E+03 | 154.67 |
| | 10 | 1170.96 | | |
| | 20 | 1204.87 | | |
| | 40 | 1265.30 | | |

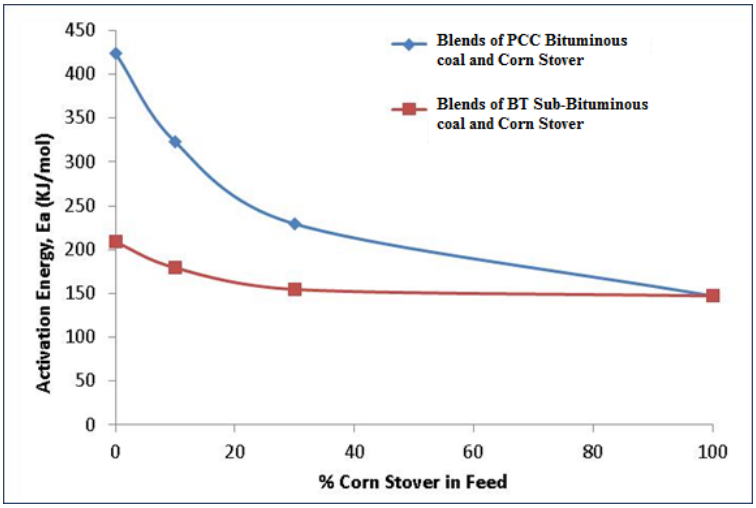



Figure 11-42. Variation in activation energy of Boudouard reaction with increasing percentage of Corn Stover in blends with Bituminous and Sub-bituminous coals

Values of the kinetic parameters and peak temperatures obtained, as seen from Table 11-7, indicate that temperature at which the char-$CO_2$ reaction occurs decreases with increasing percentage of corn stover in the blend. Clearly, the activation energy decreases with increasing percentage of corn stover in the feedstock as shown in Figure 11-42. Assessment of the kinetics indicated that while the overall range of activation energy had not reduced significantly in blends with sub-bituminous coal, the amount of material reacting with the more reactive kinetics within the reaction system had increased after addition of corn stover. This indicates certain positive synergistic behavior exists between the blends. The shift in mass fraction and lowered temperature range of the reaction, all serve to confirm this hypothesis for these particular samples. A possible cause for the effect could be the fact that the mineral content inherently present in biomass has catalytic effects which improves the $CO_2$ reactivity during gasification of biomass and of coal-biomass blends and that the activation energies obtained are lowered compared to those of coals, implying that biomass is a viable fuel source for co-gasification (Zhu et al., 2008; Vamvuka et al., 2011; Vittee, 2012).

### 11.6.2 Kinetic Analysis of Boudouard Reaction – Matrix Inversion Algorithm

The single first order reaction model described in Section 11.6.1 is applicable only in the high temperature zone where only the char or fixed carbon of the solid fuel remaining after devolatilization reacts with $CO_2$. Hence, the model may not be able to predict the weight loss characteristics when pure $CO_2$ is used as the sweep gas over the full temperature range where devolatilization of the feedstock followed by char gasification occurs. In order to overcome this drawback and predict the weight loss of the solid feedstock reacting in a $CO_2$ environment, the matrix inversion algorithm (described in Section 11.5.3), previously utilized for accurately predicting the devolatilization reaction kinetics in an inert nitrogen atmosphere, was further extended for predicting the kinetics of any feedstock material undergoing thermal degradation in a $CO_2$ atmosphere. Since it has already been established that both devolatilization and char gasification can be represented with first order kinetics, utilizing this algorithm is logically viable.

For illustrative purposes, the results of the algorithm are presented for one coal (PCC Bituminous coal), one biomass (corn stover) and one blend of both single fuels (10% corn stover blended with 90% PCC bituminous coal). Figure 11-43 describes the mass loss of PCC

Bituminous coal in a $CO_2$ atmosphere on a dry basis (i.e. after the complete removal of moisture and letting the initial temperature for the algorithm to be 400 K). The inversion algorithm was then applied to the TGA data at various heating rates and kinetic parameters were obtained at various conversions. Similar to the results described for the pyrolysis model, obtained kinetic parameters were then used to model the reactions at unknown heating rates that were not used in the algorithm. The obtained weight loss data was then compared with real TGA data for comparison and accuracy of the method.

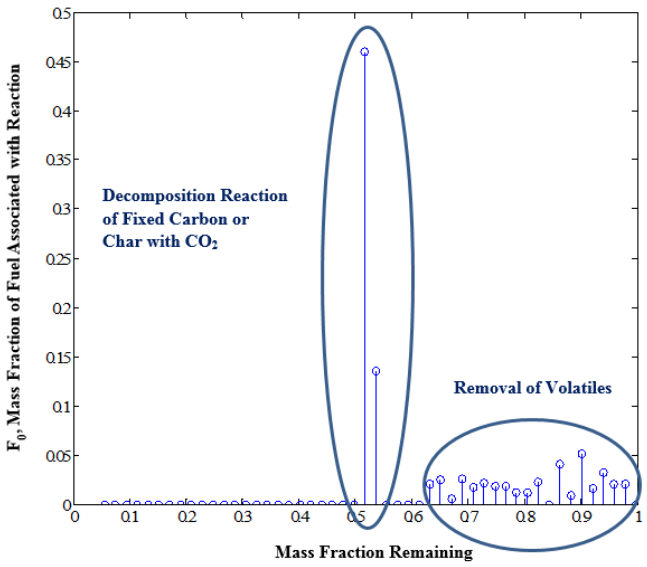



Figure 11-43. Stem plot of mass fraction of fuel associated with each reaction occurring during decomposition of PCC Bituminous coal in $CO_2$ atmosphere obtained using DAEM (matrix inversion algorithm)

Clearly, certain differences can be observed when comparing mass loss of bituminous coal in $N_2$ and $CO_2$ environments as seen from Figure 11-25 and Figure 11-43, respectively. Two separate mass loss zones are present when the coal is decomposing in $CO_2$ environment as opposed to just one zone occurring during pyrolysis in $N_2$ atmosphere. The second region in Figure 11-43 where a sharp loss in mass occurs and the mass fraction of fuel associated with the decomposition reaction is high, is the region corresponding to the reaction between fixed carbon or remaining char and $CO_2$.

## 11.7 Summary and Conclusions

Thermogravimetric analysis was performed on nine feed materials (i.e. three single fuels and four blends), and the pyrolysis characteristics were analyzed. The kinetic parameters were determined for the pyrolysis reaction using a non-isothermal mode of operation and single first order reaction model at a heating rate of 5 °C/min. The lower final weight loss of sub-bituminous coal is related to the high content of fixed carbon which is not decomposed in this temperature range. Also, it can be observed that corn stover has the highest weight loss percentage. This trend is due to the high volatile content and low fixed carbon content in corn stover as compared to coals. Furthermore, the pyrolysis temperature range decreased with an increase in the concentration of corn stover in the blends due to the fact that corn stover has a much higher weight loss rate when compared to that of the coals.

The pyrolysis of both coals can be reasonably described as a process with three consecutive first order reactions with distinct temperature zones while corn stover and the blends have two and four distinct temperature zones respectively, where the first-order kinetic analysis can be applied. Also, it was observed that the second thermal event during the coal pyrolysis has the highest activation energy of 149 kJ/mol for PCC Bituminous coal and 78 kJ/mol for BT Sub-Bituminous coal. As for corn stover, the major pyrolysis region is in the temperature range of 136-350 °C where a majority (77%) of the mass fraction is removed with an activation energy of 104 kJ/mol. It can also be seen that the activation energies of the blends are not simply additive in nature further indicating a possibility of interactions between the individual fuels. Apart from this, a thorough investigation into the synergistic behavior between single fuels in the blends has been performed with the conclusion that there are definite interactions between the PCC Bituminous coal and corn stover in the temperature range of 230-450 °C. But, in the case of blends of BT Sub-Bituminous coal and corn stover, minimal synergistic behavior was observed only at lower concentrations of corn stover starting at a temperature of about 320 °C and no synergistic interactions were observed during devolatilization of switchgrass blends.

Finally, three different kinetic models for pyrolysis in $N_2$ atmosphere have been discussed in this chapter of which the matrix inversion algorithm predicts the kinetic parameters such that the weight loss characteristics can be best represented for both single fuels as well as blends of coals and biomass materials. Also, weight loss characteristics of unknown fuel blends at unknown heating rates can be effectively predicted within 1% error through the use of this

algorithm. Also, the weight loss characteristics of coal-biomass blends in a $CO_2$ environment have been compared with those of $N_2$ atmosphere and the kinetic parameters for the Boudouard reaction have been predicted using a single first order reaction and maximum decomposition rate at temperatures greater than 500 °C.

# Chapter 12

# Experimental Moving Bed Gasification of Coal–Biomass Blends

## 12.1 Laboratory Scale Moving Bed Gasifier: Design & Operation

A laboratory-scale gasification system was designed and constructed for the purpose of gasifying the blends of coal and biomass discussed in Chapter 11. The core of the system is an updraft gasifier, where pressure and temperature profiles are measured by a pressure transducer and a set of thermocouples, respectively. Coal/biomass is fed at the top of the gasifier by means of a quick-open flange. Air/oxygen and steam is fed at the bottom of the gasifier and its rate is measured by a rotameter. The design utilizes a single condenser wherein the hot outlet gas enters a cold zone controlled using a refrigerator so that unreacted water and other solids can be collected more efficiently ensuring that clean gas enters the gas chromatograph. The air is sent in through the middle of the reactor so that heat coming out of the reactor can be used to preheat the air entering the reactor ensuring better use of waste heat. The stainless steel tube was utilized in order to improve the heat transfer upwards in the reactor.

The gasifier is a 0.9 meter (3 ft) long cylindrical stainless steel modular flange assembly having an internal diameter of 34.8 millimeters (1.37 in) fitted with another stainless steel tube of 1.9 millimeters (0.075 in) thick on the inside to promote better heat transfer in the axial direction. An initial comparative study was also performed with an inner quartz tube of similar dimensions as that of the stainless steel tube and the outlet product gas compositions were analyzed for the gasification of both coals at various oxygen/steam ratios. The inner tube is fitted with a stainless steel grate with holes large enough to let the ash pass through but small enough to hold the feed material. The grate is connected to a mechanical rotary linear feedthrough to periodically remove ash. The bottom zone, under the grate, has another cylindrical stainless steel flange with a height of about 127 millimeters (5 in) to collect and then discharge the ash produced in the process. The grate at the bottom of the gasifier is used not only for holding the solid particles together but also

as an oxidant distributor. The oxidant, fed at the bottom of the reactor, flows along the channels and exits through the small holes along the grate, so it is distributed across the whole section of the gasifier. At the bottom, a small tube allows the use of pre-heated steam to enter the bed. Temperature profiles along the gasifier axis are measured by a set of K-type thermocouples placed within a steel protective tube.

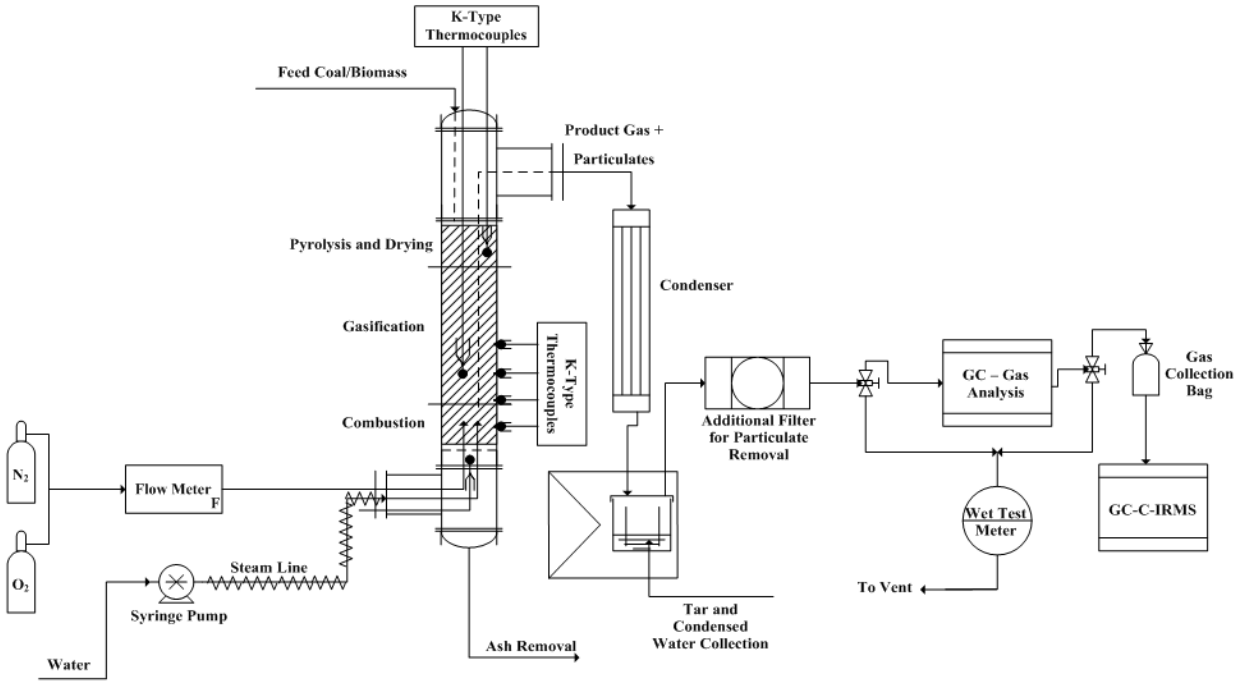



Figure 12-1. Schematic of the laboratory scale moving bed gasification system

The feeding system is constituted by a conical chamber enclosed in a quick-open flange about 127 millimeters (5 in) in height. The product gas stream flows through two condensers where the condensed liquids flow down the tubes and also capture the solid particles entrained by the gas. At the bottom, the liquid phase is discharged and collected for analysis. Condensers, wet scrubbing, packed bed, and cartridge filters constitute the gas-cleaning system, which though not optimized, guarantees a gas sufficiently clean for gas-chromatographic analysis (GOWMAC Auto System GC equipped with thermal conductivity detector (TCD) and a packed column). Gas sampling and analysis are carried out at selected times during the whole duration of the tests.

There are two possible operation modes of the gasifier, corresponding to a constant or a variable bed height. In the first modality, after ignition, the bed height is brought to the desired value and maintained constant. This is achieved by feeding the solid material at proper time

intervals. Therefore, as a consequence of variations in the oxidant flow rate, the oxidant-to-fuel ratio will also vary, given that the fuel feed rate is the adjustable variable to control the (constant) bed height. The feeding process is an important aspect in the operation of fixed-bed gasifiers. The rate of feed consumption is essentially dependent on the intrinsic reactivity and the rate of oxidant supply. Sufficient feed can be added to keep the bed height at a constant value. However, as the rate of feed consumption increases with the oxidant flow rate, the feeding frequency should also be properly adjusted. In particular, a limit is expected at very high flow rates, when the feeding frequency becomes so high that a semi-continuous procedure is no longer possible. The rate of feed consumption can also be adjusted by choosing a proper rate of solid discharge at the grate, but this may be problematic for small-scale systems. Indeed, frequent solid discharge causes significant heat loss (the discharged solid is at a high temperature), with the introduction of instabilities in the gasification process.

In the second modality, gasification tests can be made for different oxidant-to-fuel ratios, thus allowing the bed height to vary. For instance, after the selection of the oxidant flow rate, the fuel feed rate can be varied and, consequently, the bed height will also vary. However, it can be understood that there is again a limit at very low fuel feed rates, when the continuous operation approaches the behavior of a batch system and the processes of drying/devolatilization, on one side, and gasification/combustion, on the other side, tend to become uncoupled.

The first step in the gasification process is the ignition of the bed. This is caused by adding small amounts of externally heated charcoal particles onto the grate while supplying the oxidant at low flow rates of approximately 100 ml/min to 150 ml/min. The feed material is then added onto the charcoal particles and the oxidant flow rate is increased, thus causing ignition of the bed. Once the bed is ignited, pre-heated steam is allowed to enter the bed through the grate at the bottom. Experiments have been performed with varying oxygen flow rates ranging from 150 ml/min to 650 ml/min and varying steam flow rates of 150 ml/min to 1600 ml/min. Apart from varying the oxygen to steam ratio, tests have also been performed with varying oxygen partial pressure on PCC Bituminous coal.

## 12.2 Gasification with Varying Oxygen/Steam Ratio

### 12.2.1 Quartz Insulation

The gasification of PCC Bituminous coal was first carried out in the moving bed gasifier using an internal quartz insulation with varying oxygen to steam ratios. The oxygen flow rate was constant at 650 ml/min while the flow rates of steam were varied from 0 to 1625 ml/min. The average composition of the product gases and the calculated energy efficiency values are provided in Table 12-1 and Table 12-2 respectively.

Table 12-1. Average composition of product gases obtained during gasification of PCC Bituminous coal with varying oxygen to steam ratios

| Feedstock Weight, g | $H_2O:O_2$ | Average Values | | | | | | |
|---|---|---|---|---|---|---|---|---|
| | | $H_2:CO$ | $CO:CO_2$ | $(H_2+CO):CO_2$ | $H_2$ % | CO % | $CH_4$% | $CO_2$ % |
| 75 | 0.00 | 0.14 | 0.90 | 1.02 | 5.39 | 39.52 | 1.43 | 44.02 |
| 115 | 1.00 | 0.37 | 0.78 | 1.07 | 12.35 | 33.57 | 1.35 | 42.93 |
| 110 | 1.50 | 0.48 | 0.72 | 1.08 | 15.09 | 30.26 | 1.31 | 42.16 |
| 85 | 2.00 | 0.81 | 0.49 | 0.88 | 17.31 | 21.36 | 1.58 | 41.81 |
| 235 | 2.50 | 0.91 | 0.47 | 0.90 | 18.23 | 20.12 | 1.29 | 40.78 |

Table 12-2. Calculated energy efficiency during gasification of PCC Bituminous coal with varying oxygen to steam ratios

| $H_2O:O_2$ | Max $H_2:CO$ | Max $CO:CO_2$ | Energy Input (kJ) | Energy Output (kJ) | Efficiency, % |
|---|---|---|---|---|---|
| 0.00 | 0.15 | 1.03 | 1504 | 378 | 27.9 |
| 1.00 | 0.55 | 0.82 | 2614 | 953 | 42.9 |
| 1.50 | 0.59 | 0.74 | 2499 | 1067 | 49.8 |
| 2.00 | 0.90 | 0.46 | 1990 | 676 | 40.4 |
| 2.50 | 1.20 | 0.46 | 5437 | 1922 | 40.4 |

Once the composition of the product species is obtained, the gross heating value of the gases and the energy conversion efficiency of the gasifier can be calculated using the following equations (Gordillo et al., 2009).

$$GHV_{gases} = \sum_i GHV_i X_i \quad \text{(Eq. 12-1)}$$

where, $GHV_i$ is the gross heating value in kJ/m$^3$ and $X_i$ is the mole fraction of the fuel gases (i = CO, $CH_4$ and $H_2$).

$$\eta_{gas} = GHV_{gases} \,/\left[N_{fuel} * GHV_{fuel} + N_{steam} * 18\{\lambda + 4.18(373 - 298)\}\right] \quad \text{(Eq. 12-2)}$$

where, $N_{fuel}$ and $N_{steam}$ correspond to the moles of fuel and steam supplied, respectively, to the gasifier and $\lambda$ is the enthalpy of vaporization. $GHV_{fuel}$ is the gross heating value of the fuel in kJ/kg and $\eta$ is the energy conversion efficiency.

Figure 12-2 through Figure 12-4 describe the results obtained during the gasification of bituminous coal for varying steam to oxygen ratios. As seen from Figure 12-2, the increase in the amount of steam fed to the gasifier at constant oxygen flow rate (increased atoms of hydrogen supplied to the gasifier) results in an increase in the hydrogen percentage and a decrease in the percentage of carbon monoxide and carbon dioxide. The amount of methane produced should also increase with the steam supplied to gasifier. However, as the amount of methane produced during all the experiments was less than 2%; it was difficult to establish a trend for methane using the obtained data.

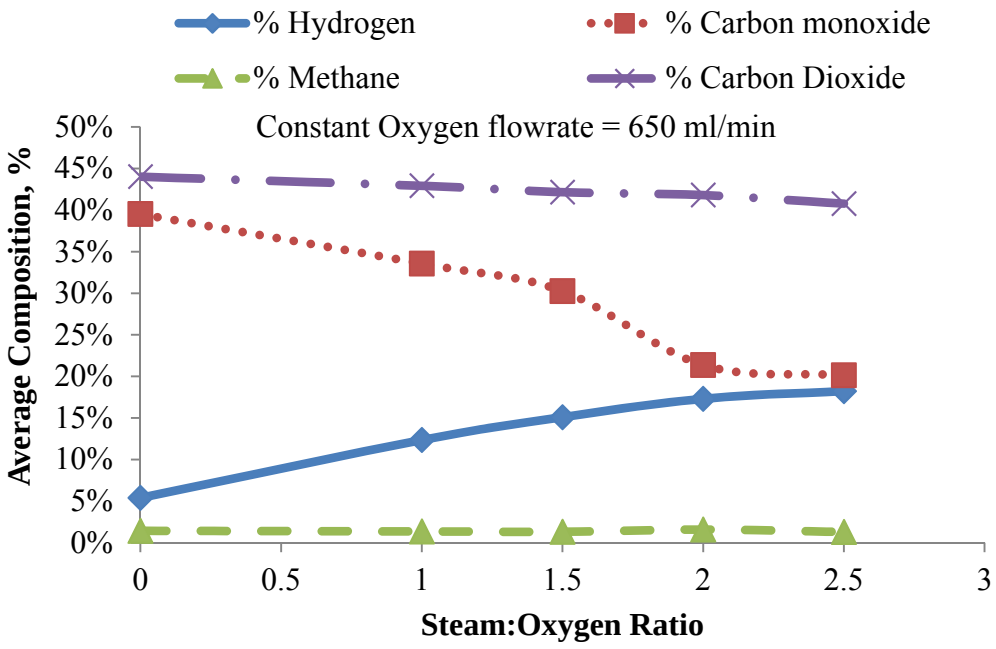



Figure 12-2. Average compositions of the product gases obtained during gasification of bituminous coal with varying steam to oxygen ratios

When experiments were performed with a steam to oxygen ratio above 2.5 in the non-externally heated moving-bed gasifier, the combustion zone at the bottom of gasifier was extinguished in a very short period of time. Increasing steam flow rates to higher values imply

decreasing the oxygen supplied to the gasifier. Thus, the exothermic reaction heat is not sufficient to maintain self-sustained reaction.

Figure 12-3, using the data from the same experiment, shows that the ratio of carbon monoxide to carbon dioxide in the product stream decreases with an increase of steam supplied to the gasifier. Similarly, the ratio of syngas produced to the amount of carbon dioxide produced, increases up to a certain value of steam to oxygen ratio (Steam:$O_2$ = 1.5) and then decreases. This is due to the reason that the production of carbon monoxide diminishes with increasing steam ratio.

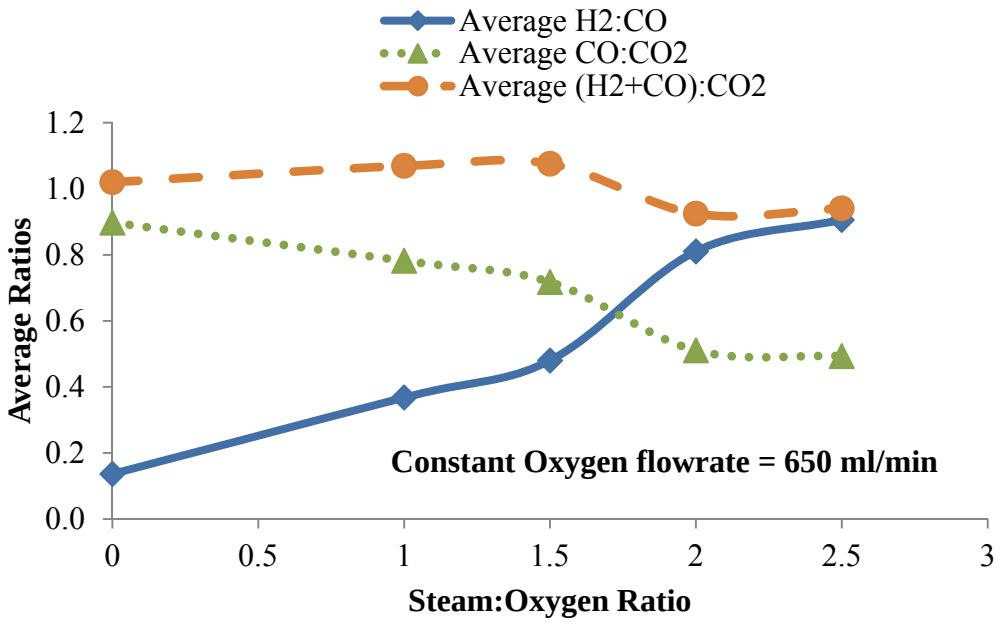



Figure 12-3. Average ratios of the product gases obtained during gasification of sub-bituminous coal with varying steam to oxygen ratios

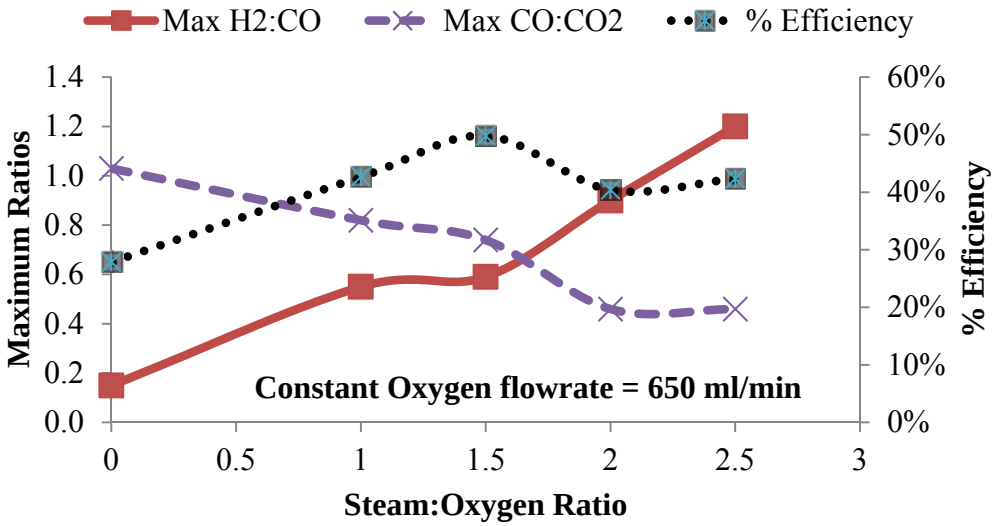



Figure 12-4. Maximum ratios of the product gases and efficiency obtained during gasification of sub-bituminous coal with varying steam to oxygen ratios

It can be observed from Figure 12-4. that the energy conversion efficiency, as described in Equation 12-2, increases up to a steam ratio of 1.5 and then decreases with higher steam ratios. The highest energy conversion efficiency obtained is approximately 50% at a steam ratio of 1.5. The efficiency decreases for steam ratios above 1.5 since the exothermic zone at the bottom of the bed is either no longer available or that the endothermic zone is much more prevalent at higher steam ratios.

### 12.2.2 Stainless Steel Reactor

As previously stated, a comparative study on the effectiveness of using an inner stainless steel tubing in place of quartz tubing was performed at various oxygen/steam ratios for PCC Bituminous coal. This was done in order to improve the heat transfer in the axial direction and thereby improve the useful product gas composition in the outlet gas and also improve the overall efficiency of the gasifier. The product gas compositions and efficiency at various O2/steam ratios for gasification of PCC bituminous coal are presented in Table 12-3.

Table 12-3. Average composition of product gases obtained during gasification of bituminous coal at varying $O_2$/steam ratios in the lab scale stainless steel moving bed gasifier

| Material | Air Flow Rate, ml/min | $O_2$ Flow Rate, ml/min | Steam Flow, ml/min | Steam: $O_2$ | $H_2$:CO | CO: $CO_2$ | ($H_2$+CO): $CO_2$ | Avg. Product Gas Composition | | | | Efficiency % |
|---|---|---|---|---|---|---|---|---|---|---|---|---|
| | | | | | | | | $H_2$ % | CO % | $CH_4$ % | $CO_2$ % | |
| PCC Bituminous Coal | | 650 | 0 | 0 | 0.39 | 0.79 | 1.10 | 12.85 | 32.96 | 3.50 | 41.71 | 47.2 |
| | | 650 | 325 | 0.5 | 0.66 | 0.75 | 1.24 | 20.53 | 31.27 | 3.21 | 41.69 | 45.9 |
| | | 650 | 650 | 1 | 0.93 | 0.63 | 1.21 | 24.39 | 26.13 | 3.09 | 41.68 | 53.6 |
| | | 650 | 1300 | 2 | 1.23 | 0.51 | 1.13 | 26.65 | 21.63 | 2.53 | 42.66 | 58.3 |
| | 1400 | 300 | 0.00 | 0 | 0.84 | 0.42 | 0.78 | 4.94 | 5.90 | 0.00 | 13.92 | 19.6 |
| | 1400 | 300 | 150 | 0.5 | 0.96 | 0.40 | 0.78 | 5.27 | 5.48 | 0.00 | 13.83 | 21.0 |
| | 1400 | 300 | 300 | 1 | 1.19 | 0.37 | 0.80 | 5.95 | 5.01 | 0.00 | 13.68 | 23.1 |
| | 1400 | 300 | 600 | 2 | 1.64 | 0.33 | 0.88 | 7.35 | 4.48 | 0.28 | 13.51 | 23.9 |

Clearly, with an increase in the concentration of steam in the gasifier the trends of the product gas compositions are similar to those obtained using an inner quartz lining. But, it must be noted here that the percentage of hydrogen generated at same operating conditions is much higher due to the increase in bed temperature (complete consumption of oxygen which was not achieved when using a quartz insulation) and transfer of heat upwards in the axial direction and thus, better heat utilization which improved the overall efficiency by at least 20% when the steam concentration was at its maximum in the gasifier. Also, unlike the quartz insulation where the efficiency increased only until a certain point and the maximum steam/$O_2$ ratio that could be utilized was 1.5, in this experimental set-up, the efficiency increased steadily until a steam/$O_2$ ratio of 2:1. Apart from this, the ratios of $H_2$/CO, CO/$CO_2$ and syngas/$CO_2$, which dictate the quality of the product gas, are markedly higher as compared with the previous experimental set-up. Hence, the current experimental set-up was utilized for analyzing the product gas trends during the gasification of various blends of coals and biomass materials.

#### 12.2.2.1 Blends with Corn Stover

Corn Stover was blended with both coals at various percentages, the maximum composition being 30% by weight of corn stover. Blending higher concentrations of corn stover (>30% by weight was not feasible) resulted in the reactions inside the gasifier being extinguished due to low temperatures achieved at the bottom of the gasifier. The blends of both coals with corn stover were gasified at various $O_2$/steam ratios and air/steam ratios and the product gas trends analyzed accordingly. Table 12-4 and Table 12-5 provide an insight into these compositions and effect of addition of biomass to coal on these compositions.

Table 12-4. Average composition of product gases obtained during gasification of blends of bituminous coal and corn stover at varying $O_2$/steam ratios in the lab scale stainless steel moving bed gasifier

| Material | Air Flow Rate, ml/min | $O_2$ Flow Rate, ml/min | Steam Flow, ml/min | Steam: $O_2$ | $H_2$:CO | CO:$CO_2$ | ($H_2$+CO): $CO_2$ | Avg. Product Gas Composition | | | | Efficiency % |
|---|---|---|---|---|---|---|---|---|---|---|---|---|
| | | | | | | | | $H_2$ % | CO % | $CH_4$ % | $CO_2$ % | |
| 90% PCC + 10% CS | | 650 | 325 | 0.5 | 0.61 | 0.74 | 1.19 | 19.41 | 31.94 | 6.79 | 43.29 | 48.5 |
| | | 650 | 650 | 1 | 0.87 | 0.61 | 1.14 | 23.19 | 26.58 | 6.18 | 43.69 | 51.1 |
| | | 650 | 1300 | 2 | 1.18 | 0.51 | 1.12 | 26.11 | 22.17 | 5.46 | 43.13 | 53.3 |
| | 1400 | 300 | 150 | 0.5 | 1.35 | 0.24 | 0.57 | 4.54 | 3.36 | 0.00 | 13.91 | 20.5 |
| | 1400 | 300 | 300 | 1 | 1.21 | 0.38 | 0.85 | 6.57 | 5.45 | 0.07 | 14.17 | 44.6 |
| | 1400 | 300 | 600 | 2 | 1.27 | 0.42 | 0.96 | 7.83 | 6.18 | 0.17 | 14.59 | 48.2 |
| 80% PCC + 20% CS | | 650 | 325 | 0.5 | 0.54 | 0.53 | 0.81 | 13.79 | 25.34 | 6.01 | 48.17 | 20.3 |
| | | 650 | 650 | 1 | 0.69 | 0.48 | 0.81 | 15.64 | 22.56 | 5.94 | 47.43 | 32.4 |
| | | 650 | 1300 | 2 | 0.92 | 0.43 | 0.82 | 18.43 | 20.11 | 5.83 | 47.11 | 37.1 |
| | 1400 | 300 | 150 | 0.5 | 0.97 | 0.35 | 0.69 | 4.59 | 4.74 | 0.11 | 13.50 | 23.1 |
| | 1400 | 300 | 300 | 1 | 1.22 | 0.43 | 0.95 | 7.23 | 5.92 | 0.00 | 13.80 | 47.1 |
| | 1400 | 300 | 600 | 2 | 1.22 | 0.45 | 0.99 | 7.45 | 6.11 | 0.00 | 13.73 | 50.4 |
| 70% PCC + 30% CS | | 650 | 325 | 0.5 | 0.67 | 0.32 | 0.54 | 12.19 | 18.13 | 5.08 | 56.67 | 21.0 |
| | | 650 | 650 | 1 | 0.91 | 0.28 | 0.53 | 14.27 | 15.73 | 4.29 | 56.79 | 25.0 |
| | | 650 | 1300 | 2 | 1.29 | 0.23 | 0.53 | 16.93 | 13.09 | 4.00 | 56.17 | 28.6 |
| | 1400 | 300 | 150 | 0.5 | 1.33 | 0.22 | 0.51 | 4.34 | 3.25 | 0.00 | 14.86 | 25.3 |
| | 1400 | 300 | 300 | 1 | 1.36 | 0.34 | 0.81 | 7.18 | 5.28 | 0.00 | 15.44 | 41.3 |
| | 1400 | 300 | 600 | 2 | 1.44 | 0.41 | 1.00 | 8.91 | 6.21 | 0.00 | 15.13 | 43.5 |

Table 12-5. Average composition of product gases obtained during gasification of blends of sub-bituminous coal and corn stover at varying $O_2$/steam ratios in the lab scale stainless steel moving bed gasifier

| Material | Air Flow Rate, ml/min | $O_2$ Flow Rate, ml/min | Steam Flow, ml/min | Steam: $O_2$ | $H_2$:CO | CO:$CO_2$ | ($H_2$+CO): $CO_2$ | Avg. Product Gas Composition | | | | Efficiency % |
|---|---|---|---|---|---|---|---|---|---|---|---|---|
| | | | | | | | | $H_2$ % | CO % | $CH_4$ % | $CO_2$ % | |
| BT Coal | - | 650 | 0 | 0 | 0.35 | 0.78 | 1.05 | 12.40 | 35.73 | 2.39 | 45.97 | 58.1 |
| | | 650 | 325 | 0.5 | 0.47 | 0.74 | 1.09 | 16.14 | 34.43 | 1.95 | 46.37 | 55.2 |
| | | 650 | 650 | 1 | 0.75 | 0.61 | 1.06 | 20.81 | 27.58 | 1.73 | 45.47 | 58.8 |
| | | 650 | 1300 | 2 | 1.17 | 0.48 | 1.04 | 25.83 | 22.03 | 0.95 | 45.90 | 61.9 |
| | 1400 | 300 | 0 | 0 | 0.57 | 0.51 | 0.80 | 4.37 | 7.65 | 0.00 | 14.95 | 31.1 |
| | 1400 | 300 | 150 | 0.5 | 0.87 | 0.51 | 0.94 | 6.45 | 7.45 | 0.00 | 14.72 | 35.9 |
| | 1400 | 300 | 300 | 1 | 1.17 | 0.47 | 1.03 | 8.20 | 6.98 | 0.00 | 14.80 | 41.7 |
| | 1400 | 300 | 600 | 2 | 2.03 | 0.39 | 1.19 | 11.37 | 5.60 | 0.00 | 14.20 | 52.1 |
| 90% BT + 10% CS | | 650 | 325 | 0.5 | 0.44 | 0.69 | 1.00 | 14.14 | 32.18 | 7.21 | 46.45 | 41.4 |
| | | 650 | 650 | 1 | 0.65 | 0.59 | 0.97 | 17.73 | 27.20 | 6.03 | 46.20 | 49.4 |
| | | 650 | 1300 | 2 | 0.93 | 0.47 | 0.91 | 20.19 | 21.64 | 5.81 | 46.05 | 58.3 |
| | 1400 | 300 | 150 | 0.5 | 0.79 | 0.59 | 1.05 | 6.30 | 8.00 | 0.00 | 13.66 | 35.9 |
| | 1400 | 300 | 300 | 1 | 1.26 | 0.65 | 1.47 | 10.87 | 8.62 | 0.00 | 13.26 | 57.2 |
| | 1400 | 300 | 600 | 2 | 1.41 | 0.75 | 1.82 | 13.83 | 9.81 | 0.00 | 13.01 | 64.6 |
| 80% BT + 20% CS | | 650 | 325 | 0.5 | 0.56 | 0.47 | 0.73 | 13.41 | 23.93 | 7.43 | 51.12 | 36.2 |
| | | 650 | 650 | 1 | 0.79 | 0.40 | 0.71 | 16.43 | 20.68 | 6.22 | 51.94 | 42.3 |
| | | 650 | 1300 | 2 | 1.04 | 0.35 | 0.71 | 18.78 | 18.14 | 5.19 | 51.74 | 48.0 |
| | 1400 | 300 | 150 | 0.5 | 0.79 | 0.66 | 1.18 | 6.64 | 8.38 | 0.00 | 12.71 | 37.5 |
| | 1400 | 300 | 300 | 1 | 1.55 | 0.58 | 1.48 | 11.94 | 7.73 | 0.00 | 13.33 | 52.8 |
| | 1400 | 300 | 600 | 2 | 2.28 | 0.46 | 1.49 | 13.98 | 6.14 | 0.00 | 13.48 | 61.1 |
| 70% BT + 30% CS | | 650 | 325 | 0.5 | 0.75 | 0.28 | 0.49 | 12.92 | 17.14 | 6.93 | 60.93 | 29.2 |
| | | 650 | 650 | 1 | 1.00 | 0.25 | 0.50 | 15.18 | 15.14 | 6.51 | 61.17 | 34.5 |
| | | 650 | 1300 | 2 | 1.45 | 0.20 | 0.50 | 18.01 | 12.39 | 5.06 | 61.11 | 38.4 |
| | 1400 | 300 | 150 | 0.5 | 0.98 | 0.98 | 1.94 | 13.73 | 14.05 | 0.00 | 14.34 | 66.5 |
| | 1400 | 300 | 300 | 1 | 0.93 | 1.11 | 2.14 | 12.03 | 12.94 | 0.00 | 11.65 | 64.1 |
| | 1400 | 300 | 600 | 2 | 0.92 | 0.39 | 0.74 | 5.22 | 5.69 | 0.00 | 14.76 | 29.1 |

#### 12.2.2.2 Blends with Switchgrass

The gasification of blends of both coals with switchgrass was also performed under similar conditions as that of corn stover and the results were compared for compositions and efficiencies obtained as shown in Table 12-6 and Table 12-7.

Table 12-6. Average composition of product gases obtained during gasification of blends of PCC bituminous coal and switchgrass at varying $O_2$/steam ratios in the lab scale stainless steel moving bed gasifier

| Material | Air Flow Rate, ml/min | $O_2$ Flow Rate, ml/min | Steam Flow, ml/min | Steam: $O_2$ | $H_2$:CO | CO:$CO_2$ | ($H_2$+CO): $CO_2$ | Avg. Product Gas Composition | | | | Efficiency % |
|---|---|---|---|---|---|---|---|---|---|---|---|---|
| | | | | | | | | $H_2$ % | CO % | $CH_4$ % | $CO_2$ % | |
| 90% PCC + 10% SG | | 650 | 325 | 0.5 | 0.61 | 0.63 | 1.02 | 17.76 | 28.91 | 5.21 | 45.86 | 27.1 |
| | | 650 | 650 | 1 | 0.89 | 0.53 | 1.00 | 21.78 | 24.35 | 5.75 | 46.02 | 30.4 |
| | | 650 | 1300 | 2 | 1.15 | 0.49 | 1.05 | 26.32 | 22.83 | 4.68 | 46.62 | 53.5 |
| | 1400 | 300 | 150 | 0.5 | 0.96 | 0.28 | 0.55 | 4.15 | 4.32 | 0.00 | 15.49 | 17.3 |
| | 1400 | 300 | 300 | 1 | 1.15 | 0.28 | 0.61 | 5.04 | 4.38 | 1.18 | 15.45 | 25.7 |
| | 1400 | 300 | 600 | 2 | 1.50 | 0.26 | 0.65 | 6.19 | 4.12 | 1.78 | 15.93 | 29.8 |
| 80% PCC + 20% SG | | 650 | 325 | 0.5 | 0.72 | 0.37 | 0.63 | 14.16 | 19.72 | 5.42 | 53.68 | 23.5 |
| | | 650 | 650 | 1 | 1.01 | 0.32 | 0.63 | 16.60 | 16.45 | 4.50 | 52.11 | 30.7 |
| | | 650 | 1300 | 2 | 1.22 | 0.28 | 0.62 | 18.11 | 14.88 | 4.65 | 53.57 | 33.3 |
| | 1400 | 300 | 150 | 0.5 | 0.73 | 0.23 | 0.40 | 3.01 | 4.14 | 0.00 | 17.68 | 16.4 |
| | 1400 | 300 | 300 | 1 | 0.92 | 0.25 | 0.47 | 3.96 | 4.33 | 0.70 | 17.58 | 24.8 |
| | 1400 | 300 | 600 | 2 | 1.05 | 0.26 | 0.53 | 4.87 | 4.65 | 0.00 | 17.98 | 28.9 |
| 70% PCC + 30% SG | | 650 | 325 | 0.5 | 0.65 | 0.26 | 0.33 | 10.34 | 16.00 | 5.73 | 62.52 | 21.8 |
| | | 650 | 650 | 1 | 0.82 | 0.23 | 0.43 | 11.89 | 14.50 | 4.28 | 62.03 | 26.8 |
| | | 650 | 1300 | 2 | 1.31 | 0.16 | 0.46 | 13.09 | 10.02 | 4.78 | 63.43 | 28.3 |
| | 1400 | 300 | 150 | 0.5 | 0.43 | 0.32 | 0.46 | 3.19 | 7.43 | 0.00 | 23.18 | 14.8 |
| | 1400 | 300 | 300 | 1 | 0.64 | 0.29 | 0.47 | 4.61 | 7.21 | 0.00 | 24.91 | 22.1 |
| | 1400 | 300 | 600 | 2 | 0.71 | 0.29 | 0.50 | 4.98 | 7.01 | 0.00 | 24.13 | 27.7 |

Table 12-7. Average composition of product gases obtained during gasification of blends of BT sub-bituminous coal and switchgrass at varying $O_2$/steam ratios in the lab scale stainless steel moving bed gasifier

| Material | Air Flow Rate, ml/min | $O_2$ Flow Rate, ml/min | Steam Flow, ml/min | Steam: $O_2$ | $H_2$:CO | CO:$CO_2$ | ($H_2$+CO): $CO_2$ | Avg. Product Gas Composition | | | | Efficiency % |
|---|---|---|---|---|---|---|---|---|---|---|---|---|
| | | | | | | | | $H_2$ % | CO % | $CH_4$ % | $CO_2$ % | |
| 90% BT + 10% SG | | 650 | 325 | 0.5 | 0.55 | 0.56 | 0.87 | 16.63 | 30.05 | 5.96 | 53.65 | 37.1 |
| | | 650 | 650 | 1 | 0.72 | 0.46 | 0.80 | 17.55 | 24.41 | 5.62 | 52.58 | 50.7 |
| | | 650 | 1300 | 2 | 0.82 | 0.43 | 0.78 | 18.38 | 22.38 | 4.82 | 52.07 | 59.0 |
| | 1400 | 300 | 150 | 0.5 | 0.78 | 0.40 | 0.72 | 5.75 | 7.33 | 0.00 | 18.22 | 30.3 |
| | 1400 | 300 | 300 | 1 | 0.84 | 0.37 | 0.68 | 5.91 | 7.01 | 0.00 | 18.99 | 33.1 |
| | 1400 | 300 | 600 | 2 | 0.88 | 0.38 | 0.71 | 6.08 | 6.91 | 0.00 | 18.19 | 38.0 |
| 80% BT + 20% SG | | 650 | 325 | 0.5 | 0.60 | 0.30 | 0.48 | 11.52 | 19.05 | 5.44 | 63.23 | 34.4 |
| | | 650 | 650 | 1 | 0.94 | 0.24 | 0.46 | 14.49 | 15.34 | 4.00 | 64.18 | 36.7 |
| | | 650 | 1300 | 2 | 1.23 | 0.20 | 0.44 | 15.68 | 12.74 | 4.51 | 64.06 | 46.5 |
| | 1400 | 300 | 150 | 0.5 | 0.72 | 0.25 | 0.43 | 3.29 | 4.55 | 0.00 | 18.41 | 24.1 |
| | 1400 | 300 | 300 | 1 | 0.70 | 0.38 | 0.65 | 4.37 | 6.24 | 0.00 | 16.32 | 34.9 |
| | 1400 | 300 | 600 | 2 | 0.72 | 0.44 | 0.76 | 5.15 | 7.18 | 0.00 | 16.18 | 39.7 |
| 70% BT + 30% SG | | 650 | 325 | 0.5 | 0.44 | 0.21 | 0.30 | 6.35 | 14.34 | 3.51 | 69.80 | 20.1 |
| | | 650 | 650 | 1 | 0.67 | 0.18 | 0.30 | 8.53 | 12.81 | 3.00 | 70.94 | 21.9 |
| | | 650 | 1300 | 2 | 0.78 | 0.16 | 0.29 | 9.13 | 11.69 | 3.00 | 71.14 | 25.5 |
| | 1400 | 300 | 150 | 0.5 | 0.59 | 0.22 | 0.34 | 2.02 | 3.44 | 0.00 | 15.89 | 14.6 |
| | 1400 | 300 | 300 | 1 | 0.58 | 0.23 | 0.36 | 2.48 | 4.30 | 0.00 | 18.90 | 19.0 |
| | 1400 | 300 | 600 | 2 | 0.59 | 0.26 | 0.42 | 2.96 | 5.00 | 0.00 | 18.92 | 23.0 |

## 12.3 Gasification with Varying Oxygen Partial Pressure

The gasification of bituminous coal was carried out with varying oxygen partial pressures by introducing nitrogen into the feed stream. Steam was not used in these experiments. Three types of experiments were performed:

1. Varying the oxygen percentage in the feed stream (40%, 60% and 100%) at a constant total flow rate of 650 ml/min.
2. Varying the oxygen percentage in the feed stream (21%, 40% and 60%) at a constant total flow rate of 1400 ml/min.
3. Varying the total flow rate of the inlet gas stream and thus the oxygen fraction (40%, 60%, 80% and 100%) at a constant oxygen flow rate of 650 ml/min.

The results of these gasification tests with varying partial pressure are summarized in Table 12-8 and Table 12-9 for sub-bituminous coal and bituminous coal, respectively.

Table 12-8. Average composition of product gases obtained during gasification of sub bituminous coal with varying oxygen partial pressures

| Total Flow Rate ml/min | $N_2$ % | $O_2$ % | Average Values | | | | | |
|---|---|---|---|---|---|---|---|---|
| | | | $CO:CO_2$ | $(H_2+CO):CO_2$ | $H_2$ % | CO % | $CH_4$ % | $CO_2$ % |
| 650 | 60 | 40 | 0.59 | 0.66 | 1.61 | 12.70 | 0.31 | 21.53 |
| 650 | 30 | 70 | 0.62 | 0.70 | 3.18 | 23.99 | 1.27 | 38.84 |
| 650 | 0 | 100 | 0.90 | 1.02 | 5.39 | 39.52 | 1.43 | 44.02 |
| 1400 | 78 | 21 | 0.62 | 0.62 | 0.00 | 7.20 | 0.00 | 11.59 |
| 1400 | 60 | 40 | 1.42 | 1.60 | 2.67 | 20.65 | 0.95 | 14.58 |
| 1400 | 40 | 60 | 1.59 | 1.79 | 3.86 | 31.63 | 1.12 | 19.88 |
| 1625 | 60 | 40 | 2.16 | 2.39 | 2.75 | 25.11 | 0.38 | 11.64 |
| 1083.33 | 40 | 60 | 1.26 | 1.42 | 3.59 | 28.87 | 0.67 | 22.90 |
| 812.5 | 20 | 80 | 1.00 | 1.11 | 3.86 | 32.17 | 1.00 | 32.33 |
| 650 | 0 | 100 | 0.90 | 1.02 | 5.39 | 39.52 | 1.43 | 44.02 |

Table 12-9. Calculated energy efficiency during gasification of bituminous coal with varying oxygen partial pressures

| Total Flow Rate ml/min | $N_2$ % | $O_2$ % | Max $CO:CO_2$ | Energy Input kJ | Energy Output kJ | Efficiency % |
|---|---|---|---|---|---|---|
| 650 | 60 | 40 | 0.77 | 2591 | 226 | 8.7 |
| 650 | 30 | 70 | 0.79 | 2082 | 315 | 15.1 |
| 650 | 0 | 100 | 1.03 | 1504 | 378 | 25.2 |
| 1400 | 78 | 21 | 1.37 | 1295 | 120 | 9.3 |
| 1400 | 60 | 40 | 1.88 | 2591 | 735 | 28.4 |
| 1400 | 40 | 60 | 2.27 | 2637 | 895 | 33.9 |
| 1625 | 60 | 40 | 3.12 | 3170 | 1136 | 35.8 |
| 1083.33 | 40 | 60 | 1.79 | 2036 | 591 | 29.1 |
| 812.5 | 20 | 80 | 1.71 | 2128 | 543 | 25.5 |
| 650 | 0 | 100 | 1.03 | 1504 | 378 | 25.2 |

From Figure 12-5 and Figure 12-6, it can be seen that the average carbon monoxide and carbon dioxide concentrations in the gasifier exit stream increase with increasing oxygen percentage in the feed gas stream. The average composition values vary not only as a function of the partial pressure of oxygen but also vary as a function of the total flow rate of the feed stream.

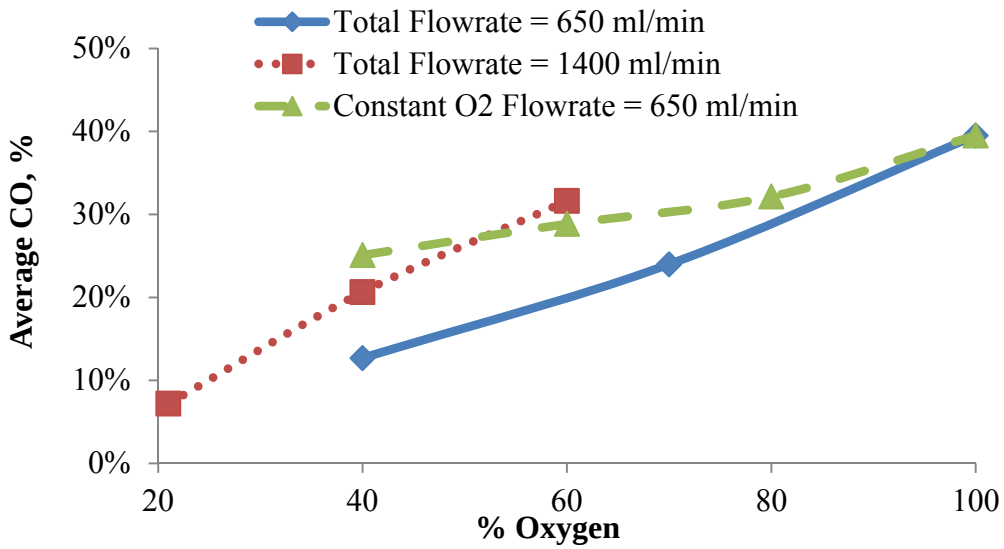



Figure 12-5. Average carbon monoxide concentration in exit stream obtained during gasification of bituminous coal with varying oxygen partial pressures

As the total flow rate of the inlet gas stream is increased, the concentrations of carbon monoxide and carbon dioxide in the product gas increase for the same oxygen percentage in the feed stream. For example, if the feed stream contains 40% oxygen and 60% nitrogen, the percentage of carbon monoxide in the product gas is 12.7% for a total inlet gas flow rate of 650 ml/min, 20.65% for a total inlet gas flow rate of 1400 ml/min and 25.11% for a total inlet gas flow rate of 1625 ml/min. This is believed to be caused because higher gas feed stream flow rate can propagate heat axially upwards at a much faster rate, causing the coal particles to react with oxygen at a higher rate.

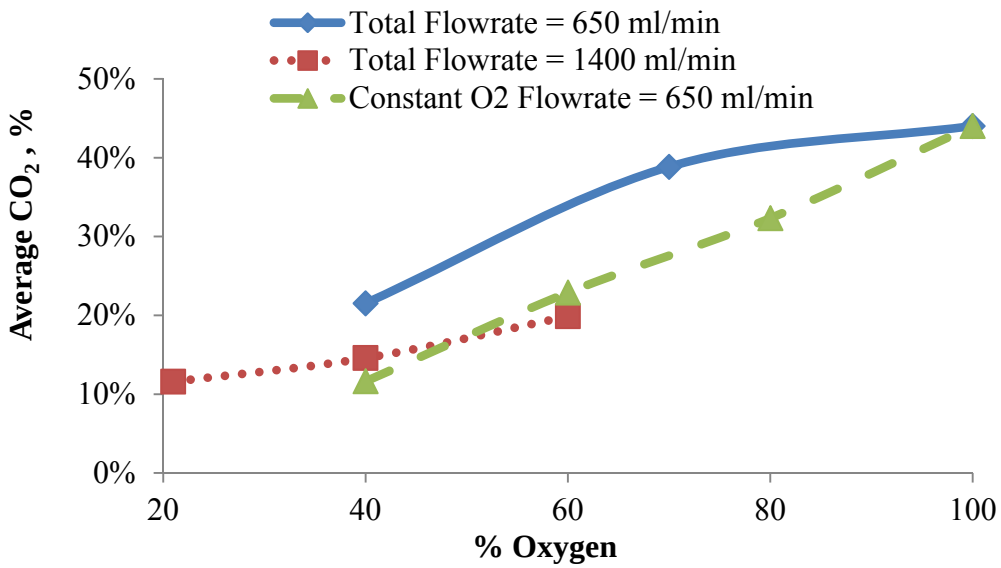



Figure 12-6. Average carbon dioxide concentration in exit stream during gasification of bituminous coal with varying oxygen partial pressures

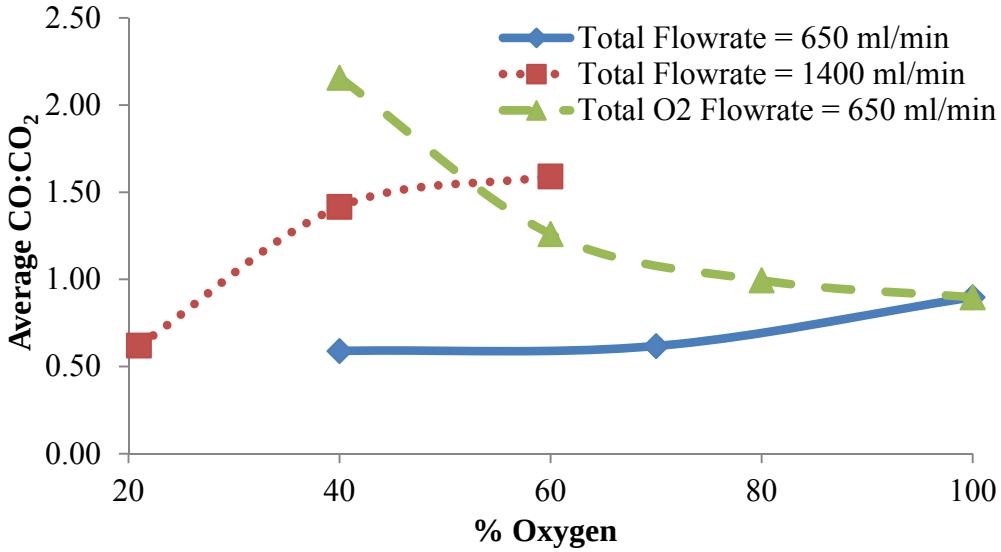



Figure 12-7. Average CO:$CO_2$ ratios in the exit gas stream obtained during gasification of sub bituminous coal with varying oxygen partial pressures

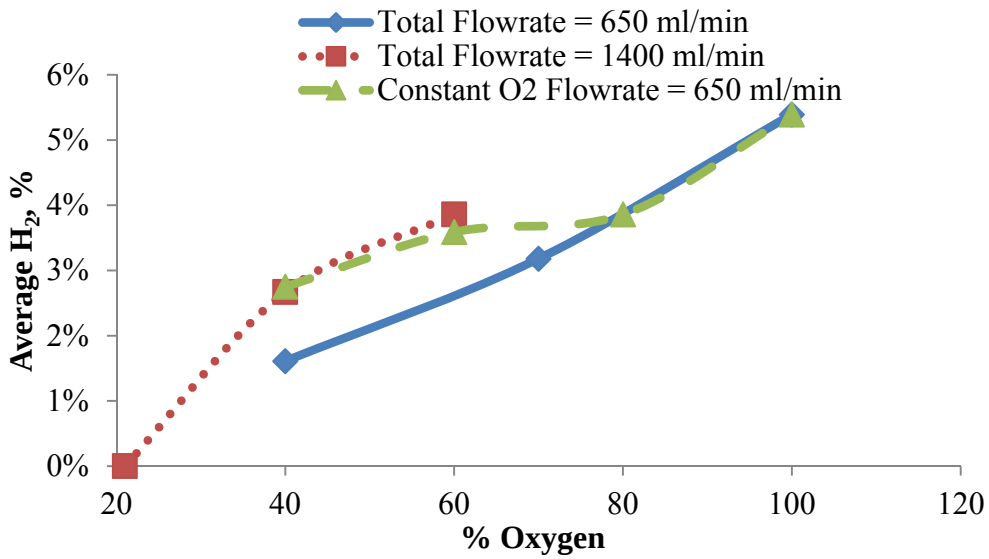



Figure 12-8. Average hydrogen concentration obtained during gasification of sub bituminous coal with varying oxygen partial pressures

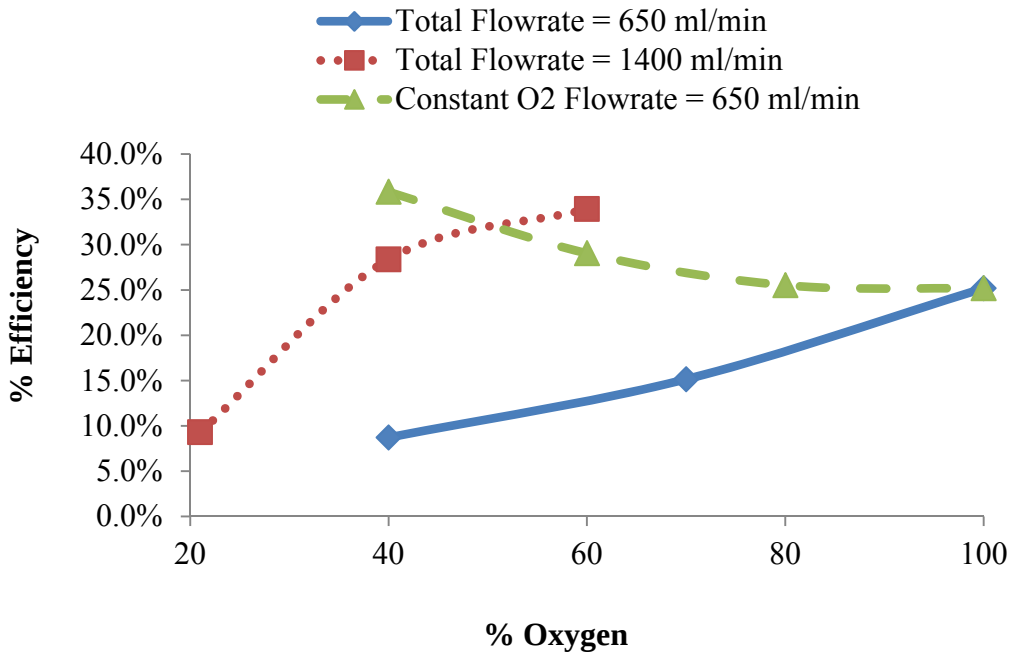



Figure 12-9. Energy conversion efficiency obtained during gasification of sub bituminous coal with varying oxygen partial pressures

Since these set of experiments were conducted in the absence of steam, it can be inferred that hydrogen would be present only in small amounts in the product gas stream. The percentage of hydrogen in the outlet gas stream was a function of the oxygen partial pressure in the feed gas stream as well as the total flow rate of the feed gas stream and followed the same trends as

observed for carbon monoxide and carbon dioxide. The efficiency of the gasification reaction increased with increase in the inlet gas flow rate and oxygen partial pressure for the same reason that more heat was believed to be carried upwards to produce higher heating value gas.

Based on the above results, the optimal gasification conditions in the laboratory scale moving bed gasifier are:

1. Using pure oxygen and steam in the inlet gas stream, the highest energy conversion efficiency obtained is approximately 50% at a steam to oxygen ratio of 1.5.
2. Using a mixture of nitrogen and oxygen in the feed gas stream, the inlet gas stream flowrate of 1625 ml/min and oxygen percentage of 40% provides the highest energy conversion efficiency and a max CO: $CO_2$ ratio of approximately 3:1.
3. The bed temperature range during the gasification of sub-bituminous coal was generally observed to be between 600 ºC and 800 ºC for the experiments with varying steam ratios and between 800 ºC and 1000 ºC for the experiments with varying oxygen partial pressures.

## 12.4 Gasification of Briquettes

The gasification of four different briquette types was studied in a moving bed reactor under different oxygen to steam and air to steam ratios. The four briquette types are as follows:

1. EM-SD: Clean coal from Emerald Mine (EM), Pennsylvania blended with 20% by weight of kiln dried eastern white pine (pinus strobus) sawdust/shavings (SD) from sawmill (Turman Lumber Company) in Hillsville, Virginia. The coal was crushed and screened to 1.0 mm top size and air dried for 1 week to 1.6% moisture before briquetting while the sawdust was screened to 1.2 mm top size before oven drying to reduce the moisture content from approximately 11% to 0.2%.
2. EM-SD-G97: The briquettes obtained by blending Emerald Mine clean coal and pine sawdust were then coated with a wood derived chemical resin (G97). The coating was performed by dipping the briquettes in resin which was heated to approximately 150 °C.
3. EB-CS: Raw coal from Eagle Butte Mine (EB), Wyoming blended with 20% by weight of corn stover (CS) obtained from Piedmont Bioproducts, VA. The raw coal was crushed and screened to 1.0 mm top size and air dried for 1 week and oven dried for 48 hours at 105 °C to reduce the moisture content to 1.7%. Corn stover, on the other hand, was

processed in a knife mill across a 4.76 mm screen and was blended with the coal without drying.

4. EB-CS-G97: The blends of EB and CS were then coated with G97 resin as described above and used as feed for the moving bed gasifier.

Experiments were performed at atmospheric pressure with varying oxygen flow rates ranging from 300 ml/min (Air flow rate of 1400 ml/min equates to approximately 300 ml/min of oxygen) to 650 ml/min and varying steam flow rates of 150 ml/min to 1300 ml/min, the results of which would be discussed in the following sections. A ratio of 2:1 (steam:$O_2$) was chosen because beyond this, the endothermic zone was prevalent inside the gasifier and the gasification of the feedstocks was not sustained.

### 12.4.1 Product Gas Analysis – Briquette Gasification

The gasification of the four types of briquettes was carried out in the moving bed gasifier with varying oxygen to steam ratios. The oxygen flow rate was constant at 650 ml/min while the flow rates of steam were varied from 0 to 1625 ml/min. In order obtain a baseline for this analysis, different known concentrations of the product gases ($H_2$, CO, $CH_4$ and $CO_2$) were first analyzed to obtain the times at which their respective peaks were occurring. A plot of volume percent versus peak area gives the calibration curve for obtaining the concentrations of the product gases. The average composition of the product gases is calculated using a calibration curve for each species. Once the composition of the product species is obtained, the gross heating value of the gases and the energy conversion efficiency of the gasifier can be calculated. The average composition of the product gases and the calculated energy efficiency values are provided in Table 12-10 through Table 12-13.

Table 12-10. Average composition of product gases obtained during gasification of EM-SD briquettes with varying oxygen to steam ratios

| Material | Air Flow Rate, ml/min | $O_2$ Flow Rate, ml/min | Steam Flow, ml/min | Steam: $O_2$ | $H_2$:CO | CO:$CO_2$ | ($H_2$+CO): $CO_2$ | Average Product Gas Compositions | | | | Efficiency % |
|---|---|---|---|---|---|---|---|---|---|---|---|---|
| | | | | | | | | $H_2$ % | CO % | $CH_4$ % | $CO_2$ % | |
| EM-SD | | 650 | 325 | 0.50 | 0.56 | 0.20 | 0.31 | 6.71 | 12.00 | 3.63 | 59.94 | 16.70 |
| | | 650 | 450 | 0.70 | 0.56 | 0.21 | 0.33 | 6.75 | 12.12 | 3.98 | 57.82 | 18.71 |
| | | 650 | 650 | 1.00 | 0.58 | 0.22 | 0.35 | 6.86 | 11.86 | 4.29 | 53.50 | 20.12 |
| | | 650 | 975 | 1.50 | 0.59 | 0.32 | 0.50 | 9.63 | 16.27 | 6.39 | 51.32 | 26.10 |
| | | 650 | 1300 | 2.00 | 0.61 | 0.39 | 0.62 | 11.20 | 18.25 | 9.37 | 47.14 | 28.12 |
| | 1400 | 300 | 150 | 0.50 | 0.68 | 0.59 | 0.99 | 4.59 | 6.74 | 0.00 | 11.50 | 25.98 |
| | 1400 | 300 | 300 | 1.00 | 0.90 | 0.64 | 1.22 | 6.23 | 6.92 | 0.00 | 10.80 | 31.40 |
| | 1400 | 300 | 600 | 2.00 | 1.05 | 0.66 | 1.36 | 7.45 | 7.11 | 0.00 | 10.73 | 43.04 |

Figure 12-10 through Figure 12-14 describe the product gas compositions obtained during the gasification of EM-SD briquettes as an example. All the briquettes follow similar trends in the product gas compositions with the average values being different. As seen from Figure 12-10, the increase in the amount of steam fed to the gasifier at constant oxygen flow rate, implies increased atoms of hydrogen supplied to the gasifier. This results in a gradual increase in the hydrogen percentage. Also, the percentage of carbon monoxide increases with increasing steam concentration. This is due to the fact that the reaction of solid carbon or char with steam (Water gas reaction) and char with carbon dioxide (Boudouard Reaction) are predominant. These reactions are endothermic in nature and are favored at high temperatures > 900 $^{\circ}$C as described earlier. The combustion of solid carbon at the bottom of the gasifier results in a highly exothermic reaction releasing carbon dioxide initially. As the temperature inside the gasifier increases and attains a steady value of around 900 $^{\circ}$C, the char present reacts with the carbon dioxide generated from combustion and thus results in an increased concentration of carbon monoxide and decreased carbon dioxide in the producer gas.

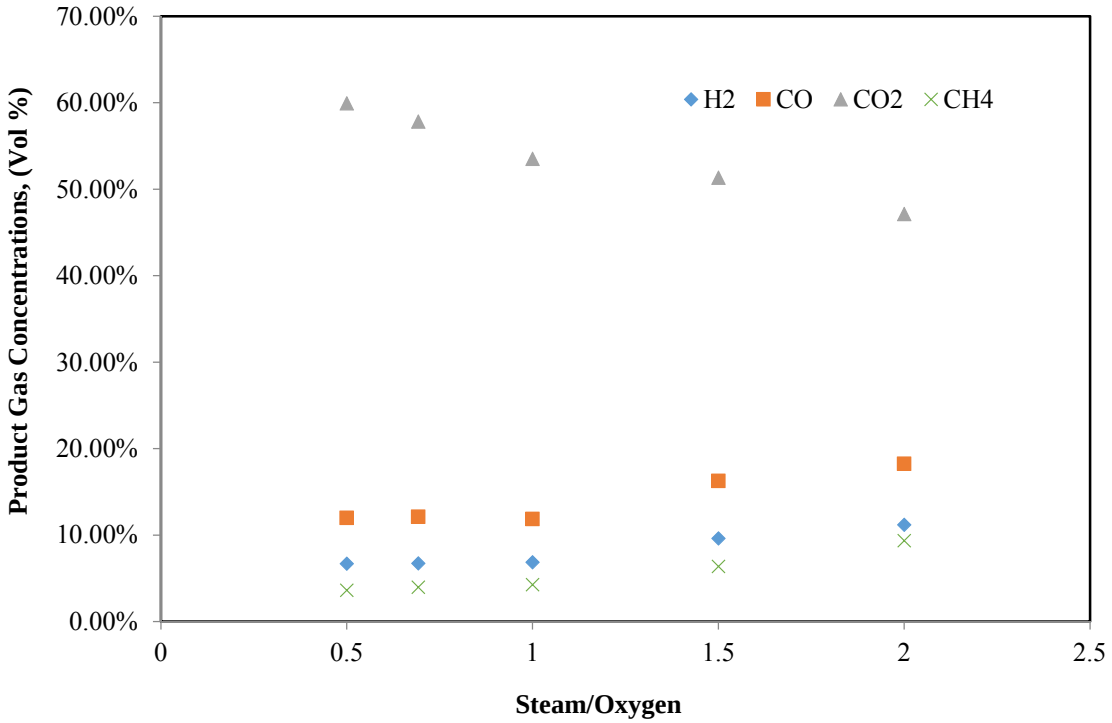



Figure 12-10. Average compositions of the product gases obtained during gasification of EM-SD briquettes with varying steam to oxygen ratios

Experiments with a steam to oxygen ratio of greater than 2.0 were also performed, but they resulted in the bed being extinguished in a very short period of time. Increasing steam flowrates to very high values implies decreasing the oxygen supplied to the gasifier. Thus, the exothermic reaction of carbon and oxygen which supplies the necessary heat for the gasification reaction to proceed is not favored resulting in temperatures not high enough for hydrogen to be stripped from steam. Hence, no gasification reaction occurred at higher flow rates of steam.

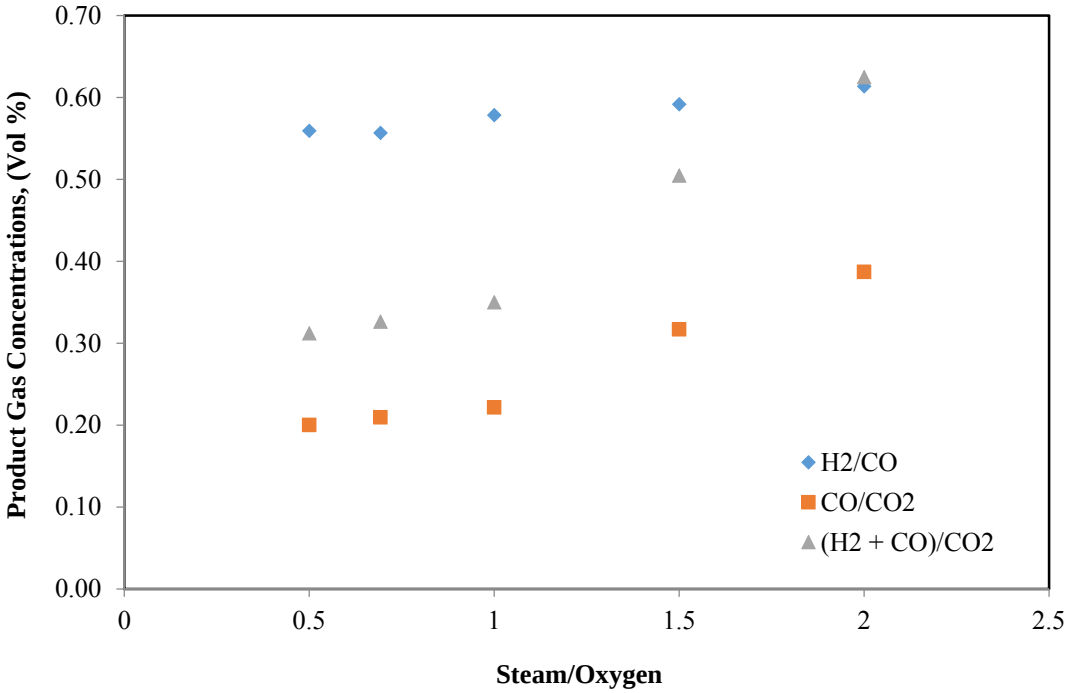



Figure 12-11. Average ratios of the product gases obtained during gasification of EM-SD briquettes with varying steam to oxygen ratios

It can be observed from Figure 12-11 that the $H_2/CO$ ratio is almost constant even with increasing steam concentration, while the ratio of $CO/CO_2$ and syngas/$CO_2$ increases. This is another proof of the fact that water-gas reaction and Boudouard reaction are predominant for the conditions at which the gasifier was operated. It is necessary to operate the gasifier at a nominal oxygen/carbon ratio. Even though high oxygen concentration results in increased carbon conversion, too much oxygen results in complete combustion and does not favor the production of syngas which will lower the heating value of the producer gas. A comparison of the product gas compositions was also made by replacing oxygen with air as the gasifying agent. Air at much higher flow rate (1400 ml/min or 300 ml/min of $O_2$) was introduced to improve the heat transfer axially upward through the reactor so that char a higher temperature falls into the gasifying zone. This was done in order to verify if the cold gas efficiencies improve with increasing steam concentrations.

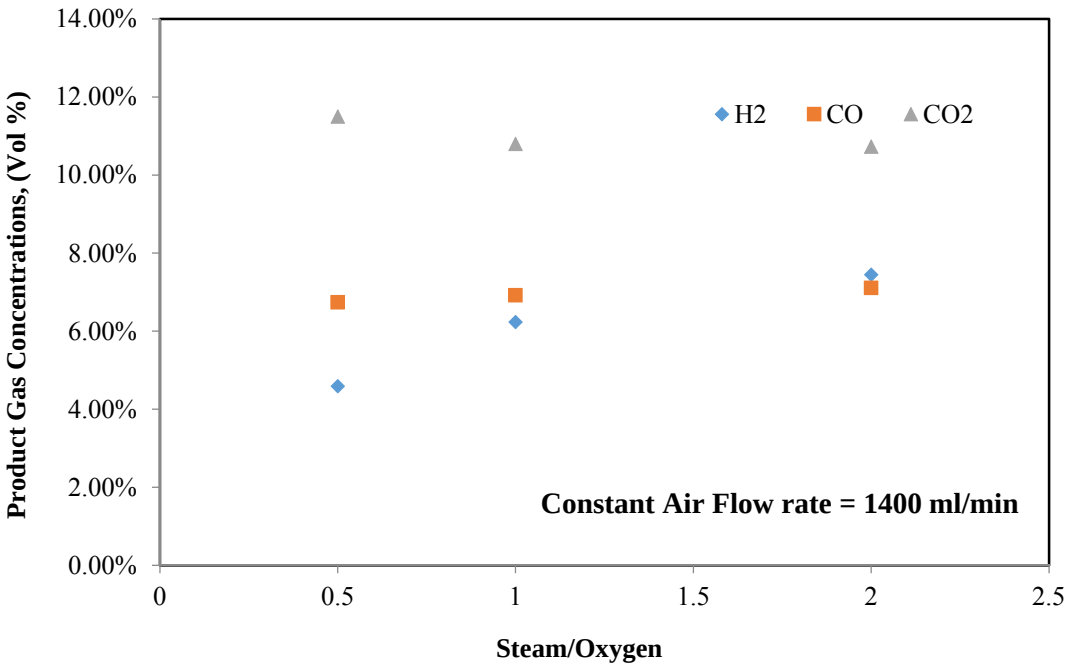



Figure 12-12. Average compositions of the product gases obtained during gasification of EM-SD briquettes with varying steam to oxygen ratios at a constant air flow rate of 1400 ml/min

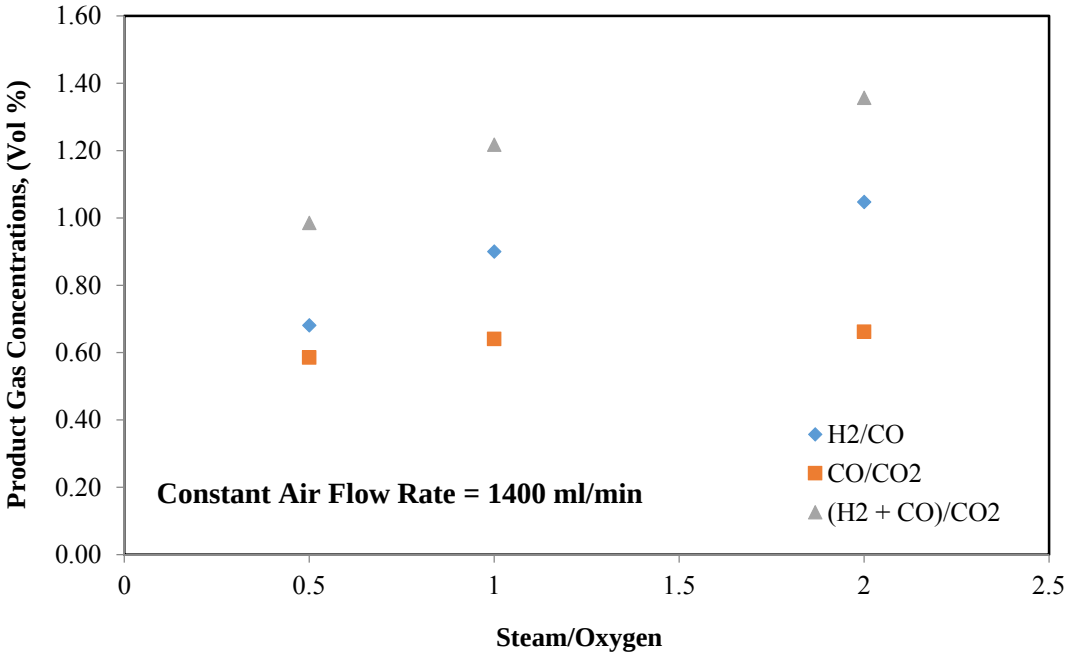



Figure 12-13. Average ratios of the product gases obtained during gasification of EM-SD briquettes with varying steam to oxygen ratios

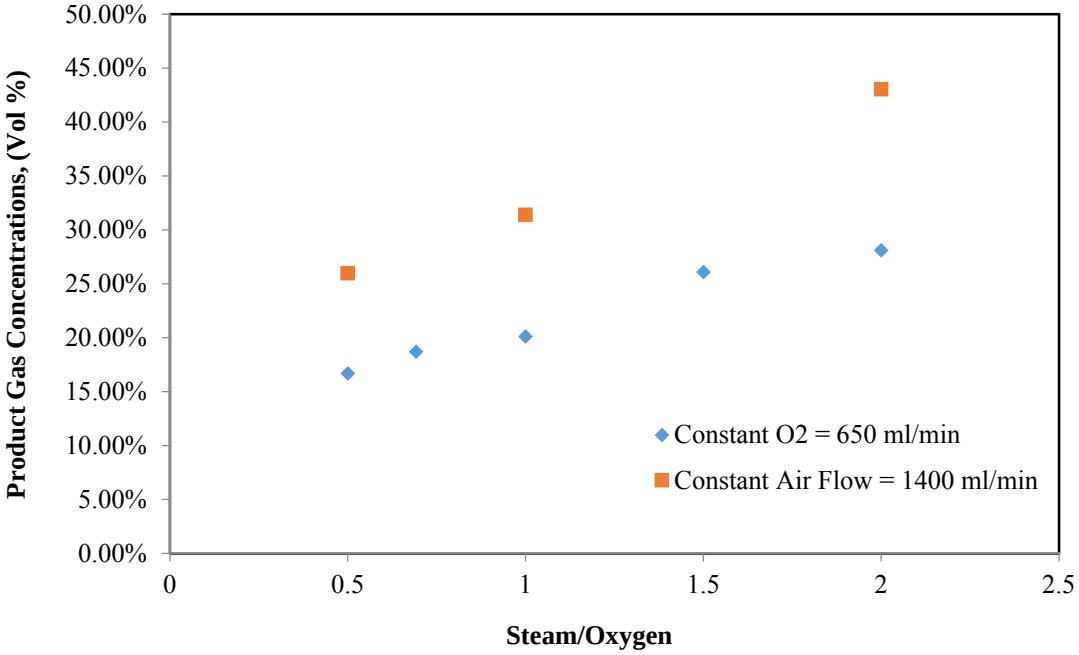



Figure 12-14. Comparison of cold gas efficiencies for gasification of EM-SD briquettes

From Figure 12-12 through Figure 12-14, it can be clearly seen that the addition of air as the gasifying agent resulted in an increased $H_2/CO$, $CO/CO_2$ and syngas/$CO_2$ ratio thereby improving the maximum cold gas efficiency from 28% to 43% as a consequence of lower $CO_2$ concentration in the product gas. It may be observed that the product gas also contains unreacted nitrogen from air (1100 ml/min) and the average product gas compositions are actual values and not normalized.

Table 12-11. Average composition of product gases obtained during gasification of EM-SD-G97 briquettes with varying oxygen to steam ratios

| Material | Air Flow Rate, ml/min | $O_2$ Flow Rate, ml/min | Steam Flow, ml/min | Steam: $O_2$ | $H_2$:CO | CO:$CO_2$ | ($H_2$+CO): $CO_2$ | Average Product Gas Compositions | | | | Efficiency % |
|---|---|---|---|---|---|---|---|---|---|---|---|---|
| | | | | | | | | $H_2$ % | CO % | $CH_4$ % | $CO_2$ % | |
| EM-SD-G97 | | 650 | 325 | 0.50 | 0.51 | 0.19 | 0.29 | 6.06 | 11.77 | 5.04 | 61.29 | 16.86 |
| | | 650 | 450 | 0.70 | 0.62 | 0.19 | 0.31 | 7.14 | 11.52 | 5.46 | 60.04 | 18.67 |
| | | 650 | 650 | 1.00 | 0.69 | 0.25 | 0.42 | 10.13 | 14.65 | 6.15 | 58.38 | 25.44 |
| | | 650 | 975 | 1.50 | 0.71 | 0.27 | 0.47 | 11.18 | 15.64 | 6.32 | 57.14 | 26.91 |
| | | 650 | 1300 | 2.00 | 0.72 | 0.33 | 0.58 | 13.32 | 18.44 | 7.40 | 55.09 | 27.91 |
| | 1400 | 300 | 150 | 0.50 | 0.68 | 0.46 | 0.77 | 4.01 | 5.91 | 0.00 | 12.83 | 20.50 |
| | 1400 | 300 | 300 | 1.00 | 1.10 | 0.57 | 1.19 | 6.98 | 6.34 | 0.00 | 11.21 | 32.38 |
| | 1400 | 300 | 600 | 2.00 | 1.26 | 0.70 | 1.59 | 8.95 | 7.11 | 0.00 | 10.13 | 47.65 |

On the addition of G-97 resin to the EM-SD briquettes, it was observed that although slightly higher concentrations of hydrogen and carbon dioxide were obtained at any given steam/$O_2$ ratio, the efficiencies were almost the same and the addition of the resin did not improve the product gas concentrations drastically.

Table 12-12. Average composition of product gases obtained during gasification of EB-CS briquettes with varying oxygen to steam ratios

| Material | Air Flow Rate, ml/min | $O_2$ Flow Rate, ml/min | Steam Flow, ml/min | Steam: $O_2$ | $H_2$:CO | CO:$CO_2$ | ($H_2$+CO): $CO_2$ | Average Product Gas Compositions | | | | Efficiency % |
|---|---|---|---|---|---|---|---|---|---|---|---|---|
| | | | | | | | | $H_2$ % | CO % | $CH_4$ % | $CO_2$ % | |
| EB-CS | | 650 | 325 | 0.50 | 0.56 | 0.30 | 0.47 | 10.53 | 18.67 | 3.55 | 61.80 | 20.84 |
| | | 650 | 450 | 0.70 | 0.58 | 0.33 | 0.52 | 11.45 | 19.74 | 3.53 | 59.47 | 24.94 |
| | | 650 | 650 | 1.00 | 0.60 | 0.42 | 0.67 | 14.19 | 23.68 | 3.72 | 56.52 | 34.12 |
| | | 650 | 975 | 1.50 | 0.73 | 0.45 | 0.78 | 17.45 | 24.03 | 3.72 | 53.41 | 39.27 |
| | | 650 | 1300 | 2.00 | 0.79 | 0.50 | 0.90 | 19.47 | 24.80 | 3.81 | 49.20 | 45.48 |
| | 1400 | 300 | 150 | 0.50 | 0.79 | 0.66 | 1.18 | 6.64 | 8.38 | 0.00 | 12.71 | 36.78 |
| | 1400 | 300 | 300 | 1.00 | 1.23 | 0.79 | 1.76 | 11.94 | 9.73 | 0.00 | 12.33 | 51.89 |
| | 1400 | 300 | 600 | 2.00 | 1.38 | 0.97 | 2.30 | 13.98 | 10.14 | 0.00 | 10.48 | 63.50 |

Table 12-13. Average composition of product gases obtained during gasification of EB-CS-G97 briquettes with varying oxygen to steam ratios

| Material | Air Flow Rate, ml/min | $O_2$ Flow Rate, ml/min | Steam Flow, ml/min | Steam: $O_2$ | $H_2$:CO | CO:$CO_2$ | ($H_2$+CO): $CO_2$ | Average Product Gas Compositions | | | | Efficiency % |
|---|---|---|---|---|---|---|---|---|---|---|---|---|
| | | | | | | | | $H_2$ % | CO % | $CH_4$ % | $CO_2$ % | |
| EB-CS-G97 | | 650 | 325 | 0.50 | 0.85 | 0.26 | 0.49 | 12.80 | 14.99 | 3.76 | 57.07 | 20.45 |
| | | 650 | 450 | 0.70 | 0.89 | 0.28 | 0.53 | 14.42 | 16.15 | 3.84 | 57.41 | 27.39 |
| | | 650 | 650 | 1.00 | 0.98 | 0.30 | 0.59 | 16.74 | 17.07 | 4.83 | 57.58 | 35.28 |
| | | 650 | 975 | 1.50 | 1.05 | 0.34 | 0.69 | 19.12 | 18.27 | 4.15 | 54.26 | 40.81 |
| | | 650 | 1300 | 2.00 | 1.35 | 0.37 | 0.87 | 24.63 | 18.30 | 4.06 | 49.55 | 50.43 |
| | 1400 | 300 | 150 | 0.50 | 0.92 | 0.45 | 0.85 | 5.22 | 5.69 | 0.00 | 12.76 | 31.69 |
| | 1400 | 300 | 300 | 1.00 | 1.10 | 0.94 | 1.97 | 12.03 | 10.94 | 0.00 | 11.65 | 55.32 |
| | 1400 | 300 | 600 | 2.00 | 1.33 | 1.07 | 2.49 | 14.73 | 11.05 | 0.00 | 10.34 | 64.75 |

The briquettes of EB-CS and EB-CS-G97 were also gasified under similar operating conditions. A comparison of EM-SD and EB-CS determines that the blends of EB-CS are much more reactive when compared to blends of EM-SD. This can be seen in the fact that the concentrations of syngas are much higher in blends with CS and therefore the cold gas efficiencies are also much higher at any given steam/$O_2$ ratio. Likewise, the addition of resin even in the case of EB-CS did not alter the product gas compositions and efficiencies to a great extent.

## 12.5 Summary and Conclusions

A laboratory-scale moving gasification system was designed and constructed for the purpose of gasifying the feedstock materials. The efficiency and product gas compositions obtained reveal that utilizing an inner stainless steel tubing better promotes heat transfer upwards in the axial direction when compared to utilizing a quartz insulation. The trends of the product gas compositions are similar to those obtained using an inner quartz lining. But, the percentage of hydrogen generated at same operating conditions is much higher due to the increase in bed temperature (complete consumption of oxygen which was not achieved when using a quartz insulation) and transfer of heat upwards in the axial direction and thus, better heat utilization which improved the overall efficiency by at least 20% when the steam concentration was at its maximum in the gasifier. Also, unlike the quartz insulation where the efficiency increased only until a certain point and the maximum steam/$O_2$ ratio that could be utilized was 1.5, in this experimental set-up, the efficiency increased steadily until a steam/$O_2$ ratio of 2:1. Apart from this, the ratios of $H_2$/CO, CO/$CO_2$ and syngas/$CO_2$, which dictate the quality of the product gas, are markedly higher as compared with the experimental design utilizing an inner quartz lining.

# Chapter 13

# Source Apportionment of Carbon using Stable Carbon Isotope Analysis

## 13.1 Abstract

Stable carbon isotope analysis, a unique analytical technique, has been utilized for distinguishing and quantifying the individual contributions of coal and biomass feedstock materials in the generation of carbon containing gases during the gasification of their blends. For this purpose, two different biomass samples, namely, corn stover (CS) and switchgrass (SG), were physically blended up to 30% by weight with two coals, namely, PCC Bituminous coal (PCC) and BT Sub-Bituminous coal (BT). The blended samples were then gasified in a moving bed gasifier operating at atmospheric pressure and varying $O_2$/steam ratios. The ratio of $CO/CO_2$ in the product gas decreased with decreasing $O_2$/steam ratio and increasing amount of biomass in the blends. Gasifying at a constant $O_2$/steam ratio with increasing percentage of biomass in the feedstock, resulted in an increasing trend of $\delta^{13}C$ (‰) values for the carbon containing product gases. An increase in the concentration of oxygen in the feed stream at a constant biomass percentage leads to the depletion of $^{13}CO$ and enrichment of $^{13}CO_2$ in the blends with corn stover while an enrichment of both $^{13}CO$ and $^{13}CO_2$ was observed in blends with switchgrass. For blends with corn stover, there exists the possibility of a carbon isotope equilibrium between CO and $CO_2$ only at temperatures over 1000 °C at an $O_2$:steam ratio of 2:1 and corn stover percentage not exceeding 20% while for blends with switchgrass, the gases are not in isotopic equilibrium. Based on isotope mass balance considerations, for the operating conditions utilized, the contribution of corn stover was in the range of 1-40% for CO generation and 6-69% for $CO_2$ generation. Switchgrass, on the other hand, contributed up to 53% for CO generation and only 46% for $CO_2$ generation.

## 13.2 Introduction

### 13.2.1 Background

The past few years have seen an upsurge in interest in the gasification of biomass and coal-biomass mixtures for several reasons. They include:

1. Reduction in greenhouse gas emissions caused by the combustion of fossil fuels,
2. A need for energy independence due to the depleting resources and fluctuating prices of oil and natural gas, and
3. Developing interest in renewable energy resources (Basu, 2010).

Although there is an abundance of coal in the United States and several other countries and it will continue to be a major source of energy for many years to come, there is still great interest in replacing part of the coal used in energy generation with renewable biomass or plant-derived organic matter available on a renewable basis (Brown, 2003). Many countries have initiated incentives in recent years to encourage the co-utilization of biomass and coal for energy production (Fernando, 2009). Biomass fuels (BF) are to be sustainable natural resources if they renew themselves at such a rate that they will be available for future use. That is, if the rate of consumption of BF is less than or equal to the rate at which it is generated. These BF resources can be either grown and harvested biomass such as switchgrass or waste biomass such as corn stover, wood wastes from forestry and lumbering operations, wastes from paper production, and landscaping wastes (Brown, 2003).

The idea of gasifying mixtures of coal and biomass is relatively new with almost zero commercial experience since the properties of coal and biomass differ significantly from each other (Gordillo et al., 2009; Di Blasi et al., 1999; Klass, 1998). Co-processing these feedstocks, with oxygen and steam in relevant proportions with respect to the amount of carbon results in the formation of mainly CO, $CO_2$, $H_2$ and small quantities of lower hydrocarbons. Prins et al. (2007) reported that fuels with higher oxygen to carbon ratios have larger energy losses due to their high ratio of available chemical energy to heating value. Also, such fuels are over-oxidized (combusted) in the gasifier in order to reach the required gasification temperature. Therefore, highly oxygenated fuels are not ideal for gasifiers keeping in view the energy losses that can be incurred and hence, solid biomass can be more readily gasified if it is co-gasified with coal (Fernando, 2009). Hence, co-gasification of blends of coal and biomass to produce syngas (CO-

$H_2$ mixtures) that can be used as feedstock for processes such as Fischer-Tropsch Synthesis used for producing liquid fuels, is a major area of research.

Also, as is well known, the emission of $CO_2$ during the burning of BF is neutralized by the removal of $CO_2$ from the atmosphere by the process of photosynthesis during biomass growth. Therefore, it is imperative to quantify the contribution of these biomass feedstocks in the generation of greenhouse gases. Stable carbon isotope analysis is one such technique that can be utilized to obtain the source from which these gases are generated during co-processing of different feedstocks (Buczynska et al., 2013; Okuda et al., 2002; McRae et al., 1999; Matthews & Hayes, 1978).

### 13.2.2 Theory

Stable carbon isotope composition is determined as the ratio of $^{13}C/^{12}C$ in a substance relative to Pee Dee Belemnite (PDB), a cretaceous marine fossil having an anomalously high $^{13}C/^{12}C$ ratio, which is an internationally established reference standard for the stable isotope composition of carbon in natural materials. Carbon isotope ratios are commonly reported using delta notation (as $\delta^{13}C$ values) in parts per thousand (per mil, ‰) as shown in Equation 13-1 (Buczynska et al., 2013; Brasseur et al., 2002; Lancet et al., 1993; Bottrell et al., 1990; Hoefs & Usdowski, 1987; Steer et al., 1987; Matthews & Hayes, 1978; Craig, 1957).

$$\delta^{13}C = \left( \frac{\left( {}^{13}C/_{12}C \right)_{Sample}}{\left( {}^{13}C/_{12}C \right)_{Standard}} - 1 \right) \times 1000\ ‰ \qquad \text{(Eq. 13-1)}$$

Most plants can be divided into three groups based on the photosynthetic pathway by which they fix carbon (Follett et al., 2012; Bechtel et al., 2008; Robinson & Hesselbo, 2004):

1. $C_3$: Almost 95% of the plants on earth fall under this category. They fix carbon dioxide by the Calvin cycle and have $\delta^{13}C$ values that generally range between -23 and -34‰. Examples of these plants include temperate shrubs and trees, and grasses.
2. $C_4$: These plants fix carbon dioxide by the Hatch-Slack cycle. Their $\delta^{13}C$ values are less negative and range between -8 and -16‰. Plants like corn, switchgrass and warm weather grasses, predominantly, belong to this category.
3. CAM: The third group of plants fix carbon dioxide by the Crassulacean Acid Metabolism pathway, and have $\delta^{13}C$ values that are intermediary compared with $C_3$ and $C_4$ plants.

Fossil fuels such as coal and oil are made primarily of $C_3$ plant material and are depleted in $^{13}C$ relative to the atmosphere, because they were originally formed from living organisms (Singh et al., 2012; Whiticar, 1996). Therefore, the carbon from fossil fuels that is returned to the atmosphere through combustion is depleted in $^{13}C$ when compared to atmospheric carbon dioxide. The values of $\delta^{13}C$ vary by measurable amounts for different carbonaceous materials depending on their carbon source, fixation pathway, environment of formation and post depositional history. These values differ by about by about 10-15‰ for coal and biomass materials with the $\delta^{13}C$ for coal being more negative than that of biomass. This means that the carbon contained in coal is richer in $^{12}C$, as is the case with all fossil fuels. Surprisingly, the carbon isotope composition of coal typically does not vary much with increasing coal rank which implies that significant fractionation does not occur during its decomposition (Thomas et al., 1993).

Most of the previous works involving coal co-processing that utilizes isotope mass spectrometry are related to the sourcing of coal-bitumen or coal-oil co-processing or gasification of carbon composite materials (Lancet et al., 1993; Bottrell et al., 1990; Steer et al., 1987). Steer et al. (1987) studied the efficacy of Highvale coal and Suncor bitumen co-processing using this technique and provided a valid isotope mass balance method to quantify the amount of coal incorporated in each distillate fraction of their liquefaction process. The synthetic oil generated from their process had intermediate isotope ratios which were directly proportional to the amount of coal incorporated in the feedstock. Lancet et al. (1993) determined the individual contributions of various coal/petroleum feedstocks under varied conditions and demonstrated that stable carbon isotope analysis can be a quantitative tool to independently assess the relative reactions of carbonaceous feedstocks during co-processing (Winschel et al., 1990). In these studies, the isotope ratios of product gas samples were not obtained directly; instead, a forced carbon balance was utilized to obtain information on the gas products. These studies concluded that during actual co-processing, considerable bond breaking occurs. Because $^{13}C$-$^{12}C$ bonds are slightly stronger than $^{12}C$-$^{12}C$, heavier organic residues like tar and vacuum bottoms were presumed to be enriched in $^{13}C$ while lighter hydrocarbon gas products were enriched in $^{12}C$ relative to the feed. Therefore, the isotope ratios in such cases would never be intermediate to the parent sources. Further complications may arise if isotope ratios in product materials change over time depending on the extent of the reactions.

For cases in which the generation of light hydrocarbons such as methane is very low and when isotopic mass balances are not affected in a huge way, the isotope analysis would still be very useful for envisaging product trends that occur during co-processing. Thomas et al. (1993) performed isotope ratio mass spectrometry to study the gasification of carbon composites manufactured from the co-processing of coal tar pitch fibers and petroleum pitch matrix. They observed that heat treating the composite produced changes in the carbon isotope composition of the reactant which may be due to different $\delta^{13}C$ values for the product gas and solid phases. Partially gasifying the carbon composites lowered their $\delta^{13}C$ values by about 4 ‰ due to the loss of $^{12}C$ enriched gases such as methane and that the $\delta^{13}C$ values for the composites change as function of gasification temperature. Also, the products had intermediate $\delta^{13}C$ values compared with the parent materials and hence, reactions occurring during co-processing were easily distinguishable (Thomas et al., 1993).

This chapter describes the utilization of stable carbon isotope analysis for distinguishing and quantifying the individual contributions of coal and biomass feedstocks towards the generation of carbonaceous product gases, in particular, CO and $CO_2$. Although this application has been available for many years and used mostly in bio-geo-chemical studies, very limited information is available in literature with regards to this particular analysis for blends of coal and biomass. Experimental data obtained by this method can provide valuable information for analyzing the interactions and synergy between the feedstocks and also for process modeling and optimization of production methods.

## 13.3 Experimental

### 13.3.1 Materials

For the purpose of this work, two different biomass samples, namely, corn stover (CS) and switchgrass (SG) were blended individually up to 30% by weight with two different ranks of coals, namely, PCC Bituminous coal (PCC) and BT Sub-Bituminous coal (BT). The proximate and elemental analysis of all the feedstock samples used in this study were listed earlier in Chapter 11. These feedstocks were then gasified in a moving bed gasifier operating at atmospheric pressure and varying $O_2$/steam ratios. Gasification of blends of higher percentages of biomass (in excess of 30% by weight) was not possible for the conditions at which the gasifier

was operated since biomass is a low density, low heating value fuel and addition of more biomass would make the gasification process less efficient. Hence, a maximum of 30% by weight of biomass was chosen for this process.

### 13.3.2 Process Parameters and Reactions

The gasification of the feedstock materials was performed at atmospheric pressure using three different volumetric ratios of $O_2$:steam (0.5, 1.0 and 2.0) which correspond to an $O_2$:steam mass ratio of 1.0, 2.0 and 4.0, respectively. One hundred grams of solid feedstock was gasified during each experimental run. The oxygen flow rate was maintained constant at 650 ml/min while the flow rate of steam was maintained between 325 ml/min to 1300 ml/min and the corresponding product gas compositions obtained. The $O_2$/solid feedstock mass ratio was, therefore, constant at 0.625 while the corresponding steam/solid feedstock mass ratios were 0.624, 0.312 and 0.156, respectively. For the purpose of discussion, the $O_2$:steam ratios are further presented as volumetric ratios.

An increase in the $O_2$:steam ratio was seen to result in an increase in the gasification temperature. Since, the gasification was performed auto-thermally, it was necessary that the percentages of oxygen and steam were varied in such a way so as to not let the endothermic zone dominate. Therefore, a minimum $O_2$:steam ratio of 0.5:1 was utilized, below which endothermic zone would prevail and the gasification would not proceed further. The product gas compositions (response variables) were analyzed in two ways: (1) by varying the $O_2$:steam ratios at constant biomass weight percent, and (2) by varying the biomass weight percent at constant $O_2$:steam ratios (treatment factors). Each experimental run was replicated 5 times (n=5) and average product gas compositions were obtained within 95% confidence interval. A list of all the treatment factors and response variables along with values of standard deviations for product gas compositions is provided in Table 13-1.

In any gasifier, char gasification takes place following coal pyrolysis. The remaining carbonaceous solids from the pyrolysis reactions are further oxidized through heterogeneous reactions with carbon dioxide, carbon monoxide, steam, oxygen, and hydrogen. The major reactions that occur during the gasification process are described in Equations 13-2 through 13-8.

Combustion:

$$C + O_2 \rightarrow CO_2 \quad \Delta H = -394 \text{ kJ/mol} \qquad \text{(Eq 13-2)}$$

$$C + \tfrac{1}{2} O_2 \rightarrow CO \quad \Delta H = -111 \text{ kJ/mol} \qquad \text{(Eq. 13-3)}$$

$$CO + \tfrac{1}{2} O_2 \rightarrow CO_2 \quad \Delta H = -283 \text{ kJ/mol} \qquad \text{(Eq. 13-4)}$$

Boudouard Reaction:

$$C + CO_2 \leftrightarrow 2CO \quad \Delta H = +172 \text{ kJ/mol} \qquad \text{(Eq. 13-5)}$$

Vapor-gasification:

$$C + H_2O \leftrightarrow CO + H_2 \quad \Delta H = +131 \text{ kJ/mol} \qquad \text{(Eq. 13-6)}$$

Water gas shift:

$$CO + H_2O \leftrightarrow CO_2 + H_2 \quad \Delta H = -41 \text{ kJ/mol} \qquad \text{(Eq. 13-7)}$$

Methanation:

$$C + 2H_2 \leftrightarrow CH_4 \quad \Delta H = -75 \text{ kJ/mol} \qquad \text{(Eq. 13-8)}$$

Sensible heating of the hot gas provides the heat required for the two endothermic gasification reactions given by Equations 13-5 and 13-6. These are responsible for most of the gasification products like hydrogen and carbon monoxide. Equation 13-7, known as the water gas shift reaction, is an exothermic reaction and has an effect on the $H_2$/CO ratio of the gasification product which is very important when the gas is used for synthesis in downstream processes such as Fischer-Tropsch synthesis. High conversion of CO and steam to $CO_2$ and $H_2$ is favored at low temperatures. The reaction of char with hydrogen to produce methane proceeds at a very slow rate except at very high pressures which is not the case in this study and hence very low concentrations of methane are observed in all the experiments that were performed.

### 13.3.3 Apparatus

The laboratory-scale updraft gasification system, described in Chapter 12, was designed and constructed for this study. The gasifier is a 0.9 meters (3 ft) long cylindrical stainless steel modular flange assembly having an internal diameter of 34.8 millimeters (1.4 in) fitted with another stainless steel tube of 1.9 millimeters (0.08 in) thick on the inside to promote better heat transfer in the axial direction. Temperature profiles along the gasifier axis are measured by a set of K-type thermocouples placed within a steel protective tube.

Coal/biomass is fed at the top of the gasifier by means of a quick-open flange while oxygen and steam are fed from the bottom of the gasifier at atmospheric pressure. The design utilizes a single condenser wherein the hot outlet gas at a temperature of approximately 120 °C enters a cold zone maintained at a temperature of about 10 °C so that unreacted water and other solids can be removed efficiently ensuring that clean product gas which is a mixture of hydrogen, carbon monoxide, carbon dioxide and small amounts of methane, is analyzed using a GOW-MAC Series 600 Auto System GC equipped with a dual thermal conductivity detector (TCD). Nitrogen was used as the carrier gas for the isothermal separation of diatomic hydrogen using a packed HAYESEP Q 60/80 column (1.2 m), while helium was used for the isothermal separation of all other carbonaceous gases using a packed HAYESEP N 60/80 column (2.7 m). Both carrier gases were regulated at 30 ml/min and analytes were detected every six minutes. The temperature of the thermal conductivity detector was maintained constant at 150 °C while the columns were constant at 140 °C.

The first step in the gasification process is the ignition of the bed by adding small amounts of externally heated charcoal particles onto the gasifier bed while supplying the oxidant at a low flow rate of approximately 100 ml/min to 150 ml/min. The feed material is then added onto the charcoal particles and the oxidant flowrate is increased, causing ignition of the bed. Once the bed is ignited, pre-heated steam enters the bed from the bottom of the gasifier. The outlet of the GC is connected to a 500 cc TEDLAR gas sampling bag using a two-way valve. Once the oxygen in the product gas stream is depleted, the valve is opened so that the product gases are collected in the sampling bag. The collected gases are then analyzed for their isotopic composition using GC-C-IRMS.

The GC-C-IRMS analyses were performed using a modified Thermo Fisher Trace GC Ultra connected to a Delta$^{PLUS}$XP isotope ratio mass spectrometer by GC Isolink interface. All carbonaceous compounds eluting from the GC column (30 m Carboxen 1010 PLOT column) were oxidized to $CO_2$ in a capillary combustion reactor maintained at 1030 °C. Helium, flowing at 0.5 ml/min, was used as the carrier gas while the temperature of the GC was ramped at a rate of 10 °C/min from 50-150 °C and held at that temperature for 30 minutes. The product gas samples from the gasifier were loaded onto the GC using 50 µL gas tight syringes through a PVT injector held at 200 °C in split/splitless mode at a split ratio of 30:1. All isotope analyses were

performed in duplicate to provide an estimate for precision and the standard deviation obtained for all $\delta^{13}C$ values was less than ± 0.2 ‰ (n = 5).

## 13.4 Results and Discussion

The product gas compositions of CO and $CO_2$ for all experimental runs are shown in Table 13-1. A major fraction of the product gas contains hydrogen, and methane is also formed in small quantities ($CH_4$ < 5% of total product gas for all experiments). Since hydrogen and methane are not analyzed using stable isotope analysis, their compositions are not listed in Table 13-1.

Table 13-1. Product gas compositions for CO and $CO_2$ produced during the gasification of various coal/biomass blends at different $O_2$/steam ratios

| **Operating Conditions** | | **Average Gasifier Product Gas Composition, % (σ values calculated for n = 5)** | | | | | | | | | | | |
|---|---|---|---|---|---|---|---|---|---|---|---|---|---|
| **$O_2$:Steam** | | **Pure PCC Bituminous Coal** | | | | | | **Pure BT Sub-Bituminous Coal** | | | | | |
| | | **CO % (σ)** | | **$CO_2$ % (σ)** | | **$CO/CO_2$** | | **CO % (σ)** | | **$CO_2$ % (σ)** | | **$CO/CO_2$** | |
| 2.0 | | 31.27 (1.51) | | 41.69 (1.24) | | 0.75 | | 34.43 (2.02) | | 46.37 (1.15) | | 0.74 | |
| 1.0 | | 26.13 (1.13) | | 41.68 (1.33) | | 0.63 | | 27.58 (1.93) | | 45.47 (1.29) | | 0.61 | |
| 0.5 | | 21.63 (1.28) | | 42.66 (1.41) | | 0.51 | | 22.03 (1.58) | | 45.90 (1.17) | | 0.48 | |
| **$O_2$:Steam** | **Biomass Wt %** | **PCC + CS** | | | **PCC + SG** | | | **BT + CS** | | | **BT + SG** | | |
| | | **CO %** | **$CO_2$ %** | **$CO/CO_2$** | **CO %** | **$CO_2$ %** | **$CO/CO_2$** | **CO %** | **$CO_2$ %** | **$CO/CO_2$** | **CO %** | **$CO_2$ %** | **$CO/CO_2$** |
| 2.0 | | 31.94 | 43.29 | 0.74 | 28.91 | 45.86 | 0.63 | 32.18 | 46.45 | 0.69 | 30.05 | 53.65 | 0.56 |
| 1.0 | | 26.58 | 43.69 | 0.61 | 24.35 | 46.02 | 0.53 | 27.20 | 46.20 | 0.59 | 24.41 | 52.58 | 0.46 |
| 0.5 | | 22.17 | 43.13 | 0.51 | 22.83 | 46.62 | 0.49 | 21.64 | 46.05 | 0.49 | 22.38 | 52.07 | 0.43 |
| | 10 | **σ (CO) %** | | **σ ($CO_2$) %** | **σ (CO) %** | | **σ ($CO_2$) %** | **σ (CO) %** | | **σ ($CO_2$) %** | **σ (CO) %** | | **σ ($CO_2$) %** |
| 2.0 | | 1.09 | | 2.15 | 1.38 | | 2.18 | 1.65 | | 1.98 | 1.61 | | 2.32 |
| 1.0 | | 1.71 | | 1.24 | 2.11 | | 2.27 | 2.01 | | 1.43 | 1.88 | | 1.76 |
| 0.5 | | 1.13 | | 1.78 | 1.93 | | 2.82 | 2.23 | | 2.07 | 1.72 | | 1.91 |
| **$O_2$:Steam** | **Biomass Wt %** | **PCC + CS** | | | **PCC + SG** | | | **BT + CS** | | | **BT + SG** | | |
| | | **CO %** | **$CO_2$ %** | **$CO/CO_2$** | **CO %** | **$CO_2$ %** | **$CO/CO_2$** | **CO %** | **$CO_2$ %** | **$CO/CO_2$** | **CO %** | **$CO_2$ %** | **$CO/CO_2$** |
| 2.0 | | 25.34 | 48.17 | 0.53 | 19.72 | 53.68 | 0.37 | 23.93 | 51.12 | 0.47 | 19.05 | 63.23 | 0.30 |
| 1.0 | | 22.56 | 47.43 | 0.48 | 16.45 | 53.11 | 0.32 | 20.68 | 50.94 | 0.40 | 15.34 | 64.18 | 0.24 |
| 0.5 | | 20.11 | 47.11 | 0.43 | 14.88 | 53.57 | 0.28 | 18.14 | 51.74 | 0.35 | 12.74 | 64.06 | 0.20 |
| | 20 | **σ (CO) %** | | **σ ($CO_2$) %** | **σ (CO) %** | | **σ ($CO_2$) %** | **σ (CO) %** | | **σ ($CO_2$) %** | **σ (CO) %** | | **σ ($CO_2$) %** |
| 2.0 | | 2.02 | | 1.26 | 1.99 | | 2.29 | 2.10 | | 1.23 | 2.63 | | 2.07 |
| 1.0 | | 1.78 | | 1.69 | 2.52 | | 1.98 | 2.79 | | 1.95 | 2.42 | | 1.64 |
| 0.5 | | 1.91 | | 1.17 | 1.44 | | 1.26 | 2.59 | | 1.47 | 2.59 | | 1.92 |
| **$O_2$:Steam** | **Biomass Wt %** | **PCC + CS** | | | **PCC + SG** | | | **BT + CS** | | | **BT + SG** | | |
| | | **CO %** | **$CO_2$ %** | **$CO/CO_2$** | **CO %** | **$CO_2$ %** | **$CO/CO_2$** | **CO %** | **$CO_2$ %** | **$CO/CO_2$** | **CO %** | **$CO_2$ %** | **$CO/CO_2$** |
| 2.0 | | 18.13 | 56.67 | 0.32 | 16.00 | 62.52 | 0.26 | 17.14 | 60.93 | 0.28 | 14.34 | 69.80 | 0.21 |
| 1.0 | | 15.73 | 56.79 | 0.28 | 14.50 | 62.03 | 0.23 | 15.14 | 61.17 | 0.25 | 12.81 | 70.94 | 0.18 |
| 0.5 | | 13.09 | 56.17 | 0.23 | 10.02 | 63.43 | 0.16 | 12.39 | 61.11 | 0.20 | 11.69 | 70.14 | 0.16 |
| | 30 | **σ (CO) %** | | **σ ($CO_2$) %** | **σ (CO) %** | | **σ ($CO_2$) %** | **σ (CO) %** | | **σ ($CO_2$) %** | **σ (CO) %** | | **σ ($CO_2$) %** |
| 2.0 | | 2.14 | | 2.29 | 2.87 | | 1.93 | 1.29 | | 1.97 | 2.10 | | 1.93 |
| 1.0 | | 2.08 | | 1.98 | 2.61 | | 2.18 | 1.85 | | 1.38 | 1.72 | | 1.77 |
| 0.5 | | 1.92 | | 1.26 | 2.06 | | 2.22 | 2.27 | | 2.11 | 1.66 | | 2.03 |

The $\delta^{13}C$ values for all the feedstock samples used in this analysis are listed in Table 13-2. For sourcing applications in co-processing, it is necessary that the co-processing feedstocks, which in this case are coal and biomass, have sufficiently different carbon isotope ratios. The idea is that, two isotopically different materials undergoing thermal degradation in a closed system would generate products that would have an isotopic signature intermediary to the parent materials, thus, reflecting the relative amounts of each material utilized. As it can be seen from Table 13-2, bituminous coal and sub-bituminous coal are similar in isotope composition (-25.31 and -24.71‰) as are corn stover and switchgrass (-11.05 and -11.13‰). The difference in

the carbon isotope ratios is relatively large between the coals and corn stover/switchgrass when compared to that of softwoods like pine and poplar which have isotopic compositions of -24.62 and -23.93‰ respectively, similar to that of the coals. This is due to the fact that fossil fuels and most woody biomass materials belong to a similar class of biological material (i.e., $C_3$ plants) as discussed earlier. Therefore, corn stover and switchgrass were chosen to be mixed with the coals in different proportions in this study.

Table 13-2. $\delta^{13}C$ values of various feedstock materials

| **Feedstock** | **$\delta^{13}C$, ‰** |
|---|---|
| PCC Bituminous Coal | -25.31 |
| BT Sub-Bituminous Coal | -24.71 |
| Corn Stover | -11.05 |
| Switchgrass | -11.13 |
| Pine | -24.62 |
| Poplar | -23.93 |

Under the GC experimental method used, carbon monoxide elutes around 318 seconds after injection followed by methane and carbon dioxide at 606 seconds and 1350 seconds respectively as shown in Figure 13-1. The amount of methane generated is relatively low, in the range of approximately 2-4% of the total product gas, and hence it is difficult to quantify its isotopic signature without the injection volume being too large. This would require pre-concentration of methane from the sample gas and heavy water tracer tests may be used in such cases to determine the origin of methane which is out of the scope of this work (Dufaux et al., 1990). Therefore, the IRMS analysis is limited to CO and $CO_2$ which are the major carbon containing gases produced.

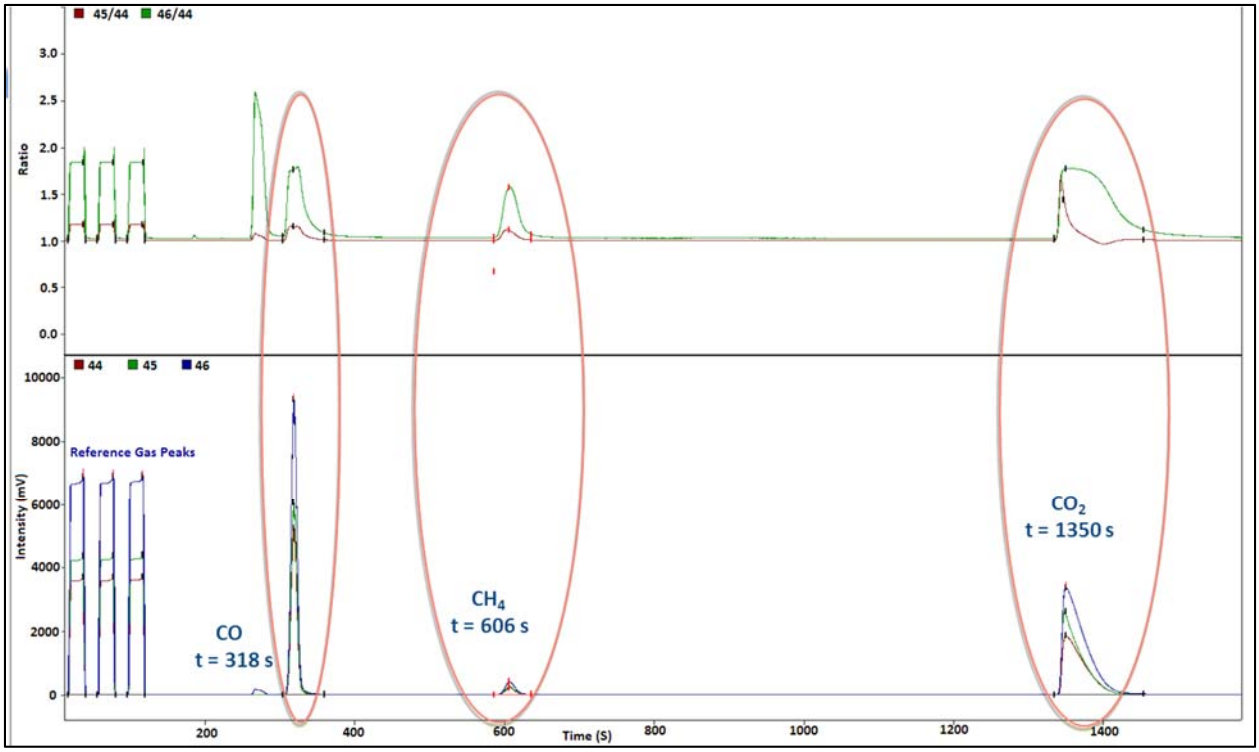



Figure 13-1. Typical GC-C-IRMS chromatogram of the gasification products (CO elutes at t = 318 s followed by $CH_4$ at 606 s and $CO_2$ at 1350 s)

The $\delta^{13}C$ values of the gaseous products (i.e., CO and $CO_2$) were analyzed as described in Section 13.3 and they are listed in Table 13-3. The isotope values of CO from the gasification of each pure source coal are extremely close to the isotope values of the parent materials and are only slightly more negative by about 0.3‰. On the contrary, $CO_2$ under same gasification conditions is enriched in $^{13}C$ by about 2‰ when compared with the source coals. This can be caused due to the effect of isotopic fractionation occurring during gasification. These shifts in isotopic values can be used in the estimation of isotopic equilibrium temperatures and compare them to the actual temperatures attained in the gasifier so as to verify the presence of an isotopic equilibrium between the gaseous compounds.

Table 13-3. Carbon isotope ratios for CO and $CO_2$ produced during the gasification of various coal/biomass blends at different $O_2$/steam ratios

| δ $^{13}C$, ‰ (σ values calculated for n = 5) | | | | | | | | | | | | | | | | | |
|---|---|---|---|---|---|---|---|---|---|---|---|---|---|---|---|---|---|
| $O_2$/Steam | Biomass Wt % | Pure PCC Bituminous Coal | | | | | | | | Pure BT Sub-Bituminous Coal | | | | | | | |
| | | CO | | St. Dev (σ) | | $CO_2$ | | St. Dev (σ) | | CO | | St. Dev (σ) | | $CO_2$ | | St. Dev (σ) | |
| - | 0% | -25.36 | | 0.11 | | -23.46 | | 0.21 | | -24.75 | | 0.17 | | -23.26 | | 0.19 | |
| $O_2$/Steam | Biomass Wt % | PCC + CS | | | | PCC + SG | | | | BT + CS | | | | BT + SG | | | |
| | | CO | (σ) | $CO_2$ | (σ) | CO | (σ) | $CO_2$ | (σ) | CO | (σ) | $CO_2$ | (σ) | CO | (σ) | $CO_2$ | (σ) |
| 2.0 | 10% | -24.47 | 0.15 | -17.90 | 0.14 | -22.59 | 0.09 | -20.91 | 0.08 | -24.61 | 0.07 | -17.37 | 0.07 | -23.58 | 0.13 | -20.85 | 0.05 |
| 1.0 | | -24.04 | 0.11 | -20.51 | 0.07 | -23.02 | 0.13 | -21.11 | 0.17 | -24.38 | 0.04 | -22.23 | 0.14 | -24.21 | 0.09 | -21.13 | 0.06 |
| 0.5 | | -23.91 | 0.18 | -21.04 | 0.20 | -23.38 | 0.12 | -21.35 | 0.05 | -24.06 | 0.06 | -23.96 | 0.04 | -24.52 | 0.11 | -21.28 | 0.12 |
| 2.0 | 20% | -23.47 | 0.16 | -16.92 | 0.18 | -20.35 | 0.09 | -20.19 | 0.05 | -23.72 | 0.10 | -16.19 | 0.09 | -22.49 | 0.07 | -19.74 | 0.08 |
| 1.0 | | -22.34 | 0.08 | -19.51 | 0.09 | -21.78 | 0.06 | -20.49 | 0.04 | -23.42 | 0.19 | -20.81 | 0.20 | -24.00 | 0.10 | -20.13 | 0.09 |
| 0.5 | | -21.26 | 0.16 | -20.38 | 0.09 | -22.81 | 0.13 | -20.65 | 0.13 | -23.23 | 0.15 | -22.74 | 0.06 | -24.40 | 0.04 | -20.34 | 0.07 |
| 2.0 | 30% | -21.56 | 0.22 | -16.73 | 0.13 | -17.84 | 0.14 | -18.90 | 0.04 | -22.43 | 0.14 | -15.24 | 0.02 | -19.16 | 0.12 | -18.44 | 0.05 |
| 1.0 | | -20.72 | 0.12 | -18.97 | 0.06 | -20.43 | 0.09 | -19.15 | 0.08 | -21.88 | 0.09 | -17.96 | 0.09 | -22.89 | 0.06 | -19.07 | 0.11 |
| 0.5 | | -19.54 | 0.17 | -20.17 | 0.06 | -22.10 | 17 | -19.26 | 0.05 | -20.99 | 0.05 | -22.28 | 0.02 | -23.88 | 0.08 | -19.54 | 0.07 |

### 13.4.1 Blends with Corn Stover

For blends of both coals with corn stover, from Table 13-1, it may be observed that with a decrease in $O_2$:steam ratio, the composition of CO decreases while $CO_2$ remains constant in all experiments indicating that Boudouard reaction (Equation 13-5), water gas reaction (Equation 13-6) and water gas shift reaction (Equation 13-7) may be taking precedence. For instance, in blends of bituminous coal and corn stover, holding the percentage of corn stover constant at 30% and varying the $O_2$:steam ratios from 2:1 to 0.5:1 results in a significant drop in the fraction of carbon monoxide in the dry product gas from approximately 18% to 13% whereas the fraction of carbon dioxide remains fairly constant at approximately 56%. In other words, the ratio of $CO/CO_2$ decreases with the addition of steam to the gasifier. This can be attributed to the fact that addition of excess steam to the gasifier lowers the temperatures which favors the conversion of CO to $CO_2$ through water gas shift reaction. The gas compositions can also be compared by increasing the corn stover percentage in the blend, and holding the $O_2$:steam ratio constant. An increase in corn stover percentage yields lower carbon monoxide while increasing the carbon dioxide yield in the product gas. Considering an $O_2$:steam ratio of 2:1, the fraction of carbon monoxide decreases from 32% to 18% while carbon dioxide increases from 42% to 56% when corn stover is increased from 0% to 30% in blends with bituminous coal. This observed effect is significant with confidence intervals greater than 95%. The P-values were calculated by

performing an analysis of variance (ANOVA) of the obtained product gas compositions with respect to varying $O_2$:steam ratios and varying corn stover percentages in the blended feedstock (Section 0).

Similar trends are observed in blends of corn stover with sub-bituminous coal. A comparison of corn stover blends with bituminous and sub-bituminous coal suggests that the ratio of $CO/CO_2$ is slightly lower in sub-bituminous blends. This is because, addition of corn stover to both coals reduces the amount of char reacting in the gasifier and in the presence of excess oxygen, the generation of $CO_2$ is favored. Also, a possible reason for this effect could be the fact that blends of sub-bituminous coal with corn stover have a lower hydrogen content. This results in lower energy content material which burns or combusts readily in the presence of oxygen to emit more $CO_2$ as compared to blends of bituminous coal and corn stover. This result is also in accordance with the average $CO_2$ emission factors supplied by U.S Energy Information Administration which states that anthracite emits the largest amount of $CO_2$ followed by Lignite, Sub-Bituminous and Bituminous (Quick, 2010; Hong & Slatick, 1994).

To support the fact that addition of corn stover to the coals affects the product gas compositions, the carbon isotope composition of the gaseous products CO and $CO_2$ are plotted with respect to the amount of corn stover in the two feedstocks (Figure 13-2 and Figure 13-3). With an increase in the amount of corn stover in the feed, gasification at a constant $O_2$:steam ratio results in a steady increase in the carbon isotope composition of the carbon containing gases, or the product gas becomes isotopically heavier during gasification. On the contrary, the isotope values for decreasing $O_2$:steam ratios at any constant corn stover percentage results in CO being enriched and $CO_2$ being depleted in $^{13}C$. The implication is that carbon from both sources (coals and corn stover) is contributing in the generation of CO and $CO_2$. Although all blends follow a similar trend, distinctions are observed in the isotopic signatures. For example, in blends of corn stover with bituminous coal, the CO in the product gas is enriched in $^{13}C$ compared to pure coal by a maximum of about 6‰ whereas $CO_2$ is only enriched by about 3‰ when 30% corn stover is added and gasified at an $O_2$:steam ratio of 0.5:1 while there is only an increase of about 4‰ in CO and 1‰ in $CO_2$ when corn stover is blended with sub-bituminous and treated under similar conditions. This indicates that corn stover is more readily converted to CO in the presence of bituminous coal than sub-bituminous coal at lower $O_2$:steam ratios. Although the gas composition data in Table 13-1 shows that the difference in the CO

compositions are very little between the two coals, the isotope analysis provides better distinctions in comparing the interactions between corn stover and coals.

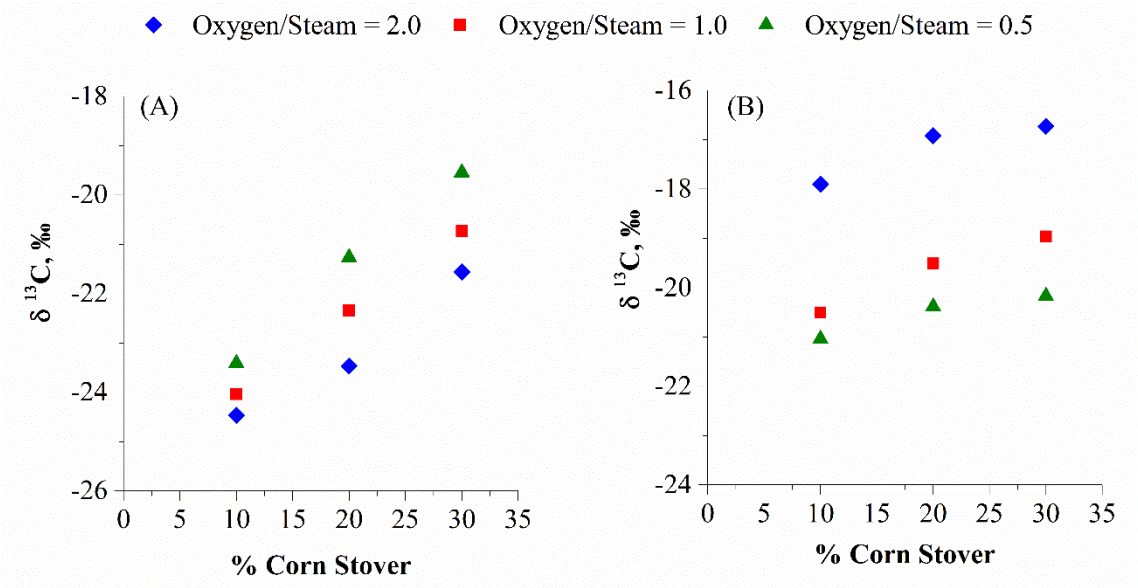



Figure 13-2. Effect of increasing percentage of corn stover and varying oxygen/steam ratios on the isotopic signatures of product gases in its blends with PCC Bituminous coal: (a) Isotopic signature of CO, and (b) Isotopic signature of $CO_2$.

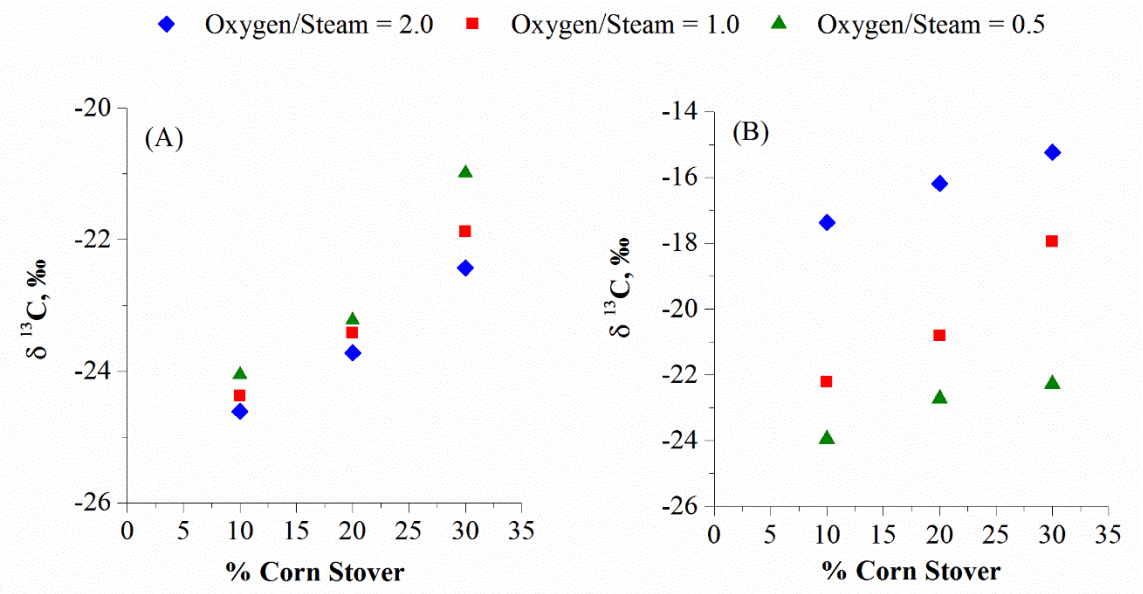



Figure 13-3. Effect of increasing percentage of corn stover and varying oxygen/steam ratios on the isotopic signatures of product gases in its blends with BT Sub-Bituminous coal: (a) Isotopic signature of CO, and (b) Isotopic signature of $CO_2$

On the other hand, at higher $O_2$:steam ratio of 2:1, as an illustration, in blends of corn stover and bituminous coal, $CO_2$ is enriched in $^{13}C$ compared to pure coal by a maximum of 7‰

at an $O_2$:steam ratio of 2:1 (30% corn stover blend) whereas CO is only enriched by 4‰, a decrease by about 2‰ when compared with lower $O_2$:steam ratio of 0.5:1. The isotope values of $CO_2$ in blends of corn stover with bituminous coal are slightly lower in $\delta\ ^{13}C$ value (17.90‰,-16.92‰,-16.73‰) than $CO_2$ generated from the blends with sub-bituminous coal (-17.37‰, -16.19‰, -15.24‰) at a 2:1 $O_2$:steam and corn stover percentages of 10, 20 and 30% respectively. When compared, CS blends with each of the coals do not show much variation in $\delta\ ^{13}C$ (CO) values even with change in $O_2$/steam ratio at lower percentages of corn stover, but the differences are clearly evident at higher loadings of corn stover. But, the same cannot be said for $CO_2$ whose isotope value is enriched in $^{13}C$ with increasing $O_2$:steam ratio at any blend percentage of corn stover. This indicates that at higher $O_2$:steam ratios, corn stover is more readily converted to $CO_2$ while most of the CO is generated via coal. The results shown in Table 13-3, thus indicate that corn stover is definitely contributing towards the generation of these gases and a probable interactions may be existing between the blended feedstock materials.

### 13.4.2 Blends with Switchgrass

As in the case of corn stover, blends of both coals with switchgrass follow similar trends in the generation of the carbonaceous gases although the $CO/CO_2$ ratios are much lower in blends with switchgrass implying higher carbon dioxide generation when compared with corn stover at any constant $O_2$:steam ratio or blend percentage (Table 13-1). The exact reason for this occurrence is speculative but the removal of higher percentage of volatile matter from switchgrass during pyrolysis may be resulting in char with higher void fraction due to which the interaction with incoming steam is reduced, thereby, generating more carbon dioxide through combustion in the bottom zone of the gasifier. The isotopic signature (Table 13-3) of the carbonaceous gases produced during the gasification of coal-switchgrass blends is shown in Figure 13-4 and Figure 13-5.

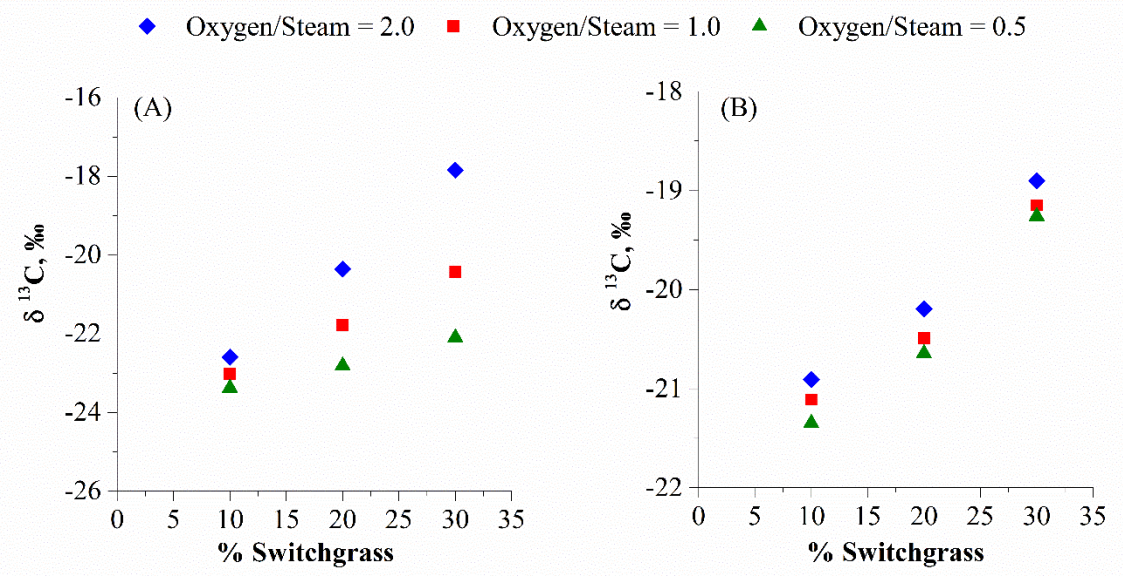



Figure 13-4. Effect of increasing percentage of switchgrass and varying oxygen/steam ratios on the isotopic signatures of product gases in its blends with PCC Bituminous coal: (a) Isotopic signature of CO, and (b) Isotopic signature of $CO_2$

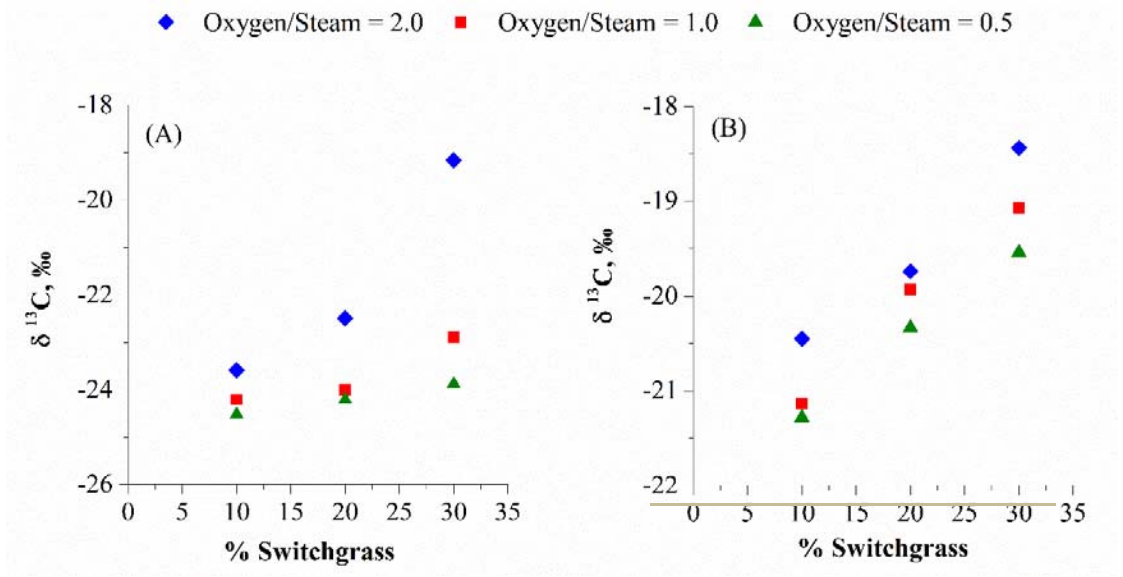



Figure 13-5. Effect of increasing percentage of switchgrass and varying oxygen/steam ratios on the isotopic signatures of product gases in its blends with BT Sub-Bituminous coal: (a) Isotopic signature of CO, and (b) Isotopic signature of $CO_2$

The results obtained show similar trends when compared with coal-corn stover blends (Figure 13-6), that is, the isotope values increase with increasing percentage of switchgrass in the feedstock at any constant $O_2$/steam ratio. An interesting observation is that, based on the isotope results, the affinity of switchgrass towards the production of CO increases with increasing $O_2$:steam ratio in the feed stream. The shift in isotope values is only about 1-1.5‰ at lower

switchgrass percentages (10% and 20%), whereas, the difference increases to about 5‰ when the switchgrass percentage in the blends is 30%. This is contrary to the results obtained for corn stover where in the isotope values for CO increase at a constant rate with increasing steam concentration in the feed stream and the shift in isotope values is only about 1‰ even at higher percentages of corn stover. This may be due to the fact that switchgrass inherently has higher volatile content when compared to corn stover which evolves at higher temperatures causing a shift in the isotopic abundance of CO.

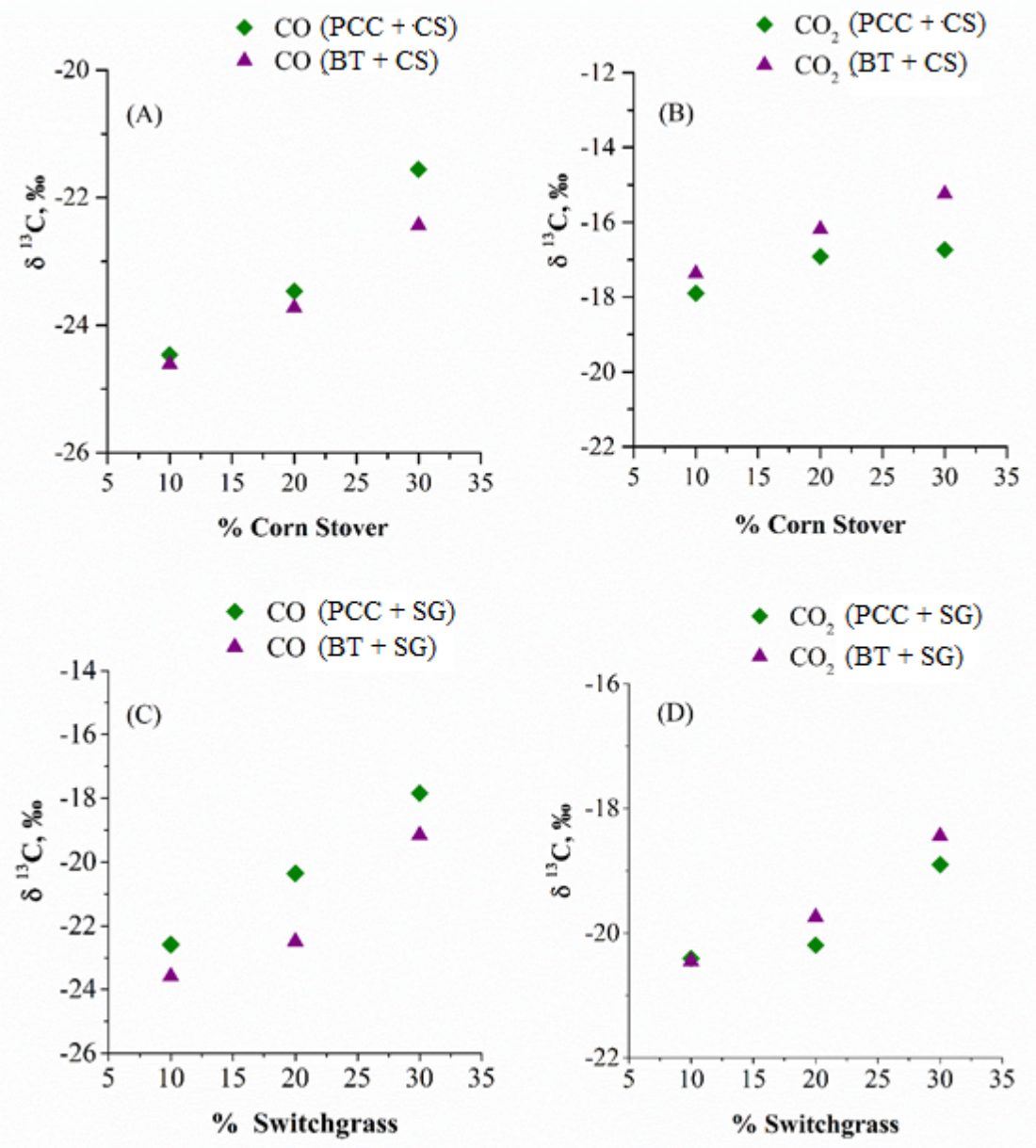



Figure 13-6. Comparison of Isotopic Signatures at an $O_2$:steam ratio of 2:1: (a) and (b): Blends with Corn Stover, and (c) and (d): Blends with Switchgrass

## 13.5 Statistical Significance of Experimental Data

Analysis of variance (ANOVA) was performed on the experimental results using Design Expert® 9.0 software to analyze the statistical significance of the data and also verify the effect of the treatment factors (% Biomass and $O_2$/steam ratio) on the response variables (% CO, % $CO_2$, CO/$CO_2$ ratio, $\delta^{13}C$ (CO) and $\delta^{13}C$ ($CO_2$)). The advantage of using ANOVA lies in the fact that multiple factors affecting a system's performance can be analyzed simultaneously using all the experimental data, rather than analyzing one factor at a time (Karimipour et al., 2013). Typically, linear or quadratic equations are used for estimating the relationship between treatment factors and response variables while the coefficients are estimated using a least-squares fit of the experimental data. The p-value determines the probability of a particular case that the coefficient for a specific term does not have a significant effect. In other words, a small p-value (generally less than 0.05) indicates that the individual terms in the model have a significant effect on the response and p-values larger than 0.1 indicate that the specific term is insignificant and does not have any effect on the response.

In Table 13-4, p-values are provided for the whole model and also for each specific term of the model used. These p-values indicate that both the treatment factors have a significant effect on the percentage of CO generated during gasification of all the feedstocks (very low p-values $<< 0.05$), but, the ratio of $O_2$/steam does not have a significant effect on the percentage of $CO_2$ that is generated (p-values $>> 0.05$). Similarly, very low p-values ($<< 0.05$) have been obtained for the other response variables (CO/$CO_2$, $\delta^{13}C$ (CO) and $\delta^{13}C$ ($CO_2$)) indicating that the desired output variables are significantly influenced by a change in the process variables. R-squared values obtained for different models have also been provided in Table 13-4. These values are close to 1 in most cases and thus, indicate a very good fit of the suggested models.

Table 13-4. Analysis of Variance (ANOVA) for models generated based on experimental data and estimating the statistical significance (p-values) between treatment factors and response variables

| Feedstock | Treatment Factors | Response Variables | | | | | | | | | |
|---|---|---|---|---|---|---|---|---|---|---|---|
| | | % CO | | % $CO_2$ | | $CO/CO_2$ | | δ $^{13}C$ (CO) | | δ $^{13}C$ ($CO_2$) | |
| | | P-Value | | P-Value | | P-Value | | P-Value | | P-Value | |
| PCC + CS | Suggested Model | Quadratic | <0.0001 | Quadratic | <0.0001 | Quadratic | <0.0001 | 2FI | <0.0001 | Quadratic | <0.0001 |
| | A - % CS | < 0.0001 | | < 0.0001 | | < 0.0001 | | < 0.0001 | | < 0.0001 | |
| | B - $O_2$/Steam | < 0.0001 | | 0.7596 | | < 0.0001 | | 0.0003 | | 0.0008 | |
| | AB | 0.0014 | | 0.0802 | | 0.0009 | | 0.0015 | | 0.0132 | |
| | $A^2$ | < 0.0001 | | < 0.0001 | | < 0.0001 | | - | | 0.0018 | |
| | $B^2$ | 0.0348 | | 0.7675 | | 0.0682 | | - | | 0.7042 | |
| | R-Squared | 0.9937 | | 0.9960 | | 0.9936 | | 0.9831 | | 0.9620 | |
| BT + CS | Suggested Model | Quadratic | <0.0001 | Quadratic | <0.0001 | Quadratic | <0.0001 | Linear | 0.0002 | Linear | <0.0001 |
| | A - % CS | < 0.0001 | | < 0.0001 | | < 0.0001 | | < 0.0001 | | 0.0027 | |
| | B - $O_2$/Steam | < 0.0001 | | 0.7253 | | < 0.0001 | | 0.0275 | | < 0.0001 | |
| | AB | 0.0016 | | 0.1244 | | 0.0064 | | - | | - | |
| | $A^2$ | 0.0017 | | < 0.0001 | | 0.0033 | | - | | - | |
| | $B^2$ | 0.0483 | | 0.9149 | | 0.1390 | | - | | - | |
| | R-Squared | 0.9887 | | 0.9979 | | 0.9843 | | 0.9410 | | 0.9671 | |
| PCC + SG | Suggested Model | Linear | <0.0001 | Quadratic | <0.0001 | Linear | <0.0451 | Quadratic | <0.0001 | Quadratic | < 0.0001 |
| | A - % SG | < 0.0001 | | < 0.0001 | | 0.0229 | | < 0.0001 | | 0.0003 | |
| | B - $O_2$/Steam | 0.0006 | | 0.7388 | | 0.0492 | | < 0.0001 | | 0.0018 | |
| | AB | - | | 0.8713 | | - | | < 0.0001 | | 0.5420 | |
| | $A^2$ | - | | < 0.0001 | | - | | 0.1234 | | 0.0017 | |
| | $B^2$ | - | | 0.0076 | | - | | 0.0209 | | 0.4035 | |
| | R-Squared | 0.9601 | | 0.9985 | | 0.9523 | | 0.9996 | | 0.9992 | |
| BT + SG | Suggested Model | 2FI | <0.0001 | Linear | 0.0001 | 2FI | <0.0001 | 2FI | 0.0015 | 2FI | <0.0001 |
| | A - % SG | < 0.0001 | | < 0.0001 | | < 0.0001 | | 0.0023 | | < 0.0001 | |
| | B - $O_2$/Steam | 0.0005 | | 0.9270 | | 0.0014 | | 0.0189 | | 0.0002 | |
| | AB | 0.0391 | | - | | 0.0250 | | 0.0106 | | 0.0021 | |
| | R-Squared | 0.9544 | | 0.9885 | | 0.9671 | | 0.9440 | | 0.9978 | |

## 13.6 Isotope Equilibrium

The generation of CO and $CO_2$ during gasification can therefore be explained via two possible theories (Table 13-1 and Table 13-3). One possibility is that there might be an existence of a partial isotopic equilibrium between $CO_2$ and CO according to the following isotope exchange reaction:

$$^{12}CO_2 + {}^{13}CO \leftrightarrow {}^{13}CO_2 + {}^{12}CO \quad \text{(Eq. 13-9)}$$

These two gases, CO and $CO_2$ could be produced in isotope equilibrium or they may form due to the gasification of solid carbon and re-equilibrate isotopically in the gasifier according to Equation 13-9. Using the observed $\delta^{13}C$ values for $CO_2$ and CO and the carbon isotope

fractionation factor reported as a function of temperature by Richet et al (1977), apparent equilibrium temperatures (AET) for the isotope exchange reaction can be estimated (Brasseur et al., 2002; Sato et al., 2002; Bottinga, 1969). Based on the values of fractionation factor for CO-$CO_2$ isotope exchange provided by Richet et al. (1977), with an increase in temperature, the difference between the $\delta^{13}C$ values of $CO_2$ and CO decreases (Bottinga, 1969).

An increase in the $O_2$:steam ratio implies an increase in the gasification temperature. For blends of corn stover with both coals, only when the percentages of corn stover in the blend are lower (10% and 20%) and high temperatures in excess of 1000 °C at an $O_2$:steam ratio of 2:1 are attained in the gasifier, there exists the potential for an isotopic equilibrium between CO and $CO_2$ as the observed average gasifier temperatures are close to the calculated isotopic equilibrium temperatures (Table 13-5). For lower gasifier temperatures (i.e. lower $O_2$:steam ratios) and higher corn stover loadings (30%), the calculated apparent equilibrium temperature deviates from the observed gasifier temperatures. Moreover, the difference in $\delta^{13}C$ values between $CO_2$ and CO increases with increasing temperatures which is opposite in direction to the expected trend of convergence in carbon isotope composition as temperature increases. Thus, an isotope exchange equilibrium does not exist.

The carbon isotope results may be explained by two chemical reactions: (1) Boudouard reaction (Equation 13-5), and (2) Water Gas Shift reaction (Equation 13-7). Boudouard reaction is endothermic by nature, therefore from thermodynamics, the formation of CO would result in a decrease in temperature of the gasification zone. This reduction in temperature would, therefore, favor the water gas shift reaction which is exothermic by nature and high conversions of CO and steam to $CO_2$ and $H_2$ can be obtained. From the product gas compositions shown in Table 13-1 and maximum gasifier temperatures shown in Table 13-5, the ratio of $CO/CO_2$ decreases with decreasing temperature (decreasing $O_2$:steam ratios) for corn stover blends and therefore, the relationship between CO-$CO_2$ proceeds via the kinetic conversion of CO to $CO_2$, and no isotope exchange is occurring between CO and $CO_2$ in these chemical reactions.

A similar argument may be made for interpreting the carbon isotope composition of CO and $CO_2$ in blends with switchgrass. As shown in Table 13-3, Figure 13-4, and Figure 13-5, although CO is enriched in $^{13}C$ with increasing temperature at a given percentage of switchgrass, and the variation in the $\delta^{13}C$ values of $CO_2$ is minimal (i.e. the difference in $\delta\ ^{13}C$ values of $CO_2$ and CO is decreasing with increasing temperatures), the calculated isotopic equilibrium

temperatures from CO and $CO_2$ are unreasonably high (Table 13-5). Also, the data from the product gas composition (Table 13-1) of the gasifier shows that the ratio of $CO/CO_2$ decreases with decreasing temperature which is in conjunction with the results obtained for corn stover blends. The calculated AETs for all sample blends are much higher than the actual gasifier temperatures and from Table 13-5, it is evident that the temperatures achieved in the gasifier are far from equilibrium and therefore, isotopic equilibrium is not achieved even with blends of switchgrass.

Table 13-5. Comparison of isotopic equilibrium temperatures of $CO_2$-CO product gases and experimental gasifier temperatures

| $O_2$:Steam | % CS Added to PCC | Temperature, °C | | % CS Added to BT | Temperature, °C | |
|---|---|---|---|---|---|---|
| | | Gasifier | Equilibrium | | Gasifier | Equilibrium |
| 2 | 10 | 1055.4 | 1089.8 | | 1081.3 | 1029.5 |
| 1 | | 900.8 | > 1300 | 10 | 1010.9 | > 1300 |
| 0.5 | | 853.5 | > 1300 | | 912.9 | > 1300 |
| 2 | 20 | 1029.3 | 1090.6 | | 1041.5 | 1002.9 |
| 1 | | 894.1 | > 1300 | 20 | 890.9 | > 1300 |
| 0.5 | | 825.6 | > 1300 | | 852.1 | > 1300 |
| 2 | 30 | 900.7 | 1143.1 | | 883.2 | 1078.2 |
| 1 | | 867.8 | > 1300 | 30 | 826.2 | > 1300 |
| 0.5 | | 803.3 | > 1300 | | 739.7 | > 1300 |
| $O_2$:Steam | % SG Added to PCC | Temperature, °C | | % SG Added to BT | Temperature, °C | |
| | | Gasifier | Equilibrium | | Gasifier | Equilibrium |
| 2 | 10 | 1010.6 | > 1300 | | 1037.3 | > 1300 |
| 1 | | 962.1 | > 1300 | 10 | 995.2 | > 1300 |
| 0.5 | | 901.1 | > 1300 | | 908.1 | > 1300 |
| 2 | 20 | 959 | > 1300 | | 927.7 | > 1300 |
| 1 | | 933 | > 1300 | 20 | 847.3 | > 1300 |
| 0.5 | | 879.1 | > 1300 | | 811.3 | > 1300 |
| 2 | 30 | 912.8 | > 1300 | | 882.1 | > 1300 |
| 1 | | 899.7 | > 1300 | 30 | 733.4 | > 1300 |
| 0.5 | | 823.5 | > 1300 | | 680.9 | > 1300 |

## 13.7 Carbon Sourcing

To interpret the amount of each parent source incorporated into the carbon containing gases, the following expression has been utilized:

$$(\delta^{13}\,C\,X)_{Biomass} + (\delta^{13}\,C\,X)_{Coal} = \delta^{13}\,C_{Product} \quad \text{(Eq. 13-10)}$$

and,

$$X_{Biomass} + X_{Coal} = 1 \quad \text{(Eq. 13-11)}$$

where *X* is the fraction of parent material incorporated into product gas. Therefore,

$$\left(\%\ Biomass\ Carbon = \frac{\delta^{13}\,C_{Product} - \delta^{13}\,C_{Biomass}}{\delta^{13}\,C_{Biomass} - \delta^{13}\,C_{Coal}}\right) \quad \text{(Eq. 13-12)}$$

For this analysis, it is assumed that the $\delta^{13}C$ values of the parental material and the gaseous products are equivalent over the course of the experiment (i.e. no isotope fractionation occurs during the reaction) (Steer et al., 1987; Schoell, 1980). The contribution of each parent material in the generation of CO and $CO_2$ is shown in Figure 13-7. The results of this analysis suggest that the contribution of biomass in the generation of both CO and $CO_2$ is greater in blends with bituminous coal as compared with blends of sub-bituminous coal.

Using Equation 13-12, it can be clearly seen, that the addition of biomass has had a definite impact in the generation of carbon containing gases. If no interactions are present between biomass and coals, then the resultant product gas mixture would have isotope values that are closer to the source coal and enriched in $^{12}C$. As this is not occurring, it may be suggested that the synergy between corn stover and coals is higher at higher $O_2$:steam ratios (2:1), with corn stover contributing almost up to 60% and 70% with respect to the generation of $CO_2$ in its blends with bituminous coal and sub-bituminous coal respectively, while, the blends of switchgrass with coals contribute only about 45% at the same $O_2$:steam ratio (2:1). At lower $O_2$:steam ratios (0.5:1), however, the contribution of switchgrass (43% in blends with PCC and 38% in blends with BT) is higher than corn stover (36% in blends with PCC and 18% in blends with BT) with respect to the generation $CO_2$. Considering the generation of CO, the contribution of corn stover is maximum at an $O_2$:steam ratio of 0.5:1 (40% and 27% in blends with PCC and BT respectively) while the contribution from switchgrass is maximum at a 2:1 ratio of $O_2$:steam (53% and 41% in blends with PCC and BT respectively). These comparisons are being made at 30% biomass blend ratios where the contribution of biomass towards the generation of CO and $CO_2$ is the highest. These results are particularly important to know during co-gasification of coal/biomass blends as one of the major reasons for blending biomass with coal is to mitigate the emission of greenhouse gases. Moreover, the interpretation of these data would only help in process modeling and optimization of co-gasification processes. Ultimately, the usage of the data from this analysis depends on the end product one would like to achieve by heat treating or chemical conversion of coal/biomass blends.

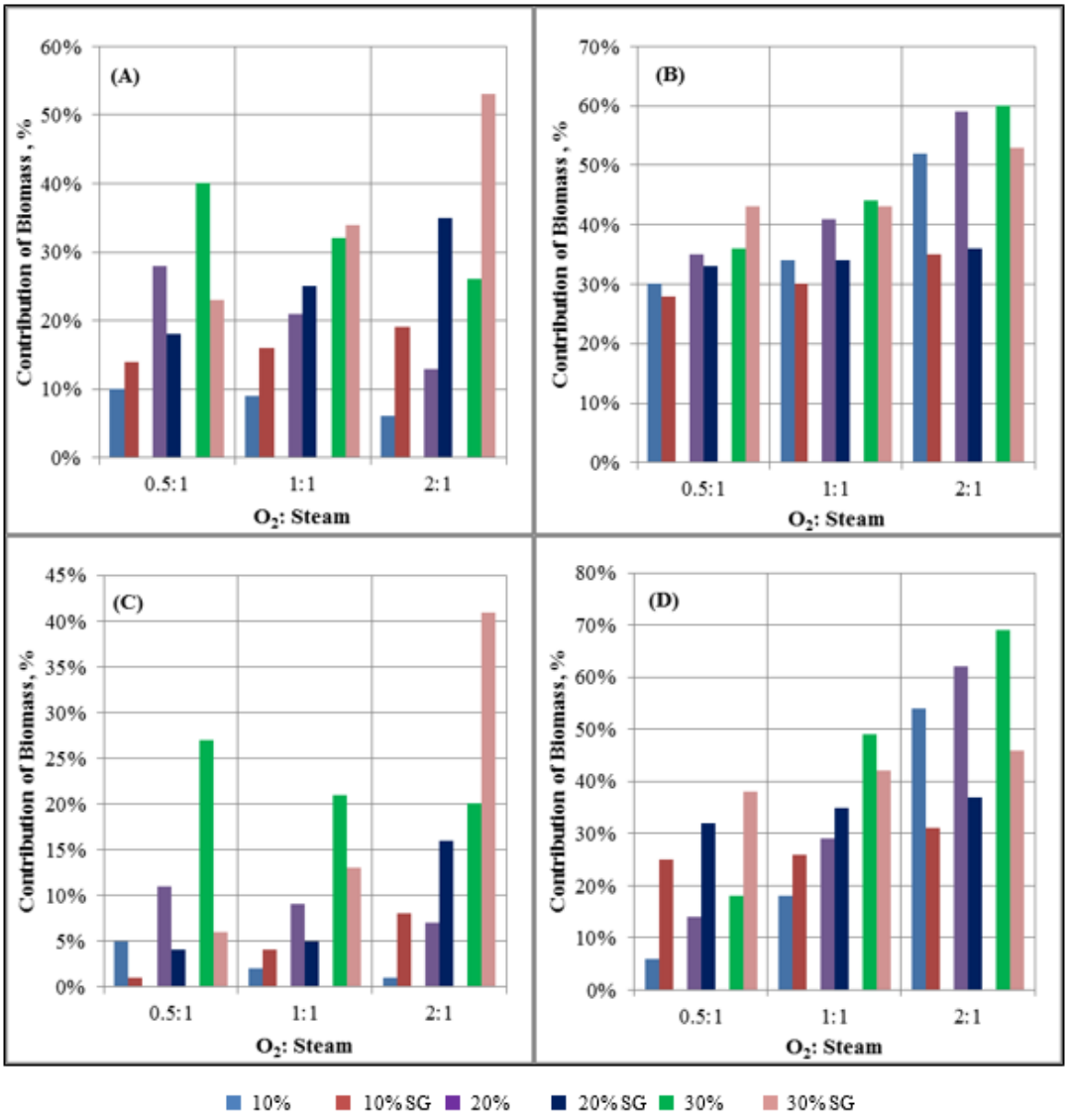



Figure 13-7. Individual contribution of each biomass source towards generation of product gases at different $O_2$/steam ratios: (a) Contribution in the generation of CO in blends with PCC Bituminous coal, (b) Contribution in the generation of $CO_2$ in blends with PCC Bituminous coal, (c) Contribution in the generation of CO in blends with BT Sub-Bituminous coal, and (d) Contribution in the generation of $CO_2$ in blends with BT Sub-Bituminous coal

## 13.8 Summary and Conclusions

An effective method has been utilized for analyzing and distinguishing the individual contributions of coal and biomass towards the generation of carbonaceous gases using the differences in their carbon isotope ratios. Corn stover and switchgrass were used as the biomass materials and were blended up to 30% by weight with two different ranks of coal (i.e. PCC bituminous coal and BT sub-bituminous coal). The gasification of these blends was performed at

varying $O_2$/steam ratios in a moving bed gasifier and the generated carbon gases were effectively analyzed using stable carbon isotope ratio mass spectrometry.

It was observed that an increase in the amount of biomass in the feed, led to a steady increase in the isotopic value of the carbon containing gases, implying that the product gas becomes isotopically heavier during gasification. This is also an indication of probable synergistic effects between the blended materials. Furthermore, the correlation between the $\delta^{13}C$ values and gasifier temperatures suggests that $CO/CO_2$ ratio proceeds via a kinetic mechanism rather than an isotopic exchange. The amount of each parent material utilized for the generation of the product gases was calculated using a simple mixing equation. The addition of biomass had a definite impact in the generation of carbon containing gases. For blends with corn stover, higher $O_2$:steam ratios result in the contribution of almost up to 70% of carbon from corn stover in the generation of $CO_2$, while, the blends of switchgrass with coals prove to be much effective at lower oxidant ratios with respect to the generation $CO_2$ and vice versa for the generation of CO. Finally, it can be stated that the data obtained utilizing this unique analytical technique would provide valuable insights not only pertaining to the synergy between the blended feedstock materials but also towards process modeling, optimization and reaction pathways in the field of co-gasification of coal and biomass.

# Chapter 14

# Physiochemical Characterization of Coal and Biomass Feedstocks

## 14.1 Introduction

An organized methodology is required to qualitatively and quantitatively understand the pyrolysis and combustion behavior of coal-biomass fuel blends. The blend pyrolysis-combustion behavior must be understood in terms of its physicochemical changes, kinetic parameters, evolved gas aspects and associated pyrolysis-combustion energetics. Based on these main aspects of analysis, a fuel pyrolysis and combustion performance model must be developed to compare the performance of different fuel blends. This understanding of pyrolysis-combustion behavior of fuel blends is developed in the subsequent chapters.

Accurate physicochemical characterization of blended fuel, their char and ash samples is necessary to determine the interactions between fuel constituents during pyrolysis and combustion. The understanding of physicochemical properties of fuel blends, their char and ash will assist predicting their pyrolysis-combustion performance and resolving the issues related to emissions and molten ash in a scaled-up reactor (Wornat et al., 1995). The physical properties, such as the size, shape and porosity of fuel particles are important parameters that define the fuel reactivity and residence time (Biagini et al., 2008). Similarly, chemical properties such as the composition of char material, and the distribution of carbon, hydrogen and oxygen elements directly influences the issues related to char ignition, combustion rate and flame-out related problems in combustors (van Alphen, 2007).

The differences in physicochemical properties of coal and biomass fuels needs to be quantified for proper understanding the pyrolysis-combustion behavior of fuels. Coal and biomass fuels contain organic elements (macerals) and inorganic components (minerals). The elemental composition of macerals (including C, H, O and organically bound inorganic elements) is directly dependent on the rank of the coal. Whereas the ash composition comprises

of minerals and aluminosilicate glasses, which is directly related to the fuel source (van Alphen, 2007). There are certain differences between the inorganic composition of coals and biomasses. While in coal most of the inorganic material is present as minerals, in biomasses these can exist as salts or organically bound to macerals (Zolin et al., 2001). Thus, the amount of inorganic material vaporizing in biomass samples is much higher (75% by weight) than those of coal samples (4% by weight) at high temperatures (1200°C) (Zolin et al., 2001).

It has been demonstrated in many studies that the presence of the inorganic salts influence the primary reactions during the devolatilization process (Park et al., 2010; Khelfa et al., 2008; Sonobe & Worasuwannarak, 2008; Zolin et al., 2001; Janse et al., 2000). While most of the inorganic salts act as catalysts, many other acts as inhibitors (Khelfa et al., 2008). Usage of biomass feedstocks in furnaces lead to operational problems such as slagging and fouling; however, usage of small amount (10-15%) of biomass with coal mixtures in co-firing applications does not show such negative effects (Zolin et al., 2001). Another way of reducing the influence of inorganic salts on biomass pyrolysis is to leach the feedstocks with water (Giuntoli et al., 2009; Gomez et al., 2009; Várhegyi et al., 2004; Manyà et al., 2002; Stenseng et al., 2001; Teng & Wei, 1998). This process removes most of the potassium and chlorine based salts among many others, and also reduces the nitrogen-oxide content in the resultant chars. However, the combustion behavior of leached biomass has not been investigated or verified in scaled-up gasifiers/furnaces (Zolin et al., 2001). Thus, the effect of biomass water leaching and its influence on co-firing must be properly quantified from physicochemical perspective.

Traditional analysis techniques, such as proximate and ultimate analysis, can be used to estimate the elemental composition of fuels and chars. However, the inherent limitations of these techniques and the sampling and analytical errors associated may lead to misleading interpretations (van Alphen, 2007). Thus, van Alphen et al. (2007) recommended detailed, accurate, and automated physicochemical characterization of fuel and ash properties using scanning electron microscope (SEM) techniques as a viable solution. SEM images can provide enlarged vision of fuel, char or ash samples with minor loss in precision. SEM instrument can be used with Backscattered Electron Imaging (BEI) and Energy Dispersive X-Ray Spectroscopy (EDX) stages to provide the elemental distribution of the sample. Hence, a series of experiments were performed to quantify the effects of biomass leaching, differences in individual biomass

and coal samples, and the impact of blending coal and biomass fuels from physicochemical perspective.

## 14.2 Experimental

### 14.2.1 Materials and Preparation

Samples used in this study included corn stover (CS) and switchgrass (SG) biomass feedstocks, as well as bituminous US eastern steam coal (EC), namely, McClure River. The proximate and ultimate analyses for these samples are provided in Table 14-1 and Table 14-2, respectively.

Table 14-1: Proximate analysis (dry basis) of coal and biomass samples

| Fuel | EC | SG-Raw | CS-Raw |
|---|---|---|---|
| % Ash | 10.50 | 2.86 | 5.01 |
| % Sulfur | 0.88 | 0.08 | 0.10 |
| % Volatile | 28.28 | 82.58 | 82.13 |
| % Fixed carbon | 61.22 | 14.56 | 12.86 |
| Calorific value (kJ/kg) | 32734 | 18873 | 18778 |
| MAF calorific value (kJ/kg) | 36574 | 19429 | 19769 |

Table 14-2: Ultimate analysis (dry basis) of coal and biomass samples

| Fuel | EC | SG-Raw | CS-Raw |
|---|---|---|---|
| % Carbon | 82.26 | 48.81 | 53.27 |
| % Hydrogen | 4.75 | 6.32 | 5.67 |
| % Nitrogen | 1.56 | 0.35 | 0.62 |
| % Sulfur | 0.88 | 0.08 | 0.10 |
| % Ash | 10.50 | 2.86 | 5.01 |
| % Oxygen | 0.05 | 41.58 | 35.33 |

Biomass feedstocks were milled to produce finely ground samples. The finely ground biomass particles were sieved through calibrated sieves within 400-500 μm range. To examine the influence of inorganic salts, the biomass samples were tested in both untreated (Raw) and distilled water washed (Leached) states, as mentioned in the literature (Giuntoli et al., 2009; Gomez et al., 2009; Várhegyi et al., 2004; Manyà et al., 2002; Stenseng et al., 2001; Teng & Wei, 1998). For this purpose, sieved biomass samples were leached at 110 ºC temperature in a

well stirred container for two hours before air drying them at 110ºC. All four biomass samples were dried at 110 ºC in air before experimentation.

Eastern coal was received in the form of powder with the mean diameter being less than 400 μm sieve. The EC sample was received in a wet state (about 30% moisture by weight), and thus was thoroughly dried in air at 110 ºC for four hours before use. Two more test samples were prepared by mixing EC with leached biomass samples in the ratio of 80:20 by mass to investigate interactions between coal and salt-free biomass samples. The biomass sample weight ratio was restricted to 20% by mass as per the guidelines mentioned in the literature (Biagini et al., 2002; Zolin et al., 2001). Thus, in total seven test samples were developed and experimented, including, EC, SG-Raw, CS-Raw, SG-Leached, CS-Leached, EC & SG-Leached mix (80:20 by mass) and EC & CS-Leached mix (80:20 by mass).

### 14.2.2 Instrumentation and Procedure

An Environmental Scanning Electron Microscope (ESEM) was used to conduct the physicochemical characterization of the samples, while a Simultaneous Thermogravimetric Analyzer (STA) was used to produce the pyrolyzed char and char oxidized ash samples from the fuel for physicochemical analysis. The physicochemical characterization of the solid fuels, pyrolyzed char and char oxidized ash samples was conducted using a Quanta 600 ESEM (Figure 14-1). ESEM images provided an enlarged vision of samples with a minor loss in precision, thus enabling the qualitative characterization of the microstructure of fuel, char and ash samples. Multiple images of the samples were collected at 100X, 1000X, 5000X and 10000X magnification levels.



Figure 14-1. Quanta 600 FEG ESEM

The ESEM instrument was further used with an Energy Dispersive X-ray Spectroscopy (EDX) stage to provide the elemental distribution at the surface of the sample. The major elements quantified on the sample surface included C, O, Si, Al, S, P, Na, Ca, K, Cl, Fe and Ti (for EC sample). Any other elements, if found in substantial amount in a sample, were also quantified. The hydrogen element was not quantified due to the limitations of the instrument. A rectangular area, spanning the maximum possible width and height of the particle at a particular magnification, was used to represent the elemental composition of the sample using EDX. The measurements were repeated for several particles of the sample, and an average composition value was used for the analysis. The aforementioned elements were quantified on the basis of mass percentage. The tested fuel, char and ash samples were sputter coated with gold and platinum prior to the ESEM testing to enable imaging. The estimated sputter coated gold and platinum amounts were appropriately deducted from the subsequent elemental analysis of the sample.

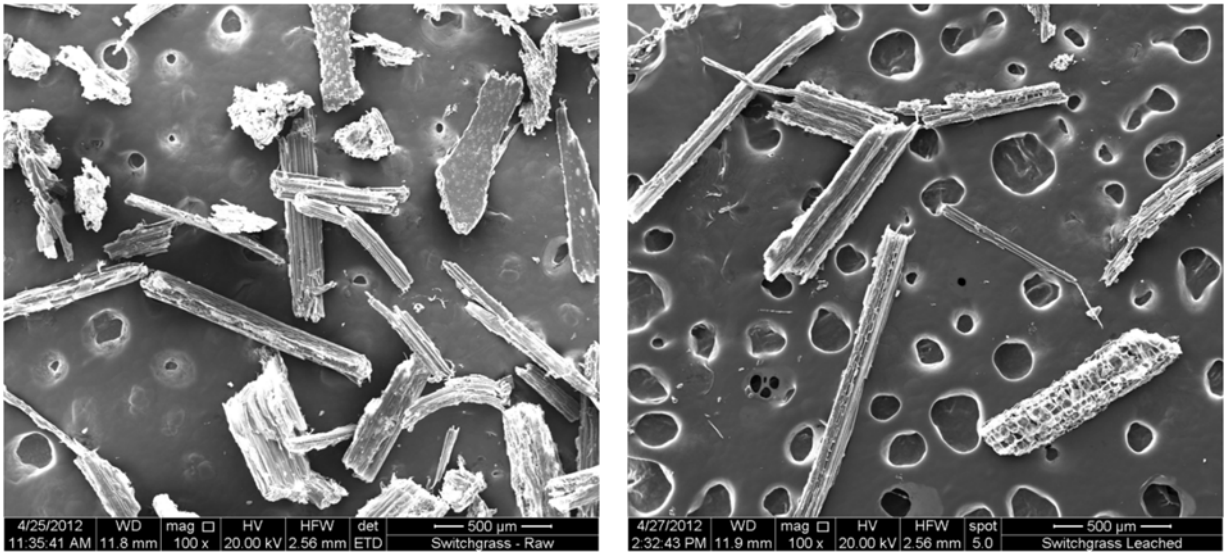
The pyrolyzed char and char oxidized ash samples were prepared using the STA. The fuel samples were first pyrolyzed in inert nitrogen atmosphere by heating the samples at 20 K/min to 1073 K with a five minute residence time interval to prepare pyrolyzed char samples. Additional pyrolyzed char samples were further oxidized in 99.999% pure air at 1073 K for 30 minutes to prepare char oxidized ash samples. These samples were then used for physicochemical characterization in the ESEM.

## 14.3 Results and Discussion

The physical effect of pyrolysis and char oxidation on different samples was investigated on a microscopic level using an ESEM. In addition, EDX was used to quantify the solid composition changes due to pyrolysis and char oxidation.

### 14.3.1 Biomass Leaching

Figure 14-2(a) and Figure 14-2(b) shows the ESEM images of untreated (Raw) and washed (Leached) SG samples at 100X magnification, respectively. In these images, the samples can be seen sitting on top of an adhesive carbon tape. As observed from the figure, biomass particles have high aspect ratio, and the particles are roughly cylindrical and straight along the length. The particles of both samples remained straight along the length after washing and drying in air, and there were no physical differences observed at 100X magnification. Same observations were made for CS Raw and CS-Leached samples.

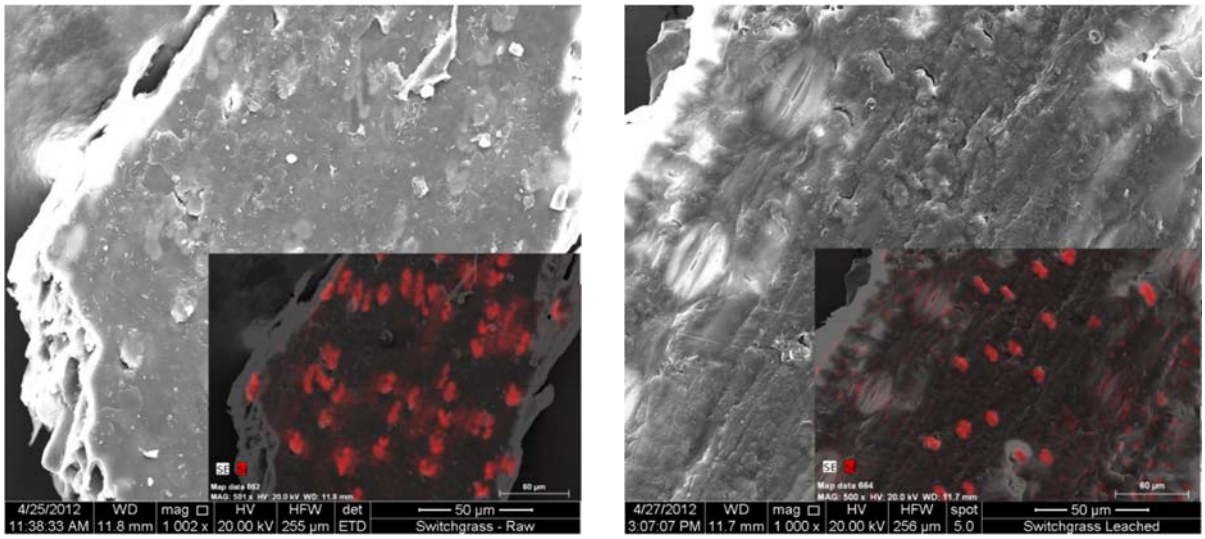



(a) (b)

Figure 14-2. Switchgrass biomass at 100X magnification on top of a carbon tape: (a) Raw, and (b) Water leached

ESEM images of raw and leached SG biomass at 1000X magnification are shown in Figure 14-3(a) and Figure 14-3(b), respectively. Also included in the inset of Figure 14-3 are the X-ray images of the particle for the Si element scan. As observed from Figure 14-3(a), small spherical particles of inorganic K and Mg based salts are present on top of the smoother surface

of raw SG particle. These K and Mg particles were washed out during the water leaching process, as observed from their absence in Figure 14-3 (b). The X-ray inset in Figure 14-3(a) shows Si and O based patches that are present in the SG particle. These patches disappear considerably during the water leaching process, as observed from Figure 14-3(a). Figure 14-4(a) and Figure 14-4(b) show the effect of water leaching on the major inorganic elements in SG and CS samples. As observed from Figure 14-4(a), the Si concentration decreased by almost 42%, while the Mg and K elements were nearly eliminated on water leaching of SG. Potassium (K) was the major inorganic element found on the surface of CS particles, the concentration of which decreased by almost 68% on water leaching. However, the complete elimination of K element was not possible with just one water leaching cycle on CS sample, thus indicating higher amount of impurities in CS. A slight increase in Cl element was observed on leaching of both biomass samples, which may be attributed to the decrease in concentration of other inorganic elements.




(a) (b)

Figure 14-3. SG particle at 1000X magnification with Si element X-ray scan in the inset: (a) SG-Raw, and (b) SG-Leached

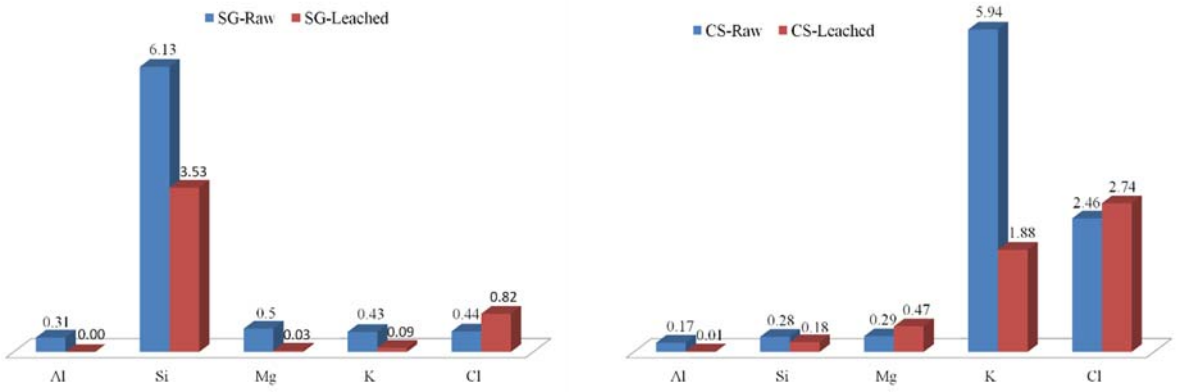



Figure 14-4. Effect of water leaching on major inorganic element concentrations of biomass samples: (a) SG, and (b) CS

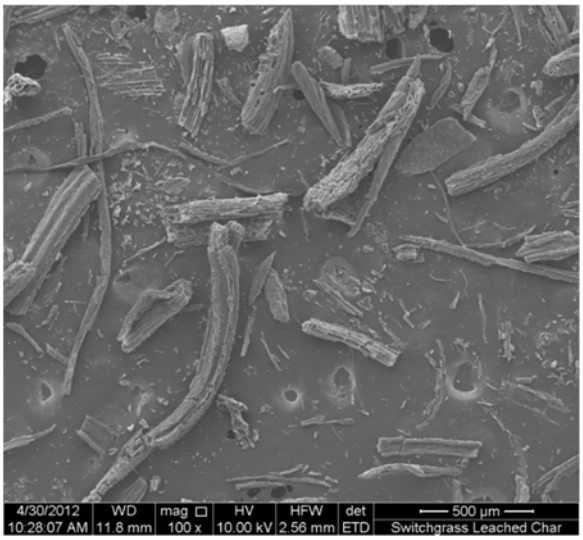
Table 14-3 shows the C%, O% and C/O percentage ratio for the raw and water leached biomass samples. As observed, the C% for biomass samples remains unchanged after water leaching. The O% of biomass samples was found to increase on water leaching (7% to 23%). Thus, water leaching caused a drop in the C/O ratio for biomass samples. The C/O ratio of CS was found to be a little higher than that for SG sample and this was primarily due to the large amount of Si-O patches found in the SG sample. This indicated that the energy density of CS sample is higher than that of SG sample, and is consistent with the MAF calorific value for the two biomass samples reported in Table 14-1. Another point noted from the Table 14-3 is regarding the accuracy of the C% (+0.9% to +2.6 % error) and O% (+0.6% to -3.8 % error) measured by the ESEM instrument compared to that measured through the ultimate analysis of Raw biomass samples provided in Table 14-2. This validates the accuracy of measurement methodology used in this analysis.

Table 14-3: Effect of leaching on biomass (C%, O% and C/O in mass percentage)

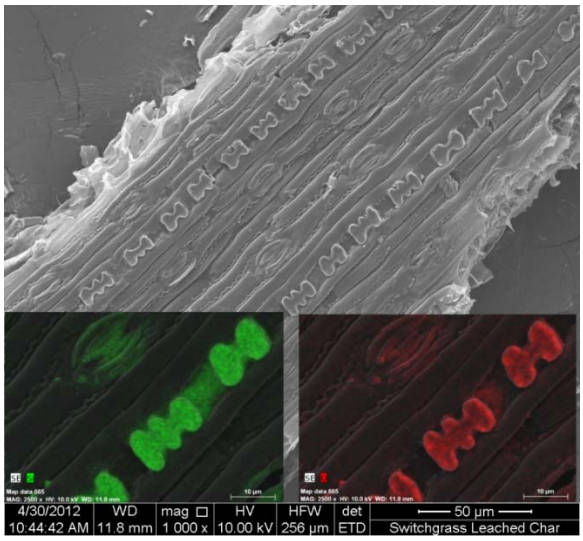
| Sample @ 20 K/min | C % | O % | C/O |
|---|---|---|---|
| SG-Raw | 49.7 | 42.2 | 1.2 |
| SG-Leached | 50.2 | 45.0 | 1.1 |
| CS-Raw | 56.1 | 31.6 | 1.8 |
| CS-Leached | 54.2 | 38.9 | 1.4 |

Figure 14-5(a) shows the char of SG-Leached samples at 100X magnification. As observed from Figure 14-5 (a), the char particles of SG-Leached sample were found to be

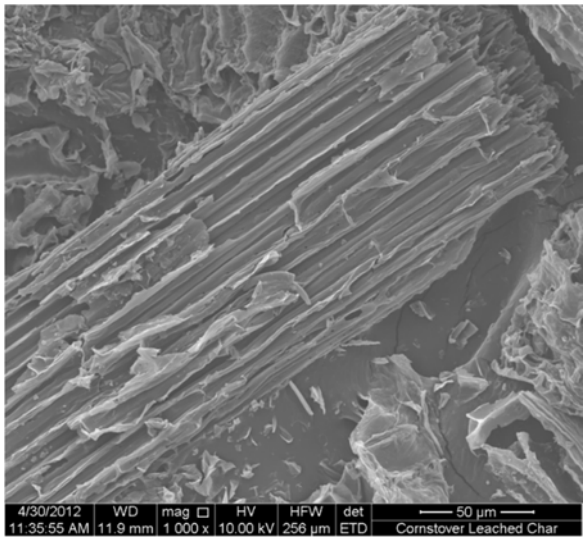
deformed in shape and more curved along the length than the original sample. There was also an emergence of smaller chipped char particles in Figure 14-5 (a), thus indicating a decrease in average aspect ratio of biomass particles following pyrolysis. A similar observation was made by Wornat et al. (1995) for SG samples. Figure 14-5(b) contains the 1000X magnified image for a SG-Leached char particle. The X-ray scan for Si and O elements is also included in the inset of Figure 14-5(b). The same Si-O patches, as previously observed in Figure 14-3(b) for unpyrolyzed SG, were now more clearly visible on the surface of pyrolyzed char in Figure 14-5(b). Thus, these patches indicated high concentration of Si and O elements in the SG-Leached sample. In comparison, the CS-Leached char particles did not show Si element patch pattern on its surface. This is consistent with Figure 14-4(b) where the Si concentration for CS samples is calculated to be substantially lower than SG samples. Instead, the char particles of CS-Leached sample show hollow zones which indicate the loss of organic matter during pyrolysis, as shown in Figure 14-5(c).




(a)




(b)

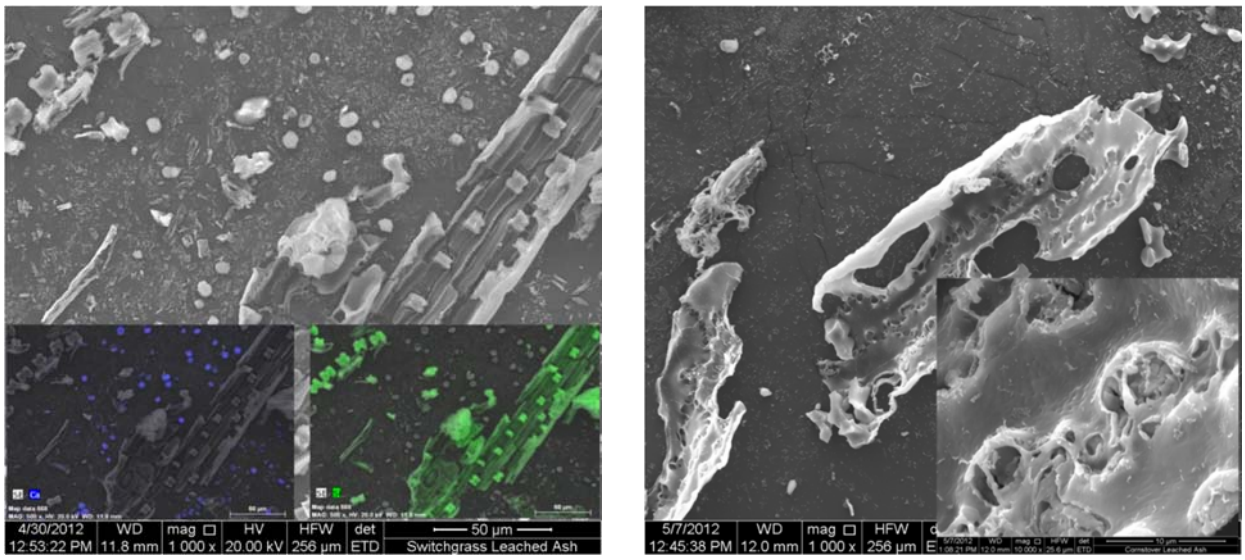



(c)

Figure 14-5. Pyrolyzed leached biomass samples: (a) SG-Leached char at 100X magnification, (b) SG-Leached char sample at 1000X magnification with Si (Green) and O (Red) element X-ray scans in the inset, and (c) CS-Leached char at 1000X magnification

Figure 14-6(a) includes the ESEM image for ash particles generated from SG-Leached sample at 1000X. The inset of Figure 14-6(a) contains the X-ray scan for Ca (Blue) and Si (Green) element. As observed from Figure 14-6(a), the Ca spheres break off from the main organic body of SG ash sample. It is important to note that the Ca element was not visible on the surface of leach SG or its char sample. A scan for O element (not shown in the figure) indicated the spheres to likely be CaO salts. It is also observed that the Si-O patches remain organically bound to the main biomass shell even after oxidation, unlike the CaO spheres (Zolin et al., 2001). In comparison, Figure 14-6(b) contains the ESEM image of for ash particles generated from CS-

Leached sample at 1000X magnification. There was neither the presence of CaO particles, nor the pattern for Si-O patches on the CS ash shell.




(a) (b)

Figure 14-6. Ash samples at 1000X magnification: (a) SG-Leached ash with Ca and Si element X-ray scans in the inset, and (b) CS-Leached ash particle

This is further evident from Figure 14-7, where the major elements in biomass ash samples are shown in their mass fraction percentages. As observed from Figure 14-7, the C, O and Si elements forms more than 90% of composition by mass in biomass ash samples. The amount of Si in SG ash is found to be approximately 62% higher than that of CS due to the presence of Si-O patches in SG. This is also indicated with a high amount of O element in the SG sample in comparison to the CS sample. However, this results in the amount of C element in the CS sample to be about 82% higher than the C content of SG sample.

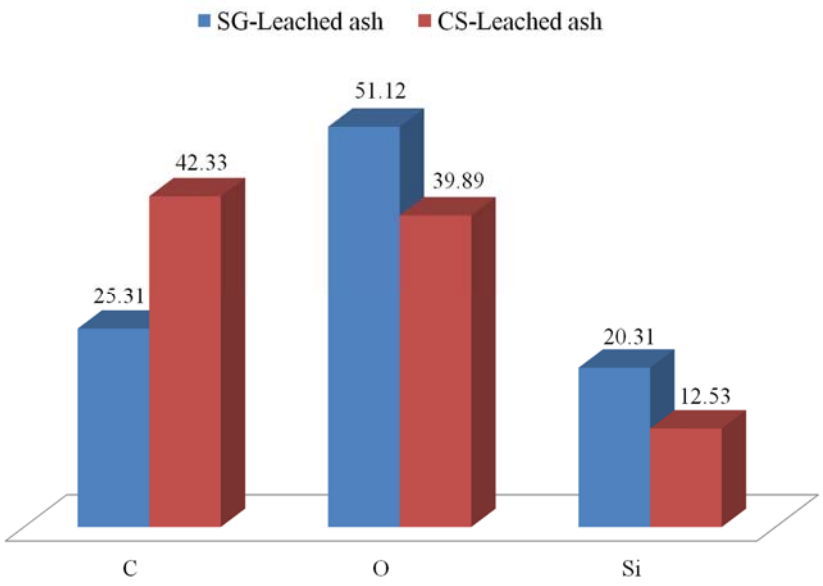
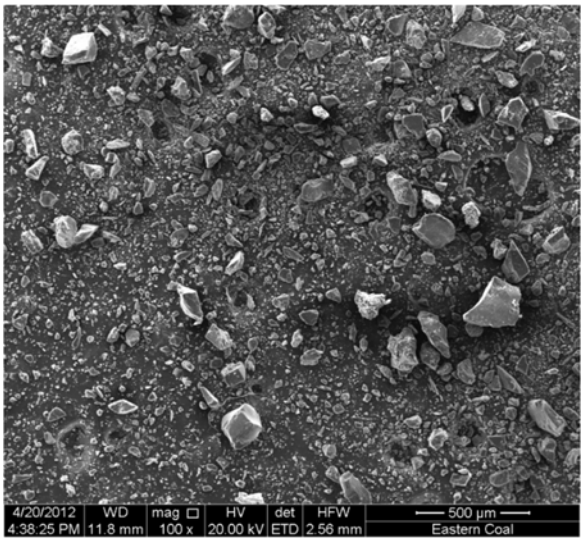


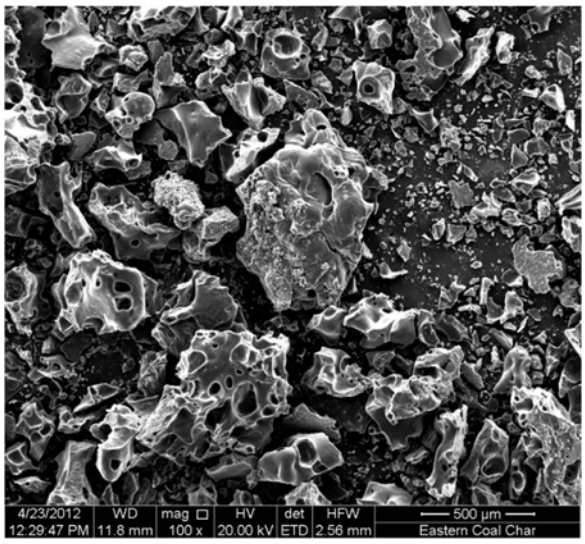

Figure 14-7. Major compounds in leached biomass ash samples

### 14.3.2 Coal and Biomass Comparison

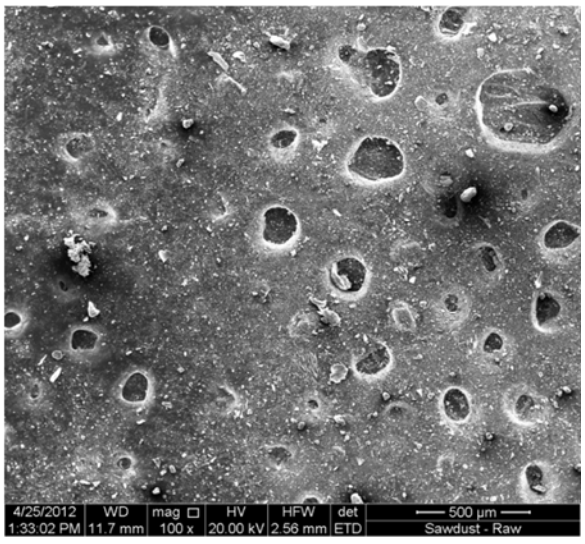
Figure 14-8(a), (b) and (c) shows the EC, EC char and EC ash sample ESEM images at 100X magnification respectively. As seen from Figure 14-8(a), the EC particles are more homogenous and have lower aspect ratio than the biomass particles. The EC particles, shown to be segregated in Figure 14-8(a), fuse with adjacent particles on pyrolysis and increase in size, as shown in Figure 14-8(b). This is in contrast to the biomass samples, where the average particle size and aspect ratio slightly decreased on pyrolysis. The EC char particles also differ from the charred biomass particles for their change in the surface morphology. A clear appearance of fissures is seen on the surface of EC char samples along with the swelling, unlike any such phenomena occurring on the biomass char particles shown in Figure 14-5(b) and (c). Such phenomena was also reported by Biagini et al. (2008), where fissures and small holes were found to appear on the swollen coal char samples due to volatiles released during the pyrolysis process. Figure 14-8(c) shows that EC ash particles are much smaller in size than EC char or unpyrolyzed EC particles; however, the EC ash particles were found to be in lumped state even after oxidation. This is in accordance to the literature where Hurt et al. (1995) reported a significant amount of fused ash on the surface of char samples of Illinois coal, thus suggesting an advanced degree of oxidation.




(a)




(b)




(c)

Figure 14-8. ESEM images for EC sample at 100X magnification: (a) Un-pyrolyzed EC, (b) EC char, and (c) EC ash

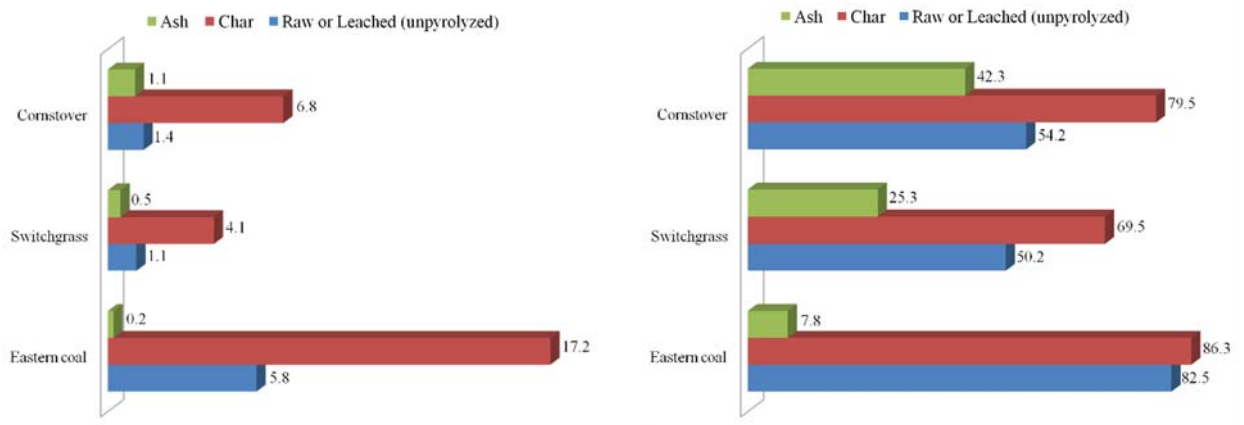
The difference in the elemental composition of coal and leached biomass samples is evident from the elemental analysis of ash compounds of these fuels, as shown in Table 14-4. As discussed in previous section and also observed from Table 14-4, the biomass ash consists of considerable amount of C, O and Si elements which keeps the ash predominantly organic. Unlike biomass samples, the coal ash is found to be predominantly inorganic with Fe (33%), Al(15%), Si(10%) forming the major oxides among other elements in smaller amounts. While the major oxides in EC ash are that of Fe, Al and Si, that of biomass ash consists of C, Si, K, Mg and Na. Also contrary to biomass, the C element percentage in the EC ash particle was found be as low

as 6%, with O element percentage increasing to almost 34%, thus indicating the inorganic nature of EC ash in comparison to biomass.

Table 14-4. Elemental composition of EC, SG-Leached and CS-Leached ash samples

| Ash % | C | O | Si | Al | Na | Mg | K | Ca | Cl | S | Fe | Ti |
|---|---|---|---|---|---|---|---|---|---|---|---|---|
| EC | 7.80 | 34.11 | 8.79 | 14.30 | 0.73 | 1.10 | 0.00 | 0.48 | 0.00 | 1.03 | 31.11 | 0.28 |
| SG-Leached | 25.31 | 51.12 | 20.31 | 0.02 | 0.09 | 0.49 | 0.27 | 1.58 | 0.81 | 0.00 | 0.00 | 0.00 |
| CS-Leached | 42.33 | 39.89 | 12.53 | 0.01 | 0.05 | 0.99 | 1.71 | 1.94 | 0.56 | 0.00 | 0.00 | 0.00 |

Figure 14-9(a) shows the C/O percentage ratio of EC, SG-Leached and CS-Leached samples, as well as their char and ash samples. As observed from the Figure 14-9(a), the C/O ratio for EC is 4-5 times higher than that of biomass samples. This indicates the high carbon density of coal in comparison to biomass, which is also evident from the differences in the calorific values reported for these samples in Table 14-1. Once pyrolyzed, the C/O ratio for the char increase for all fuels, as also observed in the literature (Hurt et al., 1995; Wornat et al., 1995). Again, the C/O ratio for EC char was found to be much higher than that of leached biomass char samples. C/O ratio for all ash samples was observed to be nearly equal. However, as discussed earlier, the C element percentage for EC ash sample is by far the lowest of all fuels indicating better burnout and its inorganic nature. This can also be observed from C element percentage for all fuels in Figure 14-9(b).

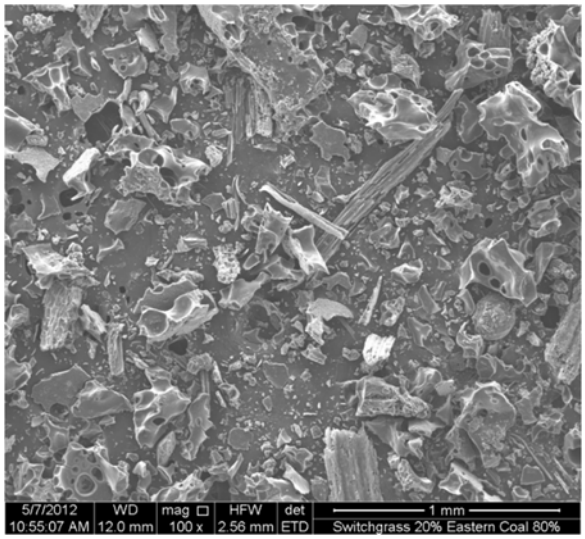



(a) (b)

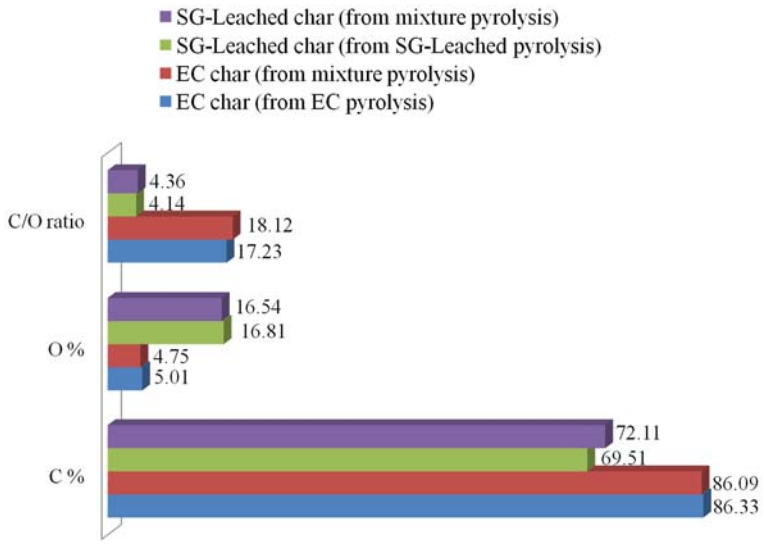
Figure 14-9. (a) C/O ratio for EC, SG leach and CS leach samples in unpyrolyzed, char and ash states, and (b) C% for EC, SG leach and CS leach samples in unpyrolyzed, char and ash states

### 14.3.3 Coal-Biomass Moisture Interactions

Figure 14-10(a) shows the ESEM image for char generated from the pyrolysis of EC and SG Leached mixture (80:20 ratio) at 100X magnification. As observed from Figure 14-10(a), no interaction or fusion was found between the individual fuel char generated from the mixture of two types of fuels. Both types of char samples can be identified separately with no apparent difference from their respective chars formed in their standalone runs. There was no fusion between coal and biomass particles despite fusion between coal particles.




(a)




(b)

Figure 14-10. Effect of EC and leached SG biomass co-pyrolysis: (a) SEM image of char from EC and SG-Leached mixture pyrolysis, and (b) C%, O% and C/O ratio of EC-char, SG-Leached char and char sample from co-pyrolysis of EC and SG-Leached sample in 80:20 mass ratio

Figure 14-10(b) shows the C%, O% and C/O ratio measured for EC-char sample, SG-Leached char sample and char sample formed by co-pyrolysis of EC and SG-leached sample. For the char sample from EC-SG mixture, the C%, O% and C/O ratio was separately evaluated for EC char and SG-Leached char particles found in the mixture char. From Figure 14-10(b), the EC char sample formed from the coal-biomass mixture, and the char formed from the standalone pyrolysis of EC sample have similar C%, O%, and C/O ratio within an error margin of ±3%. In addition, the SG-Leached char samples from the mixture and standalone run have similar elemental composition within an error of ±1%. These results show that the interactions between coal and leached biomass sample on co-pyrolysis are minimal when mixed in 80:20 ratio, both from physical and chemical aspects. Similarly, no physical and chemical interactions were found for the EC and CS leached mixture co-pyrolysis test case.

## 14.4 Summary and Conclusions

The ESEM was used to analyze the physicochemical properties of the fuel, char and pyrolyzed ash samples. The effects of biomass water leaching on the physicochemical behavior of biomass fuels and coal-biomass fuel mixtures were also studied. A significant reduction in inorganic salts and increase in oxygen element percentage was observed due to biomass leaching, while the carbon element percentage was found to be unchanged following water leaching. Physicochemical property differences between coal and biomass samples were demonstrated in their un-pyrolyzed, char and ash phases. The physicochemical interactions between coal and leached biomass sample, following co-pyrolysis, were found to be minimal.

# Chapter 15

# Pyrolysis Chemical Kinetics of Coal and Biomass Feedstocks

## 15.1 Introduction

A thorough understanding of pyrolysis kinetics is imperative for the scaling of thermochemical conversion reactors (White et al., 2011). The pyrolysis process of solid fuels is classified as heterogeneous reactions. However, it has been proven that Arrhenius kinetics satisfactorily describes the temperature dependence of the overall degradation constant for solid fuels such as biomass (Ravindra, 1985). The debate on the applicability of Arrhenius kinetics for coal-biomass pyrolysis is out-of-scope of the present research and can be traced back elsewhere (White et al., 2011; Ravindra, 1985; Brown, 1982). The current literature review discusses the coal, biomass and mixture kinetics, the tools to obtain kinetic parameters, and the dependence of kinetic parameters on operating conditions.

### 15.1.1 Pyrolysis Process

Pyrolysis is a complex process that represents the first step for all thermochemcial conversion processes (combustion, gasification and pyrolysis). The pyrolysis process of solid fuels is briefly described below (Biagini et al., 2008; Sinha et al., 2000; Kansa et al., 1977). An excellent analysis of detailed pyrolysis process is mentioned elsewhere (Colomba, 1993).

1. Energy from the heat source increases the temperature of solid fuel.
2. Initiation of primary pyrolysis reaction leading to release of volatile matter and formation of char.
3. Internal convection of volatiles causing heat transfer between hot volatiles and cooler virgin fuel.
4. Condensation of vapors in the pores of un-pyrolyzed fuel causing formation of tar.

5. Auto-catalytic secondary reactions between the volatile vapor, tar, and char at higher temperature.

The primary pyrolysis reactions are governed by the local solid fuel temperature. In case of biomass pyrolysis, the primary pyrolysis process results in several parallel and consecutive reactions signifying the decomposition of three major components (cellulose, hemicelluloses and lignin). The secondary reactions occur due to the interaction between solid fuel and hot vapors produced from primary reactions. The secondary reactions are generally auto-catalytic in nature. The auto-catalytic secondary reactions are difficult to predict and model because their experimental information is difficult to obtain from standard tools. Besides, the secondary reactions are promoted due to other factors which includes increased residence time of volatiles in the reactor, larger fuel particle size causing higher temperature gradients and longer residence time of volatiles inside the solid fuel matrix (Sinha et al., 2000; Pyle & Zaror, 1984).

In the present work, the major focus is on primary pyrolysis reactions and other factors (particle size, residence time, alkali salts) will be controlled to reduce the occurrence of secondary reactions. The primary pyrolysis process is complex due to several consecutive and parallel reactions occurring in a very narrow temperature range. However, as discussed in the later sections, the pyrolysis behavior can be simplified in terms of global representative reactions.

### 15.1.2 Kinetics Analysis Approaches

Traditionally, the kinetic analyses of solid fuel pyrolysis were conducted in the literature through instruments using an isothermal heating approach. However, recently the interest in isothermal methods has waned because of the difficulty to map all temperature regimes using this method in comparison to non-isothermal techniques (e.g. constant heating rates) (Agarwal, 1992). The two possible formats of non-isothermal data, that are commonly used to investigate pyrolysis kinetics, are the thermogravimetric (TG) data using a TGA or calorimetric data using DSC. The thermogravimetric data reports the mass loss of the pyrolysis sample, while the calorimetric data provides the energetic transitions in the samples with the application of a heating rate program. The TG data provides more accurate data and is commonly used for kinetics research. There is another approach of using differential TG (DTG) data for kinetics analysis, but this method is approximated due to the smoothing issues of DTG curves (Várhegyi

et al., 2009). As per the International Confederation for Thermal Analysis and Calorimetry (ICTAC) directive, the non-isothermal data must be obtained at multiple heating rates to provide the most accurate kinetics data (Brown et al., 2000; Burnham, 2000; Marek, 2000; Rodult, 2000; Sergey, 2000).

Various mathematical tools can be used to convert the non-isothermal TG data to kinetic parameters. These include model free methods (ASTM E698, Ozawa-Flynn-Wall analysis and Friedman analysis) and the non-linear regression method. The model free methods provide reasonably accurate data for the simple reactions which does not involve any complex reaction pathways (consecutive, parallel or independent reactions) (Opfermann et al., 2002). On the other hand, the kinetic parameters obtained from non-linear regression analysis provide a best fit to the assumed kinetic model, irrespective of the complexity of the kinetics involving multiple consecutive, parallel or independent reactions (Opfermann, 2000). The majority of kinetics data for coal-biomass pyrolysis in the older literature has been obtained through model free methods (Aboyade et al., 2011; Biagini et al., 2008; Osvalda, 2007). The non-linear regression analysis is recently emerging as a more popular technique for accurate coal-biomass kinetics investigation (Hashimoto et al., 2011; Sadhukhan et al., 2008; Manyà et al., 2002; Völker & Rieckmann, 2002; Teng & Wei, 1998; Cozzani et al., 1995). Some other studies have recently implemented a distributed activation energy model (DAEM) for the kinetic analysis of pyrolysis process (Cai et al., 2011; Shen et al., 2011; Várhegyi et al., 2010; Li et al., 2009; Li & Suzuki, 2009; Navarro et al., 2009; Várhegyi et al., 2009; Biagini et al., 2008; Sonobe & Worasuwannarak, 2008; Becidan et al., 2007). This model assumes an infinite number of irreversible 1$^{st}$ order parallel reactions to generate a distributed activation energy function for complex reactions. However, the pre-exponential factor (frequency parameter) is considered to be constant for the temperature range. It has also been claimed that the application of DAEM model is not suitable for oxidative pyrolysis of biomass (Shen et al., 2011). Inclusion of large number of parameters for kinetics analysis is another criticism of DAEM model (Sadhukhan et al., 2008). The main advantage of DAEM is that it can give a more objective representation of activation energy for the real process (Li & Suzuki, 2009; Sonobe & Worasuwannarak, 2008).

### 15.1.3 Biomass Pyrolysis

Many authors have investigated biomass pyrolysis kinetics in various levels of details and the work done on this aspect is diverse. The below subsections discuss the biomass pyrolysis literature review from various aspects.

#### 15.1.3.1 Slow and Fast Biomass Pyrolysis

Pyrolysis can be classified as slow pyrolysis (heating rates of the order 10 °C/min) and flash (fast) pyrolysis (heating rate 1000 °C/min) (Sinha et al., 2000). Both types of pyrolysis have been experimentally investigated in the literature (Radmanesh et al., 2006; Mészáros et al., 2004). The volatile matter residence time is shorter for fast pyrolysis, thus the pyrolysis kinetics is best described by primary reactions (Saddawi et al., 2009). Milosavljevic et al (1995) conducted both slow and fast pyrolysis tests, and concluded that the derived biomass kinetics parameters are sensitive to the heating rate of the experiments. The experiments with fast pyrolysis provided lower activation energy (140-155 kJ/mol) and those with slow pyrolysis gave higher activation energy (~220 kJ/mol). Many authors have noticed the activation energies of biomass pyrolysis falling into both of these two categories (Saddawi et al., 2009; Milosavljevic & Suuberg, 1995; Roberts, 1970). Milosavljevic et al (1995) attributed the lower activation energy to the pyrolysis of biomass shells (surface layer) and the higher activation energy to the pyrolysis of the sample interior. The effect of heating rate has also been observed in other aspects of pyrolysis. The char yield has often been found higher for slow pyrolysis (Strezov et al., 2003; Sinha et al., 2000). This is due to the reduction in pressure driven flows inside the sample increasing the volatile residence time, and thus promoting secondary reactions and formation of char. In addition, the increase of volatile formation for fast pyrolysis also promotes secondary reactions due to similar reasons (Radmanesh et al., 2006).

#### 15.1.3.2 Biomass Pyrolysis Process

The devolatilization temperature of lignocellulosic biomass materials is low in the range of 200-400 °C. There are three main regimes of weight loss during the slow pyrolysis process, namely, moisture release, followed by hemicellulose and cellulose decomposition. The decomposition of lignin is over a wide temperature range and does not exhibit a specific peak value at any particular temperature (Radmanesh et al., 2006; Mészáros et al., 2004; Grønli et al.,

2002). Various researchers use the temperature recordings at the decomposition initiation, shoulder, peak and termination to characterize different biomass fuels (Radmanesh et al., 2006; Grønli et al., 2002).

The pyrolysis of biomass deliver additive kinetics as those from the additive weight based ratio of biomass constituents. The deviations found, if any, are reported due to the presence of inorganic salts causing catalysis of the primary reactions (Aboyade et al., 2011; Park et al., 2010; Biagini et al., 2006; Mészáros et al., 2004; Cozzani et al., 1995). Thus, the interactions between decomposing cellulose, hemicellulose and lignin have been found to be negligible for slow pyrolysis studies (Navarro et al., 2009; Radmanesh et al., 2006; Manyà et al., 2002).

#### 15.1.3.3 Pretreatment Effect on Biomass Pyrolysis

Water leaching is generally used to remove inorganic salts in biomass samples, thus decreasing the probability of the occurrence of secondary reactions during pyrolysis. However, it has been noticed that water leaching significantly affects the pyrolysis process by elevating the peak temperature and activation energy for the decomposition of each biomass constituent (cellulose, hemicellulose and lignin). The DTG peak for each component becomes more distinguished from another on water leaching. Also, the char yield decreases and volatile yield increases on water treatment (Giuntoli et al., 2009; Várhegyi et al., 2004; Teng & Wei, 1998). Thus, water leached sample devolatilize at higher temperature, but at a faster rate, thus yielding a lower char and higher volatile percentages. The removal of inorganic salts (ash) increases the fixed carbon percentage, and thus increases the energy density of the fuel. All these factors together produce a desirable effect for the plant operation (Giuntoli et al., 2009). It has also been reported that the biomass particle size has no significant effect on the TGA pyrolysis for the mean diameter smaller than 1 mm and initial sample mass less than 15 mg (Radmanesh et al., 2006).

#### 15.1.3.4 Models used for Biomass Pyrolysis

The biomass kinetic studies can be classified into three main groups, namely, one step global models, one-stage multi reaction models and two-stage semi global models (Colomba, 1993). A representation for these models is given in Figure 15-1. One step global models represent simplified biomass pyrolysis process. One-stage multi reaction models are used to

describe the primary pyrolysis of fuel into char, gas and tar using independent parallel reactions. Two-stage semi global models are used when both primary and secondary reactions are present during pyrolysis (Colomba, 1993). The pros, cons and other details on application of these models on biomass pyrolysis are given elsewhere (Radmanesh et al., 2006; Colomba, 1993).

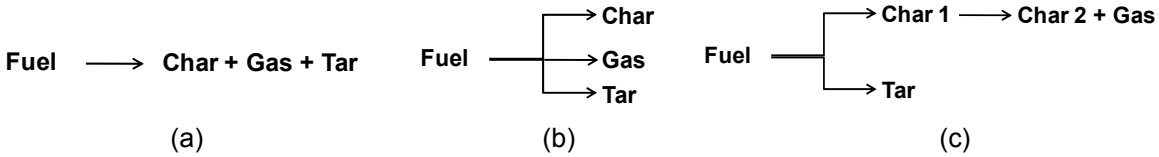



Figure 15-1. Types of decomposition models: (a) One-step global model (simplified), (b) One-stage multi reaction model (primary reactions), and (c) Two-stage semi global model (primary and secondary reactions)

Depending on the case, all three models have been satisfactorily applied for biomass and biomass constituent pyrolysis experiments. Kansa et al. (1977) and Saddawi et al. (2009) assumed that the 1st order global reaction is adequate to describe the decomposition of biomass into char and volatiles, neglecting the secondary reactions. Hashimoto et al. (2011) used a single nth-order reaction model for biomass pyrolysis and successfully correlated it with the TG data. Cozzani et al. (1995) assumed that each of the biomass constituents decompose into char and volatile matter through two independent parallel reactions (Figure 14-5(a)). The most popular model for primary pyrolysis reactions is the three independent parallel reaction model, in which each reaction corresponds to the weight loss of each biomass constituent (Seo et al., 2010; Radmanesh et al., 2006; Branca et al., 2005; Grønli et al., 2002; Manyà et al., 2002; Vovelle et al., 1982). Teng et al. (1998) included the fourth independent parallel reaction to account for the moisture release step. Although many models have been presented in the literature to account for the secondary reactions as shown in Figure 14-5(b)-(d), the one presented by Shafizadeh (1968) has been widely accepted as the most appropriate and accurate representation of biomass pyrolysis. Most of these models are presented for cellulose pyrolysis, as the cellulose form the major weight proportion of biomass and for its kinetics being similar to that of hemicellulose (Van de Velden et al., 2010).

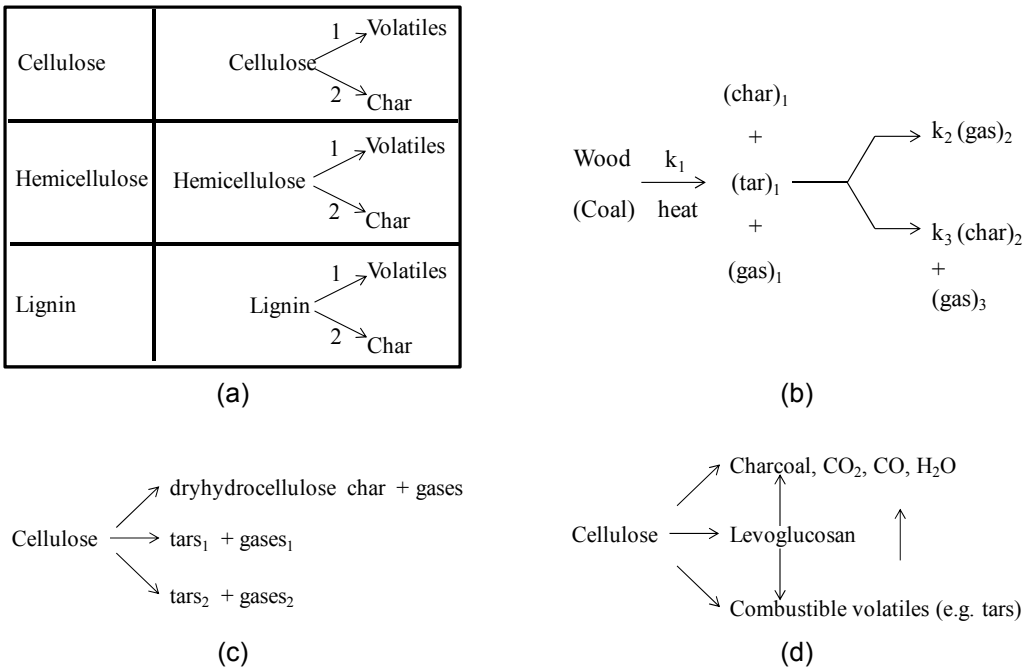



Figure 15-2. Biomass pyrolysis models: (a) Cozzani et al. (2009), (b) Kansa et al. (1977) and Kanury et al. (1970), (c) Milosavljevic et al. (1995), and (d) Shafizadeh (1968)

## 15.1.4 Coal-Biomass Co-Pyrolysis

The devolatilization of coal is fundamentally different than biomass. Coal samples devolatilize with a single main weight loss step followed by a long tail of weight loss (Biagini & Tognotti, 2006). Coal samples devolatilize at temperatures much higher than biomass. The devolatilization of coal starts at about 400 °C and it cannot be considered complete even at temperatures as high as 1000 °C due to the long tail of weight loss. Thus, the pyrolysis duration of coal is much longer than biomass and occurs at higher temperatures as well (Sadhukhan et al., 2008). The pyrolysis char yield of coals is much higher and volatile yield is much lower in comparison to biomass. The devolatilization rate (weight loss rate) of biomass particles is also higher than that of coals (Park et al., 2010). The difference in devolatilization rate is due to the bond structure of biomass and coal fuels. The lignocellulosic biomass constituents are linked with relatively weak ether bonds (bond energy of 380-420 kJ/mol) that break at low temperature range. The coal structure is made of dense polycyclic aromatic hydrocarbons which are linked by alternate single and double bonds with extra resonance stability. Thus, coal samples are more resistant to thermal decomposition and have higher bond energy (1000 kJ/mol) (Sadhukhan et

al., 2008). Thus, the activation energy for coal pyrolysis is also higher than that of biomass (Sütcü & Pişkin, 2011).

Bradley et al. (2011) investigated the kinetics of co-pyrolysis of coal biomass mixture. The kinetic model was developed to simulate the weight loss profile of mixture based on its C, H and O molar ratios. However, it was concluded that it was not possible to develop a co-pyrolysis model based on such approach.

Sadhukhan et al. (2008) developed a kinetic model based on parallel reactions to analyze the coal-biomass pyrolysis using a TGA. The blended samples were prepared with coal and biomass ratios of 100:0, 50:50, 40:60, 10:90, and 0:100, respectively. The analysis of mass loss data of mixtures and individual fuels showed a lack of interaction between the coal and biomass samples. The kinetic parameters of the blend were also found to be similar to those of the respective individual samples. The residual char mass fraction of coal biomass blend was also found to be additive of the weight average values of individual coal and biomass samples.

A similar conclusion was derived by Biagini et al. (2002), where the primary reactions for thermal decomposition of coal and biomass were found to be independent of each other. The TG curve of the coal-biomass blend was determined to lie between those of individual samples and as the weighted profile of the two fuels. The primary reactions of biomass were not found to be significantly affected by those of coal due to the difference in the devolatilization temperatures. The differences in the devolatilization temperature of coal and biomass lead to the absence of volatile species from one fuel component during the pyrolysis of the other. At lower temperatures, the blend behavior was found to be similar to that of biomass and at higher temperature the weight loss was governed by coal TG profile. Similar conclusions have been derived in various other studies (Sütcü & Pişkin, 2011; Di Nola et al., 2010; Gil et al., 2010; Yanfen & Xiaoqian, 2010; Lester et al., 2007).

However, interactions between coal and biomass samples have also been noticed in the literature. Ulloa et al. (2009) co-pyrolyzed an equal weight ratio blend of coal and pine-sawdust at multiple heating rates. Interactions in the blend indicated higher than expected volatile yield. The interactions were attributed to the secondary reactions between coal and biomass vapors at temperatures above 400 °C. Similarly, interactions were found between the coal and sawdust blends prepared by Park et al. (2010), revealing higher than expected char yield of the blend. This time an additional weight loss step was observed at 700 °C for the blend. A difference in

weight loss rate for the blends was also observed, in comparison to individual samples. Park et al. (2010) attributed these interactions to the presence of excess hydrogen donors in the volatile matter from sawdust, because the molar H/C ratio of sawdust is twice as higher than that of coal. Park et al. (2010) also attributed these interactions to the difference in heat transfer characteristics of coal and biomass. It was suggested that since the heat transfer through coal is lower than biomass, the uneven temperature distribution in the blend may cause longer residence of vapor inside the blend, thus causing secondary reactions.

Folgueras et al. (2003) found an additive behavior for 50% weight based coal and sludge blends in oxidative atmosphere, where the decomposition reactions were found to be independent for both samples. Fermoso et al. (2010) pyrolyzed coal-chestnut and coal-olive blends in 70% $N_2$ and 30% steam atmosphere. The blend ratio was 70% coal and 30% biomass for the two samples. No significant interactions were observed for the coal-chestnut blends; however, deviations from the additive behavior were found for the coal-olive blend.

## 15.2 Experimental

The materials used in this research and their preparation method is described in Chapter 14. A NETZSCH 449 F1 Jupiter STA was used to characterize the gravimetric (TGA) response of fuels during pyrolysis. Experiments were conducted in an inert atmosphere to avoid oxidation reactions during heating. For this purpose, the furnace was vacuumed and refilled with 99.999% pure nitrogen two times before analysis. Nitrogen flow rate of 80 ml/min was maintained during the analysis. The fuel samples were tested in the mass range of 4.5 to 5.5 mg. The initial and final sample mass was measured with a ±0.01 mg accuracy balance. The tests were carried out from 298 K up to temperatures sufficiently above the pyrolysis temperature of the fuels at atmospheric pressure (1073 K). To determine the Arrhenius kinetic parameters of fuel pyrolysis, the STA tests were conducted at 5, 10, 20 and 40 K/min heating rates. A five minute residence time at 1073 K was provided to all the experimental and sample preparation (char and ash) runs conducted in this study. The tests were conducted multiple times to ensure repeatability. The kinetic model parameters were obtained by non-linear regression analysis on TGA data using the NETZSCH Thermokinetics software. The STA experimental procedure and its calibration methodology have been explained in a previous publication (Agarwal & Lattimer, 2012).

## 15.3 Results and Discussion

The effects of leaching biomass and blending biomass and coal were evaluated through the use of thermogravimetric analysis (TGA). The thermogravimetric (TG) and differential TG (DTG) data for fuels and blends were measured at different heating rates and used to quantify kinetic parameters.

### 15.3.1 Gravimetric Response of Fuels

Figure 15-3 shows the TG and DTG signals for the pyrolysis of untreated and water leached SG samples at the heating rate of 20 K/min. The devolatilization temperature of biomass samples was found to be low in the range of 200-400 °C. As observed from Figure 15-3, the biomass samples are comprised of a high amount of volatile mass with almost 80% of the sample decomposing during the pyrolysis process. Despite the wide variety of biomass feedstocks, biomass as a lignocellulosic material mainly consists of three major constituents, cellulose (30-60%), hemicellulose (20-35%) and lignin (15-30%) (Van de Velden et al., 2010; Zinoviev et al., 2010; Kumar et al., 2009). As shown in Figure 15-3, there are three main regimes of weight loss during the pyrolysis process, which are associated with the decomposition of these three major components. Hemicellulose decomposition occurs initially (at 312 °C for the SG-Raw sample) followed by cellulose decomposition (at around 365 °C for the SG-Raw sample). The pyrolysis of lignin occurs over a wide temperature range and did not exhibit a specific peak value at any particular temperature.

From Figure 15-3, it is noticed that the water leaching significantly affects the peak temperature for the decomposition of biomass constituents (hemicellulose elevated by 13.5 ºC and cellulose by 1.1 ºC in the case of SG). The char yield decreased (from 19.4% to 14.5% in case of SG) and volatile yield increased due to water treatment (Giuntoli et al., 2009; Várhegyi et al., 2004; Teng & Wei, 1998). This was primarily due to removal of alkali salts during water leaching process and decrease in the secondary reactions during pyrolysis due to the same reason. This decrease in char yield was also accompanied by an increase in the peak decomposition rate of hemicellulose (about 1.5%) and cellulose (about 2.5%) constituents of the SG sample. Thus, water leached samples devolatilized at higher temperatures but at a faster rate, resulting in lower char yield. A similar observation was made for leaching of CS samples, where the char amount decreased from 22.4% to 13.7% on water leaching. The hemicellulose

decomposition temperature increased from 311 °C to 323 °C and cellulose decomposition temperature increased from 354°C to 362°C. Although CS leaching resulted in an increase in the peak rate of cellulose decomposition (from -16.9% to -23.7%), the hemicellulose peak decomposition rate increased by only 0.55%.

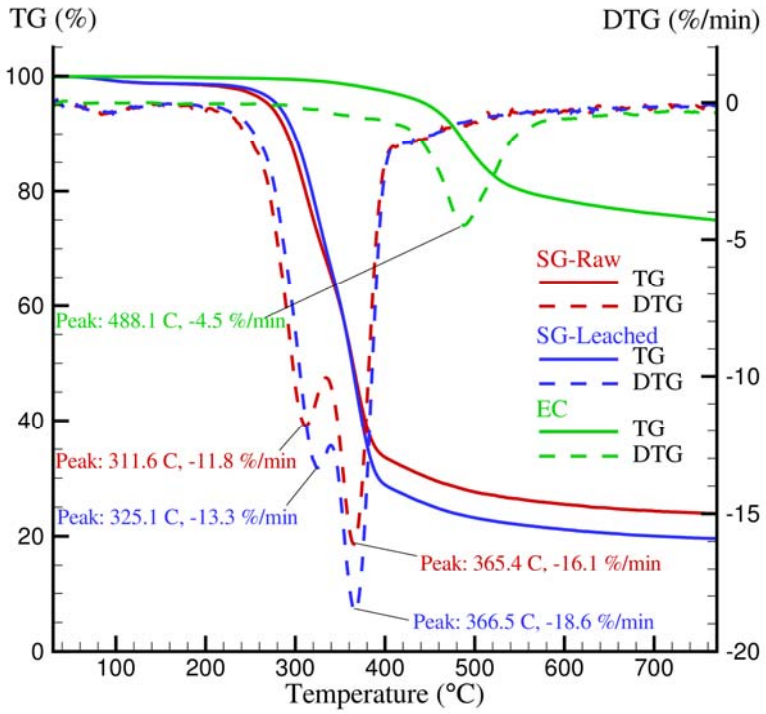



Figure 15-3. TG and DTG analysis of fuel pyrolysis at 20 K/min heating rate: SG-Raw, SG-Leached and EC samples

The gravimetric signals of the EC sample is also shown in Figure 15-3. The pyrolysis of EC is fundamentally different than SG-Leached biomass sample. EC devolatilized with a single main weight loss step followed be a long tail of weight loss. The devolatilization of EC starts at about 400 °C and it cannot be considered complete even at temperatures as high as 800 °C due to char gasification at higher temperatures. Thus, the pyrolysis duration of coal is much longer than biomass and occurs at higher temperatures as well. The pyrolysis char yield of coal was measured to be 74.7%, which is higher in comparison to the char yield of biomass samples (e.g. SG-leached 14.5%). In addition, the devolatilization rate of SG biomass particles was also found to be higher than that of EC. The difference in devolatilization rate is due to the difference in bond structure of biomass and coal fuels. The lignocellulosic biomass constituents are linked with relatively weak ether bonds (bond energy of 380-420 kJ/mol) that break at low temperature

range. The coal structure is made of dense polycyclic aromatic hydrocarbons which are linked by alternate single and double bonds with extra resonance stability. Thus, coal samples are more resistant to thermal decomposition and have higher bond energy (1000 kJ/mol) (Sadhukhan et al., 2008).

Figure 15-4 shows the gravimetric signals for the pyrolysis of 80:20 fuel mixture of EC and SG-Leached samples. At the tested mixture ratio and inert environment conditions, the coal-biomass fuel mixture decomposed as the sum of its constituents. The DTG peaks for decomposition of hemicellulose, cellulose and EC are apparent from the coal-biomass fuel mixture pyrolysis and located approximately at the same temperature as the peak temperatures of individual sample runs. The TG profile of a simulated weighted sum run for EC and SG-Leached sample in 80:20 ratio was generated from their individual gravimetric data. The simulated weighted sum TG profile matched sufficiently with the TG profile of the EC and SG-Leached fuel mixture. Thus, the mixture of EC and SG-Leached biomass sample delivered an additive thermogravimetric data during pyrolysis.

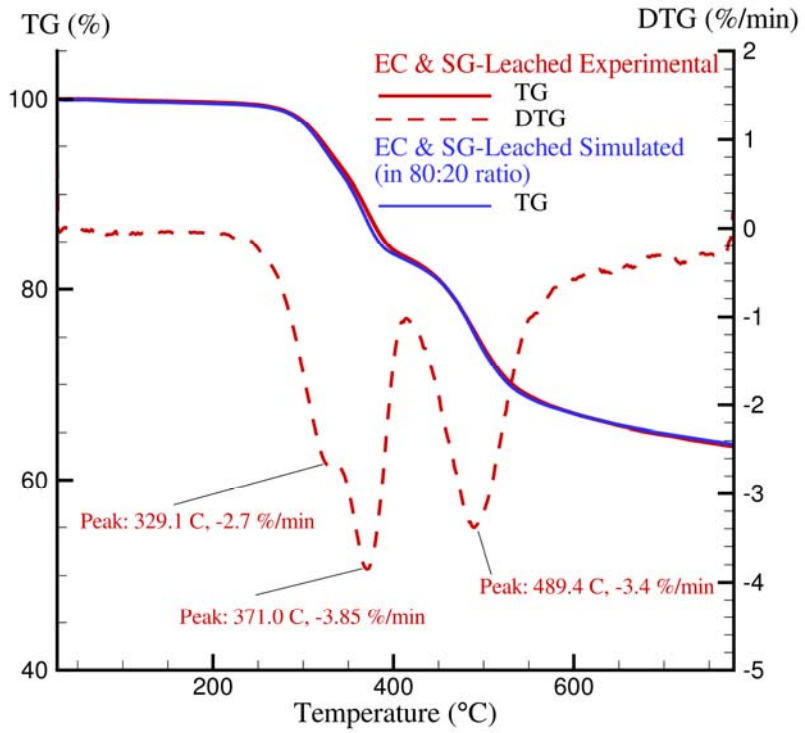



Figure 15-4. TG and DTG signals for pyrolysis of EC-SG-Leached mixture (80:20 by mass)

### 15.3.2 Model Development and Kinetic Parameters

The biomass kinetic models can be classified into three main groups, namely, one step global models, one-stage multi reaction models and two-stage semi global models (Colomba, 1993). Depending on the fuel, all three models have been satisfactorily applied for biomass pyrolysis experiments *viz.* one step global models (Hashimoto et al., 2011; Saddawi et al., 2009; Kansa et al., 1977), one-stage multi reaction models (Radmanesh et al., 2006; Grønli et al., 2002; Cozzani et al., 1995) and two-stage semi global models (Shafizadeh, 1968).

The most popular model for biomass primary pyrolysis reactions is the three independent parallel reaction model, in which each reaction corresponds to the weight loss of each biomass constituent (Radmanesh et al., 2006; Grønli et al., 2002; Cozzani et al., 1995). In the current study, as per the analysis from the Section 15.3.1 for the biomass samples, it was found that the hemicellulose, cellulose and lignin constituents pyrolyzed independently irrespective of its pretreatment with water. Hence, the three nth order independent parallel reaction model was selected to represent the pyrolysis of each biomass constituent. Figure 14-2(a) and Figure 14-2(b) shows the TG data at multiple heating rates for CS-Raw and CS-Leached samples respectively. Figure 14-2 also shows the selected model kinetic fit for these TGA runs using the non-linear regression analysis. As observed from the Figure 14-2, the three independent nth order parallel reaction model fits satisfactorily with the TGA data. The non-linear regression analysis was also conducted for several other kinetic models mentioned in this section, and fits were compared statistically using the F-test. The three nth order independent parallel reaction model was found to be statistically best fit model for the biomass TGA data. The hemicellulose and cellulose decomposition peak temperatures also matched for the TGA and the fitted kinetic model. Similar results were obtained for the SG-Raw and SG-Leached biomass samples. Table 15-1 reports the kinetic fit parameters for the four biomass samples tested in the study.

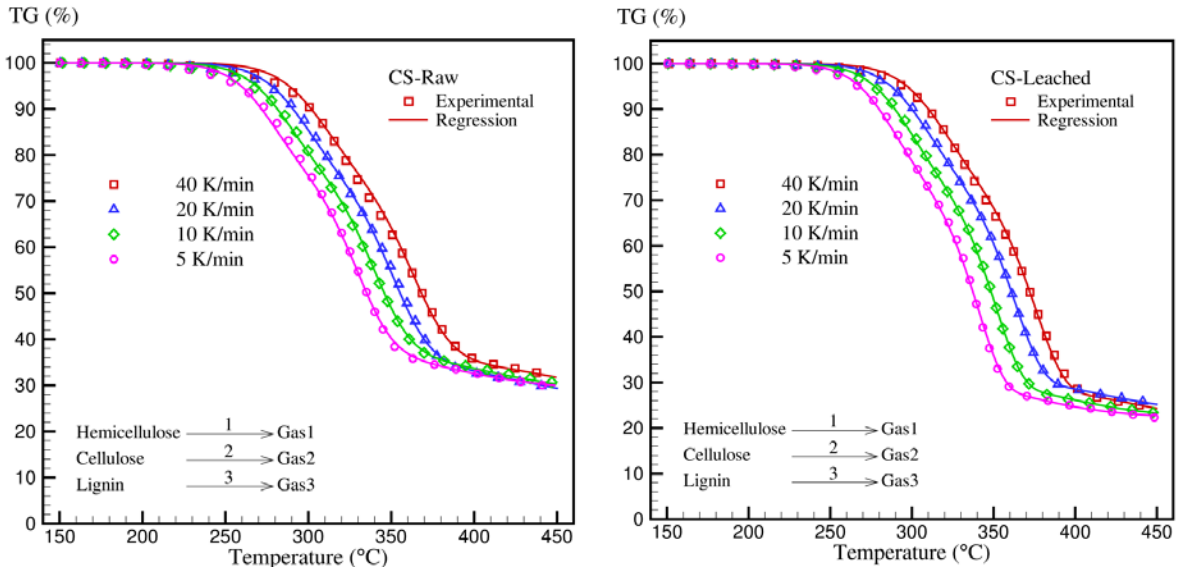



Figure 15-5. TG runs at multiple heating rates and kinetic fit estimation for biomass samples using non-linear regression: (a) CS Raw, and (b) CS-Leached

Table 15-1. Kinetic parameters for pyrolysis of biomass and EC samples

| Parameters | SG - Raw | SG - Leached | CS - Raw | CS - Leached | EC |
|---|---|---|---|---|---|
| log $A_1$ ($s^{-1}$) | 13.35 | 13.22 | 14.42 | 14.77 | 10.88 |
| $Ea_1$ (kJ/mol) | 166.02 | 167.51 | 175.66 | 182.58 | 155.56 |
| $n_1$ | 2.00 | 2.00 | 2.00 | 2.00 | 3.00 |
| log $A_2$ ($s^{-1}$) | 14.34 | 14.50 | 14.60 | 14.25 | 13.83 |
| $Ea_2$ (kJ/mol) | 195.75 | 198.79 | 195.01 | 194.41 | 227.49 |
| $n_2$ | 1.10 | 1.01 | 1.29 | .94 | 3.00 |
| log $A_3$ ($s^{-1}$) | 7.35 | 7.64 | 6.12 | 6.49 | - |
| $Ea_3$ (kJ/mol) | 123.95 | 127.92 | 108.98 | 111.87 | - |
| $n_3$ | 2.00 | 2.00 | 2.00 | 2.00 | - |
| Fr. Mass $Loss_1$ | .42 | .42 | .34 | .34 | .14 |
| Fr. Mass $Loss_2$ | .45 | .47 | .51 | .54 | .86 |
| Fr. Mass $Loss_3$ | .13 | .11 | .15 | .12 | - |

For the biomass samples, the subscripts '1', '2' and '3' represents the reactions concerning the decomposition of hemicellulose, cellulose and lignin into gases respectively. The pre-exponential factor (A), activation energy ($E_a$) and reaction order (n) for each of these three decomposition reactions was obtained using non-linear regression analysis. The parameters named 'Fr. Mass Loss' represents the fraction of mass lost from the initial fuel mass due to each constituent decomposition reaction. As observed from Table 15-1 and also confirmed from the DTG data in Figure 15-3, the maximum mass loss of the biomass sample is contributed by

cellulose decomposition and the minimum mass loss is contributed by the lignin decomposition reaction. This is consistent with the decomposition behavior of these individual constituents in the literature, where the lignin component has been identified as the major char contributor in biomass pyrolysis (Sinha et al., 2000). It was also observed that the major impact of water leaching was on the contribution from cellulose decomposition, which increased for both biomass samples (SG and CS) due to the removal of alkali salts and secondary reactions from the pyrolysis process. The increase in decomposition fraction of cellulose due to leaching was countered by reduced contribution from lignin, whereas the fraction of hemicellulose decomposition remained nearly the same. Thus, higher decomposition of cellulose and lower contribution of lignin resulted in lower char amounts for biomass samples after leaching. It is also noted from the Table 15-1 that the CS sample contains a higher amount of cellulose and a lower amount of hemicellulose compared with SG. The lignin amount is nearly same for both biomass samples. A similar observation was made by Radmanesh et al. (2006) for beechwood and rice husk biomass samples, where cellulose and hemicellulose were identified as the major contributor to the fuel mass loss during pyrolysis.

Table 15-1 also reports the Arrhenius kinetic parameters for biomass pyrolysis. As noted from Table 15-1, the activation energy for hemicellulose decomposition is found to be lower than that of cellulose, thus indicating earlier decomposition temperature for hemicellulose. The activation energy and pre-exponential factor are noted to be the lowest for lignin decomposition reaction. No kinetics literature data was found for the SG and CS pyrolysis using three independent parallel reaction model. The activation energy and pre-exponential factors for three independent reactions were found in agreement with those reported by Koufopanos et al. (1989) and Cozzani et al. (1995) for wood samples. Although, the calculated hemicellulose and cellulose pyrolysis Arrhenius parameters also matched reasonably with some other studies reported in the literature, the literature lignin decomposition activation energy and pre-exponential factors were found to be significantly lower than those determined in the current study (Radmanesh et al., 2006; Manyà et al., 2002; Teng & Wei, 1998). However unlike the current study, these studies assumed the order for all the independent decomposition reactions to be constant at 1 while implementing the regression analysis (Radmanesh et al., 2006; Manyà et al., 2002; Teng & Wei, 1998). In the current study, an increase in the activation energy (1-7 kJ/mol) has been observed for all biomass constituents on water leaching.

Similarly, EC sample pyrolysis runs were evaluated at multiple heating rates using the non-linear regression analysis. Various kinetic models were tested, including one global reaction model, one-stage multi reaction models and two-stage semi global models mentioned in the literature (Colomba, 1993). The statistical best fit to the kinetic data was obtained using a two nth-order independent parallel reaction model. The model fit to the TG data for EC sample is shown in Figure 15-6(a) and the Arrhenius parameters are reported in Table 15-1. The model predicts the first decomposition step takes place at a lower temperature range of 300-400 °C accounting for 14% of the total mass loss during the pyrolysis. The rest of the 86% of mass loss is due to a higher activation energy primary step occurring from 400 °C until the end of pyrolysis temperature. The primary step activation energy of EC sample (227.5 kJ/mol) was found to be higher than that of biomass samples (195-198 kJ/mol), thus owing to the higher bond dissociation energy of coals in comparison to biomass (Sütcü & Pişkin, 2011; Sadhukhan et al., 2008). The DTG peak obtained from the kinetics model for EC primary step also matched that of the TG data.

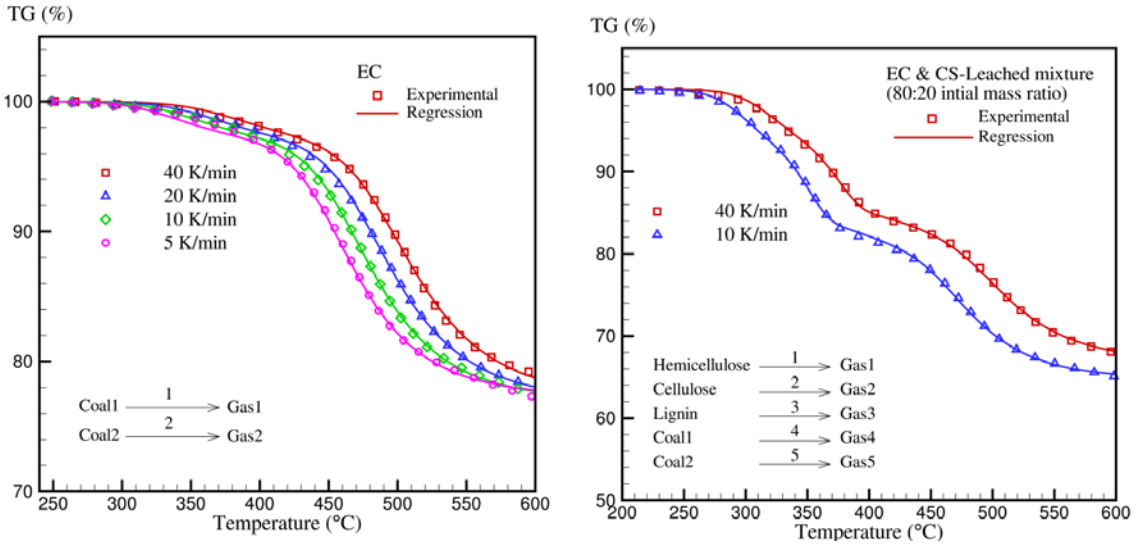



Figure 15-6. TG runs and kinetic fit estimation for fuel samples: (a) EC with three $n^{th}$ order independent parallel reaction model, and (b) EC & CS-Leached mixture at 80:20 initial mass ratio using five $n^{th}$ order independent parallel reaction model

The physicochemical and TG-DTG analysis of co-pyrolysis of coal-biomass mixture samples indicate minimal interaction between the two types of fuels. As a result, an additive kinetic model was used for the coal-biomass co-pyrolysis. A five nth order independent parallel

reaction model was selected for coal-biomass co-pyrolysis. The first three independent reactions simulated those regarding to hemicellulose, cellulose and lignin decomposition in biomass. The last two reactions corresponded to the decomposition of EC sample. The Arrhenius kinetic parameters (A, $E_a$ and n) reported in Table 15-1 were used in the five independent reaction model of coal-biomass mixtures, and the 'Fr. Mass Loss' term for each independent reaction was obtained using regression analysis. The fractional mass loss terms for all five reactions were found to be within ±15% to that reported in Table 15-1, when accounting for EC and biomass mixtures in 80:20 ratio. The resulting regression fit for the five independent reaction model was found to be in good agreement with the TG data for the coal-biomass mixture, as shown in Figure 15-6(b).

Thus, EC and leached biomass mixtures, when pyrolyzed in 80:20 mixture ratio, exhibited weighted additive devolatilization behavior. However, interactions between coal and biomass samples have been noticed in the literature for higher biomass ratio in the mixture, e.g. 50:50 ratio (Ulloa et al., 2009) and 60:40 ratio (Park et al., 2010) coal-biomass mixtures. Park et al. (2010) attributed these interactions to the presence of excess hydrogen donors in the volatile matter from biomass, and also to the difference in heat transfer characteristics of coal and biomass fuels causing secondary reactions.

## 15.4 Summary and Conclusions

The focus of this study was to characterize the samples based on its kinetic parameters using thermal analysis of the fuel undergoing devolatilization. The effects of biomass water leaching on the kinetics of biomass fuels and coal-biomass fuel mixtures were also studied. The water leaching of biomass samples mitigated the secondary reactions during pyrolysis, shifted the primary decomposition reactions to higher temperatures, and reduced the char yield of biomass fuel samples. An increase in the rate of devolatilization was noticed on biomass water leaching due to removal of secondary autocatalytic reactions.

An independent parallel reaction model of three $n^{th}$ order reactions best described the biomass pyrolysis statistically, where each reaction signified the pyrolysis of a biomass constituent viz. hemicellulose, cellulose and lignin. A small increase in the activation energy of each constituent pyrolysis reaction was found on water leaching. Coal pyrolysis was statistically best represented by a two independent nth order reaction model. It was found that the co-

pyrolysis of coal and leached biomass fuel mixtures exhibited a weight additive thermogravimetric and kinetic behavior, when pyrolyzed on an 80:20 initial mass proportion.

# Chapter 16

# Pyrolysis and Combustion Energetics of Coal and Biomass Feedstocks

## 16.1 Introduction

Predicting the thermal response of solid fuels undergoing pyrolysis and combustion has historically been of primary interest in the areas of energy recovery and gasification applications. Proper knowledge of the energetic response of such fuels is needed in order to optimize and predict gasifier performance. The energetic parameters of a fuel undergoing pyrolysis-combustion includes the amount of heat required to pyrolyze the fuel (heat of pyrolysis and heat of gasification) and the amount of heat generated by the fuel upon combustion (heat of combustion). Hence, a methodology needs to be developed for an accurate energetic characterization of fuel mixtures undergoing thermochemical conversion processes.

The co-firing of multiple fuels, such as coal and biomass mixtures, has emerged as an alternative fuel route to improve the economics, environmental impact and performance of gasifiers. Efforts have been directed in the literature towards realizing efficient coal-biomass co-firing (Sütcü & Pişkin, 2011; Kumabe et al., 2007; Ghosh et al., 2006; Minchener, 2005; Sami et al., 2001; Robinson et al., 1998). However, problems related to co-firing of fuel mixtures are less understood due the intricate pyrolysis and combustion behavior of multiple fuels. Moreover, the energetic characterization of coal-biomass mixtures is not as well understood as the other aspects of their pyrolysis process *viz.* kinetics (Bradley et al., 2011; Sadhukhan et al., 2008; Folgueras et al., 2003; Milosavljevic & Suuberg, 1995; Shafizadeh, 1968). This is primarily attributed to lack of validated pyrolysis energetics models and consistent experimental methodologies for the accurate energetic characterization of solid fuels (Agarwal & Lattimer, 2012). The reactivity of a fuel requires a total energy balance on the fuel, which includes the energy required for pyrolysis of the material as well as the heat released from combustion of the evolved gases and char. A method was developed to quantify energy for pyrolysis of materials using thermogravimetric

analysis (TGA), differential scanning calorimetry (DSC), and a pyrolysis model (Agarwal & Lattimer, 2012). The approach was validated with liquid chemicals, plastics, and composite materials, and is noted in the reference (Agarwal & Lattimer, 2012). Recently, a micro-scale combustion calorimeter (MCC) has been developed to measure the heat release rate from milligram size samples as a function of temperature (Lyon & Walters, 2004). This has also primarily been used on plastic materials and has not considered the effects of energy required for pyrolysis in the evaluation of fuels.

Research has also been performed on the effects of biomass water leaching on the energetics of biomass fuels and coal-biomass fuel mixtures. The water leaching process removes most of the inorganic salts from the biomass samples (Giuntoli et al., 2009; Gomez et al., 2009; Várhegyi et al., 2004; Stenseng et al., 2001; Teng & Wei, 1998). The removal of inorganic salts increases the fixed carbon percentage, and thus increases the energy density of the fuel. The removal of these salts reduces the drawbacks of biomass gasification operation problems associated with fouling, slagging and corrosion (Kumar et al., 2009; van Alphen, 2007; Wornat et al., 1995). All these factors together produce a desirable effect for the plant operation (Giuntoli et al., 2009). However, the co-pyrolysis energetics behavior of leached biomass with coal has not been thoroughly investigated in the literature (Zolin et al., 2001).

The focus of this section is to present a methodology to quantify the energetic response of biomass, coal, and coal-biomass blends. Different than much of the previous work, these materials have significant char that must be accounted for in the analysis to obtain correct property values and accurate prediction of coal-biomass mixture behavior. A method is presented to quantify energy to decompose samples from a simultaneous thermogravimetric analyzer (STA) that includes a TGA and DSC. In addition, an approach is presented on quantifying the heat of combustion of these charring materials based on the temperature dependent heat release rate from the MCC. These methods are used to determine the energetic properties of coal, biomass and coal-biomass blends. An approach is then presented on predicting properties of coal-biomass blends from individual material properties.

## 16.2 Experimental

Details on the materials used in this study and their preparation method is discussed in Chapter 14. A NETZSCH 449 F1 Jupiter STA, shown in Figure 14-5(a), was used to characterize

the gravimetric (TGA) and energetic (DSC) response of fuels during pyrolysis. Experiments were conducted in an inert atmosphere to avoid oxidation reactions during heating. For this purpose, the furnace was vacuumed and refilled with 99.999% pure nitrogen two times before analysis. Nitrogen flow rate of 80 ml/min was maintained during the analysis. The fuel samples were tested in the mass range of 4.5 to 5.5 milligrams. Pt-Rh cups with lids (two holes) were used for these experiments. The initial and final sample mass was measured with a ±0.01 mg accuracy balance.

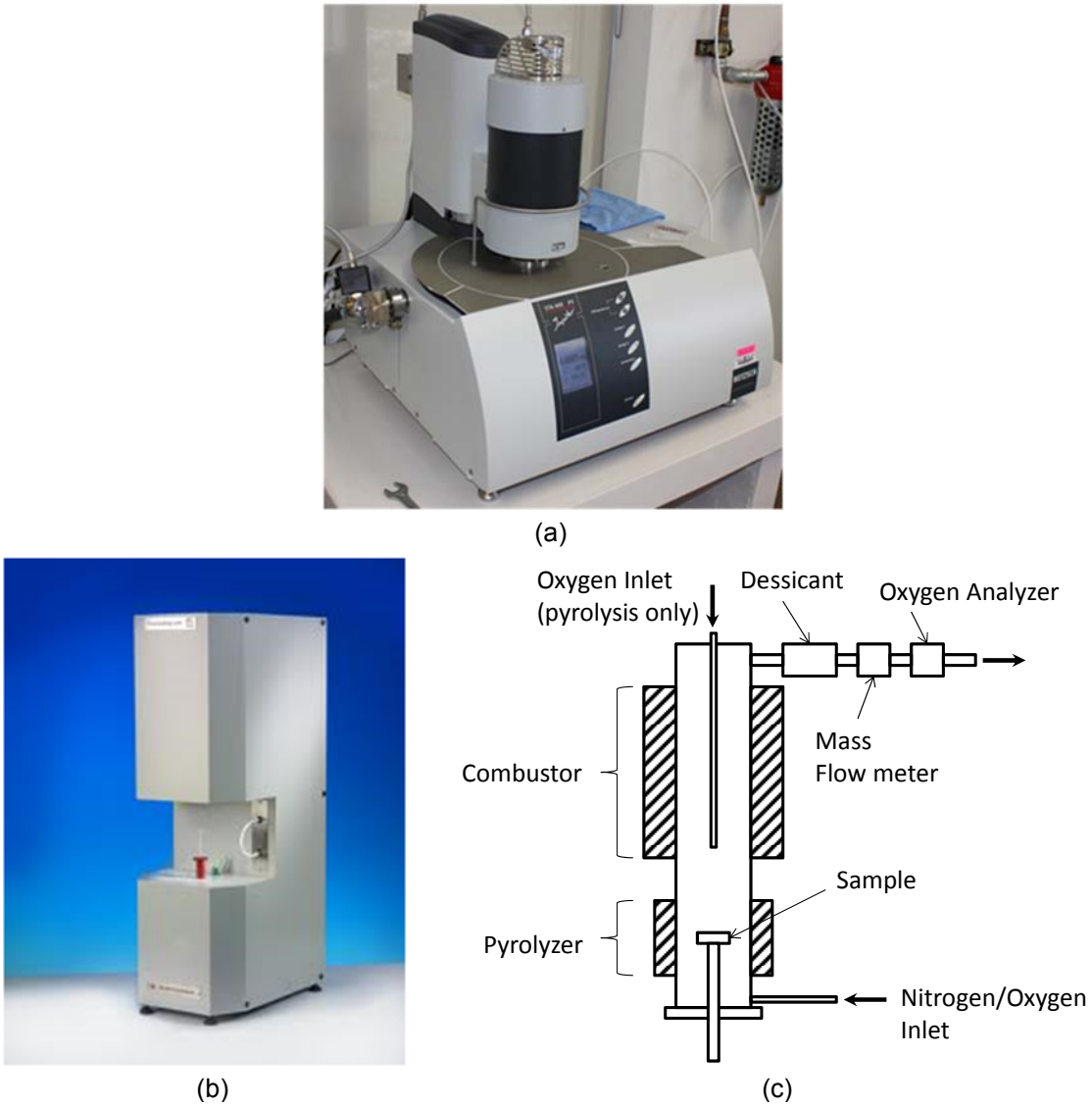



Figure 16-1. Instruments for energetic properties: (a) STA, (b) MCC, and (c) MCC schematic

The tests were carried out from 298 K up to temperatures sufficiently above the pyrolysis temperature of the fuels at atmospheric pressure (1073 K). The sample heating rate was kept

constant at 20 K/min. A five minute residence time at 1073 K was provided to all the experimental runs conducted in this study. The tests were conducted multiple times to ensure repeatability. The STA experimental procedure and its calibration methodology has been explained in reference (Agarwal & Lattimer, 2012).

A micro-scale combustion calorimeter (MCC) was used to quantify the heat release rate (HRR) from the combustion of the gases produced during the pyrolysis process, and heat release rate from the char combustion. A MCC is used by Federal Aviation Administration (FAA) to determine flammability characteristics for plastics and other composite materials used in the Aviation industry, and is carried out by ASTM D7309 (2011). A few modifications were made to this ASTM standard in order to test coal and biomass fuels in the current study. One of the main changes was to use the same Pt-Rh cups and lids (with two holes) as were used for the STA experiments. This change allowed the DTG and DSC peaks obtained from the STA experiments, and the HRR peaks obtained from the MCC experiments to be at the same temperature points. Other changes included the reduction in gas flow rates ($N_2$ and $O_2$) to get optimal accuracy from the HRR signals due to relatively low volatility of coal-biomass samples in comparison to plastics and composites.

For pyrolysis gas combustion, a nitrogen purge flow rate of 44 ml/min was used to pyrolyze the fuel samples at 20 K/min heating rate. The gases produced during the pyrolysis of fuels were instantaneously combusted in an oxygen atmosphere of 10 ml/min at 900 °C, as shown in Equation 16-1. The resultant data was used to calculate the heat of combustion for pyrolysis gas of the fuel, $\Delta h_{comb,p}$.

$$Fuel \xrightarrow{N_2,\Delta 20K/\min} Char + gas \xrightarrow{O_2,900°C} CO_2 + H_2O \qquad \text{(Eq. 16-1)}$$

The principle of oxygen consumption calorimetry was then used to calculate the HRR of the solid fuel during pyrolysis, after the correction for baseline drifts. The resultant heat release rate provided the measurement of heat output as a function of temperature per initial weight of the solid fuel.

Similar procedure was applied for char combustion experiments. A fuel char sample was kept on the sample carrier, and then oxidized at 20 K/min atmosphere in 18.5% $O_2$ environment. The 18.5% $O_2$ atmosphere was selected due to the limitation of the STA instrument in producing up to 20.95% $O_2$ atmospheres. Thus, to keep the oxidation environment common in both setups, an 18.5% $O_2$ environment was selected for char oxidation. The remnant gas was completely

oxidized in the combustor set at 900 °C, as shown in Equation 16-2. The resultant data was used to calculate the heat of char combustion, $\Delta h_{comb,cc}$.

$$Char \xrightarrow{18.5\%O_2,\Delta 20K/\min} Ash + gas \xrightarrow{O_2,900°C} CO_2 + H_2O \qquad \text{(Eq. 16-2)}$$

The MCC experimental procedure, calibration and apparatus description is provided elsewhere (Lyon & Walters, 2004). The sample preparation method and the temperature program were the same as that used in the STA analysis.

## 16.3 Energetic Models

Heat of pyrolysis, $\Delta h_{pyr}$, heat of gasification, $\Delta h_{gas}$, heat of pyrolysis gas combustion, $\Delta h_{comb,p}$, heat of char combustion, $\Delta h_{comb,cc}$, and effective total heat of combustion, $\Delta h_{comb}$, were the energetic properties determined in the current study. A brief description of models and property determination procedure is provided below.

### 16.3.1 Pyrolysis Model

The fuel pyrolysis mathematical model, its derivation, validation and application onto chemicals, polymers and composites is shown in reference (Agarwal & Lattimer, 2012). In this section, the pyrolysis model relevant to calculating the heat of pyrolysis and heat of gasification for fuel samples is discussed in brief.

The heat of pyrolysis is defined as the difference of heat of formations of pyrolysis gas and the active solid material. Hence, the heat of pyrolysis is positive for an endothermic decomposition process. The heat of gasification is defined as the amount of energy required to vaporize a unit mass of volatile matter in the solid material, originally at the ambient temperature. The heat of gasification can be calculated for solid fuels as the sum of sensible heat required to raise the material temperature and the latent heat of pyrolysis, as shown in Equation 16-3 (Agarwal & Lattimer, 2012).

$$\Delta h_{gas} = \Delta h_{sen} + \Delta h_{pyr} \qquad \text{(Eq. 16-3)}$$

Many studies in the literature have calculated the heat of pyrolysis of materials using the STA instrument. In these studies, the heat of pyrolysis was calculated as the area difference between the apparent and sensible specific heat capacity curves, $\Delta h_{area,DSC}$, or as the area difference under the apparent and specific heat flow DSC curves (Gomez et al., 2009; Stoliarov

& Walters, 2008; Yu et al., 2007; Strezov et al., 2004; Rath et al., 2003; Strezov et al., 2003; Stenseng et al., 2001; Strezov et al., 2000; Henderson & Emmerich, 1991; Henderson et al., 1982; Frederick & Mentzer, 1975). This calculation method of $\Delta h_{area,DSC}$ is shown in Equation 16-4 (Agarwal & Lattimer, 2012).

$$\Delta h_{area,DSC} = \int_{T_{in}}^{T} c_{app} d\theta - \int_{T_{in}}^{T} c_{sen} d\theta \quad \text{(Eq. 16-4)}$$

In recent publication, it was validated and concluded that the heat of pyrolysis is different from the area difference under the apparent and sensible specific heat curves, or area difference under the apparent and sensible heat flow DSC curves for the degradation of a charring material (Agarwal & Lattimer, 2012). Unlike $\Delta h_{area,DSC}$, the heat of pyrolysis, $\Delta h_{pyr}$, is defined on the basis of per unit volatile mass lost, and can be calculated by applying the STA data onto a pyrolysis mathematical model (Agarwal & Lattimer, 2012). Alternatively, it was proved that the $\Delta h_{pyr}$ can be calculated for charring samples by using the $\Delta h_{area,DSC}$ data, and then accounting for the loss of volatile mass by implementing Equation 16-5 (Agarwal & Lattimer, 2012).

$$\Delta h_{pyr} = -\Delta h_{area,DSC} / \ln\left(Y_c\right) \quad \text{(Eq. 16-5)}$$

In Equation 16-5, $Y_c$ represents the final char yield of the fuel sample at the end of pyrolysis. Equation 16-5 also complies with the findings in literature (Gomez et al., 2009; Rath et al., 2003; Stenseng et al., 2001; Strezov et al., 2001; Strezov et al., 2000) where the $\Delta h_{area,DSC}$ values were calculated for different fuels, and were found to be dependent on the final char yield of the fuel sample. The heat of gasification value, $\Delta h_{gas}$, is calculated by adding the sensible heat to and the heat of pyrolysis (Equation 16-3). Similar to $\Delta h_{pyr}$, the $\Delta h_{gas}$ property is calculated on per unit volatile mass loss basis (Agarwal & Lattimer, 2012).

### 16.3.2 Combustion Model

The heat of combustion is defined as amount of heat released from the combustion of volatiles released during the solid fuel pyrolysis (Lyon, 2000). MCC data was analyzed by calculating the $\Delta h_{area,MCC,p}$ and $\Delta h_{comb,p}$ properties. The $\Delta h_{area,MCC,p}$ property was calculated by integrating the HRR signal over the pyrolysis temperature range and dividing it by the heating rate of the sample, as shown in Equation 16-6 and described elsewhere (Lyon & Walters, 2004).

$$\Delta h_{area,MCC,p} = \int_{T_{in}}^{T} \left(HRR\right) d\theta / \left(dT / dt\right) \quad \text{(Eq. 16-6)}$$

The $\Delta h_{area,MCC}$, similar to HRR, is based on the initial mass of the sample. The effective heat of combustion is calculated on the basis of volatile mass for charring materials. Thus, the $\Delta h_{comb}$ property was calculated as per Equation 16-7 (Agarwal & Lattimer, 2012).

$$\Delta h_{comb,p} = \Delta h_{area,MCC,p}\left(\frac{1}{1-Y_c}\right) \quad \text{(Eq. 16-7)}$$

Similarly, heat of char combustion is calculated as per Equation 16-8:

$$\Delta h_{comb,cc} = \Delta h_{area,MCC,cc}\left(\frac{1}{1-Y_{cc}}\right) \quad \text{(Eq. 16-8)}$$

and the total heat of combustion for a fuel sample is calculated as shown in Equation 16-9:

$$\Delta h_{comb,cc} = \left(1-Y_c\right)\Delta h_{comb,p} + Y_c \Delta h_{comb,cc} \quad \text{(Eq. 16-9)}$$

## 16.4 Energetic Signals

This discussion is divided in two parts. Firstly, the DSC-DTG signals obtained from the STA data are presented. Next, the HRR signals from MCC are discussed.

### 16.4.1 STA Signal Analysis

Figure 16-2 shows the DTG and DSC signals for pyrolysis of CS-Raw and CS-Leached samples. The DSC signal is shown in per unit initial sample mass basis. For the CS-Leached sample, the DTG peak temperatures for hemicellulose and cellulose decomposition are noted to be accompanied with endothermic DSC peaks at the same temperature points. However, the energetics for the pyrolysis of CS-Raw sample produces different results. Although, the hemicellulose decomposition DTG peak temperature is accompanied by a DSC peak at around 308ºC, the direction of DSC peak suggests an exothermic reaction. On the other hand, the cellulose decomposition DTG peak temperature does not accompany any corresponding peak in its DSC signal for the CS-Raw sample. Similar results were observed for the leaching of SG biomass samples as well. The lack of endothermic peaks in raw biomass samples have been attributed to the occurring of secondary exothermic reactions due to the presence of alkali salts in their untreated state (Gomez et al., 2009). Overall, the decomposition reactions shifted to higher temperatures and became highly endothermic on biomass leaching.

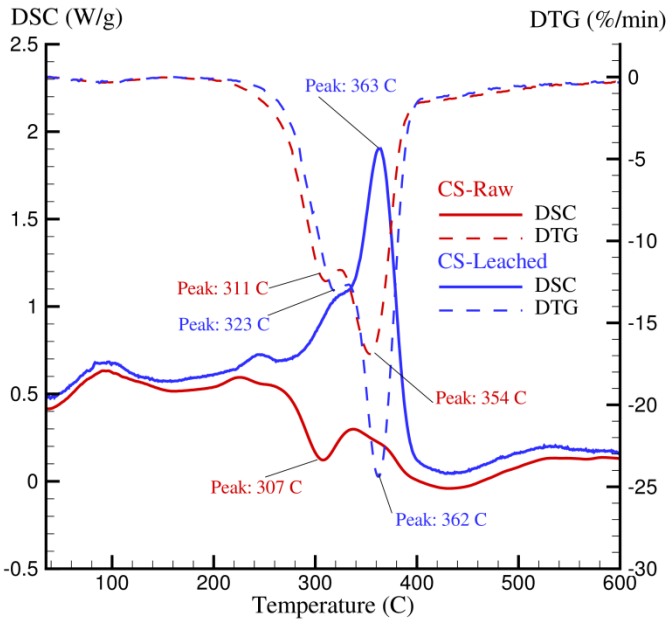



Figure 16-2. DSC and DTG signals for pyrolysis of CS-Raw and CS-Leached samples

Figure 16-3 shows the DTG and DSC signals for the EC and CS-Leached samples. Unlike leached biomass samples, the DTG peak temperature for EC sample at 488 ºC did not accompany any DSC peak. The devolatilization of coal is much more complex than biomass, where various stages of softening, physical transitions, and coal swelling takes place apart from the primary pyrolysis reactions (Strezov et al., 2000; Yun & Suuberg, 1993).

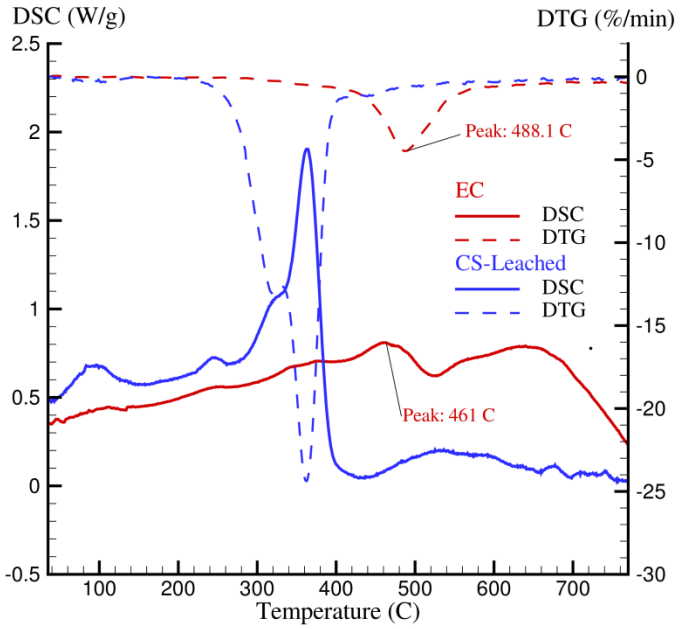



Figure 16-3. DSC and DTG signals for pyrolysis of EC and CS-Leached samples

As observed from Figure 16-3, EC pyrolysis resulted in a smaller endothermic peak than the CS-Leached sample. The smaller endothermic peak value of coal samples is partially due to much lower amount of volatile matter present in comparison to biomass samples. However, the DSC peak value for EC was comparable to the DSC peak value of CS-Raw sample despite the higher char yield of the coal sample.

Figure 16-4 shows the DSC signals obtained from the pyrolysis of 80:20 fuel mixture of EC and CS-Leached samples. The DSC profile for a simulated weighted sum of individual EC and CS-Leached sample DSC signals in 80:20 ratio was also generated. The simulated weighted sum DSC profile matched sufficiently the DSC profile of EC and CS-Leached fuel mixture, under the tested conditions. Thus, the mixture of EC and CS-Leached biomass sample delivered an additive pyrolysis energetics data. A similar conclusion was made out for EC and SG-Leached mixture STA data.

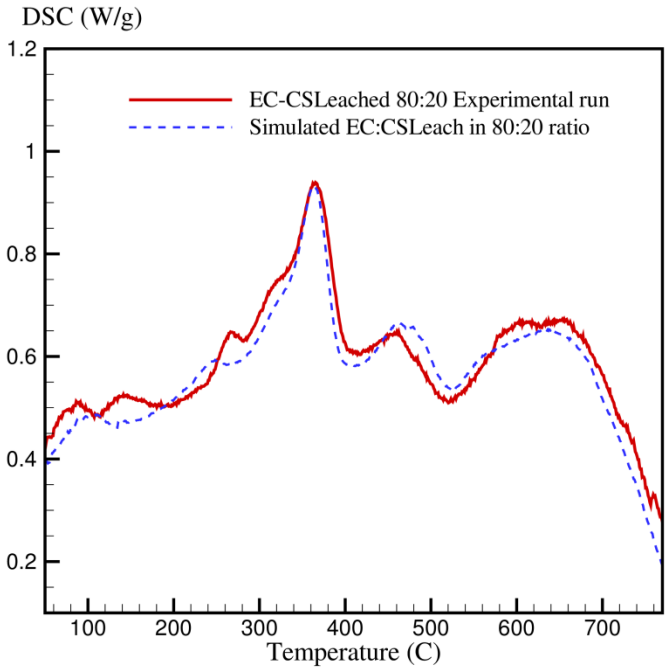



Figure 16-4. DSC signals for EC and CS-Leached mixture pyrolysis at 20 K/min heating rate

## 16.4.2 MCC Signal Analysis

Pyrolysis gas combustion heat release rate signals of CS-Wash, CS-Leached and EC samples are shown in Figure 16-5. The HRR, similar to the DSC signal, is measured on the basis of per unit initial mass of the sample. As observed from Figure 16-5, the peak temperature for

HRR of these fuels matches their respective peak temperature of DTG signal. As expected, this signifies that the rate of production of pyrolysis gases is proportional to the heat generated during the combustion of those gases.

Figure 16-5 demonstrates the effect of leaching on the pyrolysis gas combustion HRR signals of biomass samples. As observed from Figure 16-5, the peak HRR value of CS-Leached sample (58.2 W/g) is found to be much higher than that of the CS-Raw sample (37.5 W/g). This is in agreement with the DTG data presented in Chapter 15, where it can be observed that the devolatilization rate increases on biomass leaching.

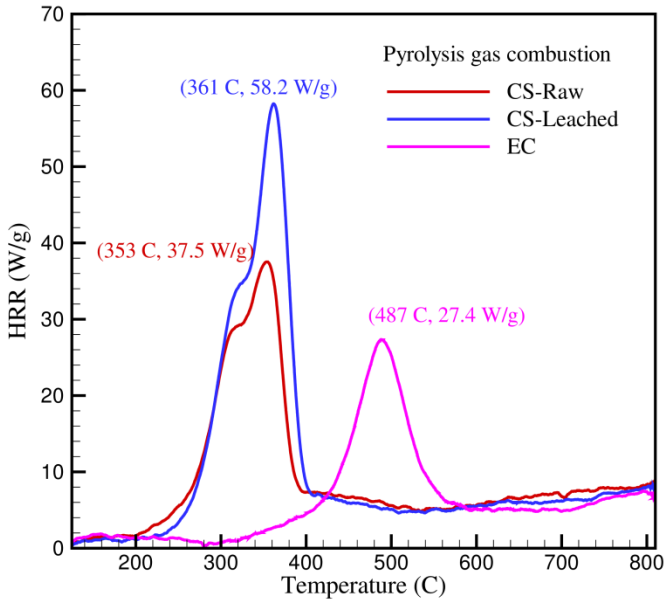



Figure 16-5. HRR for pyrolysis gas combustion of CS-Raw, CS-Leached and EC samples

A larger difference between the energy density of the samples is seen from comparing HRR signals of EC and biomass samples in Figure 16-5. As known from the previous discussion, the amount of volatile matter released from EC pyrolysis is substantially lower than that released by biomass samples (~20% volatile matter for EC in compared to ~80% for biomass samples). With a relatively very low devolatilization rate for EC sample, as observed in Figure 16-5, the peak height for HRR signal of EC was comparable in comparison to biomass samples shown in Figure 16-5.

Figure 16-6 contains the initial mass based HRR signals obtained from the pyrolysis of 80:20 fuel mixture of EC and CS-Leached samples. The HRR profile for a simulated weighted sum of individual EC and CS-Leached sample HRR signals in 80:20 ratio was also generated.

The simulated weighted sum HRR profile matched sufficiently the HRR profile of EC and CS-Leached fuel mixture. Thus, the mixture of EC and CS-Leached biomass sample delivered additive combustion energetics. A similar conclusion was determined for EC and leached SG co-pyrolysis HRR data.

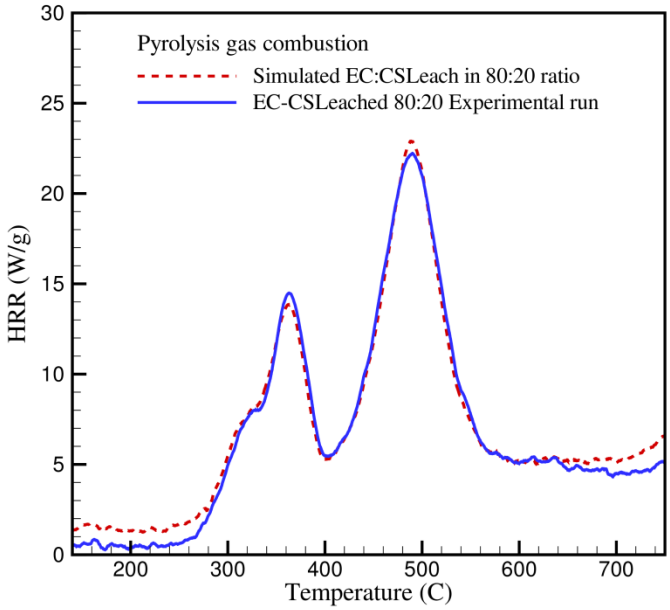



Figure 16-6. HRR for pyrolysis gas combustion of EC and CS-Leached mixture pyrolysis at 20 K/min heating rate

Figure 16-7 includes the char combustion heat release rate signals for the CS-Raw, CS-Leached and EC samples. As observed from Figure 16-7, the peak temperature and shape profile for char combustion signals is different than those of pyrolysis signals. The char combustion experiments conducted in MCC are non-flaming in nature. Therefore, there are no sharp peaks associated with the ignition of the samples and the oxidation is uniform over a wide temperature range. The biomass char combustion HRR peak and profile changes on water leaching, as seen from Figure 16-7. The leached biomass char oxidized at higher temperatures due to the removal of autocatalytic alkali salts. The peak HRR for leached biomass is lower than that of raw biomass, however the leached biomass sample oxidizes at over a broader temperature range than that of raw biomass.

The char combustion signal for EC is different than that of biomass samples. The EC char oxidizes at a higher temperature, with higher peak HRR and over a broader temperature range.

The oxidation of EC char is not complete even at temperature as high as 750 °C (the limit of MCC).

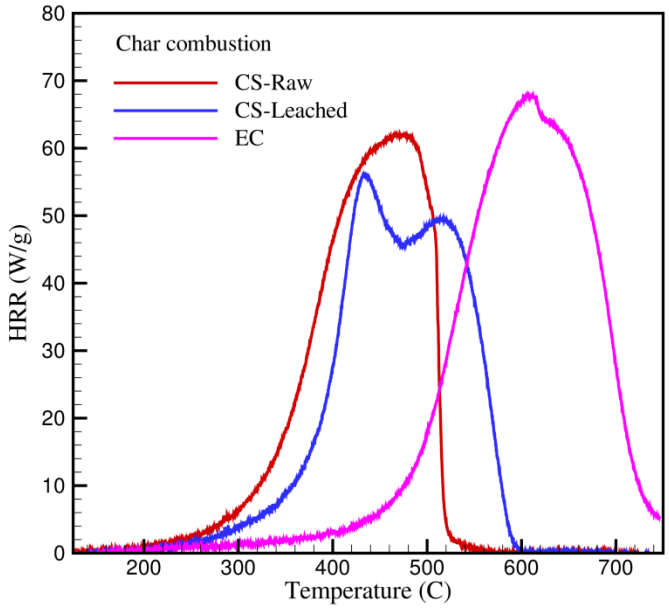



Figure 16-7. Char combustion heat release rate signals for CS-Raw, CS-Leached and EC samples

# 16.5 Energetic Properties Evaluation

## 16.5.1 Heat of Pyrolysis and Heat of Gasification

Table 16-1 reports the $\Delta h_{area,DSC}$ (initial mass basis), $\Delta h_{pyr}$ (volatile mass basis), $\Delta h_{gas}$ (volatile mass basis) and $Y_c$ values calculated for all samples at 20 K/min heating rate. $Y_c$ values were calculated form ratio of final and initial mass of sample in Pt-Rh pan.

Table 16-1. Pyrolysis energetic properties of fuel samples pyrolysis at 20 K/min heating rate

| **Experimental Runs** | $\Delta h_{area,DSC}$ **(J/g)** | $\Delta h_{pyr}$ **(J/g)** | $\Delta h_{gas}$ **(J/g)** | $Y_c$ |
|---|---|---|---|---|
| SG-Raw | 125 ± 1.2% | 77 ± 1.2% | 903 ± 1.2% | 0.194 |
| CS-Raw | 19 | 13 | 731 | 0.225 |
| SG-Leached | 374 | 194 | 1235 | 0.146 |
| CS-Leached | 538 | 271 | 1133 | 0.137 |
| EC | 389 | 1336 | 5312 | 0.747 |
| EC & SG-Leached in 80:20 Mixture | 320 | 766 | 3894 | 0.658 |
| EC & CS-Leached in 80:20 Mixture | 461 | 900 | 3276 | 0.599 |

The quantities were calculated per the pyrolysis model application (Equation 16-3, 16-4 and 16-5) onto the STA data (Agarwal & Lattimer, 2012). Based on lower char yield from biomass pyrolysis (0.14-0.22 for different samples), the $\Delta h_{pyr}$ values are noted to be lower than the corresponding $\Delta h_{area,DSC}$ values. Contrarily, the $\Delta h_{pyr}$ value for EC sample is noted to be much higher than its $\Delta h_{area,DSC}$ value, owing to its high char yield ($Y_c$ = 0.75). Thus, the $\Delta h_{pyr}$ values for EC sample was found to be much higher than $\Delta h_{pyr}$ values for biomass samples.

Consequently, as the $\Delta h_{pyr}$ directly contributes to the heat of gasification (Equation 16-3), the $\Delta h_{gas}$ values for EC sample was found to be much higher than $\Delta h_{gas}$ values for biomass samples. The high value of $\Delta h_{gas}$ values for EC is also attributed to the fact that the coal pyrolysis takes place at higher temperature ranges than biomass samples, thus resulting in a higher sensible heat for EC pyrolysis. Between the two leached biomass samples, even though the $\Delta h_{pyr}$ value was higher for the CS-Leached sample, the $\Delta h_{gas}$ value was found to be higher for the SG-Leached sample due to its higher sensible heat.

Table 16-1 also contains $\Delta h_{area,DSC}$, $\Delta h_{pyr}$ and $\Delta h_{gas}$ values for the two fuel mixture test cases of EC and leached biomass samples. An interesting point noted from the data for the two fuel mixture samples is related to comparing their $\Delta h_{area,DSC}$ and $\Delta h_{pyr}$ values. For the 80:20 initial mass mixture ratio of EC and leached biomass samples, the $\Delta h_{area,DSC}$ value was not found to be close to the two values from the individual runs of each coal and leached biomass runs. In the case of EC and SG-Leached mixture, the $\Delta h_{area,DSC}$ (320.1 J/g) was found to be lower than the $\Delta h_{area,DSC}$ values for each EC (389 J/g) and SG-Leached samples (374 J/g). However, the $\Delta h_{pyr}$ and $\Delta h_{gas}$ values for each of the mixtures were found to be in between energetic values for the individual fuels. This was in part attributed to correct calculation of energetic properties on their per unit volatile mass basis using the validated pyrolysis model (Agarwal & Lattimer, 2012). Thus, $\Delta h_{pyr}$ and $\Delta h_{gas}$ properties were able to more accurately characterize the energetic properties of fuel in comparison to the traditional approach of using $\Delta h_{area,DSC}$ values.

To further assert the above mentioned point, weight additive values of $\Delta h_{pyr}$ and $\Delta h_{gas}$ properties were compared for fuel mixture data. It has already been shown in previous sections that the mixture of EC and leached biomass samples deliver additive TGA and DSC curves. Thus, the energetic properties derived from the EC and leached biomass mixture runs should also deliver weight additive energetic properties of individual coal and leached biomass samples. These values were calculated for weighted additions of energetic properties of individual EC and

leached biomass samples and are reported in Table 16-2. The simulated values reported in Table 16-2 are compared with those present in Table 16-1 for the coal and leached biomass mixtures and presented as error percentage in brackets. The weighted simulations, presented in Table 16-2, were calculated for two types of weighted additions. The first type of weight addition, for EC and leached biomass samples, was conducted per the initial weight contribution of each fuel (i.e. in 80:20 ratio). The second type of weight addition was carried out on the basis of the volatile mass contribution of the respective fuels. The volatile contribution for an initial mass mixture of EC and leached biomass in 80:20 ratio yielded volatile matter in 54:46 ratio for both test cases involving different biomass samples. The rationale behind using the second weighted addition methodology lies in the definition of $\Delta h_{pyr}$ and $\Delta h_{gas}$ properties, which are both calculated on the volatile mass loss basis.

Table 16-2. Weighted additions of $\Delta h_{pyr}$ and $\Delta h_{gas}$ properties for individual fuel samples to estimate the energetic properties for the two fuel mixture test cases

| **Estimation Methodology** | **80:20 ratio property addition from individual fuel samples (J/g)** | | **54:46 ratio property addition from individual fuel samples (J/g)** | |
|---|---|---|---|---|
| **Fuels simulated** | **$\Delta h_{pyr}$ (Error %)** | **$\Delta h_{gas}$ (Error %)** | **$\Delta h_{pyr}$ (Error %)** | **$\Delta h_{gas}$ (Error %)** |
| EC & SG-Leached (80:20) | 1107.8 (+43.7%) | 4496.54 (+15.5%) | 810.8 (+5.9%) | 3436.4 (-11.7%) |
| EC & CS-Leached (80:20) | 1123.1 (+24.8%) | 4476.3 (+36.6%) | 846.1 (-6.0%) | 3389.8 (+3.5%) |

The second and third columns in Table 16-2 provide the energetic properties estimated by the first type of weighed addition in 80:20 ratio. These were compared with the calculated energetic properties reported for the two fuel mixture test cases reported in Table 16-1. As seen from Table 16-2, large errors were observed in the property estimation by the initial mass based weighted addition. In comparison, the properties estimated on the volatile mass contribution basis are shown in Table 16-2 to be closer to those measured for the actual fuel mixture runs reported in Table 16-1. A validation for weighted energetic property addition has not been conducted in the literature for coal and biomass samples. These analyses validate that $\Delta h_{pyr}$ and $\Delta h_{gas}$ properties must be calculated on the volatile mass loss basis. In addition, it also asserts that the predictions for energetic properties of fuel mixtures must be made on the basis of their volatile mass contribution, instead of their initial mass proportion.

## 16.5.2 Heat of Pyrolysis Gas Combustion and Heat of Char Combustion

Table 16-3 reports the $\Delta h_{area,MCC,p}$ (initial mass basis), $\Delta h_{comb,p}$ (volatile mass basis), $\Delta h_{area,MCC,cc}$ (initial mass basis), $\Delta h_{comb,cc}$ (volatile mass basis), $\Delta h_{comb}$ (volatile mass basis), $Y_c$ and $Y_{cc}$ values calculated for all samples at 20 K/min heating rate using MCC. The definition, and method of calculation of these properties has previously been described from Equation 16-6 through 16-9.

Table 16-3. Energetic combustion properties of fuel samples from MCC

| Experimental Runs | $\Delta h_{area,MCC,p}$ (J/g) | $\Delta h_{comb,p}$ (J/g) | $\Delta h_{area,MCC,cc}$ (J/g) | $\Delta h_{comb,cc}$ (J/g) | $\Delta h_{comb}$ (J/g) | $Y_c$ | $Y_{cc}$ |
|---|---|---|---|---|---|---|---|
| SG-Raw | 10,542 | 12,570 | 26,659 | 30,206 | 15,416 | 0.161 | 0.118 |
| CS-Raw | 9,641 | 11,274 | 26,840 | 30,461 | 14,052 | 0.145 | 0.119 |
| SG-Leached | 10,275 | 12,170 | 27,247 | 30,295 | 14,992 | 0.156 | 0.101 |
| CS-Leached | 9,641 | 12,501 | 26,840 | 30,324 | 15055 | 0.143 | 0.086 |
| EC | 9,185 | 36,038 | 35,424 | 40,307 | 39,219 | 0.745 | 0.121 |
| EC & SG-Leached in 80:20 Mixture | 9,277 | 24,045 | 29,067 | 33,531 | 29,871 | 0.614 | 0.133 |
| EC & CS-Leached in 80:20 Mixture | 9,545 | 26,129 | 29,892 | 34,641 | 31,532 | 0.635 | 0.137 |

*Uncertainty in heat of combustion = ±3%; Uncertainty in area values = ±2%;

For biomass samples, the $\Delta h_{area,MCC,p}$ values were found to be slightly lower than their corresponding $\Delta h_{comb,p}$ values, owing to their lower char yield as per Equation 16-7. Contrarily for EC sample, the $\Delta h_{area,MCC,p}$ value are much higher than its $\Delta h_{comb,p}$ value, owing to its high char yield. Thus the heat of pyrolysis gas combustion, $\Delta h_{comb,p,}$ for EC sample is measured to be much higher than that of biomass samples, when calculated on the basis of volatile mass. This is in agreement with the similar observation made in the previous section regarding the $\Delta h_{pyr}$ values of fuel samples. Also, the heat of char combustion, $\Delta h_{comb,cc}$, for EC is higher than that of biomass counterparts. Consequently as per Equation 16-9, the total heat of combustion, $\Delta h_{comb}$, for EC was found to be much higher than biomass samples.

As observed from Table 16-3, the $\Delta h_{comb,p}$ values for leached biomass sample are not significantly different than the corresponding values of their untreated counterparts. This is in clear contrast to the observations in the previous section, where a substantial increase in the $\Delta h_{pyr}$ values was observed on biomass leaching, primarily due to the absence of secondary exothermic reactions (Table 16-1). Thus, leaching of biomass samples does not necessarily increase the pyrolysis gas energy density of the biomass fuel. However, the $\Delta h_{area,MCC,p}$ values for biomass

samples show a clear increase due to water leaching. This happens due to $\Delta h_{area,MCC,p}$ values been calculated on the initial sample mass basis, where as $\Delta h_{comb,p}$ is calculated on the volatile mass basis of the pyrolyzing fuel. Similarly, the $\Delta h_{comb,cc}$ values do not change on biomass water leaching. This observation signifies that the absence of salts does not significantly affect the quality of the biomass char. Consistent with the two observations, the $\Delta h_{comb}$ values were not significantly affected on biomass water leaching.

The difference between the measurement of $\Delta h_{area,MCC,p}$ and $\Delta h_{comb,p}$ values is also evident from the property values reported for coal and leached biomass mixture runs in Table 16-3. Here, $\Delta h_{comb,p}$ values for mixture samples show a better representation of weighted sum of $\Delta h_{comb,p}$ values of individual fuels, in contrast to the $\Delta h_{area,MCC,p}$ properties.

To further assert the above mentioned point, weight additive $\Delta h_{comb,p}$ values of individual fuels were compared to those of fuel mixture runs. It has already been shown through Figure 16-6 that the mixture of EC and leached biomass samples deliver additive HRR curves. Thus, the $\Delta h_{comb,p}$ values derived from the EC and leached biomass mixture runs must also deliver weight additive $\Delta h_{comb,p}$ values of individual coal and leached biomass samples. Thus, the simulated weighted sum values of the fuel mixtures were calculated and are reported in Table 16-4. The simulated values reported in Table 16-4 are compared with those present in Table 16-3 for the coal and leached biomass mixture runs (last two rows in Table 16-3) and presented as error percentage in brackets. The weighted simulations, presented in Table 16-4, were calculated for two types of weighted additions. Similar to the previous section, these additions were based on the initial weight contribution of the individual coal and biomass fuels, and volatile mass contributions for coal and biomass samples. A similar exercise was run for $\Delta h_{comb,cc}$ values for coal and leached biomass mixtures, and the results are shown in Table 16-4.

Table 16-4. Weighted additions of $\Delta h_{comb,p}$ and $\Delta h_{comb,cc}$ properties for individual fuel samples to estimate the energetic properties for the two fuel mixture test cases. Additions in initial mass ratio (80:20) and volatile mass ratio (54:46) basis

| **Estimation Methodology** | **80:20 ratio property addition from individual fuel samples (J/g)** | | **Volatile ratio property addition from individual fuel samples (J/g)** | |
|---|---|---|---|---|
| **Fuels simulated** | **$\Delta h_{comb,p}$ (Error %)** | **$\Delta h_{comb,cc}$ (Error %)** | **$\Delta h_{comb,p}$ (Error %)** | **$\Delta h_{comb,cc}$ (Error %)** |
| EC & SG-Leached (80:20) | 31264 (+30.0%) | 38305 (+14.2%) | 25059 (+4.2%) | 35701 (+6.5%) |
| EC & CS-Leached (80:20) | 31331 (+19.9%) | 38310 (+10.6%) | 25211 (-3.5%) | 35715 (+3.1%) |

Table 16-4 provides the energetic properties estimated by the first type of weighed addition in 80:20 ratio. Large errors were observed in the property estimation by the initial mass based weighted addition. In comparison, the properties estimated based on the volatile mass contribution basis, shown in Table 16-4, were closer to those calculated for the actual fuel mixture runs reported in Table 16-3. This is in agreement with the conclusions from the previous section where the $\Delta h_{pyr}$ property addition on the basis of volatile mass contributions of individual fuel samples, accurately predicted the $\Delta h_{pyr}$ properties of the fuel mixture. This is due to both $\Delta h_{pyr}$ and $\Delta h_{comb}$ properties being calculated on the fuel volatile mass basis. These analyses firstly validate that the $\Delta h_{comb}$ property must be calculated on the volatile mass loss basis. Secondly, it asserts that the predictions for combustion energetic properties of fuel mixtures must be made on the basis of their volatile mass contribution, instead of their initial mass proportion.

## 16.6 Summary and Conclusions

The focus of this study was to accurately characterize the pyrolysis and combustion energetics of decomposing solid fuel samples. The energetic properties of coal, biomass and coal-biomass mixture samples were investigated using a STA and a MCC. The effects of biomass water leaching on the energetics of biomass fuels and coal-biomass fuel mixtures were also studied.

The water leaching of biomass samples mitigates the secondary reactions during pyrolysis, shifted the primary decomposition reactions to higher temperatures, and reduced the char yield of biomass fuel samples. An increase in the heat of pyrolysis was noticed on biomass water leaching due to removal of secondary exothermic reactions. However, the heat of combustion of leached biomass was not measured to be significantly higher than that of untreated biomass samples. Thus, leaching of biomass samples does not necessary increase the energy density of biomass fuels.

It was found that the co-pyrolysis of coal and leached biomass fuel mixtures exhibited a weight additive energetic behavior, when pyrolyzed on an 80:20 initial mass proportion. It was further validated and concluded that the weighted sum prediction for the heat of pyrolysis and the heat of combustion for coal-biomass fuel mixtures must be conducted on the basis of their individual volatile mass contributions and not on the basis of initial fuel mixture proportion.

# Chapter 17

# Combustion Performance of Coal and Biomass Feedstocks

## 17.1 Introduction

Questions about the long-term availability of traditional fossil fuels, their geopolitical availability, and the tightening environmental restrictions have resuscitated the need to explore renewable and clean sources of energy to alleviate the concerns of ever increasing energy demand. Addition of renewable fuels such as biomass (Gil et al., 2010; Lapuerta et al., 2008; Kumabe et al, 2007; Ghosh et al., 2006; Minchener, 2005; Ayhan, 2003; Sami et al., 2001; Robinson et al., 1998), industrial wastes from biodiesel production such as glycerol (Yun & Suuberg, 1993), and municipal solid waste (Muthuraman et al., 2010; Heikkinen et al., 2004; Folgueras et al., 2003; Otero et al., 2002; Ndaji et al., 1999), including wide range of plastics (Sharma & Ghoshal, 2010), waste wood (Kumabe et al., 2007; Ayhan, 2003; Robinson et al., 1998), cardboard (Loulou et al., 2003), paper (Yanfen & Xiaoqian, 2010) etc. have been recently investigated for co-combustion usage with coal. The pyrolysis of blends of alternate sources of fuels with traditional fossil fuels, such as coals, leads to improved energy and chemical recovery from the lifecycle of these products (Folgueras et al., 2003). Additionally, it also provides an alternative to the current disposal techniques of wastes such as land filling and incineration, which has raised issues related to soil fertility, land price depreciation and environmental pollution (Ndaji et al., 1999).

Predicting the thermal response of solid fuels and blends undergoing pyrolysis and combustion has historically been of primary interest in the areas of fire flammability and gasification applications. Proper characterization of such fuels is needed in order rank the fuel performance and customize the fuel blends in for efficient usage. However, the literature studies have been limited to the characterization of blends and identification of interactions between different fuel samples during co-pyrolysis (Sütcü & Pişkin, 2011; Di Nola et al., 2010; Gil et al.,

2010; Yanfen & Xiaoqian, 2010; Lester et al., 2007; Biagini, 2002). There is a lack of approach in the literature to design and customize fuel bends for efficient combustion along the pyrolysis temperature range and predict its performance using simple experiments and mathematical models.

As a first step to the customization of fuel blends, a system to indicate the rank based performance of an individual fuel needs to be developed. In the literature, the fuels have primarily been distinguished on the basis of their char yields (Rath et al., 2003; Gomez et al., 2009), pyrolysis temperature range (Radmanesh et al., 2006; Grønli et al., 2002; Otero et al., 2002), Arrhenius kinetic parameters (Hashimoto et al., 2011; Bradley et al., 2011; Fermoso et al., 2010; Saddawi et al., 2009; Ulloa et al., 2009; Sadhukhan et al., 2008; Becidan et al., 2007; Folgueras et al., 2003; Völker & Rieckmann, 2002; Milosavljevic & Suuberg, 1995), HHV (from bomb calorimeter data) (Naik et al., 2010; Parikh et al., 2005; Sheng & Azevedo, 2005; Demirbaş, 1997; Raveendran & Ganesh, 1996) and evolved gas analysis (Di Nola et al., 2010; Barneto et al., 2009; Biagini, 2002; Otero et al., 2002; Ndaji et al., 1999). However, the energetic characterization (in terms of heat of pyrolysis and heat of combustion) of fuel and blends is not as well understood as the other aspects of their pyrolysis process. Proper characterization of fuels, both from pyrolysis and combustion perspectives, is necessary to develop such fuel performance model. Hence, a methodology needs to be developed for complete characterization of fuels, including proper energetic characterization, and integrate it with a validated process that determines the ranking of fuels.

The reactivity of a fuel requires a total energy balance on the fuel, which includes the energy required for pyrolysis of the material as well as the heat released from combustion of the evolved gases and char. These quantities are required as a function of temperature in order to estimate the performance of fuel and blends, which decompose at different temperature ranges. The methodology of calculating accurate heat of pyrolysis and heat of combustion has been discussed in Chapter 16 using simultaneous thermogravimetric analyzer (STA) and micro-scale combustion calorimeter (MCC) instruments, respectively. These two instruments also combines the fuel properties based on their temperature dependent char yields (using TGA data), pyrolysis temperature (using STA data), Arrhenius kinetic parameters (using TGA data), evolved gas analysis (estimating gas quality from MCC data), pyrolysis energetics (using DSC data) and combustion energetics (using MCC data) simultaneously. Integrating the fuel characterization

with a fuel decomposition and combustion model will provide the tools necessary to estimate the performance of fuels and blends.

Therefore, with the help of these instruments both temperature based, as well as integrated energetic properties of the fuels can be determined for fuel ranking. The data acquired from these techniques can be applied onto an energy balance model for a single fuel particle to determine the fuel performance, and hence the ranking, along the decomposition temperature range of the fuel.

## 17.2 Experimental

The coal and biomass feedstocks used for this study, and their preparation method, is discussed in Chapter 14. The instrumentation and analysis procedure for STA and MCC is discussed in Chapter 16. In addition to the coal and biomass feedstocks, glycerol (99% purity CAS# 56-81-5) and Polystyrene (PS; MW = 250,000) were used in this study. Both samples were obtained from Sigma Aldrich. PS granules were of irregular form and crushed to -1 mm diameter range using liquid nitrogen cooled mortar. The powdered PS was tested in the mass range of 4-6 mg in STA and MCC. Glycerol was used in its viscous liquid form and its sample mass was on the order of 10-15 mg.

## 17.3 Fuel Performance Model

Solid fuels when sufficiently heated will produce gas volatiles through pyrolysis. This includes non-charring materials such as many plastics as well as charring materials.

$$Fuel \xrightarrow{N_2,\Delta} char + gas \qquad \text{(Eq. 17-1)}$$

Based on the energy balance of a single fuel particle undergoing pyrolysis, a model for the transient temperature rise of a fuel with lumped model analysis is (Agarwal et al., 2013; Agarwal & Lattimer, 2012):

$$\dot{Q}_{net} = \left[ mc\frac{dT}{dt} + \dot{m}_{pyr}\left(-\Delta h_{pyr}\right) \right] \qquad \text{(Eq. 17-2)}$$

Here $\dot{Q}_{net}$ is the net heat transfer rate to the fuel (W), $m$ is the instantaneous fuel mass (g), $c$ is the specific heat of the fuel (J/g-K), $T$ is the fuel temperature (K), $t$ is time (s), $\dot{m}_{pyr}$ is the fuel mass loss rate due to pyrolysis (g/s), and $\Delta h_{pyr}$ is the heat of pyrolysis (J/g). The first term on

the right hand side of the Equation 17-2 represents the sensible energy to heat up the fuel while the second term is the latent heat to generate volatiles. An endothermic reaction is defined here to be a positive value. For certain plastics, an additional term for the heat of melting can also be added to Equation 17-2 (Agarwal & Lattimer, 2012).

The heat of combustion of volatiles generated during pyrolysis of fuels is calculated by:

$$\dot{Q}_{c,p} = \dot{m}_{pyr} \Delta h_{comb,p} \qquad \text{(Eq. 17-3)}$$

Here $\dot{Q}_{c,p}$ is the heat release rate of the volatiles due to combustion (W) and $\Delta h_{com,pb}$ is the effective heat of combustion of the volatiles generated from fuel pyrolysis (J/g) (Lyon, 2000; Lyon & Walters, 2004). Since the combustion process is exothermic, $\Delta h_{comb,p}$ is a negative value.

The fuel pyrolysis performance parameter represents the rate of energy released from the combustion of pyrolysis gases, to the rate of energy required to generate pyrolysis gases. An expression for fuel pyrolysis performance was derived by solving the Equation 17-2 and Equation 17-3 for $\dot{m}_{pyr}$ and rearranging to obtain:

$$\eta_p = \frac{\dot{Q}_{c,p}}{\dot{Q}_{net}} = \left( 1 - \frac{mc\dfrac{dT}{dt}}{\dot{Q}_{net}} \right) \left( \frac{-\Delta h_{comb,p}}{\Delta h_{pyr}} \right) \qquad \text{(Eq. 17-4)}$$

Note that the pyrolysis performance parameter in Equation 17-4 is temperature dependent. From Equation 17-4, the fuel pyrolysis performance parameter is dependent on the fuel temperature during pyrolysis, the heat transfer rate for sensible heating of the fuel, and the ratio of the heat of combustion to heat of decomposition. An integrated form of Equation 17-4 provides a single value that represents the total pyrolysis performance of the fuel.

$$\eta_{p,tot} = \frac{Q_{c,p}}{Q_{net}} = \left( 1 - \frac{\int mc\dfrac{dT}{dt}\,dt}{Q_{net}} \right) \left( \frac{-\Delta h_{comb,p}}{\Delta h_{pyr}} \right) \qquad \text{(Eq. 17-5)}$$

For current experiments, the heating rate ($dT/dt$) has been kept constant at 20 K/min. The instantaneous mass ($m$) and specific heat ($c$), along with the $\dot{Q}_{net}$ given to the fuel sample for complete pyrolysis was obtained using the STA data (Agarwal et al., 2013; Agarwal & Lattimer, 2012). The measurement procedure for heat of pyrolysis and heat of combustion was described in Chapter 16.

The fuel pyrolysis performance expressions listed in Equation 17-4 and Equation 17-5 assimilates the contribution of char yield, pyrolysis temperature, mass loss kinetics, evolved gas quality, pyrolysis energetics and combustion energetic, apart from other temperature dependent properties. This is in contrast with many literature studies where some of these individual properties have been evaluated to compare and characterize the performance of fuels.

The char combustion performance parameter can similarly be calculated for the following reaction:

$$Char \xrightarrow{O_2,\Delta 20K/\min} ash + gas \qquad \text{(Eq. 17-6)}$$

The temperature dependent char combustion performance parameter is defined as ratio of heat released during char oxidation to the sensible heat required to heat the char sample up to its gasification temperature. Assuming the latent heat of pyrolysis of a char sample to be negligible, the expression for char combustion performance is defined as follows:

$$\eta_{cc} = \frac{\left(-\Delta h_{comb,cc}\right)\frac{dm}{dt}}{\left(m_c c_c + m_{ash} c_{ash}\right)\frac{dT}{dt}} \qquad \text{(Eq. 17-7)}$$

The total char performance parameter can then be calculated as:

$$\eta_{cc,tot} = \frac{\left(-\Delta h_{comb,cc}\right)\left(M_{in,cc} - M_{fin,cc}\right)}{\int\left(m_c c_c + m_{ash} c_{ash}\right)dT} \qquad \text{(Eq. 17-8)}$$

The cumulative fuel performance as a sum of pyrolysis performance and char performance can be calculated by Equation 17-9 on temperature basis and Equation 17-10 on total basis, as depicted below:

$$\eta_{cum} = \left(1 - Y_c\right)\eta_p + Y_c \eta_{cc} \qquad \text{(Eq. 17-9)}$$

$$\eta_{cum,tot} = \left(1 - Y_c\right)\eta_{p,tot} + Y_c \eta_{cc,tot} \qquad \text{(Eq. 17-10)}$$

## 17.4 Results and Discussion

### 17.4.1 Fuel Pyrolysis Performance

Figure 14-3(a) contains the ratio of the pyrolysis gas combustion heat release rate and heat transfer rate to heat the fuel (i.e., fuel pyrolysis performance parameter, $\eta_p$). In general, a higher fuel pyrolysis performance indicates a better fuel for pyrolysis application. As seen in

Figure 14-3(a), these different types of fuels undergo pyrolysis over a wide range of temperature. The glycerol evaporates between 150-300 ºC while the SG-Raw undergoes the majority of pyrolysis at temperatures of 220-500 ºC. The pyrolysis of PS occurs over a narrow temperature of 350-450 ºC while EC undergoes pyrolysis over a broader temperature range (300-600ºC) with the primary degradation between 400 ºC and 550 ºC. The advantage of fuels pyrolyzing over such a wide temperature range is that it could assist in designing customized fuel blends for consistent performance over a wide temperature range, e.g. the coal-biomass blend as shown in Figure 14-3(b).

The complexities of defining the fuel performance parameter based on its $\Delta h_{pyr}$ and $\Delta h_{comb,p}$ values have been discussed in the Chapter 16, where there were increases in $\Delta h_{pyr}$ property values on biomass water leaching, and decrease in $\Delta h_{pyr}$ and $\Delta h_{comb,p}$ property values due to biomass mixing in coal. In such definitions of performance, the fuel ranking becomes uncertain.

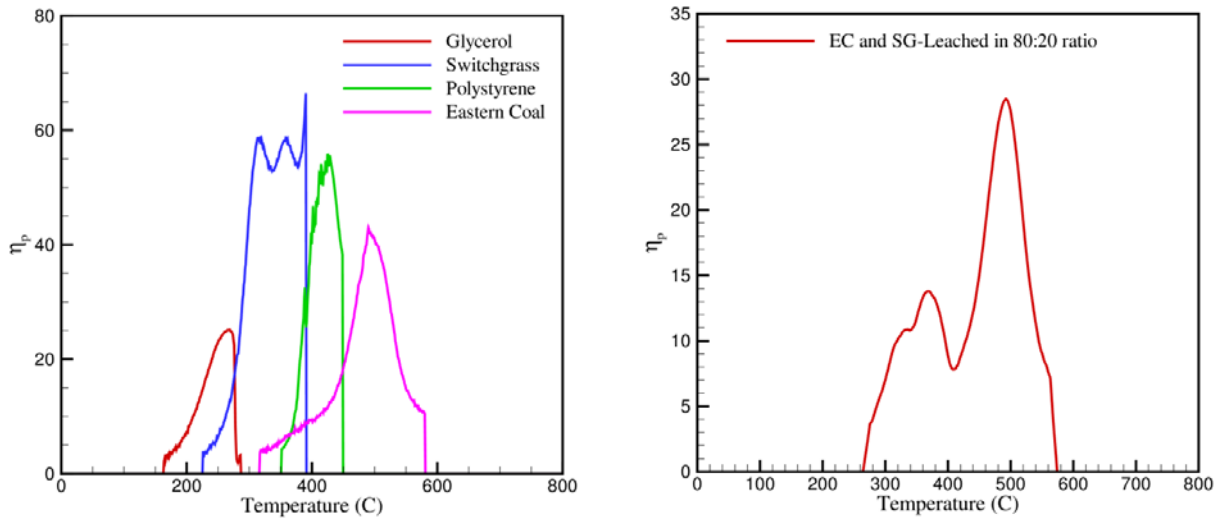



Figure 17-1. Temperature dependent fuel pyrolysis performance parameter $\eta_p$: (a) Glycerol, PS, SG-Raw and EC samples, and (b) EC & SG-Leached mixture in 80:20 ratio

Table 17-1 reports the peak heat release rate ($HRR_{peak}$), $\Delta h_{comb,p}/\Delta h_{pyr}$ and $\eta_{p,tot}$ pyrolysis properties of glycerol. PS, SG-Raw, and EC fuel samples. Many studies in the literature have used the peak heat release rate, heat of pyrolysis, heat of combustion or $\Delta h_{com,p}/\Delta h_{pyr}$ as an indicator of fuel performance. However, as indicated in the Table 17-2, all these criteria reveal a different fuel performance order with no two criteria providing the same answer. However, as

discussed in the previous sections, all these properties, including the temperature dependent fuel properties (such as $m$, $c$ etc.) play an important role in defining the total performance of the fuel in terms of Equation 17-4 and Equation 17-5 as $\eta_p$ and $\eta_{p,tot}$. As per the total fuel pyrolysis efficiency, the pyrolysis performance order for the fuels become PS > SG-Raw > Glycerol > EC.

The model also clarifies the effect of leaching on biomass in terms of pyrolysis performance change. From the previous analysis, it was shown that $\Delta h_{pyr}$ values increase due to biomass leaching and $\Delta h_{com,p}$ values remained relatively constant upon biomass water leaching. Also, as per Table 17-1, the $HRR_{peak}$ increased for both biomass samples due to water leaching; whereas, the $\Delta h_{com,p}/\Delta h_{pyr}$ values showed decline on water leaching. The $\eta_{p,tot}$ property evaluation for biomass samples reveal a net decline of 31-46% in total pyrolysis performance due to water leaching. This indicates that the water leaching of biomass feedstocks is not advantageous in terms of fuel pyrolysis performance.

Table 17-1. Pyrolysis performance indicating energetic properties of fuel samples

| Fuel | $HRR_{peak}$ (W/g) | $\Delta h_{comb,p}$ / $\Delta h_{pyr}$ | $\eta_{p,tot}$ |
|---|---|---|---|
| Glycerol | 169.4 | 25.1 | 12.7±5.2% |
| PS | 389.8 | 62.1 | 29.3 |
| SG-Raw | 42.7 | 164.3 | 18.7 |
| CS-Raw | 37.3 | 895.0 | 19.1 |
| SG-Leached | 50.3 | 62.7 | 10.1 |
| CS-Leached | 58.2 | 46.2 | 13.2 |
| EC | 26.7 | 27.0 | 7.0 |

Table 17-2. Fuel pyrolysis performance ranking order as per different criteria

| Property basis | Ranking Order based on property |
|---|---|
| $\Delta h_{pyr}$ | SG-Raw > Glycerol > PS > EC |
| $\Delta h_{com,p}$ | PS > EC > Glycerol > SG-Raw |
| $\Delta h_{com,p}/\Delta h_{pyr}$ | SG-Raw > PS > Glycerol > EC |
| $HRR_{peak}$ | PS > Glycerol > SG-Raw > EC |
| $\eta_{p,tot}$ | PS > SG-Raw > Glycerol > EC |

The pyrolysis performance model also defines the difference between the performance of CS and SG biomass samples. Consistent with the MAF BTU values for the biomass samples listed in Chapter 14, the data in Table 17-1 shows that the CS-Raw performance is slightly

higher, if not equal, to the SG-Raw performance. After water leaching, however, the performance of CS-Leached is higher than the SG-Leached sample by a factor of 1.3.

Another point of discussion in this analysis is regarding the impact of addition of biomass with coal samples onto the pyrolysis performance of blended fuel. This matter is of high importance for currently operating industrial coal based gasification plants, where the economics of biomass addition in small quantities is needed to be understood more closely. Similar to previous analysis, the evaluation of performance based on traditional criteria such as peak heat release rate, heat of pyrolysis, heat of pyrolysis gas combustion or $\Delta h_{comb,p}/\Delta h_{pyr}$ revealed conflicting results, as shown in Table 17-3. However, the application of fuel pyrolysis performance model provides a more definitive answer to the question, as the model is based on the actual physics of the fuel pyrolysis.

Table 17-3. Pyrolysis performance evaluation of fuel blends

| Fuel | $HRR_{peak}$ (W/g) | $\Delta h_{pyr}$ (J/g) | $\Delta h_{com,p}$ (J/g) | $\Delta h_{comb,p} / \Delta h_{pyr}$ | $\eta_{p,tot}$ |
|---|---|---|---|---|---|
| EC | 26.7 | 1336.2 | 36038 | 27.0 | 7.0±5.2% |
| EC & SG-Leached in 80:20 Mixture | 20.4 | 765.8 | 24045 | 31.4 | 8.5 |
| EC & CS-Leached in 80:20 Mixture | 21.1 | 900.1 | 26129 | 29.0 | 9.3 |

Table 17-3 presents the pyrolysis performance based energetic properties of EC and blends of EC with leached biomass samples in 80:20 ratio. As observed from Table 17-3, the addition of 20% biomass to EC samples decreased the peak HRR and $\Delta h_{comb,p}$ values, while simultaneously increasing the $\Delta h_{comb,p}/\Delta h_{pyr}$ values for the mixtures. However, the fuel pyrolysis performance model reveals that the performance ranking of the fuel blend increased on biomass addition. For an addition of 20% biomass to the EC sample, the total fuel blend pyrolysis performance increased by 21% for SG-Leached addition and by 33% for CS-Leached addition. This increase in the fuel pyrolysis performance is somewhat expected based on the relatively high pyrolysis performance of the biomass, but it would not be anticipated based on the evaluating the fuel on parameters such as heat of combustion or peak heat release rate. This increase in pyrolysis performance of the fuel blend is a significant number while considering the economics of transforming a coal based reactor to coal-biomass based reactor.

### 17.4.2 Char Combustion and Cumulative Performance

For many co-firing plants, where instead of fuel gasification the fuel is completely combusted in air, the performance of the fuel must also be understood in terms of char combustion performance and cumulative performance. Figure 17-2(a) shows the temperature dependent char combustion performance for SG-Raw and SG-Leached samples calculated using Equation 17-7. As observed from the Figure 17-2(a), the leaching affects the char combustion performance of fuel char at the peak temperatures of hemicellulose and cellulose decomposition. Figure 17-2(a) also shows the char combustion performance of EC char and EC-SG Leached mixture char samples. The peak values for char performance for both EC and coal-biomass mixture samples are lower than those of biomass only char samples. However, Figure 17-2(a) does not consider the effect of amount of char produced by a unit amount of fuel at the start of pyrolysis. To equate the starting amount of fuel used for a fair comparison of combustion performance, the $\eta_{cc}$ factor should be multiplied by the char yield of the fuel, $Y_c$, as shown in Figure 17-2(b). From Figure 17-2(b), it can be observed that the EC char sample combustion performance is higher than those of biomass samples. Also, the EC-SG Leached mixture char sample produces its highest combustion performance at a higher temperature than that of EC char. However, the peak value of the char combustion performance of the coal-biomass mixture char is lower than that of EC.

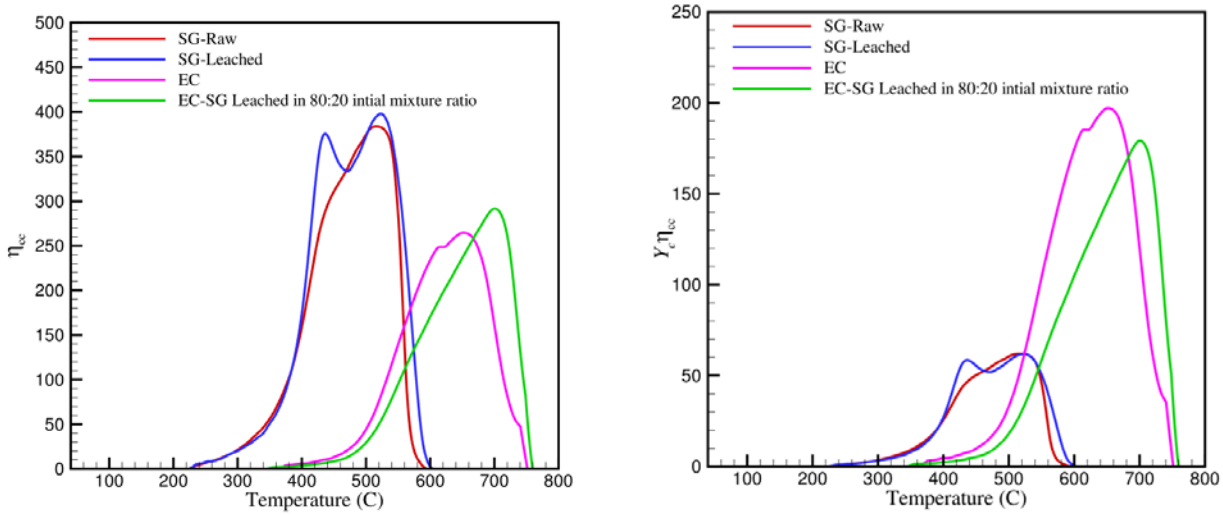



Figure 17-2. Temperature dependent fuel pyrolysis performance parameter $\eta_p$: (a) Glycerol, PS, SG-Raw and EC samples, and (b) EC & SG-Leached mixture in 80:20 ratio

To compare the combustion performance of fuel resulting from both pyrolysis and char combustion, the cumulative fuel performance can be used, as shown in Figure 17-3. The cumulative fuel performance, $\eta_{cum}$, is calculated using Equation 17-9 and considers the factor of char yield of a fuel while calculating its cumulative combustion performance. It can be observed from Figure 17-3 that for lignocellulosic fuels such as biomass, where a substantial amount of pyrolysis gases are produced, the cumulative performance is significantly directed by both combustion of pyrolysis gases and char combustion. However, for fuels such as EC and their 80:20 mixtures with biomass, where char yields are much higher, the total fuel performance is primarily governed by the char combustion performance. Hence, considering the total combustion of fuel (pyrolysis + char combustion), the combustion performance of EC samples is found to be much higher than that of biomass samples and slightly higher than that of EC and biomass mixtures in 80:20 ratio.

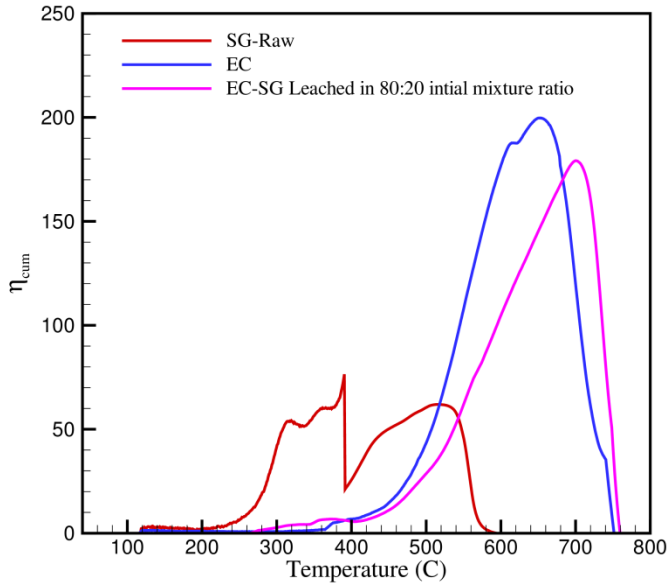



Figure 17-3. Temperature dependent cumulative fuel performance ($\eta_{cum}$)

Table 17-4 contains the comparison of all performance parameters of tested coal, biomass and mixture fuels. Looking at the $Y_c.\eta_{cc,tot}$ parameter to compare the char combustion performance of fuel char formed from same amount of initial fuel, it can be observed that the biomass water leaching decreases the char combustion performance by 23-26%. The char combustion performance for CS samples, both in raw and water leached states, were found to be slightly higher than SG samples. The char combustion performance of EC char samples was

found to be three times higher than that of biomass samples in raw form, as consistent with Figure 17-2(b). Thus, the addition of leached biomass onto EC samples produced ~28% lower char combustion performance.

Table 17-4. Fuel combustion performance parameters for coal and biomass fuels

| Fuel | $\eta_{p,tot}$ | $\eta_{cc,tot}$ | $(1-Y_c)\eta_{p,tot}$ | $Y_c.\eta_{cc,tot}$ | $\eta_{cum,tot}$ |
|---|---|---|---|---|---|
| SG-Raw | 18.7 | 63.1 | 15.7 | 10.2 | 25.9 |
| CS-Raw | 19.1 | 51.9 | 16.4 | 7.5 | 23.9 |
| SG-Leached | 10.1 | 67.9 | 8.6 | 10.6 | 19.1 |
| CS-Leached | 13.2 | 57.1 | 11.3 | 8.2 | 19.5 |
| EC | 7.0 | 43.8 | 1.8 | 32.6 | 34.4 |
| EC & SG-Leached in 80:20 Mixture | 8.5 | 36.9 | 3.3 | 22.7 | 26.0 |
| EC & CS-Leached in 80:20 Mixture | 9.3 | 37.6 | 3.4 | 23.9 | 27.3 |

The last column in Table 17-4 compares the cumulative total combustion performance, $\eta_{cum,tot}$, of different fuels, as calculated by Equation 17-10. As per the $\eta_{cum,tot}$ performance factor, the water leaching process decreases the cumulative fuel performance of biomass fuels by 18-26%. The difference between the cumulative combustion performance of SG and CS samples were found to be statistically negligible. The cumulative combustion performance of EC sample was found to be ~28% higher than raw biomass samples and ~44% higher than the water leached biomass samples. Upon mixing biomass in coal samples in 80:20 ratio, the cumulative combustion performance of the mixture decreased by ~22% of the EC only value. This number signifies the amount of extra mass of mixture fuel that would needed to be fed into a co-firing plant in order to obtain the same performance as coal-alone combustion plant.

## 17.5 Summary and Conclusions

The focus of this study was to quantify the combustion performance index of fuel and blends by developing a model based on its gravimetric, pyrolysis and combustion energetics data. The models were developed for fuel pyrolysis performance, char combustion performance and cumulative fuel combustion performance. The models were developed to calculate both temperature based performance and total integrated performance of fuels and blends. The experimental data was generated using a simultaneous thermogravimetric analyzer and a micro-scale combustion calorimeter. The fuels tested in this study included coal, biomass, polystyrene

and glycerol. The effects of biomass water leaching, as well as, coal-biomass blending, was also investigated in terms of fuel performance.

Using temperature dependent performance parameters, it was shown that different fuels produce peak performance at different temperatures. Thus, the mixing of various fuels will help blended fuels in generating consistent performance over a wider temperature range, which in turn can be advantageous for power plant operation. It was found that the pyrolysis performance of a biomass fuel decreased 31-46% on water leaching. The char combustion performance of biomass decreases 23-26% on water leaching. Thus, the cumulative combustion performance of biomass samples decreased 18-26% on water leaching. Hence, it was found that the water leaching may not be advantageous in terms of fuel pyrolysis or combustion performance.

The blending of coal and leached biomass fuels in 80:20 ratio was also evaluated in terms of total integrated performance parameters. It was found that the blending of biomass increases the pyrolysis performance of coal by 21-33%. However, the blending of biomass decreased the char combustion performance of coal samples by 28%. Thus, blending of biomass decreased the cumulative fuel combustion performance of coal by 22%. This performance drop due to blending signifies the amount of extra mass of mixture fuel that would needed to be fed into a co-firing plant in order to obtain the same performance as coal-alone combustion plant.

# Chapter 18

# Combustion Characterization of Coal-Biomass Briquettes

## 18.1 Introduction

Alternative fuels to coal are being explored for use in existing power plants as well as more advanced systems such as gasifiers (Jenkins et al., 1998). In this respect, co-firing of coal and biomass fuels into existing coal based reactors has generated substantial interest (Gil et al., 2010; Samuelsson et al., 2009; Larsson et al., 2008; Peksa et al., 2007; Sami et al., 2001; Spliethoff & Hein, 1998). However, there are many challenges related to the co-firing of two very different types of fuels, both in terms of reactor operations and fuel handling. One option being explored is the manufacturing of briquettes or pellets that contain one or more types of fuels (Bratton et al., 2010a; Bratton et al., 2010b; Luttrell et al., 2000). Briquettes containing biomass are attractive because they not only increase the density of the fuel allowing for a higher energy content fuel to be delivered to the facility, but also improve the fuel handling, storage, fuel injection and issues related to biomass degradation over time (Wang et al., 2009; Rhén et al., 2007). In addition, briquettes containing mixtures of coal and biomass have been developed for use in existing power plants to reduce the carbon footprint and decrease emissions (Gil et al., 2010; Nussbaumer, 2003). Some gasifiers have also been powered by pellets of municipal waste containing plastics, paper, and cardboard products (Biagini, 2002; Jenkins et al., 1998).

The understanding of briquette combustion behavior to date has been largely based on details of the solid combustion for individual materials without much consideration of the briquette properties. It is thus often assumed that the combustion behavior of individual fuels will dictate the combustion behavior of blended pellets (Gil et al., 2010a; Gil et al., 2010b). Most of the literature studies focus on thermogravimetric (TGA) analysis of pellet combustion behavior (Vamvuka & Sfakiotakis, 2011; Gil et al., 2010a; Gil et al., 2010b; Zhang et al., 2009; Biagini, 2002). The usage of TGA requires the tested sample to be of milligram size, thus

requiring the tested briquette to be crushed. This procedure will not accurately reflect the properties of an uncrushed briquette subjecting to its mechanical durability and non-thermally thin behavior during combustion process. The usage of TGA primarily provides the decomposition data of fuels when subjected to low heating rates (5-50 K/min) in a controlled environment. This analysis is also different to the real-time conditions that briquettes encounter while entering a furnace/reactor. In a reactor, the briquettes are instantaneously subjected to a very high heat flux and the briquette temperature rise rate is substantially higher. The fuel briquette reacts to its high temperature flames and is also affected by flames and radiation from other adjacent burning briquettes. Thus, the popular assertions that the combustion properties behavior can be simulated from the sum of its contributing constituent (Gil et al., 2010b), may not turn out to be true in reactor operations involving briquettes. The same questions also arise over the applicability of emission gas data (such as $NO_x$, CO and $CO_2$) from the TGA-MS studies (Gil et al., 2010b).

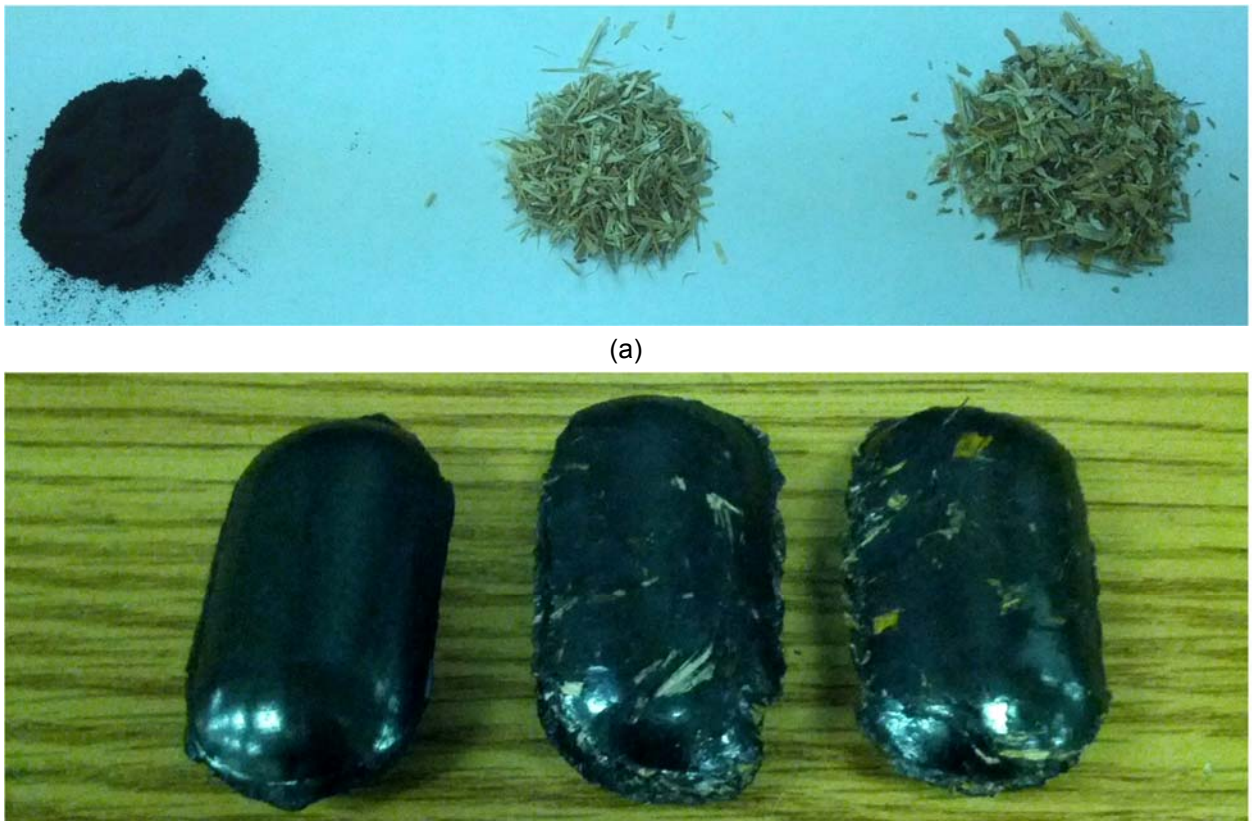
One of the primary motivation to study the briquette combustion behavior was the interest in co-firing biomass with coal in the Virginia Tech (VT) power plant. The VT power plant is a coal based CHP cycle plant that has been recently authorized to co-fire coal and biomass fuels (up to 15%). In a recent trial, the boiler was co-fired with coal and biomass that was loosely mixed prior to feeding into the hopper. During co-firing, the temperature in the boiler increased and the $NO_x$ levels increased as well. This increase in $NO_x$ is contradictory to many of the studies in the literature (Munir et al., 2010; Osvalda, 2007) that indicate including biomass in the fuel reduces the $NO_x$ levels in the flue gases due to the lower levels of nitrogen in biomass compared with coal.

This study focused on evaluating the influence of blending biomass with coal on the heat production, ignitability, and emission gas composition aspects. The research considered the effects of the manner in which the fuels were blended (i.e. loosely mixed or formed briquettes) as well as the air flow into the fuel bed. For direct comparison of performance, the experimental study was performed using full size briquettes as well as a similar mass of loosely mixed fuel under the same thermal exposure. In addition to providing insight on the impact of these parameters on the fuel combustion, the experimental data were also used to assist in understanding the behavior of co-firing coal and biomass in real-scale boilers through comparison of the small-scale data with trends noted in the VT power plant.

## 18.2 Experimental

### 18.2.1 Materials and Preparation

The fuels tested for the study included EC, SG-Raw and CS-Raw feedstocks, which are the same as those mentioned in Chapter 14. However, the heat treatment of the feedstocks in this study was different than described in Chapter 14 to simulate the fuel conditions encountered during operation of a power plant. The feedstocks were air dried for about one day before further processing. Coal particles obtained were fine enough to pass through a 400 µm sieve (40 mesh) while biomass particles were sieved between 2.38-2.81 mm particle size (7-8 mesh), as shown in Figure 14-2(a). The resultant moisture in EC-Raw was 2.35% by weight after natural drying. Moisture in SG-Raw was 16% and CS-Raw was 13% by weight after natural drying.



(a)

(b)

Figure 18-1. Fuel samples tested in this study, as shown from left to right: (a) EC, SG-Raw and CS-Raw, and (b) EC briquette, EC & SG-Raw 80:20 blend briquette and EC briquette, EC & CS-Raw 80:20 blend briquette

Powdered EC sample was blended with milled raw biomass feedstocks in an 80:20 coal-to-biomass ratio to form coal-biomass raw blends. The fuels and blends were also tested in briquetted forms. Pill shaped briquettes were prepared using a roll press briquetting machine (Komarek B-100R) without using any binding material. The method of briquette preparation and its durability analysis is discussed elsewhere (Dohm et al., 2013; Bratton et al., 2010a; Bratton et al., 2010b).

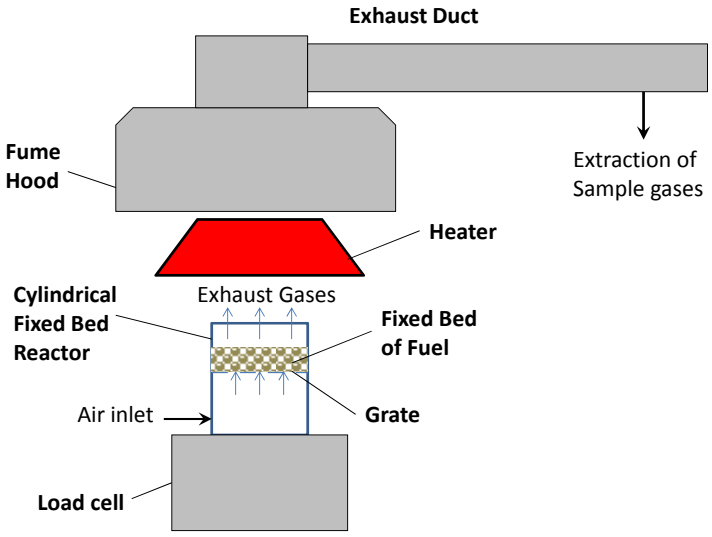
In the current study, briquettes of EC, briquettes of EC and SG Raw mix in 80:20 ratio, and briquettes of EC and CS Raw mix in 80:20 ratio were developed to compare the combustion behavior of blended briquettes versus the combustion behavior of raw blends. These three types of briquettes are shown in Figure 14-2(b). The average dimensions of briquettes were 43 x 23 x 13.5 mm with blend briquettes ~2 mm thicker than the coal pellets. On an average, the mass of a single briquette was 9.15 g. The density of EC briquettes was calculated to be 800 kg/m$^3$, while that of blend briquettes was calculated to be 635 kg/m$^3$ for SG-Raw blend briquette and 650 kg/m$^3$ for CS-Raw blend briquette.

### 18.2.2 Instrument and Procedure

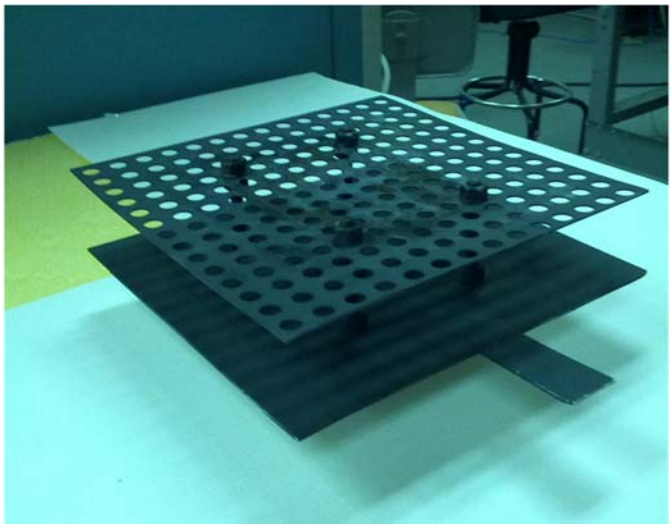
A bench-scale fixed-bed reactor was fabricated to quantify the performance of the fuels in a more realistic environment. As shown in Figure 18-2(a), a grate system was placed in the test chamber of the cone calorimeter on top of the scale balance. The grate system was constructed from stainless steel, as shown in Figure 18-2(b), and was insulated around the perimeter with high temperature ceramic fiber insulation board during tests to reduce heat losses to the surroundings. Air was naturally drawn up through the bottom of the grate to the fuel, which rested on an aluminum (Al) alloy plate. The Al alloy plate permits free air flow up through the fuel bed. The aluminum plate also collects any ash that falls through the grate so that the mass of the fuel during combustion can be accurately monitored. The heater in the cone calorimeter was set to 50 kW/m$^2$. Assuming a radiation dominated environment in a furnace, this heat flux is consistent with a furnace exposure temperature of approximately 738 ºC.

Placing the grate system inside the cone calorimeter allows for continuous measurement of the mass loss rate of the fuel, time to fuel ignition, fuel burn time, heat release rate, and combustion products downstream of the reactor. The flammability behavior of a fuel can be monitored from clear glass windows surrounding the setup. The load cell in the cone calorimeter

has an accuracy of 0.1 g, allowing for accurate mass measurements during the combustion experiments. A spark igniter was located between the fuel and the heater to ignite flammable combustion products during the experiment. The combustion products from the reactor were sampled in the exhaust and the $NO_x$ (Range 0-5000 ppb), CO (0-2000 ppm), $CO_2$ (0-5 volume %) and $O_2$ (0-25 volume %) concentrations were continuously measured. These concentrations along with the mass flow rate in the duct were used to determine the heat release rate applying the oxygen consumption principle in accordance with ASTM E-1354 (2013). The heat release rate data was used to calculate the effective heat of combustion of fuel.




(a)



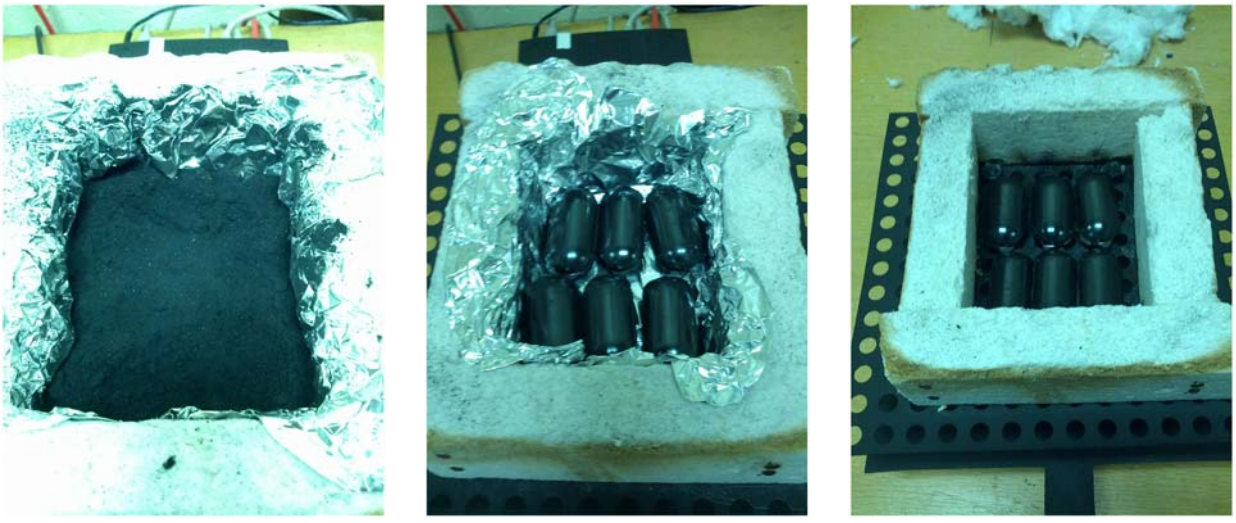
(b)

Figure 18-2. (a) Bench-scale fixed bed reactor inside the cone calorimeter, and (b) Stainless steel open grate system with aluminum pan at bottom (The system is painted with high temperature high emissivity black paint)

The cone heater temperature was set to 50 kW/m$^2$ for these experiments. The fuels, when kept in the reactor, were exposed to the heat flux for up to a duration of 1.5 hours. The fuels were combusted in two types of operating conditions that varies the combustion environment of fuels:

1. Al foil experiments: In these experiments, the fuel samples were kept on top of an aluminum foil. Thus, there was less oxygen available during the experiment. This case simulated a limited air supply condition that is being evaluated for low $NO_x$ emissions for the VT power plant. An example of this setup is shown in Figure 18-3(a) and Figure 18-3(b).
2. Open grate experiments: In these experiments, the grates are open at the bottom (no Al foil). Air was naturally drawn up through the bottom of the grate to the fuel and more air was available for combustion. An example of this setup is shown in Figure 18-3(c). This case simulated the current conditions at the VT power plant where sufficient air is supplied during fuel combustion. However, only briquettes were tested for this configuration as the raw samples would just fall through the grate to the ash plate.

In both operating conditions, a ceramic insulation wall was applied to reduce heat losses. For briquette tests, six briquettes were kept in adjacent position while testing, as shown in Figure 18-3(b). While testing raw fuel samples, an equivalent amount of raw fuel (~55 gm) was tested in the same operating conditions, as shown in Figure 18-3(a). The test matrix in Table 18-1 demonstrates all tests conducted in the study with an 'X' mark.



(a) (b) (c)

Figure 18-3. Three types of test conditions using EC fuel: (a) Raw fuel in Al foil, (b) Briquettes in Al foil, and (c) Briquettes in open grate system

Table 18-1. Test matrix for fuel briquetting study

| Fuel type and nomenclature | Al foil system | Open grate |
|---|---|---|
| EC | X | |
| SG-Raw | X | |
| CS-Raw | X | |
| EC & SG-Raw 80:20 blend (Raw EC-SG blend) | X | |
| EC & CS-Raw 80:20 blend (Raw EC-CS blend) | X | |
| EC briquettes | X | X |
| EC & SG-Raw 80:20 blend briquette (EC-SG blend briquette) | X | X |
| EC & CS-Raw 80:20 blend briquette (EC-CS blend briquette) | X | X |

## 18.3 Results and Discussion

### 18.3.1 Flammability and Combustion Performance

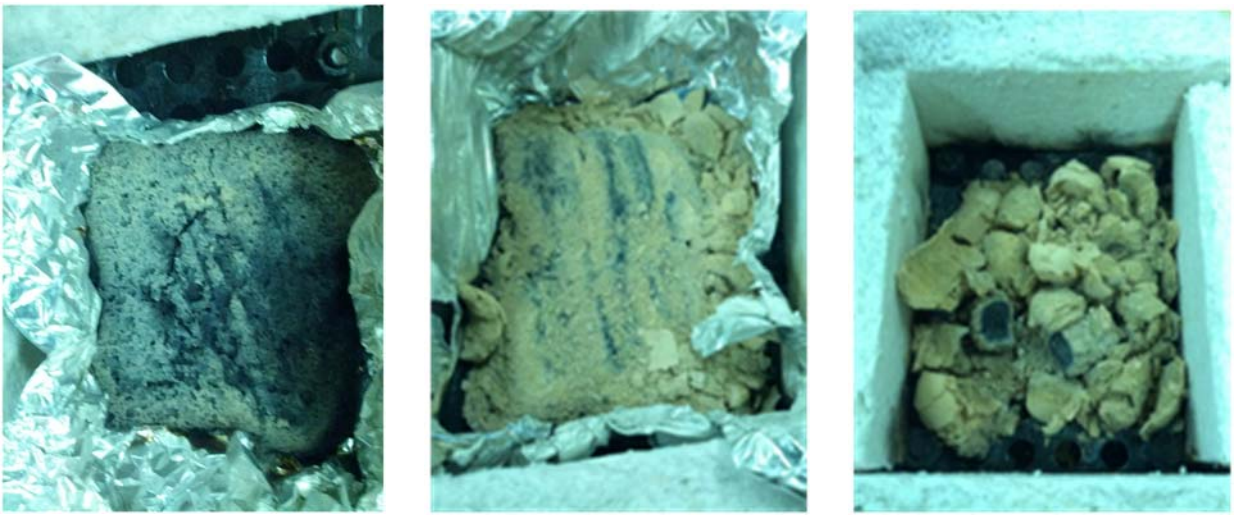
Figure 18-4(a), (b) and (c) shows the final ash from the test cases shown in Figure 18-3. When combusted in Al foil, EC-Raw fuel in Figure 18-4(a) burnt with low flames. The coal particles on the upper layer swelled and shielded the inner coal particles from combusting. Upon further combustion, the upper swollen layer cracked and short flames emerged through the cracks until the fuel burnt out. After combustion, the topmost ash layer was removed and an un-burnt layer of lower level EC sample was found, as shown in Figure 18-5(a).

When burnt as a briquette in Al foil, the EC-Raw fuel shown in Figure 18-4(b) showed more complete combustion. Since more surface area was available for combustion, the flame heights were found to be high. The flames not only originated from the top of the briquette but also from the bottom due to briquette shape. During the burning process, the upper layer of briquettes were combusting and peeling off with time while revealing the inner briquette layers. However, a small amount of char sample was left at the bottom of the Al foil when the upper layer of ash was removed, as shown in Figure 18-5(b). This analysis shows that briquettes provides a better flammability performance than raw samples, but the briquette size can be made smaller for more efficient combustion.



(a) (b) (c)

Figure 18-4. After-combustion three types of test conditions using EC fuel: (a) Raw fuel in Al foil, (b) Briquettes in Al foil, and (c) Briquettes in open grate system



(a) (b) (c)

Figure 18-5. After-combustion three types of test conditions using EC fuel upon ash removal from upper surface: (a) Raw fuel in Al foil, (b) Briquettes in Al foil, and (c) Briquettes in open grate system

When EC briquette was burnt in an open grate system, the fuel showed even more complete combustion. As shown in Figure 18-4(c) and Figure 18-5(c), the briquettes were completely combusted. With more air available for the combustion from bottom of the grate, the briquettes in this test cracked along the width instead of peeling. The flame size in this test was also found to be lower than that of briquettes with Al foil. Figure 18-5(c) also shows that even though most of the briquettes were completely burnt in the 1.5 hour test, some of them had un-

burnt interior left behind. Hence, development of smaller briquettes may provide more efficient combustion in open grate tests as well.

Figure 18-6(a) and Figure 18-6(b) provides the after combustion pictures of both blended briquettes (EC:SG-Raw and EC:CS-Raw) from open grate experiments. When compared to burnt briquette pictures of EC briquettes shown in Figure 18-5(c), the biomass blended briquettes depicted complete combustion even on the inside of the sample. This was made possible due to the presence of high ignitability biomass in the briquettes, which provided higher flames and thus higher flame temperature to completely combust the insides of the blended briquettes. A similar result was found when same briquette combustion was compared for Al foil experiments, where higher flames and better combustion was found with the presence of biomass in the briquettes.



(a) (b)

Figure 18-6. After-combustion two types of test conditions using blend briquettes upon ash removal: (a) EC and SG-Raw briquette, and (b) EC and CS-Raw briquette

When the post-combustion results were compared for coal-biomass raw blends and coal-biomass briquette blends in the Al foil test, it was found that the briquette blends provided more complete combustion than raw mixture coal-biomass blends. The raw EC-biomass blend's

flammability was hampered by the emergence of coal swelling on the upper layer of mixture. This in turn prohibited the lower levels of coal-biomass raw blends to completely combust.

These analyses shows flammability and combustion performance of briquettes were found to be better than that of raw fuel samples. It was also confirmed that the presence of biomass in briquettes favored the flammability and combustion performance of fuels in reactor operations. This assertion was further validated with comparing the effective heat of combustion, $\Delta h_{com}$, data from different tests. The effective heat of combustion is calculated on the basis of amount of matter combusted during the process, i.e. total amount of energy released during combustion process divided by the total mass lost during the process. The effective heat of combustion for different tests for blended fuels is presented in Table 18-2.

Table 18-2. Effective heat of combustion for different blended fuel tests

| Fuel Blend | Methodology | | | |
|---|---|---|---|---|
| | Raw Blend (Al foil) | Briquette blends (Al foil) | Briquette blends (Open grate) | MCC[a] |
| EC:CS (80:20) | 20.5 | 27.5 | 34.9 | 31.5 |
| EC:SG (80:20) | 23.5 | 26.0 | 30.8 | 30.0 |

[a] for Leached biomass blends with EC as reported in Chapter 16

As observed from Table 18-2, the $\Delta h_{com}$ for briquette blends were found to be 10-25% higher than that for raw blends, when combusted in similar conditions (Column 2 and Column 3). This data confirms higher combustion performance of briquette blends in comparison raw blends. Table 18-2 also confirms that the combustion performance from open grate experiments (Column 4) provided better combustion performance than Al foil experiments for briquette blends (Column 3). The heat of combustion data from MCC (Column 5) for similar coal and leached biomass blends provided the similar $\Delta h_{com}$ (reported in Chapter 16) as that for the briquetted blends in open grate conditions. Although the $\Delta h_{com}$ values reported in Chapter 16 was calculated as a weighted sum of pyrolysis and char combustion processes, the results are still close for complete combustion of fuel blends. This analysis proves: (1) open grate combustion of blended briquettes do indeed go to complete combustion, and (2) there is no loss in calorific value of fuels after briquetting. The heat of combustion data from MCC reported in Chapter 16, although from blend of EC and leached biomass, can be compared to that of blended EC and unwashed biomass briquettes because $\Delta h_{com}$ of biomass is not affected due to water leaching.

A further proof of combustion performance is provided by the final mass yield data of these runs. The final mass yield is defined as the ratio of final sample mass after combustion and the initial sample mass before combustion. A lower yield reveals a better combustion performance from a fuel blend. Table 18-3 provides the final mass yield data for the runs mentioned in Table 18-2.

Table 18-3. Final mass yield for different blended fuel tests

| Fuel Blend | Methodology | | | |
|---|---|---|---|---|
| | Raw Blend (Al foil) | Briquette blends (Al foil) | Briquette blends (Open grate) | MCC[a,b] |
| EC:CS (80:20) | 0.43 | 0.27 | 0.08 | 0.09 |
| EC:SG (80:20) | 0.41 | 0.31 | 0.06 | 0.08 |

[a] for Leached biomass blends with EC; [b] $=Y_c * Y_{cc}$ from Chapter 16

As observed from Table 18-3, the blended briquettes provide 24-37% lower mass yield than raw blend combustion, thus confirming better performance from blended briquettes. The final yield of briquetted blends in open grate experiments was found close to that reported from MCC data as multiplication of $Y_c$ and $Y_{cc}$, thus confirming more complete combustion of briquettes due to the presence of high flammability performing biomass.

The analysis from this section indicates the following: (1) flammability and combustion performance of briquettes is better than raw fuel, (2) presence of biomass in coal briquettes improves the performance of briquettes, (3) flammability, combustion performance, heat of combustion and final mass yield for blended briquettes is better than raw blends, and (4) decreasing the briquette size may improve the flammability and combustion of briquettes.

### 18.3.2 Ignitability and Burn Duration

The ignitability, or the ignition time ($t_{ig}$), of a fuel is an important parameter that determines how quickly the fuel catches fire. Not only does this parameter determine the flame height, temperature, stability, extinction and emissions (Vamvuka & Sfakiotakis, 2011; Sun & Koziński, 2000), but a significant set of operating conditions of a reactor as well. Fuel with very low $t_{ig}$ may burn before reaching the optimal position in a reactor, or may even ignite during fuel injection inside the fuel feeding chute. This kind of change in ignitibility of fuel is likely to happen in the case of coal and biomass co-firing and may lead to unsuspected drop in performance or unit failure/shutdown.

Ignitibility of a fuel is closely related to the off-gassing time ($t_{off}$) of the fuel, which is the time at which fuel starts producing pyrolysis gases when subjected to heat flux. An earlier off-gassing of fuel may release gases at non-optimal location where a significant part of it may remain un-combusted, thus leading to drop in reactor efficiency. An earlier off-gassing may also release gases at unsafe locations and lead to suffocation or fire related accidents.

The burn duration of a fuel ($t_{burn}$) represents the amount of time a fuel takes to completely burn out after ignition. A fuel with lower $t_{burn}$ may indicate presence of flashpoints at which the significant part of fuel will burn in a short duration. Such flashpoints are undesirable for operation of reactors and may affect the life of critical components such as refractory. A lower burn time may also indicate that the fuel is not burning along the full length of conveyer belt, which may result in drop in plant efficiency. Thus, the change in operation of a furnace is be closely linked with the $t_{burn}$ of the fuel.

In all coal based reactors, the operation of a plant is closely linked to $t_{off}$, $t_{ig}$ and $t_{burn}$ of the coal fuel. With the introduction of diverse fuel such as biomass, these parameters are bound to change and thus the operation of coal based plants should be changed in accordance. However, it is always desired that the amount of changes in the plant operation should be minimal. This is both due to limitations of the current coal based plants and also the costs associated with the same. Thus, a closer $t_{off}$, $t_{ig}$ and $t_{burn}$ of blended fuel to that of coal would be considered as a preferred fuel in terms of least changes in the plant operating conditions.

The present section seeks to determine the effect of biomass addition to changes in these parameters for a coal based plant. It will then be evaluated whether the briquetting of fuel further brings $t_{off}$, $t_{ig}$ and $t_{burn}$ closer to that of coal-only operation. Table 18-4 reports the $t_{off}$, $t_{ig}$ and $t_{burn}$ parameters for all fuels tested in this study using the Al foil setup.

Table 18-4. The $t_{off}$, $t_{ig}$ and $t_{burn}$ parameters for all fuels tested using Al foil setup

| Case | Fuel type and nomenclature | $t_{off}$ (s) | $t_{ig}$ (s) | $t_{burn}$ (s) |
|---|---|---|---|---|
| (I) | EC-Raw | 17 | 45 | 935 |
| | SG-Raw | 2 | 4 | 466 |
| | CS-Raw | 2 | 3 | 317 |
| (II) | EC & SG-Raw 80:20 blend (Raw EC-SG blend) | 2 | 4 | 976 |
| | EC & CS-Raw 80:20 blend (Raw EC-CS blend) | 2 | 3 | 867 |
| (III) | EC briquettes | 20 | 70 | 1610 |
| (IV) | EC & SG-Raw 80:20 blend briquette (EC-SG blend briquette) | 14 | 21 | 1059 |
| | EC & CS-Raw 80:20 blend briquette (EC-CS blend briquette) | 10 | 33 | 1407 |

The first data in Table 18-4 provides the $t_{off}$, $t_{ig}$ and $t_{burn}$ parameters of EC-Raw burn at 50kW/m$^2$ as 17, 45 and 935 s respectively. These times represent the parameters for which an EC based power plant operating conditions must be designed. The times represent a delay in off-gassing of coal fuel, further delay in its ignition time and considerable burn duration, after which the coal fuel will undergo char oxidation.

The discussion for Table 18-4 is divided in four parts from (I) to (IV). In each part, the effect of change in fuel is understood in terms of change in its $t_{off}$, $t_{ig}$ and $t_{burn}$ parameters from those of EC parameters. Based on the analysis, the effects of such changes on the possible operation of an EC based plant is discussed. Lastly, it is analyzed whether burning a certain fuel would be feasible in an EC based plant with minimal changes in plant's operating conditions.

#### 18.3.2.1 Case I: Feeding Raw Biomass in an EC Based Plant

The first discussion entails a situation where biomass feedstocks are fed into an EC based power plant. The $t_{off}$, $t_{ig}$ and $t_{burn}$ parameters for such scenario are listed in Row I of Table 18-4. It can be seen from the results that why feeding biomass into a coal-based reactor provides a huge number of operational challenges. It can be seen that the $t_{off}$, $t_{ig}$ and $t_{burn}$ parameters for biomass are significantly lower than those of EC fuel. The fuel will off-gas and ignite at non-optimal locations (possibly the feeding chute) that will lead to a series of operational problems mentioned earlier in this section. The $t_{burn}$ of biomass feedstocks is also very low, thus making it practically unfeasible to burn biomass feedstocks in a coal based plant with minimal operational changes.

#### 18.3.2.2 Case II: Feeding Coal-Biomass Blends in an EC Based Plant

The second discussion entails a situation where coal and biomass feedstocks are fed into an EC based plant in 80:20 ratio (Row II). This scenario is similar to the one recently encountered by VT power plant where a series of operational issues were observed with the same situation. Even though the coal-biomass blends deliver near identical $t_{burn}$ in comparison to that of EC samples, the $t_{off}$ and $t_{ig}$ times for blend burn correspond to those of biomass feedstocks. Thus the blended fuel will off-gas and ignite at non-optimal locations, providing high flames and emissions due to high flame temperature. This kind of operation will lead to loss in plant efficiency and other maintenance/safety issues. Thus, changing the operating conditions of the coal-based reactors to suit those of blended fuels would be an expensive and challenging task.

#### 18.3.2.3 Case III: Feeding EC Briquettes in an EC Based Plant

In the third scenario, a situation where EC briquettes are fed into a power plant designed for EC-raw feedstock is discussed. It can be seen from Row III in Table 18-4, that the $t_{off}$ of the EC-briquette (20 s) is similar to that of EC-Raw feedstock (17 s). The $t_{ig}$ and $t_{burn}$ time for EC-briquette are 55% and 70% higher than those of EC-Raw sample. Even though these differences are high, the change in operating conditions of EC-Raw based power plant to suit the EC-briquette based operation should not be as difficult as in Case I and II. The changes that may be required to suit the new briquetted fuel may include lowering of conveyer belt speed or having higher heat fluxes to combust the briquette faster, among others.

However, as more and more coal based power plants are required to burn coal-biomass blends, the effect of biomass in a briquette must be understood in terms of changes in plant operation. This case will be important as in the previous discussion (Case II), the presence of biomass dominated the burning characteristic of a blend, thus rendering it unfeasible.

#### 18.3.2.4 Case IV: Feeding EC-Biomass Blend Briquettes in an EC Based Plant

In the fourth and final situation, a scenario is discussed where EC and biomass blend briquettes are fed into a power plant designed for EC-Raw feedstock. As observed from Row (IV) of Table 18-4, the $t_{off}$ decreases slightly (by 3-7 s) for blended briquettes in comparison to $t_{off}$ of EC-Raw sample. Also, the $t_{ig}$ for blended briquettes (21 and 33 s) is comparable to that of EC-Raw sample (45 s). Both of these parameters ($t_{off}$ and $t_{ig}$) for blended briquettes in Row (IV) are an improvement from the same parameters from raw blends in Row (II), and are much closer

to the parameters of EC-Raw sample. This analysis indicates that blended briquettes would require significantly lesser amount of operational changes in the EC based power plant, in comparison to if a raw coal-biomass blended fuel were used. Thus, the briquetting of biomass with a coal sample controls the ignitability properties of biomass and provides a better combustion/flammability behavior as well (Section 18.3.1).

In terms of $t_{burn}$ parameter, the burn time of a blended briquette (1059-1407 s) is higher than that for EC-Raw sample (935 s). However, the $t_{burn}$ of a blended briquette (1059-1407 s) in Row IV is also significantly lower than $t_{burn}$ of EC-only briquette (1610 s) in Row III. This shows that usage of a blended briquette may be preferred over an EC-only briquette to keep the burn time as close to EC-Raw as possible. Thus, blended EC-biomass briquettes (in 80:20 ratio) may provide easier operation of power plant in comparison to EC-only briquettes.

#### 18.3.2.5 Summary of Ignitability and Burn Duration Results

The main points from the discussion in this section includes: (1) Feeding biomass or coal-biomass mixtures in raw form may require highest amount of changes in coal-based plant operating conditions, (2) Feeding coal briquettes as a substitute fuel in a coal-based power plant will require less changes in the coal-based plant operating conditions. However, the high ignition delay and slow burn rate must be considered for such scenario. Also, the operation of coal-only briquettes will not earn carbon credits for not using renewable fuels. Finally, (3) Usage of coal-biomass blended briquettes will not only provide a scenario where least amount of changes would be required to operating conditions of a coal based power plant, but it was also improve the ignition delay and burn time in comparison to that of coal-only briquettes. Thus, the usage of coal-biomass blended briquettes not only improves the flammability and combustion performance of a coal-based power plant (Section 18.3.1), but it also requires lower amount of changes in the operating conditions of the same by controlling the ignitability properties of biomass fuels.

### 18.3.3 Emission Gas Profiles and Yields

In the previous sections, it was determined that the flammability, combustion performance, ignitability and burn duration of blended briquettes is better than those of raw blends. In this section, the emissions entailing different fuels and operating conditions are analyzed. Understanding the emission behavior of a fuel is very important in terms of its

feasibility to use it in coal-based power plants. Even if the fuel provides better combustion performance and thermal efficiency, if the emissions from the combustion of fuels are higher than the regulatory standards then such fuel is not suitable for use in reactors.

In the literature, the understanding of emission behavior from coal-biomass blends has primarily been conducted in terms of data from a TGA setup. Usually the DTG peaks from thermogravimetric data are correlated to peak data of certain emissions (Huang et al., 2011; Barneto et al., 2009; Sonobe & Worasuwannarak, 2008; Worasuwannarak et al., 2007; Radmanesh et al., 2006; Biagini, et al., 2002; Otero et al., 2002; Ndaji et al., 1999). Other literature studies have conducted blend emission analysis in order to determine additive evolved gas behavior of coal and biomass samples on co-pyrolysis or co-combustion (Di Nola et al., 2010; Park et al., 2010; Biagini et al., 2006). As discussed in previous sections, these analyses do not provide adequate data regarding briquette combustion in high heat flux environment. Some studies have characterized the emission data from fixed bed or other gasification setups (Branca et al., 2003; Spliethoff & Hein, 1998). However, these studies have not conducted work on emission comparison from coal-biomass blend briquettes and other briquetted fuels.

As mentioned in Section 18.1, one of the primary motivations for this study was to solve the coal-biomass co-combustion problems related to the VT power plant. In a recent operation at VT power plant, it was found that the $NO_x$ levels increased when a coal-biomass co-firing was performed. Hence, the current section primarily focuses on $NO_x$ peak data from coal-biomass co-firing. The reasons behind the difference in $NO_x$ behavior from different fuels will be evaluated in terms of heat release rate (HRR) of the sample. Then the analysis of other important emission gases, such as $CO_2$ and CO will also be conducted.

Figure 18-7 shows the $NO_x$ profile behavior as a function of time for different tests conducted in this study. The average room $NO_x$ level (10-20 ppb) was subtracted from the actual $NO_x$ data to present data in Figure 18-7. The Savitzky-Golay smoothing (Staggs, 2005) was applied on all cone calorimeter data collected in the experiments as a function of time ($NO_x$, CO, $CO_2$, HRR). The time, t =0, represents the instant when the sample was introduced to 50 $kW/m^2$ heat flux. Only the first 1100 s of data is showed in the below plot (and other plots in this section) in order to capture the main moments of $t_{ig}$ until $t_{burn}$ for most fuels.

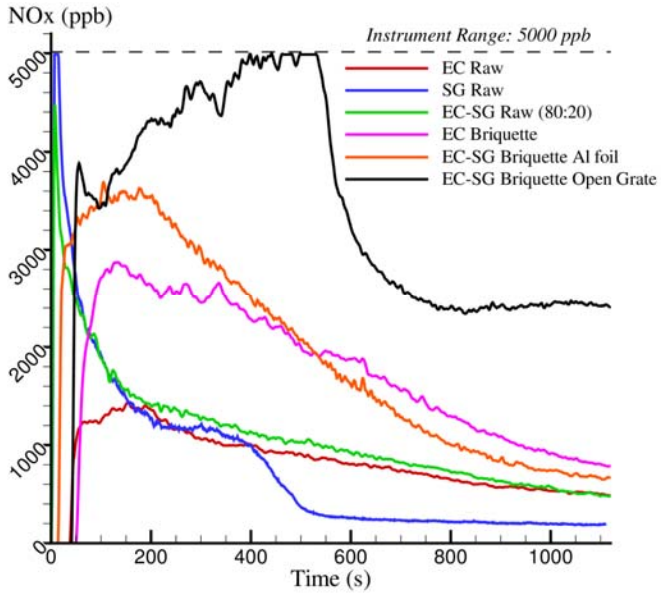



Figure 18-7. $NO_x$ profiles (in ppb) as a function of time for various experiments (All experiments conducted with Al foil except for last legend)

The major observations from Figure 18-7 are discussed below in the decreasing order of the plot legend.

1. The first curve shows the $NO_x$ profile from combusting EC-Raw sample in its powdered form (red curve). As shown, the EC-Raw sample burns at $t_{ig}$ of 45 s, thus providing increase in $NO_x$ level from zero ppb. The $NO_x$ levels gradually reach the peak levels of ~1400 ppb at ~150 s. Thereafter, the $NO_x$ levels gradually decrease with time until fuel burnout and subsequent char oxidation. This profile will be used as a representative of $NO_x$ data from a coal based power plant, and will be compared with data from other fuels.
2. The second curve (in blue) shows the $NO_x$ data for SG-Raw burning in same operating conditions. As observed, the SG sample burns instantaneously ($t_{ig}$ = 3 s), thus producing high flames and high sample temperature. The $NO_x$ levels suddenly rises up to more than the range of the $NO_x$ instrument (5000 ppb). These kind of peaks can cross the regulatory limits and lead to furnace shutdowns, thus showing the incompatibility of biomass fuels in coal based furnaces. After initial peak, the $NO_x$ levels immediately decreases until burn-out time ($t_{burn}$ = 466 s). During char oxidation phase, the $NO_x$ levels stays low and decreases gradually.
3. The third curve (in green) shows the $NO_x$ profile for EC and SG Raw blend combustion. As observed, and as previously described in Sections 18.3.1 and 18.3.2, the coal-biomass raw

blend burns in a manner similar to that of biomass rather than coal. Thus, the raw blend sample produces initial high flames and leads the peak $NO_x$ levels to as high as 4500 ppb. This high peak level of $NO_x$ simulates the similar problem encountered by the VT power plant while co-combusting coal and biomass raw blends. After the initial peak, the $NO_x$ levels gradually decrease in a manner similar to that of EC rather than biomass. This behavior of $NO_x$ pattern concurs with the $t_{ig}$ and $t_{burn}$ data for coal-biomass blend, where $t_{ig}$ was found to be same as that of biomass and $t_{burn}$ same as that of EC-Raw burn in Table 18-4.

4. The fourth curve (pink) shows the $NO_x$ profile for EC-briquette burnt in similar conditions. As seen from Figure 18-7, the $NO_x$ profile for EC-briquette combustion follows the similar profile as that of EC-Raw combustion. However, due to higher flames in EC-briquette (Section 18.3.1), the peak $NO_x$ levels (2800 ppb) produced are higher than that of EC-Raw sample. The decrease in $NO_x$ levels after peak is less gradual than that of EC-Raw sample combustion. Hence, it can be seen that usage of EC-briquettes would provide a similar combustion profile than that of EC-Raw sample which in turn will help the operational changes of the plant. The higher peak level of $NO_x$ from EC-briquette, if not higher than the regulatory standards, will require further changes in the operational procedure of a power plant.
5. The fifth curve (shown in orange) depicts the $NO_x$ profile for EC-SG briquette blend in same conditions. This curve follows the same profile as that of EC-Raw and EC-briquette combustion, and would require lesser changes in the operating conditions of a power plant. Although, the $NO_x$ peak level for blend briquette combustion is found to be higher than that of EC-Raw sample combustion, the peak levels for the blend briquette combustion were also found to be much lower than peak levels from raw blend combustion (green curve). Thus, the present study favors the usage of blended briquettes in comparison to that of raw blends for lower peak $NO_x$ emissions.
6. The sixth and the last curve (black) represents the blended briquette combustion in Open Grate experiments where higher amount of air (and hence $N_2$) was available for fuel combustion. This is the only case in Figure 18-7 that depicts profile for Open Grate combustion as the rest of the five tests were conducted with Al Foil, where limited air is available during fuel combustion. As shown for this case, the $NO_x$ levels at the initial ignition of the fuel were higher than that of blended briquette burning with Al foil (5th case, orange).

The $NO_x$ levels then gradually increase to more than the range of $NO_x$ instrument. The $NO_x$ levels remain more than 5000 ppb for significant time (~150 s) during combustion before the sample burns out and char oxidation takes place. This experiment shows that in order to obtain lower peak level of $NO_x$ from coal-biomass briquette combustion, the amount of air and hence the amount of $N_2$ available should be reduced. In an existing coal-based power plant like that at Virginia Tech, this operating condition can be controlled by lowering the air blower speed of fans located at the bottom of the conveyer belt.

The last analysis shows that $NO_x$ generation during coal-biomass fuel combustion is dependent of $N_2$ level (in air) and not particularly on the N content of the fuel. Figure 18-8 shows the HRR data for all the test cases shown in Figure 18-7. As observed, the profiles of HRR and $NO_x$ data are similar in nature. This observation depicts that the $NO_x$ levels are controlled by the Zeldovich (or thermal) mechanism, where the higher flame temperature in presence of $N_2$ produces higher $NO_x$ during hydrocarbon combustion (Turns, 1996).

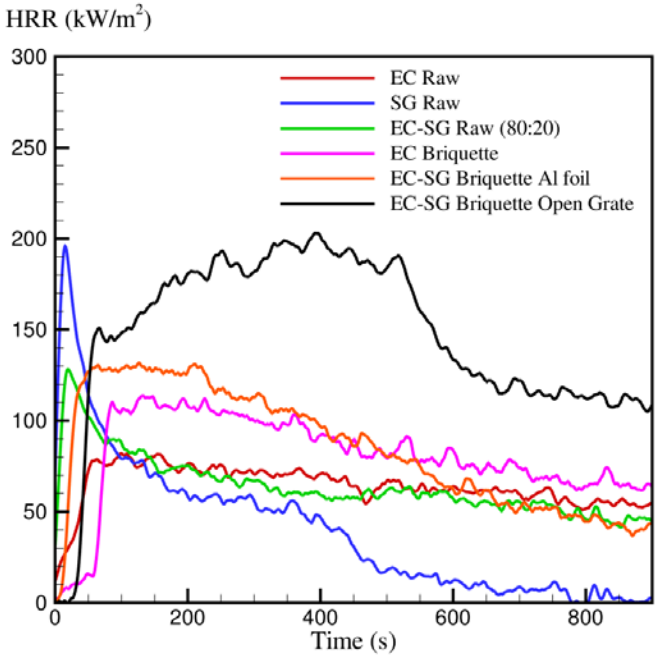



Figure 18-8. HRR profiles (in kW/m$^2$) as a function of time for various experiments (All experiments conducted with Al foil except for last legend)

Figure 18-8 also provides important data regarding fuel combustion. It can be seen that as combustion of EC-Raw (red curve) provides a uniform and high HRR with time, the biomass combustion (blue curve) provides a flash of heat at ignition and substantially lower HRR

afterwards. The EC-briquette combustion (pink curve) provides higher HRR than that of EC-Raw combustion (red curve), which indicates better combustion performance from coal briquettes in comparison to raw coal. The HRR of blended briquettes (orange curve) was found much higher and uniform along time than the HRR of raw blends (green curve). The presence of more air in Open grate system (black curve) provided more HRR than that in Al foil for blended briquettes (pink curve).

Figure 18-9 shows the $CO_2$ profiles for all the test cases depicted in Figure 18-7. As observed, the $CO_2$ profiles for all the tests are similar to those of $NO_x$ and HRR profiles shown in Figure 18-8 and Figure 18-9, respectively. Hence, the discussion for the $CO_2$ profiles is also similar in nature. However, for gases like CO and $CO_2$ the power plants are more concerned about the total yields rather than the peak values. The yield discussion for these gases will be conducted later in this section.

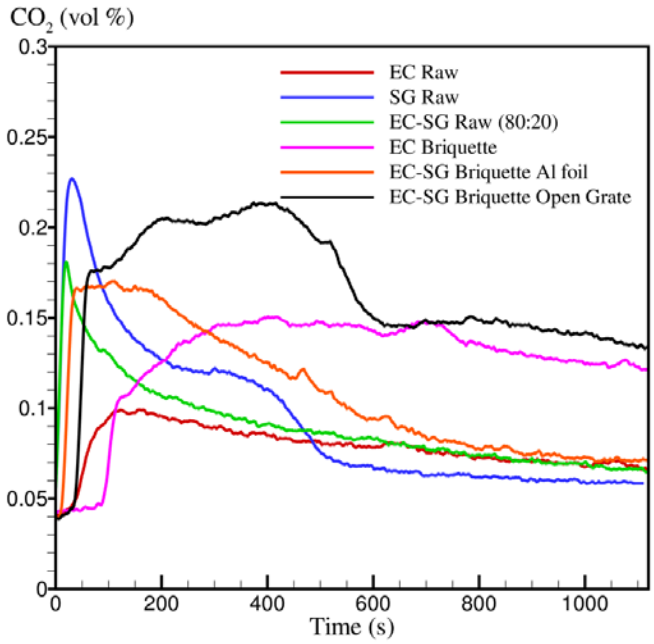



Figure 18-9. $CO_2$ profiles (in volume %) as a function of time for various experiments (All experiments conducted with Al foil except for last legend)

Figure 18-10 shows the CO profiles for all the test cases depicted in Figure 18-7. The CO profiles are different than those of $NO_x$, HRR and $CO_2$. This is because $CO_2$ formation is predominant during the flaming combustion and CO formation is dominant during the non-flaming char oxidation after sample burn out (smoldering). Thus in all test cases, the CO profiles have been seen rising as the combustion progresses. As seen from CO profile for biomass

combustion (blue) which shows full cycle of fuel burn, the CO levels increase with time until the sample burns ($t_{burn}$ = 466 s). During char smoldering, the CO levels decrease gradually or remain relatively constant (as in case for coal based fuels) until the end of tests. For some coal based fuel CO profile (all except pink curve), an initial spike in the CO formation was observed with an instantaneous decrease, which may indicate a different mechanism of CO generation for ignition instant when high flames were present.

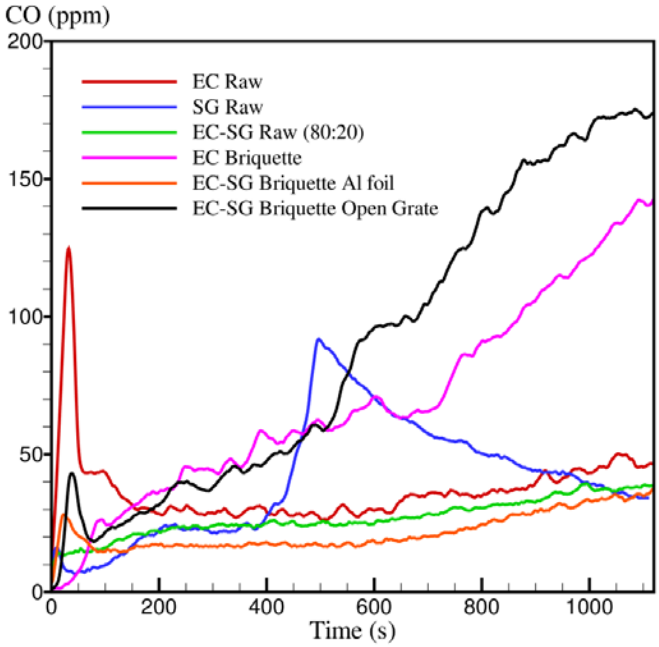



Figure 18-10. CO profiles (in ppm) as a function of time for various experiments (All experiments conducted with Al foil except for last legend)

The yields for $NO_x$, $CO_2$ and CO gases were calculated as per the Equation 18-1:

$$Yield = \frac{\int X_{gas} \times \dot{m}_e}{\Delta m_{fuel}} \qquad \text{(Eq. 18-1)}$$

where *Yield* represents a unitless yield for emission gas ($NO_x$, $CO_2$ or CO), $X_{gas}$ represents the mass fraction of the gas in exhaust stream of cone calorimeter, $\dot{m}_e$ is the mass flow rate in the exhaust stream, and $\Delta m_{fuel}$ is the net mass loss of the fuel during the combustion process. The yield data for gases ($NO_x$, $CO_2$ and CO) is mentioned in Table 18-5 for the tests discussed in Figure 18-7.

Looking at the yield values for $NO_x$ test, it was found that the EC-briquette provides higher $NO_x$ yield than yield form the EC-Raw combustion, and similarly blend Briquette

provides higher $NO_x$ yield than raw blend. Therefore, although the peak $NO_x$ values are lower for briquette combustion, their $NO_x$ yields are higher than combustion of raw fuel. However, as discussed previously, the peak values of $NO_x$ may be more significant parameter for a power plant rather than the $NO_x$ yield values. The coal-biomass blending reduced the $NO_x$ yields, both in comparison to EC-Raw and EC-briquette cases. It was also found that limiting the air (and hence $N_2$) during combustion significantly reduces the $NO_x$ yield of the briquetted fuel.

Table 18-5. Yield data for $NO_x$, $CO_2$ and CO gases for various experiments

| **Fuel and process** | **Yield** | | |
|---|---|---|---|
| | **$NO_x$ (*0.001)** | **$CO_2$ (*1.0)** | **CO (*0.1)** |
| EC-Raw (Al foil) | 4.57 | 7.60 | 3.64 |
| SG-Raw (Al foil) | 2.21[+] | 2.65 | 7.00 |
| EC-SG Raw in 80:20 ratio (Al foil) | 3.83 | 5.88 | 2.67 |
| EC-Briquette (Al foil) | 6.49 | 6.99 | 2.32 |
| EC-SG Briquette (Al foil) | 5.39 | 5.47 | 1.68 |
| EC-SG Briquette (Open grate experiment) | 8.04[+] | 5.22 | 3.04 |

[+] NOx levels crossed the range of the instrument, hence underestimated values

The data on $CO_2$ yield reveals that $CO_2$ yields are lower for biomass combustion that coal combustion. Hence, combustion of coal and biomass blend in raw form produces lower $CO_2$ yield than the combustion of EC-Raw. Similarly, combustion of blended briquettes produced lower $CO_2$ yield than combustion of EC-briquette. It is also observed that the $CO_2$ yield from combustion of briquetted fuel is lower than that of raw fuel. Thus, the combustion of briquetted fuel may be favored for reducing the greenhouse gas emissions.

The data on CO yield reveals that CO yields are higher for biomass combustion than coal combustion. However, the CO yields for blended fuel combustion (both in raw and briquetted forms) was found to be lower than the CO yield of EC-Raw combustion. The CO yields for briquetted fuels were found to be lower than the CO yields for similar constituent fuels. It was also observed that limiting the air supply during combustion reduced the CO yield for blended briquetted fuel.

## 18.4 Summary and Conclusions

A combustion setup was develop to understand the effect of fuel briquetting on the flammability, ignitability, combustion performance, burn duration and emissions of the fuel.

Coal, biomass feedstock and blends were used in the study. Coal briquettes and coal-biomass blend briquettes were also tested. The fuels were tested in different combustion environments to study its effects on fuel combustion behavior.

The fuel flammability observations were made from flame behavior. The combustion performance of the fuel was evaluated in terms of final mass yield and effective heat of combustion, $\Delta h_{com}$. It was found that the flammability and combustion performance of blended briquettes were better than those of raw blended fuels. It was further noticed that reducing the size of briquettes may help improve the flammability and combustion performance of tested briquettes.

The fuel off-gassing time, ignitability and burn duration were measured in these tests. It was found that the fuel off-gassing time, fuel ignition time and fuel burn duration for blended coal-biomass briquettes were close to that of coal. It was further concluded that for an existing coal-based power plant, usage of blended briquettes may require least amount of changes in its operation conditions. In turn, usage of just raw blends of coal and biomass will require considerable operational challenges in a coal-based power plant.

In terms of peak $NO_x$ emissions, it was concluded that the usage of blended briquettes will provide lower $NO_x$ peak values than raw blends of coal and biomass fuels. The $CO_2$ and CO yields from blended briquette combustion were found to be lower than that from raw coal and biomass blend combustion. Additionally, the heat release rate profile for blended briquette was higher and more uniform than the heat release rate profile for coal-biomass raw blends. These profiles for blended briquettes were also found to be more similar to that of coal and coal briquette heat release rate profiles.

Together with all these factors, it was determined that usage of coal-biomass blended briquettes will not only provide a scenario where least amount of changes would be required to operating conditions of a coal based power plant, but it will also improve the combustion behavior of fuels in terms of flammability, combustion performance, ignitability, burn duration and emissions from constituent raw fuels.

# SECTION IV

# FEASIBILITY ASSESSMENT AND CONCLUSIONS

# Chapter 19

# Feasibility Assessment

## 19.1 Abstract

A study was conducted to evaluate the feasibility to design and construction a coal-biomass production facility. A processing circuit simulator and a project cost simulator were developed to estimate the capital and operating costs associated with the facility. Simulations were conducted to evaluate the production of briquettes using a premium blend coal/wood related biomass feedstock and a low rank coal/agriculture related biomass feedstock in the eastern and western region of the U.S., respectively. Detailed flowsheet simulations and costs analyses were developed for 10%, 20% and 30% blends of biomass in each region. The feasibility analysis indicated that a 100 ton per hour (dry) briquetting facility could be developed for $5.9 million. The operating cost for the facility was estimated to be $7-10 per ton in the eastern region and $30-40 per ton in the western region.

## 19.2 Circuit Simulation

In order to conduct the feasibility for designing and operating a facility to produce coal-biomass briquettes for various feedstocks, a flowsheet simulator was developed to evaluate a conceptual processing circuit design and processing strategies. The simulation program was developed using Microsoft Excel in order to take advantage of the optimization routines incorporated within this software.

Simulations were conducted to evaluate the production of briquettes using a premium blend coal and a low rank coal. The Emerald coal was selected as the premium coal and mixed with saw dust. The Eagle Butte coal was selected as the low rank coal and mixed with corn stover. The mixtures were selected to represent the optimal blends identified by the bench-scale

testing, and to geographically pair the Emerald coal in the East with the wood/forest industry and pair the Eagle Butte coal with the agriculture industry in the West.

## 19.3 Conceptual Circuit Design

A conceptual processing circuit design (flowsheet) was developed to provide a mass and energy balance for the production facility. The circuit design was selected to process either the premium or the low rank feedstock. The circuit (flowsheet) simulation was then used to evaluate the equipment loading and energy demands for each type of feedstock.

The flowsheet and conceptual design for the facility are based on the following state-of-the-art processing technologies, accepted industry practice parameters, processing facility requirements:

- A briquette production capacity of 100 ton per hour (tph, dry) of combined coal/biomass feedstock.
- The coal feed is delivered by rail and the biomass feed is delivered by truck, considering that the facility should located within or near the biomass supply region. This arrangement reduces transportation costs by moving only the high-energy density material (coal) long distances.
- Storage and surge hoppers, automated feeding equipment and conveyors are provided to move the feed stocks to the processing equipment.
- Crushing and grinding equipment is provided to reduce the coal to the optimal top particle size.
- Shredding, grinding and drying equipment is provided to reduce the biomass to the biomass to the optimal top particle size and moisture content.
- The crushed coal and shredded/dried biomass feeds will be automatically blended in the proper ratio and mixed in a pug mill or other mixing/blending unit.
- The briquetting machine has a rated production capacity of 150 tph (as-received) of “raw” briquettes (required for the low rank, high moisture coal).
- The “raw” briquettes will report to a vibrating screen to remove edge remnants and small pieces. The undersize particles from the screen will be recycled back to the mixing unit.

The additional briquetting machine capacity allows for 2-5% of the "raw" briquettes to be recycled back to the pug mill.

- All the processing equipment will be selected from commercial-scale "off-the-shelf" options.
- The "finished" briquettes will report to a storage unit for either rail or truck loading.
- The process control and instrumentation system will provide a fully automated facility which maximizes processing efficiency and minimizes worker involvement.

The conceptual flowsheet simulations for the various briquette production options provided operating data for the feasibility analysis. The capacity of 100 tph (dry basis) of "finished" briquettes was established to provide a facility that would be adequate as a stand-alone operation and to be evaluated as a module unit for higher capacity demands.

## 19.4 Processing Simulations

### 19.4.1 Coal and Biomass Feedstock Properties

The coal feedstocks selected for the simulations were from the Emerald Preparation Plant in southwestern Pennsylvania to represent the premium (high rank bituminous) thermal coals and from the Eagle Butte Mine in southern Wyoming to represent the low rank (subbituminous) thermal coals. The typical properties for the feed coals and biomass used as the input parameters for in the flowsheet simulation routines are summarized in Table 19-1. As stated previously, two sets of simulations were conducted. The first set was performed using a likely eastern U.S. scenario involving the high-rank eastern Emerald coal together with saw dust (or other wood products) as the source of biomass. The three different levels of wood biomass addition were evaluated in simulation runs (i.e., 30%, 20% and 10% biomass for simulation runs A1, A2 and A3, respectively). The second set of simulation runs were conducted of a likely western U.S. scenario involving the low-rank Eagle Butte coal together with three different additions of corn stover biomass (i.e., 30%, 20% and 10% agricultural biomass for simulation runs B1, B2 and B3, respectively).

### 19.4.2 Briquetting Process Flowsheet Simulations

The simplified flowsheet simulations were developed to provide preliminary data to conduct a feasibility study for a commercial-scale briquetting facility. Simulations were conducted for the

two regions with three blending options for each region. The simulations conducted for the eastern region, represented by the Emerald coal and sawdust (EM-SD) feedstock, are shown in Figures 19-1, 19-2 and 19-3 for feedstock blends with 30%, 20% and 10% biomass, respectively.

The flowsheet simulations conducted for the western region, represent by the Eagle Butte coal and corn stover (EB-CS) feedstock, are shown in Figures 19-4, 19-5 and 19-6 for feedstock blends with 30%, 20% and 10% biomass, respectively. The simulations utilize the feedstock properties and operating conditions provided in Table 19-1.

## 19.5 Economic Feasibility

An economic analysis were conducted to evaluate the viability of the proposed circuit design. For the purpose of this study, the briquette production rate was set at 100 tph, dry product. The plant was assumed to operate for three 8-hour shifts per day for 250 days per year with an operating availability of 90%, i.e., 5400 hrs/yr. The facility was assumed to have a life span of 20 years.

The major equipment items for the facility include coal and biomass feedstock handling and storage systems ($530,000), a raw coal crusher ($400,000), fine coal pulverizer ($400,000), biomass shredding and drying systems (for the biomass material only to minimize abrasion of the equipment) ($200,000), weigh belt feeders ($100,000), binding and coating reagent systems ($35,000), pug mill or mixing/blending equipment ($100,000), briquetting machine ($300,000), briquette dressing screen ($50,000 each), transfer and recycle conveyors ($75,000), briquette storage and train/truck loadout ($150,000), miscellaneous chutes and piping ($50,000), process control system and instrumentation ($85,000) and building with heat/ventilation ($150,000). The total capital cost of the plant equipment was calculated to be $2,575,000. The total installed cost was estimated by doubling the total equipment cost. This rule-of-thumb estimation procedure is often used by local fabricators within the coalfields. Other costs considered in the capital estimation included a 10% fee for engineering/permitting and an overhead rate of 20%. The estimated total installed cost is $5,922,500.

Table 19-1. Summary of feedstock properties and operating parameters used for the flowsheet simulations.

| | A1 | A2 | A3 | B1 | B2 | B3 |
|---|---|---|---|---|---|---|
| FEED COAL | | | | | | |
| Type | Emerald | Emerald | Emerald | Eagle Butte | Eagle Butte | Eagle Butte |
| Rate (t/hr Dry) | 70 | 80 | 90 | 70 | 80 | 90 |
| Moisture (% AR) | 8 | 8 | 8 | 29 | 29 | 29 |
| Ash (% Dry) | 9.5 | 9.5 | 9.5 | 8 | 8 | 8 |
| Heat (kcal/kg MAF) | 8490 | 8490 | 8490 | 6935 | 6935 | 6935 |
| Topsize (mm) | 50 | 50 | 50 | 50 | 50 | 50 |
| FEED BIOMASS | | | | | | |
| Type | Sawdust | Sawdust | Sawdust | Corn Stover | Corn Stover | Corn Stover |
| Rate (t/hr Dry) | 30 | 20 | 10 | 30 | 20 | 10 |
| Moisture (% AR) | 24 | 24 | 24 | 13 | 13 | 13 |
| Ash (% DRY) | 1 | 1 | 1 | 5 | 5 | 5 |
| Heat (kcal/kg MAF) | 4780 | 4780 | 4780 | 4725 | 4725 | 4725 |
| Topsize (mm) | 50 | 50 | 50 | 50 | 50 | 50 |
| BINDER | | | | | | |
| Addition (%) | 0 | 0 | 0 | 3 | 3 | 3 |
| Moisture (% AR) | 0 | 0 | 0 | 12 | 12 | 12 |
| Ash (% AR) | 0 | 0 | 0 | 0.3 | 0.3 | 0.3 |
| Heat (kcal/kg AR) | 0 | 0 | 0 | 4180 | 4180 | 4180 |
| COATING | | | | | | |
| Addition (%) | 0.5 | 0.5 | 0.5 | 0 | 0 | 0 |
| Moisture (% AR) | 12 | 12 | 12 | 0 | 0 | 0 |
| Ash (% AR) | 4.8 | 4.8 | 4.8 | 0 | 0 | 0 |
| Heat (kcal/kg AR) | 3825 | 3825 | 3825 | 0 | 0 | 0 |
| SIZING RATIO | | | | | | |
| Shredder | 40 | 40 | 40 | 40 | 40 | 40 |
| Dryer | 1.05 | 1.05 | 1.05 | 1.05 | 1.05 | 1.05 |
| Crusher | 6 | 6 | 6 | 6 | 6 | 6 |
| Pulverizer | 8 | 8 | 8 | 8 | 8 | 8 |
| SCREEN U/S SPLIT | | | | | | |
| Biomass (%) | 3.5 | 3.5 | 3.5 | 3.5 | 3.5 | 3.5 |
| Coal (%) | 3.5 | 3.5 | 3.5 | 3.5 | 3.5 | 3.5 |
| Binder (%) | 3.5 | 3.5 | 3.5 | 3.5 | 3.5 | 3.5 |
| MOISTURE DROP (%) | | | | | | |
| Shredder | 1 | 1 | 1 | 1 | 1 | 1 |
| Dryer | 70 | 70 | 70 | 70 | 70 | 70 |
| Crusher | 1 | 1 | 1 | 1 | 1 | 1 |
| Pulverizer | 2 | 2 | 2 | 2 | 2 | 2 |
| Briquetter | 6 | 6 | 6 | 6 | 6 | 6 |
| SIZE DATA | | | | | | |
| Briquette Size (mm) | 50 | 50 | 50 | 50 | 50 | 50 |
| Screen Size (mm) | 5 | 5 | 5 | 5 | 5 | 5 |
| Screen Degradation (%) | 1 | 1 | 1 | 1 | 1 | 1 |

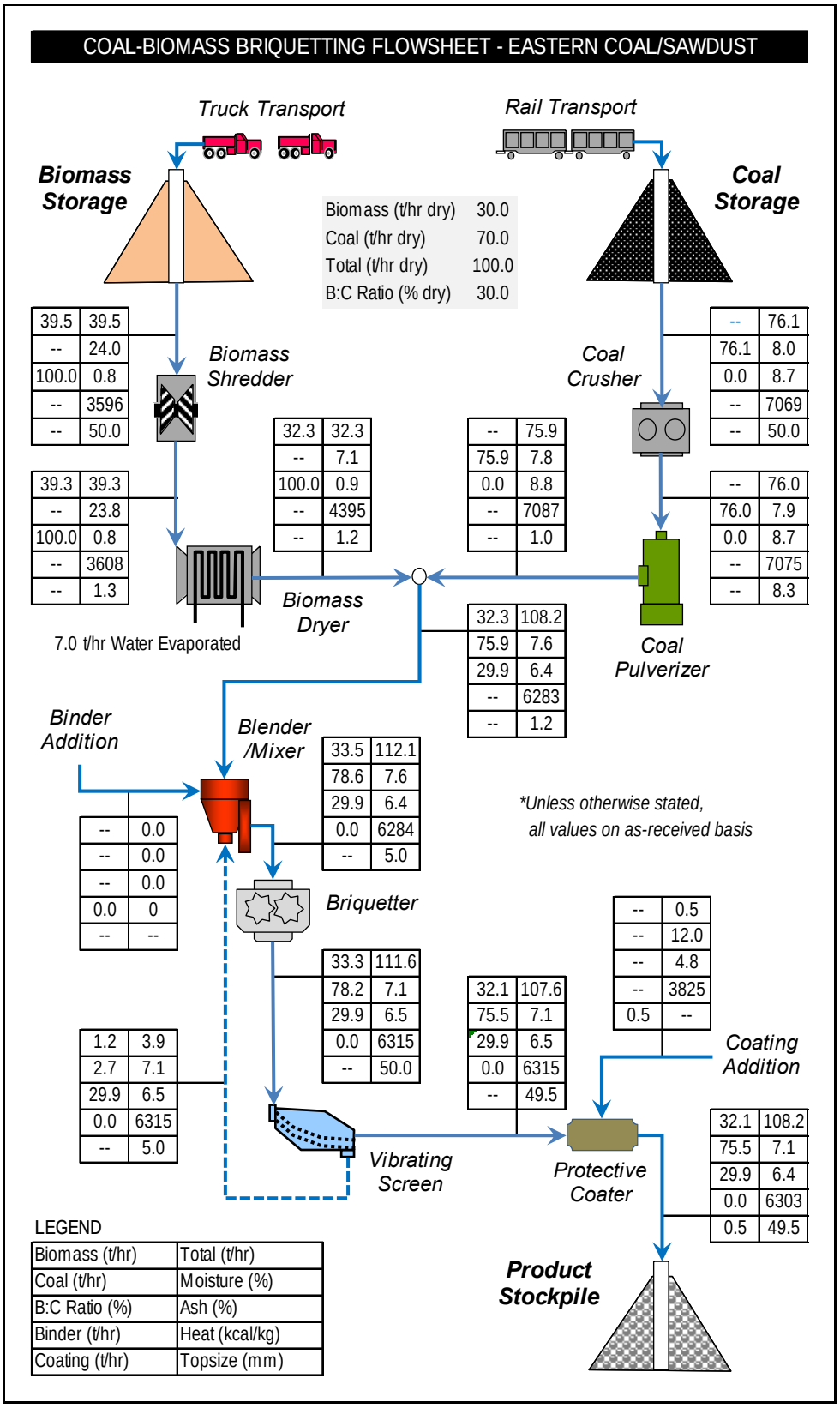



Figure 19-1. Flowsheet simulation for the EM-SD feedstock with 30% biomass.

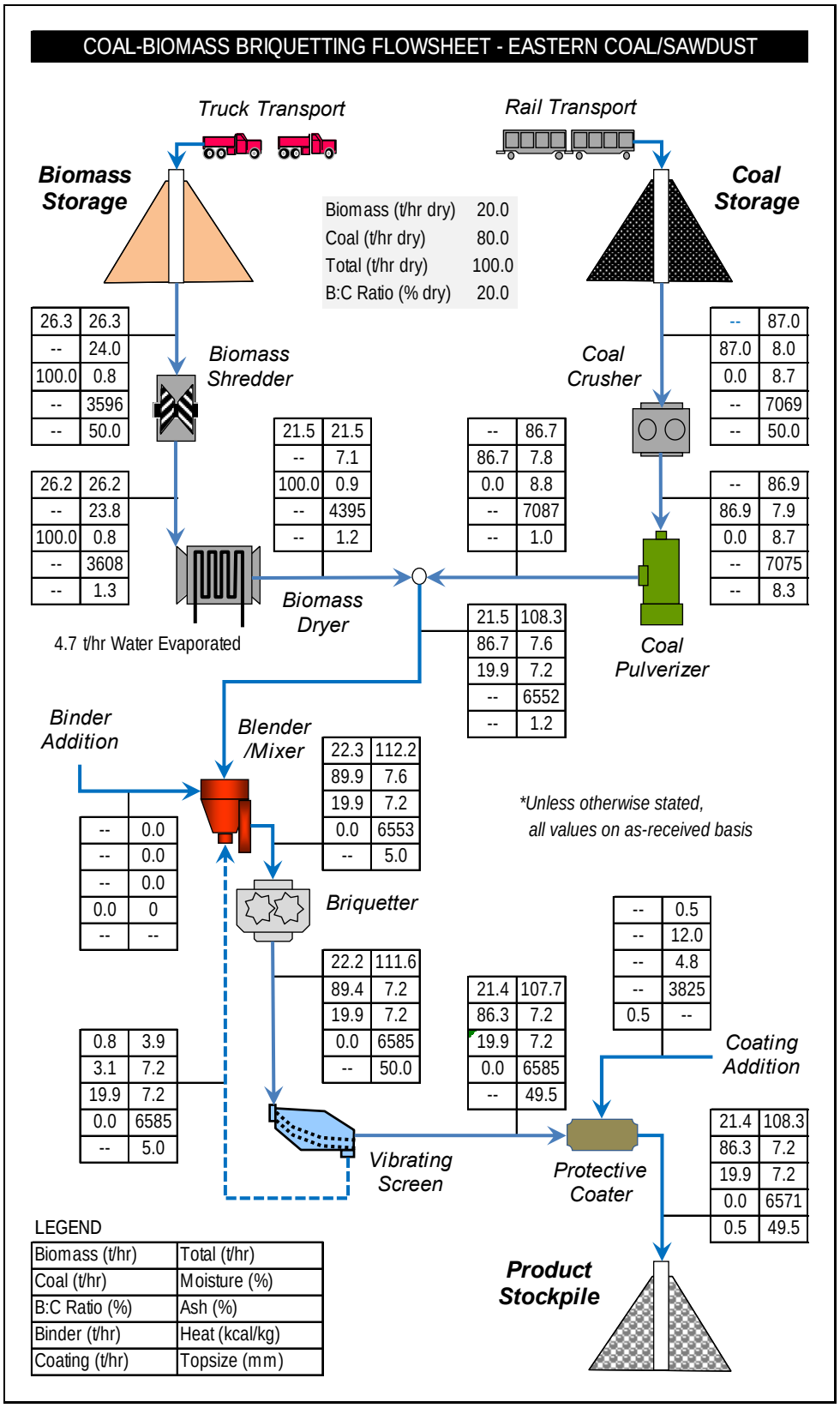



Figure 19-2. Flowsheet simulation for the EM-SD feedstock with 20% biomass.

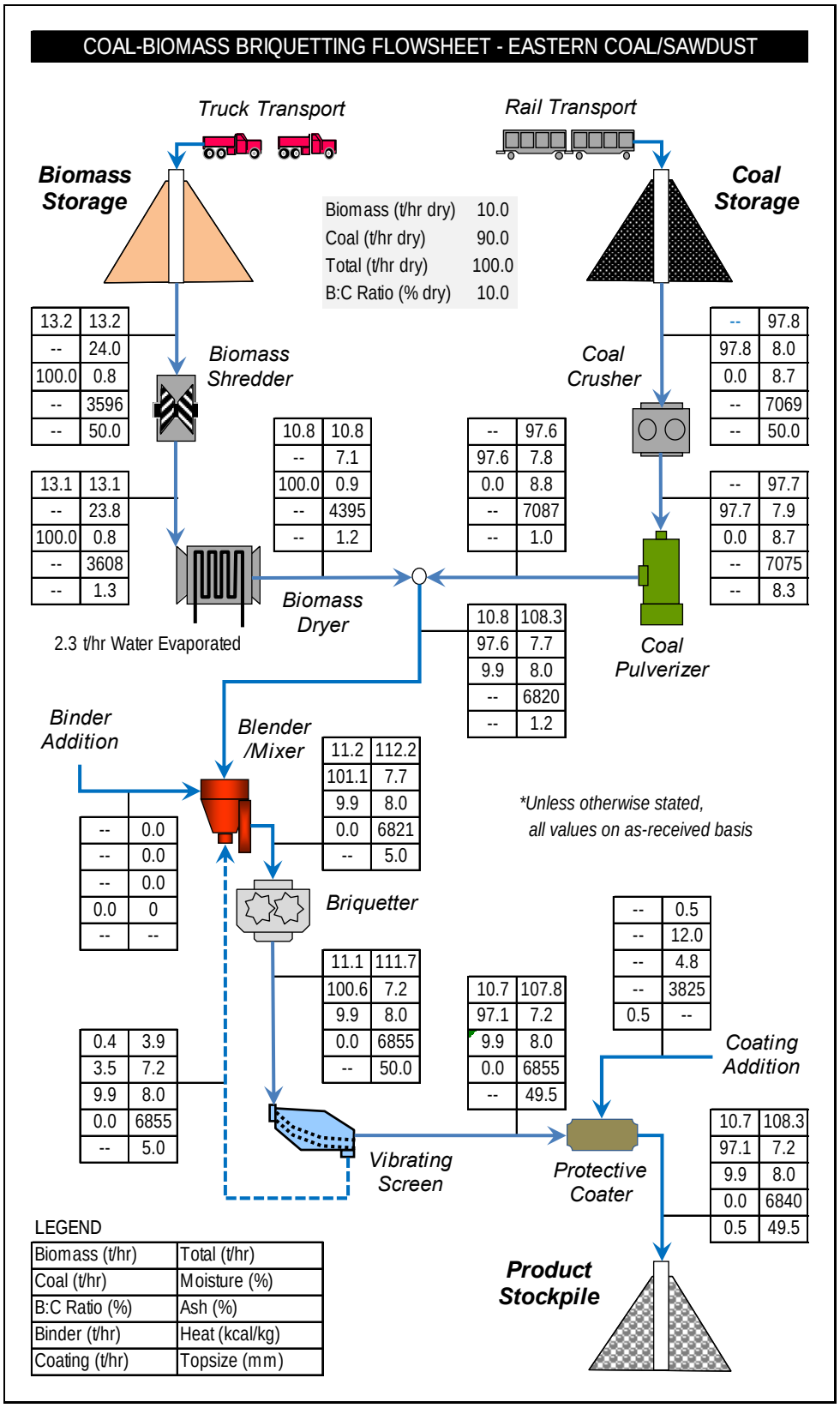



Figure 19-3. Flowhseet simulation for the EM-SD feedstock with 10% biomass.

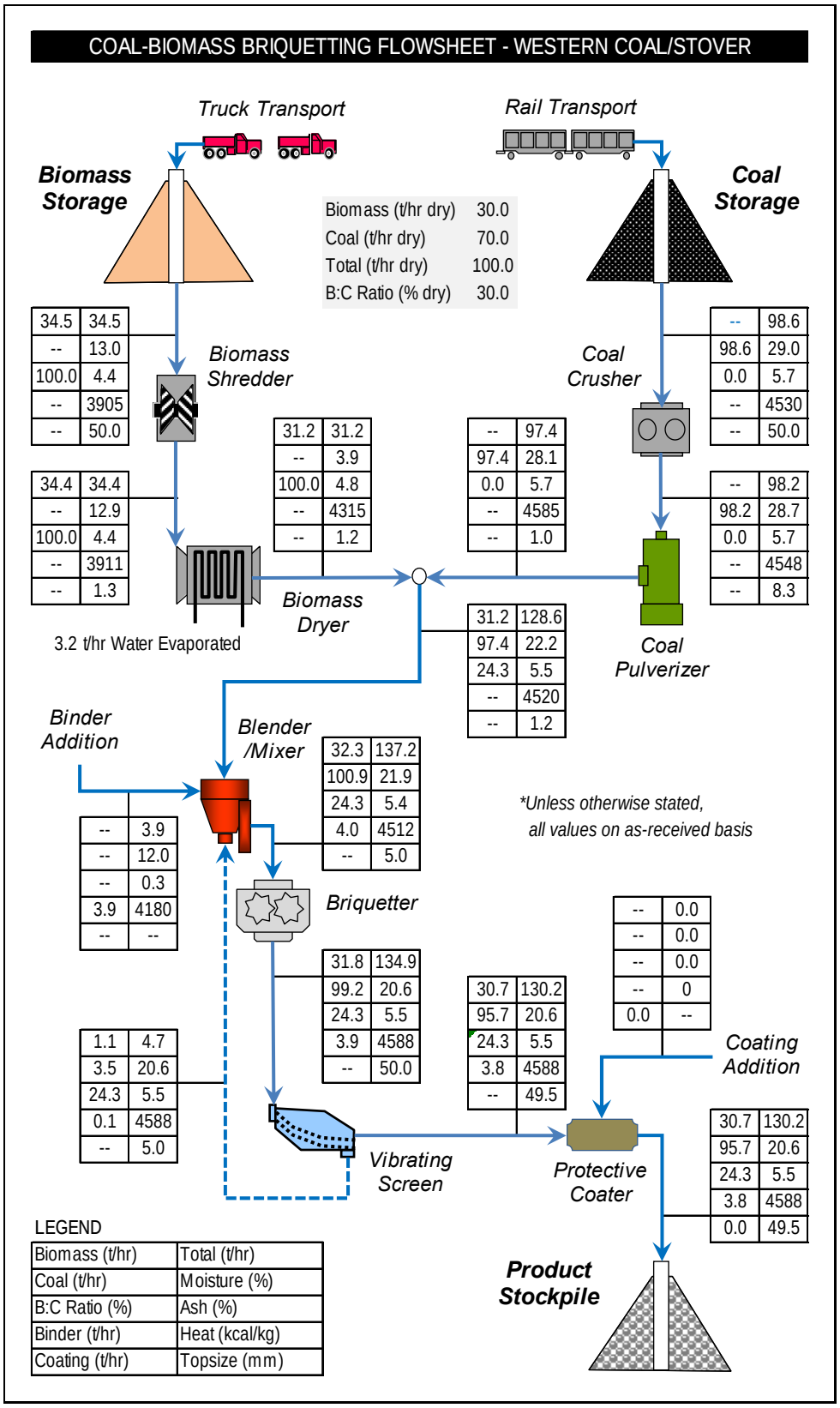



Figure 19-4. Flowsheet simulation for the EB-CS feedstock with 30% biomass.

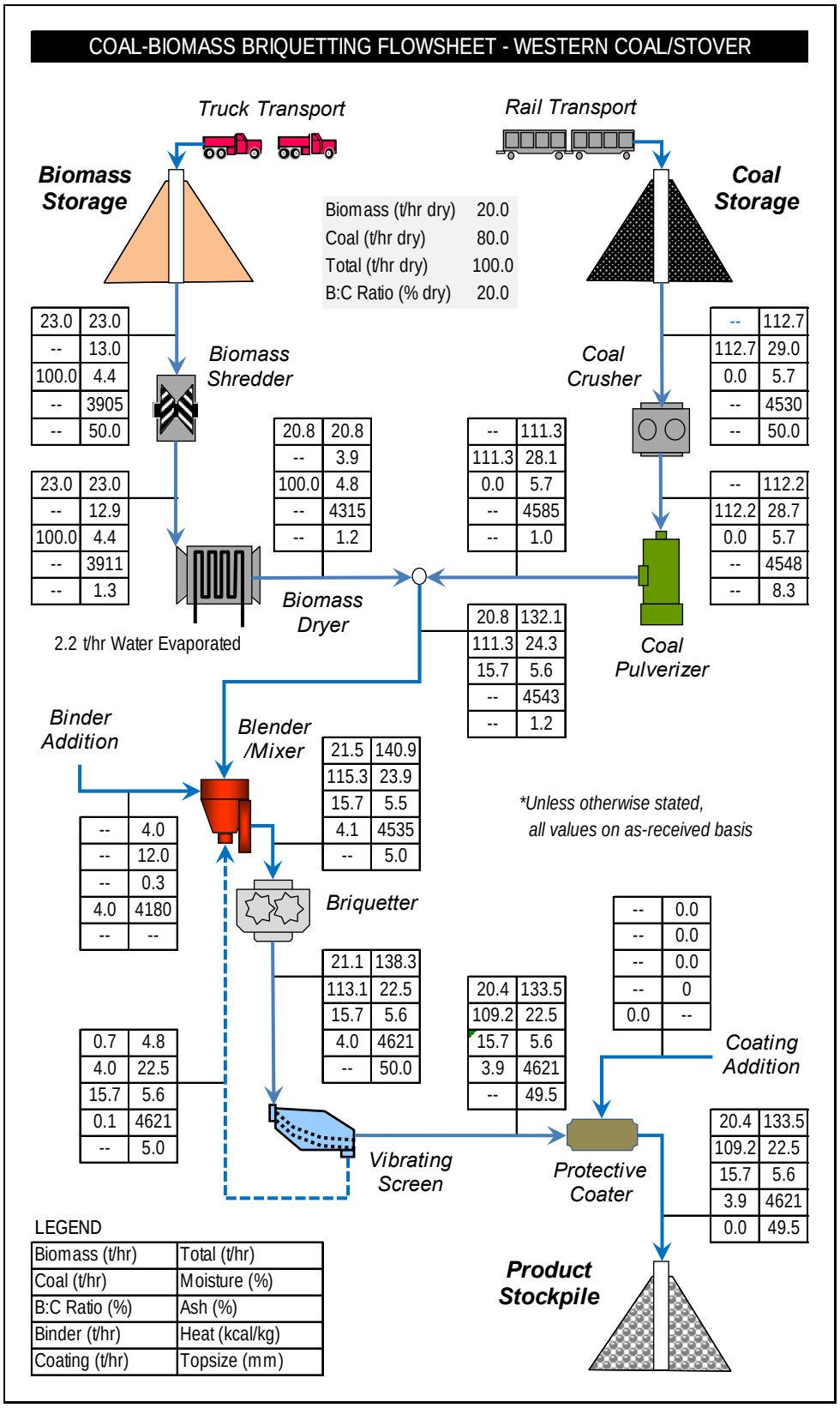



Figure 19-5. Flowsheet simulation for the EB-CS feedstock with 20% biomass.

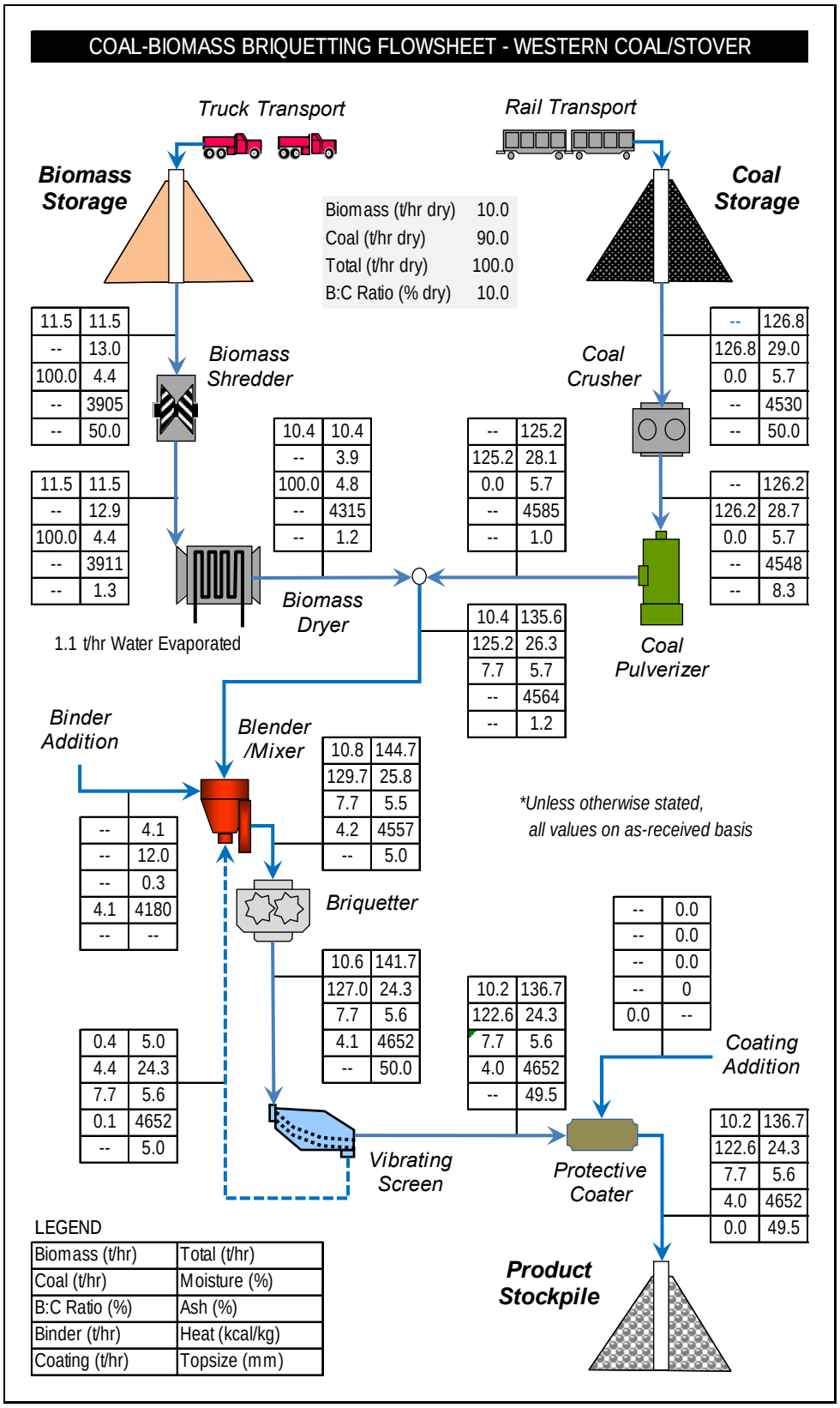



Figure 19-6. Flowsheet simulation for the EB-CS feedstock with 10% biomass.

Annual operating costs were estimated for power consumption, equipment maintenance, personnel and miscellaneous consumables (i.e., reagents, lubricants, etc.). Electrical power consumption was estimated for all primary units and ancillary operations. The largest power consumers were the coal crusher (60 kW), coal pulverizer (120 kW) and briquetting machine (150 kW). For primary unit operations, a power load factor of 80% was used to estimate actual power requirements, while a power factor of 15% was used for heat/light and small reagent pumps. Power costs were estimated at an industrial rate of $0.04/kW-hr. The cost to operate the biomass dryer is estimated to be $1.00/ton of water evaporated. The major consumable items included in the operating costs were the binding and coating reagents at $1.00/kg and $1.00/kg, respectively. An additional $0.01/ton of product was also allocated to account for oils and lubricants. Annual equipment maintenance costs were estimated as 10% of the total capital cost of the proposed circuitry.

The plant staff was assumed to consist of a one full-time shift foreman ($80,000/yr), plant operator ($60,000/yr) and mechanic/electrician ($60,000/yr) for each working shift. Personnel benefits were estimated as 50% of the base salary. Total salaries/wages were estimated to be $900,000 per year.

## 19.6 Feasibility Study Results

The results of the six simulations are summarized in Table 19-2. . Three different levels of the Emerald coal with sawdust biomass addition for the eastern U.S. were evaluated in the simulation runs (i.e., 30%, 20% and 10% biomass for simulation runs A1, A2 and A3, respectively). The second set of simulation runs were conducted of a likely western U.S. scenario involving the low-rank Eagle Butte coal together with three different additions of corn stover biomass (i.e., 30%, 20% and 10% biomass for simulation runs B1, B2 and B3, respectively). The difference in the as-received production rates between the regions (eastern, 108 tph versus western, 130-137 tph) are due to the high (inherent) moisture of the low rank coal.

Table 19-2. Results of the flowsheet simulations for the eastern region (Emerald/sawdust, A1-A3) and the western region (Eagle Butte/corn stover, B1-B3).

| | A1 | A2 | A3 | B1 | B2 | B3 |
|---|---|---|---|---|---|---|
| PRODUCT (AS-RECEIVED) | | | | | | |
| Rate (t/hr) | 108.2 | 108.3 | 108.3 | 130.2 | 133.5 | 136.7 |
| Moisture (%) | 7.1 | 7.2 | 7.2 | 20.6 | 22.5 | 24.3 |
| Ash (%) | 6.4 | 7.2 | 8.0 | 5.5 | 5.6 | 5.6 |
| Heat (kcal/kg) | 6303 | 6571 | 6840 | 4588 | 4621 | 4652 |
| PRODUCT (DRY) | | | | | | |
| Rate (t/hr) | 100.5 | 100.5 | 100.5 | 103.4 | 103.5 | 103.6 |
| Moisture (%) | 0.0 | 0.0 | 0.0 | 0.0 | 0.0 | 0.0 |
| Ash (%) | 6.9 | 7.8 | 8.6 | 6.9 | 7.2 | 7.4 |
| Heat (kcal/kg) | 6737 | 7084 | 7435 | 4853 | 4892 | 4930 |
| REAGENT (AS-RECEIVED) | | | | | | |
| Binder (t/hr) | 0.0 | 0.0 | 0.0 | 3.9 | 4.0 | 4.1 |
| Coating (t/hr) | 0.5 | 0.5 | 0.5 | 0.0 | 0.0 | 0.0 |
| REAGENT (DRY) | | | | | | |
| Binder (t/hr) | 0.0 | 0.0 | 0.0 | 3.4 | 3.5 | 3.6 |
| Coating (t/hr) | 0.5 | 0.5 | 0.5 | 0.0 | 0.0 | 0.0 |

The results of the feasibility analysis for the EM-SD facility are summarized in Table 19-3. The estimated capital cost for the facility is $5.9 million, including engineering, equipment, installation, and overhead. The life of the facility is set at 20 years. The annual operating cost is estimated at $5.3 million, including the fixed costs associated with capital cost of the facility. Based on the estimated costs, and a briquette production of 100 tph dry or 108 tph as-received, the operating cost for the EM-SD briquetting facility is estimated to be ~$8.45 per ton on a dry product basis and ~$7.80 per ton on an as-received basis for the three biomass blends.

The results of the feasibility analysis for the EB-CS operation are summarized in Table 19-4. The estimated capital cost for the facility is $5.9 million, including engineering, equipment, installation, and overhead. The life of the facility is set at 20 years. The annual operating cost is estimated at $22.8 million, including the fixed costs associated with capital cost of the facility. Based on the estimated costs, and a briquette production of 100 tph dry or 130-137 tph as-received, the cost for the EB-CS briquetting operation is $42-43 per ton on a dry product basis and $31-33 per ton on an as-received basis for the three biomass blends. It may be possible to reduce the operating cost by incorporating a drying unit for the low rank coal or by routing the coal-biomass mixture through a dryer.

Table 19-3. Feasibility analysis for the eastern region (EM-SD) facility.

**PRODUCTION DATA:**

| | | | |
|---|---|---|---|
| Biomass Ratio (%) | 10.0 | 20.0 | 30.0 |
| Coal (tph), dry | 90.0 | 0.0 | 0.0 |
| Biomass (tph), dry | 10.0 | 0.0 | 0.0 |
| Total (tph), dry | 100.0 | 100.0 | 100.0 |
| Moisture (%) | 7.2 | 7.2 | 7.1 |
| Water Evaporation (tph) | 7.0 | 4.7 | 2.3 |
| Binder (tph) | 0.0 | 0.0 | 0.0 |
| Coating (tph) | 0.5 | 0.5 | 0.5 |
| Total (tph), AR | 108.3 | 108.3 | 108.1 |
| Total (tpy), AR | 584,597 | 584,597 | 583,970 |

**FIXED COSTS:**

| | | | |
|---|---|---|---|
| Equipment Cost ($): | $2,575,000 | $2,575,000 | $2,575,000 |
| Installed Cost ($): | $2,575,000 | $2,575,000 | $2,575,000 |
| Overhead ($): | $515,000 | $515,000 | $515,000 |
| Engineering Cost ($): | $257,500 | $257,500 | $257,500 |
| Total Fixed Cost ($): | $5,922,500 | $5,922,500 | $5,922,500 |
| Total FIxed Cost ($/yr): | $296,125 | $296,125 | $296,125 |

**O&M COSTS:**

| | | | |
|---|---|---|---|
| Maintenance Cost ($/yr): | $257,500 | $257,500 | $257,500 |
| Power Cost ($/yr): | $175,185 | $175,185 | $175,185 |
| Consumables Cost ($/yr): | $2,916,756 | $2,916,756 | $2,913,617 |
| Dryer Cost ($/yr) | $37,800 | $25,380 | $12,420 |
| Personnel Cost ($/yr): | $900,000 | $900,000 | $900,000 |
| Total O&M Cost ($/yr): | $4,287,242 | $4,274,822 | $4,258,722 |
| Total O&M Cost ($): | $85,744,830 | $85,496,430 | $85,174,437 |

**TOTAL PREPARATION COSTS:**

| | | | |
|---|---|---|---|
| Annual ($/yr) | $4,583,367 | $4,570,947 | $4,554,847 |
| Product ($/ton), dry | $8.49 | $8.46 | $8.43 |
| Product ($/ton), AR | $7.84 | $7.82 | $7.80 |
| Total ($) | $91,667,330 | $91,418,930 | $91,096,937 |

Table 19-4. Feasibility analysis for the western region (EB-CS) facility.

**PRODUCTION DATA:**

| | | | |
|---|---|---|---|
| Biomass Ratio (%) | 10.0 | 20.0 | 30.0 |
| Coal (tph), dry | 90.0 | 3.1 | 2.7 |
| Biomass (tph), dry | 10.0 | 0.8 | 1.1 |
| Total (tph), dry | 100.0 | 100.0 | 100.0 |
| Moisture (%) | 24.3 | 22.5 | 20.6 |
| Water Evaporation (tph) | 7.0 | 4.7 | 2.3 |
| Binder (tph) | 4.0 | 3.9 | 3.8 |
| Coating (tph) | 0.0 | 0.0 | 0.0 |
| Total (tph), AR | 136.7 | 133.5 | 130.2 |
| Total (tpy), AR | 734,942 | 717,834 | 700,621 |

**FIXED COSTS:**

| | | | |
|---|---|---|---|
| Equipment Cost ($): | $2,575,000 | $2,575,000 | $2,575,000 |
| Installed Cost ($): | $2,575,000 | $2,575,000 | $2,575,000 |
| Overhead ($): | $515,000 | $515,000 | $515,000 |
| Engineering Cost ($): | $257,500 | $257,500 | $257,500 |
| Total Fixed Cost ($): | $5,922,500 | $5,922,500 | $5,922,500 |
| Total FIxed Cost ($/yr): | $296,125 | $296,125 | $296,125 |

**O&M COSTS:**

| | | | |
|---|---|---|---|
| Maintenance Cost ($/yr): | $257,500 | $257,500 | $257,500 |
| Power Cost ($/yr): | $175,185 | $175,185 | $175,185 |
| Consumables Cost ($/yr): | $21,409,181 | $21,543,999 | $21,027,380 |
| Dryer Cost ($/yr) | $37,800 | $25,380 | $12,420 |
| Personnel Cost ($/yr): | $900,000 | $900,000 | $900,000 |
| Total O&M Cost ($/yr): | $22,779,666 | $22,902,064 | $22,372,485 |
| Total O&M Cost ($): | $455,593,320 | $458,041,276 | $447,449,709 |

**TOTAL PREPARATION COSTS:**

| | | | |
|---|---|---|---|
| Annual ($/yr) | $23,075,791 | $23,198,189 | $22,668,610 |
| Product ($/ton), dry | $42.73 | $42.96 | $41.98 |
| Product ($/ton), AR | $31.40 | $32.32 | $32.36 |
| Total ($) | $461,515,820 | $463,963,776 | $453,372,209 |

The high consumption of binding reagent is the primary factor for the high operating cost for the briquetting facility in the western region. In addition, the high inherent moisture content and low heating value of the low rank coal, coupled with the high operating cost, will pose a major challenge in justifying a production facility in that region.

## 19.7 Summary and Conclusions

A feasibility analysis was conducted to estimate the cost to construct a coal-biomass briquetting facility for each of the optimal blends discussed in previous chapters, namely the Emerald coal/sawdust feedstock in the eastern region and the Eagle Butte/corn stover feedstock in the western region.

As a result of this study, the following conclusions can be drawn regarding the construction and operation of a facility to produce coal-biomass briquettes on a commercial scale in the eastern and western regions:

- The estimated cost to develop and construct a modular-style briquetting facility rated at 100 tph dry product capacity is $5.9 million. The estimate was based on utilizing "off-the-shelf" commercial-scale processing equipment and designed as a module.
- The preliminary estimates for developing a modular-style briquetting facility indicate the processing cost in the eastern region would be less than $10 per ton. The region would be a source for premium thermal coals and wood related biomass feedstocks.
- The estimated processing cost for a briquetting facility in the western region is significantly higher at $30-40 per ton, primarily due to the higher (inherent) moisture content of the low rank coal which requires a high binding reagent dosage.
- The operating cost for the briquetting facility is largely dependent on the required dosage of the binding and coating reagents, especially the binding reagent.
- The operating cost for the western facility could be reduced by incorporating a drying unit for the low rank coal or by routing the coal-biomass mixture through a dryer.

# Chapter 20

# Conclusions and Recommendations

## 20.1 Summary of Research Activities

Co-utilization of biomass with coal in existing coal-fired facilities presents a unique opportunity to reduce greenhouse gas emissions and increase energy production from renewable resources. Significant interest in this opportunity has led to more than 150 coal-fired power stations across the world co-firing coal and biomass on a commercial or trial basis. These co-firing experiences have revealed a number of feedstock challenges that must be addressed to improve the potential for this growing technology. Recent studies suggest that many of these challenges can be mitigated by reconstituting coal-biomass mixtures into larger particles. Specifically, roll press briquetting has been investigated to produce homogeneous, free-flowing feedstocks that minimize handling and segregation problems often encountered with combustion and gasification systems. However, several technical and economic barriers require further investigation prior to industrial utilization of coal-biomass briquettes.

The research activities presented in this report are intended to address the most critical technical challenges pertaining to coal-biomass briquette feedstocks. As with any product of an agglomeration process, the primary technical challenge regarding coal-biomass briquettes is achieving and maintaining a high level of physical quality from production to utilization. Additional challenges include developing a proper understanding of the co-firing behavior of blended coal-biomass fuels, and optimizing the operation of advanced gasification systems for converting coal-biomass blends into useable energy. Several detailed research investigations were conducted to address these challenges, which included:

1. Identification, development and refinement of methods to characterize physical properties of coal-biomass briquettes;
2. Development of a methodology to identify the optimum water content of coal-biomass blends prior to briquette production;

3. Evaluation and optimization of feedstock variables, additive variables and roll press operating parameters in the production of coal-biomass briquettes from various coal and biomass types;
4. Development and evaluation of methods to improve the water resistance of coal-biomass briquettes using proprietary wood-derived chemicals;
5. Development of a novel sequential coal pelletization, drying, and briquetting process to improve the strength and durability of coal-biomass briquettes;
6. Evaluation of the potential to use bio-oil and biochar produced from the pyrolysis of woody biomass as a coal-biomass briquette binder and filler, respectively;
7. Evaluation of the impact of coal particle-size distribution on the strength and durability of coal-biomass briquettes;
8. Validation of the results of selected laboratory-scale briquetting test work through a series of pilot-scale briquetting tests;
9. Thermogravimetric analysis of coal-biomass blends for evaluation of the thermal evolution profiles and estimation of the kinetic parameters for pyrolysis and Boudouard reaction;
10. Conducting a series of experimental moving bed gasification tests on coal-biomass blends;
11. Evaluation of the source apportionment of carbon during gasification of coal-biomass mixtures using stable carbon isotope analysis;
12. Physiochemical characterization of the effects of biomass leaching, differences in individual coal and biomass samples, and the impact of blending coal and biomass fuels;
13. Kinetic characterization of coal and biomass fuels, including water leached biomass, using thermal analysis of the fuels while undergoing devolatilization;
14. Characterization of the pyrolysis and combustion energetics of coal, biomass, and coal-biomass blends using a STA and a micro-scale combustion calorimeter (MCC);
15. Quantification of the combustion performance index of coal, biomass, and coal-biomass blends by developing a model based on gravimetric, pyrolysis and combustion energetics data;

16. Investigation of the effect of briquetting on the flammability, ignitability, combustion performance, burn duration, and emissions of coal briquettes and coal-biomass briquettes; and
17. Determination of the economic feasibility of a commercial-scale coal-biomass briquette production facility.

The study of briquette characterization methods included a detailed review of briquette properties to determine the most important properties for characterization of coal-biomass briquettes. The briquette properties that were identified as most significant are: (1) tensile strength, (2) crushing strength, (3) elasticity, (4) mechanical durability, (5) attritability, (6) friability, (7) water content, (8) particle density, (9) bulk density and (10) water resistance. Experimental evaluations were conducted to adapt, evaluate and refine established methods that appeared suitable for coal-biomass briquette evaluations. This was accomplished by measuring briquette properties at different test conditions to determine the most accurate and precise configuration of each test method. Additional work was conducted to develop novel characterization methods to quantify briquette properties when suitable established methods were not applicable or available.

The moisture optimization study was conducted to develop a new experimental approach to identify the optimum water content of coal-biomass briquettes. The Briquette Proctor Test was developed based on the Proctor Test for clay soils, in which briquettes are produced at different water contents using a hydraulic press to determine the point at which dry particle density reaches a maximum value. Briquette Proctor Tests were conducted over a range of water contents (0.01 to 0.25) for blends of sawdust and both bituminous and sub-bituminous coals. Further work was conducted to evaluate the influence of a similar range of water contents on the particle density, crushing strength and mechanical durability of briquettes produced with a roll press. The results of the hydraulic press briquette production and roll press briquette production were compared to determine the feasibility of using the Briquette Proctor Test to indicate optimum water contents for roll press briquette production. The results were also analyzed to determine the relationship between particle density and briquette quality (i.e. crushing strength and mechanical durability).

The evaluation and optimization of briquette production variables study was conducted to examine the most significant feedstock, additive and roll press variables in coal-biomass

briquette production. For evaluation of feedstock variables, the effects of biomass content (10 to 30%), water content (0.02 to 0.20) and biomass top size (1.20 to 4.75 mm) on the quality (particle density, crushing strength and mechanical durability) of briquettes were studied. For evaluation of additive variables, the effects of binder content (0.0 to 5.0%) and cure time (0 to 7 days) on the quality of coal-biomass briquettes were investigated. For evaluation of roll press operating parameters, the effects of roll force (50 to 100 kN), roll torque (600 to 1800 N-m) and roll motor speed (300 to 900 rpm) on the quality of coal-biomass briquettes were studied. The results of these investigations were analyzed to develop mathematical models that can be used to predict the quality of coal-biomass briquettes. In addition, work was conducted to compare and contrast the quality of briquettes composed of four coal types and five biomass types. Finally, a comprehensive series of tests were conducted to characterize the physical properties, flow properties and gasification behavior of selected coal-biomass briquettes to verify the enhanced quality of co-briquetted feedstocks.

The water resistance study was conducted to evaluate the potential for several proprietary wood-derived chemicals to improve the water resistance of coal-biomass briquettes. Two methods for application of the chemicals were examined: (1) conventional binder application as a powder prior to briquette production and (2) briquette coating. For the conventional binder application method, the effects of binder content (0.0 to 5.0%) was evaluated for six wood-derived chemicals and pregelatinized wheat starch to determine the impact of each chemical on the water resistance, crushing strength and mechanical durability of briquettes. For the briquette coating method, the effects of coating individual briquettes with heated chemicals were evaluated for five wood-derived chemicals and paraffin wax to determine the impact of each coating on the water resistance and mechanical durability of briquettes. Additional work was conducted to fully characterize the coated briquettes and to compare the physical properties of coated and uncoated briquettes.

The sequential pelletization, drying and briquetting study was conducted to develop a novel process to dry coal fines, and more importantly to improve the strength and durability of coal-biomass briquettes. For this study, wet coal fines were formed into spherical pellets, which were subsequently thermally or air dried prior to briquette production. To determine the impact of the pre-pelletization step on briquette durability, numerous comparisons were made including comparisons of briquettes made with air dried coal fines, with air dried coal pellets, and with

thermally dried coal pellets. Further investigations were performed to compare the durability of briquettes formed from hot versus cooled pellets. The impact of adding a starch binder and co-briquetting these feedstocks with various types of biomass was also evaluated.

The bio-oil and biochar study was conducted to evaluate the potential to use bio-oil and biochar produced from the pyrolysis of woody biomass as a coal-biomass briquette binder and filler, respectively. For this study, several kilogram samples of bio-oil and biochar were produced in a series of batch reactor runs using a kiln dried sawdust feedstock. The bio-oil sample was evaluated both as collected and after thermal treatment that was intended to remove lighter components and increase viscosity. Briquettes containing either 10 or 30% biomass were produced from various combinations of screen-bowl coal fines, the two bio-oil binders, and the sawdust biochar, all of which were tested for strength and durability. For comparison, evaluations were also conducted on coal-biomass briquettes produced with a conventional wheat starch binder, miscanthus, and corn stover.

The coal particle-size distribution study was conducted to evaluate the impact of coal particle-size distribution on the strength and durability of coal-biomass briquettes. In this study, an ultra-fine coal sample was systematically blended with two larger size screen-bowl coal samples at targeted ratios to achieve a series of coal particle-size distributions. Two biomass types that differed in shape and texture (corn stover and wheat straw) were added at 10% by weight to each of the blended coal samples and briquetted, both with and without a starch binder. The strength and durability of the produced briquettes was measured to determine the combined impact of coal particle-size distribution, binder addition, and biomass type on coal-biomass briquette quality.

The pilot-scale briquette performance study was conducted to compare the physical performance characteristics for commercial-scale briquettes with the performance characteristics obtained for the briquettes produced during the bench-scale testing. Two coal-biomass batches were prepared based on the optimal formulation for a premium eastern thermal coal and a low rank western coal. The eastern coal was mixed with sawdust and the western coal was mixed with corn stover. Both batches were formulated with 70% coal and 30% biomass. The pilot-scale briquettes were then subjected to the same physical performance testing as the bench-scale briquettes.

The thermogravimetric analysis study was conducted to investigate the thermal evolution profiles and kinetic parameters for the pyrolysis of coal-biomass feedstocks. Non-isothermal thermogravimetric analyses were performed on all the feed materials to establish the effect of heating rates on devolatilization. The thermogravimetric analysis was performed at four different heating rates (5, 10, 20, and 40 ºC/min) in an inert nitrogen atmosphere. Non-isothermal thermogravimetric analysis in carbon dioxide atmosphere was also performed at relatively higher temperatures and varying heating rates ranging between 5 ºC/min and 40 ºC/min to study the effects of heating rates and temperatures on the Boudouard reaction. Using MATLAB, complex models for devolatilization of the blends were developed to estimate and predict global kinetic parameters, such as activation energy and pre-exponential factor. Three different models, namely, single first order reaction model, distributed activation energy model and its extension, called matrix inversion method, where no prior assumption of the activation energy curve is made, were utilized and compared.

The moving bed gasification study was conducted to study the thermochemical conversion of coal-biomass blends. Two different low rank coals (Perry County bituminous coal and Black Thunder sub-bituminous coal) and biomass feedstocks (corn stover and switchgrass) were utilized for this purpose. The biomass feedstocks were blended up to a maximum of 30% by weight with each of the coal feedstocks. These blended feedstocks were gasified auto-thermally in the laboratory scale moving bed gasifier operating at atmospheric pressure and various steam to oxygen/air ratios (0 to 2.5:1). Initially, a comparative study was performed with quartz and stainless steel tubes within the gasifier, and the outlet product gas compositions were analyzed to determine the better material of construction. Next, the effect of steam content in the inlet gas stream on the gasification products was analyzed. Additional tests were conducted to investigate the effect of partial pressure of oxygen on the gasification products. This was accomplished by varying the oxygen percentage in the inlet gas stream from 20 to 100% (i.e. from pure air to pure oxygen). Finally, experimental results were examined for potential synergistic effects between blends of coal and biomass for production of liquid and gaseous fuels. This involved analysis of thermogravimetric data and actual product gas composition obtained at various operating conditions using the laboratory scale moving bed gasifier.

The source apportionment of carbon study was conducted to qualitatively and quantitatively measure individual contributions of coal and biomass feedstock materials in the

generation of carbon containing gases during gasification. Gas Chromatography-Combustion-Isotope Ratio Mass Spectrometry (GC-C-IRMS) was used to perform stable carbon isotope analysis, which is a unique analytical technique for measuring the carbon contribution of coal and biomass. This technique was also used to check for the existence of isotopic equilibrium during moving bed gasification.

The physiochemical characterization study was conducted to quantify the effects of biomass leaching, differences in individual coal and biomass samples, and the impact of blending coal and biomass fuels. The physicochemical properties of blended fuel, char and pyrolyzed ash samples were analyzed using an Environmental Scanning Electron Microscope (ESEM). The effects of biomass water leaching on the physicochemical behavior of biomass fuels and physicochemical interactions within coal-biomass fuel mixtures during pyrolysis were investigated.

The pyrolysis chemical kinetics study was conducted to investigate and understand the devolatilization process of coal, biomass and coal-biomass blends. Thermogravimetric (TG) data was obtained from a simultaneous thermogravimetric analyzer (STA) for coal-biomass fuel blends undergoing co-pyrolysis at multiple constant heating rates. Non-linear regression analysis was conducted on the TG data to determine the Arrhenius kinetic parameters for fuel blend co-pyrolysis.

The pyrolysis and combustion energetics study was conducted to accurately characterize the energetics of coal, biomass and coal-biomass blends during pyrolysis and combustion processes. The energetic behavior of coal-biomass fuel blends undergoing pyrolysis-combustion process was investigated using a STA and a micro-scale combustion calorimeter (MCC). The instruments were used to generate differential scanning calorimetry (DSC) and heat release rate (HRR) signals for the blended fuels. Mathematical models were developed for fuels undergoing pyrolysis-combustion, and experimental signal data was applied onto the models to calculate the heat of pyrolysis and heat of combustion properties for the fuel blends. The mathematical models and the approach developed in this work was applied on samples such as glycerol, polymers, composites and cardboard. The heat of pyrolysis and heat of combustion data generated from these tests was validated against the literature findings to properly understand their energetic behavior during pyrolysis-combustion. The approach was then applied onto coal-biomass fuel

blends to quantify their energetic behavior in terms of the properties of constituent fuels of the blends.

The combustion performance study was conducted to further the understanding of coal-biomass blend pyrolysis-combustion behavior. Lumped mathematical models were developed to calculate fuel pyrolysis performance, char combustion performance and cumulative fuel combustion performance. The models were developed to calculate both temperature based performance and total integrated performance of fuels and blends. The experimental data for model application was generated using a simultaneous thermogravimetric analyzer (STA) and a micro-scale combustion calorimeter (MCC). The fuels tested in this study included coal, biomass, polystyrene and glycerol. The effects of biomass water leaching, as well as, coal-biomass blending, was also investigated in terms of total integrated performance parameters.

The study of combustion characteristics of coal-biomass briquettes was conducted to understand the effect of fuel briquetting on the flammability, ignitability, combustion performance, burn duration and emissions of the fuel. Coal-biomass blend briquettes were developed and their combustion behavior was compared against raw coal-biomass blends of same mixture proportion. The fuel blends were also tested in different combustion environments to study the effects of operating conditions on combustion behavior.

A feasibility study was conducted to develop a conceptual processing flowsheet and to provide estimated costs for a commercial-scale briquette production facility rated at 100 tph dry product. Simulations, using Excel spreadsheet optimization routines, were developed to provide operating parameters (equipment loading and energy demands) for the conceptual flowsheet and to estimate the capital and operating costs based on the conceptual flowsheet. The simulations were used to evaluate the costs for an eastern premium thermal coal mixed with wood related biomass (sawdust) and for a western low rank coal mixed with agricultural related biomass (corn stover). Simulations were conducted for three blend ratios (30%, 20% and 10% biomass) for each coal type.

## 20.2 Original Contributions

As a result of the research presented in this report, several original contributions have been made in the field of solid fuel agglomeration and gasification technologies:

1. *Novel Characterization Methods for Water Resistance, Attritability and Elasticity of Coal-Biomass Briquettes.* The methods developed to quantify each of these properties were independently developed and refined during the course of this research. These methods describe unique theoretically sound procedures and apparatuses to characterize coal-biomass briquettes.
2. *A Novel Low-Cost Method to Quickly Determine the Optimum Water Content of Coal-Biomass Briquettes.* The Briquette Proctor Test presents a unique approach to maximize the quality of coal-biomass briquettes by determining the optimum feedstock water content. This test greatly reduces the time and materials required to locate the optimum water content, and thus provides a significant opportunity to reduce research and development costs.
3. *A Novel Post-Production Method to Improve the Water-Resistance of Coal-Biomass Briquettes using Wood-Derived Chemicals.* The coating of coal-biomass briquettes with heated wood-derived chemicals presents a significant opportunity to improve the water-resistance of coal-biomass briquettes. Water resistant coal-biomass briquettes could be transported and stored using existing coal infrastructure, which would minimize required capital expenditures upstream of the gasifier.
4. *A Novel Pre-Pelletization, Drying, and Briquetting Process to Dry Coal Fines and Produce High Quality Coal-Biomass Briquettes.* Forming wet coal fines into spherical pellets before thermally drying and briquetting the pellets at an elevated temperature offers several advantages over direct briquetting of wet or dry coal fines. These advantages include a significant improvement in the physical quality of briquettes, the ability to dry coal fines in an approved moving bed dryer, and enhanced flow properties for feeding a briquette press.
5. *Matrix Inversion Algorithm.* A mathematical algorithm, called matrix inversion method, which is essentially a model-free distributed activation energy method, for solving the complex devolatilization equations and estimating the kinetic parameters of both pyrolysis as well as gasification of blends of coal and biomass. This method greatly

reduces the number of validation experiments, accurately predicts the weight loss of complex fuel blends with an error of less than 1%, and estimates the total number of reactions and the amount of each reaction occurring during devolatilization of the fuel blends. Also, the advantage of using this method lies in the fact that the algorithm can be utilized for predicting the devolatilization of unknown fuel blends at unknown heating rates. Hence, this method can be extremely useful on an industrial scale where the instantaneous heating rates are unknown.

6. *Stable Carbon Isotope Analysis*. A unique analytical technique, stable carbon isotope analysis, has been utilized for distinguishing and quantifying the individual contributions of coal and biomass feedstock materials in the generation of carbon containing gases during the gasification of their blends. The utilization of this technique is unique and takes a very interesting approach towards assessing coal-biomass gasification characteristics. The analysis takes advantage of the fact that coal and biomass belong to different class of plants (C3 and C4 plants respectively) which have different carbon isotope values. Therefore, when such fuels are blended together and subjected to thermal decomposition, the gases generated have carbon isotope compositions that are distributed within those of the single fuels. Hence, the greenhouse gases generated can be easily distinguished and individual contributions of single fuels can be quantified. This is important to know as one of the main objectives of adding biomass to coal is to reduce the amount of greenhouse gases released into the atmosphere as it is a $CO_2$ neutral and sustainable fuel. Furthermore, correlating the carbon isotope values and gasifier temperatures provides insights into estimating whether the gasification is proceeding via an isotope exchange mechanism or a chemical reaction mechanism. Finally, it can be stated that the data obtained utilizing this unique analytical technique would provide valuable insights not only pertaining to the synergy between the blended feedstock materials but also towards process modeling, optimization and reaction pathways in the field of co-gasification of coal and biomass.

## 20.3 Final Conclusions

The following conclusions were drawn from the results of the research presented in this report:

1. *Briquette Characterization Methods.* Crushing strength and mechanical durability are the most widely used indicators of the physical quality of coal-biomass briquettes, and thus both properties should be measured for all experimental and industrial briquette production operations.
2. *Optimization of Briquette Water Content.* The influence of water content of coal-biomass mixtures on the dry density of briquettes determined by the Briquette Proctor Test is very similar to the influence of water content on the dry density of compacted clay soils as determined by the standard Proctor Test. The optimum crushing strength and mechanical durability of coal-biomass briquettes can be determined by using the Briquette Proctor Test for optimization of water content. Hydraulic press briquette production is representative of roll press briquette production, and thus the Briquette Proctor Test can be used to indicate the optimum water content of coal-biomass mixtures prior to roll press briquetting evaluations. The dry density of briquettes composed of bituminous coal and biomass exhibits a strong positive correlation with crushing strength and mechanical durability. An exhaustive experimental study of water content optimization for roll press briquetting coal-biomass mixtures can be streamlined by simply determining the water content that results in the highest dry density because maximum crushing strength and mechanical durability likely exist at or near this value as well.
3. *Briquetting Comparison of Coal and Biomass Types.* Differences in the quality of coal-biomass briquettes composed of different types of bituminous coal with identical top sizes can be attributed to differences in the distribution modulus and ash content of the coals, where briquette quality increases with a corresponding increase in distribution modulus and decrease in ash content. Bituminous coals generally produce higher quality briquettes than sub-bituminous coals. Corn stover exhibits the best properties of the biomass types studied with regard to the crushing strength and mechanical durability of coal-biomass briquettes.
4. *Influence of Feedstock Variables on Briquette Quality.* Biomass content is the most statistically significant mixture variable with regard to the particle density of coal-

biomass briquettes. For all types of coal and biomass evaluated, an increase in biomass content causes a direct reduction in particle density. Biomass content is the most statistically significant mixture variable with regard to the crushing strength of binderless coal-biomass briquettes. For all types of coal and biomass evaluated, an increase in biomass content causes a direct increase in crushing strength. Water content is the most statistically significant mixture variable with regard to the mechanical durability of binderless coal-biomass briquettes. For all types of coal and biomass evaluated, a clear optimum water content can be identified where mechanical durability reaches a maximum value. Biomass top size is not a statistically significant mixture variable with regard to the particle density, crushing strength and mechanical durability of coal-biomass briquettes.

5. *Statistical Influence of Additive Variables on Briquette Quality.* Starch content is a very statistically significant mixture variable with regard to the crushing strength and mechanical durability of coal-biomass briquettes. An increase in starch content causes a direct increase in crushing strength and mechanical durability. Cure time is a statistically significant process variable with regard to the crushing strength of coal-biomass briquettes. A period of 6 days is recommended to cure the briquettes for which this variable was statistically studied.
6. *Influence of Roll Press Operating Parameters on Briquette Quality.* Roll torque is the most statistically significant roll press operating variable with regard to the particle density, crushing strength and mechanical durability of coal-biomass briquettes. An increase in roll torque causes a direct increase in particle density, crushing strength and mechanical durability. Roll force is a statistically significant roll press operating variable with regard to the particle density, crushing strength and mechanical durability of coal-biomass briquettes. An increase in roll torque causes a direct increase in particle density, crushing strength and mechanical durability. Roll speed is a statistically significant roll press operating variable with regard to the particle density of coal-biomass briquettes. An increase in roll speed causes a direct reduction in particle density.
7. *Characteristics of Optimum Binderless Briquettes.* Binderless coal-biomass briquettes produced at optimized conditions exhibit very high crushing strength and mechanical durability values, which indicate that the briquettes would largely remain competent in

the presence of forces encountered in handling, storage and transportation. Binderless coal-biomass briquettes produced at optimized conditions exhibit poor water resistance, which indicates that additional investigation of this matter is required. Binderless coal-biomass briquettes produced at optimized conditions exhibit excellent flow properties, which indicates that proper hopper design is straightforward. Binderless coal-biomass briquettes produced at optimized conditions exhibit excellent gasification behavior with regard to product gas composition and cold gas efficiency. This confirms that coal-biomass briquettes are exceptional gasification feedstocks for the co-production of power and synthetic fuels.

8. *Wood-Derived Chemicals to Improve Briquette Water Resistance.* Wood-derived chemicals added to coal-biomass mixtures prior to briquette production can improve the water resistance of coal-biomass briquettes by up to 77% at a binder content of 5%. Wood-derived chemicals applied to the exterior of coal-biomass briquettes as a coating can improve the water resistance of the briquettes by up to 97% and the weathered mechanical durability by up to 400% with a coating dosage of 8%.
9. *Influence of Ambient Temperature Coal Pellets on Briquette Quality.* At ambient temperature, briquette strength and durability are improved by forming blends of binder and fine coal into pellets and then drying prior to briquetting, as opposed to briquetting dried blends of fines and binder directly. This is presumably due to more uniform dispersal of the binder during pelletization. The optimum moisture for briquettes produced from pelletized coal fines ranges from about 1 to 4% for the four bituminous coals evaluated. Crushing strength is generally higher for 30% biomass briquettes compared to their 10% counterparts. The opposite trend is true for briquette durability, which classifies as acceptable to good for briquettes made with 10% biomass and poor to acceptable for briquettes made with 30% biomass.
10. *Influence of Thermally Dried Coal Pellets on Briquette Quality.* Substantial improvements in briquette quality can be obtained by briquetting thermally-dried coal pellets while hot as compared to briquettes formed at ambient temperature in the form of air-died fines, air-dried pellets, or thermally dried pellets. These improvements are more pronounced for briquettes made with a binder and with larger particle size coals. The

magnitude of improvement depends on the type of binder added and any potential thermal activation properties.

11. *Potential for Bio-Oil as a Briquette Binder.* Coal-biomass briquettes made with a sawdust-derived bio-oil binder exhibit good resistance to water degradation as opposed to binderless briquettes or briquettes made with a wheat starch binder. Thermally modifying as-collected bio-oil to remove a portion of the more volatile oil components results in an increase in oil viscosity and subsequent improvement in binding characteristics. However, the strength and durability of briquettes made with as-collected and thermally treated bio-oil are not improved, and often are worse than obtained without adding a binder. Despite the ability to impart water resistance, bio-oil characteristics appear to be more akin to those of a lubricant than to those of a binder. Thus, bio-oil is deemed unacceptable as a binding agent at this time.
12. *Potential for Biochar as a Briquette Filler.* The strength and durability of coal-biomass briquettes made with a sawdust-derived biochar are unacceptably low on both an absolute as well as a relative basis compared to briquettes made with equivalent amounts of miscanthus or corn stover. Production of coal-biochar briquettes with 30% of sawdust-derived biochar is not feasible as the briquettes do not survive the fines removal step across a mechanical screener, even when a starch binder is added. Thus, the sawdust-derived bio-char used in this study is unsuitable for producing coal-biomass briquettes.
13. *Influence of Coal Particle-Size Distribution on Binderless Briquette Quality.* The highest briquette strength and durability is obtained with an ultra-fine coal regardless of the biomass type added. At relatively low biomass addition rates of 10%, the particle-size distribution of the coal component has a greater impact on briquette properties than does the type of biomass added. Without binder, stronger briquettes are formed from ultra-fine flotation coal compared to the briquettes formed with larger-particle-size screen bowl samples or with blends of the flotation and screen bowl coals.
14. *Influence of Coal Particle-Size Distribution on Binder-Infused Briquette Quality.* Significant improvements in briquette durability are obtained when ultra-fine flotation coal is blended with screen-bowl fines when a binder is added compared to binderless briquettes made from the same blends. This difference is more pronounced as the proportion of the larger sized fines is increased. This is attributed to good overlap of the

particle size distributions, which allows for more efficient particle packing coupled with a reduction in the total surface area, thereby requiring less binder to obtain effective binder coverage. This improvement is not observed when flotation coal is blended with a much larger particle size sample of fines in which there is a gap in the particle size distribution of the two coal samples. It is speculated that the mismatch in particle size distributions leads to inefficient in-filling of the voids between the larger coal particles, which results in a reduction of crushing strength. This speculation is supported by a correlation between the average briquette weight and briquette strength for the various combinations of fine coal samples.

15. *Curing Characteristics of Briquettes.* The durability of briquettes made with fine coal and raw biomass declines as the briquettes cure in contrast to briquettes made with fine coal without biomass or that are made with fine coal and bio-char, which remain relatively constant or increase slightly as the briquettes cure. The difference in aging characteristics is attributed to expansion and/or moisture absorption by the raw biomass as the briquettes cure.
16. *Performance Testing of Pilot-Scale Coal-Biomass Briquettes.* The crushing strength and the mechanical durability of the pilot-scale briquettes were very similar to the bench-scale briquettes. The evaluation suggests that bench-scale testing can be used to obtain valid preliminary predictions for commercial-scale briquette performance.
17. *Weight Loss Profile of Individual Fuels*. The weight loss profiles in the $N_2$ atmosphere illustrate that the thermal evolution profiles of the individual fuels are different from that of the blends. The thermal evolution profiles of PCC Bituminous coal (PCC) and BT Sub-Bituminous coal (BT) display only one major peak over a wide temperature distribution (152-814 °C for PCC and 175-818 °C for BT), whereas the thermal decomposition profile for corn stover falls in a much narrower band than that of the coals, (226-608 °C), and the maximum weight loss rate of corn stover is almost an order of magnitude higher than both coals. Also, the maximum weight loss rate of BT is much lower than that of PCC. This can attributed to the fact that the volatile matter or the immobile phase present in BT coal are bonded together with much higher molecular bond energy than that of PCC coal, and hence will be removed at a slower rate under similar temperatures.

18. *Weight Loss Profile of Coal-Corn Stover Blends*. For blends of PCC and corn stover, the first peak occurs at a maximum peak temperature of approximately 326-330 °C, representing the devolatilization of corn stover (evolution of hemicellulose and cellulose components). The second peak occurs at a maximum peak temperature of 419-430 °C, representing the devolatilization of PCC. Similar trends are observed for blends of BT and corn stover, with maximum peak temperatures ranging from 318-336 °C for the devolatilization of corn stover and 411-423 °C for the devolatilization of BT. Also, the maximum weight loss rate (%/min) for the corn stover devolatilization profile increases with increasing concentration of corn stover in the blends, and vice versa for the coal devolatilization profile. Interestingly, this occurs without an apparent change in the shape and position of the peaks when compared to that of the single fuels. Also, the change in the maximum devolatilization rate is not linear with the increase in corn stover percentage, which indicates the possibility of interactions between the blended fuels.
19. *Weight Loss Profile of Coal-Switchgrass Blends*. The weight loss curves of coal-switchgrass blends follow a similar pattern as that of blends with corn stover. The devolatilization interval for switchgrass starts around 175 °C with the decomposition of hemicellulose and ends around 650 °C with the slow decomposition of lignin. When compared with blends of corn stover, a clear distinction in the DTG profiles can be observed. For these blends of coals and switchgrass, three different peaks are clearly observed, where the low temperature peaks can be attributed to the decomposition of switchgrass and the high temperature peaks correspond to the decomposition of coals. This is different from the trend observed for blends with corn stover where the two low temperature peaks merge, which is an indication that some components in coal interact with corn stover in the low temperature range of around 220-380 °C. There is a clear distinction in the hemicellulose and cellulose peaks when switchgrass is blended with coal, which suggests that no significant interactions occur and that the two components decompose separately.
20. *Synergistic Effects of Coal-Biomass Co-Gasification*. The non-linearity in the evolution of volatile matter with increasing percentage of corn stover in the blends verifies the possibility of synergistic behavior in the blends with bituminous coal. Deviations of 2-7% from the predicted yield were observed for bituminous coal blends, whereas very little

deviations (1-3%) from predicted yield were observed in blends with sub-bituminous coal, which indicated no significant interactions with corn stover. Similar to corn stover blends, the blends containing switchgrass also show a clear increase in the amount of volatile matter with increasing percentage of switchgrass in the blend. However, the deviations from the predicted and experimental yield is minimal, which suggests that no significant interactions are present during devolatilization of blends of coals and switchgrass.

21. *Effect of Gaseous Atmosphere on Devolatilization*. When compared with devolatization of the feedstock materials utilizing a $N_2$ atmosphere, the TGA curves with respect to temperature follow a similar pattern until approximately 500 °C even when pure $CO_2$ is utilized as the sweeping gas. Although the mass loss rates at low temperatures are higher in pure $CO_2$ atmosphere, the differences are only marginal. At higher temperatures, however, a significant increase in mass loss rate is observed in pure $CO_2$ atmosphere. This may be understood by the stages of coal pyrolysis process. In the case of 100% $N_2$ environment, the coal pyrolysis process has two stages: release of moisture content and devolatilization but the process of coal pyrolysis in pure $CO_2$ environment can be divided into three stages: moisture release, devolatilization and char gasification or Boudouard reaction with $CO_2$ to form CO in high temperature zone (> 500 °C). Also, this difference may be explained due to the density difference and transport properties of these gases which are quite different (the mass of the $CO_2$ molecule is different from that of $N_2$). Moreover, the formation of char particles is larger and its surface area is also higher than that of the $N_2$ char particles. Hence, the weight loss observed in $CO_2$ environment is much higher.
22. *Comparison of Kinetic Decomposition Models*. The matrix inversion algorithm predicts the kinetic parameters of decomposition such that the weight loss characteristics can be best represented for both single fuels as well as blends of coals and biomass materials. Also, weight loss characteristics of unknown fuel blends at unknown heating rates can be effectively predicted within 1% error through the use of this algorithm. The distributed activation energy model can also be used to predict the weight loss of the feedstocks in a $CO_2$ atmosphere over the whole temperature range of the experimental procedure (~35 °C to 1000 °C).

23. *Comparison of Quartz and Stainless Steel Reactor Tubes*. The efficiency and product gas compositions obtained reveal that utilizing an inner stainless steel tubing better promotes heat transfer upwards in the axial direction when compared to utilizing a quartz insulation. The trends of the product gas compositions are similar to those obtained using an inner quartz lining. However, the percentage of hydrogen generated at same operating conditions is much higher due to the increase in bed temperature (complete consumption of oxygen occurs) and transfer of heat upwards in the axial direction. Thus, better heat utilization occurs, which improves the overall efficiency by at least 20% when the steam concentration is at its maximum in the gasifier. Also, unlike the quartz insulation where the efficiency increased only until a certain point and the maximum steam/$O_2$ ratio that could be utilized was 1.5, in this experimental setup, the efficiency increased steadily until a steam/$O_2$ ratio of 2:1. Apart from this, the ratios of $H_2$/CO, CO/$CO_2$ and syngas/$CO_2$, which dictate the quality of the product gas, are markedly higher as compared with the experimental design utilizing an inner quartz lining.
24. *Optimum Moving Bed Gasifier Operating Conditions*. Using pure oxygen and steam in the inlet gas stream, the highest energy conversion efficiency obtained is approximately 50% at a steam to oxygen ratio of 1.5. Using a mixture of nitrogen and oxygen in the feed gas stream, an inlet gas flow rate of 1625 ml/min and oxygen percentage of 40% provides the highest energy conversion efficiency and a max CO:$CO_2$ ratio of approximately 3:1. The bed temperature range during the gasification of sub-bituminous coal was generally observed to be between 600 ºC and 800 ºC for the experiments with varying steam ratios and between 800 ºC and 1000 ºC for the experiments with varying oxygen partial pressures.
25. *Source Apportionment of Carbon*. An increase in the amount of biomass in the feed leads to a steady increase in the isotopic value of the carbon containing gases, implying that the product gas becomes isotopically heavier during gasification. This is also an indication of probable synergistic effects between the blended materials. Furthermore, the correlation between the $\delta^{13}C$ values and gasifier temperatures suggests that CO/$CO_2$ ratio proceeds via a kinetic mechanism rather than an isotopic exchange. The addition of biomass had a definite impact in the generation of carbon containing gases. For blends with corn stover, higher $O_2$:steam ratios result in up to 70% of the carbon contribution coming from the

corn stover in the generation of $CO_2$. In contrast, gasification of blends of switchgrass with coals are much more effective at lower oxidant ratios with respect to the generation $CO_2$ and vice versa for the generation of CO.

26. *Physiochemical Characterization of Coal and Biomass Feedstocks.* A significant reduction in inorganic salts and increase in oxygen element percentage occurs as a result of biomass leaching, while the carbon element percentage is unchanged following water leaching. Physicochemical properties of coal and biomass samples are unchanged in their un-pyrolyzed, char and ash phases. The physicochemical interactions between coal and leached biomass sample, following co-pyrolysis, are minimal.
27. *Pyrolysis Chemical Kinetics of Coal and Biomass Feedstocks.* The water leaching of biomass samples mitigates the secondary reactions during pyrolysis, shifting the primary decomposition reactions to higher temperatures, and reducing the char yield of biomass fuel samples. An increase in the rate of devolatilization occurs as a result of biomass water leaching due to removal of secondary autocatalytic reactions. An independent parallel reaction model of three $n^{th}$ order reactions best described the biomass pyrolysis statistically, where each reaction signifies the pyrolysis of a biomass constituent (i.e. hemicellulose, cellulose, and lignin). A small increase in the activation energy of each constituent pyrolysis reaction occurs on water leaching. Coal pyrolysis is statistically best represented by two independent $n^{th}$ order reaction models. Five independent $n^{th}$ order reactions statistically best describes the co-pyrolysis behavior of fuel blends, with the first three reactions corresponding to the decomposition of biomass and the last two corresponding to the decomposition of coal. The Arrhenius parameters for coal-biomass blend co-pyrolysis fits experimental TG data, which shows that an additive thermogravimetric and kinetics behavior model best fits coal-biomass fuel blends.
28. *Pyrolysis and Combustion Energetics of Coal and Biomass Feedstocks.* The water leaching of biomass samples mitigates the secondary reactions during pyrolysis, shifting the primary decomposition reactions to higher temperatures, and reducing the char yield of biomass fuel samples. An increase in the heat of pyrolysis occurs on biomass water leaching due to removal of secondary exothermic reactions. The pyrolysis-combustion energetic signals and properties for coal-biomass blended fuel exhibit a weight additive behavior. The weighted sum prediction for the heat of pyrolysis and the heat of

combustion properties for coal-biomass fuel blends must be conducted on the basis of their individual volatile mass contributions from constituent fuels and not on the basis of initial fuel mixture proportion. The energetic properties such as heat of pyrolysis and heat of combustion must be calculated on the volatile mass basis of the fuel samples, instead on their initial mass basis.

29. *Combustion Performance of Coal and Biomass Feedstocks.* Different fuels produce peak performance at different temperatures. Thus, the mixing of various fuels will help blended fuels in generating consistent performance over a wider temperature range, which in turn can be advantageous for power plant operation. The blending of coal and leached biomass increases the pyrolysis performance of coal by 21-33%. However, the blending of biomass decreases the char combustion performance of coal samples by as much as 28%. Thus, blending of biomass decreases the cumulative fuel combustion performance of coal by up to 22%. This performance drop due to blending signifies the amount of extra mass of mixture fuel that would need to be fed into a co-firing plant to obtain the same performance as a coal combustion plant.
30. *Combustion Characterization of Coal-Biomass Briquettes.* The flammability and combustion performance of blended briquettes is better than those of raw blended fuels. The off-gassing time, ignitability and burn duration of blended coal-biomass briquettes combustion is close to that of coal combustion. The heat release rate profile for blended briquettes is higher and more uniform than the heat release rate profile for coal-biomass raw blends. The use of blended briquettes provides lower $NO_x$ peak values than raw blends of coal and biomass fuels. The $CO_2$ and CO yields from blended briquette combustion is lower than that from raw coal and biomass blend combustion. For an existing coal-based power plant, usage of blended briquettes may require the least amount of changes in its operating conditions. In contrast, usage of just raw blends of coal and biomass will require considerable operational challenges in a coal-based power plant. Usage of coal-biomass blended briquettes will not only provide a scenario where the least amount of changes would be required to operating conditions of a coal based power plant, but it will also improve the combustion behavior of fuels in terms of flammability, combustion performance, ignitability, burn duration and emissions from constituent raw fuels.

31. *Feasibility Analysis for a Commercial-Scale Briquetting Facility.* Flowsheet simulations and costs estimates indicate that a facility could be developed in the eastern region for $5.9 million in capital with less than $7-10 per ton operating cost. The same facility developed in the western region will have an estimated operating cost of $30-40 per ton, due primarily to the higher reagent dosage required for the low rank coal feedstock.

## 20.4 Recommendations for Further Investigation

Based on the research work performed and current technology status of coal-biomass blend briquetting, combustion, and gasification, the following recommendations are suggested for future work in this field to promote the co-utilization of coal and biomass feedstocks:

1. *Briquette Characterization Methods.* Although a general consensus has been reached regarding the most important physical properties of fuel briquettes, specific test methods to quantify these parameters are highly variable. It is common for researchers to independently develop assessment procedures appropriate to the nature of the particular investigations performed at their laboratories. This makes it extremely difficult to compare the quality of briquettes produced and tested in separate laboratories. In support of this challenge, stakeholders in the fuel briquetting industry must work with organizations that develop and publish standard test methods (e.g. ASTM, CEN, ISO) to standardize common briquette characterization methods (e.g. crushing strength, mechanical durability). Additional investigation is also recommended for methods to characterize the effects of other weather conditions (i.e. humidity, freezing) on the quality of coal-biomass briquettes.
2. *Influence of Moisture Content.* Additional research is needed to determine the influence of surface and inherent moisture (in addition to total moisture) on the quality of briquettes composed of sub-bituminous coal and biomass.
3. *Influence of Coal Particle-Size Distribution.* Future work on particle size evaluations could benefit from studies focused on differentiating the impact of clay content versus the coal particle size distribution, and on an evaluation of the impact of the roller force used during production of briquettes from coal samples with a broad particle size distribution.
4. *Potential for Bio-Oil as a Briquette Binder.* Further research to develop an effective bio-oil binder should focus on treatments to increase the average molecular weight and

viscosity through aggressive removal of the lighter components and/or methods to induce cross-linking reactions.

5. *Potential for Biochar as a Briquette Filler.* Two promising areas for further research on coal-biochar briquetting are production of biochar at lower temperatures than used in this study and production of biochars with a morphology better suited to the production of durable coal-biochar briquettes, such as those formed from wheat straw or miscanthus feedstocks.
6. *Wood-Derived Chemicals to Improve Water Resistance.* Additional research is needed to improve the method used to coat coal-biomass briquettes with heated wood-derived chemicals. Improvement is needed to reduce the chemical dosage applied to individual briquettes to ultimately improve the economic feasibility of this technique. Further research is required to develop a continuous process for coating coal-biomass briquettes with heated wood-derived chemicals. The batch process described in this report is not ideal for industrial applications and scaling the process to higher capacity would present challenges.
7. *Feedstock Logistics, Sustainability and Economics.* Several additional studies should be conducted to investigate the market potential for coal-biomass briquettes. Specific investigation is required in the areas of logistics, biomass sustainability (i.e. life-cycle analysis), and economic feasibility to determine the potential role of coal-biomass briquettes in the global energy market. The results of this work would provide invaluable information for future energy policy decisions.
8. *Performance Testing of Pilot-Scale Coal-Biomass Briquettes.* Additional studies should be conducted to evaluate the effect of the shape of the pilot-scale briquettes when comparing the crushing strength and physical durability of bench-scale briquettes to pilot-scale briquettes and to develop correlations for applying bench-scale performance data to pilot-scale briquettes for various shapes.
9. *A Mechanistic Model for Various Biomass Feedstocks.* The work performed in this research involved the utilization of two coal ranks and two biomass sources. It is a known fact that each carbonaceous feedstock varies greatly in its physical and chemical properties. Hence, a mechanistic model needs to be developed and evaluated to provide a

database of the availability of various biomass feedstocks and segregate these based on their properties which may be useful during scaling up of the process.

10. *Kinetic Devolatilization Model Enhancement.* To improve upon the devolatilization models suggested in this research, future work can involve utilization of thermogravimetric analysis coupled with other analytical techniques such as mass spectrometry or infra-red spectroscopy (TGA-MS or TGA-FTIR) so that specific models pertaining to each component evolving during the devolatilization stage can be evaluated. The kinetic models coupled with component-specific models would be extremely useful in moving this research to the next stage.
11. *High Pressure Laboratory Gasification Experiments.* The laboratory scale gasifier experiments were performed at atmospheric pressure in this research. To develop the process for a commercial scale, experiments need to be performed at moderate and high pressures and also evaluate the performance of the gasifier under similar operating conditions using an appropriate catalyst so that tar yields are significantly reduced.
12. *Process and Hydrodynamic Models.* ASPEN process models and hydrodynamic models (1-D and 2-D) congregating all the processes during gasification need to be developed and evaluated. The stable carbon isotope analysis utilized in this work, also, needs to be incorporated into process models to better understand reaction pathways. It is important to mathematically model the moving bed gasification results to establish the effects of mass, heat and momentum. The new data should account for different operating conditions and biomasses to have enough points to cover the whole range and variability that needs to be modelled.
13. *Economic Feasibility of Coal-Biomass Gasification.* A thorough investigation into the costs and economics involved in the process of gasifying coal-biomass blends needs to be evaluated if the process is to be commercially viable.
14. *More Realistic Reactor Conditions to Develop Comprehensive Models and Experiments.* The experiments to understand the coal-biomass behavior can be done on larger scale setups and with higher heat fluxes or heating rates (similar to those in the power plant) than used in the present study. These experiments will help the research group in developing more comprehensive mathematical models that can quantify the kinetics,

energetics, performance and evolved gas behavior of thermally thick samples, rather than milligram size samples covered in the present study.

15. *A More Sophisticated Approach to Determine Decomposition Process for Briquettes*. Therefore, the models and experiments will be able to quantify the briquette combustion process in terms of briquette cracking, volatile gas production, fuel ignition, flame spread and radiation effects, re-radiation from adjacent briquettes, and their subsequent effect on the modeled/experimented briquette. The physicochemical analysis in such a study will focus more on briquette physicochemical behavior while under exposure from extreme thermal conditions. The thermo-mechanical properties of briquettes must be analyzed to determine briquette cracking, peeling and crumbling while under thermo-mechanical stress. The elemental analysis of the un-pyrolyzed, charred, and ash briquette must be conducted to understand its thermo-chemical behavior during the combustion process.
16. *More Comprehensive Energetic Models*. Such models must be developed that can simultaneously quantify the energetic properties of fuel relating to both pyrolysis and combustion. As mentioned previously, any such approach should be developed for thermally thick samples that can include the effects of briquette cracking, flame spread and re-radiation effects from adjacent briquettes. This approach should be developed based on the actual kinetics of the briquette combustion process, and thus should be flexible for varying combustion atmospheric levels.
17. *Emission Gas Behavior Correlations*. The emission gas behavior must be correlated with the physicochemical, kinetic and energetic behavior and similar models must be developed to complete the understanding of emission gas behavior. Apart from $NO_x$, $CO_2$ and CO gases, other pollutant gases (such as $SO_x$) and non-pollutant gases (such as $CH_4$, $H_2$ and $H_2O$) must also be quantified to completely understand the emission gas behavior. Advanced chromatography techniques such as GC-MS, GC-FID and GC-TCD can be used apart from rack analyzers to attain this objective. Such models will be able to better predict the performance of different briquetted fuel blends in actual power plant environment, and will also be able to indicate possible improvements in the fuels, briquetting process and reactor operating conditions that will be beneficial for the power plant efficiency.

18. *Briquette Size Optimization*. The briquette size must be optimized for complete combustion of the fuel during the limited time of the combustion process in the power plant, as any un-combusted inner parts of briquettes will decrease the efficiency of the plant. This study would also require a better understanding of the thermo-mechanical and thermo-chemical behavior of the briquettes, thus leading to a future study related to briquette size optimization. The improvement briquetting technology should also be understood in terms of trying different coal-biomass blend ratios, testing briquette blends with more than two fuels, and analyzing different binding agents/techniques to make optimized briquettes for future power operation.
19. *Feasibility Analysis for a Commercial-Scale Briquetting Facility.* Additional studies should be conducted to evaluate the cost benefit for constructing briquetting facilities in various regions, based on feedstock sources (coal and biomass) and to evaluate potential markets for the coal-biomass products.

# References


Aboyade, A., Görgens, J., Carrier, M., Meyer, E., & Knoetze, J. (2013). Thermogravimetric study of the pyrolysis characteristics and kinetics of coal blends with corn and sugarcane residues. *Fuel Processing Technology, 106*, 310-320.

Aboyade, A., Hugo, T., Carrier, M., Meyer, E., Stahl, R., Knoetze, J., & Görgens, J. (2011). Non-isothermal kinetic analysis of the devolatilization of corn cobs and sugar cane bagasse in an inert atmosphere. *Thermochimica acta, 517*(1–2), 81-89.

Agarwal, G., & Lattimer, B. (2012). Method for measuring the standard heat of decomposition of materials. *Thermochimica acta, 545*(0), 34-47.

Agarwal, G., Lattimer, B., & Liu, G. (2013). Pyrolysis and combustion characterization of coal-biomass fuel blends. *Proceedings of the ASME 2013 power conference*.

Agrawal, R. (1992). Analysis of non-isothermal reaction kinetics: Part 1. Simple reactions. *Thermochimica acta, 203*, 93.

Ahmed, S., & Whalley, B. (1978). Analytical procedures for sulfur in coal desulfurization products. In Karr, C., Jr. (Ed.), *Analytical methods for coal and coal products.* San Diego, CA: Academic Press.

Ahuja, P., Kumar, S., & Singh, P. (1996). A model for primary and heterogeneous secondary reactions of wood pyrolysis. *Chemical engineering technology, 19*(3), 272-282.

Allardice, D., & Evans, D. (1978). Moisture in coal. In Karr, C., Jr. (Ed.), *Analytical methods for coal and coal products.* San Diego, CA: Academic Press.

ANSI/ASAE S424.1 (1992). *Method of determining and expressing particle size of chopped forage materials by screening.* St. Joseph, MI: American Society of Agricultural and Biological Engineers.

Anthony, D., & Howard, J. (1976). Coal devolatilization and hydrogasification. *AIChE journal, 22*(4), 625-656.

ASAE D274.1 (1992). *Flow of grain and seeds through orifices.* St. Joseph, MI: American Society of Agricultural and Biological Engineers.

ASAE S358.3 (2012). *Moisture measurement − Forages.* St. Joseph, MI: American Society of Agricultural and Biological Engineers.

ASTM C518-10 (2010). *Standard test method for steady-state thermal transmission properties by means of the heat flow apparatus.* West Conshohocken, PA: ASTM International.

ASTM D167-12a (2012). *Standard test method for apparent and true specific gravity and porosity of lump coke.* West Conshohocken, PA: ASTM International.

ASTM D1875/D1875M-04 (2010). *Standard test method for fusibility of coal and coke ash.* West Conshohocken, PA: ASTM International.

ASTM D2639-08 (2008). *Standard test method for plastic properties of coal by the constant-torque Gieseler plastometer.* West Conshohocken, PA: ASTM International.

ASTM D2766-95 (2009). *Standard test method for specific heat of liquids and solids.* West Conshohocken, PA: ASTM International.

ASTM D291-07 (2012). *Standard test method for cubic foot weight of crushed bituminous coal.* West Conshohocken, PA: ASTM International.

ASTM D3172-07a (2007). *Standard practice for proximate analysis of coal and coke.* West Conshohocken, PA: ASTM International.

ASTM D3173-11 (2011). *Standard test method for moisture in the analysis sample of coal and coke.* West Conshohocken, PA: ASTM International.

ASTM D3174-12 (2012). *Standard test method for ash in the analysis sample of coal and coke.* West Conshohocken, PA: ASTM International.

ASTM D3175-11 (2011). *Standard test method for volatile matter in the analysis sample of coal and coke.* West Conshohocken, PA: ASTM International.

ASTM D3176-09 (2009). *Standard practice for ultimate analysis of coal and coke.* West Conshohocken, PA: ASTM International.

ASTM D3177-02 (2007). *Standard test methods for total sulfur in the analysis sample of coal and coke.* West Conshohocken, PA: ASTM International.

ASTM D3302/D3302M-12 (2012). *Standard test method for total moisture in coal.* West Conshohocken, PA: ASTM International.

ASTM D3682-01 (2006). *Standard test method for major and minor elements in combustion residues from coal utilization processes.* West Conshohocken, PA: ASTM International.

ASTM D409/D409M-12 (2012). *Standard test method for grindability of coal by the Hardgrove-machine method.* West Conshohocken, PA: ASTM International.

ASTM D4208-02 (2007). *Standard test method for total chlorine in coal by the oxygen bomb combustion/ion selective electrode method.* West Conshohocken, PA: ASTM International.

ASTM D440-07 (2012). *Standard test method of drop shatter test for coal*. West Conshohocken, PA: ASTM International.

ASTM D5373-08 (2008). *Standard test methods for instrumental determination of carbon, hydrogen, and nitrogen in laboratory samples of coal.* West Conshohocken, PA: ASTM International.

ASTM D5865-12 (2012). *Standard test method for gross calorific value of coal and coke.* West Conshohocken, PA: ASTM International.

ASTM D6128-06 (2006). *Standard test method for shear testing of bulk solids using the Jenike shear cell.* West Conshohocken, PA: ASTM International.

ASTM D6683-08 (2008). *Standard test method for measuring bulk density values of powders and other bulk solids as function of compressive stress.* West Conshohocken, PA: ASTM International.

ASTM D6773-08 (2008). *Standard shear test method for bulk solids using the Schulze ring shear tester.* West Conshohocken, PA: ASTM International.

ASTM D7309-11 (2011). *Standard test method for determining flammability characteristics of plastics and other solid materials using microscale combustion calorimetry*. West Conshohocken, PA: ASTM International.

ASTM D7481-09 (2009). *Standard test methods for determining loose and tapped bulk densities of powders using a graduated cylinder.* West Conshohocken, PA: ASTM International.

ASTM E1354-14 (2014). *Standard test method for heat and visible smoke release rates for materials and products using an oxygen consumption calorimeter*. West Conshohocken, PA: ASTM International.

ASTM E1534-93 (2006). *Standard test method for determination of ash content of particulate wood fuels.* West Conshohocken, PA: ASTM International.

ASTM E1755-01 (2007). *Standard test method for ash in biomass.* West Conshohocken, PA: ASTM International.

ASTM E775-87 (2008). *Standard test method for total sulfur in the analysis sample of refuse-derived fuel.* West Conshohocken, PA: ASTM International.

ASTM E777-08 (2008). *Standard test method for carbon and hydrogen in the analysis sample of refuse-derived fuel.* West Conshohocken, PA: ASTM International.

ASTM E778-08 (2008). *Standard test method for nitrogen in the analysis sample of refuse-derived fuel.* West Conshohocken, PA: ASTM International.

ASTM E870-82 (2006). *Standard test methods for analysis of wood fuels.* West Conshohocken, PA: ASTM International.

ASTM E871-82 (2006). *Standard test method for moisture analysis of particulate wood fuels.* West Conshohocken, PA: ASTM International.

ASTM E872-82 (2006). *Standard test method for volatile matter in the analysis of particulate wood fuels.* West Conshohocken, PA: ASTM International.

Ayhan, D. (2003). Sustainable cofiring of biomass with coal. *Energy conversion and management, 44*(9), 1465-1479.

Barkia, H., Belkbir, L., & Jayaweera, S. (2004). Thermal analysis studies of oil shale residual carbon. *Journal of thermal analysis and calorimetry, 76*(2), 615-622.

Barneto, A., Carmona, J., Alfonso, J., & Ferrer, J. (2009). Use of thermogravimetry/mass spectrometry analysis to explain the origin of volatiles produced during biomass pyrolysis. *Industrial & engineering chemistry research, 48*(15), 7430-7436.

Basu, P. (2010). *Biomass gasification and pyrolysis: Practical design and theory*. Burlington, MA: Academic Press.

Basu, P., Butler, J., & Leon, M. (2011). Biomass co-firing options on the emission reduction and electricity generation costs in coal-fired power plants. *Renewable energy*, *36*(1), 282-288.

Bates, A., Heng, S., & Perry, G. (1988). *Australian Patent No. 1988016577*. Wooden, ACT: Australian Patent Office.

Baughman, G. (1978). *Synthetic fuels data handbook: U.S. oil shale, U.S. coal, oil sands.* Denver, CO: Cameron Engineers.

Bechtel, A., Gratzer, R., Sachsenhofer, R., Gusterhuber, J., Lucke, A., & Puttmann, W. (2008). Biomarker and carbon isotope variation in coal and fossil wood of central Europe through the Cenozoic. *Palaeogeography, palaeoclimatology, palaeoecology, 262*(3-4), 166-175.

Becidan, M., Várhegyi, G., Hustad, J., & Skreiberg, Ø. (2007). Thermal decomposition of biomass wastes. A kinetic study. *Industrial & engineering chemistry research, 46*(8), 2428-2437.

Beker, U. (1997). Briquetting of Afsin-Elbistan lignite of Turkey using different waste materials. *Fuel processing technology, 51*(1-2), 137-144.

Beker, U., Kucukbayrak, S., & Ozer, A. (1998). Briquetting of Afsin-Elbistan lignite. *Fuel processing technology, 55*(2), 117-127.

Bell, D., Towler, B., & Fan, M. (2011). *Coal gasification and its applications*. London, England: William Andrew.

Bennett, R. (1981). Gas conditioning. In T. Reed (Ed.), *Biomass gasification: Principles and technology*. Park Ridge, NJ: Noyes Data Corporation.

Berenbaum, R., & Brodie, I. (1959). Measurement of the tensile strength of brittle materials. *British journal of applied physics, 10*(6), 281-287.

Berkowitz, N. (1994). *An introduction to coal technology*. (2nd ed.). San Diego, CA: Academic Press.

Bhagavatula, A., Huffman, G., Shah, N., & Honaker, R. (2014). Evaluation of thermal evolution profiles and estimation of kinetic parameters for pyrolysis of coal/corn stover blends using thermogravimetric analysis. *Journal of fuels, 2014*, 1-12.

Bhagavatula, A. (2013). [Gasification of coal-biomass briquettes]. Unpublished raw data.

Biagini, E. (2002). *Energy and material recovery by thermal treatments of biomasses and wastes (co-combustion, pyrolysis and gasification)*. (Doctoral dissertation, Università di Pisa).

Biagini, E., Barontini, F., & Tognotti, L. (2006). Devolatilization of biomass fuels and biomass components studied by TG/FTIR technique. *Industrial & Engineering Chemistry Research, 45*(13), 4486-4493.

Biagini, E., Fantei, A., and Tognotti, L. (2008). Effect of the heating rate on the devolatilization of biomass residues. *Thermochimica acta, 472*(1–2), 55-63.

Biagini, E., Lippi, F., Petarca, L., & Tognotti, L. (2002). Devolatilization rate of biomasses and coal-biomass blends: An experimental investigation. *Fuel, 81*(8), 1041-1050.

Biagini, E., Narducci, P., & Tognotti, L. (2008). Size and structural characterization of lignin-cellulosic fuels after the rapid devolatilization. *Fuel, 87*(2), 177-186.

Biagini, E., & Tognotti, L. (2006). Comparison of devolatilization/char oxidation and direct oxidation of solid fuels at low heating rate. *Energy & fuels, 20*(3), 986-992.

Boley, C. & Rice, N. (1949). Methods of evaluating briquet quality. *Proceedings of a coal briquetting conference*, 31-47, Laramie, WY: University of Wyoming.

Bottinga, Y. (1969). Calculated fractionation factors for carbon and hydrogen isotope exchange in the system calcite-carbondioxide-graphite-methane-hydrogen-water vapor. *Geochimica et cosmochimica acta, 33*(1), 49-64.

Bottrell, S., Louie, P., Bartle, K., Taylor, N., Wallace, S., Kemp, W., & Steedman, W. (1990). Differentiation of forward and back reactions during co-processing of coal and petroleum by isotope mass balance analysis, *Fuel, 69*(10), 1332-1333.

Boylan, D. (1996). Southern company tests of wood/coal cofiring in pulverized coal units. *Biomass and bioenergy, 10*(2-3), 139-147.

Bradley, L., Miller, S., Miller, B., & Tillman, D. (2011). A study on the relationship between fuel composition and pyrolysis kinetics. *Energy & fuels, 25*(5), 1989-1995.

Branca, C., Albano, A., & Di Blasi, C. (2005). Critical evaluation of global mechanisms of wood devolatilization. *Thermochimica acta, 429*(2), 133-141.

Branca, C., Giudicianni, P., & Di Blasi, C. (2003). GC/MS characterization of liquids generated from low-temperature pyrolysis of wood. *Industrial & engineering chemistry research, 42*(14), 3190-3202.

Brar, J., Singh, K., Wang, J., & Kumar, S. (2012). Cogasification of coal and biomass: A review. *International journal of forestry research, 2012*(1), 1-10.

Brasseur, A., Antenucci, D., Bouquegneau, J., Coëme, A., Dauby, P., Létolle, R., Mostade, M., Pirlot, P., & Pirard, J. (2002). Carbon stable isotope analysis as a tool for tracing temperature during the El Tremedal underground coal gasification at great depth. *Fuel, 81*(1), 109-117.

Bratton, R., Luttrell, G., Kasindorf, H., McGraw, G., & McAllister, M. (2010a). Evaluation of a novel fine coal briquetting process at GreenFields Coal Company. In R. Honaker (Ed.), *International coal preparation congress 2010 conference proceedings*. Littleton, CO: Society for Mining, Metallurgy, and Exploration.

Bratton, R., Luttrell, G., Kasindorf, H., McGraw, G., & Robbins, R. (2010b) Evaluation of a novel fine coal dry cleaning process at Greenfields Coal Company. *International journal of coal preparation & utilization, 30*(2-5), 145-153.

Brown, D. (1982). The questionable use of the Arrhenius equation to describe cellulose and wood pyrolysis. *Thermochimica acta, 54*(3), 377-379.

Brown, D., & Atkin, B. (2000). A method for the rapid on-site assessment of handleability. *Coal preparation, 21*(3), 299-313.

Brown, D., Atkin, B., Miles, N., & Creasey, D. (1997). Determination of the handleability of a coal blend using an extrusion trough. *Fuel, 76*(13), 1183-1186.

Brown, D., & Miles, N. (2004). Assessment of coal handleability. *Coal preparation, 24*(3-4), 99-122.

Brown, M., Maciejewski, M., Vyazovkin, S., Nomen, R., Sempere, J., Burnham, A., Opfermann, J., Strey, R., Anderson, H., Kemmler, A., Keuleers, R., Janssens, J., Desseyn, H., Li, C.-R., Tang, T., Roduit, B., Malek, J., & Mitsuhashi, T. (2000). Computational aspects of kinetic analysis.: Part A: The ICTAC kinetics project – data, methods and results. *Thermochimica acta, 355*(1–2), 125-143.

Brown, R. (2003). *Biorenewable resources: Engineering new products from agriculture.* Ames, IA: Blackwell Publishing.

Browning, J. (1967). Agglomeration. *Chemical Engineering, 74*(25), 147-170.

Buczynaska, A., Geypens, B., Van Grieken, R., & De Wael, K. (2013). Stable carbon isotopic ratio measurement of polycyclic aromatic hydrocarbons as a tool for source identification and apportionment - A review of analytical methodologies. *Talanta, 105*, 435-450.

Burnham, A. (2000). Computational aspects of kinetic analysis.: Part D: The ICTAC kinetics project – multi-thermal-history model-fitting methods and their relation to isoconversional methods. *Thermochimica acta, 355*(1–2), 165-170.

Cai, J., Jin, C., Yang, S., & Chen, Y. (2011). Logistic distributed activation energy model – Part 1: Derivation and numerical parametric study. *Bioresource technology, 102*(2), 1556-1561.

Cai, J., Wang, Y., Zhou, L., & Huang, Q. (2008). Thermogravimetric analysis and kinetics of coal/plastic blends during co-pyrolysis in nitrogen atmosphere. *Fuel Processing Technology, 89*(1), 21-27.

Capes, C. (1980). Particle size enlargement. In J. Williams & T. Allen (Eds.), *Handbook of powder technology* (Vol. 1). Amsterdam, Netherlands: Elsevier Scientific Publishing Company.

Carpenter, A. (2008). Polygeneration from coal. London, England: IEA Clean Coal Centre.

Carslaw, H., & Jaeger, J. (1959). *Conduction of heat in solids.* (2nd ed.). Oxford, England: Oxford University Press.

Casper, J. (2010). *Fossil fuels and pollution: The future of air quality*. New York, NY: Facts on File.

CEN/TS 15370-1 (2006). *Solid biofuels − Method for the determination of ash melting behavior − Part 1: Characteristic temperatures method.* Brussels, Belgium: European Committee for Standardization.

Cercone, K., Deming, D., & Pollack, H. (1996). Insulating effect of coals and black shales in the Appalachian Basin, Western Pennsylvania. *Organic chemistry, 24*(2), 243-249.

Channiwala, S., & Parikh, P. (2002). A unified correlation for estimating HHV of solid, liquid, and gaseous fuels. *Fuel, 81*(8), 1051-1063.

Coats, A., & Redfern, J. (1964). Kinetic parameters from thermogravimetric data. *Nature, 201*(1), 68-69.

Collazo, J., Pazo, J., Granada, E., Saavedra, A., & Eguia, P. (2012). Determination of the specific heat of biomass materials and the combustion energy of coke by DSC analysis. *Energy, 45*(1), 746-752.

Collot, A. (2002). *Matching gasifiers to coals*. London, England: IEA Clean Coal Centre.

Collot, A. (2006). Matching gasification technologies to coal properties. *International journal of coal geology, 65*(3), 191-212.

Colomba, D. (1993). Modeling and simulation of combustion processes of charring and non-charring solid fuels. *Progress in energy and combustion science, 19*(1), 71-104.

Conkle, H. (1992). *Pelletization/reslurrying as a means of distributing and firing clean coal: Final report*. USDoE contract DE-AC22-PC90166. Submitted to Pittsburgh Energy Technology Center, U.S. Department of Energy, Pittsburgh, PA.

Couch, G. (2008). *Coal to liquids*. London, England: IEA Clean Coal Centre.

Cozzani, V., Petarca, L., & Tognotti, L. (1995). Devolatilization and pyrolysis of refuse derived fuels: Characterization and kinetic modelling by a thermogravimetric and calorimetric approach. *Fuel, 74*(6), 903-912.

Craig, H. (1957). Isotopic standards for carbon and oxygen and correction factors for mass-spectrometric analysis of carbon dioxide. *Geochimica et cosmochimica acta, 12*(1-2), 133-149.

Crooks, E. (2012). *EPA seeks strict limits on coal plants.* London, England: The Financial Times Limited (FT.com).

Cummer, K., & Brown, R. (2002). Ancillary equipment for biomass gasification. *Biomass and bioenergy, 23*(2), 113-128.

Dec, R., & Komarek, R. (1997). Testing and scaling up compaction process using small laboratory roll press. *Proceedings of the 25th biennial conference of the Institute for Briquetting and Agglomeration*, 97-106, Albuquerque, NM: Institute for Briquetting and Agglomeration.

Demirbaş, A. (2003). Sustainable cofiring of biomass with coal. *Energy conversion and management, 44*(9), 1465-1479.

Demirbaş, A. (1997). Calculation of higher heating values of biomass fuels. *Fuel, 76*(5), 431-434.

Desrosiers, R. (1981). Thermodynamics of gas-char reactions. In T. Reed (Ed.), *Biomass gasification: Principles and technology*. Park Ridge, NJ: Noyes Data Corporation.

Di Blasi, C. (2008). Modeling chemical and physical processes of wood and biomass pyrolysis. *Progress in energy and combustion science, 34*(1), 47-90.

Di Blasi, C., Signorelli, G., & Portoricco, G. (1999). Countercurrent fixed-bed gasification of biomass at laboratory scale. *Industrial and engineering chemistry research, 38*(7), 2571-2581.

Di Nola, G., de Jong, W., & Spliethoff, H. (2010). TG-FTIR characterization of coal and biomass single fuels and blends under slow heating rate conditions: Partitioning of the fuel-bound nitrogen. *Fuel processing technology, 91*(1), 103-115.

Dohm E., Luttrell G., Karmis M., and Ripepi N. (2013). Optimization of binderless briquetting coal-biomass mixtures. *Proceedings of the 6th international conference on clean coal technologies*.

Doroodchi, E., Zulfiqar, H., & Moghtaderi, B. (2013). A combined experimental and theoretical study on laboratory-scale comminution of coal and biomass blends. *Powder technology, 235*(1), 412-421.

Drzymala, Z. (1993). *Industrial briquetting: Fundamentals and methods*. Warsaw, Poland: Polish Scientific Publishers.

Dufaux, A., Gaveau, B., Létolle, R., Mostade, M., Noël, M., & Pirard, J. (1990). Heavy water tracing test in the underground coal gasification process at Thulin. *Fuel, 69*(11), 1454-1456.

Dutta, A., & Leon, M. (2011). Pros and cons of torrefaction of woody biomass. *Proc. of: Short-Rotation Afforestation and Agroforestry Systems for Energy Purposes and GHG Reduction: Joint ecoETI & CEF Projects Workshop*, Turfgrass Inst., University of Guelph.

Dutta, S., Wen, C., & Belt, R. (1977). Reactivity of coal and char. 1. In carbon dioxide atmosphere. *Industrial and engineering chemistry process design and development, 16*(1), 20-30.

Eckerd, J. (1967). Development of standard procedures for testing fuel briquets. *Proceedings of the 10th biennial briquetting conference*, 95-99, Albuquerque, NM: Institute for Briquetting and Agglomeration.

EN 14774-1 (2009). *Solid biofuels − Determination of moisture content − Oven dry method − Part 1: Total moisture − Reference method.* Brussels, Belgium: European Committee for Standardization.

EN 14774-2 (2009). *Solid biofuels − Determination of moisture content − Oven dry method − Part 2: Total moisture − Simplified method.* Brussels, Belgium: European Committee for Standardization.

EN 14774-3 (2009). *Solid biofuels − Determination of moisture content − Oven dry method − Part 3: Total moisture − Moisture in general analysis sample.* Brussels, Belgium: European Committee for Standardization.

EN 14775 (2009). *Solid biofuels − Determination of ash content.* Brussels, Belgium: European Committee for Standardization.

EN 14918 (2009). *Solid biofuels − Determination of calorific value.* Brussels, Belgium: European Committee for Standardization.

EN 15103 (2009). *Solid biofuels − Determination of bulk density.* Brussels, Belgium: European Committee for Standardization.

EN 15104 (2011). *Solid biofuels − Determination of total content of carbon, hydrogen and nitrogen − instrumental methods.* Brussels, Belgium: European Committee for Standardization.

EN 15148 (2009). *Solid biofuels − Determination of the content of volatile matter.* Brussels, Belgium: European Committee for Standardization.

EN 15149-2 (2010). *Solid biofuels − Determination of particle size distribution − Part 2: Vibrating screen method using sieve apertures of 3,15 mm and below.* Brussels, Belgium: European Committee for Standardization.

EN 15150 (2011). *Solid biofuels − Determination of particle density.* Brussels, Belgium: European Committee for Standardization.

EN 15210-2 (2010). *Solid biofuels – Determination of mechanical durability of pellets and briquettes – Part 2: Briquettes.* Brussels, Belgium: European Committee for Standardization.

EN 15289 (2011). *Solid biofuels − Determination of total content of sulfur and chlorine.* Brussels, Belgium: European Committee for Standardization.

Ergun, S. (1951). Determination of particle density of crushed porous solids. *Analytical chemistry, 23*(1), 151-156.

Ettinger, I., & Zhupakhina, E. (1960). Method of determining porosity of mineral coals. *Fuel, 39*(5), 387-392.

Fell, J., & Newton, J. (1968). The tensile strength of lactose tablets. *Journal of pharmacy and pharmacology, 20*(8), 657-659.

Fermoso, J., Arias, B., Gil, M., Pevida, C., Pis, J., & Rubiera, F. (2010). Co-gasification of different rank coals with biomass and petroleum coke in a high-pressure reactor for $H_2$-rich gas production. *Bioresource technology, 101*(9), 3230-3235.

Fermoso, J., Gil, M., Pevida, C., Pis, J., & Rubiera, F. (2010). Kinetic models comparison for non-isothermal steam gasification of coal–biomass blend chars. *Chemical engineering journal, 161*(1–2), 276-284.

Fernando, R. (2005). *Fuels for biomass cofiring*. London, England: IEA Clean Coal Centre.

Fernando, R. (2008). *Coal gasification*. London, England: IEA Clean Coal Centre.

Fernando, R. (2009). *Co-gasification and indirect cofiring of coal and biomass*. London, England: IEA Clean Coal Centre.

Folgueras, M., Díaz, R., Xiberta, J., & Prieto, I. (2003). Thermogravimetric analysis of the co-combustion of coal and sewage sludge. *Fuel, 82*(15-17), 2051-2055.

Follett, R., Vogel, K., Varvel, G., Mitchell, R., & Kimble, J. (2012). Soil carbon sequestration by switchgrass and no-till maize grown for bioenergy. *Bioenergy research, 5*(4), 866-875.

Frederick, W., & Mentzer, C. (1975). Determination of heats of volatilization for polymers by differential scanning calorimetry. *Journal of applied polymer science, 19*(7), 1799-1804.

Freeman, E., & Carroll, B. (1958). The application of thermoanalytical techniques to reaction kinetics: The thermogravimetric evaluation of the kinetics of the decomposition of calcium oxalate monohydrate. *The journal of physical chemistry, 62*(4), 394-397.

Freitag, W. (1996). Principles of application. In D. Stoye & W. Freitag (Eds.), *Resins for coatings: Chemistry, properties and applications*, 40-44. Cincinnati, Ohio: Hanser/Gardner Publications.

Gan, H., Nandi, S., & Walker, P., Jr. (1972). Nature of the porosity in American coals. *Fuel, 51*(4), 272-277.

Gaston, K., Jarvis, M., Pepiot, P., Smith, K., Frederick, W., Jr., & Nimlos, M. (2011). Biomass pyrolysis and gasification of varying particle sizes in a fluidized-bed reactor. *Energy & fuels, 25*(8), 3747-3757.

Geyer, W., DeWyke, J., & Walawender, W. (2000). Biomass and gasification properties of young populous clones. *Wood and fiber science, 32*(3), 375-384.

Ghosh, D., Sagar, A., and Kishore, V. (2006). Scaling up biomass gasifier use: An application-specific approach. *Energy policy, 34*(13), 1566-1582.

Gil, M., Casal, D., Pevida, C., Pis, J., & Rubiera, F. (2010a). Thermal behaviour and kinetics of coal/biomass blends during co-combustion. *Bioresource technology, 101*(14), 5601-5608.

Gil, M., Oulego, P., Casal, M., Pevida, C., Pis, J., & Rubiera, F. (2010b). Mechanical durability and combustion characteristics of pellets from biomass blends. *Bioresource technology, 101*(22), 8859-8867.

Giuntoli, J., Arvelakis, S., Spliethoff, H., de Jong, W., & Verkooijen, A. (2009). Quantitative and kinetic thermogravimetric Fourier transform infrared (TG-FTIR) study of pyrolysis of agricultural residues: Influence of different pretreatments. *Energy & fuels, 23*(11), 5695-5706.

Goleczka, J., Harris, W., & Pringle, J. (1988). *U. S. Patent No. 4,738,685*. Washington, DC: U.S. Patent and Trademark Office.

Gomez, C., Velo, E., Barontini, F., & Cozzani, V. (2009). Influence of secondary reactions on the heat of pyrolysis of biomass. *Industrial & engineering chemistry research, 48*(23), 10222-10233.

Gomez-Barea, A., & Leckner, B. (2010). Modeling of biomass gasification in fluidized bed. *Progress in energy and combustion science, 36*(4), 444-509.

Gopalakrishnan, S., & Sujatha, R. (2011). Comparative thermoanalytical studies of polyurethanes using Coats-Redfern, Broido and Horowitz-Metzger methods. *Der Chemica Sinica, 2*(5), 103-117.

Gorbaty, M., Kelemen, S., George, G., & Kwiatek, P. (1992). Characterization and thermal reactivity of oxidized organic sulphur forms in coals. *Fuel, 71*(11), 1255-1264.

Gordillo, G., Annamalai, K., & Carlin, N. (2009). Adiabatic fixed-bed gasification of coal, dairy biomass, and feedlot biomass using an air-steam mixture as an oxidizing agent. *Renewable energy, 34*(12), 2789-2797.

Goss, W. (1938). *U.S Patent No. 2,114,377*. Washington, DC: U.S. Patent and Trademark Office.

Graboski, M. (1981). Kinetics of char gasification reactions. In T. Reed (Ed.), *Biomass gasification: Principles and technology*. Park Ridge, NJ: Noyes Data Corporation.

Graboski, M., & Bain, R. (1981). Properties of biomass relevant to gasification. In T. Reed (Ed.), *Biomass gasification: Principles and technology*. Park Ridge, NJ: Noyes Data Corporation.

Grigorova, I., & Kuzev, L. (2003). Briquetting of brown coals with a binding agent modified amylum with soluble colophony, Annual of University of Mining and Geology "St. Ivan Rilski", *Mining and Mineral Processing, 46*(II).

Grønli, M., Várhegyi, G., & Di Blasi, C. (2002). Thermogravimetric analysis and devolatilization kinetics of wood. *Industrial & engineering chemistry research, 41*(17), 4201-4208.

Gryczka, O., Heinrich, S., Miteva, V., Deen, N., Kuipers, J., Jacob, M., & Mörl, L. (2008). Characterization of the pneumatic behavior of a novel spouted bed apparatus with two adjustable gas inlets. *Chemical engineering science, 63*(3), 791-814.

Guigon, P., & Simon, O. (2003). Roll press design – influence of force feed systems on compaction. *Powder technology, 130*(1-3), 41-48.

Hale, S., Kelly, S., & Tayler, R. (1989). *European Patent Application No. 0377995 A2*. Munich, Germany: European Patent Office.

Hall, D., & Cutress, J. (1960). The effect of fines content, moisture and added oil on the handling of small coal. *Journal of the institute of fuel, 33*(1), 63-72.

Hanson, S., Patrick, J., & Walker, A. (2002). The effect of coal particle size on pyrolysis and steam gasification. *Fuel, 81*(5), 531-537.

Hashimoto, K., Hasegawa, I., Hayashi, J., & Mae, K. (2011). Correlations of kinetic parameters in biomass pyrolysis with solid residue yield and lignin content. *Fuel, 90*(1), 104-112.

Haslbeck, J., Kuehn, N., Lewis, E., Pinkerton, L., Simpson, J., Turner, M., Varghese, E., & Woods, M. (2010). *Cost and performance baseline for fossil energy plants − Volume 1: Bituminous coal and natural gas to electricity.* Washington, DC: U.S. Department of Energy.

Hatakeyama, T. & Quinn, F. (1999). *Thermal analysis: Fundamentals and applications to polymer science.* Chichester, England: John Wiley and Sons.

Hattingh, B., Everson, R., Neomagus, H., & Bunt, J. (2011). Assessing the catalytic effect of coal ash constituents on the $CO_2$ gasification rate of high ash, South African coal. *Fuel processing technology, 92*(10), 2048-2054.

Heikkinen, J., Hordijk, J., de Jong, W., & Spliethoff, H. (2004). Thermogravimetry as a tool to classify waste components to be used for energy generation. *Journal of analytical and applied pyrolysis, 71*(2), 883-900.

Henderson, J., & Emmerich, W. (1991). Measurement of specific heat and energetic characterization of materials up to high temperatures. *Journal of thermal analysis and calorimetry, 37*(8), 1979-1985.

Henderson, J., Wiebelt, J., Tant, M., & Moore, G. (1982). A method for the determination of the specific heat and heat of decomposition of composite materials. *Thermochimica acta, 57*(2), 161-171.

Herrin, J., & Deming, D. (1996). Thermal conductivity of U.S. coals. *Journal of geophysical research, 101*(B11), 25381-25386.

Higman, C., & van der Burgt, M. (2003). *Gasification*. Burlington, MA: Gulf Professional Publishing.

Higman, C., & van der Burgt, M. (2008). *Gasification*. (2nd ed.) Burlington, MA: Elsevier Inc.

Hoefs, J., & Usdowski, E. (1987). C-13/C-12 Fractionation and kinetics of $CO_2$ absorption by hydroxide solutions. *Fortschritte der mineralogie, 65*, 76-76.

Holley, C., & Antonetti, J. (1977). Agglomeration of coal fines. *Proceedings of the 15th biennial conference of the Institute for Briquetting and Agglomeration*, 1-12, Albuquerque, NM: Institute for Briquetting and Agglomeration.

Honaker, R., Parekh, B., Taulbee, D., & Tao, D. (2005). *Premium fuel production from mining and timber waste using advanced separation and pelletizing technologies*. Washington, DC: U.S. Department of Energy.

Hong, B., & Slatick, E. (1994). *Carbon dioxide emission factors for coal*. Quarterly Coal Report, U.S. Energy Information Administration, Washington, DC.

Huang, F., Kuan, H., Chiueh, T., & Lo, L. (2011). Pyrolysis of biomass by thermal analysis–mass spectrometry (TA–MS). *Bioresource technology, 102*(3), 3527-3534.

Hunt, E., Prinzing, D., Battista, J., & Hughes, E. (1997). The shawville coal/biomass cofiring test: A coal/power industry cooperative test of direct fossil-fuel $CO_2$ mitigation. *Energy conversion and management, 38*(Supplement), S551-S556.

Hurst, H., Novak, F., & Patterson, J. (1999). Viscosity measurements and empirical predictions for some model gasifier slags. *Fuel, 78*(4), 439-444.

Hurt, R., Davis, K., Yang, N., Headley, T., & Mitchell, G. (1995). Residual carbon from pulverized-coal-fired boilers. 2. Morphology and physicochemical properties. *Fuel, 74*(9), 1297-1306.

Idris, S., Abd Rahman, N., Ismail, K., Alias, A., Abd Rashid, Z., & Ariz, M. (2010). Investigation of thermochemical behavior of low rank Malaysian coal, oil palm biomass and their blends during pyrolysis via thermogravimetric analysis (TGA). *Bioresource technology, 101*(12), 4584-4592.

Janse, A., Westerhout, R., & Prins, W. (2000). Modelling of flash pyrolysis of a single wood particle. *Chemical engineering and processing: Process intensification, 39*(3), 239-252.

Jeguirim, M., & Trouve, G. (2009). Pyrolysis characteristics and kinetics of Arundo donax using thermogravimetric analysis. *Bioresource technology, 100*(17), 4026-4031.

Jenike, A. (1964). Storage and flow of solids, *University of Utah engineering experiment station, Bulletin number 123*.

Jenkins, B. (1989). Physical properties of biomass. In O. Kitani & C. Hall (Eds.), *Biomass handbook.* New York, NY: Gordon and Breach Science Publishers.

Jenkins, B., Baxter, L., Miles, T., Jr., Miles, T. (1998). Combustion properties of biomass. *Fuel processing technology, 54*(1-3), 17-46.

Jerez, A. (1983). A modification to the Freeman and Carroll method for the analysis of the kinetics of non-isothermal processes. *Journal of thermal analysis, 26*(2), 315-318.

Jong, W., Nola, G., Venneker, B., Spliethoff, H., & Wojtowicz, M. (2007). TG–FTIR pyrolysis of coal and secondary biomass fuels: determination of pyrolysis kinetic parameters for main species and NOx precursors. *Fuel, 86*(15), 2367-2376.

Kaliyan, N., & Morey, R. (2008). *Binding mechanisms of corn stover and switchgrass in briquettes and pellets*. ASABE Paper No. 084282. St. Joseph, MI: ASABE.

Kaliyan, N., & Morey, R. (2009). Factors affecting strength and durability of densified biomass products. *Biomass and bioenergy, 33*(3), 337-359.

Kansa, E., Perlee, H., & Chaiken, R. (1977). Mathematical model of wood pyrolysis including internal forced convection. *Combustion and flame, 29*(0), 311-324.

Kanury, A., & Blackshear, P. (1970). Some considerations pertaining to the problem of wood-burning. *Combustion science and technology, 1*(5), 339-356.

Karimipour, S., Gerspacher, R., Gupta, R., & Spiteri, R. (2013). Study of factors affecting syngas quality and their interactions in fluidized bed gasification of lignite coal. *Fuel, 103*, 308-320.

Katzer, J., Ansolabehere, S., Beer, J., Deutch, J., Ellerman, A., Friedmann, S., Herzog, H., Jacoby, H., Joskow, P., Mcrae, G., Lester, R., Moniz, E., & Steinfeld, E. (2007). *The future of coal − Options for a carbon-constrained world*. Cambridge, MA: Massachusetts Institute of Technology.

Khambeckar, J., Barnum, R., & Hossfeld, R. (2010). Achieving reliable material flow in coal preparation plants. *CPSA journal, 9*(2), 12-15.

Khelfa, A., Finqueneisel, G., Auber, M., & Weber, J. (2008). Influence of some minerals on the cellulose thermal degradation mechanisms. *Journal of thermal analysis and calorimetry, 92*(3) 795-799.

Kim, Y., Seo, D., & Hwang, J. (2011). Study of the effect of coal type and particle size on char-$CO_2$ gasification via gas analysis. *Energy & fuels, 25*(11), 5044-5054.

Kissinger, H. (1957). Reaction kinetics in differential thermal analysis. *Analytical chemistry, 29*(11), 1702-1706.

Klass, D. (1998). *Biomass for renewable energy, fuels, and chemicals*. San Diego, CA: Academic Press.

Komarek, R. (1991). Binderless briquetting of peat, lignite, sub-bituminous and bituminous coals in roll press. *Proceedings of the 22nd biennial conference of the Institute for Briquetting and Agglomeration*, 233-242, Albuquerque, NM: Institute for Briquetting and Agglomeration.

Koppejan, J., & Brem, G. European Commission, Intelligent Energy − Europe. (2008). *Cofiring and co-processing biomass with coal* (WP2B Deliverable 2B-5).

Koppejan, J., Sokhansanj, S., Melin, S., & Madrali, S. (2012). Final report: Status overview of torrefaction technologies. *IEA Bioenergy Task 32 Report,* Enschede, Netherlands.

Koufopanos, C., Lucchesi, A., & Maschio, G. (1989). Kinetic modelling of the pyrolysis of biomass and biomass components. *The Canadian journal of chemical engineering, 67*(1), 75-84.

Koufopanos, C., & Papayannakos, N. (1991). Modeling of the pyrolysis of biomass particles: studies on kinetics thermal and heat transfer effects. *Canadian journal of chemical engineering, 69*(4), 907-915.

Kriech, A., & Dobbs, T. (2003). *U. S. Patent No. 6,530,966*. Washington, DC: U.S. Patent and Trademark Office.

Kristiansen, A. (1996). *Understanding coal gasification*. London, England: IEA Clean Coal Centre.

Kumabe, K., Hanaoka, T., Fujimoto, S., Minowa, T., & Sakanishi, K. (2007). Co-gasification of woody biomass and coal with air and steam. *Fuel, 86*(5-6), 684-689.

Kumar, A., Jones, D., & Hanna, M. (2009). Thermochemical biomass gasification: A review of the current status of the technology. *Energies, 2*(3), 556-581.

Lancet, M., Winschel, R., & Burke, F. (1993). Stable carbon-isotope analysis of coprocessing materials. *Fuel, 72*(8), 1209-1217.

Lapuerta, M., Hernández, J., Pazo, A., & López, J. (2008). Gasification and co-gasification of biomass wastes: Effect of the biomass origin and the gasifier operating conditions. *Fuel processing technology, 89*(9), 828-837.

Larsson, S., Thyrel, M., Geladi, P., & Lestander, T. (2008). High quality biofuel pellet production from pre-compacted low density raw materials. *Bioresource technology, 99*(15), 7176-7182.

Lester, E., Gong, M., & Thompson, A. (2007). A method for source apportionment in biomass/coal blends using thermogravimetric analysis. *Journal of analytical and applied pyrolysis, 80*(1), 111-117.

Li, C., & Suzuki, K. (2009). Kinetic analyses of biomass tar pyrolysis using the distributed activation energy model by TG/DTA technique. *Journal of thermal analysis and calorimetry, 98*(1), 261-266.

Li, Z., Liu, C., Chen, Z., Qian, J., Zhao, W., & Zhu, Q. (2009). Analysis of coals and biomass pyrolysis using the distributed activation energy model. *Bioresource technology, 100*(2), 948-952.

Liang, C., Chen, X., Xu, P., Liu, B., Zhao, C., & Xu, C. (2011). Effect of moisture content on conveying characteristics of pulverized coal for pressurized entrained flow gasification. *Experimental thermal and fluid science, 35*(6), 1143-1150.

Lindeburg, M. (1989). *Civil engineering reference manual* (5th ed.). Belmont, CA: Professional Publications, Inc.

Liu, K., Song, C., & Subramani, V. (2010). *Hydrogen and syngas production and purification technologies*. Hoboken, NJ: John Wiley and Sons.

Long, H., III, & Wang, T. (2011). *Case studies for biomass/coal co-gasification in IGCC applications*. Vancouver, Canada: ASME Turbo Expo 2011.

Loulou, T., Salvador, S., & Dirion, J. (2003). Determination of reaction parameters for cardboard thermal degradation using experimental data. *Chemical engineering research and design, 81*(9), 1265-1270.

Lundwall, A. (1939). *U.S. Patent No. 2,155,500*. Washington, DC: U.S. Patent and Trademark Office.

Luo, S., Xiao, B., Guo, X., Hu, Z., Liu, S., & He, M. (2009). Hydrogen-rich gas from catalytic steam gasification of biomass in a fixed bed reactor: Influence of particle size on gasification performance. *International journal of hydrogen energy, 34*(3), 1260-1264.

Luttrell, G., Kohmuench, J., & Yoon, R.-H. (2000). An evaluation of coal preparation technologies for controlling trace element emissions. *Fuel processing technology, 65–66*(0), 407-422.

Lyon, R. (2000). Heat release kinetics. *Fire and materials, 24*(4), 179-186.

Lyon, R., & Walters, R. (2004). Pyrolysis combustion flow calorimetry. *Journal of analytical and applied pyrolysis, 71*(1), 27-46.

Mahajan, O., & Walker, P., Jr. (1978). Porosity of coals and coal products. In Karr, C., Jr. (Ed.), *Analytical methods for coal and coal products.* San Diego, CA: Academic Press.

Major, B., & Radu, G. (1998). *U. S. Patent No. 6,013,116*. Washington, DC: U.S. Patent and Trademark Office.

Mangena, S., & du Cann, V. (2007). Binderless briquetting of some selected South African prime coking, blend coking and weathered bituminous coals and the effect of coal properties on binderless briquetting. *International journal of coal geology, 71*(2-3), 303-312.

Mani, S., Tabil, L., & Sokhansanj, S. (2003). An overview of compaction of biomass grinds. *Powder handling and processing, 15*(3), 160-168.

Manyà, J., Velo, E., & Puigjaner, L. (2002). Kinetics of biomass pyrolysis: A reformulated three-parallel-reactions model. *Industrial & engineering chemistry research, 42*(3), 434-441.

Marek, M. (2000). Computational aspects of kinetic analysis.: Part B: The ICTAC kinetics project – the decomposition kinetics of calcium carbonate revisited, or some tips on survival in the kinetic minefield. *Thermochimica acta, 355*(1–2), 145-154.

Matthews, D., & Hayes, J. (1978). Isotope-ratio-monitoring gas chromatography-mass spectrometry. *Analytical chemistry, 50*(11), 1465-1473.

McRae, C., Sun, C., Snape, C., Fallick, A., & Taylor, D. (1999). $\delta^{13}C$ values of coal-derived PAHs from different processes and their application to source apportionment. *Organic geochemistry, 30*(8), 881-889.

Meesri, C., & Moghtaderi, B. (2002). Lack of synergetic effects in the pyrolytic characteristics of woody biomass/coal blends under low and high heating rate regimes. *Biomass and bioenergy, 23*(1), 55-66.

Mehrotra, V. (1980). *Pelletization of coal fines - kinetic and strength aspects*. (Doctoral dissertation, University of California, Berkeley).

Mehta, R. (1996). *Pelletization studies of ultra-fine clean coal.* (Master's thesis, University of Kentucky).

Messman, H. (1977). Introduction. In H. Messman & T. Tibbetts (Eds.), *Elements of briquetting and agglomeration*. Las Cruces, NM: Institute for Briquetting and Agglomeration.

Mészáros, E., Várhegyi, G., Jakab, E., & Marosvölgyi, B. (2004). Thermogravimetric and reaction kinetic analysis of biomass samples from an energy plantation. *Energy & fuels, 18*(2), 497-507.

Mikka, A., & Smitham, J. (1985). Coal handleability assessment. *Proceedings of the third Australian coal preparation conference*, 12-27.

Miller, M., & Martin, D. (1980). *U. S. Patent No. 4,235,603*. Washington, DC: U.S. Patent and Trademark Office.

Mills, J. U.S. Department of the Interior, United States Geological Survey. (1908). *Binders for coal briquets: Investigations made at the fuel-testing plant: St. Louis, Mo.* (Bulletin 343).

Mills, K., & Rhine, J. (1989a). The measurement and estimation of the physical properties of slags formed during coal gasification. 1. Properties relevant to fluid flow. *Fuel, 68*(2), 193-200.

Mills, K., & Rhine, J. (1989b). The measurement and estimation of the physical properties of slags formed during coal gasification. 2. Properties relevant to heat transfer. *Fuel, 68*(7), 904-910.

Milosavljevic, I., & Suuberg, E. (1995). Cellulose thermal decomposition kinetics: Global mass loss kinetics. *Industrial & engineering chemistry research, 34*(4), 1081-1091.

Minchener, A. (2005). Coal gasification for advanced power generation. *Fuel, 84*(17), 2222-2235.

Moore, J. (1957). Proposals of the standards committee. *Proceedings of the 5th biennial briquetting conference*, 37-40, Laramie, WY: International Briquetting Association.

Mondal, P., Dang, G., & Garg, M. (2011). Syngas production through gasification and cleanup for downstream applications − Recent developments. *Fuel processing technology, 92*(8), 1395-1410.

Montagnaro, F., Brachi, P., & Salatino, P. (2011). Char-wall interaction and properties of slag waste in entrained-flow gasification of coal. *Energy & fuels, 25*(8), 3671-3677.

Motaung, S., Mangena, S., de Korte, G. (2007). Effects of coal composition and flotation reagents on the water resistance of binderless briquettes. *Coal preparation, 27*(4), 230-248.

Mulvaney, D., & Robbins, P. (Eds.). (2011). *Green energy: An a-to-z guide.* Thousand Oaks, CA: SAGE Publications.

Munir, S., Nimmo, W., & Gibbs, B. (2010). Co-combustion of agricultural residues with coal: Turning waste into energy. *Energy & fuels, 24*(3), 2146-2153.

Muthuraman, M., Namioka, T., & Yoshikawa, K. (2010). A comparative study on co-combustion performance of municipal solid waste and Indonesian coal with high ash Indian coal: A thermogravimetric analysis. *Fuel processing technology, 91*(5), 550-558.

Naik, S., Goud, V., Rout, P., Jacobson, K., & Dalai, A. (2010). Characterization of Canadian biomass for alternative renewable biofuel. *Renewable energy, 35*(8), 1624-1631.

Nattermann, C., & Hutinger, K. (1994). Correlations between coal reactivity and inorganic matter content for pressure gasification with steam and carbon dioxide. *Fuel, 73*(10), 1682-1684.

Navarro, M., Murillo, R., Mastral, A., Puy, N., & Bartroli, J. (2009). Application of the distributed activation energy model to biomass and biomass constituents devolatilization. *AIChE journal, 55*(10), 2700-2715.

Ndaji, F., Ellyatt, W., Malik, A., & Thomas, K. (1999). Temperature programmed combustion studies of the co-processing of coal and waste materials. *Fuel, 78*(3), 301-307.

Nowok, J. (1994). Viscosity and phase transformation in coal ash slags near and below the temperature of critical viscosity. *Energy & fuels, 8*(6), 1324-1336.

Nussbaumer, T. (2003). Combustion and co-combustion of biomass: Fundamentals, technologies, and primary measures for emission reduction. *Energy & fuels*, *17*(6), 1510-1521.

Okuda, T., Kumata, H., Naraoka, H., & Takada, H. (2002). Origin of atmospheric polycyclic aromatic hydrocarbons (PAHs) in Chinese cities solved by compound-specific stable carbon isotopic analyses. *Organic geochemistry, 33*(12), 1737-1745.

Opfermann, J. (2000). Kinetic analysis using multivariate non-linear regression. I. Basic concepts. *Journal of thermal analysis and calorimetry, 60*(2), 641-658.

Opfermann, J., Kaisersberger, E., & Flammersheim, H. (2002). Model-free analysis of thermoanalytical data-advantages and limitations. *Thermochimica acta, 391*(1–2), 119-127.

Osborne, D. (1988). *Coal preparation technology*. London, England: Graham & Trotman.

Osvalda, S. (2007) Kinetics of pyrolysis, combustion and gasification of three biomass fuels. *Fuel processing technology, 88*(1), 87-97.

Otero, M., Díez, C., Calvo, L., García, A., & Morán, A. (2002). Analysis of the co-combustion of sewage sludge and coal by TG-MS. *Biomass and bioenergy, 22*(4), 319-329.

Ozum, B., Kovacik, G., & Chambers, A. (1993). Coal gasification gas cleanup. *International journal of hydrogen energy, 18*(10), 847-851.

Pan, Y., Velo, E., Roca, X., Manya, J., & Puigjaner, L. (2000). Fluidized-bed co-gasification of residual biomass/poor coal blends for fuel gas production. *Fuel, 79*(11), 1317-1326.

Parikh, J., Channiwala, S., & Ghosal, G. (2005). A correlation for calculating HHV from proximate analysis of solid fuels. *Fuel, 84*(5), 487-494.

Park, D., Kim, S., Lee, S., & Lee, J. (2010). Co-pyrolysis characteristics of sawdust and coal blend in TGA and a fixed bed reactor. *Bioresource technology, 101*(15), 6151-6156.

Patil, D., Taulbee, D., Parekh, B., & Honaker, R. (2009). Briquetting of coal fines and sawdust – Effect of particle-size distribution. *International journal of coal preparation and utilization, 29*(1), 251-264.

Peksa, M., Dolzan, P., Grassi, A., Heinimö, J., Junginger, H., Ranta, T.-M., & Walter, A. (2007). Global wood pellets markets and industry: Policy drivers, market status and raw material potential. *IEA bioenergy task 40.*

Perry, R., & Chilton, C. (1973). *Chemical engineer's handbook*. (5th ed.). Tokyo, Japan: McGraw-Hill Kogakusha.

Petrakis, L., & Grandy, D. (1980). Coal analysis, characterization and petrography. *Journal of chemical education, 57*(10), 689-694.

Phanphanich, M., & Mani, S. (2012). Impact of torrefaction on the grindability and fuel characteristics of forest biomass. *Bioresource technology, 102*(2), 1246–1253.

Pickard, E., Roll, W., & Ramser, J. (1961). Fundamentals of hay wafering. *Transactions of the American Society of Agricultural Engineers, 4*(1), 65-68.

Pietsch, W. (2002). *Agglomeration processes: Phenomena, technologies, equipment*. Weinheim, Germany: Wiley-VCH.

Pietsch, W. (2005). *Agglomeration in industry: Occurrence and applications*. Weinheim, Germany: Wiley-VCH.

Pinto, F., Andre, R., Franco, C., Lopes, H., Carolino, C., Costa, R., & Gulyurtlu, I. (2010). Co-gasification of coal and wastes in a pilot-scale installation. 2: Effect of catalysts in syngas treatment to achieve sulphur and nitrogen compounds abatement. Fuel, 89(11), 3340-3351.

Plancher, H., Agarwal, P., & Severns, R. (2002). Improving form coke briquette strength. Fuel processing technology, 79(2), 83-92.

Please, C., McGuinness, M., & McElwain, D. (2003). Approximations to the distributed activation energy model for the pyrolysis of coal. *Combustion and flame, 133*(1-2), 107-117.

Prescott, J., & Barnum, R. (2000). On powder flowability. Pharmaceutical technology, 24, 60-84.

Prins, M., Plasinski, K., & Janssen, F. (2007). From coal to biomass gasification: Comparison of thermodynamic efficiency. *Energy, 32*(7), 1248-1259.

Prostel, E., (1953). Report on physical tests used by operating briquetting plants. Proceedings of the 3rd biennial briquetting conference, 67-70, Laramie, WY: International Briquetting Association.

Pyle, D., & Zaror, C. (1984). Heat transfer and kinetics in the low temperature pyrolysis of solids. *Chemical engineering science, 39*(1), 147-158.

Quick, J. (2010). Carbon dioxide emission factors for U.S. coal by origin and destination. *Environmental science and technology, 44*(7), 2709-2714.

Rabier, F., Temmerman, M., Bohm, T., Hartmann, H., Jensen, P., Rathbauer, J., & Fernandez, M. (2006). Particle density determination of pellets and briquettes. Biomass and bioenergy, 30(11), 954-963.

Radmanesh, R., Courbariaux, Y., Chaouki, J., & Guy, C. (2006). A unified lumped approach in kinetic modeling of biomass pyrolysis. *Fuel, 85*(9), 1211-1220.

Rastogi, S., & Klinzing, G. (1994). Characterizing the rheology of powders by studying dynamic avalanching of the powder. *Particle and particle systems characterization, 11*(6), 453-456.

Ratafia-Brown, J., Manfredo, L., Hoffmann, J., & Ramezan, M. (2002). *Major environmental aspects of gasification-based power generation technologies*. Washington, DC: U.S. Department of Energy.

Rath, J., Wolfinger, M., Steiner, G., Krammer, G., Barontini, F., & Cozzani, V. (2003). Heat of wood pyrolysis. *Fuel, 82*(1), 81-91.

Raveendran, K., & Ganesh, A. (1996). Heating value of biomass and biomass pyrolysis products. *Fuel, 75*(15), 1715-1720.

Ravindra K. (1985). On the use of the arrhenius equation to describe cellulose and wood pyrolysis. *Thermochimica acta, 91*(0), 343-349.

Records, A., & Sutherland, K. (2001). *Decanter centrifuge handbook.* (1st ed.). New York, NY: Elsevier Science Inc.

Reed, T. (1981). Recommendations for future gasification research and development. In T. Reed (Ed.), *Biomass gasification: Principles and technology*. Park Ridge, NJ: Noyes Data Corporation.

Rhén, C., Öhman, M., Gref, R., & Wästerlund, I. (2007). Effect of raw material composition in woody biomass pellets on combustion characteristics. *Biomass and bioenergy, 31*(1), 66-72.

Richards, S. (1990). Physical testing of fuel briquettes. *Fuel processing technology, 25*(2), 89-100.

Richet, P., Bottinga, Y., & Javoy, M. (1977). A review of hydrogen, carbon, nitrogen, oxygen, sulfur, and chlorine stable isotope fractionation among gaseous molecules. *Annual review or earth and planetary sciences, 5*, 65-110.

Roberts, A. (1970). A review of kinetics data for the pyrolysis of wood and related substances. *Combustion and flame, 14*(2), 261-272.

Robinson, S., & Hesselbo, S. (2004). Fossil-wood carbon-isotope stratigraphy of the non-marine Wealden Group (Lower Cretaceous, southern England). Journal of the geological society of London, 161(1), 133-145.

Robinson, A., Junker, H., Buckley, S., Sclippa, G., & Baxter, L. (1998). Interactions between coal and biomass when cofiring. *Symposium (international) on combustion, 27*(1), 1351-1359.

Rodult, B. (2000). Computational aspects of kinetic analysis.: Part E: The ICTAC kinetics project – numerical techniques and kinetics of solid state processes. *Thermochimica acta, 355*(1-2), 171-180.

Rumpf, H. (1962). The strength of granules and agglomerates. In W. Knepper (Ed.), *Agglomeration*, 379-418. New York, NY: John Wiley and Sons.

Sadd, M. (2009). *Elasticity – Theory, applications, and numerics.* (2nd ed.). Burlington, MA: Academic Press.

Saddawi, A., Jones, J., Williams, A., & Wójtowicz, M. (2009). Kinetics of the thermal decomposition of biomass. *Energy & fuels, 24*(2), 1274-1282.

Sadhukhan, A., Gupta, P., Goyal, T., & Saha, R. (2008). Modelling of pyrolysis of coal–biomass blends using thermogravimetric analysis. *Bioresource technology, 99*(17), 8022-8026.

Sadhukhan, A., Gupta, P., & Saha, R. (2008). Modeling and experimental studies on pyrolysis of biomass particles. *Journal of analytical and applied pyrolysis, 81*(2), 183-192.

Saglam, M., Yuksel, M., Yanik, J., Tutas, M., Karaduman, M., & Ustun, G. (1990). Production of water-resistant briquettes from Turkish lignites using sulphite liquor binders. *Fuel, 69*(1), 60-64.

Saloojee, F. (2011). *Kinetics of pyrolysis and combustion of a South African coal using the distributed activation energy model*. (Master's thesis, University of Witwatersrand).

Sami, M., Annamalai, K., & Wooldridge, M. (2001). Co-firing of coal and biomass fuel blends. *Progress in energy and combustion science*, *27*(2), 171-214.

Samuelsson, R., Thyrel, M., Sjöström, M., & Lestander, T. (2009). Effect of biomaterial characteristics on pelletizing properties and biofuel pellet quality. *Fuel processing technology, 90*(9), 1129-1134.

Sato, M., Mori, T., Shimoike, Y., Nagao, K., & Notsu, K. (2002). Carbon isotope systematics of $CO_2$, CO and $CH_4$ in fumarolic gases from Satsuma-Iwojima volcanic island, Japan. *Earth, planets and space, 54*(3), 257-263.

Schoell, M. (1980). The hydrogen and carbon isotopic composition of methane from natural gases of various origins. *Geochimica et cosmochimica acta, 44*(6), 649-661.

Schulze, D. (2008). *Powders and bulk solids: Behavior, characterization, storage and flow.* Berlin, Germany: Springer-Verlag.

Schwedes, J., & Schulze, D. (1990). Measurement of flow properties of bulk solids. *Powder technology, 61*(1), 59-68.

Scott, G., & Kilgour, D. (1969). The density of random close packing of spheres. *Journal of physics D: Applied physics, 2*(6), 863-866.

Scott, S., Dennis, J., Davidson, J., & Hayhurst, A. (2006a). An algorithm for determining the kinetics of devolatilisation of complex solid fuels from thermogravimetric experiments. *Chemical engineering science, 61*(8), 2339-2348.

Scott, S., Dennis, J., Davidson, J., & Hayhurst, A. (2006b). Thermogravimetric measurements of the kinetics of pyrolysis of dried sewage sludge. *Fuel, 85*(9), 1248-1253.

Seggiani, M. (1998). Modelling and simulation of time varying slag flow in a Prenflo entrained-flow gasifier. *Fuel, 14*(14), 1611-1621.

Seo, D., Park, S., Hwang, J., & Yu, T.-U. (2010). Study of the pyrolysis of biomass using thermo-gravimetric analysis (TGA) and concentration measurements of the evolved species. *Journal of analytical and applied pyrolysis, 89*(1), 66-73.

Sergey, V. (2000). Computational aspects of kinetic analysis.: Part C. The ICTAC kinetics project – The light at the end of the tunnel?. *Thermochimica acta, 355*(1–2), 155-163.

Shafizadeh, F. (1968). Pyrolysis and combustion of cellulosic materials. In M. Wolfrom & R. Tipson (Eds.) *Advances in carbohydrate chemistry*, 419-474. New York, NY: Academic Press.

Sharma, S., & Ghoshal, A. (2010). Study of kinetics of co-pyrolysis of coal and waste LDPE blends under argon atmosphere. *Fuel, 89*(12), 3943-3951.

Shen, D., Gu, S., Jin, B., & Fang, M. (2011). Thermal degradation mechanisms of wood under inert and oxidative environments using DAEM methods. *Bioresource technology, 102*(2), 2047-2052.

Sheng, C., & Azevedo, J. (2005). Estimating the higher heating value of biomass fuels from basic analysis data. *Biomass and bioenergy, 28*(5), 499-507.

Shimasaki, K., Deguchi, T., Sugita, S., & Makino, E. (2003). *U.S. Patent No. 6,626,966*. Washington, DC: U.S. Patent and Trademark Office.

Sima-Ella, E., Yuan, G., & Mays, T. (2005). A simple kinetic analysis to determine the intrinsic reactivity of coal chars. *Fuel, 84*(14-15), 1920-1925.

Simbeck, D., Korens, D., Biasca, F., Vejtasa, S., & Dickenson, R. (1993). *Coal gasification guidebook: Status, applications, and technologies*. Palo Alto, CA: Electric Power Research Institute.

Singh, P., Singh, M., Prachiti, P., Kalpana, M., Manikyamba, C., Lakshminarayana, G., Singh, A., & Naik, A. (2012). Petrographic characteristics and carbon isotopic composition of Permian coal: Implications on depositional environment of Sattupalli coalfield, Godavari Valley, India. *International journal of coal geology, 90–91*, 34-42.

Sinha, S., Jhalani, A., Ravi, M., & Ray, A. (2000). Modeling of pyrolysis in wood: A review. *SESI Journal, 10*(1), 41-62.

Sjostrom, K., Chen, G., Yu, Q., Brage, C., & Rosen, C. (1999). Promoted reactivity of char in co-gasification of biomass and coal: Synergies in the thermochemical process. *Fuel*, *78*(10), 1189-1194.

Smith, I. (2001). *Potential for economic greenhouse gas reduction in coal-fired power generation.* London, England: IEA Clean Coal Centre.

Smith, I., & Rousaki, K. (2002). *Prospects for co-utilization of coal with other fuels − GHG emissions reduction.* London, England: IEA Clean Coal Centre.

Snow, N. (2012). Former ambassadors cite foreign policy impacts from oil imports. *Oil and gas journal*, *110*(5), 27-28.

Song, W., Sun, Y., Wu, Y., & Zhu, Z. (2011). Measurement and simulation of flow properties of coal ash slag in coal gasification. *AIChE journal, 57*(3), 801-818.

Song, W., Tang, L., Zhu, X., Wu, Y., Zhu, Z., & Koyama, S. (2010a). Effect of coal ash composition on ash fusion temperatures. *Energy & fuels, 24*(1), 182-189.

Song, W., Tang, L., Zhu, X., Wu, Y., Zhu, Z., & Koyama, S. (2010b). Flow properties and rheology of slag from coal gasification. *Fuel, 89*(7), 1709-1715.

Sonobe, T., & Worasuwannarak, N. (2008). Kinetic analyses of biomass pyrolysis using the distributed activation energy model. *Fuel, 87*(3), 414-421.

Speight, J. (1994). *The chemistry and technology of coal.* (2nd ed.). New York, NY: Marcel Dekkar.

Speight, J. (2005). *Handbook of coal analysis.* Hoboken, NJ: John Wiley and Sons.

Speight, J. (2008). *Synthetic fuels handbook: Properties, process, and performance.* New York, NY: McGraw-Hill.

Spliethoff, H., & Hein, K. (1998). Effect of co-combustion of biomass on emissions in pulverized fuel furnaces. *Fuel processing technology, 54*(1–3), 189-205.

Staggs, J. (2005). Savitzky-Golay smoothing and numerical differentiation of cone calorimeter mass data. *Fire safety journal, 40*(6), 493-505.

Standish, N., Yu, A., & He, Q. (1991a). An experimental study of the packing of a coal heap. *Powder technology, 68*(2), 187-193.

Standish, N., Yu, A., & Zou, R. (1991b). Optimization of coal grind for maximum bulk density. *Powder technology, 68*(2), 175-186.

Steer, J., Ohuchi, T., & Muehlenbachs, K. (1987). Efficacy of coal-bitumen co-processing as determined by isotopic mass balance calculations. *Fuel processing technology, 15*, 429-438.

Stenseng, M., Jensen, A., & Dam-Johansen, K. (2001). Investigation of biomass pyrolysis by thermogravimetric analysis and differential scanning calorimetry. *Journal of analytical and applied pyrolysis, 58–59*(0), 765-780.

Stoliarov, S., & Walters, R. (2008). Determination of the heats of gasification of polymers using differential scanning calorimetry. *Polymer degradation and stability, 93*(2), 422-427.

Strezov, V., Lucas, J., & Strezov, L. (2000). Quantifying the heats of coal devolatilization. *Metallurgical and materials transactions b, 31*(5), 1125-1131.

Strezov, V., Moghtaderi, B., & Lucas, J. (2004). Computational calorimetric investigation of the reactions during thermal conversion of wood biomass. *Biomass and bioenergy, 27*(5), 459-465.

Strezov, V., Moghtaderi, B., & Lucas, J. (2003). Thermal study of decomposition of selected biomass samples. *Journal of thermal analysis and calorimetry, 72*(3) 1041-1048.

Sun, L., & Koziński, A. (2000). Ignition behaviour of pulp and paper combustible wastes. *Fuel, 79*(13), 1587-1593.

Sun, Y., Mukherjee, A., Kuznetsov, O., Thaner, R., Alemany, L., & Billups, W. (2011). Functionalization by reductive alkylation and mapping of a subbituminous coal by energy dispersive x-ray spectroscopy. *Energy & fuels, 25*(4), 1571-1577.

Sütcü, H., & Pişkin, S. (2011). The pyrolytic characteristics and kinetics of agricultural waste, bituminous coal, and their blends. *Materials and manufacturing processes, 26*(1), 99-103.

Syed, S., Qudaih, R., Talab, I., & Janajreh, I. (2011). Kinetics of pyrolysis and combustion of oil shale sample from thermogravimetric data. *Fuel, 90*(4), 1631-1637.

Taulbee, D. (2012). *U.S Patent Application Pub. No. US 2012/0317878 A1*. Washington, DC: U.S. Patent and Trademark Office.

Taulbee, D., Hodgen, R., & Aden, N. (2012). Co-briquetting of coal and biomass. *29th Annual Pittsburgh Coal Conference*, October 15-18, 2012. B. Morsi, ed., University of Pittsburgh, Swanson School of Engineering, Pittsburgh, PA.

Taulbee, D., Hodgen, R., & Patil, D. (2014). Drying and agglomeration of high-moisture coals and coal fines. *Proceedings of the 33nd Biennial Conference of the Institute for Briquetting and Agglomeration*, November, 2013. D. Taulbee, ed., Institute for Briquetting and Agglomeration, San Francisco, CA.

Taulbee, D., Neather, J., Patil, D., Sowder, N., O'Daniel, B., & Montross, M. (2010). Combustion of briquettes and fuel pellets prepared from blends of biomass and fine coal. In R. Honaker (Ed.), *International coal preparation congress 2010 conference proceedings*. Littleton, CO: Society for Mining, Metallurgy, and Exploration.

Taulbee, D., Patil, D., Honaker, R., & Parekh, B. (2009). Briquetting of coal fines and sawdust Part I: Binder and briquetting-parameters evaluations. *International journal of coal preparation and utilization, 29*(1), 1-22.

Teng, H., & Wei, Y.-C. (1998). Thermogravimetric studies on the kinetics of rice hull pyrolysis and the influence of water treatment. *Industrial & engineering chemistry research, 37*(10), 3806-3811.

Thomas, K., Dillon, F., Bottrell, S., Louie, P., & Bartle, K. (1993). The use of $^{13}C/^{12}C$ isotope mass-spectrometry in the study of the gasification of carbon composite-materials. *Carbon, 31*(2), 273-277.

Trechock, J. (1973). *U.S. Patent No. 3,711,318*. Washington, DC: U.S. Patent and Trademark Office.

Tremel, A., Haselsteiner, T., Nakonz, M., & Spliethoff, H. (2012). Coal and char properties in high temperature entrained flow gasification. *Energy, 45*(1), 176-182.

Tumuluru, J., Wright, C., Hess, J., & Kenney, K. (2011). A review of biomass densification systems to develop uniform feedstock commodities for bioenergy application. *Biofuels, bioproducts and biorefining, 5*(6), 683-707.U.K. Department of Trade and Industry, Cleaner Coal Technology Programme. (2002). *Guaranteed bunker flow using the Edinburgh Cohesion Tester, Case study 008,* London, England.

Turns, R. (1996). *An introduction to combustion*. New York, NY: McGraw-Hill.

U.S. Department of Energy, National Energy Technology Laboratory. (2010). *2010 Worldwide gasification database*. Pittsburgh, PA.

U.S. Energy Information Administration. (2012). *Annual energy review 2011*. Pittsburgh, PA.

U.S. Environmental Protection Agency. (2012). Standards of performance for greenhouse gas emissions for new stationary sources: Electric utility generating units. *Federal register 77*(72), 22392-22441.

Ulloa, C., Gordon, A., & García, X. (2009). Thermogravimetric study of interactions in the pyrolysis of blends of coal with radiata pine sawdust. *Fuel processing technology, 90*(4), 583-590.

Vamvuka, D., Karouki, E., & Sfakiotakis, S. (2011). Gasification of waste biomass chars by carbon dioxide via thermogravimetry. Part I: Effect of mineral matter. *Fuel, 90*(3), 1120-1127.

Vamvuka, D., & Sfakiotakis, S. (2011) Combustion behaviour of biomass fuels and their blends with lignite. *Thermochimica acta, 526*(1–2), 192-199.

van Alphen, C. (2007). Automated mineralogical analysis of coal and ash products – Challenges and requirements. *Minerals engineering, 20*(5), 496-505.

Van de Velden, M., Baeyens, J., Brems, A., Janssens, B., & Dewil, R. (2010). Fundamentals, kinetics and endothermicity of the biomass pyrolysis reaction. *Renewable energy, 35*(1), 232-242.

van Heek, K., & Muhlen, H. (1987). Effect of coal and char properties on gasification. *Fuel processing technology, 15*(1), 113-133.

van Heek, K., & Muhlen, H. (1985). Aspects of coal properties and constitution important for gasification. *Fuel, 64*(10), 1405-1414.

Várhegyi, G., Chen, H., & Godoy, S. (2009). Thermal decomposition of wheat, oat, barley, and brassica carinata straws. A kinetic study. *Energy & fuels, 23*(2), 646-652.

Várhegyi, G., Bobály, B., Jakab, E., & Chen, H. (2010). Thermogravimetric study of biomass pyrolysis kinetics. A distributed activation energy model with prediction tests. *Energy & fuels, 25*(1), 24-32.

Várhegyi, G., Grønli, M., & Di Blasi, C. (2004). Effects of sample origin, extraction, and hot-water washing on the devolatilization kinetics of chestnut wood. *Industrial & engineering chemistry research, 43*(10), 2356-2367.

Vittee, T. (2012). *Determination of kinetics of char reactivity with carbon dioxide using thermogravimetry and the distributed activation energy model*. (Doctoral dissertation, University of Witwatersrand).

Voitkevich, O., Kabo, G., Blokhin, A., Paulechka, Y., & Shishonok, M. (2012). Thermodynamic properties of plant biomass components. Heat capacity, combustion energy, and gasification equilibria of lignin. *Journal of chemical and engineering data, 57*(7), 1903-1909.

Völker, S., & Rieckmann, T. (2002). Thermokinetic investigation of cellulose pyrolysis – impact of initial and final mass on kinetic results. *Journal of analytical and applied pyrolysis, 62*(2), 165-177.

Vovelle, C., Mellottée, H., & Delbourgo, R. (1982) Kinetics of the thermal degradation of cellulose and wood in inert and oxidative atmospheres. *Symposium (international) on combustion, 19*(1), 797-805.

Vuthaluru, H. (2004). Investigations into the pyrolytic behaviour of coal/biomass blends using thermogravimetric analysis. *Bioresoure Technology, 92*(2), 187-195.

Waitzman, D., Faucett, H., Kindahl, E., Tomlinson, S., & Nichols, D. (1975). *Evaluation of fixed-bed, low-BTU coal gasification systems for retrofitting power plants*. Palo Alto, CA: Electric Power Research Institute.

Wang, C., Wang, F., Yang, Q., & Liang, R. (2009). Thermogravimetric studies of the behavior of wheat straw with added coal during combustion. *Biomass and bioenergy, 33*(1), 50-56.

Wang, H., Zhu, S., Bai, Z., & Yang Y. (2011). Effect of heat treatment on water resistance of lignite briquettes. *Power and energy engineering conference (APPEEC)*, 2011 Asia-Pacific, 1-3.

Weast, R. (Ed.) (1960). *Handbook of chemistry and physics*. Cleveland, OH: The Chemical Rubber Company.

White, D. (1999). *U.S. Patent No. 5,916,826*. Washington, DC: U.S. Patent and Trademark Office.

White, J., Catallo, W., & Legendre, B. (2011). Biomass pyrolysis kinetics: A comparative critical review with relevant agricultural residue case studies. *Journal of analytical and applied pyrolysis, 91*(1), 1-33.

Whiticar, M. (1996). Stable isotope geochemistry of coals, humic kerogens and related natural gases. *International journal of coal geology, 32*(1-4), 191-215.

Wild, M. (2014). Torrefaction - International overview of developments in this novel technology. *IEA Task 40 Torrefaction Workshop*, CEBC, Grax, Austria.

Winschel, R., Burke, F., & Lancet, M. (1990). Application of stable carbon isotope analysis to continuous coal oil coprocessing. *Abstracts of papers of the American chemical society, 200*, 62.

Worasuwannarak, N., Sonobe, T., & Tanthapanichakoon, W. (2007). Pyrolysis behaviors of rice straw, rice husk, and corncob by TG-MS technique. *Journal of analytical and applied pyrolysis, 78*(2), 265-271.

Wornat, M., Hurt, R., Yang, N., & Headley, T. (1995). Structural and compositional transformations of biomass chars during combustion. *Combustion and flame, 100*(1–2), 131-143.

Wright, C. U.S. Department of the Interior, Bureau of Mines. (1911). *Briquetting tests at the United States fuel-testing plant: Norfolk, Virginia, 1907-8*. (Bulletin 385).

Yaman, S., & Haykiri-Acma, H. (2010). Interaction between biomass and different rank coals during co-pyrolysis. *Renewable energy, 35*(1), 288-292.

Yaman, S., & Haykiri-Acma, H. (2007). Synergy in devolatilization characteristics of lignite and hazelnut shell during co-pyrolysis. *Fuel, 86*(3), 373-380.

Yanfen, L., & Xiaoqian, M. (2010). Thermogravimetric analysis of the co-combustion of coal and paper mill sludge. *Applied energy, 87*(11), 3526-3532.

Yildirim, M., & Ozbayoglu, G. (2002). Environmentally sound coal-derived binder for coal briquetting. *Coal preparation, 22*(5), 269-276.

Yin, R., Liu, R., Wu, J., Wu, X., Sun, C., & Wu, C. (2012). Influence of particle size on performance of a pilot-scale fixed-bed gasification system. *Bioresource technology, 119*(1), 15-21.

Yu, A., Standish, N. (1993) A study of the packing of particles with a mixture size distribution. *Powder Technology, 76*(2), 113-124.

Yu, A., Standish, N., Lu, L. (1995) Coal agglomeration and its effect on bulk density. *Powder Technology, 82*(2), 177-189.

Yu, B., Till, V., & Thomas, K. (2007). Modeling of thermo-physical properties for FRP composites under elevated and high temperature. *Composites science and technology, 67*(15-16), 3098-3109.

Yun, Y., & Suuberg, E. (1993). New applications of differential scanning calorimetry and solvent swelling for studies of coal structure: Prepyrolysis structural relaxation. *Fuel, 72*(8), 1245-1254.

Zhang, Y., McKechnie, J., Cormier, D., Lyng, R., Mabee, W., Ogino, A., & MacLean, H. (2009). Life cycle emissions and cost of producing electricity from coal, natural gas, and wood pellets in Ontario, Canada. *Environmental science & technology, 44*(1), 538-544.

Zhou, J., Masutani, S., Ishimura, D., Turn, S., & Kinoshita, C. (2000). Release of fuel-bound nitrogen during biomass gasification. *Industrial & engineering chemistry research, 39*(3), 626-634.

Zhou, L., Wang, Y., Huang, Q., & Cai, J. Thermogravimetric characteristics and kinetics of plastic and biomass blends co-pyrolysis., *Fuel Processing Technology, 87*(11), 963-969.

Zhu, W., Song, W., & Lin, W. (2008). Catalytic gasification of char from co-pyrolysis of coal and biomass, *Fuel Processing Technology, 89*(9), 890-896.

Zinoviev, S., Müller-Langer, F., Das, P., Bertero, N., Fornasiero, P., Kaltschmitt , M., Centi , G., & Miertus, S. (2010). Next-generation biofuels: Survey of emerging technologies and sustainability issues. *ChemSusChem, 3*(10), 1106-1133.

Zolin, A., Jensen, A., Jensen, P., Frandsen, F., & Dam-Johansen, K. (2001). The Influence of inorganic materials on the thermal deactivation of fuel chars. *Energy & fuels, 15*(5), 1110-1122.

# Appendix A. Additional Mathematical Models for Coal–Biomass Briquette Production

## A.1 EM-SG Model

### A.1.1 Particle Density Model

| | | | | | | | |
|---|---|---|---|---|---|---|---|
| Use your mouse to right click on individual cells for definitions. | | | | | | | |
| Response | 1 | Particle density | | | | | |
| ANOVA for Response Surface Linear Model | | | | | | | |
| Analysis of variance table [Partial sum of squares - Type III] | | | | | | | |
| | Sum of | | Mean | F | p-value | | |
| Source | Squares | df | Square | Value | Prob > F | | |
| Model | 0.022801167 | 3 | 0.0076 | 14.6876 | 0.0004 | significant | |
| A-Water content | 0.010879574 | 1 | 0.01088 | 21.02456 | 0.0008 | | |
| B-Biomass top size | 0.001067386 | 1 | 0.001067 | 2.062702 | 0.1788 | | |
| C-Biomass content | 0.01312521 | 1 | 0.013125 | 25.36421 | 0.0004 | | |
| Residual | 0.005692166 | 11 | 0.000517 | | | | |
| Cor Total | 0.028493333 | 14 | | | | | |
| | | | | | | | |
| The Model F-value of 14.69 implies the model is significant. There is only | | | | | | | |
| a 0.04% chance that a "Model F-Value" this large could occur due to noise. | | | | | | | |
| | | | | | | | |
| Values of "Prob > F" less than 0.0500 indicate model terms are significant. | | | | | | | |
| In this case A, C are significant model terms. | | | | | | | |
| Values greater than 0.1000 indicate the model terms are not significant. | | | | | | | |
| If there are many insignificant model terms (not counting those required to support hierarchy), | | | | | | | |
| model reduction may improve your model. | | | | | | | |
| | | | | | | | |
| Std. Dev. | 0.02274796 | | R-Squared | 0.800228 | | | |
| Mean | 1.059333333 | | Adj R-Squ | 0.745745 | | | |
| C.V. % | 2.147384491 | | Pred R-Sq | 0.617834 | | | |
| PRESS | 0.010889172 | | Adeq Prec | 12.31524 | | | |
| | | | | | | | |
| The "Pred R-Squared" of 0.6178 is in reasonable agreement with the "Adj R-Squared" of 0.7457. | | | | | | | |
| | | | | | | | |
| "Adeq Precision" measures the signal to noise ratio. A ratio greater than 4 is desirable. Your | | | | | | | |
| ratio of 12.315 indicates an adequate signal. This model can be used to navigate the design space. | | | | | | | |
| | | | | | | | |
| | Coefficient | | Standard | 95% CI | 95% CI | | |
| Factor | Estimate | df | Error | Low | High | VIF | |
| Intercept | 1.05798162 | 1 | 0.00603 | 1.04471 | 1.071254 | | |
| A-Water content | -0.036909706 | 1 | 0.00805 | -0.05463 | -0.01919 | 1.011591 | |
| B-Biomass top size | 0.011283541 | 1 | 0.007856 | -0.00601 | 0.028576 | 1.004282 | |
| C-Biomass content | -0.040652704 | 1 | 0.008072 | -0.05842 | -0.02289 | 1.007309 | |
| | | | | | | | |
| | | | | | | | |
| | | | | | | | |
| Final Equation in Terms of Coded Factors: | | | | | | | |
| | | | | | | | |
| | Particle density | = | | | | | |
| | 1.05798162 | | | | | | |
| | -0.036909706 | * A | | | | | |
| | 0.011283541 | * B | | | | | |
| | -0.040652704 | * C | | | | | |
| | | | | | | | |
| Final Equation in Terms of Actual Factors: | | | | | | | |
| | | | | | | | |
| | Particle density | = | | | | | |
| | 1.181891355 | | | | | | |
| | -1.230323545 | * Water content | | | | | |
| | 0.006356925 | * Biomass top size | | | | | |
| | -0.00406527 | * Biomass content | | | | | |

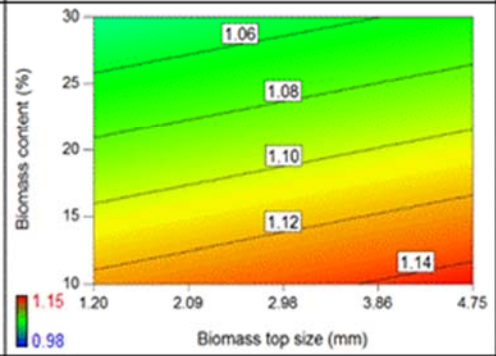
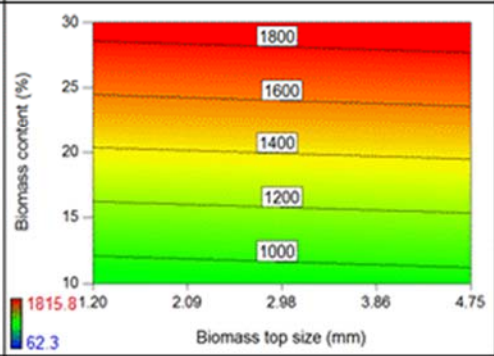
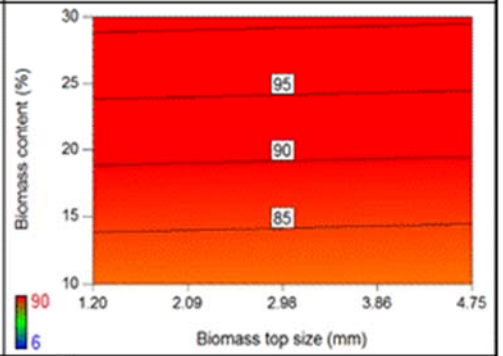
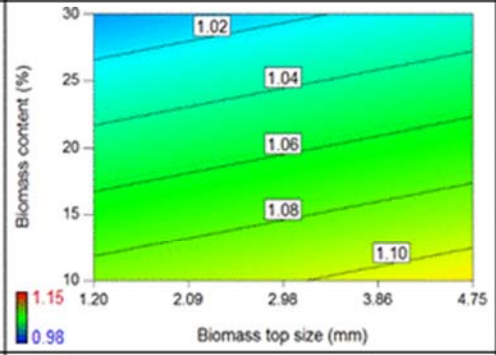
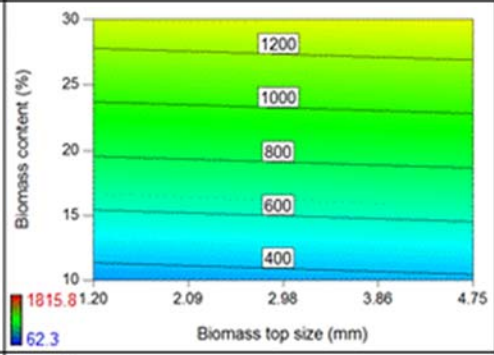
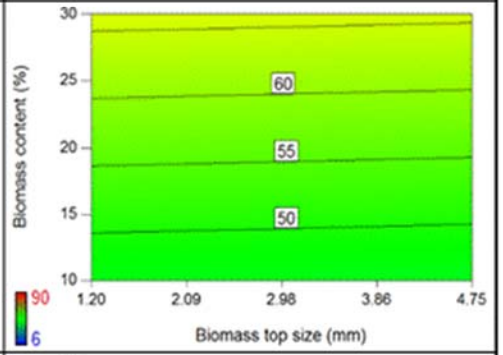
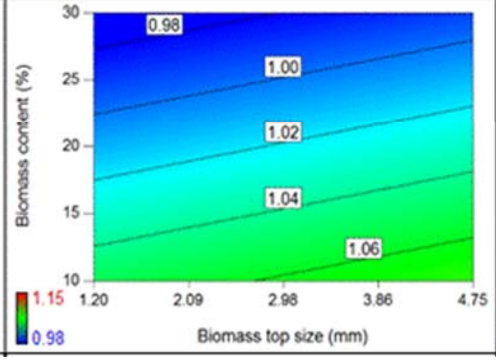
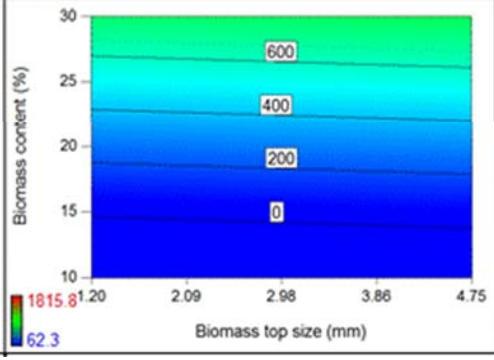
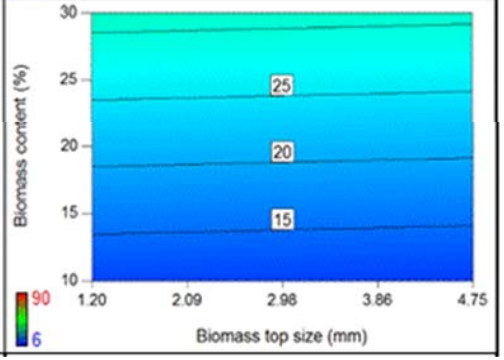
## A.1.2 Crushing Strength Model

| | | | | | | | |
|---|---|---|---|---|---|---|---|
| Use your mouse to right click on individual cells for definitions. | | | | | | | |
| Response | 2 | Crushing strength | | | | | |
| ANOVA for Response Surface Linear Model | | | | | | | |
| Analysis of variance table [Partial sum of squares - Type III] | | | | | | | |
| | Sum of | | Mean | F | p-value | | |
| Source | Squares | df | Square | Value | Prob > F | | |
| Model | 4797285.809 | 3 | 1599095 | 26.59629 | < 0.0001 | significant | |
| A-Water content | 2516664.149 | 1 | 2516664 | 41.85737 | < 0.0001 | | |
| B-Biomass top size | 3943.153703 | 1 | 3943.154 | 0.065583 | 0.8026 | | |
| C-Biomass content | 1874166.421 | 1 | 1874166 | 31.17129 | 0.0002 | | |
| Residual | 661372.2867 | 11 | 60124.75 | | | | |
| Cor Total | 5458658.096 | 14 | | | | | |
| | | | | | | | |
| The Model F-value of 26.60 implies the model is significant. There is only | | | | | | | |
| a 0.01% chance that a "Model F-Value" this large could occur due to noise. | | | | | | | |
| | | | | | | | |
| Values of "Prob > F" less than 0.0500 indicate model terms are significant. | | | | | | | |
| In this case A, C are significant model terms. | | | | | | | |
| Values greater than 0.1000 indicate the model terms are not significant. | | | | | | | |
| If there are many insignificant model terms (not counting those required to support hierarchy), | | | | | | | |
| model reduction may improve your model. | | | | | | | |
| | | | | | | | |
| Std. Dev. | 245.2034937 | | R-Squared | 0.87884 | | | |
| Mean | 887.5684872 | | Adj R-Squ | 0.845796 | | | |
| C.V. % | 27.62643078 | | Pred R-Sq | 0.754069 | | | |
| PRESS | 1342455.699 | | Adeq Prec | 16.83524 | | | |
| | | | | | | | |
| The "Pred R-Squared" of 0.7541 is in reasonable agreement with the "Adj R-Squared" of 0.8458. | | | | | | | |
| | | | | | | | |
| "Adeq Precision" measures the signal to noise ratio. A ratio greater than 4 is desirable. Your | | | | | | | |
| ratio of 16.835 indicates an adequate signal. This model can be used to navigate the design space. | | | | | | | |
| | | | | | | | |
| | Coefficient | | Standard | 95% CI | 95% CI | | |
| Factor | Estimate | df | Error | Low | High | VIF | |
| Intercept | 843.5567147 | 1 | 64.99865 | 700.4956 | 986.6178 | | |
| A-Water content | -561.3675038 | 1 | 86.76834 | -752.343 | -370.392 | 1.011591 | |
| B-Biomass top size | 21.68735324 | 1 | 84.68595 | -164.705 | 208.0799 | 1.004282 | |
| C-Biomass content | 485.7808507 | 1 | 87.00876 | 294.2759 | 677.2858 | 1.007309 | |
| | | | | | | | |
| | | | | | | | |
| | | | | | | | |
| Final Equation in Terms of Coded Factors: | | | | | | | |
| | | | | | | | |
| | Crushing strength | = | | | | | |
| | 843.5567147 | | | | | | |
| | -561.3675038 | * A | | | | | |
| | 21.68735324 | * B | | | | | |
| | 485.7808507 | * C | | | | | |
| | | | | | | | |
| Final Equation in Terms of Actual Factors: | | | | | | | |
| | | | | | | | |
| | Crushing strength | = | | | | | |
| | 771.2582938 | | | | | | |
| | -18712.25013 | * Water content | | | | | |
| | 12.21822718 | * Biomass top size | | | | | |
| | 48.57808507 | * Biomass content | | | | | |

## A.1.3 Mechanical Durability Model

| | | | | | | | |
|---|---|---|---|---|---|---|---|
| Response | 3 | Mechanical durability | | | | | |
| ANOVA for Response Surface Linear Model | | | | | | | |
| Analysis of variance table [Partial sum of squares - Type III] | | | | | | | |
| | Sum of | | Mean | F | p-value | | |
| Source | Squares | df | Square | Value | Prob > F | | |
| Model | 11077.63789 | 3 | 3692.546 | 32.6465 | < 0.0001 | significant | |
| A-Water content | 9687.306228 | 1 | 9687.306 | 85.64731 | < 0.0001 | | |
| B-Biomass top size | 0.870660776 | 1 | 0.870661 | 0.007698 | 0.9317 | | |
| C-Biomass content | 785.8871181 | 1 | 785.8871 | 6.948177 | 0.0232 | | |
| Residual | 1244.176484 | 11 | 113.107 | | | | |
| Cor Total | 12321.81437 | 14 | | | | | |
| | | | | | | | |
| The Model F-value of 32.65 implies the model is significant. There is only | | | | | | | |
| a 0.01% chance that a "Model F-Value" this large could occur due to noise. | | | | | | | |
| | | | | | | | |
| Values of "Prob > F" less than 0.0500 indicate model terms are significant. | | | | | | | |
| In this case A, C are significant model terms. | | | | | | | |
| Values greater than 0.1000 indicate the model terms are not significant. | | | | | | | |
| If there are many insignificant model terms (not counting those required to support hierarchy), | | | | | | | |
| model reduction may improve your model. | | | | | | | |
| | | | | | | | |
| Std. Dev. | 10.63517527 | | R-Squared | 0.899027 | | | |
| Mean | 59.01533333 | | Adj R-Squ | 0.871488 | | | |
| C.V. % | 18.02103737 | | Pred R-Sq | 0.825413 | | | |
| PRESS | 2151.232328 | | Adeq Prec | 16.7288 | | | |
| | | | | | | | |
| The "Pred R-Squared" of 0.8254 is in reasonable agreement with the "Adj R-Squared" of 0.8715. | | | | | | | |
| | | | | | | | |
| "Adeq Precision" measures the signal to noise ratio. A ratio greater than 4 is desirable. Your | | | | | | | |
| ratio of 16.729 indicates an adequate signal. This model can be used to navigate the design space. | | | | | | | |
| | | | | | | | |
| | Coefficient | | Standard | 95% CI | 95% CI | | |
| Factor | Estimate | df | Error | Low | High | VIF | |
| Intercept | 56.02383857 | 1 | 2.819177 | 49.81887 | 62.22881 | | |
| A-Water content | -34.82861077 | 1 | 3.763391 | -43.1118 | -26.5454 | 1.011591 | |
| B-Biomass top size | -0.322262068 | 1 | 3.673071 | -8.40664 | 7.762113 | 1.004282 | |
| C-Biomass content | 9.947556164 | 1 | 3.773818 | 1.641438 | 18.25367 | 1.007309 | |
| | | | | | | | |
| | | | | | | | |
| | | | | | | | |
| Final Equation in Terms of Coded Factors: | | | | | | | |
| | | | | | | | |
| | Mechanical durability | = | | | | | |
| | 56.02383857 | | | | | | |
| | -34.82861077 | * A | | | | | |
| | -0.322262068 | * B | | | | | |
| | 9.947556164 | * C | | | | | |
| | | | | | | | |
| Final Equation in Terms of Actual Factors: | | | | | | | |
| | | | | | | | |
| | Mechanical durability | = | | | | | |
| | 94.71654024 | | | | | | |
| | -1160.953692 | * Water content | | | | | |
| | -0.181556095 | * Biomass top size | | | | | |
| | 0.994755616 | * Biomass content | | | | | |

## A.1.4 Model Graphs

| Water Content | Particle Density (g/cm³) | Crushing Strength (N) | Mechanical Durability (%) |
|---|---|---|---|
| 0.02 |  |  |  |
| 0.05 |  |  |  |
| 0.08 |  |  |  |

# A.2 EM-MC Model

## A.2.1 Particle Density Model

| | | | | | | | |
|---|---|---|---|---|---|---|---|
| Response | 1 | Particle density | | | | | |
| ANOVA for Response Surface Linear Model | | | | | | | |
| Analysis of variance table [Partial sum of squares - Type III] | | | | | | | |
| | Sum of | | Mean | F | p-value | | |
| Source | Squares | df | Square | Value | Prob > F | | |
| Model | 0.020546812 | 3 | 0.006849 | 29.5848 | < 0.0001 | significant | |
| A-Water content | 0.005146391 | 1 | 0.005146 | 22.23045 | 0.0006 | | |
| B-Biomass top size | 2.92358E-05 | 1 | 2.92E-05 | 0.126288 | 0.7290 | | |
| C-Biomass content | 0.015746156 | 1 | 0.015746 | 68.01739 | < 0.0001 | | |
| Residual | 0.002546521 | 11 | 0.000232 | | | | |
| Cor Total | 0.023093333 | 14 | | | | | |
| | | | | | | | |
| The Model F-value of 29.58 implies the model is significant. There is only | | | | | | | |
| a 0.01% chance that a "Model F-Value" this large could occur due to noise. | | | | | | | |
| | | | | | | | |
| Values of "Prob > F" less than 0.0500 indicate model terms are significant. | | | | | | | |
| In this case A, C are significant model terms. | | | | | | | |
| Values greater than 0.1000 indicate the model terms are not significant. | | | | | | | |
| If there are many insignificant model terms (not counting those required to support hierarchy), | | | | | | | |
| model reduction may improve your model. | | | | | | | |
| | | | | | | | |
| Std. Dev. | 0.015215187 | | R-Squared | 0.889729 | | | |
| Mean | 1.097333333 | | Adj R-Squ | 0.859655 | | | |
| C.V. % | 1.386560202 | | Pred R-Sq | 0.786177 | | | |
| PRESS | 0.004937874 | | Adeq Prec | 17.81544 | | | |
| | | | | | | | |
| The "Pred R-Squared" of 0.7862 is in reasonable agreement with the "Adj R-Squared" of 0.8597. | | | | | | | |
| | | | | | | | |
| "Adeq Precision" measures the signal to noise ratio. A ratio greater than 4 is desirable. Your | | | | | | | |
| ratio of 17.815 indicates an adequate signal. This model can be used to navigate the design space. | | | | | | | |
| | | | | | | | |
| | Coefficient | | Standard | 95% CI | 95% CI | | |
| Factor | Estimate | df | Error | Low | High | VIF | |
| Intercept | 1.096100877 | 1 | 0.00403 | 1.087231 | 1.104971 | | |
| A-Water content | -0.02743922 | 1 | 0.00582 | -0.04025 | -0.01463 | 1.003664 | |
| B-Biomass top size | 0.001866274 | 1 | 0.005252 | -0.00969 | 0.013425 | 1.003049 | |
| C-Biomass content | -0.044378815 | 1 | 0.005381 | -0.05622 | -0.03254 | 1.000615 | |
| | | | | | | | |
| | | | | | | | |
| | | | | | | | |
| Final Equation in Terms of Coded Factors: | | | | | | | |
| | | | | | | | |
| | Particle density | = | | | | | |
| | 1.096100877 | | | | | | |
| | -0.02743922 | * A | | | | | |
| | 0.001866274 | * B | | | | | |
| | -0.044378815 | * C | | | | | |
| | | | | | | | |
| Final Equation in Terms of Actual Factors: | | | | | | | |
| | | | | | | | |
| | Particle density | = | | | | | |
| | 1.227462562 | | | | | | |
| | -0.914640679 | * Water content | | | | | |
| | 0.001051422 | * Biomass top size | | | | | |
| | -0.004437882 | * Biomass content | | | | | |

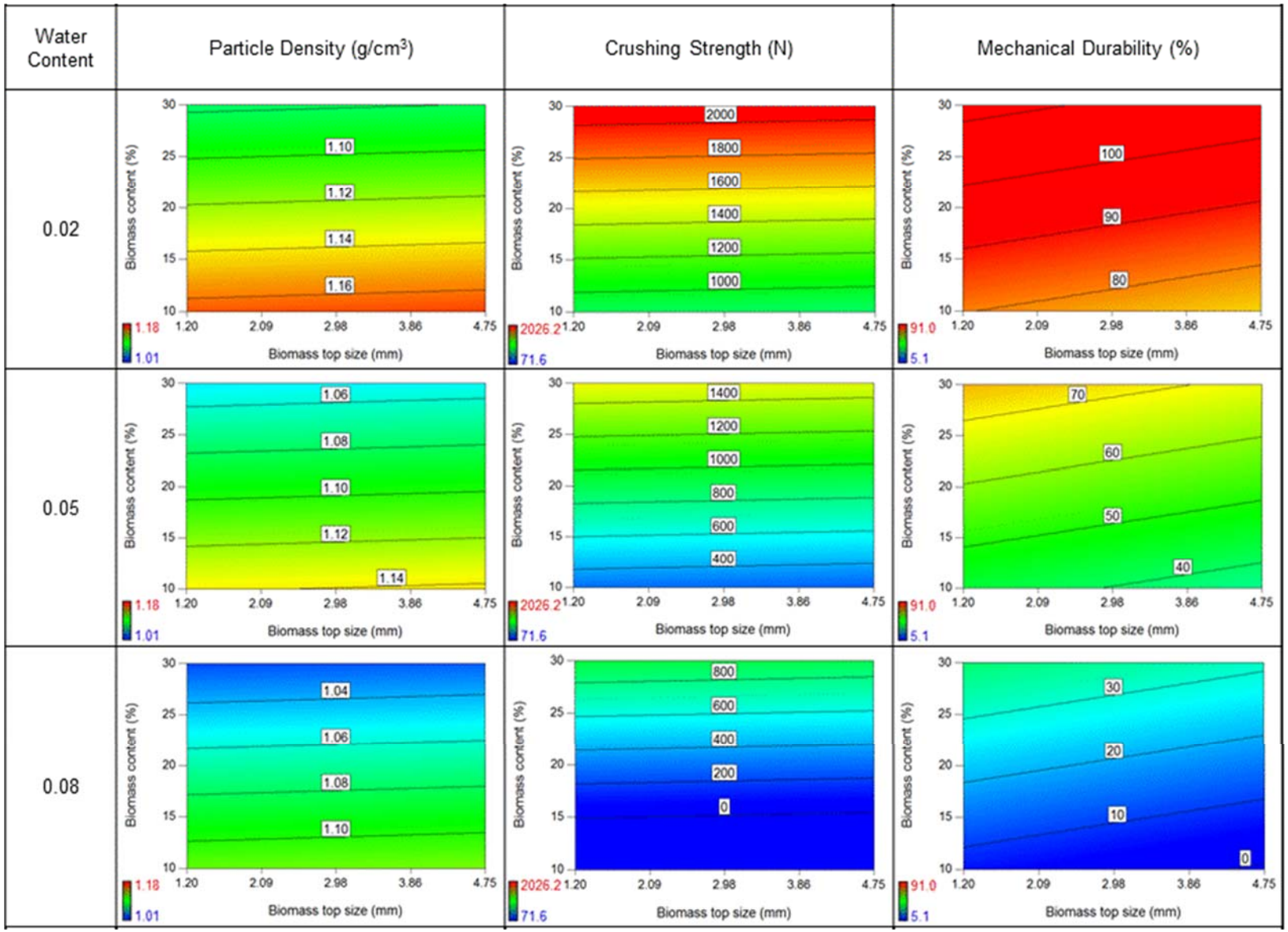
## A.2.2 Crushing Strength Model

| Response | 2 | Crushing strength | | | | |
|---|---|---|---|---|---|---|
| ANOVA for Response Surface Linear Model | | | | | | |
| Analysis of variance table [Partial sum of squares - Type III] | | | | | | |
| | Sum of | | Mean | F | p-value | |
| Source | Squares | df | Square | Value | Prob > F | |
| Model | 5644655.92 | 3 | 1881552 | 53.31607 | < 0.0001 | significant |
| A-Water content | 2481821.007 | 1 | 2481821 | 70.32542 | < 0.0001 | |
| B-Biomass top size | 2615.776263 | 1 | 2615.776 | 0.074121 | 0.7905 | |
| C-Biomass content | 3022329.598 | 1 | 3022330 | 85.64139 | < 0.0001 | |
| Residual | 388195.7508 | 11 | 35290.52 | | | |
| Cor Total | 6032851.671 | 14 | | | | |
| | | | | | | |
| The Model F-value of 53.32 implies the model is significant. There is only | | | | | | |
| a 0.01% chance that a "Model F-Value" this large could occur due to noise. | | | | | | |
| | | | | | | |
| Values of "Prob > F" less than 0.0500 indicate model terms are significant. | | | | | | |
| In this case A, C are significant model terms. | | | | | | |
| Values greater than 0.1000 indicate the model terms are not significant. | | | | | | |
| If there are many insignificant model terms (not counting those required to support hierarchy), | | | | | | |
| model reduction may improve your model. | | | | | | |
| | | | | | | |
| Std. Dev. | 187.8577196 | | R-Squared | 0.935653 | | |
| Mean | 925.1707873 | | Adj R-Squ | 0.918104 | | |
| C.V. % | 20.30519361 | | Pred R-Sq | 0.865558 | | |
| PRESS | 811070.9928 | | Adeq Prec | 23.54583 | | |
| | | | | | | |
| The "Pred R-Squared" of 0.8656 is in reasonable agreement with the "Adj R-Squared" of 0.9181. | | | | | | |
| | | | | | | |
| "Adeq Precision" measures the signal to noise ratio. A ratio greater than 4 is desirable. Your | | | | | | |
| ratio of 23.546 indicates an adequate signal. This model can be used to navigate the design space. | | | | | | |
| | | | | | | |
| | Coefficient | | Standard | 95% CI | 95% CI | |
| Factor | Estimate | df | Error | Low | High | VIF |
| Intercept | 888.9333333 | 1 | 49.75927 | 779.4139 | 998.4527 | |
| A-Water content | -602.5673383 | 1 | 71.85374 | -760.716 | -444.418 | 1.003664 |
| B-Biomass top size | -17.65298743 | 1 | 64.84059 | -160.366 | 125.0602 | 1.003049 |
| C-Biomass content | 614.8360856 | 1 | 66.43814 | 468.6067 | 761.0655 | 1.000615 |
| | | | | | | |
| | | | | | | |
| | | | | | | |
| Final Equation in Terms of Coded Factors: | | | | | | |
| | | | | | | |
| | Crushing strength | = | | | | |
| | 888.9333333 | | | | | |
| | -602.5673383 | * A | | | | |
| | -17.65298743 | * B | | | | |
| | 614.8360856 | * C | | | | |
| | | | | | | |
| Final Equation in Terms of Actual Factors: | | | | | | |
| | | | | | | |
| | Crushing strength | = | | | | |
| | 693.1274607 | | | | | |
| | -20085.57794 | * Water content | | | | |
| | -9.945345032 | * Biomass top size | | | | |
| | 61.48360856 | * Biomass content | | | | |

## A.2.3 Mechanical Durability Model

| | | | | | | | |
|---|---|---|---|---|---|---|---|
| Use your mouse to right click on individual cells for definitions. | | | | | | | |
| Response | 3 | Mechanical durability | | | | | |
| ANOVA for Response Surface Linear Model | | | | | | | |
| Analysis of variance table [Partial sum of squares - Type III] | | | | | | | |
| | Sum of | | Mean | F | p-value | | |
| Source | Squares | df | Square | Value | Prob > F | | |
| Model | 11957.08044 | 3 | 3985.693 | 32.08396 | < 0.0001 | significant | |
| A-Water content | 9625.412059 | 1 | 9625.412 | 77.48246 | < 0.0001 | | |
| B-Biomass top size | 116.0219322 | 1 | 116.0219 | 0.933951 | 0.3546 | | |
| C-Biomass content | 2074.024161 | 1 | 2074.024 | 16.69544 | 0.0018 | | |
| Residual | 1366.496804 | 11 | 124.227 | | | | |
| Cor Total | 13323.57724 | 14 | | | | | |
| | | | | | | | |
| The Model F-value of 32.08 implies the model is significant. There is only | | | | | | | |
| a 0.01% chance that a "Model F-Value" this large could occur due to noise. | | | | | | | |
| | | | | | | | |
| Values of "Prob > F" less than 0.0500 indicate model terms are significant. | | | | | | | |
| In this case A, C are significant model terms. | | | | | | | |
| Values greater than 0.1000 indicate the model terms are not significant. | | | | | | | |
| If there are many insignificant model terms (not counting those required to support hierarchy), | | | | | | | |
| model reduction may improve your model. | | | | | | | |
| | | | | | | | |
| Std. Dev. | 11.14571587 | | R-Squared | 0.897438 | | | |
| Mean | 58.512 | | Adj R-Squ | 0.869466 | | | |
| C.V. % | 19.04859835 | | Pred R-Sq | 0.811102 | | | |
| PRESS | 2516.793937 | | Adeq Prec | 17.00645 | | | |
| | | | | | | | |
| The "Pred R-Squared" of 0.8111 is in reasonable agreement with the "Adj R-Squared" of 0.8695. | | | | | | | |
| | | | | | | | |
| "Adeq Precision" measures the signal to noise ratio. A ratio greater than 4 is desirable. Your | | | | | | | |
| ratio of 17.006 indicates an adequate signal. This model can be used to navigate the design space. | | | | | | | |
| | | | | | | | |
| | Coefficient | | Standard | 95% CI | 95% CI | | |
| Factor | Estimate | df | Error | Low | High | VIF | |
| Intercept | 55.84564782 | 1 | 2.952248 | 49.34779 | 62.3435 | | |
| A-Water content | -37.52580561 | 1 | 4.263128 | -46.9089 | -28.1427 | 1.003664 | |
| B-Biomass top size | -3.717816595 | 1 | 3.847033 | -12.1851 | 4.749445 | 1.003049 | |
| C-Biomass content | 16.10628362 | 1 | 3.941817 | 7.430404 | 24.78216 | 1.000615 | |
| | | | | | | | |
| | | | | | | | |
| | | | | | | | |
| Final Equation in Terms of Coded Factors: | | | | | | | |
| | | | | | | | |
| | Mechanical durability | = | | | | | |
| | 55.84564782 | | | | | | |
| | -37.52580561 | * A | | | | | |
| | -3.717816595 | * B | | | | | |
| | 16.10628362 | * C | | | | | |
| | | | | | | | |
| Final Equation in Terms of Actual Factors: | | | | | | | |
| | | | | | | | |
| | Mechanical durability | = | | | | | |
| | 92.40735999 | | | | | | |
| | -1250.860187 | * Water content | | | | | |
| | -2.094544561 | * Biomass top size | | | | | |
| | 1.610628362 | * Biomass content | | | | | |

## A.2.4 Model Graphs



# A.3 EM-WS Model

## A.3.1 Particle Density Model

| | | | | | | | |
|---|---|---|---|---|---|---|---|
| Use your mouse to right click on individual cells for definitions. | | | | | | | |
| Response | 1 | Particle density | | | | | |
| ANOVA for Response Surface Linear Model | | | | | | | |
| Analysis of variance table [Partial sum of squares - Type III] | | | | | | | |
| | Sum of | | Mean | F | p-value | | |
| Source | Squares | df | Square | Value | Prob > F | | |
| Model | 0.026415377 | 3 | 0.008805 | 14.36053 | 0.0004 | significant | |
| A-Water content | 0.01357929 | 1 | 0.013579 | 22.14686 | 0.0006 | | |
| B-Biomass top size | 5.5221E-05 | 1 | 5.52E-05 | 0.090062 | 0.7697 | | |
| C-Biomass content | 0.011244693 | 1 | 0.011245 | 18.3393 | 0.0013 | | |
| Residual | 0.006744623 | 11 | 0.000613 | | | | |
| Cor Total | 0.03316 | 14 | | | | | |
| | | | | | | | |
| The Model F-value of 14.36 implies the model is significant. There is only | | | | | | | |
| a 0.04% chance that a "Model F-Value" this large could occur due to noise. | | | | | | | |
| | | | | | | | |
| Values of "Prob > F" less than 0.0500 indicate model terms are significant. | | | | | | | |
| In this case A, C are significant model terms. | | | | | | | |
| Values greater than 0.1000 indicate the model terms are not significant. | | | | | | | |
| If there are many insignificant model terms (not counting those required to support hierarchy), | | | | | | | |
| model reduction may improve your model. | | | | | | | |
| | | | | | | | |
| Std. Dev. | 0.024761815 | | R-Squared | 0.796604 | | | |
| Mean | 1.096 | | Adj R-Squ | 0.741132 | | | |
| C.V. % | 2.259289727 | | Pred R-Sq | 0.573784 | | | |
| PRESS | 0.014133328 | | Adeq Prec | 12.44086 | | | |
| | | | | | | | |
| The "Pred R-Squared" of 0.5738 is in reasonable agreement with the "Adj R-Squared" of 0.7411. | | | | | | | |
| | | | | | | | |
| "Adeq Precision" measures the signal to noise ratio. A ratio greater than 4 is desirable. Your | | | | | | | |
| ratio of 12.441 indicates an adequate signal. This model can be used to navigate the design space. | | | | | | | |
| | | | | | | | |
| | Coefficient | | Standard | 95% CI | 95% CI | | |
| Factor | Estimate | df | Error | Low | High | VIF | |
| Intercept | 1.099923387 | 1 | 0.006576 | 1.08545 | 1.114397 | | |
| A-Water content | -0.04343098 | 1 | 0.009229 | -0.06374 | -0.02312 | 1.003665 | |
| B-Biomass top size | 0.002561188 | 1 | 0.008534 | -0.01622 | 0.021345 | 1.000149 | |
| C-Biomass content | -0.037557007 | 1 | 0.00877 | -0.05686 | -0.01825 | 1.003516 | |
| | | | | | | | |
| | | | | | | | |
| | | | | | | | |
| Final Equation in Terms of Coded Factors: | | | | | | | |
| | | | | | | | |
| | Particle density | = | | | | | |
| | 1.099923387 | | | | | | |
| | -0.04343098 | * A | | | | | |
| | 0.002561188 | * B | | | | | |
| | -0.037557007 | * C | | | | | |
| | | | | | | | |
| Final Equation in Terms of Actual Factors: | | | | | | | |
| | | | | | | | |
| | Particle density | = | | | | | |
| | 1.243129672 | | | | | | |
| | -1.447699321 | * Water content | | | | | |
| | 0.001442923 | * Biomass top size | | | | | |
| | -0.003755701 | * Biomass content | | | | | |

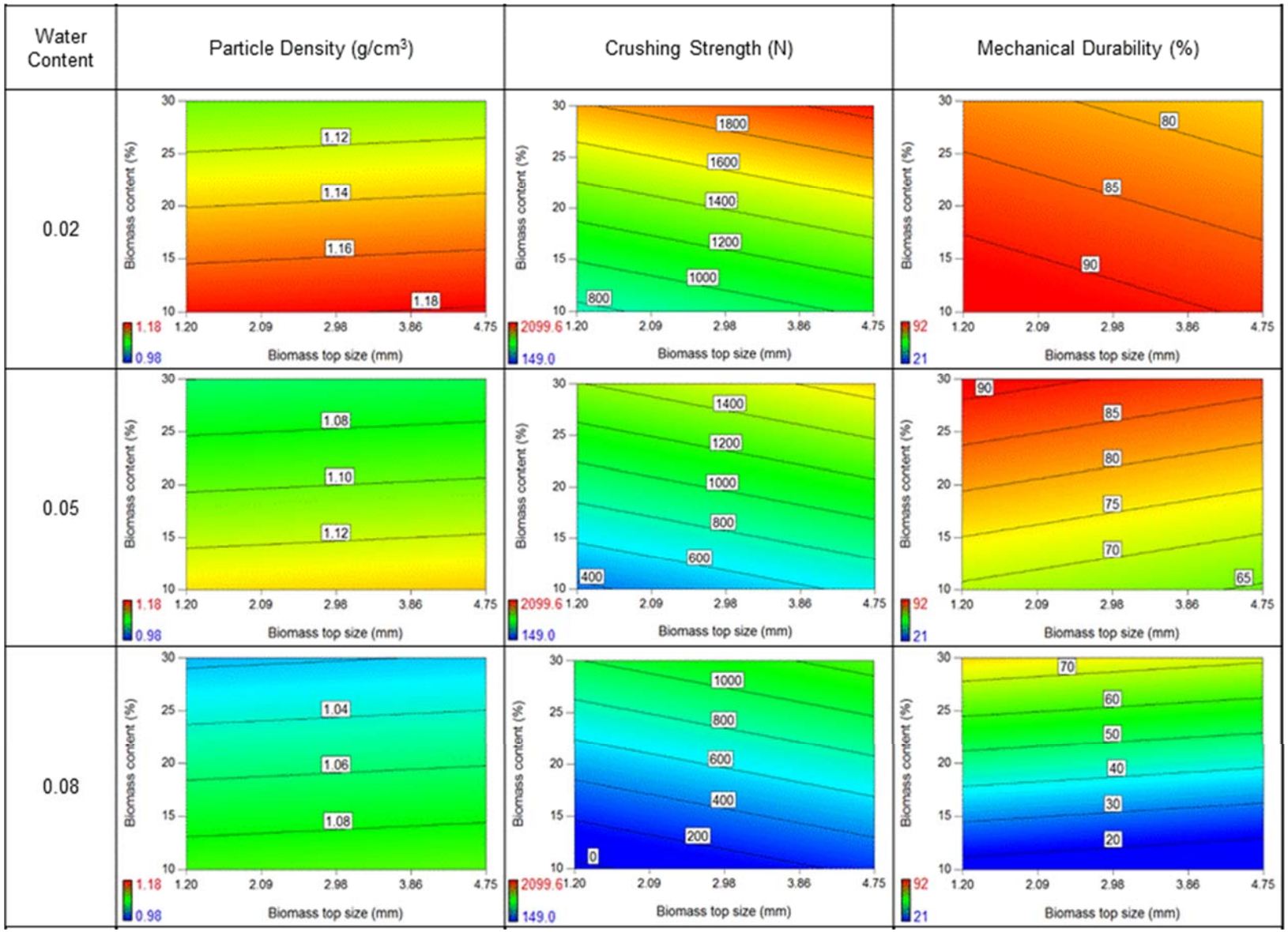
## A.3.2 Crushing Strength Model

| Response | 2 | Crushing strength | | | | |
|---|---|---|---|---|---|---|
| ANOVA for Response Surface Linear Model | | | | | | |
| Analysis of variance table [Partial sum of squares - Type III] | | | | | | |
| | Sum of | | Mean | F | p-value | |
| Source | Squares | df | Square | Value | Prob > F | |
| Model | 3246551.783 | 3 | 1082184 | 20.05681 | < 0.0001 | significant |
| A-Water content | 1160670.945 | 1 | 1160671 | 21.51146 | 0.0007 | |
| B-Biomass top size | 168499.0488 | 1 | 168499 | 3.122902 | 0.1049 | |
| C-Biomass content | 2102089.906 | 1 | 2102090 | 38.95939 | < 0.0001 | |
| Residual | 593515.1735 | 11 | 53955.92 | | | |
| Cor Total | 3840066.956 | 14 | | | | |
| | | | | | | |
| The Model F-value of 20.06 implies the model is significant. There is only | | | | | | |
| a 0.01% chance that a "Model F-Value" this large could occur due to noise. | | | | | | |
| | | | | | | |
| Values of "Prob > F" less than 0.0500 indicate model terms are significant. | | | | | | |
| In this case A, C are significant model terms. | | | | | | |
| Values greater than 0.1000 indicate the model terms are not significant. | | | | | | |
| If there are many insignificant model terms (not counting those required to support hierarchy), | | | | | | |
| model reduction may improve your model. | | | | | | |
| | | | | | | |
| Std. Dev. | 232.2841468 | | R-Squared | 0.845441 | | |
| Mean | 965.9461522 | | Adj R-Squ | 0.803289 | | |
| C.V. % | 24.0473184 | | Pred R-Sq | 0.668861 | | |
| PRESS | 1271594.108 | | Adeq Prec | 14.64304 | | |
| | | | | | | |
| The "Pred R-Squared" of 0.6689 is in reasonable agreement with the "Adj R-Squared" of 0.8033. | | | | | | |
| | | | | | | |
| "Adeq Precision" measures the signal to noise ratio. A ratio greater than 4 is desirable. Your | | | | | | |
| ratio of 14.643 indicates an adequate signal. This model can be used to navigate the design space. | | | | | | |
| | | | | | | |
| | Coefficient | | Standard | 95% CI | 95% CI | |
| Factor | Estimate | df | Error | Low | High | VIF |
| Intercept | 1020.646148 | 1 | 61.68763 | 884.8726 | 1156.42 | |
| A-Water content | -401.5278299 | 1 | 86.57264 | -592.073 | -210.983 | 1.003665 |
| B-Biomass top size | 141.4776917 | 1 | 80.05875 | -34.7304 | 317.6858 | 1.000149 |
| C-Biomass content | 513.502799 | 1 | 82.2691 | 332.4297 | 694.5759 | 1.003516 |
| | | | | | | |
| | | | | | | |
| | | | | | | |
| Final Equation in Terms of Coded Factors: | | | | | | |
| | | | | | | |
| | Crushing strength | = | | | | |
| | 1020.646148 | | | | | |
| | -401.5278299 | * A | | | | |
| | 141.4776917 | * B | | | | |
| | 513.502799 | * C | | | | |
| | | | | | | |
| Final Equation in Terms of Actual Factors: | | | | | | |
| | | | | | | |
| | Crushing strength | = | | | | |
| | 425.7290183 | | | | | |
| | -13384.261 | * Water content | | | | |
| | 79.70574183 | * Biomass top size | | | | |
| | 51.3502799 | * Biomass content | | | | |

## A.3.3 Mechanical Durability Model

| | | | | | | |
|---|---|---|---|---|---|---|
| Use your mouse to right click on individual cells for definitions. | | | | | | |
| Response | 3 | Mechanical durability | | | | |
| ANOVA for Response Surface Reduced Quadratic Model | | | | | | |
| Analysis of variance table [Partial sum of squares - Type III] | | | | | | |
| | Sum of | | Mean | F | p-value | |
| Source | Squares | df | Square | Value | Prob > F | |
| Model | 6302.570065 | 5 | 1260.514 | 42.93803 | < 0.0001 | significant |
| A-Water content | 3062.125181 | 1 | 3062.125 | 104.3079 | < 0.0001 | |
| B-Biomass top size | 57.61790497 | 1 | 57.6179 | 1.962691 | 0.1948 | |
| C-Biomass content | 1046.805413 | 1 | 1046.805 | 35.65828 | 0.0002 | |
| AC | 1219.600216 | 1 | 1219.6 | 41.54435 | 0.0001 | |
| A^2 | 517.2217521 | 1 | 517.2218 | 17.61859 | 0.0023 | |
| Residual | 264.2092679 | 9 | 29.35659 | | | |
| Cor Total | 6566.779333 | 14 | | | | |
| | | | | | | |
| The Model F-value of 42.94 implies the model is significant. There is only | | | | | | |
| a 0.01% chance that a "Model F-Value" this large could occur due to noise. | | | | | | |
| | | | | | | |
| Values of "Prob > F" less than 0.0500 indicate model terms are significant. | | | | | | |
| In this case A, C, AC, A ++2 +- are significant model terms. | | | | | | |
| Values greater than 0.1000 indicate the model terms are not significant. | | | | | | |
| If there are many insignificant model terms (not counting those required to support hierarchy), | | | | | | |
| model reduction may improve your model. | | | | | | |
| | | | | | | |
| Std. Dev. | 5.418171769 | | R-Squared | 0.959766 | | |
| Mean | 70.79666667 | | Adj R-Squ | 0.937413 | | |
| C.V. % | 7.653145302 | | Pred R-Sq | 0.881287 | | |
| PRESS | 779.5644052 | | Adeq Prec | 21.68401 | | |
| | | | | | | |
| The "Pred R-Squared" of 0.8813 is in reasonable agreement with the "Adj R-Squared" of 0.9374. | | | | | | |
| | | | | | | |
| "Adeq Precision" measures the signal to noise ratio. A ratio greater than 4 is desirable. Your | | | | | | |
| ratio of 21.684 indicates an adequate signal. This model can be used to navigate the design space. | | | | | | |
| | | | | | | |
| | Coefficient | | Standard | 95% CI | 95% CI | |
| Factor | Estimate | df | Error | Low | High | VIF |
| Intercept | 78.03491642 | 1 | 2.068501 | 73.35564 | 82.71419 | |
| A-Water content | -20.7563553 | 1 | 2.032321 | -25.3538 | -16.1589 | 1.01659 |
| B-Biomass top size | -2.656514419 | 1 | 1.896209 | -6.94604 | 1.633008 | 1.031225 |
| C-Biomass content | 11.57112631 | 1 | 1.93774 | 7.187655 | 15.9546 | 1.023235 |
| AC | 18.47532215 | 1 | 2.866395 | 11.99109 | 24.95956 | 1.022669 |
| A^2 | -13.3622752 | 1 | 3.183426 | -20.5637 | -6.16086 | 1.042219 |
| | | | | | | |
| | | | | | | |
| | | | | | | |
| Final Equation in Terms of Coded Factors: | | | | | | |
| | | | | | | |
| | Mechanical durability | = | | | | |
| | 78.03491642 | | | | | |
| | -20.7563553 | * A | | | | |
| | -2.656514419 | * B | | | | |
| | 11.57112631 | * C | | | | |
| | 18.47532215 | * A * C | | | | |
| | -13.3622752 | * A^2 | | | | |
| | | | | | | |
| Final Equation in Terms of Actual Factors: | | | | | | |
| | | | | | | |
| | Mechanical durability | = | | | | |
| | 118.4060332 | | | | | |
| | -438.8694083 | * Water content | | | | |
| | -1.496627842 | * Biomass top size | | | | |
| | -1.922107727 | * Biomass content | | | | |
| | 61.58440715 | * Water content * Biomass content | | | | |
| | -14846.97245 | * Water content^2 | | | | |

## A.3.4 Model Graphs



# A.4 EM-SD Model

## A.4.1 Particle Density Model

| | | | | | | | |
|---|---|---|---|---|---|---|---|
| Use your mouse to right click on individual cells for definitions. | | | | | | | |
| Response | 1 | Particle density | | | | | |
| ANOVA for Response Surface Linear Model | | | | | | | |
| Analysis of variance table [Partial sum of squares - Type III] | | | | | | | |
| | Sum of | | Mean | F | p-value | | |
| Source | Squares | df | Square | Value | Prob > F | | |
| Model | 0.036113858 | 3 | 0.012038 | 18.75741 | 0.0001 | significant | |
| A-Water content | 0.028452389 | 1 | 0.028452 | 44.33421 | < 0.0001 | | |
| B-Biomass top size | 0.002407903 | 1 | 0.002408 | 3.751969 | 0.0788 | | |
| C-Biomass content | 0.005102399 | 1 | 0.005102 | 7.950503 | 0.0167 | | |
| Residual | 0.007059476 | 11 | 0.000642 | | | | |
| Cor Total | 0.043173333 | 14 | | | | | |
| | | | | | | | |
| The Model F-value of 18.76 implies the model is significant. There is only | | | | | | | |
| a 0.01% chance that a "Model F-Value" this large could occur due to noise. | | | | | | | |
| | | | | | | | |
| Values of "Prob > F" less than 0.0500 indicate model terms are significant. | | | | | | | |
| In this case A, C are significant model terms. | | | | | | | |
| Values greater than 0.1000 indicate the model terms are not significant. | | | | | | | |
| If there are many insignificant model terms (not counting those required to support hierarchy), | | | | | | | |
| model reduction may improve your model. | | | | | | | |
| | | | | | | | |
| Std. Dev. | 0.02533319 | | R-Squarec | 0.836485 | | | |
| Mean | 1.061333333 | | Adj R-Squ | 0.79189 | | | |
| C.V. % | 2.38692116 | | Pred R-Sq | 0.700943 | | | |
| PRESS | 0.0129113 | | Adeq Prec | 13.26808 | | | |
| | | | | | | | |
| The "Pred R-Squared" of 0.7009 is in reasonable agreement with the "Adj R-Squared" of 0.7919. | | | | | | | |
| | | | | | | | |
| "Adeq Precision" measures the signal to noise ratio. A ratio greater than 4 is desirable. Your | | | | | | | |
| ratio of 13.268 indicates an adequate signal. This model can be used to navigate the design space. | | | | | | | |
| | | | | | | | |
| | Coefficient | | Standard | 95% CI | 95% CI | | |
| Factor | Estimate | df | Error | Low | High | VIF | |
| Intercept | 1.071548878 | 1 | 0.006791 | 1.056603 | 1.086495 | | |
| A-Water content | -0.056278426 | 1 | 0.008452 | -0.07488 | -0.03768 | 1.00424 | |
| B-Biomass top size | 0.016935312 | 1 | 0.008743 | -0.00231 | 0.036179 | 1.002845 | |
| C-Biomass content | -0.025272312 | 1 | 0.008963 | -0.045 | -0.00555 | 1.001395 | |
| | | | | | | | |
| | | | | | | | |
| | | | | | | | |
| Final Equation in Terms of Coded Factors: | | | | | | | |
| | | | | | | | |
| | Particle density | = | | | | | |
| | 1.071548878 | | | | | | |
| | -0.056278426 | * A | | | | | |
| | 0.016935312 | * B | | | | | |
| | -0.025272312 | * C | | | | | |
| | | | | | | | |
| Final Equation in Terms of Actual Factors: | | | | | | | |
| | | | | | | | |
| | Particle density | = | | | | | |
| | 1.187506342 | | | | | | |
| | -1.87594752 | * Water content | | | | | |
| | 0.009541021 | * Biomass top size | | | | | |
| | -0.002527231 | * Biomass content | | | | | |

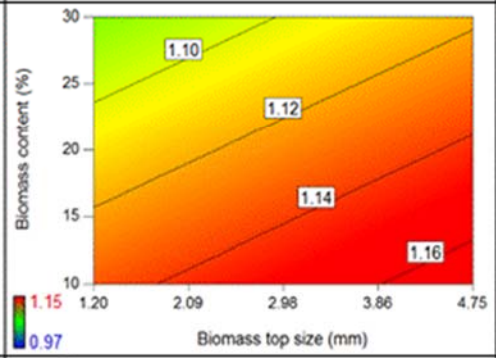
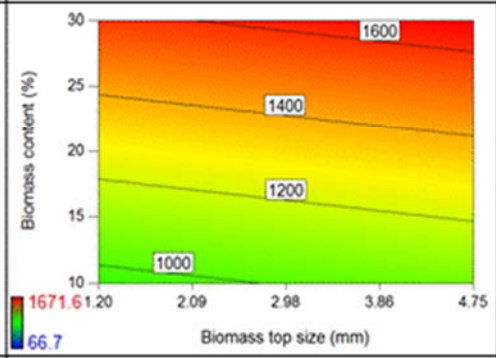
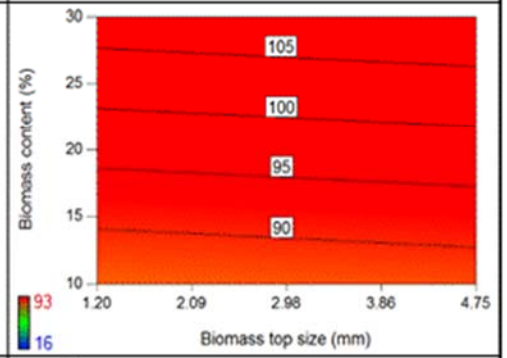
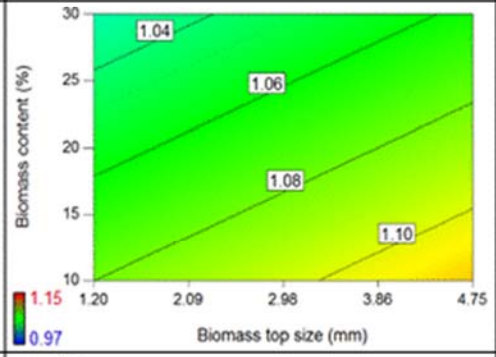
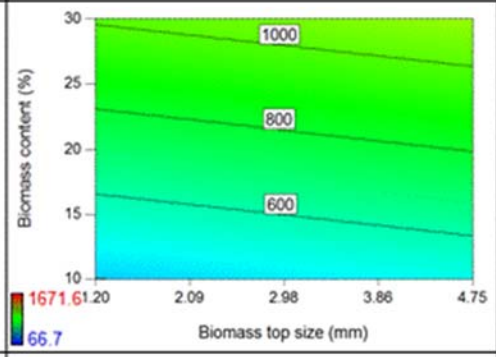
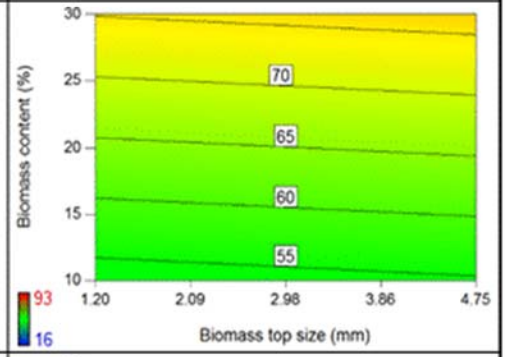
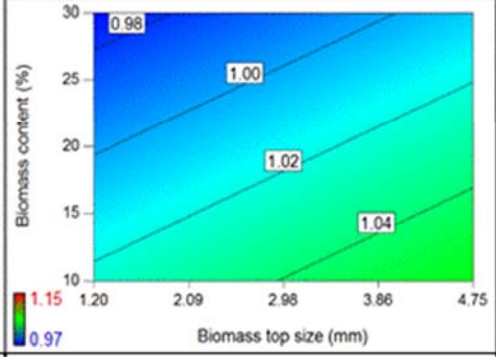
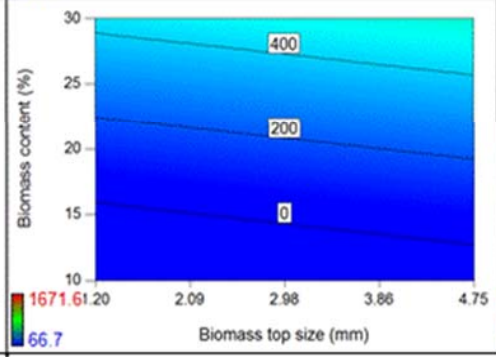
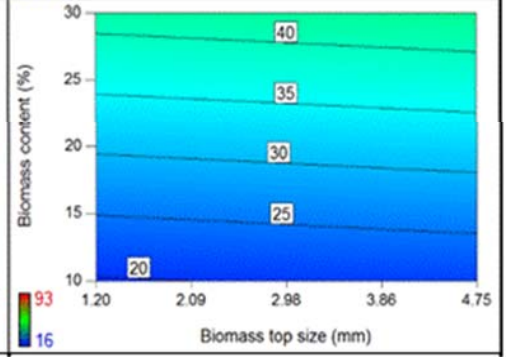
## A.4.2 Crushing Strength Model

| | | | | | | | |
|---|---|---|---|---|---|---|---|
| Response | 2 | Crushing strength | | | | | |
| ANOVA for Response Surface Linear Model | | | | | | | |
| Analysis of variance table [Partial sum of squares - Type III] | | | | | | | |
| | Sum of | | Mean | F | p-value | | |
| Source | Squares | df | Square | Value | Prob > F | | |
| Model | 3673503.485 | 3 | 1224501 | 75.89205 | < 0.0001 | significant | |
| A-Water content | 3019739.277 | 1 | 3019739 | 187.1572 | < 0.0001 | | |
| B-Biomass top size | 20600.29414 | 1 | 20600.29 | 1.276764 | 0.2825 | | |
| C-Biomass content | 759073.7641 | 1 | 759073.8 | 47.04582 | < 0.0001 | | |
| Residual | 177482.5243 | 11 | 16134.77 | | | | |
| Cor Total | 3850986.009 | 14 | | | | | |
| | | | | | | | |
| The Model F-value of 75.89 implies the model is significant. There is only | | | | | | | |
| a 0.01% chance that a "Model F-Value" this large could occur due to noise. | | | | | | | |
| | | | | | | | |
| Values of "Prob > F" less than 0.0500 indicate model terms are significant. | | | | | | | |
| In this case A, C are significant model terms. | | | | | | | |
| Values greater than 0.1000 indicate the model terms are not significant. | | | | | | | |
| If there are many insignificant model terms (not counting those required to support hierarchy), | | | | | | | |
| model reduction may improve your model. | | | | | | | |
| | | | | | | | |
| Std. Dev. | 127.0227339 | | R-Squared | 0.953912 | | | |
| Mean | 669.2794249 | | Adj R-Squ | 0.941343 | | | |
| C.V. % | 18.97902867 | | Pred R-Sq | 0.906917 | | | |
| PRESS | 358462.4223 | | Adeq Prec | 26.6346 | | | |
| | | | | | | | |
| The "Pred R-Squared" of 0.9069 is in reasonable agreement with the "Adj R-Squared" of 0.9413. | | | | | | | |
| | | | | | | | |
| "Adeq Precision" measures the signal to noise ratio. A ratio greater than 4 is desirable. Your | | | | | | | |
| ratio of 26.635 indicates an adequate signal. This model can be used to navigate the design space. | | | | | | | |
| | | | | | | | |
| | Coefficient | | Standard | 95% CI | 95% CI | | |
| Factor | Estimate | df | Error | Low | High | VIF | |
| Intercept | 754.9771788 | 1 | 34.0486 | 680.0367 | 829.9176 | | |
| A-Water content | -579.7854281 | 1 | 42.3803 | -673.064 | -486.507 | 1.00424 | |
| B-Biomass top size | 49.53479999 | 1 | 43.83845 | -46.953 | 146.0226 | 1.002845 | |
| C-Biomass content | 308.247654 | 1 | 44.94064 | 209.334 | 407.1613 | 1.001395 | |
| | | | | | | | |
| | | | | | | | |
| | | | | | | | |
| Final Equation in Terms of Coded Factors: | | | | | | | |
| | | | | | | | |
| | Crushing strength | = | | | | | |
| | 754.9771788 | | | | | | |
| | -579.7854281 | * A | | | | | |
| | 49.53479999 | * B | | | | | |
| | 308.247654 | * C | | | | | |
| | | | | | | | |
| Final Equation in Terms of Actual Factors: | | | | | | | |
| | | | | | | | |
| | Crushing strength | = | | | | | |
| | 1021.767802 | | | | | | |
| | -19326.18094 | * Water content | | | | | |
| | 27.90692957 | * Biomass top size | | | | | |
| | 30.8247654 | * Biomass content | | | | | |

## A.4.3 Mechanical Durability Model

| | | | | | | |
|---|---|---|---|---|---|---|
| Use your mouse to right click on individual cells for definitions. | | | | | | |
| Response | 3 | Mechanical durability | | | | |
| ANOVA for Response Surface Linear Model | | | | | | |
| Analysis of variance table [Partial sum of squares - Type III] | | | | | | |
| | Sum of | | Mean | F | p-value | |
| Source | Squares | df | Square | Value | Prob > F | |
| Model | 10847.05827 | 3 | 3615.686 | 42.86629 | < 0.0001 | significant |
| A-Water content | 10083.19517 | 1 | 10083.2 | 119.5428 | < 0.0001 | |
| B-Biomass top size | 4.813477412 | 1 | 4.813477 | 0.057067 | 0.8156 | |
| C-Biomass content | 972.5751261 | 1 | 972.5751 | 11.53051 | 0.0060 | |
| Residual | 927.8280214 | 11 | 84.348 | | | |
| Cor Total | 11774.88629 | 14 | | | | |
| | | | | | | |
| The Model F-value of 42.87 implies the model is significant. There is only | | | | | | |
| a 0.01% chance that a "Model F-Value" this large could occur due to noise. | | | | | | |
| | | | | | | |
| Values of "Prob > F" less than 0.0500 indicate model terms are significant. | | | | | | |
| In this case A, C are significant model terms. | | | | | | |
| Values greater than 0.1000 indicate the model terms are not significant. | | | | | | |
| If there are many insignificant model terms (not counting those required to support hierarchy), | | | | | | |
| model reduction may improve your model. | | | | | | |
| | | | | | | |
| Std. Dev. | 9.18411683 | | R-Squared | 0.921203 | | |
| Mean | 60.28933333 | | Adj R-Squ | 0.899713 | | |
| C.V. % | 15.23340253 | | Pred R-Sq | 0.845826 | | |
| PRESS | 1815.386808 | | Adeq Prec | 18.42803 | | |
| | | | | | | |
| The "Pred R-Squared" of 0.8458 is in reasonable agreement with the "Adj R-Squared" of 0.8997. | | | | | | |
| | | | | | | |
| "Adeq Precision" measures the signal to noise ratio. A ratio greater than 4 is desirable. Your | | | | | | |
| ratio of 18.428 indicates an adequate signal. This model can be used to navigate the design space. | | | | | | |
| | | | | | | |
| | Coefficient | | Standard | 95% CI | 95% CI | |
| Factor | Estimate | df | Error | Low | High | VIF |
| Intercept | 64.91205264 | 1 | 2.461814 | 59.49364 | 70.33047 | |
| A-Water content | -33.50284273 | 1 | 3.06422 | -40.2471 | -26.7585 | 1.00424 |
| B-Biomass top size | 0.75718704 | 1 | 3.169648 | -6.21916 | 7.733536 | 1.002845 |
| C-Biomass content | 11.03365419 | 1 | 3.24934 | 3.881905 | 18.1854 | 1.001395 |
| | | | | | | |
| | | | | | | |
| | | | | | | |
| Final Equation in Terms of Coded Factors: | | | | | | |
| | | | | | | |
| | Mechanical durability | = | | | | |
| | 64.91205264 | | | | | |
| | -33.50284273 | * A | | | | |
| | 0.75718704 | * B | | | | |
| | 11.03365419 | * C | | | | |
| | | | | | | |
| Final Equation in Terms of Actual Factors: | | | | | | |
| | | | | | | |
| | Mechanical durability | = | | | | |
| | 97.41372733 | | | | | |
| | -1116.761424 | * Water content | | | | |
| | 0.426584248 | * Biomass top size | | | | |
| | 1.103365419 | * Biomass content | | | | |

## A.4.4 Model Graphs

| Water Content | Particle Density (g/cm³) | Crushing Strength (N) | Mechanical Durability (%) |
|---|---|---|---|
| 0.02 |  |  |  |
| 0.05 |  |  |  |
| 0.08 |  |  |  |

# Appendix B. Briquette Flow Properties Report

This appendix includes the Flow Properties Report prepared by Solids Handling Technologies, Inc. A summary and discussion of this information is provided in Chapter 5. The report describes the flow properties of coal-biomass briquettes. The properties are expressed in terms of bin dimensions required to ensure dependable flow and maximum hopper angles for mass flow. All dimensions represent limiting conditions for flow: therefore, larger outlets and steeper hoppers are acceptable. An additional section follows the main results section of the report that explains how to properly interpret the results.

Solids Handling TECHnologies Inc.

# Virginia PolyTechnic Institute and State University

## Flow Properties Report

Project # 133060

1631 Caille Ct., Fort Mill, SC 29708 Telephone: (803) 802-5527 Fax: (803) 802-0193
E-mail email@solidshandlingtech.com www.solidshandlingtech.com

Tuesday, November 12, 2013

## INTRODUCTION

This report describes the flow properties of your materials. These properties are expressed in terms of bin dimensions required to ensure dependable flow and maximum hopper angles for mass flow. All dimensions represent limiting conditions for flow: therefore, larger outlets and steeper hoppers are acceptable. In case you are unfamiliar with the use of this type of data an appendix follows the main body of this report.

## GENERAL COMMENTS

Samples of EB CS Briquettes, EM SD Briquettes, EB CS and EM SD Coal Mix Fines were received for testing. Cohesive property tests and wall friction tests were run to determine the opening sizes required to prevent arching, and the required angle for mass flow. In addition, a compressibility test was run to determine the materials' bulk density/pressure relationship.

The field of bulk solids handling was developed due mainly to the work of Dr. Andrew W. Jenike, who pioneered the theory of bulk solids flow. Flow property testing is required to ensure reliable solids flow. A Jenike Shear Tester is used to provide the information required to solve solids flow problems. This device is a direct shear tester similar to that used in soil mechanics analyses. The Jenike method is now the standard for evaluating a bulk solid's flow properties, in the United States through ASTM (D-6128-97). It has also been the standard in Europe for many years.

A bulk solid's cohesive properties (ability to develop strength in a bin) and friction properties are measured on this bench scale test apparatus. As well, environmental conditions such as temperature, moisture content, etc. and time of storage at rest, are simulated to ensure a representative test and accurate evaluation of actual storage conditions.

**Temperature—**The following tests were run at 72°F.
**Funnel Flow**—when material flows in a funnel flow pattern a major concern is ratholing. As such, an example of the opening size required to collapse a rathole is indicated here
Note: we assumed an effective head (EH) of 10' for this summary.

| Material | Time at Rest Hours | Conical Opening to Prevent Ratholing, ft |
|---|---|---|
| EB CS Briquettes | 0 | 7.4 |
| | 24 | 8.3 |
| EM SD Briquettes | 0 | 7.7 |
| | 24 | 8.7 |
| EB CS Coal Mix Fines | 0 | 9.7 |
| | 24 | 14.0 |
| EM SD Coal Mix Fines | 0 | 9.8 |
| | 24 | 11.9 |

**Mass Flow**—when material flows in mass flow the opening size to prevent arching and the hopper angle to ensure flow along the walls is critical. The tests indicate the following opening sizes to prevent arching in mass flow:

| Material | Time at Rest Hours | Conical Opening to Prevent Arching, ft | Slot Opening to Prevent Arching, ft |
|---|---|---|---|
| EB CS Briquettes | 0 | 1.0 | 0.5 |
| | 24 | 1.0 | 0.5 |
| EM SD Briquettes | 0 | 1.0 | 0.5 |
| | 24 | 1.0 | 0.5 |
| EB CS Coal Mix Fines | 0 | 0.5 | 0.2 |
| | 24 | 0.7 | 0.4 |
| EM SD Coal Mix Fines | 0 | 0.0 | 0.0 |
| | 24 | 0.1 | 0.0 |

Wall friction tests (to determine hopper slopes for **mass flow**) were run on 2B Stainless Steel and Carbon Steel The values listed below are given as an example of how to use the results of the testing, such that, if a conical or wedge shaped hopper was fabricated from or lined with the tested wall materials, had a circular opening 1' in diameter or a slot 0.5' wide by 1.5' long, the following hopper angles would be required for mass flow:

**Note, the opening sizes were selected for use as an example only of how to interpret wall friction test results and do not necessarily indicate the required opening to prevent arching. Please refer to the appropriate table for opening size requirements, and then determine the required hopper angle for mass flow.**

The tests indicate the following hopper angles to ensure mass flow, for each sample tested:

| Material | Wall Surface | Recommended Conical Hopper Angle for Mass Flow, **(deg. from vertical)** | Recommended Wedge Hopper Angle for Mass Flow, **(deg. from vertical)** |
|---|---|---|---|
| EB CS Briquettes | 2B Stainless Steel | 30 | 42 |
| | Carbon Steel | 19 | 29 |
| EM SD Briquettes | 2B Stainless Steel | 28 | 40 |
| | Carbon Steel | 12 | 22 |
| EB CS Coal Mix Fines | 2B Stainless Steel | 24 | 35 |
| | Carbon Steel | 16 | 26 |
| EM SD Coal Mix Fines | 2B Stainless Steel | 29 | 41 |
| | Carbon Steel | 12 | 22 |

Bulk material: EB CS Briquettes
Particle size: 1.75"x.75"x.5"
Moisture content: As Rec'd
Temperature: 72 F

**Section 1: Arching and Rathole Dimensions**
**Continuous flow** (0 storage hours)

Arching Dimensions (ft)

| P factor | Bc | Bp | Bf |
|---|---|---|---|
| 1.0 | 1.0 | 0.5 | 0.5 |
| 1.25 | 1.0 | 0.5 | 0.5 |
| 1.5 | 1.1 | 0.5 | 0.6 |

Note: If arching dimension = 0 then opening size should be based on flow rate and/or feeder size requirements
***** = no dimension given by tests

Rathole Dimensions (ft)

Critical rathole diameters Df given as a function of effective head and P factor (overpressure)

| Effective head (ft): | | 5 | 10 | 20 | 30 | 40 |
|---|---|---|---|---|---|---|
| P factor = | 1.0 | 4.4 | 7.4 | 9.2 | 9.8 | 10.4 |
| P factor = | 1.25 | 5.2 | 8.9 | 10.5 | 11.2 | 12.0 |
| P factor = | 1.5 | 5.9 | 10.4 | 10.8 | 11.7 | 12.6 |

Bc = Recommended minimum outlet diameter for a conical hopper
Bp = Recommended minimum slot outlet width in a wedge shaped hopper
Bf = Minimum width of a rectangular outlet in a funnel flow bin
Df = Minimum size of flow channel in funnel flow bin to prevent stable rathole
P factor = Multiplier (of gravity) acting to consolidate bulk solid

We typically use a Jenike Shear Tester, which is the ASTM standard in the US and is as well the standard in Europe to measure flow properties; however, because of the size of the briquettes, we cannot use this equipment to measure cohesive properties. We will instead, use a hopper that is specially designed for large particles and has variable sized openings, to determine the briquettes cohesive properties.

Bulk material: EB CS Briquettes
Particle size: 1.75"x.75"x.5"
Moisture content: As Rec'd
Temperature: 72 F

**Section 1: Arching and Rathole Dimensions**

**After 24 hours at rest**

Arching Dimensions (ft)

| P factor | Bc | Bp | Bf |
|---|---|---|---|
| 1.0 | 1.0 | 0.5 | 0.5 |
| 1.25 | 1.1 | 0.5 | 0.6 |
| 1.5 | 1.2 | 0.6 | 0.6 |

Note: If arching dimension = 0 then opening size should be based on flow rate and/or feeder size requirements
***** = no dimension given by tests

Rathole Dimensions (ft)

Critical rathole diameters Df given as a function of effective head and P factor (overpressure)

| Effective head (ft): | | 5 | 10 | 20 | 30 | 40 |
|---|---|---|---|---|---|---|
| P factor = | 1.0 | 4.9 | 8.3 | 10.4 | 11.0 | 11.7 |
| P factor = | 1.25 | 5.7 | 10.0 | 10.7 | 11.6 | 12.4 |
| P factor = | 1.5 | 6.6 | 11.7 | 11.0 | 12.1 | 13.1 |

Bc = Recommended minimum outlet diameter for a conical hopper
Bp = Recommended minimum slot outlet width in a wedge shaped hopper
Bf = Minimum width of a rectangular outlet in a funnel flow bin
Df = Minimum size of flow channel in funnel flow bin to prevent stable rathole
P factor = Multiplier (of gravity) acting to consolidate bulk solid

Bulk material: EB CS Briquettes
Particle size: 1.75"x.75"x.5"
Moisture content: As Rec'd
Temperature: 72 F

**Section 2: Bulk Density (Compressibility)**

| | | | | | | | |
|---|---|---|---|---|---|---|---|
| $\sigma_1$ (psf) | 45 | 105 | 315 | 615 | 1215 | 1815 | 2415 |
| EH (ft) | 1.1 | 2.5 | 7.6 | 14.8 | 29.1 | 43.4 | 57.6 |
| $\gamma$ (pcf) | 41.3 | 41.4 | 41.5 | 41.6 | 41.7 | 41.8 | 41.9 |

$$\gamma = \gamma_0 * (\sigma / \sigma_0) \text{ ^ BETA}$$

where: $\gamma_0$ = 41.1 pcf
$\sigma_0$ = 13.0 psf
BETA = 0.0034

$\sigma_1$ = Major consolidating pressure

EH = Effective head of material ($\sigma_1 / \gamma$ )

$\gamma$ = Bulk density

| | | | |
|---|---|---|---|
| Bulk material: | EB CS Briquettes | Moisture content: | As Rec'd |
| Hopper material: | 2B Stainless Test | Particle size: | 1.75"x.75"x.5" |
| | | Temperature: | 72 F |

**Section 3: Recommended Hopper Angles for Mass Flow**

**Storage time at rest: 0 hours**

| Outlet Dia, Cone, ft | 0.5 | 1 | 2 | 4 | 8 | 16 |
|---|---|---|---|---|---|---|
| Outlet Width, Slot, ft | 0.25 | 0.5 | 1 | 2 | 4 | 8 |
| Φ' (deg) | 14 | 14 | 13 | 13 | 13 | 13 |
| θc (deg) | 30 | 30 | 30 | 31 | 31 | 31 |
| θp (deg) | 42 | 42 | 42 | 42 | 43 | 43 |

**Storage time at rest: NT**

| Outlet Dia, Cone, ft | 0.5 | 1 | 2 | 4 | 8 | 16 |
|---|---|---|---|---|---|---|
| Outlet Width, Slot, ft | 0.25 | 0.5 | 1 | 2 | 4 | 8 |
| Φ' (deg) | - | - | - | - | - | - |
| θc (deg) | - | - | - | - | - | - |
| θp (deg) | - | - | - | - | - | - |

Φ' = Angle of sliding friction on wall material
θc = Recommended slope of conical hopper wall for mass flow (from vertical)
θp = Recommended slope of wedge hopper wall for mass flow (from vertical)
NT = Not tested

7

| | | | |
|---|---|---|---|
| Bulk material: | EB CS Briquettes | Moisture content: | As Rec'd |
| Hopper material: | Carbon steel | Particle size: | 1.75"x.75"x.5" |
| | | Temperature: | 72 F |

**Section 3 (cont):** **Recommended Hopper Angles for Mass Flow**

**Storage time at rest:** **0 hours**

| Outlet Dia, Cone, ft | 0.5 | 1 | 2 | 4 | 8 | 16 |
|---|---|---|---|---|---|---|
| Outlet Width, Slot, ft | 0.25 | 0.5 | 1 | 2 | 4 | 8 |
| Φ' (deg) | 23 | 23 | 23 | 22 | 22 | 22 |
| θc (deg) | 19 | 19 | 19 | 20 | 20 | 20 |
| θp (deg) | 29 | 29 | 30 | 30 | 30 | 31 |

**Storage time at rest:** **NT**

| Outlet Dia, Cone, ft | 0.5 | 1 | 2 | 4 | 8 | 16 |
|---|---|---|---|---|---|---|
| Outlet Width, Slot, ft | 0.25 | 0.5 | 1 | 2 | 4 | 8 |
| Φ' (deg) | - | - | - | - | - | - |
| θc (deg) | - | - | - | - | - | - |
| θp (deg) | - | - | - | - | - | - |

Φ' = Angle of sliding friction on wall material
θc = Recommended slope of conical hopper wall for mass flow (from vertical)
θp = Recommended slope of wedge hopper wall for mass flow (from vertical)
NT = Not tested

Bulk material: EM SD Briquettes
Particle size: 1.75"x.75"x.5"
Moisture content: As Rec'd
Temperature: 72 F

**Section 1: Arching and Rathole Dimensions**

**Continuous flow** (0 storage hours)

Arching Dimensions (ft)

| P factor | Bc | Bp | Bf |
|---|---|---|---|
| 1.0 | 1.0 | 0.5 | 0.5 |
| 1.25 | 1.0 | 0.5 | 0.5 |
| 1.5 | 1.0 | 0.5 | 0.5 |

Note: If arching dimension = 0 then opening size should be based on flow rate and/or feeder size requirements
***** = no dimension given by tests

Rathole Dimensions (ft)

Critical rathole diameters Df given as a function of effective head and P factor (overpressure)

| Effective head (ft): | | 5 | 10 | 20 | 30 | 40 |
|---|---|---|---|---|---|---|
| P factor = | 1.0 | 4.3 | 7.7 | 8.3 | 8.9 | 9.5 |
| P factor = | 1.25 | 5.0 | 8.7 | 9.5 | 10.2 | 10.9 |
| P factor = | 1.5 | 5.7 | 8.9 | 9.8 | 10.6 | 11.5 |

Bc = Recommended minimum outlet diameter for a conical hopper
Bp = Recommended minimum slot outlet width in a wedge shaped hopper
Bf = Minimum width of a rectangular outlet in a funnel flow bin
Df = Minimum size of flow channel in funnel flow bin to prevent stable rathole
P factor = Multiplier (of gravity) acting to consolidate bulk solid

Bulk material: EM SD Briquettes
Particle size: 1.75"x.75"x.5"
Moisture content: As Rec'd
Temperature: 72 F

**Section 1: Arching and Rathole Dimensions**
**After 24 hours at rest**

Arching Dimensions (ft)

| P factor | Bc | Bp | Bf |
|---|---|---|---|
| 1.0 | 1.0 | 0.5 | 0.5 |
| 1.25 | 1.1 | 0.5 | 0.6 |
| 1.5 | 1.2 | 0.6 | 0.7 |

Note: If arching dimension = 0 then opening size should be based on flow rate and/or feeder size requirements
***** = no dimension given by tests

Rathole Dimensions (ft)

Critical rathole diameters Df given as a function of effective head and P factor (overpressure)

| Effective head (ft): | | 5 | 10 | 20 | 30 | 40 |
|---|---|---|---|---|---|---|
| P factor = | 1.0 | 4.8 | 8.7 | 9.3 | 10.0 | 10.6 |
| P factor = | 1.25 | 5.6 | 8.8 | 9.6 | 10.5 | 11.3 |
| P factor = | 1.5 | 6.5 | 9.0 | 10.0 | 10.9 | 11.9 |

Bc = Recommended minimum outlet diameter for a conical hopper
Bp = Recommended minimum slot outlet width in a wedge shaped hopper
Bf = Minimum width of a rectangular outlet in a funnel flow bin
Df = Minimum size of flow channel in funnel flow bin to prevent stable rathole
P factor = Multiplier (of gravity) acting to consolidate bulk solid

Bulk material: EM SD Briquettes
Particle size: 1.75"x.75"x.5"
Moisture content: As Rec'd
Temperature: 72 F

**Section 2: Bulk Density (Compressibility)**

| $\sigma_1$ (psf) | 45 | 105 | 315 | 615 | 1215 | 1815 | 2415 |
|---|---|---|---|---|---|---|---|
| EH (ft) | 1.0 | 2.3 | 6.8 | 13.3 | 26.2 | 39.0 | 51.9 |
| $\gamma$ (pcf) | 46.2 | 46.3 | 46.3 | 46.4 | 46.4 | 46.5 | 46.6 |

$$\gamma = \gamma_0 * (\sigma / \sigma_0) \text{ ^ BETA}$$

where: $\gamma_0$ = 46.1 pcf
$\sigma_0$ = 13.0 psf
BETA = 0.0019

$\sigma_1$ = Major consolidating pressure

EH = Effective head of material ($\sigma_1 / \gamma$)

$\gamma$ = Bulk density

| | | | |
|---|---|---|---|
| Bulk material: | EM SD Briquettes | Moisture content: | As Rec'd |
| Hopper material: | 2B Stainless Test | Particle size: | 1.75"x.75"x.5" |
| | | Temperature: | 72 F |

**Section 3: Recommended Hopper Angles for Mass Flow**

**Storage time at rest: 0 hours**

| | | | | | | |
|---|---|---|---|---|---|---|
| Outlet Dia, Cone, ft | 0.5 | 1 | 2 | 4 | 8 | 16 |
| Outlet Width, Slot, ft | 0.25 | 0.5 | 1 | 2 | 4 | 8 |
| Φ' (deg) | 17 | 15 | 14 | 12 | 10 | 9 |
| θc (deg) | 26 | 28 | 30 | 32 | 34 | 36 |
| θp (deg) | 38 | 40 | 42 | 44 | 46 | 48 |

**Storage time at rest: NT**

| | | | | | | |
|---|---|---|---|---|---|---|
| Outlet Dia, Cone, ft | 0.5 | 1 | 2 | 4 | 8 | 16 |
| Outlet Width, Slot, ft | 0.25 | 0.5 | 1 | 2 | 4 | 8 |
| Φ' (deg) | - | - | - | - | - | - |
| θc (deg) | - | - | - | - | - | - |
| θp (deg) | - | - | - | - | - | - |

Φ' = Angle of sliding friction on wall material
θc = Recommended slope of conical hopper wall for mass flow (from vertical)
θp = Recommended slope of wedge hopper wall for mass flow (from vertical)
NT = Not tested

12

| | | | |
|---|---|---|---|
| Bulk material: | EM SD Briquettes | Moisture content: | As Rec'd |
| Hopper material: | Carbon steel | Particle size: | 1.75"x.75"x.5" |
| | | Temperature: | 72 F |

**Section 3 (cont):** **Recommended Hopper Angles for Mass Flow**

**Storage time at rest:** **0 hours**

| Outlet Dia, Cone, ft | 0.5 | 1 | 2 | 4 | 8 | 16 |
|---|---|---|---|---|---|---|
| Outlet Width, Slot, ft | 0.25 | 0.5 | 1 | 2 | 4 | 8 |
| Φ' (deg) | 29 | 28 | 28 | 27 | 26 | 26 |
| θc (deg) | 12 | 12 | 13 | 14 | 15 | 15 |
| θp (deg) | 22 | 22 | 23 | 24 | 25 | 26 |

**Storage time at rest:** **NT**

| Outlet Dia, Cone, ft | 0.5 | 1 | 2 | 4 | 8 | 16 |
|---|---|---|---|---|---|---|
| Outlet Width, Slot, ft | 0.25 | 0.5 | 1 | 2 | 4 | 8 |
| Φ' (deg) | - | - | - | - | - | - |
| θc (deg) | - | - | - | - | - | - |
| θp (deg) | - | - | - | - | - | - |

Φ' = Angle of sliding friction on wall material
θc = Recommended slope of conical hopper wall for mass flow (from vertical)
θp = Recommended slope of wedge hopper wall for mass flow (from vertical)
NT = Not tested

Bulk material: EB-CS Coal Mix fines
Particle size: As Rec'd
Moisture content: As Rec'd
Temperature: 72 F

**Section 1: Arching and Rathole Dimensions**

**Continuous flow** (0 storage hours)

Arching Dimensions (ft)

| P factor | Bc | Bp | Bf |
|---|---|---|---|
| 1.0 | 0.5 | 0.2 | 0.2 |
| 1.25 | 0.6 | 0.3 | 0.3 |
| 1.5 | 0.6 | 0.3 | 0.4 |

Note: If arching dimension = 0 then opening size should be based on flow rate and/or feeder size requirements
***** = no dimension given by tests

Rathole Dimensions (ft)

Critical rathole diameters Df given as a function of effective head and P factor (overpressure)

| Effective head (ft): | | 5 | 10 | 20 | 30 | 40 |
|---|---|---|---|---|---|---|
| P factor = | 1.0 | 4.9 | 9.7 | 19.4 | 29.7 | 30.7 |
| P factor = | 1.25 | 6.1 | 12.1 | 24.2 | 41.1 | 42.3 |
| P factor = | 1.5 | 7.3 | 14.5 | 29.0 | 41.8 | 43.3 |

Bc = Recommended minimum outlet diameter for a conical hopper
Bp = Recommended minimum slot outlet width in a wedge shaped hopper
Bf = Minimum width of a rectangular outlet in a funnel flow bin
Df = Minimum size of flow channel in funnel flow bin to prevent stable rathole
P factor = Multiplier (of gravity) acting to consolidate bulk solid

Bulk material: EB-CS Coal Mix fines
Particle size: As Rec'd
Moisture content: As Rec'd
Temperature: 72 F

**Section 1: Arching and Rathole Dimensions**
**After 24 hours at rest**

Arching Dimensions (ft)

| P factor | Bc | Bp | Bf |
|---|---|---|---|
| 1.0 | 0.7 | 0.4 | 0.4 |
| 1.25 | 0.9 | 0.4 | 0.5 |
| 1.5 | 1.0 | 0.5 | 0.7 |

Note: If arching dimension = 0 then opening size should be based on flow rate and/or feeder size requirements
***** = no dimension given by tests

Rathole Dimensions (ft)

Critical rathole diameters Df given as a function of effective head and P factor (overpressure)

| Effective head (ft): | | 5 | 10 | 20 | 30 | 40 |
|---|---|---|---|---|---|---|
| P factor = | 1.0 | 7.4 | 14.0 | 27.4 | 41.5 | 42.8 |
| P factor = | 1.25 | 9.0 | 17.4 | 34.0 | 42.5 | 44.1 |
| P factor = | 1.5 | 10.7 | 20.7 | 40.7 | 43.5 | 45.5 |

Bc = Recommended minimum outlet diameter for a conical hopper
Bp = Recommended minimum slot outlet width in a wedge shaped hopper
Bf = Minimum width of a rectangular outlet in a funnel flow bin
Df = Minimum size of flow channel in funnel flow bin to prevent stable rathole
P factor = Multiplier (of gravity) acting to consolidate bulk solid

Bulk material: EB-CS Coal Mix fines
Particle size: As Rec'd
Moisture content: As Rec'd
Temperature: 72 F

**Section 2: Bulk Density (Compressibility)**

| $\sigma_1$ (psf) | 45 | 105 | 315 | 615 | 1215 | 1815 | 2415 |
|---|---|---|---|---|---|---|---|
| EH (ft) | 1.7 | 3.9 | 11.0 | 20.6 | 38.9 | 55.3 | 71.6 |
| $\gamma$ (pcf) | 26.1 | 27.3 | 28.7 | 29.8 | 31.3 | 32.8 | 33.7 |

$$\gamma = \gamma_0 * (\sigma / \sigma_0) \text{ ^ BETA}$$

where: $\gamma_0$ = 23.9 pcf
$\sigma_0$ = 13.0 psf
BETA = 0.0624

$\sigma_1$ = Major consolidating pressure

EH = Effective head of material ($\sigma_1 / \gamma$)

$\gamma$ = Bulk density

| | | | |
|---|---|---|---|
| Bulk material: | EB-CS Coal Mix fines | Moisture content: | As Rec'd |
| Hopper material: | 2B Stainless Steel | Particle size: | As Rec'd |
| | | Temperature: | 72 F |

**Section 3: Recommended Hopper Angles for Mass Flow**

**Storage time at rest: 0 hours**

| Outlet Dia, Cone, ft | 0.5 | 1 | 2 | 4 | 8 | 16 |
|---|---|---|---|---|---|---|
| Outlet Width, Slot, ft | 0.25 | 0.5 | 1 | 2 | 4 | 8 |
| Φ' (deg) | 20 | 19 | 17 | 16 | 14 | 13 |
| θc (deg) | 22 | 24 | 26 | 28 | 29 | 31 |
| θp (deg) | 33 | 35 | 37 | 39 | 41 | 43 |

**Storage time at rest: NT**

| Outlet Dia, Cone, ft | 0.5 | 1 | 2 | 4 | 8 | 16 |
|---|---|---|---|---|---|---|
| Outlet Width, Slot, ft | 0.25 | 0.5 | 1 | 2 | 4 | 8 |
| Φ' (deg) | - | - | - | - | - | - |
| θc (deg) | - | - | - | - | - | - |
| θp (deg) | - | - | - | - | - | - |

Φ' = Angle of sliding friction on wall material
θc = Recommended slope of conical hopper wall for mass flow (from vertical)
θp = Recommended slope of wedge hopper wall for mass flow (from vertical)
NT = Not tested

| | | | |
|---|---|---|---|
| Bulk material: | EB-CS Coal Mix fines | Moisture content: | As Rec'd |
| Hopper material: | Carbon Steel | Particle size: | As Rec'd |
| | | Temperature: | 72 F |

**Section 3 (cont):** **Recommended Hopper Angles for Mass Flow**

**Storage time at rest:** **0 hours**

| Outlet Dia, Cone, ft | 0.5 | 1 | 2 | 4 | 8 | 16 |
|---|---|---|---|---|---|---|
| Outlet Width, Slot, ft | 0.25 | 0.5 | 1 | 2 | 4 | 8 |
| Φ' (deg) | 26 | 25 | 25 | 24 | 24 | 23 |
| θc (deg) | 15 | 16 | 17 | 17 | 18 | 19 |
| θp (deg) | 25 | 26 | 27 | 27 | 28 | 29 |

**Storage time at rest:** **NT**

| Outlet Dia, Cone, ft | 0.5 | 1 | 2 | 4 | 8 | 16 |
|---|---|---|---|---|---|---|
| Outlet Width, Slot, ft | 0.25 | 0.5 | 1 | 2 | 4 | 8 |
| Φ' (deg) | - | - | - | - | - | - |
| θc (deg) | - | - | - | - | - | - |
| θp (deg) | - | - | - | - | - | - |

Φ' = Angle of sliding friction on wall material
θc = Recommended slope of conical hopper wall for mass flow (from vertical)
θp = Recommended slope of wedge hopper wall for mass flow (from vertical)
NT = Not tested

Bulk material: EM-SD Coal Mix fines
Particle size: As Rec'd
Moisture content: As Rec'd
Temperature: 72 F

**Section 1: Arching and Rathole Dimensions**

**Continuous flow** (0 storage hours)

Arching Dimensions (ft)

| P factor | Bc | Bp | Bf |
|---|---|---|---|
| 1.0 | 0.0 | 0.0 | 0.0 |
| 1.25 | 0.0 | 0.0 | 0.0 |
| 1.5 | 0.0 | 0.0 | 0.0 |

Note: If arching dimension = 0 then opening size should be based on flow rate and/or feeder size requirements
***** = no dimension given by tests

Rathole Dimensions (ft)

Critical rathole diameters Df given as a function of effective head and P factor (overpressure)

| Effective head (ft): | | 5 | 10 | 20 | 30 | 40 |
|---|---|---|---|---|---|---|
| P factor = | 1.0 | 4.9 | 9.8 | 19.6 | 29.1 | 30.1 |
| P factor = | 1.25 | 6.1 | 12.2 | 24.5 | 35.4 | 36.6 |
| P factor = | 1.5 | 7.3 | 14.7 | 29.4 | 36.1 | 37.6 |

Bc = Recommended minimum outlet diameter for a conical hopper
Bp = Recommended minimum slot outlet width in a wedge shaped hopper
Bf = Minimum width of a rectangular outlet in a funnel flow bin
Df = Minimum size of flow channel in funnel flow bin to prevent stable rathole
P factor = Multiplier (of gravity) acting to consolidate bulk solid

Bulk material: EM-SD Coal Mix fines
Particle size: As Rec'd
Moisture content: As Rec'd
Temperature: 72 F

**Section 1: Arching and Rathole Dimensions**
**After 24 hours at rest**

Arching Dimensions (ft)

| P factor | Bc | Bp | Bf |
|---|---|---|---|
| 1.0 | 0.1 | 0.0 | 0.0 |
| 1.25 | 0.1 | 0.0 | 0.0 |
| 1.5 | 0.1 | 0.0 | 0.0 |

Note: If arching dimension = 0 then opening size should be based on flow rate and/or feeder size requirements
***** = no dimension given by tests

Rathole Dimensions (ft)

Critical rathole diameters Df given as a function of effective head and P factor (overpressure)

| Effective head (ft): | | 5 | 10 | 20 | 30 | 40 |
|---|---|---|---|---|---|---|
| P factor = | 1.0 | 6.0 | 11.9 | 23.7 | 35.3 | 36.5 |
| P factor = | 1.25 | 7.4 | 14.8 | 29.6 | 36.2 | 37.6 |
| P factor = | 1.5 | 8.9 | 17.8 | 35.6 | 37.0 | 38.8 |

Bc = Recommended minimum outlet diameter for a conical hopper
Bp = Recommended minimum slot outlet width in a wedge shaped hopper
Bf = Minimum width of a rectangular outlet in a funnel flow bin
Df = Minimum size of flow channel in funnel flow bin to prevent stable rathole
P factor = Multiplier (of gravity) acting to consolidate bulk solid

Bulk material: EM-SD Coal Mix fines
Particle size: As Rec'd
Moisture content: As Rec'd
Temperature: 72 F

**Section 2: Bulk Density (Compressibility)**

| | | | | | | | |
|---|---|---|---|---|---|---|---|
| $\sigma_1$ (psf) | 45 | 105 | 315 | 615 | 1215 | 1815 | 2415 |
| EH (ft) | 1.8 | 4.2 | 11.7 | 21.7 | 39.3 | 57.3 | 74.6 |
| $\gamma$ (pcf) | 24.3 | 25.3 | 27.0 | 28.3 | 30.9 | 31.7 | 32.4 |

$$\gamma = \gamma_0 * (\sigma / \sigma_0) \text{ ^ BETA}$$

where: $\gamma_0$ = 21.7 pcf
$\sigma_0$ = 13.0 psf
BETA = 0.0746

$\sigma_1$ = Major consolidating pressure

EH = Effective head of material ($\sigma_1 / \gamma$)

$\gamma$ = Bulk density

| | | | |
|---|---|---|---|
| Bulk material: | EM-SD Coal Mix fines | Moisture content: | As Rec'd |
| Hopper material: | 2B Stainless Steel | Particle size: | As Rec'd |
| | | Temperature: | 72 F |

**Section 3:** **Recommended Hopper Angles for Mass Flow**

**Storage time at rest:** **0 hours**

| Outlet Dia, Cone, ft | 0.5 | 1 | 2 | 4 | 8 | 16 |
|---|---|---|---|---|---|---|
| Outlet Width, Slot, ft | 0.25 | 0.5 | 1 | 2 | 4 | 8 |
| Φ' (deg) | 15 | 15 | 14 | 13 | 12 | 11 |
| θc (deg) | 28 | 29 | 30 | 31 | 32 | 33 |
| θp (deg) | 39 | 41 | 42 | 43 | 44 | 45 |

**Storage time at rest:** **NT**

| Outlet Dia, Cone, ft | 0.5 | 1 | 2 | 4 | 8 | 16 |
|---|---|---|---|---|---|---|
| Outlet Width, Slot, ft | 0.25 | 0.5 | 1 | 2 | 4 | 8 |
| Φ' (deg) | - | - | - | - | - | - |
| θc (deg) | - | - | - | - | - | - |
| θp (deg) | - | - | - | - | - | - |

Φ' = Angle of sliding friction on wall material
θc = Recommended slope of conical hopper wall for mass flow (from vertical)
θp = Recommended slope of wedge hopper wall for mass flow (from vertical)
NT = Not tested

| | | | |
|---|---|---|---|
| Bulk material: | EM-SD Coal Mix fines | Moisture content: | As Rec'd |
| Hopper material: | Carbon Steel | Particle size: | As Rec'd |
| | | Temperature: | 72 F |

**Section 3 (cont):** **Recommended Hopper Angles for Mass Flow**

**Storage time at rest:** **0 hours**

| Outlet Dia, Cone, ft | 0.5 | 1 | 2 | 4 | 8 | 16 |
|---|---|---|---|---|---|---|
| Outlet Width, Slot, ft | 0.25 | 0.5 | 1 | 2 | 4 | 8 |
| Φ' (deg) | 30 | 29 | 27 | 26 | 25 | 24 |
| θc (deg) | 10 | 12 | 13 | 15 | 17 | 18 |
| θp (deg) | 20 | 22 | 24 | 25 | 27 | 28 |

**Storage time at rest:** **NT**

| Outlet Dia, Cone, ft | 0.5 | 1 | 2 | 4 | 8 | 16 |
|---|---|---|---|---|---|---|
| Outlet Width, Slot, ft | 0.25 | 0.5 | 1 | 2 | 4 | 8 |
| Φ' (deg) | - | - | - | - | - | - |
| θc (deg) | - | - | - | - | - | - |
| θp (deg) | - | - | - | - | - | - |

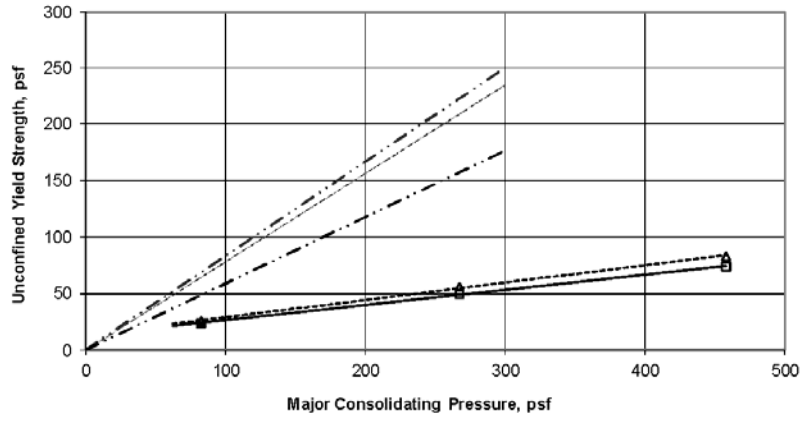
Φ' = Angle of sliding friction on wall material
θc = Recommended slope of conical hopper wall for mass flow (from vertical)
θp = Recommended slope of wedge hopper wall for mass flow (from vertical)
NT = Not tested

*Solids Handling Technologies, Inc.*

**Flow functions - Strength vs Consolidating Pressure**

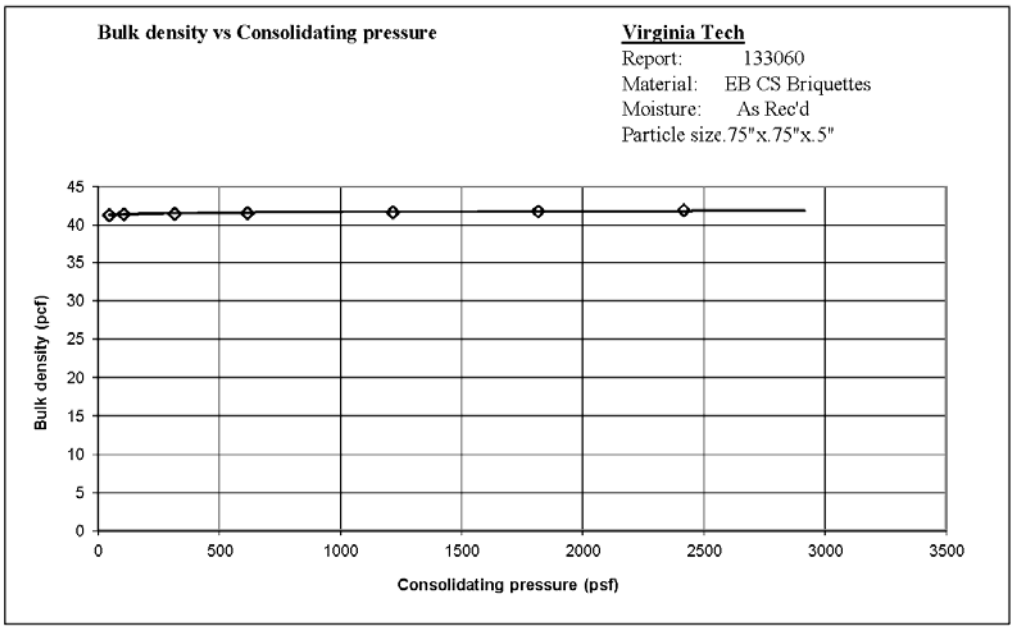
Continuous flow
Time at rest: 24 hours
Temperature: 72 F

**Virginia Tech**
Report: 133060
Material: EB CS Briquettes
Moisture: As Rec'd
Particle size:.75"x.75"x.5"




24

*Solids Handling Technologies, Inc.*



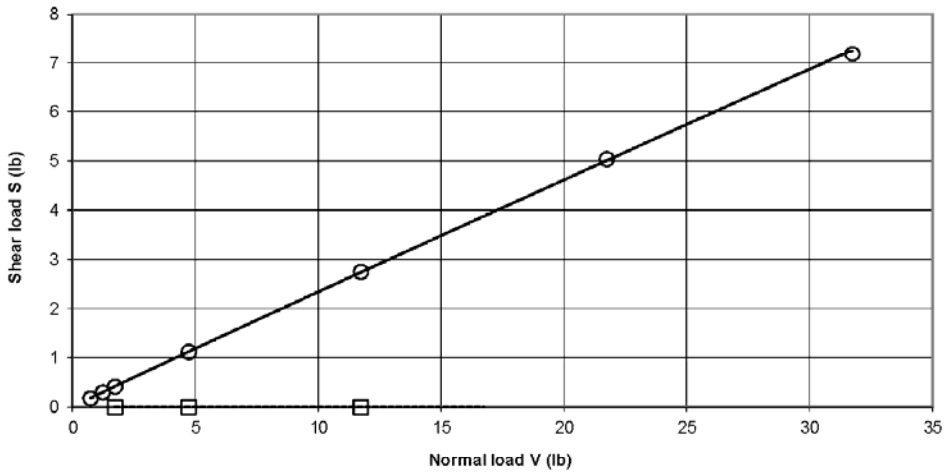

25

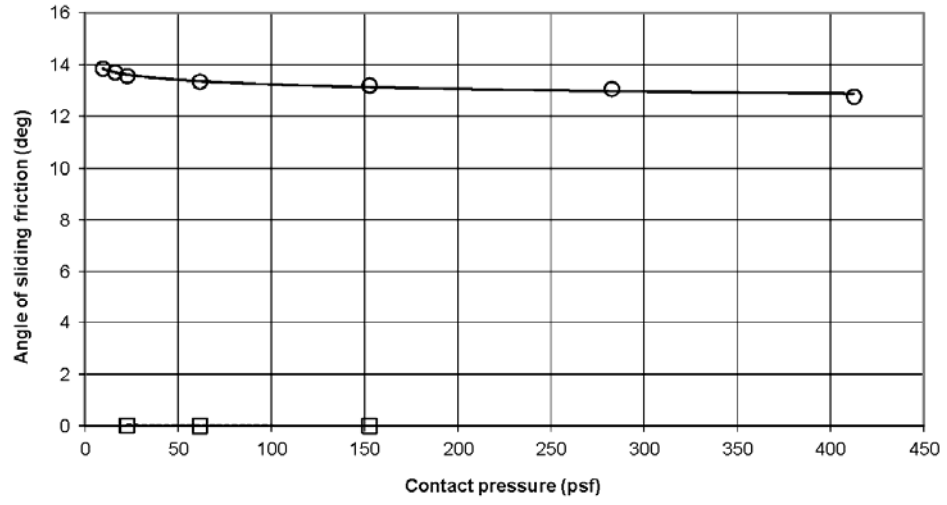
*Solids Handling Technologies, Inc.*

**Friction between**
EB CS Briquettes
2B Stainless Test

**Virginia Tech**
Report: 133060
Moisture: As Rec'd
Particle size: .75"x.75"x.5"
Temperature: 72 F

Continuous flow
Adhesion after NT



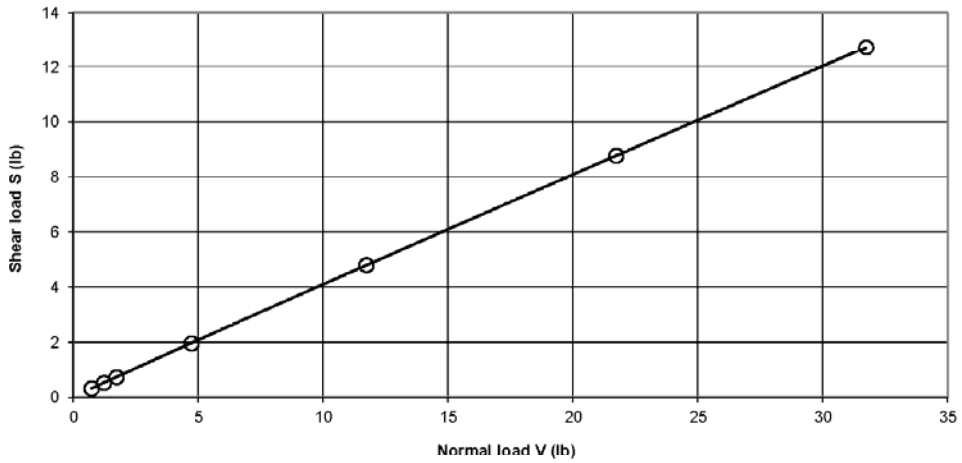

26

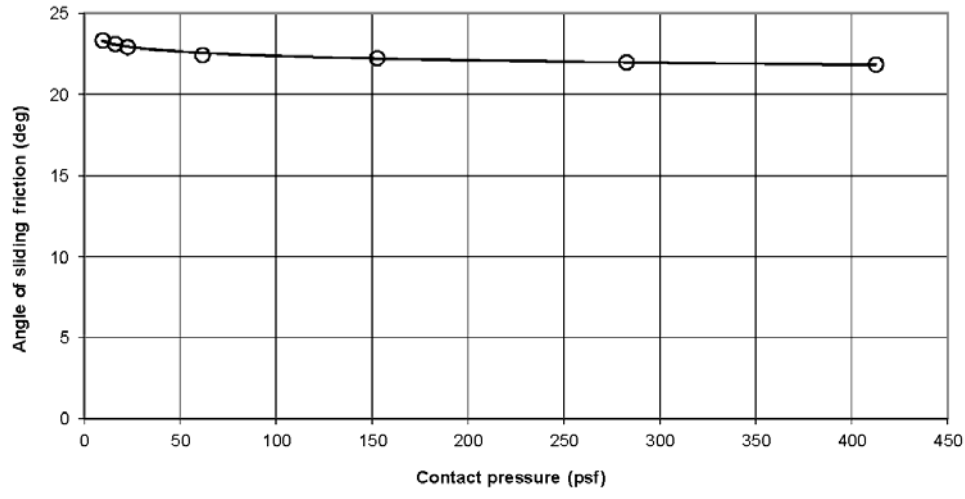
*Solids Handling Technologies, Inc.*

**Friction between**
EB CS Briquettes
Carbon steel

**Virginia Tech**
Report: 133060
Moisture: As Rec'd
Particle size: .75"x.75"x.5"
Temperature: 72 F

Continuous flow
Adhesion after NT



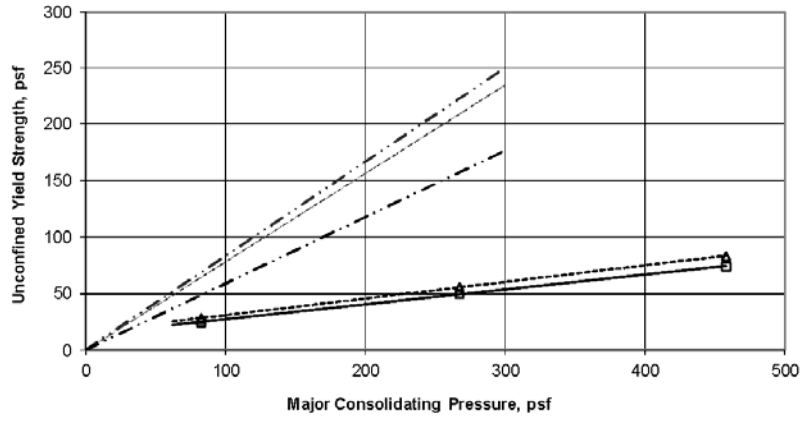

27

*Solids Handling Technologies, Inc.*

**Flow functions - Strength vs Consolidating Pressure**

Continuous flow
Time at rest: 24 hours
Temperature: 72 F

**Virginia Tech**
Report: 133060
Material: EM SD Briquettes
Moisture: As Rec'd
Particle size:.75"x.75"x.5"

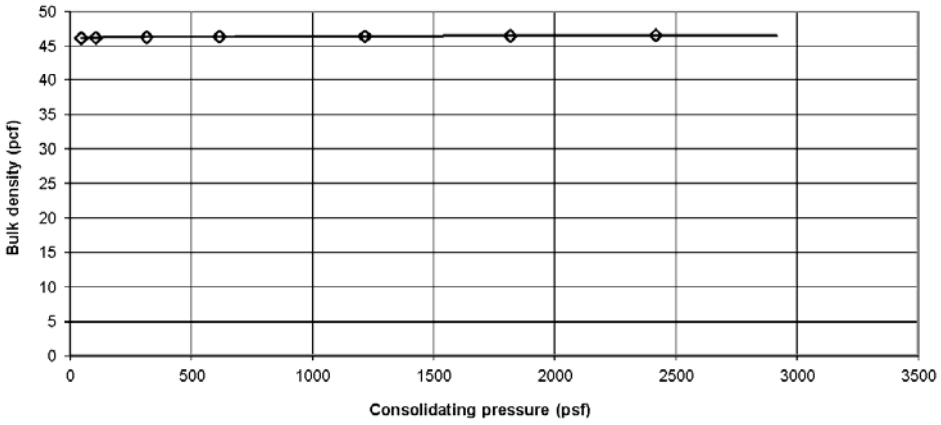



28

*Solids Handling Technologies, Inc.*

**Bulk density vs Consolidating pressure**

**Virginia Tech**
Report: 133060
Material: EM SD Briquettes
Moisture: As Rec'd
Particle size. 75"x.75"x.5"



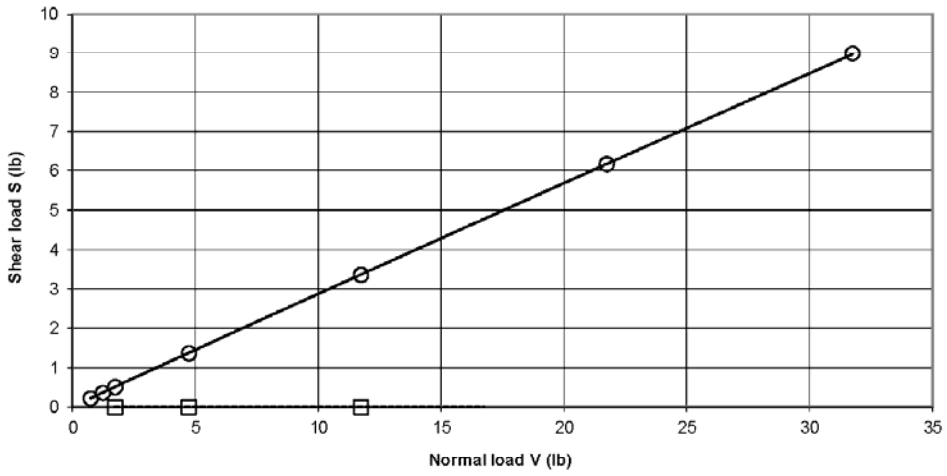

29

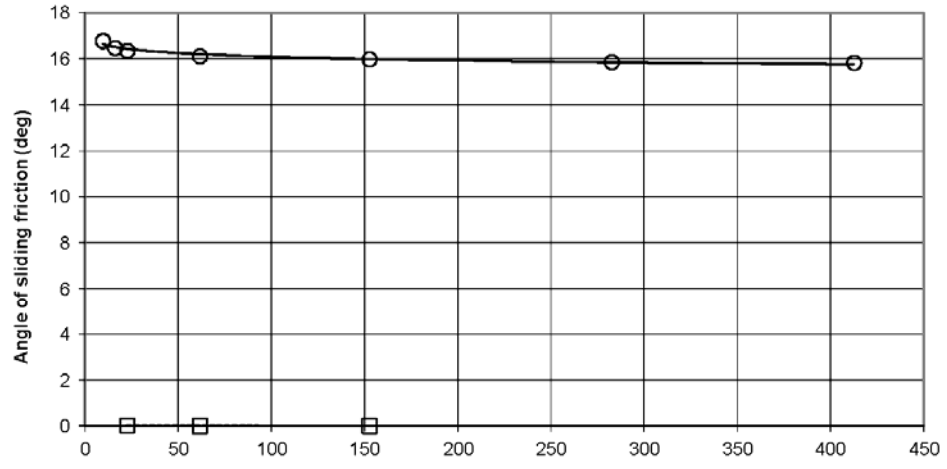
*Solids Handling Technologies, Inc.*

**Friction between**
EM SD Briquettes
2B Stainless Test

**Virginia Tech**
Report: 133060
Moisture: As Rec'd
Particle size: .75"x.75"x.5"
Temperature: 72 F

Continuous flow
Adhesion after NT



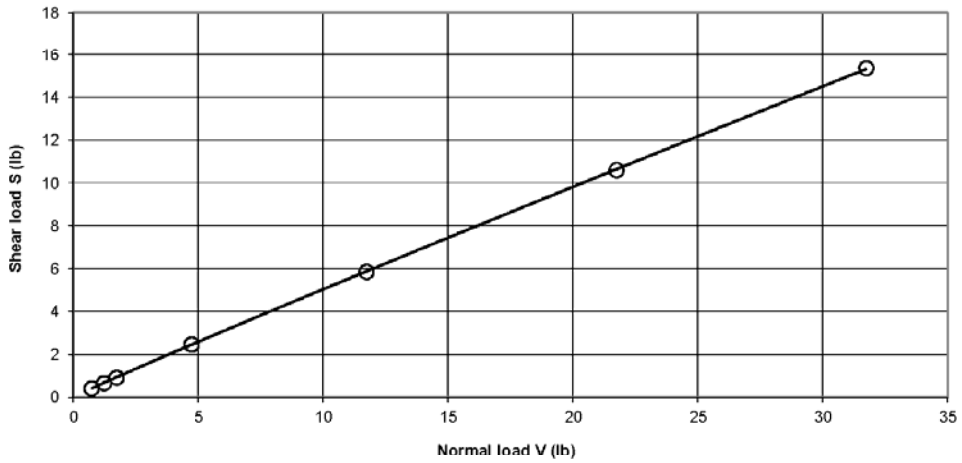

30

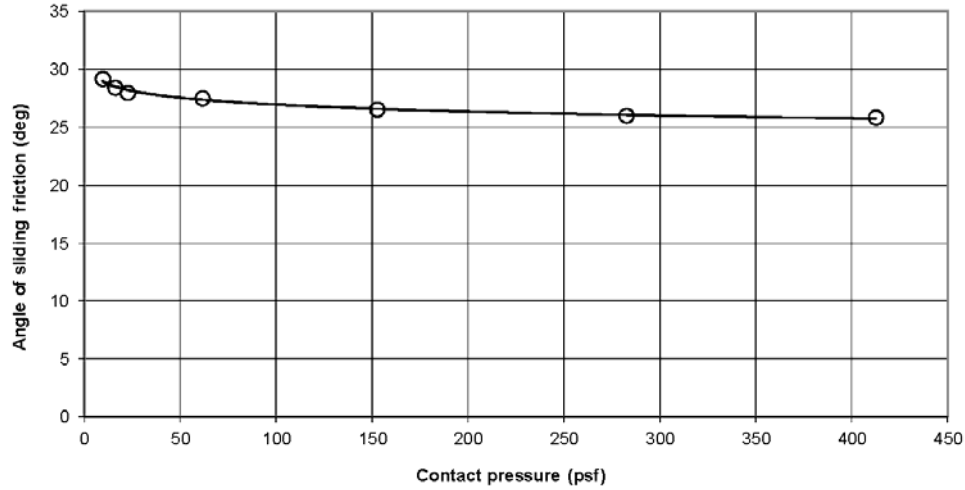
*Solids Handling Technologies, Inc.*

**Friction between**
EM SD Briquettes
Carbon steel

**Virginia Tech**
Report: 133060
Moisture: As Rec'd
Particle size: .75"x.75"x.5"
Temperature: 72 F

Continuous flow
Adhesion after NT



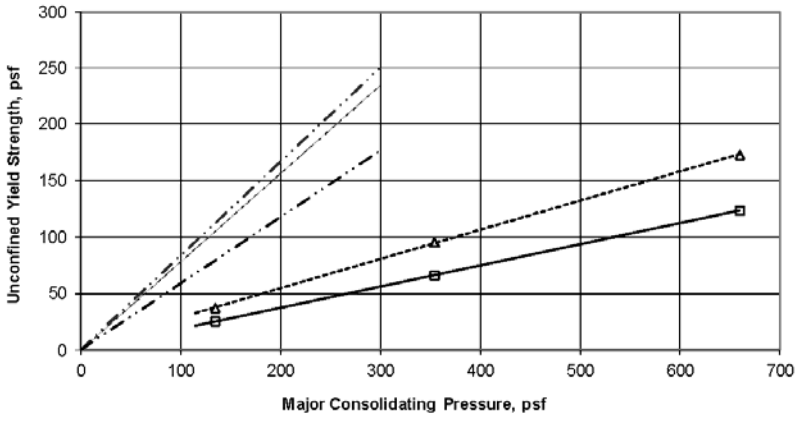

31

*Solids Handling Technologies, Inc.*

**Flow functions - Strength vs Consolidating Pressure**

Continuous flow
Time at rest: 24 hours
Temperature: 72 F

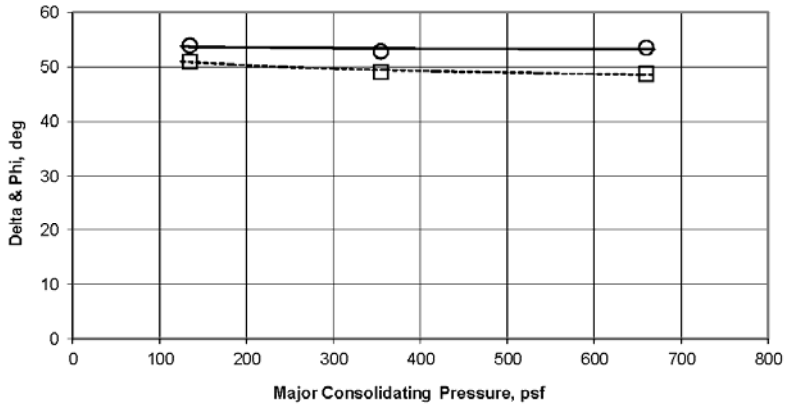
**Virgina Tech**
Report: 133060
Material: EB-CS Coal Mix fines
Moisture: As Rec'd
Particle size: As Rec'd




**Angles Delta and Phi**

Delta Phi

**Virgina Tech**
Report: 133060
Material: EB-CS Coal Mix fines
Moisture: As Rec'd
Particle size: As Rec'd



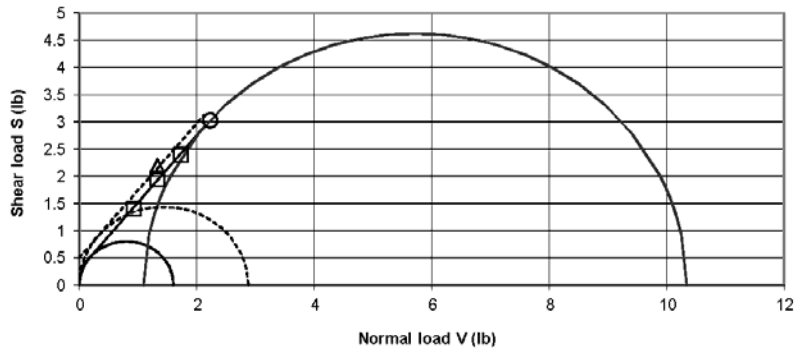

32

*Solids Handling Technologies, Inc.*

**Yield locus 1**

Continuous flow
Time at rest: 24 hours
Temperature: 72 F

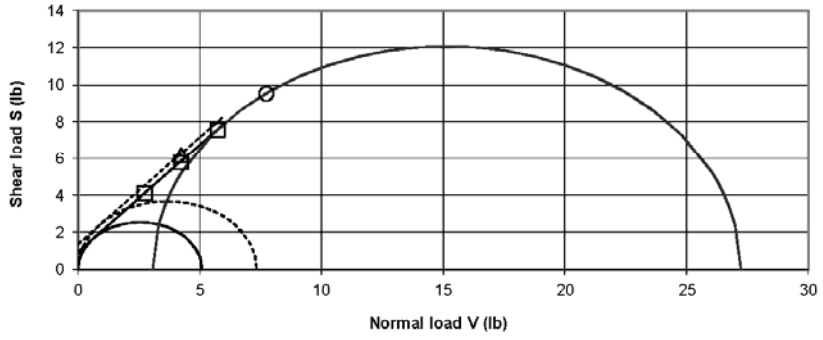
**Virgina Tech**
Report: 133060
Material: EB-CS Coal Mix fines
Moisture: As Rec'd Delta: 54
Particle size: As Rec'd Phi: 51




**Yield locus 2**

Continuous flow
Time at rest: 24 hours
Temperature: 72 F

**Virgina Tech**
Report: 133060
Material: EB-CS Coal Mix fines
Moisture: As Rec'd Delta: 53
Particle size: As Rec'd Phi: 49



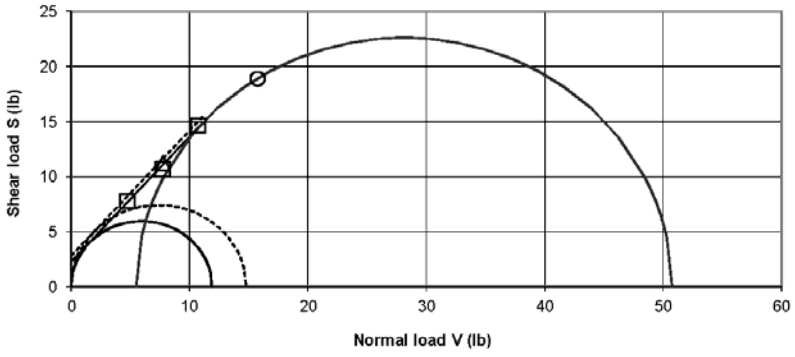

33

*Solids Handling Technologies, Inc.*

**Yield locus 3**

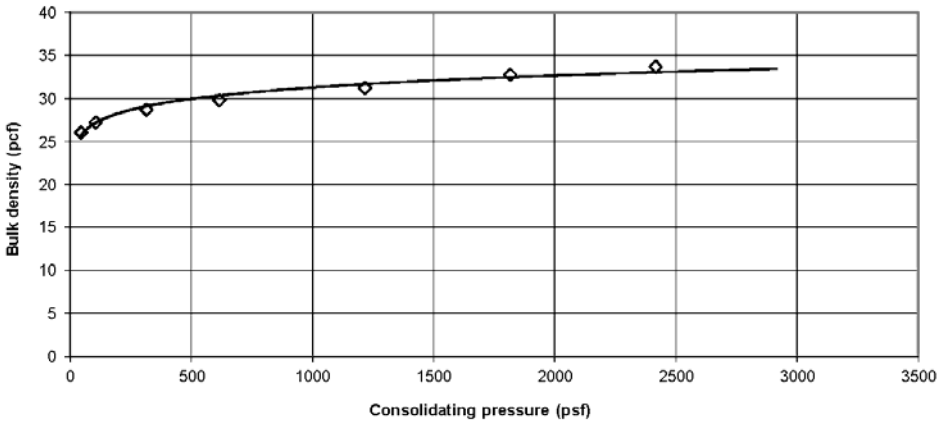
Continuous flow
Time at rest: 24 hours
Temperature: 72 F

**Virgina Tech**
Report: 133060
Material: EB-CS Coal Mix fines
Moisture: As Rec'd Delta: 54
Particle size: As Rec'd Phi: 49




**Bulk density vs Consolidating pressure**

**Virgina Tech**
Report: 133060
Material: EB-CS Coal Mix fines
Moisture: As Rec'd
Particle size As Rec'd



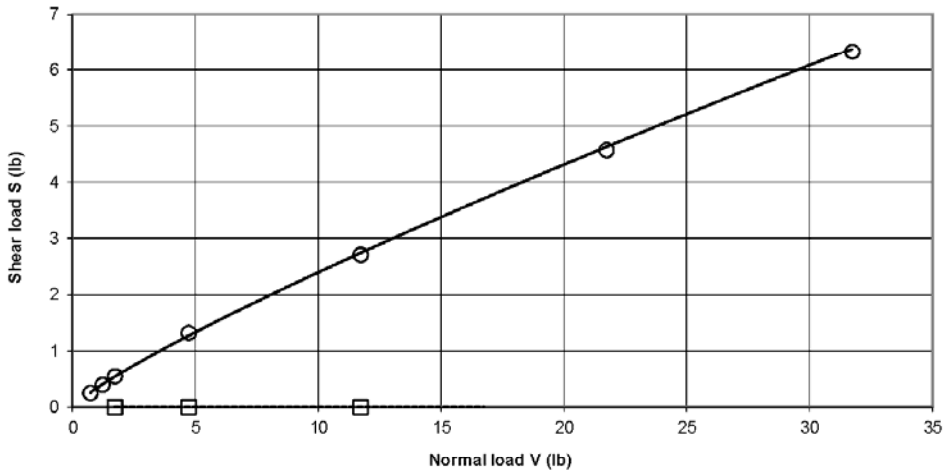

34

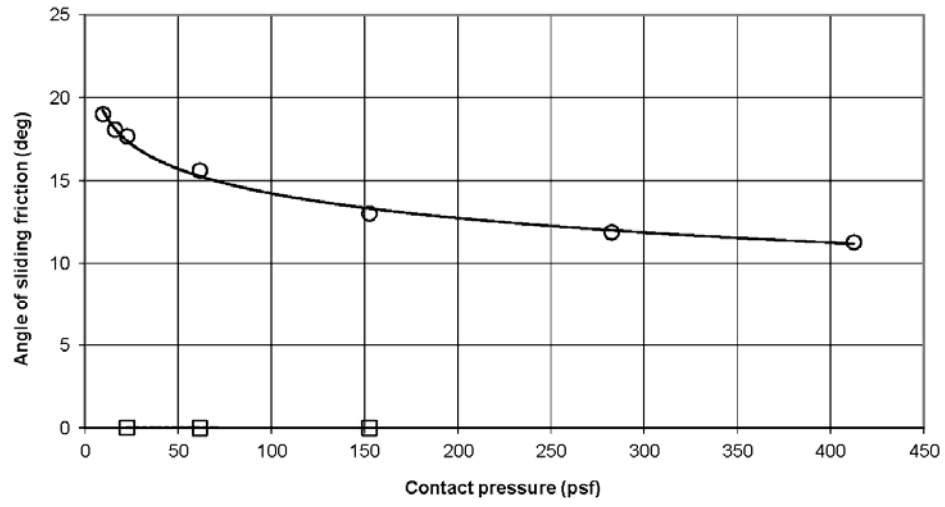
Solids Handling Technologies, Inc.

**Friction between**
EB-CS Coal Mix fines
2B Stainless Steel

**Virgina Tech**
Report: 133060
Moisture: As Rec'd
Particle size: As Rec'd
Temperature: 72 F

Continuous flow
Adhesion after NT



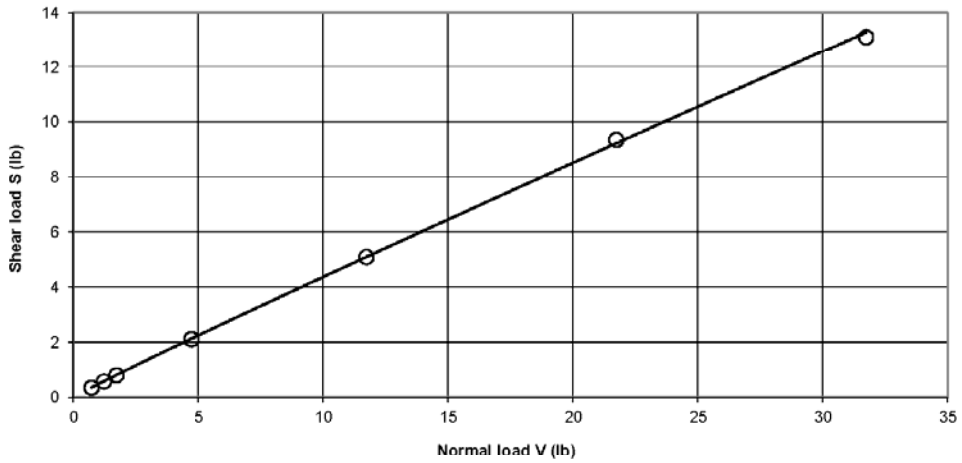

35

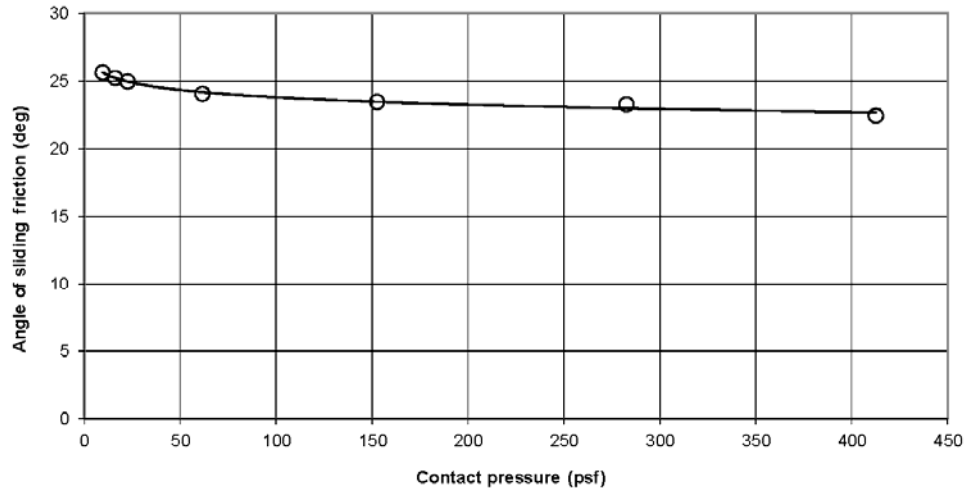
*Solids Handling Technologies, Inc.*

**Friction between**
EB-CS Coal Mix fines
Carbon Steel

Continuous flow
Adhesion after NT

**Virgina Tech**
Report: 133060
Moisture: As Rec'd
Particle size: As Rec'd
Temperature: 72 F



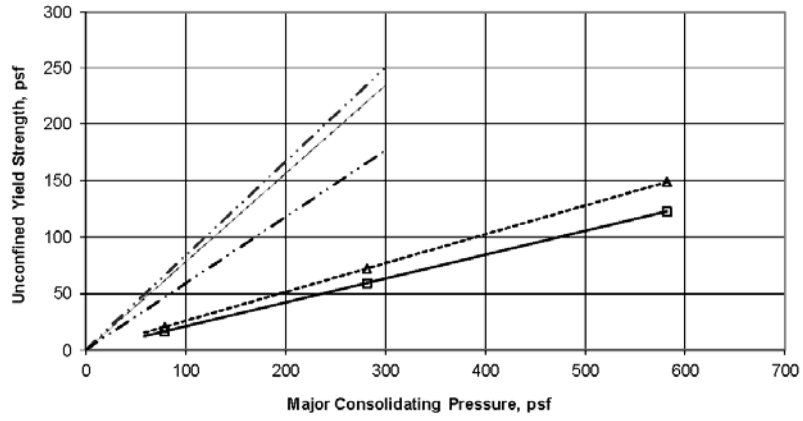

36

*Solids Handling Technologies, Inc.*

**Flow functions - Strength vs Consolidating Pressure**

Continuous flow
Time at rest: 24 hours
Temperature: 72 F

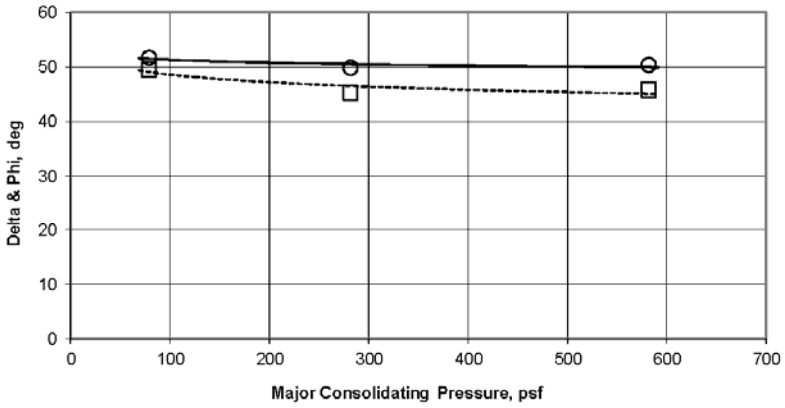
**Virgina Tech**
Report: 133060
Material: EM-SD Coal Mix fines
Moisture: As Rec'd
Particle size: As Rec'd




**Angles Delta and Phi**

Delta Phi

**Virgina Tech**
Report: 133060
Material: EM-SD Coal Mix fines
Moisture: As Rec'd
Particle size: As Rec'd



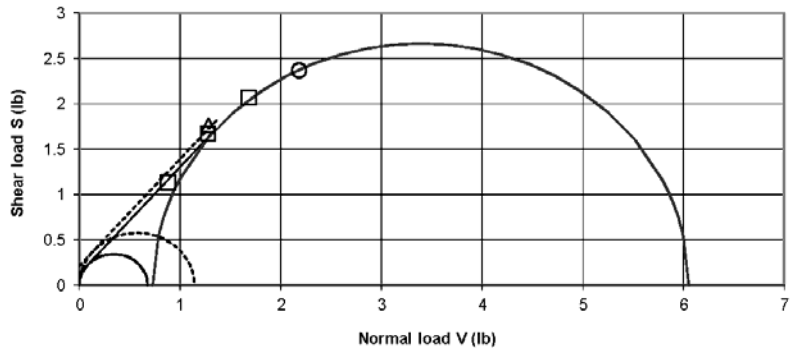

37

*Solids Handling Technologies, Inc.*

**Yield locus 1**

Continuous flow
Time at rest: 24 hours
Temperature: 72 F

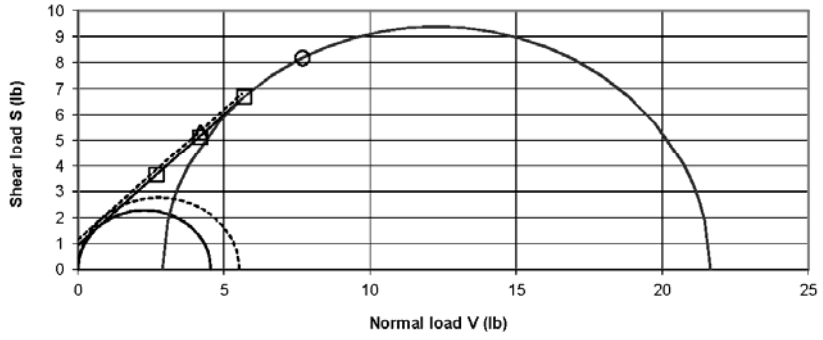
**Virgina Tech**
Report: 133060
Material: EM-SD Coal Mix fines
Moisture: As Rec'd Delta: 52
Particle size: As Rec'd Phi: 50




**Yield locus 2**

Continuous flow
Time at rest: 24 hours
Temperature: 72 F

**Virgina Tech**
Report: 133060
Material: EM-SD Coal Mix fines
Moisture: As Rec'd Delta: 50
Particle size: As Rec'd Phi: 45



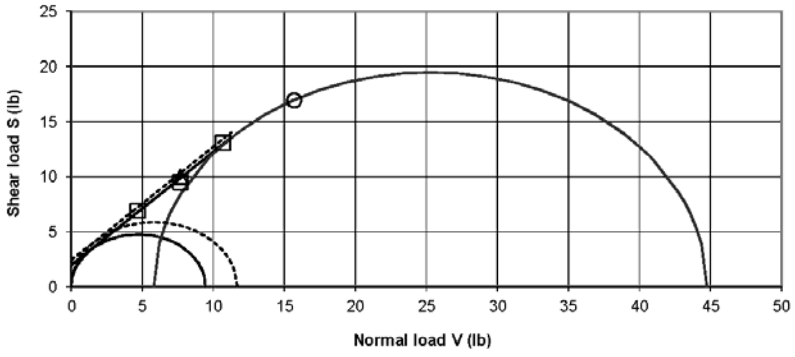

38

*Solids Handling Technologies, Inc.*

**Yield locus 3**

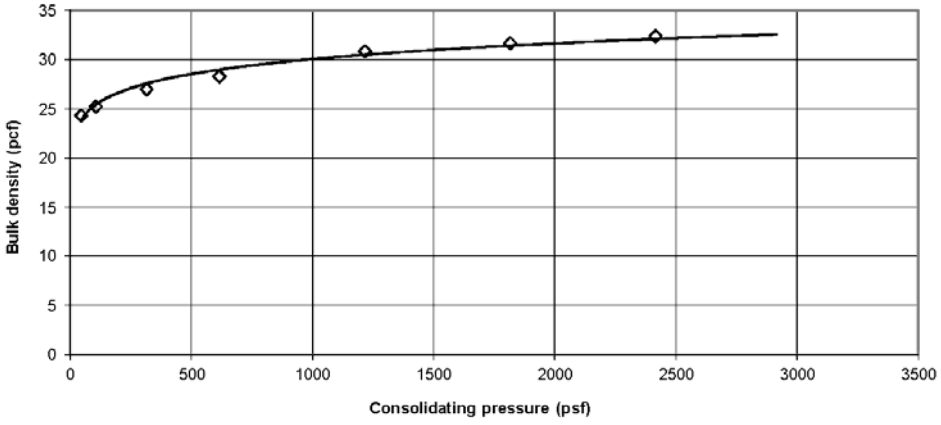
Continuous flow
Time at rest: 24 hours
Temperature: 72 F

**Virgina Tech**
Report: 133060
Material: EM-SD Coal Mix fines
Moisture: As Rec'd Delta: 50
Particle size: As Rec'd Phi: 46



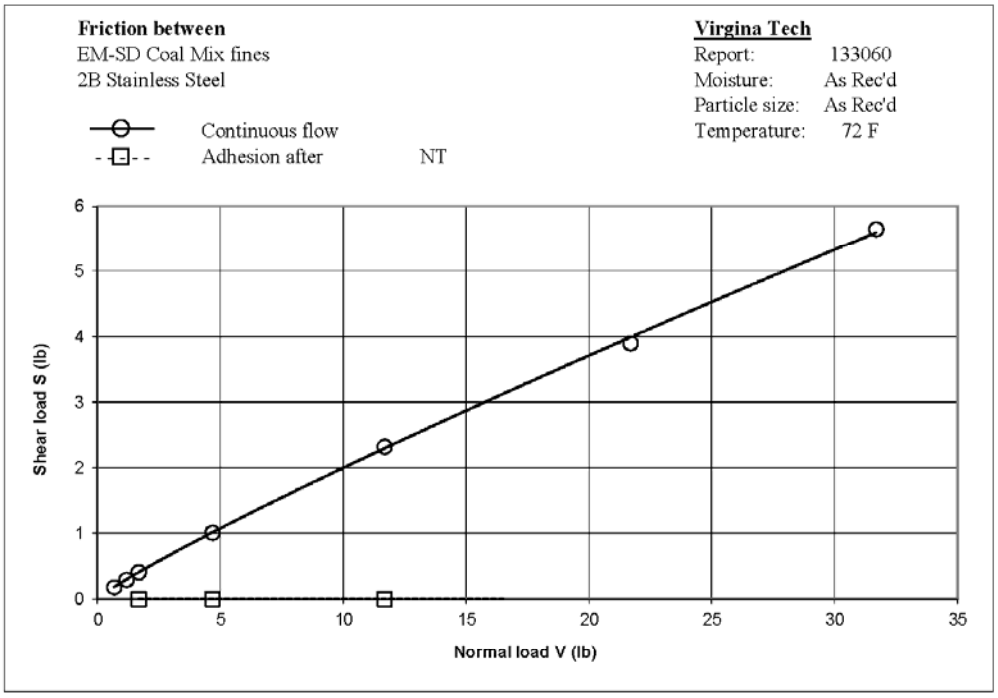

**Bulk density vs Consolidating pressure**

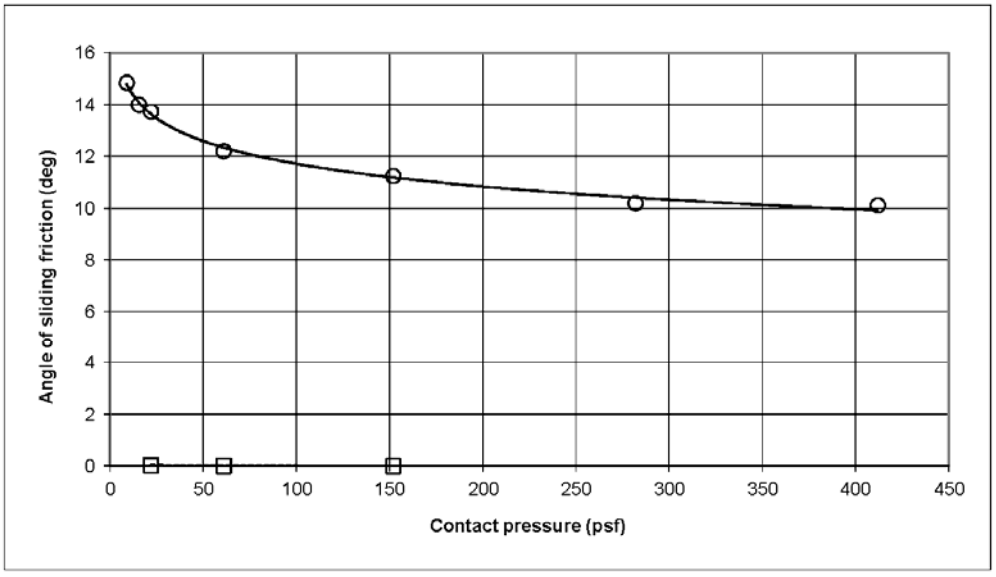
**Virgina Tech**
Report: 133060
Material: EM-SD Coal Mix fines
Moisture: As Rec'd
Particle size As Rec'd




39

*Solids Handling Technologies, Inc.*



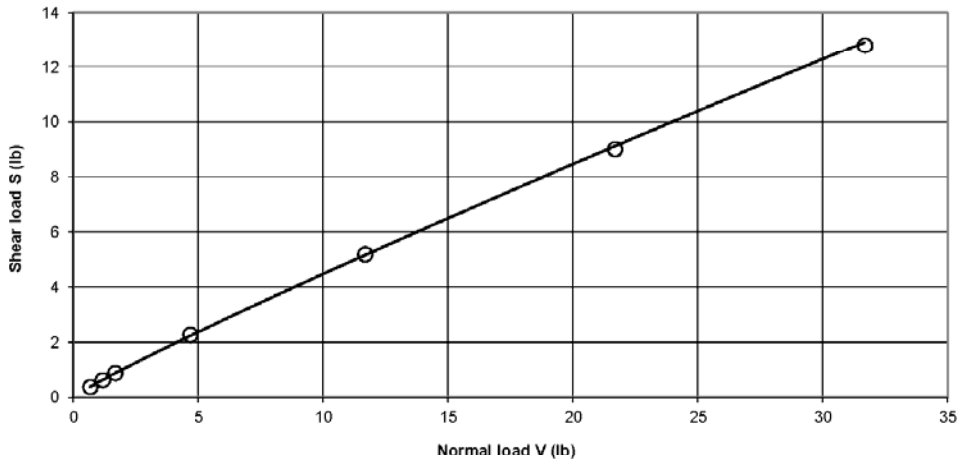

40

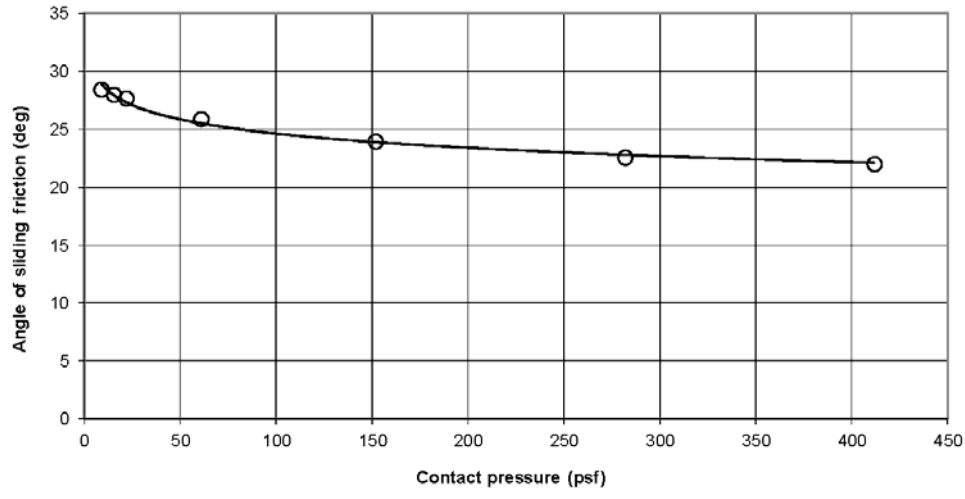
*Solids Handling Technologies, Inc.*

**Friction between**
EM-SD Coal Mix fines
Carbon Steel

**Virgina Tech**
Report: 133060
Moisture: As Rec'd
Particle size: As Rec'd
Temperature: 72 F

Continuous flow
Adhesion after NT




41

## APPENDIX

**How to Interpret a Flow Report**

In order to determine if a new bin or silo will work reliably or to be able to make modifications to an existing troublesome bin or silo, you need to know:

- What type of flow pattern can develop (modes of flow)
- Your material's flow properties.

Modes of Flow

There are two modes of flow that can develop in a bin or silo, funnel flow and mass flow (expanded flow is another but is simply a combination of a mass flow pattern and a funnel flow pattern).

*Funnel Flow*

Funnel flow occurs because the hopper is not sufficiently steep and smooth enough to ensure sliding along its walls. In funnel flow, material flows toward the outlet through a channel that forms within stagnant material caused by friction on the shallow and/or rough walls. With a cohesive solid, this channel expands upward from approximately the hopper outlet, potentially to silo cylinder walls Even if the outlet is fully live, the preferential flow channel may empty out and form a stable rathole. This may:

- limit your live capacity
- cause materials to agglomerate or spontaneously ignite
- cause powders to flood or flow uncontrolled
- enhance particle segregation
- cause silo failure.

Generally, a funnel flow pattern is only suitable for coarse, free-flowing, non-degrading solids when segregation is unimportant.

*Mass Flow*

In mass flow, the hopper is steep and smooth enough to ensure flow of all the material whenever any solid is withdrawn, thereby overcoming the friction that develops between the material and the hopper wall surface.

Where there are many disadvantages to funnel flow, mass flow has certain advantages, as follows:

- flow is uniform
- pressures acting at the outlet are practically independent of the head of solid in the bin

- segregation of particles is minimized by the first-in- first-out flow sequence associated with mass flow and segregated particles are re-mixed as they discharge from the outlet
- fine powders tend to deaerate and flooding is avoided, due to increased residence time

Generally, a mass flow pattern is recommended when handling cohesive materials, powders that can flood, materials which degrade with time and when segregation needs to be minimized.

Material Flow Properties

There are two major considerations for reliable flow; namely, cohesive strength and wall friction properties. Cohesive strength is measured using a bench scale laboratory testing device such as a direct shear tester (Jenike Shear Tester) seen here:



This device is used to determine a material's "Flow Function", whereby the material's cohesive strength is measured as a function of applied consolidation pressure (pressure/ strength relationship). The sample's moisture content and particle size are controlled while the direct shear tester is capable of determining the effects of temperature and time of storage at rest. This information is then used to determine the opening size required to prevent arching and ratholing in a bin or hopper.

The Jenike Shear Tester is also used to measure wall friction properties. Consider that friction develop between a solid and the walls of a bin or hopper. Wall friction determines whether the solid will slide on the wall (mass flow) or adhere to the wall forcing it to flow preferentially on itself (funnel flow) rather than at the walls.

Additionally, the material's compressibility (bulk density/pressure relationship) is determined. A Flow Report is created describing the material's flow properties. This report indicates values to be used to design a new bin or modify and existing one. A Flow Report typically consists of the following:

*Page 1: Title Page*

The first page is obviously a title page with a description of the project, company, etc.

*Pages 2 & 3: Introduction and General Comments*

This contains a General Comments section and is meant to provide general information regarding the flowability of the particular material being tested. These comments are given without any bin geometry in mind and serve to help explain tabulated data in the following pages and how to interpret it.

*Pages 4 & 5: Cohesive Properties Test Results*

**Section 1 Arching and Ratholing Dimensions** of the Flow Report indicates the arching and ratholing dimensions of your material as a function of time at rest, temperature, etc, as follows:

*Arching Dimensions*

Time at Rest, hrs---In the example report, the material was tested to simulate 0 hrs storage (continuous flow) or as if the material was put in a bin and flow initiated immediately, shown on page 4. As well, some period of storage at rest was simulated, such as overnight, 72 hr, etc.

Temp., ºF---The material was tested at 90 °F for 0 hrs and at 90 ºF cooling to room temperature after 3 days at rest to simulate actual storage conditions.

Particle size---An estimate of the material's particle size is given here just to indicate whether the material is coarse or fine. In this case it would be considered fairly fine as it is considered -10 mesh.

Moisture content---The material's total moisture content was measured according to an ASTM standard.

**Arching Dimensions**

P-Factor---P-Factor is an estimation of the effect of excess pressure on your material. The magnitude of the excess pressure or overpressure factor can be estimated for vibration and impact during charging into the bin as follows:

Bulk material: Sample 1
Particle size: -10 mesh
Moisture content: 6.2%
Temperature: 90F

**Section 1: Arching and Rathole Dimensions**
**Continuous flow (0 storage hours)**

Arching Dimensions (ft)

| P factor | Bc | Bp | Bf |
|---|---|---|---|
| 1.0 | 1.0 | 0.5 | 0.6 |
| 1.25 | 1.2 | 0.6 | 0.9 |
| 1.5 | 1.6 | 0.7 | 1.7 |

Note: If arching dimension = 0 then opening size should be based on flow rate and/or feeder size requirements
***** = no dimension given by tests

Vibration
Vibrators can affect flow two ways as follows:
(1) While vibrators are commonly used as flow aid devices, they also pack materials in bins and hoppers. It is recommended that a P-Factor of 1.5 be used to calculate arching dimensions when vibrators are in use.

(2) Vibrators sometimes work well when your material gains strength with time but is easy handling during continuous flow (0 hrs storage). Vibrators should be used only to initiate flow and should be turned off once flow is initiated. The following equations can be used to estimate P-Factor due to vibrator use as described here:

P-Factor = (1 + x/g) or P-Factor = y/g, whichever is larger, where:

x = vertical upward component of acceleration
y = horizontal component of acceleration
g = gravity constant

Impact on filling.

If you are filling your bin with a fine material and it drops close to the outlet,
the P-Factor should be calculated as follows:

P-FACTOR = (1 = m) $[w/(A\ B\ \gamma)]\sqrt{2h/g}$ where:
w = weight flow rate into bin
h = height of fall
m = 0 for a rectangular outlet
m = 1 for a circular outlet
A = impact area
B = outlet size of cone or slot
$\gamma$ = bulk density

Bulk material: Sample 1
Particle size: -10 mesh
Moisture content: 6.2%
Temperature: 90F to room

**Section 1: Arching and Rathole Dimensions**
**After 72 hours at rest**

Arching Dimensions (ft)

| P factor | Bc | Bp | Bf |
|---|---|---|---|
| 1.0 | 2.1 | 1.0 | 1.6 |
| 1.25 | 2.8 | 1.3 | 4.0 |
| 1.5 | 4.7 | 1.9 | ***** |

Note: If arching dimension = 0 then opening size should be based on flow rate and/or feeder size requirements
***** = no dimension given by tests

Mass Flow Bc, ft---"B" is the hopper opening and "c" stands for conical, such that these dimensions are given for 0 hrs and for some period of storage at rest. These are the minimum arching dimensions for a conical hopper that is designed for mass flow.

Mass Flow Bp, ft---"B" again is the hopper opening, while "p" stands for planar or wedge type hoppers, such that these dimensions are given for 0 hrs and for some period of storage at rest. These are the minimum arching dimensions for the width of a slotted opening in a wedge hopper, designed for mass flow. Remember that the slot length should be at least three times the width.

Funnel Flow Bf, ft---"B" is the hopper opening and "f" stands for a funnel flow slotted opening, such that these dimensions are given for 0 hrs and for some period of storage at rest. These are the arching dimensions for a slotted opening in a funnel flow bin, such as a long slot on a flat bottom bin.

**Ratholing Dimensions**

Time at Rest, hrs---Same as above
Temp., °F---Same as above

$\sigma$1, psf---This is the major consolidation pressure acting on the material as it remains in a bin. This pressure is simulated in the laboratory tests.

EH, ft---Effective Head (EH) is determined as a result of material sliding on the cylinder walls. As it slides, the material loses some of its head pressure due to shear along the walls and is referred to as EH rather than the actual head of material. The effective head in the example report ranges from 5' to 40'.

The critical rathole diameter DF is a function of the major consolidating pressure that acts on the solid in the bin, which is expressed in terms of EH, the effective consolidating head of solid in the bin, as follows:

Rathole Dimensions (ft)

Critical rathole diameters Df given as a function of effective head and P factor (overpressure)

| Effective head (ft): | 5 | 10 | 20 | 30 | 40 |
|---|---|---|---|---|---|
| P factor = 1.0 | 6.5 | 12.1 | 18.3 | 19.4 | 20.5 |
| P factor = 1.25 | 7.9 | 14.9 | 23.6 | 25.0 | 26.4 |
| P factor = 1.5 | 9.3 | 17.7 | 24.2 | 25.9 | 27.6 |

$$EH = [R/(u\,k)]\ [\,1 - EXP(-uk\,H/R)]$$

R = hydraulic radius of the cylindrical portion of the bin,
i.e. ratio of cross sectional area to circumference
R= D/4 for a circular cylinder of diameter D or a square cylinder of side D
R = W/2 for a long rectangular cylinder of width W.

u= tan (PHI-PRIME), coefficient of friction between the stored solid and the cylinder walls

k= ratio of horizontal to vertical solids pressure. A value of 0.4 is usually acceptable within cylinders.

h= height of the cylindrical portion of a bin.

Critical Rathole Diameters, Df, ft---"D" is the diameter of the opening required to collapse a rathole, while "f" stands for funnel flow. If your effective is 20' after 3 days at rest the rathole dimension is 18.3', meaning that an 18.3' diameter opening is required to collapse a rathole, even at this low head.

*Page 5: Compressibility Test Results*

**Section 2 Bulk Density / Pressure Relationship** of the Flow Report on Page 5 indicates the bulk density of your material as a function of consolidation pressure or head of material as follows:

Section 2: Bulk Density (Compressibility)

| σ1 (psf) | 45 | 105 | 315 | 615 | 1215 | 1815 | 2415 |
|---|---|---|---|---|---|---|---|
| EH (ft) | 1.2 | 2.6 | 7.2 | 13.5 | 25.9 | 37.8 | 49.4 |
| γ (pcf) | 38.2 | 40.3 | 43.6 | 45.4 | 47.0 | 48.1 | 48.9 |

$\gamma = \gamma 0 * (\sigma / \sigma 0)^{\beta}$

where: γ0 = 35.5 pcf
σ0 = 13.0 psf
β = 0.0610

σ1, psf---Same as above

EH, ft---Same as above

γ, pcf---γ is the Greek symbol used for bulk density. There are a range of bulk densities when dealing with solids, not just loose density and packed density. In this case, γ ranges from 38.2 pcf to 48.9 pcf. γ is used in opening size and hopper angle calculations along with bin and feeder load calculations.

*Page 6: Wall Friction Properties Test Results*

**Section 3 Recommended Hopper Angles for Mass Flow** of the Flow Report beginning on Page 6, indicates the conical and wedge hopper angles required to ensure flow along the walls i.e. mass flow, as follows:

Outlet Dia., Cone, ft - Is usually interpreted as the conical opening size; however, it could be any span in the hopper, not just the opening.

Outlet Width, Slot, ft - Is usually interpreted as the slot opening size; however, it could be any span in the hopper, not just the opening.

$\phi'$ - This is the wall friction angle generated during a wall friction on a particular wall surface. It is given in degrees from horizontal.

$\theta c$ - This is the hopper angle (degrees from vertical) required for mass flow in a conical hopper.

$\theta p$ - This is the hopper (degrees from vertical) required for mass flow along the sidewall of a wedge type hopper.

**Section 3: Recommended Hopper Angles for Mass Flow**

**Storage time at rest: 0 hours**

| | | | | | | |
|---|---|---|---|---|---|---|
| Outlet Dia, Conc, ft | 0.5 | 1 | 2 | 4 | 8 | 16 |
| Outlet Width, Slot, ft | 0.25 | 0.5 | 1 | 2 | 4 | 8 |
| $\Phi'$ (deg) | 25 | 25 | 25 | 25 | 25 | 25 |
| $\theta c$ (deg) | 16 | 16 | 16 | 16 | 16 | 16 |
| $\theta p$ (deg) | 27 | 27 | 27 | 27 | 27 | 27 |

As an example of using these dimensions, you could design a mass flow conical hopper with a 2.1' diameter opening (to prevent arching) or a slot that is 1.0 ft wide, that would require the following hopper slopes (depending on the wall surface preferred):

| Wall Surface | $\theta c$ | $\theta p$ |
|---|---|---|
| 2B stainless steel | 16 | 27 |
| TIVAR 88 | 23 | 33 |
| Carbon steel | 7 | 16 |

To summarize, the Flow Report essentially describes the geometry required to ensure reliable flow. It yields opening sizes to prevent arching and ratholing, bulk density values, and hopper angles required for mass flow.

A Note about Feeders and Gates

If flow from the bin is controlled by means of a feeder, the feeder must be so designed as to draw uniformly from the entire cross section of the outlet.

Uniform withdrawal is especially important when feeding fine powders from slotted outlets. Typical commercial designs tend to draw material either from the front or the back of the slot resulting in a preferential flow channel which will convert a bin intended to mass flow, to a funnel flow bin with the potential to form a stable rathole. The powder may also fluidize within this channel and flood upon discharging from the bin.

Initial fill pressures occur when a bin is filled after being emptied. This can cause significantly higher solids pressures to act on your feeders and you will require approximately 2.5 times more power at startup. Once started, initial fill pressures will convert to flow pressures which are typically lower.

Gates should be used with caution. A gate should be operated fully opened or fully closed and not used to meter or control the rate of withdrawal from a hopper. Partially opened gates create preferential flow channels that cause funnel flow and my jeopardize the structural integrity of your silo.

Glossary of Terms and Symbols

Arching - a no-flow condition whereby material forms a stable arch/bridge over the opening.

Bin - container for bulk solids also referred to as a silo, tank, bunker, vessel, etc.

Bin Discharger -device used to enhance material flow from a bin.

Effective head - convenient way to express consolidating pressure.

Expanded Flow - flow pattern which is a combination of mass flow and funnel flow.

Feeder - device for controlling the rate of withdrawal of bulk solid from a bin.

Funnel flow - flow pattern in which some material flows but most remains stagnant.

Hopper - converging part of a bin.

Mass flow - flow pattern in which all the material is in motion whenever any it is withdrawn.

Ratholing - a no-flow condition in which material forms a stable vertical hole within the bin.

B - span across a bin at any elevation of the bin, ft

Bc - minimum diameter of a circular outlet in a mass flow bin, ft

Bf - minimum width of a rectangular outlet in a funnel flow bin, ft

Bp - minimum width of an slotted outlet in a mass flow bin, ft

D - diameter of cylindrical portion of a bin, ft



DF - critical rathole dimension, ft

EH - effective consolidating head, ft

h - height of cylinder, ft

k - ratio of horizontal to vertical pressure, usually 0.4

R - hydraulic radius, ft

$\gamma$ - bulk density, pcf

$\theta c$ - maximum recommended angle (degrees from vertical ) of conical hoppers and end walls of transition hoppers for mass flow.

$\theta p$ - maximum recommended angle (degrees from vertical) of side walls of wedge, chisel or transition hoppers for mass flow

$\mu$ - coefficient of friction between solid and wall surface.

$\sigma_1$ - major consolidation pressure, psf

$\phi'$ - kinematic angle of friction between a solid and a wall, degrees

# Appendix C. MATLAB Codes used for Estimating Gasification Kinetic Parameters

In Appendix C, all the MATLAB codes used for estimating the kinetic parameters of devolatization are presented. Firstly, the codes used for estimating the weight loss profiles using the Gaussian distribution method are presented. Secondly, the elaborate codes used for the matrix inversion algorithm are presented. Any comments preceded by % are part of a description and do not actually belong to the code.

## C.1 Distributed Activation Energy Model – Gaussian Distribution of Activation Energy

```
%  DAEM using Miura's method
function Vmodel = miura2()
clear;
clc;
format short
global E T1 T2 T3 T4 alpha beta H1 H2 H3 H4

alpha = exp(16.209);
beta = 0.068;
% Heating rate, C/min
H1 = 5;
H2 = 10; H3 = 20; H4 = 40;
% Initial Temperature, K
To = 400.5;
[E] = xlsread('SBrates_miura.xls','Data','A5:A24'); % Obtained Activation Energy, KJ/mol
[Vexp] = xlsread('SBrates_miura.xls','Data','g5:g24'); % Exp weight loss

 n = size(E);

[T1] = xlsread('SBrates_miura.xls','Data','c5:c24');
[T2] = xlsread('SBrates_miura.xls','Data','d5:d24');
[T3] = xlsread('SBrates_miura.xls','Data','e5:e24');
[T4] = xlsread('SBrates_miura.xls','Data','f5:f24');

z1  = zeros(size(E));
z2  = zeros(size(E));
z3  = zeros(size(E));
z4  = zeros(size(E));
```

```
Ko = zeros(size(E));

int1 = zeros(size(E));
int2 = zeros(size(E));
int3 = zeros(size(E));
int4 = zeros(size(E));

Vmodel = zeros(size(E));


for i=1:size(E)

z1(i) = quadgk(@temp, To, T1(i));
z2(i) = quadgk(@temp, To, T2(i));
z3(i) = quadgk(@temp, To, T3(i));
z4(i) = quadgk(@temp, To, T4(i));

Ko(i) = alpha*exp(E(i)*beta) ;
int1(i) = -(Ko(i)/H1)*z1(i);
int2(i) = -(Ko(i)/H2)*z2(i);
int3(i) = -(Ko(i)/H3)*z3(i);
int4(i) = -(Ko(i)/H4)*z4(i);
Vmodel(i)= quadgk(@integral,0,E(i));
end
plot(T1,Vexp,'-r',T2,Vexp,'-b',T3,Vexp,'-g',T4,Vexp,'-c',
T1,Vmodel,'or',T2,Vmodel,'ob',T3,Vmodel,'og', T4,Vmodel,'oc')

title('Comparison of Experimental and Calculated V/Vf for Sub-Bituminous Coal')
xlabel('Temperature, K')
ylabel('V/Vf')
legend('5 C/min', '10 C/min','20 C/min','40 C/min')

function y  = temp(T)
global E
for i=1:size(E)
y=exp(-E(i) *1000./(8.314*T)); % The exponential term
end

function p = integral(X)
global E

% Parameters obtained from logistic distribution
fo = 0.000298051;
A=0.84114;
w=123.06867;
```

```
Ec=267.37791;
 p = zeros(size(E));
for i=1:size(E)
p =(((fo + (A/(1.2533*w))*exp(-2*((X-Ec)/w).^2))));
end
```

The same code is used for determining the weight loss profiles of all feedstock materials by inputting the required data sets of those particular feedstocks.

## C.2 Matrix Inversion Algorithm

The codes presented here are shown for BT sub-bituminous coal only as an illustration. The same codes are used for estimating the kinetic parameters of all other feedstocks, both single fuels as well as blended feedstocks, by inputting the appropriate TGA data sets at different heating rates.

1. Matmodel2: This code uses the inversion algorithm described in Chapter 2 and calculates the values of activation energy, pre-exponential factor and initial mass fraction of each reaction occurring during devolatilization. This code is a part of several other codes used in the calculation of these kinetic parameters. Both real TGA data and simulated data can be used in this code.

```
function c= Matmodel2(T1,T2,B,Tr,xx,B1,B2,T0)
% T1 and T2 are the temperature data sets corresponding to the values of X
% for the specified number of reactions.

% B1 and B2 are the heating rates corresponding to T1 and T2
% Tr is the reduced set of temperature data selected for the calculation of PE.
% B is the heaitng rate corresponding to Tr
% xx is the set of X values chosen by specifying the number of reactions

warning off
options2=optimset('MaxIter',100000,'TolFun',1e-4,'TolX',1e-4,'MaxFunEvals',100000);

% This defined the error tolerance of the calculations
n=length(T1); % This specifies how many calculations there will be for E and PE

for i=1:n
E(i)=fminbnd('AEerror2',0,1200,options2,T1(i),T2(i),T0,B1,B2);
% This applies the built-in solver 'FMINBND' to the program 'AEerror2' with the
% specified parameters. The minimum and maximum values of E that can be found by
iteration
% are 0 and 1200 respectively. Options2 defines the tolerance of the iteration.
```

```
PE(i)=Ai2(E(i),T1(i),T2(i),T0,B1,B2);
% This uses the code Ai2 with the specified parameters to calculate the value of PE using the
calculated value of E

PE(1)=0.0000001; % Initial guess for PE

chi_check20(i)=chi(E(i),PE(i),T1(i),T0,B,B2);
chi_check100(i)=chi(E(i),PE(i),T2(i),T0,B,B2);
% the above two commands provide a check of the matrix Ψ.
end

check=[chi_check20' chi_check100']

a=isfinite(PE'); % This find all the finite values of PE
PE=PE(a);
E=E(a);

q=length(Tr); % reduces no of data points in TGA set
npoints=q;
nn=length(E);
Tr1i=Tr;

for i=1:npoints
for j=1:nn
term1(j)=quad(@term,T0,Tr1i(i),[],[],E(j));
chi1(i,j)=exp((-PE(j)/B)*(term1(j)));
chi1(i,nn+1)=1;
chi_1(i,j)=chi(E(j),PE(j),Tr1i(i),T0,B,B2); %Uses the code 'chi' to create 9
chi_1(i,nn+1)=1;
end
end
% The above loop creates the chi matrix using the obtained E and PE. The function 'term'
% represents the temperature integral.

options3=optimset('TolX',10);
f0=lsqnonneg(chi_1,xx) %This uses matrix inversion to calculate the values of f0.

m=100;
T=linspace(T0,1167,m);
for i=1:m
for j=1:nn
term1(j)=quad(@term,T0,T(i),[],[],E(j));

chi2(i,j)=exp((-PE(j)/B1)*(term1(j)));
chi2(i,nn+1)=1;
chi_2(i,j)=chi(E(j),PE(j),T(i),T0,B,B2); % Uses the code 'chi' to create chi
```

```
chi_2(i,nn+1)=1;
end
end
% This loop creates the chi matrix for the other heating rate.

[length(f0) length(E') length(PE')];

E(n+1)=0;PE(n+1)=0;
% This defined the last E and PE values as 0 since they represent ash.

c=[f0 E' PE'];
% The final output of this code. These are the values of f0, E and PE for each reaction.
```

2. AError2: This function solves each term of the temperature integral defined in Eq. 2.4.26 in Chapter 2 using the inbuilt EXPINT function.

```
function error = AEerror2(E,T1,T2,T0,B1,B2)
% This uses the EXPINT function to find the integral from X to inf of exp(-t)/t dt

R=8.314; % Universal gas constant in j/molK
% Each term in the temperature integral is defined here.

first=T0*exp(-E*1000/(R*T0));
aa=E*1000/(R*T0);
bb=exp(-aa)/aa;
second=(-E*1000/R)*expint(aa);
third=T1*exp(-E*1000/(R*T1));
cc=E*1000/(R*T1);
dd=exp(-cc)/cc;
fourth=(E*1000/R)*expint(cc);
fifth=first;
sixth=second;
seventh=T2*exp(-E*1000/(R*T2));
ee=E*1000/(R*T2);
ff=exp(-ee)/ee;
eighth=(E*1000/R)*expint(ee);
ls=(1/B1)*(first-second-third+fourth); %LHS of EQ 2.17
rs=(1/B2)*(fifth-sixth-seventh+eighth); %RHS of EQ 2.17
error = sqrt((1-rs/ls)^2);
```

3. Ai2: The value of pre-exponential factor is estimated using this code by combining Eq. 2.4.22 through Eq. 2.4.26 of Chapter 2.

```
function y = Ai2(E,T1,T2,T0,B1,B2)
R=8.314; % Universal gas constant in j/molK
% terms in Eq 2.26
```

```
first=T0*exp(-E*1000/(R*T0));
aa=E*1000/(R*T0);
bb=exp(-aa)/aa;
second=(E*1000/R)*expint(aa);
third=T1*exp(-E*1000/(R*T1));
cc=E*1000/(R*T1);
dd=exp(-cc)/cc;
fourth=(E*1000/R)*expint(cc);
Ai=-B1/(first-second-third+fourth);
y=Ai;
```

4. Chi: This code calculates the matrix Ψ described in Chapter 2.

```
function error = chi(E,PE,T2,T0,B1,B2);
%This uses the approximation for integral from X to inf of exp(-t)/t dt to
% create the matrix chi.
A=PE;
R=8.314; % Universal gas constant in j/molK
first=T0*exp(-E*1000/(R*T0));
aa=E*1000/(R*T0);bb=exp(-aa)/aa;
second=(E*1000/R)*expint(aa);

third=T2*exp(-E*1000/(R*T2));
cc=E*1000/(R*T2);dd=exp(-cc)/cc;
fourth=(E*1000/R)*expint(cc);
rhs=(A/B1)*(first-second-third+fourth);
error = exp(rhs);
```

5. Term:

```
% This code simply defines the exponential term ‘exp(-E/RT)

function y=term(T,E)
y=exp(-E*1000./(8.314*T)); % The exponential term
```

6. Orates: The TGA curves for known and unknown heating rates are created using this code. The kinetic parameters obtained using Matmodel.m are used as inputs to this code. The matrix Ψ is created and mass fraction remaining is obtained by multiplying with mass fraction associated with each reaction.

```
function z=orates(f0,T0,E,PE,b,Tup,m)
% b is the heating rate in K/min
% Tup is the maximum temperature that the curve should reach
% m is the number of points on the curve


B=b/60; %K/sec
```

```
s=size(E');
nn=s(:,1);
T=linspace(T0,Tup,m); % This selects a number of evenly spaced temperature points
for i=1:m
for j=1:nn
term1(j)=quad(@term,T0,T(i),[],[],E(j));
chi2(i,j)=exp((-PE(j)/B)*(term1(j)));
chi2(i,nn+1)=1;
end
end
% This loop creates the matrix chi using kinetic and temperature data

M=chi2*f0
z=[T' M]

x=z(:,1);y=100.*z(:,2);
deriv=-diff(y)./diff(x) % This calculates the discreet derivatives of the data sets
x=x(2:length(x));
hold on
plot(x,deriv,'m--') % This plots the derivative curve on the same axes
ylabel('Derivative Mass Fraction Remaining')
plot(T,M,'b.') % This plots the TGA curve
```

7. Pyrolysis: This code applies the DAEM algorithm to actual TGA data. Data from any two heating rates can be used as input to this code.

```
function c = pyrolysis()
clear;
clc;
% Heating Rates, C/min
 b1=5;
 b2=40;
B1=b1/60; % heating rate K/sec
B2=b2/60;% heating rate K/sec
T0=300; % Initial temp
R=8.314; %j/molK
 nrxns=50;
 rnTGA=100;
% Real TGA data for lower heating rate
 [TT1,Temp1,alldata] = xlsread('SBrates.xls','5 C min','d154:d18220'); % Temp Data
 [x1,MF1,alldata] = xlsread('SBrates.xls','5 C min','h154:h18220'); % Weight loss data

% Real TGA data for higher heating rate
[TT2,Temp2,alldata] = xlsread('SBrates.xls','40 C min','d167:d6726');
[x2,MF2,alldata] = xlsread('SBrates.xls','40 C min','h167:h6726');

Tr1=linspace(TT1(1),TT1(length(TT1)),rnTGA)'; % reducing TGA points
```

```
Tr2=linspace(TT2(1),TT2(length(TT2)),rnTGA)'; % reducing TGA points

 Xr1=interp1q(TT1,x1,Tr1);
 Xr1(1)=0.998;

 Xr2=interp1q(TT2,x2,Tr2);
 Xr2(1)=0.998;
 Xr2(end)=0.56;
%
% %Initial and end values need to be specified to allow calculations
%
 TT1=Tr1;
 TT2=Tr2;
 x1=Xr1
 x2=Xr2
 x1(length(x1))=x1(length(x1)-1);
 X=linspace(0.998,0.56,nrxns)' % Choosing conversions
%
 T1=interp1q(flipud(x1),flipud(TT1),X);
 T2=interp1q(flipud(x2),flipud(TT2),X);
%
 plot(T1,X,'go')
 hold on
 plot(T2,X,'ro')
 plot(TT1,x1,'g')
 plot(TT2,x2,'r')
%
 deriv1=-100*diff(x1)./diff(TT1) %Calculating Derivatives
 Tt1=TT1(2:length(TT1))';
 deriv2=-100*diff(x2)./diff(TT2)
 Tt2=TT2(2:length(TT2))';
  plot(Tt1,deriv1,'g')
  plot(Tt2,deriv2,'r')

 Xtga=x1; % Data for either heating rate may be used to calculate E and PE
 data3=Matmodel2(T1,T2,B1,Tr1,Xtga,B1,B2,T0) % Applying DAEM algorithm to data
 f0=data3(:,1)
 E=data3(:,2)
 PE=data3(:,3)
 c=[f0 E PE];

% Plotting kinetic parameters as a function of conversion
f0=f0(1:50);
X=X(1:50);
figure(2);
stem(X,f0)
```

```
xlabel('Mass Fraction Remaining');
ylabel('f0, Mass Fraction of Fuel Associated with Reaction');

E=E(1:50); X=X(1:50);
figure(3);
stem(X,E)
xlabel('Mass Fraction Remaining');
ylabel('E (KJ/mol)');

PE=PE(1:50);
X=X(1:50);
figure(4);hold on
stem(X,PE,'.b')
xlabel('Mass Fraction Remaining');
ylabel('A (/sec)');
```

8. Pyrolysis1: This code is used for estimating the weight loss profiles at unknown heating rates not used in the algorithm. The kinetic parameters obtained for real TGA data at known heating rates using previous codes are used as inputs to this code.

```
function c = pyrolysis1()
% nrxns is the number of points at which to calculate the kinetics, or the number of reactions
% rnTGA is the number of points that the TGA data should be reduced to
% nTGA is the number of points that orates.m uses to create the data
% b1 and b2 are the heating rates used in K/min
clear;
clc;

b1=10;
b2=20;
B1=b1/60;
B2=b2/60;

T0=300;
R=8.314; % Universal gas constant in j/molK

nTGA=100;
rnTGA=100;

f0= [0.54894922  0.00370381   0.021526785  0.007376867  0.006970187  0.026344887
     0.016856559 0.011701375  0.022369799  0.012156829  0.022985722  0.019675679
     0.007490796 0.042997369  0.003156278  0.027915627  0.011575587  0.0097363
     0.014827114 0.004765505  0.010518342  0.008007697  0.008804414  0.008575667
```

```
    0.00905741   0.008390065  0.009093133  0.00779559   0.009968905  0.007247496
    0.011794159  0.005119809  0.008592462  0.012718192  0.030654896 0]';

E = [293.810372  523.6464203  439.7116109  4.85895261   92.83742045  66.94006184
    59.85523809  223.0812877  1199.999906  24.80397376  41.08870387  100.0708152
    119.5127056  182.4481902  197.6091577  243.7077374  262.3374918  305.2370132
    330.345946   356.970629   382.4309661  403.9481959  410.872351   398.9204904
    376.3977433  350.659064   328.0705123  305.8166101  284.0888109  263.640219
    245.7139639  230.57669    216.8757918  200.5473982  141.6867706];

PE= [1.00E-07    6.34E+87     1.45E+73     0.026853079  1.11335E+12  34108032.39
    1896602.687  1.18E+28     1.20E+156    1.795308473  18.96809319  612261.6267
    15991778.85  3.93468E+11  4.2429E+12   4.97E+15     8.43E+16     5.16E+19
    2.06E+21     9.46E+22     3.14E+24     4.80E+25     6.35E+25     4.05E+24
    5.06E+22     4.04E+20     5.55E+18     8.62E+16     1.57E+15     3.71694E+13
    1.34296E+12  74485045041  5207872042   278720029.2  38041.67707];
% Kinetic Parameters obtained using known heating rates

data1=orates(f0,T0,E,PE,B1*60,1200,nTGA); % Generates TGA data at heating rate B1
TT1=data1(:,1); x1=data1(:,2); % Defines temperature and weight percent data sets

data2=orates(f0,T0,E,PE,B2*60,1200,nTGA); % Generates TGA data at heating rate B2
 TT2=data2(:,1); x2=data2(:,2); % Defines temperature and weight percent data sets

c = [data1 data2]; % Temperature and weight loss data at unknown heating rates

deriv1=-100*diff(x1)./diff(TT1) %Calculating Derivatives
 Tt1=TT1(2:length(TT1))';
 deriv2=-100*diff(x2)./diff(TT2)
 Tt2=TT2(2:length(TT2))';
  plot(Tt1,deriv1,'g')
  plot(Tt2,deriv2,'r')
```